THE NIGERIAN INSTITUTION OF PROFESSIONAL ENGINEERS AND SCIENTISTS

IN COLLABORATION WITH

NATIONAL CENTRE FOR ENERGY, ENERGY COMMISSION OF NIGERIA

PRESENTS

BOOK OF PROCEEDINGS

2nd International Conference

theme:

EMERGING TRENDS IN SCIENCE AND TECHNOLOGY

TOWARDS INDUSTRY 4.0 REVOLUTION

15TH - 17TH FEB 2023

9:00AM DAILY

VENUE: NATIONAL CENTER FOR ENERGY AND ENVIRONMENT, UNIVERSITY OF BENIN

CHIEF HOST
PROF. D.I. IGBINOMWANHIA
NCEE (ENERGY COMMISSION OF NIGERIA)
UNIBEN, BENIN CITY.

HOST
DR. O.O IGHODARO
CHIEF EXECUTIVE OFFICER NIPES

INTERNATIONAL KEYNOTE SPEAKER
DR. SHIVAN CHETTEY
Director, Biomedical Industrialisation & Globalization Division, Wits Health Consortium, South Africa

NATIONAL KEYNOTE SPEAKER
PROF. IKUOBASE EMOVON
Dean College Of Engineering, Federal University Of Petroleum Resources, Effurun, Delta State

ABOUT NIPES

Nigerian Institution of Professional Engineers and Scientist (NIPES) is a research community which combines the engineering and science profession. It is the National Division of the incorporated Trustees of the International Association of Professional Engineers and Scientists which is registered in accordance with the provision of the Allied Matters Act. Cap C20, laws of the Federation of Nigeria. NIPES stands to promote and facilitate the exchange of research information among engineers and scientists and provide opportunities for interaction among members in the industry.

ABOUT NCEE

National Centre for Energy and Environment is an agency of the Energy Commission of Nigeria. It was established by the federal Government of Nigeria on the 12th of March 2009, through the 2009 appropriation bill. The Centre is situated in University of Benin, Benin City in the South-South region of Nigeria. The Centre's mandate is to promoted renewable energy sources through research and developmental initiatives in Bioenergy production and Environmental Forensics/Management, supported by technology transfer.

ABOUT THE CONFERENCE

The Second International Conference was held both physically and virtually from the 15th to 17th of February 2023. The conference theme was entitled: "Emerging Trends in Science and Engineering towards Industry 4.0 Revolution". The aim is to bring together academicians, experts, scholars, policy makers and industrialists to discuss contemporary and cutting-edge research issues in engineering and science geared towards meeting key Sustainable Development Goals. The Conference will also provide participants the opportunity to develop new collaborative initiatives in different areas of sciences and engineering

CONFERENCE SUBTHEMES

- Energy and Power (EP)
- Environmental Sustainability (ES)
- Renewable energy & Carbon Capture (RCC)
- Material and Industrial Process (MI)
- Modelling and Simulation (MS)
- Local Content in Manufacturing (LC)
- Mathematics-Industrial Physics (MP)
- Nanoscience and Nanotechnology (NN)
- ICT and Smart Systems (ICT)
- Waste Management (WM)

CONTENTS

NIPES-NCEE Conference Proceedings
The 2nd International Conference 15th-17th Feb. 2023
1-11
www.nipesjournals.org.ng

DEVELOPMENT OF SOLID WASTE MANAGEMENT STRATEGY FOR AUCHI POLYTECHNIC NEW STAFF QUARTERS, AUCHI, EDO STATE, NIGERIA

A. Rawlings[1]*, S. Seghosime[2]

[1]*Department of Civil Engineering, Faculty of Engineering, University of Benin, Benin City, Edo State, Nigeria
[2]Department of Civil Engineering, School of Engineering, Auchi Polytechnic, Auchi, Edo State, Nigeria.
Corresponding Author E-mail Address: seghosimeh@gmail.com

Abstract

Proper management of solid waste is essential for environmentally sustainable living conditions, but it remains a challenge for many developing countries like Nigeria including their tertiary institutions and environs. Therefore, this study has developed a solid waste management strategy for Auchi Polytechnic new staff quarters based on information on their existing solid waste management and the rate of waste generation in the quarters. Information on the existing waste management in the new staff quarters was gathered via interviews conducted in some selected sections of the Polytechnic community (Administrative block, Environmental and Sanitation Department and Works and Maintenance Department) while waste generation analysis was used to obtain data on the rate of waste generation in the quarters. The findings from the studies revealed that currently, there is no well-structured collection/disposal mechanism of solid waste in the new staff quarters. Results from waste generation rate showed that the amount of solid waste generated in the new staff quarters on a daily basis is quite high with values ranging from 352.09kg/day to 732.76kg/day and on a weekly basis per component, values ranges from 281.18kg/week to 1600.80kg/week. The solid waste consists of various components with generating rate of 1125.73kg/month (6.33%), 1328.74kg/month (7.47%), 5357.47kg/month (30.12%), 3471.96kg/month (19.52%), 6503.26kg/month (36.56%) for paper, aluminium, plastic, polythene and organic wastes respectively. Organic waste comprises the highest composition of the waste and the least was paper. In decreasing order, the composition of the waste is organic waste> plastics>polythene> aluminium>paper. Based on the findings from the study, possible solid waste management strategies for a sustainable management of the waste in the new staff quarters was developed to include the practice of the 3R (reduce, reuse and recycle) concept, composting, proper training, provision of incentive and other fiscal policies.

***Key Words**: Solid Waste Management, Waste Generation Rate, Auchi Polytechnic New Staff Quarters, Waste Collection, Waste Disposal, Decomposable.*

1.0 Introduction

Solid waste refers to any type of garbage, trash, refuse or solid material that is discarded because it has served its purpose or is no longer useful [1,2]. It can be categorized according to where the waste is generated (source). The sources of solid waste include residential, commercial, institutional, and industrial activities [3,4]. Certain types of wastes that cause immediate danger to exposed individuals or environments are classified as hazardous. All non-hazardous solid waste from a community that requires collection and transport to a processing or disposal site is called refuse or municipal solid waste (MSW). Refuse includes garbage and rubbish. Garbage is mostly decomposable food waste while rubbish is mostly dry material such as glass, paper, cloth, or wood. Garbage is highly putrescible or decomposable, whereas rubbish is not. Trash is rubbish that includes bulky items such as old refrigerators, couches, or large tree stumps. Trash requires special collection and handling.

Around the world, waste generation rates are rising. Over 2 billion tons of municipal solid waste are produced annually [5]. In 2020, the world was estimated to generate 2.24 billion tonnes of solid waste, amounting to a footprint of 0.79 kilograms per person per day [6]. With rapid population growth and urbanization, annual waste generation is expected to increase by 73% from 2020 levels to 3.88 billion tonnes in 2050 [7]. This is indicating that solid waste is continuously increasing, thus their management has proved to be a rather challenging issue in the 21st century [8] and this has become a major concern for researchers in the world. Because of its sticky nature, solid waste has the quality of accumulating, and physically insulting the environment [9]. Most of the solid wastes like plastic, rubber etc. are non-biodegradable which means that they do not get broken down through organic processes, hence when they accumulate, they pose a health threat to the people.

Solid waste management is the collecting, treating, and disposing of solid material that is discarded because it has served its purpose or is no longer useful [10]. Improper disposal can lead to adverse health outcomes, for example through water, soil and air contamination. Vulnerable groups such as children are at increased risk of adverse health outcomes. About 54 million tons of e-waste, such as TVs, computers and phones, are created annually (2019 data) with an expected increase to 75 million tons by 2030 [11]. In 2019 only 17% of e-waste was documented as being properly collected and recycled. Exposure to improperly managed e-waste and its components can cause multiple adverse health and developmental impacts especially in young children. Compared to those in developed nations, residents in developing countries (such as Nigeria), especially the urban poor (like Auchi), are more severely impacted by unsustainably managed waste. In Auchi town, municipal solid waste is often disposed in unregulated dumps or openly burned [12] and such is the case for Auchi Polytechnic New Staff Quarters. These practices create serious health, safety, and environmental consequences. Poorly managed waste serves as a breeding ground for disease vectors, contributes to global climate change through greenhouse gas emission, and can even promote urban violence. Poor waste collection leads to environmental and marine pollution and can block water drains, thus resulting to flooding. Also standing waters in waste items favour cholera and vector-borne diseases such as malaria and dengue. Therefore, managing waste properly is essential for building sustainable and livable cities, but it remains a challenge for many developing countries and cities.

In modern society, majority of the items which are used on a daily basis are design as disposable material after use. This change in life style coupled with agricultural waste has increased the problem of solid waste management in Auchi Polytechnic New Staff Quarters. Also dumping of solid waste in some places such as corners and backs of buildings in the New Staff Quarters has resulted in an unpleasant odour in the surrounding. It has also created unsanitary conditions and these conditions in turn can lead to pollution of the environment and outbreaks of vector-borne disease (that is, diseases spread by rodents and insects). Hence, there is need for a solid waste management plan for the new staff quarters which will provides a complete way and sets a path to achieve new waste minimization, diversion and disposal targets [13,14] in the new staff quarters. Therefore, this study is aimed at developing a potential solid waste management strategy for the new staff quarters in Auchi Polytechnic, Auchi, Edo State, Nigeria. This strategy will be beneficial in defending the environment from the harmful effects of improper solid waste management.

2.0 Materials and Methods

2.1 Study Area

Auchi Polytechnic New Staff Quarters is situated in Auchi Polytechnic which is sited in Auchi. Auchi is located in the northern part of Edo state and is the headquarters of Etsako-west Local Government Area of Edo State. It has an elevation of 188m [15] and covers a total land area of 94,562 kilometer square [16]. Auchi lies between latitude 7^0 10' to 7^0 20' N and longitude 6^0 16' to 6^0 36'E [17]. It is bounded to the north by Jattu, to the south by Aviele, to the east by Iyakpi and Iyakpe and to the west by Owan LGA [18]. Auchi has a sub humid climate with mean annual rainfall in the range of 1000mm to 1500mm and the mean monthly temperature varying from 20°C to 25°C with diurnal temperature range of about 12.4°C [19]. Auchi is underlain by sedimentary formation of the Miocene-Pleistocene age [20,21] and it constitute part of the south central (Lower Niger sedimentary rock areas). The geology is generally marked by top red or reddish-brown earth, composed of ferruginized or literalized clay sand [22]. Auchi has two distinct seasons. These are the wet (rainy) season and the dry season. The rainy season occurs between the months of April and October with a short break in August. The dry season on the other hand lasts from November to April with cold harmattan winds in December [23], but with the effect of global warming and climate change, rains have been observed to fall irregularly almost in every month of the year with double peak periods in July and September. Auchi has a population of about 197,609 persons [24].

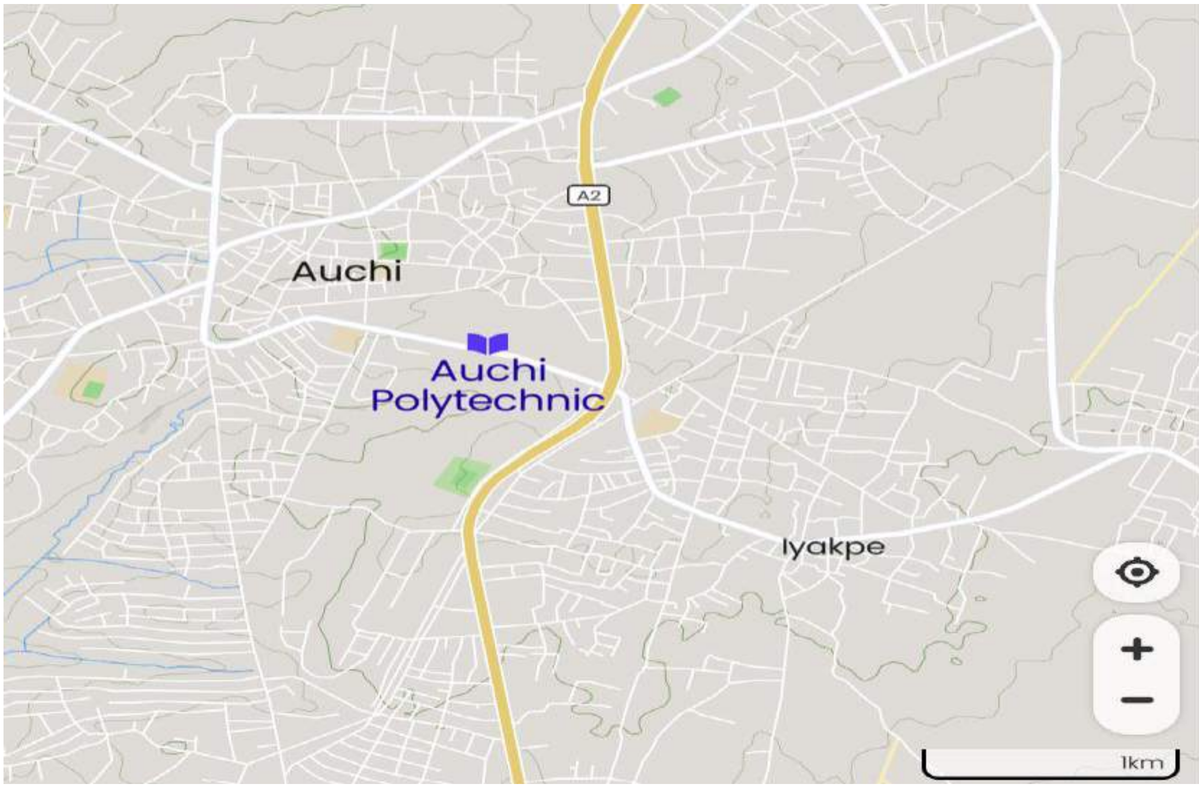

Figure 1: Map Showing Auchi Polytechnic, Auchi (Source: Mapcarta, 2023b)

Figure 2: Map Showing Auchi Polytechnic New Staff Quarters (Source: WorldPlaces, 2023)

2.2 Data Collection

Data were collected via interviews from the administrative block (administrative office), environmental and sanitation department and works and maintenance department (health care centre), all in Auchi Polytechnic, Auchi. These data include the number of buildings/population and the existing solid waste management system in the new staff quarters. Also, studies on waste generated in the new staff quarters for a period of one month (September, 2022) was carried out. This was to obtained data on the rate of generation of waste and the type of waste generated in the new staff quarters (so as to be able to propose a method for disposing them).

2.3 Solid Waste Generation Rate

In this study, quantification at the point of waste collection was employed to estimate the amount of waste generated in the new staff quarters. This is because, information from the interview revealed that the actual population of the new staff quarters was unavailable (but both academic and non-academic staffs were 150 in number) and that there are no records and well-structured collection/disposal mechanism of solid waste in the new staff quarters. Using this method, the wastes were sorted, weighed and categorized. The new staff quarters is composed of different buildings including bungalow and storey buildings with about 170 apartments, but about 100 apartments agreed to participate in this study, thus waste collection containers/bins were placed at each apartment to serve as collection locations. The targeted apartments were provided with two waste bins each with labels as organic and inorganic waste. The waste collection process was done by collecting wastes on a daily basis directly from each apartment considered for a week. Sorting and weighing of the solid wastes were carried out on a daily basis at respective collection locations. Sorting was done manually by hand with the use of hand gloves and weighing was carried out with a weighing balance. The various solid waste components at each collection location were aggregated respectively to obtain the total amount of the waste component generated daily. This procedure was repeated for three more weeks in order to cover the duration of the study (one month). The collected wastes were sorted accordingly into 5 categories namely: Paper, Aluminium (tins), Plastic, Polythene and Organic Waste (food waste). Using arithmetic mean the average daily total weight of each solid waste component for a period of one month was estimated. The percentage composition of the solid waste components was estimated using the following formulae as specified by Spangler (2018):

$$\%\ composition\ of\ solid\ waste\ component = \frac{Weight\ of\ solid\ waste\ component\ generated}{Total\ weight\ of\ solid\ waste\ generated} \times 100 \qquad \text{.......... (1)}$$

3.0 Results and Discussion

The results from this study will be discussed in two sections as indicated below:

3.1 Current Solid Waste Management in Auchi Polythenic New Staff Quarters

Currently, solid waste management in Auchi Polythenic New Staff Quarters is basically controlled and managed by the Works and Maintenance Department in the polytechnic. This department revealed that the new staff quarters was design in such a way that an apartment is supposed to generate 6.01kg of solid waste per day and this was used to plan the solid waste management practice in the new staff quarters. With the limited numbers of sanitation workers and the alarming rate of waste generation in the new staff quarters, there are few major collection locations with dumpsters to collect all the wastes generated in the new staff quarters for transport to disposal site, thus no recycle bins are provided at the waste collection locations. The frequency of transporting the bulky waste collected to disposal site is once in every month or two months and when transportation services are not available, the wastes (including recyclable materials) are burnt directly at the collection location. The findings from this study indicated that the waste generated in the new staff quarters is made up of different components (organic and non-organic). At present the new staff quarters do not practice segregation of waste into recycle bins. All the wastes are gathered in a garbage plastic bags and disposed of directly into dumpsters which are situated at the collection location with no recycle bins. The substantial amount of organic waste (food waste) that is dumped at these collection locations gets mixed with all other kinds of dry and wet waste. Consequently, resulting in a polluted landscape (that is an eyesore) with lots of dirt and bad smells (pungent). This situation might discourage the residents to practice waste segregation and it might as well hinder recycling awareness.

3.2 Solid Waste Generation Rate/Composition in the New Staff Quarters

The results of solid waste generation rate in the new staff quarters are presented in Table 1 and 2. Table 1 show the average daily/weekly solid waste generation rate in the new staff quarters while Table 2 show the average solid waste generation rate and percentages composition of solid waste in the new staff quarters.

Table 1: Average Daily/Weekly Waste Generation in the New Staff Quarters

Days	**Components**					**Daily Total (kg/day)**
	Paper	**Aluminium**	**Polythene**	**Plastic**	**Organic Waste**	
Monday	40.51	50.42	110.71	80.30	70.15	352.09
Tuesday	21.12	30.01	90.11		93.41	234.65
Wednesday	2.85		90.43	69.48	261.32	424.08
Thursday	50.05	50.14	150.5	52.83	105.76	409.28
Friday	30.47	28.09	100.05	60.22	260.37	479.20
Saturday	70.52	130.66	165.35	971.47	448.96	1786.96
Sunday	65.66	50.36	155.84	100.07	360.83	732.76
Weekly Total (kg/week)	281.18	339.68	862.99	1334.37	1600.8	4419.02

Table 2: Average Solid Waste Generation and Percentage Composition of Solid Waste in the New Staff Quarters for a Month

Components	**Generation Rate (kg/month)**	**Percentage Composition of Waste (%)**
Paper	1125.73	6.33
Aluminium	1328.74	7.47
Polythene	3471.96	19.52
Plastics	5357.47	30.12
Organic Waste	6503.26	36.56

Results from Table 1 indicated that the amount of solid waste generated in the new staff quarters on a daily basis is quite high with values ranging from 352.09kg/day to 732.76kg/day and on a weekly basis per component, values ranges from 281.18kg/week to 1600.80kg/week. There were slight variations in the amount of waste generated per day (daily) in the new staff quarter. According to Dikole and Letshwenyo (2020) the different living style of people may affect waste generation rate. It was observed that wastes generation rate was low during the weekdays and high during weekends. Monday (352.09kg/day) and Tuesday (234.65kg/day) have the least total waste generated per day while Saturday (1786.96kg/day) and Sunday (732,76kg/day) have the highest total waste generated per day. This is implying that the rate of wastes generated during the weekdays differs from that generated during the weekends. This might be attributed to the indoor activities (such as cleaning the house for the week, parties etc.) involved by the residents in the new staff quarters on Saturdays and Sundays. The more time spend at home by residence and shopping at weekends for more goods and food to be consumed both at weekends and weekdays might also account for the increase in waste generation during weekends [25]. Studies on household waste generation have reported high waste generation during weekends [26,27,28].

Results from Table 2 showed that for a period of one month, the composition of solid waste generated in the new staff quarters was mostly dominated by organic waste (36.56%) followed by plastic (30.12%), polythene (19.52%), Aluminium (7.47%) and paper (6.33%) which is the least solid waste generated. Higher generation rate of organic waste (food waste) may be attributed to food wastage especially on the part of children and this is also suggesting a culture of cooking large quantities of food [26] as an essential need for people [27]. Studies have also reported organic waste as the highest composition of solid waste generated in households [28,29,30]. High quantity of food waste has been reported to pose environmental problems as leachate at landfills and dumpsites results from the organic fraction of the solid wastes [1] and this may impact water sources such as surface and ground water. organic waste (food waste) has the potential for recovery to produce fertilizers which can be used for crop production, thus this may help to reduce the cost of crop production. Therefore, food waste composting should be conducted/practice in the new staff quarters since food waste comprise the highest composition of waste generated in the area. Although the current practice of not using waste segregation recycle bins in the new staff quarters may impede this method of waste disposal, however, recycle bins should be adequately provided and appropriately located at accessible areas to facilitate and encourage residents to utilize them as it may encourage food waste composting in the area.

Plastic and Polythene wastes following organic waste as the second and third dominated components suggested that the wastes are from packaging of some items (such as food, water etc.) which are bought from the market and commercial areas by the residents. Plastics are mostly used for packing water, liquors and soft drinks etc. They are also used for making household materials such as plastic chairs, buckets, plates and other cooking utensils. This might account for the high amount of plastics in the waste generated in the new staff quarters. Sachet water (sanitised water packed in polythene bag) is the common and the cheapest form of selling portable water in Nigeria and as such it is found in most home and this might be behind the high quantity of polythene waste. Another major contributing factor is the use of polythene bags known as "water proof" for packaging items bought from the market and commercial areas. As found in this study, high amount of plastic and polythene components have also been reported in household waste [2,3]. It takes many years for plastic and polythene to decompose [4], thus if not properly disposed pose serious environmental danger to human and animal health. They release toxic substances into the soil when they perish under sunlight [4], if they are landfilled or buried, they affect the soil structure, composition and the level of microbial activities in the soil [5] and if they are burned, they release toxic substances into the air causing ambient air pollution [1,6]. Hence, a proper method of disposing plastic and polythene wastes such as recycling should be adopted in the new staff quarters as majority (87%) of the plastic and polythene sold are thermoplastic [7]. Thermoplastic are among the recyclable form of plastics because they can be re-melted and reprocessed, usually with only minor changes in their properties [5]. Since Auchi Polytechnic is the owner and distributor of the dominant brand of sachet water in the polytechnic community, they should consider recycling of the plastics and polythene generated in their community for reuse in packing of their water brand. Also, plastics can be sold to the local markets for their use in bottling locally made beverage drinks in the polytechnic like Zobo, Soya beans and Qunu [8]. The practise of selling plastic bottles to local re-users is common in most parts of Nigeria. The high rate of plastics generated in the new staff quarters implies that the residents are not involved in this practise.

Aluminium and Paper waste are the lowest solid waste components generated in the new staff quarters. The low rate of aluminium waste might be implying that residents consumed low amount of processed food and can drinks while the use of digital alternatives might account for the low rate of paper waste. This finding is suggesting the culture of waste reduction at source among residents. Because paper wastes have high reduction potential, various prevention and reduction strategies can be used to minimize the generation rate of papers at source [4]. Hence the culture of waste reduction at source should be encourage among residents of new staff quarters. Apart from reduction, recycling can be used to manage aluminium waste in order to reuse them.

4.0 Conclusion

Information on existing waste management and the rate of waste generation are essential in developing a solid waste management strategy (plan). In this regard, the findings from this study revealed that there is no well-structured collection and disposal mechanism of solid waste in the new staff quarters. The collection locations are very few and these locations are only provided with dumpsters to collect all the solid waste generated in the staff quarters. No recycle bins are provided at these locations, thus segregation of solid waste at the source is not currently practiced. The frequency of transporting the bulky waste collected to disposal site is once in every month or two months and when transportation services are not available, the wastes (including recyclable materials) are burnt directly at the collection location. Results from waste generation rate showed that the amount of solid waste generated in the new staff quarters on a daily basis is quite high with values ranging from 352.09kg/day to 732.76kg/day and on a weekly basis per component, values ranges from 281.18kg/week to 1600.80kg/week. The solid waste consists of various components with generating rate of 1125.73kg/month (6.33%), 1328.74kg/month (7.47%), 5357.47kg/month (30.12%), 3471.96kg/month (19.52%), 6503.26kg/month (36.56%) for paper, aluminium, plastic, polythene and organic wastes respectively. It was observed that organic waste comprises the highest composition of the waste and the least was paper. In decreasing order, the composition of the waste is organic waste> plastics>polythene> aluminium>paper. Based on the aforementioned findings from this study, a solid waste management strategy was developed for proper management of waste in the new staff quarters and it entails:

i. The Works and Maintenance Department should develop zero waste policies for a sustainable environment by encouraging the practice of the 3R (reduce, reuse and recycle) concept.
ii. Recycle bins should be adequately provided and appropriately located at accessible areas to facilitate and encourage residents to utilize the recycle bins and thus encourage the practice of waste segregation for recycling.
iii. Labelled bags should be provided to residents to encourage separation at the source for compostable/ organic waste from the other non-biodegradable wastes. Organic waste composting is very crucial since organic waste comprised the highest composition of waste generated in the new staff quarters. Organic waste has the potential for recovery to produce fertilizers which can be used for crop production.
iv. Plastics and Polythene which also accounted for high composition of waste generated in the new staff quarters should be recycled as majority of the plastic and polythene sold are thermoplastic. Since Auchi Polytechnic is the owner and distributor of the dominant brand of sachet water in the polytechnic community, they should consider recycling of the plastics and polythene generated in their community for reuse in packing of their water brand. Also, plastics can be sold to the local markets for their use in bottling locally made beverage drinks in the polytechnic like Zobo, Soya beans and Qunu etc.

v. Aluminium and Paper wastes which are among the components of solid waste generated in the new staff quarters, but at low rates should be reduce at the point of generation. Reuse of papers for packaging materials should be encouraged. However, these wastes can also be recycled.
vi. The frequency of transporting the collected waste to a disposal site outside the Polytechnic community should be upgraded to at least four times in a month. This can be achieved by increasing the number of staff and compactor vehicles. The Polytechnic authority can consider constructing an engineered solid waste disposal site in the area.
vii. Residents of the Polytechnic community should be sensitized regularly on the benefits of waste minimization and recycling and the strategies for safer and cleaner environments. This will upgrade the culture of proper waste disposal among residents of the new staff quarters.

References

[1] Ajayi, A. S., Ibrahim, R., Brai, M, A. and Seghosime, S. (2019). Overview of the Anthropogenic Causes of Soil Erosion in Auchi, Edo State, Nigeria. Merit Research Journal of Agricultural Science and Soil Sciences, 7(8): 087-090.
[2] Asikihia, M. O., Balogun, T. F. and Etu, M. O. (2011). Socio-Economic Impacts of Soil Erosion in Auchi,Nigeria. Academic Scholarship Journal, 4(1): 169-17.9
[3] Babatunde, B. B., Vincent-Akpu, I. F., Woke, G. N., Atarhinyo, E., Aharanwa, U. C., Green A. F., and Isaac-Joe, O. (2013). Comparative analysis of municipal solid waste (MSW) composition in three local government areas in Rivers State, Nigeria. African Journal of Environmental Science and Technology, 7(9): 874-881.
[4] Bolaji, V. (2022). Solid Waste Management and Disposal Systems. Available online: www.schoolthesis.com [Accessed 31st January, 2023]
[5] Dalil, M., Ilegieuno, A. A., Babangida, M. U. and Husain, A. (2016). Assessment of the Impacts of Gully Erosion on Auchi Settlement, Southern Nigeria. Journal of Geography and Regional Planning, 9(7): 128-138.
[6] Dikole, R. and Letshwenyo, M. W. (2020). Household Solid Waste Generation and Composition: A Case Study in Palapye, Botswana. Journal of Environmental Protection,11: 10-123
[7] Halkos, G. and Petrou, K. N. (2016). Efficient Waste Management Practices: A Review. Munich Personal RePEc Archive, 71518: 1-34
[8] Ibrahim, F. K., Kolo, B. S., Fulata, A. M., Adam, S. and Goni, H. B. (2020). The Environmental Effects of Dumped Sachet (Polyethene) Water on Soil. International Journal of Scientific and Engineering Research, 11(1): 624-636.
[9] Idiata, D. J. and Iyasele, J. U. (2014). The Environmental Threat of Sachet Water Package (Waste) on Agricultural Land. Journal of Multidisciplinary Engineering, Science and Technology, 1(4): 81-87.
[10] Jadoon, A., Adila, S. and Chaudry, M.N. (2014). Assessment of Factors Affecting Household Solid Waste Generation and Its Composition in Gulberg Town, Lahore, Pakistan. Journal of Materials Cycles Waste Management, 16, 73-81.
[11] Kadir, A. A. and Abidin, S. S. S. Z. (2015). Solid Waste Composition and Quantification at Taman Melewar, Parit Raja, Batu Pahat. Soft Soil Engineering International Conference 2015 (SEIC2015), IOP Conf. Series: Materials Science and Engineering, 136 (2016):012047.
[12] Katiyar, M. (2016). Solid Waste Management. Journal of Construction and Building Materials Engineering, 3 (2): 1-6.

[13] Magnus, O. O. and Eseigbe, J. O. (2012). Categorisation of Urban Centres in Edo State, Nigeria. I0SR Journal of Business and Management, 3(6): 19-25.
[14] Mapcarta, (2023a). Auchi Map-Edo State, Nigeria. Available online: https://www.mapcarta.com [accessed 2nd February, 2023]
[15] Mapcarta, (2023b). Auchi Polytechnic Map-Edo State, Nigeria. Available online: https://www.mapcarta.com [accessed 4th February, 2023]
[16] Mohd-Rodzi, R., Mohd-Nopiah, Z., Ezlin, N. and Basri, A. (2019). Analysis of Solid Waste Generation and Composition in Malaysia TVET Campus. International Journal of Integrated Engineering,11 (2): 158–170.
[17] Mondol, E. F., Hasan, Md. R., Rahman, Md. S., Alam, Md. S., Rahman, Sm. A., and Sinthia, T. T. (2013). Solid Waste Management Strategy & Improvement of Existing Scenario Based on Market Waste. Global Journal of Researches in Engineering,13(4): 1-5.
[18] Nathanson, J. A. (2023). Solid Waste Management. Available online: https://www.britannica.com/technology/solid-waste-management [Accessed 31st January, 2023]
[19] NPC-National Population Commission of Nigeria, (2006). Nigeria Population and Housing Census. Development Economics Data Group, Version 01 (July 2013).
[20] Owamah, I.H., Izinyon, O.C. and Igbinewekan, P. (2017) Characterization and Quantification of Solid Waste Generation in the Niger Delta Region of Nigeria: A Case Study of Ogbe-Ijoh Community in Delta State. Journal of Material Cycles and Waste Management, 19, 366-373.
[21] Palanivel, T.M. and Sulaiman, H. (2014) Generation and Composition of Municipal Solid Waste (MSW) in Muscat, Sultanate of Oman. APCBEE Procedia, 10, 96-102.
[22] Roy, T. K., (2013). Management of Park Solid Wastes in Khulna City. Proceedings of the Waste Safe 2013, 3rd International Conference on Solid Waste M management in the Developing Countries 10-12 February 2013, KhuIna, Bangladesh.
[23] Simmons, S. (2005). It's in the Bag: An Estimate of the Effect of CO2 Emission of the Irish Plastic Bag Tax. Available online: www.bestfootforward.com [Accessed, 10th February 2023]
[24] Spangler, J. (2018). How to Calculate the Waste Diversion Rate of an Event. Ecosystem Events. Available online: https://www.ecosystemevents.com. [Accessed 5th February, 2023]
[25] Thanh, N.P., Matsui, Y. and Fujiwara, T. (2010). Household Solid Waste Generation and Characteristic in a Mekong Delta City, Vietnam. Journal of Environmental Management, 91, 2307-2321.
[26] Ugwu, C. O., Chigbogu, G. O., and Ozor, P. A. (2020). Solid Waste Quantification and Characterization in University of Nigeria, Nsukka Campus, and Recommendations for Sustainable Management. Heliyon, 6: e04255.
[27] Ujeh, K. C. (2023). The Negative Environmental Effects of Plastic Shopping Bags. Available online: www.ibnet.org [Accessed, 10th February 2023]
[28] WHO, (2023). Guidance on Solid Waste and Health. Compendium of WHO and other UN Guidance on Health and Environment
[29] World Bank, (2022). Solid Waste Management. Available online: www.worldbank.org [Accessed 31st January, 2023]
[30] WorldPlaces, (2023). New Staff Quarters Auchi Polytechnic Nigeria. Available online: https//nigeria.worldplaces.me

PERFORMANCE EVALUATION OF CHICKEN LITTERS BIOCHAR IN DIRECT CARBON FUEL CELL

[a]*Ejedegba, G.O., [a]Adeniyi O. D., [a]Otaru A.J., [a]Adeniyi M.I., [a]Muhammed A. A. and [b]Yusuff A.S.

[a] Chemical Engineering Department, Federal University of Technology Minna, Nigeria
[b]Chemical and Petroleum Engineering Department, Afe Babalola University, Ado-Ekiti, Nigeria
*Corresponding author's Email: ejedegbagodwin@gmail.com
Tel: +2348035930444

Abstract

As fossil fuels (a non-renewable energy resource) dominate the world's electrical power generation, we are not only exposed to inadequate energy at a high cost but we are also exposed to high exhaust emissions that contribute to the greenhouse effect. Therefore, exploring alternative renewable energy sources that are more reliable, cheaper, and less reliant on fossil fuels has become imperative. Through electrochemical reactions, direct carbon fuel cells (DCFC) convert carbon from a wide range of carbon-rich biomass, including biochar derived from animal waste, into electricity. Therefore, this study explores the possibility of generating electricity from a biomass-classified waste known as chicken litter. Chicken litters were pyrolyzed at 750°C, yielding 46wt.% biochar, before tests were conducted on proximate and ultimate weights and calorific values. The average moisture content obtained was 4.26wt.%, volatile matter was 21.90wt.%, and fixed carbon was 61.51 wt.%, with an average calorific value of 28.79 MJ/kg and a carbon value of 57.501wt.%. When operated within a temperature range of 300 to 700°C, it produced an Open Circuit Voltage (OCV) peak of 1.18 Volt at 600°C. The results of this study demonstrate that solid carbon sourced from chicken litter can be converted directly in a single step using DCFCs.

***Keyword**: Chicken litters, Biochar, DCFC, pyrolysis, Open Circuit Voltage.*

1 Introduction

Energy is regarded as the fuel of life, because it is the most essential needs of man. As such, decisions on its sources are carefully considered. Generally, energy resources are classified as finite (exhaustible) and infinite (perpetual) resources. The finite energy resources are energy obtained from exhaustible sources like Coal, Crude oil, Natural gas, Uranium among others. While infinite energy resource are energy gotten from perpetual sources like Solar, Wind, Geothermal, Marine, Bio-energy (Biomass energy) just to mention few. For several decades, the world has greatly relied on fossil fuel -a finite energy resource- for its energy needs [1]. Concerns about its dwindling supplies, its unstable and rising cost, and environmental challenges of high exhaust emission have motivated researchers to seek a more eco-friendly and renewable energy source. To this end, bio-energy (biomass energy) source and fuel cell technology are under consideration [2,3,4].

Bio-energy or biomass energy is a renewable energy source that is not only known for its replenishment but also efficient in energy supply and at the same time environmentally friendly.

Fuel Cell is an electrochemical device that continually converts chemical energy into electricity for as long as fuel and oxygen are available [5]. Fuel cell, therefore, bears similarities both to batteries, with which they share the electrochemical nature of the power generation process, and to plant engine which (unlike batteries) will continuously work by consuming fuel. It is a zero-emission engine that produces power and drinking water when hydrogen is used as fuel but generates power and pure carbon dioxide when pure carbon is utilized as fuel [6,7,8].

The use of carbons for electricity production in Carbon Fuel Cells has been shown to provide conversion efficiencies of up to 80%. Direct Carbon Fuel Cell (DCFC) is a special kind of high temperature fuel cell that directly converts solid carbonaceous fuels to electricity [9]. It offers great thermodynamic advantages over other fuel cell types, have almost 100% fuel utilization efficiency; it reduces carbon emissions by 50%, off-gas volume by 10 times compared with convectional coal-fired power plant and with efficiency twice as that of a steam plant [10]. DCFC can be fed with a wide range of carbon-rich fuels but biomass (animal wastes) is the centre of attention because they are renewable and can be processed into char (carbon fuel). As a fuel, animal waste char has the advantage of being inexpensive and easy to produce, easily stored, readily available to consumers, devoid of mercury, almost no sulphur, low nitrogen, and produces little ash when burned. Its high electrical conductivity, large surface area, and many bonds make it very reactive at relatively low temperatures [11,12,13,14,15,16,17]. In Nigeria, animal wastes are readily available and abundant, and carbon produced from them can be operated on a Direct Carbon Fuel Cell (DCFC) with high efficiency, while simultaneously addressing waste management issues. Therefore, a Direct Carbon Fuel Cell containing carbon from chicken litter is being considered in this research. Chicken litter is a solid waste generated from the rearing of chicken. Physically, Poultry litter is a mixture of bedding materials (wood shavings, saw dust and peanut hull), bird excreta, feathers, feed spills and chemical treatments (alum, sodium bisulphate).

2.0 Materials and Method

The method adopted involves the collections of samples of chicken litters, pyrolysed them to obtain char and then characterized the produced biochar. The method also involved the DCFC set-up, carbon electrolyte preparation and carbon fuel particles production.

2.1 Collection of Chicken litters

The animal waste of chicken litters was choicely selected due to its availability and good carbon content, which is a one of the parameter for a substantial energy generation.

Figure 1: Chicken litters Sample

2.2 Sample Preparation

The freshly obtained chicken litters had very high moisture content. Since the energy conversion route to be employed in this study is not anaerobic digestion, but pyrolysis, the sample were sun dried in order to reduce their moisture content because high moisture content.

2.3 Sample Biomass Pyrolysis

The chicken litters sample was oven dried for an hour at an operating temperature of 100^{o}C. A crucible containing Nitrogen gas in its cylinder was employed to hold the dry sample before being inserted into the furnace at 400-600^{o}C. The Nitrogen help to starve the sample of any oxygen so as to obtain a high solid carbon yield which is suitable for DCFC operation. The sample pyrolysis process was carried out at an increasing temperature rate of 10^{o} C/min up to 500 ^{o}C/min to obtain biochar.

Figure 2: Pyrolysed chicken litters (Biochar)

2.4 Biochar Characterization

The characterization of biochar is vital in determining the energy (proximate) and chemical (ultimate) properties of a sample, which influence its performance. Consequently, proximate, ultimate analysis and calorific value were carried out on the biochar produced from chicken litters.

2.5 DCFC Set-up, Electrolyte and Carbon Fuel preparation

The cell design arrangement of this research work is similar to the work of Adeniyi 2014, but incorporated double cells in serial connection known as "stacking" where each anode is connected to the cathode of the next cell. The said design is advantageous in terms of cost and availability of material and/with ease of fabrication.

The cells have corrugated flow channels (two gas pipe) each attached at both ends of the cells which serve as inlet and outlet of purging gas (anode) and oxidizing gas or air (cathode) passage. These anode(s) and cathode(s) were made from steel pipes with conscious consideration of operating temperature of the cell and melting point (2600^{o}F or 1427^{o}C) of the steel.

A molten binary mixture of $LiCO_3$ and K_2CO_3 in a mixture ratio of 38 mol% and 62 mol% ranges were employed as the electrolyte, biochar carbon mixed with the salts in a mixture proportion of 3g of $LiCO_3$, 3g of K_2CO_3 and 4 g of carbon were combined to produce the fuel, while copper wires were used as current collectors on the electrode (anode and cathode). Refractive crystal beads were used to insulate the copper wire from high temperature. The electrolyte was made up of a porous alumina mesh of 1.5 mm thickness, 25 mm diameter and about 40% void, which provided the conductive surface for effective carbonate ion transportation. Carbon fuel is supplied to the negative electrode (anode) and oxidant to the positive electrode (cathode). The electrolyte is sandwiched between these electrodes, then carbon fuel is fed to the anode where a catalyst separates carbon negatively charged electrons from positively charged ions (protons). The electrons from the anode side of the cell cannot pass through the membrane to the positively charged cathode; they must travel via an electric circuit to reach the other side of the cell thereby generate electricity.

Figure 3: DCFC Set-up

3.0 Results and Discussion

All analyses involving the characterisation were conducted in duplicate and the average value recorded. Also, the results from DCFC performance tests on Open Circuit Voltage for the chicken litters were obtained.

3.1 Biochar yield

The biochar is the quantity of char obtained after pyrolysis of the chicken litters .The percentage yields is given Table 1.

Table 1: Percentage yield of biochar

Sample Description	Weight before Pyrolysis (g)	Weight after Pyrolysis (g)	% Yield (%)
Chicken Litters	60	28	46.6

3.2 Proximate Ultimate and Calorific Value Analyses

The results of the proximate, ultimate and the calorific value of the chicken litters and composite are given in Table 2. The analyses were conducted in duplicates and the average values recorded. From the table, the low ash and moisture content of the chicken litters with good fixed carbon after pyrolysis and a favourable calorific value made it more suitable for thermal electrochemical operation.

Table 2: Characterisation analyses results

Analysis	**Proximate analysis**				**Calorific**	**Ultimate analysis**	
	Moisture Content Wt.%	**Ash content** Wt.%	**Volatile matter** Wt.%	**Fixed carbon** Wt.%	**Value (CV)** MJ/kg	**Carbon (C)** Wt.%	**(H_2)** Wt.%
1	4.16	13.18	21.90	60.82	28.62	57.74	5.10
2	4.34	13.12	21.90	61.20	28.96	57.86	4.50
Average	4.25	13.15	21.90	61.51	28.79	57.80	4.80

3.3 Carbon Electrolyte and Carbon Fuel Particle

The electrolyte was prepared using a molten carbonate mixture of $LiCO_3$ and K_2CO_3 [18,19,20]. A measurement of 12.4 g of K_2CO_3 granule was mixed with 7.6g of $LiCO_3$ powder in a stainless steel plate, amounting to 20g of the mixture. The electrolyte was made with the mixture being stirred continuously under heat and an aluminum wire mesh into the melted mixture of K_2CO_3 and $LiCO_3$ so as to saturate it. The saturated wire mesh was removed and placed on a flat surface to cool.

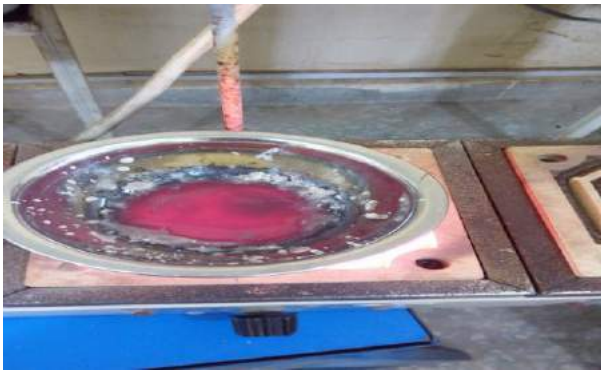
Figure 5: Carbon Fuel Particles

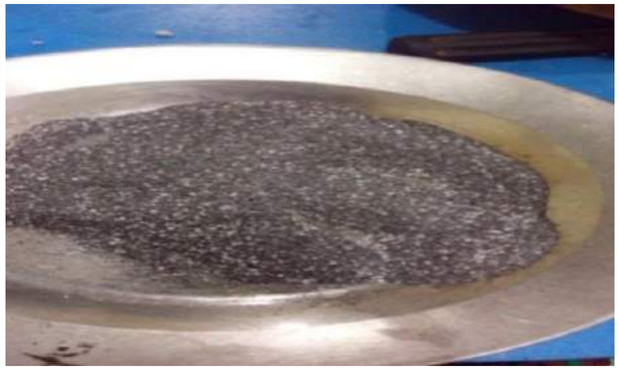
Figure 4: Carbon Electrolyte

While th**e** fuel used in the DCFC was a mixture of carbon and carbonate [12]. The carbon (biochar) was the actual fuel butwas mixed with carbonates and the mixture turned molten at the operating temperature of the DCFC which offers the required electrochemical reaction in the cell.

3.4 DCFC Performance Test

Results of Voltage obtained from MCDCFC using the Chicken litters

The preliminary results obtained from the assembled molten carbonate Direct Carbon Fuel Cell running on the chicken litters biochar fuels was based on the fuel cell potential to generate open circuit voltage at different temperature. Tables 3 represent the open circuit voltage (OCV) for Chicken litters at different operational temperature.

Table 3: Open Circuit Voltage value chicken litters biochar fuel

Time (Min)	Temp. °C	OCV(V)
44	300	0.58
68	400	0.69
93	500	0.86
116	600	1.18
132	700	0.91

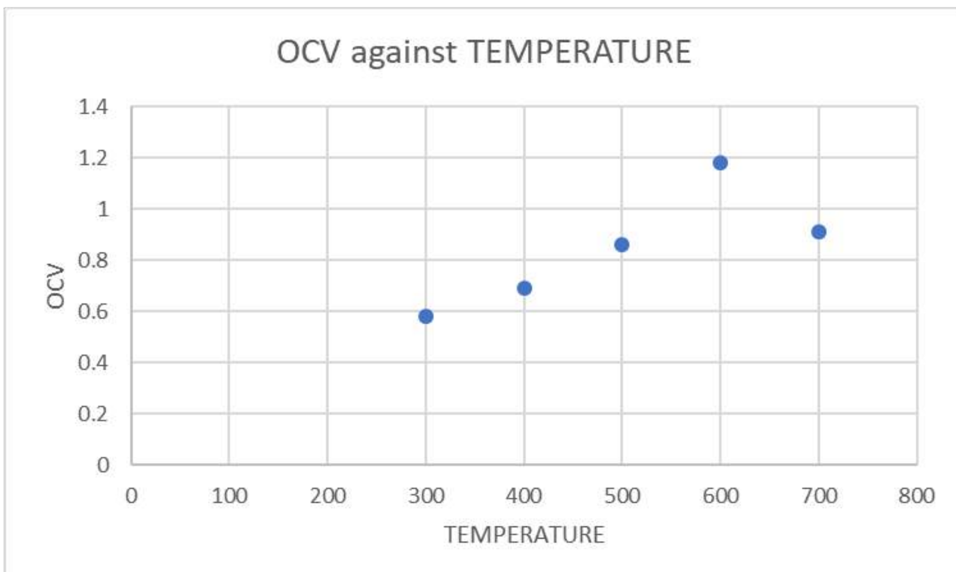

Figure 6: Plot of DCFC OCV against Temperature

Based on the DCFC set-up in Figure 3, the heat that is required for the electrochemical reaction to occur in the electrolyte that is sandwich between the cathode and the anode component of the cell is supplied by the furnace. Since the electrolyte is sandwiched between these electrodes, and the carbon fed into the anode, the electrolyte separates the carbon negatively charged electrons from positively charged ions (protons). Then, the electrons from the anode side of the cell cannot pass through the membrane to the positively charged cathode. As such they travel through the electric circuit to reach the other side of the cell thereby generating electricity. So at 300^{o}C, the Open Circuit Voltage (OCV) generated was 0.58V. This OCV value increase as the the temperature increases and attained an optimal voltage 1.18 V at 600^{o}C. Further increase in temperature to

700°C witnessed a decline in voltage value to 0.91 V . This is as a result of drop in reaction as the fuel is being used up rapidly due to the high reactive atmosphere created by high temperature.

4.0 Conclusion

This study demonstrate that solid carbon sourced from chicken litter can be converted directly in a single step using DCFCs. Chicken litters were pyrolyzed at 750°C, yielding 46 wt.% biochar, before tests were conducted on proximate and ultimate weights and calorific values. The average moisture content obtained was 4.26 wt.%, volatile matter was 21.90 wt.%, and fixed carbon was 61.51 wt.%, with an average calorific value of 28.79 MJ/kg and a carbon value of 57.501 wt.%. When operated within a temperature range of 300 to 700°C, it produced an Open Circuit Voltage (OCV) peak of 1.18 Volt at 600°C.

REFERENCE

[1] Adeniyi O. D., Ngozichukwu, B, Adeniyi M.I., Olutoye M.A., Musa U., & Ibrahim M.A. (2020), Power Generation from Melon Seed Husk Biochar using Fuel Cell, *Ghana Journal of Science*, 61(2), 38-44, https://dx.doi.org/10.4314/gjs.v6li2.4.

[2] Adeniyi O.D., Ewan, B.C.R., Adeniyi M.I. and Abdulkadir M. (2014) The behaviour of biomass char in two direct carbon fuel cell designs, *Journal of Energy Challenges & Mechanism* 1(4), 1-6, http://www.nscj.co.uk/JECM/PDF/1-4-6-Adeniyi.pdf .

[3] Ahn S.Y., Eom S.Y., Rhie Y.H., Sung Y.M., Moon C.E., Choi G.M. and Kim D.J. (2013), Application of refuse fuels in a direct carbon fuel cell system, *Energy*, 51:447-457, http://dx.doi.org/10.1016/j.energy.2012.12.025 .

[4] Behling N.H., Managi S., & Williams M.C. (2019), Updated look at the DCFC: the fuel cell technology using solid carbon as the fuel, *Mining, Metallurgy & Exploration*, 36:181-187, https://doi.org/10.1007/s42461-018-0022-x .

[5] Cao D., Sun Y., Wang G. (2007) "Direct carbon fuel cell: Fundamentals and recent developments", *Journal of Power Sources*, 167(2), 250-257, doi:10.1016/j.jpowsour.2007.02.034.

[6] Cherepy N.J., Krueger R., Fiet K.J., Jankowski A.F. & Cooper J.F. (2005) "Direct conversion of carbon fuels in a molten carbonate fuel cell", *Journal of the Electrochemical Society*, 152(1) A80-A87.

[7] Cooper J.F. & Cherepy N. (2008) Carbon fuel particles used in direct carbon conversion fuel cells. US Patent Pub. No. US 2008/0274382 A1.

[8] Cui C., Li S., Gong J., Wei K, Hou X., Jiang C., Yao Y., & Ma J. (2021), Review of molten carbonate based direct carbon fuel cells, *Materials for Renewable and Sustainable Energy*, 10:12, https://doi.org/10.1007/s40243-021-00197-7.

[9] Deleebeeck L, Hanson K.K, (2014) Hybrid direct carbon fuel cells and their reaction mechanisms -a review. J Solid State Electrochem. 18:861-882

[10] Dicks A.L. (2006) "The role of carbon in fuel cells", *Journal of Power Sources*, 156, 128-141.

[11] Dudek M., Adamczyk B., Sitarz M., Śliwa M., Lach R., Skrzypkiewicz M., Raźniak A.,

Ziąbka M., Zuwała J. and Grzywacz P. (2018), The usefulness of walnut shells as waste biomass fuels in direct carbon solid oxide fuel cells, Biomass and Bioenergy 119 (2018) 144–154, https://doi.org/10.1016/j.biombioe.2018.09.026 .

[12] Hackett G.A., Zondlo J.W. and Svensson R. (2007) "Evaluation of carbon materials for use in a direct carbon fuel cell", *Journal of Power Sources*, 168, 111-118, doi:10.1016/j.jpowsour.2007.02.021.

[13] Henriksson G., Li J., Zhang L. and Lindström M.E. (2010) "Lignin utilization", in M. Crocker (ed.) *Thermochemical Conversion of Biomass to Liquid Fuels and Chemicals*, RSC Energy and Environment Series No. 1, Royal Society of Chemistry, Cambridge, pp.222-259.

[14] Jafri N., Wong W.Y., Doshi V., Yoon L.W. and Cheah K.H. (2018), A review on production and characterization of biochars for application in direct carbon fuel cells, *Process Safety and Environmental Protection*, 118:152-166, https://doi.org/10.1016/j.psep.2018.06.036.

[15] Jia L., Tian Y., Liu Q., Chun X., Yu J., Wang Z., Zhao Y. and Li Y. (2010) "A direct carbon fuel cell with (molten carbonate)/(doped ceria) composite electrolyte", *Journal of Power Sources*, 195, 5581-5586, doi:10.1016/j.jpowsour.2010.03.016.

[16] Klass D.L. (1998) "*Biomass for renewable energy, fuels, and chemicals*", San Diego, CA, Academic Press.

[17] Li C., Shi Y, and Cai N. (2011a) "Mechanism for carbon direct electrochemical reactions in a solid oxide electrolyte direct carbon fuel cell", *Journal of Power Sources*, 196, 754-763.

[18] Li C., Shi, Y and Cai N. (2011b) "Effect of contact type between anode and carbonaceous fuels on direct carbon fuel cell reaction characteristics", *Journal of Power Sources*, 196, 4588-4593.

[19] Li X., Zhu Z, Chen J., De Marco R., Dicks A., Bradley J. and Lu G. (2009) "Surface modification of carbon fuels for direct carbon fuel cells", *Journal of Power Sources*, 186, 1-9, doi:10.1016/j.jpowsour.2008.09.070.

[20] Meher, L.C., Sugar, D.V., Naik, S.N (2006)."Technical aspects of Biodiesel Production by Transesteification"- A review. *Renewable Sustainable Energy*. 10:3, 248-268.

NIPES-NCEE Conference Proceedings
The 2nd International Conference 15th-17th Feb. 2023
22-32
www.nipesjournals.org.ng

CHARACTERIZATION, KINETICS, AND THERMODYNAMICS STUDIES OF OIL EXTRACTION FROM PALM KERNEL

Charity Aghariagbonse Osagiede and George Chidozie Nwagu

Department of Chemical Engineering, University of Benin, Benin City, Nigeria
Corresponding email: aghariagbonse.osagiede@eng.uniben.edu

Abstract
The inadequate availability of kinetics and thermodynamic data in the design stage of oil extractors contributes to the inefficiency often encountered. The kinetics and thermodynamics of oil extraction from palm kernel seeds were investigated in this study. The mass transfer kinetic power model and the laws of thermodynamics were applied to describe the kinetics and the thermodynamics of the oil extraction process, respectively. The physicochemical parameters of the palm kernel oil extracted were determined according to the methods recommended by AOAC (1990). The results showed that a maximum oil yield of 48.56% was obtained from the dried palm kernels under optimum conditions of 70 °C, a particle size of 2.0 mm, and an extraction duration of 90 min, using 250 ml of n-hexane. The oil extraction process was found to follow second-order kinetics, whose rate constant is dependent on temperature, and the activation energy (Ea) was 54.69 kJ/mol. The thermodynamic parameters of the extraction process were an enthalpy change (ΔH) of 24.94 kJ/mol, an entropy change (ΔS) of 0.08 kJ/mol, and negative values of Gibbs' free energy change (ΔG) at each prevailing temperature value. The results of the thermodynamic study implied that the palm kernel oil extraction process is endothermic and requires a constant supply of energy for effective and efficient extraction. Also, the physicochemical properties of the oil showed that it is edible and also suitable for use in soap production, pharmaceutical industries, and as a feedstock in the production of biodiesel.

1.0 Introduction
The need for oil has resulted in a comprehensive analysis of various oils [1]. Vegetable seed oils play a crucial role in the production of items such as soaps, paints, varnishes, lacquers, lubricants, hydraulic fluids, printing inks, dyes, pesticides, and insecticides [2 - 4]. The growing expense and insecurity of petroleum products have prompted the use of vegetable oil as a replacement fuel and in biodiesel manufacturing, thus resolving the energy shortage issue [5]. According to data, the global output of vegetable oil has continuously increased from around 90.5 million metric tons in the year 2000/2001 to 207.5 million metric tons in 2019/2020, and a similar upward trend is forecast to continue in the future [6].

The palm kernel seed, which comes from the oil palm fruit tree (Elaeis guineensis), contains roughly 75-80% oil that can be extracted through several processes or a combination of techniques including mechanical screw-pressing, solvent extraction, and traditional methods. However, the mechanical screw-press method is considered the most effective, as it can extract all available drops of oil, while the solvent extraction method is the next best option [7].

Palm kernel oil is a yellowish oil obtained from the kernels of the nuts of the palm tree (Elaeis guineensis), which is native to tropical regions in Africa and Asia. When processed locally, it takes on a dark brown color. The oil is a rich source of fats, with its primary fatty acid being the saturated lauric acid, which makes up 48.20% of the oil [8]. Due to its high content of lauric acid, palm kernel oil is sometimes referred to as lauric oil. Other significant fatty acids in the oil include myristic acid (16%) and oleic acid (15%) [9, 10]. In addition to being used as a lubricant or biodiesel in rural areas, palm kernel oil is also used in the food processing industry, soap production, cosmetics, pharmaceuticals, and traditional medicine [11].

A significant number of authors have dedicated their research to exploring the extraction of oils from seeds of various kinds, as well as conducting investigations into the characterization, kinetics, and thermodynamics of the process. For example, Osagiede et al. [12] conducted a study on the kinetics and thermodynamics of mango seed oil extraction, which resulted in a 12.15 wt% oil yield, and the oil extraction process was reported to follow first-order kinetics. Orhevba et al. [13] investigated the extraction and characterization of Moringa oleifera seed based on solvent extraction method and found that Moringa oleifera contained 35 wt% oil. In a separate study, Ochi et al. [14] and Uzoh et al. [15] studied the extraction of Gmelina arborea oil and reported an oil yield of 52.60 and 49.90 wt%, respectively. Based on their findings, Uzoh et al. [2] reported that the extraction process follows a second-order rate mechanism.

The inadequate information regarding the kinetics data of extractors for seed oil extraction can result in suboptimal performance. To improve the design of efficient extractors for palm kernel seed oil extraction, it is crucial to conduct a study that generates kinetic and thermodynamic data. This data is essential in the design process and can significantly contribute to improving the performance of the extractors. This work is, therefore, aimed at investigating the kinetics and thermodynamics of oil extraction from palm kernel seeds using the solvent extraction method.

2.0 Methodology

2.1 Materials Collection and Preparation

The palm kernel nuts were collected from Nigeria Institute for oil palm Research (NIFOR), Benin city, Edo state, Nigeria. They were of Dura and Tenera varieties with thin and thicker mesocarps respectively. They were then cracked to separate the shells from the kernels. Afterward, a manual grinding machine was utilized to grind the kernels and the ground kernel was made to pass through a laboratory test sieve to obtain particles size of 2.0 mm [16]. To decrease the moisture content to the minimum level possible, the ground seeds were dried in an electric oven held at a constant temperature of 105 °C for 2 hours.

2.2 Methods

The palm kernel oil was extracted from its kernels using the solvent extraction method, which involved the use of a Soxhlet extractor and n-hexane as the solvent. To investigate the kinetics and thermodynamics of the extraction process, a total of 15 experimental runs were conducted. The extraction time was varied from 30 to 90 minutes, with 15-minute intervals, while keeping the volume of solvent and particle size constant at 250 ml and 2.0 mm, respectively, for each run. The extraction temperature was also varied from 50 °C to 70 °C, with 10 °C intervals, while maintaining the volume of solvent and particle size constant. In all 15 runs, a fixed weight of 100 g of ground palm kernel was used, and the percentage oil yield was calculated using Equation 1.

$$Y = \frac{W_o}{W_s} \times 100 \qquad 1$$

Where: Y = yield of the oil (%), W_o = weight of pure oil extracted (g), and W_s = weight of the seed sample (g).

2.3 Characterization of the extracted palm kernel oil

The physicochemical characteristics of the extracted palm kernel oil were evaluated, which included its specific gravity, oil content, refractive index, density, viscosity, moisture content, peroxide, iodine and acid values, free fatty acid content, saponification value, and ester value. These properties were measured using techniques specified by the standard association of official analytical chemists (AOAC).

2.4 Kinetic Modelling

The kinetics of the oil extraction process was investigated using the mass transfer kinetic power model shown in Equation 2.

$$\frac{dY}{dt} = kY^n \tag{2}$$

Where: t = extraction time (minutes); k = rate constant for the extraction, n = the extraction order, and $\frac{dY}{dt}$ = rate of change of oil yield (Y) with respect to time (t).
Equation 2 is then linearized to produce Equation 3.

$$\ln\left(\frac{dY}{dt}\right) = n\ln Y + \ln k \tag{3}$$

$\ln\left(\frac{dY}{dt}\right)$ was plotted against ln Y and the values of n and k were obtained from slope and intercept, respectively [17].

2.5 Thermodynamics Studies

The thermodynamic parameters of the process of oil extraction from palm kernel were determined using the Arrhenius equation which establishes the relationship between the rate constant (k) and temperature (T) as shown in Equation 4. The Arrhenius equation was then linearized to produce Equation 5, which was used to determine the activation energy and Arrhenius's constant. The changes in enthalpy (ΔH) and Entropy (ΔS) were determined using Equation 6 while Equation 7 was used to determine Gibb's free energy change (ΔG) at various temperatures [18].

$$k = Ae^{\left[\frac{-E_a}{RT}\right]} \tag{4}$$

$$\ln k = \left(\frac{-Ea}{R}\right)\frac{1}{T} + \ln A \tag{5}$$

$$\ln k = \frac{-\Delta H}{RT} + \frac{\Delta S}{R} \quad 6$$

$$\Delta G = \Delta H - T\Delta S \quad 7$$

where k = extraction rate constant, A = Arrhenius's constant (frequency factor); E_a = Activation energy; R= Universal gas constant; T = absolute Temperature.

3.0 Results and Discusion

The results of the study showed that the palm kernel seeds contained 49.02% oil by mass, as determined through exhaustive extraction (repeated extraction of the same sample until all oil was extracted). However, a one-step extraction process using 250 ml of n-hexane and 100 g of 2.0 mm palm kernel seed particles at 70 °C for 90 minutes resulted in a maximum oil yield of 48.56%. In a similar study, Ibiam and Anosike [19] reported a maximum oil content of 47.5 wt% in the oil extraction from dura species of palm kernel, which is close to the value reported in this work. However, in another study, a yield of 75-80% was reported in the extraction of oil from palm kernel oil [20]. The wide discrepancy observed may be attributed to the difference in the mode of extraction and the species of palm fruit used, which unfortunately were not specified in the study [19, 21].

.1 Physicochemical properties of the palm kernel oil

The physicochemical properties of the extracted palm kernel oil are presented in Table 1. The specific gravity of the oil was found to be 0.901 and this value is comparable to those of other oils such as shea butter oil (0.920) and rubber seed oil (0.92) [22]. The specific gravity (0.901), obtained is close to those obtained for PKO by Ibiam et al. [19] and Olaniyi et al [23], which were 0.910 and 0.904, respectively.

Table 1: Physicochemical properties of the palm kernel oil

Property	**Value**
Specific gravity	0.9014
Refractive index	1.409
Oil content (%)	49.02
Viscosity of the oil at 35 ^oC (cP or mpa-s)	29.3
Moisture content of the oil (wt%)	0.91
Odour	Not offensive
Colour	Brown
Peroxide value (Meq/kg)	5.988
Acid value (mg KOH/g)	5.11
Free fatty acid (%)	2.555
Saponification value	240.43

Saponification value (mg KOH)	240.43
Iodine value (gI_2 /100g)	13.106
Ester value (mg KOH/g)	235.32

The refractive index measures the extent to which a light ray is bent as it passes from air into the oil, and its measurement is typically influenced by the oil's density. The refractive index of the oil was determined to be 1.409. This result can be compared with the refractive indices of other oils, such as coconut oil (1.449) and groundnut oil (1.47) [23], and fluted pumpkin seed oil (1.476) [16]. Furthermore, the value of 1.409 was found to be comparable to the 1.412 refractive index obtained for PKO [23].

The extracted palm kernel oil had a brown color and a non-offensive odor. The moisture content of the PKO obtained in this study was 0.91%, which was slightly higher than the 0.89% obtained by Ibiam and Anosike [19], but much lower than the values found in red palm oil (5%) and other vegetable oils such as cashew nut oil (8%), shea butter oil (10%), and rubber seed oil (8.60%) [20]. Low moisture content indicates a longer shelf life for the oil. The effectiveness of the distillation apparatus used to recover the oil might have contributed to the low moisture content [24].

The viscosity value of 29.3 cP that was determined in this study is an indication of the oil's resistance to shear stress. This value is higher than the values obtained for most other oils, except for fluted pumpkin seed oil (119 cP) as reported by Nwabanne [16]. For instance, the viscosity values for rubber seed oil (10.32 cP), castor oil (13.02 cP), and shear butter oil (17.78 cP) were lower than the value obtained in this study.

The peroxide value determined in this study was 5.988 meq/kg. This value is higher than the peroxide value of sesame seed oil (0.34 meq/kg) reported by Adeyemi et al. [25]. However, it is lower than the peroxide values for soybean oil (10 meq/kg) and sunflower oil (10 meq/kg) reported by Ebewele et al. [26], and shea butter oil (7.41 meq/kg) reported by Adeyemi et al. [25]. The peroxide value is a measure of the degree of deterioration of vegetable oils, where lower values indicate fresher oils and higher values suggest greater rancidity [27].

The iodine value of 13.106 gI2/100g obtained was lower than those of other oils such as fluted pumpkin seed oil (123.83gI2/100g), rubber seed oil (142.45 gI2/100g), soyabean oil (124-139 gI2/100g) and sunflower oil (110-144 gI2/100g) [16, 26]. The lower iodine value (13.106 gI2/100g) observed, was an indication of a low degree of unsaturation of the palm kernel oil. The iodine value measures the degree of unsaturation of a particular vegetable oil. The palm kernel oil extracted in this study was in good condition.

The saponification value is a measure of the weight of alkalis required to saponify a fixed amount of oil. The saponification value obtained in this study was 240.43 mg KOH/g, which falls within the range of 230-254 mg KOH/g recommended by the Codex Alimentarius Commission [28]. The saponification value for PKO obtained in this study is similar to that of other oils such as coconut oil (257.5 mg KOH/g) and rubber seed oil (226.02 mg KOH/g) [23, 26]. This high saponification value of 240.43 mg KOH/g suggests that palm kernel oil has the potential for use in the industry and is suitable for soap production [29]. Additionally, it may be used for producing other cosmetic products, such as shampoo.

The acid value is the amount of free fatty acid present in fat as measured by the milligrams of potassium hydroxide needed to neutralize it. The lower the acid value of oil, the fewer the free fatty acids it contains, and vice versa [24]. The acid value of an oil may be used as a measure of quality. However, the acid value of the oil must not be too high, as this denotes an excessively high content of free fatty acids, which causes the oil to turn sour and may also lead to discoloration of the oil. The acid value obtained in this study for palm kernel oil was 5.11 mg KOH/g while the FFA was 2.55%. The acid value of 5.11 mg KOH/g obtained in this study was close to that obtained for coconut oil which was (5.5±0.5 mg KOH/g) (Olaniyi, Babalola and Mary, 2014), but was lower than those obtained for groundnut oil (9.0±0.5 mg/KOH/g), castor seed oil (14.8 mg KOH/g) and rubber seed oil (37.96 mg KOH/g) [23, 24, 26]. A low acidic value implies rather stable oil at the extraction temperature.
Ester value is the number of milligrams of potassium hydroxide (KOH) required to saponify the esters in 1 g of a sample. It is the difference between the saponification value and the acid value. The ester value of 235.32 mg KOH/g obtained was lower than that of coconut oil (252 mg KOH/g) but was higher than that of groundnut oil (182.5 mg KOH/g), rubber seed oil (191.93 mg KOH/g), shea butter oil (183.4) and castor seed oil (163.2) [20, 22, 23, 30]. The high ester value of the PKO 235.32 mg KOH/g) obtained in this study indicates the presence of a high amount of ester and low molecular weight fatty acid content.

4.2 Kinetics and thermodynamics study

The linearized form of the nth power model given by Equation (3) was used to obtain a linear plot of $\ln\left(\frac{dY}{dt}\right)$ versus lnY. Second-order kinetics was obtained from the slope of the straight lines. The extraction rate constants (k) were also determined from the intercepts of the plots as shown in Figure 1, with an average R^2 value of 0.9894, and the values are shown in Table 2.

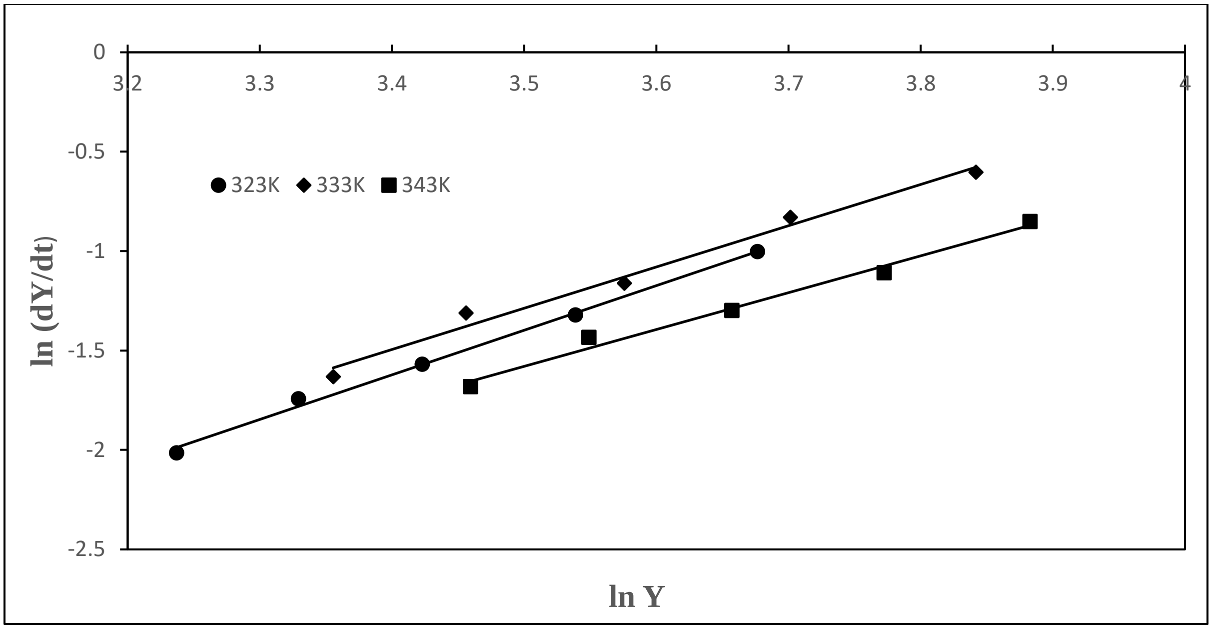

Figure 1: Plots of ln (dY/dt) Versus ln (Y) at 323, 333, and 343 K

Table 2: Estimated values of n and k at various temperatures

S/N	Temperature (K)	Slope(n)	Intercept (ln k)	k (min^{-1})	R^2
1	323	2.2429	-9.2481	0.00009629	0.9962
2	333	2.0747	-8.5486	0.00019382	0.9851
3	343	1.8522	-8.0622	0.00031523	0.9869

From the plot of ln k against 1/T shown in Figure 2, the activation energy (Ea), Arrhenius' constant (A), and thermodynamic parameters (ΔH and ΔS) of the extraction process were determined from the slope and intercept using Equations 5 and 6. The result is presented in Table 3. The Gibbs' free energy change ΔG of the extraction process, at each temperature value, was also calculated from Equation (7), and the results are shown in Table 4.

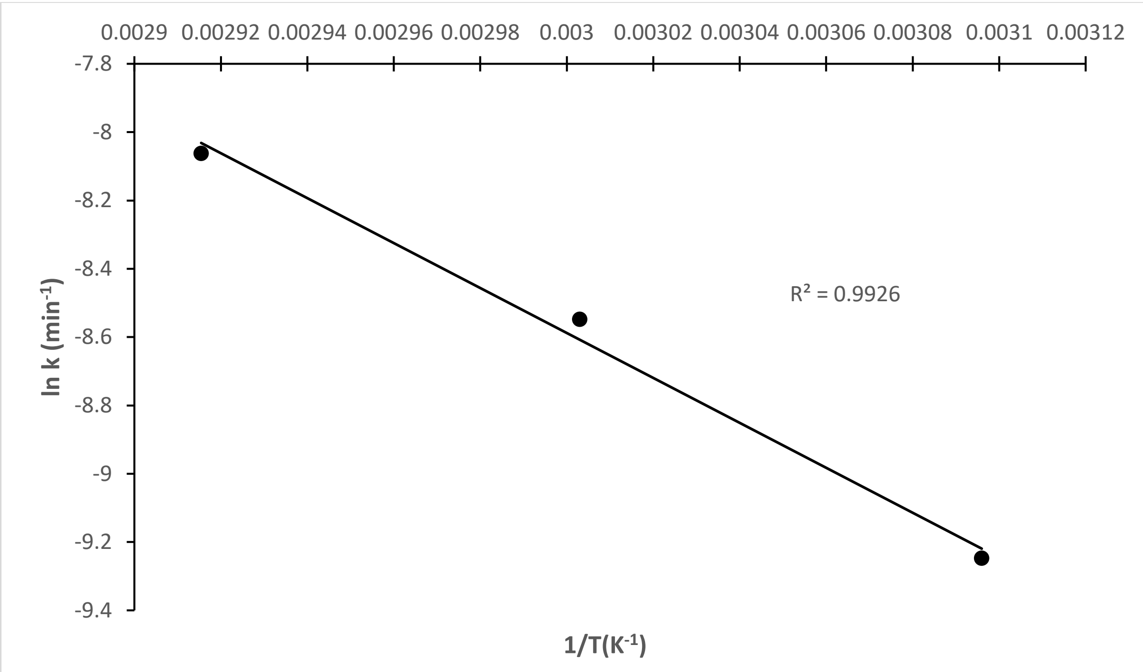

Figure 2: A Plot of ln k Versus 1/T for palm kernel oil extraction

Table 3: Comparison of thermodynamic parameters

Reference	ΔH (kJ/mol)	ΔS (kJ/mol.K)
This study	24.94	0.08
Osagiede et al. [12]	32.78	0.108
Nwabanne [16]	78.84	0.234
Liauw et al. [31]	25.33	0.09

Table 4: Estimated values of change in Gibb's free energy at various temperatures

Temperature. (K)	323	333	343
ΔG (kJ/mol)	-0.90	-1.70	-2.50

The activation energy and the frequency factor for the palm kernel oil extraction process were found to be 54.69 kJ/mol and 6.96×10^4 min^{-1}. The values of the thermodynamic parameters obtained in this study in comparison with those reported in the literature are shown in Table 3. It can be seen from Table 3 that the values of ΔH and ΔS obtained in this study compare favorably with the results reported by Liauw et al. [31] in the study of the extraction of neem seed oil using n-hexane. Also, the values of ΔH and ΔS in this study are lower than those reported by Osagiede et al. [12] for the extraction of oil from mango seed, Nwabanne [16] for the extraction of oil from fluted pumpkin seed, and Liauw et al. [31] for the extraction of oil from neem seed. The lower values of the thermodynamic parameters obtained in this study suggest that the extraction of palm kernel oil is an energy-efficient process that requires less energy input when compared to the extraction of oil from seeds such as mango seed, fluted pumpkin, and neem seed. The negative values of Gibb's free energy shown in Table 4 indicate there is a decrease in the free energy with an increase in temperature. This observation suggests that the extraction process is spontaneous, which is consistent with earlier studies [17, 18, 31, 32]. This also suggests that the process is thermodynamically viable.

5.0 Conclusion

The present study has demonstrated that palm kernel seeds are oil-rich, containing approximately 49.02% total oil content, and thus hold promise as a commercially valuable source of vegetable oil. The oil yield from the extraction of palm kernel oil using n-hexane as solvent is affected by operating conditions such as temperature and time under constant particle size and volume of solvent. The palm kernel oil possesses desirable qualities that render it appropriate for various applications, including pharmaceuticals, soap production, margarine production, and consumption. The low iodine value, indicating a low degree of unsaturation, as observed in this study, makes it feasible to store the palm kernel oil in a plastic container for an extended period without the risk of rancidity. Furthermore, the evaluation of kinetic and thermodynamic parameters revealed that the extraction data of palm kernel oil were suitably described by a second-order kinetics model, where the rate constant was significantly influenced by the extraction temperature. The positive value of entropy implies that the extraction process is characterized by randomness, whereas the positive value of enthalpy and the negative value of the Gibbs free energy change indicate that the extraction process is endothermic and spontaneous, respectively

References

[1] Agu, C. M., Agu, C. C., Ani, K. A., Agulanna, A. C., and Dzarma, G. W. (2022). Process thermodynamic, kinetics and statistical analysis of Gmelina arborea seed oil extraction as clean environmental friendly industrial base-oil. *Case Studies in Chemical and Environmental Engineering*, 6, https://doi.org/10.1016/j.cscee.2022.100216

[2] Hlaing, N., and Oo, M. (2008). Manufacture of alkyd resin from castor oil. *In proceedings of world academy of science, engineering and technology*, 36, pp. 928-934.

[3] Silva, G., Camargo, F., and Ferreira, A. (2011). Application of response surface methodology for optimization of biodiesel production by transesterification of soyabean oil with ethanol. *Fuel processing technology*, 92(3), pp. 407–413.

[4] Uzoh, C. F., Onukwuli, O. D., Odera, R. S., and Ofechebe, S. (2013). Optimization of polyesterification process for production of palm oil modified alkyd resin using response surface methodology. *Journal of Environmental Chemical Engineering*, 1(4), pp. 777–785.

[5] Sangay, B., Priyanka, B. and Dibakar, O. (2014). Gmelina arborea and Tarbernaemontanna divaricate seed oils as non-edible feedstock for biodiesel production. *Journal of chem Tech Research*, 6(2), pp. 1440-1445.
[6] Statista (2019). Global vegetable oil production. https://www.statista.com/statistics.
[7] Jin, Q., Zhang, T. and Shan, L. (2008). Palm kernel oil extraction. *Oil Chemical Society*, 85, pp. 23–28.
[8] Tooley, P. (1971). Experiment in Applied Chemistry. *John Moray*, pp. 29.
[9] Pantzaris, T., and Ahmed, M. J. (2004). Palm kernel oil. palm oil Research Institute of Malaysia, *Porim Europe*, pp. 220.
[10] Ugbogu, O. C., Onyeagba, R., and Chigbu, O. A. (2006). Lauric acid content and inhibitory effect of palm kernel oil on two bacterial isolates and Candida albicans. *African Journal of Biotechnology*, 5(11), pp. 1045–1047.
[11] Alander, I. (2004). Palm kernel oil: A Multifunctional Ingredient for food and cosmetics. *Lipid Technology*, 16(9), pp. 2002–2005.
[12] Osagiede, C. A., Akerele, O. O., Ogbeide, S. E. and Onaifo, J. O. (2019). Mango Seeds Oil Extraction: Effects of Operating Variables, Kinetics and Thermodynamics Studies. Nigerian Research Journal of Engineering and Environmental Sciences, 4(1), pp. 243–250.
[13] Orhevba, B. A., Sunmonu, M. O., Iwunze, H. I. (2013). Extraction and characterization of Moringa oleifera seed oil, *J. Food Dairy Technol*., 1 (1), pp. 22–27.
[14] Ochi, D. O., Mahmud, H., Nworie, C. E. Aliu, S. O. (2019). Extraction, characterization and transesterification of *Gmelina arborea* seed oil using clinker as catalyst, *Niger. Res. J. Chem. Sci*. 7, pp. 357–371.
[15] Uzoh, C. F., Onukwuli, O. D., Nwabanne, J. T. (2014). Characterization, kinetics and statistical screening analysis of Gmelina seed oil extraction process, Mater. Renew. Sustain. Energy, 3 (38), pp. 1–12.
[16] Nwabanne, J. T. (2012) 'Kinetics and Thermodynamics Study of Oil Extraction from Fluted Pumpkin Seed', International Journal of Multidisciplinary sciences and Engineering, 3(6), pp. 11–15.
[17] Topallar, H. and Gecgel, U. (2000). Kinetics and Thermodynamics of Oil Extraction from Sunflower Seeds in the Presence of Aqueous Acidic. *Turkish Journal of chemistry*, 24, pp. 247–253.
[18] Agu, C. M., Menkiti, M. C., Ohale, P. E., and Ugonabo, V. I. (2021). Extraction modeling, kinetics, and thermodynamics of solvent extraction of *Irvingia gabonensis* kernel oil, for possible industrial application. *Engineering Reports*, pp. 1–25.
[19] Ibiam, J. A. and Anosike, O. P. (2014). Extraction and characterization of palm kernel oil from the kernel of palm tree (*elaeis guineensis*). *International Journal of Current Research*, 6(5), pp. 6696–6698.
[20] Asuquo, J. (2008). Studies on the adsorption of some selected metallic soaps onto hematite. Palm Kernel Oil extraction oil. *Chem. Soc*., 85, pp. 23–28.
[21] Paulin, Y. and Irène, K. (2019). Physico-chemical Characterization of Palm Kernel Oil Extracted from the Seeds of Two Varieties of Oil Palm (*Elaeis guineensis Jacq* .) for Possible Use in Feed or Food. *European journal of nutrition and food safety*, 9(4), pp. 341–353. doi: 10.9734/EJNFS/2019/v9i430081.
[22] Asuquo, J., Anusiem, A. and Etim, E. (2012) 'Extraction and Characterization of Rubber Seed Oil.', International Journal of modern Chemistry, 1(3), pp. 109–115.
[23] Olaniyi, A., Babalola, O. and Mary, O. (2014) 'Physicochemical Properties of Palm Kernel Oil', Current Research Journal of Biological Sciences., 6(5), pp. 205–207.
[24] Asuquo, J., Anusiem, A. C. and Etim, E. (2010). Extraction and characterization of Shea butter oil. *World journal OF Applied Science and Technology*, 2(2), pp. 282–288.
[25] Adeyemi, A. ., Ogunwole, O. . and Oladimeji, S. . (2020) 'Chemical characterisation of palm kernel (Elaeis guineensis Jacq .) , shea butter (Vitellaria paradoxa C . F . Gaertn .) and sesame (Sesamum indicum L .) seed oils as ingredients in breeding broiler diets', Nigerian J. Anim. Sci, 22(3), pp. 191–198.
[26] Ebewele, R. O., Iyayi, A. F. and Hymore, F. K. (2010) 'Considerations of the extraction process and potential technical applications of Nigerian rubber seed oil', international journal of physical sciences, 5(June), pp. 826–831.
[27] Dawodu, F. (2009). Physico – chemical studies on oil extraction processes from some Nigerian grown plant seeds. *EJAFChe*, 8(2), pp. 102–110.
[28] Codex Alimentarius Commission (2015). Standard for named vegetable oils', Codex Stan 210-1999.

[29] Amoo, I. F., Eleyinmi, A. F., Ilelaboye, N. A. O., and Akoja, S. S. (2004). Characteristics of oil extract from gourd (*Curcurbita maxima*) seed. *Food, Agriculture & Environment*, 2, pp. 38–39.
[30] Abitogun, A., Alademeyin, O., and Oloye, D. (2009). Extraction and Characterization of Castor Seed Oil. *The internet Journal of Nutrition and Wellness*., 8(2), pp. 1–10.
[31] Liauw, M. Y., Natan, F. A, Widiyanti, P., Ikasari, D., Indraswati, N., Soetaredjo, F. E. (2008). Extraction of neem oil (*azadirachta indica ajuss*) using n-hexane and ethanol: studies of oil quality, kinetic and thermodynamic. *ARPN journal of Engineering and Applied sciences*., 3(3), pp. 49–54.
[32] Khraisha, Y. H. (2000) 'Reporting of Oil Shale Followed by Solvent Extraction of Spent Shale: Experiment and Kinetic Analysis.', Journal of Energy Sources, 22, pp. 374–355.

NIPES-NCEE Conference Proceedings
The 2nd International Conference 15th-17th Feb. 2023
33-36
www.nipesjournals.org.ng

SYNYHESIS OF HIERARCHICAL ZEOLITE Y FROM ALOJI KAOLIN.

[1]R. A. Usman, [1,2]A. S. Kovo, [1,2] A. S. Abdulkareem and [1]M. U Garba.

[1]Department of Chemical Engineering, Federal University of Technology, PMB. 65, Minna, Niger State, Nigeria
[2]Nanotechnology Research Group, Africa Center of Excellence for Mycotoxin and Food Safety, Federal University of Technology, PMB 65, Minna, Niger State, Nigeria
[*]Corresponding author's E-mail: rukiyausman3@gmail.com

Abstract
Zeolites has emerged as a main heterogeneous catalyst in most chemical industries. Its diffusion limitation causes ineffective utilization of the catalyst, leading to early coking and subsequent deactivation of the zeolites. Hierarchical zeolites have been identified as suitable advanced material that addresses the limitations encountered with microporous zeolites in the catalytic reaction. It has an enlarged pore improved surface area and reduced channel that speed up the reaction in many applications. The development of hierarchical zeolite Y from Aloji kaolin as a possible catalyst in reactions is the focus of this work. The bottom-up synthesis approach of hierarchical zeolites Y denoted by (YB) involved the use of pluronic-123(copolymer) as mesopores directing agent. The crystallized hierarchical zeolites (YB6) were characterized with XRD, SEM, TEM, and BET. The crystallite size of the YB6 is 35.69nm with a percentage crystallinity of 73.50%. The pore distribution of 0.2nm to 90nm was observed with the synthesized hierarchical zeolite. The SAED images of synthesized hierarchical zeolitesYB6 depict a polycrystalline material with distinct rings showing grains of different sizes. The hierarchical zeolite Y has a surface area of 6.2817m2/g, pore volume of 0.013655cm3/g, and pore size of 8.4194nm.

1.0 **Introduction**
Zeolites are porous multi-dimensional crystalline aluminosilicate materials with a defined framework containing silicon, aluminum, oxygen alkaline or alkaline earth metals, and water stuck in between them. Zeolites are made from interweaved tetrahedra of alumina and silica. They have open pores and cavities arranged regularly. Zeolites are microporous (>2nm) and have a large specific surface area and pore volume that are accountable for their adsorption capacity and catalysis in general [1]. They have numerous applications in chemical industries due to their ability to preferentially adsorb certain gaseous molecules in gas separation and their ability to act as 'sieves' for a reactant or product molecules based on their pore sizes and difference in the diffusion rates of competing molecules within their channel system [2]. Zeolites are synthesized from sodium aluminosilicate gel formed from various silica and alumina sources by hydrothermal treatment. However, the source of synthetic aluminosilicate reagents for the preparation of synthetic zeolites has higher cost implications and generates waste to the environment [3]. The search for a cheap source of silica and alumina for the synthesis of zeolite motivated most researchers to use different geological materials and industrial wastes like coal fly ash[4] and kaolin[5]. The use of kaolin as the source of natural aluminosilicate for the synthesis of zeolite has continued to interest researchers over the years due to its easy accessibility, low impurities, and environmental friendliness. The development of hierarchical zeolite with qualities such as a longer lifetime, high catalytic performance, postponed coking and deactivation will reduce the constrain observed in the conventional zeolite catalyst [6].

Hierarchically structured zeolites combine the qualities of microporous zeolites and mesoporous materials to offer enhanced molecular diffusion and mass transfer without compromising the inherent catalytic activities and selectivity of zeolites. They are defined by the difference in their physical properties mainly pore size distribution. It contains more types of pores of different sizes (micropores, mesopores, and macro-pores) which can overcome mostly the transport limitation of the smaller pore's zeolites. It encompasses zeolite with at least a secondary pore structure system.

2.0 Material and Methods

Aloji kaolin was beneficiated and calcined at a temperature of 650^{o}C in a furnace for 3 hours to obtain a reactive metakaolin. Synthesis of Hierarchical zeolite Y was done by Bottom-up

Approach (Soft templating). 1.3g of sodium hydroxide pellets were dissolved in 2 grams of distilled water. The above solution was divided into two halves. 2.46 grams of sodium metasilicate was added to one and 1 gram of metakaolin and 0.005P123 to the other solution. The P123 was acting as a structural directing agent. The two mixtures were rigorously stirred for a complete dissolution of sodium metasilicate. The combined aluminosilicate gel was aged for 10 hours and crystalline in a Teflon-line stainless steel autoclave at 110^{o}C crystallization temperatures for 9 hours. The crystallized zeolite was washed with deionized water to a pH of 9 and dried at 110^{o} C for 8h. The sample obtained above was calcined in air at 550^{o}C for 6 h to remove the template. This mesoporous zeolite Y was protonated by ion exchange with 10ml 1.0 M NH_2SO_4 solution per gram of synthesized zeolite by soaking in the above solution for 24 h. This was later filtered and dried in the oven at 100^{o}C for 3 h and calcined at 550^{0} C for 2h and denoted as YB6. The crystallized Hierarchical zeolite YB6 was characterized by XRD, SEM, TEM, and BET.

3.0 Results and Discussions

From the XRD pattern (A) the peaks at 2 theta values of 6.13^{o}, 10.34^{o}, 12.14$^{o.}$ and more denotes zeolites Y [7]. However, the peaks of 26.65^{0} and 36.55^{0} denote the presence of quartz which is an impurity in the synthesis of zeolites from kaolin [8].The SEM Images (B) of Hierarchical zeolite Y (Bottom-up approach) show a spherical shape of hierarchical zeolites Y, percentage crystallinity of 73.50%, and Si/ Al ratio of 1.996 from the EDX values [9]. The higher distribution between 200 to 600nm gives an average diameter of 551.45nm. The higher magnification of the HRTEM images of synthesized zeolites(C) has notable numbers of grains typical of polycrystalline or nanomaterial. The Selected area diffraction (SAED) has many small spots forming a ring. This phenomenon rings are that of polycrystalline or hierarchical material [10]. The adsorption isotherm is a type IV and hysteresis of H4 according to the IUPAC classification for a porous material. The hysteresis loop H4 is associated with narrow pores and internal voids of irregular shape that are connected. The narrow hysteresis loop observed at the low-pressure region of p/p^o of less than 0.2, is evidence of the presence of mesopores. The presence of a hysteresis loop at the high-pressure region of p/p^o greater than 0.2 is an indication of macro-pores in the as-synthesized zeolite YB6. The BJH pore size distribution revealed the presence of hierarchical porosity ranging from 0.2 to 90nm. The synthesized zeolite YB6 has a BET surface area of 6.2817m^2/g, pore volume of 0.013655cm^3/g, and pore size of 8.4194nm.

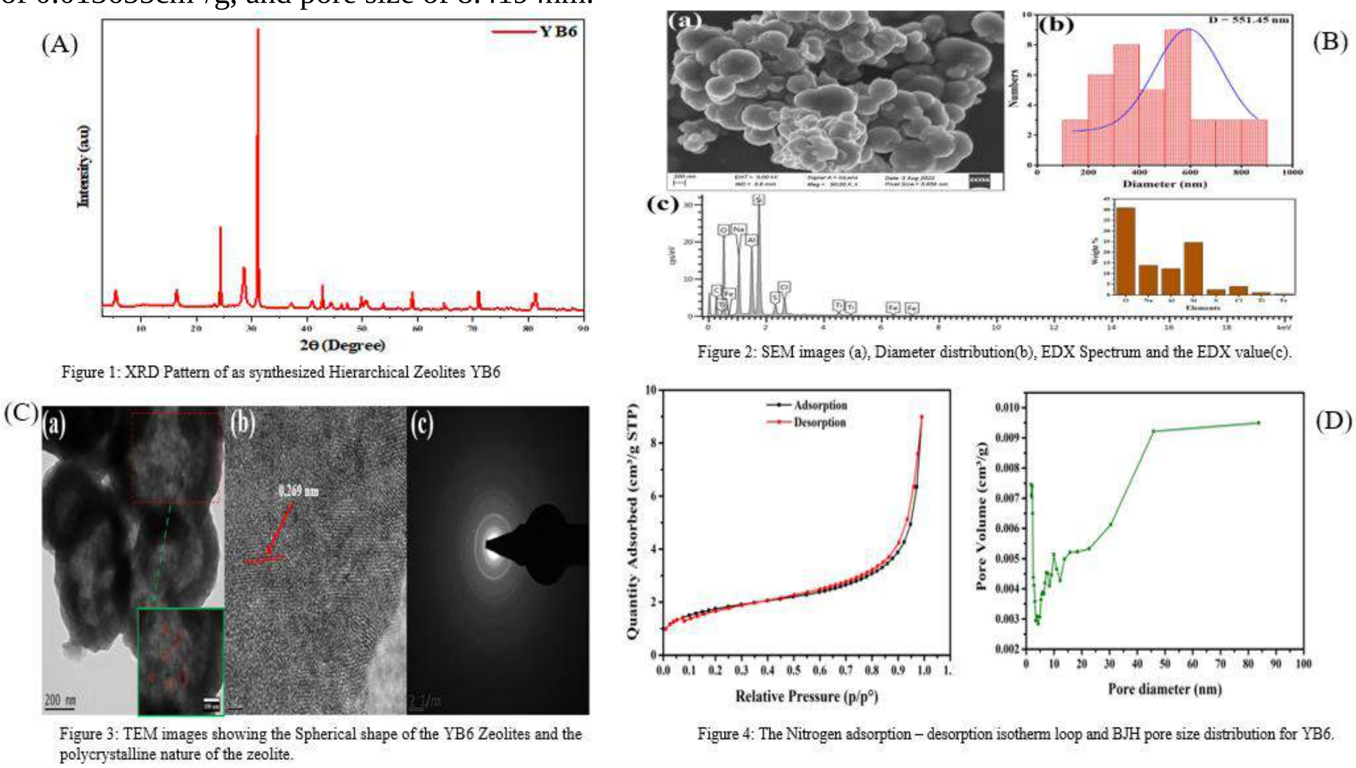

Figure 1: XRD Pattern of as synthesized Hierarchical Zeolites YB6

Figure 2: SEM images (a), Diameter distribution(b), EDX Spectrum and the EDX value(c).

Figure 3: TEM images showing the Spherical shape of the YB6 Zeolites and the polycrystalline nature of the zeolite.

Figure 4: The Nitrogen adsorption – desorption isotherm loop and BJH pore size distribution for YB6.

Figure 1: Characterization of Synthesized Hierarchical Zeolite YB6

Conclusion

A hierarchical zeolite Y has been successfully synthesized from Aloji Kaolin for possible application in catalytic, separation processes and any other reactions involving the utilization of heterogeneous nano-catalyst. The pore size distribution of this synthesized zeolite Y ranges from 0.2 nanometers to 90 nanometers. This nanomaterial has been prepared from an abundant locally sourced material with the simplest methodology.

References

[1] Perla S. L., Yulia K., Rosario I. Y., Joel A. G., Ramesh K. C., Vitalii P., and Sergio F. M.(2021)Recent Advances in Catalysis Based on Transition Metals Supported on Zeolites(Review) *Front. Chem. Sec. Catalysis and Photocatalysis*
doi.org/10.3389/fchem.2021.716745

[2] Jan-Paul G., Katharina K., Bastian R., Wilhelm S. and Alexandra I. (2021). Layer-Like Zeolite X as Catalyst in a Knoevenagel Condensation: The Effect of Different Preparation Pathways and Cation Exchange. Institute of Chemical Reaction Engineering, Friedrich-Alexander University Erlangen-Nürnberg, 91058 Erlangen, Germany *Catalysts*, *11*(4), 474. 484.

[3] Krisnandi Y. K., Indah, R., Saragi I. R., Sihombing R., Ekananda R., Sair R., Benjamin E., Griffith and John V. Hanna (2019). Synthesis and Characterization of Crystalline NaY-Zeolite from Belitung Kaolin as Catalyst for n-Hexadecane Cracking. *Crystals.*

[4] Wei F., Guoping H., Eric F. M. and Gang K. L. (2022) Synthesis of zeolites from circulated fluidized bed coal fly ash. *Inorganic Chemistry Frontiers*. Issue 8,

[5] Norsuhailizah S. and Zawati H. (2022) One Shot of the Hydrothermal Route for the Synthesis of Zeolite LTA Using Kaolin. *Journal of Inorganic and Organometallic Polymers and Materials* volume 32, pages 3508–3520

[6] Wen Q. J., Wen H. F., Xiao M. L., Yi M. W., and Ming-Yuan H. (2014)Preparation of hierarchically structured Y zeolite with low Si/Al ratio and its applications in acetalization reactions. *RSC Advances*, Issue 102.

[7] Yuan H., Shenghui G., Shiwei L., and …., Shaohua Y. (2022) Green and efficient synthesis of high-purity Y zeolite using natural raw material-kaolin activated by microwave heating. *Applied Physics A*, volume 128, Article number: 1077

[8] Younesse H., Hicham M., Said M., Youssef T., Rachid B., Mina O., and Hassan H. (2021) Effect of Sodium Hexafluorosilicate Addition on the Properties of Metakaolin Based Geopolymers Cured at Ambient Temperature. *Silicon* 13(5) DOI:10.1007/s12633-020-00536-9

[9] Belaabed R., Elknidi H., Elkhalfaouy R., Addaou A., Laajab A. and Lahsini A. (2017) Zeolite Y synthesis without an organic template: The effect of synthesis parameters *Journal of Material and Environmental Sciences*, Volume 8, Issue 10, Page 3550-355

[10] Alessia A., Matteo S., Francesca B., Pierluigi Q., Silvia B., Johan A. M. and Valentina C. (2021) Insights on a Hierarchical MFI Zeolite: A Combined Spectroscopic and Catalytic Approach for Exploring the Multilevel Porous System Down to the Active Sites. Appl. Mater. Interfaces 13, 41, 49114–49127

NIPES-NCEE Conference Proceedings
The 2nd International Conference 15th-17th Feb. 2023
37-47
www.nipesjournals.org.ng

PERFORMANCE EVALUATION OF 11KV GOVERNMENT RESERVE AREA (G.R.A), ETETE FEEDER IN BENIN ELECTRICITY DISTRIBUTION COMPANY(BEDC), BENIN CITY, EDO STATE, NIGERIA

[1]R.O. Edokpia and [2]O.C.Onuigbo

Department of Production Engineering, University of Benin, Nigeria
ralphedokpia@yahoo.com and ositadimma.onuigbo@gmail.com

Abstract

In this present time where the demand of electric energy is increasing rapidly with technological and economic growth. The energy demands of the customers supposed to be met, however, Nigeria's power supply has been experiencing incessant interruptions due to failures in the distribution system which constitutes about 80%. The reliability of the power system is the major challenge to meet the customers demand. In this research work, the performance of an 11kv feeder in Benin Electricity Distribution Company (BEDC), Edo State Nigeria were evaluated. These was carried out by collating the failure data which includes; outage duration, time of failure, causes of failure, and load interruption from the Injection substations G.R.A Injection substations for the year, 2020 and 2021. Monthly and yearly trend analysis (involving Mean time between failure(MTBF), Mean time to repair(MTTR), failure rate, repair rate, availability), Non parametric method, Customer based reliability indices, and parametric method were deployed for the analysis.

The analysis from this study reveals that there was a decrease for MTBF for the feeders (which implies decline in Performance). The year 2021 had the accumulated higher MTTR than 2020 as a result of decline in response to faults. Lambda (λ) increased in magnitude in the year 2021 for the feeder. There were also decrease in the scale parameter (also known as 'life characteristics') in the year 2021 relative to 2020. The results showed that the year 2020 had a better performance than the year 2021.

Keywords:
Reliability, Availability, Maintainability, Mean Time between Failure (MTBF), Mean Time to Repair (MTTR), Failure rate.

NOMENCLATURE AND SYMBOL

$R(t)$	Reliability Function
$f(t)$	Probability Density Function
$F(t)$	Failure Function/Cumulative Density Function (CDF)
$\lambda(t)$	Hazard Rate/Failure rate
$H(t)$	Repair Distribution Function
MTBF	Mean Time between Failures
MTTF	Mean Time to Failure
MTTR	Mean Time to Repair
n	number of failure/repair times
t_i	time of failure of ith unit
t_n	time of failure of nth unit

FIT	Failure in time
RAM	Reliability, Availability, and Maintainability
SAIFI	System Average Interruption Frequency Index
SAIDI	System Average Interruption Duration Index
CAIDI	Customer Average Interruption Duration Index
CAIFI	Customer Average Interruption Frequency Index
ASAI	Average System Availability Index
ASUI	Average System Unavailability Index
β	shape parameter (slope)
ŋ	scale parameter (characteristics life)
Y	location parameter (the displacement of the time origin)

1. Introduction

Over the last half-century, power systems have been growing exponentially around the globe, creating a pathway for industrial development [1]. There has been modification of Electric Power System since the year 1896 till date. There has been restructuring and reorganization of power sector down to President Buhari's administration yet the energy demands of the country is yet to be met [2,3]. A stable and reliable electric power supply system is a pre-requisite for the technological and economic growth of any nation. Nigeria's power supply has been experiencing incessant power interruptions caused by a failure in the distribution system. Electric power is a vital element in any modern economy. The availability of reliable power supply at a reasonable cost is crucial for the economic growth and development of a country [4]. The satisfaction and importance of availability of electricity supply to consumers at the time of usage cannot be over-emphasized. A reliable power supply boost productivity and reduces waste in any system [5, 6, 7]. The electric power supply in the feeder under study has become alarming and a source of concern to all stakeholders.

Distribution systems are large-scale systems that comprises many components and assets which need periodic maintenance to work properly and provide reliable energy and power to customers [8]. Although relevance of distribution system fault/failure are much greater than other parts of power systems like generation and transmission. Analysis throughout the world shows that around 90% of all customer reliability problems are due to the problem in the distribution system, hence, improving distribution reliability is the key to improving customer reliability. Many power systems Engineers have carried out different optimization studies via heuristic, network configuration, integration of renewable energy resources, and coordination of distributed generation aimed at improving the system network. Therefore, improving distribution reliability is the key to improving customer reliability [4, 9, 10].

The aim of this research is to carry out the performance evaluation of the feeder under study. Despite the realization of the importance of the distribution sector, the performances of Nigerian distribution utilities of these feeders have not been measured empirically. The performance evaluation of the distribution sector is important in order to assess the impact of reform measures.

The Reliability availability and maintainability (RAM) of electric power supply is crucial for economic development because of electricity's role as a powerful engine of social and economic change. 78% of firms in Africa experienced power outages yearly. Also, 41% of firms identified electricity as a major constraint to their business operations [11, 12, 13, 14]. The predominant factor that differentiate modern man from his ancestor is the ability to manage energy/power [14].

2. Performance evaluations have been carried out with the use of reliability, availability, and maintainability (RAM) assessment for Electric Power generation, transmission, and distribution. Having gone through various articles and researches that have been published on RAM assessment within and outside the country, only few worked on the feeders of distribution system. And to the best of my knowledge, the performance evaluation of the feeders have not been carried out by comparing the use of Non Parametric approach, Customer based reliability indices and Parametric Method.**METHODOLOGY**

The interruption data (comprising of the time power went off and the time it was restored) were gotten from G.R.A injection substation for G.R.A Etete Feeder [15]. The anaysis started with computing the repair time which implies subtracting the time power was restored from the time power went off. The failure time is the time the restored power lasted. Then, reliability, availability, and maintainability (RAM) is analysed graphically using Microsoft Excel. The flow chart of the experiment is represented in figure 1 below

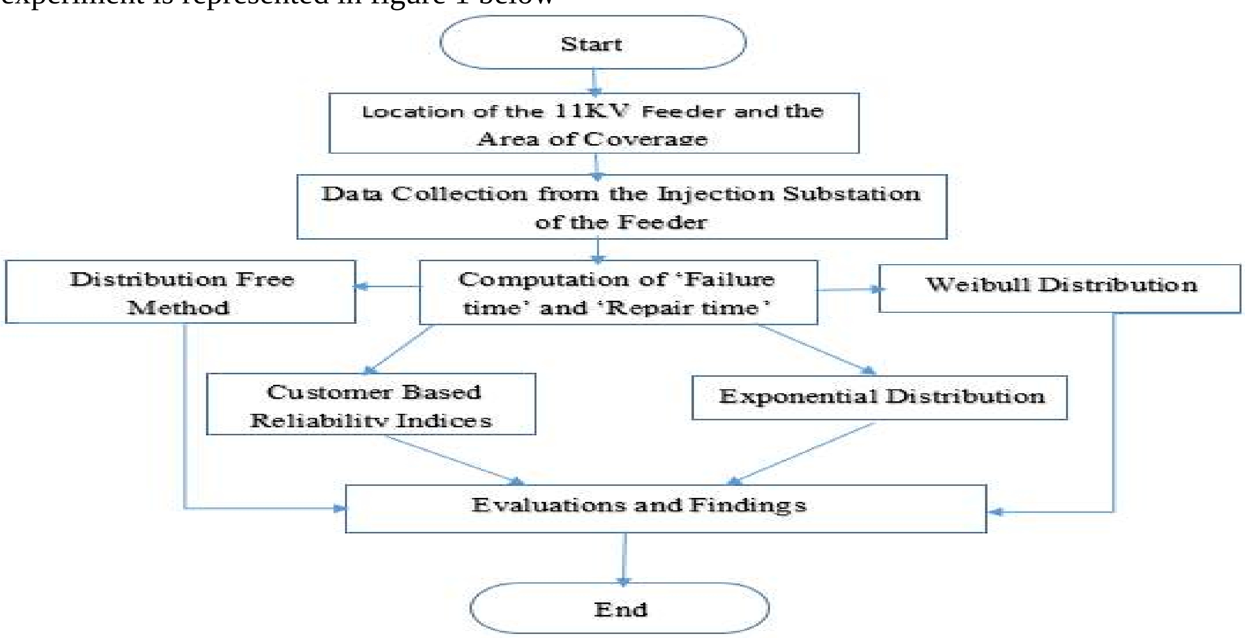

3. Figure 1: Research flow diagram [16, 17, 18, 19, and 20]**RESULTS AND DISCUSSION**

3.1 Results

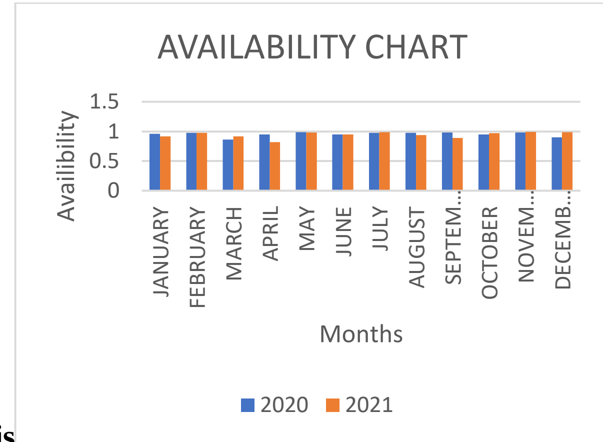

Monthly Trend Analysis

Figure 2: G.R.A Etete Availability

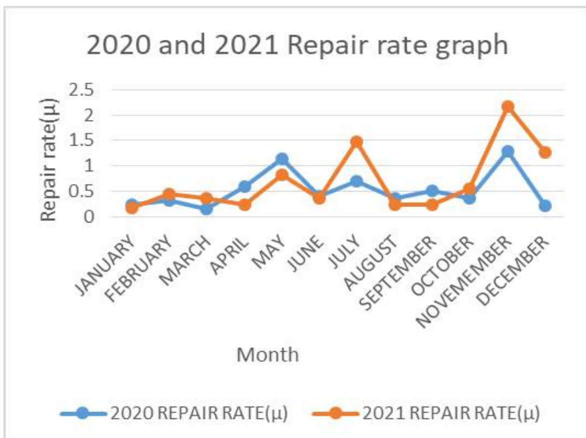

Figure 3: 11kv Feeder Repair rate graph for 2020 and 2021

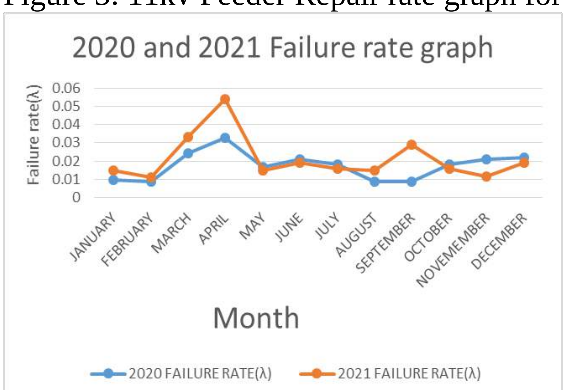

Figure 4: 11kv Feeder Failure rate graph for 2020 and 2021

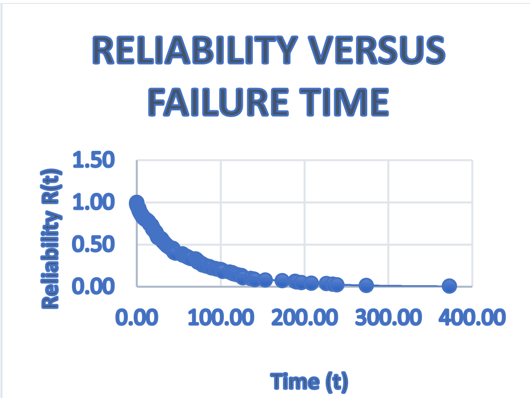

Figure 5: Reliability curve for 2020

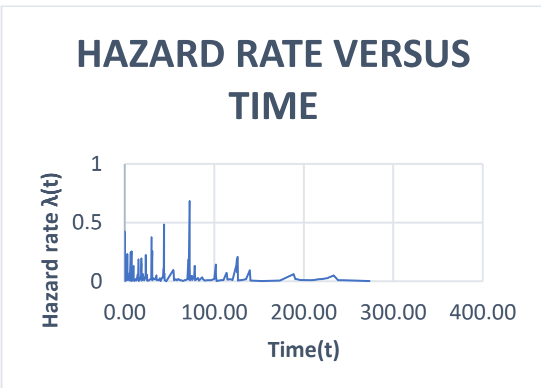

Figure 6: Hazard rate curve for 2020

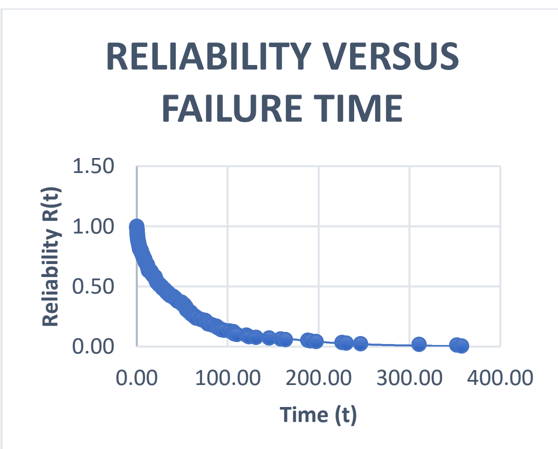

Figure 7: Reliability curve for 2021

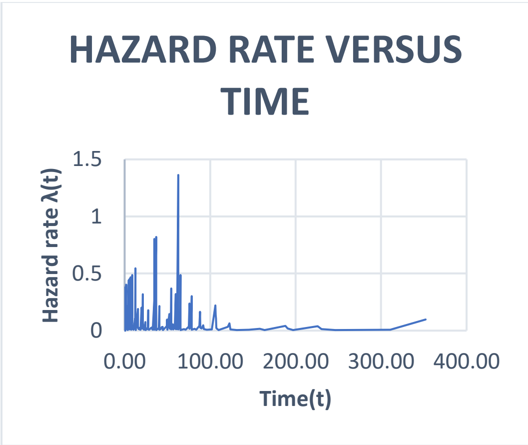

Figure 8: Hazard rate curve for 2021

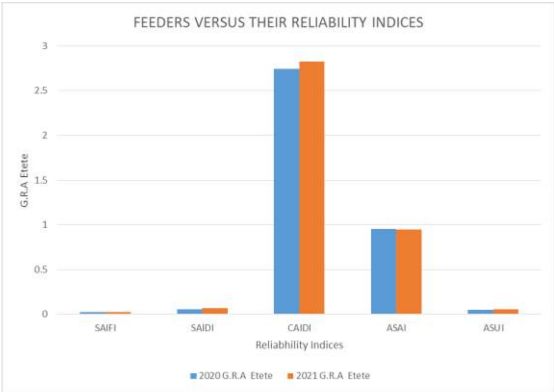

Figure 9: Customer based reliability indices charts

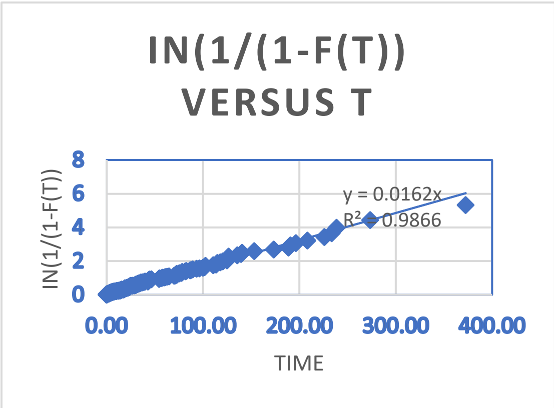

Figure 10: Exponential plot for 2020

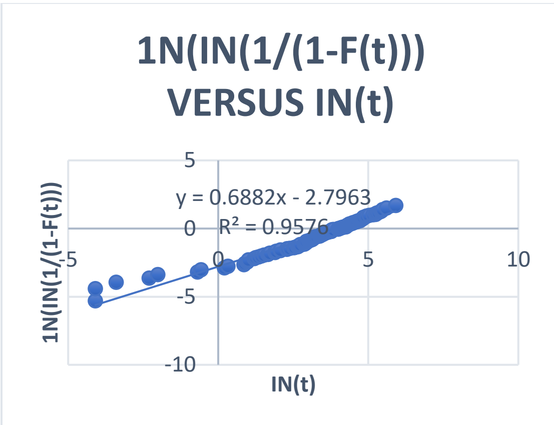

Figure 11: Weibull plot for 2020

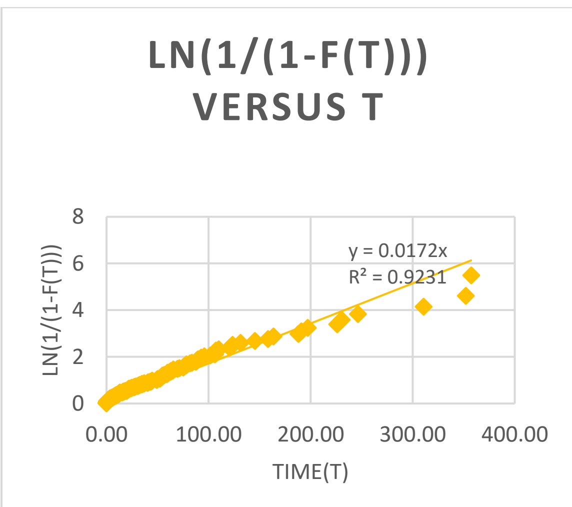

Figure 12: Exponential plots 2021

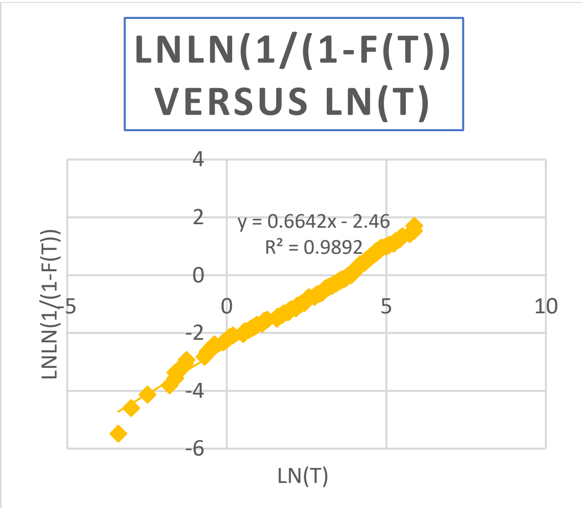

Figure 13: Weibull plots 2021Table 1: Yearly Reliability, Availability, and Maintainability (RAM) parameters for 2020

FEEDERS	MTBF	Failure Rate(λ)	MTTR	REPAIR RATE(μ)	AVAILABILITY
G.R.A Etete	57.71	0.0173	2.8	0.3569	0.9537

Table 2: Yearly Reliability, Availability, and Maintainability (RAM) parameters for 2021

FEEDERS	MTBF	Failure Rate(λ)	MTTR	REPAIR RATE(μ)	AVAILABILITY
G.R.A Etete	48.5	0.0206	2.84	0.3521	0.9447

Table 3: Exponential Parameter for the year 2020 and 2021

LAMBDA(λ)		
FEEDERS	**2020**	**2021**
G.R.A ETETE	0.0I62	0.0172

Table 4: Weibull Parameters for the year 2020 and 2021

	2020		2021	
FEEDERS	SHAPE PARAMETRE(β)	SCALE PARAMETER (η)	SHAPE PARAMETER (β)	SCALE PARAMETE R(η)
G.R.A ETETE	0.6882	58.16	0.6642	40.5972

3.2 Discussion of Results

The availability chart as in Figure 2 shows that February, March, July, October, November, and December. On a yearly basis, the availability of the Feeder in the year 2020 is 0.9537 where as that of 2021 is 0.9447. From the value of availability for the two (2) years, it is observed that the performance is better in 2020 than 2021 (as shown in Table 1 and 2). Therefore, an investigation need to be made for the root cause analysis (RCA) that led to the drop in performance such that the proper root cause action will be taken.

Figures 3 and 4 describes the repair and failure rates respectively for 2020 and 2021. In 2020; From May to June, and November to December, there is a drastic decline in repair rate which indicates less response to resolution of faults and vice versa. This (drastic decline in repair rate) replicated in July to August, and November to December. The decline in the repair rates shows decrease in the overall availability of supply to the G.R.A Etete feeder as well as making the customers to spend more money in fuel thereby reducing the total revenue of the distribution company (BEDC). There are drastic decline in failure rate from April to May concurrently in 2020 and 2021. The same is also seen in July to August, 2020 and September to October, 2021. The decline in failure rates implies less outages which will always trigger the customers to pay there by increasing the revenue of the distribution company and vice versa.

The Reliability curve for the year 2020 and 2021 (as represented in figure 5 and 7) shows that reliability R (t) is a step function which decreases by $1/(n + 1)$ just after each observed failure time. The hazard rates (as in figure 5 and 7) are not showing consistent trends (as Increasing, Decreasing, or Constant failure rates).

Figure 8 reveals that the customer based reliability index (SAIFI, SAIDI, and CAIDI) for the year 2021 is higher than that of the year 2020. This implies higher reliability in the year 2020 than in 2021. The same also applies to ASAI implying more power availability in the year 2020 than 2021.

Figure 10, 11, 12, and 13 captured the result of linearization of Exponential and Weibull distribution function. The parameter, 'lambda (λ)' in Exponential distribution actually increased in the year 2021 in comparison with the year 2020 which also signifies decrease in performance. The same is also applicable in Weibull distribution more especially in the scale parameter (η) (also known as the Characteristic life is measured in hours) also decreased in the year 2021 which also depicts drop in Performance. Since the shape parameters (β) are less than one (1) for the both years. This connotes that the feeder is exhibiting decreasing failure rates.

The exponential and Weibull distributions revealed that the plots formed approximately a straight line and the coefficient of determination (R^2) above 0.9 in both plots implies that the data are well fitted

4. Conclusion

Two (2) years failure data for the feeder (which consist of the following; time of outage, time outage was restored, causes of outages, load interrupted) were collated and collected from the Injection sub-station. 'Time to repair' and, 'Time between failures' were computed from the data collected. The causes of the failure were attributed to a number of factors such as transient reasons, earth fault, over current, load limitation, load shedding, Work permit, and in some cases failure from the transmission company of Nigeria (TCN). The analysis from this study revealed that there was a decrease in MTBF for the feeder (which implies decline in performance). The year 2021 had the accumulated higher MTTR (which means there was decline in response to outages). The Feeder actually had a decline in the availability performance when you compare the year 2020 and 2021 performance. Exponential and Weibull distribution was also applied in the analysis, it was observed that 'lambda (λ)' which signifies 'failure rates' increased in magnitude in the year 2021 which depicts increase in the frequency of failure. There were also decrease in the scale parameter (also known as 'life characteristics') in the year 2021. Having applied these approaches; monthly trend analysis, Parametric, Non-parametric approaches and Customer-based reliability approaches. It is observed that the year 2020 have the best performance than 2021.

References

[1]. Alvarez-Alvarado M.S., Donaldson D.L, Recalde A.A., Noriega H.H., Khan Z.A., Washington V. and Rodriguez-Gallegos C.D. (2022). Power System Reliability and Maintenance Evolution: A Critical Review and Future Perspectives, Open Access Journal, Vol 10, pp 51922-51950

[2]. Adejumobi, I.A. (2021), Electricity, Man, and Development: The Complexity of the Distribution System Management in a Power Network, FUNAB Inaugural lecture, Series No 64, Pp.7-81, ISBN: 978-978-992-948-1

[3]. Akpan,P (2006), Electricity and Water supply in Nigeria: A case study of Markudi Town. Journal of Historical Society of Nigeria, Vol.16, pp. 48-71

[4]. Nweke, J.N., Gusau, A.G, and Isah, L. M. (2020), Reliability and Protection in Distribution Power System considering Customer-Based Indices, Nigerian Journal of Technology (NIJOTECH), Vol.39, No 4, pp.1198-1205

[5]. Akpojedje F.O., Abu Y.O., and Onowighose. O. (2021). Tripping Profile Analysis of the 33 KV Feeder of Ugbowo 2 x 15 MVA, 33/11 kV Injection Substation, Equity Journal of Science and Technology, Vol 8 No 1, pp 19 – 26, ISSN 2354-1814; E-ISSN 2682-5961, Available online at www.equijost.com

[6]. Ohajianya, A.C., Abumere, O.E., Owate, I.O., and Osarolube, E. (2014), Erratic Power Supply in Nigeria: Causes and Solutions, International Journal of Engineering Science and Innovation, Vol 3, Issue 7, and pp.51-55, ISSN: 2319 – 6726

[7]. Momoh Z., Anuga J.A., and Obidi J.A. (2018). Implications of Poor Electricity Supply on Nigeria's National Development. Vol.6, No.2, PP.31-40, ISSN (p): 2312-5659 DOI:10.18488/journal.73.2018.62.31.40

[8]. Olajuyin E. A. and Eniola O. (2022). Reliability and Maintenance of Assets in Electric Power Distribution Network, Current Journal of Applied Science and Technology, Volume 41, no 9, pp 8-17, *Article no.CJAST.80761* ISSN*: 2457-1024*

[9]. Mirhosseini M. and Keynia F. (2021) Asset management and maintenance programming for Power distribution systems: a review. Pp 2287–2297 https://doi.org/10.1049/gtd2.12177

[10]. Mirhosseini M., Azim Heydari1 A., 2 · Davide Astiaso Garcia D. A., Mancini F. and Keynia F (2022). Reliability based maintenance programming by a new index for electrical Distribution system components ranking, Optimisation and Engineering, Research Article, pp 2315-2333, https://doi.org/10.1007/s11081-022-09767-8

[11]. Oseni, M.O., & Pollitt, M.G., (2015). A firm-level analysis of outage loss differentials and self-generation: Evidence from African business enterprises. Energy Economics (52).

[12]. Airoboman A. E., Salihu-Ango H., Ibrahim, S. O and Ahmed H. (2021). Risk Assessment of Injection Substation within Kaduna Metropolis using Failure Mode and Effect Critical Analysis (FMECA), Journal of Sciecnce Technology And Education, Vol 9, No 2, pp 308-319, ISSN: 2277-0011; Journal homepage: www.atbuftejoste.com

[13]. Airoboman A.E. (2022). Reliability Assessment of Power System Network: A Detailed Review, International Journal of Engineering Technologies-IJET Vol.7, No.4, pp90-103

[14]. Olusuyi K., Oluwole A.S., Temitope Adefarati T. and Babarinde A.K. (2014). A fault analysis of 11kv distribution system (a case study of ado Ekiti electrical power distribution district), American Journal of Electrical Power and Energy Systems.Volume 3,No 2,

pp. 27-36. doi: 10.11648/j.epes.20140302.13
[15]. Log Book Data Outages of Benin Electricity Distribution Company Plc, G.R.A Unit., 2020 and 2021 (G.R.A, Etete, and Iyekogba Injection Sub-station).
[16]. Adediran, Y. A. (2014). Introduction to Reliability Engineering. Finom Associates, ISBN: 978 – 978 - 52341- 2-1, First Edition,
[17]. Lewis, E.E. (1994), Introduction to Reliability Engineering, John Wiley and Sons, Inc, 2nd Edition, Pp.1-9; 145-153
[18]. Marko, C. (2011), Assessment of Power System Reliability (Methods and Application), pp.28, 52-56, 215-224, ISBN: 978-0-85729-687-0, DOI: 10.1007/978-0-85729-688-7
[19]. Troyer, D.D. (2019), Reliability Engineering Principles for Plant Engineers, Article, pp.1-13
[20]. Urdhwareshe, H. (2020), Weibull Distribution, Online Video, Institute of Quality and Reliability

NIPES-NCEE Conference Proceedings
The 2nd International Conference 15th-17th Feb. 2023
48-63
www.nipesjournals.org.ng

DEVELOPMENT OF A ZIGBEE TYRE PRESSURE MONITORING SYSTEM SENSOR UNIT WITH AN EFFICIENT BATTERY SCHEDULING ALGORITHM

Kingsley Okeoghene Enalume,[1] Kingsley Osaro Ogbeide,[2]

[1]Department of Electrical and Electronic Engineering, Federal University of Petroleum Resources, Nigeria
[2]Department of Electrical and Electronic Engineering, University of Benin, Nigeria
Corresponding email: enalume.kingsley@fupre.edu.ng

Abstract

Proper tyre pressure is very important for even tread wear, fuel economy, safe driving and better braking performance. To ensure the effective monitoring of tyre pressure, tyre pressure monitoring systems (TPMS) was developed. However, powering the sensor unit which is enclosed by the tyre has continued as a challenge. In this work, we developed an algorithm to extend the battery life of a sensor unit for TPMS. Besides, the frequency used by most original equipment manufacturers (OEM) of TPMS in the US and Europe is 315 MHz and 433 MHz respectively, which is within the frequency band of TV signal transmission in Nigeria (41MHz – 960 MHz). Hence, we chose a 2.4 GHz unlicensed frequency for our work. We chose ZigBee over Bluetooth technology as it consumes lesser power and has a wider range. Then we designed and developed the sensor unit, measured the sleep and wake-up currents of the unit and used the values to develop an idle and active mode operation for the sensor unit which was implemented in the program code. We compared the results of the system when it was continuously transmitting data with the system when our algorithm was implemented. We observed that there was a 99.97 % power savings between the current in the sleep mode and wake-up mode thereby extending the battery life without reducing the efficiency of the system. Using a 700 mAH Li-ion battery, the battery lifespan could be increased from 1.34 – 1.77 years to 4.69 – 6.195 years which is large enough to cover the 4 years lifespan of a tyre.

Keywords*: Tyre pressure, ZigBee, sensor unit, TPMS battery, algorithm*

1.0 Introduction

Tyre is the only part of a car that makes contact with the road. For the tyre to function properly, its inflation pressure must be maintained within an acceptable range. Underinflated tyre flex excessively, generates excessive heat, wears rapidly around the shoulders, reduces the tyre lifespan, and lead to blowout [1]–[4]. An overinflated tyre, on the other hand, leads to excessive inner wear, reduced braking and cornering performance, and blowout. If it runs over a pothole or other hard substances on the road, it could be damaged [5]–[7]. But a properly inflated tyre leads to even wear of the threads thereby increasing the lifespan of the tyre and better fuel economy. To ensure proper monitoring of tyre inflation pressure, a tyre pressure monitoring system (TPMS) was developed. TPMS is a system that monitors tyre inflation pressure and passes the information to the driver through some form of display mainly as warning symbols or digital readouts.

There are two types of TPMS, which are direct and indirect TPMS. Indirect TPMS uses some of the sensory information already present in the car to estimate tyre pressure. This type of TPMS is not very accurate. However, it does present information that is accurate enough to alert a driver on the condition of their tyre pressure and it is cost-effective [8]–[10]. The direct TPMS uses additional sensors and other circuitry, known as sensor units, that are attached to the wheel of the car to measure the tyre pressure. This type of TPMS is very accurate and is mainly powered by batteries [11]–[13]. One of the major challenges in TPMS is the wireless transmission of signals. For effective transmission of the signal, the antenna must be properly designed [14], [15]. Another major challenge of the TPMS is power. Since the sensor unit is enclosed by the tyre it is difficult to access it for battery change. How to power the sensor unit to ensure it is long-lasting since battery change is almost impossible has been the subject of research for decades [16]–[18]. This has led to the development of some battery-less technologies to power the sensor unit. However, developing energy harvesting systems for TPMS has some challenges which have not made it widely accepted as an alternative power supply for TPMS[17], [19]. As a result, battery-powered TPMS is still very popular.

To improve the battery life of the sensor unit, some use the accelerometer to determine the operation of the sensor unit [20], [21]. If there is no motion, the sensor unit goes to sleep but when a motion of the vehicle is detected, then the sensor unit measures the tyre inflation pressure and transmits it to be displayed for the user. The drawback of this system is that it does not transmit information about the tyre inflation pressure when the vehicle is parked or stationary. Chen et al. [22] developed a low-frequency wake-up receiver that acts on a signal received from the main control module to wake up the sensor unit. The drawback is that an additional circuitry that requires power is used, which increases the overall power requirement. Also, the system has not been demonstrated to work effectively in the dynamic environment of the tyre. Kuncoro et al. [23] developed a prototype wireless battery charger to charge the battery of the sensor unit to prolong the life of the battery. But it was simply an experimental setup that will need to be scaled up for commercial use. Investigation into how the system can function as the tyre rotates also needs to be carried out to determine the reliability and efficiency of the wireless charger. Bowen and Arafa [17] reviewed various battery-less systems such as electromagnetic, piezoelectric, electret, triboelectric and many more energy harvesters to power the sensor unit. Although such harvesters look promising, challenges such as variable driving frequencies of automobiles, frequencies as low as 20 Hz, how to make the energy harvester compact, and discontinuous and unregulated output power which is not suitable to power the sensor unit is affecting its implementation.

In this paper, we designed and developed a ZigBee-based TPMS sensor unit that could last for 4.69 – 6.195 years using a novel battery scheduling algorithm. ZigBee is a standard for low power, low cost, low rate, and short-range wireless personal area networks (LR-WPANs). It is based on the IEEE 802.15.4 standard that operates in the Industrial, Scientific, and Medical (ISM) radio bands with frequencies of 868 MHz band in Europe, 915 MHz in the US and 2.4 GHz worldwide. TPMS operates at 315 MHz in the US and 434 MHz in Europe which is within the frequency band of TV signal transmission in Nigeria (41MHz – 960 MHz) [24], [25]. ZigBee was chosen over Bluetooth because of its low power and long range compared with Bluetooth [26]–[29]. A TPMS sensor unit was proposed, designed and developed. A novel power scheduling algorithm was implemented on the program code to extend the battery life. The system was tested and the result shows that the sensor unit can efficiently be powered using the algorithm developed. The methodology of the research was discussed in section 2. Detailed design and fabrication of the wheel sensor unit were covered in this section. The battery algorithm to significantly increase the battery life was also highlighted in section 2. The results of the research were presented in section 3. While section 4 shows the conclusion of the paper.

2.0 Materials and Methods

2.1 Choice of The Wireless Communication Protocol

In this research, we chose ZigBee technology over Bluetooth technology because of the low power requirement. The power requirement for Bluetooth is 0 – 10 dBm while that for ZigBee is -25 – 0 dBm. As a result, batteries needed for ZigBee applications can last several years while that for Bluetooth would require constant charging. The data rate for ZigBee is 250 kbps against that of Bluetooth, which stands at 1 Mbps. The low data rate of ZigBee also leads to fewer computational resources. The time to join a network for ZigBee is 100 times faster than that of Bluetooth technology. ZigBee is at 30 ms while Bluetooth is at 3 s. The range for ZigBee is from 10 – 100 m against that of Bluetooth which is 10 m maximum. [26], [27], [30]–[32]. ZigBee technology was used as the communication technology between the master and sensor units. Figure 3 shows the ZigBee network topology that is used in this research. A star topology was deployed to implement the master section as the ZigBee coordinator and the sensor units as the ZigBee end devices. There are five sensor units. One for each tyre including the spare. The TPMS master unit is installed in the car where the driver can see the status of each tyre.

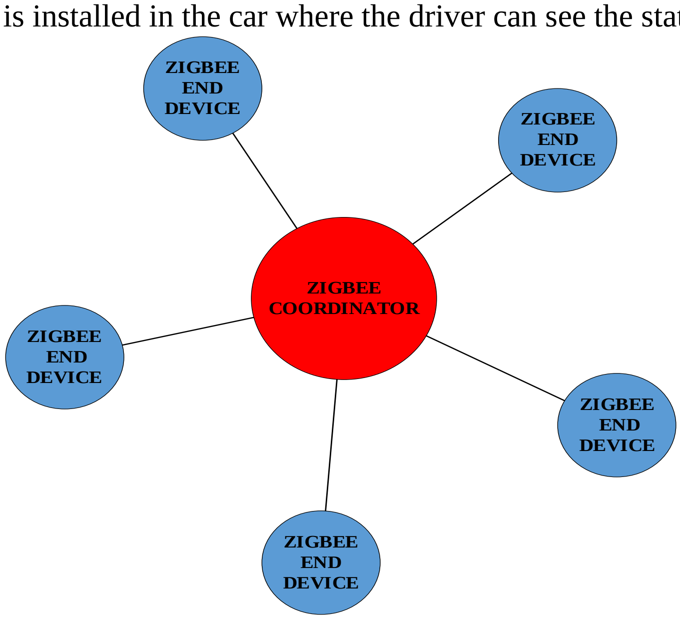

Figure 3: ZigBee star topology

2.2 Sensor Unit Circuit Design

Shown in Figure 4 is the block diagram of the entire TPMS. It contains the master section or receiver unit and the slave section which is the sensor unit. The focus of this paper was on the

NIPES-NCEE Conference Proceedings
The 2nd International Conference 15th-17th Feb. 2023
48-63
www.nipesjournals.org.ng

development of the sensor unit or the slave section. The sensor unit consists of a pressure sensor to measure the pressure of the tyre, a temperature sensor to measure the tyre temperature, a microcontroller to process the information and an XBEE module with an antenna radiating at 2.4 GHz to transmit/receive the appropriate signals.

Figure 5: Circuit diagram of the sensor unit shows the circuit diagram of the sensor unit. The pressure sensor used in this design was the MPXHZ6400AC6T1 piezoresistive pressure sensor. It is a small lightweight device with an operating temperature of -40°C to +125°C and a pressure range of 3.0 – 58 psi, which met the design criteria for this work. It is an 8-pin device, with pins 2, 3 and 4 as V_s, GND, and V_{out}. While pins 1, 5, 6, 7, and 8 are internal device connections and are not connected to any external devices. It has an accuracy of ±1.5 %V_{FSS}.

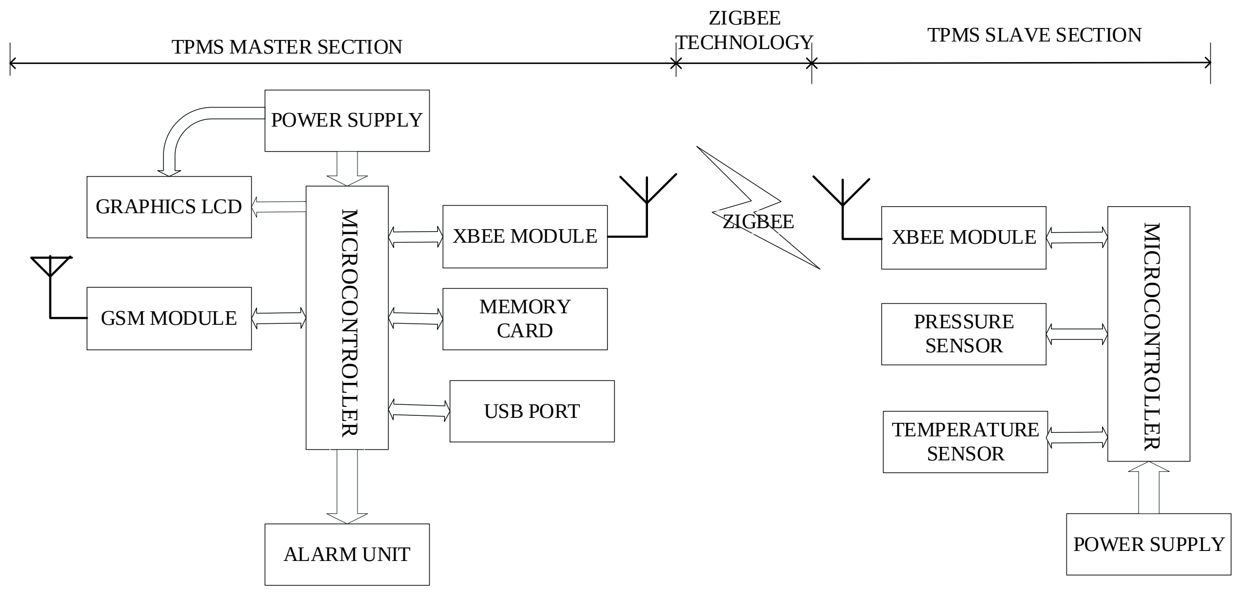

Figure 4: Block diagram of the TPMS

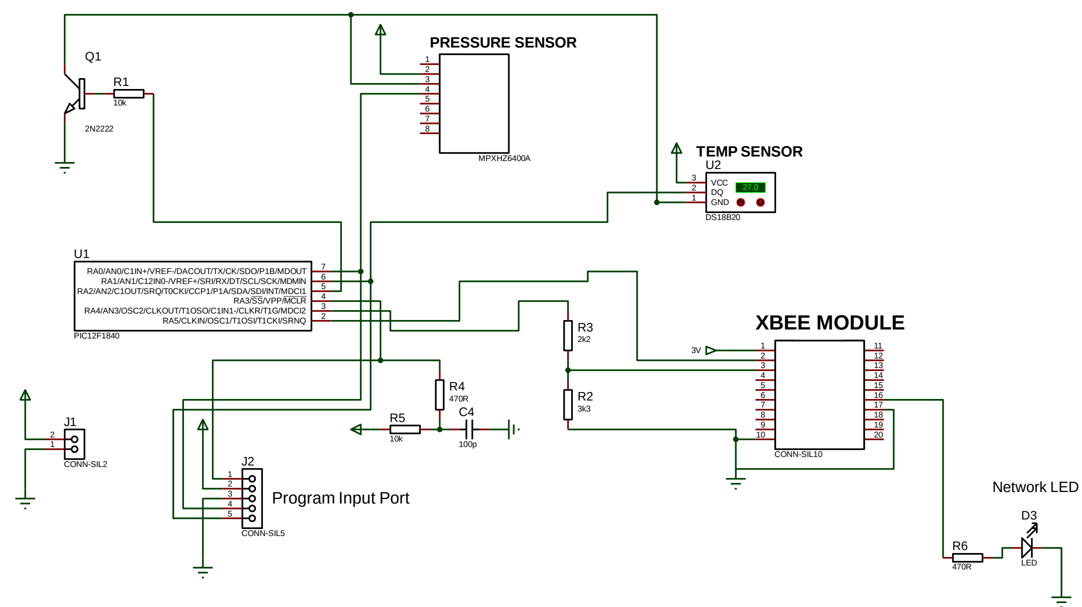

Figure 5: Circuit diagram of the sensor unit

The temperature sensor used was the DS18B20. It is a 3-pin device with pins 1, 2 and 3 as GND, Data input/output and V_{DD}. The range of temperature measurement is from -55°C to +125°C with an accuracy of ±0.5°C from -10°C to +85°C. The temperature sensor was well suited for the design because it can function adequately in a harsh environment.

The PIC12F1840 microcontroller, which is an 8-pin microcontroller, processes the pressure and temperature data and also does the analogue to digital conversion (ADC). The microcontroller is also responsible for the sleep and wake-up instructions of the sensor unit. PIC microcontroller was used because of its low power consumption and high-performance ability. It is small in size and can effectively interface with all the peripherals needed in the TPMS sensor unit. The pin connections of the PIC12F1840 with other units in the Slave modules are such that the output pin 4 of the MPXHZ6400AC6T1 piezoresistive pressure sensor is connected to port RA0 (pin 7) of the microcontroller, while Pin 2 of the DS18B20 is connected to port RA1 (pin 6) of the microcontroller. Pin 7 and 6 of the microcontroller act as input for the analogue pressure and temperature data respectively. They also carry out analogue-to-digital conversion (ADC) of the pressure and temperature data. Pin 2 (DO-Data Out) of the XBEE module is interfaced to pin 2 (USART asynchronous receive) of the microcontroller, and it is used to transmit data from the XBEE module to the PIC12F1840 microcontroller. Pin 3 (USART asynchronous transmit) of the microcontroller is connected to pin 3 (DI-Data In) of the XBEE module to receive data from the module. The transmit data pin of the microcontroller is connected to the receive data pin of the XBEE module. In contrast, the microcontroller's receive data pin is connected to the transmit data pin of the XBEE module. The microcontroller works with 5V, but the XBEE module data lines work with 3.3 V, so there is a need to step down any voltage signal from the microcontroller to the

XBEE module achieved by using a 3.3k and 2.2k resistor network. (See Equations (1.1) and (1.2))

Design for the slave module

$$V_{10} = V_3 \frac{R_2}{R_2 + R_3} \quad \textbf{(0.1)}$$

Where**,**

V_{10} = Input voltage to pin10 of XBEE module

V_3 = 5 V (Output voltage from pin3 of the PIC12F1840 microcontroller)

$$V_{10} = V_3 \frac{R_2}{R_2 + R_3} = 5\frac{3.3}{3.3 + 2.2} = 3 \text{ V} \quad \textbf{(0.2)}$$

After designing the circuit using Proteus software, the 2D and 3D PCB layouts were generated, as shown in Figure 6 and sent for etching. Then the components were soldered to the respective vias. Five sensor units were developed as shown in Figure 7.

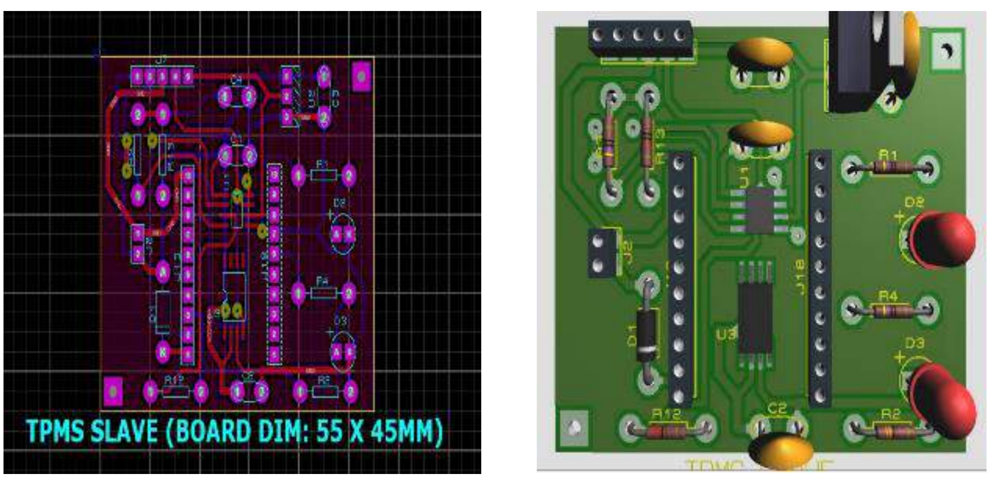

a **b**

Figure 6: 2D and 3D PCB layout of the sensor unit

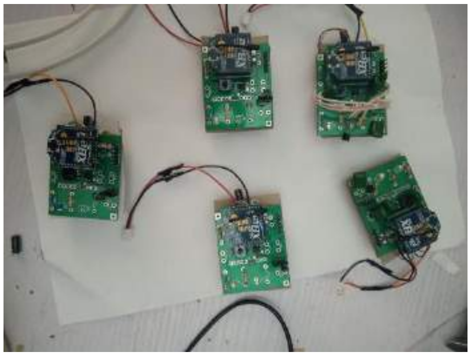

Figure 7: TPMS sensor units

2.3 Power Supply of The Sensor Unit

Each of the sensor units is powered by a 200 mA, 3.3 V, CR2032 Li-ion coin battery. They have excellent energy density against the weight ratio. The CR-type battery was used because of its superior high-temperature performance, better durability, lower weight and ease of availability [19]. Power management is critical in the TPMS module since the module containing the battery is enclosed by the tyre, and replacing the battery is almost impossible. Thus an efficient battery with good lifespan power management was chosen for this research. In this research, two sets of algorithms were developed to manage the power consumption of the batteries of the slave module. The first was the wake-up/sleep schedule, and the other was the active/idle mode. These sets of algorithms work together to reduce the power consumption of the batteries of the slave modules

2.3.1 Wake–up and Sleep Schedule

The TPMS slave module is wrapped around the rim with a band clamp. A SLEEP/WAKE–UP schedule algorithm was developed through a set of program instructions to the microcontroller unit (MCU) to TURN OFF or TURN ON the sensor unit at an appropriate time interval to increase the battery's lifespan. These instructions led to having the high-power WAKE–UP mode and low-power SLEEP mode for the slave section. Figure 8 shows the flowchart of the WAKE–UP and SLEEP Schedule. During the WAKE–UP mode, data transmission was done, after which the transmitter entered SLEEP mode for a predefined time interval, after successfully transmitting data packets. It remains in the SLEEP mode for ten minutes before entering the WAKE–UP mode again if the ignition is ON. Otherwise, it enters the SLEEP mode for one hour if the ignition is OFF before entering the WAKE–UP mode again. This intermittent transmission of data reduces the amount of current drawn from the battery, reducing power consumption.

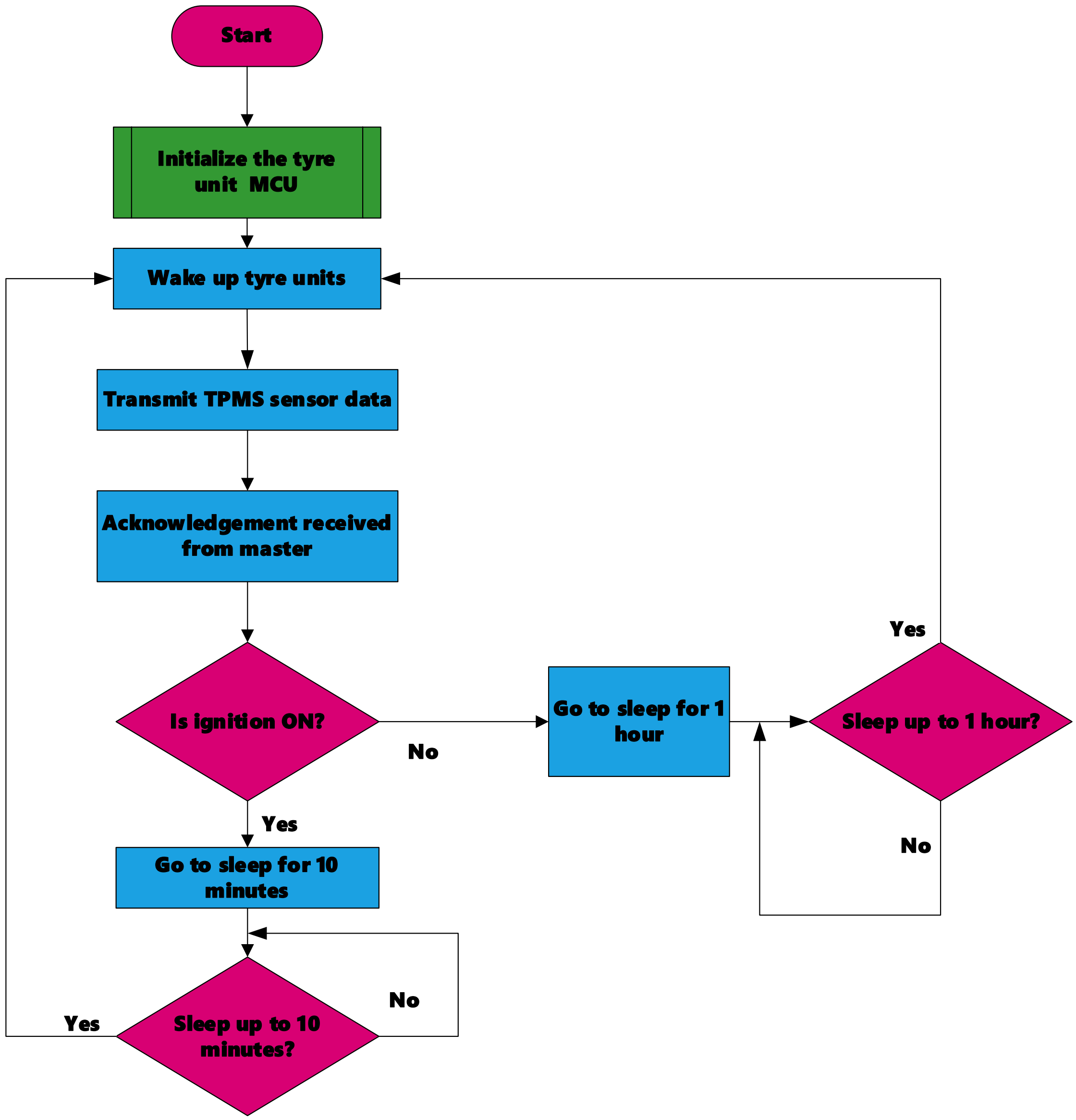

Figure 8: Flow chart of the WAKE–UP and SLEEP Schedule

As shown in Figure 9, the measured maximum current consumption was 48.8 mA in the WAKE-UP mode and 12 µA in the SLEEP. Other values of current measured in the WAKE-UP mode were 17 mA and 25 mA. As shown in Equation (1.3) there is a 99.97 % power savings between the current required in the WAKE-UP mode and SLEEP mode. This is a huge power saving which is very significant in this research to prolong the life of the sensor unit battery.

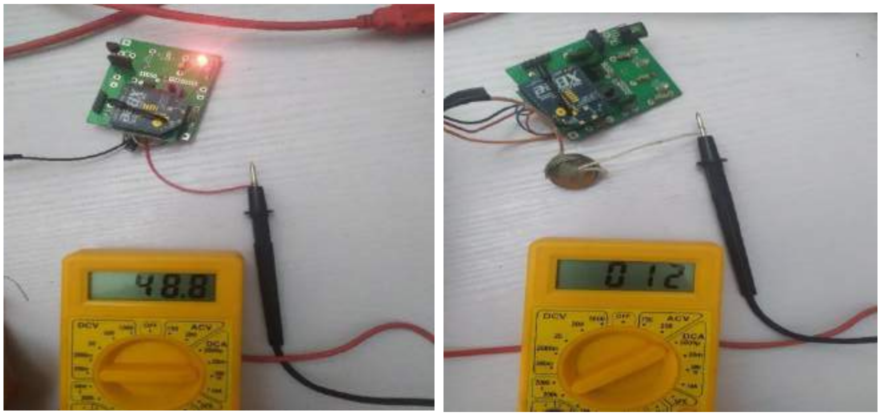

(a) (b)

Figure 9: Measured values of current in (a) wake-up and (b) sleep mode

$$i_{con}\ savings = \frac{i_w - i_s}{i_w} = \frac{48.8m - 12\varphi}{48.8m} = 0.9997 \qquad \textbf{(0.3)}$$

i_{con} = *current flowing*

i_w = *maximum current in wake-up mode*

i_s = *current in sleep mode*

The average current consumed $i_{average}$, by the TPMS sensor is given by Equation (1.4)

$$i_{average} = \frac{i_{wake}T_{wake} + i_{sleep}T_{sleep}}{T_{wake} + T_{sleep}} \qquad \textbf{(0.4)}$$

i_{wake} = *current in wake-up mode*

i_{sleep} = *current in sleep mode*

T_{wake} =*period in wake-up mode*

T_{sleep} = *period in sleep mode*

The battery life expectancy can be calculated using Equation (1.5)

$$Battery\ life\ in\ hours = \frac{Battery\ capacity\ in\ mAH}{load\ current\ in\ mA} \quad \textbf{(0.5)}$$

Active mode worst-case scenario average current.

From Equation (0.4), the $i_{average}$ is:

$$i_{average} = \frac{i_{wake}T_{wake} + i_{sleep}T_{sleep}}{T_{wake} + T_{sleep}}$$

i_{wake} = 48.8 mA, i_{sleep} = 12 µA, T_{wake} =100 ms, T_{sleep} = 10 minutes = 600 s. Substituting these values into Equation (0.4) gives

$$i_{average} = \frac{i_{wake}T_{wake} + i_{sleep}T_{sleep}}{T_{wake} + T_{sleep}} = \frac{48.8m \times 100m + 12\mu \times 600}{100m + 600}$$

$$i_{average} = \frac{4.88mAs + 7.2mAs}{600.1s} = 20.13\ \mu\text{A}$$

The estimated battery life is given by the Equation (0.5)

$$Battery\ life\ in\ hours = \frac{Battery\ capacity\ in\ mAh}{load\ current\ in\ mA} = \frac{200mAh}{20.13\mu} = 9935.42$$

$$Battery\ life\ in\ years = \frac{9935.42}{24 \times 365} = 1.134$$

Active mode best-case scenario average current.

From Equation (0.4), the $i_{average}$ is:

$$i_{average} = \frac{i_{wake}T_{wake} + i_{sleep}T_{sleep}}{T_{wake} + T_{sleep}}$$

i_{wake} = 17 mA, i_{sleep} = 12 µA, T_{wake} =100 ms, T_{sleep} = 10 minutes = 600 s. Substituting these values into Equation (0.4) gives

$$i_{average} = \frac{i_{wake}T_{wake} + i_{sleep}T_{sleep}}{T_{wake} + T_{sleep}} = \frac{17m \times 100m + 12\mu \times 600}{100m + 600}$$

$$i_{average} = \frac{1.7mAs + 7.2mAs}{600.1s} = 14.83\ \mu\text{A}$$

The estimated battery life is given by the Equation (0.5)

$$Battery\ life\ in\ hours = \frac{Battery\ capacity\ in\ mAh}{load\ current\ in\ mA} = \frac{200mAh}{14.83\mu} = 13485.39$$

$$Battery\ life\ in\ years = \frac{13485.39}{24 \times 365} = 1.539$$

Idle mode worst-case scenario average current.

From Equation (0.4), the $i_{average}$ is:

$$i_{average} = \frac{i_{wake}T_{wake} + i_{sleep}T_{sleep}}{T_{wake} + T_{sleep}}$$

i_{wake} = 48.8 mA, i_{sleep} = 12 µA, T_{wake} =100 ms, T_{sleep} = 60 minutes = 3600 s. Substituting these values into Equation (0.4) gives

$$i_{average} = \frac{i_{wake}T_{wake} + i_{sleep}T_{sleep}}{T_{wake} + T_{sleep}} = \frac{48.8m \times 100m + 12\mu \times 3600}{100m + 3600}$$

$$i_{average} = \frac{4.88mAs + 43.2mAs}{3600.1s} = 13.36\ \mu\text{A}$$

The estimated battery life is given by the Equation (0.5)

$$Battery\ life\ in\ hours = \frac{Battery\ capacity\ in\ mAh}{load\ current\ in\ mA} = \frac{200mAh}{13.36\mu} = 14970$$

$$Battery\ life\ in\ years = \frac{14970}{24 \times 365} = 1.709$$

Idle mode best-case scenario average current.

From Equation (0.4), the $i_{average}$ is:

$$i_{average} = \frac{i_{wake}T_{wake} + i_{sleep}T_{sleep}}{T_{wake} + T_{sleep}}$$

i_{wake} = 17 mA, i_{sleep} = 12 µA, T_{wake} =100 ms, T_{sleep} = 60 minutes = 3600 s. Substituting these values into Equation (0.4) gives

$$i_{average} = \frac{i_{wake}T_{wake} + i_{sleep}T_{sleep}}{T_{wake} + T_{sleep}} = \frac{17m \times 100m + 12\mu \times 3600}{100m + 3600}$$

$$i_{average} = \frac{1.7mAs + 43.2mAs}{3600.1s} = 12.47\ \mu\text{A}$$

The estimated battery life is given by the Equation (0.5)

$$Battery\ life\ in\ hours = \frac{Battery\ capacity\ in\ mAh}{load\ current\ in\ mA} = \frac{200mAh}{12.47\mu} = 16038.49$$

$$Battery\ life\ in\ years = \frac{16038.49}{24 \times 365} = 1.831$$

$$The\ ACTIVE\ mode\ average\ battery\ life = \frac{1.134 + 1.539}{2} = 1.34\ years$$

$$The\ IDLE\ mode\ average\ battery\ life = \frac{1.709 + 1.831}{2} = 1.77\ years$$

2.3.2 Active and Idle Mode Algorithm

The ACTIVE mode is the state of the vehicle when the ignition is turned ON. Turning the ignition OFF puts the system in IDLE mode. Figure 10 shows the flowchart of the ACTIVE and IDLE modes. The charging voltage is the decision criteria for determining the ACTIVE mode. When the ignition is ON, the system enters ACTIVE mode. The master unit gets powered by the electrical system of the vehicle through the cigarette lighter terminal. During this time the backup battery of the master unit starts charging and continues charging until the battery is fully charged. At full charge, the battery is disconnected from the charging voltage and it starts charging again when the battery voltage drops below the maximum.

Data transmission between the TPMS sensor and the master unit is done both in the ACTIVE and IDLE mode. In the ACTIVE mode, the SLEEP/WAKE-UP schedule of the sensor unit was done at 10 minutes intervals. In the ACTIVE mode (fast data transmission rate), the sensor unit could get the pressure/temperature data and transmit it at 10 minutes intervals if the ignition was ON.

The master unit waits to receive data from the sensor unit (TPMS sensor). On receiving the data, the master sends an ACK that contains the timing sequence to the sensor unit. Then the sensor unit transmit at 10 minutes intervals as long as the ignition is ON. Each time the TPMS sensor data is received by the master, it sends an ACK that either maintains or updates the timing sequence of data transmission between the slave and the master unit.

If the master receives the TPMS sensor data and the ignition is OFF, it will send an ACK that updates the timing sequence from 10 minutes to 1-hour intervals. The system thus enters the IDLE mode. It will continue this slow data transmission rate as long as the ignition is OFF. But if the master receives sensor data when the ignition is again turned ON, it will send an ACK that would again update the timing sequence from the slow to fast data transmission rate. This different rate of transmission continues depending on whether the ignition is turned ON or OFF.

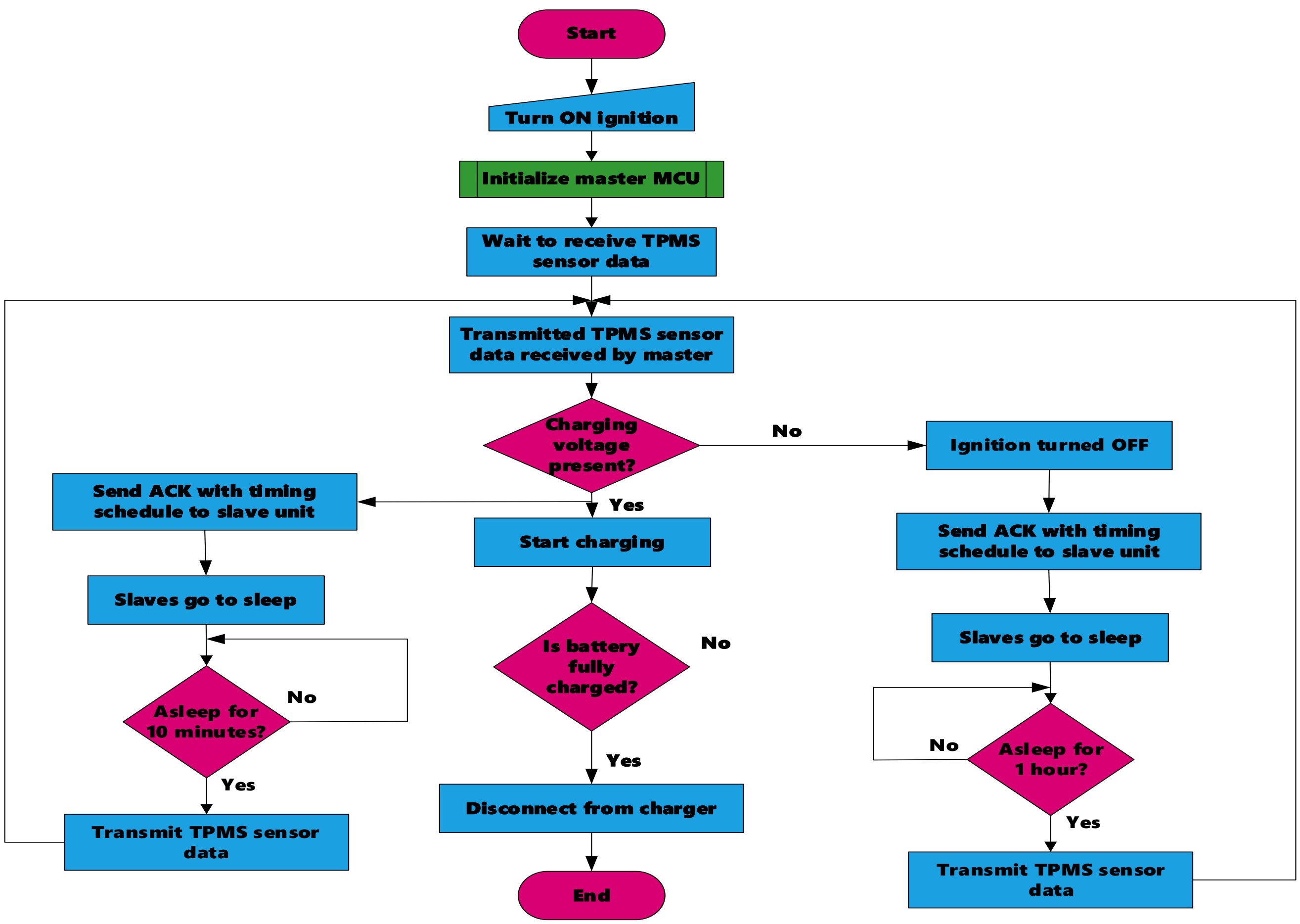

Figure 10: Flowchart of the ACTIVE and IDLE modes

3.0 Results and Discussion

As shown in Equation (0.3) there is a 99.97 % power savings from the current consumption in the WAKE-UP mode as opposed to that of the SLEEP mode. This is a huge power saving which is very significant in this research to prolong the life of the sensor unit's battery.

According to Lange et.al. [19], motion detection consumes 13% of the sensor unit battery's energy in its lifetime. In most OEM TPMS, the accelerometer is measured to know when the vehicle is in motion. This determination serves to help with the power reduction mechanism since vehicles are parked about 90% of the time, and it is essential to know when the vehicle is in motion [33], [34]. When the vehicle is parked, there is no need for frequent transmission of data. Thus, energy is conserved. However, the energy consumption for the detection of motion is also very high. The algorithm to determine the rate of data transmission depends on vehicle motion and the rate of acceleration. If the acceleration rate is constant, then data transmission is slower when driving in the expressway. If acceleration is continually changing, such as driving in busy urban areas, data transmission is faster. For a micro-machined sensor unit, the large power drawn by the accelerometer could be accommodated since the overall power of the system is small. But using discrete components, such as in this paper, adding an accelerometer to the design would sap the sensor unit of much-needed energy. Hence, an accelerometer was not included in the design of the sensor unit. Since the algorithm of the TPMS in this research did not include motion detection, considerable energy is conserved. All these algorithms were developed to increase the battery's lifespan while still providing useful data as needed.

There are two algorithms used in this work to improve the power requirement of TPMS sensors. One is the WAKE-UP and SLEEP schedule while the other is the ACTIVE and IDLE mode. During the ACTIVE mode, the WAKE-UP and SLEEP schedule occurs every 10 minutes but in the IDLE mode, the WAKE-UP and SLEEP schedule takes place at 1-hour intervals. We chose 10 minutes because previous research shows that sensor unit can transmit their information every 10 minutes to update the tyre status [35]–[37]. To determine the battery life expectancy, the worst-case and best-case scenario of the average current was determined both for the ACTIVE and IDLE mode.

As shown in section 0 the 200 mAh battery would have a life expectancy of 1.34 – 1.77 years. Using a 700 mAh battery which is a typical battery used in a TPMS sensor, the life expectancy of the battery would be 4.69 – 6.195 years [23]. Thus the algorithm implemented in the design can lead to having a TPMS sensor with a life span of four to six years if a 700 mAh Li-ion battery was used. The duration is long enough to cover the lifespan of a tyre which is typically four years.

4.0 Conclusion

A TPMS sensor unit was designed and developed to measure the tyre pressure and temperature. However, since the sensor unit would be placed on the wheel and enclosed by the tyre, it is imperative to have a power scheduling that would prolong the lifespan of the battery since they are not rechargeable. In this work, we used a low-power communication standard known as ZigBee over Bluetooth to transmit tyre pressure information to the receiver. We eliminated the motion detection mechanism in our design to reduce the power requirement of the sensor unit. We also developed a battery scheduling algorithm that efficiently prolonged the life of the sensor unit battery. The algorithms were the SLEEP and WAKE-UP mode and the ACTIVE and IDLE modes. With these algorithms, we achieved 99.97 % power savings between the SLEEP and WAKE-UP mode. Using a 200 mAh battery, its life expectancy was 1.34 – 1.77 years. But if a 700 mAh battery were used then, the life expectancy of the battery would be 4.69 – 6.195 years

References

[1] H. Köylü, "Experimental study on development of smart algorithm based on tire deflection to detect the drops in tire pressure," *International Journal of Automotive Engineering and Technologies*, vol. 6, no. 2, pp. 104–115, 2017, doi: 10.18245/ijaet.438134.
[2] B. S. Chethan, K. S. Kishor, K. B. v Kiran, and K. N. Chethan, "Design and development of running wheel air pressure monitoring system for vehicles," *Imperial Journal of Interdisciplinary Research (IJIR)*, vol. 3, no. 6, pp. 100–106, 2017.
[3] O. A. Egaji, S. Chakhar, and D. Brown, "An innovative decision rule approach to tyre pressure monitoring," *Expert Syst Appl*, vol. 124, pp. 252–270, 2019, doi: 10.1016/j.eswa.2019.01.051.
[4] Transport and Environment, "EU drivers at risk of under-inflated tyres : New tests show failure of tyre pressure monitoring systems on the road," 2018.
[5] P. P. G. Salunkhe, H. R. Kulthe, S. N. Kolhe, and A. A. Khan, "Automatic tyre pressure monitoring system using wireless communication," in *International Conference on Recent Trends in Civil Engineering, Science and Management*, 2017, no. March, pp. 140–148.
[6] M. G. Elnour and H. A. Laz, "Tire inflation rate modeling," *Int J Eng Sci Res Technol*, vol. 3, no. 11, pp. 542–555, 2017.
[7] A. A. Ogunwemimo, "Economic analysis of continuous monitoring of commercial truck tire pressure using Tire Pressure Monitoring Systems (TPMS) and RFID technologies," M.Sc, University of Nebraska, 2011.
[8] K. Thiriez, "Evaluation of indirect tire pressure monitoring systems using data from NCSA's tire pressure special study," 2003. [Online]. Available: http://www-nrd.nhtsa.dot.gov/pdf/nrd-01/esv/esv18/CD/Files/18ESV-000259.pdf
[9] S. Velupillai and L. Güvenç, "Tire pressure monitoring," *IEEE Control Systems Magazine*, vol. 27, no. 6, pp. 22–25, 2007, doi: 10.1109/MCS.2007.909477.
[10] A. Wyglinski, Alexander Arnold, and S. Piscitelli, "TPMS receiver hacking (Bachelor of Science Thesis)," Bachelor of Science Thesis, Worcester Polytechnic Institute, 2015. [Online]. Available: http://www.wpi.edu/academics/ugradstudies/project-learning.html.
[11] S. Mule and K. S. Ingle, "Review of wireless tyre pressure monitoring system for vehicle using wireless communication," *International Journal of Innovative Research in Computer and Communication Engineering*, vol. 5, no. 3, pp. 4163–4168, 2017, doi: 10.15680/IJIRCCE.2017.
[12] L. M. Silalahi, M. Alaydrus, A. D. Rochendi, and M. Muhtar, "Design of tire pressure monitoring system using a pressure sensor base," *Sinergi*, vol. 23, no. 1, p. 70, 2019, doi: 10.22441/sinergi.2019.1.010.
[13] T. Xiangjun, "The design and research of tire pressure monitoring system," in *2016 International Conference on Intelligent Transportation, Big Data and Smart City, ICITBS 2016*, 2017, pp. 479–481. doi: 10.1109/ICITBS.2016.45.
[14] K. O. Enalume, J. Emagbetere, F. Edeko, G. Ofualagba, and G. Uzedhe, "Design and analysis of a 2.4 GHz whip antenna for tyre pressure monitoring system;," *Biom Biostat Int J*, vol. 11, no. 3, pp. 105–109, 2022, doi: 10.15406/bbij.2022.11.00362.
[15] K. O. Enalume, J. Emagbetere, and F. Edeko, "Experimental analysis of a 2.4 Ghz antenna for tyre pressure monitoring system," *Journal of Engineering Studies and Research*, vol. 28, no. 4, p. 51, 2022, doi: 10.29081/jesr.v28i4.006.
[16] A. L. Chait, "Solving the last milli-mile " problem in vehicle safety: The EoPlex approach to powering wireless tire pressure sensors." Accessed: Feb. 04, 2023. [Online]. Available: http://www.eoplex.com/images/eoplex_whitepaper_tire.pdf

[17] C. R. Bowen and M. H. Arafa, "Energy harvesting technologies for tire pressure monitoring systems," *Adv Energy Mater*, pp. 1–17, 2014, doi: 10.1002/aenm.201401787.
[18] A. Vasanthara and K. Krishnamoorthy, "Tire pressure monitoring system using SoC and low power design," *Circuits and Systems*, vol. 07, no. 13, pp. 4085–4097, 2016, doi: 10.4236/cs.2016.713337.
[19] T. Lange, M. Löhndorf, and T. Kvisterøy, "Intelligent low-power management and concepts for battery-less direct tire pressure monitoring systems (TPMS)," in *Advanced Microsystems for Automotive Applications 2007*, J. Valldorf and W. Gessner, Eds. Springer, 2007, pp. 237–249. doi: 10.1007/978-3-540-71325-8.
[20] B. Zhu, J. Han, and J. Zhao, "Tire-pressure identification using intelligent tire with three-axis accelerometer," *Sensors (Switzerland)*, vol. 19, no. 11, Jun. 2019, doi: 10.3390/s19112560.
[21] A. Kolodgie *et al.*, "Enhanced TPMS security through acceleration timed transmissions," *Proceedings - IEEE Military Communications Conference MILCOM*, vol. 2017-Octob, pp. 35–39, 2017, doi: 10.1109/MILCOM.2017.8170841.
[22] X. F. Chen, L. J. Wu, and X. M. Zhang, "A low-power low-frequency wake-up receiver for tire pressure monitoring system," in *ICSICT 2012 - 2012 IEEE 11th International Conference on Solid-State and Integrated Circuit Technology, Proceedings*, 2012, pp. 5–7. doi: 10.1109/ICSICT.2012.6467613.
[23] B. D. C. Kuncoro, M.-F. Sung, and Y.-D. Kuan, "Battery charger prototype design for tire pressure sensor battery recharging," *Sensors*, vol. 19, no. 1, p. undefined-3, Jan. 2019, doi: 10.3390/s19010124.
[24] Z. A. Adetona, T. O. Koledoye, and M. I. Alebiosu, "Television broadcasting transmission in Nigeria: Application of technical data for re-planning," *Electrical and Electronic Engineering*, vol. 3, no. 6, pp. 173–177, 2013, doi: 10.5923/j.eee.20130306.05.
[25] I. B. Oluwafemi, A. P. Bamisaye, and M. A. Faluru, "Quantitative estimation of TV white space in Southwest Nigeria," *Telkomnika (Telecommunication Computing Electronics and Control)*, vol. 19, no. 1, pp. 36–43, Feb. 2021, doi: 10.12928/TELKOMNIKA.V19I1.17881.
[26] J. Kooker, "Bluetooth, ZigBee, and Wibree: A comparison of WPAN technologies," *Ww.Cse.Ucsd.Edu/Classes/Fa08/Cse237a/Topicresearch*, pp. 1–4, 2008.
[27] J. S. Lee, Y. W. Su, and C. C. Shen, "A comparative study of wireless protocols: Bluetooth, UWB, ZigBee, and Wi-Fi," *IECON Proceedings (Industrial Electronics Conference)*, vol. 4, no. March, pp. 46–51, 2007, doi: 10.1109/IECON.2007.4460126.
[28] N. A. Somani and Y. Patel, "Zigbee : a Low Power Wireless Technology for Industrial," *International Journal of Control Theory and Computer Modelling*, vol. 2, no. May, pp. 27–33, 2012, doi: 10.5121/ijctcm.2012.2303.
[29] S. Farahani, *ZigBee wireless networks and transceivers*. Elsevier, 2008.
[30] K. Y. Rashmi Singh, Pradeep Singh, "Wireless communications enlargement: A review of advancement in technologies," *International Journal of Current Engineering and Technology*, vol. 4, no. 4, pp. 2703–2710, 2014, doi: 10.13140/RG.2.1.3024.0242.
[31] Zigbee Alliance, "ZigBee specification," 2015.
[32] J. Armstrong and C. R. Helps, "Comparative evaluation of ZigBee and Bluetooth : Embedded wireless network technologies for students and designers," *American Society for Engineering Education*, 2007.
[33] L. D. Burns, "A vision of our transport future," *Nature*, pp. 181–182, May 2013.
[34] T. A. Litman, "Parking management comprehensive implementation guide," 2021. [Online]. Available: www.vtpi.org
[35] P. A. Grygier, S. Daniel, R. L. Hoover, and T. R. van Buskirk, "Tire pressure monitoring system tests for medium and heavy trucks and buses," 2010. [Online]. Available: www.ntis.gov
[36] P. Grygier *et al.*, "An evaluation of existing tire pressure monitoring systems," Washington, 2001.
[37] S. van Zyl, S. van Goethem, S. Kanarachos, M. Rexeis, S. Hausberger, and R. Smokers, "Study on tyre pressure monitoring systems (TPMS) as a means to reduce light-commercial and heavy-duty vehicles fuel consumption and CO2 emissions," 2013. [Online]. Available: www.tno.nl

NIPES-NCEE Conference Proceedings
The 2nd International Conference 15th-17th Feb. 2023
64-70
www.nipesjournals.org.ng

PRODUCTION, OPTIMIZATION OF BIODIESEL FROM DESERT DATE SEED OIL VIA TRANSESTERIFICATION

*S. O. Ohile, A. A. Aboje, H. M. Uthman, A. D. Dirisu, Ibrahim Yusuf.

Department of Chemical Engineering, Federal University of Technology, PMB. 65, Minna, Niger State, Nigeria
Corresponding author's E-mail: ohile.susan@gmail.com

Abstract

Due to the adverse effect of exhaust emissions from the combustion of petroleum-based fuels, the global warming phenomenon and greenhouse effect has escalated in recent decades. These problems have necessitated the use of alternative fuels more than ever in today's ever-changing world. Furthermore, convectional fossil fuels such as coal, petroleum and natural gas are constantly being depleted. Nevertheless, the world's dependency on these fuels is still growing and this problem has prompted the need for this research, which is aimed at the production of biodiesel from desert date seed oils as an alternative source of fuel since they are readily available and environmentally friendly. The study reports the yield of biodiesel from the transesterification of desert date seed oil using methanol as the alcohol and NaOH as the catalyst for the reaction. Optimization was carried out via response surface methodology (RSM) using the Box-Behnken approach with the software, Design Expert 13. The results of the analysis of the produced biodiesel, which were found to agree very well with the standard values, indicated that the liquid produced from the desert date seed oil by transesterification process was indeed, biodiesel with a yield of 82 %, which is in a close agreement with results reported in the literature.

Keywords*: Transesterification, Biodiesel, desert date, optimization.*

1.0 Introduction

The finite nature of petroleum-derived fuels, global energy crisis and climate change, have necessitated the search for green bio-fuels that are renewable, eco-friendly and can serve as substitute to petro-derived fuels. In this regard, bio-ethanol and biodiesel are believed to have great potential and a promising future, especially for the transportation sector. As a result, research interest is being focused on this area [4].

Growing concern due to environmental pollution caused by conventional fossil fuels and their depletion has led to a search for more environmentally friendly and renewable fuels, among various options investigated for diesel fuel, biodiesel obtained from vegetable oils and other sources has been recognized worldwide as one of the best alternatives for reducing exhaust emissions [5].

Biodiesel, as an alternative fuel, has been currently receiving much attention owing to the limited availability of conventional petroleum diesel and environmental concerns. It can be directly used to replace petroleum diesel without modifying diesel engines since their properties, for example, specific gravity, cetane number, viscosity, cloud point, and flash point, are similar, it is a promising alternative or extender to conventional petroleum-based diesel fuel. Furthermore, it has a number of advantages such as reducing carbon dioxide emissions by about 78%, nontoxicity and biodegradability. These benefits have made the fuel a very good environmentally benign one. Furthermore, biodiesel is a renewable energy source [2].

The first ASTM D6751 was published in 2002. In October of the following year, a new biodiesel standard DIN EN14214 was published in Europe. Later in September of the next year The US state of Minnesota sold the diesel fuel that contained 2% biodiesel and then in 2008 October ASTM published the first biodiesel blend specification standard. The present version of the European standard EN 14214 was published in November 2008 [3].

Desert date seed (*Balanites aegyptiaca*) belongs to the Kingdom: Plantea; Division: Spermatophyta; Subdivision: Angiospermea; Class: Dicotyledonea; order: Balanitales; family: Balanitaceae; Genus: Balanites; Species: aegyptiaca;[1].

Balanites aegyptiaca tree is distributed in West Africa, especially in West African arid and semi-arid regions where the climatic environment and soil are not suitable to produce plants commonly used for the production of biofuel, In Nigeria, Balanites aegyptiaca is commonly found in the northern part of the country with mean temperature of 20-30°C and mean annual rainfall of 250–400 mm^3, it is one of the most neglected common trees, usually found throughout the dried regions of Africa, especially Nigeria [6].

2.0 Methodology

2.1 Materials

The materials used in the current study include magnetic stirrer, ground sample of the *Balanites aegyptiaca* seed kernel. Other materials include, *n*-hexane, methanol, vegetable oil extracted from the plant's seed kernel, sodium hydroxide pellets (caustic soda), Soxhlet extractor was the equipment used for the oil extraction. Brookfield viscometer was used to determine the kinematic viscosity, other equipment used for oil extraction and biodiesel production includes: electronic weighing balance, water bath shaker.

Figure 1 Desert Date seed

2.2 Methods

Oil was extracted from desert date (*Balanites aegyptiaca*) seed kernel according to the methods and procedures described by [2]. 100g of the seed sample was weighed using electric weighing balance and placed into the thimble of the Soxhlet extraction apparatus. 175cm^3 of *n*-hexane solvent was poured into the thimble and allowed to extract the oil at 68°C for about 2–4 hours. The extract (mixture of oil and solvent) was then taken to an oven which facilitates evaporating of the solvent and the pure oil was obtained.

Figure 2 Soxhlet apparatus setup

One hundred cm^3 of the oil was measured and poured into a 250 cm^3 conical flask and heated to a temperature of 50°C using a water bath. A solution of sodium methoxide was prepared in a 150 cm^3 beaker using 0.08g of NaOH pellet and 19 cm^3 of methanol. The sodium methoxide solution produced was then poured gently into the warm oil and stirred vigorously for about 90 minutes using a water bath shaker. The mixture was then poured in a separating funnel and allowed to settle for about 24 hours. After settling, the upper layer (biodiesel) was decanted into a separate beaker while the lower layer which consists of glycerol and soap were collected from the bottom of the funnel. The decanted biodiesel was washed with warm water of about 45°C in order to eliminate soluble methanol, excess catalyst and other impurities. The washing process left the biodiesel looking a bit cloudy which indicated the presence of moisture. The biodiesel was heated slowly to a temperature slightly above 105°C in the oven until all moisture present evaporated.

Response surface methodology (RSM) with Box-Behnken module was applied to optimize is to maximize production of biodiesel from Mango, desert date and the blend of both oils using ‘Design Expert®, (Version 13.0.0, Stat Ease, Inc., USA) software. In this study four factors were considered which are methanol to oil ratio, catalyst loading, temperature and reaction time.

Table 3: Independent factors used for Box-Behnken in transesterification of the extracted oil

Variables	Low	High	Unit
Temperature	35	75	^{O}C
Time	60	180	Minutes
Catalyst Concentration	0.3	0.7	%wt/vol
Methanol to Oil Ratio	3:1	9:1	vol/vol

3.0 Results and Discussions

One kg of desert date seed (*Balanites aegyptiaca*) seed kernel obtained from about 12 kg of its fruits collected yielded an average of 396 g (426 cm^3) oil using Soxhlet extractor, the extracted crude desert date oil was dark brown in colour with a yield of 46.86 %. The oil after being trans-esterified with 119 g (128 cm^3) sodium methoxide solution produced 426 g (458 cm^3) biodiesel and 82 g (88 cm^3) glycerol, translated to give 82.7% biodiesel yield.

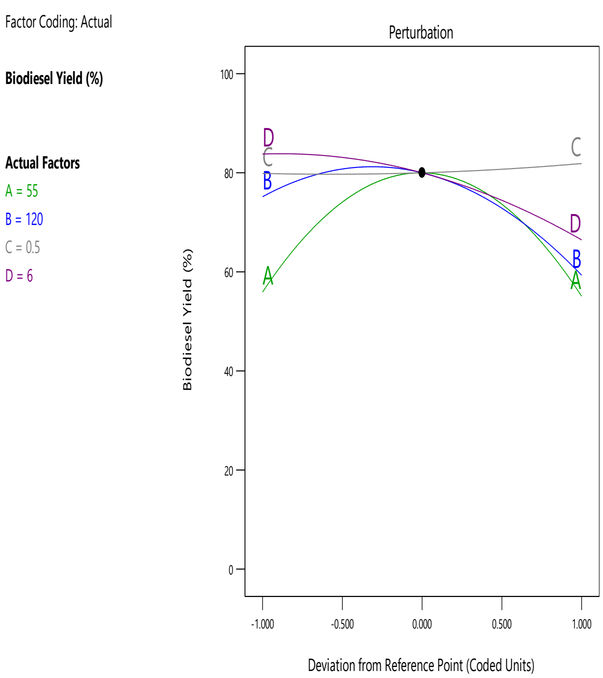

Figure 3: Perturbation of the biodiesel yield between A&B

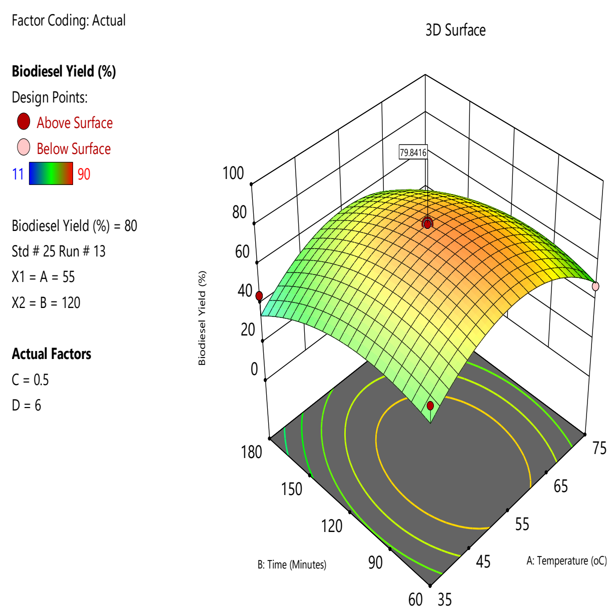

Figure 4: 3D of the biodiesel yield

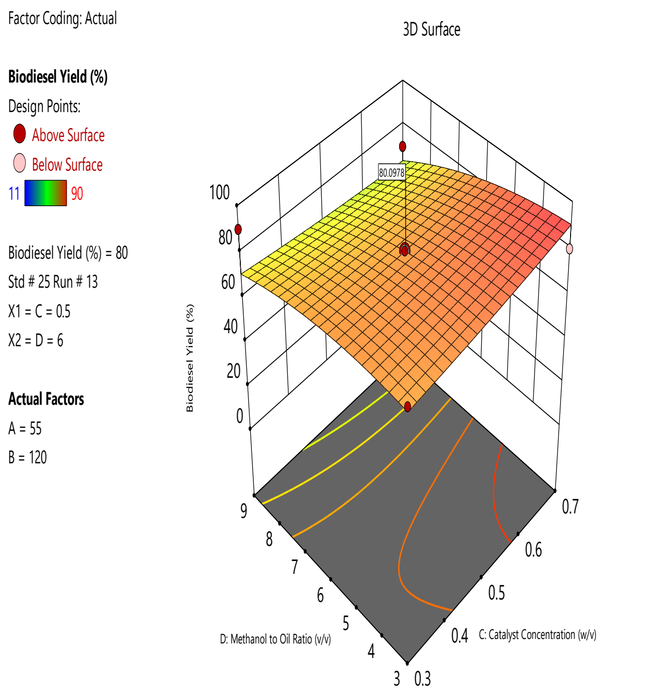

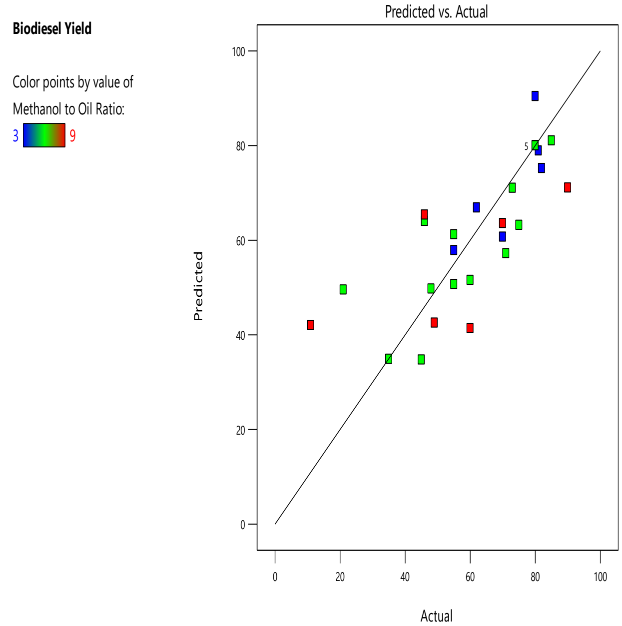

Figure 5: 3D of the biodiesel yield between C&D **Figure 6: Predicted versus actual reading**

4.0 Conclusion

After the optimum results were achieved, it was concluded that the industrial utilization of *Balanites aegyptiaca* oil for the production of biodiesel is favourable because of its oil yield capacity from the plant and its limitation for utilization as edible oil. The promising plant having oil yield of 396 g/kg (42%) with 88% extraction efficiency revealed high oil yield, and fact that the Soxhlet extractor could extract about 88% of the available oil present in the seed. The oil having biodiesel yield of about 82.7% shows the effectiveness of alkali catalyzed transesterification method in synthesizing biodiesel from the plant oil, its prospect as better alternative raw material for biodiesel production, and promise for local farmers in dry land areas.

References

[1] Dass, P.M., Louis, H., Alheri, A.1., Amos, P.I., Bifam, M. & Ago, M.A. (2018). Production of Biodiesel Oil from Desert Dates (*Balanites aegyptiaca*) Seeds Oil Using a Heterogeneous Catalyst Produced from Mahogany (*Khaya Senegalensis*) Fruit Shells. *Analytical Chemistry Indian Journal*, *18*(1), 129.

[2] Giwa, S.O., Ibrahim, M., Akaagerger, S.M., & Giwa, A. (2016). Production of Biodiesel from Desert Date Seed Oil. *International Journal of ChemTech Research*, *9*(6), 453-463.

[3] Mahmudul, H.M., Hagos, F.Y., Mamat, R., Adam, A.A, Ishak, W.F.W, Alenezi, R. (2017), Production, characterization and performance of biodiesel as an alternative fuel in diesel engine-A review, *Renewable and Sustainable Energy Review*, *72*(2017), 497 – 509, dx.doi.org/10.1016/j.rser.2017.01.001

[4] Nnaji, J.C. (2020), Advances in Biodiesel Synthesis: The role of various catalyst, *Open Journals for Engineering sciences*,1(10), 53-71.

[5] Onukwuli, D.O., Umeuzuegbu, J.C., Ude, C.N., Nwobi-Okoye, C.C. (2020), Homogeneous catalyzed transesterification of neem seed oil to biodiesel and its kinetic modelling, *Wiley Online Library (wileyonlinelibrary.com);* DOI: 10.1002/bbb.2171; Biofuels, Bioprod. Bioref.

[6] Usman, A., Rufai, I.A. (2020), Properties of Balanites Aegyptiaca Biodiesel as a potential energy carrier in the dry land of Nigeria, *International Journal of Energy Engineering*, 10(4), 95-101, DOI: 10.5923/j.ijee.20201004.01.

NIPES-NCEE Conference Proceedings
The 2nd International Conference 15th-17th Feb. 2023
71-83
www.nipesjournals.org.ng

CERVICAL CANCER PREDICTION USING ENSEMBLE MODELS

Efosa Charles Igodan [1], Samuel Ebosetale Ojietohamen [2] and Rose Iyonawan Izevbizua

1,2,3 Department of Computer Science, Faculty of Physical Sciences, University of Benin, Benin City, Nigeria.
Correspondence email: charles.igodan@uniben.edu

Abstract

Feature selection is one of the ways for data dimensionality reduction a requisite machine learning task. Most existing studies only concentrated on a centralized fashion in its application, i.e., using the entire benchmark datasets all at once in the feature selection process before machine learning is applied. As a result, the issues facing data with enormity on size, noise, missing values, redundancy, and relevance are partially unattended to. In this research, a new approach for creating a homogeneously-centralized feature selection referred to as cascaded ensemble feature selectors is proposed. Chi-squared, information gain, and ReliefF are homogeneously combined and then embedded feature selector- Recursive Features Elimination-Support Vector Machine (RFE-SVM) is centrally used in determining the final distinctive feature subsets for ensemble classifiers prediction. The adequacy of our proposal is applied on cervical cancer dataset, which is a challenge for researchers due to its similarities among others as well as its effect the world over. The standard metrics was used to measure performance of our model and comparison done. Our proposed cascaded ensemble feature selectors-classifier shows improved performance obtaining accuracies of 97.6% and 97.7% for bagging and boosting respectively, and showing future improvement.

***Keywords**: Filter-Method, Embedded-Method, Ensemble-Learning, RFE-SVMs, and Cervical cancer*

1.0 Introduction

Cancer is caused by certain mutations in the genetic materials within the cells of the human body. These cells divide rapidly in an unregulated way due to the abnormalities in the genetic content and fail to die after the normal life span. Such uncontrolled proliferation of the cells give rise to malignant growth. However, these genetic changes can be spontaneous without any definite cause or may be induced by certain known common risk factors like tobacco; overweight; harmful alcohol use; outdoor and indoor air pollution; occupational carcinogens; and Epstein-barr virus [1,2]. According to [3], it is predicted that by 2020, the rate of death from cancer alone would be about thirteen million as a result of the global burden caused which is expected to give rise to over twenty-one million new cases. In the majority of these cases, cervical cancer develops unnoticeably at its early stage and spreads quickly to other body parts, hindering its treatment [4]. The Human Papilloma Virus (HPV), Thinprep-Cytologic Test (TCT), and biopsy are traditional techniques used for treatment [5,6]. These techniques take a minimum of four weeks and during high demand, periods take up to 33 weeks to obtain results [7]. These techniques take a longer time to obtain results and suffer from accurate results as a result of the dearth of medical experts mostly in African countries like Nigeria [5,8,62]. The issue associated with larger data dimensionality also leads to irrelevant, redundant, and noisy data as a result occupying large storage and high computational cost, which may also pose a problem in the cervical cancer diagnoses [8]. However, with the advent of machine learning these diseases can be properly diagnosed early to enhance their detection, cure, and survival rates [2,4,5,7,9,59]. To deal with a dataset's high dimensionality with its high impact on the model's performance, FS ensemble technique is adopted. In general, two different approaches for FS can be distinguished: filter and wrapper approaches. While filtering identifies informative and descriptive features fast, the wrapper approach selects features based on the classifier's accuracy. Although, filter approach might be faster in terms of speed, when combined with the wrapper approach better classification result is achieved through diversity and accuracy [10,11,12,13,57,58,60,63]. This is referred to as ensemble of FS methods overcoming the disadvantages of either method [10,14,15,16,17,18,19,20]. Ensemble of FS methods and classifiers [21] are two types of ensemble learning that aim to improve learning by integration and improves on the poor performance of a single model [22]. The degree/level of integration of ensemble method play an essential role in offering superior classification accuracy as a result of the rich information derived in use of either feature-feature and feature-target learning process. In data mining community, support vector machines (SVMs) are among the influential algorithms robustly used due to its high accuracy and sound foundation theoretically rooted in statistical learning theory [11,12,61]. Justification for the use of SVMs is in [56]. Due to the scarcity of study on the use of ensemble methods both for FS and learning algorithms, this study is motivated to apply the knowledge to classify cervical cancer. The rest sections are arranged as follows. Section two reports the reviewed literature, whilst the methodology is described in section three. Section four detailed the experimental results. The paper concludes in section four.

2.0 Literature Review

Many researchers have applied different FS techniques on learning algorithms achieving different results [2,10,40]. However, their integration scopes are still limited [4,23,24] as most efforts are concentrated in a single layer combination [25]. Despite FS techniques combined with data cleaning takes away 60-95% of the total time of the learning process [16,17,22], most authors still obtain suboptimal results. Using recursive feature elimination with SVM and Multiple-SVM, the authors in [26] obtained improved unmeasured model with high time complexity. The authors in [27] only applied filter-based methods on three models with inability to generalize. The wrapper-based PSO was applied on three models in [28] to obtain accuracies between 96%-100%, but lacks diversity. In [29], two models were built without FS to achieve 91.67%. In [30], an ensemble classifier without FS technique obtains 96% accuracy. Wrapper based RFE- and PCA-SVM was implemented in [31], and 94.13% accuracy was obtained. However, the models suffered from high computational cost. Five models were used in [32] to diagnose ovarian cancer recurrence, however, the study suffered under fitting problem. The poor results in [32] were not validated after using boosted tree classifier for the early detection of cancer. An investigation into cervical cancer was carried out in [2] obtaining. In [4], random forest was used both for FS and prediction of cervical cancer to achieve 97.6% accuracy but with low diversity. The authors in [34] used six algorithms without FS techniques and obtain 77.97% accuracy. While in [6], five models with PCA algorithm obtained 83.16% and was limited by experimental support. Both in [7,9,36,37,39] data imbalanced techniques were applied on the dataset only on various learning algorithms to achieve 99.09%, 94.59%, 94.10%, 98.49% and 95.67% respectively without FS methods. However, the study was characterized by high computational cost as a result of data noise, and omitted attributes. An ensemble of naïve Bayes and decision trees were built in [35] for cervical cancer classification with no FS technique applied to obtain 95.92%, but suffered under fitting issues. Also, in [8] a prediction model using risk factors of cervical cancer was built apply ensemble of five algorithms without FS methods and showed 87.21% accuracy. A fuzzy rank-based ensemble of CNN models was used to classify cervical cancer images and an accuracy of 99.23% [39]. The application of MLP with optimized parameter using BP algorithm was investigated in [64] showing promising results. However, results were not reported in the study. In general, none of the reviewed study create an ensemble of FS methods in handling the dataset.

3.0 Methodology

The level of integration of ensemble of FS techniques involves different methods combined either in serial or parallel to obtain optimal subset [15,21]. The justification of our approach is found in [10,20,43] respectively. The framework of our suggested model is described in Fig. 1.

3.1 Benchmark Dataset Analysis

The dataset was taken from https://archive.ics.uci.edu/ml/machine-learning-databases/00383/risk_factors_cervical_cancer.csvwebsite website. It contains 344 patients' demographics, habits, and medical records, 35 risk factors on four classes. The missing values are substituted with the median value using the Median Imputation algorithm. By synthetically increasing the minority class, the Synthetic Minority Oversampling Technique (S M O T E) in Equation 1 to reduce the risk of overfitting as described in [20,65]. The dataset is normalized using the min-max normalization

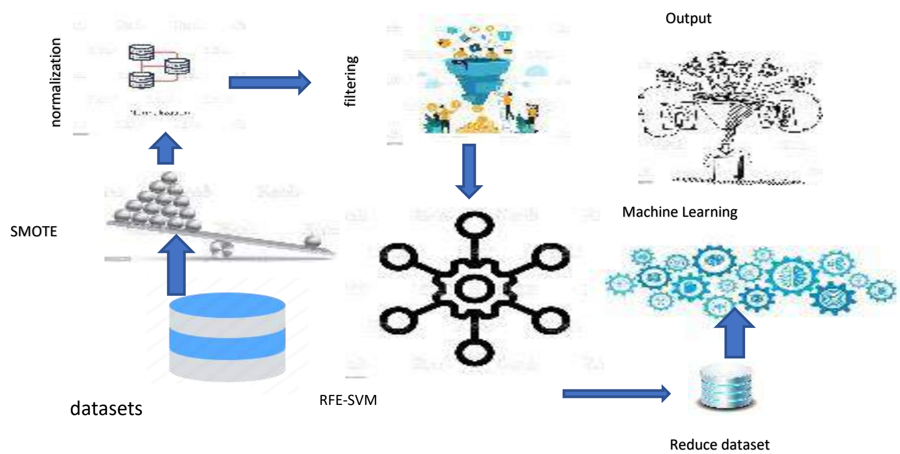

Fig. 1 Framework of Hybrid Feature Ensemble Learning Model

method as shown in equation 2. A total of 344 records were used for the biopsy with 15 risk factors after the feature selection technique was applied to the dataset.

$$x_{syn} = x_i + (x_{knn} - x_i) * t \quad (1)$$

$$f(x) = \frac{x_i - X_{min}}{(X_{max} - X_{min})}$$

where x_i is the feature vector, x_{knn} for the k-nearest neighbors and a randomized number (0,1) t . x_i are the process values, X_{min} and X_{max} are the min and max values in the dataset, whilst $f(x)$ is the normalized value.

3.2 The Feature Selection Methods

Our proposed hybrid feature ensemble method integrates the output of three filter-based methods that is Info-Gain, chi-Square, ReliefF, and RFE-SVM to obtain the final feature subset [43].

3.2.1 Information Gain: The information gain calculates the difference in entropy between the prior and the posterior entropies [44,45].

$$IG(X) = H(X) - H(Y|X) \quad (3)$$

where $H(X)$ is Entropy of Y and $H(Y|X)$ is t Entropy of Y given X.

$$H(Y) = -\sum_{i=1}^{m} p(y)\, log_2 p(y_i) \quad (4)$$

$$H(Y|X) = -\sum_{j=1}^{m} p(\frac{y_i}{x_i}).\, log_2 p\left(\frac{y_i}{x_i}\right) \quad (5)$$

where n represents the size of instances in the cervical cancer set, $p(y_i)$ is the occurrence probability of class label value of instance I, and $p\left(\frac{y_i}{x_i}\right)$ is the probability of the class label value of instance i will occur given the occurrence of attribute value x of the instance i.

3.2.2 Chi-Square (x2): The Chi-Square, based on the $\boldsymbol{x^2}$ statistic measures the feature's independence from the class label. Chi-square score for a feature with x different values and $\boldsymbol{y}$ classes is defined as shown in Equation 6 [24,46,47]:

$$x^2 = \sum_{i=1}^{x} \sum_{j=1}^{y} \frac{(A_{ij} - E_{ij})^2}{E_{ij}} \quad (6)$$

where the number of actual patterns in t he i-th attribute is A_{ij}; j-th class, E_{ij} is the number of expected observations of $A_{ij} = R_i * C_j / N$, R_i is the number of patterns in the i-th interval $= \sum_{j=1}^{y} A_{ij}$. The degree of freedom of the x^2-statistic is one less the number of classes.

3.2.3 ReliefF: ReliefF is a supervised feature selector that finds features in multi-class, noisy/noise-free, dependent, and incomplete data by using the k-nearest neighbor algorithm. Equation 7 determines attribute quality depending on how well its values discriminate between instances that are similar to one another [11,17, 24,40,44].

$$W[A] = W[A_0] - \frac{\sum_{J=1}^{k} diff(A,\ x_i,\ H)}{(m,k)} + \sum_{c \neq class(x_i)} \frac{p(C)}{1-p(class(x_i))} \cdot \frac{\sum_{j=1}^{k} diff(A, x_i, M_j(C))}{(m,k)} \quad (7)$$

where attribute weight is W_x, randomly sampled instances are X, R, the nearest hit H, the nearest miss M, m is the number of randomly sampled instances and $diff(A, X_i, H)$ calculates the gap between the values of R for two instances.

3.2.4 RFE-SVM: The SVM-RFE selection approach employs the SVM classifier for features ranking and discard least informative features recursively. This approach suggests recursively deleting features by reranking them based on their contribution to the SVM classifier after each iteration [20,24,48]. For linear SVMs the classification boundary coomputed by equation 8 is:

$$\hat{y}(x) = w^T . x + b \quad (8)$$

where sign[$\hat{y}(x)$] is the expected class feature vector (x), w is the weight vector, and b is a constant.

The SVM training process takes as inputs a training set of feature vectors and their corresponding class labels and a set of outputs (N_{train}) parameters, $\{\alpha_i\} = \{\alpha_1, \dots, \alpha_{N_{train}}\}$, where (N_{train}) is the number of training points. The parameters $\{\alpha_i\}$ can be used to calculate the weight vector w in the classification boundary equation 9:

$$w = \sum_{i=1}^{N_{train}} \alpha_i y_i x_i \quad (9)$$

$$c_j = (w_i)^2 \quad (10)$$

The SVM-RFE uses equations 9 and 10 to calculate the ranking criterion values c_j after the SVM training with the entire set of features for each feature j. The feature having the lowest c_j value is removed from the training set and placed at the bottom of the ranked feature set, and the process continues until the training list is empty of any features. The ranked features list now contains the entire feature set in a logical order [26].

4.0 SVM Classification Algorithm

SVM is used as a supervised ML algorithm that groups data based on the support vectors [11,16]. It uses fewer parameters; the $cost\ of\ error\ C$, and the gamma value γ, to tune, [11,24,29,55] whose values influence each support vector and decides the intended curvature of decision boundary. In this research, these parameters are set to C =100 and γ = 10-14 as they are adequate to ensure numerical stability [21,22,32,40,50,51,52,53]. Given a training set of cervical cancer data of instance labeled pairs (x_i, y_i) where $x_i \in R_n$ and $y_i \epsilon \{-1,1\}$, where the $y_i$is either 1 or -1, x_i belongs as indicated in Equation 11:

$$\min_{w,b,\xi} \frac{1}{2}\omega^T\omega + C\sum_{i=1}^{l}\xi_i \text{ where} C > 0 \quad (11)$$

$$subject\ to \qquad y_i(\Phi\ (\mathrm{x}_i) + \mathrm{b}\ ) \geq 1 - \xi,\ \text{where}\ \xi > 0,\ \mathrm{i} = 1, \dots, \mathrm{l},$$

where $\Phi\ (\mathrm{x}_i)$ maps x_i into a hig her di mensional space, $C > 0$ is the regulari zation (cost) para meter, ω the vector variable, and $\xi > 0$ is the slack variable.

5.0 The Proposed methodology

The three filter methods were initially used in scoring and ranking the features of the original set creating a mutually exclusive subsets and three-fourth (3/4) of the ranked features (i.e., 23 features) were selected from individual method. The RFE-SVM was applied on each subset and common features were combined selecting 15 features using a threshold of T=2. The proposed HEFS method is shown in algorithm 1.

Algorithm 1: Proposed HEFS Implementation procedure

Input: Training dataset D, feature set $F = \{ f_1, f_2, \dots, f_n\}$, grouped sample set S, majority vote V, no of filter methods n, size of an entity { }, Information content $I(\,)$.

Output: Subset of m features

Procedure:

For $i = 1\ to\ n$ //for each filter method

For $j = 1\ to\ size\{F\}$

Computer filter's ranking scores for features on $S_{i,j}$

End for

$S_{i,j}$ = Select high feature scores

End f o r

For $i = 1\ to\ n$

For $j = 1\ to\ size\{S_{i,j}\}$

$S_{i,j}' = obtain\frac{3}{4}split$ //based on the feature size)

End f or

End f or

For $j =\ 1\ to\ size\ \{S_{i,j}'\}$

$S'' = \{S_{1,j}U\ S_{2,j}US_{3,j}\}$ //combine all filtered features

End for

Compute majority vote $V = \arg Max\ I(S'')$

Perform SVM-RFE on V //automatically select best features subset for ensemble methods

5.1 Ensemble Methods

In this study, two widely used techniques which are boosting and bagging are adopted.

Adaboost: Adaboost, [49,54,65] combines naive classifiers to produce a stable, effective classifier using the iterative ensemble approach. The fundamental principle of Adaboost is to train data samples and create classifier weights to precisely forecast a c lass target.

*Bagging***:** An ensemble method efficient in variance reduction of prediction by combination of multiple classifiers generated from resampling of same dataset. During the bagging process, datasets are split up into multiple bootstrap replicates. Each replication is created by substituting data from the original dataset, and the process involves repeatedly running a series of bootstraps on naive learners [49,65].

6.0 Experiments

Our model was implemented using Python 3.7 running on core i5, 64-bit windows 10pro with 1.9 Giga Hz. To understand how well our models performed, we adopted confusion matrix. The performances of both the individual and ensemble models are shown in table 1. Both the bagging and boosting models performed better than the individual models. The accuracies for bagging and Adaboost are 97.6% and 97.7% respectively and be improved upon. The individual RBF SVM performed better than the linear, polynomial, and sigmoid SVM models. The accuracy of the linear SVM is 96.2%, while RBF, Polynomial, and Sigmoid SVM have 96.7%, 94.5%, and 94.5% respectively and indicated in table 1. However, no study has shown the type of integration level we used for our classifier ensemble method—combining filter and embedded methods. Table 2 shows the comparative analysis of our proposed study perform better when compared with others, especially with the size of the features used in achieving the accuracy. From the table, only the authors in [4] compete with the proposed work but with many features which has high time and space complexity as disadvantage.

Table 1 Performance Analysis

Model	**Acc**	**Pre**	**Recall**	**F1**	**No. of Mislabeled Points**	**AUC**
Linear (SVM)	0.962	0.962	0.962	0.962	13	0.9027
RBF(SVM)	0.967	0.977	0.984	0.94	18	0.8687
Polynomial (SVM)	0.944	0.945	0.945	0.945	19	0.8637
Sigmoid (SVM)	0.944	0.945	0.945	0.945	19	0.8383
Bagging-Linear (SVM)	0.976	0.987	0.974	**0.98**	**19**	**0.9810**
Boosting-Linear (SVM)	**0.977**	**0.99**	**0.977**	**0.98**	**19**	**0.9844**

Table 2 Comparative Analysis

Studies	**Acc.**	**Studies**	**Acc.**
Proposed Study	**97.7%**	Fayz et al. 2018	97.6%
Sahu and Mishra, 2012	96%	Singh and Sharma, 2019	77.97%
Okaka, 2017	96%	Liu et al. 2019	83.16%
Salo et a. 2018	91.67%	Alam et al. 2019	95.92%

Wu et al. 2017	94.13%		

7.0 Concluding

Our study developed a prediction model to diagnose and analyze risk factors using ensemble of FS methods and RFE-SVM (with boosting and bagging) using different kernel functions. While the filter methods handled redundancy, the embedded method takes care of both redundancy and relevancy of features selected. Accuracy, precision, recall, f1-score, and AUC curve were used as performance evaluation criteria. The bagging and boosting ensemble methods obtained accuracies of 97.6% and 97.7% respectively higher than others. This proves that with the few features, high accuracies can be achieved with reduced time and space complexity. Compared with existing works, our proposed model showed improvement after the used of ensemble feature selectors applied. For future work, we hope to improve the performance by introducing other feature selection methods that will automatically determine the feature subset and also try other class of classification learning algorithms and their ensembles with regard to using optimized parameters to scale-up their performance.

References

[1] World Health Oorganization. (2021). Cervical cancer. Retrieved May 21, 2021, from WHO: https://www.who.int/health-topics/cervical-cancer#tab=tab_1, 2021

[2] Raina, R. (2017). An Investigation into Cervical Cancer using Ensemble Learning Approach. MSc Research Project. Ireland.

[3] World Health O:rganization (WHO). (2014). Comprehensive Cervical Cancer Control: A guide to essential practice, 2nd Edition, last assessed 2021/05/21

[4] Fayz, S. Aborizka, M. & Maghraby, F. (2018). Cervical Cancer Diagnosis using Radom Forest Classifier with SMOTE and Feature Reduction Tchniques. IEEE Access. Vol. XX.

[5] Devi, A.M. Ravi, S., & Punitha, V.S. (2016). Detection of Cervical Cancer using the Image Classification Algorithms. IJCTA, International Science Press, 9(3), pp. 1589-1602.

[6] Lu, J., Aong, W., Ghoneim, A., & Alrashoud, M. (2019). Machine Learning for Assisting Cervical Cancer Diagnosis: An Ensemble Approach, Springer.

[7] Quinlan, S., Afli, H., & O'Reilly, (2019). A Comparative Analysis of Classification Techniques for Cervical Cancer Utilizing at Risk Factors and Screening Test Results. CEUR-WS.org/Vol-2563/aics_37.pdf.

[8] Ahishakiye, E., Wario, R., Mwangi, W., & Taremwa, D. (2020). Prediction of Cervical Cancer Basing on Risk Factors using Ensemble Learning. IST-Africa 2020 Conference Proceedings Mirian Cunningham and Paul Cunningham (Eds). IST-Africa Institute and IMC, pp. 1-12.

[9] Sharma, M. (2019). Cervical Cancer Prognosis using Genetic Algorithm and Adaptive Boosting Approach. Health and Technology Retrieved May 21, 2021, from https://doi.org/10.1007/s12553-019-00375-8.

[10] Ugwu, C.C., Obe, O.O., Popoola, O.S., & Adetunmbi, A.O. (2020). Adistriuted denial of service attack detection system using long short term memory with Singular Value Decomposition. Proceedings of the 2020 IEEE 2nd International Conference on Cyberspace, CYBER NIGERIA, pp. 112-118, 9428870.

[11] Villacampa, O. (2015). Feature Selection and Classification Methods for Decision Making: A Comparative Analysis. Ph.D. Thesis.

[12] Matthew, F. T., Adepoju, A.I., Ayodele, O. Obe, O.O. Olaniyan, O., Esan, O., Omodunbi, B. & Egbetola, F. (2018). Development of Mobile-Interfaced Machine Learning-Based Predictive Models for Improving Students' Performance in Programming Courses. International Journal of Advanced Computer Science and Applications(ijacsa), 9(5). http://dx.doi.org/10.14569/IJACSA.2018.090514

[13] Mera-Gaona, M., López, D.M., & Vargas-Canas, R. Neumann, U. (2021). Framework for the Ensemble of Feature Selection Methods. Appl. Sci., 11, 8122. Retrieved May 21, 2021, from https://doi.org/10.3390/app11178122

[14] Kumari, B., Swarkar, T. (2011). Filter versus Wrapper Feature Subset Selection in Large Dimensionality Microarray: A Review. International Journal of Computer Science and Information Technologies, Vol. 2(3), 1048-1053.

[15] Hoque, N., Singh, M., & Bhattacharyya, D.K. (2017). EFS-MI: and Ensemble Feature Selection Method for Classification. Complex Intelligent System. Springer. DOI:10.1007/s40747-017-0060-x.

[16] Dziuda, M.A. (2010). Data Mining for Geneomics and Proteomics Analysis of Gene and Protein Expression Data. Wiley.

[17] Oreski, D & Novosel, T. (2014). Comparison of Feature Selection Techniques in Knowledge Discovery Process", TREM Journal, Volume 3, Number 4, pp.285-290.

[18] Weston, J., Mukheriee, S., Chapelle, O. Pontil, M., Poggio, T., & Vapnik, V. (2000). Feature Selection for SVMs. NIPS' 00: Proceedings of the 13th International Conference on Neural Information Processing Systems. pp. 647-653.

[19] Mahajan, S. Abhishek, Singh, S. (2016). Review of Feature Selection Approaches using Gene Expression Data. Imperial Journal of Interdsciplinary Research (IJIR), Vol. 2, Issue 3, pp. 356-364.

[20] Rustam, Z. & Kharis, S.A.A. (2017). Comparison of Support Vector Machine Recursive Feature Elimination and Kernel Function as feature selection using Support Vector Machine for lung cancer classification. Basic and Applied Science Interdisciplinary Conference. pp.1-6. doi:10.1088/1742-6596/1442/1/012027.

[21] Kang, J., Ullah, Z., & Gwak, J. (2021). MRI-Based Brain Tumor Classification Using Ensemble of Deep Features and Machine Learning Classifiers. Sensors, 21, 2222. https//doi.org/10.3390/s21062222.

[22] Guyon, I. & Weston, J. Barnhill, S., & Vapnik, V. (2002). Gene Selection for Cancer Classification using Support Vector Machines. Machine Learning. 46 (1-3), 2002, 389-422.

[23] Diaz, E. Ccope, A., & Wong, L. (2020). Cervical Cancer: Machine Learning Techniques for Detection, Risk Factors, and Prevention Measures. International Journal of Recent Technology and Engineering (IJRTE). Volume 9, Issue 3, pp. 158-163.

[24] Alelyani, S. (2021). Stable Bagging Feature Selection on Medical Data. Journal of Big Data, Springer, 8, 11.

[25] Verma, A.K., Pal, S., & Tiwari, B.B. (2020). Skin Disease Prediction Using Ensemble Methods and A New Hybrid Feature Selection Technique", Iran Journal of Computer Science. Springer.

[26] Duan, K-B., & Rajapause, J.C. (2005). Multiple SVM-RFE for Gene Selection in Cancer Classification with Expression Data. IEEE Transactions on Nanobioscience. Vol. 4, No. 3, pp. 228-234.

[27] Bolon-Canedo, V. Sanchez-Marono, N., & Alonso-Betanzos, A. (2012). An Ensemble of Filters and Classifiers for Microarray Data Classification. Pattern Recognition. Elsevier, 45, 2012, 531-539. DOI: 10.1016/j.patcog.2011.06.006.

[28] Sahu, B., & Mishra, D. A Novel Feature Selection Algorithm using Particle Swarm Optimization for Cancer Microarray Data", Procedia Engineering, Volume 38, pp. 27-31.

[29] Salo, F., Nassif, A.B., & Essex, A.B. (2018). Dimensionality Reduction with IG-PCA and Ensemble Classifier for Network Intrusion Detection. Computer Networks. Vol. 148, 2018, pp.164-175.

[30] Okaka, R.A. (2017). A Comparative Analysis of Advanced Ensemble Models in Cervical Cancer Prediction. Springer.

[31] Wu, W., & Zhou, H. (2017). Data-Driven Diagnosis of Cervical Cancer with Supoort Vector Machine –Based Approachs. IEEE Access, Volume 5, pp. 25189-25190.

[32] Tseng, C-J., Liu, C-J., Chen, G-D., & Cheewakriangkrai, C. (2017). Integration of Data Mining Classification Techniques and Ensemble Learning to Identify Risk Factors and Diagnose Ovarian Cancer Recurrence. Artificial Intelligence in Medicine, 78, pp. 47-54.
[33] Zarei, N., Cox, D., & Lane, P., Cantor, S., Atkinson, N., Yamel, J-M., Fradkin, L., Serachitopol, D., Lam, S., Niekerk, D., Miller, D., McAlpine, J., Castaneda, K., Castandefa, F., Follen, M., & Miller, C. (2017). Boosted Tree Classifier for in Vivo Identification of Early Cervical Cancer Using Multispectral Digital Colposcopy", In proceeding of the 10th International Joint Conference on Biomedical Engineering Systems and Technologies (BIOSTEC 2017), pp.85-91.
[34] Singh, J., & Sharma, S. (2019). Prediction of Cervical Cancer using Machine Learning Techniques", International Journal of Applied Engineering Research. Volume 14, Number 11, pp. 2570-2577.
[35] Alam, T.M., Milhan, M., Khan, A., Iqbal, A.A., Wahab, A., Mushtag, M. (2019). Cervical Cancer Prediction Through Different Screening Methods Using Data Mining. International Journal of Advanced Computer Science and Applications, Vol., 10, No. 2, pp.388-396.
[36] Punjani, D.N., & Atkotiya, K. (2019). Ensemble Classifier for Cervical Cancer Required Test Prediction. International Journal of Research and Analytical Reviews, Volume 6, Issue 1, pp311-316.
[37] Alsmariy, R., Hearly, G., & Abdelhafez. (2020). Predicting Cervical Cancer using Machine Learning Methods. International Journal of Advanced Computer Science and Applications. Vol. 11, No. 7, pp.173-184.
[38] Diniz, D.N., Rezenda, M.T., Bianchi, G.C., Carneiro, C.M., Ushizima, D.M., de Medeiros, F.N.S., & Souza, M.J.F. (2021). A Hierarchical Feature-based Methodology to Perform Cervical Cancer Classification. Applied Sciences, 11, 409. Retrieved May 21, 2021, from https://doi.org/10.3390/app11094091.
[39] Manna, A., Kundu, R., Kaplun, D., Sinitca, A., & Sarkar, R. (2021). A Fuzzy rank-based Ensemble of CNN Models for classification of Cervical Cancer. Scientific Reports, 11, 14538. Retrieved May 21, 2021, from https:// doi.org/10.1038.s41598-021-93783-8.
[40] Sanchez-Marono, N., Alonso-Betanzos, A., & Tombella-Sanroman, M. (2007). Filter methods for feature selection – a comparative study. International Conference on Intelligent Data Engineering and Automated Learning-IDEAL 2007, Springer, Birmingham, pp. 178–187.
[41] Aazi, F.Z., Abdesselam, R., Achchab, B., & Elouardighi, B. (2017). Feature Selection for Multiclass Support Vector Machines", AI Communications, 29, 583-593. DOI 10.3233/AIC-160707.
[42] Jia, L. (2018). A Hybrid Feature Selection Method for Software Defect", IOP Conference Series: Materials Science and Engineering, 394, pp. 1-9. DOI:10.1088/1757-899X/394/3/032035.
[43] Vergara, J.R., & Estevez, P.A. (2013). A Review of Feature Selection Methods based on Mutual Information. Neural Computation & Application. Springer. 2013, Doi 10.1007/s00521-013-1368-0.
[44] Kononenko, I. (1994). Estimating Attributes: Analysis and Extensions of Relief. Berlin: Springer, 171-182.
[45] Rim, P., & Liu, E. (2020). Optimizing the C4.5 Decision Trees Algorithm Using MSD-Splitting", International Journal of Advanced Computer Science and Application, Vol. 11, No. 10, pp. 41-47.
[46] Liu, H., & Setiono, R. (1995). CHi2: Feature Selection and Discretization of Numeric Attributes. IEEE 7th International Conference of Tools with Artificial Intelligence, pp. 388-392.
[47] Zhao, Z., Morstatter, F. Sharmer, S., Alelyani, S., Anand, A., & Liu, H. (2010). Advancing Feature Selection Research. ASU Feature Selection Repository. Pages 1-28.
[48] Seijo-Pardo, B., Porto-Diaz, I., Bolon-Canedo, V., & Alonso-Betanzos, A. (2017). Ensemble Feature Selection: Homogeneous and Heterogeneous Approaches. Knowledge-Based Systems, Vol. 118, pp.124-139.
[49] Zhang, C., & Ma, Y. (2012). Ensemble Machine Learning: Methods and Applications. Springer, New York.
[50] Li, G-Z., Yang, J., Ye, C-Z.., & Geng, D-Y. (2005). Degree Prediction of Malignancy in Brain Glioma Using Support Vector Machines. Computer in Biology and Medicine, pp. 313-325.
[51] Li, G-Z.& Liu, T-Y. (2006). Feature Selection for Bagging of Support Vector Machine", Proceedings of 9th Biennial Pacific Rim International Conference on Artificial Intelligence (PRICAI2006), Vol. 4099, Springer, pp. 271-277.
[52] Vapnik, C.V. (1995). Support-vector networks. Machine Learning 20, 3, 1995, 273. doi:10.1007/BF00994018.
[53] Cristianini, N., & Shawe-Taylor, J. (2000). An Introduction to Support Vector Machines and Other Kernel-based Learning Methods. Cambridge.
[54] Schapire, R.E. (2012). Boosting: Foundations and Algorithms. Cambridge, Massachusetts, London.

[55] Aldahiri, A., Alrashed, B., & Hussain, W. (2021). Trends in Using IoT with Machine Learning in Health Prediction System. Forecasting, 3, 181-206. Retrieved May 21, 2021, from https://doi.org/10.3390/forecast3010012

[56] Wu, X., & Kumar, V. (2009). The Top Ten Algorithms in Data Mmining, Chapman and Hall/CRC, New York, pp. 37-59.

[57] Jabali, V.K., Rahbari, M., & Kashkouli, A. (2017). Taxonomy of Feature selection in Intrusion Detection System. IJCSNS International Journal of Computer Science and Network Security, VOL.17 No.6, pp. 88-102.

[58] Igodan, E.C., Obe, O., Thompson, A.F-B.., & Owolafe, O. (2022). Erythemato Squamous Disease Prediction using Ensemble Multi-Feature Selection Approach. International Journal of Computer Science and Information Security (IJCSIS), Vol. 20, No. 2, pp. 95-106.

[59] Sobar, Machmud, R., & Wijaya, A. (2016). Behavior Determinant based Cervical Cancer Early Detection with Machine Learning Algorithm. Advanced Science Letter. Vol. 22, 3120-3123.

[60] Oduntan, O.E., Adeyanju, I.A. Falohun, A.S., & Obe, O.O. (2018). A comparative analysis of euclidean distance and cosine similarity measure for automated essay-type grading", Journal of Engineering and Applied Sciences, 13(11), pp. 4198–4204.

[61] Wang, S. Tang, J., & Liu, H. (2016). Feature Selection. Encyclopedia of Machine Learning and Data Mining. Springer. DOI:10.10007/978-1-4899-7502-7-101-1

[62] Akinloye, F. O., Obe, O. O., & Boyinbode, O. K. (2020). Development of an affective-based e-healthcare system for autistic children. Elsevier Science Direct, Scientific African, Volume 9 (1): 1-9.

[63] Asogbon, Y. A., Oluwarotimi, W. S., Nsugbe, E. Jarrah, Y. A., Obe, O. O., Geng, Y., & Li, G. (2021). A Deep Learning-based Model for Decoding Motion Intent of Traumatic Brain Injured Patients' using HD sEMG Recordings", 2021 IEEE International Workshop on Metrology for Industry 4.0 and IoT.

[64] Igodan, C.E., & Ukaoha, K.C. (2019). Using Multilayer Perceptron and Deep Neural Networks for the Diagnosis of Breast Cancer Classification", 2019 IEEE Africon, pp. 1-7, doi:101109/AFRICON46755.2019.9133873.

[65] Igodan, E.C., Obe, O., Thompson, A.F-B.., & Owolafe, O. (2023). A Cascaded Ensemble Learning Approach for Cancer Prediction. Unpublished.

NIPES-NCEE Conference Proceedings
The 2nd International Conference 15th-17th Feb. 2023
84-99
www.nipesjournals.org.ng

DETECTING MOTORCYCLING NEAR MISS INCIDENTS USING COMPUTER VISION AND IMAGE PROCESSING BASED SYSTEM

Rotimi-Williams Bello[1*], Daniel A. Olubummo[2]

[1]Department of Mathematics and Computer Science, University of Africa, 561101 Sagbama, Bayelsa State, Nigeria
[2]Department of Computer and Information Systems, Robert Morris University, Moon-Township, Pennsylvania, United States of America
[*]Corresponding email: sirbrw@yahoo.com

Abstract
Commercial motorcycling is one of the economical means of transportation in many countries, although many perceive it as a dangerous means of transportation, which is affirmed by the number of casualties recorded daily. This life threatening record has greatly hindered continuous support for commercial motorcycling as an affordable means of transportation. Information retrieved from near miss datasets can be a telltale of potential hazards and how to prevent them from happening. However, many researchers have come up with different definitions for near misses, and this has created a gap in understanding the right definition for near misses, thereby making it statistically difficult to address the situation for a safer commercial motorcycling. In this paper, we present near misses as corrective and preventive measures to safety events. Our focus is on the risk factors of commercial motorcycling near miss incidents, which we address by proposing near miss detection framework based on deep learning and its models. Video streams in form of near miss dataset were collected for the experiment. The research contributes to the different approaches employed in literature for solving near miss incidents with the proposed computer vision-based camera embedded system for detecting and analyzing near miss incidents in a complex environment, which can be extended to other safety related events.

Keywords: *Accident, Computer vision, Image processing, Near miss*

1.0 Introduction
Although many researchers have come up with different definitions for near misses, but the most suitable definition among them all is defined as an unexpected event that results neither in dangerous hazard, damage, injury, nor death but if ignored or unreported, has the tendency to result to any of them in future. The reporting and investigation of a near miss incident by a detailed accident investigation helps in applying preventive measures to forestall reoccurrence of such incident. Figure 1 shows a typical implication of ignored or unreported near miss incident. Near miss events are not uncommon, they are more common than sickness, hazard, damage, injury and fatality any statistics may present. According to the Federal Road Safety Corps (FRSC), near miss events precede road safety incidents. The responsiveness of urban planners, practitioners, commercial motorcyclists, drivers, road users and road safety corps to near miss events can be corrective and preventive measures to future safety incidents.

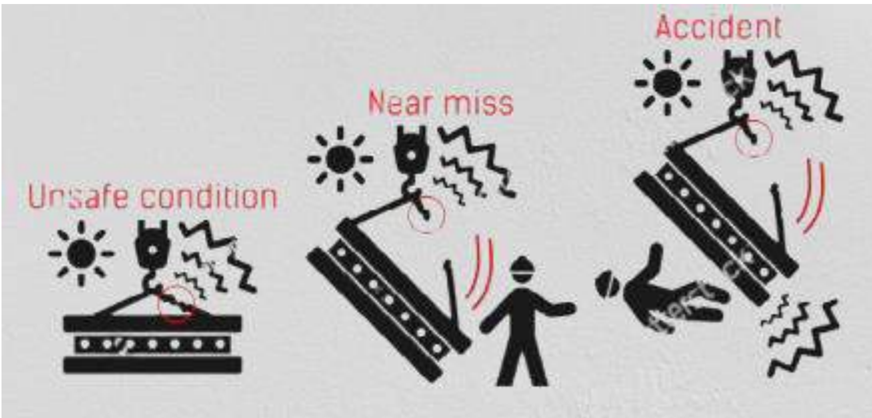

Figure 1 Unreported or ignored scenarios of near miss incident leading to accident. Source: Internet

According to [1] there is potential ability in the newly emerging urban data sources to handle image-related urban modeling tasks. Utilizing such data for urban scenes analysis helps in understanding the dynamic nature of cities and controlling incidents relating to traffic or overcrowding in such cities. Several attempts have been made by urban researchers to model cities by multi-agent models using science of complexity and theory of network [2]. The implication of these models, most of the time, is over-simplification of the urban systems' initial settings and cities exploration from a perspective that is one-dimensional [3]. Lack of large-scale and public accessible dataset, open source modifiable code and graphic processing unit (GPU) are mitigating the robustness of these models from feeding simulations that are unusually large in scope. However, the advent of the artificial intelligence based computer vision and image processing algorithms has changed the whole systems by paving the way for data/video analytics and analytical techniques that can handle urban-related problems.

The emergence of computer vision and image processing, and their applications have helped in understanding the complexity of the attributes of the city dynamic for prompt detection of motorcycling near miss incidents. Various problems confronting urban settlement can be resolved through large-scale datasets of analyzed digital images, whereby essential information and image elements can be tracked and extracted as if performed by human experts for the overall benefit of transportation industry. Some of the risks caused by the congestion and incidents of traffic to the urban dwellers are due to the nature of road and transport networks put in place. According to [4], to control these ugly incidents, for couple of years, measures were put in place such as safety awareness programmes for sensitizing the urban dwellers on road safety, and monitoring the networks of urban transport using technology-based road signs and traffic lights. However, these measures could not give detail account of the unpalatable consequences such as congestion or incidents of traffic of the agents' behavior such as motorcycles, pedestrians, and automobile, all within the city environment.

Having such detail account is essential and beneficial to the motorcyclists, who are mostly exposed to road accidents, with little or no near misses data. Motorcycling is a major occupation among many youths in Nigeria and elsewhere [5]. However, incessant motorcycling road crash is worrisome; a total of 689 people were killed, over 200 injured in 1,500 road crashes involving motorcycles and tricycles between 2015 and 2019 on Lagos roads alone, according to the state government [6]. Although other means of transportation have been encouraged globally to ease challenges of transportation and reduce air pollution caused by automobiles [7, 8], motorcycling has not been favorably considered in that category due to numerous near miss incidents involving motorcycles as a result of little or no formal training received by the motorcyclists regarding rules guiding roads and their usage. In another perspective, motorcycling is perceived as dangerous mode of transportation in that, only a few passengers can withstand the trauma of its near miss incidents or the risk of dodging its crash [9]. Just as found in many places of the world, motorcyclists and their passengers are not likely to get to their destinations without experiencing one form of near miss incidents or another [10], thereby hindering the wider acceptance of commercializing motorcycling as a mode of transportation [11-13].

Although most of the near miss incidents are reported, not recording them contributes to the difficulty in accessing their data as information source for investigating and identifying the associating factors responsible for the accidents risked by individual motorcyclists such as visibility, physical conditions of the roads and the motorcycles, mental and psychological state of the motorcyclists and the pedestrians. Camera-trap images and video data of commuting motorcyclists can be a good source of the data and information needed to address the aforementioned tasks, especially the video data, which provide the replica of the original near miss scenes for their features extraction [11, 12, 14, 15, 16]. In all combination, incidents of motorcycling near misses are factors- and events-based, which in actual fact, are not all the time caused by transportation alone. In-depth understanding of these factors and events will ease the problem of analyzing motorcycling near miss incidents. Due to the small number recorded for near miss incidents, and the impact of prejudice on reporting data pertaining to road crash, where only the near miss incidents that lead to crash or death are reported while the near miss incidents that do not lead to crash or death are either ignored or under-reported, it is an herculean task to give quantitative analysis of the risk of motorcycling [12, 17, 18].

Too many ignored or unreported near miss incidents lead to motorcycling crash. By using this analogy, if data on these near misses can be recorded, then they can provide a rich source of information with which to study motorcyclists' crash risks and identify the factors that are most associated with them. Among the many walks-of-life that have adopted computer vision in tackling the most difficult part of their career are urban planners. Among the catalysts that are responsible for the computer vision accuracy and efficiency in practical settings are the logics of the models; computer vision models are constructed in multiple hidden layers with high graphic processing capabilities to handle the large datasets [19-21]. The models logical construction enables computer vision to posses the capabilities of overcoming even the most herculean vision tasks of recognizing and extracting features from digital images more than any natural vision [22-24]. Urban scene elements such as those based on a collection of themes as found in our natural environment such as sky and built environment such as infrastructure need to be understood; and this can be achieved by computer vision represented by parsing and semantic segmentation for the localization of the objects in cities [25, 26].

Computer vision has shown a dramatic improvement on how cities complexity can be tackled. According to [24], computer vision as a field of artificial intelligence (AI) can be defined as an artificial method of training computers to learn to interpret and understand the features representation of the visual objects for their accurate identification and classification. Computers react to what they see, just as human eyes react, computer vision leverages artificial intelligence (AI) to enable computers to extract meaningful data from visual inputs such as images and videos. The insights gained from computer vision are then employed to take automated actions. Just like AI allows computers to possess thinking ability, computer vision gives them the ability to see. Computer vision, through the region-based convolutional neural network has been able to solve various visual issues that are related to videos and images accurately [24, 27].

We combined YOLOv4 (You Only Look Once version 4 [28] and DeepSort [29] to YOLOv4-DeepSort [30] for the detection and tracking tasks, and the tracked images and identity information were stored. Every 1s, the sequence of image was fetched into the VGG16 (Visual Geometry Group [31] and BiLSTM [32] model (VGG16 and BiLSTM were combined to VGG16-BiLSTM and used for extraction of image feature information and near misses recognition respectively). LSTM (Long Short Term Memory [33] is a unique recurrent neural network (RNN). We evaluate the method by testing 444 sequential video frames of motorcycling near miss incidents in urban environment, and approximately 96% recognition accuracy rate is achieved. The results of the study indicate practicality for automatic detection of motorcycling near misses in urban environment, and it could assist in providing resourceful technical reference for analyzing the risk factors of motorcycling near misses. The work in this paper is a step towards alleviating near miss incidents among motorcyclists and those that are directly affected in the complex urban environment.

2.0 Methodology

In collecting and analyzing road safety data and the risk factors, there are methodological challenges that are involved [34]. The approach used in the existing methods for understanding near misses has limitations; therefore, this section presents the conceptual framework for understanding near misses occurrence and detection in urban environment using the proposed models as shown in Figure 2.

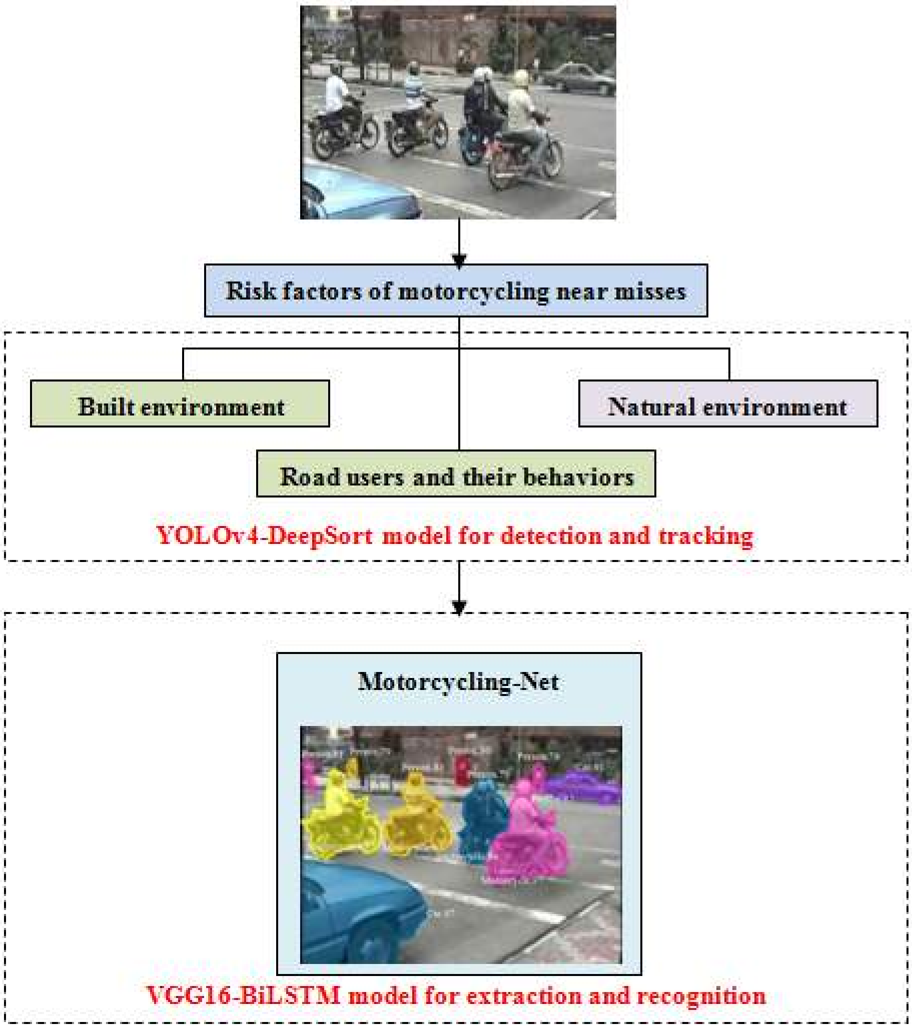

Figure 2 Conceptual framework for understanding near misses occurrence and detection in urban environment

2.1 Datasets

PCAH The proposed framework employed two different datasets; 1) the dataset for training and testing the models, and 2) the dataset for validating the models. The datasets were labeled using LabelMe [35], which provides an online annotation tool to label image(s) for computer vision research as applied in this study for best performance. Datasets related to road users and motorcycling near misses, and risk factors (i.e., built and natural environment) were employed for the training, testing and validation of the models (YOLOv4-DeepSort and VGG16-BiLSTM models) that are proposed in this study. Both YOLOv4-DeepSort and VGG16-BiLSTM models were trained and tested on the aforementioned datasets in ratio 30:70.

Fog as one of the risk factors has 628 images and 2876 non-fog images, which were extracted from among the dataset of weather images that consist of more than 180, 000 images of four classes of weather such as rainy, sunny, cloudy and foggy [36]. Moreover, the datasets are only representations of urban settlements at daytime for intensity of the clouds (other weather and visual factors are not considered in this study). For the road users and motorcycling near misses, approximately 444 sequential video frames in urban environment captured by mobile and immobile cameras were employed. This is in-line with the Multi-Object Tracking (MOT) dataset [37] employed by the DeepSort method to conduct the tracking experiment. MOT dataset comprises 5500 sequential frames of training dataset with approximately 39,905 bounding boxes, and the 5,783 sequential frames of test dataset with approximately 61,440 bounding boxes.

ILSVRC CLS-LOC dataset [21] was used in training the weights of the base network of VGG16 model, and COCO dataset [20] was used in training the model by adapting the network of the last fully connected layers that were converted to layers of convolution after shortening the base network. To make up the limited datasets and improve the performance of the models, data augmentation technique was appropriately applied for two reasons; 1) for the training enhancement of the models, and the accountability for the class disparity of each model without changing the image class [24, 38]. The framework is built with one input of video frames based on the bootstrap aggregating (or bagging) technique [38] in which multi-models are trained in isolation but integrated to improve generalization. The system specifications for carrying out the experiment are as follows: (1) Software; 64-bit Windows 10 Operating System, Jupyter IDE, and Open CV Python library, (2) Hardware; Intel Core i5 processor@2.4GHz CPU, 16 Gigabytes RAM, GeForce GTX 1080 Ti Graphics card, 2 Terabytes hard-disk, and 10.1 inch IPS HD Portable LCD Gaming Monitor PC display VGA HDMI interface for PS3/PS4/XBOx360/CCTV/Camera.

2.2 YOLOv4-DeepSort for detection and tracking

This stage comprises the detection and tracking of road users (i.e., pedestrians, automobiles, and motorcycles) and motorcycling near misses, and their risk factors (i.e., built and natural environment). The qualities possessed by YOLOv4 make it different from other approaches for detecting objects. We adopted DeepSort algorithm tracking method, which is based on SORT [39] algorithm. The simple Kalman filter was used in SORT algorithm for predicting state, and intersection over union (IOU) was used in constructing the cost matrix. Then the detection boxes and trajectory associations were made possible by using Hungarian algorithm. This algorithm in its simplicity performs excellently well in high frame rates videos.

But there is limitation to what SORT could handle; one of its limitations is ignoring the surface features of the object that was detected, its accuracy is solely depended on the low uncertainty of the state of the object. The extraction of appearance information was carried out in DeepSort, and the correlative metrics were replaced with more reliable metrics. The convolutional neural network (CNN) was trained for the extraction of appearance feature information; this increased the network robustness and greatly reduced the identification switch occurrence for an improved tracking accuracy. In this study, YOLOv4-DeepSort was employed as the multi-target tracking algorithm to track the detected road users in the video. Figure 3 shows the flowchart of the multi-target tracking algorithm.

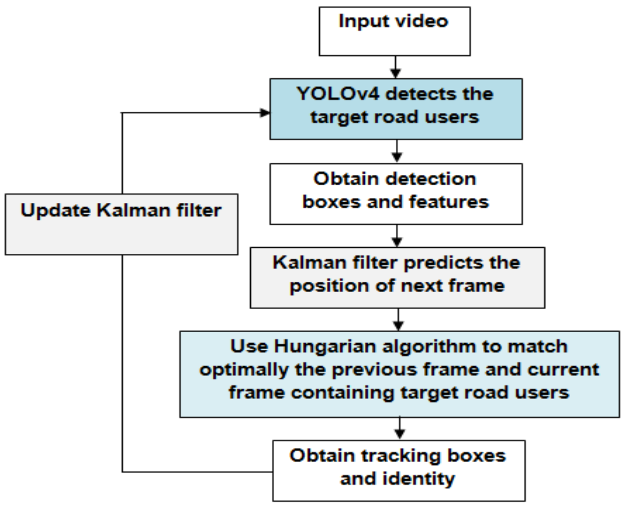

Figure 3 Flowchart of multi-target tracking algorithm showing the contributions of the proposed models to detecting and tracking the road users for near misses analysis

In Figure 3, the video was converted to video frames after it has been inputted into the model network, then, YOLOv4 algorithm for object detection was used to extract the deep features, followed at this stage was obtainment of candidate boxes. Non-maximum value suppression (NMS) algorithm was employed in removing the overlapping frames, thereby obtaining the final detection boxes and features. Kalman filter was used in predicting the position and state of the target road users in the next frame of the video, and the prediction result was assigned to the detection box with higher confidence after comparing the confidences of detection boxes provided by the detector. The target road users between the previous frame and the current frame were matched optimally by the Hungarian algorithm, thereby associating the tracking boxes in the previous frame with the detections in the current frame, leading to obtainment of the target trajectories in the video for the extraction of the appearance information. Concurrently, the results of the tracking were generated and the tracker's parameters were updated for target redetection.

The model's objective loss function is calculated based on the confidence loss' weighted sum and the localization loss [40]. In this study, the detection accuracy of the model is evaluated based on the centre error of performance measures of the detected object for every time-frame (1 to n). The centre error in the video for every time-frame (first frame to the last frame) is calculated based on the threshold values. The precision and recall metrics which measure the accuracy of object detection in terms of the centre error are employed. The percentage of precision, recall, false negatives and false positives is calculated as

$$\text{Precision}=\frac{\text{True Positive}}{\text{True Positive}+\text{False Positive}} \quad (1)$$

$$\text{Recall}=\frac{\text{True Positive}}{\text{True Positive}+\text{False Negative}} \tag{2}$$

Precision otherwise known as positive predictive value is the fraction of relevant objects among the total number of relevant and irrelevant retrieved objects, that is, precision is defined as the percentage of correct instances produced by a model. Recall otherwise known as sensitivity is the fraction of relevant objects that were retrieved. A true positive is an outcome where the model correctly predicts the positive class. A false positive is an outcome where the model incorrectly predicts the positive class. A false negative is an outcome where the model incorrectly predicts the negative class. Based on the precision-recall percentile of each track object, a similarity function is employed as the metrics for evaluating the performance of the object tracking model.

The similarity function is used for evaluating tracking performance of the DeepSort in the object tracking models (YOLOv4-DeepSort). The tracking accuracy of the Deep-Sort is established if the similarity function satisfies

$$\text{SIM}\ (T_o, C_o) \geq Th_1 \tag{3}$$

where T_o is the target object and C_o is the candidate (detected) object. Th_1 is a pre-defined threshold for checking the tracking accuracy. By using Bhattacharyya coefficient, the SIM (T_o, C_o) is calculated for computing the similarity in distance between the colour distributions of the object tracking models (YOLOv4-DeepSort) and the detected objects, the similarity function is denoted by

$$\text{SIM}\ (T_o, C_o) = \sum_{u=1}^{b} \sqrt{\text{HTo}(u) * \text{HCo}(u)} \tag{4}$$

where HTo is the colour distribution of the object tracking models (YOLOv4-DeepSort) and HCo is the colour distribution of the detected object, b denotes the total number of histogram bins. The value of threshold for occlusion detection is set between 0 and 1. Mean Average Precision (mAP) [20] is employed as the metric for evaluating the performance of the segmentation model based on the precision-recall curve of each object class. By carrying out the evaluation, the first precision-recall curve is produced, and for that particular object class, an Area Under the Curve (AUC) is calculated and referred to as Average Precision (AP). To produce the precision-recall curves, it is compulsory for the predicted instance to match with the image's ground-truth annotated object. If both the produced instance and the ground-truth instance possess the same class, and the IOU is greater in value than the predefined value, this means that there is a match between the produced instance from the model and the ground-truth instance.

The rate of overlapping between the predicted value and the ground-truth value is measured using IOU in the instance segmentation problem [41]. The IOU equation is

$$\text{IOU}=\frac{\text{Area of Intersection}}{\text{Area of Union}} \tag{5}$$

The instance with the highest score of IOU is chosen if the instance produced by the model matches with many ground-truth values. The IOU values considered for this work is from 0.50 to 0.95 with mAP at X notation, where X is the threshold value employed in computing the metric. By removing from consideration of the ground-truth instance which matches with the produced instance, the repeated instance is penalized and considered as false positive as no other produced instance can be matched with the removed ground-truth instance object. The precision-recall is computed only after establishing all the matches for the image. Once the precision-recall points are produced using the various threshold IOU values, the average precision (AP) will be calculated. AP is calculated using

$$\mathrm{AP} = \sum_{n=1}^{N} [\mathrm{R(n)} - \mathrm{R(n-1)}].\max \mathrm{P(n)} \quad (6)$$

where N is the number of precision-recall points produced, P(n) and R(n) are the precision and recall with the lowest nth recall respectively.

$$m\mathrm{AP} = \frac{1}{\mathrm{N}}\sum_{i=1}^{N} AP_i$$

(7)

where AP_i = the *AP* of class *i*, *and* N = the number of classes.

2.3 Motorcycling-Net (VGG16-BiLSTM model)

The different environmental factors with potential to influence the motorcyclist safety and cause near misses were addressed at this stage using the proposed method with a sensor-based detector for sensing the qualitative measures, which are associated with the built environment and natural environment such as fog and road infrastructure. A fog is an atmospheric environment in which visibility is reduced because of a cloud of some substance. The framework proposed in this study for this stage is according to the work in [42], which relies on 3D-Convolutional Neural Network (3D-CNN) and VGG16-BiLSTM model based computer vision and image processing for extracting the information pertaining to risk factors (i.e., fog, bad road infrastructure, carefree motorcyclist and pedestrian) from road-captured images using a merged method.

The classification of the risk factors is also carried out at this stage irrespective of the foggy and visibility conditions. The convolution neurons of the model were trained using error back-propagation with a batch size of 32, an initial learning rate of 0.001, momentum of 0.9, 50 epochs, and Adam optimizer. Figure 4 shows the random samples for foggy type of weather carefully acquired to suit the purpose of the study.

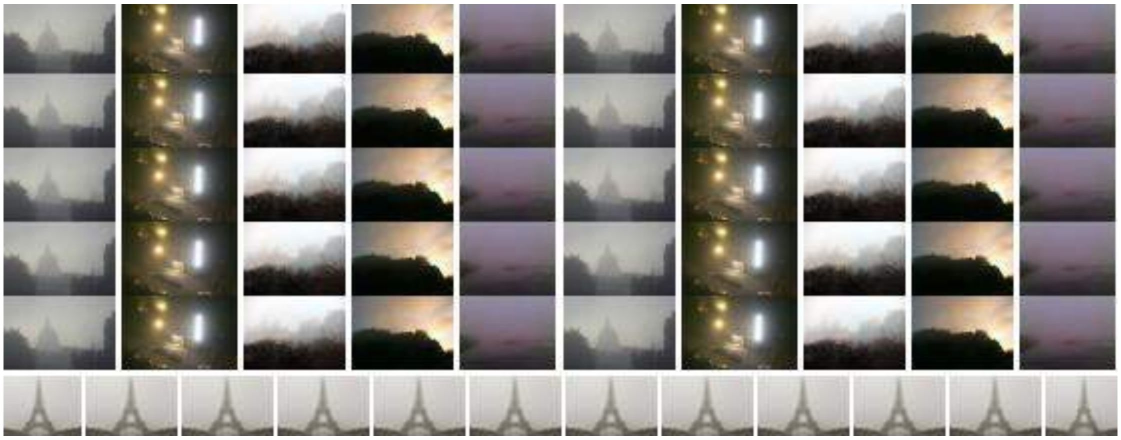

Figure 4 Random samples for foggy weather type

This stage provides a proposed model called Motorcycling-Net for the extraction and segmentation of the detected road users and motorcycling near misses from the generated video. Motorcycling-Net is a model that is based on computer vision which itself is based on structure of convolution embedded with VGG16-BiLSTM model blocks for recognizing near miss actions from scene images. BiLSTM model was employed for the recognition of near misses in this study. BiLSTM has a better effect when it comes to time series data processing by combining the forward LSTM and backward LSTM. In this study, the pre-trained VGG16 model for Image-Net was used for extracting the image sequence features.

The feature sequences are inputted into the network model of BiLSTM after normalizing them for model effects testing. To recognize near misses, the model needs to learn some elements such as the relative motions of the objects in the scene, and the recognition of past events. The finalized hyper-parameters of the model after many experiments are a batch size of 32, dropout of 0.5, decay of 0.00005, hidden unit of 256, an initial learning rate of 0.001, momentum of 0.9, 50 epochs, and Adam optimizer. The primary motive behind the proposed model is to serve as an information generator from which important conclusions can be drawn with respect to how motorcycling behaves in urban areas, for the overall benefit of policy makers and urban planners in understanding what is required for safety measures during the course of designing urban infrastructure. Figure 5 is an image sample of urban environment showing road users and built environment.

Figure 5 An image sample of urban environment showing road users and built environment

3.0 Results and Discussion

This section presents and discusses the results of the experiments conducted in this study where the first stage was responsible for detection and tracking of road users and motorcycling near misses, and risk factors for the extraction and classification of the detected objects at the second stage. As shown in Table 1, the detection models achieved 96% accuracy for motorcycle, 89% for car, and 81% for person with lower false-positive rates on the test datasets based on the aforementioned parameters used in training the CNN model. Likewise, Table 2 shows the result achieved by YOLOv4-DeepSort model for fog detection. Figure 6 shows the visual result of the detection experiment conducted on image sample of road users and motorcycling near misses, and risk factors (i.e., built and natural environment).

Figure 6 Sample of testing images showing segmentation of cars, motorcycles, persons as road users

After the testing stage, we evaluated our models by comparing our results with the results achieved by other related methods. [43] achieved overall score of 0.91 by using CNN-LSTM model to detect fog and four classes of weather (rainy, sunny, cloudy, snowy); they could not detect night time and glare. [44] achieved overall score of 0.80 by using different types of CNN models to detect fog and two classes of weather (snowy and rainy); they could not detect night time and glare. [45] achieved overall score of 0.93 by using multiple residual deep models to detect the following; night time, glare, fog and weather classes (clear, rain, snow).

The proposed models are limited in performance in some instances when compared with the existing work; for example, the unavailability and inconsideration of other classes of weather datasets such as weather at night-time, snow, rain and glare images in this study affected the general performance of the models. However, narrowing the data acquisition to only road users and motorcycling near misses dataset, and fog dataset as one of the risk factors under weather condition makes the proposed models essential in addressing the current challenges reported in the existing work and for the analysis of the variations in images of urban scenes by computer vision and deep learning, which may assist city planners.

Table 1 object detection result using VGG16-BiLSTM model

	Class		
Model	**AP for Motorcycle**	**AP for Car**	**AP for Person**
VGG16-BiLSTM	0.96	0.89	0.81

Table 2 fog detection result using YOLOv4-DeepSort model

Model	**Loss (cross entropy)**	**Accuracy (%)**	**Precision**	**True positive**	**False positive**
YOLOv4-DeepSort	0.88	96	0.96	0.95	0.28

The tracking models achieved 34.3 Multi-Object Tracking Accuracy (MOTA) on the test set and Multi-Object Tracking Precision (MOTP) of 0.77.

4.0 Conclusion

Detecting motorcycling near miss incidents using computer vision and image processing based system has been proposed in this study. YOLOv4-DeepSort was employed for the detection and tracking of road users (i.e., pedestrians, automobiles, and motorcycles) and motorcycling near misses, and their risk factors (i.e., built and natural environment). The qualities possessed by YOLOv4 make it different from other approaches for detecting objects. The extraction and recognition experiments were conducted by using Motorcycling-Net (VGG16-BiLSTM model). While the detection models achieved 96% accuracy for motorcycle, 89% for car, and 81% for person with lower false-positive rates on the test datasets, the tracking models achieved 34.3 MOTA on the test set and MOTP of 0.77. Although these results justify the objectives of the research, we intend to utilize more datasets of different classes of weather and other risk factors of near misses with their agents in future work.

References

[1] Arribas-Bel, D., 2014. Accidental, open and everywhere: Emerging data sources for the understanding of cities. Appl. Geogr. 49, 45–53. https://doi.org/10.1016/j.apgeog.2013.09.012

[2] Zhou, W., Li, Q., 2013. Complexity and dynamic modeling of urban system. Int. J. Mach. Learn. Comput. 3, 440–444. https://doi.org/10.7763/IJMLC.2013.V3.356

[3] Batty, M., Torrens, P.M., 2001. Modelling complexity : The limits to prediction. Cybergeo. https://doi.org/10.4000/cybergeo.1035

[4] Tarigan, J., Nadia, Diedan, R., Suryana, Y., 2017. Plate recognition using backpropagation neural network and genetic algorithm. Procedia Comput. Sci. 116, 365–372. https://doi.org/10.1016/j.procs.2017.10.068

[5] Dozza, M., Schwab, A., Wegman, F., 2017. Safety science special issue on cycling safety. Saf. Sci. 92, 262–263. https://doi.org/10.1016/j.ssci.2016.06.009

[6] https://www.vanguardngr.com/2020/01/689-dead-over-250-injured-in-over-1500-okada-tricycle-accidents-within-four-years-reports/

[7] Pucher, J., Dill, J., Handy, S., 2010. Infrastructure, programs, and policies to increase bicycling: An international review. Prev. Med. 50, S106–S125. https://doi.org/10.1016/j.ypmed.2009.07.028

[8] Savan, B., Cohlmeyer, E., Ledsham, T., 2017. Integrated strategies to accelerate the adoption of cycling for transportation. Transp. Res. Part F Traffic Psychol. Behav. 46, 236–249. https://doi.org/10.1016/j.trf.2017.03.002

[9] Blaizot, S., Papon, F., Haddak, M.M., Amoros, E., 2013. Injury incidence rates of cyclists compared to pedestrians, car occupants and powered two-wheeler riders, using a medical registry and mobility data, Rhône County, France. Accid. Anal. Prev. 58, 35–45. https://doi.org/10.1016/j.aap.2013.04.018

[10] Aldred, R., Crosweller, S., 2015. Investigating the rates and impacts of near misses and related incidents among UK cyclists. J. Transp. Health 2, 379–393. https://doi.org/10.1016/j.jth.2015.05.006

[11] Aldred, R., 2016. Cycling near misses: Their frequency, impact, and prevention. Transp. Res. Part Policy Pract. 90, 69–83. https://doi.org/10.1016/j.tra.2016.04.016

[12] De Rome, L., Boufous, S., Georgeson, T., Senserrick, T., Richardson, D., Ivers, R., 2014. Bicycle crashes in different riding environments in the Australian Capital Territory. Traffic Inj. Prev. 15, 81– 88. https://doi.org/10.1080/15389588.2013.781591

[13] Winters, M., Branion-Calles, M., 2017. Cycling safety: Quantifying the under reporting of cycling incidents in Vancouver, British Columbia. J. Transp. Health 7, 48–53. https://doi.org/10.1016/j.jth.2017.02.010

[14] Beck, B., Stevenson, M., Newstead, S., Cameron, P., Judson, R., Edwards, E.R., Bucknill, A., Johnson, M., Gabbe, B., 2016. Bicycling crash characteristics: An in-depth crash investigation study. Accid. Anal. Prev. 96, 219–227. https://doi.org/10.1016/j.aap.2016.08.012

[15] Imprialou, M., Quddus, M., 2017. Crash data quality for road safety research: Current state and future directions. Accid. Anal. Prev. https://doi.org/10.1016/j.aap.2017.02.022

[16] Teschke, K., Frendo, T., Shen, H., Harris, M.A., Reynolds, C.C., Cripton, P.A., Brubacher, J., Cusimano, M.D., Friedman, S.M., Hunte, G., Monro, M., Vernich, L., Babul, S., Chipman, M., Winters, M., 2014. Bicycling crash circumstances vary by route type: a cross-sectional analysis. BMC Public Health 14. https://doi.org/10.1186/1471-2458-14-1205

[17] Aldred, R., 2018. Inequalities in self-report road injury risk in Britain: A new analysis of National Travel Survey data, focusing on pedestrian injuries. J. Transp. Health 9, 96–104. https://doi.org/10.1016/j.jth.2018.03.006

[18] Abay, K.A., 2015. Investigating the nature and impact of reporting bias in road crash data. Transp. Res. Part Policy Pract. 71, 31–45. https://doi.org/10.1016/j.tra.2014.11.002

[19] Cordts, M., Omran, M., Ramos, S., Rehfeld, T., Enzweiler, M., Benenson, R., Franke, U., Roth, S., Schiele, B., 2016. The cityscapes dataset for semantic urban scene understanding, in: Proceedings of the IEEE Conference on Computer Vision and Pattern Recognition. pp. 3213–3223.

[20] Lin, T.-Y., Maire, M., Belongie, S., Bourdev, L., Girshick, R., Hays, J., Perona, P., Ramanan, D., Zitnick, C.L., Dollár, P., 2014. Microsoft COCO: Common Objects in Context, in: Computer Vision – ECCV 2014, Springer, pp. 740–755. https://doi.org/10.1007/9783-319-10602-1_48

[21] Russakovsky, O., Deng, J., Su, H., Krause, J., Satheesh, S., Ma, S., Huang, Z., Karpathy, A., Khosla, A., Bernstein, M., Berg, A.C., Fei-Fei, L., 2015. ImageNet large scale visual recognition challenge. Int. J. Comput. Vis. 115, 211–252. https://doi.org/10.1007/s11263-015-0816-y
[22] Guo, Y., Liu, Y., Oerlemans, A., Lao, S., Wu, S., Lew, M.S., 2016. Deep learning for visual understanding: A review. Neurocomputing 187, 27–48. https://doi.org/10.1016/j.neucom.2015.09.116
[23] Kuo, C.-C.J., 2016. Understanding convolutional neural networks with a mathematical model. J. Vis. Commun. Image Represent. 41, 406–413
[24] LeCun, Y., Bengio, Y., Hinton, G., 2015. Deep learning. Nature 521, 436–444. https://doi.org/10.1038/nature14539
[25] Chaurasia, A., Culurciello, E., 2017. LinkNet: Exploiting encoder representations for efficient semantic segmentation. 2017 IEEE Vis. Commun. Image Process. VCIP 1–4. https://doi.org/10.1109/VCIP.2017.8305148
[26] Zhou, B., Zhao, H., Puig, X., Fidler, S., Barriuso, A., Torralba, A., 2017. Scene Parsing through ADE20K Dataset, in: 2017 IEEE Conference on Computer Vision and Pattern Recognition (CVPR), IEEE, Honolulu, HI, pp. 5122–5130. https://doi.org/10.1109/CVPR.2017.544
[27] He, K., Zhang, X., Ren, S., Sun, J., 2016. Deep Residual Learning for Image Recognition, in: 2016 IEEE Conference on Computer Vision and Pattern Recognition (CVPR), IEEE, Las Vegas, NV, USA, pp. 770–778. https://doi.org/10.1109/CVPR.2016.90
[28] Bochkovskiy, A., Wang, C.Y., Liao, H.Y.M. 2020. Yolov4: Optimal speed and accuracy of object detection. arXiv preprint arXiv:2004.10934. https://doi.org/10.48550/arXiv.2004.10934
[29] Wojke, N., Bewley, A., Paulus, D., 2017. Simple online and realtime tracking with a deep association metric. In 2017 IEEE international conference on image processing (ICIP); pp. 3645-3649. IEEE. https://doi.org/10.1109/ICIP.2017.8296962
[30] Zhang, X., Hao, X., Liu, S., Wang, J., Xu, J., Hu, J., 2019. Multi-target tracking of surveillance video with differential YOLO and DeepSort. In: Proceedings of 11th International Conference on Digital Image Processing; Guangzhou, China; vol.11179, pp. 701-710. https://doi.org/10.1117/12.2540269
[31] Simonyan, K., Zisserman, A., 2014. Very deep convolutional networks for large-scale image recognition. arXiv preprint arXiv:1409.1556. https://doi.org/10.48550/arXiv.1409.1556
[32] Schuster, M., Paliwal, K.K., 1997. Bidirectional recurrent neural networks. IEEE Transactions on Signal Processing. 45(11):2673-2681. https://doi.org/10.1162/neco.1997.9.8.1735
[33] Hochreiter, S., Schmidhuber, J., 1997. Long short-term memory. Neural Computation. 9(8):1735-1780. https://doi.org/10.1109/78.650093
[34] Schlögl, M., Stütz, R., 2017. Methodological considerations with data uncertainty in road safety analysis. Accid. Anal. Prev. https://doi.org/10.1016/j.aap.2017.02.001
[35] Russell, B.C., Torralba, A., Murphy, K.P., Freeman, W.T., 2008. LabelMe: a database and web-based tool for image annotation. International Journal of Computer Vision, 77(1), 157-173
[36] Chu, W.-T., Zheng, X.-Y., Ding, D.-S., 2016. Image2Weather: A large-scale image dataset for weather property estimation, in: 2016 IEEE Second International Conference on Multimedia Big Data (BigMM), IEEE, Taipei, Taiwan, pp. 137–144. https://doi.org/10.1109/BigMM.2016.9
[37] Leal-Taixé, L., Milan, A., Reid, I., Roth, S., Schindler, K., 2015. MOTChallenge 2015: Towards a benchmark for multi-target tracking. ArXiv150401942 Cs
[38] Goodfellow, I., Bengio, Y., Courville, A., 2017. Deep Learning, Adaptive computation and machine learning series. The MIT Press, Cambridge, Massachusetts
[39] Bewley, A., Ge, Z., Ott, L., Ramos, F., Upcroft, B., 2016. Simple online and realtime tracking. 2016 IEEE Int. Conf. Image Process. ICIP 3464–3468. https://doi.org/10.1109/ICIP.2016.7533003
[40] Liu, L., Silva, E.A., Wu, C., Wang, H., 2017. A machine learning-based method for the large-scale evaluation of the qualities of the urban environment. Comput. Environ. Urban Syst. 65, 113– 125. https://doi.org/10.1016/j.compenvurbsys.2017.06.003
[41] He, K., Gkioxari, G., Dollár, P., Girshick, R., 2020. Mask R-CNN. IEEE Transactions on Pattern Analysis and Machine Intelligence, 42(2), 386-397. doi:10.1109/TPAMI.2018.2844175

[42] Kamangir, H., Collins, W., Tissot, P., King, S. A., Dinh, H. T. H., Durham, N., Rizzo, J., 2021. FogNet: A multiscale 3D CNN with double-branch dense block and attention mechanism for fog prediction. Machine Learning with Applications, 5, 100038

[43] Zhao, B., Li, X., Lu, X., Wang, Z., 2018. A CNN–RNN architecture for multi-label weather recognition. Neurocomputing 322, 47–57. https://doi.org/10.1016/j.neucom.2018.09.048

[44] Villarreal Guerra, J.C., Khanam, Z., Ehsan, S., Stolkin, R., McDonald-Maier, K., 2018. Weather classification: A new multi-class dataset, data augmentation approach and comprehensive evaluations of convolutional neural networks, in: 2018 NASA/ESA Conference on Adaptive Hardware and Systems (AHS), IEEE, Edinburgh, pp. 305–310. https://doi.org/10.1109/AHS.2018.8541482

[45] Ibrahim, M.R., Haworth, J., Cheng, T., 2019. WeatherNet: Recognising weather and visual conditions from street-level images using deep residual learning. ISPRS Int. J. Geo-Inf. 8, 549. https://doi.org/10.3390/ijgi8120549

NIPES-NCEE Conference Proceedings
The 2nd International Conference 15th-17th Feb. 2023
100-129
www.nipesjournals.org.ng

FLEXURAL ANALYSIS OF RECTANGULAR PLATE UNDER LOAD USING EXACT POLYNOMIAL DISPLACEMENT FUNCTION

Festus Chukwudi Onyeka[1] and Thompson Edozie Okeke [2]

[1]Edo State University Uzairue, Edo Sate, 312102, Nigeria.
[2]University of Nigeria, Nsukka, 410101, Nigeria.
[1]onyeka.festus@edouniversity.edu.ng, [2]edozie.okeke@unn.edu.ng,

Abstract

Failure in the structures exists in the world today is attributed to the inability of the de-signers to perform a thorough structural analysis to obtain the design moment and stresses that are induced due to loads subjected to the structure. Previous studies have applied two-dimensional (2-D) model, but analysis of plate requires a three-dimensional (3-D) analogy. This study presents a static flexural analysis of a rectangular plate that is clamped at the second and fourth edge, simply supported and freely supported at the first and third edge using an analytical polynomial model developed from the 3-D plate theory. In the developed model, the elastic static principle was applied in the coupling the 3-D kinematics and constitutive relations to formulate the total potential energy equation. The formulated energy equation was transformed into the equilibrium equation which was used to obtain the shape function of the plate. An exact polynomial deflection of the plate which is a product of its coefficient and shape function was obtained analytically through the principle of general variation. Furthermore, the formula for calculation of the dis-placements and stresses induced due to application of a uniformly distributed load in the plate was obtained by the direct variation of the total potential energy equation to produce a reliable solution for the statically bending analysis of the plate. The outcome of the numerical analysis revealed that increase in the span-thickness ratio led to the decrease in the value of displacement and stresses induced in the plate. On the other hand, as the longest-breadth ratio of the plate increased, the value of the displacement and stresses in the plate increases. The result showed that the present model developed gives distinct and satisfactory solution but still followed an identical pattern when compared with previous studies, this shows the credibility of the derived relationships. Based on the percentage error evaluation, it can be said that the present model, unlike the 2-D model and numerical model provide a reliable solution in the analysis such type of boundary condition. Thus, the present model can be used with confidence for the analysis of any type of rectangular plate under the same loading configuration.

Keywords*: Typical bending analysis 3-D plate, exact polynomial function, displacement and stress analysis in a thick plate*

1.1 Introduction

Plates are three-dimensional structural members having spatial dimensions along x, y, z-axes whose thickness is geometrically less compared to other dimensions [1-2]. They are vastly applied in aeronautical, naval, mechanical, Geotechnical and structural engineering for modelling water tanks, bridge deck slabs, turbine disks, ship hulls, retaining walls, machine parts, architectural structures [3-5].

Plates can be classified according to shapes such as; quadrilateral, square, circular or rectangular; they can be classified based on the integral constituents as homogeneous, non-homogeneous, orthotropic, anisotropic or isotropic [6-7]. Considering boundary status, plates are either fixed, free or simply supported, and they can be thin, moderately thick or thick according to their weight [8-10].

Rectangular plates $a/t \leq 20$ are addressed as thick plate, while $20 \leq a/t \leq 50$ as moderately-thick plates and $50 \leq a/t \leq 100$ as thin plate, where a/t is the span-to-depth ratio [11]. There is increasing research interest for thick plates in engineering structures among scholars due to their pertinence and captivating attributes, features such as lightweight, heavy loads carrying-capacities, cost reduction, high mechanical properties and ability to be customized to the desired state [12]. The properties of thick plates can be improved with adequate perspicacity of its failure form and structural trait.

The investigation on thick plates can be generally and thoroughly made through bending, vibration or buckling [13-15]). The deformation of plates, due to the application of lateral loads or external forces on the plate, at right angles towards the surface of the plate is considered as a bending phenomenon. Deformation extends as the induced load exceeds the critical load [16-17]. This results to plate failure. This study is of great essence because the bending mannerism of thick plates requires adequate attention to circumvent structural instability emanating from deformations and obtain an exact solution.

Several theories such as the classical plate theory (CPT), refined plate theories (RPTs), and three-dimensional theory (3-D) [18] were formulated and deployed by diverse scholars to solve the plight of instability arising from bending. RPTs consist of FSDT [19-20], TSDT [21-22], ESDT [23], PSDT [24] and HSDT [25-26]. An accurate solution for the bending of thick plates cannot be actualized using Kirchhoff plate theory (CPT) [27] because it neglects transverse shear effects. Although RPTs give a better analytical result, their solution is incomplete and inconsistent as they overlook the normal stress and strain along the thickness axis of the plate.

The solutions of the 3D model are accurate and reliable as the limitations of 2D-RPT is terminated with the comprehensive system of fifteen governing equations which consists of material constitutive laws for generalized stress - strain equations, the kinematic relations for six strains and displacements and the three differential equations of equilibrium [28-30]. This study is needful as thick plate analysis a three-dimensional problem and it is advantageous as it investigates thick plates with SCFC support order.

Studies on bending can be carried out numerically, analytically or using an energy approach or a miscellany of any [31]. In the analytical approach, the outcome of the bending issue covers the edge requirements of the plate in the governing equations at different positions of the plate surface. This method includes; Integral transforms, Eigen expansion, Naiver and Levy series [1, 32], while the numerical approach whose solutions are approximate [33-34], consists of; Galerkin, Collocation, Bubnov-Galerkin, truncated double Fourier series, Kantorovich methods, boundary element, Ritz, and finite difference. The energy method whose total energy is equal to the sum of strain and potential energy or external work on the continuum [35]; can be in an analytical or a numerical form.

Unlike the preceding works, this study evaluates the deflection, shear stresses at the x-y axis, x-z axis and y-z axis, the normal stresses along x, y and z co-ordinates produced due to the applied load on the plate, as well as the in-plane displacement in the direction of x and y co-ordinates. Inexact solutions were obtained by past authors that employed assumed displacement-shape functions and others that used an exact process only applied it to the solution of the 2-D bending problem of the thick plate. The nature of the shape functions used during analysis matters so much to the designer as it affects the applicability and performance of the structure; to enhance the robustness of the process and at the same time ensure structural integrity and accuracy of solutions in the plate bending problem, a 3-D polynomial theory is required. This study also addresses this gap by excellently combining RPT of fourth order polynomial with a 3-D elasticity plate theory which is an improvement to past works and more advantageous as it can easily be employed to analyze plates with any boundary condition. A thick plate that is subjected to a uniformly-distributed transverse loads, and simply supported at one edge, free at one edge and clamped at the two other edges (SCFC) were evaluated herein, using a 3-D polynomial plate theory and exact polynomial displacement function to determine value of displacements, moments and stresses along x, y and z co-ordinate at arbitrary nodes of plates.

2. Review of Previous Studies

Bi-directional bending investigation of thick isotropic plates was carried out by Bhaskar *et al.*, [36] using a new inverse TSDT and a finite element solution was developed, considering the effects of transverse shear deflection and rotating inertia. With the application of the dynamic version of the virtual work principle, the dominant equations and edge conditions of the theory were obtained. Although their model showed precise predictions of stresses-displacements when collated with other RPTs, it was unable to capture thick plates with SCFC-support order, polynomial functions, and an analytical and 3D approach.

Neglecting the use of shear correction elements connected with FSDTs, Sayyad and Ghugal [37], as well as Ghugal and Gajbhiye [38] captured the effect of shear and strain deformation in their bending study. The phenomenon of zero-shear transverse stresses was satisfactory. Polynomial displacement functions with 3D theory and SCFC plates were not considered in their assessment.

Simply-supported plates under transverse bi-sinusoidal loads were evaluated by Mantari and Soares [39] using the precept of virtual work and HSDT with an assumed variation of the mechanical properties of the plates in the thickness axis. The authors obtained a Navier-type analytical solution which showed a level of accuracy compared to the previous shear deformation model. The 3D theory and polynomial shape functions were not applied. Plates with SCFC edge status were not covered.

Both trigonometric and polynomial displacement functions were employed by Onyeka and Okeke [40] to formulate the governing differential equation for SSFS plates. They used the direct energy method in their bending analysis and the deflection and stresses obtained in their study were in good agreement with the other RPTs. 3-D theory and SCFC plates were not encapsulated in their study. Mantari *et al.* [41] employed trigonometric functions and shear deformation plate theory to obtain the displacement and stresses in thick rectangular plate. The approach applied by the authors cannot be reliable for a thick plate analysis as they cannot give an exact solution. The authors did not apply 3D theory, neither were polynomial functions incorporated. Plates with SSFS support status was not addressed in their study. An alternate refined plate model was developed by Onyeka *et al.*, (2021) [42] for analyzing the effect of bending CCFC thick plates using the energy method. The authors obtained exact solutions as 3-D kinematic and constitutive relations were applied to formulate the equilibrium equations and total energy function. The beauty of their analytical approach and solutions is undeniable but their model was not a blend of the polynomial RPT and the 3D plate theory rather a trigonometric displacement function was used. In addition, plates with SCFC edge status were not considered in their study.

The spline-collocation method with two-coordinate directions and a numerical approach based on the 3-D theory was employed by Grigorenko *et al.,* [43] to get the bending solutions of a thick plate. They determined the displacements-stresses in clamped plates. Their approach did not capture accurately the value for out-of-plane displacements at any given point in the plate. They did not cover plates with the SCFC support - condition. Onyeka *et al.* [1], Onyeka and Mama [44] presented a 3D trigonometric model for CSCS and SSSS plates respectively. The authors solved the bending issue of these plates using a direct variational energy approach. The solutions obtained in their study validate the accuracy of 3D prediction. But a combination of 2D-RPT and 3D theory with the polynomial function were not considered in their study. Plates with the SCFC boundary condition was also not addressed.

The 3-D model was adopted by Hadi *et al.,* [45] to examine the bending characteristics of functionally graded rectangular plates with variable exponential properties. The authors numerically expressed the impact of different functionally-graded inequality on the stress and displacement fields. They presented the exact solutions of the stresses-displacements and the effects of the graded-material's properties on the plate's behavior, without considering polynomial functions and SCFC isotropic thick rectangular plates.

The study of the behavior of plates using non-classical elasticity theories, have gained more attention in recent times. Many authors have investigated nanostructures using nonlocal elasticity, strain gradient and nonlocal strain gradient theory. Functionally graded material has been the subject of concentration.

These studies include those of Farajpour *et al.* [46], Rahmani *et al.* [47], Shishesaz *et al.* [48], Ebrahimi and Haghi [49], Hosseini *et al.* [50], Nejad and Hadi [51, 52], Nejad *et al.* [53], Farajpour and Rastgoo [54], Farajpour *et al.* [55, 56], Hosseini *et al.* [57], Ebrahimi and Salari [58], Ebrahimi and Barati [59, 60], Hadi *et al*. [61], Asemi and Farajpour [62]. Plate bending features was not considered by these authors, neither was isotropic thick SCFC rectangular plates covered. The 3D elasticity plate theory was also not addressed in their studies.

Antecedently, refined plate theories were mostly used by many scholars in the bending investigation of rectangular plates while 3D model was used by few authors as shown in the available literatures. The solutions obtained by those that employed 2D-RPTs were inexact because the stresses along the thickness axis were not analyzed. Although those who applied 3D theory had exact solutions, polynomial displacement-shape functions were not deployed. This study addressed these research gaps and distinctively presented the coalescence of 3-D and RPT of fourth-order polynomial function which was not seen in preceding studies. The assumed shape functions applied in prior studies birthed erroneous and unreliable solutions as the functions were not derived from the governing compatibility equation that was obtained from the first principle. Close-form solutions, safe and cost-effective analysis is achieved in this work as it employed exact displacement functions. Discordant to other studies that used trigonometric functions to proffer solutions to bending problems, this work utilized polynomial shape functions, which is an accurate, easy and simplified approach that can solve any boundary condition of thick plates.

An exact bending solution for thick plates under uniformly distributed transverse loads with one simply supported edge, one free edge and clamped at the two outer edges (SCFC), is presented in this study using 3-D polynomial-RPT model. Exact polynomial-displacement-functions were used to determine the displacements and stresses in the plate. The effect of span - depth ratios and length-breadth aspect ratios were also examined.

3. Methodology

3.1 Model Formulation

The model of this study was formulated by considering a rectangular plate in Figure 1 as a three-dimensional element in which the deformation exists in the three axis: length (a), width (b) and thickness (t). The displacement field which includes the displacements along x, y and z-axes: p, q and U are obtained assuming that the x-z section and y-z section, which are initially normal to the x-y plane before bending go off normal to the x-y plane after bending of the plate (see Figure 1).

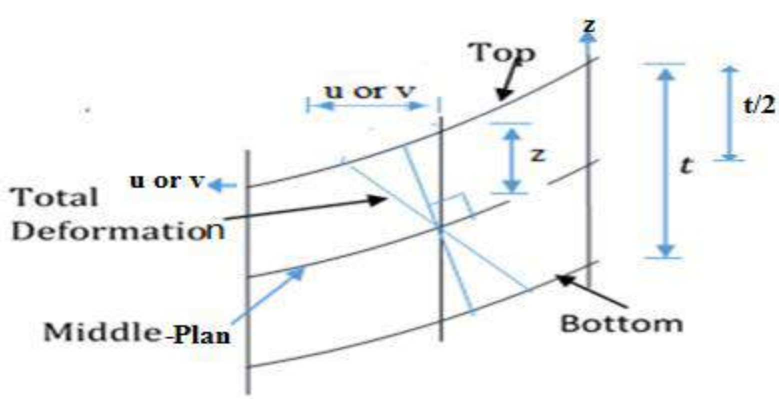

Figure 1: Displacement of x-z (or y-z) section after bending [4].

3.2. Kinematics

The kinematics of the study if formulated by taking the assumption of the plate that the x-z section and y-z section, is no longer normal to the x-y plane after bending. Thus, the 3-D displacement kinematics along x, y and z axis are obtained in line with the work of Onyeka *et al.* [2], as:

$$p = z.\emptyset_x \qquad (1)$$

$$q = z.\emptyset_y \qquad (2)$$

Given that:

$$z = kt \qquad (3)$$

$$\beta = \frac{\mathrm{a}}{t} \qquad (4)$$

$$\gamma = \frac{\mathrm{b}}{a} \qquad (5)$$

Thus, the six non-dimensional coordinates strain components were derived using strain-displacement expression according to Hooke's law and presented in Equation (6) - (11):

$$\varepsilon_x = \frac{1}{\mathrm{a}}.\frac{\partial p}{\partial u} \qquad (6)$$

$$\varepsilon_y = \frac{1}{\mathrm{a}\gamma} \cdot \frac{\partial q}{\partial v} \qquad (7)$$

$$\varepsilon_z = \frac{1}{\mathrm{t}} \cdot \frac{\partial \cup}{\partial k} \qquad (8)$$

$$\gamma_{xy} = \frac{1}{\mathrm{a}} \cdot \frac{\partial q}{\partial u} + \frac{1}{\mathrm{a}\gamma} \cdot \frac{\partial p}{\partial v} \qquad (9)$$

$$\gamma_{xz} = \frac{1}{\mathrm{a}} \cdot \frac{\partial \cup}{\partial u} + \frac{1}{\mathrm{t}} \cdot \frac{\partial p}{\partial k} \qquad (10)$$

$$\gamma_{yz} = \frac{1}{\mathrm{a}\gamma} \cdot \frac{\partial \cup}{\partial v} + \frac{1}{\mathrm{t}} \cdot \frac{\partial q}{\partial k} \qquad (11)$$

3.3. Constitutive Relations

The three dimensional constitutive relation for isotropic material is given as (see [65]):

$$\begin{bmatrix} \varepsilon_x \\ \varepsilon_y \\ \varepsilon_z \\ \gamma_{xz} \\ \gamma_{yz} \\ \gamma_{xy} \end{bmatrix} = \frac{1}{E} \begin{bmatrix} 1 & -\mu & -\mu & 0 & 0 & 0 \\ -\mu & 1 & -\mu & 0 & 0 & 0 \\ -\mu & -\mu & 1 & 0 & 0 & 0 \\ 0 & 0 & 0 & 2(1+\mu) & 0 & 0 \\ 0 & 0 & 0 & 0 & 2(1+\mu) & 0 \\ 0 & 0 & 0 & 0 & 0 & 2(1+\mu) \end{bmatrix} \begin{bmatrix} \sigma_x \\ \sigma_y \\ \sigma_z \\ \tau_{xz} \\ \tau_{yz} \\ \tau_{xy} \end{bmatrix} \qquad (12)$$

The six stress components were obtained by substituting Equations 6 to 11 into Equation 12 and simplifying the outcome gave:

$$\sigma_x = \left[\mu \frac{\mathrm{kt}}{\gamma \mathrm{a}} * \frac{\partial \emptyset_y}{\partial v} + (1-\mu)\, \frac{\mathrm{kt}}{\mathrm{a}} * \frac{\partial \emptyset_x}{\partial u} + \mu \frac{1}{\mathrm{t}} * \frac{\partial \cup}{\partial \mathrm{k}}\right] \frac{\mathrm{E}}{(1+\mu)(1-2\mu)} \qquad (13)$$

$$\sigma_y = \left[\mu k\mathrm{t} * \frac{\partial \emptyset_x}{a\partial u} + \frac{\mu}{t} * \frac{\partial \cup}{\partial k} + \frac{(1-\mu)\mathrm{kt}}{\gamma a} * \frac{\partial \emptyset_y}{\partial v}\right] \frac{\mathrm{E}}{(1+\mu)(1-2\mu)} \quad (14)$$

$$\sigma_z = \left[\frac{\mu k\mathrm{t}}{\gamma a} * \frac{\partial \emptyset_y}{\partial v} + \frac{(1-\mu)}{t} * \frac{\partial \cup}{\partial k} + \mu k\mathrm{t} * \frac{\partial \emptyset_x}{a\partial u}\right] \frac{\mathrm{E}}{(1+\mu)(1-2\mu)} \quad (15)$$

$$\tau_{xy} = \left[\frac{\mathrm{kt}\partial \emptyset_y}{a2\partial u} * \frac{\mathrm{kt}}{2\gamma a}\frac{\partial \emptyset_x}{\partial v}\right] \frac{E(1-2\mu)}{(1+\mu)(1-2\mu)} \quad (16)$$

$$\tau_{yz} = \left[\frac{1}{a2\gamma}\frac{\partial \cup}{\partial Q} + \frac{\emptyset_y}{2}\right] \frac{(1-2\mu)E}{(1+\mu)(1-2\mu)} \quad (17)$$

$$\tau_{xz} = \left[\frac{1}{a}\frac{\partial \cup}{2\partial u} + \frac{\emptyset_x}{2}\right] \frac{(1-2\mu)E}{(1+\mu)(1-2\mu)} \quad (18)$$

3.4. Formulation of Energy

The potential energy which is the summation of all the external work done on the body of the material and strain energy generated due to the applied load on the plate is mathematically defined as:

$$\nexists = \in - \ni \quad (19)$$

Given that;

$$\ni = wab \cap \int_0^1 \int_0^1 \complement \, du \, dv \quad (20)$$

And;

$$\in = \frac{tab}{2}\int_0^1\int_0^1\int_{-0.5}^{0.5}\left(\sigma_x\varepsilon_x + \sigma_y\varepsilon_y + \sigma_z\varepsilon_z + \tau_{xy}\gamma_{xy} + \tau_{xz}\gamma_{xz} + \tau_{yz}\gamma_{yz}\right) du\, dv\, dk \qquad (21)$$

Substituting Equations 22 and 25 into Equation 24 to get the energy equation as:

$$\begin{aligned} \nexists = \frac{\mathrm{E}t^3\gamma}{24(1+\mu)(1-2\mu)}\int_0^1\int_0^1 \Bigg[\left(\frac{\partial\emptyset_y}{\partial u}\right)^2\frac{(1-2\mu)}{2} + \frac{1}{\gamma}\frac{\partial\emptyset_x}{\partial u} * \frac{\partial\emptyset_y}{\partial v} + \frac{(1-\mu)}{\gamma^2}\left(\frac{\partial\emptyset_y}{\partial v}\right)^2 \\ + \frac{(1-\mu)}{t^2} * \left(\frac{\partial \cup}{\partial k}\right)^2\beta^2 + \frac{(1-2\mu)}{2\gamma^2}\left(\frac{\partial\emptyset_x}{\partial v}\right)^2 \\ + \frac{6(1-2\mu)}{t^2}\Bigg\{a^2{\emptyset_x}^2 + \left(\frac{\partial \cup}{\partial u}\right)^2 + a^2{\emptyset_y}^2 + \left(\frac{\partial \cup}{\partial v}\right)^2\frac{1}{\gamma^2} \\ + a\left(\frac{\partial \cup}{\partial u}\right)2\emptyset_x + \left(\frac{\partial \cup}{\partial v}\right)2a * \frac{\emptyset_y}{\gamma}\Bigg\} + \left(\frac{\partial\emptyset_x}{\partial u}\right)^2(1-\mu)\Bigg]\partial u\partial v \\ - w\gamma a^2\int_0^1\int_0^1 \complement S\,\partial u\partial v \end{aligned} \qquad (22)$$

3.5. Solution to the Equilibrium Equation

The two compatibility equations were obtained by minimizing the total potential energy functional with respect to rotations in x-z and in y-z plane to give:

$$\begin{aligned} \frac{\mathrm{E}t^3\gamma}{24(1+\mu)(1-2\mu)}\int_0^1\int_0^1\Bigg[2(1-\mu)\frac{\partial^2\emptyset_x}{\partial u^2} + \frac{\partial^2\emptyset_y}{\partial u\partial v} * \frac{1}{\gamma} + \frac{(1-2\mu)}{\gamma^2}\frac{\partial^2\emptyset_x}{\partial v^2} \\ + \left(2\mathrm{a}^2\theta_{sx} + 2\mathrm{a}.\frac{\partial \cup}{\partial u}\right)\frac{6(1-2\mu)}{\mathrm{t}^2}\Bigg]\partial u\partial v = 0 \end{aligned} \qquad (23)$$

$$\frac{\mathrm{Et}^3\gamma}{24(1+\mu)(1-2\mu)}\int_0^1\int_0^1\left[\frac{\partial^2\emptyset_x}{\partial u\partial v}*\frac{1}{\gamma}+2\frac{\partial^2\emptyset_y}{\partial v^2}*\frac{(1-\mu)}{\gamma^2}+2\frac{(1-2\mu)}{2}\frac{\partial^2\emptyset_y}{\partial u^2}+\left(2\mathrm{a}^2\emptyset_y+\frac{2\mathrm{a}.}{\gamma}\frac{\partial\cup}{\partial v}\right)\frac{6(1-2\mu)}{\mathrm{t}^2}\right]\partial u\partial v=0 \tag{24}$$

The solution of the equilibrium differential equation gives the characteristics trigonometric displacement and rotation functions as presented in the Equation 25-27 as:

$$\cup=[1\ \ u\ \ Cos\,(uc_1)\ \ Sin\,(uc_1)]\begin{bmatrix}a_0\\a_1\\a_2\\a_3\end{bmatrix}.[1\ \ v\ \ Cos\,(vc_1)\ \ Sin\,(vc_1)]\begin{bmatrix}b_0\\b_1\\b_2\\b_3\end{bmatrix} \tag{25}$$

$$\emptyset_x=\frac{c}{a}.\mathrm{H}_0.[1\ \ c_1Sin\,(uc_1)\ \ c_1Cos\,(uc_1)]\begin{bmatrix}a_1\\a_2\\a_3\end{bmatrix}.[1\ \ v\ \ Cos\,(vc_1)\ \ Sin\,(vc_1)]\begin{bmatrix}b_0\\b_1\\b_2\\b_3\end{bmatrix} \tag{26}$$

$$\emptyset_y=\frac{c}{a\beta}.H_0.[1\ \ u\ \ Cos\,(uc_1)\ \ Sin\,(uc_1)]\begin{bmatrix}a_0\\a_1\\a_2\\a_3\end{bmatrix}.[1\ \ \ c_1Sin\,(vc_1)\ \ c_1Cos\,(vc_1)]\begin{bmatrix}b_1\\b_2\\b_3\end{bmatrix} \tag{27}$$

Considering a transversely loaded rectangular thick plate whose Poisson's ratio is 0.3 under uniformly distributed load as shown in the Figure 2, the derived trigonometric deflection functions is subjected to a SCFC boundary condition to get the particular solution of the deflection.

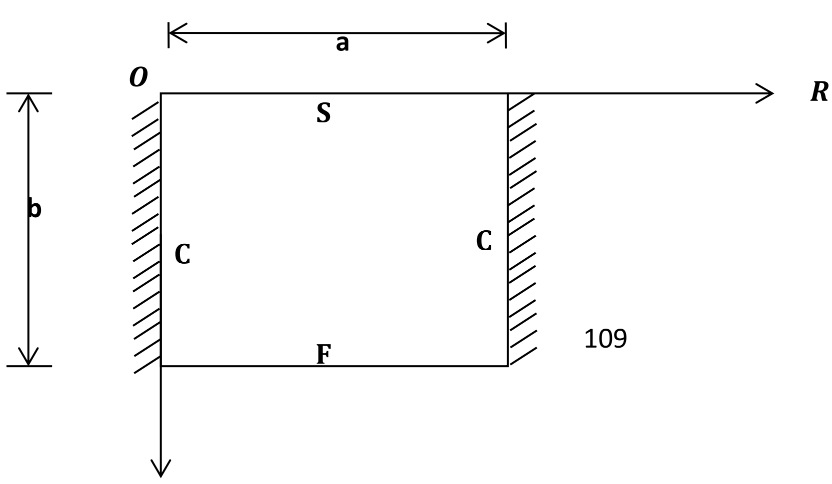

Figure 2: SCFC Rectangular Plate

Applying the initial conditions of the plate in Figure 2, the relationship between the displacement and shape function of the plate as:

$$\cup = C.\cap \tag{28}$$

$$\emptyset_x = \frac{h}{a}.\frac{\partial C}{\partial u} \tag{29}$$

$$\emptyset_y = \frac{g}{\gamma a}.\frac{\partial C}{\partial v} \tag{30}$$

The in trigonometric form of the shape function of the plate after satisfying the boundary conditions is given as:

$$C = (Sin\,\pi u).\left(Cos\frac{\pi v}{2} - 1\right) \tag{31}$$

Substituting Equation 28, 29 and 30 into 22, gives:

$$∄ = \frac{\mathrm{Et}^3\gamma}{24(1+\mu)(1-2\mu)}\Bigg[(1-\mu)h^2 r_x + \frac{1}{\gamma^2}\left[h.g + \frac{(1-2\mu)h^2}{2} + \frac{(1-2\mu)g^2}{2}\right] r_{xy} + \frac{(1-\mu)g^2}{\gamma^4} r_y + 6(1-2\mu)\beta^2\left([h^2 + \cap^2 + 2\cap h].r_z + \frac{1}{\gamma^2}.[g^2 + \cap^2 + 2\cap g].r_{2z}\right) - \frac{2qa^4 r_c \cap}{D^*}\Bigg] \tag{32}$$

Where:

$$r_x = \int_0^1\int_0^1 \left(\frac{\partial^2 \mathrm{C}}{\partial u^2}\right)^2 \partial u \partial v \tag{33}$$

$$r_{xy} = \int_0^1\int_0^1 \left(\frac{\partial^2 \mathrm{C}}{\partial u \partial v}\right)^2 \partial u \partial v \tag{34}$$

$$r_y = \int_0^1\int_0^1 \left(\frac{\partial^2 \mathrm{C}}{\partial v^2}\right)^2 \partial u \partial v \tag{35}$$

$$r_z = \int_0^1\int_0^1 \left(\frac{\partial \mathrm{C}}{\partial u}\right)^2 \partial u \partial v \tag{36}$$

$$r_{2z} = \int_0^1\int_0^1 \left(\frac{\partial \mathrm{C}}{\partial v}\right)^2 \partial u \partial v \tag{37}$$

$$r_c = \int_0^1\int_0^1 \mathrm{C}\, \partial u \partial v \tag{38}$$

Minimizing Equation 32 with respect to h gives:

$$\frac{1}{2\gamma^2}[g + h(1-2\mu)]r_{xy} + hr_x(1-\mu) \ = -6(1-2\mu)\beta^2[h + \cap].r_z \tag{39}$$

Minimizing Equation 32 with respect to g gives:

$$\frac{1}{2\gamma^2}[h + g(1-2\mu)]r_{xy} + \frac{(1-\mu)g}{\gamma^4}k_y = +\frac{6}{\gamma^2}(1-2\mu)\beta^2([g + \cap].r_{2z}) \tag{40}$$

Re-write the Equation (39) and (40) and simplifying to give:

$$h = \cap \frac{(k_{12}k_{23} - k_{13}k_{22})}{(k_{12}k_{12} - k_{11}k_{22})} \tag{41}$$

$$g = \cap \frac{(k_{12}k_{13} - k_{11}k_{23})}{(k_{12}k_{12} - k_{11}k_{22})} \tag{42}$$

Where;

$$k_{11} = (1-\mu)r_x + \frac{1}{2\gamma^2}(1-2\mu)r_{xy} + 6(1-2\mu)\beta^2 r_z \tag{43}$$

$$k_{12} = k_{21} = \frac{1}{2\gamma^2}r_{xy};\ k_{13} = -6(1-2\mu)\beta^2 r_z \tag{44}$$

$$k_{22} = \frac{(1-\mu)}{\gamma^4}r_y + \frac{1}{2\gamma^2}(1-2\mu)r_{xy} + \frac{6}{\gamma^2}(1-2\mu)\beta^2 r_{2z} \tag{45}$$

$$k_{23} = k_{32} = -\frac{6}{\gamma^2}(1-2\mu)\beta^2 r_{2z} \tag{46}$$

Minimizing Equation 32 with respect to ∩ gives:

$$\frac{\mathrm{Et}^3\gamma}{24(1+\mu)(1-2\mu)}\left[6(1-2\mu)\beta^2\left([2\cap+2h].r_z+\frac{1}{\gamma^2}.[2\cap+2g].r_{2z}\right)\right]-\frac{24wa^4r_c(1+\mu)(1-2\mu)}{\mathrm{Et}^3}=0 \tag{47}$$

$$\frac{(1-2\mu)\beta^2\mathrm{Et}^3\gamma}{4(1+\mu)(1-2\mu)}\left\{\left[\cap+\cap\frac{(k_{12}k_{23}-k_{13}k_{22})}{(k_{12}k_{12}-k_{11}k_{22})}\right].r_z+\frac{1}{\beta^2}.\left[\cap+\cap\frac{(k_{12}k_{13}-k_{11}k_{23})}{(k_{12}k_{12}-k_{11}k_{22})}\right].r_{2z}\right\}=\frac{wa^4r_c(1+\mu)(1-2\mu)\beta^3}{\mathrm{E}} \tag{48}$$

Factorizing Equations (48) and simplifying gives:

$$\cap=\frac{2q(1+\mu)(1-2\mu)\beta^3}{E}\left\{\frac{ar_c}{(1-2\mu)\left(\frac{a}{t}\right)^2\left(\left[1+\frac{(k_{12}k_{23}-k_{13}k_{22})}{(k_{12}k_{12}-k_{11}k_{22})}\right].r_z+\frac{1}{\beta^2}.\left[1+\right.\right.}\right. \tag{49}$$

3.6. Exact Displacement and Stress Expression

By substituting the value of ∩ in Equation 49 into Equation 28, the deflection equation after satisfying the boundary condition of CSFS plate is given as:

$$\cup=\cap\,(Sin\,\pi u).\left(Cos\frac{\pi v}{2}-1\right) \tag{50}$$

Similarly, the in-plane displacement along x-axis becomes:

$$p=\frac{(k_{12}k_{23}-k_{13}k_{22})}{(k_{12}k_{12}-k_{11}k_{22})}\left\{\frac{12q(1+\mu)(1-2\mu)\beta^2kr_c}{(1-2\mu)\left(\frac{a}{t}\right)^2\left(\left[1+\frac{(k_{12}k_{23}-k_{13}k_{22})}{(k_{12}k_{12}-k_{11}k_{22})}\right].r_z+\frac{1}{\beta^2}.\left[1+\frac{(k_{12}k}{(k_{12}k}\right.\right.}\right. \tag{51}$$

$$p = \frac{12q(1+\mu)(1-2\mu)\beta^2}{E}\left(\frac{kMr_c}{L}\right)\frac{\partial C}{\partial u} \tag{52}$$

Where;

$$L = 6(1-2\mu)\beta^2\left([1+h].r_z + \frac{1}{\gamma^2}.[1+g].r_{2z}\right) \tag{53}$$

$$N = \frac{(r_{12}r_{23} - r_{13}r_{22})}{(r_{12}r_{12} - r_{11}r_{22})} \tag{54}$$

$$M = \frac{(r_{12}r_{13} - r_{11}r_{23})}{(r_{12}r_{12} - r_{11}r_{22})} \tag{55}$$

Similarly, the in-plane displacement along y-axis becomes;

$$q = \frac{12q(1+\mu)(1-2\mu)\beta}{E}\left(\frac{kNr_c}{L}\right)\frac{\partial C}{\partial v} \tag{56}$$

The six stress elements after satisfying the boundary condition are presented in Equations (57) – (62) as:

$$\sigma_x = \frac{E}{(1+\mu)(1-2\mu)}\left[\frac{k}{\beta}.\frac{\partial^2 C}{\partial u^2}(1-\mu) + \mu\beta^4 * \frac{12q(1+\mu)(1-2\mu)}{E}\left(\frac{r_c}{L}\right)\frac{\partial C}{\partial k} + \frac{\mu k}{\gamma\beta}.\frac{\partial^2 C}{\partial v^2}\right] \tag{57}$$

$$\sigma_y = \frac{E}{(1+\mu)(1-2\mu)}\left[\frac{\mu k}{\beta}.\frac{\partial^2 C}{\partial u^2} + \mu\beta^4 * \frac{12q(1+\mu)(1-2\mu)}{E}\left(\frac{r_c}{L}\right)\frac{\partial C}{\partial k} + \frac{(1-\mu)k}{\gamma\beta}.\frac{\partial^2 C}{\partial v^2}\right] \tag{58}$$

$$\sigma_z = \frac{\mathrm{E}}{(1+\mu)(1-2\mu)}\left[\frac{\mu \mathrm{k}}{\beta}.\frac{\partial^2 \mathrm{C}}{\partial u^2} + (1-\mu)\beta^4 * \frac{12q(1+\mu)(1-2\mu)}{\beta}\left(\frac{r_c}{L}\right)\frac{\partial \mathrm{C}}{\partial \mathrm{k}} + \frac{\mu \mathrm{k}}{\gamma\beta}.\frac{\partial^2 \mathrm{C}}{\partial v^2}\right] \quad (59)$$

$$\tau_{xy} = \frac{E(1-2\mu)}{(1+\mu)(1-2\mu)}.\left[\frac{\mathrm{k}}{2\beta}.\frac{\partial^2 \partial \mathrm{C}}{\partial u\, \partial v} + \frac{\beta^2 \mathrm{k}}{2a\gamma}.\frac{12q(1+\mu)(1-2\mu)}{E}\left(\frac{r_c}{L}\right)\frac{\partial^2 \partial \mathrm{C}}{\partial u\, \partial v}\right] \quad (60)$$

$$\tau_{xz} = \frac{(1-2\mu)E}{(1+\mu)(1-2\mu)}.\left[\frac{1}{2}\frac{\partial \mathrm{C}}{\partial \mathrm{u}} + \frac{\beta^3}{2} * \frac{12q(1+\mu)(1-2\mu)}{E}\left(\frac{r_c}{L}\right)\frac{\partial \mathrm{C}}{\partial u}\right] \quad (61)$$

$$\tau_{yz} = \frac{(1-2\mu)E}{(1+\mu)(1-2\mu)}.\left[\frac{1}{2}\frac{\partial \mathrm{C}}{\partial v} + \frac{\beta^3}{2\gamma} * \frac{12q(1+\mu)(1-2\mu)}{E}\left(\frac{r_c}{L}\right)\frac{\partial \mathrm{C}}{\partial v}\right] \quad (62)$$

4. Results and Discussion

A 3-D polynomial shear deformation model was developed to obtain the numerical outcome for the non-dimensional values of displacements, perpendicular and shear stresses of SCFC thick plate subjected to a transverse load. The variation of the displacements and stresses in a different span-depth ratio varying length-breadth ratio, was presented in Figures 3 to 11. The range of span-thickness ratio is considered between 4, 5, 10, 15, 20, 50, 100 and CPT, which covers the span of thick, moderately thick and thin plates. The length-breadth aspect ratio captured in this study is 1.0, 1.5 and 2.0.

The plot in Figures 3 to 5 showed that as the span-depth ratio increased, the out-of-plane displacements (Ս) decreased positively while the in-plane displacements (p and q) increased negatively. Considering a span - depth ratio of 4 to 20, the result as presented in figures showed that the deflection values varied from 0.0041 & 0.0023, 0.0036 & 0.0025 and 0.0043 & 0.0024 at length-breadth ratio of 1.0, 1.5 and 2.0 respectively. It is observed that the value of deflection varies less as the span-depth ratio increases under the same loading capacity/condition. Plates at a span - depth ratio between 4 and 20 can be regarded as thick plates while span-thickness ratio of 50 and beyond can be considered as moderately-thick or thin plates as they are almost equivalent to the value of the CPT. The plate structure tends to fail when the reductions continues to the point where the deflection exceeds the elastic yield stress.

The stresses perpendicular to the x and z axis (σ_x, and σ_z) decreased positively while the ones in the y-axis (σ_y) increased negatively with an increase in span-thickness ratio, as shown in Figure 6. In Figure 7, the stresses perpendicular to the x-axis (σ_x) reduced positively while stresses perpendicular to the y-axis (σ_y) increased negatively as the span-depth ratio kept rising. Between span-depth ratios of 4 and 5, the normal stress in the z-plane (σ_z) increased negatively, dropped in the negative order at a span - depth ratio of 10 with a gradual negative increment till span-depth ratio of 20 and a constant value of 0.0114 at span-depth ratio of 50 and beyond. The normal stresses in the x-axis (σ_x), as shown in Figure 8 decreased in the positive coordinate as the span-thickness ratio increased, perpendicular stresses in the y-axis (σ_y) increased negatively from span-depth ratio of 4 to 15 with a positive increase from span-depth of 20 to CPT. Figure 8 equally showed that stresses perpendicular to the z-axis (σ_z) dropped positively span-depth ratio of 4 and 5, with an increase in the negative sense between span-depth ratio of 10 till 20, maintaining a positive value of 0.0154 for span-depth ratio of 50, 100 and CPT.

The non-dimensional parameters for the shear stresses in the in the x-y plane (τ_{xy}) increased in the negative order with each rise in the span - depth ratio and the shear stresses in the x-z, and y-z plane (τ_{xz} and τ_{yz}) reduced positively as presented in Figure 9. In Figure 10, there was a negative increase for the shear stresses in the x-y plane (τ_{xy}) for a span - depth ratio of 4 to 5 and 50 to CPT, with a reduction in the positive sense of span-depth ratio of 10 till 20. The same chart revealed the reduction of shear stresses in the x-z plane (τ_{xz}) positively. It also showed a positive reduction for span-depth ratio of 4 to 5, a negative rise in the span - depth ratio of 10 to 20 and a positive decrease for span-thickness ratio of 50 till CPT for shear stresses in the y-z plane (τ_{yz}).

In Figure 11, shear stresses in the x-y plane (τ_{xy}) increased in the negative order from span-depth ratio of 4 to 5, with a positive reduction in the span - depth ratio of 10 till 20, and a constant negative value of 0.019 for a span - depth ratio of 50 till CPT. The same plot showed that there was a positive reduction in the shear stresses at x-z plane (τ_{xz}) for the span-depth ratio of 4 to 5, with a rise in the negative sense in span-depth ratio of 10 till 20 and a positive reduction of the values of the shear stresses. For span-depth ratio between 4 and 5, the values of the shear stresses in the y-z plane (τ_{yz}) increased negatively with the same occurrence at a span - depth ratio of 10 till 20 and had a constant negative value of 0.0036 for span-depth ratio of 50 and beyond.

In a nutshell, it can be deduced that there are categorically three rectangular plates. Plates whose deflection and transverse shear stress vary greatly from zero are considered as thick plates while thin plates can be categorized as plates whose vertical shear stress and deflection do not differ largely from zero; their values being almost the same as CPT values. Plates that lie in between the thick and thin plates are considered as moderately-thick plates. Taking a/t to represent the span-thickness ratio for the plate categories; $a/t \geq 50$ are thin plates, $15 \leq a/t \leq 50$ are moderately thick plate, while $a/t \leq 15$ are thick plates. This attestation can be applied to depict the boundary between thin and thick plate. From this study, it can be inferred that thick plate is one whose span-depth ratio value is 4 up to 15.

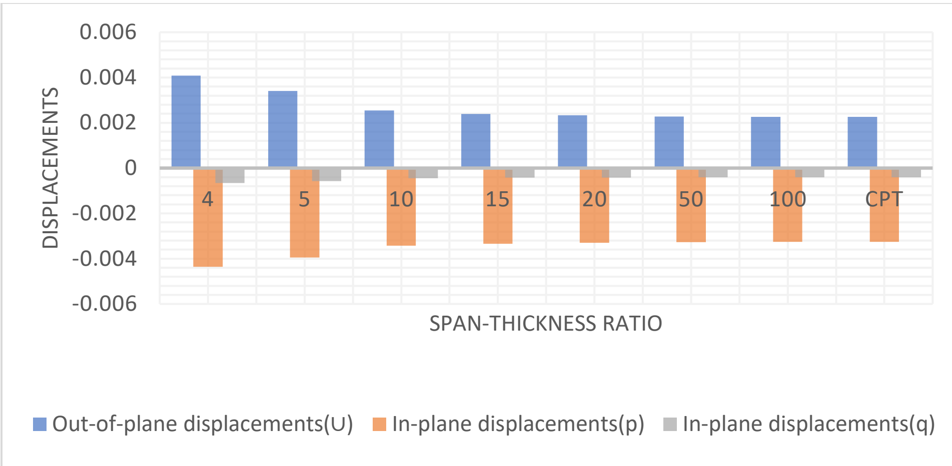

Figure 3: Graph of displacements versus span-depth ratio of the plate at length-breadth ratio of 1.0

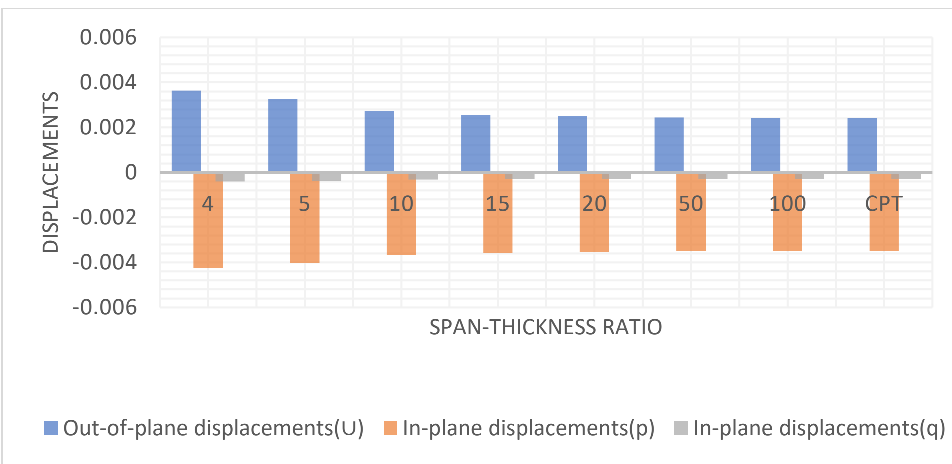

Figure 4: Graph of displacements versus span-depth ratio of the plate at length-breadth ratio of 1.5

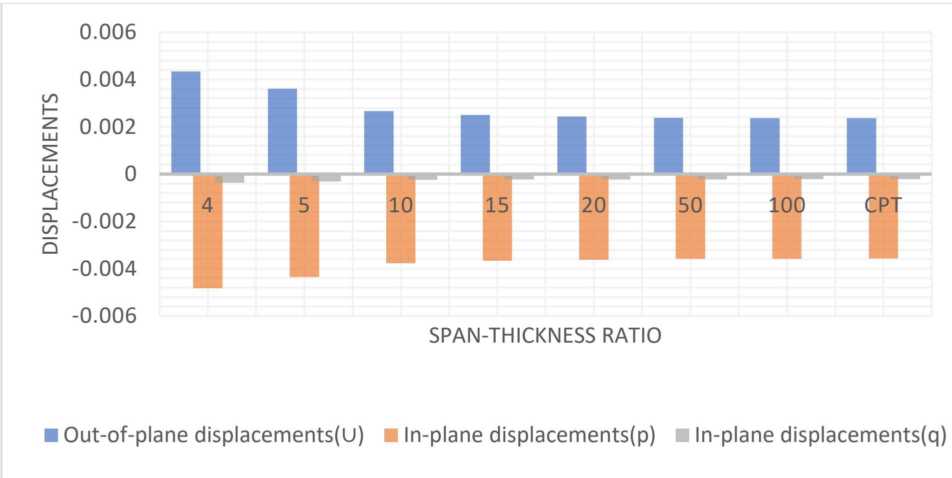

Figure 5: Graph of displacements versus span-depth ratio of the plate at length-breadth ratio of 2.0

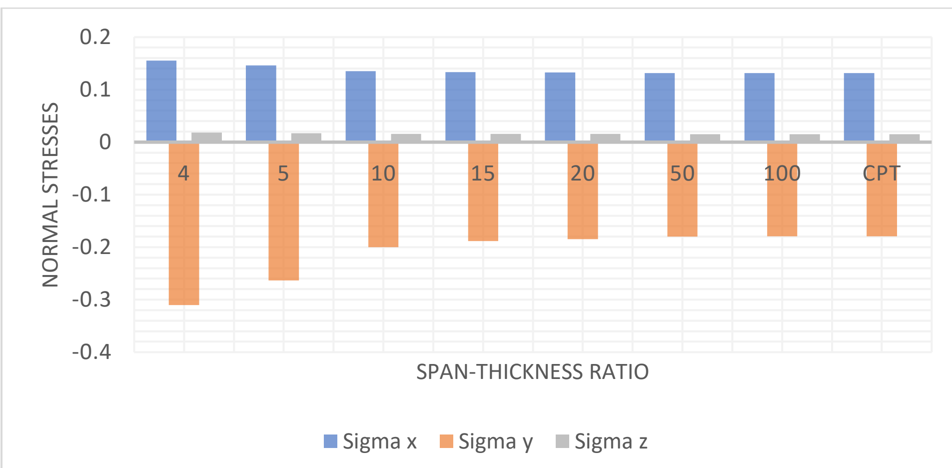

Figure 6: Graph of normal stresses versus span-depth ratio of the plate at length-breadth ratio of 1.0

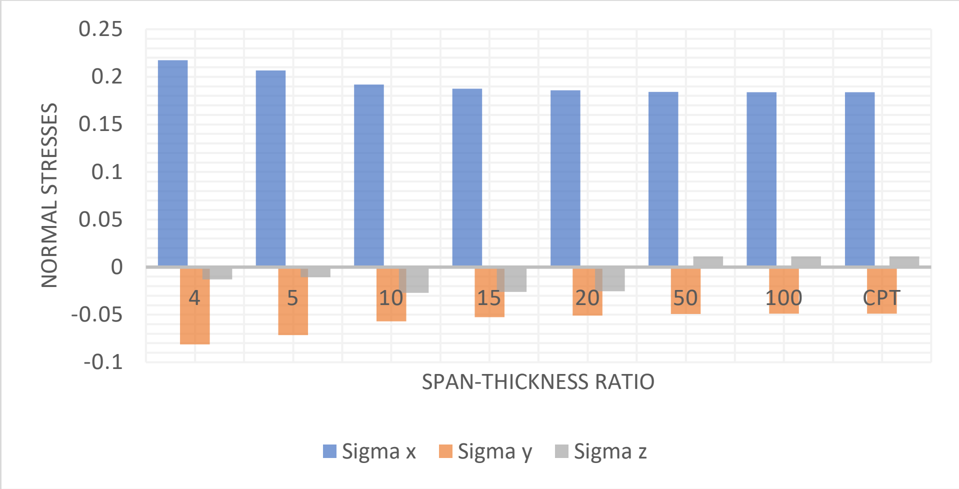

Figure 7: Graph of normal stresses versus span-depth ratio of the plate at length-breadth ratio of 1.5

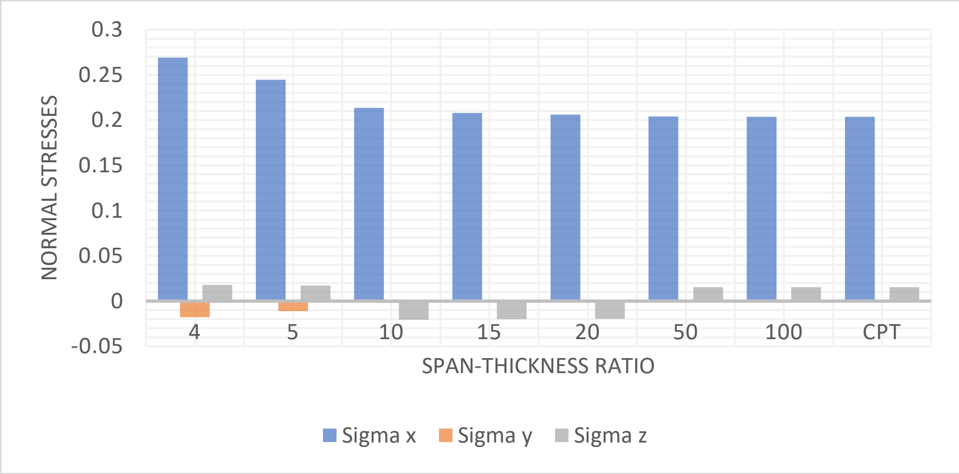

Figure 8: Graph of normal stresses versus span-depth ratio of the plate at length-breadth ratio of 2.0

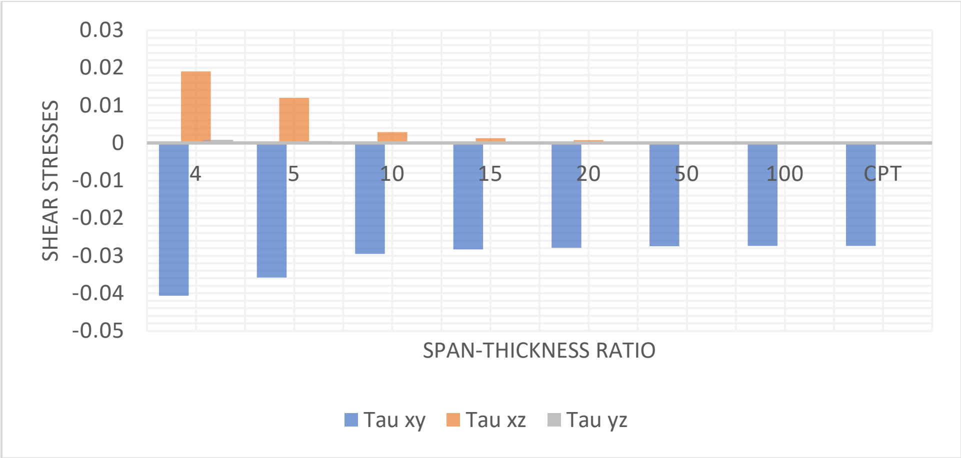

Figure 9: Graph of shear stresses versus span-depth ratio of the plate at length-breadth ratio of 1.0

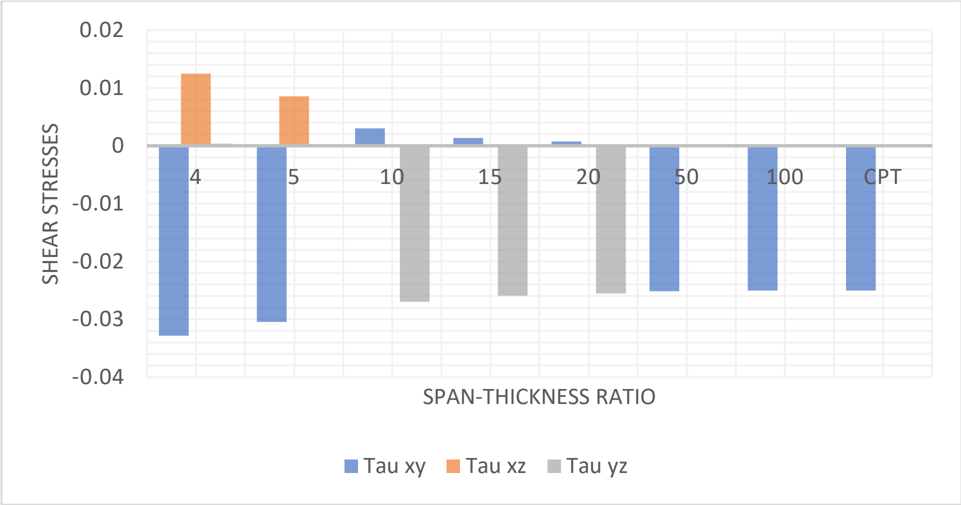

Figure 10: Graph of shear stresses versus span-depth ratio of the plate at length-breadth ratio of 1.5

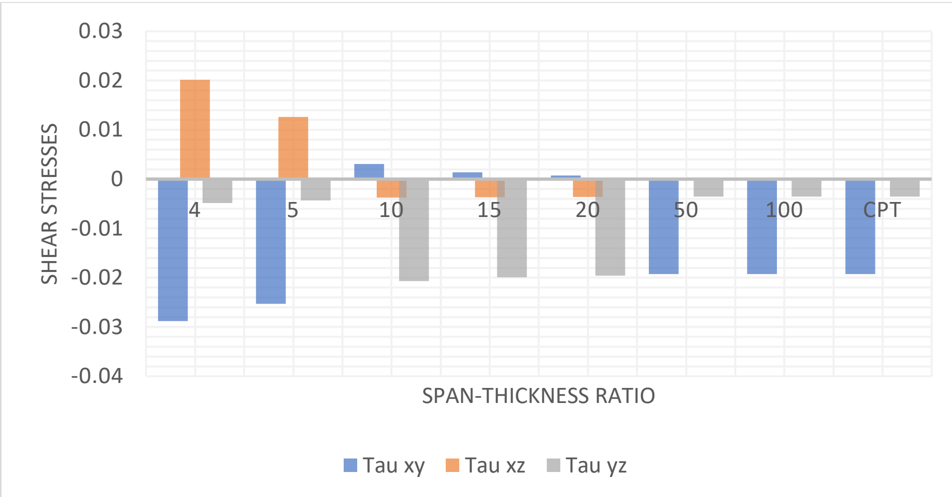

Figure 11: Graph of shear stresses versus span-depth ratio of the plate at length-breadth ratio of 2.0

The result of the comparative evaluation tabulated in Table 1 and Figure 12 clearly showed the contrariety of this model and those of previous scholars. To validate the derived relationships in the deflection analysis, an assessment of the percentage difference was adopted and recorded in the table. As the span-depth ratio increased, it was observed that the non-dimensional values of deflection for both present and previous studies decreased. The table and the diagram in Figure 12 revealed that the study of Gwarah (2019) varied a little from the present work while that of Onyeka and Okeke (2020) varied much. The reason for these variations is that Gwarah (2019) employed RPT with an assumed polynomial shape function, while Onyeka and Okeke (2020) applied a third-order polynomial shear deformation theory with a derived shape function. Significantly, both previous studies did not apply the amalgam of 3-D elasticity plate theory and fourth-order polynomial shear-deformation theory; a feat documented in this work.

Table 1 and Figure 12 revealed the over-estimation and underestimation of the RPT-solutions obtained by previous researchers. This confirms the reliability of this model and the approach considered herein as it gives accurate and exact solutions. This model is worth adopting for safe, cost-effective and accurate analysis of thick plates of any boundary condition. The average percentage difference obtained in this work and Onyeka and Okeke (2020) is 9.27%, while that of Gwarah (2019) is 6.83%. The overall percentage variation is 8.05%. This implies that the present study is equivalent to those of Onyeka and Okeke (2020) and Gwarah (2019) at 90.7% and 93.2% respectively. With this confidence level, the approach presented in this study should be espoused for adequate investigation of thick plates.

Table 1: Comparative deflection analysis of square plate between present studies and past studies at different span-depth ratio

β = a/t	Present Work [P.W]	Onyeka and Okeke (2020) [64]	Gwarah (2019) [63]	Percentage difference between [P.W] & [64]	Percentage difference between [P.W] & [63]
4	0.004084	0.004465	0.003713	9.3291	9.0842
5	0.003407	0.003726	0.003147	9.3631	7.6313
10	0.002544	0.002786	0.002381	9.5126	6.4072
15	0.002389	0.002570	0.002238	7.5764	6.3206
20	0.002335	0.002559	0.002188	9.5931	6.2955
50	0.002277	0.002496	0.002134	9.6179	6.2802
100	0.002269	0.002487	0.002126	9.6078	6.3023
CPT	0.002266	0.002482	0.002123	9.5322	6.3107
				9.27	6.83
Average Percentage difference					
Total Percentage difference				8.05%	

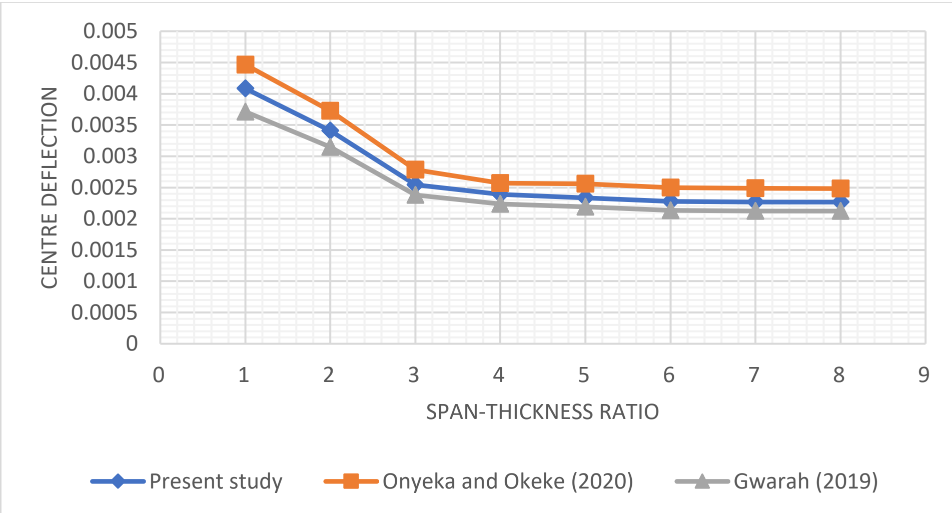

Figure 12: Comparative variation of deflection and span-depth ratios of present study and previous studies

Nomenclature

k	non-dimensional parameters of z-axis
u	non-dimensional parameters of x-axis
v	non-dimensional parameters of y-axis
t	thickness of the plate,
p	in-plane displacement along x-axis
q	in-plane displacement along y-axis
h	coefficient of shear deformation along x-axis of the plate
g	coefficient of shear deformation along y-axis of the plate
ε_x	normal strain along x-axis
ε_y	normal strain along y-axis
ε_z	normal strain along z-axis
γ_{xy}	shear strain in the plane parallel to the x-y plane
γ_{xz}	shear strain in the plane parallel to the x-z plane
γ_{yz}	shear strain in the plane parallel to the y-z plane

τ_{xy}	shear stress in the plane parallel to the x-y plane
τ_{xz}	shear stress in the plane parallel to the x-z plane
τ_{yz}	shear stress in the plane parallel to the y-z plane
E	modulus of elasticity
µ	Poisson's ratio
∄	Potential energy of the plate
∈	Strain energy of the plate
∋	External work done on the plate
C	Plate's shape function
w	Uniformly distributed load
∪	Deflection function of the plate
∩	Coefficient of deflection
$\emptyset_x$	Coefficient of shear deformation along x-axis
$\emptyset_y$	Coefficient of shear deformation along y-axis
p	In-plane displacement along x-axis
q	In-plane displacement along y-axis
β	Span-thickness ratio
α	Aspect ratio

References

[1]. F. C. Onyeka, B. O. Mama, C. D. Nwa-David and T. E. Okeke (2022). Exact Analytic Solution for Static Bending of 3-D Plate under Transverse Loading. Journal of Computational Applied Mechanics, Vol. 53, No. 3, pp. 309-331. DOI: 10.22059/jcamech.2022.342953.721.

[2]. K. Chandrashekhara (2001). Theory of plates. University Press (India) Limited.

[3]. I. C. Onyechere, O. M. Ibearugbulem, C. U. Anya, K. O. Njoku, A. U. Igbojiaku and L. S. Gwarah (2020). The Use of Polynomial Deflection Function in The Analysis of Thick Plates using Higher Order Shear Deformation Theory. Saudi Journal of Civil Engineering, Vol.4, no.4, pp. 38-46. DOI: 10.36348/sjce. 2020. v04i04.001.

[4]. F. C. Onyeka, B. O. Mama and C. D. Nwa-David (2022). Application of Variation Method in Three-Dimensional Stability Analysis of Rectangular Plate Using Various Exact Shape Functions. Nigerian Journal of Technology (NIJOTECH), Vol. 41, no. 1, pp. 8-20. DOI: http://dx.doi.org/10.4314/njt.v41i1.2.

[5]. F. C. Onyeka, C. D. Nwa-David and E. E. Arinze (2021). Structural Imposed Load Analysis of Isotropic Rectangular Plate Carrying a Uniformly Distributed Load Using Refined Shear Plate Theory. FUOYE Journal of Engineering and Technology (FUOYEJET), Vol.6, no. 4, pp. 414-419. DOI: http://dx.doi.org/10.46792/fuoyejet.v6i4.719.

[6]. J. N. Reddy (2006). Classical theory of plates, In Theory and Analysis of Elastic Plates and Shells, CRC Press. DOI: 10.1201/9780849384165-7

[7]. F. C. Onyeka and T. E. Okeke (2020). Application of Higher Order Shear Deformation Theory in The Analysis of Thick Rectangular Plate. International Journal of Emerging Technologies, Vol. 11, no. 5, pp. 62-67.

[8]. R. Szilard (2004). Theories and Applications of Plates Analysis: Classical, Numerical and Engineering Methods. John Wiley and Sons Inc. DOI: 10.1002/9780470172872.

[9]. E. Ventsel and T. Krauthammer (2001). Thin plates and shells theory, analysis and applications, Maxwell Publishers Inc, New York.

[10]. F. C. Onyeka, T. E. Okeke and C. D. Nwa-David (2022). Static and Buckling Analysis of a Three-Dimensional (3-D) Rectangular Thick Plates Using Exact Polynomial Displacement Function. European Journal of Engineering and Technology Research, Vol. 7, no. 2, pp.29-35. DOI: http://dx.doi.org/10.24018/ejeng.2022.7.2.2725.

[11]. F. C. Onyeka, B. O. Mama and C. D. Nwa-David (2022). Analytical Modelling of a Three-Dimensional (3D) Rectangular Plate Using the Exact Solution Approach. IOSR Journal of Mechanical and Civil Engineering (IOSR-JMCE), Vol.19, no. 1, pp. 76-88. DOI: 10.9790/1684-1901017688.

[12]. F. C. Onyeka, F. O. Okafor and H. N. Onah (2021). Buckling Solution of a Three-Dimensional Clamped Rectangular Thick Plate Using Direct Variational Method. IOSR Journal of Mechanical and Civil Engineering (IOSRJMCE), Vol. 18, no.3, pp.10-22. DOI: 10.9790/1684-1803031022.

[13]. S. P. Timoshenko and J. M. Gere (1963). Theory of elastic stability, 2nd Edition, McGraw-Hill Books Company, New York. DOI: 10.1115/1.3636481.

[14]. F. C. Onyeka (2020). Critical Lateral Load Analysis of Rectangular Plate Considering Shear Deformation Effect. Global Journal of Civil Engineering, Vol. 1, pp. 16-27. DOI: 10.37516/global.j.civ.eng.2020.012.

[15]. F. C Onyeka and T. E Okeke (2021). Analytical Solution of Thick Rectangular Plate with Clamped and Free Support Boundary Condition using Polynomial Shear Deformation Theory. Advances in Science, Technology and Engineering Systems Journal, Vol.6, no. 1, pp. 1427-1439. DOI: 10.25046/aj0601162.

[16]. P. S. Gujar and K. B. (2015). Ladhane, Bending Analysis of simply supported and clamped circular plate. International Journal of Civil Engineering (SSRG-IJCE), Vol. 2, no. 5, pp. 45-51. DOI: 10.14445/23488352/IJCE-V2I5P112.

[17]. F. C. Onyeka (2021). Effect of Stress and Load Distribution Analysis on an Isotropic Rectangular Plate. Arid Zone Journal of Engineering, Technology and Environment, Vol. 17, no. 1, pp. 9-26.

[18]. F. C. Onyeka and T. E. Okeke (2021). Analysis of critical imposed load of plate using variational calculus. Journal of Advances in Science and Engineering Vol. 4, no. 1, pp. 13–23. DOI: https://doi.org/10.37121/jase.v4i1.125.

[19]. E. Reissner (1945). The Effect of Transverse Shear Deformation on the Bending of Elastic Plates. Journal of Applied Mechanics, Vol. 12, no. 2, pp. A69–A77. DOI:10.1115/1.4009435.

[20]. M. Zenkour (2003). Ashraf, Exact Mixed-Classical Solutions for the Bending Analysis of Shear Deformable Rectangular Plates. Applied Mathematical Modelling, Vol. 27, no. 7, pp. 515-34. DOI: 10.1016/S0307-904X(03)00046-5.

[21]. F. C. Onyeka, F. O. Okafor and H. N. Onah (2021). Application of a New Trigonometric Theory in the Buckling Analysis of Three-Dimensional Thick Plate. International Journal of Emerging Technologies, Vol. 12, no. 1, pp. 228-240.

[22]. Y. M. Ghugal and A. S. Sayyad (2011). Free vibration of thick isotropic plates using trigonometric shear deformation theory. J. Solid Mech, Vol. 3, no. 2, pp. 172-182.

[23]. A. S. Sayyad and Y. M. Ghugal (2012). Bending and Free Vibration Analysis of Thick Isotropic Plates by Using Exponential Shear Deformation Theory. Applied and Computational Mechanics, Vol. 6, no. 1, pp. 65-82, 2012.

[24]. F. C. Onyeka and D. Osegbowa (2020). Stress analysis of thick rectangular plate using higher order polynomial shear deformation theory, FUTO Journal Series-FUTOJNLS, Vol. 6, no. 2, pp. 142-161.

[25]. I. I. Sayyad (2013). Bending and Free Vibration Analysis of Isotropic Plate Using Refined Plate Theory. Bonfring International Journal of Industrial Engineering and Management Science, Vol. 3, no. 2, pp. 40-46. DOI:10.9756/bijiems.4390.

[26]. O. M. Ibearugbulem and F. C. Onyeka (2020). Moment and Stress Analysis Solutions of Clamped Rectangular Thick Plate. European Journal of Engineering Research and Science, Vol. 5, no. 4, pp. 531-534. DOI:10.24018/ejers.2020.5.4.1898.

[27]. G. Kirchhoff (1850). Ueber Die Schwingungen Einer Kreisförmigen Elastischen Scheibe. Annalen Der Physik, Vol. 157, no.10, pp. 258-64. DOI:10.1002/andp.18501571005.

[28]. F. C. Onyeka, T. E. Okeke and C. D. Nwa-David (2022). Buckling Analysis of a Three-Dimensional Rectangular Plates Material Based on Exact Trigonometric Plate Theory. Journal of Engineering Research and Sciences, Vol. 1, no. 3, pp. 106-115. DOI: https://dx.doi.org/10.55708/js0103011.

[29]. F. C. Onyeka, B. O. Mama and T. E. Okeke (2022). Exact three-dimensional stability analysis of plate using a direct variational energy method. Civil Engineering Journal, Vol. 8, no. 1, pp. 60-80. DOI: http://dx.doi.org/10.28991/CEJ-2022-08-01-05.

[30]. M. Kashtalyan (2004). Three-dimensional elasticity solution for bending of functionally graded rectangular plates. European Journal of Mechanics A/Solids, Vol. 23, no. 5, pp. 853-864.

[31]. F. C. Onyeka, D. Osegbowa and E. E. Arinze (2020). Application of a New Refined Shear Deformation Theory for the Analysis of Thick Rectangular Plates. Nigerian Research Journal of Engineering and Environmental Sciences, Vol. 5, no. 2, pp. 901-917.

[32]. B. O. Mama, C. U. Nwoji, C. C. Ike and H. N. Onah (2017). Analysis of Simply Supported Rectangular Kirchhoff Plates by the Finite Fourier Sine Transform Method. International Journal of Advanced Engineering Research and Science (IJAERS), Vol. 4, no. 3, pp. 285-291. DOI https://doi.org/10.22161/ijaers.4.3.44.

[33]. C. U. Nwoji, B. O Mama, C. C Ike and H. N. Onah (2017). Galerkin-Vlasov method for the flexural analysis of rectangular Kirchhoff plates with clamped and simply supported edges. IOSR Journal of Mechanical and Civil Engineering (IOSR JMCE), Vol. 14, no. 2, pp. 61-74. DOI: https://doi.org/10.9790/1684-1402016174.

[34]. N. N. Osadebe, C. C. Ike, H. N. Onah, C. U. Nwoji and F. O. Okafor (2016). Application of Galerkin-Vlasov Method to the Flexural Analysis of Simply Supported Rectangular Kirchhoff Plates under Uniform Loads. Nigerian Journal of Technology (NIJOTECH), Vol. 35, no. 4, pp. 732-738. DOI: https://doi.org/10.4314/njt.v35i4.7.

[35]. N. G. Iyengar (1988). Structural Stability of Columns and Plates, New York: Ellis Horwood Limited; 1988.

[36]. D. P. Bhaskar, A. G. Thakur, I. I. Sayyad and S. V. Bhaskar (2021). Numerical Analysis of Thick Isotropic and Transversely Isotropic Plates in Bending using FE Based New Inverse Shear Deformation Theory. International Journal of Automotive and Mechanical Engineering (IJAME), Vol.18, no. 3, pp. 8882-8894. DOI: https://doi.org/10.15282/ijame.18.3.2021.04.0681.

[37]. A. S. Sayyad and Y. M. Ghugal (2012). Bending and free vibration analysis of thick isotropic plates by using exponential shear deformation theory. Applied and Computational Mechanics, Vol. 6, pp. 65-82.

[38]. Y. M. Ghugal and P. D. Gajbhiye (2016). Bending Analysis of Thick Isotropic Plates by Using 5th Order Shear Deformation Theory. Journal of Applied and Computational Mechanics, Vol. 2, no. 2, pp. 80-95. DOI: 10.22055/jacm.2016.12366.

[39]. J. L. Mantari and C. G. Soares (2012). Bending Analysis of Thick Exponentially Graded Plates Using A New Trigonometric Higher Order Shear Deformation Theory. Composite Structures, Vol. 94, no. 6, pp. 1991-2000. DOI: https://doi.org/10.1016/j.compstruct.2012.01.005.

[40]. F. C. Onyeka and T. E. Okeke (2021). New Refined Shear Deformation Theory Effect on Non-Linear Analysis of a Thick Plate Using Energy Method. Arid Zone Journal of Engineering, Technology & Environment, Vol. 17, no. 1, pp.121-140.

[41] J. L. Mantari, A. S. Oktem, C. Guedes Soares (2012). A New Trigonometric Shear Deformation Theory for Isotropic, Laminated Composite and Sandwich Plates. International Journal of Solids and Structures, Vol. 49, no. 1, pp. 43-53. DOI: http://doi.org/10.1016/j.ijsolstr.2011.09.008.

[42]. F. C. Onyeka, B. O. Mama and T. E. Okeke (2021). Elastic Bending Analysis Exact Solution of Plate using Alternative I Refined Plate Theory. Nigerian Journal of Technology (NIJOTECH), Vol. 40, no. 6, pp. 1018-1029. DOI: http://dx.doi.org/10.4314/njt.v40i6.4.

[43]. A.Y. Grigorenko, A. S. Bergulev, S. N. Yaremchenko (2013). Numerical solution of bending problems for rectangular plates. International Applied Mechanics, Vol. 49, no.1, pp.81-94. DOI: https://doi.org/10.1007/s10778-013-0554-1.

[44]. F. C. Onyeka and B. O. Mama (2021). Analytical Study of Bending Characteristics of an Elastic Rectangular Plate using Direct Variational Energy Approach with Trigonometric Function. Emerging Science Journal, Vol. 5, No. 6, pp. 916-928. DOI: http://dx.doi.org/10.28991/esj-2021-01320.

[45]. A. Hadi, A. Rastgoo, A. Daneshmehr and F. Ehsani (2013). Stress and strain analysis of functionally graded rectangular plate with exponentially varying properties. Indian Journal of Materials Science, Vol. 2013, 2013.

[46]. M. R. Farajpour, A. Rastgoo, A. Farajpour and M. Mohammadi (2016). Vibration of piezoelectric nanofilm-based electromechanical sensors via higher-order non-local strain gradient theory. Micro. Nano Lett., Vol. 11, no. 6, pp. 302-307. DOI: https://doi.org/10.1049/mnl.2016.0081.

[47]. O. Rahmani, S. Norouzi, H. Golmohammadi and S. Hosseini (2017). Dynamic response of a double, single-walled carbon nanotube under a moving nanoparticle based on modified nonlocal elasticity theory considering surface effects. Mech. Adv. Mater. Struct., Vol. 24, no. 15, pp. 1274-1291. DOI: https://doi.org/10.1080/15376494.2016.1227504.

[48]. M. Shishesaz, M. Hosseini, K. N Tahan and A. Hadi (2017). Analysis of functionally graded nanodisks under thermoelastic loading based on the strain gradient theory. Acta Mechanica, Vol. 228, no. 12, pp. 4141-4168. DOI: https://doi.org/10.1007/s00707-017-1939-8.

[49]. F. Ebrahimi and P. Haghi (2018). Elastic wave dispersion modelling within rotating functionally graded nanobeams in thermal environment. Adv. Nano Res., Int. J., Vol. 6, no. 3, pp. 201-217. DOI: https://doi.org/10.12989/anr.2018.6.3.201.

[50]. M. Hosseini, M. Shishesaz, K. N. Tahan and A. Hadi (2016). Stress analysis of rotating nano-disks of variable thickness made of functionally graded materials. Int. J. Eng. Sci., Vol. 109, pp. 29-53. DOI: https://doi.org/10.1016/j.ijengsci.2016.09.002.

[51]. M. Z. Nejad, A. Hadi (2016). Eringen's non-local elasticity theory for bending analysis of bi-directional functionally graded Euler–Bernoulli nano-beams. Int. J. Eng. Sci., Vol. 106, pp. 1-9. DOI: https://doi.org/10.1016/j.ijengsci.2016.05.005

[52]. M. Z. Nejad, A. Hadi (2016). Non-local analysis of free vibration of bi-directional functionally graded Euler–Bernoulli nano-beams. Int. J. Eng. Sci., vol. 105, pp. 1-11. DOI: https://doi.org/10.1016/j.ijengsci.2016.04.011

[53]. M. Z. Nejad, A. Hadi and A. Rastgoo (2016). Buckling analysis of arbitrary two-directional functionally graded Euler–Bernoulli nano-beams based on nonlocal elasticity theory. Int. J. Eng. Sci., Vol. 103, pp. 1-10. DOI: https://doi.org/10.1016/j.ijengsci.2016.03.001

[54]. A. Farajpour and A. Rastgoo (2017). Influence of carbon nanotubes on the buckling of microtubule bundles in viscoelastic cytoplasm using nonlocal strain gradient theory. Results Phys., Vol. 7, pp. 1367-1375. DOI: https://doi.org/10.1016/j.rinp.2017.03.038

[55]. A. Farajpour, A. Rastgoo and M. Farajpour (2017). Nonlinear buckling analysis of magneto-electro-elastic CNT-MT hybrid nanoshells based on the nonlocal continuum mechanics. Compos. Struct., Vol. 180, pp.179-191. DOI: https://doi.org/10.1016/j.compstruct.2017.07.100

[56]. A. Farajpour, A. Rastgoo and M. Mohammadi (2017). Vibration, buckling and smart control of microtubules using piezoelectric nanoshells under electric voltage in thermal environment. Physica B: Condensed Matter, Vol. 509, pp. 100-114. DOI: https://doi.org/10.1016/j.physb.2017.01.006

[57]. M. Hosseini, H. H Gorgani, M. Shishesaz, A. Hadi (2017). Size-dependent stress analysis of single-wall carbon nanotube based on strain gradient theory. Int. J. Appl. Mech., vol.9, no. 6. DOI: https://doi.org/10.1142/S1758825117500879

[58]. F. Ebrahimi, P. Haghi (2018). Elastic wave dispersion modelling within rotating functionally graded nanobeams in thermal environment. Adv. Nano Res., Int. J., Vol. 6, no. 3, pp. 201-217. DOI: https://doi.org/10.12989/anr.2018.6.3.201

[59]. F. Ebrahimi and M. R. Barati (2018). Buckling Analysis of nonlocal strain gradient axially functionally graded nanobeams resting on variable elastic medium. Proc. Inst. Mech. Eng. Pt. C J. Mech. Eng. Sci., Vol. 232, no. 11, pp. 2067-2078. DOI: https://doi.org/10.1177/0954406217713518.

[60]. F. Ebrahimi and M. R. Barati (2018). Stability analysis of functionally graded heterogeneous piezoelectric nanobeams based on nonlocal elasticity theory. Adv. Nano Res., Int. J., vol. 6, no. 2, pp. 93-112. DOI: https://doi.org/10.12989/anr.2018.6.2.093.

[61]. A. Hadi, M. Z Nejad, M. Hosseini (2018). Vibrations of three-dimensionally graded nanobeams. Int. J. Mech. Sci., Vol. 128, pp. 12-23. DOI: https://doi.org/10.1016/j.ijengsci.2018.03.004.

[62]. S. R. Asemi, A. Farajpour (2014). Vibration Characteristics of double-piezoelectric-nanoplate-systems. Micro. Nano Lett., Vol. 9, no. 4, pp. 280-285. DOI: https://doi.org/10.1049/mnl.2013.0741.

[63]. L. S. Gwarah (2019). Application of shear deformation theory in the analysis of thick rectangular plates using polynomial displacement functions. PhD Thesis Presented to the School of Civil Engineering, Federal University of Technology, Owerri, Nigeria.

[64]. F. C. Onyeka and T. E Okeke (2020). Effect of load, shear and bending analysis of rectangular plate using polynomial displacement function. Journal of Research and Innovations in Engineering, Vol. 5, pp. 145-158.

[65]. T. E. Okeke, F. C. Onyeka and C. D. Nwa-David (2022). Characteristic Trigonometric Function Application to the Direct Variation Method for Clamped, Simply and Freely Supported Plate under Uniform Load Distributions. Journal of Materials Engineering, Structures and Computation, Vol.1, no. 1, pp. 40-58, 2022.

NIPES-NCEE Conference Proceedings
The 2nd International Conference 15th-17th Feb. 2023
130-145
www.nipesjournals.org.ng

DESIGN, FABRICATION AND PERFORMANCE EVALUATION OF A WASTE PLASTIC SHREDDER

Azamosa Harry, Albert Obanor, Osamudiame Rapahel, Ataman Raphael, Idiahi Lumen, Asemosa Esosa

Department of Mechanical Engineering, University of Benin, Benin city, Nigeria.
Corresponding author's email: johnharry238@gmail.com

Abstract

It is a common thing in societies today to see plastic materials discarded inappropriately with consequential effects of degradation of the environment through drainage blockage, emission of human unfriendly gases when combusted by locals amongst other negative impacts. Arising from this, it became pertinent to recycle these plastic wastes for the production of new economic materials through processes which include shredding, sorting, controlled melting, moulding, extrusion and so on. Some of these processes and the relevant machines for executing them are imported and not easily accessible to many.

This has in turn led to the need to research cheap and local methods of producing the machines using locally sourced materials. In order to achieve this goal, a plastic shredding machine was designed and fabricated. It consists of a loading hopper, shaft with 3 shredding blades at $120\,^o$ *apart, sieve, bearings and an electric motor.*

Results obtained from the operational testing of the machine showed that it took an average time of 73.7 minutes for the plastic shredding machine to shred 25kg of plastic waste. The fabricated plastic shredder had machine throughput capacity of 1170kg/h. The efficiency of the machine was calculated as 95.7%. The comparative analysis of the results with other research findings showed that it was well within optimum operating capacity and suitable for use in small to medium scale plastic shredding.

Keywords*: Design, fabrication, performance evaluation, plastic, shredder, waste.*

1.0 Introduction

Polymers are the primary component of plastics, which are synthetic or semi-synthetic materials. These materials can be moulded, extruded, or pressed into solid objects of various shapes due to their fluidity. They are used widely because of their adaptability as well as a variety of other qualities, including their light weight, toughness, flexibility, and low production costs. However, more contemporary industrial methods employ versions made from renewable resources, such as corn- or cotton-derived products. Most contemporary plastics are produced using chemicals derived from fossil fuels like natural gas or petroleum. Engineering and technology involves the development, design, production and conversion of materials into useful products that are of domestic and economic value.

One can clearly understand that the various products of engineering and technology are themselves outcome of the processing, refinement and fabrication of other materials which are referred to as raw materials. Such raw materials may be recycled plastics which are further processed through shredding, melting and remould to bring about other finished products. Raw materials as utilized in engineering and technology may be natural (originating from natural source, renewable and abundant) or synthetic (originated by subsequent conversion). These materials are further classified into metals (iron, steel, copper etc.) and non-metals (polymers such as plastic and rubber, ceramics, wood, glass etc.). Natural polymers processing may have its few demerits, but its renewability and less environmental degradation as well as its properties may prove a great deal as to why it is still far preferable to the synthetic polymers derived from the petrochemicals. In a search for sources of raw materials such as plastic and other natural polymer to meet the demand of a rapidly expanding polymer based industries and to curb the problem of environmental degradation it has become pertinent for plastics to be recycled. Recycling is the process of repurposing waste materials and products to make new goods. Nigeria is amongst the top rubber cultivators around the world; hence; the utilization of rubber and its products have been a huge investment for income generation. Due to their distinctive qualities, which include durability, elasticity, abrasion and impact resistance, effective heat dispersion, and malleability at low temperatures, polymers like plastics utilized in large number of consumer products, including medical equipment. This has forced an increase in the demand for such materials as raw products for the manufacture of other products which in turn end up as wastes after use. Such polymer waste includes plastic chairs, water containers, packaging polymers, toys, electrical appliances and household wares etc. These materials constitute a mess in society and degrades the environment by blocking of drainages, emission of poisonous gasses when combusted and littering of passage ways due to their inability to easily decay.

The demand for raw materials and the negative environmental impact of these materials have necessitated a paradigm shift to recycling them and one method of their recycling is shredding. Polymer or plastic shredding is the breakdown of large sizes of plastic materials into reusable smaller sizes for ease of processing into other useful product. The shredding process could be done manually by humans which is time consuming, unsafe and with low throughput, hence the need for the development of machines otherwise called plastic shredding machines that are motorized and have the ability to shred large volume of plastics in lesser time. Many of the existing plastic shredding machines are imported and expensive and not amenable to many rural manufacturers. To curb this and many of the setbacks on plastics usages, waste and recycling machine acquisition, the present research therefore is focused on study, design and fabrication of a low cost plastic shredding machine for use in small and medium scale plastic shredding.

2.0 Materials and Methodology

2.1 Materials

The plastic shredding machine design and production involve the use of computer aided design software for the production of conceptual designs. Various components of the machine that were drafted include the following:

i. Hopper
ii. Shafts
iii. Bearing
iv. Shredding blades
v. Pulley

vi. Pulley belts
vii. Mesh

2.2 Methods

The first step was to find a feasible design which could be taken as the basis for the waste plastic shredder. The design is a modification of both the single shaft plastic shredder and the double shaft plastic shredder. This is to take advantage of the merit of both designs, especially the ease of waste plastic feeding into the plastic shredder via the open top feed. A 2 Horsepower electric motor was chosen after technical consideration.

2.2.1 Bulk material properties of plastic

Proposed product output = 25kg

Density of plastics = 970kg/m^3

Shredding force of plastic = 680.547N (David and Joel, 2018)

2.2.2 Volume of hopper (V_h)

$$V_h = \frac{W_p}{g p_p} \qquad \text{eqn. (1)}$$

Where V_h =Volume of the machine hopper unit, w_p =weight of the plastic material in N, p_p = bulk density of plastic material and g = 9.81 m/s^2

$$V_h = \frac{25 \text{ x } 10}{9.8 \, x \, 970} = 0.0263\text{m}^3$$

2.2.2 The shredding unit

This is the compartment where the shredding process takes place. It consists of a shaft on which are mounted blades which are equally spaced as shown in Figure 1 and a stationary blade which rubs against the rotating blade to induce shredding. The compartment is made of two halves of a cylinder as shown in Figure 2. the upper half of the cylinder allows for un-shredded plastic intake and the lower half is perforated to allow for shredded plastic outlet. The size of the shredded plastic is dependent on the size of the perforations.

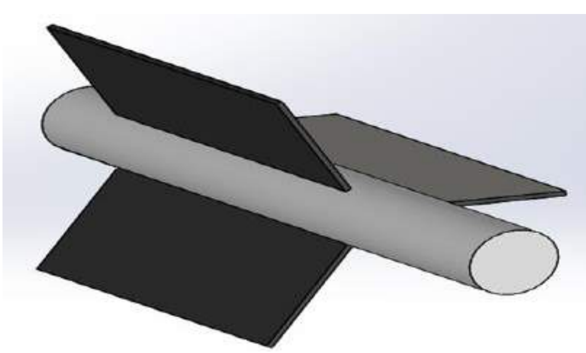

Figure 1: Shaft with shredding blades

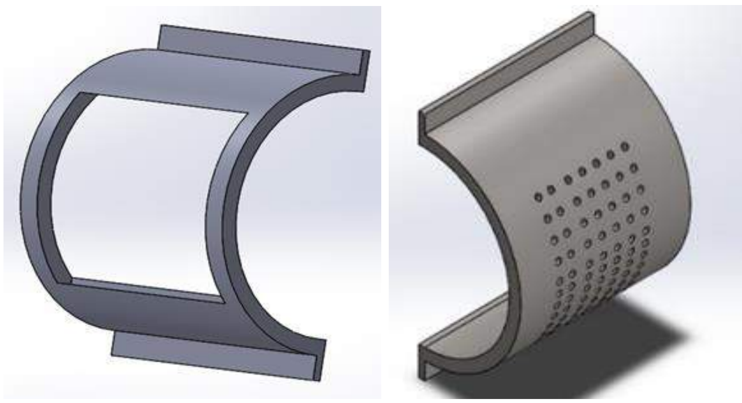

Fig. 2: Upper and lower halves of shredding compartment.

Basically there are two forces that exist on the impeller blade depending on its state of motion. These are the centrifugal force (F_C) on the rotor blade associated with dynamic motion of the blade and weight (W_g) of the blade associated with the static state of the blade. [1]. The centrifugal force (F_c) is responsible for the shredding of plastic. It is given by

$F_c = m\varpi^2 r = e V\varpi^2 r$ eqn. (2)

$F_c = 1423.25Nm^{-2}$ (Oke, 2007]

ρ = density of the blade material (mild steel=$7850kgm^{-3}$)

$\varpi = \frac{2\pi N}{60}$ = angular velocity of the blade (rad/s)

N = speed of rotation (rpm)

$V_c = \varpi r$ = peripheral velocity = $2\pi rN = 2 \times 3.142$

V= volume of the blade = l x b x t eqn. (3)

Where;

l = length of blade (mm) = 100mm

b = breadth of blade (mm) = 90mm

t = thickness of blade (mm) = 12mm

V= 100 x 90 x 12 = $108000mm^3$ and

Weight of single blade $W_b = (7850x10.8x10^{-5} \text{ x } 9.8) = 8.31N$

Weight of 3 blades $W_b = 8.31 \text{ x } 3 = 24.93N$

2.2.3 Load bearing on shaft

The blade and plastic exert bearing loads on the shaft when stationary or during operation. The total load bearing on the shaft = $(W_s + W_p + W_b + W_n)$ (4).

where W_s = weigth of shaft, W_p = weight of pulley, W_n= weight of plastic and W_b = weight of blade.

Weight = mg eqn, (5)

g = acceleration due to gravity

m = mass of the element given as = ρV eqn. (6)

where ρ is the density of the material and V the volume

But V= (breadth x width x thickness) {for the blades} eqn. (7)

Hence equation (3.7) becomes m = ρ x (l x b x t) eqn. (8)

g = acceleration due to gravity

Therefore W = ρ x 3lbt (for the three blades eqn. (9)

The expression in equation (9) is considered for the 3 blades exerting load alone, but in the case of additional load by the plastic shrapnel on the shaft, equation (9) can be evaluated as

$W_t = (\rho \text{ x } 3btr) + W_p + W_{n\,+} W_s$ eqn. (10)

Where W_t = total weight of blades, pulley, shaft and plastic. The term (ρV) is the product of the bulk density (ρ) of the plastic and the volume (V) of the plastic contained in the shredding chamber per batch.

But w_p = (pV)g = 7850 x vol. of pulley = (7850 x 28.278 x 10-5m^3) x 9.8 = 21.75N

Weight of the shaft (w_s) = mass of shaft x 9.8 = 2.2 x 9.8 = 11.76N

Weight of plastic (w_p) = 250N (assuming material input = material output)

Therefore; W_t = 11.6N + 21.75N + 24.93N + 250N =308.23N

2.2.4 Power required for driving the shaft

The power (P_c) required for driving the shaft = (Ws + Wp+Wb + Wn) Vc [2] eqn. (11)

The hurling speed of 30 m/s and 26m/s were required to shred plastic less than or equal to 20 mm and greater than 20 mm respectively [3]

Therefore, P_c= (11.6N + 21.75N + 24.93N + 35.28N) 30 = 2806.80 = 2.81kW

Multiply by factor of safety of 1.5 =4.215 kW

A motor of 5kW is chosen for improved shredding efficiency.

2.2.5 Belt design

Center distance between driver and driven pulleys = C = A + $[(A^2 + B^2)^{1/2}]$ eqn. (12)

Where A = $\frac{LP}{4} - \frac{\pi}{8}(D_1-D_2)$ and B = $\frac{(D1-D2)^2}{2}$

Length of the belt (LP) = 1500 mm

Diameter of the machine (driven) pulley (D_1) = 60mm

Diameter of electric motor (driver) pulley (D_2) = 30mm

A = 363.22 mm, B = 112.50 mm

Therefore, C = 743.46 mm

$\cos \theta/2 = [(D_1-D_2)/C]$, and $\theta = 175.4^0$

$\sin \beta= [(D_1-D_2)/C]$ and $\beta = 2.31^0$

the angle of wraps $\alpha_1 = [180 - \beta] = 177.69^0$ and $\alpha_2 = [180 + \beta] = 182.31^0$

The tensions in the belt are T_1 and T_2 which are tensions in the tight and slack side respectively

$T_1/T_2 = [\varrho^{u\theta}]$ eqn. (13)

But $P = [(T_1-T_2) V]$

μ = coefficient of friction of the belt material (convass stitched)

$T_c = [T_1/3]$

$(T_1 - T_c)/(T_2 - T_c) = [(\varrho^{u\theta/\sin\theta/2})]$

Therefore, $T_1 = 337.50$ and $T_2 = 230.72$

And the combined tension = 568.22N

2.2.6 Length of pulley belt

The pitch length or length of the belt is given by

$$L = 2C + 1.57\,(D_2 + D_1) + \frac{(D1 - D2)}{2C} \qquad \text{eqn. (14)}$$

where L is the belt's length in millimeters and C is the space between the driving and driven pulley centers (mm).

A belt with the designation A50 was selected from a standard table based on the power rating of the prime mover, the length of the belt, the distance between centers, and the correction factor for belt and angle of wrap.

2.2.7 Shaft design

Strength, rigidity, and stiffness may be taken into consideration when designing the shafts.

If these are considered for the plastic shredder, the following conditions have to be put into consideration

a. If the shaft is subjected to twisting moment or torque only

b. If it is subjected to bending moment only

c. If it is subjected to fluctuating loads

d. If it is subjected to combined twisting and bending moments

e. If it is subjected to axial loads in addition to combined torsion and bending loads

The shaft is built to withstand varied loads due to the machine's type of operation. This is because it experiences variable bending moments from the movement of bulk materials in plastic, as well as variable torque from rotation at its neutral axis.

The Torsion equation for shafts

$$\frac{T}{J} = \frac{\tau}{r} \qquad \text{eqn. (15)}$$

Where T = Twisting moment or torque acting upon the shaft

τ = Torsion shear stress and r= Distance from neutral axis to the outermost fibre and it is given by the expression d/2, where d is the diameter of the shaft

J=Polar moment of inertia of the shaft about the axis of rotation and for our shaft selection which is a round solid shaft, and

$J= \frac{\pi}{32} x\ d^{4}$

The equation (17) from substitution of the above expressions can now be written as

$\frac{T}{\frac{\pi d^4}{32}} = \frac{\tau}{\frac{d}{2}}$ or $T= \frac{\pi}{16} x\ \tau\ x\ d^3$

Therefore; $T= \frac{\pi}{16} x\ \tau\ x\ d^3$ eqn. (16)

For the mild steel shaft material in focus, τ =440mpa=440N/mm^2, and d = 20mm

Equation (14) may be used to determine the diameter of the round solid shaft assuming it is subjected to twisting moment only.

Also if the shaft is subject to bending moment only, with plastic, then the diameter can be determined as follows from first principle,

$M/I = \sigma_b/y$. eqn. (17)

Where M = bending moment, I= moment of inertia of cross sectional area of the shaft about the axis of rotation, σ = bending stress and y = distance from neutral axis to the outer most fiber.

Thus for round solid shaft, $I = \frac{\pi}{64} x\ d^4$ and y = d/2, Hence substituting these values into equation (15) we have

$\frac{M}{\frac{\pi d^4}{64}} = \frac{\sigma_b}{\frac{d}{2}}$ or $M= \frac{\pi}{32} x\ \sigma_b\ x\ d^3$

Therefore; $M = \frac{\pi}{32} x\ \sigma_b\ x\ d^3$ eqn. (18)

However, as previously said, our shaft is supposed to be subjected to varying loads, which results in varying torque and bending moment; as a result, the total of the shock and fatigue factors is taken into consideration to compute the twisting moment (T) and bending moment (M).

The corresponding twisting moment for the bending and torsion coupled,

$T_e = \sqrt{\{(K_m\ x\ M)^2 + (K_t\ x\ T)^2\}}$ eqn. (19)

And the equivalent bending moment is given as

$M_e = \frac{1}{2}[K_m\ x\ M + \sqrt{(K_m\ x\ M)^2 + (K_t\ x\ T)^{2}}$. eqn. (20)

where:

K_m = Combined shock and fatigue factor for bending

K_t = Combined shock and fatigue factor for torsion

M = Bending moment, and T = Twisting moment or Torque

For recommended values for K_m and K_t see appendix one of this literature.

For the shaft to transmit a power of 5kW = 5 x 10^3W

The diameter of the shaft to transmit the power is calculated thus

Vertical forces acting on the shaft are:

a. Weight of plastic inside hopper acting within a length of 200 mm

b. Weight of shaft

c. Weight of pulley

Length of shaft used = 400 mm

Using moment about a rigid supported shaft, R_1= 44.65N

Vertical bending moment (Mv) at point A (weight of plastic) and B (weight of pulley) = 0

Taking moment about the shaft weight at a point c

35.28 x 0.1 = 3.53Nm

And at point d (moment about R_1) = 21.75 x 0.15 = 3.26N

Horizontal forces acting on the shaft are:

a. Weight of a pair of hammer

b. Weight of shaft

c. Tension on the belt (T1 + T2) = 568.22 N

Taking moment about B (point of active belt tension)

R_2 = 32.42, moment at point of shaft weight = 24.93 x 0.1 = 2.49Nm

Moment about R_2 = 568.22 x 0.15 = 85.23Nm

Resultant bending moment at point where weight of shaft acts

$= M_b = [(M_v)^2 + (M_h)^2]^{1/2}$

$= 3.53^2 + 2.49^2 = 4.31$Nm

And at point R_2, $M_b = [(M_v)^2 + (M_h)^2]^{1/2} = 3.26^2 + 85.23^2 = 85.30$

The maximum is taken of the bending moment = 85.30

Torsional moment = P/2πn

Where n = speed (rev/h)

Maximum speed of the machine = 30 m/s

But 2πrad = 1rev,

$V_c = \frac{2\pi N}{60}$

Hence, M_t = 23.84 Nm

The diameter of the shaft which is given as $d^3 = 16/\pi S_s[(K_bM_b)^2 + (K_tM_t)^2]^{1/2}$

Where d = diameter of shaft

Ss = allowable stress (55 MN/m^2 for shaft without keyway and 40 MN/m2 for shaft with keyway

Therefore, d = 28.5mm.

A shaft of diameter 40mm was utilized to optimize the machine efficiency since the electric motor power rating was also increased.

Kb factor for suddenly applied load = 2

Kt factor for suddenly applied load = 2

2.2.8 Critical speed of the shaft

Even in the absence of an external load, every rotating shaft experiences rotational deflection. At a particular speed, referred to as the Critical Speed, the combined weight of a shaft and wheel might cause deflection that will produce resonant resonance.

Using the Rayleigh-Ritz formula,

Critical speed of the shaft is $N_c = (30/\pi)\sqrt{g/\delta st}$ eqn. (21) [4]

Where g = acceleration due to (9.81 m/s2) and δst = total maximum static deflection

According to best practices, the maximum operation speed shouldn't be higher than 75% of the critical speed.

The maximum static deflection of the rotating I shaft and (ii) load are added to give the total maximum static deflection (st).

For the palm kernel cracking machine, the shaft assemble is of the type below

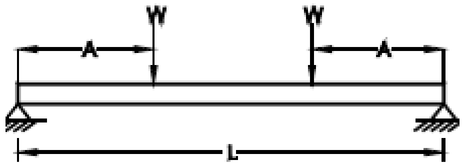

Maximum static deflection on the shaft (δstI) = $5wL^3/384EI$ eqn. (22)

= $5x(0.4x15.40)x0.4^3/384x200x10^8x306.79 \times 10^{-9} = 8.36x10^{-7}$

b) Maximum static deflection on load = WA $(3L^2 - 4A^2)/24EI$ eqn. (23)

Where: W_s = weight of shaft, kg, W_w = weight of wheel in kg, E = modulus of elasticity, kg/m^2 (for steel shaft=200 x108 kg/m^2), I = moment of inertia=ðD4/64 = 306.79 x 10^{-9} for shaft diameter of 50mm and L = length of shaft = 400mm

= $2.175 \times 0.25(3x0.4^2 - 4x0.25^2)/24x200\ x10^8x306.79 \times 10^{-9} = 1.76 \times 10^{-7}$

Total maximum static deflection (δ_{st})

$\delta st = \delta st_1 + \delta st_2$ = 0.000000836 + 0.000000176 = 0.0001012

Nc = (30/π) √g/δst = 2971rpm

Safety factor is 25%, hence maximum operation speed = 0.75x2971 = 2228

2.2.9 Torsional rigidity of the shaft

Depending on the application for solid circular shafts, the permitted angle of twist is either 0.3 or less than or equal to 3.0.

A torsion solid shaft's angular deflection can be represented as

$\theta = 584M_tL/ Gd^4$ eqn. (24)

Where

θ = angular shaft deflection (degrees)

L = length of shaft (m)

G = torsional modulus of elasticity, (kg/m^2) = 7.30 GN/m^2 of the shaft material

D = diameter of shaft

$=584 \times 0.4 \times 23.84/ 7.3x\ 0.04^4 = 2.03^0$

2.2.10 Bearing selection

An evaluation of some governing conditions guided the selection of the bearings used for supporting the rotating shafts. The conditions evaluated includes the followings

a) The roller contact bearings were selected rather than the slider contact bearing for the following reasons; It's low starting and running friction within the desired low speed, its ability to withstand momentary shock loads, accuracy of shaft alignment and low cost of maintenance.

b)The desired speed to be transmitted from the shaft as supplied from the motor is less than 2000rpm

c) The bearings required needed to have ability to bear load at this speed

d) The minimum static and dynamic load rating of the bearing has to exceed the bearing load of the shaft.

The aforementioned information alongside other conditions as coefficient of friction and bore diameter of the bearing, which are calculated and matched from reference and manufacturers manual gives a better selection from series of potential bearing for the nature of machine.

2.2.11 Dynamic equivalent load for rolling contact bearings (del)

Under this constant stationary axial or radial load, a bearing with a rotating inner ring and a stationary outer ring would have the same lifespan as it would under the actual load and rotation conditions. [5]

For the radial and angular contact bearings operating under a combined constant radial load (W_R) and constant axial or thrust load (W_A), the total load W is given by equation (25).

$$W = X.V.W_R + Y.W_A \qquad \text{eqn. (25)}$$

Where;

V = A rotation factor = 1 for all types of bearings when the inner race is rotating

2.2.12 Rolling contact bearing dynamic load rating under variable loads dlr

C stands for the constant stationary load (constant axial load for radial ball or roller bearings) that a collection of allegedly comparable bearings with a stationary outer ring can support throughout the course of 500 hours of operation at 33.3 rpm or one million rotations, whichever comes first (in the case of thrust ball or roller bearings). [5]

It is given as

$$C = W (L / 10^6)^{1/k} \qquad \text{eqn. (26)}$$

where W= equivalent dynamic load

L= service life rating of the ball or roller bearing

The relationship between the life in revolution L and the life in working hours L_H is given by

$L = 60N.L_H$ revolutions where N = the speed in rpm

k = 3, for ball bearings and 10/3 for roller bearings

3.0 Fabrication

In the course of fabrication of the plastic shredding machine, various manufacturing processes were carried out. Some of the manufacturing operations include the followings:

1. Marking out;
2. Cutting Operation
3. Fitting
4. Joining Operation
5. Grinding Operation
6. Drilling and Boring
7. Finishing

Figure 3: Fabricated waste plastic shredder

4.0 Results and Discussion

S/N	Reading)	Test operation 1	Test operation 2	Test operation 3	Average
1	Mean weight of plastic fed into machine (kg)	25	25.02	25.02	25.01
2	Average shredding time (min)	72	75	74	73.7
3	Mean weight of shredded plastic waste (kg)	24.2	23.7	23.9	23.93

Table 1: Test results for bulk material balance of plastic shredding.

Stress analysis also carried out on the shaft and blade assembly is shown in Figure 4.

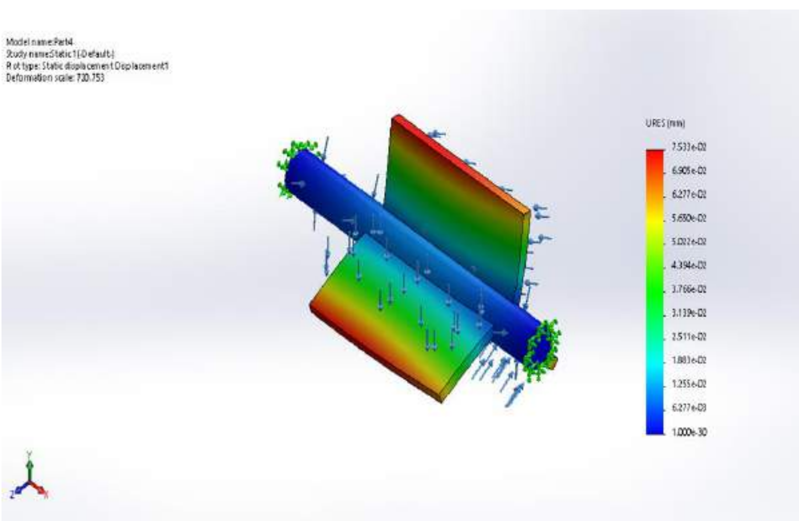

Figure 4: Static 1-Displacement-Displacement1

Machine throughput capcity = $\frac{Average\ weiht\ of\ shredded\ plastic}{Average\ time\ for\ plastic\ shredding} = \frac{23.93}{73,7}$ = 0.325kg/min

$$\text{Machine shredding efficiency} = \frac{Mean\ weight\ of\ shredded\ plastic\ (output)}{Mean\ weight\ of\ un{-}shredded\ plstic\ loded\ in\ nachine\ (input)} \times 100$$

$$= \frac{23.93}{25.01} = 95.7\%$$

Tables 1 shows the result for bulk material balance of plastic shredding. It was observed that it took an average time of 73.7 minutes for the plastic shredding machine to shred the given amount of load input of 25kg of plastic waste. This gave a machine throughput capacity of 0.325kg per second. Also the efficiency of the machine was calculated as 95.7% which was in close agreement with other research works done by various authors like David and Joel (2018) who reported plastic shredding machine efficiency of 98%,

Figure 4 shows the stress analysis carried out on the shaft and blade assembly. It was observed that the stress concentration was at the sharp edges of the blade (coloured red) which are the edges which does the actual shredding of the plastic by shearing them against stationary blades. The ease of shredding of plastic is aided by pre pressing of the plastic waste such as PET bottles before being fed into the machine to avoid loss of grip by the blades since the smooth body of the pet bottles may limit their firm hold by the blades and they can bounce off.

5.0 Conclusion

The plastic shredding machine was successfully designed, fabricated and tested. Preliminary results from its test operation showed that it is effective in the shredding of plastics bottles made from polyethylene terephthalate which are common plastic materials that litter our environment because of their abundant and commercial use for water and other liquid holding wares in our environment. The plastic shredding machine is a viable waste recycling machine that can be commercialized to recycle plastic waste as a raw material for new plastic ware production. In Europe (EU-27), 59.6% of plastics were recovered and recycled in 2011, while 61.9% were recycled in 2012 (EU-Plastics). However, in Africa less than 4% of its plastics waste despite its annual generation of about 16million tones of plastic waste which is 6% of plastic waste generated globally [6,7]. In Nigeria, a large proportion of the plastic garbage produced is not recycled. Instead, a large portion of it winds up in bodies of water like rivers, lakes, drains, lagoons, and the ocean. Considering these, the present research remains a viable means of plastic recycling in Nigeria.

References

[1] Babatunde, O. O., and Okoli, J. O., (1988). Investigation into the Effect of Nut Size on the Speed needed for Cracking Palm Nut in Centrifugal Nut Cracker. Nigerian journal of palm and oil seeds, 9(1): 84 – 88.

[2] David, A and Joel, O.O. (2018). Design and Construction of a Plastic Shredder Machine for Recycling and Management of Plastic Wastes. International Journal of Scientific & Engineering Research Volume 9, Issue 5, May-2018 1379 ISSN 2229-5518.

[3] Jimoh, M. O. and Olukunle, O. J. (2013). Design of an effective automated Machine for quality palm kernel production. Journal of Mechanical and Civil Engineering (IOSR– JMCE). ISSN: 2278 – 1684, Vol. 6, Issue.1, pp. 89-97, www.iosr journals.org.

[4] Khurmi, R.S. and Gupta, J.K. (2005) A Textbook of Machine Design. 14th Edition, Eurasia Publishing House (PVT.) Ltd, Ram Nagar, New Delhi.
[5] Kruger (1998). Critical speeds shafts. Technical bulletin tbn017.0/1998
[6] Oke, P.K. (2007). Development and Performance Evaluation of Indigenous Palm Kernel Dual Processing Machine. Journal of Engineering and Applied Science 2(4): 701-705. Copyright Medewell Journals.
[7] Olakanmi, E. O. (2004). Development and Performance Testing of a Palm Kernel Cracker. Compendium of Engineering Monographs, pp. 11

NIPES-NCEE Conference Proceedings
The 2nd International Conference 15th-17th Feb. 2023
146-157
www.nipesjournals.org.ng

SECURITY ISSUES IN DIGITAL LEARNING SPACES AND PREVENTIVE MEASURES

(A CASE STUDY OF NATIONAL OPEN UNIVERSITY OF NIGERIA)

UMAR MUKHTAR[1]; AMINU TUKUR[2]

[1] *Directorate of Management Information Systems, National Open University, Abuja.*
[2]*Department of Mathematics and Computer Science Borno State University, Maiduguri.*
[1]*umakhtar@noun.edu.ng*, [2]*tukuraminu@bosu.edu.ng*

Abstract

During the COVID-19 pandemic the demand for digital learning space became higher like never before for academic institutions of learning, with learning institutions going fully online for the delivery of training and education, cybercriminals have more opportunities in taking advantage of vulnerable LMS to steal sensitive information or deploy ransomware. Irrespective of the cybercriminals motive, a compromised system has serious consequences on institutions. Institutions need to invest in choosing the most secured LMS and apply the required security controls as recommended in this paper. The National Open University of Nigeria (NOUN) implements its digital learning spaces using the Moodle LMS. Based on the 2022 CVE and the 2021 OWASP top ten analysis, vulnerabilities are found in some specific versions of Moodle. The 2021 OWASP top 10 vulnerabilities are: Broken Access Control, Cryptographic Failures, Injection, Insecure Design, Security Misconfiguration, Vulnerable and Outdated Components, Identification and Authentication Failures, Software and Data Integrity Failures, Security Logging and Monitoring Failures, and Server-Side Request Forgery. A secured learning platform should incorporate all the aspects of security without affecting too much the system performance. Security risks in learning institutions increased significantly with the COVID-19 and it is very important to consider security during design. A system needs to implement security services such as authentication, encryption, access control, and managing users and their permissions. This paper studied the CVSS of Moodle and recommended the implementation of all preventive measures recommended for the 2021 OWASP top 10 vulnerabilities.

Keywords:

LMS: Learning Management System

CVE: Common Vulnerability and Exposure

CVSS: Common Vulnerability Scoring System

OWASP: Open Web Application Security Project

1. INTRODUCTION

National Open University of Nigeria (NOUN), is the most comprehensive Open and Distance Learning (ODL) institution in Nigeria, with about five hundred and thirty-three thousand eight hundred and forty-nine (533,849) student enrollment [1]. Presently, NOUN operates one hundred and three (103) study centers spread across the geopolitical zones of Nigeria equipped with requisite physical infrastructure, human and material resources with top-notch ICT competencies for learning, in compliance with the best global standards of education in all accredited programmes [1]. It is the only university mandated for the delivery of education in the ODL mode, thus, it is a single-mode ODL university. NOUN has a comprehensive and very impressive ICT infrastructure through which it achieves all its ICT mandates. These ICT infrastructures are managed through its three (3) directorates, the Directorate of Information and Communications Technologies (DICT), the Directorate of Management Information Systems (DMIS) and the Directorate of Learning Content Management Systems (DLCMS). The dynamic nature of ICT has continued to extend the shape and scope of ODL, and ODL institutions have a lot to achieve. With ODL, learners would not be obligated to join lessons or even active interactions, except there are convincing explanations to validate the interaction, such interaction may be periodic online facilitation, scheduled practical contacts and examinations [2].

The internet facilitates and enhances the learning process through the use of devices such as computers and digital mobile devices, such as smart phone and tablets. Educational resources are available on the internet through text, images, links to other online resources, audio and video presentations. These educational resources together with other features such online forums and chats make up a digital learning space or in another setting a virtual classroom coordinated by a facilitator who plans the activity for the students and discusses aspects of the course using a discussion section of the virtual class [3].

Security is at the top of the priority list of any institution or any organization that utilizes information technology, phishing is still one of the most current and effective techniques that attackers use to compromise accounts and gain access to company data and resources [4]. With the rapid change and massive disruption in the development of educational systems and the necessity of developing applications that can be accessed over the internet, the security of digital learning space has become a serious concern, IT teams are facing increased pressure to navigate the challenges, bad actors are creating new techniques to attacks and scams unsuspecting victims every day. Meeting the security requirements in a digital learning space is an extremely compound problem because it is necessary to protect contents, services, personal data and other infrastructure from external and internal threats [5]. The surge in remote work due to the COVID-19 pandemic, cyber-attacks and data breaches have taken a significant leap forward [6]. For example, the most targeted areas by attacks are healthcare, energy, financial, pharmaceutical, technology, industrial, online service providers, entertainment, and education [7]. Between March 2021 and March 2022, the average cost of a data breach in the healthcare sector amounted to over 10 million U.S. dollars, up from 9.23 U.S. dollars between May 2020 and March 2021. As of 2022, the average cost of a data breach in the financial industry worldwide was 5.97 million U.S. dollars, up from 5.72 U.S. dollars in 2021. The global average cost of a data breach across all studied industries was 4.35 million U.S. dollars, data breaches in the public sector cost an average of 2.07 million U.S. dollars during the measured period [8]. The educational systems are among the sectors most affected by cyberattacks and are even more so since the arrival of coronavirus [9], where with education is now more online. According to [10], 28% of critical infrastructure organizations included those in the financial services, industrial, technology, energy, transportation, communication, healthcare, education and public sector industries experienced a destructive or ransomware attack, while 17% experienced a breach because of a business partner being compromised. According to [11] in 2021 the most common type of cybercrime as reported to the U.S. Internet Crime Complaint Center was phishing and similar fraud, with approximately 324 thousand individuals affected. In addition, nearly 52 thousand cases of personal data breaches were reported to the IC3 during that year.

2. METHODOLOGY

2.1 Research Methodology

Qualitative research methodology was used to find the vulnerabilities and the exposures of the Moodle LMS using the OWASP top 10 2021 vulnerabilities classification and Common vulnerabilities and exposure (CVE) of Moodle LMS.

2.2 Moodle LMS

Moodle is a learning platform designed to provide educators, administrators and learners with a single robust, secure and integrated system to create personalised learning environments. Users can download the software onto personal web server. Moodle is built by the Moodle project which is led and coordinated by Moodle HQ, which is financially supported by a network of over 80 Moodle Partner service companies worldwide. Moodle is trusted by institutions and organisations large and small, including Shell, London School of Economics, State University of New York, Microsoft and the Open University. Moodle has a worldwide number of more than 213 million users (As of 2020-06-15) across both academic and enterprise level usage makes it the world's most widely used learning platform [12].

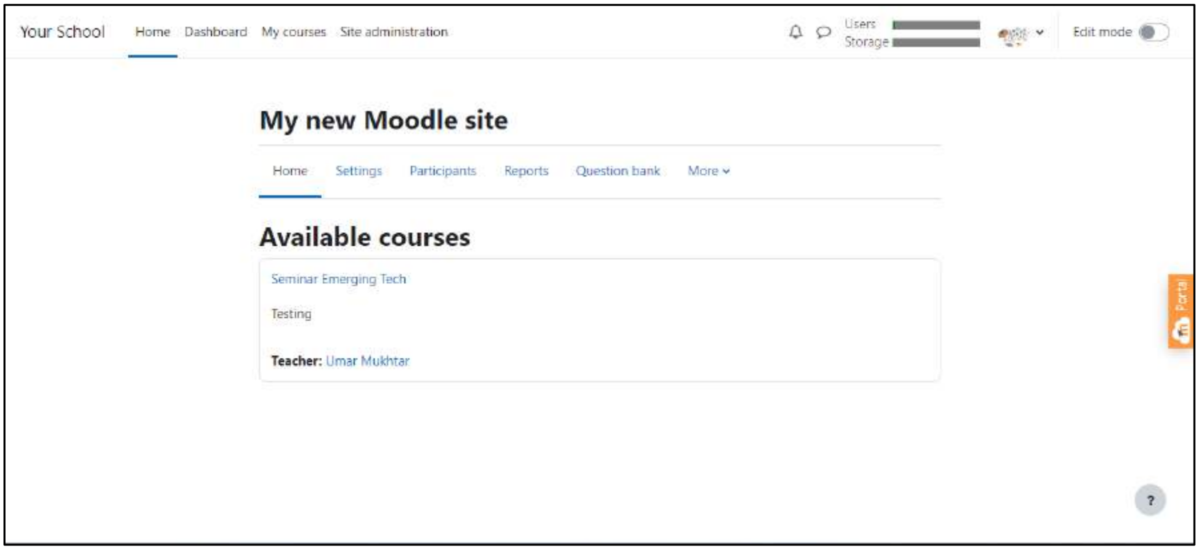

Figure 1. Sample Moodle Site

The main delivery channel of education and training in the National Open University of Nigeria is through the internet using the Moodle Learning Management System (LMS) platform, so maintaining the security of the LMS is essential through finding and fixing vulnerabilities. LMS, being a web application, it is evident that it inherits all security issues of software, web applications and video conferencing tools, thus all digital educational services, contents and personal data are exposed to internal and external threats. Digital learning spaces have faced issues connected to security, availability, and reliability during the covid19 crisis. Educational institutions had move in full gear towards digital learning immediately with no or partial security strategies. It is important to ensure the security and privacy of digital learning space data and information with a consistent and practical knowledge of these security issues, as well as how to avoid and or practically manage such security issues. To overcome challenges, a practical prevention knowledge is required to protect data and information of all digital learning spaces users.

3. Results and Discussion

Below are the OWASP top 10 2021 classification, the most common web-based application vulnerabilities and recommended preventive strategies:

1. Broken Access Control: Access controls are critical for securing applications against unauthorized access to data and resources. Broken access controls can lead to data compromise, obtaining permissions beyond what's intended for standard users, or account takeover attacks where outsiders hijack user accounts and initiate fraudulent transactions. This vulnerability jumped from 5th position in 2017 to 1st in 2021, reflecting that it was found in 94% of tested applications. Common vulnerabilities in this risk category include application logic faults that bypass access control checks by allowing users to change parameter values or force browse to certain URLs. From a decision-making perspective, it's critical to emphasize the importance of shifting security left in the development cycle. Access controls are harder to implement later, so communicate the importance of implementing proper access controls, such as denying requests by default and rate limiting APIs early on in web app development. Access control is only effective in trusted server-side code or server-less API, where the attacker cannot modify the access control check or metadata.

2. Cryptographic Failures: Cryptographic failures refer to either a bad implementation of encryption or a complete lack of encryption. The major consequence of a cryptographic failure is that you can potentially expose sensitive data. The exposure of sensitive data can pose compliance, reputational, or competitive business risks depending on what information is not adequately protected by encryption. With the average data breach cost at an all-time high of $4.35 million in 2022, businesses can't afford to slip up with cryptography. Critical to preventing cryptographic failures is first classifying the data that any web app processes, stores, or transmits. Then, you can identify the sensitive data assets and ensure they're encrypted both at rest and in transit. A modern encryption solution that uses up-to-date and strong standard algorithms centralizes encryption and encryption key configuration, and manages the encryption key lifecycle is a prudent investment. Minimal prevention is to classify data processed, stored, or transmitted by an application. Identify which data is sensitive according to privacy laws, regulatory requirements, or business needs.

3. Injection: Injection is a risk category that refers to the ability of threat actors to provide malicious input to web applications that result in the app executing unexpected and unwanted commands. Injection occurs when the app can't distinguish malicious input from its code. Common injection attacks include SQL injections that insert malicious SQL queries into input fields or JavaScript injections that load malicious code into the client-side of the web app. Injection attacks can lead to various negative outcomes, including denial of service, privilege elevation, and data breaches. An important strategic element of mitigation is encouraging the use of tools that help to detect injection vulnerabilities in code. Since there are several different injection attacks, you may need more than one tool for thorough testing. Injection can be prevented by keeping data separate from commands and queries.

4. Insecure Design: This is an entirely new category for the OWASP Top Ten, focusing broadly on application design and architectural flaws that lead to increased security risks. When an application is inherently designed in an insecure way, even a perfect implementation of security controls and risks can't compensate for those design weaknesses. Sophisticated threat actors will eventually find and exploit design flaws. At a high level, one of the most important mitigation tips is to mandate the use of threat modeling for software development teams. Threat modeling should use the structure and data flow inherent to a specific web app to trace out the key technical threats that could exploit the system. To trace out the threats, try to answer the question, “what can go wrong here?” The STRIDE model is a good place to brainstorm because it focuses on important types of application security threats and controls for preventing them. Establish and use a secure development lifecycle with AppSec professionals to help evaluate and design security and privacy-related controls.

5. Security Misconfiguration: This category of risks relates to the security components in an application being incorrectly configured. Misconfigurations are increasingly common due to the cloud being used as a development environment and web apps being built with container images. The infrastructural complexity adds more points at which security misconfigurations can occur. In the data gathered by OWASP, current Top Ten, there were over 200,000 detected instances of security misconfigurations in web apps. The challenge with mitigating security misconfiguration risks from a strategic standpoint is that they cover the whole application stack and the app’s infrastructure. Individual errors are often at play here, such as opening unnecessary ports, not changing default passwords, or leaving cloud storage buckets open. A pivotal strategic change is to ensure you have a repeatable process for hardening configurations and a tool or process that automatically audits and verifies those configurations across on-premise and cloud environments. Secure installation processes should be implemented, a repeatable hardening process makes it fast and easy to deploy another environment that is appropriately locked down. Development, QA, and production environments should all be configured identically, with different credentials used in each environment. This process should be automated to minimize the effort required to set up a new secure environment. A minimal platform without any unnecessary features, components, documentation, and samples. Remove or do not install unused features and frameworks.

6. Vulnerable and Outdated Components: Web apps comprise many components or building blocks from external sources (libraries, frameworks, etc.). These components handle both back-end and front-end functionality. When threat actors try to compromise an application, they look at its component parts and attempt to exploit any vulnerabilities. Often, these vulnerabilities come from using out-of-dated frameworks or libraries that are easy to exploit. The overall strategic mitigation here is to ensure an effective patch management strategy is in place. Part of that strategy entails maintaining an inventory of all the components in your apps and the respective versions of those components the app is running. Ideally, is to to automate the inventory step with a digital inventory solution. There should be a patch management process in place to remove unused dependencies, unnecessary features, components, files, and documentation.

7. Identification and Authentication Failures: Failures in authentication and identity management make applications vulnerable to threat actors masquerading as legitimate users. Some examples of vulnerabilities include not setting validity periods for session IDs, permitting weak passwords that are easy to guess, and not rate limiting login attempts against automated attacks. The solutions include implementing multi-factor authentication in apps and communicating the importance of complying with recommended password length, complexity, and rotation policies to developers and do not ship or deploy with any default credentials, particularly for admin users.

8. Software and Data Integrity Failures: This is another new risk category in the OWASP Top Ten, and it's all about making faulty default assumptions within development pipelines about the integrity of software or data. Since web apps regularly rely on plugins and libraries from external sources, a lack of verification of the integrity of these sources introduces the risk of malicious code, unauthorized access, and compromise. The main mitigation strategy is ensuring external code or data hasn't been tampered with by requiring digital signatures.

9. Security Logging and Monitoring Failures: Logging and monitoring help to provide security accountability, visibility into events, incident alerting, and forensics. When there are failures in these capabilities, your company's ability to detect and respond to application breaches becomes severely compromised. To mitigate, use open source or proprietary tools to correlate logs, implement monitoring and alerting, and create an incident recovery and response strategy using established guidelines, such as National Institute of Standards and Technology (NIST) 800-61r2 or later.

10. Server-Side Request Forgery (SSRF): SSRF is one of the two OWASP Top Ten risks added based on the community survey rather than data from web apps. Most web apps today require external resources for their functionality, which are usually accessed at URLs. SSRF occurs when hackers can get servers to make requests that they control. The typical vulnerability is that the web application doesn't validate the user-supplied URL, potentially allowing access to internal services or resources by bypassing access controls. The strategic concept of defense in depth is important here; multiple controls at the application and network layers can help to prevent SSRF. Client-supplied input data should be validated and sanitized, while network segmentation can also help.

3.1 Common Vulnerabilities and Exposures

Common vulnerabilities and exposure (CVE) give a unique name to known vulnerabilities. The objective of CVE is to facilitate sharing information over different databases and make available a common platform to evaluate security tools [13]. Its mission is to identify, define, and catalog publicly disclosed cybersecurity vulnerabilities [14]. Security experts and researchers examine applications to find vulnerabilities, and when they find a new vulnerability, they give a unique identifier to each one to help security analysts to deal with them. The format of the CVE consists of three portions: the first one is fixed "CVE", the second part is the year of release, and the third is a serial number, for example, CVE-2022-0334 was a flaw found in Moodle, in versions 3.11 to 3.11.4, 3.10 to 3.10.8, 3.9 to 3.9.11 and earlier unsupported versions, the description of the vulnerability is "insufficient capability checks could lead to users accessing their grade report for courses where they did not have the required gradereport/user: view capability."

CVE makes a unique definition of each vulnerability to allow sharing this information between tools and services, when a new vulnerability is discovered, it is assigned an ID according to the CVE Numbering Authority (CAN) that writes a description and references, and then this information is posted on CVE website, the description includes the software versions that are affected and the impact of the vulnerability, CVE is designed to allow vulnerability databases. The US Department of Homeland Security funded MITRE to copyright the CVE list for the benefit of the community to assure that this database is available for everyone as an open-source through their website https://www.cve.org.

According to the CVE 2022 classification, the top 25 most dangerous software weaknesses are out-of-bounds write, improper neutralization of input during web page generation (cross-site scripting), improper neutralization of special elements used in an SQL command (SQL injection), improper input validation, out-of-bounds read, improper neutralization of special elements used in an OS command (OS command injection), use after free, improper limitation of a pathname to a restricted directory (path traversal), cross-site request forgery (CSRF), unrestricted upload of file with dangerous type, null pointer dereference, deserialization of untrusted data, integer overflow or wraparound, improper authentication, use of hard-coded credentials, missing authorization, improper neutralization of special elements used in a command (command injection), missing authentication for critical function, improper restriction of operations within the bounds of a memory buffer, incorrect default permissions, server-side request forgery (SSRF), concurrent execution using shared resource with improper synchronization (race condition), uncontrolled resource consumption, improper restriction of XML external entity reference, improper control of generation of code (code injection).

Table 3.1: Comparison between Vulnerability and Exposures

Sn.	Vulnerability	Exposures
1.	Allows the hacker to intrude a system or network due to an error in the software code.	Make the data accessible to the attacker to be misused or sold.
2.	Allows the hacker to execute commands with unauthorized permissions.	Facilitate data gathering activities for the attacker.
3.	Allows the hacker to get information that is restricted.	Allows the hacker to conceal activities.
4.	Allows the hacker to act like another entity.	Is considered as the main entry point by an attacker to access the information.
5.	Allows the hacker to deny service.	Is an issue in the security policy.

[15]

3.1.2 Common Vulnerability Scoring System

Common Vulnerability Scoring System (CVSS) is an open framework that was launched in 2005 to measure the characteristics and severity of CVEs. CVSS supply a qualitative measure of severity. CVSS is not a measure of risk. CVSS consists of three metric groups: Base, Temporal, and Environmental. The Base metrics produce a score ranging from 0 to 10, where 10 is the most severe, which can then be modified by scoring the Temporal and Environmental metrics. A CVSS score is also represented as a vector string, a compressed textual representation of the values used to derive the score. Thus, CVSS is well suited as a standard measurement system for industries, organizations, and governments that need accurate and consistent vulnerability severity scores. Two common uses of CVSS are calculating the severity of vulnerabilities discovered on one's systems and as a factor in prioritization of vulnerability remediation activities. The National Vulnerability Database (NVD) provides CVSS scores for almost all known vulnerabilities. The NVD provides CVSS 'base scores' which represent the innate characteristics of each vulnerability. The NVD does not currently provide 'temporal scores' (metrics that change over time due to events external to the vulnerability) or 'environmental scores' (scores customized to reflect the impact of the vulnerability on your organization). However, the NVD does supply a CVSS calculator to allow individuals and organisations to add temporal and environmental score data. CVSS is owned and managed by FIRST.Org, a US-based non-profit organization, whose mission is to help computer security incident response teams across the world, [16].

Table 3.2 Vulnerability Severity Levels

Sn.	**Severity Level**	**Score Range**
1.	Critical	9 - 10
2.	High	7.0 – 8.9
3.	Medium	4 – 6.9
4.	Low	0.1 – 3.9
5.	Information	0

[17]

The National Vulnerability Database (NVD) is the U.S. government repository of standards-based vulnerability management data represented using the Security Content Automation Protocol (SCAP). This data enables automation of vulnerability management, security measurement, and compliance. The NVD includes databases of security checklist references, security-related software flaws, misconfigurations, product names, and impact metrics.

3.2 OWASP Top 10 Vulnerabilities 2021

Open Web Application Security Project (OWASP), is a nonprofit organization focused on software security. Their projects include a number of open-source software development programs and toolkits, local chapters and conferences, among other things. One of their projects is the maintenance of the OWASP Top 10, a list of the top 10 security risks faced by web applications. It is a list of the 10 most common web application security risks. Developers can create secure applications that keep their users' confidential data safe from attackers with these risks in mind, by writing code and performing robust testing. The OWASP top 10 isn't just a list, it assesses each flaw class using the OWASP Risk Rating methodology and provides guidelines, examples, best practices for preventing attacks, and references for each risk. By learning the flaws on the OWASP Top 10 chart and how to resolve them, application developers can take concrete steps toward a more secure application that helps keep users safe when it comes to malicious attacks [18].

3.3 Learning Management System (LMS)

LMS is a technology tool that provides functionalities beyond the instructional context such as management tracking, personalized instruction, and facilitative learning [19]. It is used by education institutes, and other organizations to manage the whole learning process and deliver e-Learning material, it can be used by any organization to deliver training for internal employees, LMS has a lot of benefits in terms of cost reduction, flexibility, and mobility. There are many Learning Management Systems, widely used LMS's include, Moodle, SAP Litmos, and TalentLMS [20].

Table 3.1 Some 2021-2022Moodle Common Vulnerability Score with high scores

Sn.	**CVE ID**	**Vulnerability Type(s)**	**Score**	**Description**
1.	CVE-2021-21809	Exec Code	9	A command execution vulnerability exists in the default legacy spellchecker plugin in Moodle 3.10. A specially crafted series of HTTP requests can lead to command execution. An attacker must have administrator privileges to exploit these vulnerabilities.
2.	CVE-2021-3943	Exec Code	7.5	A flaw was found in Moodle in versions 3.11 to 3.11.3, 3.10 to 3.10.7, 3.9 to 3.9.10 and earlier unsupported versions. A

				remote code execution risk when restoring backup files was identified.
3.	CVE-2022-0332	Sql	7.5	A flaw was found in Moodle in versions 3.11 to 3.11.4. An SQL injection risk was identified in the h5p activity web service responsible for fetching user attempt data.
4.	CVE-2022-30599	Sql	7.5	A flaw was found in Moodle where an SQL injection risk was identified in Badges code relating to configuring criteria.
5.	CVE-2022-30600	Bypass	7.5	A flaw was found in Moodle where logic used to count failed login attempts could result in the account lockout threshold being bypassed.

(CVE, 2022)

4. CONCLUSION AND RECOMMENDATION

Organizations and institutions need to have control over all the systems they deploy. It is very important to apply higher security measures at all levels, to manage who does what, when, where and why. It will as well allow the organization to manage the security physical of physical infrastructure. This study was limited to only the security vulnerability of Moodle Learning Management Systems (LMS) based on the 2022 Common Vulnerability Exposure (CVE) and the 2021 OWASP Top Ten, there are a lot more available LMS systems that are widely used by institutions and organizations, e.g. TalentLMS, Blackboard and Canvas, are widely used and their vulnerability assessment can be carried out.

References

[1] Alexei Scerbakov, F. K. (2019). SECURITY VULNERABILITIES IN MODERN LMS. *Researchgate Conference Paper.* Researchgate.
[2] Bradley, V. M. (2021). Learning Management System (LMS) use with online instruction. *International Journal of Technology in Education (IJTE)*.
[3] CGI Cyber Security Team. (2020, 9 15). Retrieved from CGI Website: https://www.cgi.com/uk/en-gb/blog/cyber-security/helping-defend-against-a-30000-increase-in-phishing-attacks-related-to-covid-19-scams
[4] Ciobanu (Defta) Costinela - Luminita, C. (.-M. (2012). E-learning Security Vulnerabilities. *Elsevier*.
[5] CVE. (2022, 12 14). Retrieved from CVE: Common vulnerabilities and exposures: https://www.cve.org/
[6] Essohanam DJEKI, J. D. (2022). Preventive Measures for Digital Learning Spaces' Security Issues. *IEEE Technology and Engineering Management Conference (TEMSCON EUROPE)* (pp. 49-55). IEEE.

[7] Habib Ibrahim, S. K. (2020). A Study on Cybersecurity Challenges in E-learning and Database Management System. *Researchgate Conference Paper.* Researchgate.
[8] IBM Security. (2022). *Cost of a Data Breach Report 2022.* NY: IBM.
[9] Moodle. (2022, 12 16). Retrieved from About Moodle: https://docs.moodle.org/400/en/About_Moodle
[10] Ms. Shikha Dua, M. S. (2016). Issues, Trends & Challenges of Digital Education: An Empowering Innovative Classroom Model for Learning. *International Journal of Science Techology and Management*, 142.
[11] Neil Kumaran, S. L. (2020, 4 17). *Google Cloud.* Retrieved from Google Cloud Blog: https://cloud.google.com/blog/products/identity-security/protecting-against-cyber-threats-during-covid-19-and-beyond
[12] NOUN. (2019). *National Open University of Nigeria (NOUN) Annual Report, 2016-2018.* Abuja: NOUN Press.
[13] NOUN. (2022, 12 11). *National Open University of Nigeria*. Retrieved from NOUN Website: https://nou.edu.ng/
[14] NUC. (2009). Guidelines for Open and Distance Learning in Nigerian Universities. *National Universities Commission*.
[15] NVD. (2023, 2 6). *The National Vulnerability Database*. Retrieved from https://nvd.nist.gov/vuln-metrics/cvss
[16] OWASP Top 10. (2022, 12 16). Retrieved from OWASP Website: https://owasp.org/www-project-top-ten/
[17] Priyanka Sharma, K. A. (2021). E-Learning Platform Security Issues And Their Prevention Techniques: A Review. *International Journal of Advance Scientific Research and Engineering Trends*, 51-59.
[18] Rabie, M. (2021). Cyber Security Vulnerability Assessment In Learning Management System. *California State University, San Bernardino, Electronic Theses, Projects, and Dissertations.* California.
[19] Statista Research Department. (2022, 9 6). Retrieved from Statista: https://www.statista.com/statistics/387861/cost-data-breach-by-industry/
[20] Yuldasheva, N. (2019). Security issues in E-Learning system. *Researchgate Conference Paper.* Researchgate.

DESIGN AND DEVELOPMENT OF A COST-EFFECTIVE AUTOMATED METAL SHEET BENDING MACHINE

[1]Eke, Lawrence Azundah and [2]Ashiedu, Festus Ifeanyi

[1, 2] Department of Mechanical Engineering, Federal University of Petroleum Resources Effurun, Delta State Nigeria.
[1] Email: ekelawrence32@gmail.com [2] Email: ashiedu.ifeanyi@fupre.edu.ng

Abstract

In the Metal Production industry, metal sheet fabrication is crucial. This involves manufacturing products like hinges, tools, vehicles, and machine plates. A single flat sheet of metal can be folded into different shapes without being stretched or chopped. Numerous research studies have been carried out to design metal sheet bending machines using techniques ranging from manual, semiscale metal, and metal product makers is a crucial job driven by the worldwide movement towards intermediate technology and sustainable development. Generally, in large-scale manufacturing and construction Industries, Metal Sheet Bending machines are expensive due to their enormous work. In most cases, the power consumption of the machine is always high and a larger space is occupied during installation. However, in small and medium-scale industries (artisan workshops), metal bending imposes greater challenges for business owners. Metal bending is done with aid of a vice and hammer. The difficulty of using human effort results in workplace accidents, man-hour loss, and a reduction in revenue. This work focuses on the development of a cost-effective automated metal sheet bending machine. This design will comprise several sections, the microcontroller unit, the display unit, the power supply unit, rollers, bending components, the rigid frame, etc. The device is aimed at effortlessly bending aluminum sheet that is 0.5 to 0.7mm thick in a small and medium-scale workshop if put into practice. It is expected to lead to a short cycle time, lower cost of production, high-quality product, manpower reduction, increase in the safety of bending machine operators, and increase in revenue of business owners.

***Keywords**: fabrication, bending machine, micro-controller, power supply*

1.0 Introduction

Any nation's economy depends heavily on the production of iron and steel. This is so because the iron and steel industry, which serves as the foundation for all other industries, directly impacts the creation of a sustainable society. This is achieved by exerting stress on a metal sheet, which causes it to bend into the required shape, the bending process—also known as metalworking—produces a V-shaped (channel or U-shape) shape along the axis of a material, conducted using ductile materials. Such materials are employed in machine processes such as brake presses, pan brakes, and specialist machinery [6]. When utilizing a pressure pad to hold the sheet against the die, wipe bending causes the sheet to bend against the radius of the edge.

As a result, the trend in steel production and consumption is seen as a sign of the health of the national economy. For this reason, steel is sometimes referred to as the "backbone" of an economy [5]. Thus, by increasing steel production, a significant contribution to the expansion of the economy of a nation can be achieved.

The sheet metal sector relies heavily on cutting and punching equipment, and since large-scale enterprises are well-established, they can afford to outfit themselves with hydraulically controlled cutting and punching machines that produce a lot of force and are simple to automate. Consequently, the vast production output of large-scale industries. The same is not true for

medium-sized to small-scale industries. Most of these sectors are limited to solely utilizing handoperated cutting or punching machines because hydraulic machinery is too expensive. The adaptability of the sheet metal process has led to its widespread use as a metal-forming technique worldwide [4]. Because sheet metal forming is one of the most crucial semi-finished and finished products utilized in the steel industry, sheet metal forming technology is a crucial technical discipline within the field of mechanical engineering. As a result, sheet metal forming products are today used in a wide range of industries, including infrastructure, domestic appliances, buildings, airplanes, and the manufacturing industry [2]. Given that the sheet metal process is extremely productive and that its use grows yearly, [3].
The aim of this project is to design and construct an automated metal sheet bending machine which uses actuators to drive the bending mechanism. This involves: implementing a Computer Aided Diagram (CAD), selecting a hydraulic system capable of delivering a sufficient load for 0.7mm sheet metal bending, selecting and assembling the appropriate electronic components for the automation, and evaluating the performance of the developed system using the sheet metal dimension. The metal sheet is automated and calibrated to minimize manpower. This calls for the use of Programmable logic circuit as an interface for controlling mechanical movements through electronic systems. Several metal sheet bending machine designs have been implemented including the design and development of a bicycle-integrated pipe bending system [1]. However, the previous designs require extensive manpower.

2.0 Methodology

Research articles, books, periodicals, manuals, and electronic sources that describe the design, manufacture, and mechanics of the metal sheet production process served as the basis for the study's literature evaluation. To increase productivity and the comparativeness of the sheet metal production sectors, comprehensive reviews were ensured on metal sheet machine techniques. There are diverse metal bending techniques, but this research is focused solely on developing a cost-effective metal sheet bending machine using a v-shaped technique. To achieve the objectives of this work, the design implementation is subdivided into control circuit and mechanical sections. Figure 1 below shows the basic block diagram of the proposed automated metal sheet bending machine. The block diagram highlights the basic control and mechanical components required for the design of the set objectives. The actuator will replace the manpower used in previous designs for the bending of metal sheets on machines, while the controller; a programmable electronic device will be used to control all of the machine operations.

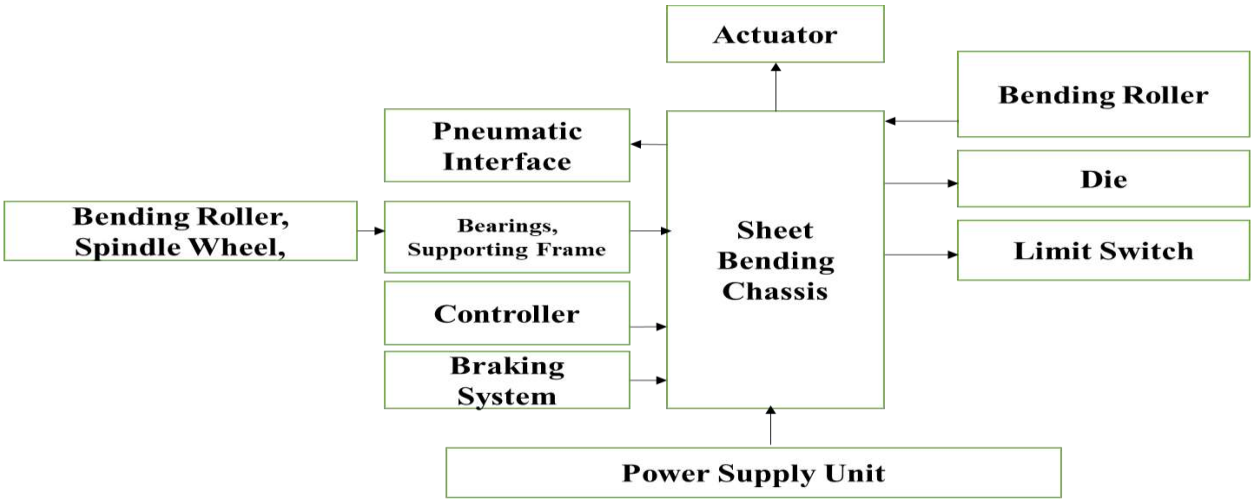

Figure 1: Block Diagram of the Automated Metal Sheet Bending Machine

2.1 V-shaped Die

The V-shaped bending technique will be considered in this research as it is the most crucial diebending procedure, where the deformed shape is produced as a result of the sheet being driven into the die by the punch until it is in as much contact as possible with the sides of the die. Air bending and coining are the two independent stages of the V-die bending process. The sheet first experiences the air-bending stage. As the bending continues, it reaches a point where the bent sheet's edges are tangent to the die's sides close to both support points. The coining stage officially starts at this moment.

The spring-forward or spring-back bend angle in a precise component of bending depends on process variables, such as the tensile qualities, geometrical parameters, and the coining process. In a bending process, coining can lessen the amount of unloaded spring-back or spring-forward. The following factors will be considered for the V-shaped metal bending machine.

2.1.1 Factors to be Considered for V-shaped Bending Procedure

- **i.** BA = bend allowance
- **ii.** BD = bend deduction
- **iii.** R = inside bend radius **iv.** K = K-Factor, which is t / T
- **v.** T = material thickness
- **vi.** t = distance from the inside face to the neutral line
- **vii.** A = bend angle in degrees (the angle through which the material is bent)

The absence of any internal forces is symbolized by the neutral line, which is an illustrative line that can be drawn through the cross-section of the workpiece and is also known as the neutral axis. The forces employed to produce the part, as well as the yield and tensile strengths of the material, all affect where it is located inside the material. The material between the neutral line and the inside radius will be compressed during the bend at the bend zone. During the bend, tension will be applied to the material between the neutral line and the outside radius. The material's needed length before bending is shown by the neutral line or flat pattern, which is the difference between the created bend and the bend allowance.

2.2 Control Circuit

Automation and control of machines play a crucial role in eliminating manpower, and safety, and also increasing productivity. The machine control console will have an emergency stop button. These ought to be lock-in models, which prevent restarting unless a manual reset has been performed. The machine shouldn't start after resetting the emergency stop button until the regular start control is used. To ensure that they are entirely conversant with the machine, its controls, guards and safety devices, hazards associated with the equipment, and any other control measures, operators should receive thorough instruction.

An electronic circuit that consists of discrete components such as resistors, capacitors, solid-state relays, and high-gain amplifiers with an integrated circuit will be designed, assembled, analyzed, and critically tested to ensure the optimum performance of the metal sheet-bending machine. The software section will include the Arduino Integrated Development Environment (IDE) for programming and Proteus software as a circuit simulator, while the hardware interface comprises a sensing unit, an amplification unit, a filtering section, and the microcontroller unit. Table 1 below shows the list of the electronic components for the design.

There are two classes of power supply required for the design; a direct current (dc) power source and an alternating current (ac) power source. The ac power source is 220 V/50 Hz obtainable from mains, generator, and inverter, while the dc power supply will be obtained after rectification and voltage reduction of the ac mains. The dc supply is subdivided into two namely; 5 V AND 12 V supplies. This is a result of the voltage requirement of different electronic components required for the machine's operation.

Table 1: Components List for the Automated Metal Sheet Bending Machine

Electronic Components	Specifications
Controller	Arduino Mega
Limit Switch	5V
Relay	5V, 30 A
Power supply unit	220V/50 Hz
Liquid Crystal Display	5V
Actuator	12V

Button (Emergency)	5V
1.5 mm and 2.5 mm electrical cable	220V
Cat-6 cable	5V

2.3 Solenoid Valve

A solenoid is an electrical device that uses electricity to create force and motion in a straight line. Additionally, this will be utilized to run a mechanical process that controls the valve mechanism.

Solenoids come in push or pull varieties. The plunger is pushed when the solenoid is electrically energized in a push-type solenoid. The plunger is pulled when the solenoid is energized in a pulltype solenoid. The solenoid will be used in addition to the actuator to eliminate the manual operation of metal sheet bending by humans.

Figure 2: Solenoid Valve

2.4 DC Motor

An electromechanical tool known as a stepper motor transforms discrete electrical pulses into discrete mechanical movements. When electrical command pulses are supplied to a stepper motor's shaft or spindle in the correct order, the motor rotates at an identical angle of increment known as steps. The motor shaft's direction of rotation, its speed, the frequency of the applied input pulses, and the total radiation at a stretch are all closely tied to the applied input pulse sequence, frequency, and number. A shaft angle increment of 30°, 15°, 5°, 25°, 2°, and 1.8° each step is possible with stepper motors having steps of 12, 24, 72, 144, 180, and 200 per revolution. To automate the metal sheet bending system, a dc motor with the specifications listed below will be used.

2.4.1 Specification of DC Motor

- Length:80mm
- Torque: 1.5 kg/cm
- Shaft Diameter:6mm

• Weight:130.00 g

• Supply Voltage:12V

• Speed=3.5 RPM

2.5 Mechanical Unit

Any machine part preparation requires careful material selection while taking design and safety into account. Table 2 shows the mechanical materials required for the design of the metal bending machine, while Table 3 shows the specifications of the metal sheet to be used on the machine. Equations i and ii highlight metal sheet cutting force calculation and metal sheet bending force calculation.
The following considerations determine the choice of material for engineering applications:

Table 2: Mechanical Components for the Design of an Automated Metal Sheet Bending Machine

Components	Engineering Standard	Specifications
Bending Rollers	alloy steel	Length = 155 mm, Diameter= 70 Ø
Joints	AISI 4037	Diameter = 40 Ø, width = 10 Mm
Screw	AISI 4037	Length = 135mm , Height =22mm
Bearings	52100 chrome steel	Diameter = 30 Ø, Thickness= 9 mm
Spindle Wheel	410 stainless	Length = 173.20 mm , width = 25 mm, Diameter = 10 Ø
Moving Roller	alloy steel	Length = 155 mm, Diameter = 70 Ø
Supporting Frame		

Pneumatic Actuator		
Die, Pneumatic valve, Pneumatic pipe, screws and bolts		

Table 3: Metal Sheet Specifications

Metal Sheet Material	**Aluminum Sheet**
Max Shear stress of the Aluminum sheet (τmax)	25 N/ mm^2
Length (L)	20 mm
Thickness (t)	0.7 mm
Tensile Strength for Aluminum	400N/mm^2

2.5.1 Metal Sheet Cutting Force Calculation

Force = L X t X τmax

Metal sheet thickness = 0.7mm

Force, F = 20 X 0.7 X 25

F = 350 N (This is the force needed to cut the sheet metal)

2.5.2 Metal Sheet Bending Force Calculation

The force required to bend the sheet metal = (L× K ×ut × t) / (w)

Where, ut = Tensile Strength of Aluminum (400N/mm^2)
K = Die opening Factor (1.33 for V-Bending) w = Width of Die Opening, For the value of K=1.33, w=16t
Force required = (25 × 1.33 × 400 × 0.7) / (16 × 1) = 9310/16

F = 582N

Therefore, the Maximum force required to bend 0.5 -0.7mm thickness of the metal sheet is 582N

3.0 Results and Discussion

After the assembling and testing of the control and mechanical components, the machine will be subjected to the metal sheet of 0.5 mm, and 0.7mm to validate the performance of the system. The source of power for the machine, the electric motor, will be an electrical ac mains source (220 V); and the gears will convert the electrical energy into mechanical energy, supplying the speed required by the actuator for the metal sheet bending.

4.0 Evaluation of The Performance of The Automated Metal Sheet Bending Machine

The evaluation of the performance of the metal sheet bending machine will be carried out using a software simulator and comparison analysis by calibrating the developed metal sheet bending machine against a standard.

5.0 Conclusion

This research will produce an efficient cost-effective automated metal sheet bending machine capable of manpower reduction, increase in safety of the operators, less expensive to purchase, easy to maintain, service, and repair when faulty.

References

[1] Ahmed K., Zied A., Nader H. and Khaled E. Modeling and computation of the three-roller bending process of steel sheets, Journal of Mechanical Science and Technology 26 (1) (2012) 123-128
[2] Anas Muzamil Bin, Hamiddin, Design, and Fabrication of Multipurpose machine, Universiti

Malaysia Pahang November 2009

[3] Groche P., A. Zettler, S. Berner: Development of a One-Step-Model for The Design of flexible

[4] Michael Lindgren, Experimental and Computational Investigation of the Roll Forming

Process, Luleå University of Technology 2009

[5] Xiaoyun Liao, Evolutionary Path Planning for Robot-Assisted Part Handling in Sheet Metal Bending, Dept. of Mechanical & Industrial Engineering, The University of Manitoba, 2007.
[6] Wanisevic A, Milutinovi M, Strbac B, Skakum P (2013) Stress state and spring back bending operations. J Technol Plast 39(2):157–168

NIPES-NCEE Conference Proceedings
The 2nd International Conference 15th-17th Feb. 2023
167-181
www.nipesjournals.org.ng

DESIGN AND FABRICATION OF AN IMPROVED AUTOMATIC WHITE BOARD CLEANING SYSTEM

Loyalty Akpeti [a], Efe Orumwense [b], Ukpong Iyeneobong Daniel, Jimoh Hamza, Edegbo Maro Felix

[a] Department of Mechanical Engineering, University of Benin, P.M.B. 1154, Benin City, Nigeria. Email Address: loyaltyakpeti@gmail.com

[b] Department of Mechanical Engineering, University of Benin, P.M.B. 1154, Benin City, Nigeria. Email Address: efe.orumwense@uniben.edu

Abstract

In recent times, whiteboards have gradually replaced the conventional blackboards used in various schools and educational institutions and the ease of cleaning is a major driving force that led to these changes. Whiteboards with automatic cleaning devices have also been gaining popularity in most parts of the world and one with an effective cleaning device is expected to totally erase conventional cleaning methods off the markets. In this work, we introduce, design and develop an effective and cheap automatic whiteboard cleaner made with locally sourced materials. A lot of design factors were put into consideration so as to outperform the currently existing systems. Testing and results showed that our design is capable of cleaning specific areas of a whiteboard and not just the whole board at once as is common with other automatic whiteboard cleaners currently available. The cleaning time is recorded at 18 seconds and the device is capable of leaving zero residue after a few sweeps of the board. In conclusion, our whiteboard cleaning system performed efficiently and effectively, and it easily meets market standards.

***Keywords**: Whiteboard, Duster, Automatic, Arduino, Cleaner, Board.*

1. INTRODUCTION

Since its inception, the whiteboard has proven to be useful in both professional and non-professional settings. It should come as no surprise that, in comparison to the black and green chalkboards, it offers a number of advantages, making it a popular choice for personal study, business presentations, and knowledge transfer. Whiteboards were designed and made with enamel-hard surfaces and melamine in the 1950s and 1960s, based on the level of expertise and resources that were readily available at the time. This was the first-time whiteboards were used, and since then, people all over the world have started using them and black and green chalkboards are being phased out.

Despite the whiteboard's advantages over the black and green chalkboards, they all faced the same problem: "The difficulty and unease in cleaning off what has been written on its surface," specifically between 1950 and 1975. As a result, the porcelain-on-steel whiteboard was introduced. In the years that followed, porcelain became the preferred and most widely used surface material for the production of whiteboards. The substitution of dry-erase markers for wet-erase markers was another limitation addressed during this process. Professionals in the academic, business, and industrial sectors now find it simple to use the whiteboard for daily tasks thanks to modern surface finishes and wipe-clean markers.

In today's technologically advanced world, the whiteboard is one of a few manually relevant items that has remained distinctive. Cleaning the board is always necessary because every letter, number, symbol, or other entity written on it is only temporary. This can be tedious in a fast-paced learning environment or when the need to increase usage speed arises. As a result, reducing the use of manual cleaning techniques and increasing cleaning speed are major strategies for combating this persistent issue. The time and energy aspects are addressed simultaneously in this manner; using an automated system to handle the whiteboard cleaning process is the best way to accomplish these goals.

At the moment, automated cleaning techniques are barely used at all, especially in the University of Benin where this research project was carried out. The main objective of this project is to provide a standardized and improved automatic whiteboard cleaning system through this project that will clean whiteboards relatively quickly and easily.

After considering the immediate needs of our environment and the current methods of board cleaning being used, we have been able to itemize the following key issues:

a) Cleaning whiteboards after usage consumes a lot of time while teaching.
b) Energy is expended by the lecturer or student when cleaning manually.
c) Dusters can get stolen or go missing due to carelessness.
d) Manual cleaning is inconsistent and leaves black residue on the board.

These are the main issues but the above list is by no means all-encompassing. The problems above will serve as our launching pad for this work. Being able to solve them will classify this project as a success. This project aims to design and fabricate an automated whiteboard cleaning system that will be suitable for use in classrooms and other places where whiteboards are regularly used. This project aims to design an automated cleaning mechanism that cleans the entire board automatically with just the push of a button, saving a lot of time and effort.

2. METHODOLOGY

The design was targeted towards achieving the following: producing a faster and easier way to clean white boards, high cleaning efficiency, availability of locally sourced materials, and cost of the machine.

During the course of this project, three distinct concepts were proposed as analyzed below.

CONCEPT ONE: HORIZONTAL DESIGN (MOVING RACK)

This concept is called the moving rack horizontal design and it consists of a DC Motor as the prime-mover and a single set of rack and pinion to convert the rotational motion of the DC Motor into linear motion of the duster. When the DC motor rotates, it transfers motion to the pinion. The pinion then moves the rack, and the rack in turn pushes the duster. The duster moves left-to-right across the board cleaning everything in its path.

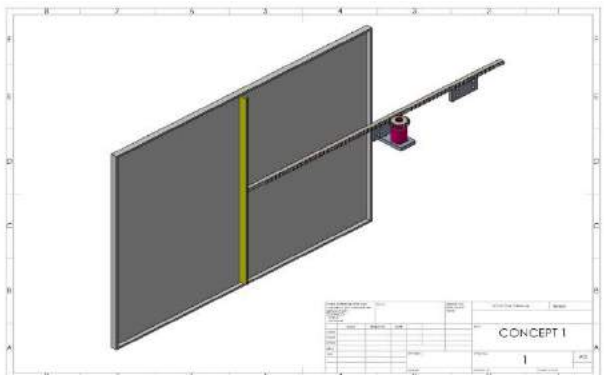

Figure 11 - CONCEPT ONE: HORIZONTAL DESIGN (MOVING RACK)

CONCEPT TWO: HORIZONTAL DESIGN (FIXED RACK)

This is what we called the fixed rack horizontal design and it consists of two sets of rack and pinion located at the top and bottom of the board. The pinions are connected with a shaft. The shaft is also connected to the prime-mover, a DC Motor. As the DC Motor spins, the shafts spins, as the shaft spins, the pinions spin, as the pinions spin, they move along the racks thus moving the duster along the board.

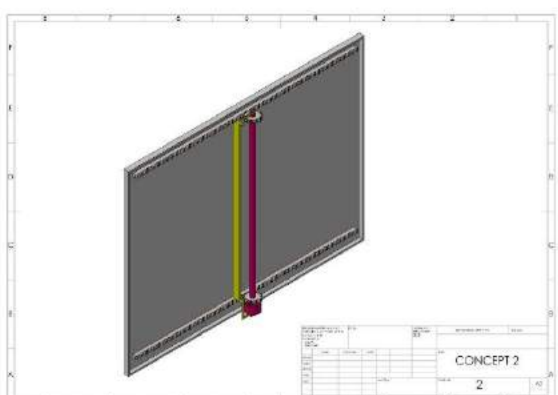

Figure 12 - CONCEPT TWO: HORIZONTAL DESIGN (FIXED RACK)

CONCEPT THREE: VERTICAL DESIGN

This concept is called the vertical design and it is driven by one motor that connects two pulleys with a shaft. The shaft helps to transfer motion from the motor to the pulleys. The pulleys move the belt and the belt moves the duster vertically across the board cleaning it. The duster doesn't cover the entire board, rather it covers a third of the width of the board. There is another motor placed on the duster, which will be responsible for moving the duster from left to right. This way, the duster can pick specific parts of the board to wipe, not having to clean the whole thing while moving.

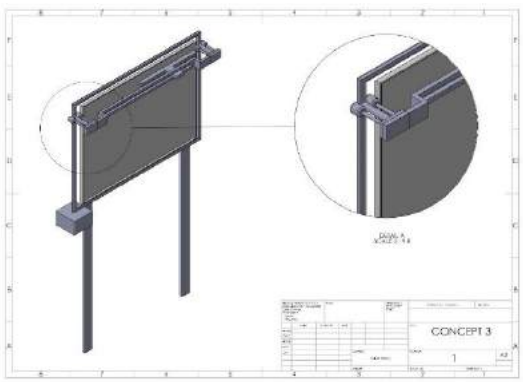

Figure 13 - CONCEPT THREE: VERTICAL DESIGN

DECISION MATRIX

Of the 3 proposed concepts, only one can be used for the prototype. Hence a decision matrix was employed to help us make the choice. We based our decision matrix on 5 major criteria that we considered to be most important for whatever design we choose. The criteria are:

a) Cost
b) Efficiency
c) Practicality
d) Flexibility
e) Aesthetics

We then assigned each criteria a weight ranging from 1 to 5 with 1 being the least important and 5 being the most important. Let's discuss the criteria and how each concept was rated.

a. COST

Cost was our most important criteria when choosing a concept. Cost was assigned a weight of 5 to signify this. Concept one consists of one motor, one rack and one pinion as its major components. Thus, making it the cheapest of our three concepts. Concept one was assigned a cost rating of 5 for being the cheapest. Concept two consists of one motor, two racks, two pinions and one shaft as its major components. Thus, making it the second cheapest of our three concepts. Concept two was assigned a cost rating of 2 for being the second cheapest. Concept three consists of three motors, four pulleys, four bearings, two belts, and a relay board as its major components. Thus, making it the most expensive of our three concepts. Concept three was assigned a cost rating of 1 for being the most expensive.

b. EFFICIENCY

Efficiency was the second most important criteria when selecting a concept. We assigned it a weight of 4. The efficiency of the concepts is defined as the ability of the design to properly clean all parts of the board. Concepts two and three were given a rating of 5 each for being the most efficient. They have a shaft that presses the duster against the board at all times thus ensuring a smooth clean. Concept one was assigned a value of 2 for being less efficient. It doesn't possess the shaft that the other two concepts have to continuously exert pressure on the duster against the board. The duster is free and could clean less efficiently when the rack is fully extended.

c. PRACTICALITY

We defined practicality of our design as the ability of the system to be installed in any classroom. We gave this criterion a weight of 3. Concept one is very impractical because of the way it works. It extends fully to the right of the board at the base of its motion, and this extension cannot be accommodated in most classrooms. Some classrooms have many boards next to each other, so this extension will cover the next board. Other classrooms don't have enough space to the right of their board to accommodate this extension. For these reasons, concept one was given a rating of 1 for practicality. Concepts two and three were given ratings of 5 because they are more practical and don't take up a lot of unnecessary space.

d. FLEXIBILITY

We defined flexibility here as the ability of the device to clean specific areas of the board and not just the whole board. Most lecturers like to divide the board when writing so they don't clean the entire thing when they are done, just specific parts. Being able to meet this need is a very important criteria that our design has to have. We gave this criterion a weight of 2. Concepts one and two are not capable of this. They clean the entire board and not specific bits. We gave concepts one and two ratings of 2 for flexibility. Concept three on the other hand is very flexible. The duster in this design is a third of the length of the board and it has a motor to move the duster from left to right. For this flexibility, concept three was given a rating of 5.

e. AESTHETICS

Of the five criteria we used, aesthetics was the least important. We gave it a weight of 1. All designs appealed to us aesthetically so all three concepts were given a rating of 5 for aesthetics.

CRITERIA	WEIGHT	CONCEPT 1		CONCEPT 2		CONCEPT 3	
		RATING	WEIGHTED SCORE	RATING	WEIGHTED SCORE	RATING	WEIGHTED SCORE
COST	5	5	25	2	10	1	5
EFFICIENCY	4	2	8	5	20	5	20
PRACTICALITY	3	1	3	5	15	5	15
FLEXIBILITY	2	2	4	2	4	5	10
AESTHETICS	1	5	5	5	5	5	5
TOTAL SCORE			45		54		55

Figure 14 - DECISION MATRIX

DESIGN CALCULATIONS

Our prototype was constructed on a frame for transportation. The eventual machine will be designed to be attached to the wall beneath the board. The height of the "legs" of the frame is **91.44cm**. The top of the frame that houses the board is **107cm x 168cm.** The motors used are **50Watts, 12V** motors. They have a mechanical horsepower of **6hp**. The battery used to power the prototype is **12V, 7Ah.** The pulleys are **6cm** in diameter and the bearings are **5.5cm** in diameter. The belts used are **215cm** in length by measurement. The distance between the belts is **142cm.** The relay switches used are **12V**. Center-to-center distance of the pulleys is **98cm**.

Belt Parameters

b = 12mm, t = 8mm, w/l = 1.06

NIPES-NCEE Conference Proceedings
The 2nd International Conference 15th-17th Feb. 2023
167-181
www.nipesjournals.org.ng

D_1 = diameter of driving pulley, 60mm

D_2 = Diameter of driven pulley, 60mm.

$P_{belt} = 1250kg/m^3$

Rotational Speed of driver pulley, N_1 = 319.998rpm

S_s = 3.0MPa

μ = 0.25

Groove angle of pulley = 30° = 2β

Length of belt by calculation,

$$\mathbf{L} = \frac{\pi(D_1 + D_2)}{2} + 2C + \left(\frac{(D_1 + D_2)^2}{4C}\right) \qquad \textbf{[6]}$$

We use a center, C, 980mm.

$$L = \frac{\pi(60+60)}{2} + 2\times 980 + \left(\frac{(60+60)^2}{4\times 980}\right)$$ = **2152.169mm = 215.2169cm** (close to the **215cm** obtained via measurement)

A standard belt is then chosen as the nearest match is 2158 mm which is a type **A83 belt.**

Operational Acceleration

$N_s = 319.998RPM$

$$\omega = \frac{2\pi N}{60} = \frac{2\times\pi\times 319.998}{60} \qquad \textbf{[6]}$$

$\omega = 33.51 \,{}^{\text{rads}}/_{\text{s}}$

$$\boldsymbol{\alpha} = \frac{\boldsymbol{\omega}}{\mathbf{t}} = \frac{\mathbf{33.51}}{\mathbf{6}} \qquad \textbf{[10]}$$

$\alpha = 5.585 \,{}^{\text{rads}}/_{\text{s}^2}$

Bearing Parameters

The single row deep groove ball bearing was chosen because of its high load carrying capacity and suitability for high running speed. The specific static load rating or capacity C_o is:

$$Co = \frac{1}{5} \times ko \times i \times z \cos \alpha Dw^2 \qquad \textbf{[7]}$$

Where:

C_o = Specific Static Load rating or Capacity = 40kN

K_o = Factor depending on the type of bearing = 12.3

D_w = Diameter of the ball

α = Nominal angle of contact = 0

i = Number of rows of the ball in any one bearing = 1

z = Number of balls per row in the groove = 6

$$Ko = \frac{Q\max}{\mathrm{Dw}^2} \qquad \textbf{[7]}$$

Qmax = Maximum bearing load.

From the above data, the ball diameter can be calculated

$$Dw = \sqrt{\left(\frac{Co \times 5}{Ko \times i \times z \cos \alpha}\right)} \qquad \textbf{[3]}$$

$$= \sqrt{\left(\frac{40 \times 10^3 \times 5}{12.3 \times 1 \times 6 \cos 0}\right)}$$

$$= \sqrt{2710.0271}$$

= 52.06mm

The next available market diameter was **55mm**.

Then the maximum bearing load Q_{max} becomes:

$$Ko = \frac{Qmax}{\mathrm{Dw}^2}$$

$$Q_{max} = K_o \times D_w^2$$

$$= 12.3 \times 2710.0271$$

$$= \mathbf{33333.3333N}$$

The bearing with identification number 6206, which is has an inner diameter of 25mm and outer diameter of 55mm, was then chosen. The bearing number interpreted as 200 means a light-bearing of the bore that is the inner diameter of 5 × 5 = 25mm. Also, in the selection of this bearing, the radial load of which the bearing can carry was put into consideration. However, for the ball lubrication, grease is used at low and medium speed when the temperature is not over 20ºC while oil is used at higher speed. Hence, for this design, grease is regarded as the most satisfactory lubricant, because the temperature rarely exceeds 20ºC during operation.

THE PROTOTYPE

Concept three was chosen with the aid of the decision matrix. The materials needed were identified and then purchased. Then fabrication began.

The frame was the first to be fabricated. Lengths of metal were bought. The metal was cut to the desired measurements and the welded together to the desired shape.

Figure 15 - THE FRAME

Once the frame was standing, the rest of the materials were attached to it. The board was mounted to the frame. Next the pocket for the battery was fabricated and welded to the back of the frame.

Figure 16 - BOARD MOUNTED ON THE FRAME

The driving pulleys were welded to the motors and the motors had pockets fabricated to house them. The driving and driven pulleys were then connected with the belts.

Figure 17 - DC MOTOR

The driven pulleys were then set up between two bearings each to aid rotation. The bearings are set in a ‘cup’ which was in turn welded to the frame. The cup holds the outside of the bearing firm while allowing the inside rotate freely.

Figure 18 - DRIVEN PULLEY AND BEARINGS

Next, a holder was fabricated for the duster. The wood was cut to the required dimensions (1.75ft) and the felt from the dusters we bought was glued to the wood. The duster was then set on the holder and the two induction motors and two wheels were attached to the duster.

Figure 19 - DUSTER HOLDER

The duster holder was then fastened to the belts of the device using bolts and nuts. A hole was first punched in the belts as the desired locations in order to give room for the bolts and nuts to be placed. At the sites of the holes, the duster was then fastened. Wheels were then placed at the back of the holder to give the holder freedom to ascend and descend the frame. The wheels are there to make the motion smooth.

Figure 20 - DUSTER HOLDER ATTACHED TO THE BELT

The electrical work and the coding were then done next. The H-bridge relays were built. The aim of this is to reverse the polarity of the motors so the duster can both ascend and descend. The Arduino code was then done and the board was assembled to enable the system to be operated with the push of a button form a distance. Finishing touches were added to the device, the welded joints were sanded. The belts were tensioned.

Figure 21 - FINISHED DESIGN

ARDUINO CODE

The following is the code used to assign functions to various keys on the remote. 4 keys were needed in total: UP, DOWN, LEFT and RIGHT. We assigned **UP** to button **2, DOWN** to button **8, LEFT** to button **4, RIGHT** to button **6.**


```
#include <IRremote.hpp>

#define first_key 48703
#define second_key 58359
#define third_key 539
#define fourth_key 25979
int receiver_pin = 3;

int first_led_pin = 7;
int second_led_pin = 6;
int third_led_pin = 5;
int fourth_led_pin = 4;
int led[] = {0,0,0,0};
IRrecv receiver(receiver_pin);
decode_results output;

void setup()
{
Serial.begin(9600);
receiver.enableIRIn();
pinMode(first_led_pin, OUTPUT);
pinMode(second_led_pin, OUTPUT);
pinMode(third_led_pin, OUTPUT);
pinMode(fourth_led_pin, OUTPUT);
}

void loop() {
if (receiver.decode(&output)) {
unsigned int value = output.value;
switch(value) {
case first_key:
if(led[1] == 1) {
digitalWrite(first_led_pin, LOW);
```

```
digitalWrite(first_led_pin, LOW);
led[1] = 0;
} else {
digitalWrite(first_led_pin, HIGH);
led[1] = 1;
}
break;
case second_key:

if(led[2] == 1) {
digitalWrite(second_led_pin, LOW);
led[2] = 0;
} else {
digitalWrite(second_led_pin, HIGH);
led[2] = 1;
}
break;
case third_key:

if(led[3] == 1) {
digitalWrite(third_led_pin, LOW);
led[3] = 0;
} else {
digitalWrite(third_led_pin, HIGH);
led[3] = 1;
}
break;
case fourth_key:

if(led[4] == 1) {
digitalWrite(fourth_led_pin, LOW);
led[4] = 0;
} else {
```

```
if(led[2] == 1) {
digitalWrite(second_led_pin, LOW);
led[2] = 0;
} else {
digitalWrite(second_led_pin, HIGH);
led[2] = 1;
}
break;
case third_key:

if(led[3] == 1) {
digitalWrite(third_led_pin, LOW);
led[3] = 0;
} else {
digitalWrite(third_led_pin, HIGH);
led[3] = 1;
}
break;
case fourth_key:

if(led[4] == 1) {
digitalWrite(fourth_led_pin, LOW);
led[4] = 0;
} else {
digitalWrite(fourth_led_pin, HIGH);
led[4] = 1;
}
break;
}
Serial.println(value);
receiver.resume();
}
}
```

Figure 22 - REMOTE CONTROL **Figure 233 – ARDUINO CODE**

3. RESULTS AND DISCUSSION

The following calculations were performed to first ascertain that our device would be able to clean faster than conventional methods. We spent a week collecting data from two lecture theatres in the University of Benin, namely: Old 1000 LT and LT2. We then were able to determine the average amount of time it would take to clean a board using conventional methods.

Average time taken to clean a 4ft x 8ft board manually = 54s

Ratio of the area of our prototype board to the area of a standard board used in the University of Benin = $\frac{3 \times 4}{4 \times 8} = 0.375$

Time taken to clean a 3ft x 4ft board manually = $0.375 \times 54 = 20.25s$

Time taken for our device to slide top-to-bottom = 6s

Time taken to clean a 3ft x 4ft board with our machine = 6s x 3 = 18s

Percentage time saved = $\frac{20.25 - 18}{20.25} \times 100 = 11.11\%$

Secondly, we performed calculations to find out how long a fully charged battery can be used to power the device in the average University of Benin lecture theatre. We collected date from the two aforementioned lecture theatres over the course of three weeks and determined the average numbers of times a board is cleaned in each of those theatres per week.

Average number of times a week the board is cleaned in Old 1000 LT = 54

Average number of times a week the board is cleaned in LT2 = 51

Battery = 12V, 7Ah

Time to charge with a 12V, 1A charger = $\frac{7Ah}{1A} = 7hours$ **[2]**

Current needed by both motors = 4.2 amps x 2 = 8.4A

Time both motors will run on a fully charged battery = $\frac{7Ah}{8.4A} = 0.8333hours = 50\ minutes$

Number of times the machine can clean the board on a full battery = $\frac{50\ x\ 60}{18} \approx 167\ times$

At an average of 52.5 cleans per week, number of weeks the machine can last on a full battery = 3.18 weeks $\approx 16\ school\ days$

Lastly, we determined the torque in our motors.

Time taken to slide top-to-bottom = 6s

Distance from top-to-bottom = 0.98m

Velocity = $\frac{0.98m}{6s} = 0.16m/s$ **[8]**

Radius of the pulley = 0.03m

Revolutions = $\frac{0.16m/s}{0.03m} = 5.3333rev/s = 319.998rev/min$ **[5]**

Angular velocity = $\frac{2\ x\ \pi\ x\ 319.998}{60} = 33.51rad/s$ **[4]**

Mechanical Horsepower = 6hp = 6 x 745.7 = 4474.2Watts **[1]**

Torque = $\frac{P}{\omega} = \frac{4474.2}{33.51}$ = 133.52Nm **[9]**

The time taken for the machine to clean (18s) will be slightly more on a 4ft x 8ft board due to the increased length of the shaft and the extra weight. Although there will be an increase, we expect it to still be considerably less than the 54s taken to clean it manually. Thus, the machine will remain efficient even at full scale.

At full scale, and taking losses into consideration, the 16-day battery life of the machine should drop but not so much as to make the 7-hour charging time seem wasted.

4. CONCLUSION

We were able to achieve our objectives:

a) Our device cleans faster than a person cleaning using conventional means.
b) Manpower was saved because the device is almost fully automated, only the push of a button is required and sliding of the duster is required.
c) The entire device can be fixed to the wall above and under the board to prevent theft.
d) The duster applies enough pressure on the board to ensure no residue is left behind after cleaning.

REFERENCES

[1] Avallone, E., Baumeister, T. & Sadegh, A., 2006. *Marks' Standard Handbook for Mechanical Engineers.* 11th ed. s.l.:McGraw-Hill.

[2] Bird, J., 2003. *Electrical Circuit Theory and Technology.* Revised 2nd ed. s.l.:Newnes.

[3] Budynas, R. G. & Nisbett, J. K., 2015. *Shigley's Mechanical Engineering Design.* 10th ed. s.l.:McGraw-Hill Education.

[4] Hibbeler, R. C., 2009. *Engineering Mechanics.* Upper Saddle River, New Jersey: Pearson Prentice Hall.

[5] Kelly, S. G., 2012. *Mechanical Vibrations: Theory and Applications.* s.l.:Cengage Learning.

[6] Khurmi, R. & Gupta, J., 2005. *A Textbook of Machine Design.* 14th ed. New Delhi: Eurasia Publishing House (PVT.) Ltd.

[7] Palmgren, A., 1945. *Ball and Roller Bearing Engineering.* 2nd ed. Sweden: SKF Industries.

[8] Resnick, R. & Walker, J., 2004. *Fundamentals of Physics.* 7 ed. s.l.:Wiley.

[9] Serway, R. A. & Jewett, J. J., 2003. *Physics for Scientists and Engineers.* 6th ed. s.l.:Brooks-Cole.

[10] Singh, S. K., 2022. *Physics for K-12.* s.l.:OpenStax CNX.

NIPES-NCEE Conference Proceedings
The 2nd International Conference 15th-17th Feb. 2023
182-192
www.nipesjournals.org.ng

NEURAL NETWORK MODEL APPROACH TO INTRUSION DETECTION IN INFORMATION SYSTEMS: *NETSHIELD*

Osa Edosa
Department of Electrical/Electronic Engineering
Faculty of Engineering
University of Benin, Benin City, Nigeria.
eddyedos@yahoo.com
+2348168307508

Pimeh Daniel
Information Technology Department
Distribution Operations
Procter and Gamble, Lagos, Nigeria.
pimehD@gmail.com
+2348109842917

*Corresponding Author: Osa Edosa.

Abstract

Security of information Systems has become a top priority since the present trend for record keeping in almost all spheres of human operations is fast becoming electronic. Data such as human or animal patient records, research data, database of environmental or agricultural variables, weather patterns, finance data and the like are mostly housed in various personal or network computer systems for ease of management or collaboration amongst other purposes. However, criminal elements are found to go after such data for one of many reasons such as ransom, competition, naughtiness, political maneuvers and so on. There is the need therefore to protect such systems. Various traditional interventions have been used over the years such as firewalls, legacy Intrusion Detection systems and the like. However, such systems lack capacity to keep up with the large amounts of data being generated in the fast paced information sphere we currently live in. Moreover, they find it difficult to detect zero-day attacks. Such problems can be overcome by applying artificial intelligence interventions. This work aims to present an artificial intelligence solution to detect attacks in information networks namely a Neural Network Model. It is designed in a Google Colab environment using tools such as Python programming language and Tensorflow. It also implements the SparseCategoricalCrossentropy method. Results show up to 99.7% accuracy. This presents an excellent model for detecting intrusion in computer information networks.

Keywords*: Data, Neural Network, Intrusion, Artificial Intelligence.*

1. INTRODUCTION

Besides the benefits of digital technology for the advancement of the human life experience, there exist a subset of malicious users who manipulate such technology for exploitation. Such exploitations could be attempts to remotely access a computer network and compromise the confidentiality, integrity or availability of the system. These exploitations can result in detrimental effects to the victims and huge gain for the malicious intruder. One solution to this menace is to implement an Intrusion Detection System (IDS) in the network. Network IDS analyze network traffic and distinguish patterns that can cause damage to systems or networks. A recent design of such a system especially in this era of big data is by implementation of Deep Neural Networks. Deep Neural Networks which possess simultaneous multiple layers of feature extraction have gained wide popularity and impacted the scientific world significantly [1]. Application of these algorithms in the theatre of network IDS presents improved detection accuracy over a range of datasets. Due to security and privacy concerns, there is a dearth of openly available labeled datasets for intrusion-detection. This limitation made artificial intelligence IDS researchers to simulate network traffic with real-life feature representations, resulting in a pioneer IDS dataset namely, KDDCup, which was a DARPA project. Lincoln Lab-created this dataset via tcpdump from closed network generated traffic that included manual injected attacks. It was designed to simulate network traffic in U.S. Air Force bases. However, because this simulated dataset failed to validate real network traffic and had several redundant records especially for attacks, the next version NSL-KDD was created [2]. Other network IDS datasets include NSL-KDD, Kyoto, WSN-DS, CICIDS-2017, etc. The Canadian Institute for Cybersecurity at the University of New Brunswick developed CICIDS 2017 (Intrusion Detection Evaluation Dataset). This dataset is made up of a 5-day data stream (3rd–7th July 2017) on a network formed by machines running current operating systems like Windows Vista / 7 /8.1 / 10, Mac, Ubuntu 12/16 and Kali Linux. Information about the CICIDS-2017 dataset can be found at the official website. Our paper focuses on developing a Deep Neural Network model over the CICIDS-2017 Dataset.

1.1.STATEMENT OF PROBLEM

Traditional Intrusion Detection Systems (IDSs) are signature-based, since they rely on existing signatures of already known attacks. However, huge amounts of data need to be processed daily in order to develop new signatures. This characteristic makes the task of generating such systems on time a difficult one. Furthermore, generating signatures for many complex attacks that have evolved from their previously known threats is not quite straightforward and also requires some additional effort by cybersecurity specialists. Traditional IDSs cannot also respond to zero-day attacks since they have no pre-existing signature. To overcome the aforesaid challenges, IDS researchers employ Behaviour Analysis to detect intrusions. Machine learning techniques are employed to model system behaviour and thus detect malicious activity as abnormalities in system behaviour. When compared to signature-based IDSs, these machine learning models can detect large families of attack variants no matter the level of complexity. Using such systems, an IDS more accurately recognizes attacks on the network by the features of the attack [3]. Classification could be binary (i.e., normal or malicious) or multi-class where the model can also detect the attack type by the classes/labels in the training set. Some researchers have also employed machine learning (ML) to reduce false alarms in IDSs [4,5]. Unfortunately, complexity of modern networks such as the IoT have rendered some limitations on classical ML algorithms when used to process increasing volumes of data [5]. Moreover, MLs are poor at feature-learning when it comes to extracting meaningful information from big data [6,7]. As a result, predictive analytics solution namely, Deep Learning (DL) is required to surmount the disadvantages of machine learning-based IDSs with regards to big data. Deep learning involves the development of artificial neural network algorithms with several hidden layers for extracting meaningful information from big data repositories. The DL technique possesses the advantage of extracting large numbers of data features making it highly suitable for attack detection and classification in networks [8].

2. METHODOLOGY

The methodology involved design, training, and testing of the Deep Neural Network over five epochs. The flowchart is described in figure 1.

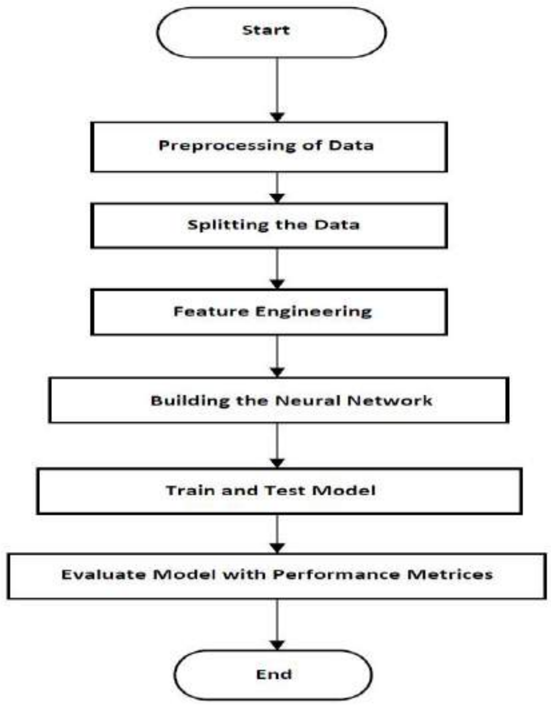

Figure 1: Flowchart of Methodology

2.1. Experimental Design

This project was implemented using the Python programming language, Google's TensorFlow library, and all programming done on one Jupyter Notebook. Python 3 and TensorFlow 2.8.2 versions were deployed while other libraries such as Pandas, Numpy, Seaborn and Matplotlib were used also. The Google Colab cloud environment was used to train and test our model as we needed fast and secure computing resources. Data pre-processing is described in sections 2.2 to 2.4 below.

2.2.Dataset Acquisition

The dataset for this project was the CICIDS-2017 dataset developed by the Canadian Institute for Cybersecurity at the University of New Brunswick. It is made up of a 5-day data stream (3rd–7th July 2017) on a network formed by machines running operating systems like Windows Vista / 7 /

8.1 / 10, Mac, Ubuntu 12/16 and Kali Linux. Information about the CICIDS-2017 dataset can be found at the website (Canadian Institute for Cybersecurity, 2017). This dataset consists of eight CSV files, with seven of the files containing two types of network traffic; BENIGN and a particular attack malicious network traffic, while one of the files contains only BENIGN network traffic. Since the project concept was to build a singular classifier that could identify any of the attack scenarios, all eight CSV files were imported and merged as one. Figure 2 describes the download and merging of the dataset.

```python
# importing all 8 datasets
df1 = pd.read_csv("/content/drive/MyDrive/IDS with TensorFlow/MachineLearningCSV.zip (Unzipped Files)/MachineLearningCVE/Tuesday-WorkingHours.pcap_ISCX.csv")
df2 = pd.read_csv("/content/drive/MyDrive/IDS with TensorFlow/MachineLearningCSV.zip (Unzipped Files)/MachineLearningCVE/Monday-WorkingHours.pcap_ISCX.csv")
df3 = pd.read_csv("/content/drive/MyDrive/IDS with TensorFlow/MachineLearningCSV.zip (Unzipped Files)/MachineLearningCVE/Wednesday-workingHours.pcap_ISCX.csv")
df4 = pd.read_csv("/content/drive/MyDrive/IDS with TensorFlow/MachineLearningCSV.zip (Unzipped Files)/MachineLearningCVE/Thursday-WorkingHours-Afternoon-Infilteration.pcap_ISCX.csv"
df5 = pd.read_csv("/content/drive/MyDrive/IDS with TensorFlow/MachineLearningCSV.zip (Unzipped Files)/MachineLearningCVE/Thursday-WorkingHours-Morning-WebAttacks.pcap_ISCX.csv")
df6 = pd.read_csv("/content/drive/MyDrive/IDS with TensorFlow/MachineLearningCSV.zip (Unzipped Files)/MachineLearningCVE/Friday-WorkingHours-Afternoon-DDos.pcap_ISCX.csv")
df7 = pd.read_csv("/content/drive/MyDrive/IDS with TensorFlow/MachineLearningCSV.zip (Unzipped Files)/MachineLearningCVE/Friday-WorkingHours-Afternoon-PortScan.pcap_ISCX.csv")
df8 = pd.read_csv("/content/drive/MyDrive/IDS with TensorFlow/MachineLearningCSV.zip (Unzipped Files)/MachineLearningCVE/Friday-WorkingHours-Morning.pcap_ISCX.csv")
```
Python

```python
# merging datasets into 1
list_of_df = [df1, df2, df3, df4, df5, df6, df7, df8]
IDS_df = pd.concat(list_of_df, axis=0, ignore_index=True)
```
Python

Fig.2: Dataset Download and Merging

2.3.Data Exploration (Exploratory Data Analysis)

Exploratory Data Analysis involves the inspection and visualisation of our data in order to spot errors and trends that could affect model performance. While the data in its raw form had been well arranged and was very valuable, there were certain aspects that would have made building a reliable classification model challenging. Data exploration involved the following steps:

- Checking for duplicates
- Checking for Columns and data types
- Checking for Infinity and Null values
- Checking for Constant Features
- Checking sample size

Upon checking the dataset, it was apparent that the BENIGN classes had far more samples than the other (attack) classes. With the dataset being skewed, grouping and oversampling of the other classes was required during the feature engineering phase of the project. Figure 3 below displays the high data skew.

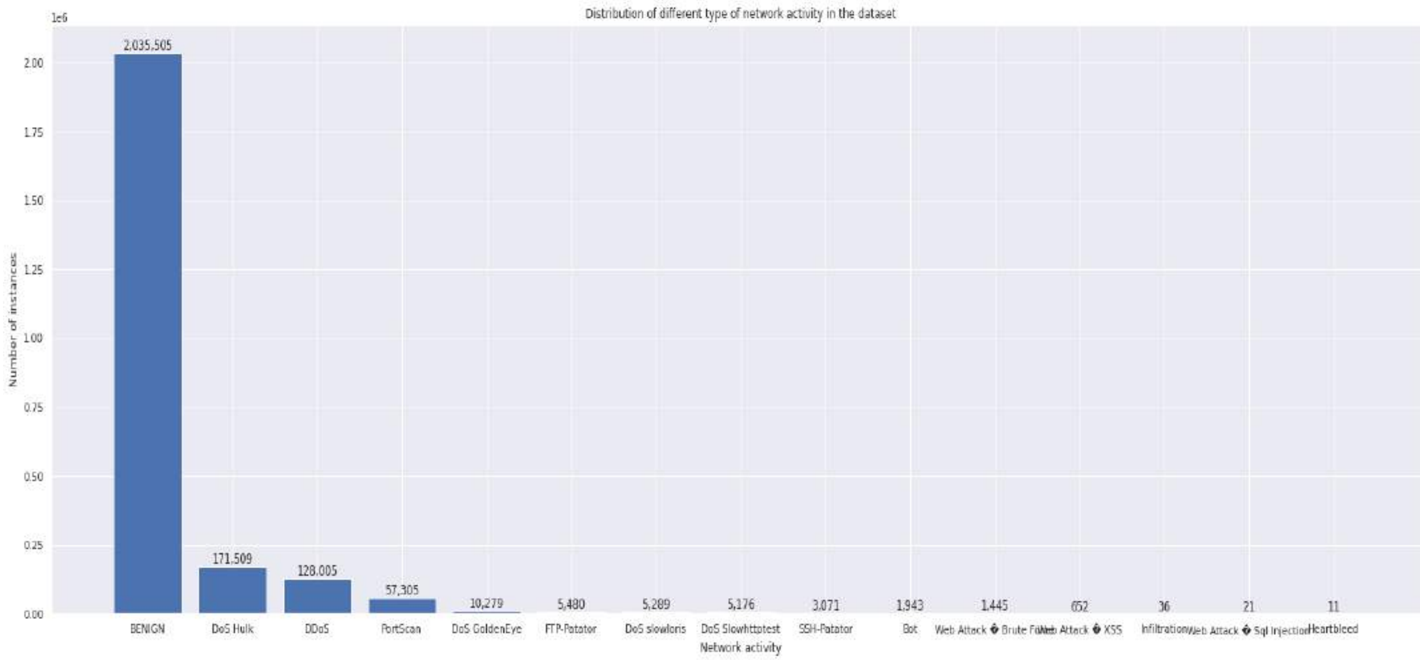

Figure 3: High skew of Dataset

2.4.Data Cleaning

Having identified the above issues with the dataset, it was therefore necessary to carry out consequent data cleaning. This was done by the following steps:

- Handling Duplicates
- Changing Column Size
- Removing Null and Infinity Values
- Dropping Constant Features
- Inspection of Label
- Correcting Heavy Dataset Skew

New grouping of the target classes in order to reduce the heavy skew in the dataset was carried out and the resultant distribution is shown in figure 4.

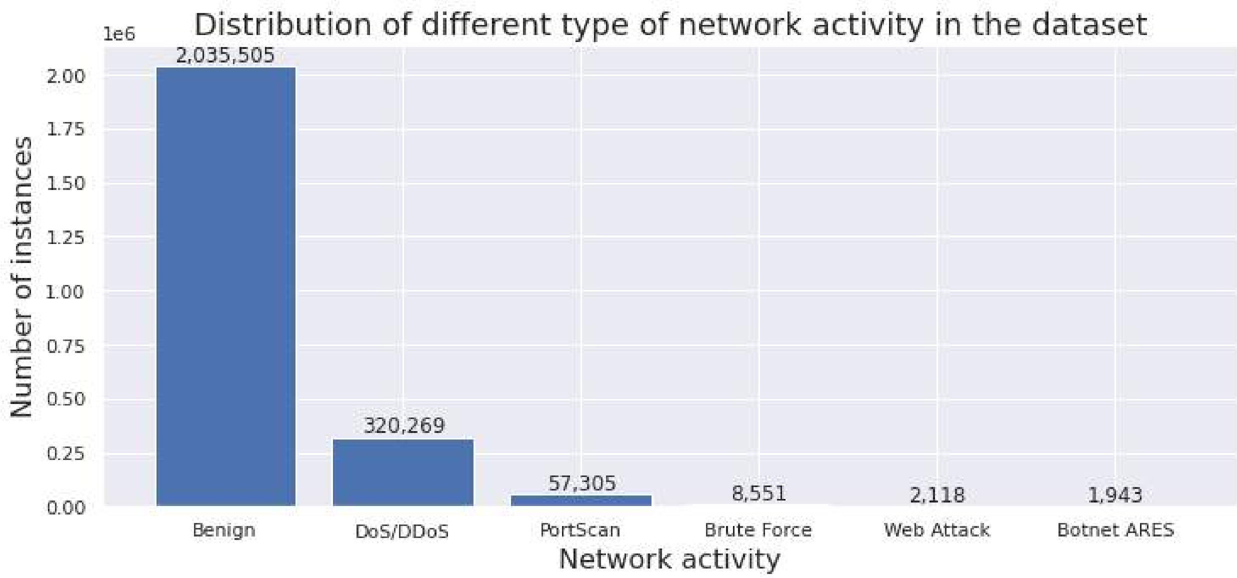

Figure 4: Bar Chart showing New Data Distribution

2.5.Splitting the Dataset

Every machine learning algorithm requires data for training as well as test data to evaluate the performance of the algorithm and to see how well it works. At this stage, we split the dataset into two; training and testing datasets. This common practice helps determine whether the model is overfitting the dataset or not. The algorithm trains a model on the training data and applies it to the test data. The result of the test data is the performance of the machine learning algorithm [9]. The CICIDS2017 dataset does not contain separate training and test data, but rather a single unbundled dataset. As a result, the data needed to be separated into training and test sections. The train test split Sklearn tool was used to separate the dataset into a twenty-percent test and eighty-percent training data split (see Appendix 1). As the BENIGN classes were far more than other label classes, we had to stratify the split to ensure all classes were included in the same ratio between the training and test datasets.

2.6.Feature Engineering

In order to make our model train faster and resolve its skewed nature totally, we had to numerically encode the labels and employ an oversampling and undersampling strategy for the target label classes. Numerical encoding of the "label" is carried out as shown in appendix 2. Application of Undersampling and Oversampling strategy to balance the training dataset further resulted in a numerical data collection (see appendix 3). Evaluation metrices were set afterwards.

2.7.Building the Neural Network

The Deep Neural Network model was configured with six Hidden Dense layers, all using the "relu" activation. The output layer was configured with "softmax" activation since we are dealing with more than two classes.

2.8.Training and Evaluating Model performance

Before training our model, we first compiled it using the 'SparseCategoricalCrossentropy' loss function since the classes in our target label are all mutually exclusive. Next, we used the 'Adam optimizer' and set the learning rate to 0.001, and then trained the model for 5 epochs (see appendix 4).

3. RESULTS AND DISCUSSION

The Test portion of the dataset was used as the basis for validating model performance. It represents twenty percent of the overall dataset. Five metrics were used to validate the performance of Neural Network model. They are Loss, Accuracy, F1-Measure, Precision and Recall-measure. Results for the five epochs considered are described in Table 1, while Accuracy is further described in figure 5.

Table 1: Result of Model Performance

EPOCH	TIME TAKEN (secs.)	LOSS	ACCURACY (%)	F1-MEASURE	PRECISION	RECALL-MEASURE
1	110	0.0230	98.85	0.2740	0.1621	1.0041
2	108	0.0336	98.65	0.2735	0.1618	1.0028
3	109	0.0140	99.63	0.2755	0.1630	1.0104
4	110	0.0131	99.71	0.2728	0.1614	1.0003
5	106	0.0260	99.20	0.2730	0.1615	1.0010

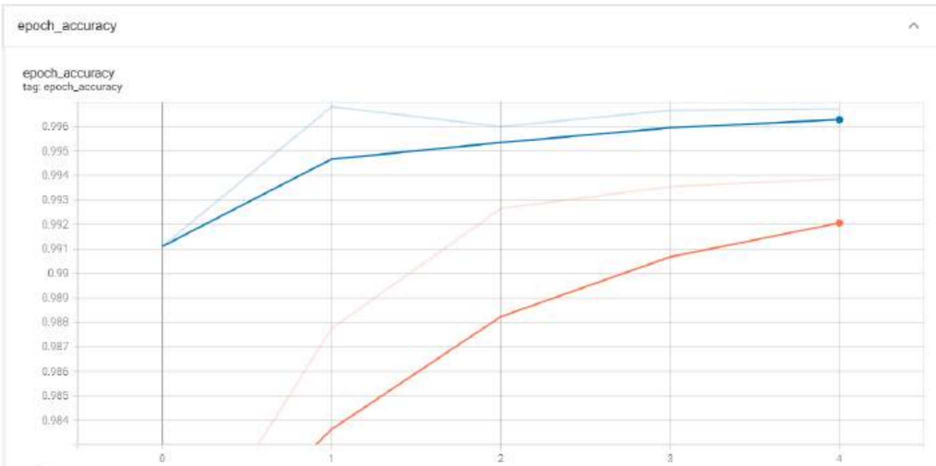

Figure 5: Model Accuracy

As can be seen in Table 1, the model had the highest accuracy (99.71%) at the 4th epoch. While the average accuracy is approximately 99.2% representing a high accuracy model.

CONCLUSION

This paper describes the development and testing of a Deep Neural Network model for intrusion Detection in Computer Networks namely, NETSHIELD. The CICIDS 2017 dataset was implemented and results show that the model is highly accurate.

REFERENCES

[1] Feurer, M. and Hutter, F. (2019) Hyperparameter optimization. In: Hutter F, Kotthoff L, Vanschoren J, editors. Automated machine learning: methods, systems, challenges. Springer International Publishing; p. 3–33. http://dx.doi.org/10.1007/978-3-030-05318-5_1.

[2] Géron, A. (2017) Hands-on machine learning with Scikit-Learn and TensorFlow: concepts, tools, and techniques to build intelligent systems. " O'Reilly Media, Inc."

[3] McHugh, John. (2000) 'Testing Intrusion Detection Systems: A Critique of the 1998 And 1999 DARPA Intrusion Detection System Evaluations as Performed by Lincoln Laboratory.' ACM Transactions on Information and System Security (TISSEC) 3, no. 4: 262-294.

[4] Masduki, B.W., Ramli, K., Saputra, F.A. and Sugiarto, D. (2015) 'Study on Implementation of Machine Learning Methods Combination for Improving Attacks Detection Accuracy on Intrusion Detection System (IDS).' *In: 2015 International conference on quality in research. IEEE;* p. 56–64.

[5] Mishra, P., Varadharajan, V., Tupakula, U. and Pilli, E.S. (2018) 'A Detailed Investigation and Analysis of Using Machine Learning Techniques for Intrusion Detection.' IEEE Commun. Surv. Tutor 2018;21(1):686–728.

[6] Najafabadi, M.M., Villanustre, F., Khoshgoftaar, T.M., Seliya, N., Wald, R. and Muharemagic, E. (2015) 'Deep Learning Applications and Challenges in Big Data Analytics.' J Big Data 2015;2(1):1.
[7] Osken, S., Ecem, N. Y., Gozde, K. and Levent, C.. (2019) 'Intrusion Detection Systems with Deep Learning: A Systematic Mapping Study.' *2019 Scientific Meeting on Electrical-Electronics & Biomedical Engineering and Computer Science (EBBT)*, 1-4. IEEE.
[8] Canadian Institute for Cybersecurity, (2017) 'Intrusion Detection Evaluation Dataset (CIC-IDS2017).' Available at: www.unb.ca/cic/datasets/ids-2017.html. Accessed 24 September 2022.
[9] Xie, J. Song, Z. Li, Y. Zhang, Y. Yu, H. and Zhan, J. et al. (2018) 'A Survey on Machine Learning Based Mobile Big Data Analysis: Challenges and Applications.' Wirel. Commun. Mobile Comput.

APPENDIX

1. Splitting the Dataset

```
labels = IDS_df['label_category']
features = IDS_df.drop(labels=['label', 'label_category'], axis=1)
```

```
from sklearn.model_selection import train_test_split

X_train, X_test, y_train, y_test = train_test_split(features, labels, test_size=0.2, random_state=42, stratify=labels)
#X_test, X_val, y_test, y_val = train_test_split(X_test, y_test, test_size=0.5, random_state=42)
```

```
X_train.shape, X_test.shape#, X_val.shape
```

```
((1940552, 68), (485139, 68))
```

2. Label Encoding

```
columns = numeric_features.tolist()

X_train = pd.DataFrame(preprocessor.fit_transform(X_train), columns=columns)
X_test = pd.DataFrame(preprocessor.transform(X_test), columns=columns)
#X_val = pd.DataFrame(preprocessor.transform(X_val), columns=columns)


le = LabelEncoder()

y_train = pd.DataFrame(le.fit_transform(y_train), columns=["label"])
y_test = pd.DataFrame(le.transform(y_test), columns=["label"])
#y_val = pd.DataFrame(le.transform(y_val), columns=["label"])
```

```
y_train.value_counts()
```

```
label
0        1628403
3         256215
4          45844
2           6841
5           1694
1           1555
dtype: int64
```

3. Numerical Result of Sampling

```
undersampling_strategy = {
    0: 800000,
    3: 192161,
    4: 34383,
    2: 5131,
    5: 1271,
    1: 1166,
}

oversampling_strategy = {
    0: 800000,
    3: 212102,
    4: 44460,
    2: 50115,
    5: 50284,
    1: 50149,
}

# Balance the training set
X_train_bal, y_train_bal = balance_dataset(X_train, y_train, undersampling_strategy, oversampling_strategy)
```

4. Training and Evaluation

```
tf.random.set_seed(42)

model = tf.keras.Sequential([
    tf.keras.layers.Dense(activation="relu", units=256),
    tf.keras.layers.Dense(activation="relu", units=128),
    tf.keras.layers.Dense(activation="relu", units=64),
    tf.keras.layers.Dense(activation="relu", units=32),
    tf.keras.layers.Dense(activation="relu", units=16),
    tf.keras.layers.Dense(activation="relu", units=8),
    tf.keras.layers.Dense(activation="softmax", units=6),
])


model.compile(loss=tf.keras.losses.SparseCategoricalCrossentropy(),
              optimizer=tf.keras.optimizers.Adam(learning_rate=0.001),
              metrics=["accuracy", f1_m, precision_m, recall_m])

model.fit(X_train_bal,
          y_train_bal,
          validation_data = (X_test, y_test),
          batch_size=32,
          epochs=5)
```

NIPES-NCEE Conference Proceedings
The 2nd International Conference 15th-17th Feb. 2023
193-202
www.nipesjournals.org.ng

COMPARATIVE ANALYSIS OF MACHINE LEARNING MODELS LEVERAGING THE NSL-KDD DATASET

Osa Edosa
Department of Electrical/Electronic Engineering
Faculty of Engineering
University of Benin, Benin City, Nigeria.
eddyedos@yahoo.com
+2348168307508

Ekinkonye Ifeoma O.
Department of Mathematics and Computer Science
Western Delta University, Oghara, Nigeria.
ejinkonye.ifeoma@yahoo.com
+2348060297345.

*Corresponding Author: Osa Edosa.

Abstract

Cyber-attack on networks is a major threat to information security in the society. Various attacks are being launched continually to intrude into personal and organizational networks by attackers for malicious purposes. Intrusion detection systems act as a defensive tool in detecting such attacks on a network. Recently, machine learning algorithms are being utilized in developing such systems and one integral component of such design is the dataset. This paper is aimed at performing a comparative analysis of the performance of some machine learning models with respect to the NSL-KDD dataset. Models such as Random Forest, Logistic Regression, Support Vector Machine (SVM), Artificial Neural Network (ANN) and K-Nearest Neighbour (KNN) were considered without feature selection. Performance metrices such as Accuracy, F1-score, Precision and Recall were used as basis for comparing the models. Results show that Random Forest gives the best accuracy compared to the other models.

***Keywords**: Dataset, Machine Learning, Random Forest, Accuracy, NSL-KDD.*

1. INTRODUCTION

By January 2021, the internet had about 4.66 billion active users representing about 59.5% of the global population in comparison to year 2000 where the internet had an active user statistic of 400million representing about 4.8% of the global population at the time [1]. This high percentage increase underscores the extent to which computer networks and the internet at large have become integrated into human endeavours. From crucial applications in healthcare and military, to relative ease at which financial transactions can be made with just a swipe of a card or the touch of a button, our world has become so computer-reliant, analogous to being connected to a life support machine a trend not likely to abate in any near future. However, this increased use of the internet has also brought about the ensuing problem of cybercrime. An increasing number of cyberattacks, including phishing and malicious software make cyber security threats the downside to utilizing computer networks. Criminally motivated attackers desire ransom as rewards for money theft and identity theft. Other motives for cyber-attacks include espionage, political statements, etc. [2]. These threats are therefore highly significant issues that information technology-based organizations must address critically [3].

Cybersecurity could be defined as the practice of defending critical systems as well as sensitive data from digital attacks, due to technology, people and processes [1]. It is responsible for the protection of internet-connected systems such as hardware, software and data from cyberthreats. A lot of research into the development of network security technologies has been the focus lately. Various traditional Intrusion Detection Systems (IDS) have been employed over the years such as Signature-based IDS schemes and Anomaly-based IDS. However, more recently Artificial intelligence (AI) techniques such as Machine Learning (ML) are being utilized to detect malicious traffic in computer networks. ML is a sub- field of AI that develops systems with capability of automatic learning and improving from experience without explicit programming [4]. This model of operation is in consonance with the principle of attack detection by a self-learning system against external intrusion in order to improve detection rate and reduce the rate of false positives. Machine Learning for Network traffic intrusion detection is therefore a viable area of research.

1.1 Intrusion Detection System (IDS)

Intrusion into computer networks can be said to be the illegal attempt to gain entry into a computer system or network. Intrusion detection is the act of detecting intrusions into a network or a computer. IDS could be hardware, software or combination of both monitoring the network flow in the search of intrusions. This system reviews all outgoing and ingoing network activity and logs doubtful patterns. They can be classified into Host-based Intrusion Detection System (HIDS) [5] and Network-based Intrusion Detection System (NIDS) [6].

1.1.1. Host-based Intrusion Detection System

Host based intrusion detection takes place on a single host system such as a server or personal computer [7]. It is a software application installed in order to protect the system from intruders.

1.1.2. Network-based Intrusion Detection System

A network-based intrusion detection system (NIDS) is used to monitor as well as analyze network traffic in order to protect a system from network-based threats [8]. It reads all inbound packets and searches for any suspicious patterns. The two well-known types of NIDS are the signature-based and anomaly-based detection.

1.1.3 Signature-based Intrusion Detection System

Signature-based IDS detects attacks by checking for specific patterns such as byte sequences in network traffic, or for known malicious sequences.

1.2 Statement of Problem

Typically, signature-based IDS utilize a predefined database of security attacks' signatures and attempt to match system events and traffic to the specific attack patterns in the database [9]. However, this operation cannot detect new attacks where pattern and signature are unknown (zero-day attacks). Anomaly-based IDS on the other hand attempt to learn normal system behaviors and categorize all else as anomaly [10]. Nonetheless, they suffer from false positive problems as a normal traffic could be seen as anomaly. Machine learning based IDS could be employed to surmount the above challenges since they can self-learn and detect zero-day attacks. They also can improve on the false positive problem. One factor that has a direct impact on the effectiveness of machine learning IDS techniques is the availability of the label datasets from traffic flow [11].

2. METHODOLOGY

The methodology involved design, training, and testing some supervised machine learning classification algorithms on the NSL-KDD dataset for detecting network intrusion. The flowchart is described in figure 1.

Fig 1: Flowchart of Methodology

2.1.Exploring NSL-KDD Dataset

In machine learning operations, dataset is primary. NSL-KDD network dataset, a refined version KDD CUP 99 is employed in this paper. NSL-KDD attempts to solve the inherent problems of KDD CUP 99 [12]. The NSL-KDD records a train dataset of 125971 and test dataset of 22542 as shown from the last five records at the tail() end of the dataset (see appendix 1). These reasonable record sizes reduce the need for random selection of a small data portion for experiments.

2.2.Environmental setup

The algorithm development was implemented on a Windows 10 system with a 2.86GHZ Intel(R) Core i3 processor with 4GB of RAM. Jupyter Notebook with Python 3 installed on Anaconda Navigator was also employed as well as libraries like Pandas, Sklearn etc.

NIPES-NCEE Conference Proceedings
The 2nd International Conference 15th-17th Feb. 2023
193-202
www.nipesjournals.org.ng

2.3.Data extraction and Data Processing

The dataset was first downloaded from Kaggle.com, then checked to determine the total number of rows from both the train and the test dataset. Thereafter, the column labels were included to label the dataset for both training and testing as shown in the figure 2.

	duration	protocol_type	service	flag	src_bytes	dst_bytes	land	wrong_fragment	urgent	hot	...	dst_host_same_srv_rate	dst_host_diff_srv_rate	dst_host
0	0	udp	other	SF	146	0	0	0	0	0	...	0.00	0.60	
1	0	tcp	private	S0	0	0	0	0	0	0	...	0.10	0.05	
2	0	tcp	http	SF	232	8153	0	0	0	0	...	1.00	0.00	
3	0	tcp	http	SF	199	420	0	0	0	0	...	1.00	0.00	
4	0	tcp	private	REJ	0	0	0	0	0	0	...	0.07	0.07	

Figure 2: Dataset with Label for Easy Classification

2.4.Data Transformations

The attack field was first transformed by adding a column that encodes 'normal' values as *0* and 'attack' values as *1*. This represented a simple binary classification model that identifies any attack (see appendix 2). Each attack was classified according to attack type for a more granular prediction model. Four attack types were classified as DOS, Probe, U2R, and R2L. The training dataset consisted twenty-one different attacks which also appear in the test dataset. The known attack types are contained in the training dataset while the novel attacks are the additional attacks in the test dataset (i.e., those not included in the training dataset). An evaluation on the dataset was carried out to visualize the attack type versus the protocol type using *pd. crosstab*. Figure 3 shows that most attacks are against the TCP protocol.

protocol_type	icmp	tcp	udp
attack_map			
DOS	2847	42188	892
R2L	0	995	0
U2R	0	40	3
normal	1309	53608	12434
probe	4135	5857	1664

Figure 3: Number of Attacks versus Network Protocol

Using *plt. show()* further displayed the different protocols (i.e., icmp, tcp and udp) and their attack types as shown in figure 4.

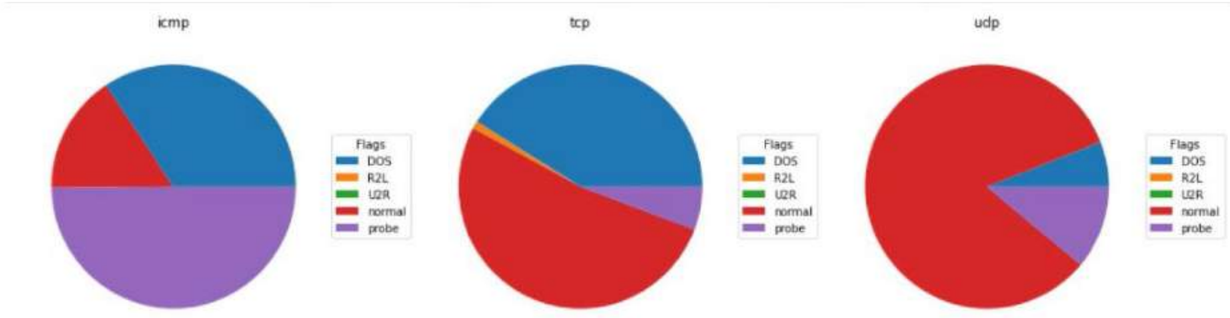

Figure 4: Pie chart of Network protocols and Attacks

2.5.Classifier Algorithms

Five different classifiers were employed namely; Random Forest, Artificial Neural Network (ANN), Support Vector Machine (SVM), K-Nearest Neighbour (KNN) and Logistic Regression. The rationale was that since each classifier belongs to a different family of classifiers, they would result in different models despite the same dataset being used as input.

2.6.Model Building

2.6.1. Data Split

Data was split into train and test set using the scikit-learn library with the train_test_split() function. Four variables were simultaneously created as follows: (x_train and y_train) for the training set and (x_test and y_test) for test set.

2.6.2. Model Fitting

Due to the nature of the dataset, Decision trees were a good starting point for building the predictive models. Random forest was first used to build the model. RandomForestClassifier() function from the sklearn.linear_model sub-module was imported to train the model. Next, the function was assigned to a variable *rf_model* and *the .fit()* function performed the actual model training on the input data x_train and y_train.

2.6.3. Prediction with Test Dataset

After successfully building the model, it was tested using the test dataset to observe its predictive ability. The test feature was passed as the *x_test* and it was allowed to predict the *y_test* after which performance metrices such as Accuracy, Precision, Recall and F1 were evaluated and the confusion matrix was plotted.

The same steps as described above were repeated for the other four classifiers.

3. RESULTS AND DISCUSSION

Following the use of the five different classifiers from different classification family, after training the model with the training dataset and testing the split data to predict it accuracy, the dataset was then tested to see how the trained model performed. It was then compared to see the classifier that has the highest prediction rate, (i.e., the confusion matrix was evaluated to see the number of true Positive, true negative, false positive and false negative of each classifier's predictions on the test dataset). Below is the confusion matrix for the test dataset of each of the classifier.

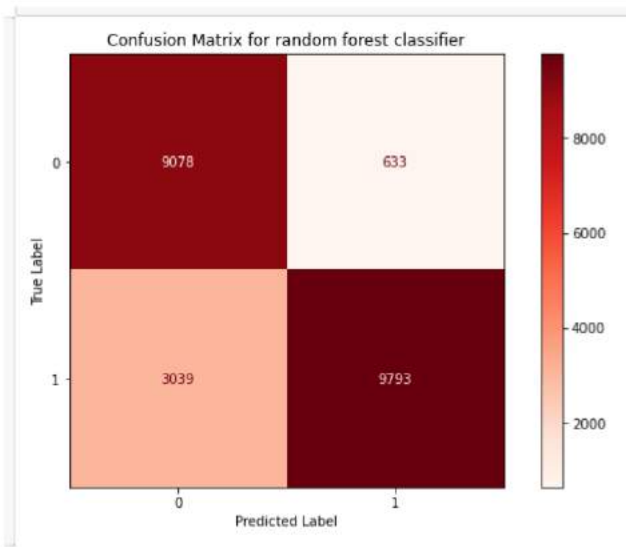

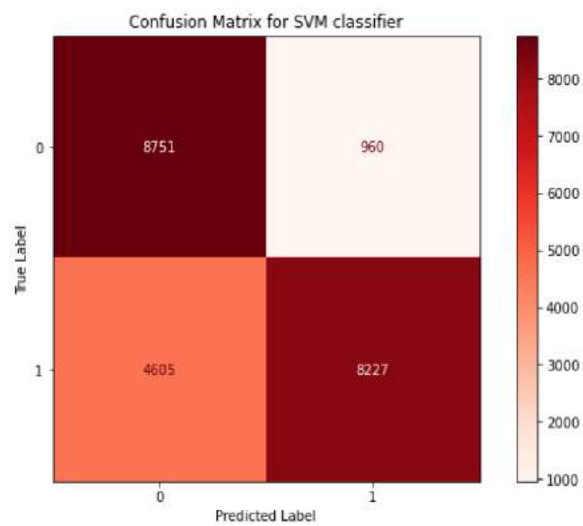

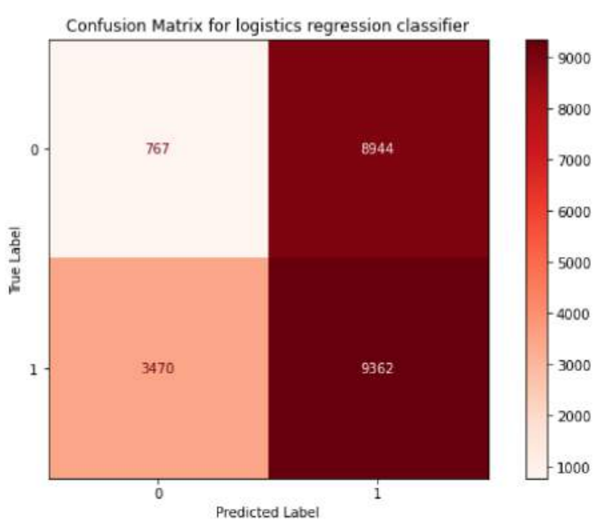

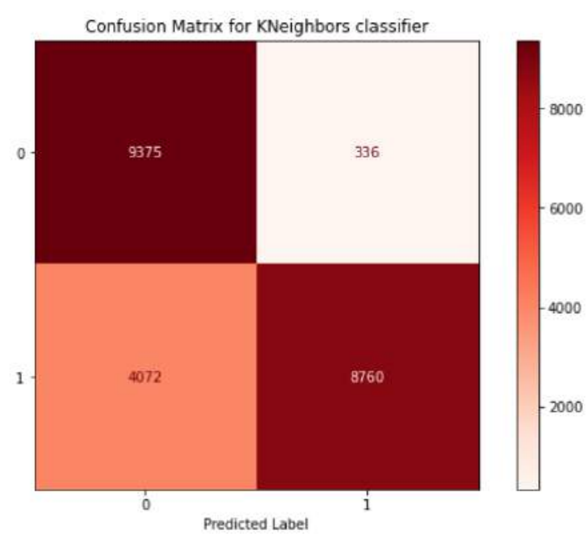

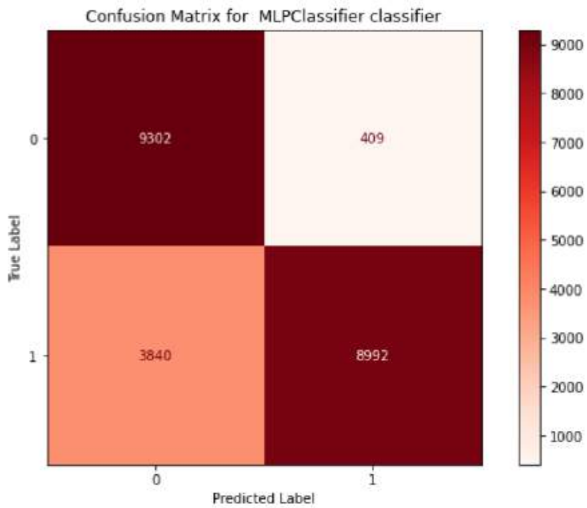

Figure 3: Confusion Matrices for the Five Classifiers

The above confusion matrix plots show information regarding the metrics (Accuracy, Precision, Recall, and F1 score) of the trained model when applied to an unknown test dataset.

Table 1 interprets the confusion matrices as it displays the metrics for the trained models when an unknown dataset (i.e., the test dataset) is passed through the model to predict the number of intrusions present in the network dataset.

Table 1: Performance Metrices of Classifier Models

Model Name	Accuracy	Precision	Recall	F1
Random Forest	0.837111	0.939286	0.763170	0.842119
SVM	0.753138	0.895505	0.641132	0.747264
Logistic Regression	0.449319	0.511417	0.729582	0.601323
ANN	0.811516	0.956494	0.700748	0.808888
KNN	0.804463	0.963061	0.682668	0.798978

From Table 1 above, Random Forest had the highest accuracy of approximately 84% followed by ANN (81%), KNN (80%), SVM (75%) and logistic regression (45%) in the order of accuracy.

CONCLUSION

This paper describes the design, implementation and testing of a network-based intrusion detection model. Five machine learning classifiers were used to rank the forty-one features in the NSL-KDD dataset and comparison was done based on prediction accuracy level. The performance of the classifier was also evaluated based on their predictive accuracy. The results show that Random Forest had the best accuracy compared to the others.

REFERENCES

[1] Ashfaq, R.A.R., Wang, X.-Z., Huang, J.Z., Abbas, H., He, Y.-L., (2017). Fuzziness based semi-supervised learning approach for intrusion detection system. *Inf. Sci.* 378, 484–497.

[2] AT&T Cybersecurity, (2021). Hosted IDS: Host-Based intrusion detection system. Available at: www.cybersecurity.att.com.

[3] Bridges, R.A., Glass-Vanderlan, T.R., Iannacone, M.D., Vincent, M.S., Chen, Q., (2019). A survey of intrusion detection systems leveraging host data. *ACM Comput. Surv*. 52, 1–35.

[4] Brownlee, J. (2018). How to think about machine learning,". Available: https://machinelearningmastery.com/think-machine-learning.

[5] IBM, 2021. WHAT IS A CYBER ATTACK? WHY CYBER ATTACKS HAPPEN. Available at: www.ibm.com.

[6] Johnson, J. (2021). Worldwide Digital Population as of January 2021. Available at: www.statista.com.

[7] Masdari, M., Khezri, H., (2020a). A Survey and Taxonomy of the Fuzzy Signature-Based Intrusion Detection Systems. Applied Soft Computing, p. 106301.

[8] Masdari, M., Khezri, H., (2021b). Towards fuzzy anomaly detection-based security: a comprehensive review. Fuzzy Optim. Decis. Making 20, 1–49.

[9] Tavallaee, M., Bagheri, E., Lu, W. and Ghorbani, A. "A Detailed Analysis of the KDD CUP 99 Data Set," *Submitted to Second IEEE Symposium on Computational Intelligence for Security and Defense Applications (CISDA)*, 2009.

[10]Sultana, N., Chilamkurti, N., Peng, W., Alhadad, R., (2019). Survey on SDN based network intrusion detection system using machine learning approaches. *Peer-to-Peer Networking and Applications* 12, 493–501.

[11]Techopedia, (2021). Network-based Intrusion Detection System (NIDS). What Does Network-based Intrusion Detection System (NIDS) Mean? Available at: www.techopedia.com.

[12]Von Solms, R., Van Niekerk, J., (2013). From information security to cyber security. *Comput. Secur.* 38, 97–102.

APPENDIX

1. NSL-KDD DATASET RECORDS

```
from sklearn.metrics import classification_report
from sklearn import metrics
```

In [74]:

```
#import the dataset to the jupyter notebook
train_data = "nsl-kdd/KDDTrain+.txt"
test_data = "nsl-kdd/KDDTest+.txt"

df_train = pd.read_csv(train_data)

df_test = pd.read_csv(test_data)

df_train.tail()
```

Out[74]:

	0	tcp	ftp_data	SF	491	0.1	0.2	0.3	0.4	0.5	...	0.17.1	0.03	0.17.2	0.00.6	0.00.7	0.00.8	0.05	0.00.9	normal	20
125967	0	tcp	private	S0	0	0	0	0	0	0	...	0.10	0.06	0.00	0.0	1.00	1.0	0.00	0.0	neptune	20
125968	8	udp	private	SF	105	145	0	0	0	0	...	0.96	0.01	0.01	0.0	0.00	0.0	0.00	0.0	normal	21
125969	0	tcp	smtp	SF	2231	384	0	0	0	0	...	0.12	0.06	0.00	0.0	0.72	0.0	0.01	0.0	normal	18
125970	0	tcp	klogin	S0	0	0	0	0	0	0	...	0.03	0.05	0.00	0.0	1.00	1.0	0.00	0.0	neptune	20
125971	0	tcp	ftp_data	SF	151	0	0	0	0	0	...	0.30	0.03	0.30	0.0	0.00	0.0	0.00	0.0	normal	21

5 rows × 43 columns

2. CREATING VARIABLES TO ALLOCATE 0 TO NORMAL AND 1 TO ATTACK

```
df_test.columns = columns
```

In [76]:

```
df_train.head()
```

Out[76]:

	duration	protocol_type	service	flag	src_bytes	dst_bytes	land	wrong_fragment	urgent	hot	...	dst_host_same_srv_rate	dst_host_diff_srv_rate	dst_host_
0	0	udp	other	SF	146	0	0	0	0	0	...	0.00	0.60	
1	0	tcp	private	S0	0	0	0	0	0	0	...	0.10	0.05	
2	0	tcp	http	SF	232	8153	0	0	0	0	...	1.00	0.00	
3	0	tcp	http	SF	199	420	0	0	0	0	...	1.00	0.00	
4	0	tcp	private	REJ	0	0	0	0	0	0	...	0.07	0.07	

5 rows × 43 columns

In [77]:

```
#create a new variable to allocate 0 to normal traffic and 1 to attack traffic
# This means you are doing 2 class classification: Attack versus No Attack

train_attack = df_train.attack.map(lambda x: 0 if x == 'normal' else 1)

testing_attack = df_test.attack.map(lambda x: 0 if x == 'normal' else 1)

#data

df_train['attack_flag'] = train_attack

df_test['attack_flag'] = testing_attack
```

NIPES-NCEE Conference Proceedings
The 2nd International Conference 15th-17th Feb. 2023
203-217
www.nipesjournals.org.ng

THE COMPREHENSIVE AND ANALYTIC STUDY OF A DUFFING OSCILLATOR WITH CUBIC, QUINTIC AND HEPTIC NONLINEARITIES. (AN ANALYSIS)

Nwamba Ikechukwu Joshua

ICT Unit, Imo State University, Owerri
nwambaik@gmail.com

Abstract

In this work, a thorough analysis of the generalized Duffing system was presented. A special case of this system, the cubic-quintic-heptic Duffing system which suitably models the restrained cargo system was treated comprehensively using analytical methods and the method of averaging (a powerful tool of nonlinear analysis). In our analysis, it was observed that the cubic-quintic-heptic Duffing system exhibits some certain behaviors not present in the dynamics of the cubic and cubic-quintic Duffing systems. The approximate solutions obtained through the use of the averaging technique were compared to the exact solutions obtained numerically using Runge-Kutta method.

Keywords *--- Method of Averaging; external excitation; negative damping; nonlinearity; cubic-quintic-heptic oscillators.*

1.0 Introduction

Understanding the dynamics of certain nonlinear differential equations plays a major role in every aspect of the engineering of physical systems. In reality physical systems are nonlinear in nature, hence the difficulty in analyzing their model equations. One of such nonlinear model differential equation used in modeling a very important class of physical systems is the Duffing equation named after the German engineer Georg Duffing. The Duffing equation which has been considered in different forms turned out useful in modeling many physical phenomena especially in engineering. The classical Duffing equation which may be generally represented by (11) containing a cubic nonlinearity, hence the name cubic Duffing equation, has been studied and researched on extensively since it appeared in literature, see [1-11].

Generally, the damped and forced Duffing system with random noise may be represented by [12,13]:

$$y = u'(t)$$
$$y' + \delta y + \frac{d\phi(u)}{du} = \sum_{i=0}^{P} F_i \cos(\omega_i t + \theta) + \zeta(t) \tag{1}$$

where, the prime denotes differentiation with respect to time t, $P < \infty$, δ is the damping coefficient, F_i and ω_i represents the amplitude and frequency of the external periodic forcing respectively, $\zeta(t)$ is the random noise and $\phi(u)$ an n-well potential may be represented as

$$\phi(u)=\sum_{n=0}^{N}\frac{a_n u^{2n+2}}{2n+2}, N<\infty \tag{2}$$

Setting $y=c(\text{constant})$ in (1), we obtain

$$c=u'$$

$$y'=\sum_{i=0}^{P}F_i\cos(\omega_i t+\theta)+\zeta(t)-\delta c-\frac{d\phi(u)}{du} \tag{3}$$

and

$$\sum_{n=0}^{N}\frac{a_n u^{2n+2}}{2n+2}+\delta c=\sum_{i=0}^{P}F_i\cos(\omega_i t+\theta)+\zeta(t) \tag{4}$$

The stability matrix of the system (3) is then obtained as

$$J=\begin{bmatrix}0 & 1\\ -\frac{d^2\phi(u)}{du^2} & -\delta\end{bmatrix} \tag{5}$$

The corresponding characteristic equation satisfied by J is $\det[J-\lambda I]=0$ which may be represented as

$$\lambda^2+\delta\lambda+\frac{d^2\phi(u)}{du^2}=0 \tag{6}$$

This paper investigates a special case of the system (1), where $N=3$ in (2), in the absence of random noise. Hence the paper is organized as follows, section 2 will present a comprehensive stability analysis of the generalized system (1), in section 3 the stability analysis of the special case mentioned above will be treated, section 4 will be concerned with obtaining an analytical approximate solution to the special case employing the method of averaging [2, 10, 14] (a powerful perturbation technique), in section 5, results obtained will be discussed in details where comparisons will be made between the analytical approximate solution obtained and the exact solution using Runge Kutta method (RK4) for different parameter values, finally the results obtained in this paper will be summarized in section 6.

2.0 Stability analysis of the generalized Duffing system

Setting $\delta = 0, F_i \neq 0$ in (1), we obtain the generalized un-damped and forced Duffing system while setting $\delta \neq 0, F_i = 0$ in (1) gives us the generalized damped and unforced Duffing system. It follows that we will obtain a generalized un-damped and unforced Duffing system when $\delta = F_i = 0$ in (1).

We may set $c = 0$ in (3) to obtain:

$$y' + \frac{d\phi(u)}{du} = \sum_{i=0}^{P} F_i \cos(\omega_i t + \theta) + \zeta(t) \tag{7}$$

Consequently,

$$\frac{d\phi(u)}{du} = \sum_{i=0}^{P} F_i \cos(\omega_i t + \theta) + \zeta(t) \tag{8}$$

Equation (8) gives us the equilibrium or stationary points of the non-autonomous dynamical system (1). We may represent (8) as

$$\phi(u) = u\left[\sum_{i=0}^{P} F_i \cos(\omega_i t + \theta) + \zeta(t)\right] + k(\text{constant}) \tag{9}$$

with the solutions $u_m, m = 0,1,\ldots$ to (8) representing the mentioned stationary points of the system. The stability dynamics of the system (1) will be determined by the solutions to (6). The possibility of obtaining complex, real or purely imaginary eigenvalues for (6) will be solely determined by the values of δ and $Z = \dfrac{d^2\phi(u)}{du^2}$.

With $\delta = 0, \lambda_{1,2} = \pm i\sqrt{Z}$

for this, the following cases were investigated, hence the following results:

1. $Z = 0$: $\lambda_{1,2} = 0$

This contradicts our assumption that $\det[J] \neq 0$ and consequently all the a_n's, $n = 0,1,\ldots$ becomes zero.

2. $Z > 0$: $\lambda_{1,2} = \pm i\sqrt{Z}$

This corresponds to critical points that are centres for which stability is guaranteed. [15]

3. $Z < 0$: $\lambda_{1,2} = \pm\sqrt{Z}$

This corresponds to saddles giving rise to instability. [15]

With $\delta > 0, \lambda_{1,2} = \frac{1}{2}\left[-\delta \pm \sqrt{\delta^2 - 4Z}\right]$

Then considering the cases below, we deduce that

1. $Z = 0$: amounts to $\lambda_{1,2} = 0, -\delta$ which goes contrary to our assumption that $\det[J] \neq 0$ and consequently all the a_n'$s, n = 0,1,\ldots$ becomes zero.

2. $Z > 0$: $\lambda_{1,2} = \frac{1}{2}\left[-\delta \pm \sqrt{\delta^2 - 4Z}\right]$

Considering the discriminant for this case, we have the following cases investigated,

a. $\delta^2 < 4Z$: $\lambda_{1,2} = \frac{1}{2}\left[-\delta \pm i\sqrt{\left(\delta^2 - 4Z\right)}\right]$

which corresponds to spirals and asymptotic stability [15].

b. $\delta^2 > 4Z$: $\lambda_{1,2} = \frac{1}{2}\left[-\delta \pm \sqrt{P}\right], P > 0$

which corresponds to nodes resulting in asymptotic stability if $\delta > \sqrt{P}$ and to saddles as well as consequent instability if $\delta < \sqrt{P}$ [15].

c. $\delta^2 = 4Z$: $\lambda_{1,2} = \pm\sqrt{Z}$

for this case, we have saddles and hence instability [15].

3. $Z < 0$: $\lambda_{1,2} = \frac{1}{2}\left[-\delta \pm \sqrt{\delta^2 + 4Z}\right]$

Considering the discriminant, we investigated two possible cases that can arise:

a. $\delta^2 + 4Z > 0$: $\lambda_{1,2} = \frac{1}{2}\left[-\delta \pm \sqrt{Q}\right], Q > 0$

this leads to the existence of nodes and asymptotic stability if $\delta > \sqrt{Q}$ and to saddles as well as consequent instability if $\delta < \sqrt{Q}$ [15].

b. $\delta^2 + 4Z = 0$: $\lambda_{1,2} = \pm i\sqrt{Z}$

this results to centres and stability [15].

Considering (2) with $N = 1$ leads to

$$\phi(u) = a_0 \frac{u^2}{2} + a_1 \frac{u^4}{4} \tag{10}$$

with $a_0 = \alpha$(proper or resonant frequency), $a_1 = \beta$(coefficient of nonlinearity).

The dynamical system having the potential (10) in the absence of random noise is known as the cubic Duffing system and may be generally represented as

$$u'' + \delta u' + \alpha u + \beta u^3 = \sum_{i=0}^{P} F_i \cos(\omega_i t + \theta) \tag{11}$$

Equation (11) has been presented in different forms, it has also received great attention over the years due to its rich and ever-interesting dynamics. See [1-11]

Considering (2) with $N = 2$ leads to

$$\phi(u) = a_0 \frac{u^2}{2} + a_1 \frac{u^4}{4} + a_2 \frac{u^6}{6} \tag{12}$$

with $a_0 = \alpha$(proper or resonant frequency), $a_1 = \beta, a_2 = \mu, \beta$ and μ being coefficients of nonlinearity.

The dynamical system having the potential (12) in the absence of random noise is known as the cubic-quintic Duffing system and may be generally represented as

$$u'' + \delta u' + \alpha u + \beta u^3 + \mu u^5 = \sum_{i=0}^{P} F_i \cos(\omega_i t + \theta) \tag{13}$$

Equation (13) has also been considered in different forms, it has also received great attention since its first appearance in literature in the early twenty-first century. The stability analysis of the special case of (13) where $\delta = 0, P = 0,1$ and 2 was treated in [10]. On the other hand, a comprehensive stability analysis of (13) was presented recently in [12] and very interesting results were discovered [16]. See [17-23]

Now considering (2) with $N = 3$, we obtain

$$\phi(u) = a_0 \frac{u^2}{2} + a_1 \frac{u^4}{4} + a_2 \frac{u^6}{6} + a_3 \frac{u^8}{8} \tag{14}$$

with $a_0 = \alpha$(proper or resonant frequency),
$a_1 = \beta, a_2 = \mu, a_3 = \sigma, \beta, \mu$ and σ being coefficients of nonlinearity.

The dynamical system having the potential (14) in the absence of random noise is known as the cubic-quintic-heptic Duffing system and may be generally represented as

$$\begin{aligned} y &= u' \\ y' + \delta y + \alpha u + \beta u^3 + \mu u^5 + \sigma u^7 &= \sum_{i=0}^{P} F_i \cos(\omega_i t + \theta) \end{aligned} \tag{15}$$

The system (15) has only appeared three times in literature to the best knowledge of the Author(s). In [16] and [24] respectively, the homotopy analysis method (HAM) as well as the iteration perturbation method (IPM) and the variational iteration method (VIM) were used to investigate (15) obtaining accurate and analytical approximate solutions. It was strongly observed and noted in [25] that (15) best models a restrained cargo system.

2.1 Stability analysis of the Duffing Oscillator with cubic, quintic and heptic nonlinearities

In this section, we employ equations (6) and (9) to investigate the stability of the dynamics of the considered nonlinear oscillator model. The equilibrium or stationary points of the cubic-quintic-heptic Duffing system employing (9) and (14) is given by

$$\alpha \frac{u^2}{2} + \beta \frac{u^4}{4} + \mu \frac{u^6}{6} + \sigma \frac{u^8}{8} = u \left[\sum_{i=0}^{P} F_i \cos(\omega_i t + \theta) \right], k = 0 \tag{16}$$

Considering the case where there are no external forces acting on the system (15), we obtain

$$C + Bu^2 + Au^4 + u^6 = 0 \tag{17}$$

where $A=\frac{4\mu}{3\sigma}, B=2\frac{\beta}{\sigma}$ and $C=4\frac{\alpha}{\sigma}$.

From (16), we obtain the first stationary point as

$$u_0 = 0 \tag{18a}$$

On the other hand, (17) is a polynomial of the sixth order in u, its solution gives the remaining equilibrium points and may be represented by

$$u_{1,2,3,4,5,6}=\sqrt{\frac{1}{2}\sqrt{\sqrt[3]{N+\sqrt{N^2-\frac{4M^3}{27}}}+\sqrt[3]{N-\sqrt{N^2-\frac{4M^3}{27}}}-\frac{A}{3}}} \tag{18b}$$

with $M=B-\frac{A^2}{3}, N=C-\frac{AB}{3}$.

Interested readers may now input different parameter values in (18b) to obtain numerical results which can be further substituted into Z to determine the type of stability possessed by the particular system.

2.2 Method of Averaging

The basic idea of the method of averaging, a powerful tool has been comprehensively discussed in [2, 10, 14].

Now considering a perturbed version of the system (15),

$$u''+\varepsilon\delta u'+\alpha u+\varepsilon\beta u^3+\varepsilon\mu u^5+\varepsilon\sigma u^7=\varepsilon\rho\cos\left(\omega_0 t+\theta\right) \tag{19}$$

where $\varepsilon << 1, \alpha=\omega_0^2$.

We seek a solution to (19) in the form

$$u=a(t)\cos\left(\omega_0 t+\theta(t)\right), u'=-\omega_0 a(t)\sin\left(\omega_0 t+\theta(t)\right) \tag{20}$$

Then according to the averaging technique, the approximate analytical solution to (19) may be represented as

$$u(t)=a\exp-\left(\frac{\varepsilon\delta t}{2}\right)\cos\left[\left(\omega_0+\frac{\varepsilon}{2\omega_0}\left[\frac{\rho}{a}+\frac{3\beta a^2}{4}+\frac{5\mu a^4}{8}+\frac{35\sigma a^6}{64}\right]\right)t+k_2\right] \tag{36}$$

$$u'(t) = -\omega_0 a \exp-\left(\frac{\varepsilon\delta t}{2}\right)\sin\left[\left(\omega_0 + \frac{\varepsilon}{2\omega_0}\left[\frac{\rho}{a} + \frac{3\beta a^2}{4} + \frac{5\mu a^4}{8} + \frac{35\sigma a^6}{64}\right]\right)t + k_2\right] \quad (37)$$

For the un-damped case where $\delta = 0$, (36) and (37) becomes respectively

$$u(t) = a\cos\left[\left(\omega_0 + \frac{\varepsilon}{2\omega_0}\left[\frac{\rho}{a} + \frac{3\beta a^2}{4} + \frac{5\mu a^4}{8} + \frac{35\sigma a^6}{64}\right]\right)t + k_2\right] \quad (38)$$

$$u'(t) = -\omega_0 a\sin\left[\left(\omega_0 + \frac{\varepsilon}{2\omega_0}\left[\frac{\rho}{a} + \frac{3\beta a^2}{4} + \frac{5\mu a^4}{8} + \frac{35\sigma a^6}{64}\right]\right)t + k_2\right] \quad (39)$$

3.0 Results and Discussion

Employing (38) and (39), the following simulations were observed:

First for the case where there is no external forcing i.e $\rho = 0$ in (38) and (39), the following behaviors were observed.

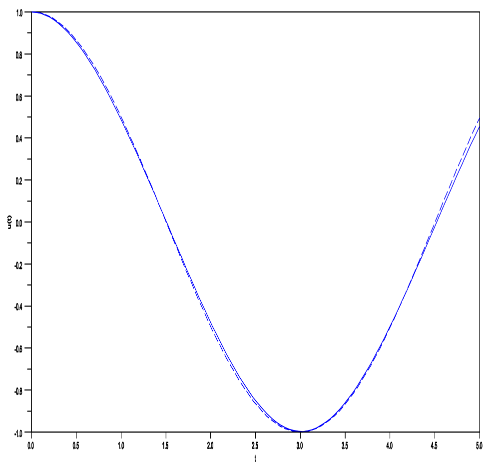

(a)

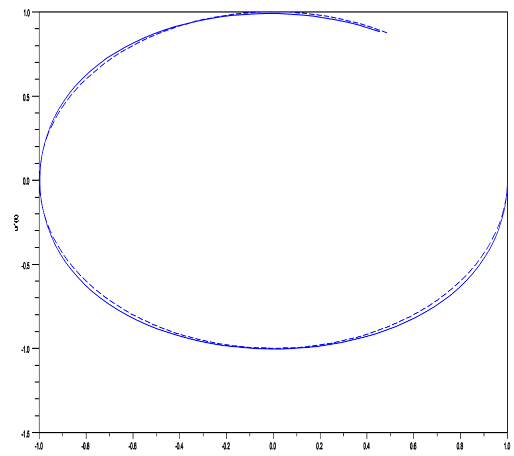

(b)

FIG I: (a) Behavior of the displacement (b) Phase portrait : for $\varepsilon = 0.1, a = \alpha = \beta = \mu = \sigma = \rho = 1$, where the thick line represents the exact solution and the dashed line represent the approximate solution.

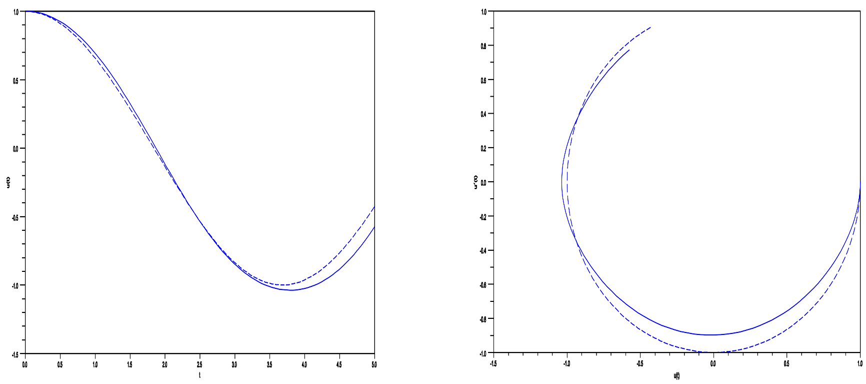

(a) (b)

FIG II: (a) Behavior of the displacement (b) Phase portrait : for $\varepsilon = 0.1, a = \alpha = \rho = 1, \beta = -1, \mu = \tau = 0.01$, where the thick line represents the exact solution and the dashed line represent the approximate solution.

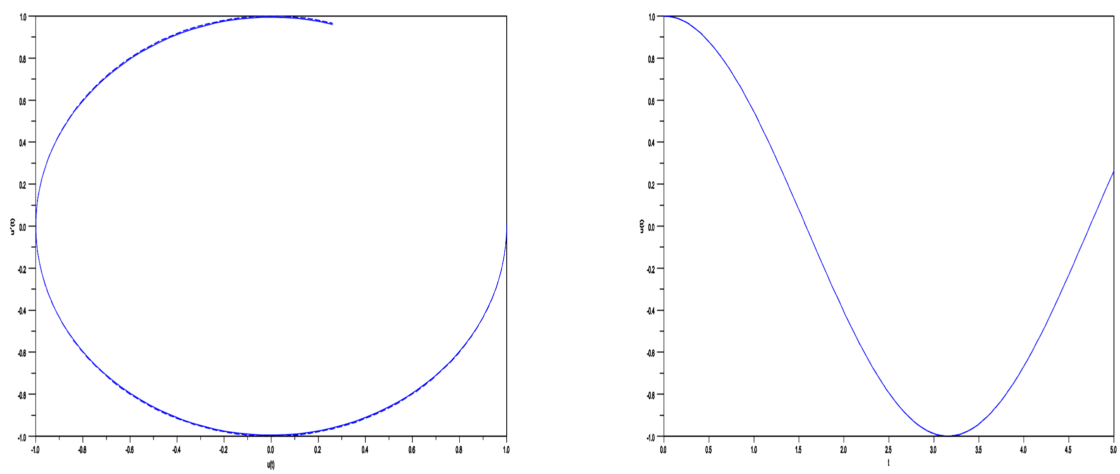

(a) (b)

FIG III: (a) Behavior of the displacement (b) Phase portrait : for $\varepsilon = 0.1, a = \alpha = \sigma = 1, \beta = -0.02, \mu = -1$, where the thick line represents the exact solution and the dashed line represent the approximate solution.

From FIGS I-III, we observed that the nonlinear effect was pronounced for the case $\sigma < 0$ in the un-damped and forced system. On the other hand, we observe also that the introduction of external excitation changes the trajectory of the particles in the system.

Employing (36) and (37), the following simulations were observed for $\delta > 0$:

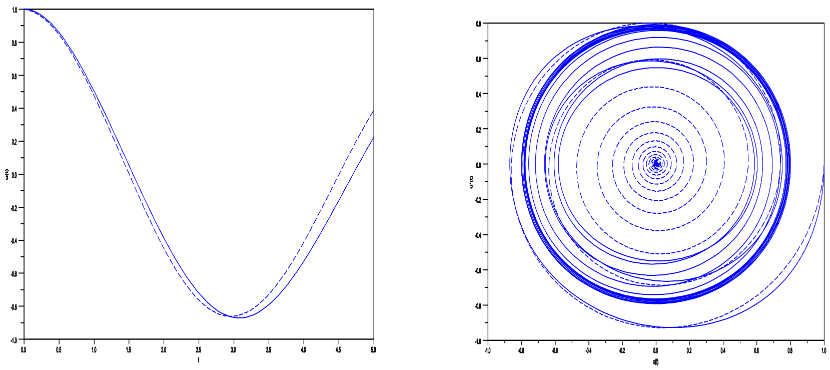

(a) (b)

FIG IV: (a) Behavior of the displacement (b) Phase portrait : for $\varepsilon = 0.1, a = \alpha = \beta = \mu = \sigma = \rho = 1$, where the thick line represents the exact solution and the dashed line represent the approximate solution.

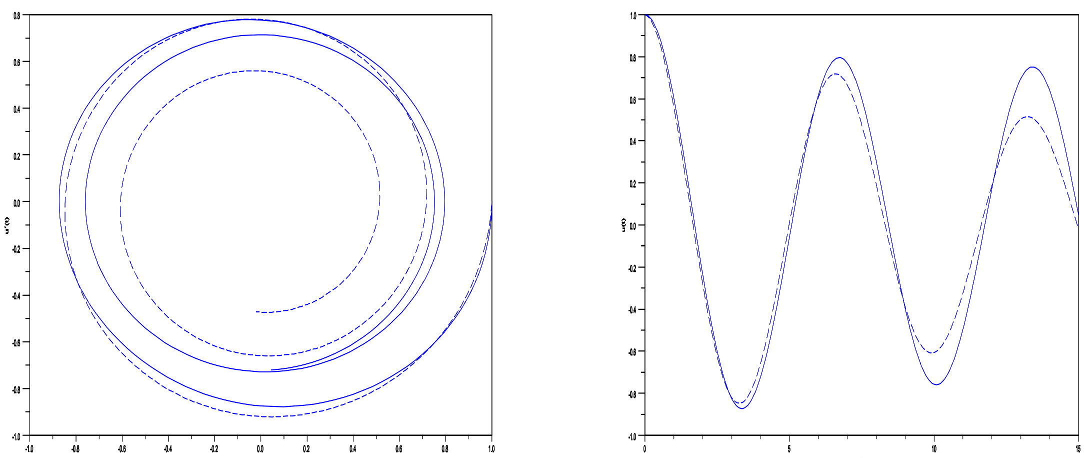

(a) (b)

FIG V: (a) Behavior of the displacement (b) Phase portrait : for $\varepsilon = 0.1, a = \alpha = \rho = \sigma = 1, \beta = -0.02, \mu = -1$, where the thick line represents the exact solution and the dashed line represent the approximate solution.

Employing (36) and (37), the following simulations were observed for $\delta < 0$:

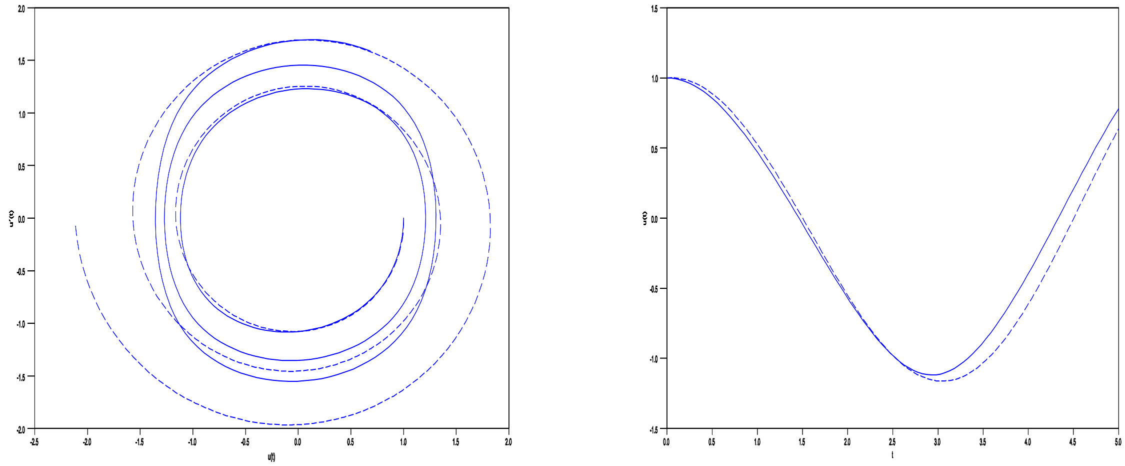

(a) (b)

FIG VI: (a) Behavior of the displacement (b) Phase portrait : for $\varepsilon = 0.1, a = \alpha = \beta = \mu = \sigma = \rho = 1$, where the thick line represents the exact solution and the dashed line represent the approximate solution.

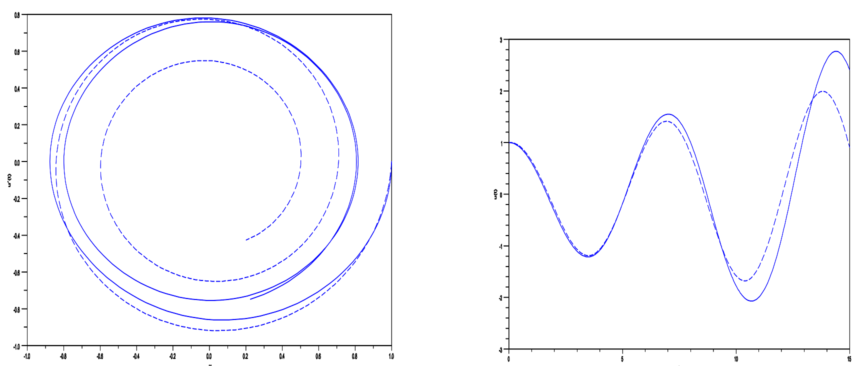

(a) (b)

FIG VII: (a) Behavior of the displacement (b) Phase portrait : for $\varepsilon = 0.1, a = \alpha = \rho = 1, \beta = -1, \mu = \tau = 0.01$, where the thick line represents the exact solution and the dashed line represent the approximate solution.

Studying and comparing FIGS. IV-VII, we observed that:

a. for the positively damped case, the trajectory paths tends to converge (move towards) to the origin while for the negatively damped case, these paths tends to diverge (move away) from the origin. These finding is in harmony with that recorded in [12,13].

b. nonlinear behavior is more pronounced for the negatively damped case compared to the positively damped case.

Here we must remark that the concept of negative damping is not a mathematical idea or an ideal phenomena introduced to simplify things but rather a reality often encountered when handling physical systems [13]. See [26-36].

We further observed from our analysis that seven equilibrium points were generated for each of the segments considered. One interesting observation is the fact that for the cubic Duffing Oscillator, one and three equilibrium point(s) were observed, also for the cubic- quintic Duffing Oscillator, three as well as five equilibria were also observed and now for the cubic-quintic-heptic Duffing Oscillator, there was no case of five equilibria recorded. Moreover as was observed in [12] for the cubic-quintic case, the negatively damped cubic-quintic-heptic Duffing Oscillator exhibited instability all through for the parameter values we used while the positively damped cubic-quintic-heptic Duffing Oscillator exhibited asymptotic stability all through as opposed to the positively damped cubic-quintic Duffing Oscillator which exhibited stability, asymptotic stability and instability, see [12]. The un-damped cubic-quintic-heptic Duffing Oscillator exhibited stability all through in our study, this corroborate the claim made in [13] that only equilibrium points that are centres can be obtained for un-damped Duffing Oscillators.

4.0Conclusion

This paper investigated the Duffing Oscillator with cubic, quintic and heptic nonlinearities presented in the un-damped, damped (positively/negatively), unforced and forced forms. It was observed analytically that unlike the previous versions of the Duffing system namely, cubic and cubic-quintic, the cubic-quintic-heptic Duffing oscillator has seven equilibria but does not have one, three or five equilibrium point(s). The positively damped cubic-quintic-heptic Duffing Oscillator exhibited asymptotic stability all through for the parameter values we used, this was not the case in the cubic-quintic case. Moreover, the effect of adding the heptic nonlinearity was stronger for the negatively damped case when compared to the positively damped case, this can be seen from the simulations presented in this paper. The method of averaging proved effective in obtaining approximate solution to the Duffing system possessing a higher degree of nonlinearity with small parameters since the comparison done in this paper with the exact solution recorded little or no difference regarding the behavior of the system. Noteworthy is the fact that, negative damping increases the effect of external excitations on the Duffing system, this is not encouraging for physical systems modeled by Duffing equations as it leads to failure if unchecked, hence the necessary need to take preventive measures while constructing physical systems. We also note that the addition of the heptic nonlinearity increases the damping effect as reported in some literatures recently, see [13, 16]. This work is the first step towards developing a complete theory on the generalized Duffing system, future works may include the effect of other important phenomena like delay and nonlinear damping on the Duffing system presented in this paper. On the other hand, more work need be done in finding suitable physical systems that can be effectively modeled by the cubic-quintic-heptic Duffing equation.

Acknowledgement

The author is very grateful to Professor M. O. Oyesanya for going through the work and the anonymous reviewers for their invaluable comments.

References

[1] A. Nayfeh, D. T. Mook. (1975). Nonlinear Oscillations. Wiley, New York.

[2] R. H. Rand, (2012). Lecture notes on nonlinear vibrations (version 53). Available from http//audiophile.tam.cornell.edu/randdocs/.

[3] J. J. Stoker, (1950). Nonlinear vibrations in mechanical and electrical systems. New York.

[4] T. K. Nagy and B. Balachandran. Forced harmonic vibration of a Duffing oscillator with linear viscous damping. Available from http://aero.tamu.edu/sites/default/files/faculty/kalmarnagy/Forced%20harmonic%20vibration%20of%20a%20Duffing%20oscillator%20with%20linear%20viscous%20damping.pdf.

[5] G. Duffing. Erzwungene Schwingungen bei veranderlicher Eigenfrequenz und ihre technische Bedeutung, Excerpt translated by O. E. Rossler. Available from http://www.atomosyd.net/spip.php?action=dw2_out&id=344.

[6] Scholarpedia (2012). Duffing Oscillator, Scholarpedia. Available from http://www.scholarpedia.org/article/Duffingoscilator.

[7] Wolfram Math World. Duffing Differential Equation. Available from Math World, http://mathworld.wolftram.com/DuffingDifferentialEquation.html.

[8] A. H. Nayfeh. (1985). Problems in Perturbation, Wiley, New York.

[9] A. H. Nayfeh. (2000). Perturbation Methods, Wiley, New York.

[10] V. Chua, (2003). Cubic-Quintic Duffing Oscillators, www.its.caltech.edu/~mason/research/duf.pdf.

[11] J. Guckenheimar, P. Holmes, (2003). Nonlinear oscillations, dynamical systems and bifurcations of vector fields, Fifth Edition, Springer, New York.

[12] M.O. Oyesanya, J.I. Nwamba, (2013). Stability analysis of damped cubic-quintic Duffing Oscillator. World Journal of Mechanics, 3, 43-57, doi:10.4236/wjm2013.31003.

[13] J. I. Nwamba, (2012). The stability analysis of the damped cubic-quintic Duffing oscillator. M.Sc project, University of Nigeria, Nsukka.

[14] T. M. Morrison and R. H. Rand, (2007). 2:1 Resonance in delayed nonlinear Mathieu equation, Nonlinear Dyn 50: 341-352. DOI 10.1007/s11071-006-9162-5.

[15] W. E Boyce and R. C Diprima, (2000). Elementary Differential Equations and Boundary Value Problems, John Wiley & Sons, Inc.

[16] M.O. Oyesanya, J.I Nwamba, (2013). Effect of heptic nonlinearity on positively damped Duffing Oscillator with single periodic forcing. International Journal of Mechanics and Applications (vol.3, no. 2).

[17] A. Barari, M. Omidvar, A. R. Ghotbi and D. D. Ganji, (2008). Application of homotopy perturbation method and variational iteration method to nonlinear oscillator differential equations. Acta Applicandae Mathematicae, 104, 161-171.

[18] J. H. He. Variational approach for nonlinear oscillators. Chaos, Solitons and Fractals 34, 2007, 1430-1439.

[19] M. Akbarzade and D. D. Ganji, (2010) Coupled method of Homotopy perturbation method and Variational approach for solution to nonlinear cubic-quintic Duffing oscillator, Adv. Theor. Appl. Mech., 3(7), 329-337.

[20] M. Momeni, N. Jamshidi, A. Barari, D. D. Ganji, (2012) Application of He's energy balance method to Duffing harmonic oscillators. Inter. J. Computer Mathematics. DOI:10,1080/00207160903337239.

[21] S. S. Ganji, A. Barari, S. Karimpour, G. Domairry, (2012). Motion of a rigid rod rocking back and forth and cubic-quintic Duffing oscillators. Journal of Theoretical and Applied Mechanics 50(1), 215-229.

[22] S.K. Lai, C.W. Lim, B.S. Wu, C. Wang, Q.C. Zeng, X.F. He, (2009). Newton-harmonic balancing approach for accurate solutions to nonlinear cubic-quintic Duffing oscillators. J. of Applied Mathematical Modelling 33, 852-866.

[23] T. Pirbodaghi, S.H. Hoseni, M.T. Ahmadian, G.H. Farrahi, (2009). Duffing equations with cubic and quintic nonlinearities. J. of Computers and Mathematics with Applications 57, 500-506.

[24] J. I. Nwamba, (2013). Application of Iteration Perturbation Method and Variational Iteration Method to a Restrained Cargo system modeled by cubic-quintic-septic Duffing equation. Int. J. Mech. and Apps. 3(4), 63-69. Doi:105923/jmechanics.20130304.01

[25] Lesage, J. C., Liu, M. C. (2008). On the investigation of a restrained cargo system modeled as a Duffing oscillator of various orders, Proceedings of ECTC (Early Career Technical Conference) ASME, Maimi, Florida, USA.

[26] A. G. Davenport and M. Novak, (2002). Vibration of structures induced by fluid flow, In: Harris' shock and vibration handbook. McGraw-Hill; p. II chapter 29.

[27] D. Coy and M. Molnar, (1997) Optically driven pendulum, fac.sponsors-R. Peters & T. Moore, USMA, West Point, Proc. 11th Nat. Conf. Undergrad. Res. 1621.

[28] E. I Rivin, (1980). Role of induction driving motor in transmission dynamics, ASME paper 80-DET-96, ASME.

[29] E. I Rivin, (2002). Machine tool vibration , In: Harris' shock and vibration handbook. McGraw-Hill; chapter 40.

[30] E. I Rivin, (2007). Dynamic overloads and negative damping in mechanical linkage: Case study of catastrophic failure of extrusion press, Engineering Failure Analysis 14, 1301-1312.

[31] J. M. Jonkman, (2008). Influence of control on the pitch damping of a floating wind turbine, available electronically at http://www.osti.gov/bridge.

[32] R. D Blevins, (2002). Vibration of structures induced by fluid flow, In: Harris' shock and vibration handbook. McGraw-Hill; p. I chapter 29.

[33] R. D Peters, (2004). Beyond the linear damping model for mechanical harmonic oscillators, http://physics.mercer.edu/petepag/debunk.html.

[34] S. A Tobias,(1965). Machine tool vibration, London: Blackie; p. 351.

[35] S. T Wu, Asymptotic behavior of solutions for nonlinear wave equations of Kirchhoff type with a positive-negative damping, Journal of Applied Mathematics Letters 25 (2012), 1082-1086.

[36] Y. M Chen, J. K Liu and G. Meng, Equivalent damping of aero-elastic system of an airfoil with cubic stiffness, Journal of Fluids and Structures 27 (2011), 1447-1.

NIPES-NCEE Conference Proceedings
The 2nd International Conference 15th-17th Feb. 2023
218-228
www.nipesjournals.org.ng

OPTIMIZATION OF SOME PROPERTIES (TENSILE STRENGTH, ELONGATION AND WATER VAPOR PERMEABILITY) OF BIODEGRADABLE FILMS PRODUCED FROM TACCA (*L. KUNZE*) STARCH AND PLASTICIZER BLENDS

Sunday, Simon Ochoyoda and Orhevba, Bosede Adelola

Department of Agricultural and Bio resources Engineering, Federal University of Technology, P.M.B. 65, Minna, Nigeria
Corresponding email: simonsunday9@gmail.com

Abstract

Tacca (L. Kunze) starch films (TSF) were developed and investigated for the effects of starch level (5-15g) w/w, glycerol (0 – 4.5g) w/v, sorbitol (0 – 4.5g) w/v and process temperature (75 – 950C) on their tensile strength, elongation and water vapour permeability using Box-Behnken experimental design in response surface methodology (RSM). Model optimization of the results and formulation for prospective food packaging applications was done using Analysis of variance (ANOVA). The linear and quadratic effects of independent variables shows that starch levels significantly affected (p<0.05) all the responses except for tensile strength with no significant effect of starch at 5% level of significance. Results also shows that plasticizer blend and concentration (sorbitol and glycerol) had significant effect (p<0.05) on all responses with interactive effects on film tensile strength. Temperature only had a significant effect on water vapor permeability (WVP). WVP of the film varied from 4.9 to 12.13 x 10-9g. s-1mPa-1 and tensile strength varied from 1.006 to 9.13MPa while elongation varied from 2.41 to 53.17%. The optimized values indicated that TSF prepared with 13.728g of starch, 4.5g of sorbitol, 4.5g of glycerol and 750C of process temperature provided TSF with improved and satisfactory response with a desirability value of 0.609. R2 (Coefficient of determination) values shows a good correlation between experimental and predicted values, revealing the adequacy and fitness of the model. The results obtained clearly illustrates that within the optimum levels of the process parameters, the suitability of the developed linear and quadratic models for optimal values of response variables are valid.

***Keywords**: Optimization, Tacca starch, Biodegradable film, Box-Behnken, Response Surface Methodology*

1.0.Introduction

A lot of efforts have been taken to develop biodegradable films from renewable and natural polymers such as starch, cellulose derivatives, gelatin, protein and lipids [1]. These biodegradable films are not meant to completely replace synthetic packaging films but they do possess potentials to replace the conventional packaging materials in some applications thereby mitigation some of the environmental menace posed by the use of conventional plastics. These films can be completely degraded by microorganisms without emission of toxic gases.

Starch is one the most studied natural polymer for the development of biodegradable films because of its provision of low-cost carbohydrate polymer, easy to obtain and good ability to form films [2]. It primarily consists of branched and linear chains of glucose molecules namely amylopectin and amylose. Thus, starch is a potential packaging material in agriculture, medicine, and packaging industries [3].

Tacca leontopetaloides also known as Polynesian arrowroot is a wild perennial herb belonging to the *Dioscoreaceae* species [4]. This plant is naturally distributed from western Africa through southern Asia to northern Australia [5]. This starch serves as an important food source for many Pacific Island cultures and additionally used to stiffen fabrics in some of the islands. Application of this starch was reported as a treatment of stomach ailments. It is also believed to treat diarrhea and dysentery [6]. The proximate composition of fresh tubers of *Tacca* includes: 1.10-1.50 % protein, 2.70-2.73 % ash, 0.28-0.68% fibre, 0.08-0.10 % fat and 95.02-95.42 % total carbohydrate on dry matter basis [6]. These values can be compared with some values on the composition of some starchy materials and promises to provide elastic properties and become an alternative to common starch in the production of biodegradable film.

2.0.Materials and methods

2.1.Raw materials

Materials used for starch production were: *Tacca* tubers obtained from a local market in Shandam Local Government Area of Plateau State, Nigeria. Other materials for the starch extraction were knife, bowl, grinder, sieves, filter clothes and distilled water. Sorbitol and glycerol were purchased from SIM BEST Scientific and Chemicals Minna, Niger State.

2.2.Starch Preparation

The method described by Ezeoha and Ezenwane (2013) for cassava starch preparation was adopted with slight modifications. The *Tacca* tubers were peeled and washed with portable water. This was followed by mechanical grating of the tuber. The grated *Tacca* was mixed with water (3 times the volume of the grated *tacca*). The mixture was sieved and filtered using coarse sieve and filter clothes respectively. Thereafter, the filtrate was allowed to settle for twelve hours. This process is known as starch washing. At the end of the twelfth hour, it was decanted. The wet starch was dewatered manually and oven-dried using Mqeco-4t4030 oven. It was dried at a temperature of 105^0C for twelve hours. This was to make sure that the starch is in the barest minimum moisture content of 12%.

2.3.Film Preparation

The method described by Muhammed *et al.* (2015) was adopted with slight modifications. The *Tacca* starch films were produced by conventional solution-casting techniques at Chemical Engineering Laboratory facility of the Ahmadu Bello University (ABU), Zaria. 5-15g (w/w) of Tacca starch were dissolved in 100ml distilled water. This was followed by heating the film forming solution at a temperature range of 75^0C to 95°C (75^OC, 85^OC and 95^OC) for 15 minutes under constant stirring in a water bath. This step helped to provide homogeneous dispersion by disintegrating the starch granules. Thereafter, the different plasticizers were added into the dispersions at 0-4.5g (w/v) of each plasticizer (Glycerol, G and Sorbitol, S) representing 0-30% (w/v starch basis). The heating process for each was continued for an additional 15 minutes for each temperature for proper gelatinization. The gelatinized film solutions were cooled down, prior to their casting in glass petri-dishes. The glass petri-dishes served as casting surfaces, enabling the film to have a smooth and flat surface. The fresh casted films were placed in an oven (45 °C) to allow evaporation. All films were prepared in triplicates including films without plasticizers, used as control. After 36 hours of drying and a constant weight, films were peeled from the casting surfaces and stored in desiccators with 53% relative humidity (RH). The selection of the above levels of the filmogenic components were based on preliminary studies and by reviewing literatures [7,8].

2.4.Characterization of Film Properties

The mechanical properties (Tensile strength and elongation) of the film were determined using the standard method of D882-02 (ASTM, 2002) while water vapour permeability (WVP) tests was conducted according to ASTM E96–95 with slight modifications.

2.4.1. Tensile strength and elongation of film

The tensile strength testing Machine (TM2101-T7) was used to test for the tensile strength of the biodegradable film. The specimens with different concentrations of glycerol and sorbitol blends were cut into the same dumbbell-shapes. Tensile strength and elongation at break were determined by using the tensile strength testing machine with a load cell of 40N. Films were cut in the form of strips with dimension of 10 × 70 mm. The strips were clamped between two tensile grips and the initial gauge length was set at 30 mm. Films were be pulled using a crosshead speed of 2 mm/min. During the stretching, force (N) and deformation (mm) were recorded. Measurements were carried out on 5 different specimens. The mechanical properties were calculated as average value from the obtained results.

2.4.2. Water Vapour Permeability (WVP)

Prior to the WVP test, the film samples were conditioned in a desiccator with relative humidity of 50% at 25 °C. Circular film samples were mounted and sealed on the open mouth of cylindrical cups containing 20g of silica gel. The test cups were measured before being kept in a relative humidity chamber (25°C, relative humidity 75%). The weight of the test cups was determined by periodic measurement until the equilibrium state is reached. Weight increments of the test cups were recorded and WVP were calculated as follows:

$$WVP = \frac{m \times d}{A \times t \times P}$$

Where:

m = weight increment of the test cup (g)
d = film thickness (mm)
A = area of film exposed (m^2)
t = duration for permeation(s) and

P = water vapor partial pressure across the films (Pa).

The results were expressed in g.mm.s^{-1} m^{-2} ·P^{-1}.

2.5 Experimental design and statistical analysis

The experimental design was conducted using Box Behnken experimental design for investigating the individual and interactive effects of process parameters (Tacca starch, temperature, glycerol and sorbitol concentration) on the tensile strength, elongation and water vapour permeability of the Tacca starch-based film in which 29 different trials were conducted. Statistical Analysis of variance (ANOVA) was done to study the effects of the different independent parameters on all dependent variables by Response Surface Methodology (RSM) using statistical design software (Design Expert 11 version 27. 3D).

3.0.Results and Discussion

3.1.Results

The result of the film's tensile strength, elongation and water vapour permeability, is presented in **Table 1.**

Table 1: Result of the Tensile strength, elongation and Water vapour permeability of Tacca-based film

Std	Runs	A Starch w/w	B Sorbitol w/v	C Glycerol w/v	D Temp ^{0}C	Tensile Strength (MPa)	Elongation E%	WVPx10^{-9}g.s^{-1}mPa^{-1}
24	1	10	4.5	2.25	95	3.051	11.735	8.64
19	2	5	2.25	4.5	85	2.699	50.415	10.74
8	3	10	2.25	4.5	95	6.666	28.578	9.98
3	4	5	4.5	2.25	85	1.418	52.35	10.86
26	5	10	2.25	2.25	85	6.086	17.514	8.56
21	6	10	0	2.25	75	5.67	3.91	5.01
18	7	15	2.25	0	85	8.35	5.38	4.39
17	8	5	2.25	0	85	7.95	6.42	5.21

7	9	10	2.25	0	95	9.13	2.57	4.68
23	10	10	0	2.25	95	6.34	2.41	5.97
12	11	15	2.25	2.25	95	6.649	14.514	8.39
16	12	10	4.5	4.5	95	2.948	8.943	12.13
2	13	15	0	2.25	85	8.37	2.68	5.43
9	14	5	2.25	2.25	85	2.225	53.174	9.37
13	15	10	0	0	75	16.15	2.041	NA
20	16	15	2.25	4.5	85	1.151	9.683	8.59
29	17	10	2.25	2.25	85	1.006	20.14	9.01
22	18	10	4.5	2.25	75	3.501	24.251	7.81
4	19	15	4.5	2.25	85	4.455	25.152	6.84
27	20	10	2.25	2.25	85	1.071	21.14	8.86
6	21	10	2.25	4.5	75	8.657	29.523	8.31
1	22	5	0	2.25	85	1.365	20.51	6.01
28	23	10	2.25	2.25	85	1.199	12.945	8.34
14	24	10	4.5	0	85	1.52	9.886	7.45
15	25	10	0	4.5	85	2.124	46.62	9.36
10	26	15	2.25	2.25	75	6.086	17.514	6.38
5	27	10	2.25	0	75	8.35	16.36	4.39
11	28	5	2.25	2.25	95	4.33	46.143	11.53
25	29	10	2.25	2.25	75	1.006	20.14	9.08

3.1.1 Tensile strength (MPa)

Tensile strength for the Tacca starch biodegradable film decreased with increase in plasticizer concentration. It was maximum (16.15MPa) at 0% plasticizers, 5g starch level, processing temperature of 85^0C and minimum at 30% glycerol concentration, 15% sorbitol, 10g starch level and a processing temperature of 85^0C. Analysis of variance (ANOVA) in Table 2 showed that Sorbitol (B), Glycerol (C), plasticizer interaction BC, and the quadratic terms of glycerol (C^2) and temperature (D^2) have significant effect ($p<0.05$) on the tensile strength of Tacca starch biodegradable film. On the other hand, starch level and temperature showed non-significant effect ($p>0.05$) on the films tensile strength. Results from taro peel starch was also found to show no significant effect on film tensile strength [8]. The phenomenon of biodegradable film having high tensile strength at low plasticizer concentration might be due to the dominance of strong intermolecular hydrogen bond formed by starch-starch intermolecular interactions over starch-plasticizer attraction.

Studies have reported that tensile strength of starch-based biopolymers diminished with increasing plasticizer content [8,9]. Tensile strength was found to have quadratic relationship with the process variables as per the following equation,

Tensile Strength = $+ 168.62540 + 0.832190A – 1.25251B – 2.38020C – 3.91480D – 0.088178AB – 0.043289AC – 0.007710AD – 0.763160BC – 0.012444BD – 0.030789CD + 0.018510A^2 + 0.137430B^2 + 0.601208C^2 + 0.024136D^2$.

The **Model P-value** of 0.0110 implies the model is significant.

3.1.2. Elongation (%)

Maximum elongation at break (53.174%) was observed for the combination of 5g starch concentration, 15% sorbitol concentration, 15% glycerol concentration (30% plasticizer concentration) and 75^0C process temperature. ANOVA shows that Elongation of the film was significantly affected by starch level and glycerol plasticizer concentration ($p<0.05$). Sorbitol and processing temperature showed no significant effects on the film elongation ($p>0.05$). Similar result was obtained by Lucio *et al.*, (2020) for effect of sorbitol and glycerol on sweet potato starch film. Glycerol plasticized film showed the highest value in elongation percentages. Glycerol has a smaller effective hydrodynamic radius (0.31nm) than sorbitol (0.39) and therefore, the distance between starch molecules in glycerol plasticized film would be the farthest. The higher values in the elongation percentage for glycerol-plasticized film can be associated with the fact that it has a smaller molecular chain which can enter the polymer network more easily than sorbitol (Dias *et al.*, 2009). The elongation was found to have a linear relationship with the process parameters as per the following equation, **Elongation** = $+ 57.80557 – 2.56815A + 2.00541B + 4.85574C – 0.32318D$.

The **Model p-value** of 0.0008 implies the model is significant.Table 2**: Analysis of variance ANOVA of the effects of process parameter on tensile strength an elongation of TSF**

Source	Sum of Squares	Df	Mean Square	F-value	p-value	R^2	Adjusted R^2	Predicted R^2	PRESS	Remarks
ELONGATION										
Model	**3780.65**	**4**	**945.16**	**6.89**	**0.0008**	**0.7346**	**0.6570**	**6.2748**	**11.7751**	**Significant**
A-starch	1978.62	1	1978.62	14.43	0.0009					
B-sorbitol	244.32	1	244.32	1.78	0.1945					
C-glycerol	1432.38	1	1432.38	10.44	0.0036					
D-temperature	125.34	1	125.34	0.9139	0.3486					
Pure Error	44.10	4	11.03							
Cor Total	7071.98	28								
TENSILE STRENGTH (MPa)										
Model	276.87	14	19.78	3.62	0.0110	**0.7836**	**0.6671**	**0.6073**	**12.6328**	**Significant**
A-starch	18.94	1	18.94	3.47	0.0837					
B-sorbitol	44.57	1	44.57	8.16	0.0127					
C-glycerol	61.68	1	61.68	11.29	0.0047					
D-temperature	0.2344	1	0.2344	0.0429	0.8389					
AB	3.94	1	3.94	0.7206	0.4102					
AC	0.9487	1	0.9487	0.1737	0.6832					
AD	0.5944	1	0.5944	0.1088	0.7464					
BC	59.71	1	59.71	10.93	0.0052					
BD	0.3136	1	0.3136	0.0574	0.8141					
CD	1.92	1	1.92	0.3514	0.5628					
A^2	1.39	1	1.39	0.2543	0.6219					
B^2	3.14	1	3.14	0.5748	0.4609					
C^2	60.09	1	60.09	11.00	0.0051					
D^2	37.79	1	37.79	6.92	0.0198					

Pure Error	20.15	4	5.04
Cor Total	353.35	28	

3.1.3. Water Vapor Permeability WVP ($g.s^{-1}MPa^{-1}$)

The water vapor permeability of Tacca starch film ranged from 4.39 to 12.13 x 10^{-9}g. $s^{-1}MPa^{-1}$. Maximum WVP (12.13 x 10^{-9}g. $s^{-1}MPa^{-1}$) was observed for the combination of 10g of Tacca starch, 60% plasticizers (30%sorbitol and 30% glycerol) and a processing temperature of 85^0C whereas a minimum WVP (4.39 x 10^{-9}g.$s^{-1}MPa^{-1}$) was observed for a combination of 10g of starch, 15% sorbitol plasticizer and a process temperature of 75^0C. The equation of response and ANOVA results shows that the mass concentration of tacca starch, plasticizers (sorbitol and glycerol) blends and processing temperature exerted significant effect ($p<0.05$) on the film WVP. According to Paramantham and Thottiam (2017), increase in level of starch and plasticizer concentration increased the WVP of cassava-based starch film significantly. Thicker films increased the resistance to water transfer along the internal surface of films equilibrium. Plasticizers consisting of a higher number of hydroxyl group increase the space among polymer mobility and cause films to have hydrophilic property, which eventually results to the increase in WVP of the films [10]. The linear model equation for WVP was,

$$WAP = +0.495564 - 0.228333A + 0.671399B + 1.08029C + 0.06600D.$$

Source	**Sum of Squares**	**df**	**Mean Square**	**F-value**	**p-value**	**R^2**	**Adjusted R^2**	**Predicted R^2**	**PRESS**	**REMARK**
WVP X 10^{-9}										
Model	**103.06**	**4**	**25.77**	**22.19**	**< 0.0001**	**0.7942**	**0.7584**	**0.6935**	**16.5022**	**Significant**
A-starch	15.64	1	15.64	13.47	0.0013					
B-sorbitol	24.80	1	24.80	21.36	0.0001					
C-glycerol	64.20	1	64.20	55.30	< 0.0001					
D-temperature	5.23	1	5.23	4.50	0.0448					
Residual	26.70	23	1.16							
Pure Error	0.3908	4	0.0977							
Cor Total	129.76	27								

The **Model P-value** of < 0.0001 implies the model is significant.

Table 3: **Analysis of Variance of the effects of process parameters on WVP of TSF**

3.2 Optimization and verification of models

Design expert software was used to analyze the responses for obtaining optimum process parameters. Model equations were developed for each response to calculate the optimum condition for both dependent and independent variables. The optimization was carried out on the basis of the following objectives (i) Maximize Tensile strength (ii) Maximize elongation (iii) Minimize water vapor permeability as shown in Table 4. It is intended to be used for food packaging applications.

Table 4: Optimization constraints

Name	Goal	Lower Limit	Upper Limit	Lower Weight	Upper Weight	Importance
A: starch	is in range	5	15	1	1	3
B: sorbitol	is in range	0	4.5	1	1	3
C: glycerol	is in range	0	4.5	1	1	3
D: temperature	is in range	75	95	1	1	3
TS	maximize	1.006	16.15	1	1	3
Elongation	maximize	2.041	53.174	1	1	3
WVP X10^{-9}	minimize	0	12.13	1	1	3

The optimal levels of process parameters obtained to be 13.728g of starch, 30% glycerol, 30% sorbitol and 75^0C process temperature resulting in 9.117MPa tensile strength, 29.047% elongation and 6.744 x 10^{-9}g. $s^{-1}MPa^{-1}$ water vapor permeability were obtained with a desired value of 0.609 as obtained from 100 optimization solutions. The response plots revealed that all four process parameters were found to influence all responses independently or interactively. The results clearly illustrate that within the optimum level of the process parameters, the suitability of the developed quadratic and linear models, the optimal values of response variable are valid.

4.0.Conclusions

The following conclusions were made from this study;

1. The tensile strength and elongation properties of the biodegradable films were affected mainly by starch level and plasticizer blends. Only water vapor permeability was significantly influenced by process temperature at 5% level of significance.
2. Film elongation increased with increase in starch level and plasticizer concentrations. Tensile strength decreased significantly with increase in plasticizer blends along with their interactive effects.
3. Linear models were developed from the experimental data for film water vapor permeability and elongation while a quadratic model was obtained for film tensile strength.
4. Results showed that the optimal formulation for the preparation of Tacca starch biodegradable film was 13.728g of starch, 30% glycerol, 30% sorbitol and 75^0C process temperature which had improved and satisfactory responses when compared with films from other tuber crops.
5. Numerical optimization based on desirability function using Design expert software shows that the optimal film has a desirability value of 0.609.

The films being made from biodegradable, non-toxic, edible natural resources, can replace synthetic polymer in certain circumstances by providing options for development of new plastic products for food packaging.

References

[1] Bertuzi, M.A., Vidaure, E.F.C., Amada, M., & Gottifredi J.C., (2007). Water vapour permeability of edible starch-based films. *Journal of Food Engineering, 80(3), 972-978.*

[2] Dias A.B., Muller C.M., Laraotonda F.D. & Laurindo J.B. (2010). Biodegradable films based on rice starch and rice flour. *Journal of cereal science* 51(2) 213-219. http//doi.org/101916/jcs.2032.11.014.

[3] Ezeoha, S.L and Ezenwanne, J.N. (2013). Production of Biodegradable Plastic Packaging Film from Cassava Starch. Department of Agricultural and Bioresources engineering, University of Nigeria, Nsukka. p-ISSN: 2278-8719 Vol. 3, Isuue 10.

[4] Muscat, D., Adhikari, B., Adhikari, R., & Chaudhary, D.S. (2012). Comparative study of film forming behaviour of low and high amylose starches using glycerol and xylitol as plasticizers. *Journal of Food Engineering*, 109(2), 189-201.

[5] Paramanantham H.P. & Thottiam V.R. (2017). Modelling and optimization of cassava starch based film for food packaging applications Pak. *J. Biotechnol. Vol*. 14 (4) 571-586.

[6] Smith, A. M. (2001). The biosynthesis of starch granules. *Biomacromolecules*, 2(2), 335-341. http://dx.doi.org/10.1021/bm000133c. PMid:11749190.

[7] Srikulkit, K., Bangyekan, C., & Aht-Ong D. (2006). Preparation and properties evaluation of Chitosan coated cassava starch film. *Carbohydrate Polymer, 63, 61-71.*

[8] Ukpabi, U.J., Ukenye, E. & Olojede, A.O. (2009). Raw-Material potentials of Nigerian wild Polynesian Arrowroot (*Taccaleontopetaloides*) tubers and starch. *Journal of Food Technology*, 7: 135-138.

[9] Abdou, E.S. & Sorou, M.A. (2014). Preparation and Characterization of starch/carrageen edible films. *International Food Research Journal, 21(1), 189-193.*

[10] Ubwa S.T., Anhawange B.A., & Chia J.T. (2011). Chemical analysis of Tacca leontopetaloides peels. *American journal of food technology* 6, 932-928. Doi:10.3928/asfj.932-938

[11] Zaku, S.G., Aguzue, O.C., Thomas, S.A. & J.T. (2009). Barminas Studies on the functional properties and the nutritive values of amura plant starch (Tacca involucrate) a wild tropical plant. *African J. of Food Science.* 2009; 3(10):320-322.
[12] Mohammad H.S., Morteza H., Mohsen J. & Ghasem N. D. (2015). Optimization of encapsulated clove oil particle size with biodegradable shell using design expert methodology. Pak. *J. Biotechnol.* 12(2): 149-160.
[13] Dutta, P. K., Tripathi, S., Mehrotra, G.K. & Dutta J. (2009). Perspectives for chitosan based anti-microbial films in food applications. *Food Chem.* 114: 1173-1182.
[14] Rhim J.W. (2011). Effect of clay contents on mechanical and water vapor barrier properties of agar-based nanocomposite films. *Carbohydrate Polymers* 86: 691–699.
[15] ASTM (2002). Designation D882-02: Standard Test Method for Water tensile strength properties of thin plastic sheeting. Annual book of ASTM standards philadephia: American Society for Testing and Materials.
[16] ASTM (1996). Standard test method for water vapor transmission of materials, method E96/E96M e 342 13. Phialdelphia: American Society for Testing and Materials
[17] Rusta B., Annur A. A., Rogelio A. B.P., & Albert L. C. (2023). Characterization of Biodegradable Films Made from Taro Peel (*Colocasia esculenta*) Starch.*Polymers 15*(2) 338; https://doi.org/10.3390/polym15020338.
[18] Lucio, B.M., Camen, P.C. & Ricardo, A. P. (2019). Effects of glycerol and sorbitol concentration on mechanical, Optical and barrier properties of sweet potato film. *NFS journal* http://doi.org/10.1016/jnfs.2020.002

NIPES-NCEE Conference Proceedings
The 2nd International Conference 15th-17th Feb. 2023
229-235
www.nipesjournals.org.ng

RETscreen FEASIBILITY ANALYSIS OF WIND POWER PLANT IN KANO, NIGERIA

Mujittapha Idris Wawo[1], Yunusa Rabiu Magaji[2], Umar Shehu[3], Abdulkadir Habib K/Naisa[4]
[1,2,3,4]Department of Electrical Engineering, Kano State Polytechnic
Corresponding email: Mujittapha.wawo@yahoo.com

Abstract

The development of the electricity sector in Nigeria continues to be fenced by high rates of inefficiencies, insufficient security of supply, low rate of RET investment including wind power plants and the need to further unbundle and liberalize the energy market is increasing, in a bid to produce and maintain a sustainable, secure, flexible in time, efficiently supplied, climate-friendly and affordable energy supply system is required. The most critical aspects of attaining energy expansion goals cannot be achieved without the promotion of carbonless power technologies reducing (GHG) emissions. As a consequence, huge investments in RET energy based power generation systems and related RET technologies are required. To overcome the barriers to clean energy technology implementation especially at the preliminary feasibility stage, the latest model of RETScreen Expert software added the ability to rapidly analyze the feasibility of wind power plant options at real site condition. This fast feature of the model enables us to analyse the real potential of the proposed 3000 KW wind farm. From the simulation executed in RETScreen Expert software, the technical and economic optimization of the proposed energy system is achieved. Environmental friendly with 0 GHG emission off-grid power plants is achieved.

Keywords*: Wind Power Plant, RETScreen Expert, Renewable energy, wind energy.*

1.0 Introduction

Recently, the cost associated with electric energy derived from fossil and nuclear fuel, and the increases in environmental regulations continue to constrain the planning and operation of electric utilities. Furthermore, the global economic and political conditions that tend to make countries more dependent on their own energy resources have caused growing interest in the development and use of renewable energy [1]. In terms of its environmental advantages, renewables generate electricity with insignificant contribution of carbon dioxide (CO2) or other greenhouse gases (GHG) to the atmosphere and they produce no pollutant discharge on water or soil [2]. Due to the rapid industrial and economic growth and increase in energy consumption, Grid extension and replacement of old plants and implementation of new power plants to cover the growth of electricity demand is the main objectives of developing nation's electricity sector in the upcoming decade [3]. It is obvious that the implementation of any strategy towards adopting renewable energy will be an essential element of national plans for achieving sustainable development and protection of the environment via upgrading energy efficiency and replacing conventional polluting resources by renewable resources [1].

Just as the fossil fuel based energy industry relies on exploration, discovery, and proven reserves of the available resources, the renewable energy sector depends upon the assessment of renewable resources for planning and selling their energy production technology [4]. For wind-based renewable energy technologies, the basic resource or fuel available is wind kinetic energy. Assessment of the wind resource for these technologies is based upon metrological data available [5].

Nigeria is endowed with large wind energy resources. Wind power or wind energy utilization is the use of wind kinetic energy to generate mechanical power through wind turbines to operate electric generators[6]. According to wind production indicators, an average wind speed of around 3.0 m/s is still sufficient to start wind energy production[7][8].

2.0 Methodology

2.1 Basic operation principle

Wind possesses energy by virtue of its motion. Any device capable of slowing down the mass of moving air, like a sail or propeller, can extract part of the energy and convert it into useful work. The spinning blades, attached to a hub and a low-speed shaft, turn along with the blades [9]. The rotating low-speed shaft is connected to a gearbox that connects to a high-speed shaft on the opposite side of the gearbox. This high-speed shaft connects to an electrical generator that converts the mechanical energy from the rotation of the blades into electrical energy [10].

Wind power can be converted in to electricity or mechanical energy using wind turbines. The rotary machine used to convert air motion into electricity is referred to as a wind turbine. Wind turbines convert the kinetic energy in the wind into mechanical power. A generator can convert mechanical power into electricity. Mechanical power can also be utilized directly for specific tasks such as pumping water [10] [11].

The power in the wind is extracted by allowing it to blow past moving blades that exert torque on a rotor. The rotor turns the drive shaft, which turns an electric generator [12]. The amount of power transferred is dependent on the rotor size and the wind speed. The types of wind power plants based on capacity are oftentimes a large number of wind turbines that are built close together, which is referred to as a wind project or wind farm. A wind farm functions as a single power plant and sends electricity to the grid [13].

In order to motivate the investors and decision makers and to show the feasibility of wind power plants, a project viability analysis is performed using RETScreen software through electric energy production analysis, financial analysis, and GHG emission analysis

2.2 Wind Turbine characteristics

The following is the characteristics of the Wind turbine used for the purpose of this study:

AAER wind turbines were used for the analysis. Each turbine had a rated power of 1000 KW and 3 units of the similar size and ratings were combined to give the desired capacity of 3000 KW. The technical characteristics of each wind turbine is given in Table 1

Table 1: Technical characteristics of AAER wind turbine

AAER	
Model	A-1000/S-50
Number of Rotor Blades	3
Hub height	70 m
Rotor Diameter	54 m
Swept Area	2,290 m^2
Capacity per unit	1000 Kw
Cut in wind speed	4m/s
Cut out wind speed	22m/s
Rated speed	22m/s

2.3 SOFTWARE

RETScreen Expert is a software tool for analyzing clean energy projects based on Microsoft Excel developed by the CANMET Energy Diversification Research Laboratory of Canada. It is used to help decision-makers quickly determine whether a renewable energy, energy efficiency and co-generation project is financially and technically viable [14]. It is powerful free software.

RETscreen is used in this paper to perform energy production analysis, and GHG emission analysis for a proposed wind off-grid power plant at the selected site. RETScreen software is capable of assessing RETs viability factors such as, energy resource available at project site, equipment performance, initial project costs, ‘‘base case’’ credits (e.g., diesel generators for remote sites), on-going and periodic project costs, avoided cost of energy, financing, taxes on equipment and income (or savings), environmental characteristics of energy displaced, environmental credits and/or subsidies, decision-maker’s definition of cost-effective [8].

The RETScreen software integrates a series of databases to help overcome the costs and difficulties associated with gathering meteorological data, product performance data .etc. Worldwide meteorological data has been incorporated directly into the RETScreen software. This meteorological database includes both the ground-based meteorological data and NASA’s satellite-derived meteorological data sets. RETScreen Expert allows three main types of analysis for different types of installations[16]. The possible analyses are: comparison, feasibility and performance. Each project analysis is done in 5 steps: establishment of the energy model, cost analysis, analysis of the emission rate of greenhouse gases, preparation of the financial summary, sensitivity and risk analysis [6].

2.4 Project Location Selection

The location was carefully selected based on the metrological data available in the RETscreen software. The power plant is located in wudil kano state, latitude 11.8° N and longitude 8.9° E as shown in the table 2 below,

Table 2: geographical location of the proposed site

Location | Climate data

Location

	Unit	Climate data location	Facility location
Name		Nigeria - Wudil	Nigeria - Kano - Wudil
Latitude	°N	11.8	11.8
Longitude	°E	8.9	8.9
Climate zone		1A - Very hot - Humid	1A - Very hot - Humid
Elevation	m	531	0

Climate data

The location climate is shown below:

Table 3: location climate data

Heating design temperature	16.3
Cooling design temperature	34.7
Earth temperature amplitude	17.2

Month	Air temperature	Relative humidity	Precipitation	Daily solar radiation - horizontal	Atmospheric pressure	Wind speed	Earth temperature	Heating degree-days	Cooling degree-days
	°C	%	mm	kWh/m²/d	kPa	m/s	°C	°C-d	°C-d
January	23.1	18.4%	1.16	5.55	95.1	3.4	25.6	0	405
February	24.9	16.4%	0.59	6.29	95.0	3.3	27.7	0	418
March	28.1	26.5%	0.97	6.65	94.8	3.6	31.2	0	561
April	28.2	51.1%	29.62	6.69	94.7	3.7	30.8	0	545
May	26.9	67.2%	94.71	6.37	94.8	3.5	28.6	0	524
June	25.1	78.1%	167.75	5.93	95.0	3.0	25.9	0	452
July	24.0	81.8%	255.15	5.45	95.1	2.8	24.6	0	434
August	23.9	81.4%	302.06	5.16	95.1	2.7	24.6	0	432
September	24.6	76.9%	192.58	5.53	95.0	2.4	25.3	0	438
October	25.8	56.6%	27.66	5.77	95.0	2.7	27.1	0	489
November	25.9	25.6%	0.56	5.65	95.0	3.1	27.8	0	477
December	23.6	20.1%	1.58	5.35	95.1	3.6	25.6	0	423
Annual	**25.3**	**50.2%**	**1,074.40**	**5.86**	**95.0**	**3.1**	**27.0**	**0**	**5,597**

The mean annual wind speed is 3.1 m/s which is strong and viable enough to set up wind power plant.

3.0 RETScreen RESULTS

In the following sections the results obtained from RETScreen are discussed. These results are based on the energy production analysis, and GHG emission analysis. Data required to run RETScreen are listed in the relevant sections.

3.1 Electric energy production

The renewable energy analysis (wind energy) was done using RETScreen software. The program uses the monthly mean values of the wind speed, to estimate the energy produce and the plant capacity factor. The electrical energy generated from the analysis is presented below.

Table 4: Energy generated by the Power Plant

Target

Summary

	Electricity exported to grid MWh	Electricity export revenue $	GHG emission reduction tCO_2
Proposed case	7,884	788,400	3,720

Propose site generates 7884MWh annually.

3.2 GHG emission analysis

The RETScreen is capable of estimating the amount of greenhouse gases (GHG) which could be avoided as a result of usage of renewable energy sources. The input required data are the fuel types used in the selected location which is chosen to be ‘‘wind energy’’ in this case. The model estimated GHG emission factor to be 0.472tCO2/MWh. The ranges of variations of both the net GHG reductions in tCO2 and its equivalent cars and light trucks not used are shown in Table below. As shown in the Table significant amount of GHG are reduced by installing wind turbine power plants of replacement of conventional generation method.

The analysis show that placement of the proposed 3000 KW wind off-grid power plant at Wudil offers good profitability, energy production, and GHG emission reduction, compared to similar power plant using fossil fuels.

Table 5: Estimated GHG emission reduction

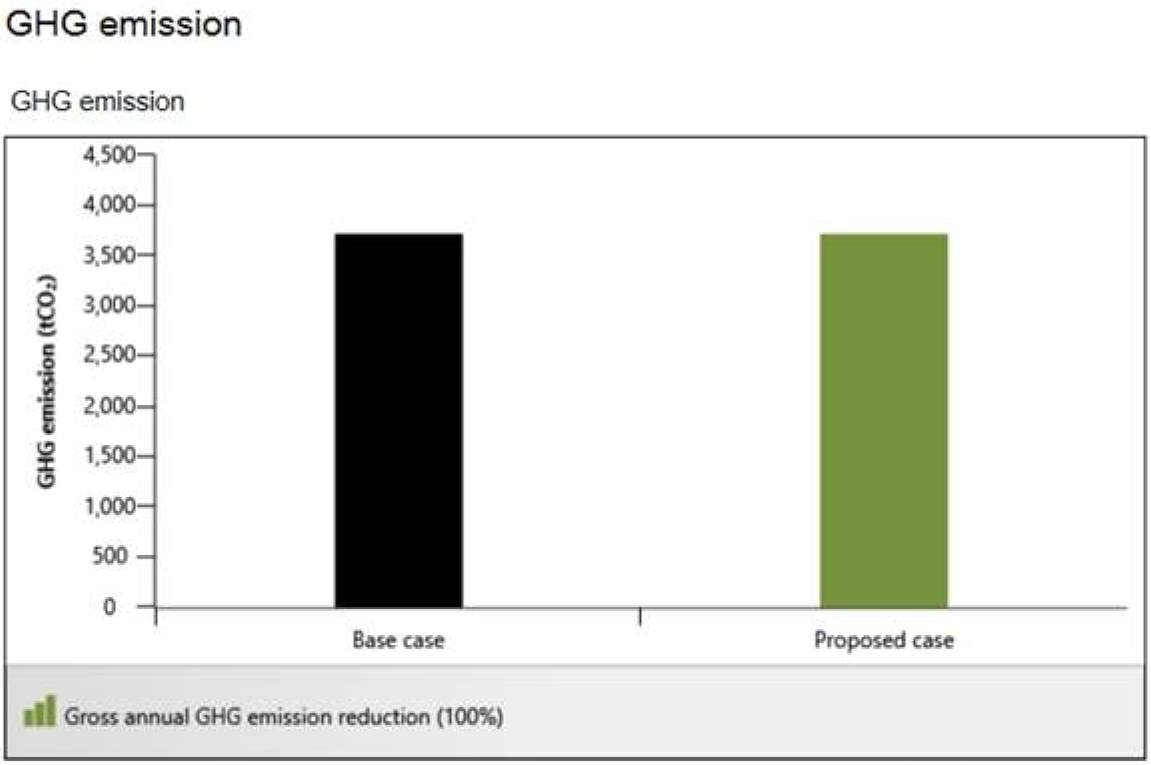

As wind energy is purely GHG emission free there is 100% reduction of GHG emission on the base case, which is equivalent to 681 cars and light trucks not used.

Table 6: Estimated number of cars and light trucks not used

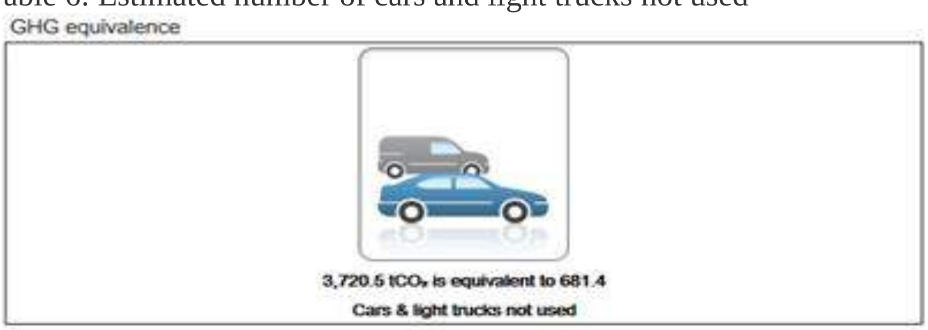

GHG emission		
Base case	3,720.5	tCO_2
Proposed case	0	tCO_2
Gross annual GHG emission reduction	**3,720.5**	**tCO_2**

4.0 Conclusion

This paper presented an extended analysis of 3000 KW wind power off-grid power plant in Wudil in search of the replacement of conventional power plant in place at the moment. In addition to profitability of wind power plant in Wudil, the environmental impact of such projects is evaluated through GHG emission analysis which show that the use of wind power plants reduce large amounts of CO2 emission to the environment or in equivalent large number of barrels of crude oil not consumed (which is also of economic value).

In response to the energy needs and environmental concerns, electricity from wind generators is considered as one of the future solutions. However, the variability and the diffuse nature of the wind power can be challenging to the operation of a power system. However the advantage of using wind energy in electric energy production has by far outweigh these challenges. Therefore, it is recommended to start building large-scale wind power plants projects.

References

[1] Roche M.Y., Ude N., Ofoegbu I.D. (2017), true cost of electricity: comparison of cost of electricity generation in Nigeria. Heinrich Böll Stiftung Nigeria.
[2] IEA, (2016) Next Generation Wind and Solar Power - From Cost to Value.
[3] Cervigni, R., Rogers, J.A., Henrion, M., (2013). Low-Carbon Development: Opportunities for Nigeria, Directions in Development - Countries and Regions. The World Bank. doi:10.1596/978-0-8213-9925-5
[4] Bertheau, P., Cader, C., Blechinger, P., (2016). *Electrification Modelling for Nigeria. Energy Procedia, Africa-EU Symposium on Renewable Energy Research and Innovation 93, 108–112. doi:10.1016/j.egypro.2016.07.157*
[5] Mentis, D., Welsch, M., Fuso Nerini, F., Broad, O., Howells, M., Bazilian, M., Rogner, H., (2015). *A GIS-based approach for electrification planning—A case study on Nigeria. Energy Sustain. Dev. 29, 142–150. doi:10.1016/j.esd.2015.09.007*
[6] NERC, (2012). The Multi Year Tariff Order for the determination of the cost of electricity generation for the period 1st of June 2012-31st May 2017 [WWW Document]. URL http://www.nercng.org/index.php/document-library/func-startdown/67/
[7] Oyewo, S. Aghahosseini, A. Breyer, C. (2017). *Assessment of energy storage technologies in transition to a 100% renewable energy system for Nigeria (PDF Download Available), in: 11th International Renewable Energy Storage Conference*.
[8] Elsayed I. and Nishi, Y. (2018). "*A feasibility study on power generation from solar thermal wind tower: Inclusive impact assessment concerning environmental and economic costs," Energies, vol. 11, no. 11, pp. 1–18, 2018*
[9] X. Chen, X. Sun, H. Wen, J. Lee, W. J. Yuan, X. Li, N. Yao, L. (2011) *Integrating wind farm to the grid using hybrid multiterminal hvdc technology, Industry Applications, IEEE Transactions on 47 (2) (2011) 965–972.*
[10] Torres-Olguin, R. E. Molinas, M. Undeland, T. (2012). *Offshore wind farm grid integration by vsc technology with lcc-based hvdc transmission, Sustainable Energy, IEEE Transactions on 3 (4) (2012) 899–907.*
[11] Lin, W. Wen, J. Liang, J. Cheng, S. Yao, M. Li, N. (2012) A three-terminal hvdc system to bundle wind farms with conventional power plants. Heinrich Böll Stiftung Nigeria.
[12] Perveen, R. Kishor, N. Mohanty, S. R(2014). *Off-shore wind farm development: Present status and challenges, Renewable and Sustainable Energy Reviews 29 (2014) 780–792*.
[13] M. Ahlstrom, M. Jones, L. Zavadil, R. Grant, W. (2005). *The future of wind forecasting and utility operations, Power and Energy Magazine, IEEE 3 (6) (2005) 57–64*
[14] Yang, N. Yu, C. W. Wen, F. Chung, C. Y. (2007). *An investigation of reactive power planning based on chance constrained programming, International Journal of Electrical Power & Energy Systems 29 (9) (2007) 650–656.*
[15] J. Carta, J. Ramirez, P. Velazquez, S. (2009) *A review of wind speed probability distributions used in wind energy analysis: Case studies in the canary islands, Renewable and Sustainable Energy Reviews 13 (5) (2009) 933 –955.*
[16] Villanueva, D. Feijo, . A. E. Pazos, J. L. (2014). *An analytical method to solve the probabilistic load flow considering load demand correlation using the dc load flow, Electric Power Systems Research 110 (2014) 1–8.*

VIABILITY ANALYSIS OF MINI OFF GRID SOLAR SYSTEM INSTALLATION IN WUDIL, KANO STATE

Mujittapha Idris Wawo[1], Auwal Salisu Yunusa[2], Abubakar Sani Muhammad[3], Abdulkadir Ahmad Yako[4]
[1,3,4]Department of Electrical Engineering, Kano State Polytechnic
[2]Department of Mechatronocs Engineering, Kano State Polytechnic
Corresponding email: Mujittapha.wawo@yahoo.com

Abstract

Energy is a very important variable that its conservation is of paramount interest to everyone nowadays. This paper work on power generation from solar source as a system that converts solar irradiance into electric energy. Researchers suggest that the amount of sunlight that strikes the Earth's surface in an hour and a half is enough to handle the entire world's energy consumption for a full year. Here solar energy is converted to electrical energy by means of a solar panel made up of transducers called solar cell. Solar energy has incredible potential to power our daily lives. Solar power system is one of the best renewable energy technology which is not only cost effective but environment friendly as well. The paper focused on the feasibility analysis of an off-grid mini power plant which can help to reduce the dependency on grid and allow isolated area to live in self-sufficient manners without reliance on one or more public utilities. Off-grid or standalone systems can be defined as independent systems that are not connected to any electrical grid. It is mostly used in location where there is little access to grid infrastructure. The feasibility study of a 300KW PV power plant at Wudil, Kano State was conducted. For this study RETScreen software is used, using the RETScreen the benchmark analysis, emission and financial analysis were made. From the bench mark analysis the energy cost of production is reduced to 0.10USD/KWh and finally emission analysis shows that 3,412.6 tCO2 will be reduced from the potential emission to the environment. Hence, this means the project is feasible financially, technically and environmental friendly and it will help the country to achieve its goal in building clean energy.

Keywords*: Photovoltaic, Power Plant, RETScreen, Renewable Energy and Solar Energy.*

1.0 Introduction

Nigeria, with its developing economy and rapidly expanding population of over 150 million, has always faced shortage of energy. Even though it is among the countries that are highly endowed with natural resources that can be converted to electricity in the world, it is hardly ever able to meet the electricity requirements of its ever-so-rapidly increasing population [1]. One hundred million Nigerians, representing 60% of the country's population, have no access to grid electricity. Those who do have grid access experience extremely unreliable Supply [1]. Efforts are underway to accelerate the transition to an adequate electricity generation capacity that can meet the current and future demand of Nigerian citizens and their businesses. It is high time Nigeria moved to renewable ways to feed its population its fair-share of electricity [2].

The renewable energy resource which is currently of most interest in Nigeria for utility-scale electricity generation is solar PV. Theoretically, Nigeria has a potential for electricity production from solar PV technology in the range of 207,000 GWh per year (ten times the production in Nigeria in 2011) if only 1% of the land area were covered with PV modules[3]

Solar energy has emerged as the most viable and environment-friendly option for Nigeria to utilize for the energy requirements of one and all—including the majority of its rural inhabitants who still live without electricity. A typical solar system is very easy to set up and just entails installing solar panels correctly in order for it to work [2]. Quite a few people were already aware of its benefits and were really quick at setting their properties up with solar systems; in fact, the utilization of solar energy in Nigeria is nothing new and has existed in some household locations for quite some time now. However, it has yet to pick up steady thrust [4].

Solar technologies convert sunlight into electrical energy through photovoltaic (PV) panels. This energy can be used to generate electricity or be stored in batteries [5]. Needless to say that the Sun is the biggest source of renewable energy for the Earth. The fact is that even though the earth receives only a part of the energy generated by the Sun (i.e. Solar energy), that part of solar energy is also tremendously huge [6]. The Earth receives solar energy in the form of light and heat. But in today's world, the words 'power' and 'energy' are leaned more towards 'electricity'[2]

2.0 Methodology

2.1 Climate data and Location of the Power Plant

The location of the power plant is at Wudil town with Latitude of 11.8°N and Longitude of 8.9° E the other details of the location are given by Table-1 the location is selected based on climate data that can justify its potential, the climate data is given by Table-2. The average daily solar radiation-horizontal of wudil is about 5.86kwh/m^2

Therefore, the wudil town has a very good amount of solar radiation which can be utilized for electric generation throughout the year. Based on the value obtained from the climate data it is easily understandable that the location is suitable for solar power production.

	Unit	Climate data location	Facility location
Name		Nigeria - Wudil	Nigeria - Kano - Wudil
Latitude	°N	11.8	11.8
Longitude	°E	8.9	8.9
Climate zone		1A - Very hot - Humid	1A - Very hot - Humid
Elevation	m	531	0

Table-1: Climate Data Location and facility location

The facility location is with an elevation of **0** meters above sea level. The climate data is extrapolated to this elevation to perform the exact calculations of the feasiblity study and the extrapolated results are given by table-2.

Table-2: Climate Data of the Facility Location

	Heating design temperature			16.3					
	Cooling design temperature			34.7					
	Earth temperature amplitude			17.2					
Month	Air temperature	Relative humidity	Precipitation	Daily solar radiation - horizontal	Atmospheric pressure	Wind speed	Earth temperature	Heating degree-days	Cooling degree-days
	°C	%	mm	kWh/m²/d	kPa	m/s	°C	°C-d	°C-d
January	23.1	18.4%	1.16	5.55	95.1	3.4	25.6	0	405
February	24.9	16.4%	0.59	6.29	95.0	3.3	27.7	0	418
March	28.1	26.5%	0.97	6.65	94.8	3.6	31.2	0	561
April	28.2	51.1%	29.62	6.69	94.7	3.7	30.8	0	545
May	26.9	67.2%	94.71	6.37	94.8	3.5	28.6	0	524
June	25.1	78.1%	167.75	5.93	95.0	3.0	25.9	0	452
July	24.0	81.8%	255.15	5.45	95.1	2.8	24.6	0	434
August	23.9	81.4%	302.06	5.16	95.1	2.7	24.6	0	432
September	24.6	76.9%	192.58	5.53	95.0	2.4	25.3	0	438
October	25.8	56.6%	27.66	5.77	95.0	2.7	27.1	0	489
November	25.9	25.6%	0.56	5.65	95.0	3.1	27.8	0	477
December	23.6	20.1%	1.58	5.35	95.1	3.6	25.6	0	423
Annual	**25.3**	**50.2%**	**1,074.40**	**5.86**	**95.0**	**3.1**	**27.0**	**0**	**5,597**

2.2 Power Plant Capacity

According to [14] peak electricity demand is expected to grow exponentially by 2025 as more people become electrified and the economy grows. The government is targeting 30-30-30 (which assume a 30% share of renewable energy in the energy mix by 2030, given a total of 30,000 MW electricity generation). To reach this amount, it is a must to do potential and feasibility assessments to help the government and interested energy sector investors. Therefore, this study will contribute a potential 300kW of power and it has its own role to help the country to reach its goal by 2030.

2.3. Software

RETScreen enables the user to facilitate project development in various renewable energy and energy-efficiency projects. It includes assessment of the potential for solar power plants based on the solar irradiation data of the selected area. It also determines the main financial information for the project, including initial capital cost and payback period, and calculates avoided CO2 emissions [7][8]. RETScreen can be downloaded for free from www.retscreen.net. The RETScreen solar power project model provides the means to assess the available energy at a potential site that could be provided to a central grid or isolated grid [9][10][11].

3.0 Results and Discussions

3.1 Benchmark Analysis

It has been said that Benchmarking analysis is a specific type of market research that allows organizations to compare their existing performance against others and adopt improvements that fit their overall approach to continuous improvement [12]. And according to[1]At present, there is no significant utility scale solar power generation in Nigeria, but this analysis shows that it can compete at the lower cost range with coal generation (before external costs are considered) at USD 10-11cents/kWh. Fourteen solar PV companies signed power purchase agreements (PPAs) at USD 0.11/kWh with NBET in 2016, with a combined capacity of 1 GW. Some controversy exists as to the feasibility of the project at this price, but our analysis shows that it is a plausible reflection of the lower-bound costs in 2017[1].

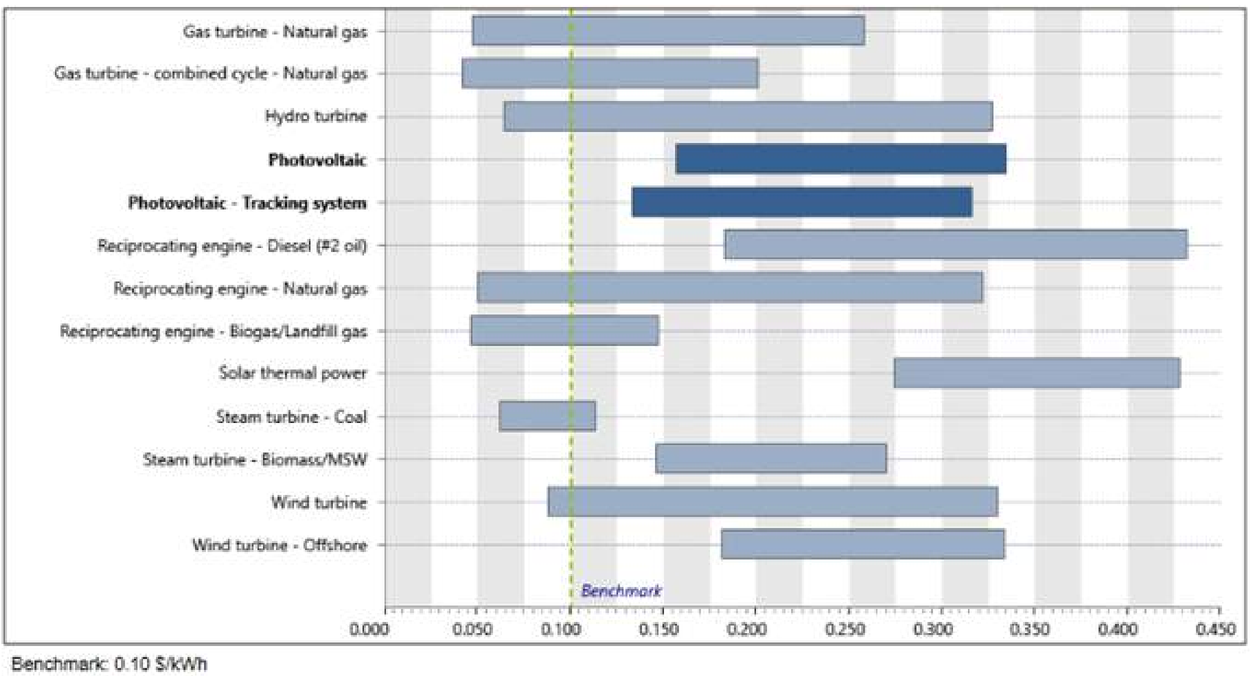

Figure-1: Benchmark Analysis

From the bench mark analysis in Fig. 1 the cost of production for 1kwh photovoltaic power plant is about 0.10 USD which is much less than the proposed planned power generation options in the country as stated by [1]. Therefore, it is clear that photovoltaic power plant at wudil, kano state is feasible regarding the cost of power production and this is a positive result.

3.2 Energy Analysis

The Energy analysis is made based on the bench mark analysis and the climate data presented in sections above. The target plant capacity is about 3,000 KW, this means the plant should deliver constantly 3000KW of power. And the electricity supplied is calculated to be 7,889 MWh and this is given by table-3 below.

Table-3: Energy Capacity

Power system - Total		
Capacity	3,003	kW
Electricity	7,889	MWh

3.3 Emission Analysis

The main target of installing renewable energy sources as power means is reducing the Greenhouse Gas emission [15]. And this study also investigates how much GHG will be reduced, if the location is solely depending on natural gases instead of renewable energy for the same amount of 7,889 MWh annually. The gross annual greenhouse gas reduction is about 93% and this is a meaningful value, this is shown in fig.2 and installing a 3,000 KW PV power plant will reduce the GHG emission from 3669.4 Tco_2 to 256.9 tCO_2 annually and this is shown in Fig.3.

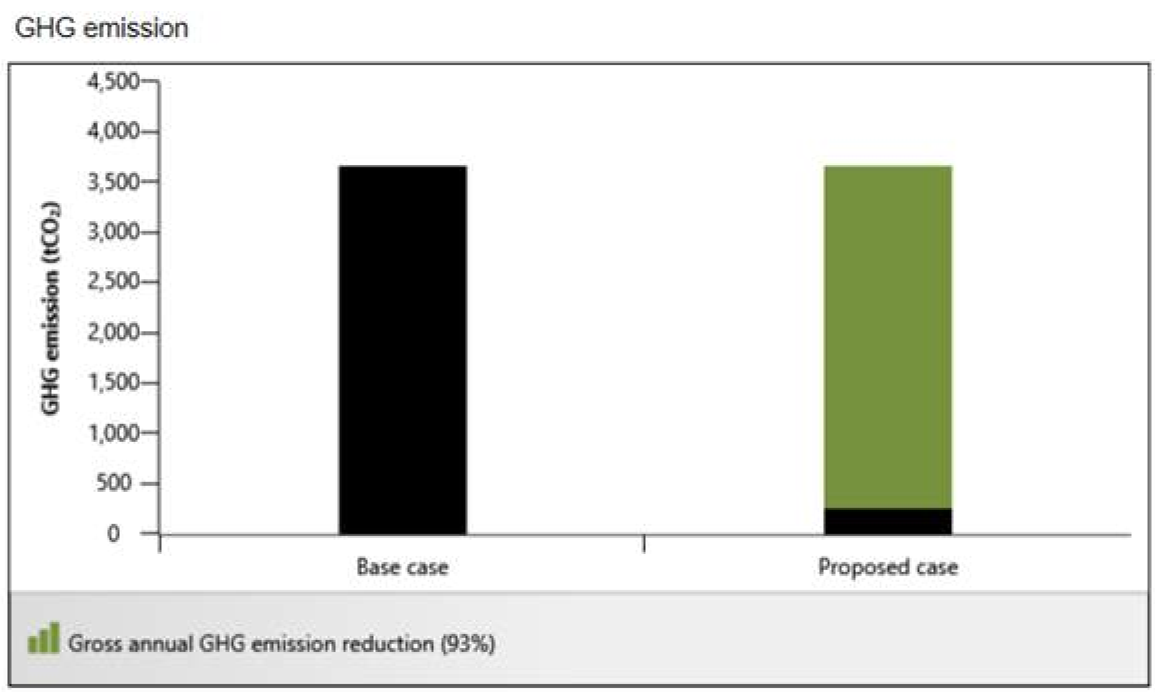

Figure-2: GHG emission reduction

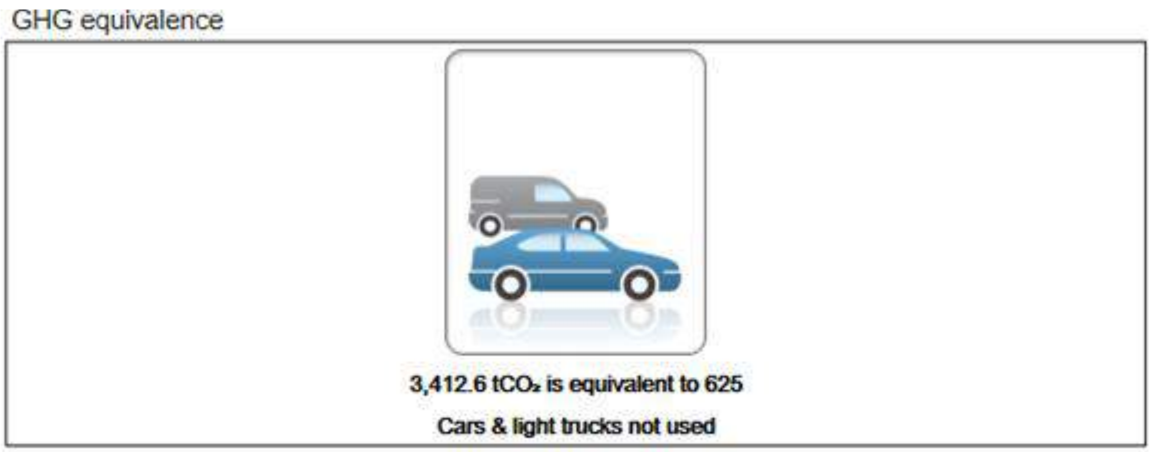

GHG emission		
Base case	3,669.4	tCO_2
Proposed case	256.9	tCO_2
Gross annual GHG emission reduction	**3,412.6**	**tCO_2**

Figure-3: GHG reduction Equivalence

4.0 Conclusion

The feasibility study of a 3,000KW PV power plant in Wudil, kano Nigeria has been completed and the following conclusions are made based on the results.

1. From bench mark analysis employing a PV power plant at Wudil will reduce the energy cost of production from 0.11 USD/KWh to 0.10 USD/KWh. And this alone can tell us the feasibility.

2. Installing this plant in Wudil, Kano Nigeria will reduce the GHG emission from 3669.4 Tco_2 to 256.9 tCO_2 anually. And, this result shows that the plant has a great role in reducing the GHG in a meaningful manner.

From the above points it is concluded that the project is feasible technically, financially and environmentally. And, it will play a great role for the country to achieve its goal of increase in energy production.

REFERENCES

[1] Roche M.Y., Ude N., Ofoegbu I.D. (2017). True cost of electricity: comparison of cost of electricity generation in Nigeria. Heinrich Böll Stiftung Nigeria.

[2] Candelise, C., M. Winskel, and R.J.K. Gross, (2013). *The dynamics of solar PV costs and prices as a challenge for technology forecasting. Renewable and Sustainable Energy Reviews*, 26: p.13 96-107.

[3] Inman, R.H., H.T.C. Pedro, and C.F.M. Coimbra, (2013*). Solar forecasting methods for renewable energy integration Progress in Energy and Combustion Science. 39(6): p. 535 - 576.*

[4] Kaur, A., et al., *(*2016*). Benefits of solar forecasting for energy imbalance markets. Renewable Energy, 86: p. 819-830.*

[5] González-Aparicio, I. and A. Zucker, (2015). *Impact of wind power uncertainty forecasting on the market integration of wind energy in Spain. Applied Energy*. 159: p. 334-349.

[6] P. Chauhan and S. T. Ghandat (2015*).* "*Feasibility Study for Setting Up of a Solar PV Power Plant in Dehradun, India," SSRN Electron. J., no. September, pp. 0–42,*

[7] Roulston, M.S., et al., (2003). *Using medium-range weather forcasts to improve the value of wind energy production. Renewable Energy. 28(4): p. 585-602.*

[8] Milligan, M.R., A.H. Miller, and F. Chapman (1995). Estimating the economic value of wind forecasting to utilities. National Renewable Energy Laboratory Golden, CO.

[9] Jonsson, T., P. Pinson, and H. Madsen, (2010). *On the market impact of wind energy forecasts. Energy Economics. 32(2): p. 313-320.*

[10] Higgins, P., et al. (2014). *Impact of offshore wind power forecast error in a carbon constraint electricity market. Energy. 76: p. 187-197.*

[11] Elsayed I. and Nishi, Y. (2018) "*A feasibility study on power generation from solar thermal wind tower: Inclusive impact assessment concerning environmental and economic costs," Energies, vol. 11, no. 11, pp. 1–18*.

[12] Aguilar L. A. (2015). "Feasibility Study of Developing Large Scale Solar PV Project in Ghana : An Economical Analysis," p. Department of Energy and Environment, Chalmers Uni.

[13] Chika, E.P, (2012). Design and Installation of 200 Watt Solar Power System. Caritas University, Amorji-Nike Enugu.

[14] https://www.get-invest.eu/market-information/nigeria/energy-sector

[15] Al-Ammar E. and Al-Aotabi A. (*2010*). "*Feasibility study of establishing a PV power plant to generate electricity in Saudi Arabia from technical, geographical and economical viewpoints," Renew. Energy Power Qual. J., vol. 1, no. 08, pp. 941–946,*

[16] Gordon, E. (2018). "The Politics of Renewable Energy in East Africa," no. August, pp. 205–224,

*[17]*Bourahla, N. A. Benghanem, M. Doumbia, M. and Bouzeboudja, H. "*The economic feasibility analysis of generated photovoltaic energy in the usto campus," Prz. Elektrotechniczny, vol. 95, no. 5, pp. 147–152, 2019.*

*[18]*Dorothal, M. (2019). *"Ethiopia Solar Report," Sol. Plaza Int., no. July, p. 18.*

*[19]*National Planning Commission, *(*2016*). "Growth and Transformation Plan II (Volume I)," Natl. Plan. Comm., vol. I, no. Gtp Ii, p. 236.*

*[20]*Benti N. E. and Tadesse, G. (2017) *"Feasibility Study of Solar Photovoltaic (PV) Energy Systems for Rural Villages of Ethiopian Somali Region (A Case Study of Jigjiga Zone)," vol. 1, no. 2, pp. 42–48.*

[21] K. Komoto et al., *Energy from the Desert: Very Large Scale PV Power Plants for Shifting to Renewable Energy Future, no. IEA PVPS T8-01:2015.*

[22] L. Marena, (2019). *Integration of Variable Renewable Energy in the National Electric System of Ethiopia, no. February 2019. 2019, p.* 18

[23] https://www.energy.gov/eere/solar/how-does-solar-work

[24] https://www.electricaleasy.com/2015/12/solar-power-system-how-does-it-work.html

[25] https://www.electricaleasy.com/2016/05/future-of-solar-energy-in-india.html

*[26]*Chauhan P. and Ghandat, S. T. (2015) "*Feasibility Study for Setting Up of a Solar PV Power Plant in Dehradun, India," SSRN Electron. J., no. September, pp. 0–42, 2015.*

NIPES-NCEE Conference Proceedings
The 2nd International Conference 15th-17th Feb. 2023
243-253
www.nipesjournals.org.ng

THE EFFECT OF MAGNETIC FLUX DENSITY AMPLITUDE ON THE OUTPUT OF A PERMANENT MAGNET MACHINE: PART I

Chukwuemeka Chijioke AWAH

Department of Electrical and Electronic Engineering, Michael Okpara University of Agriculture, Umudike, Nigeria
Corresponding email:awahchukwuemeka@gmail.com

Abstract

The effect of magnetic flux density amplitude on electromagnetic characteristics of a double stator permanent magnet machine is investigated in this study. The studied parameters are: flux linkage, electromotive force, speed characteristics, torque and inductance profiles. 2D-finite element analysis is implemented in the result predictions with the aid of MAXWELL software. It is revealed that the amount of magnetic flux density in an electric machine would determine its corresponding output performance level; however, with a direct consequence of magnetic saturation at high working conditions. The predicted amplitude of electromotive force in the analyzed machine at no-load condition using fast Fourier transform analysis is: 3.91 V, 4.87 V, 3.96 V and 3.11 V at magnetic flux density of 1.0 T, 2.0 T, 3.0 T and 4.0 T, respectively. Also, the corresponding electromagnetic output torque of the investigated machine at operating current of 15 A, simulated at 1.0 T, 2.0 T, 3.0 T and 4.0 T is: 2.05 Nm, 2.59 Nm, 2.13 Nm and 1.66 Nm, respectively. It is also observed that the fault-tolerance potential of the analyzed machine would be higher at lower magnetic flux density, based on the machine's self-inductance and mutual-inductance characteristics.

Keywords: *Electromotive force, flux density, flux linkage, inductance, speed and torque.*

1.0 Introduction

The quantity of magnetic flux density in a given electrical machine is a vital factor in determining the resulting amplitudes of the machine's electromagnetic characteristics. In particular, a given electrical machine undergoes high electromechanical energy conversion process at the air-gap region and the resulting electromagnetic products of the machine under such condition, would largely depend on the amount of magnetic flux density in such system at any given time, *t*. The investigated double stator permanent magnet machine in this current study is a classical flux-switching permanent magnet machine; and due to the dual excitation nature of typical flux-switching permanent magnet machines (FSPM), it is strongly recommended in [1] that FSPM machine should be operated within a practical flux density limits, in order to avoid the consequential effect of electromagnetic saturations on the machine's overall performance. It is worth noting that the cumulative effect of magnet flux density in a given electrical device would be contributed by both the system's magnetic core materials of steel/iron, owing to the conductor armature reactions and that of the permanent magnets. The synergy effect of the dual excitation sources are demonstrated in [2].

In addition to the quantity of magnetic flux density, the electromagnetic performance of a given electrical machine would also depend on both the implemented magnetic material's coercivity i.e. the coercive force and the machine's operating temperature, as presented in [3]. The studies in [4] noted that accurate prediction of a machine's magnetic flux is essential in the design and analysis of electrical machine, though, the adopted analytical method in could predict electromagnetic results very fast; however, it may have some slight prediction inaccuracies compared to the applied finite element analysis in this current study.

More so, the amount of flux density in a given permanent magnet machine is a function of the machine's axes currents i.e. the machine's current in either the direct-axis or quadrature-axis direction. These axes currents would eventually determine the system's overall output performance, as established in [5]. Invariably, these axes currents would influence the machines axes inductances, and the impact situation would be more intense if the current advance angle is also adjusted synchronously with the machine's working conditions, as could be inferred from [2].

Besides the impact of magnetic properties of magnets on the machine's output performance, it is demonstrated in [6] that the magnetic material or properties of the core would considerably affect the machine's mechanical strength, its loss and thermal contents, power, efficiency and magnetic saturation, to mention but a few. Similarly, large amount of magnetic flux density is proved to have positive enhancement on the electromotive force as well as on other performance indices of a given permanent magnet machine [7]. Nevertheless, an increased value of magnetic flux density could amplify the loss content of the machine, and consequently reduce the machine's efficiency. Additionally, the overall performance of an electrical machine would substantially depend on the machine's flux density [8], electrical frequency [9] and temperature effects [10]. Nevertheless, it is highlighted in [11] that the magnetic saturation intensity of a given electrical machine could be heightened by the effect of electric load and hence, increased armature reaction. The significant effect of electric loading, due to armature reaction on the machine's output is reconfirmed in [1]. It is important to note that magnetic saturation effects of flux-switching permanent magnet machine are usually evidenced on its stator and rotor teeth, particularly on the parts that are closer to the airgap zone. However, magnetic saturation in electric machine could be controlled by adopting modeling/analytical approaches such as magnetic equivalent circuit method, subdomain method, etc., as highlighted in [12]. Also, the total flux density in an electrical machine's airgap is the sum of the of machine's radial and tangential flux density components. However, the resultant electromagnetic output from such a machine would be a function of the sinusoidal nature of the flux density, and hence, the level of its anti-harmonic contents coupled to the resultant magnitude of the flux density in the system.

In general, this current investigation evaluates the effect of magnetic flux density of a given double stator permanent magnet machine; in order to guide electrical machine designers on technical implications of implementing magnetic flux density values on the prediction of electrical machine performances. The analysis is subdivided into four (4) sections i.e. introduction, methodology, results and discussion and conclusion.

2.0 Methodology

Ansoft/Maxwell-2D finite element software is adopted in estimating the results of this current study, owing to its higher level of accuracy compared to modeling and analytical methods of prediction. Meanwhile, fast Fourier transform approach is employed in calculating the amplitude and harmonics of the generated flux linkage, electromotive force (EMF), static torque and output electromagnetic torque with the aid of a MATLAB script file. The investigated machine model is displayed in Figure 1. The parameters of the analyzed machine are listed in Table 1. Note that the analyzed machine has two stators equipped with armature windings having three-phase alternating current; both the inner and outer stator windings are connected in series for improved electromagnetic output. In addition, the outer stator is furnished with permanent magnets having alternating polarities on adjacent poles, in order to ensure effective torque production. It is worth mentioning that only the magnetic flux density effect due to permanent magnets are considered in this present work; thus, influence of steel/iron core magnetic material in relation to its resulting flux density is not considered in this current investigation.

The predicted electromotive force, E is dependent upon the changing magnetic flux, $d\varphi$ of the electric machine at any given time, t. The mathematical expression of E is given in Eq. (1). It is worth noting that the core materials of the investigated machine are made of silicon steel. The torque is produced by a synergy outcome of magnetic fields from armature windings and permanent magnets using flux-switching and flux-concentration principles. However, a larger portion of torque is made by the permanent magnets during the electromagnetic energy conversion process compared to the ones from the armature windings, due to the negligible impact of reluctance torque in this type of machine owing to the machine's inherent unity saliency ratio.

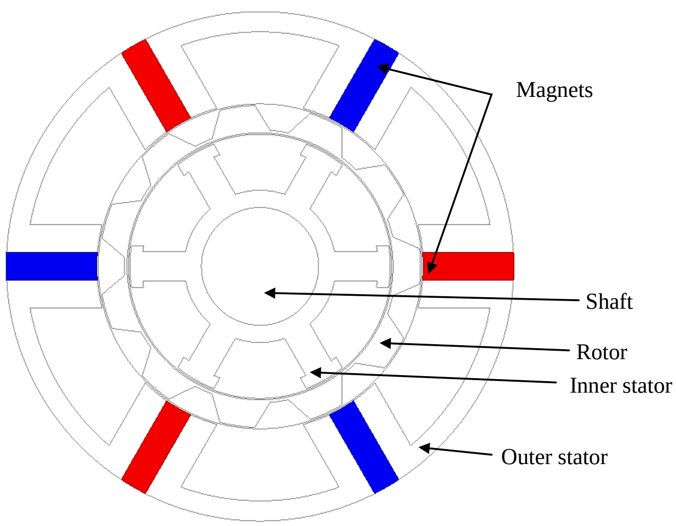

Figure 1 Diagram of the investigated machine

$$E = -N_t \, {}^{d\varphi}/_{dt} \qquad (1)$$

where: N_t is the total number of turns per phase.

Similarly, the self-inductance and mutual-inductance magnitudes of the machine are estimated with the mathematical expression of (2) and (3), respectively.

Table 1 Machine parameters

Parameter/unit	value
Number of rotor pole	11
Number of slots per stator	6

Machine axial length (mm)	25
Machine outer radius (mm)	45
Winding factor	0.6
Type of magnet	neodymium-iron-boron
Magnet relative permeability	1.05
Stator resistance (Ohms)	0.0493
Residual flux density (T)	1.2
Total number of turns per phase	72
Airgap length (mm)	0.5
Combined half-slot area (mm^2)	202.56

3.0 Results and Discussion

The resultant magnetic flux density outlines of the studied machine are depicted in Figure 2. It is observed that the magnetic flux density profiles are strong on the steel core areas, particularly in the air-gap neighbourhood, likely due to the high electromechanical energy conversion activities that are usually experienced around the air-gap. Moreover, the magnitude of magnetic flux density in the machine is seen to be directly proportional to the machine's saturation withstand ability; for instance, the machine would undergo higher saturation impact at 4.0 T than what it would experience at 0.5 T as could be inferred from Figure 2. Also, the resulting phase flux linkage and its corresponding harmonic spectra are depicted in Figure 3. It is noticed that the resultant phase flux linkage would have its largest amplitude between 1.5–2.0T of the magnetic flux density; the decrease in value beyond this point is associated to saturation effect caused by magnets as well as that from the marginal influence by armature reaction.

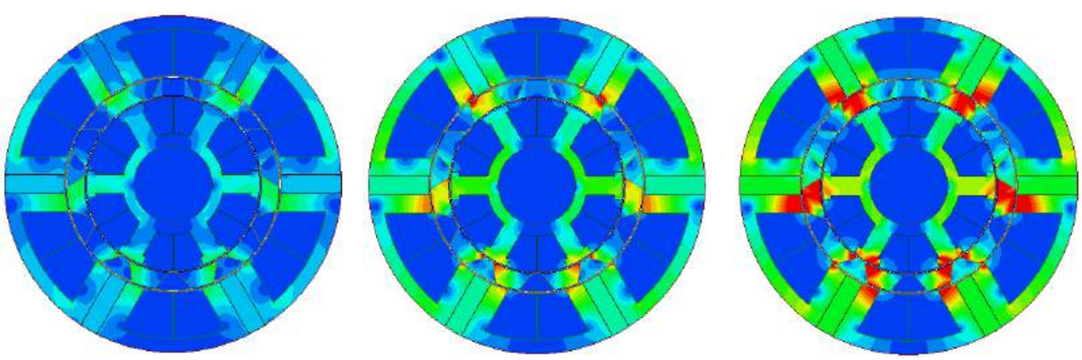

0.5T 1.0T 1.5T

NIPES-NCEE Conference Proceedings
The 2nd International Conference 15th-17th Feb. 2023
243-253
www.nipesjournals.org.ng

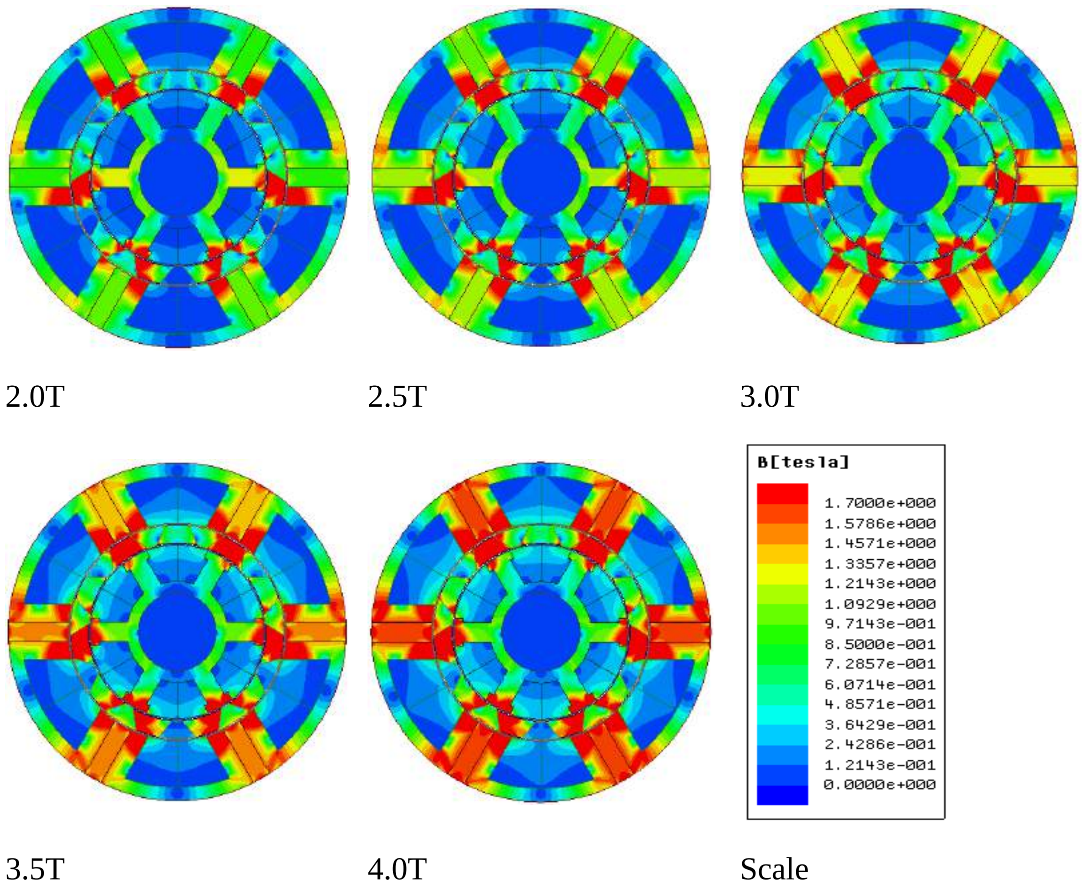

Figure 2 Magnetic flux density distributions

$$L = \frac{Excited\ phase\ A\ flux\ linkage - Open\ circuit\ phase\ A\ flux\ linkage}{Excitation\ current\ in\ phase\ A} \quad (2)$$

$$M = \frac{Excited\ phase\ A\ flux\ linkage - Open\ circuit\ phase\ B\ flux\ linkage}{Excitation\ current\ in\ phase\ A} \quad (3)$$

Where: L and M is the self- and mutual-inductance, respectively. Note that the excitation current in this study is 15A.

Similarly, the generated phase electromotive force (EMF) waveforms and harmonic orders are shown in Figure 4. Again, it is observed that in the vicinity of 1.5 T and 2.0 T of the magnetic flux density; the analyzed machine would attain its maximum EMF amplitude. It is also important to note that the investigated machine exhibits negligible harmonic spectra in both the phase flux linkage and EMF waveforms shown in Figures 3(b) and 4(b), owing to its nearly sinusoidal and symmetrical outlines. These attributes are essential for efficient control of electric machines and for effective operation in brushless alternating current mode [13]. Also, it is shown in Figure 4 (c) that the generated electromotive force would be directly proportional to the motor's rotational speed. Furthermore, similar trend to the produced flux linkage and EMF waveforms are repeated in the variation of output electromagnetic torque over time by the incremental magnetic flux density. It is concluded that magnetic saturation effect sets in the machine beyond the 2.0 T border, and this will lead to decreased overall output performance of the machine. The almost negligible torque harmonic characteristics presented in Figure 5(b), implies that the machine would most likely have low cogging torque magnitude, which is also a desirable electric machine quality. Quantitative comparison of resultant phase flux linkage, phase electromotive force, static torque and output electromagnetic torque is shown in Figure 6 at varying magnetic flux densities, in one electric period. The comparison is simulated at a rotor revolving speed of 400r/min.

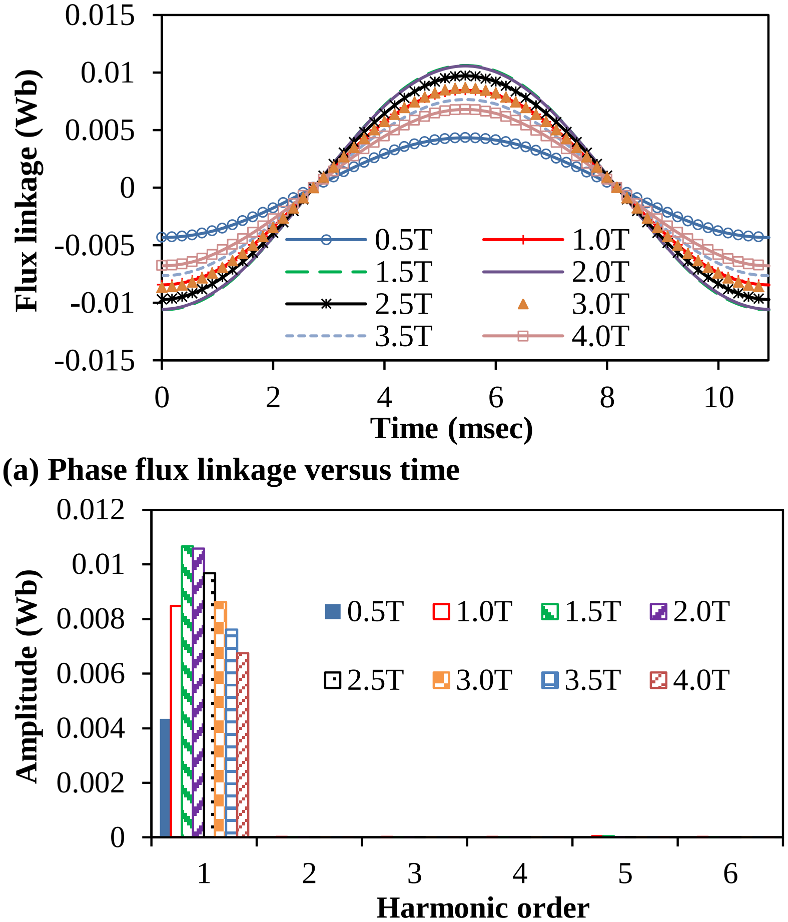

(a) Phase flux linkage versus time

(b) Flux linkage harmonics

Figure 3 Comparison of phase flux linkage

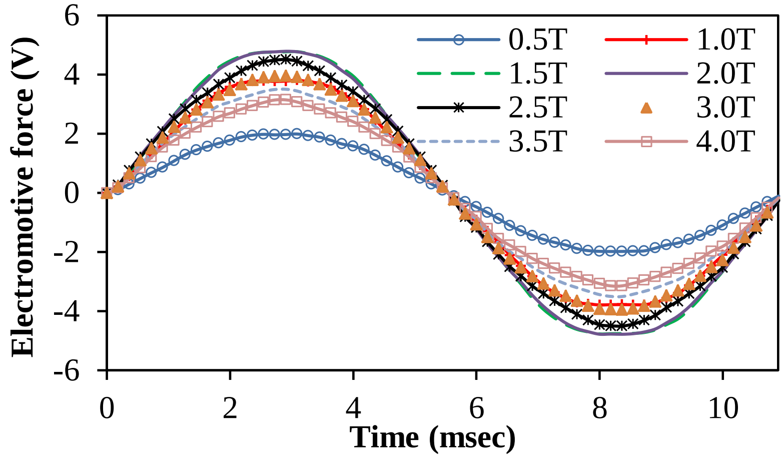

(a) Electromotive force (EMF) versus time at 400rpm

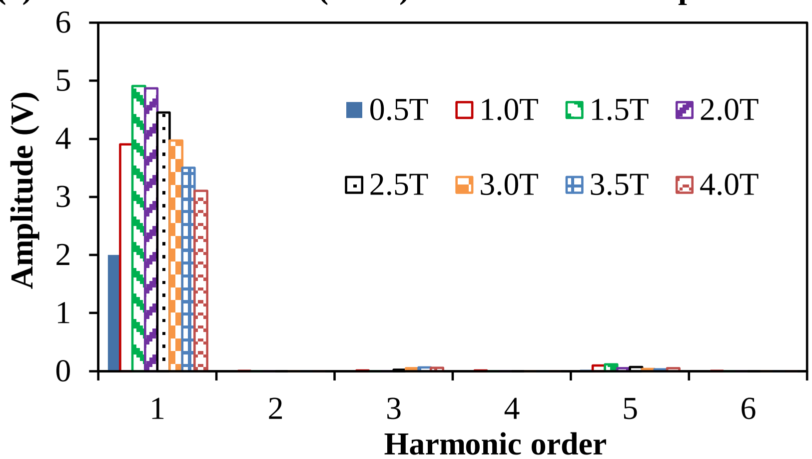

(b) EMF harmonics

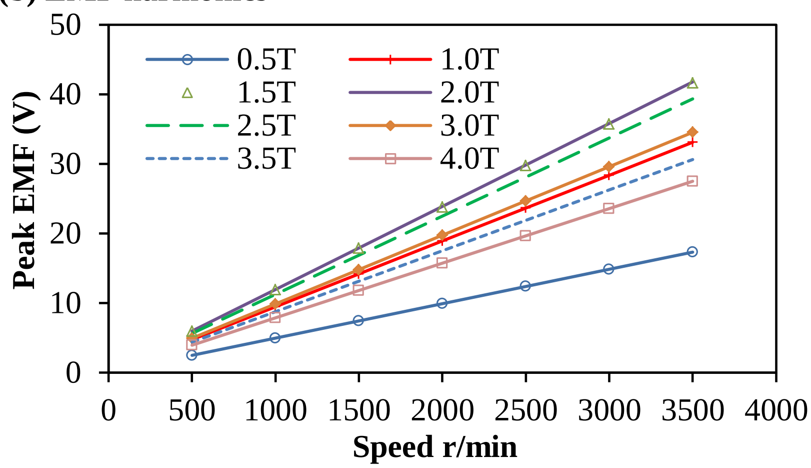

(c) Peak EMF versus speed

Figure 4 Comparison of phase electromotive force (EMF)

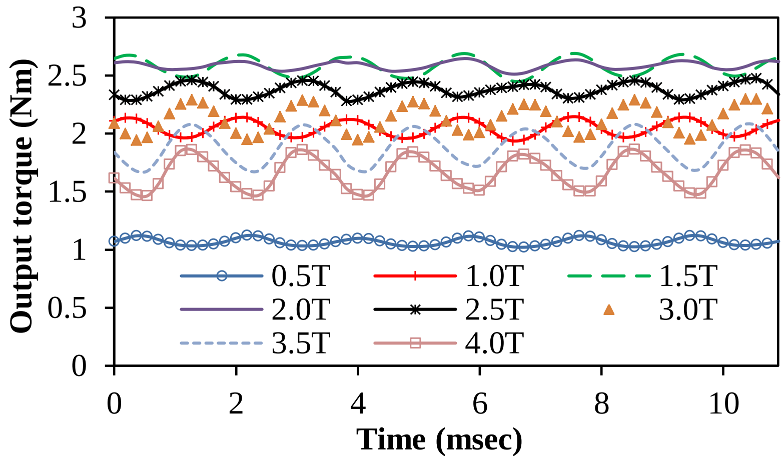

(a) Output torque versus time

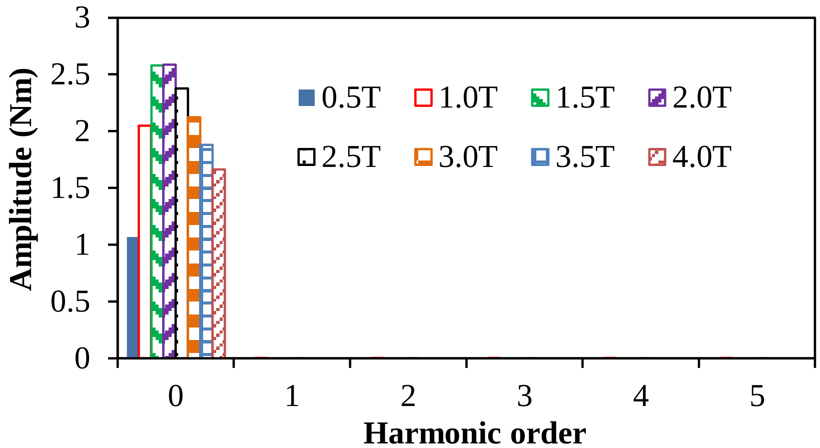

(b) Output torque harmonics

Figure 5 Comparison of output electromagnetic torque, 15A

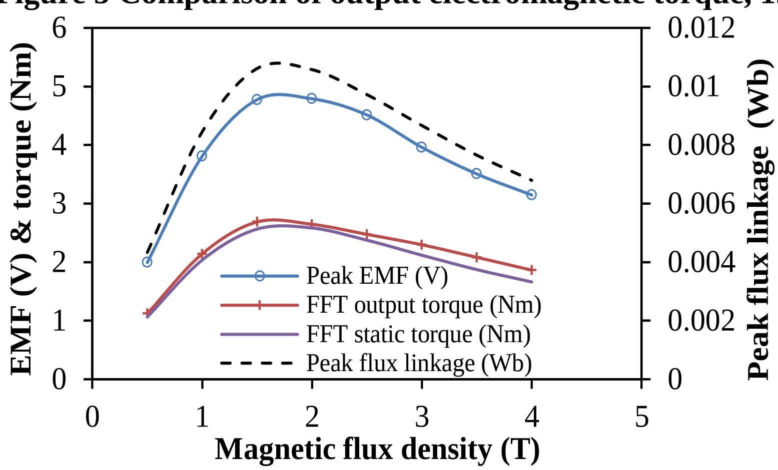

Figure 6 Comparison flux linkage, EMF, and torque

Moreover, the self- and mutual-inductance waveforms of the investigated machine over one electric period are shown in Figure 7. It is worth noting that absolute magnitude of the mutual inductance is used in judging the machine's fault-tolerance level. Note that the actual coil direction is in the reverse path, as could be inferred from the obtained negative mutual-inductance values of Figure 7(b). The results reveal that lower amount of magnetic flux density would yield higher magnitude of self-inductance, which is necessary for short circuit sustenance. Also, the estimated absolute magnitude of mutual-inductance in the system presented in Figure 7(b) shows that large amount of magnetic flux density would give rise to a corresponding low absolute mutual inductance value and vice-versa. Meanwhile, a low amount of mutual-inductance is required to achieve high level of magnetic decoupling and better fault-tolerance potential in an electrical machine, as pointed out in [14] and [15]. Hence, the investigated machine would exhibit the highest fault-tolerant ability when it exhibits the largest magnitude of self-inductance with a corresponding lowest amount of mutual-inductance.

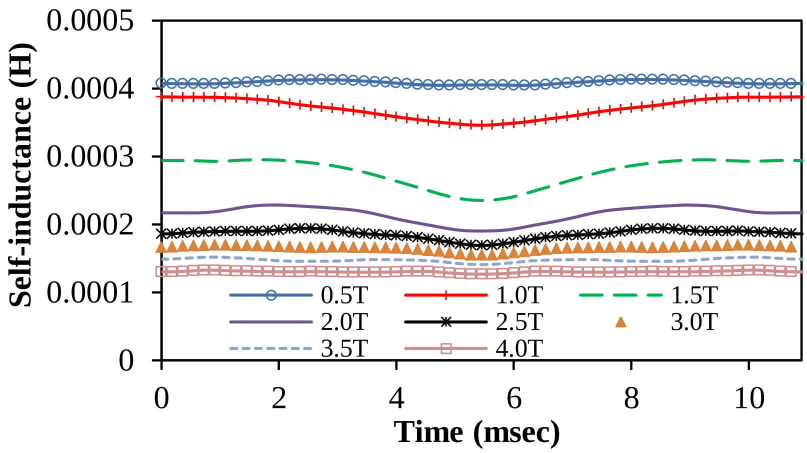

(a) Self-inductance versus time

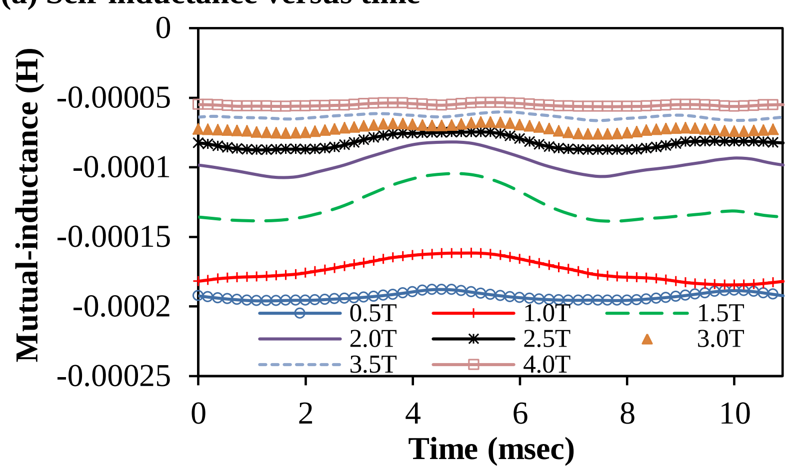

(b) Mutual-inductance versus time

Figure 7 Comparison of self- and mutual-inductances

4.0 Conclusion

The importance of magnetic flux density on output electromagnetic characteristics of a given double stator permanent magnet machine is presented. This present study would enable electrical machine designers to discern the appropriate amplitude of magnetic flux density that is required in an electrical machine, for effective and efficient output delivery. It is noted that the magnetic flux density vary directly proportional to the machine's output performance, however, an inverse relation would be developed in the machine as soon as electromagnetic saturation sets in. More so, it is revealed that the fault-tolerance capability of the analyzed machine would be determined through adequate judgment of the machine's highest self-inductance and lowest mutual-inductance values. It is also observed that the investigated double stator machine would be suitable for electric machine control applications owing to its negligible harmonic order effects. Moreover, there is a linear relationship between the machine's rotational speed and the generated electromotive force (EMF).

References

[1] Petrov, I., Lindh, P., and Pyrhönen, J. (2018). Importance of accurate iron permeability in saturated condition on performance evaluation of flux-switching permanent magnet synchronous machines. IEEE Transactions on Magnetics, 54(6), 1–7.

[2] Zeng, Z., Shen, Y., Lu, Q., Gerada, D., Wu, B., Huang, X., and Gerada, C. (2019). Flux-density harmonics analysis of switched-flux permanent magnet machines. IEEE Transactions on Magnetics, 55(6), 1–7.

[3] Wu, S., Wu, S., Zhao, W., and Cui, S. (2019). Demagnetization research on PMs in the Halbach magnetized pulsed alternator. CES Transactions on Electrical Machines and Systems, 3(2), 170–177.

[4] Li, J., Huang, X., and Jing, L. (2022). Analysis of magnetic field and torque of magnetic gear with rotor copper bar. Progress in Electromagnetics Research M, 109(3), 101–111.

[5] Valavi, M., Nysveen, A., and Nilssen, R. (2015). Effects of loading and slot harmonic on radial magnetic forces in low-speed permanent magnet Machine with concentrated windings. IEEE Transactions on Magnetics, 51(6), 1–10.

[6] Prabhu, M.A., Loh, J.Y., Joshi, S.C., Viswanathan, V., Ramakrishna, S., Gajanayake, C.J., and Gupta, A.K. (2016). Magnetic loading of soft magnetic material selection implications for embedded machines in more electric engines. IEEE Transactions on Magnetics, 52(5), 1–6.

[7] Xie, K., Li, D., Qu, R., and Gao, Y. (2017). A novel permanent magnet vernier machine with halbach array magnets in stator slot opening. IEEE Transactions on Magnetics, 53(6), 1–5.

[8] Jia, W., Xiao, L., and Zhu, D. (2020). Core-loss analysis of high-speed doubly salient electromagnetic machine for aeronautic starter/generator application. IEEE Transactions on Industrial Electronics, 67(1), 59–68.

[9] Xue, S., Feng, J., Guo, S., Peng, J., Chu, W.Q., and Zhu, Z.Q. (2018). A new iron loss model for temperature dependencies of hysteresis and eddy current losses in electrical machines. IEEE Transactions on Magnetics, 54(1), 1–10.

[10] Soleimani, J., Vahedi, A., Ejlali, A., Bafghi, M.B. (2014). Study on interior permanent magnet synchronous motors for hybrid electric vehicle traction drive application considering permanent magnet type and temperature. Turkish Journal of Electrical Engineering & Computer Sciences, 22(6), 1517–1527.

[11] Liu, H.C., Kim, I.G., Oh, Y.J., Lee, J., and Go, S.C. (2017). Design of permanent magnet-assisted synchronous reluctance motor for maximized back-EMF and torque ripple reduction. IEEE Transactions on Magnetics, 53(6), 1–4.

[12] Zhang, H.S., Deng, Z.X., Yang, M.L., Zhang, Y., Tuo, J.Y., and Xu, J. (2020). Analytical prediction of Halbach array permanent magnet machines considering finite tooth permeability. IEEE Transactions on Magnetics, 56(6), 1–10.

[13] Zhu, Z.Q., Pang, Y., Howe, D., Iwasaki, S., Deodhar, R., and Pride, A. (2005). Analysis of electromagnetic performance of flux-switching permanent-magnet machines by nonlinear adaptive lumped parameter magnetic circuit model. IEEE Transactions on Industry Applications, 41(11), 4277–4287.

[14] Bianchi, N., Bolognani, S., Pré, M.D., and Grezzani, G. (2006). Design considerations for fractional-slot winding configurations of synchronous machines, IEEE Transactions on Industry Applications, 42(4), 997–1006.

[15] Kang, M.; Xu, L.; Ji, J.; and Zhu, X. (2022). Design and analysis of a high torque density hybrid permanent magnet excited vernier machine. Energies, 15(5), 1723.

NIPES-NCEE Conference Proceedings
The 2nd International Conference 15th-17th Feb. 2023
254-264
www.nipesjournals.org.ng

THE EFFECT OF MAGNETIC FLUX DENSITY AMPLITUDE ON THE OUTPUT OF A PERMANENT MAGNET MACHINE: PART II

Chukwuemeka Chijioke AWAH

Department of Electrical and Electronic Engineering, Michael Okpara University of Agriculture, Umudike, Nigeria
Corresponding email:awahchukwuemeka@gmail.com

Abstract
The effect of magnetic flux density amplitude on electromagnetic performance of a three-phase double stator permanent magnet synchronous machine is investigated and presented in this study. Time-stepping (TS) finite element analysis (FEA) is adopted in predicting the results with the help of MAXWELL-2D computational software package. Performance indices such as: average torque, losses, efficiency and field-weakening capability etc. are considered. The results reveal that the magnetic flux density magnitude of a given electric machine would only produce the required optimum electromagnetic output in a given machine, for a limited period i.e. before saturation effect sets in. The loss and efficiency profiles of an electrical machine are also affected by this undesirable saturation effect. Moreover, there is a consequent impact of the magnetic flux density value on torque-speed and power-speed trajectories of the analyzed machine, at both constant torque and constant power operating regions. Thus, electrical machine designers and practitioners need to estimate and factor in the adverse effect(s) of high magnetic flux density value during the design and optimization phase and also during different operation modes, for improved machine output. A maximum efficiency of 89.22% is obtained from the simulated machine model at flux density amplitude of 1.6T.

Keywords: *Efficiency, electromagnetic, loss, magnet flux density and saturation*

1.0 Introduction
Magnetic flux density is an essential parameter which influences the overall output of any given electrical machine. Therefore, detailed analysis of the effects of this essential parameter on the electromagnetic output of a given electrical machine is provided in this presented study, in order to be guided on the deployment of the most appropriate magnetic flux density magnitude, so as to achieve optimal electromagnetic results. In particular, electrical machines that have negligible reluctance torque components such as the topology adopted in this present study would usually have a direct proportionality between its magnetic flux density and the resulting output torque, as pointed out in [1]. Though, extreme large amount of magnetic flux density in a given electric machine could result to high core loss consequence, irrespective of its other admirable qualities such high output torque, as provided in [2].

Also, double airgap machines would naturally generate higher magnetic flux density than that obtainable in equivalent single-airgap machines, as highlighted in [3]. It is worth mentioning that the investigated machine model in this current study has double airgap structure, for improved overall output.

The quantity of airgap magnetic flux density in an electrical machine is vital in determining its output performances, as demonstrated in [4]; thus, a dual airgap machine having improved magnetic flux density using Halbach array magnet techniques is proposed in [4], for enhanced machine mechanical stability as well as better output performance. The use of Halbach array magnet technology to boost the machine performance is reiterated in [5]; though, the significant impact of magnetic flux density magnitude is a function of its working harmonic contents. The assertion about the great relevance of working magnetic flux density harmonic contents is proven in [6], where the useful magnetic flux density harmonic elements are dominant in a machine's torque generation.

Mores so, it is pointed out in [7] that manipulation of the relative permeability of the adopted materials through suitable manufacturing processes could help in enhancing the machine's magnetic flux density amplitude, for improved overall performance. However, the deployment of new magnetic materials in electrical machines is very important, in order to achieve reduced machine losses and improved machine efficiency, as opined in [8]. Additionally, the impact of eccentricity in a rotating electrical machine would greatly influence its output characteristics, as demonstrated in [9].

Further, it is noted in [10] that the size of permanent magnet materials of an electrical machine would be proportional to its resulting magnetic flux density magnitude, within normal operating limits of the machine i.e. prior to saturation period of the system. Thus, optimal magnet thickness or size is recommended in order to achieve the best electromagnetic yield from any given electrical machine. Moreover, it is proved in [11] that electric loading of a given electric machine would hamper both its magnetic flux density amplitude as well as its resultant waveforms, owing to the adverse effects of armature reaction.

Essentially, the effect of magnetic flux density magnitude on the overall electromagnetic performance of a double stator electric machine would be analyzed in this current study; in order to have proper guide towards achieving optimal machine electromagnetic performance(s). The background of study is presented in Section 1 of this present investigation, while the implemented method(s), as well as the generated finite element analysis (FEA) results are provided in Section 2 and 3, respectively. The analyses are concluded in Section 4.

2.0 Methodology

The estimated results of this study are calculated using time-stepping (TS) finite element analysis (FEA) of Maxwell-2D software. It is worth noting that the FEA calculated results of torque-speed and power-speed curves are further post-processed using MATLAB m-file at peak voltage and current of 22.9V and 15A, respectively. The implemented machine parameters and materials are given in Table 1. The considered machine metrics include: torque, power, losses and efficiency. The estimated flux-weakening capability (k) of the investigated machine is obtained from Eq. (1). Also, the copper loss of the machine model is estimated using Eq. (2). Similarly, the estimated efficiency (η) of the simulated machine model is given in Eq. (3).

$$k = \frac{LI}{\Psi_m} \tag{1}$$

where: Ψ_m is the flux-linkage of magnet, I is the rated current and L is the d-axis inductance [12].

$$Copper\ loss = 3 \times I_{rms}^2 R_a \tag{2}$$

where: R_a is the armature phase resistance and I_{rms} is the root mean square value of the applied current.

$$\eta = \frac{Output\ power}{Output\ power + Eddy\ current\ loss + Core\ loss + Copper\ loss} \times 100 \tag{3}$$

Note that windage and friction losses are neglected in this investigation

Table 1 Machine parameters

Parameter/unit	**value**
Number of rotor pole	11
Number of slots per stator	6
Machine axial length (mm)	25
Machine outer radius (mm)	45
Winding factor	0.6
Type of magnet	neodymium-iron-boron
Magnet relative permeability	1.05
Stator resistance (Ohms)	0.0493
Residual flux density of magnet (T)	1.2
Rotor and stator material	Silicon steel
Conductor material	Copper
Operating temperature (^oC)	20
Machine split ratio	0.64
Backiron thickness (mm)	3.57
Base speed (r/min)	400
Magnet width (mm)	4.94
Rotor radial size (mm)	4.86
Shaft radius (mm)	10.4
Turns per phase	36
Number of coils per phase	2
Total number of turns per phase	72
Airgap length (mm)	0.5
Combined half-slot area (mm^2)	202.56

3.0 Results and Discussion

The magnetic flux lines of the simulated machine model on open-circuit condition are shown in Figure 1. It is observed that the resulting flux lines linking the stator and rotor parts of the machine through the air-gap are commensurate to its magnetic flux density amplitudes; although, saturation effects of the armature winding could hamper the impact of these flux density amplitudes at extreme electromagnetic load conditions.

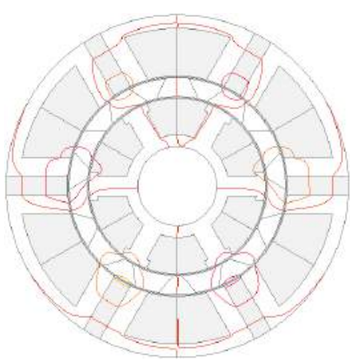

0.5T

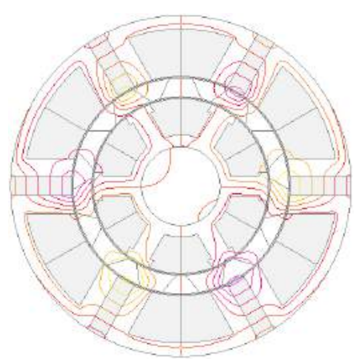

1.0T

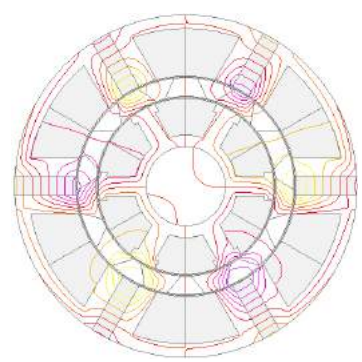

1.5T

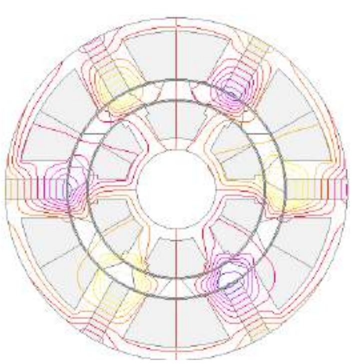

2.0T

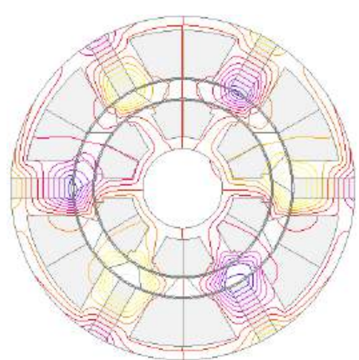

2.5T

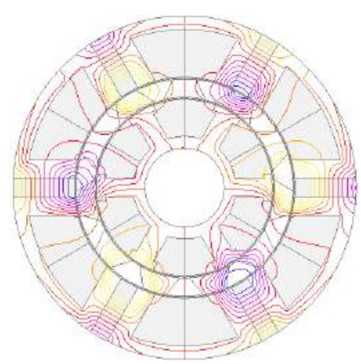

3.0T

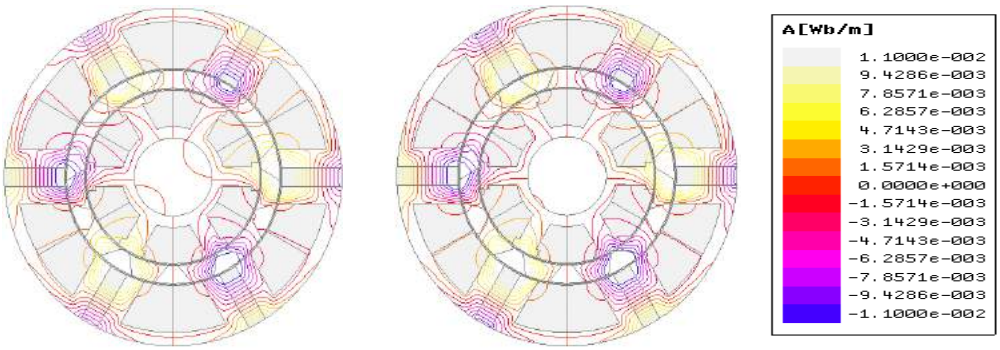

3.5T 4.0T Scale

Figure 1 Magnetic flux lines on open circuit

The average torque variation with both current and copper loss is presented in Figure 2(a) and 2(b), respectively. It is observed that average torque values tend to decrease after the 2.0T point; irrespective of the linear relation that existed before the 2.0T magnetic flux density value. Similarly, the investigated machine model outputs the largest average torque at 2.0T within the simulated current advance angle range, as displayed in Figure 3. It is important to note that in all the simulated case scenarios, the least amount of torque is obtained when 0.5T magnetic flux density magnitude is inputted in the machine.

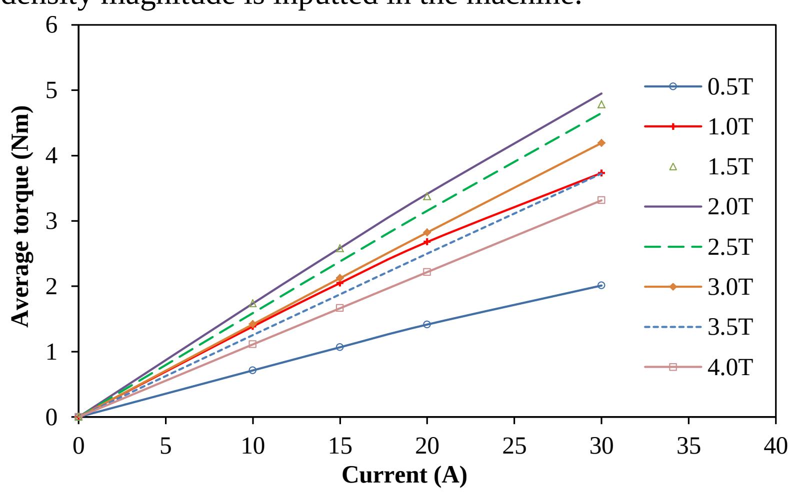

(a) Average torque versus current

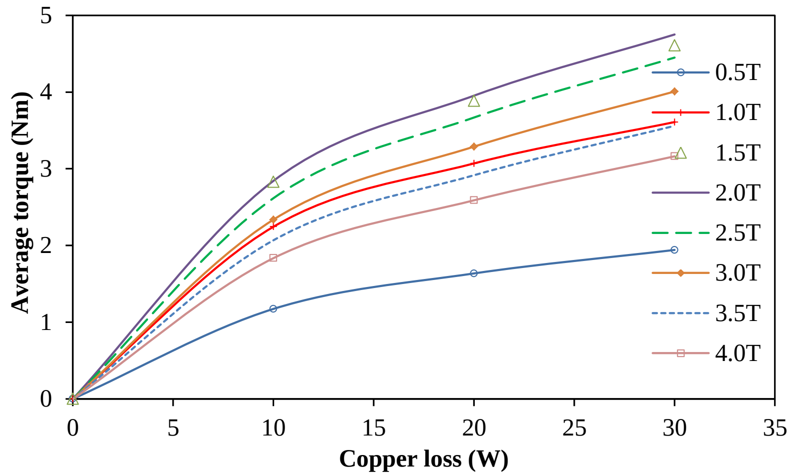

(b) Average torque versus copper loss

Figure 2 Average torque comparisons

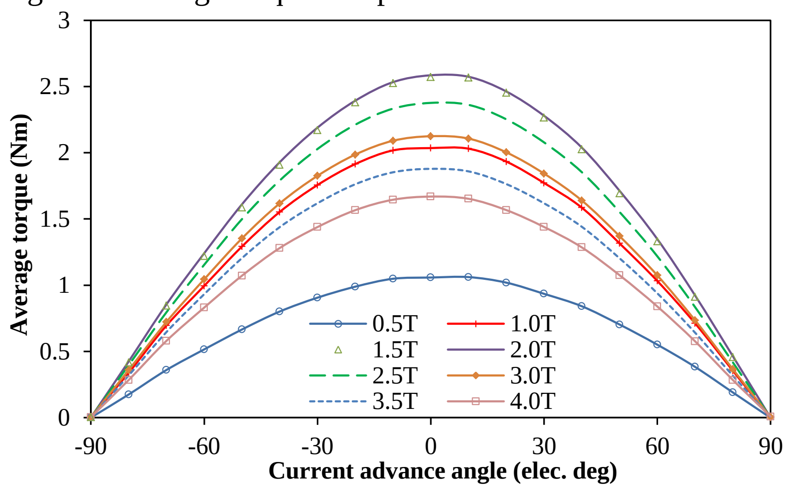

Figure 3 Average torques versus current advance angle

Further, the torque-speed and power-speed envelopes of the simulated model are shown in Figure 4. The studies show that enhanced or extended speed range of the analyzed machine is obtained at relatively low value of magnetic flux density; this attribute also characterizes the machine's flux-weakening potential, as reflected in Table 2. Nevertheless, both the largest electromagnetic torque and power are produced when the machine operates in the neighbourhood of 1.5T to 2.0T amplitudes, as shown in Figure 4. Although, the torque and power densities of a given electric machine could be improved further by using suitable magnetic material such as soft magnetic composite (SMC), as demonstrated in [13] and [14]. However, SMC materials are usually characterized by poor manufacturing tolerance and low vector magnetization quality, as highlighted in [15].

Furthermore, the computed eddy current loss and core loss values given in Figure 5(a) and 5(b) reveal that the losses rise with increasing values of magnetic flux density, up till a magnetic flux density value of about 1.6T, before experiencing a decrease owing to saturation effects in the system. Additionally, the decrease in loss at high flux density amplitudes could also be attributed to the inverse relation that exists between flux density amplitudes and loss coefficients, as inferred from [16].

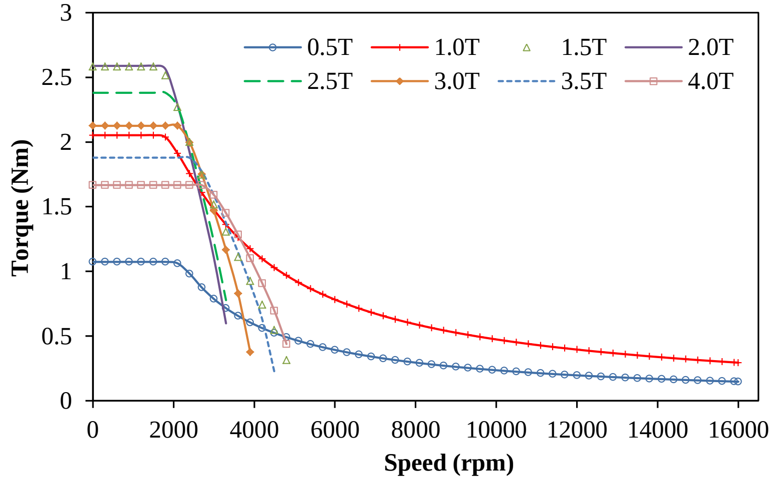

(a) Torque

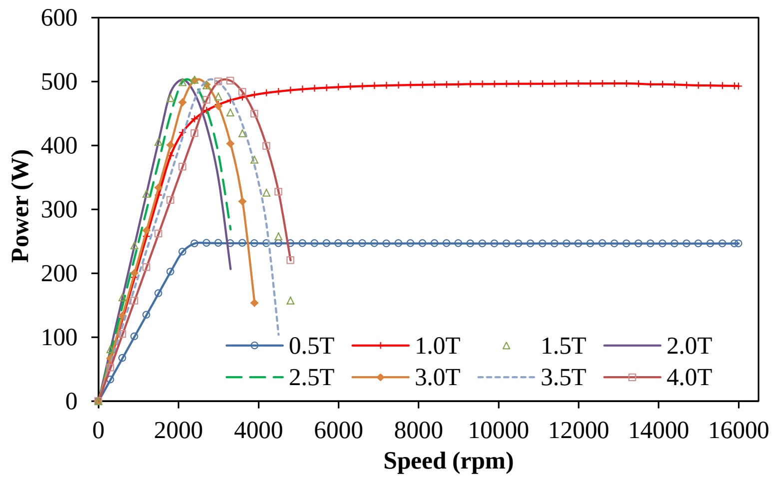

(b) Power

Figure 4 Torque speed and power speed envelopes

Figure 6(a) shows the comparison of resulting permanent magnet (PM) flux per pole at different magnetic flux density values. Again, the best output PM flux is realized within magnetic flux density range of 1.5–2.0T; in addition, there is a noticeable decrease in the resultant PM flux values due to increase influence of the supplied current which may also add some saturation impacts to that caused by the increasing magnetic flux density amplitudes. It is worth noting that the best efficiency of the analyzed machine model is obtained at a magnetic flux density value of 1.6T, as provided in Table 3. More so, efficiency of the simulated model could further be improved, if magnet segmentation is implemented; since magnet eddy current loss contributes largely to poor efficiency of any given rotating electrical machine, as revealed in [17]. The numerical values of some of the machine's performance guides are enumerated in Tables 2 and 3.

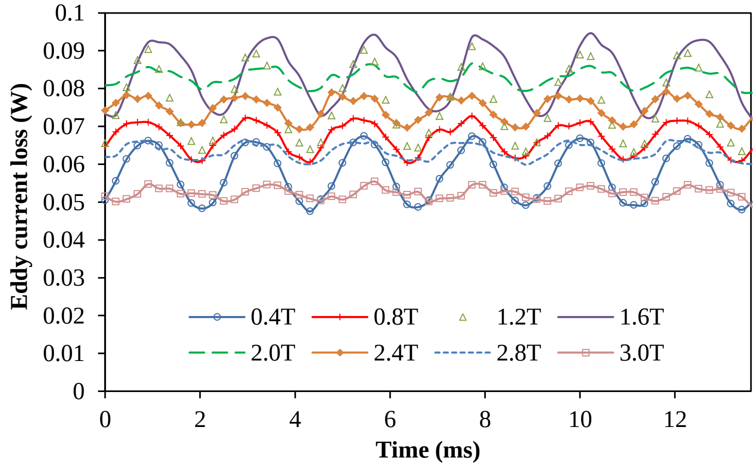

(a) Eddy current loss

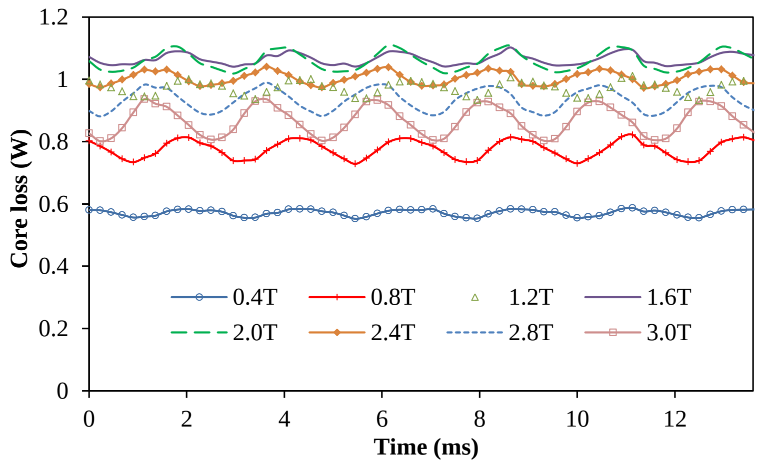

(b) Core loss

Figure 5 Loss comparisons

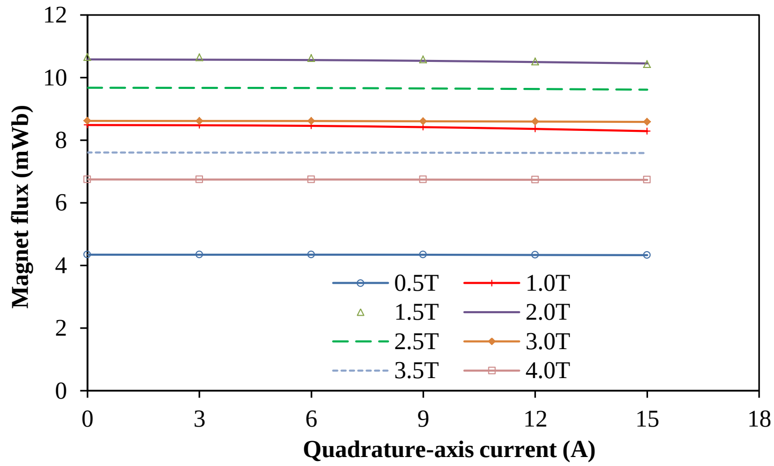

(a) Permanent magnet flux

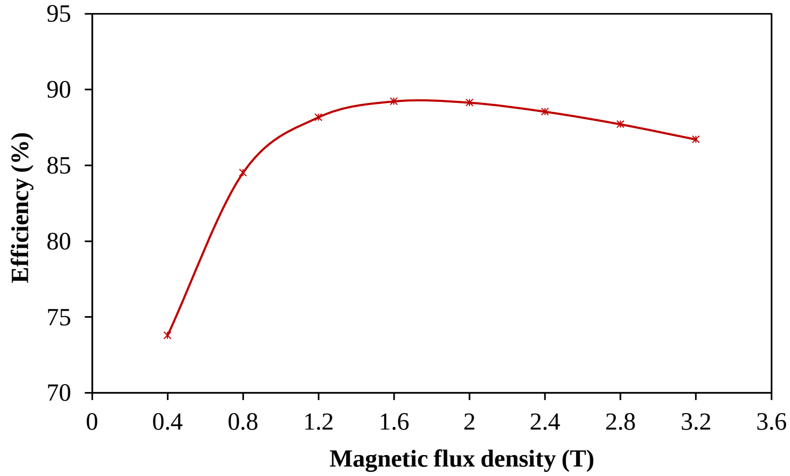

(b) Efficiency

Figure 6 Magnet flux and efficiency plots

Table 2: Torque-speed characteristics

Magnetic flux density (T)	**0.5T**	**1.0T**	**1.5T**	**2.0T**	**2.5T**	**3.0T**	**3.5T**	**4.0T**
Maximum speed (rpm)	16000	16000	4900	3400	3500	4000	4500	5000
Base speed (rpm)	2000	1700	1700	1800	1900	2100	2400	2700
Speed ratio	8.00	9.41	2.88	1.94	1.84	1.90	1.88	1.85

Field weakening capability	2.0494	1.0096	0.6360	0.4674	0.4264	0.4236	0.4252	0.4171

Table 3: Performance of the analyzed machine at 400 rpm

Magnetic flux density (T)	**0.4T**	**0.8T**	**1.2T**	**1.6T**	**2.0T**	**2.4T**	**2.8T**	**3.2T**
PM eddy current loss (W)	0.0575	0.067	0.0757	0.0836	0.0828	0.0745	0.0633	0.0523
Core loss (W)	0.5712	0.7758	0.9722	1.0642	1.0593	1.0044	0.9342	0.8673
Torque (Nm)	0.8545	1.6838	2.336	2.6133	2.5889	2.4265	2.2273	2.0241
Electromagnetic power (W)	35.79	70.53	97.85	109.46	108.44	101.64	93.3	84.79
Efficiency (%)	73.79	84.51	88.17	89.22	89.13	88.54	87.7	86.7

4.0 Conclusion

The impact of magnetic flux density amplitude on output performance of a given electric machine is analyzed and presented in this study. The studies show that there is a limit beyond which, the linear relationship between the magnetic flux density magnitudes and the machine's electromagnetic performance(s) would cease to exist, owing to saturation effects. More so, it is revealed that the largest output torque, power and efficiency of the analyzed machine model are obtained at magnetic flux density vicinity of 1.6–2.0T. Nevertheless, the machine's best flux-weakening potential is attained at relatively low magnetic flux density amplitude. Hence, electrical machine designers should take into consideration the ideal amount of magnetic flux density required in a given electrical machine, in order to achieve the most optimal performance. Experimental tests of the simulated results are recommended, for validation.

References

[1] McFarland, J.D., Jahns, T.M., and A.M. EL-Refaie. (2015). Analysis of the torque production mechanism for flux-switching permanent-magnet machines. IEEE Transactions on Industry Applications, 51(4), 3041–3049.

[2] Tsunata, R., Takemoto, M., Ogasawara, S., and Orikawa, K. (2021).Variable flux memory motor employing double-layer delta-type PM arrangement and large flux barrier for traction applications. IEEE Transactions on Industry Applications, 57(4), 3545–3561.

[3] Kim, B., and Lipo, T.A. (2016). Analysis of a PM vernier motor with spoke structure. IEEE Transactions on Industry Applications, 52(1), 217–225.

[4] Pan, Y., and Jing, L. (2021). Characteristic research on double rotor permanent magnet motor with irregular Halbach array. Progress in Electromagnetics Research M, 104 (6), 133–144.

[5] Huang, X., Guo, Y., and Jing, L. (2021). Comparative analysis of electromagnetic performance of magnetic gear. Progress in Electromagnetics Research Letters, 97(3), 69–76.

[6] Lin, S., Chang, L., Su, P., Li, Y., Hua, W., and Shen, Y. (2023). Research on high-torque-density design for axial modular flux-reversal permanent magnet machine. Energies, 16(4), 1691.

[7] Pham, T.Q., and Foster, S.N. (2020). Additive manufacturing of non-homogeneous magnetic cores for electrical machines-opportunities and challenges. 2020 International Conference on Electrical Machines (ICEM), Gothenburg, Sweden, 1623–1629.

[8] Palangar, M.F. and Soong, W.L. (2022). Future electrical machine materials: Possibilities, opportunities and challenges. 2022 IEEE Energy Conversion and Exposition (ECCE), Detroit, USA, 1–7.

[9] Wang, J., and Wang, Y. (2023). Electromagnetic torque analysis and structure optimization of interior permanent magnet synchronous machine with air-gap eccentricity. Energies, 16(4), 1665.

[10] Evans, D., Azar, Z., Wu, L.J., and Zhu, Z.Q. (2010). Comparison of optimal design and performance of pm machines having non-overlapping windings and different rotor topologies. 5th IET International Conference on Power Electronics, Machines and Drives (PEMD 2010), Brighton, UK. 1–7.

[11] Qi, J., Zhu, Z.Q, Yan, L., Jewell, G.W., Gan, C., Ren, Y., Brockway, S., and Hilton, C. (2023). Influence of armature reaction on electromagnetic performance and pole shaping effect in consequent pole PM machines. Energies, 16(4), 1982.

[12] Wei, H., Zhang, H., Cheng, M., Meng, J., and Hou, C. (2017). An outer rotor flux-switching permanent magnet machine with wedge-shaped magnets for in-wheel light traction, IEEE Transactions on Industrial Electronics, 64(1), 69–80.

[13] Fang, S., Liu, H., Wang, H., Yang, H., and Lin, H. (2019). High power density PMSM with lightweight structure and high-performance soft magnetic alloy core. IEEE Transactions on Applied Superconductivity, 29(2), 1–5.

[14] Chen, Q., Liang, D., Jia, S., Ze, Q., and Liu, Y. (2020). Analysis of winding MMF and loss for axial flux PMSM with FSCW layout and YASA topology. IEEE Transactions on Industry Applications, 56(3), 2622–2635.

[15] Guo, Y., Ba, X., Liu, L., Lu, H., Lei, G., Yin, W., Zhu, J. (2023). A review of electric motors with soft magnetic composite cores for electric drives. Energies, 16(4), 2053.

[16] Biasion, M., Peixoto, I.S.P., Fernandes, J.F.P., Vaschetto, S., Bramerdorfer, G., and Cavagnino, A. (2022). Iron loss characterization in laminated cores at room and liquid nitrogen temperature. 2022 IEEE Energy Conversion and Exposition (ECCE), Detroit, USA, 1–8.

[17] Ding, H., Zhang, L., Hembel, A., and Sarlioglu, B. (2020). Investigation of the effects of skew of an integrated flux-switching motor-compressor. 2020 IEEE Energy Conversion and Exposition (ECCE), Detroit, USA, 5545–5552.

NIPES-NCEE Conference Proceedings
The 2nd International Conference 15th-17th Feb. 2023
265-270
www.nipesjournals.org.ng

DETERMINATION OF THE SUITABILITY OF RICE HUSK ASH AS AN ALTERNATIVE TO SILICA SAND IN THE PRODUCTION OF SODIUM SILICATE

Z. S. ALIYU and **T. M. SALISU

*Department of Glass and Silicate Technology
Ahmadu Bello University, Zaria- Nigeria

**Department of Glass and Silicate Technology
Ahmadu Bello University, Zaria- Nigeria

Correspondence authors' emails: zainabsagarba@gmail.com*
tijjanisalisu201@gmail.com**

Abstract

Samples of rice husk was obtained from Zaria local government area of Kaduna state, beneficiated, ashed and analyzed using x-ray fluorescence to determine the oxides composition the rice husk ash in wt%. The result of the analysis revealed that the rice husk ash sample has a high silica content up to 92.5wt%. The concentration of silica in Zaria rice husk ash was enough to be used as a starting material for making glass and glass-ceramics using sol-gel process. A batch was formulated which constitutes rice husk ash in conjunction with chemical grade soda ash as a source of alkali oxide (Na2O). The batch was melted at 1000°C for 4 hours in a muffle furnace to produce sodium silicate glass which can be majorly used for preserving eggs.

***Key words**: Rice husk ash, analysis, melting, sodium silicate glass*

1.0 Introduction

Utilization of waste from various industries and agricultural sector have received increasing attention in the scientific, technology, ecology, economic and social spheres in the modern times. The global community suffers two types of challenges that is disappearance of natural resources and production of excess wastes [1]. The best alternative to eliminate accumulation of wastes is to put them in the main streams of production. A great deal of researches was carried out in the last few decades seeking for alternatives and sustainable materials for those products that are largely used in the society among which include food by-products and agricultural wastes have grossly gained increasing attention [2]. Corn cob ash and sugarcane bagasse have been involved for biofuel production while rice husk ash (RHA) in the production of glass due to its rich silica content. According to [1], rice husk ash (RHA) is rich in amorphous silica and contains between 85-95% SiO_2. Rice husk (RH) is a by-product of rice milling and therefore could be recycled through burning it for energy production. A wide range of silica-based wastes were identified as potential sources of silica among which include corn ash [3], Coal fly ash [8], rice husk ash [2], sugarcane bagasse ash [4], fly ash from incineration [2 & 4], blast furnace slag [5] and sewage sludge incinerated ash [6], bottom ash (Hossain et al, 2018)[1] among others.

2.0 Materials and Methods

2.1 Materials

The materials for this research was Rice husk, which were obtained from Zaria local government area of Kaduna state, additional materials include in this research are X-ray florescence, distilled water, oven, technical grade Soda ash, burners, Muffle furnace, milling machine, sieves, Crucible, Spatula, Digital weighing balance,

2.2 Methods

2.3 Sample preparation

The rice husk was obtained and sieved to eliminate clay particle. Subsequently washed thoroughly with distilled water to remove the soluble particles dust and other contaminants present in the rice husk, subsequently the heavy impurities such as sand were also removed. It was then dried under the sun for 48hours and then dried in an oven at 100°C for 24hrs. After draying, then the sample was heated in a burner at a temperature of 650°C to 750°C for five days to obtain a uniform ash known as amorphous silica. The generated ash was sieve with a sieve shaker to the particle size distribution of 75 µm.

2.3 Chemical analysis

The rice husk ash obtained was analysed using x-ray fluoresces (XRF) analytical method to determine the elemental composition present in the ash with their respective concentrations.

Table I: Chemical composition of the rice husk ash obtained from the X-ray florescence result in wt%

Oxide	**SiO_2**	**Al_2O_3**	**Cl**	**CaO**	**MgO**	**TiO_2**	**MnO**	**Fe_2O_3**
Wt%	92.5	ND	0.58	0.98	ND	0.11	0.18	0.77
Oxide	**CuO**	**ZnO**	**As_2O_3**	**Rb_2O**	**SrO**	**PbO**	**CO_3O**	**L.O.I**
Wt%	0.05	0.01	0.003	0.022	0.015	0.028	0.004	0.80

2.4 Batch Formulation

In light with the nominal and chemical composition of the (XRF) analysis from the rice husk ash whereby all exact chemical information is obtained, the rice husk ash and technical grade reagent soda ash were used for this study, the following batches were formulated.

Table 2: Batch formulation

Samples	Oxide Component	Weight Of Oxide Component	Source Raw Materials	Weight Of Raw Materials	Total weight of Raw materials	Temperature (°C)
A1	Na_2O SiO_2	40g 60g	Na_2CO_3 R.H.A	68.4g 62.3g	130.7g	1000
A2	Na_2O SiO_2	30g 70g	Na_2CO_3 R.H.A	42.8g 77.9g	120.7g	1000

2.5 Test Melting

The two batches were formulated (A1 and A2) are weighed individually to their respective masses using a digital weighing balance. Sample A1 with a total weight of 130.7g was thoroughly mixed and poured in to a clean crucible and placed in an electric furnance at a temperature of 1000°C for 4 hours at heating rate of 10°C per minute. While the corresponding sample A2 with a total weight of 120.7g was also mixed and poured in a crucible and placed in an electric furnance at a temperature of 1000°C for 4 hours at heating rate of 10°C per minute.

3.0 Results and Discussion

The rice husk ash sample after burning out at 650°C to 750°C for five days presented the highest amount of silica**,** Table 1, demonstrate the chemical composition of the rice husk ash determined using X-ray fluorescence (XRF). The constituents of the rice husk ash as identified by the XRF analytical result are; silica (SiO_2) 92.5wt.%, (Al_2O_3) NDwt.%, (Cl) 0.58wt%, (CaO) 0.98wt%, (MgO) NDwt.%, (TiO_2) 0.11wt%, (MnO) 0.18wt%, (Fe_2O_3) 0.77wt%, (CuO) 0.05wt%, (ZnO) 0.01wt%, (As_2O_3) 0.003wt%, (Rb_2O) 0.022wt%, (SrO) 0.015wt%, (PbO) 0.028wt%, (CO_3O) 0.004wt%, (L.O.I) 0.80wt%. Subsequently the sample was selected for further grinding to particle size distribution of 75 µm. The relative constituent of other elements and the percentage of loss on ignition were small after heat treatment. The most common trace element in the rice husk ash are calcium, titanium, iron, manganese, copper, zinc e.t.c. Difference in composition are due to geographical factors, year of harvest, sample preparation and analysis method [7]. The Samples A1 and A2 melted at a temperature of 1000^oC for 4 hours at heating rate of 10^oC per minute. Table 1 show X-ray fluorescence of samples A1 and A2, while Table 2 shows batch formulation of sample A1 and A2 respectively. The rice husk ash sample burned at 650^oC to 750^oC for five days as presented in plate 1, while Plate 2 & 3 shows sample A1 and A2 of sodium silicate glass melted at 1000^oC for four hours at heating rate of 10^oC per minute.

Plate 1: shows rice husk ash sample burned at 650^oC to 750^oC for five days.

Plate 2: shows sample A1 of sodium silicate glass melted at 1000^{o}C/ 4h.

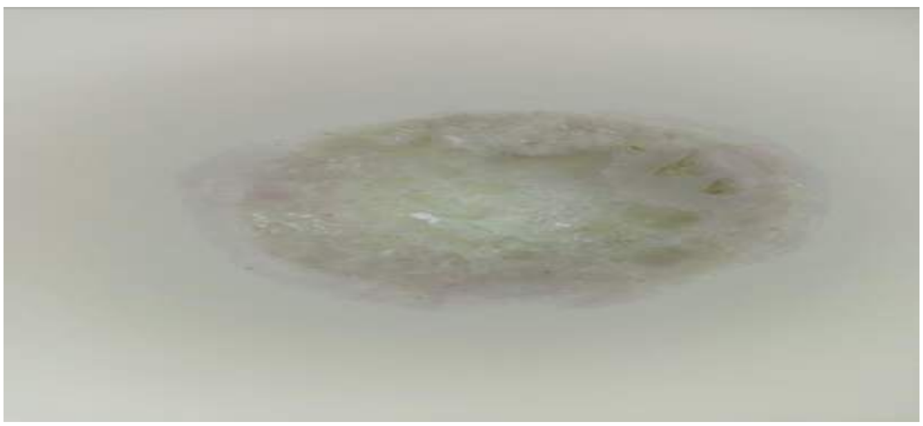

Plate 3: shows sample A2 of sodium silicate glass melted at 1000^{o}C/ 4h.

4.0 **Conclusion**

From the above descriptions the following significant facts can be drawn:

1. It was observed that the ashes are with grey particles as a result of different steps of carbon combustion during the rice husk burning.
2. It was observed from the XRF result that the rice husk ash sample contained a high concentration of silica (92.50%) and low concentrations of ion.
3. The batches were formulated in two different forms with varying concentration of ash content.
4. It was observed that the obtained sodium silicate glass in sample A1 had a presence of colour (orange- like) and bubbles. Sample A2 gave a somewhat light- brown colour with presence of larger and more bubbles and also un-melted portions, compared to sample A1.

5. It can be deduced from the results that the presence of colour in both samples A1and A2 could be as a result of colourants present in the rice husk ash and the percentage ratio of the R.H.A to soda ash. The un-melted portions and bubbles could be due to insufficient temperature and soaking time.
6. RHA is found to be the most promising waste to serve as a potential source of silica in glass and ceramics production.

References

[1]. Hossain S.K.S., Lakshya, M. and Roy, P.K. (2018). Rice husk/rice husk ash as an alternative source of silica in ceramics. A review. *Journal of Asian Ceramic Societies.* Vol.6. pp 299-313. https//: doi.org/10.1080/21870764.2018. 1539210.

[2]. Jaderson, G. and Chiara, V. (2020). Production of transparent soda-lime glass from rice husk containing iron and manganese impurities. *Journal of Ceramics.* Vol. 3, pp 494-506.

[3]. John, T. K. and Kejin, W. (2010). Investigation of corn ash as a supplementary cementitious material in concrete. *Second International Conference on Sustainable Construction Material and Technologies.* ISBN -1-4507-1490-7.

[4]. Norsuraya, S. Norhasyyimi, R. and Fazlena, H. (2017). Characterization of sodium silicate derivedfrom sugarcane baggase ash. *Malysian Journal of Analytical Sciences*. Vol. 21, No. 2, pp512-517.

[5]. Ozturk, Z. B. and Gultekin, E. (2015). Preparation of ceramic wall tiling derived from blast furnace slag. *Journal of Ceramics International.* Vol. 41, pp 12020-12026.

[6]. Sunday, A. (2011). Effect of Varying Corn Cob and Rice Husk Ashes on Properties of Moulding Sand. *Journal of Minerals & Materials Characterization & Engineering.* Vol. 10. No. 15, pp1449-1455.

[7]. Yadav, V. (2021). "Rice Husk Ash: A Systematic Review of Its Applications". *International Journal of Current Research* Vol. 13, (06), pp.17706-17713.

[8]. Zu, M. Ji, R. and Li, Z. (2016). Preparation of glass ceramic foams for thermal insulation applications from coal fly ash and waste glass. *Journal of Construction and Building Materials*. Vol. 112, pp 398-405.

NIPES-NCEE Conference Proceedings
The 2nd International Conference 15th-17th Feb. 2023
271-279
www.nipesjournals.org.ng

PRODUCTION OF BIODIESEL FROM NON-EDIBLE SEED USING IMPREGNATED CATALYST OF CALCIUM OXIDE AND ZINC OXIDE

[1] Ahmadu G. K., [2] Eterigho, E. J. & [3] Otori, A. A.

[1,3] Chemical Engineering Department, Federal Polytechnic, Bida, Niger State
[2] Chemical Engineering Department, Federal University of Technology, Minna, Niger State
Email: kaybeetechs@gmail.com

Abstract

The major part of all energy consumed worldwide comes from fossil sources. However, these sources are limited, and will be exhausted by the near future. Biodiesel (Methyl ester of fatty acids), an alternative diesel fuel, is made from renewable biological sources such as vegetable oils and animal fats. This study deals with the transesterification of Prosopis Africana seed oil with heterogeneous catalyst using CaO loaded with ZnO as solid base catalyst. Four different parameters were optimize namely: methanol to oil ratio (5:1), Temperature (50 0C), catalyst concentration (2.2 wt%) and reaction time (60 min) to have high yield of biodiesel with 95% conversion rate. The fuel properties of the produced biodiesel were compare with ASTM and EU standards and they are all in conformity with the standards.

***Keywords**: Impregnation, Calcination, Prosopis africana, Heterogeneous catalyst, Calcium oxide, Zinc oxide*

INTRODUCTION

Prior to the advent of biodiesel, petroleum fuels have remained almost entirely unchallenged since the motor vehicle was invented. However, their reserves are not uniformly distributed and their increased use contributes to a variety of local and regional air pollution problems and potential climatic change [5].

Biodiesel is most commonly made by transesterification process of the oil through the use of a catalyst and an alcohol, typically methanol. The chemical reaction that occurs through this process breaks down the oil molecules and replaces the glycerin portion of the molecule with an alcohol molecule. The glycerin separates to the bottom and is drained off resulting in biodiesel. The biodiesel is then typically washed, to remove any extra impurities and is then used as a fuel in a diesel engine without making any modifications to the engine. The use of enzymes (lipases) is timely as we embrace the practice of green production technologies (Green chemistry) which ensures sustainable use of resources, energy and maintenance of a clean environment [18].

The main advantages of using biodiesel fuels as 100 % mono alkyl esters of vegetable oil and animal fat or biodiesel blends (up to 20 % blend to the diesel fuel) are producing less smoke and particulates and having higher cetane numbers [11]. In addition, the production of biodiesel should be encouraged especially in developing countries because of the following considerations; Biodiesel is produced from sustainable/renewable biological sources; Ecofriendly and oxygenated fuel.

Biodiesel is an energy efficient, alternative fuel which can fulfill energy security needs without trading the engine's operational performance [17]. This is because it can be applied to compression-ignition diesel engines with very little or without modifications. It therefore provides possible solution to the dual crises of fossil fuel exhaustion and environmental degradation. In terms of engine emissions, it has been indicated that exhausted gas from biodiesel combustion does not contains SO_2 and relatively small amount of CO, unburned hydrocarbons when compared to the combustion products of conventional diesel fuel [19]. In addition its lubricant property can extend the engine's life. Other benefits of the biodiesel are high cetane number, high flash point, and acceptable cold filter plugging point (CFPP) (Dorado *et al.*, 2014).

EXPERIMENTAL PROCEDURE

Collection of Sample

A non-conventional feed stock of *P. africana* seed was selected for this study, as this plant is native to Bida, and there is a need to exploit the benefit of this plant as substitute feed stock for biodiesel production.

Pretreatment of *P. africana* Seeds

Seeds were first unshelled and made clean of any other impurity and sundry for seven days. The dried seeds were pulverized into uniform powdered, sieved, weighed, bottle, labeled and stored in plastic container (air-tight) to air contamination.

Extraction of *P. africana* oil

100 g of ground seeds were taken in a soxhlet apparatus on a water bath. Extraction was done in petroleum ether for 3 h and repeated twice to obtain enough quantity of oil sample. Extracted oil was made free of the solvent under vacuum in rotary evaporator (Heidolph HB digital, Laboratory 4001 efficient). The percentage oil yield was calculated using the formula:

$$\text{Oil content} = \frac{\text{weight of oil extracted}}{\text{weight of seed}} \text{x} \frac{100}{1}$$

Physicochemical Properties of *P. africana* Oil

All the test done for physicochemical chemical properties of *P. africana* were according [16]. The tests performed were iodine value, pH, free fatty acid, saponification value, peroxide value, acid value, odour, specific gravity, ash content, moisture content and colour. The test was tabulated in Table below.

Table A: Physicochemical Properties of *P. africana* oil

Properties	*P. Africana*
Yield (%)	35
pH	4.2
Colour	Bright yellow
Density (g/cm^3)	0.85
Refractive index	2.2
Specific gravity	1.5
Saponification value (mgKOH/g)	120
Acid value (mgKOH/g)	3.3

Values are mean ± SD of duplicate determinations

Catalyst Preparation

Calcium oxide was loaded onto zinc oxide at the following amounts of 20, 25, 30, 35, 40, 45 and 50 wt % by an impregnation from aqeous solution, following by drying at 100 ^{0}C for 14 h. Prior to each reaction, the catalyst were calcined at desired temperatures (400 ^{0}C) in air for 5 h.

Transesterification procedure

The oil extracted from *P. africana* seed was transesterified using transesterification reaction. 200 g of the *P. africana* oil seeds was heated to 60 ^{0}C with 100 cm^3 of methanol followed by addition of 5 w% of CaO loaded on ZnO. The reaction was carried out under reflux at a stirring speed of 250 – 350 rpm. The mixture was stirred at all-time throughout the transesterification process.

An electronic temperature controller was used to vary the reaction temperature in the range of 50 – 70 ^{0}C, reaction time 30 – 65 min. After the reaction time was over, the catalyst is filtered out and the product was poured into a separation funnel and was left overnight for separation of methyl ester and triglyceride to occur. After separation the lower layer which is triglyceride (glycerol) is drawn out of separating funnel and the methyl ester was the product obtained which is biodiesel.

RESULTS AND DISCUSSION

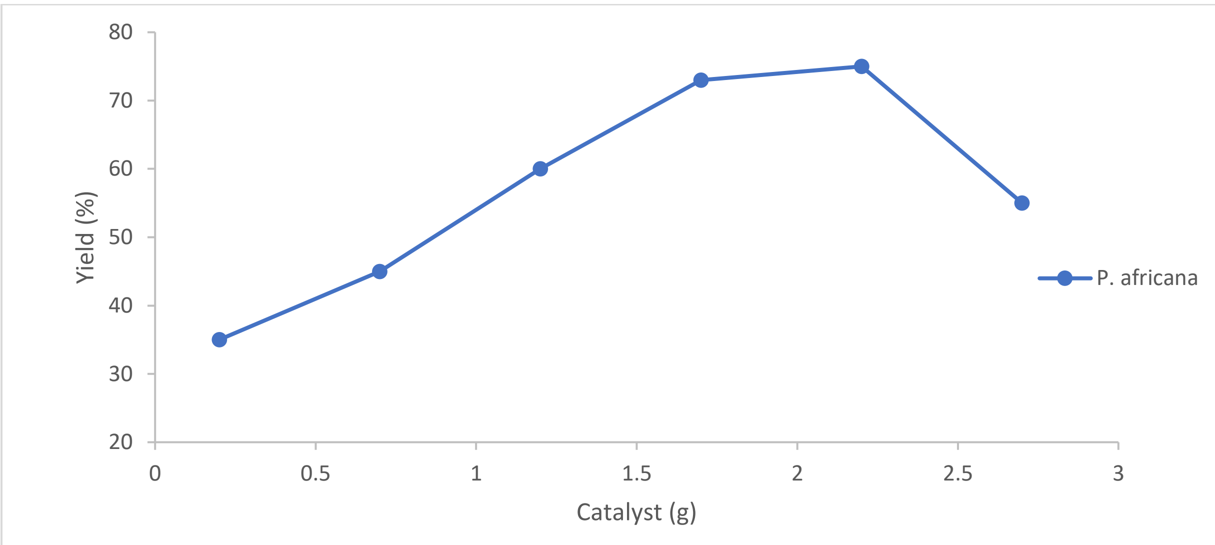

Fig. 1: Effect of catalyst concentration on the biodiesel yield. Reaction condition: temperature 50 ^{0}C, reaction time 60 min, mole ration (5:1).

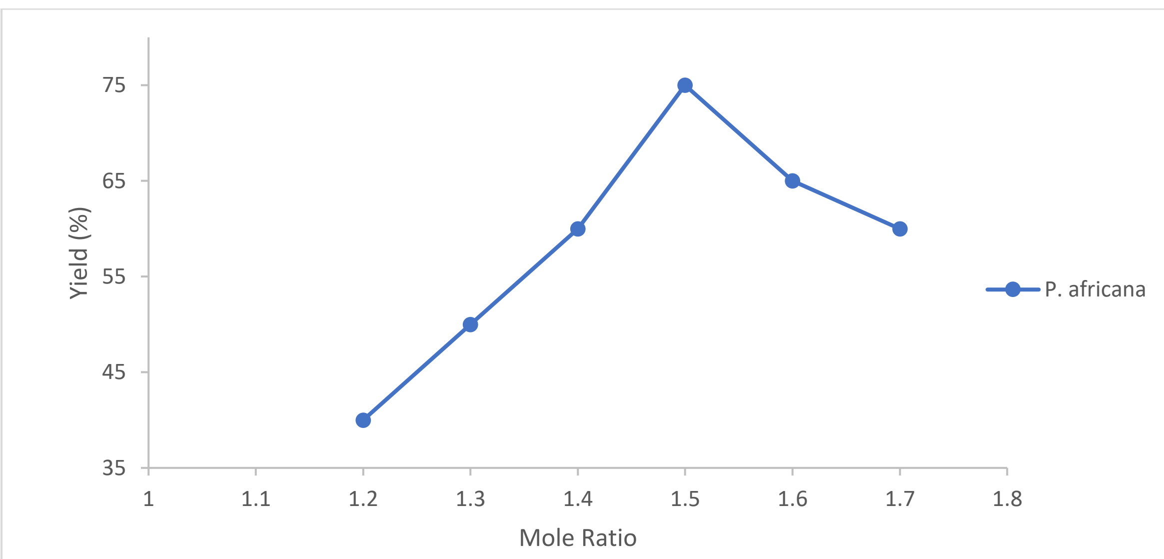

Fig. 2: Effect of methanol to oil mole ratio on the biodiesel yield. Reaction condition: catalyst concentration 2.2 wt%, reaction time 60 min, reaction temperature 50^{0}C.

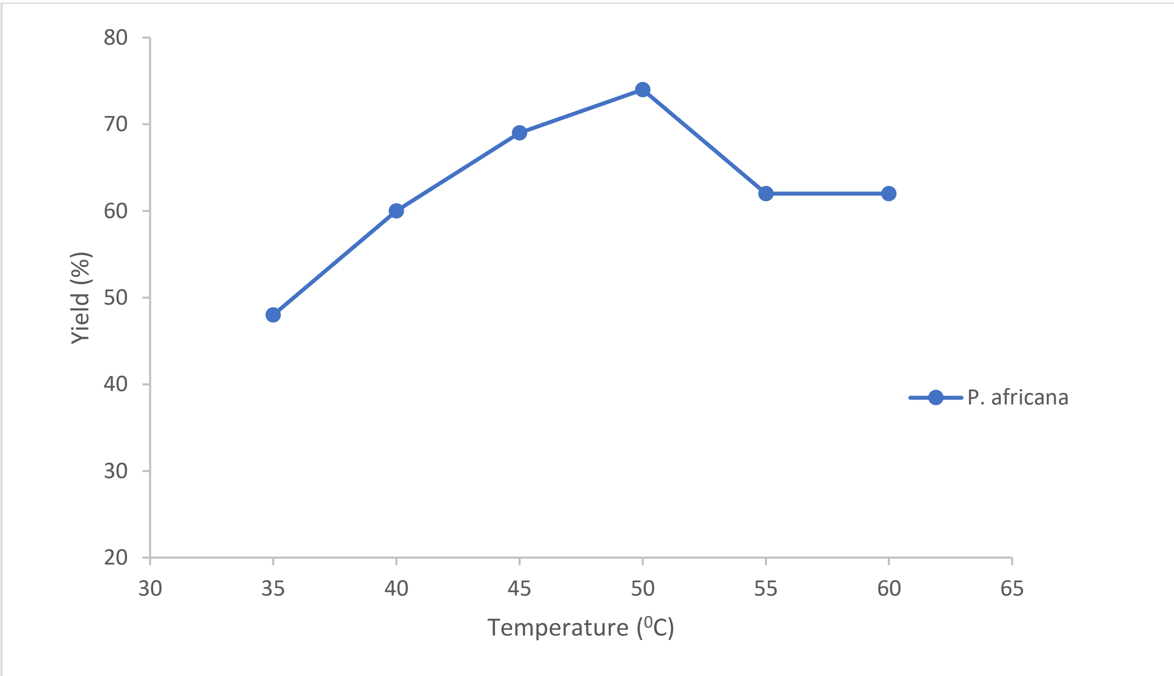

Fig. 3: Effect of reaction temperature on the biodiesel yield. Reaction condition: catalyst concentration 2.2 wt%, reaction time 60 min, mole ratio (5:1).

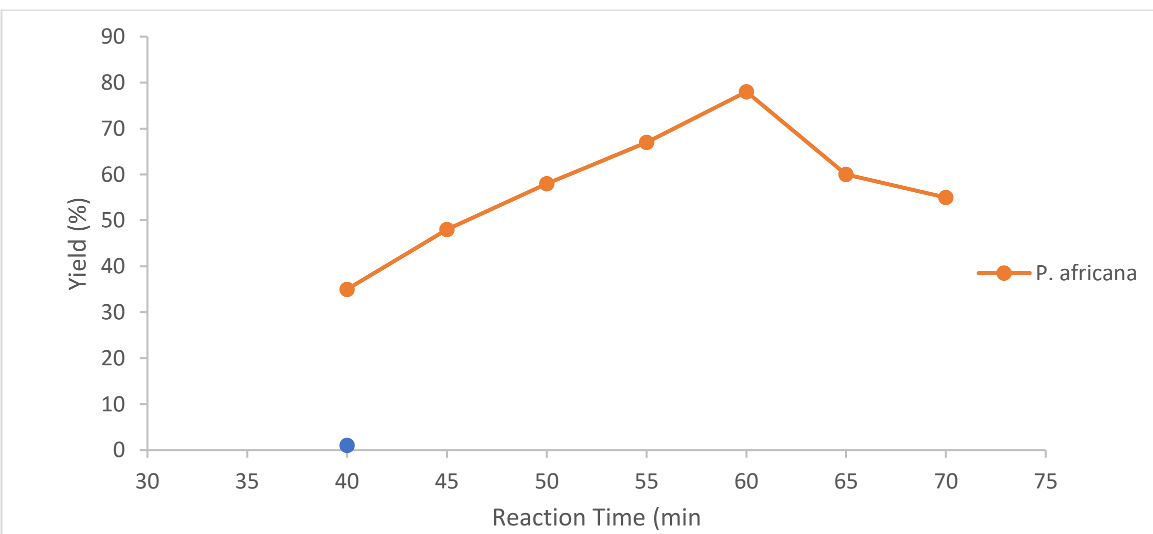

Fig. 4: Effect of reaction temperature on the biodiesel yield. Reaction condition: catalyst concentration 2.2 wt%, reaction time 60 min, mole ratio (5:1).

Table B: Fuel properties of produced biodiesel

Properties	*P. Africana*	*ASTM*
Density	0.83	0.75 – 0.84
Pour point	6.5	5 – 10
Cloud point (^{0}C)	-9.3	-1.2 - -13
Flash Point (^{0}C)	130	100 – 170
Cetane no.	38.3	38 – 64

DISCUSSION OF RESULT

Heterogeneous catalyst of impregnated CaO/ZnO prepared was calcined and tested for the production of biodiesel. In the presence of calcination at 500 ^{0}C, the catalyst were active and exhibited a higher catalytic activity. As a result, the catalyst activity is generated by loading the calcium oxide with zinc oxide followed by the calcination of the samples.

Effect of loading amount of CaO on the conversion of the *P. africana* seed oil at the loading amount range from 15 – 40 wt%. When the loading amount of CaO was increased to 25 wt%, the conversion increased and the highest conversion of 88.4% was achieved. However, when the loaded CaO was over 25 wt%, the conversion was decreased. This result could be attributed to the effect of CaO on ZnO support weakens the combination of Ca^+ and ions of O^{-2} due to the interaction of CaO and the surface of the support, which is beneficial for the decomposition of CaO. At low loading of CaO, the active base sites are more dispersed on the zinc oxide surface and strong adsorption of reactant may occur at unreactive surface sites.

The extracted oil colour is brown yellow from *P. africana*. This colour is acceptable for biodiesel production according to [9]. [16] reported brown colour for Jatropha oil for the product of biodiesel, [15] reported brown yellow colour for neem oil for the production of biodiesel which are all accepted by Codex Standard for biodiesel production.

The study shows that 3.3 mg/g was obtained for *P. africana*, and this value is low compare to that of breadfruit seed oil that is 7.38 mgKOH/g but higher than that of butter oil which is 1.79 mgKOH/g [7] but are lesser than those of cashew nut (10.7 mgKOH/g) [2], avocado seed oil 16.8 mgKOH/g. The low acid value suggest that the oil may be good for paint making [3]. The lower the acid value of oil, the few fatty acid it contains which makes it less exposed to the phenomenon rancidity [14].

The physicochemical properties and the percentage oil yield of the extracted oil were determined. After the extraction it was found that the seed contains 37.0% (*P. africana*) of oil, which was slightly higher compared to *A. africana* (35.5%) reported by [1]. The variation in the oil yield could be attributed to the extracting solvent, difference in variety of plant, cultivation climate. In this study *n*-hexane was used using soxhlet extractor. The results of the physicochemical properties of *P. africana* oil seed is presented in Table A.

Four process parameters affecting transesterification reaction namely methanol to oil ratio, temperature, catalyst and reaction time were determine for optimal biodiesel production. Figure 4.1 presented the effect of methanol to oil molar ratio. Optimum biodiesel was observed at methanol to oil ratio of 5:1 and yield of 75.3%. An increase in mole ratio beyond the optimum mole ratio of 5:1 had a negative effect on the yield. The yield decreased above this optimum point. [4] showed that the most suitable molar ratio was found to be within the range of 5:1 to 10:1, in the production of biodiesel using egg shell ash (CaO) as heterogeneous catalyst.

Figure 1 shows the catalyst concentration increases from 0.2 – 2.7 wt%, a progressive increase in percentage conversion in the reaction was achieved and thereafter experienced a decrease in yield above this concentration (2.2 wt% of CaO). It was obvious that increased in catalyst concentration beyond 2.2 wt% of CaO result to decrease in biodiesel yield [8].

Temperature plays an important role during biodiesel production; this is because the rate of reaction strongly influenced by the reaction temperature. Figure 3 shows the result of temperature variation from (35 – 60 ^{0}C) at a catalyst concentration of 2.2 wt%. As the temperature increases from (35 - 60 ^{0}C) the conversion yields of biodiesel also increases considerably. Further increase in temperature result in decrease in the yield of biodiesel. In this study, optimum temperature for the production of biodiesel took place at 50 ^{0}C. [13] reported that alkaline transesterification at temperature above 60 ^{0}C cause excessive methanol loss due to evaporation as significantly reduce overall biodiesel yield.

Some of the important fuel properties of the biodiesel produced from *P. africana* seed oils are compared with the biodiesel standard (ASTM 6751) and are presented in Table B. Flash point is the minimum temperature at which a fuel must be heated for it to ignite air-vapour mixture. The flash point for this work is 130 ^{0}C. This result shows appreciable consistency with both ASTM, EN standard for biodiesel and works of other researchers. The high value obtained in this study clearly signifies that the biodiesel produced in basically free from methanol; this is because even small quantity of methanol can reduce the flash point reasonably and also negatively affects diesel engine parts such as fuel pumps, seals and elastomers.

The cloud and pour point are criterion used for low temperature performance of a fuel. This work report 5.2 ^{0}C. This properties help to show the behavior of the biodiesel under a specified climate setting. This shows the biodiesel produced from *P. africana* can be used in cold climate region.

Cetane number is a measure of ignition quality of diesel fuel. The higher the cetane number, the easier the fuel will ignite when it is injected into the engine the better the fuel. Beside the reduction of viscosity resulting from transesterification of vegetable oil, one of the most evident changes that result from process is the significant increases in the cetane number of the fuel produced. This work indicates that the cetane number is 38.2. The value obtained is in agreement with both ASTM and EN standard. This implies the *Jatropha curcas* biodiesel produced to have high ignition quality [12].

CONCLUSION AND RECOMMENDATION

The catalytic activity of the impregnated and calcined catalyst of CaO/ZnO prepared shows that the CaO /ZnO samples present catalytic activity, as expected, due to the presence of strong basic sites on which methanolysis reaction could occur. However, after calcination at 600°C these catalysts were active and exhibited a higher catalytic activity. As a result, the catalyst activity is generated by loading the calcium oxide with zinc oxide followed by calcination of the samples. On account of the high activity of the catalysts in the transesterification reactions, the influence of catalyst preparation conditions on the conversion of *P. africana* oil was studied to find a higher activity catalyst. Four different parameters were optimize namely: methanol to oil ratio (5:1), Temperature (50 ^{0}C), catalyst concentration (2.2 wt%) and reaction time (60 min) to have high yield of biodiesel with 95% conversion rate. The fuel properties of the produced biodiesel were compare with ASTM and EU standards and they are all in conformity with the standards. In order to diversify the economy, biodiesel should be encourage and the feedstock should be domesticated for easy production of biodiesel.

REFERENCES

[1] Ajala, A. S. & Adeleke, S.A. (2014). Effect of Drying Temperatures on Physiochemical Properties and Oil Yield of African Star Apple (*Chrysophyllum Alibidum*) Seed. *International Journal of Advanced Research in Engineering and Technology (IJARET*), 3(3), 12 – 16.

[2] Akintayo, E. (2014). Characteristics and Composition of Parkia biglobosa and *Jatropha curcas* Oils and Cakes,*Bio- resource Technology*, 92, (3), 307-310.

[3] Akpan, U.G., Jimoh, A. & Mohammed, A. D. (2011). Extraction, Characterization and Modification of Castor Seed Oil. *Fuel*, 78(1-5), 1629-1623.

[4] Alamu, O.J., Waheed, M.A. & Jekayinfa, S.O. (2018). Effect of Ethanol-Palm Kernel Oil Ratio on Alkali-Catalyzed Biodiesel Yield. *Fuel*, 87(8-9), 1529-1523.

[5] Anigo, K.M., Dauda, B.M., Sallau, A. B. & Chindo, I.E. (2013). Chemical Composition of Kapok (*Ciebapentandra*) Seed and Physicochemical Properties of its Oil. *Nigerian Journal of Basic and Applied Science*, 21(2), 105 – 108.

[6] AOAC (2006). Official methods of analysis Association of Analytical Chemist 15th Edition Washington DC. 12-135.

[7] Asuquo, J. E., Anusiem, A.C. and Etim, E.E. (2012). Comparative study of the effect of temperature on the adsorption of metallic soaps of shea butter, castor and rubber seed oil onto hematie. *Int. J. Modern Chem.* 3:39-50.

[8] Birla, A., Singh, B., Upadhyay, S.N. & Sharma, Y.C. (2012). Kinetics studies of synthesis of biodiesel from waste frying oil using heterogeneous catalyst derived from snail shell. *Bioresource Technology,* 106:95-100.
[9] Codex (2013). Alimentarius Commission; Recommended International Standards for edible Arachis oil, 11, (1st ed), FAO/WHO: Rome.
[10] Dorado, M. P., Ballesteros, E., Lopez, F. J. and Mittelbach, M. (2014), Optimization of alkalicatalyzed transesterification of brassica carinata oil for biodiesel production: Article in Energy and Fuels, 18(1) 77–83.
[11] Kimilu, R. K., Nyang'nya, J. A & Onyari, J. M. (2013). The effect of temperature and blending on the specific gravity and viscosity of jatropa methyl esters. *ARPN Journal of Engineering and Applied Science*, 6(12), 150-157.
[12] Ochigo, S. S. and Paiko, Y. B. (2011). Effects of solvent blending on the characteristics of oils extracted from the seeds of *Chrysophyllumalbidium. International Journal of Science and Nature.* IJSN, 2(2), 252-358.
[13] Patil, P. D. and Deng, S. (2016). "Optimization of biodiesel production from edible and non-edible vegetable oils" "fuel", (88) 7, 1302 – 11306.
[14] Roger, A.B., Rebecca, R. A., Goerges, A. and Mathias, I. O. (2010). Chemical characterization of oil from germinated nuts of several coconut cultivars (cocosnuciferh L.). *Euro. J. Sci. Res.,* 391: 514 – 522.
[15] Sanjay, B. (2013.) Non-Conventional Seed Oils as Potential Feedstocks for Future Biodiesel Industries: A Brief Review. *Research Journal of Chemical Sciences*, 3(5), 99-103.
[16] Singh, S. P. and Singh, D. (2017). Biodiesel production through the use of different source and characterization of oils and their esters as the substitute of diesel: A review. *Energy Review,* 14, 200-216.
[17] Van Gerpen, J. H. (2015), Biodiesel processing and production: Fuel Processing Technology, 86 (10), 1097-1107.
[18] Walker, G. M. (2016). Bioethanol: Science and Technology of Fuel Alcohol. Greame M. Walker & Ventuse Publishing Aps, Dundee, Scotland.
[19] Watkins, S.R., Lee, F.A. and K. Wilson (2014) CaO catalyzed tri-glyceride transesterification for biodiesel application: Green Chemistry, 7, 335–340.

A RATIO-PRODUCT ESTIMATOR FOR ESTIMATION OF FINITE POPULATION MEAN USING KNOWN AUXILIARY VARIABLE

Muili, J. O., Babayemi, A. W. and Adamu, I. Y.
Department of Mathematics, Northwest University Sokoto, Sokoto State, Nigeria.
Department of Mathematics and Statistics, Federal Polytechnic Nasarawa, Nasarawa State, Nigeria.
Corresponding email: jamiunice@yahoo.com

Abstract
Ratio estimation is a technique that uses available auxiliary information which is positively correlated with the study variable while product estimation is a technique that uses available auxiliary information which is negatively correlated with the study variable. In this study, a ratio-product estimator has been proposed for the estimation of the finite population mean of the study variable. The purpose of this study is to develop a new ratio-product estimator to improve the precision of estimation of finite population mean in sample random sampling without replacement using the information of auxiliary variable. The properties of the proposed estimator namely Bias and Mean Square Error were derived up to the first degree of approximation by Taylors' series expansion. The empirical results show that the proposed estimator is more efficient than the sample mean, ratio estimator, and other existing estimators.

Keywords:
Median, Efficiency, Mean Square Error, Ratio Estimator, Product Estimator, and Percentage Relative Efficiency.

1.0 Introduction
Ratio estimation is a process that uses available auxiliary information which is positively correlated with the study variable. The ratio and product methods of estimation are used for the estimation of finite population mean when the correlation between the study variable and the auxiliary variable is positive and negative respectively. [1] initiated an important contribution to the modern sampling theory by suggesting methods of using the auxiliary information for the estimation of population mean to increase the precision of the estimates. Many researchers have suggested ratio and product type estimators for estimating population means of study variable using different population parameters such as [2], [3], [4], [5], [6], [7], [8], [9], [10], [11], [12], etc.

This study aims to develop an efficient estimator to improve the precision of the estimation of population mean using auxiliary information.

Let $U=\{U_1,U_2,U_3,...,U_N\}$ be a finite population having N units and each $U_i=(X_i, Y_i),\ i=1,2,3,...,N$ has a pair of values. Y is the study variable and X is the auxiliary variable which is correlated with Y. Let $y=\{y_1,y_2,...,y_n\}$ and $x=\{x_1,x_2,...,x_n\}$ be n sample values. $\bar{y}$ and $\bar{x}$ are the sample means of the study and auxiliary variables respectively. Let S_y^2 and S_x^2 be the population mean squares of Y and X respectively and s_y^2 and s_x^2 be respective sample mean squares based on the random sample of size n drawn without replacement. N :

Population size, n:Sample size, $\bar{Y},\bar{X}$:Population means of study and auxiliary variables ρ_{yx}: Coefficient of correlation, C_y, C_x: Coefficient of variations of study and auxiliary variables, $\beta_{2(x)}$: Coefficient of Kurtosis of auxiliary variable, M_d: Median of the auxiliary variable, TM:Tri-Mean

$$\bar{X}=\frac{1}{N}\sum_{i=1}^{N}X_i,\ \bar{Y}=\frac{1}{N}\sum_{i=1}^{N}Y_i,\bar{x}=\frac{1}{n}\sum_{i=1}^{n}x_i,\ \bar{y}=\frac{1}{n}\sum_{i=1}^{n}y_i, TM=\frac{(Q_1+2Q_2+Q_3)}{4},\ s_y^2=\frac{1}{n-1}\sum_{i=1}^{n}(y_i-\bar{y})^2,$$

$$s_x^2=\frac{1}{n-1}\sum_{i=1}^{n}(x_i-\bar{x})^2,\quad S_y^2=\frac{1}{N-1}\sum_{i=1}^{N}(Y_i-\bar{Y})^2,\ S_x^2=\frac{1}{N-1}\sum_{i=1}^{N}(X_i-\bar{X})^2,\ \gamma=\frac{1-f}{n},\ f=n/N,$$

$$C_y^2=\frac{S_y^2}{\bar{Y}^2},\ and\ C_x^2=\frac{S_x^2}{\bar{X}^2}$$

1.1 Some Existing Estimators of Population Mean

The usual sample mean $(\bar{y})$ in simple random sampling without replacement is given as:

$$\bar{y}=\frac{1}{n}\sum_{i=1}^{n}y_i \tag{1}$$

$$V(\bar{y})=\gamma\bar{Y}^2C_y^2 \tag{2}$$

[1] was the first to show the contribution of known auxiliary information in improving the efficiency of the estimator of the population mean $(\bar{Y})$ of the study variable (Y) in survey sampling. Assuming that the population mean $(\bar{X})$ of the auxiliary variable is known, he introduced a ratio estimator of the population mean $(\bar{Y})$ defined as

$$\bar{y}_R=\bar{y}\left(\frac{\bar{X}}{\bar{x}}\right) \tag{3}$$

$$Bias(\bar{y}_R)=\gamma\bar{Y}\left(C_x^2-\rho_{yx}C_yC_x\right) \tag{4}$$

$$MSE(\bar{y}_R)=\gamma\bar{Y}^2\left(C_y^2+C_x^2-2\rho_{yx}C_yC_x\right) \tag{5}$$

[13] proposed a product estimator for estimating the population mean $(\bar{Y})$ of the study variable (Y) given as:

$$\bar{y}_P=\bar{y}\left(\frac{\bar{x}}{\bar{X}}\right) \tag{6}$$

$$Bias(\bar{y}_P)=\gamma\bar{Y}\left(C_x^2+\rho_{xy}C_yC_x\right) \tag{7}$$

$$MSE(\bar{y}_P)=\gamma\bar{Y}^2\left(C_y^2+C_x^2+2\rho_{xy}C_yC_x\right) \tag{8}$$

[2] developed ratio and product estimators for estimation of population mean using known values of coefficient of variation (C_x) and coefficient of kurtosis $(\beta_2(x))$ of variable variables with their biases and mean squares errors (MSEs) given as:

$$\bar{y}_{us1} = \bar{y}\left(\frac{\bar{X}C_x + \beta_2(x)}{\bar{x}C_x + \beta_2(x)}\right) \quad (9)$$

$$\bar{y}_{us2} = \bar{y}\left(\frac{\bar{X}\beta_2(x) + C_x}{\bar{x}\beta_2(x) + C_x}\right) \quad (10)$$

$$\bar{y}_{us3} = \bar{y}\left(\frac{\bar{x}C_x + \beta_2(x)}{\bar{X}C_x + \beta_2(x)}\right) \quad (11)$$

$$\bar{y}_{us4} = \bar{y}\left(\frac{\bar{x}\beta_2(x) + C_x}{\bar{X}\beta_2(x) + C_x}\right) \quad (12)$$

$$Bias(\bar{y}_{us1}) = \gamma\bar{Y}\left(\lambda_1^2 C_x^2 - \lambda_1\rho_{xy}C_yC_x\right) \quad (13)$$

$$Bias(\bar{y}_{us2}) = \gamma\bar{Y}\left(\lambda_2^2 C_x^2 - \lambda_2\rho_{xy}C_yC_x\right) \quad (14)$$

$$Bias(\bar{y}_{us3}) = \gamma\bar{Y}\left(\lambda_1^2 C_x^2 + \lambda_1\rho_{xy}C_yC_x\right) \quad (15)$$

$$Bias(\bar{y}_{us4}) = \gamma\bar{Y}\left(\lambda_2^2 C_x^2 + \lambda_2\rho_{xy}C_yC_x\right) \quad (16)$$

$$MSE(\bar{y}_{us1}) = \gamma\bar{Y}^2\left(C_y^2 + \lambda_1^2 C_x^2 - 2\lambda_1\rho_{xy}C_yC_x\right) \quad (17)$$

$$MSE(\bar{y}_{us2}) = \gamma\bar{Y}^2\left(C_y^2 + \lambda_2^2 C_x^2 - 2\lambda_2\rho_{xy}C_yC_x\right) \quad (18)$$

$$MSE(\bar{y}_{us3}) = \gamma\bar{Y}^2\left(C_y^2 + \lambda_1^2 C_x^2 + 2\lambda_1\rho_{xy}C_yC_x\right) \quad (19)$$

$$MSE(\bar{y}_{us4}) = \gamma\bar{Y}^2\left(C_y^2 + \lambda_2^2 C_x^2 + 2\lambda_2\rho_{xy}C_yC_x\right) \quad (20)$$

where $\lambda_1 = \frac{\bar{X}C_x}{\bar{X}C_x + \beta_2(x)}$ *and* $\lambda_2 = \frac{\bar{X}\beta_2(x)}{\bar{X}\beta_2(x) + C_x}$

[4] developed ratio and product types estimators for estimating the population mean $(\bar{Y})$ of the study variable (Y). The biases and mean square error are given as:

$$\bar{y}_{s5} = \bar{y}\left(\frac{\bar{X} + \beta_{2(x)}}{\bar{x} + \beta_{2(x)}}\right) \quad (21)$$

$$\bar{y}_{s6} = \bar{y}\left(\frac{\bar{x} + \beta_{2(x)}}{\bar{X} + \beta_{2(x)}}\right) \quad (22)$$

$$Bias(\bar{y}_{s5}) = \gamma\bar{Y}\left(\lambda_3^2 C_x^2 - \lambda_3\rho_{xy}C_yC_x\right) \quad (23)$$

$$MSE(\bar{y}_{s5}) = \gamma\bar{Y}^2\left(C_y^2 + \lambda_3^2 C_x^2 - 2\lambda_3\rho_{xy}C_yC_x\right) \quad (24)$$

$$Bias\left(\bar{y}_{s6}\right) = \gamma\bar{Y}\lambda_3\rho_{xy}C_yC_x \quad (25)$$

$$MSE\left(\bar{y}_{s6}\right) = \gamma\bar{Y}^2\left(C_y^2 + \lambda_3^2C_x^2 + 2\lambda_3\rho_{xy}C_yC_x\right) \quad (26)$$

where $\lambda_3 = \dfrac{\bar{X}}{\bar{X} + \beta_{2(x)}}$

[14] modified product-type estimator for the estimation of population means using the information of Median as:

$$\bar{y}_{H7} = \bar{y}\left(\frac{\bar{x} + M_d}{\bar{X} + M_d}\right) \quad (27)$$

$$Bias\left(\bar{y}_{H7}\right) = \gamma\bar{Y}\lambda_4\rho_{xy}C_yC_x \quad (28)$$

$$MSE\left(\bar{y}_{H7}\right) = \gamma\bar{Y}^2\left(C_y^2 + \lambda_4^2C_x^2 + 2\lambda_4\rho_{xy}C_yC_x\right) \quad (29)$$

where $\lambda_4 = \dfrac{\bar{X}}{\bar{X} + M_d}$,

2.0 Methodology

2.1 Proposed Estimator

We proposed a ratio-cum-product estimator for estimating the population mean using the linear combination of coefficient of correlation and median as:

$$\bar{y}_{New} = \bar{y}\left[\varphi\left(\frac{\bar{X} + M_d}{\bar{x} + M_d}\right) + (1-\varphi)\left(\frac{\bar{x} + M_d}{\bar{X} + M_d}\right)\right] \quad (30)$$

To derive the bias and MSE, we define $e_0 = \dfrac{\bar{y} - \bar{Y}}{\bar{Y}}$, and $e_1 = \dfrac{\bar{x} - \bar{X}}{\bar{X}}$ such that $\bar{y} = \bar{Y}\left(1 + e_0\right)$, $\bar{x} = \bar{X}\left(1 + e\right)$, from the definitions of e_0, and e_1, we obtained

$$\left.\begin{aligned} &E\left(e_0\right) = E\left(e_1\right) = 0,\ E\left(e_0^2\right) = \gamma C_y^2 \\ &E\left(e_1^2\right) = \gamma C_x^2,\ E\left(e_0e_1\right) = \gamma\rho_{yx}C_yC_x \end{aligned}\right\} \quad (31)$$

Expressing (30) in terms of e_0 and e_1 we have

$$\bar{y}_{New} = \bar{Y}\left(1 + e_0\right)\left[\varphi\left(\frac{\bar{X} + M_d}{\left(1 + e_1\right)\bar{X} + M_d}\right) + (1-\varphi)\left(\frac{\left(1 + e_1\right)\bar{X} + M_d}{\bar{X} + M_d}\right)\right] \quad (32)$$

Reducing (32), we have

$$\bar{y}_{New} = \bar{Y}\left(1 + e_0\right)\left[\varphi\left(1 + \lambda_p e_1\right)^{-1} + (1-\varphi)\left(1 + \lambda_p e_1\right)\right] \quad (33)$$

where $\lambda_p = \dfrac{\bar{X}}{\bar{X} + M_d}$,

Simplifying (33) up to first-order approximation, it reduces to (34) as:

$$\bar{y}_{New} = \bar{Y}\left[1 + e_0 + (1-2\varphi)\lambda_p e_1 + (1-2\varphi)\lambda_p e_0 e_1 + \rho_{xy}\lambda_p^2 e_1^2\right] \quad (34)$$

Applying the results of (31) to (35) gives the bias as:

$$Bias(\bar{y}_{New}) = \gamma\bar{Y}\left[\varphi\lambda_p^2 C_x^2 + (1-2\varphi)\lambda_p \rho_{xy} C_y C_x\right] \quad (35)$$

where $\varphi = \frac{1}{2}\left(1 + \frac{\rho_{xy} C_y}{\lambda_p C_x}\right)$

Squaring and taking the expectation of (34), gives

$$MSE(\bar{y}_{New}) = \bar{Y}^2 E\left[e_0 + (1-2\varphi)\lambda_p e_1\right]^2 \quad (36)$$

Expanding and applying the results of (31) to (37), gives

$$MSE(\bar{y}_{New}) = \gamma\bar{Y}^2\left[C_y^2 + (1-2\varphi)^2 \lambda_p^2 C_x^2 + 2(1-2\varphi)\lambda_p \rho_{xy} C_y C_x\right] \quad (37)$$

Obtaining the expression for the value of φ, differentiate $MSE(\bar{y}_{New})$ partially with respect to φ and equate to zero then simplifying for φ, obtaining the optimum value of φ and Substitute in (37) gives:

$$MSE(\bar{y}_{New})_{\min} = \gamma\bar{Y}^2 C_y^2\left[1 - \rho_{xy}^2\right] \quad (38)$$

2.2 Comparison of Efficiency

The condition under which the proposed estimator will have minimum Mean Square Error (MSE) compared to the sample mean, ratio estimator, product estimator and other existing estimators have been derived as follows:

The proposed estimator of the population mean is more efficient than the sample mean if,

$$MSE(\bar{y}_{New})_{\min} < V(\bar{y})$$

$$\gamma\bar{Y}^2 C_y^2\left[1 - \rho_{xy}^2\right] < \gamma\bar{Y}^2 C_y^2 \quad (39)$$

The proposed estimator of the population mean is more efficient than the ratio estimator if,

$$MSE(\bar{y}_{New})_{\min} < MSE(\bar{y}_r)$$

$$\gamma\bar{Y}^2 C_y^2\left[1 - \rho_{xy}^2\right] < \gamma\bar{Y}^2\left(C_y^2 + C_x^2 - 2\rho_{xy} C_y C_x\right) \quad (40)$$

The proposed estimator of the population mean is more efficient than ratio-type estimators if,

$$MSE(\bar{y}_{New})_{\min} < MSE(\bar{y}_j) \qquad j = 1,2,3$$

$$\gamma\bar{Y}^2 C_y^2\left[1 - \rho_{xy}^2\right] < \gamma\bar{Y}^2\left(C_y^2 + \theta\lambda_j^2 C_x^2 + 2\lambda_j \rho_{xy} C_y C_x\right) \quad (41)$$

When conditions (39), (40) and (41) are satisfied, we conclude that the proposed estimator is more efficient than the sample mean, ratio estimator, product estimator and other existing estimators considered in the study.

2.3 Empirical Study

To access the performance of the proposed estimator, we considered the two populations as: Source: [Population I: [15]. Population II: [16]]

Study variable (Y) = Output of 80 factories

Auxiliary variable (X) = Fixed Capital.

Table 1: Parameters of the Populations

Parameter	Population I	Population II
N	30	80
n	10	20
$\bar{Y}$	17.5	51.8264
$\bar{X}$	4.4637	11.2646
ρ_{xy}	-0.1994	0.9413
C_y	0.4758	0.3542
C_x	0.8727	0.750
$\beta_{2(x)}$	0.2296	2.866
$\beta_{1(x)}$	1.36	1.05
M_d	2.27	7.575

Table 1 shows the descriptive statistics of the two populations

Table 2: The Mean Square Error (MSE) and Percentage Relative Efficiency (PRE) of the Proposed and Other Estimators

Estimator	Population I		Population II	
	MSE	PRE	MSE	PRE
[1]	341.5092	100	498.2401	100
[13]	243.4638	140.271	3151.239	15.81093
[2] $(\bar{y}_{us1})$	314.3803	108.6293	174.1301	286.1309
[2] $(\bar{y}_{us2})$	159.2658	214.4272	461.379	107.9893

[2] $(\bar{y}_{us3})$	221.7920	153.9772	2155.113	23.11898
[2] $(\bar{y}_{us4})$	106.3119	321.2333	3054.145	16.31357
[4] $(\bar{y}_{s5})$	317.5905	107.5313	223.4473	222.9788
[4] $(\bar{y}_{s6})$	224.3415	152.2274	2338.359	21.30725
[14] $(\bar{y}_{H7})$	133.5982	255.6241	1659.303	30.02707
Proposed Estimator $(\bar{y}_{New})$	**64.3549**	**530.6654**	**37.9199**	**1313.928**

The Values of MSE and PRE of the Existing and Proposed Estimators

3.0 Results and Discussion

A ratio-product estimator for the estimation of the population mean of the study variable is proposed. The mean square error (MSE) of the proposed estimator is derived up to the first order of approximation. Theoretical comparison of the proposed ratio-cum-product estimator of the population mean with sample mean, ratio estimator and other existing estimators considered in the study were established. The value of mean square errors (MSE) of the proposed estimator is smaller than the sample mean, ratio estimator, product estimator and other estimators considered in the study and with the highest percentage relative efficiency (PRE). The performance of the proposed estimator over the sample mean, ratio estimator, product estimator and other selected existing estimators using two real populations were obtained. The results show that the proposed estimator is more efficient than the sample mean, [1], [13], [2], [4] and [14] estimators.

4.0 Conclusion

The results in Table 1 clearly showed that the proposed ratio-product estimator performed better than the sample mean, [1], [13], [2], [4] and [14] estimators considered in the study having the Least Mean Square Error (MSE) and higher Percentage Relative Efficiency (PRE). Based on the results, the proposed estimator increases the efficiency of the estimate in estimating finite population mean.

References

[1] W. G. Cochran (1940). The Estimation of the Yields of the Cereal Experiments by Sampling for the Ratio of Grain to Total Produce, The Journal of Agricultural Science, Vol. 30, pp. 262–275.

[2] Upadhyaya, L. N. and Singh, H. P. (1999). Use of Transformed Auxiliary Variable in Estimating the Finite Population Mean. Biometrical Journal, Vol. 41, pp. 627 – 636.

[3] Abu-Dayyeh, W. A., Ahmed, M. S., Ahmed, R. A. & Muttlak, H. A. (2003). Some Estimators of a Finite Population Mean using Auxiliary Information, Applied Mathematics and Computation. Vol. 139, pp. 287–298.

[4] Singh, H. P., Tailor, R. & Kakran, M. S. (2004). An Improved Estimation of Population Mean using Power Transformation. Journal of the Indian Society of Agricultural Statistics, Vol. 8(2), pp. 223–230.

[5] Kadilar, C. and Cingi, H. (2004). Ratio Estimators in Simple Random Sampling. Applied Mathematics and Computation Vol. 151, pp. 893 – 902.

[6] Yan, Z. and Tian, B. (2010). Ratio Method to the Mean Estimation using Coefficient of Skewness of Auxiliary Variable. In: Information Computing and Applications. ICICA.

[7] Tailor, R., Parmar, R., Kim, J. M. & Tailor, R. (2011). Ratio-Cum-Product Estimators of Population Mean using known Population Parameters of Auxiliary Variates, Communications of the Korean Statistical Society, Vol. 18(2), pp. 155–164. DOI: https://doi.org/10.5351/CKSS.2011.18.2.155

[8] Jeelani, M. I., Maqbool, S. & Mir, S. A. (2013). Modified Ratio Estimators of Population Mean using Linear Combination of Estimators of Population Mean using Linear Combination of Coefficient of Skewness and Quartile Deviation. International Journal of Modern Mathematical Sciences. Vol. 6, pp. 174 – 183.

[9] Gupta, R. K. & Yadav, S. K. (2017). New Efficient Estimators of Population Mean Using Non-Traditional Measures of Dispersion. Open Journal of Statistics. Vol. 7, pp. 394-404.

[10] Muili, J. O. & Audu, A. (2019). Modification of Ratio Estimator for Population Mean. Annals. Computer Science Series. Vol. 17(2), pp. 74-78.

[11] Muili, J. O., Audu, A., Singh, R. V. K. & Yunusa, I. A. (2019). Improved Estimators of Finite Population Variance Using Unknown Weight of Auxiliary Variable. Annals. Computer Science Series. Vol. 17(1), pp. 148-153.

[12] Muili, J. O. Adebiyi, A. & Agwamba, E. N. (2020). Improved Ratio Estimators for Estimating Population Mean Using Auxiliary Information. International Journal of Scientific and Research Publications. Vol. 10(5), pp. 937-945.http://dx.doi.org/10.29322/IJSRP.10.05.2020.p101111

[13] Robson, D. S. (1957). Application of multivariate polykays to the theory of unbiased ratio type estimation, Journal of the American Statistical Association. Vol. 52, pp. 511–522.

[14] Hasan, M. Z., Hossian, M. A., Sultana, M., Fatema, K. & Hossain, M. M. (2019). A New Modified Product Estimator for Estimation of Population Mean when Median of the Auxiliary Variable is Known. International Journal of Scientific Research in Mathematical and Statistical Sciences. Vol.6, pp. 108 – 113.

[15] Yadav, S. K. Subramani, J., Mishra, S. S. & Shukla, A. K. (2016). Improved Ratio-Cum-Product Estimators of Population Mean Using Known Population Parameters of Auxiliary Variables. American Journal of Operational Research 2016, 6(2): 48-54 DOI: https://doi.org/10.5923/j.ajor.20160602.03

[16] Murthy, M. N. (1967). Sampling Theory and Methods. Statistical Publishing Society, Calcutta, India.

NIPES-NCEE Conference Proceedings
The 2nd International Conference 15th-17th Feb. 2023
288-302
www.nipesjournals.org.ng

ADVANCED RATIO-TYPE ESTIMATOR FOR ESTIMATING FINITE POPULATION VARIANCE

Muili, J. O.

Department of Mathematics, Northwest University Sokoto, Sokoto State, Nigeria.
Corresponding email: jamiunice@yahoo.com

Abstract

Centile or Percentile is a measure used in statistics indicating the value below which a given percentage of observations in a group of observations fall. A set of ratio estimators for estimating the finite population variance of the study variable with a known auxiliary variable in simple random sampling without replacement (SRSWOR) has been suggested. The expressions of the bias and mean square error (MSE) of the suggested estimators were derived by the Taylor series method up to the first degree of approximation. The efficiency conditions under which the suggested ratio estimators are better than sample variance, ratio estimator and other estimators considered in this study have been established. The numerical and empirical results show that the suggested estimators are more efficient than the sample variance, ratio estimator, and other existing estimators.

Keywords:
Centile, Ratio Estimator, Quartile, and Variance.

1.0 Introduction

A sampling survey is a technique that deals with the estimation of population parameters (mean, total, or variance population) under consideration. Percentiles divide a set of ordered data into hundredths. Percentiles play an important part in descriptive statistics and their use is well recommended. Appropriate use of auxiliary information results in a reduction in variance or mean square error of the estimator. In a situation where the information about an auxiliary variable X is known and the association between the study variable and the auxiliary variable is positive, the ratio estimation method is useful. Then if the relationship is negative, the product estimation method can be used efficiently. So, to determine the most efficient estimator in a set of estimators, the estimator with the least value of variance or mean square error is considered the best. The estimation of population variance has been extensively discussed by many researchers to improve and increase the precision of an estimate under consideration. The problem of estimating the population variance of the study variable when the population variance of an auxiliary variable(s) is/are known has been discussed among the statisticians in the field of sample surveys. The early work on the estimation of population variance was initiated from the work of [1], [2], and [3]. [3] developed a ratio estimator of population variance of study variable for estimation of the finite population variance. Since then many researchers/authors have been improving and modifying estimators of population variance using auxiliary information in one way or the other like [4], [5], [6], [7], [8], [9], [10], [11], [12], [13], [14]. [15], [16], etc. The purpose of this study is to develop a new class of ratio-type estimators to improve the precision of the estimate of population variance in sample random sampling without replacement using available information of auxiliary variables. Consider a finite population $U=\{U_1,U_2,U_3,...,U_N\}$ having units where each $U_i=(X_i,Y_i),\ i=1,2,3,...,N$ has a pair of values. X is the auxiliary variable which Y is the study variable and is correlated with X, where $y=\{y_1,y_2,...,y_n\}$ and $x=\{x_1,x_2,...,x_n\}$ are the n sample values. $\bar{y}$ and $\bar{x}$ are the sample means of the study and auxiliary variables respectively. Let S_y^2 and S_x^2 be the population mean squares of Y and X respectively and s_y^2 and s_x^2 be respective sample mean squares based on the random sample of size n drawn without replacement. N: Population size, n: Sample size, Y: Study variable, X: auxiliary variable, $\bar{y}$, $\bar{x}$: Sample means of study and auxiliary variables, $\bar{Y},\bar{X}$: Population means of study and auxiliary variables, f: Sampling fraction, ρ : Coefficient of correlation, C_y,C_x : Coefficient of variations of study and auxiliary variables. Q_3 :The upper quartile, Q_d :Population Quartile Deviation, $\beta_{1(x)}$:Coefficient of skewness of auxiliary variable, $\beta_{2(x)}$:Coefficient of kurtosis of auxiliary variable, $\beta_{2(y)}$:Coefficient of kurtosis of study variable, M_d : Median of the auxiliary, and P_i: Percentiles.

$$\bar{X}=\frac{1}{N}\sum_{i=1}^{N}X_i,\quad \bar{Y}=\frac{1}{N}\sum_{i=1}^{N}Y_i,\quad \bar{x}=\frac{1}{n}\sum_{i=1}^{n}x_i,\quad \bar{y}=\frac{1}{n}\sum_{i=1}^{n}y_i,\quad \gamma=\frac{1-f}{n},\ f=\frac{n}{N},\ Q_d=\frac{Q_3-Q_1}{2}$$

$$s_y^2=\frac{1}{n-1}\sum_{i=1}^{n}(y_i-\bar{y})^2,\quad s_x^2=\frac{1}{n-1}\sum_{i=1}^{n}(x_i-\bar{x})^2,\ S_y^2=\frac{1}{N-1}\sum_{i=1}^{N}(Y_i-\bar{Y})^2,$$

$$S_x^2=\frac{1}{N-1}\sum_{i=1}^{N}(X_i-\bar{X})^2,$$

$$Q_a=\frac{Q_3+Q_1}{2},\ Q_r=Q_3-Q_1\quad \gamma=\frac{1-f}{n},\ f=\frac{n}{N}$$

The sample variance of the finite population variance is defined as

$$\hat{\tau}_1^2=s_y^2 \tag{1}$$

its variance is given as:

$$Var(\hat{\tau}_1^2)=\gamma S_y^4(\beta_{2(y)}-1) \tag{2}$$

[3] was the pioneer of ratio estimator for the estimation of finite population variance when the population variance of auxiliary variable X is known. The bias and its mean squared error are given below:

$$\hat{\tau}_R^2=s_y^2\left(\frac{S_x^2}{s_x^2}\right) \tag{3}$$

$$Bias\left(\hat{\tau}_R^2\right) = \gamma S_y^2\left[\left(\beta_{2(x)} - 1\right) - \left(\lambda_{22} - 1\right)\right] \quad (4)$$

$$MSE\left(\hat{\tau}_R^2\right) = \gamma S_y^4\left[\left(\beta_{2(y)} - 1\right) + \left(\beta_{2(x)} - 1\right) - 2\left(\lambda_{22} - 1\right)\right] \quad (5)$$

[17], and [18] modified families' ratio-type estimators for finite population variance using the known parameters of the auxiliary variable as:

$$\hat{\tau}_2^2 = s_y^2\left(\frac{\beta_{1(x)}S_x^2 + \beta_{2(x)}}{\beta_{1(x)}s_x^2 + \beta_{2(x)}}\right) \quad (6)$$

$$\hat{\tau}_3^2 = s_y^2\left(\frac{\beta_{2(x)}S_x^2 + \rho}{\beta_{2(x)}s_x^2 + \rho}\right) \quad (7)$$

$$\hat{\tau}_4^2 = s_y^2\left(\frac{\beta_{1(x)}S_x^2 + S_x}{\beta_{1(x)}s_x^2 + S_x}\right) \quad (8)$$

$$\hat{\tau}_5^2 = s_y^2\left(\frac{\beta_{1(x)}S_x^2 + M_d}{\beta_{1(x)}s_x^2 + M_d}\right) \quad (9)$$

$$\hat{\tau}_6^2 = s_y^2\left(\frac{\beta_{2(x)}S_x^2 + S_x}{\beta_{2(x)}s_x^2 + S_x}\right) \quad (10)$$

$$\hat{\tau}_7^2 = s_y^2\left(\frac{\beta_{2(x)}S_x^2 + M_d}{\beta_{2(x)}s_x^2 + M_d}\right) \quad (11)$$

$$\hat{\tau}_8^2 = s_y^2\left(\frac{\beta_{2(x)}S_x^2 + \rho}{\beta_{2(x)}s_x^2 + \rho}\right) \quad (12)$$

$$\hat{\tau}_9^2 = s_y^2\left(\frac{\beta_{2(x)}S_x^2 + \beta_{1(x)}}{\beta_{2(x)}s_x^2 + \beta_{1(x)}}\right) \quad (13)$$

$$\hat{\tau}_{10}^2 = s_y^2\left(\frac{\rho S_x^2 + \beta_{2(x)}}{\rho s_x^2 + \beta_{2(x)}}\right) \quad (14)$$

$$\hat{\tau}_{11}^2 = s_y^2\left(\frac{\rho S_x^2 + \beta_{1(x)}}{\rho s_x^2 + \beta_{1(x)}}\right) \quad (15)$$

$$\hat{\tau}_{12}^2 = s_y^2\left(\frac{\rho S_x^2 + S_x}{\rho s_x^2 + S_x}\right) \quad (16)$$

$$\hat{\tau}_{13}^2 = s_y^2\left(\frac{\rho S_x^2 + M_d}{\rho s_x^2 + M_d}\right) \quad (17)$$

$$\hat{\tau}_{14}^2 = s_y^2\left(\frac{S_x S_x^2 + \beta_{2(x)}}{S_x s_x^2 + \beta_{2(x)}}\right) \quad (18)$$

$$\hat{\tau}_{15}^2 = s_y^2\left(\frac{S_x S_x^2 + \beta_{1(x)}}{S_x s_x^2 + \beta_{1(x)}}\right) \quad (19)$$

$$\hat{\tau}_{16}^2 = s_y^2\left(\frac{S_x S_x^2 + \rho}{S_x s_x^2 + \rho}\right) \quad (20)$$

$$\hat{\tau}_{17}^2 = s_y^2\left(\frac{S_x S_x^2 + M_d}{S_x s_x^2 + M_d}\right) \quad (21)$$

$$\hat{\tau}_{18}^2 = s_y^2\left(\frac{M_d S_x^2 + \beta_{2(x)}}{M_d s_x^2 + \beta_{2(x)}}\right) \quad (22)$$

$$\hat{\tau}_{19}^2 = s_y^2\left(\frac{M_d S_x^2 + S_x}{M_d s_x^2 + S_x}\right) \quad (23)$$

$$\hat{\tau}_{20}^2 = s_y^2\left(\frac{M_d S_x^2 + \rho}{M_d s_x^2 + \rho}\right) \quad (24)$$

$$\hat{\tau}_{21}^2 = s_y^2\left(\frac{M_d S_x^2 + \beta_{2(x)}}{M_d s_x^2 + \beta_{2(x)}}\right) \quad (25)$$

$$Bias\left(\hat{\tau}_i^2\right) = \gamma A_i S_y^2\left[A_i\left(\beta_{2(x)} - 1\right) - \left(\lambda_{22} - 1\right)\right], \text{ where i= 1,2, 3, … ,21} \quad (26)$$

$$MSE\left(\hat{\tau}_i^2\right) = \gamma S_y^4\left[\left(\beta_{2(y)} - 1\right) + A_i^2\left(\beta_{2(x)} - 1\right) - 2A_i\left(\lambda_{22} - 1\right)\right], \text{ where i= 1,2, 3, … ,21} \quad (27)$$

where

$$A_2=\frac{\beta_{1(x)}S_x^2}{\beta_{1(x)}S_x^2+\beta_{2(x)}},A_3=\frac{\beta_{1(x)}S_x^2}{\beta_{1(x)}S_x^2+\rho},A_4=\frac{\beta_{1(x)}S_x^2}{\beta_{1(x)}S_x^2+S_x},A_5=\frac{\beta_{1(x)}S_x^2}{\beta_{1(x)}S_x^2+M_d},\ A_6=\frac{\beta_{2(x)}S_x^2}{\beta_{2(x)}S_x^2+S_x},$$

$$A_7=\frac{\beta_{2(x)}S_x^2}{\beta_{2(x)}S_x^2+M_d},A_8=\frac{\beta_{2(x)}S_x^2}{\beta_{2(x)}S_x^2+\rho},A_9=\frac{\beta_{2(x)}S_x^2}{\beta_{2(x)}S_x^2+\beta_{1(x)}},A_{10}=\frac{\rho S_x^2}{\rho S_x^2+\beta_{2(x)}},\ A_{11}=\frac{\rho S_x^2}{\rho S_x^2+\beta_{1(x)}},$$

$$A_{12}=\frac{\rho S_x^2}{\rho S_x^2+S_x},A_{13}=\frac{\rho S_x^2}{\rho S_x^2+M_d},A_{14}=\frac{S_xS_x^2}{S_xS_x^2+\beta_{2(x)}},A_{15}=\frac{S_xS_x^2}{S_xS_x^2+\beta_{2(x)}},\ A_{16}=\frac{S_xS_x^2}{S_xS_x^2+\rho},$$

$$A_{17}=\frac{S_xS_x^2}{S_xS_x^2+M_d},A_{18}=\frac{M_dS_x^2}{M_dS_x^2+\beta_{2(x)}},A_{19}=\frac{M_dS_x^2}{M_dS_x^2+S_x},A_{20}=\frac{M_dS_x^2}{M_dS_x^2+\rho},\ A_{21}=\frac{S_xS_x^2}{S_xS_x^2+\beta_{1(x)}}$$

[19] proposed a class of ratio-type estimators for estimating finite population variance using a known auxiliary variable as:

$$\hat{\tau}_{22}^2=s_y^2\left(\frac{\rho S_x^2+M_d+Q_1}{\rho s_x^2+M_d+Q_1}\right) \tag{28}$$

$$\hat{\tau}_{23}^2=s_y^2\left(\frac{\rho S_x^2+M_d+Q_2}{\rho s_x^2+M_d+Q_2}\right) \tag{29}$$

$$\hat{\tau}_{24}^2=s_y^2\left(\frac{\rho S_x^2+M_d+Q_3}{\rho s_x^2+M_d+Q_3}\right) \tag{30}$$

$$\hat{\tau}_{25}^2=s_y^2\left(\frac{\rho S_x^2+M_d+Q_d}{\rho s_x^2+M_d+Q_d}\right) \tag{31}$$

$$\hat{\tau}_{26}^2=s_y^2\left(\frac{\rho S_x^2+M_d+Q_r}{\rho s_x^2+M_d+Q_r}\right) \tag{32}$$

$$\hat{\tau}_{27}^2=s_y^2\left(\frac{\rho S_x^2+M_d+Q_a}{\rho s_x^2+M_d+Q_a}\right) \tag{33}$$

$$Bias\left(\hat{\tau}_j^2\right)=\gamma A_jS_y^2\left[A_j\left(\beta_{2(x)}-1\right)-\left(\lambda_{22}-1\right)\right],\text{ where j = 22, 23, …, 27} \tag{34}$$

$$MSE\left(\hat{\tau}_j^2\right) = \gamma S_y^4\left[\left(\beta_{2(y)}-1\right)+A_j^2\left(\beta_{2(x)}-1\right)-2A_j\left(\lambda_{22}-1\right)\right], \text{ where j = 22, 23, …, 27} \quad (35)$$

where

$$A_{22} = \frac{\rho S_x^2}{\rho S_x^2 + M_d + Q_1},\ A_{23} = \frac{\rho S_x^2}{\rho S_x^2 + M_d + Q_2},\ A_{24} = \frac{\rho S_x^2}{\rho S_x^2 + M_d + Q_3},\ A_{25} = \frac{\rho S_x^2}{\rho S_x^2 + M_d + Q_d},$$

$$A_{26} = \frac{\rho S_x^2}{\rho S_x^2 + M_d + Q_r},\ A_{27} = \frac{\rho S_x^2}{\rho S_x^2 + M_d + Q_a}$$

2.0 Methodology

2.1 Suggested Estimators

Motivated by the work of [19], we suggested a class of new ratio-type estimators for estimating finite population variance using known information of coefficient of correlation, and Percentiles as:

$$\hat{\tau}_{p1}^2 = s_y^2\left(\frac{\rho S_x^2 + P_1}{\rho s_x^2 + P_1}\right) \quad (36)$$

$$\hat{\tau}_{p2}^2 = s_y^2\left(\frac{\rho S_x^2 + P_5}{\rho s_x^2 + P_5}\right) \quad (37)$$

$$\hat{\tau}_{p3}^2 = s_y^2\left(\frac{\rho S_x^2 + P_{10}}{\rho s_x^2 + P_{10}}\right) \quad (38)$$

$$\hat{\tau}_{p4}^2 = s_y^2\left(\frac{\rho S_x^2 + P_{15}}{\rho s_x^2 + P_{15}}\right) \quad (39)$$

$$\hat{\tau}_{p5}^2 = s_y^2\left(\frac{\rho S_x^2 + P_{20}}{\rho s_x^2 + P_{20}}\right) \quad (40)$$

$$\hat{\tau}_{p6}^2 = s_y^2\left(\frac{\rho S_x^2 + P_{25}}{\rho s_x^2 + P_{25}}\right) \quad (41)$$

$$\hat{\tau}_{p7}^2 = s_y^2\left(\frac{\rho S_x^2 + P_{30}}{\rho s_x^2 + P_{30}}\right) \quad (42)$$

$$\hat{\tau}_{p8}^2 = s_y^2\left(\frac{\rho S_x^2 + P_{35}}{\rho s_x^2 + P_{35}}\right) \tag{43}$$

$$\hat{\tau}_{p9}^2 = s_y^2\left(\frac{\rho S_x^2 + P_{40}}{\rho s_x^2 + P_{40}}\right) \tag{44}$$

$$\hat{\tau}_{p10}^2 = s_y^2\left(\frac{\rho S_x^2 + P_{45}}{\rho s_x^2 + P_{45}}\right) \tag{45}$$

$$\hat{\tau}_{p11}^2 = s_y^2\left(\frac{\rho S_x^2 + P_{50}}{\rho s_x^2 + P_{50}}\right) \tag{46}$$

$$\hat{\tau}_{p12}^2 = s_y^2\left(\frac{\rho S_x^2 + P_{55}}{\rho s_x^2 + P_{55}}\right) \tag{47}$$

$$\hat{\tau}_{p13}^2 = s_y^2\left(\frac{\rho S_x^2 + P_{60}}{\rho s_x^2 + P_{60}}\right) \tag{48}$$

$$\hat{\tau}_{p14}^2 = s_y^2\left(\frac{\rho S_x^2 + P_{65}}{\rho s_x^2 + P_{65}}\right) \tag{49}$$

$$\hat{\tau}_{p15}^2 = s_y^2\left(\frac{\rho S_x^2 + P_{70}}{\rho s_x^2 + P_{70}}\right) \tag{50}$$

$$\hat{\tau}_{p16}^2 = s_y^2\left(\frac{\rho S_x^2 + P_{75}}{\rho s_x^2 + P_{75}}\right) \tag{51}$$

$$\hat{\tau}_{p17}^2 = s_y^2\left(\frac{\rho S_x^2 + P_{80}}{\rho s_x^2 + P_{80}}\right) \tag{52}$$

$$\hat{\tau}_{p18}^2 = s_y^2\left(\frac{\rho S_x^2 + P_{85}}{\rho s_x^2 + P_{85}}\right) \tag{53}$$

$$\hat{\tau}_{p19}^2 = s_y^2\left(\frac{\rho S_x^2 + P_{90}}{\rho s_x^2 + P_{90}}\right) \tag{54}$$

$$\hat{\tau}^2_{p20} = s^2_y\left(\frac{\rho S^2_x + P_{95}}{\rho s^2_x + P_{95}}\right) \tag{55}$$

$$\hat{\tau}^2_{p21} = s^2_y\left(\frac{\rho S^2_x + P_{99}}{\rho s^2_x + P_{99}}\right) \tag{56}$$

The suggested estimators can be written in a general form as:

$$\hat{\tau}^2_{pi} = s^2_y\left(\frac{\rho S^2_x + P_j}{\rho s^2_x + P_j}\right),\ i = p1, p2, ..., p21;\quad j = 1, 5, 10, ..., 99. \tag{57}$$

2.2 Properties of the Suggested Estimators

Let $e_0 = \dfrac{s^2_y - S^2_y}{S^2_y}$ and $e_1 = \dfrac{s^2_x - S^2_x}{S^2_x}$ such that $s^2_y = S^2_y\left(1+e_0\right)$ *and* $s^2_x = S^2_x\left(1+e_1\right)$, where

$$\left.\begin{array}{l} E\left(e_0\right) = E\left(e_1\right) = 0,\ E\left(e^2_0\right) = \gamma\left(\beta_{2(y)} - 1\right) \\ E\left(e^2_1\right) = \gamma\left(\beta_{2(x)} - 1\right),\ E\left(e_0 e_1\right) = \gamma\left(\lambda_{22} - 1\right) \end{array}\right\} \tag{58}$$

Expressing (57) in error terms, we have

$$\hat{\tau}^2_{pi} = S^2_y\left(1+e_0\right)\left(\frac{\rho S^2_x + P_j}{S^2_x \rho\left(1+e_1\right) + P_j}\right) \tag{59}$$

$$\hat{\tau}^2_{pi} = S^2_y\left(1+e_0\right)\left(1 + A_{Ji} e_1\right)^{-1} \tag{60}$$

where $A_{Ji} = \dfrac{\rho S^2_x}{\rho S^2_x + P_j}$,

Simplifying (60) up to first-order approximation, it reduces to (61) as:

$$\hat{S}^2_{Ji} = S^2_y\left(1+e_0\right)\left(1 - A_{Ji} e_1 + A^2_{Ji} e^2_1 ...\right) \tag{61}$$

Removing the brackets and subtracting both sides by S^2_y

$$\hat{S}^2_{Ji} - S^2_y = S^2_y\left(e_0 - A_{Ji} e_1 - A_{Ji} e_0 e_1 + A^2_{Ji} e^2_1\right) \tag{62}$$

Taking Expectations of both sides of (62)

$$E\left(\hat{\tau}_{pi}^{2}-S_{y}^{2}\right)=S_{y}^{2}E\left(e_{0}-A_{Ji}e_{1}-A_{Ji}e_{0}e_{1}+A_{Ji}^{2}e_{1}^{2}\right) \tag{63}$$

Applying the results of (58) obtaining the bias as

$$Bias\left(\hat{\tau}_{pi}^{2}\right)=\gamma S_{y}^{2}\left[A_{Ji}^{2}\left(\beta_{2(x)}-1\right)-A_{Ji}\left(\lambda_{22}-1\right)\right] \tag{64}$$

To get the MSE, squaring both sides of (63) and ignoring e of power two as:

$$E\left(\hat{\tau}_{pi}^{2}-S_{y}^{2}\right)^{2}=S_{y}^{4}E\left(e_{0}-A_{Ji}e_{1}\right)^{2} \tag{65}$$

Expanding, and taking the expectation of (65)

$$MSE\left(\hat{\tau}_{pi}^{2}\right)=S_{y}^{4}E\left(e_{0}^{2}+A_{Ji}^{2}e_{1}^{2}-2A_{Ji}e_{0}e_{1}\right) \tag{66}$$

Applying the results of (58), obtaining $MSE\left(\hat{\tau}_{pi}^{2}\right)$ as:

$$MSE\left(\hat{\tau}_{pi}^{2}\right)=\gamma S_{y}^{4}\left[\left(\beta_{2(y)}-1\right)+A_{Ji}^{2}\left(\beta_{2(x)}-1\right)-2A_{Ji}\left(\lambda_{22}-1\right)\right] \tag{67}$$

where

$$A_{J1}=\frac{\rho S_x^2}{\rho S_x^2+P_1},\ A_{J2}=\frac{\rho S_x^2}{\rho S_x^2+P_5},\ A_{J3}=\frac{\rho S_x^2}{\rho S_x^2+P_{10}},\ A_{J4}=\frac{\rho S_x^2}{\rho S_x^2+P_{15}},\ A_{J5}=\frac{\rho S_x^2}{\rho S_x^2+P_{20}},\ A_{J6}=\frac{\rho S_x^2}{\rho S_x^2+P_{25}},$$

$$A_{J7}=\frac{\rho S_x^2}{\rho S_x^2+P_{30}},\ A_{J8}=\frac{\rho S_x^2}{\rho S_x^2+P_{35}},\ A_{J9}=\frac{\rho S_x^2}{\rho S_x^2+P_{40}},\ A_{J10}=\frac{\rho S_x^2}{\rho S_x^2+P_{45}},\ A_{J11}=\frac{\rho S_x^2}{\rho S_x^2+P_{50}},\ A_{J12}=\frac{\rho S_x^2}{\rho S_x^2+P_{55}},$$

$$A_{J13}=\frac{\rho S_x^2}{\rho S_x^2+P_{60}},\ A_{J14}=\frac{\rho S_x^2}{\rho S_x^2+P_{65}},\ A_{J15}=\frac{\rho S_x^2}{\rho S_x^2+P_{70}},\ A_{J16}=\frac{\rho S_x^2}{\rho S_x^2+P_{75}},\ A_{J17}=\frac{\rho S_x^2}{\rho S_x^2+P_{80}},\ A_{J18}=\frac{\rho S_x^2}{\rho S_x^2+P_{85}},$$

$$A_{J19}=\frac{\rho S_x^2}{\rho S_x^2+P_{90}},\ A_{J20}=\frac{\rho S_x^2}{\rho S_x^2+P_{95}},\ A_{J21}=\frac{\rho S_x^2}{\rho S_x^2+P_{99}}$$

2.3 Efficiency Comparisons

Comparison of the proposed estimators with other existing estimators considered in the study with certain conditions to determine the estimators with higher precision.

The $\hat{\tau}_{Ji}^{2}$ - estimators of the finite population variance are more efficient than $Var(\hat{\tau}_{1}^{2})$ if,

$$MSE\left(\hat{\tau}_{Ji}^{2}\right) < Var\left(\hat{\tau}_{1}^{2}\right)$$

$$\left[\left(\beta_{2(y)}-1\right)+A_{Ji}^{2}\left(\beta_{2(x)}-1\right)-2A_{Ji}\left(\lambda_{22}-1\right)\right] < \left(\beta_{2(y)}-1\right) \tag{68}$$

The $\hat{\tau}_{Ji}^{2}$ - estimators of the finite population variance are more efficient than $\hat{\tau}_{R}^{2}$ if,

$$MSE\left(\hat{\tau}_{Ji}^{2}\right) < MSE\left(\hat{\tau}_{R}^{2}\right)$$

$$\left[A_{Ji}^{2}\left(\beta_{2(x)}-1\right)-2A_{Ji}\left(\lambda_{22}-1\right)\right] < \left[\left(\beta_{2(x)}-1\right)-2\left(\lambda_{22}-1\right)\right] \tag{69}$$

The $\hat{\tau}_{Ji}^{2}$ - estimators of the finite population variance are more efficient than $\hat{\tau}_{i}^{2}$ if,

$$MSE\left(\hat{\tau}_{Ji}^{2}\right) < MSE\left(\hat{\tau}_{i}^{2}\right)$$

$$\left[A_{Ji}^{2}\left(\beta_{2(x)}-1\right)-2A_{Ji}\left(\lambda_{22}-1\right)\right] < \left[A_{i}^{2}\left(\beta_{2(x)}-1\right)-2A_{i}\left(\lambda_{22}-1\right)\right] \tag{70}$$

The $\hat{\tau}_{Ji}^{2}$ - estimators of the finite population variance are more efficient than $\hat{\tau}_{j}^{2}$ if,

$$MSE\left(\hat{\tau}_{Ji}^{2}\right) < MSE\left(\hat{\tau}_{i}^{2}\right)$$

$$\left[A_{Ji}^{2}\left(\beta_{2(x)}-1\right)-2A_{Ji}\left(\lambda_{22}-1\right)\right] < \left[A_{j}^{2}\left(\beta_{2(x)}-1\right)-2A_{j}\left(\lambda_{22}-1\right)\right] \tag{71}$$

When conditions (68), (69), (70), and (71) are satisfied, we conclude that the proposed estimators $\left(\hat{\tau}_{Ji}^{2}\right)$ are more efficient than existing estimators.

2.4 Empirical Study

An empirical study is carried out to support the efficiency comparison stated above by considering a real-life population as:

Data: [20]

Fixed capital (Auxiliary variable X) Output of 80 factories (Study variable Y)

$N = 80,\ n = 20,\ S_x = 8.4542,\ S_y = 18.3569,\ C_x = 0.7507,\ \overline{X} = 11.2624,\ \overline{Y} = 51.8264,\ \beta_{2(x)} = 2.8664,$
$\beta_{2(y)} = 2.2667,\ \beta_{1(x)} = 1.05,\ \rho = 0.9413,\ \lambda_{22} = 2.2209,\ Q_1 = 9.318,\ C_y = 0.3542,\ Q_2 = 7.5750,$
$Q_3 = 16.975,\ P_1 = 2.44,\ P_5 = 4.35,\ P_{10} = 5.9,\ P_{15} = 6.63,\ P_{20} = 7.45,\ P_{25} = 7.8,\ P_{30} = 8.7,\ P_{35} = 11.6,$
$P_{40} = 15.3,\ P_{45} = 16.9,\ P_{50} = 17.2,\ P_{55} = 19.3,\ P_{60} = 21.7,\ P_{65} = 23.55,\ P_{70} = 24.98, P_{75} = 25,\ P_{80} = 26.95,$
$P_{85} = 27.8,\ P_{90} = 29.7,\ P_{95} = 30,\ P_{99} = 34.85.$

Table1: Constant of the Existing Estimators and Suggested Estimators

Estimator	Constant	Estimator	Constant	Estimator	Constant
τ_1^2	-	τ_{17}^2	0.9876	τ_{p6}^2	0.8962
τ_2^2	0.9648	τ_{18}^2	0.9947	τ_{p7}^2	0.8855
τ_3^2	0.9882	τ_{19}^2	0.9844	τ_{p8}^2	0.8530
τ_4^2	0.9035	τ_{20}^2	0.9982	τ_{p9}^2	0.8148
τ_5^2	0.9119	τ_{21}^2	0.9979	τ_{p10}^2	0.7993
τ_6^2	0.9597	τ_{22}^2	0.8410	τ_{p11}^2	0.7965
τ_7^2	0.9639	τ_{23}^2	0.8170	τ_{p12}^2	0.7772
τ_8^2	0.9953	τ_{24}^2	0.7333	τ_{p13}^2	0.7562
τ_9^2	0.9945	τ_{25}^2	0.8406	τ_{p14}^2	0.6589
τ_{10}^2	0.9595	τ_{26}^2	0.7763	τ_{p15}^2	0.6917
τ_{11}^2	0.9837	τ_{27}^2	0.6939	τ_{p16}^2	0.6939
τ_{12}^2	0.8877	τ_{p1}^2	0.9650	τ_{p17}^2	0.7077
τ_{13}^2	0.8985	τ_{p2}^2	0.9393	τ_{p18}^2	0.7141

τ_{14}^2	0.9954	τ_{p3}^2	0.9194	τ_{p19}^2	0.7292
τ_{15}^2	0.9982	τ_{p4}^2	0.9103	τ_{p20}^2	0.7293
τ_{16}^2	0.9984	τ_{p5}^2	0.9003	τ_{p21}^2	0.7408

Table 2: Bias of the Existing Estimators and Suggested Estimators

Estimator	Bias	Estimator	Bias	Estimator	Bias
τ_1^2	-	τ_{17}^2	96.5697	τ_{p6}^2	5.1150
τ_2^2	93.0301	τ_{18}^2	97.6845	τ_{p7}^2	4.8328
τ_3^2	96.6636	τ_{19}^2	96.0691	τ_{p8}^2	4.0005
τ_4^2	87.8218	τ_{20}^2	98.2363	τ_{p9}^2	3.0872
τ_5^2	85.0561	τ_{21}^2	98.1890	τ_{p10}^2	2.7367
τ_6^2	92.2468	τ_{22}^2	74.8916	τ_{p11}^2	2.6737
τ_7^2	92.8916	τ_{23}^2	71.5866	τ_{p12}^2	2.2549
τ_8^2	97.7790	τ_{24}^2	60.5971	τ_{p13}^2	1.8203
τ_9^2	97.6531	τ_{25}^2	74.8360	τ_{p14}^2	0.0734
τ_{10}^2	92.2161	τ_{26}^2	66.1386	τ_{p15}^2	0.6128
τ_{11}^2	95.9598	τ_{27}^2	55.7128	τ_{p16}^2	0.6497
τ_{12}^2	81.5194	τ_{p1}^2	7.0754	τ_{p17}^2	0.8941
τ_{13}^2	83.0891	τ_{p2}^2	6.3170	τ_{p18}^2	1.0096

τ_{14}^2	97.7948	τ_{p3}^2	5.7521	τ_{p19}^2	1.2903
τ_{15}^2	98.2363	τ_{p4}^2	5.5004	τ_{p20}^2	1.2933
τ_{16}^2	98.2679	τ_{p5}^2	5.2280	τ_{p21}^2	1.5143

Table 3: Mean Square Error (MSE) of the Existing and Suggested Estimators

Estimator	MSE	Estimator	MSE	Estimator	MSE
τ_1^2	5393.8940	τ_{17}^2	7264.7925	τ_{p6}^2	2458.5388
τ_2^2	6941.4748	τ_{18}^2	7360.8374	τ_{p7}^2	2418.6169
τ_3^2	7272.8307	τ_{19}^2	7222.1662	τ_{p8}^2	2307.3358
τ_4^2	6281.0713	τ_{20}^2	7408.9281	τ_{p9}^2	2198.1806
τ_5^2	6377.4765	τ_{21}^2	7404.7868	τ_{p10}^2	2160.5543
τ_6^2	6907.4220	τ_{22}^2	5733.9738	τ_{p11}^2	2154.0711
τ_7^2	6958.7755	τ_{23}^2	5565.5876	τ_{p12}^2	2113.3454
τ_8^2	7369.3313	τ_{24}^2	5159.0648	τ_{p13}^2	2075.8607
τ_9^2	7358.1024	τ_{25}^2	5730.6299	τ_{p14}^2	1993.2480
τ_{10}^2	6904.5232	τ_{26}^2	5332.4920	τ_{p15}^2	2004.2851

τ_{11}^2	7212.8965	τ_{27}^2	5064.8053	τ_{p16}^2	2005.5987
τ_{12}^2	6127.9373	τ_{p1}^2	2761.1311	τ_{p17}^2	2015.8730
τ_{13}^2	6231.5274	τ_{p2}^2	2639.2940	τ_{p18}^2	2021.6302
τ_{14}^2	7370.4162	τ_{p3}^2	2552.3018	τ_{p19}^2	2037.8119
τ_{15}^2	7408.9281	τ_{p4}^2	2514.6841	τ_{p20}^2	2038.0006
τ_{16}^2	7411.6910	τ_{p5}^2	2474.8173	τ_{p21}^2	2052.7660

3.0 Results and Discussion

Tables 1, 2, and 3 show the numerical results of Constant, Bias and MSE for the existing and suggested estimators using a population set. Of all the estimators considered in the study, the suggested estimators have minimum MSEs for the population set. This implies that the suggested estimators demonstrate a high level of efficiency over others.

4.0 Conclusion

From the results of the numerical illustration, it is observed that the suggested estimators are more efficient than other estimators considered in the study and therefore, it is recommended for use for estimating the population mean when the study variable is associated with an auxiliary variable.

References

[1] Evans, W. D. (1951). On the Variance of Estimates of the Standard Deviation and Variance. Journal of the American Statistical Association. 46:220-224.

[2] Hansen, M. H., Hurwitz, W. N. & Madow, W. G. (1953). Sample Survey Methods and Theory. Wiley, New York.

[3] Isaki, C. T. (1983). Variance Estimation using Auxiliary Information. Journal of the American Statistical Association.78:117–123.

[4] Parsad, B. & Singh, H. P. (1990). Some Improved Ratio-Type Estimators of Finite Population Variance using Auxiliary Information in Sample Surveys. Communication in Statistics –Theory and Methods. Vol. 19(3), pp. 1127- 1139.

[5] Kadilar, C. & Cingi, H. (2006). Improvement in Variance Estimation using Auxiliary Information. Hacettepe Journal of Mathematics and Statistics. Vol. 35: pp. 111-115.

[6] Gupta, S. & Shabbir, J. (2008). Variance Estimation in Simple Random Sampling using Auxiliary Information. Hacettepe Journal of Mathematics and Statistics. Vol. 37, pp. 57-67.

[7] Tailor, R. & Sharma, B. (2012). Modified Estimators of Population Variance in presence of Auxiliary Information. Statistics in Transition-New Series. Vol. 13(1), pp. 37-46.

[8] Khan, M. & Shabbir, J. A. (2013). Ratio Type Estimator for the Estimation of Population Variance using Quartiles of an Auxiliary Variable. Journal of Statistics Applications and Probability. Vol. 2: 3, pp. 319-325.

[9] Yadav, S. K., Mishra, S. S. & Gupta, S. (2014). Improved Variance Estimation Utilizing Correlation Coefficient and Quartiles of an Auxiliary Variable. Communicated to American Journal of Mathematics and Mathematical Sciences.

[10] Subramani, J. (2015). Generalized Modified Ratio Type Estimator for Estimation of Population Variance. Sri-Lankan J. Appl. Statist. Vol.16(1), pp. 69-90.

[11] Audu, A., Adewara, A. A. & Singh, R. V. K. (2016). Class of Ratio Estimators with Known Functions of Auxiliary Variable for Estimating Finite Population Variance. Asian Journal of Mathematics and Computer Research. Vol.12(1), pp. 63-70.

[12] Maqbool, S. & Shakeel, J. (2017). Variance Estimation Using Linear Combination of Tri-mean and Quartile Average. American Journal of Biological and Environmental Statistics. Vol. 3(1), pp. 5-9.

[13] Muili, J. O., Singh, R. V. K. & Audu, A. (2018). Study of Efficiency of Some Finite Population Variance Estimators in Stratified Random Sampling. Continental Journal Applied Sciences. Vol. 13(2), pp. 1 – 17.

[14] Bhat, M. A., Raja, T. A., Maqbool, S., Sofi, N. A., Rauf, A. B., Baba, S. H. & Immad, A. S. (2018). Robust Estimators for Estimation of Population Variance Using Linear Combination of Downton's Method and Deciles as Auxiliary Information. Advances in Research. Vol. 15(2), pp. 1-7,

[15] Muili, J. O., Audu, A., Singh, R. V. K. & Yunusa, I. A. (2019). Improved Estimators of Finite Population Variance Using Unknown Weight of Auxiliary Variable. Annals. Computer Science Series. Vol.17(1), pp. 148-153.

[16] Muili, J. O., Agwamba, E. N., Odeyale, A. B. & Adebiyi, A. (2020). Ameliorated Class of Estimators of Finite Population Variance". Asian Journal of Probability and Statistics. Vol. 7(4), pp. 1-14.

[17] Subramani, J. & Kumarapandiyan, G. (2012a). Variance Estimation Using Median of the Auxiliary Variable. International Journal of Probability and Statistics. Vol. 1(3), pp. 36 – 40.

[18] Subramani, J. & Kumarapandiyan, G. (2012b). Variance Estimation Using Quartiles and Their Function of the Auxiliary Variable. International Journal of Statistics and Applications. Vol. 2(5), pp. 67 – 72.

[19] Ali, M., Khalil, M. Hanif, M., Jamal, N. & Shazad, U. (2018). An Improved Ratio-Type Variance Estimator by Using Linear Combination of Different Measures of Location. Oriental Journal of Physical Sciences. Vol. 2(1), pp. 24 – 32.

[20] Murthy, M. N. (1967). Sampling Theory and Methods. Calcutta Statistical Publishing House, India.

PROMOTING AN OPEN-SOURCE PROCESS SIMULATOR AS A MEANS TO DISCOURAGE THE USE OF CRACKED COMMERCIAL SIMULATORS: A STUDY OF THEIR PREDICTION AGREEMENT IN A SELECTED CHEMICAL PROCESS SIMULATION

Toyese OYEGOKE*

Chemical Engineering Department, Ahmadu Bello University Zaria, Nigeria.
*Corresponding email: OyegokeToyese@gmail.com, ORCID: https://orcid.org/0000-0002-2026-6864

Abstract
The significance of process simulators in training process engineers in petrochemical, chemical, nuclear, and biochemical processes cannot be overemphasized. It helps simplify the teaching of several chemical engineering courses like process design, thermodynamics, process integration, separation processes, safety, and a lot more. Most of these process simulators are primarily commercialized, with only a few being freeware. The commercialized ones are known for their friendliness, high publicity, and global trust gained for their predictions in several industrial applications over the years. However, they are costly for schools in low-income nations to afford. In contrast, the freeware publicity is not relatively low, less friendly, and cheaper than the commercial ones. To help promote the confidence of the institutions in the prediction of freeware process simulators, this report comparatively investigates the agreement of the prediction of commercial process simulators with freeware ones. In the analysis, a selected chemical process involving the Gibbs reactor and mixer was modelled and simulated in the COCO and Aspen HYSYS simulator. Findings from the analysis reveal good agreement in the predicted results obtained from the various process simulators. The study suggests the promotion of utilizing the freeware process simulator over the cracked version often used in low-income nations in teaching process engineers and research studies due to cost.

Keywords: *Process, Modelling, Simulation, Freeware, Plant, Chemical Process.*

1. Introduction
Chemical process simulation is essential for evaluating and analyzing chemical processes in industrial and academic settings[1]. This technology helps to optimize the chemical process and minimize environmental issues. It allows engineers and scientists to understand how chemical reactions occur, predicts their outcomes, and make informed decisions about the safety, cost, and efficiency of new processes. Chemical process simulation can help reduce the time and cost involved in developing new chemical products by providing an accurate picture of the impact of different variables on the reaction outcome[1]–[3]. Several works in the literature have deployed the use of the principle in the study of different research subjects. Some of these include

evaluating the chemical process energy efficiency [4], process integration, the impact of changing several operating parameters [5], [6], process decision-making[7]–[9], economic implications of re-designing or designing a chemical process [10]–[12], and many more subjects [13].

In most of these studies, a process simulator is application software that has successfully made many of these studies easier [14]. Examples of these process simulators include Aspen HYSYS, ChemCAD, SuperPro Designer, COCO, ChemSep, and a lot more [15]–[21]. It is essential to know that some simulators are freeware while others are commercialized. Most commercialized process simulators are well known by the public and well accepted for their good years of quality prediction, which has facilitated much advancement in the field of process engineering, unlike the cases of freeware simulators.

To help in shedding more light on the potential of the freeware process simulator as a measure of discouraging the practice of considering a cracked version of the commercial ones, especially in the low-income nation, the report presents a comparative analysis of the Aspen HYSYS (commercial) with the COCO (freeware) process simulator. A choice of the chemical process in which methane is oxidized in the presence of oxygen yields syngas with a possible composition of carbon monoxide, carbon dioxide, and hydrogen.

2. Computational Details

For this study, the choice of CAPE-OPEN to CAPE-OPEN, often abbreviated as COCO version 3.6 [16] being a selected freeware process simulator, and the commercial process simulator, the use of Aspen HYSYS [19] was considered for the study, being that it is a commercial simulator with a high reputation and wide range of industrial acceptance over past years.

2.1 Process description

The process study is a chemical process where the methane gas is oxidized in the presence of oxygen to yield carbon monoxides, carbon dioxide, and hydrogen gas as a specified reaction condition of 373K and 2 bar using a 2:1 ratio of methane to oxygen.

2.2 Simulation Basis and Conditions

In the analysis, pure methane gas was blended in a mixer (U1) with hydrogen gas in a given ratio of 2:1. The two components were fed into the mixer (U1) at 303K and 1 bar. After which, a compressor (U2) was used to increase the pressure to 2 bar. The pressurized stream (F2) was charged into a heater, raising the stream temperature to 373K, assuming no pressure loss. The resulting stream (F3) was charged into the Gibbs reactor, where methane oxidation is held in the presence of oxygen. The resulting products (F31 and F32) were mixed to give us an overall product stream (F4) in Aspen HYSYS. In COCO, the resulting product stream is only one, equating to the F4. The operation of the reactor was set to be at a constant temperature. The Soave-Redlich-Kwong (SRK) thermodynamic model was used in the simulation across each simulator. In the modeling of the reaction process, methane, oxygen, carbon monoxide, carbon dioxide, and hydrogen gas were modeled as possible reactants and products that could take part in the reaction simulation for the comparative assessment of the freeware and commercial process simulator.

2.3 Analysis of feeds ratio on the process simulated

In the analysis of the understanding of the impact of the ratio of the feed on the process, the amount of the methane feed flow rate was kept constant at 100 mol/s while varying the oxygen feed flow rate from zero to 200 mol/s. In analyzing the change effects on the yield, a design of 20 steps was spread within the chosen range of oxygen feed flow rate at constant temperature and pressure of 373 K and 2 bar, respectively.

3. Results and Discussions

3.1 Process Flow Diagram

The resulting process flow diagram (PFD) obtained from the modeling and simulation of the chosen process for the oxidation of methane to yield carbon monoxide, carbon dioxide, and hydrogen gas is presented in Figures 1 to 2. The figures displayed the corresponding PFD obtained from the process simulation run in Aspen HYSYS [19] and COCO [16] process simulators.

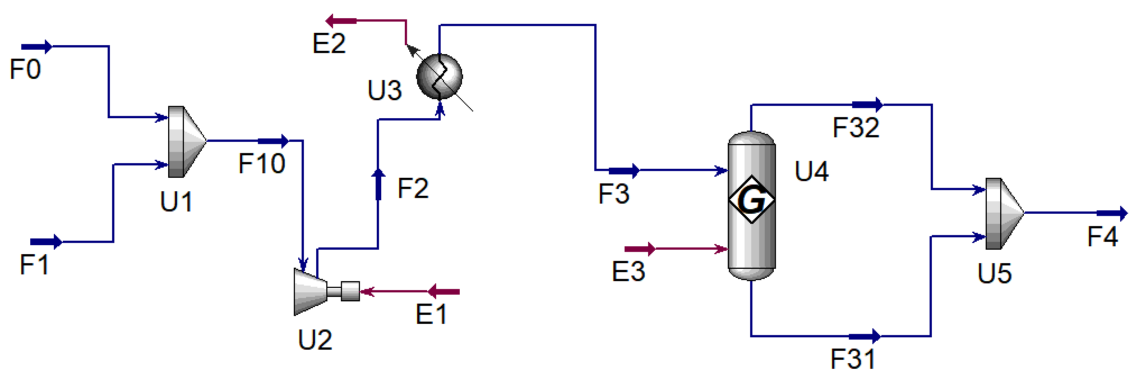

Figure 1. A PFD for the process studied in the Aspen HYSYS simulator.

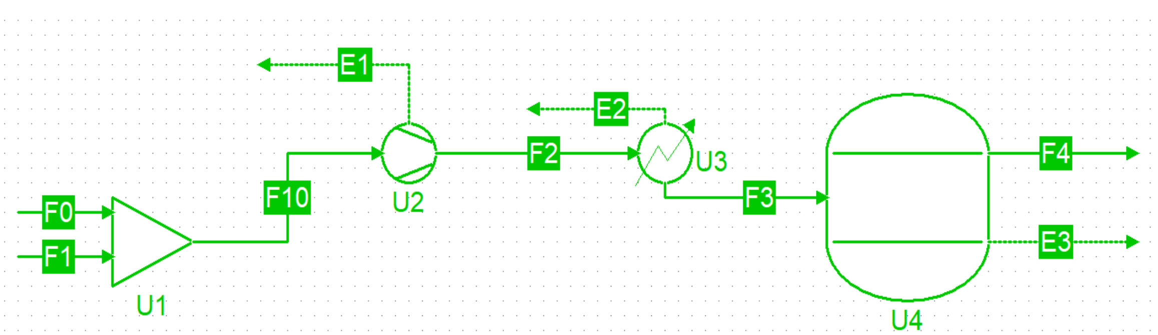

Figure 2. A PFD for the process studied in the COCO simulator.

In Figures 1 and 2, the oxygen gas is charged via the F0 stream, and the methane gas via the F1 stream is mixed in U1 to yield the resulting mixture in the F10 stream. The pressure of the F10 stream increased via the U2 compressor with a E1 compression duty to yield the F2 stream and was further heated via the U3 heater with an E2 heating duty to yield the F3 stream. The F3 stream is charged into the U4 reactor to obtain the F4 product stream with E3 reactor duty.

3.2 Effect of Molar Feed Ratio on the Carbon Dioxide Yield

The effect of the molar feed ratio (that is, the methane and oxygen gas feed ratio) is well presented in Figure 3 for the COCO [16] and Figure 4 for the Aspen HYSYS [19] process simulator.

The result obtained in Figure 3 shows that methane was fully converted at an oxygen molar flow rate of 100 mol/s, which yields 0.67 mol of hydrogen, 0 mol of oxygen, and 0.33 mol of carbon monoxide at 373 K and 2 bar. The molar feed flow rate of oxygen gas that fully converted methane was found to be equal to the methane molar feed flow rate. In accordance with the literature [22], the methane oxidation or gasification mechanism followed $CH_4+O_2 \rightarrow CO_2+2H_2$ in the process showing equal stoichiometric coefficients.

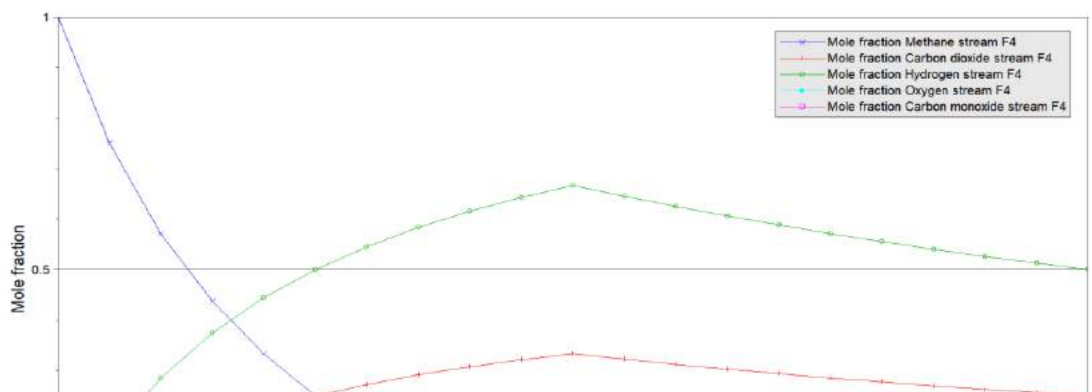

Figure 2. The plot of product composition – oxygen molar flow rate COCO simulator.

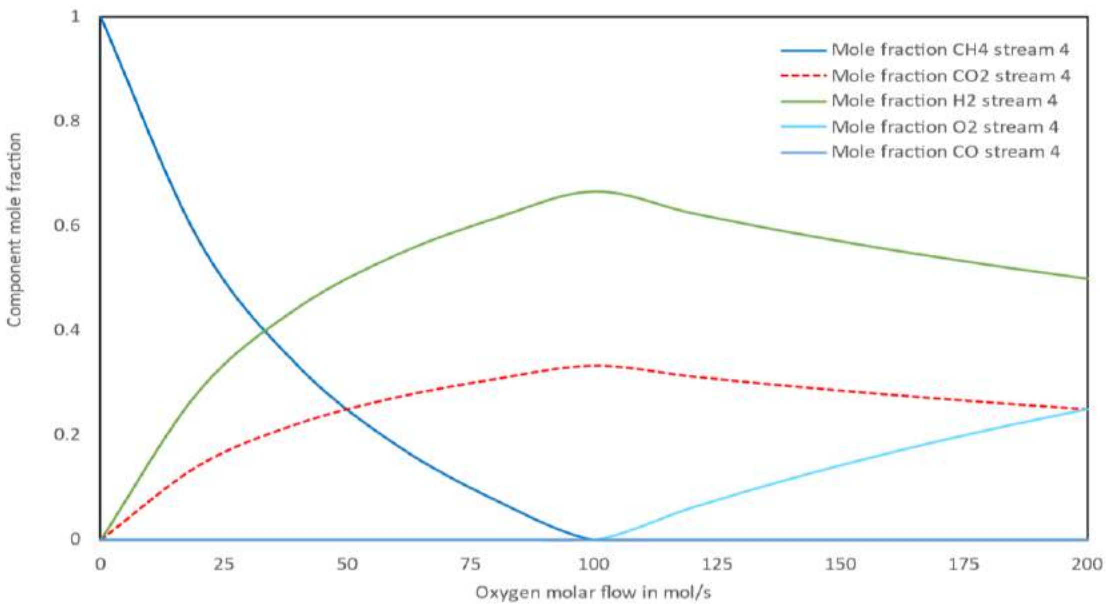

Figure 3. The plot of product composition – oxygen molar flow rate Aspen HYSYS simulator.

A study of the product evolution profile in Figures 3 and 4 indicated a higher yield of hydrogen gas [22], which could be a valuable product for other applications like energy [23], [24], and hydrogenation processes [25]. The COCO [16] process simulator's prediction profiles were obtained for the trend of the product composition as the oxygen molar flow changes from zero to 200 mol/s, which was found to have shown a similar agreement for the commercial process simulator (Aspen HYSYS).

5. Conclusions

Successful modeling and simulation of the conversion of methane to syngas in the presence of oxygen under the stated circumstances were accomplished in this work utilizing both the commercial class of the process simulator, Aspen HYSYS, and the freeware class, COCO. Also, the simulation of the process of oxidizing methane to make carbon monoxide, carbon dioxide, and hydrogen in the COCO process simulator showed a good match with the results from Aspen HYSYS. At an oxygen molar flow rate of 100 mol/s, both process simulators predict a complete conversion of methane (that is, convert 100% of the methane). In general, the process model simulated within the COCO process simulator predictions showed a good agreement with the Aspen HYSYS (a commercial process simulator).

Acknowledgment

The author acknowledges the help of the Pencil Team and thanks the creators and contributors of the COCO process simulators for making it freely accessible to everyone.

References

[1] Wikipedia, "Process simulation - Wikipedia," *Wikipedia, The Free Encyclopedia*. 2023. Accessed: Feb. 25, 2023. [Online]. Available: https://en.wikipedia.org/wiki/Process_simulation

[2] Processium, "Chemical process simulation: Processium, process simulation (chemical process simulation and conception)," 2023. https://web.archive.org/web/20150710045707/http://en.processium.com/process-simulation/chemical-process-simulation.htm# (accessed Feb. 25, 2023).

[3] Wikipedia, "Chemical process modeling ," *Wikipedia, The Free Encyclopedia*. 2023. Accessed: Feb. 25, 2023. [Online]. Available: https://en.wikipedia.org/wiki/Chemical_process_modeling

[4] S. Yanisa, R. S. Thongchai, D. Peerapan, and C. Kotchakorn, "Heat Integrated Process Design, Simulation and Control of Polymerization and Drying Sections for HDPE Production," *Applied Science and Engineering Progress*, vol. 9, no. 2, 2016, doi: 10.14416/10.14416/j.ijast.2016.03.002.

[5] M. C. Tohəneanu, V. Pleşu, P. Iancu, G. Bumbac, A. E. Bonet Ruiz, and J. B. Ruiz, "Simulation and Process Integration of Clean Acetone Plant," *Chem Eng Trans*, vol. 39, no. Special Issue, pp. 469–474, Aug. 2014, doi: 10.3303/CET1439079.

[6] D. K. Kenneth, J. Gonurubon, A. O. Michael, and N. H. Douglas, "Simulation of a Process Unit for the Recovery of Light Ends from Natural Gas Mixture," *Bioprocess Engineering*, vol. 6, no. 2, p. 33, Oct. 2022, doi: 10.11648/J.BE.20220602.14.

[7] K. Walker, "Techno-economic feasibility of propane dehydrogenation in novel membrane reactors," Eindhoven University of Technology, Eindhoven, 2020. Accessed: Dec. 10, 2022. [Online]. Available: https://pure.tue.nl/ws/portalfiles/portal/203528420/Master_Thesis_Keegan_Walker.pdf

[8] T. Oyegoke and F. Dabai, "Techno-economic feasibility study of bioethanol production from a combined cellulose and sugar feedstock in Nigeria: 2-economic analysis," *Nigerian Journal of Technology*, vol. 37, no. 4, pp. 913–920, Nov. 2018, doi: 10.4314/njt.v37i4.9.

[9] T. Oyegoke and F. Dabai, "Techno-economic feasibility study of bioethanol production from a combined cellulose and sugar feedstock in Nigeria: 1-modeling, simulation and cost evaluation," *Nigerian Journal of Technology*, vol. 37, no. 4, pp. 913–920, Nov. 2018, doi: 10.4314/njt.v37i4.8.

[10] T. Oyegoke, M. Y. Sardauna, H. A. Abubakar, and E. Obadiah, "Exploration of Biomass for the Production of Bioethanol: 'A Process Modelling and Simulation Study,'" *Renewable Energy Research and Application*, vol. 2, no. 1, pp. 51–69, 2021, doi: 10.22044/RERA.2020.10287.1042.

[11] O. O. Ajayi, K. Rasheed, A. Onadeji, and T. Oyegoke, "Techno-economic Assessment of Transforming Sorghum Bagasse into Bioethanol Fuel in Nigeria: 1-Process Modeling, Simulation, and Cost Estimation," *Journal of Engineering Studies and Research*, vol. 26, no. 3, pp. 154–164, 2020, Accessed: Mar. 18, 2021. [Online]. Available: http://jesr.ub.ro/1/article/view/219

[12] A. Abemi, T. Oyegoke, F. N. Dabai, and B. Y. Jibril, "Technical and Economic Feasibility of Transforming Molasses Into Bioethanol In Nigeria," in *National Engineering Conference*, 2018, pp. 531–537.

[13] D. J. Navarro Perez, J. C. Moreno Diaz, and P. A. Simeone Barrientos, "Emergency remote teaching in process simulation using DWSIM: a case study from DIQ-UMAG, Chilean Patagonia," *Scientia et Technica, ISSN 0122-1701, Vol. 27, Nº. 2, 2022, págs. 130-140*, vol. 27, no. 2, pp. 130–140, 2022, Accessed: Jan. 28, 2023. [Online]. Available: https://dialnet.unirioja.es/servlet/articulo?codigo=8518384&info=resumen&idioma=ENG

[14] Wikipedia, "List of chemical process simulators - Wikipedia," *Wikipedia, The Free Encyclopedia*. 2023. Accessed: Feb. 25, 2023. [Online]. Available: https://en.wikipedia.org/wiki/List_of_chemical_process_simulators

[15] UniSim, "UniSim Design | Process Simulation Software," *Honey Well Forge Report*, Jan. 28, 2023. https://www.honeywellforge.ai/us/en/products/industrials/unisim-design (accessed Jan. 28, 2023).

[16] COCO, "COCO - the CAPE-OPEN to CAPE-OPEN simulator," *CAPE-OPEN Report*, Oct. 30, 2021. https://www.cocosimulator.org/ (accessed Oct. 30, 2021).

[17] J. van Baten and L. Rozas, "An Introduction to COCO," *COCO Simulator Report*, 2007, Accessed: Jan. 28, 2023. [Online]. Available: http://www.chemsep.com/

[18] B. Jasper van, T. Ross, and K. Harry, "Using Chemsep, COCO and other modeling tools for versatility in custom process modeling," *Amsterchem Report*, 2008.
[19] Aspentech, "Aspen HYSYS Dynamics | Intuitive Dynamic Modeling | AspenTech," *Aspentech Report*, Oct. 30, 2021. https://www.aspentech.com/en/products/engineering/aspen-hysys-dynamics (accessed Oct. 30, 2021).
[20] SuperPro Designer, "Process Simulations," *Intelligen, Inc. Report*, 2020. https://www.intelligen.com/products/superpro-overview/ (accessed Jan. 28, 2023).
[21] L. Canizales, F. Rojas, C. A. Pizarro, N. H. Caicedo-Ortega, and M. F. Villegas-Torres, "SuperPro Designer®, User-Oriented Software Used for Analyzing the Techno-Economic Feasibility of Electrical Energy Generation from Sugarcane Vinasse in Colombia," *Processes 2020, Vol. 8, Page 1180*, vol. 8, no. 9, p. 1180, Sep. 2020, doi: 10.3390/PR8091180.
[22] V. Bach, F. Raganati, S. Okiemute Akpasi, and Y. Makarfi Isa, "Review of Carbon Capture and Methane Production from Carbon Dioxide," *Atmosphere (Basel)*, vol. 13, no. 12, p. 1958, Nov. 2022, doi: 10.3390/ATMOS13121958.
[23] M. O. Petinrin, M. B. Adebayo, and A. T. Adelowokan, "A Review on Hydrogen as a Fuel for Automotive Application," *International Journal of Energy Engineering*, vol. 4, no. 4, pp. 75–80, 2014, doi: 10.5923/J.IJEE.20140404.02.
[24] A. Pan, J. Liu, Z. Liu, Y. Yang, X. Yang, and M. Zhang, "Application of Hydrogen Energy and Review of Current Conditions," *IOP Conf Ser Earth Environ Sci*, vol. 526, no. 1, p. 012124, Jun. 2020, doi: 10.1088/1755-1315/526/1/012124.
[25] D. Geburtig, P. Preuster, A. Bösmann, K. Müller, and P. Wasserscheid, "Chemical utilization of hydrogen from fluctuating energy sources – Catalytic transfer hydrogenation from charged Liquid Organic Hydrogen Carrier systems," *Int J Hydrogen Energy*, vol. 41, no. 2, pp. 1010–1017, Jan. 2016, doi: 10.1016/J.IJHYDENE.2015.10.013.

NIPES-NCEE Conference Proceedings
The 2nd International Conference 15th-17th Feb. 2023
310-320
www.nipesjournals.org.ng

PERFORMANCE OF MUNICIPAL SOLID WASTE AS FUEL IN A BINARY DIRECT CARBON FUEL CELL

Ajaw A. R., Adeniyi O. D., Adeniyi M.I. and Olutoye M. A.

Department of Chemical Engineering, Federal University of Technology, PMB.65, Minna.
Niger State,Nigeria.
*Corresponding author's E-mail: ajawz16@gmail.com.Tel:+2347037888594

Abstract

A variety of abundant carbonaceous fuels such as municipal solid waste (MSW) and biochar from biomass carbonization can be utilized to generate electricity in a direct carbon fuel cell (DCFC) system.In this paper, characterized municipal solid waste of different fractions of sawdust, sugarcane bagasse and orange peel were characterized. The proximate and ultimate analysis employed to determine the High heating value (HHV). The result shows that the HHV of municipal solid waste of the different fractions of sawdust, sugarcane bagasse and orange peel were 6.79, 9.78, 7.68 and its combination which makes up the municipal solid waste to be 11.00 MJ/kg respectively . The calorific values were evaluated to be 7.0, 6.7, 5.8 and 7.9 MJ respectively .The XRD and SEM/EDX reveals that amorphous carbon were present in the analysis. it shows the possibility utilizing municipal solid waste(MSW) as fuel in a direct carbon fuel cell(DCFC) for power generation.

Keywords:*Municipal solid waste,Energy,Biochar,DCFC.*

1.0 Introduction

Population growth, migration from rural to urban areas, as well industrial growth have recently escalated, resulting in substantial increases in waste generation that is of socio-economic and environmental global concern [1]. The management of Municipal Solid Waste (MSW) is a challenging ideal that can potentially provide use-able commodities such as recycled materials and energy. The world economy is driven by consumer-based lifestyles, which generate a high quantity of waste [2]. MSW are classified into either inorganic or organic and they are further categorized in accordance with hazardousness for resource recovery. In general, some of these MSW are organic matter, paper, wood, glass, plastic, metals, rubber, fiber, medical waste and batteries [3]. The composition of MSW differs from one country to another, depending on their socio-economic and cultural status. The low income countries generate the highest amount of organic waste while the high income countries produce the highest proportion of inorganic waste [4].
Currently, the worldwide is clamoring towards less dependence on fossil fuels, due to the emission of greenhouse gases and energy security issues, has led to the strong interest in using biomass energy. As an alternative, renewable energy source, biomass absorbs the same amount of carbon dioxide (CO_2) during plant growth, contributing less to global warming. The only remaining issue, however, is how to produce energy from biomass without competing with food supply over the use of arable lands. As such, utilization of waste biomass byproducts, especially from the organic and inorganic materials is key to solving this problem [5].
The Direct Carbon Fuel Cell (DCFC) have attracted growing attention nowadays as an efficient generator of electrical power. It has the advantages of a near 100% thermodynamic efficiency and a practical efficiency of about 80 % far higher than hydrogen fuel cell technologies and coal fired generator. The overall process of generating electricity by a DCFC system is relatively compared

to other fuel cell technologies and does not require expensive preparation of any gaseous fuel, as well as accepts a variety of carbon-rich materials (coal, graphite, carbon black, coke, active carbon, etc.) as potential fuels. This cell is an interesting system because it offers the possibility to use, as fuel source, available and abundant raw materials with only minor pretreatment [6].
MSW, as a significant feed-stock of biomass fuel, possesses truly high potential as the fuel feed-stock for DCFCs due to its easy availability, low cost, and high energy content (19,800 kJ/kg), especially for the MSW after pyrolysis or compaction . The energy content of pyrolysed MSW is competitive to that of coals (30,200 kJ/kg). Waste materials in terms of weight, account for nearly half composition of the MSW, and possesses the above mentioned properties of MSW. It is highly expected that waste materials would be suitable feed-stock for DCFC. Therefore, it is well worthy to study the feasibility of municipal solid waste.

2. Methodology

2.1. Raw materials-municipal solid waste (MSW)

Municipal solid waste collected mainly from households consists of plastics, paper, metals, textiles. organic waste, leather, rubber, metals, glass, ceramics, soil materials and miscellaneous other materials. Typical household waste contains a wide range of materials that vary significantly in composition depending on the type of community and its consumers' incomes and lifestyles, and its degree of industrialization, institutionalization and commercialism. In general, the highest waste generation is correlated with the highest income. Moreover, even the season of year or the number of persons living in a household influence the amount and composition of waste. For example, more food waste and less paper is generated during summer. Additionally, the larger the community, the more garbage is produced per capita [7]. This work is being motivated by the availability of solid waste found in abundant in most part of Nigeria [8]. As a renewable energy source. The problem of instability can be resolved by using the fuel cell technology which offers a great deal of efficiency and low emissions in the production of electricity it is portable and easy to handle with level of stability at a constant fuel oxygen supply. In an attempt to investigate the electrochemical performance of the fuel cell the efficiency is obtained and it gives us an idea of the quantity of electricity that can be generated. The direct carbon fuel cell uses waste materials as its fuel source making it economically-viable for waste management and reduction of greenhouse effect.

2.2 Experimental apparatus and procedure of bio char preparation

This paper investigate the potential of selected municipal solid waste biochar as carbon fuel in DCFC.

Solid waste sample was collected at three(3) different dump site from Kaduna. The collected solid wastes was sorted into biodegradable and non-biodegradable waste. The biodegradable samples of the waste, which were sugarcane bagasse ,sawdust and orange peel. The sorted solid waste was sun dried. Particle size reduction was carried out by pounding in a mortar. The pounded sample was sieved with a 500µm (0.5mm) sieve.

Pyrolysis of the Sieved Sample

The sieved sample was pyrolysed in other to obtain the bio char. A crucible containing Nitrogen gas in its cylinder was used to hold the dry sample and later was inserted into a muffler furnace Carbolite RHF 600 at high temperature. The sample was prepared for pyrolysis. The sample pyrolysed was carried out in a muffler furnace at 500^{o}C for 30 minutes for the MSW . The nitrogen gas in the cylinder was used to purge the crucible from Oxygen so as to remain only the solid carbon for DCFC Performance. The muffler furnace was heated at an increasing rate of 10^{o}C/min to 500^{o}C for 30 minutes to complete the pyrolysis process [8]. At the end, the biochar was sieved using a 250 µm size mesh to obtain fine carbon particles.

Characterization of the Bio char

Proximate Analysis. The proximate analysis of the biocher is given in terms of four constituents namely.Moisture Content Analysis.Ash Content Analysis.Volatile Content Analysis.Fixed Carbon Analysis.

Ultimate Analysis. The elemental components of the biochar sample was detected by elemental analyzer. The elemental component includes carbon, hydrogen, oxygen, nitrogen and sulphur.

X-Ray Diffraction (XRD) Analysis.X-ray diffraction analysis was carried out to determine the structure of the various biochar obtained from the solid waste.

Scanning Electron Microscope (SEM).SEM was carried out to determine the texture, chemical composition and crystalline structure [10].

Calorific Value. The calorific value was carried out to determine the amount of chemical energy in a given waste sample.

2.3.2 Proximate Analysis of Biomass

The proximate analysis of the biomass is key to determining the chemical compositions of the biomass and to provide their various combustion characteristics of the biomass. The proximate analysis of biomass composition (by mass) is given in terms of four constituents, namely: moisture content, fixed carbon, volatile matter (the gases emitted during thermal decomposition of the biomass in an inert atmosphere) and ash (inorganic matter left after combustion). The fixed carbon is estimated by difference.

2.3.2.1 Moisture Content Analysis

The moisture content was carried out on the individual samples in order to ascertain the level of moisture (water) in the samples. An empty crucible of known weight was put in a drying oven for 30minutes at 105^{o}C to eliminate any trace of moisture. The crucible was put in a desiccator to cool down and then was reweighed, the weight was noted. Then 1g of the sample was measured out. The sample and the crucible were put in a drying oven set at 105^{o}C and left for 1hr. The crucible and its contents was removed and put in a desiccator, allowed to cool to room temperature and reweighed. This was repeated until the weight after cooling was constant within 0.3mg and was recorded as the final weight.

$$\text{Moisture Content (\%)} = 100\frac{(W2-W1)-(W3-W1)}{(W2-W1)} X\,100 \tag{1}$$

Where, W_1 = weight of clean, dry crucible (g), W_2 = weight crucible + wet sample (g), W_3= Weight of Crucible + Dried Sample (g)

2.3.2.2 **Ash Content Analysis**

1.0g of the dried test samples each was measured and heated in a furnace at 750°C for 30 minutes by following the previous weighing procedures and heating was carried out in a muffler furnace known as Carbolite RHF 1600 and left in a desicator to cool down to room temperature, and weighed. This was repeated for 1hr interval until the weight was constant. This weight each was recorded as the final weight of the ash by using Equation (2) in grams (g).

$$\text{Ash Content (\%)} = \frac{(\text{Weight of ash})}{(\text{Initial weight of dried sample})} X\,100 \tag{2}$$

2.3.2.3 Volatiles Content Analysis

The volatile matter of the sample was determined using the Meynell method. 1.0g of the residual dry sample each from moisture content determination was placed (spread evenly) on an empty crucible, after weighing the empty crucible and was then covered and place in a furnace preheated at 950°C for 30 minutes to drive off the volatile. The resulting sample was further heated at 800°C for 5minutes (just before the materials turns black, that is, before it ashed), placed in a desiccator and allowed to cool and then calculated using the equation below:

Volatile Matter = Weight of residual dry sample before heating – weight of dry sample after heating

$$\text{Volatile Matter (\%)} = \frac{\text{Loss in weight due to removal of volatile matter}}{\text{weight of sample taken}} X\,100 \tag{3}$$

2.3.2.4 Fixed Carbon Analysis

The fixed carbon analysis gives a measure of what is left of the biomass when moisture, volatile and ash have been removed. The fixed carbon content of the samples was calculated using the following relation:

$$\text{Fixed carbon content (\%)} = 100 - (\text{moisture content} + \text{volatile matter} + \text{Ash content}) \tag{4}$$

2.3.3 Ultimate Analysis

Elemental components of the fuel samples were placed in a platinum crucible and detected by an elemental analyser. A given weight (1 mg) of sample was burned at a raised temperature (°C) in an oxygen atmosphere, so the Carbon was converted into CO_2, Hydrogen in H_2O, Sulfur into SO_2 and the Nitrogen in N_2. The first three compounds were detected quantitatively by an IR detector, while N_2 was determined by a thermal conductivity detector.

2.3.3.1 Carbon and Hydrogen Contents

Big-Pregle Method was used actually to determine the Carbon and Hydrogen determination. To determine the Carbon and hydrogen content: 1g of the biomass sample was placed in quartz tube and burnt off through the absorbent Magnesium percolate to absorb water and Sodium Hydroxide to absorb Carbon Dioxide. The amount of water and carbon dioxide were determined from the difference between the weigh before and after absorption of water. The Hydrogen and Carbon (%) were evaluated thus as:

$$\%C = \frac{a(0.2727)}{g} \times 100\% \quad (5)$$

While for Hydrogen content we have

$$\%H = \frac{b(0.2727)}{g} \times 100\% \quad (6)$$

2.3.4 Calorific Value (CV) Determination

The calorific value of a given biomass is the heat released by the biomass when it is completely burnt at standard pressure (1 bar) and reference temperature (298 K). The higher the calorific value of a given biomass, the greater the heat released. The sample was analysed using a Bomb Calorimeter. The equation used to calculate the calorific value is given as:

$$\text{Calorific Value} = \frac{(\text{Rise in Temperature of Sample}) \times (\text{Water Equivalent})}{\text{weight of Sample}} \quad (7)$$

2.4 X-Ray Diffraction (XRD) Analysis

XRD is the technique for analyzing crystalline phase in solid materials. XRD can be used as a tool for measuring carbonization, as material reactivity is influenced its phase composition. The total intensity of diffracted beam from crystalline part is the remaining area under curve above background.

The powdered samples were pelletized and sieved to 0.074mm. which were later placed in an aluminium alloy grid (35 mm x 50 mm) on a flat glass plate and enclosed with a paper. Wearing hand gloves, the samples were gently compressed with the hand. Each sample was run through the Rigaku D/Max-lllC X-ray diffractometer developed by the Rigaku Int. Corp. Tokyo, Japan and set to make diffractions at scanning rate of 2 ^{0}/min in the 2 to 50^0 at room temperature with a CuKa radiation set at 40kV and 20mA.

The diffraction information (d value and relative intensity) obtained was compared to that of the standard data of minerals from the mineral powder diffraction file, ICDD which contained and includes the standard data of more than 3000 minerals. Similar diffraction information means the same minerals to standard minerals which exist in the soil sample.

2.5 SEM/EDX Analysis

Scanning Electron Microscope were taken on a JOEL-JSM 7600F with a 6587 EDS (energy dispersion X-rays spectrometer) detector, using an accelerating voltage of 15KV. The Samples are coated with platinum coating of electrically conducting material, deposited on the sample either by low-vacuum sputter coating or by high-vacuum evaporation, the samples were deposited on a sample holder with an adhesive carbon foil and sputter with gold.

2.6 Design and Assembling of the Direct Carbon Fuel Cell (DCFC)

The design arrangement in this research work is similar to the work of Cooper *et al*, 2004, experimented also by Adeniyi,*et al* 2014. which employed Direct Carbon Molten Carbonate Fuel Cell. There are similarities in the shape, size, and configuration but with a modified design similar to that of Kacprzak *et al*., 2015 and the design is advantageous in terms of cost and availability of materials, and with ease of fabrication.

The cell has a corrugated flow channels (two gas pipes) attached at both ends of the cell which serves as inlet and outlet of purging gas (anode) and oxidizing gas or air (cathode) passage, the anode and the cathode were made from steel pipes with considerations of operating temperature and melting point(2600^oF or 1427^oC) of steel, as the cell operates at high temperature.

A molten binary mixture of NaOH or KOH was used as the electrolyte. While copper wires were used as current collectors on the electrode (anode and cathode). The copper wire which was to transmit the generated power was insulated with crystal beads which are also resistant to high temperature. The anode was made up of a porous alumina mesh of area 2.5 cm^2 and about 40 % void, which provided the conductive surface for effective carbonate ions transportation.

2.6 Preparation of Carbonate Electrolyte Using a Mesh Wire

The electrolyte was prepared using molten hydroxide of Sodium and Potassium as suggested by Adeniyi*et a*l (2014). 9.5g of NaOH and 15.5g of KOH (i.e. 38 mol% of NaOH and 62 mol% of KOH) were measured and mixed together and later transferred to a stainless steel [12]. The stainless steel was then place on a hot plate where it was been prepared. The mixture was immediately stirred continuously to ensured homogeneous mixture. Molten started at a temperature of 130^{0}C and at 159^{0}C the molten hydroxide has completely formed. The 25mm Aluminium wire mesh was saturated with the melted molten hydroxide and upon cooling, the molten hydroxide stick to the aluminum wire mesh and it was used as the electrolyte.

2.7 Preparation of Carbon Fuel Particles

The carbon fuel particles used for The carbon fuel particles used for the electrochemical reaction as suggested by Copper (2008) was mixed with the mixed hydroxide salt (15 wt% of Biomass, 46.6 wt% of NaOH and 53.4 wt% of KOH. The Sodium Hydroxide (13.98 g) and Potassium Hydroxide (16.02 g) were mixed together and later mixed with 4.5 g of the biomass carbon particle to form the fuel for the DCFC [8].

3. Result and Discussion

3.1 Thermo-Gravimetric Analysis of MSW

The result of the Thermo-Gravimetric analysis involves the Proximate and Ultimate Analysis and it is represented in Tables 1 and 2;

Table 1: Proximate analysis of MSW(sawdust, sugarcane bagasse, orange peel)

Sample	Moisture Content (wt%)	Ash Content (wt%)	Volatile Matter (wt%)	Fixed Carbon (wt%)
MSW	1.36	3.57	65.10	29.97

Table 2: Ultimate Analysis of MSW(sawdust, sugarcane bagasse, orange peel)

Sample	C (wt%)	H (wt%)	O (wt%)	N (wt%)	S (wt%)
MSW	58.40	6.60	34.00	0.72	0.28

From Table 1, The result of the Thermo-gravimetric analysis carried out on the samples indicates the properties of the fuel source and which invariable is an important check for the a suitable fuel for use in the Direct Carbon Fuel Cell. The moisture content, ash content and volatile matter of the MSW are 1.36 wt%, 3.57 wt%, 65.10 wt% compared to the result gotten by Omari 2015. of 8.41 wt% 4.18 wt% respectively. The difference can be attributed to the different drying temperature and procedure being that for this research, the sample was sun dried for a week as against 60^{o}C for Omari 2015.While having a fixed carbon content of 29.97wt% ,which makes it a suitable fuel with high carbon content.

From Tables 1 and 2 the moisture content, ash content, volatile matter, carbon (C) content, hydrogen content and sulphur content obtained are 1.36 wt%, 3.57 wt%, 65.10 wt%, 29.97 wt% 6.60 wt% and 0.28 wt% respectively for the combined fuel. Higher volatile matter, hydrogen (H) content and low moisture content are suitable for short term use as substrate in the DCFC but for long term a high carbon content and low sulphur (S) content is better [13].

3.1.1 Calorific Value

This is an important characteristic in the setup of DCFC as it determines the amount of heat released during burning a unit quantity of fuel, the higher and lower heating values was determined with the help of the calorific value. The calorific values of the proposed fuel obtained are:

Table: 3.3: Calorific value of MSW(sawdust, sugarcane bagasse, orange peel)

Sample	Calorific Value (MJ/Kg)	LHV (MJ/Kg)	HHV (MJ/Kg)
MSW(sawdust, sugarcane bagasse, orange peel)	7.9	9.54	11.00

3.2 X-ray Diffraction (XRD) Pattern

The X-ray diffraction (XRD) analysis was carried out to investigate the phase composition, crystalline structure and the degree of disorderliness of the carbon fuel. This was done for the pyrolysis of the MSW sample at 500°C. The result from the XRD pattern is presented in Figure 3.1. The pattern constitute the basis for comparison for the carbonized MSW to be used in the fuel cell. It has been agreed by several researchers that less crystalline carbon contains more edges sites and defects which are considered reactive sites for carbon oxidation in DCFC [14,15,16].

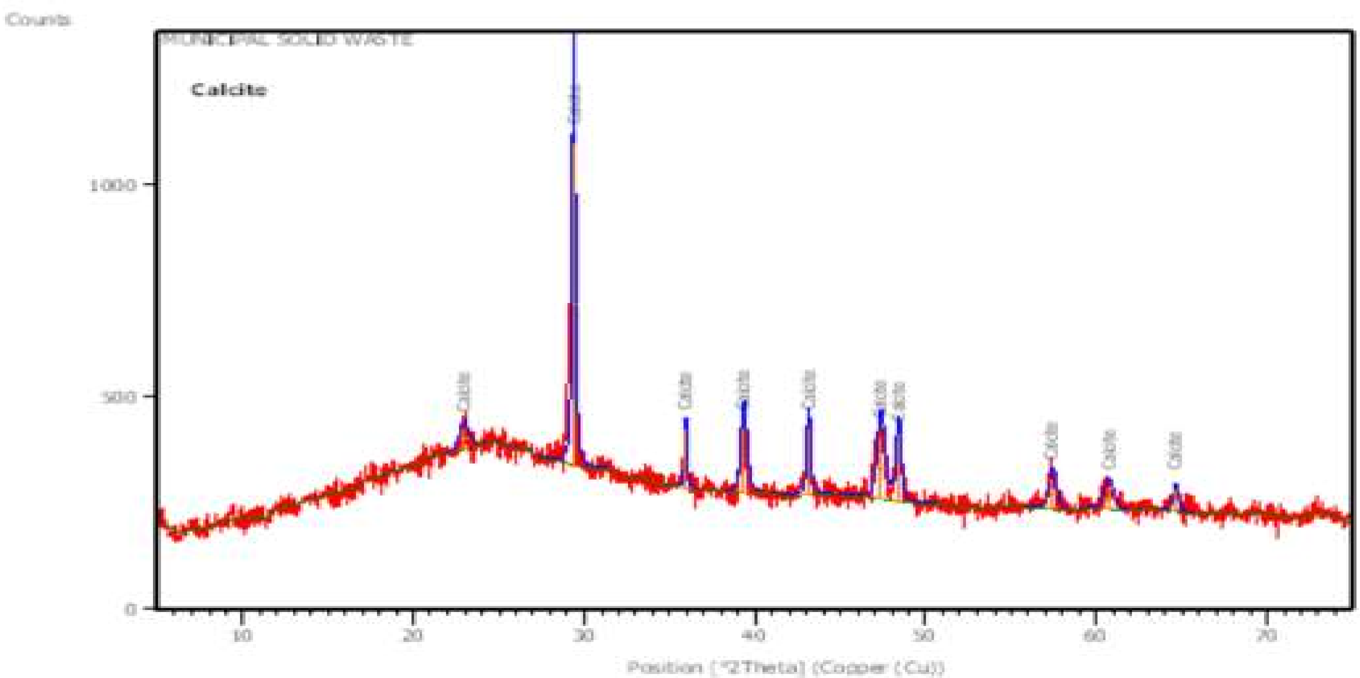

Figure 1: X-ray diffraction pattern for MSW(sawdust, sugarcane bagasse, orange peel)

The XRD pattern for MSW is in Figure .1. The crystallographic parameter are crystal system calcite(rhombohedral) with space group of R-3C and space group number of 167.The sample exhibits four prominent peaks at (2 θ) value of 24^0,29.5^0, and 58.5^0.peak 58.5^0 is in amorphous area and the remaining are in crystal area.

3.3 SEM/EDX Analysis

The SEM uses a focused beam of high energy electrons to generate a variety of signals at the surface of the solid sample.The signals that derive from electron sample interaction reveal information about the sample including texture, chemical composition and crystalline structure.The EDX shows the elemental composition of the fuel samples.

3.3.1 The Morphological analysis of carbonized MSW.

The carbon Biochar were subjected to scanning electron microscope (SEM) to obtain more understanding on the structures and size distributions of the carbon sample. Figures 2 show the SEM structure for the biomass carbon obtained after pyrolysis. The morphology of the samples was determined by Scanning Electron Microscope (SEM) and then the graded composition was analysed by energy dispersive X-ray dispersion (EDX).

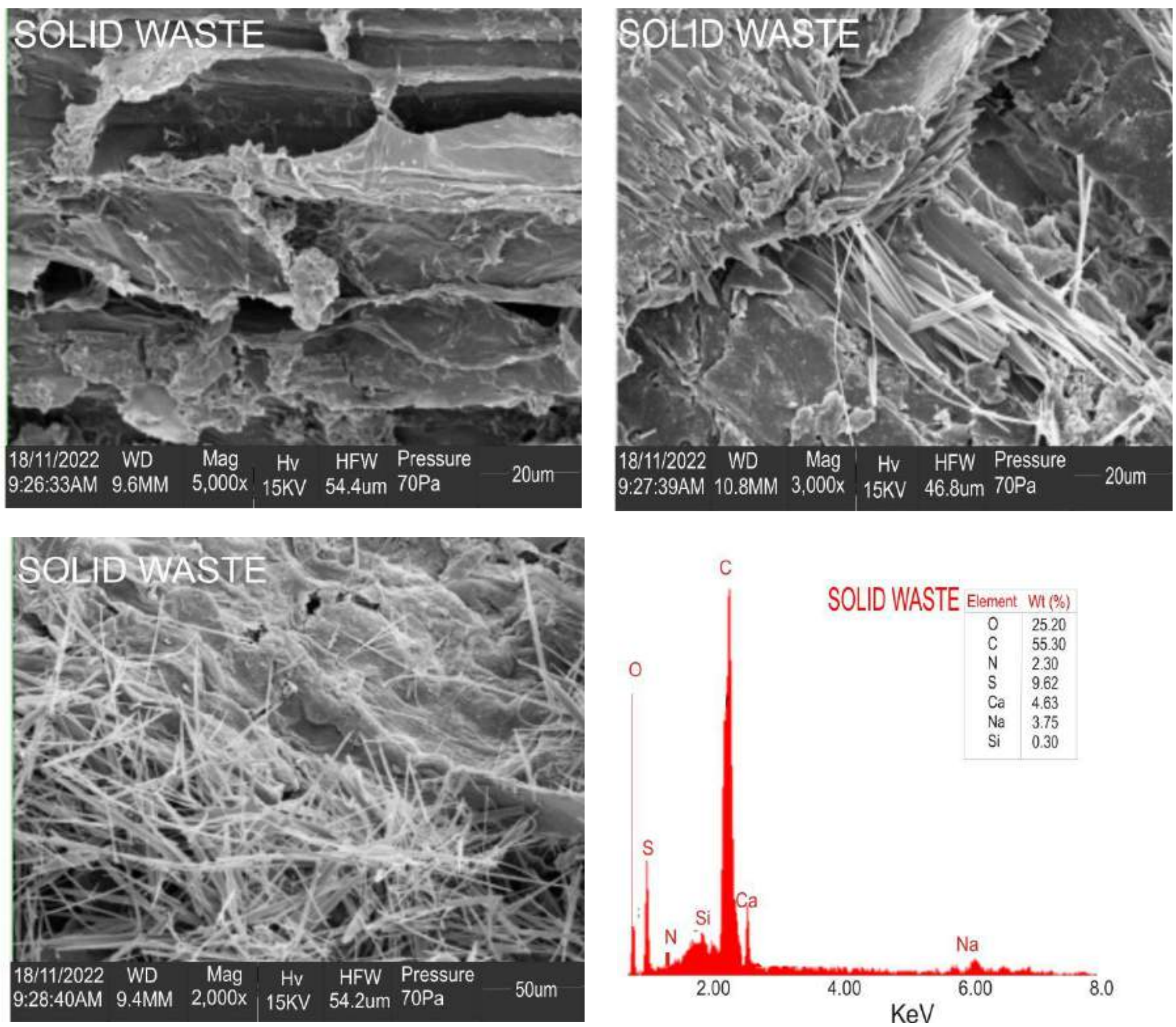

Figure 2 SEM/EDX of MSW carbon at 5000_x,3000_x and 2000_x magnification.

Figure 2 gives the morphological structure of carbonized sawdust at 500^{o}c under 5000,3000 and 2000 times magnification.The SEM micro-graph indicate that MSW is very rich in fine particles with non uniform but well developed pore structure.These features could be as a result of surface area because when the porosity increases the surface area also increase. The EDX shows the elemental composition of the fuel sample. The sawdust consist of C, O,N,S,Ca, Na and Si with a corresponding weight percent of 55.30%,25.20%,2.30 %, 9.62%,4.63%,3.75%,0.30%.

4.1 Conclusion

Municipal solid waste biochar were prepared using using a pyrolyzer at around 500 ^{0}c. the proximate and ultimate analysis was done. SEM/ EDX and XRD analysis was performed for the pyrolysed carbon which served as fuel in the DCFC. The scanning electron micrograph and X-ray diffraction reveals that the carbon fuels contain large sized particles with the highest peak of 29.6^o with corresponding d-spacing of 3.42 Å. The composition of MSW shows that there is possibility of utilizing municipal solid waste as fuel in direct carbon fuel cell(DCFC) due to having carbon content of 55.30 wt(%). The XRD and SEM/EDX results shows that these materials can be used in direct carbon fuel cell for conversion of the electrochemical properties to power generation due to amorphous carbon present. This work will prevent environmental degradation and contribute to renewable energy sustainability.

References

[1] Aleluia, J., & Ferrão, P. (2016). Characterization of urban waste management practices in developing Asian countries: A new analytical framework based on waste characteristics and urban dimension. *Waste Management*, 58, 415-429.
[2] Adeniyi, O. D., Ewan, B. C., Adeniyi, M. I., & Abdulkadir, M. (2014). The behaviour of biomass char in two direct carbon fuel cell designs. *Journal of Energy Challenges & Mechanics (JECM)*, *1*(4), 6.
[3] Axon, S. (2017). “Keeping the ball rolling”: Addressing the enablers of, and barriers to, sustainable lifestyles. *Journal of Environmental Psychology*, 52, 11-25.
[4] Bishoge, O. K., Huang, X., Zhang, L., Ma, H., & Danyo, C. (2019). The adaptation of Waste to Energy Technologies: towards the conversion of Municipal Solid Waste into a renewable energy resource. *Environmental Reviews*, 1, 1-22
[5] Cooper, J.F., & Berner, K. (2005). The carbon/air fuel cell, conversion of coal-derived carbons” in: The Carbon fuel Cell Seminar, Palm Spring, CA, Nov. 14th, UCRLPRES-216953, 1-16.
[6] Cooper, J.F., & Cherepy, N. (2008). Carbon fuel particles used in direct carbon conversion fuel cells. US Patent Publication, No. US 2008/0274382 A1.
[7] Elleuch, A., Boussetta, A., Yu, J., Halouani, K., & Li, Y. (2013). Experimental investigation of direct carbon fuel cell fueled by almond shell biochar: part I. Physico-chemical characterization of the biochar fuel and cell performance examination. *International Journal of Hydrology Energy,* 38(36), 16590e16604.
[8] Elleuch, A., Halouani, K., & Li, Y. (2015). Investigation of chemical and electrochemical reactions mechanisms in a direct carbon fuel cell using olive wood charcoal as sustainable fuel. *Journal of Power Sources,* 281, 350-361.
[9] Hamad, T. A., Agll, A. A., Hamad, Y. M., & Sheffield, J. W. (2014). Solid waste as renewable source of energy: current and future possibility in Libya. *Case Studies in Thermal Engineering,* 4, 144-152.
[10] Omari, A. M., (2015. Characterization of Municipal Solid waste for Energy recovery-a case study of Arusha, Tanzania. *Journal of Multidisciplinary Engineering Science & Technology*(JMEST),2 . ISSN:3159-0040
[11] Omisore, A. G. (2018). Attaining sustainable development goals in sub-Saharan Africa; The need to address environmental challenges. *Environmental Development*, 25, 138-145.

[12] Pichtel J. (2014). Waste Management Practice: Municipal, Hazardous, and Industrial. Second Edition. ISBN.978100762648.

[13] Raju, C. A., Jyothi, K. R., Satya, M., & Praveena, U.(2014). Studies on development of fuel briquettes for household and industrial purpose. *International Journal of Research in Engineering and Technolog,y* 3(2), 54-63.

[14] Xiangling, T., Xin, L., & Yineng, O. (2016). Spatial and temporal variation of extreme climate events in Xinjiang, China during 1961-2010. *American Journal of Climate Change .5 (3).*

[15] Zhan, H., Zhuang, X., Song, Y., Yin, X., Cao, J., Shen, Z., & Wu, C. (2018). Step pyrolysis of N-rich industrial biowastes: Regulatory mechanism of NO x precursor formation via exploring decisive reaction pathways. *Chemical Engineering Journal*, 344, 320-331.

[16]Kacprzak, A., Kobyłecki, R. & Bis, Z. (2017). The effect of coal thermal pretreatment on the electrochemical performance of molten hydroxide direct carbon fuel cell. Journal of Power Technologies 97 (5) (2017) 382–387.

NIPES-NCEE Conference Proceedings
The 2nd International Conference 15th-17th Feb. 2023
321-336
www.nipesjournals.org.ng

AIR CONDITIONING SYSTEM COMPARISON OF FUZZY LOGIC AND NEURO FUZZY ALGORITHMS

[1]Francis. M., [2]Raymond. J., [3]Bello M. A and [4]Muhammad S.

1Department of Mechanical Engineering, Faculty of Engineering, Federal Polytechnic Kaltungo, Gombe, Nigeria, maxwellkamo4life@gmail.com; +2348069707263
2Department of Telecommunications Engineering, Air force Institute of Technology, Kaduna, Nigeria, raymondjerry5@gmail.com; +23487034261116
3Department of Mechanical Engineering, Faculty of Engineering, Federal Polytechnic Kaltungo Gombe, Nigeria, abuhafsah3491@gmail.com +2348139000461
2Department of Mechanical Engineering, Faculty of Engineering, Federal Polytechnic Kaltungo Gombe, Nigeria, muhammads342@gmail.com; +2348162585765

Abstract
Fuzzy logic and neuro- fuzzy controls are commonly used to improve the performance of an air conditioning system. Two logics, fuzzy logic and neuro- fuzzy logic, were designed and used in this work. A set of rules was proposed that used two input variables, temperature and humidity and one output variable, the compressor Speed. A fuzzy logic and neuro- fuzzy comparison of the system's simulated results was used to see which of the two produced the best results.

***Key words**: (Air Conditioning System, Fuzzy Logic Algorithsm and Neuro Fuzzy Algorithsm)*

1.0 Introduction

Nowadays, Homes and public enclosed spaces are where air conditioning systems mostly found to create comfortable environment [1].

An air conditioner (often referred to as AC) is a home appliance, system, or mechanism, designed to remove heat energy from a space or building to maintain a desired air temperature that would otherwise not be achieved due to heat flows (heat gain) from interior heat sources and the exterior environment. It is a system that must achieved four objectives simultaneously. These objectives are: control of air temperature; control of air humidity; control of air circulation; and control of air quality ASHRAE (2008). Air conditioning system has advanced to integrated industry including environment, energy, machinery, electronics, and automatic control technology, so that its several major trends of development would be health, environmental protection, energy saving, intelligence and diversity [2].

There are some methods of controllers that have been developed. There are conventional control and intelligent control. There are advantages and limitations for each, some methods are often combined others to provide better performance.

Fuzzy logic is a rigorous mathematical field, and it provides an effective vehicle for modeling the uncertainty in human reasoning. In fuzzy logic, the knowledge of experts is modeled by linguistic rules represented in the form of IF-THEN logic [3]. Fuzzy Logic controller forms the base of the fuzzy control system. It basically consists of the heuristics rules those define parameters of the problem [4]. It consists of:

- Data Base: it normalizes the input crisp values and contains the fuzzy partitions of the input and output.
- Fuzzy rule base: it contains the type of fuzzy rules, source and derivation of the fuzzy

control rules.

- Fuzzy Inference machine: the basic function is to compute the overall output variable based on the individual contribution of each rule in the fuzzy rule base.
- Defuzzification: it converts the set of modified control output values into single point wise (crisp) value and denormalizes the output onto its physical domain.

One of the key issues of the fuzzy logic management is that the problem of selection and style of membership functions for a given downside.

Neural networks provide the likelihood of finding the matter of standardization. Neural fuzzy systems will generate formal logic rules and membership functions for advanced systems that a standard fuzzy approach could fail. Hence, combining the adaptive neural networks and formal logic management forms a system known as neuro-fuzzy system.

Neuro-fuzzy system is based on the neural network that learned from fuzzy if-then rules. Neural network performance is dependent on the quality and quantity of training samples presented to the network. Neural nets can solve many problems that are either unsolved or inefficiently solved by existing techniques, including fuzzy logic [5,6].

Given the limited availability of power in Nigeria, energy consumption in an air conditioning system is a critical area to focus on when designing the air conditioning system in order to ensure thermal comfort. The increased use of air conditioners conforms to an increase in electrical power consumption [7]. Air conditioning systems consume 90% of energy [8]. When input variables are considered, the functioning of the A C can be greatly modified, minimizing power consumption in the AC compressor/fan while making effective use of available resources [9].

In this work, a design for an air conditioner system was carried out using fuzzy logic and the neuro fuzzy method, with two input parameters (Temperature and Humidity) and one output variable (compressor speed) for each, and the simulation result was carried out.

The aim is to compare the simulation results of each system using fuzzy logic and neuro fuzzy management to figure out which is better.

2.0 Methodology

2.1 Fuzzy Logic control Algorithm

The major components of Fuzzy Logic Control are input and output variables, fuzzification, inference mechanism, fuzzy rule base and deffuzification [10,11]. The fuzzy input variables are the Temperature, Humidity while the output variable is the compressor speed. Figure 1 is the Fuzzy Logic Designer. Base on these inputs, an output signal is sent to control the compressor speed. The range at which the membership functions are described is 0 to 38 degrees celcius for temperature, 0% to 100% for humidity. The temperature and humidity range used for this design is for 25 days for the month of March, 2022, and the Data is collected from Nigerian meteorological department (NIMET), Maiduguri, Borno state. In the design, the temperature and humidity has five triangular membership functions each as shown in figure 2 and figure 3 those membership function are use to fuzzify the crisp input. Figure 5, shows the output (compressor speed) membership functions namely off, low, medium High. The principles base for coming up is as "If temperature is very cold AND humidity is dry THEN compressor speed is off. The rules base for the design is shown in table 1

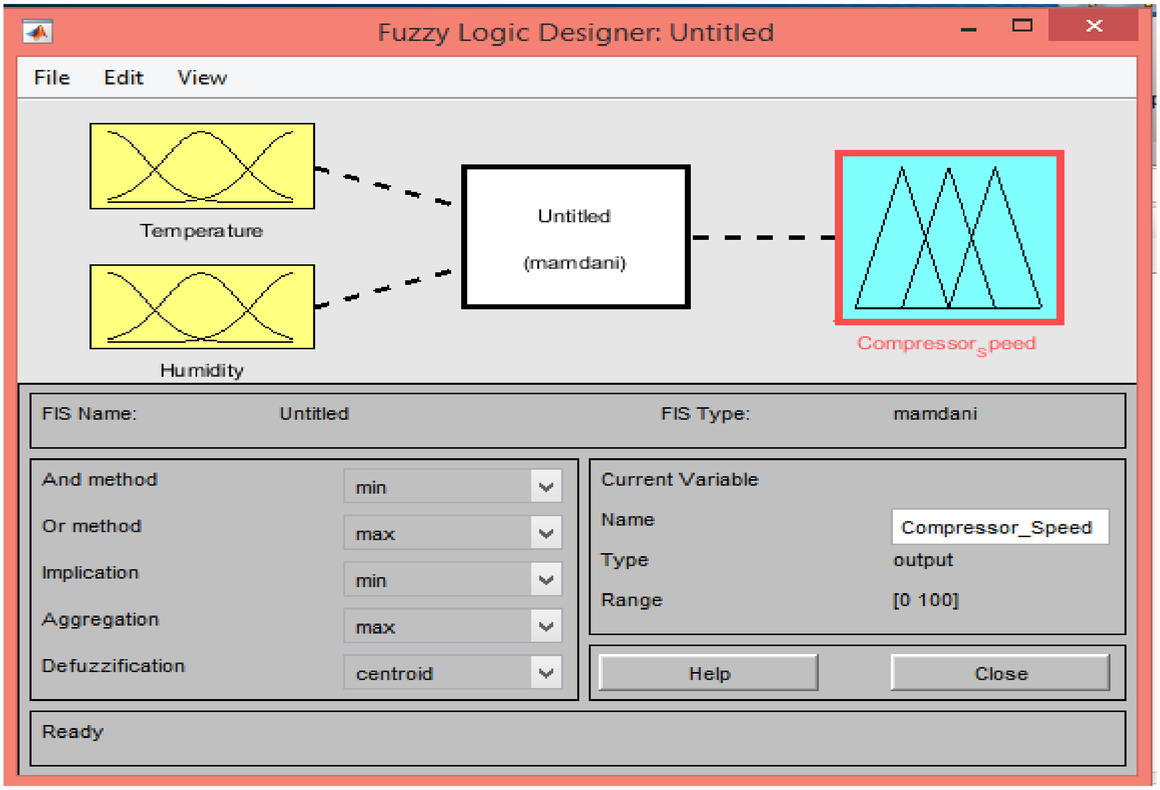

Figure 1: Fuzzy Logic Designer

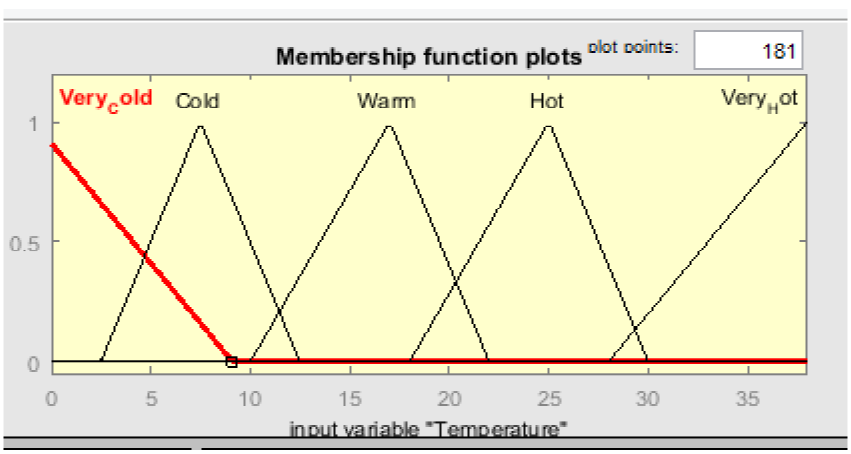

Figure 2: Temperature Membership Function

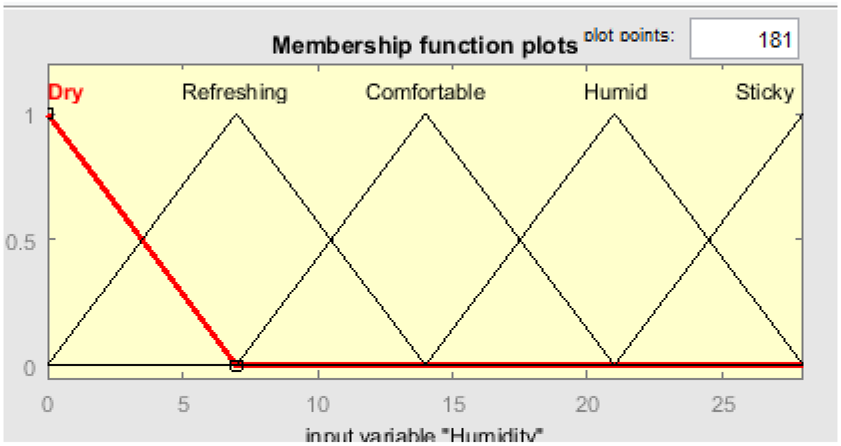

Figure 3: Humidity Membership Function

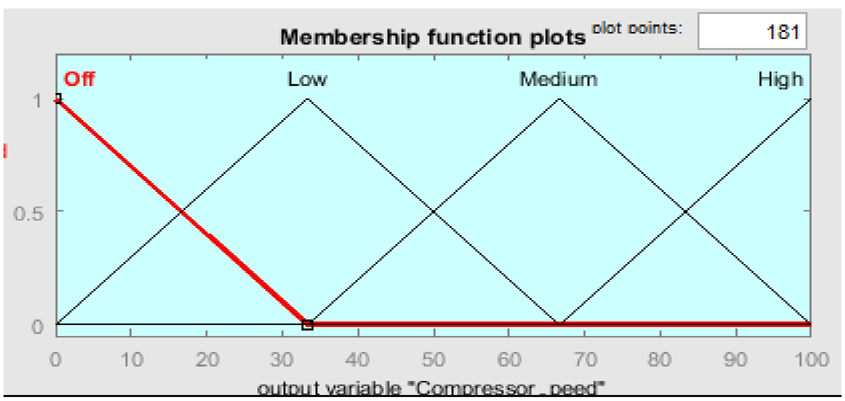

Figure 5: Compressor Speed Membership Function

Table 1: Fuzzy rules for proposed design

Rules	Input		Output
S/N	Temperature	Humidity	Compressor Speed
1	Very cold	Dry	Off
2	Very cold	Refreshing	Off
3	Very cold	Comfortable	Off
4	Very cold	Humid	Off
5	Very cold	Sticky	Low

6	Cold	Dry	Off
7	Cold	Refreshing	Off
8	Cold	Comfortable	Low
9	Cold	Humid	Low
10	Cold	Sticky	Medium
11	Warm	Dry	Medium
12	Warm	Refreshing	Medium
13	Warm	Comfortable	Low
14	Warm	Humid	Medium
15	Warm	Sticky	Medium
16	Hot	Dry	Low
17	Hot	Refreshing	Medium
18	Hot	Comfortable	Medium
19	Hot	Humid	High
20	Hot	Sticky	High
21	Very Hot	Dry	Medium
22	Very hot	Refreshing	Medium
23	Very hot	Comfortable	Medium
24	Very hot	Humid	High
25	Very hot	Sticky	High

2.2 Neuro-Fuzzy Algorithm

Neuro-fuzzy management, which is primarily based on an air conditioning system, also comprises two inputs: Temperature, and Humidity.

The temperature input is named "input1," and the range is set to 24°C to 38°C for the membership function, as shown in Figure 6.

Similarly, in figure 7, the input, humidity, is termed "input2" and the range is set to 14-30% for the membership function. The output and compressor speeds are renamed "output1" (Out1) as shown in figures 8.

For the design of the ANFIS model, selections of the following listed parameters were made.

- Membership function type
- Number of membership function
- Learning algorithm
- Epoch Size
- Data size
- Number of input variable

The listed procedure below was adopted at the ANFIS graphical user (GUI) for the design of the model.

- Obtaining training data
- Data sizing
- Data partitioning
- Loading data sets
- The ANFIS modeling criterion was adopted to effectively tune the membership function so as to minimize the output error and maximize performance index. The ANFIS structure obtained by the aforementioned parameters chosen is shown in Figure 9 while figure 10 represents the Neuro Fuzzy dialog box for rule editor.

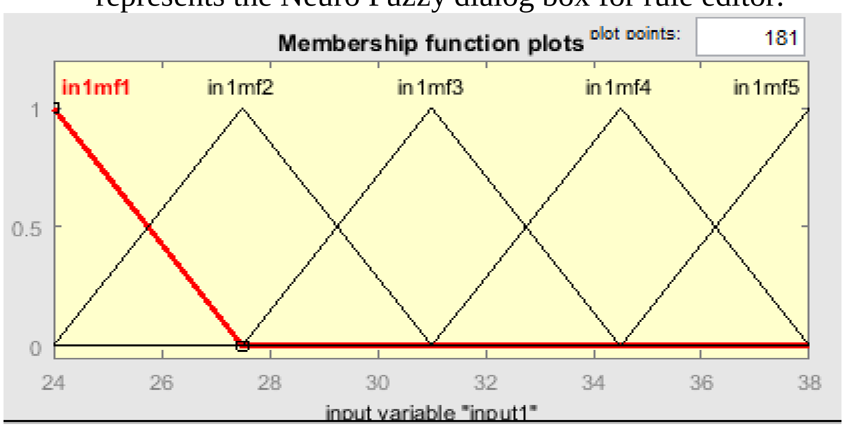

Figure 6: Input 1 Membership Function

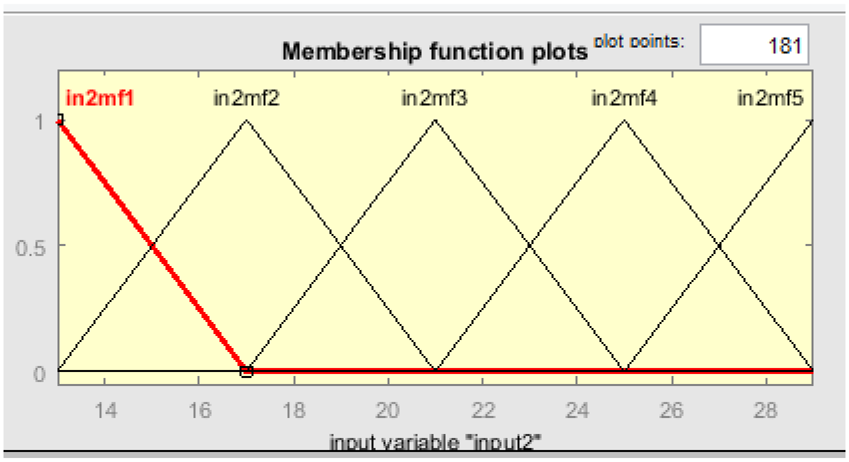

Figure 7: Input 2 Membership Function

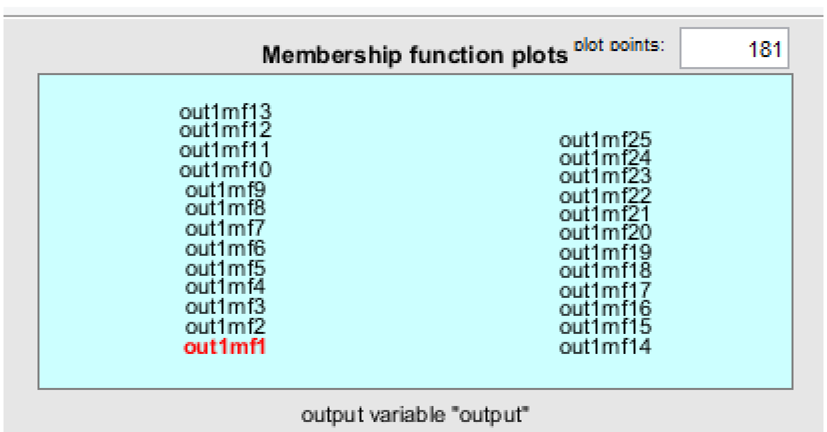

Figure 8: Output Membership Function

NIPES-NCEE Conference Proceedings
The 2nd International Conference 15th-17th Feb. 2023
321-336
www.nipesjournals.org.ng

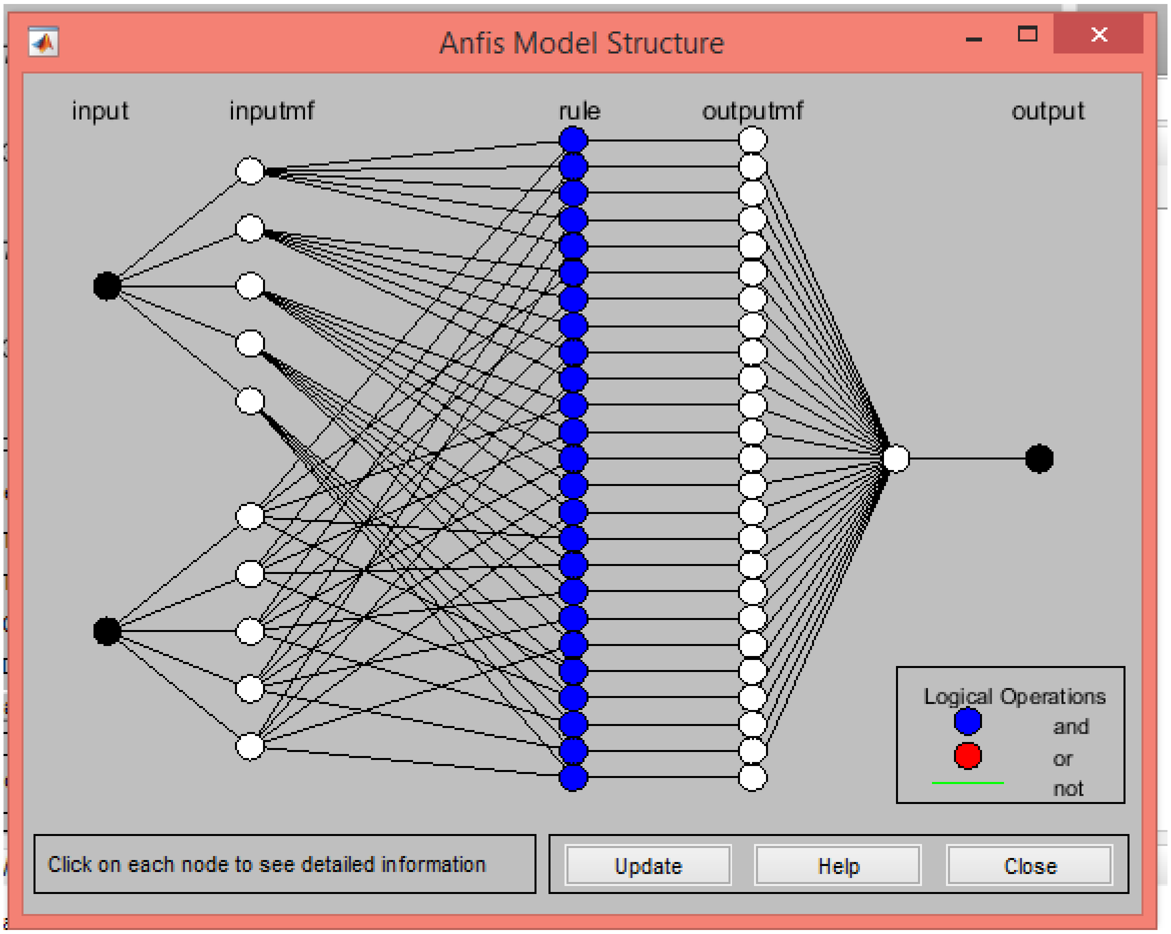

Figure 9: ANFIS models Structure for 2 Input

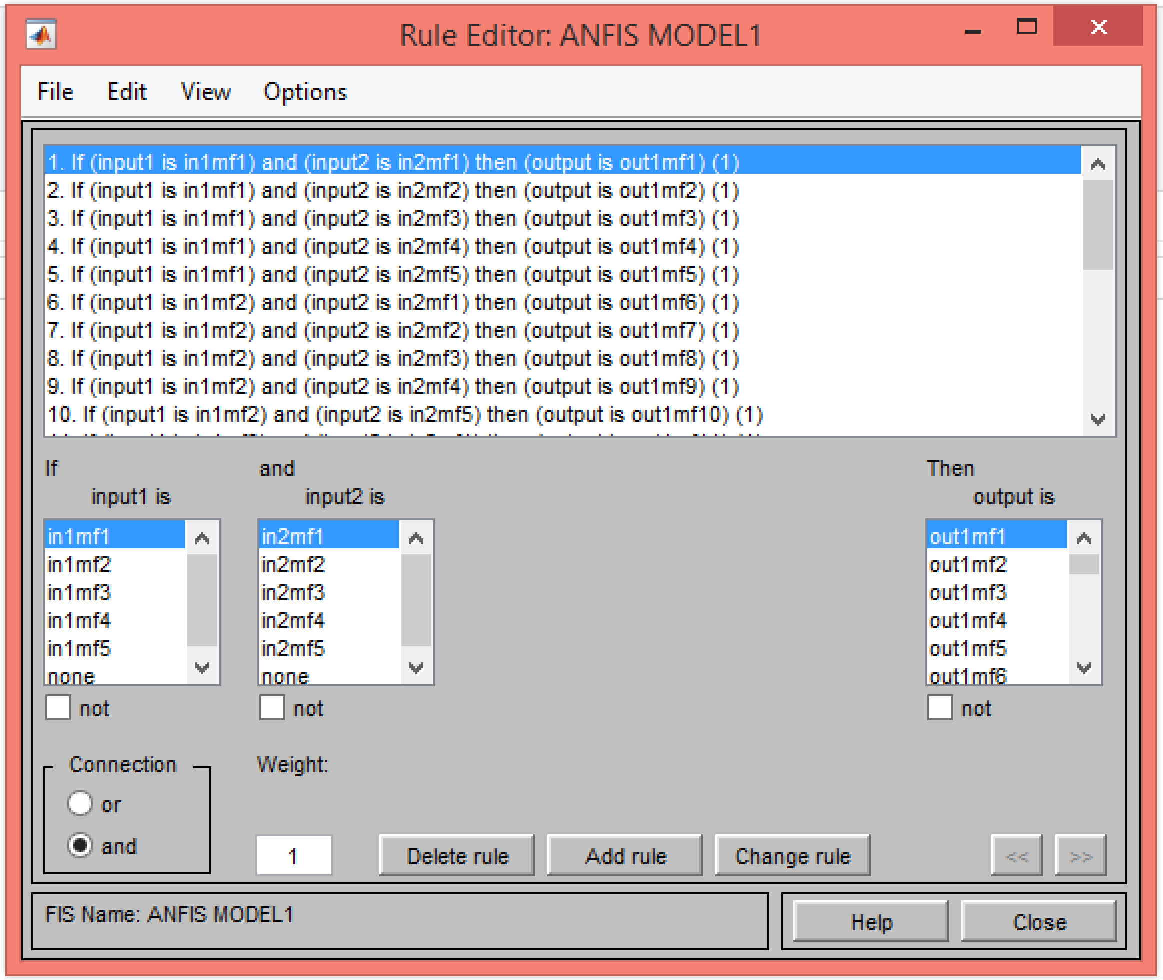

Figure 10: Neuro Fuzzy Dialog box for the Rule Editor

3.0 Results and Discussion

3.1 Experimental Results

3.1.1 Fuzzy Logic control Algorithm Simulation

The air conditioning system's results are simulated using the Mat lab Fuzzy logic tool box, which includes graphic user interface (GUI) tools.

The FIS editor, Membership Function editor, rule editor, rule viewer, and surface viewer are among the available tools.

The following are the simulation results for the fuzzy logic control base air conditioning system:

Figure 11 illustrates a surface viewer graph of humidity vs. temperature vs compressor speed.

Figure 12 illustrates a surface viewer graph temperature vs Humidity vs compressor speed.

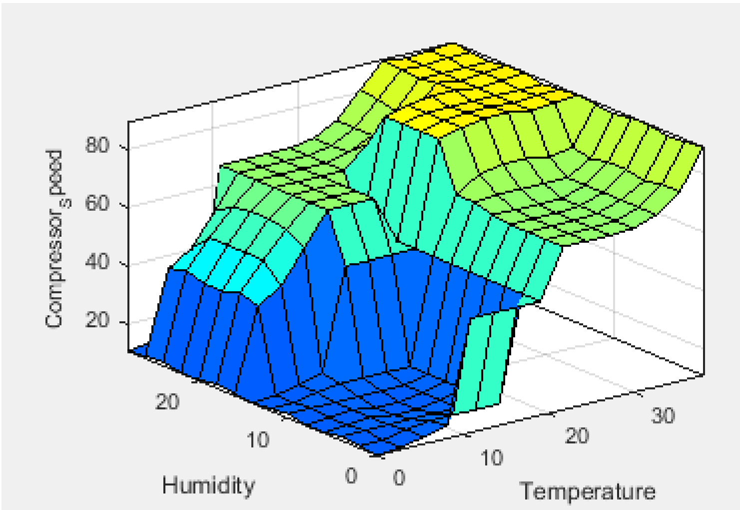

Figure 11: Surface viewer graph of No. of Humidity Vs Temperature Vs Compressor Speed

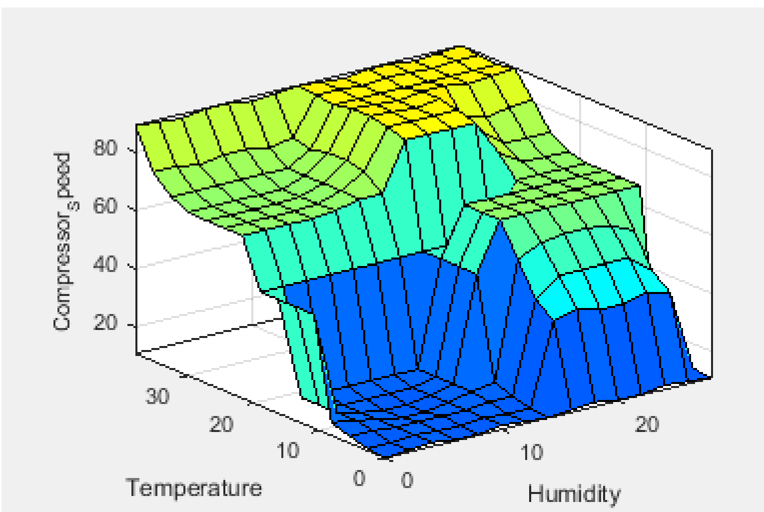

Figure 12: Surface viewer graph of No. of Temperature Vs Humidity Vs Compressor Speed
Figure 13 and 14 represents rule viewer with temperature at 38 and 31degree celcius and humidity of 21 each respectively.

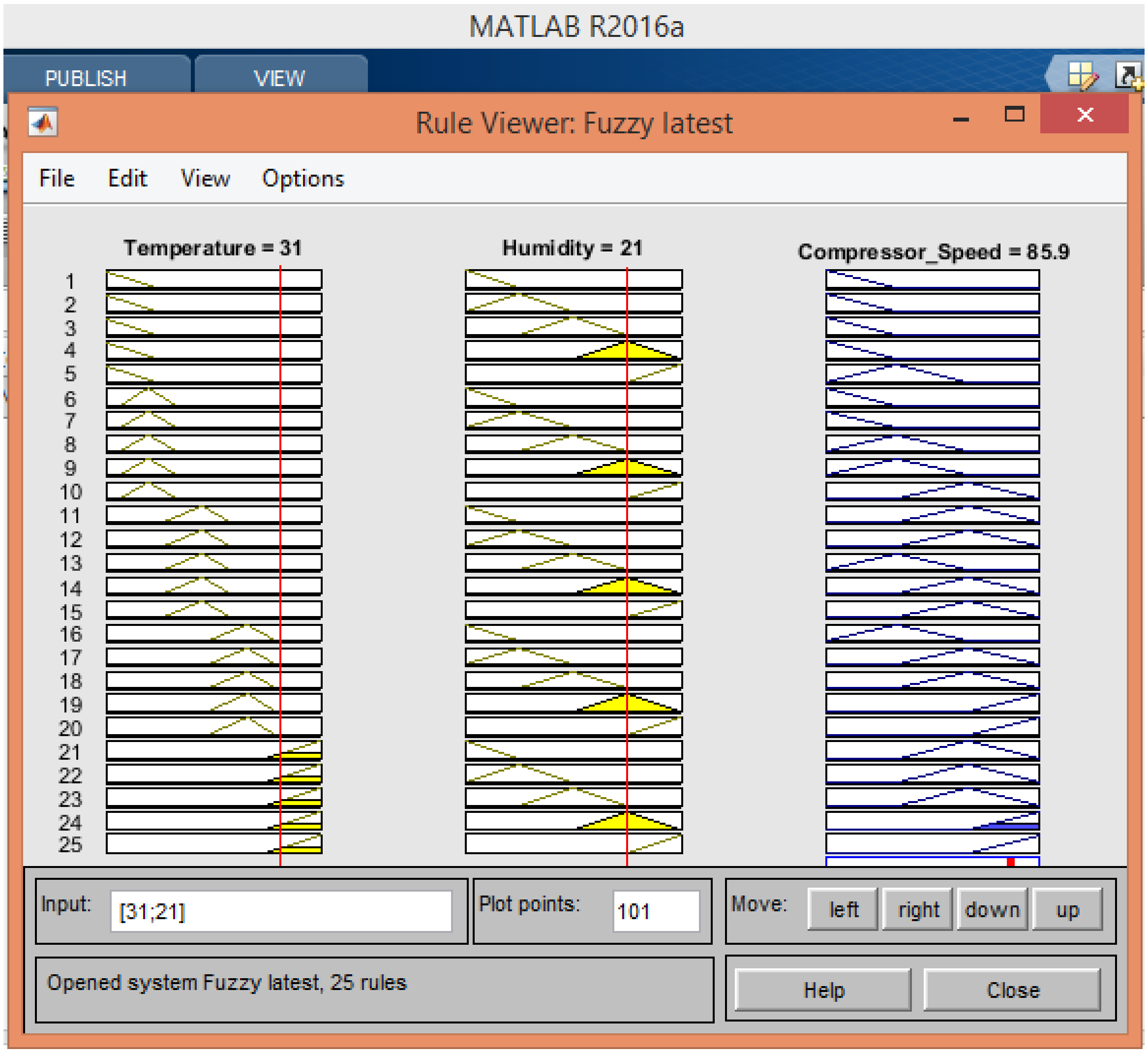

Figure 13: Rule viewer with Temperature at 31 degree celcius and 21% Humidity

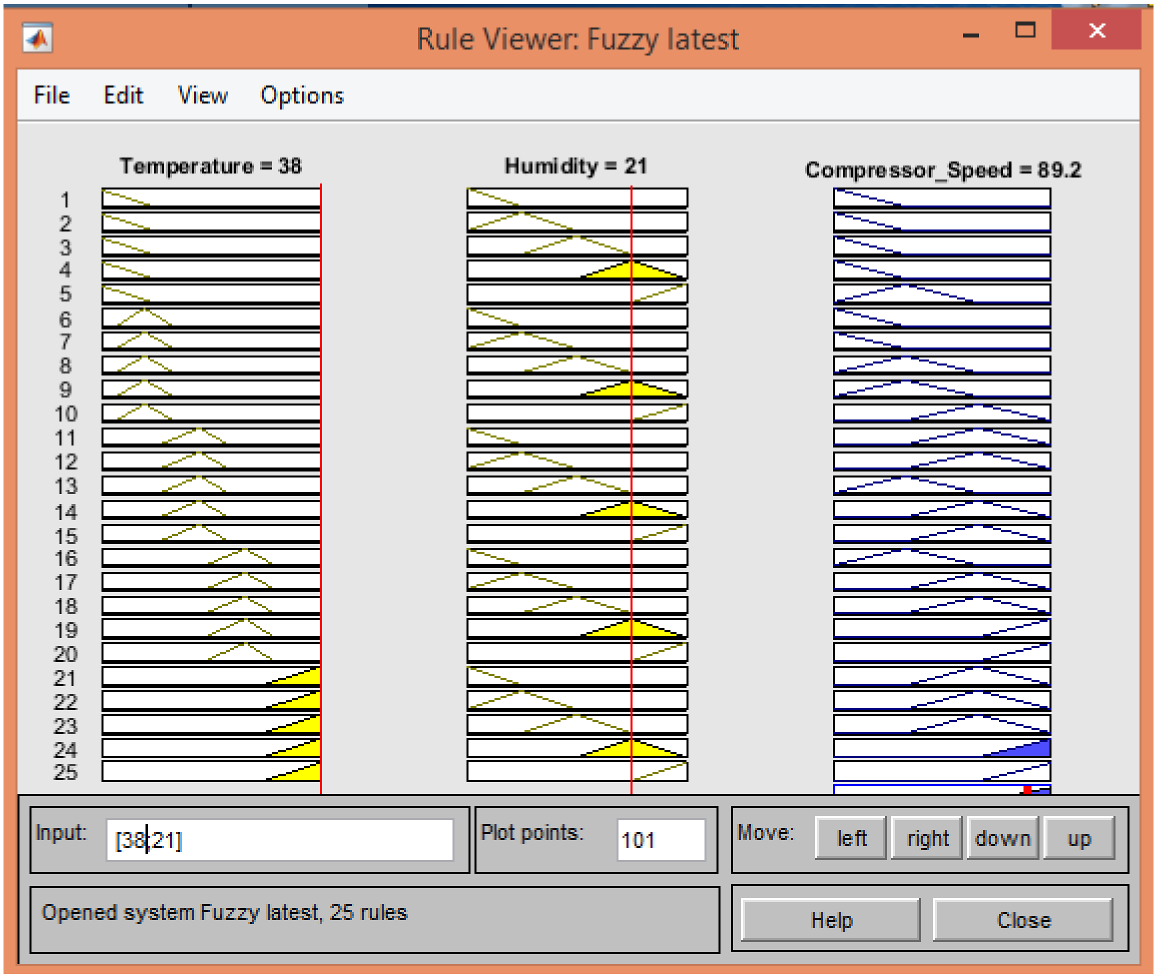

Figure 14: Rule viewer with Temperature at 38 degree celcius and 21% Humidity

3.1.1 Neuro-Fuzzy Algorithm Simulation

Neuro-fuzzy control based air conditioning system simulation results are shown in figure 15, 16, 17 and 18.

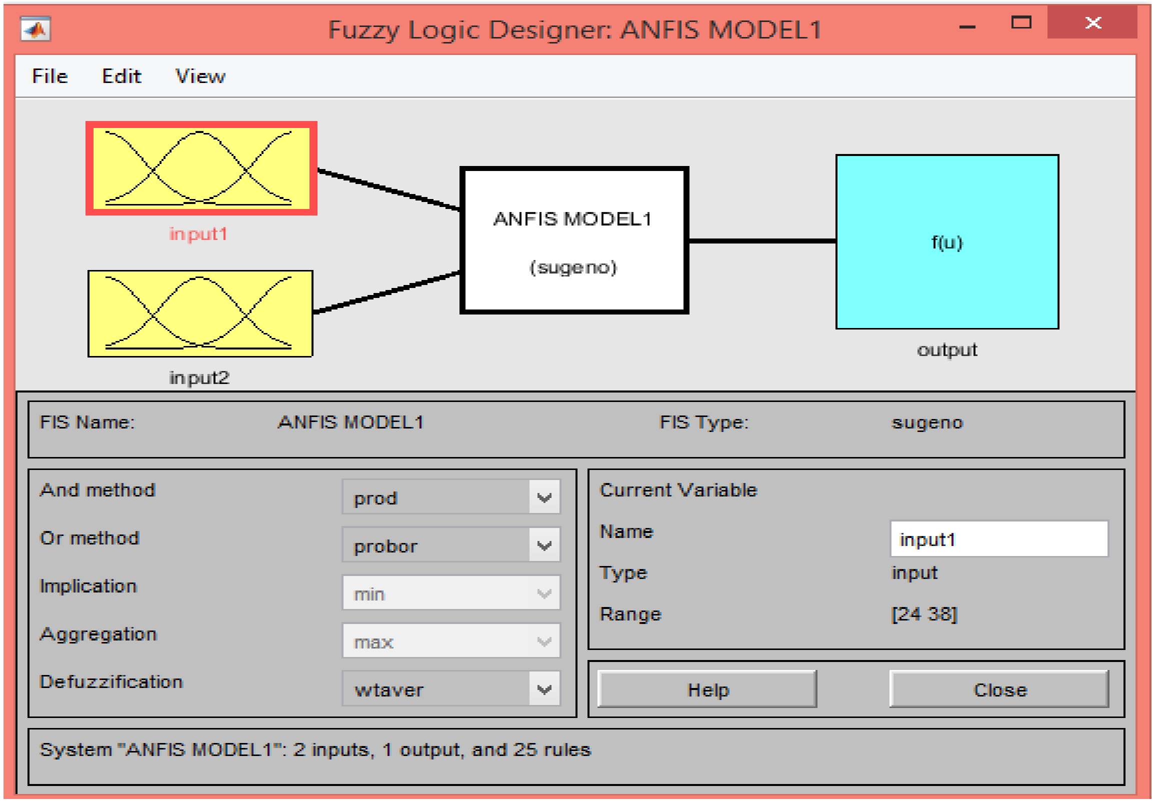

Figure 15: Fuzzy ANFIS Designer

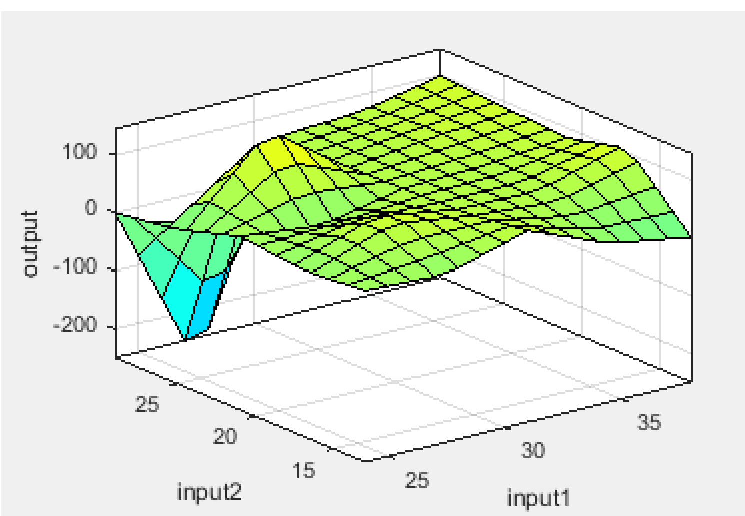

Figure 16: Surface viewer graph of No. of Input2 (Humidity) Vs Input1 (Temperature) Vs Output (Compressor Speed)

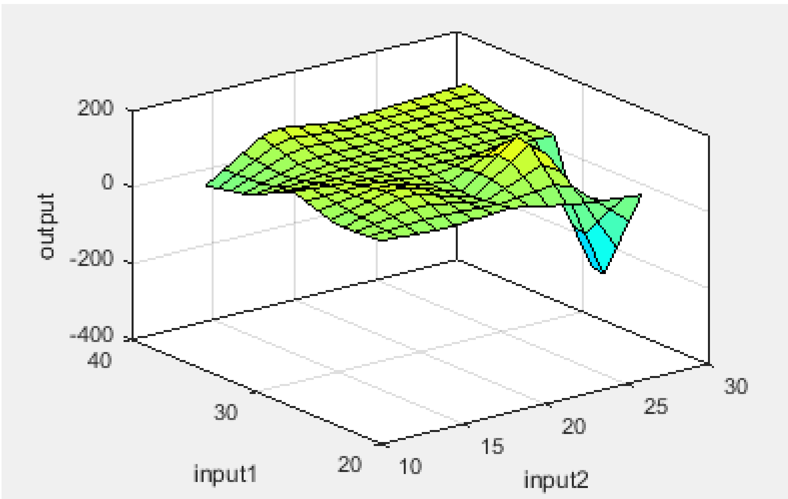

Figure 17: Surface viewer graph of No. of Input1 (Humidity) Vs Input2 (Temperature) Vs Output (Compressor Speed)

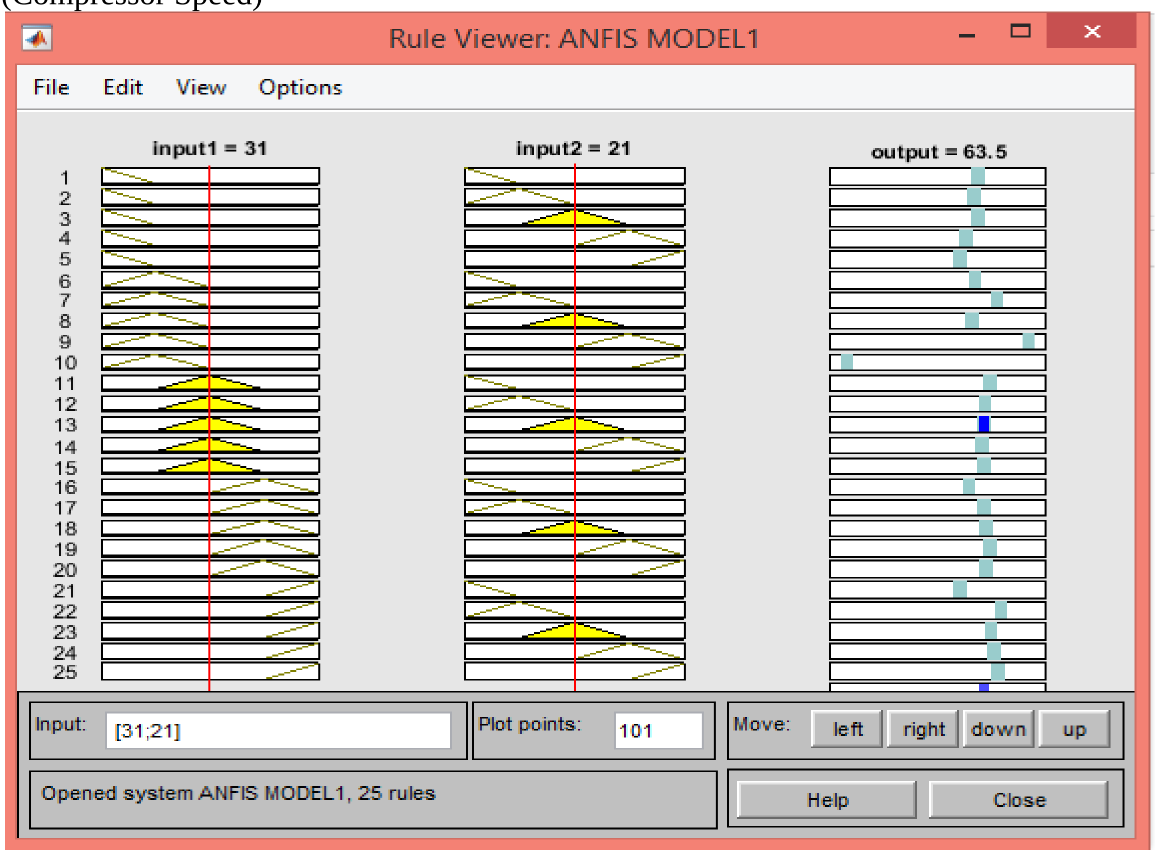

Figure 18: ANFIS Rule viewer with Temperature at 31 degree celcius and 21% Humidity

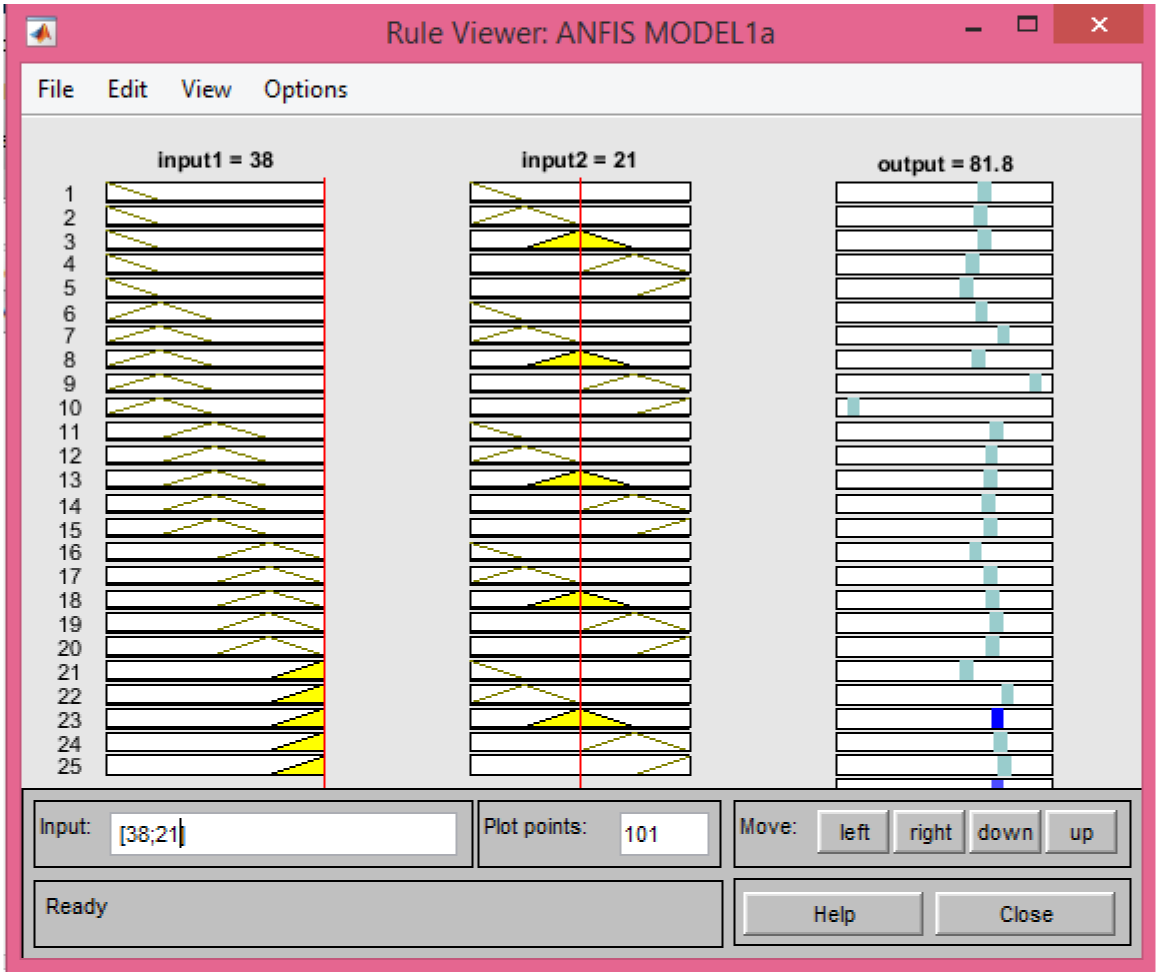

Figure 19: ANFIS Rule viewer with Temperature at 38 degree celcius and 21% Humidity

3.2 Discussion of Results

The simulation results show that the neuro fuzzy algorithm provides better control than the fuzzy logic algorithm. The compressor speed in the fuzzy logic control base design at 31 degree celcius, 21% humidity is operating at 85.9% while Neuro fuzzy is operating at 63.5%. Also at 38 degree celcius and 21% humidity, fuzzy logic algorithm output is operating at 89.2% while Neuro fuzzy is operating at 81.8%. Therefore, from the results, it is evident that neuro fuzzy provide proper output and save energy as compared with fuzzy logic algorithm.

4.0 Conclusion

The simulation has shown that the performance of the neuro-fuzzy compressor is significantly better than that of the fuzzy logic compressor; the neuro-fuzzy makes the system adaptive to the room environment and weather. It produces good results while utilizing less electricity than fuzzy logic.

References

[1] Ashrae-Handbook, *HVAC Systems and Equipment.* ASHRAE Publications, 2008.

[2] Nasution, H. Jamaluddin, H. and Syeriff J. M. (2011). “Energy analysis for air conditioning system using fuzzy logic controller”, TELKOMNIKA, Vol. 9, Issue No.1
NIMET, Nigerian Meterological Department, Maiduguri, Borno State, Nigeria

[3] Du M., Fan,T., Su, W. and Li, H. (2008). “Design of a new practical expert fuzzy controller in central air conditioning control system”, IEEE Pacific-Asia Workshop on Computational Intelligence and Industrial Application

[4] Dash S. K. and Mohanty, G. (2012). “Intelligent Air Conditioning System using Fuzzy Logic,” Int. J. Sci. Eng. Res., vol. 3, no. 12, pp. 1–6

[5] Saepullah A . (2015). “Comparative Analysis o f Mamdani, Sugeno an d Ts u k amoto Method of Fuzzy Inference System for Air Conditioner Energy Saving ,” J. Intell. Syst., vol. 1, n o. 2, pp. 143–147

[6] Islam,M.S., Sarker, Z.,AhmedRafi,K.A.,Othman,M. (2006). Development of a fuzzy logiccontroller algorithm for air conditioning system. ICSE proceedings.

[7] Batayneh, W., Al-Araidah, O., Bataineh, K. (2010). Fuzzy logic approach to provide safe and com-fortable indoor environment. Int. J. Eng. Sci. Technol.2(7)

[8] Abbas, M., Khan, M.S., Zafar, F. (2011). Autonomous room air cooler using fuzzy logic control system. Int. J. Sci. Eng. Res.2(5), 74–81

[9] Hamidi, M., Lachiver,G. (1998). Fuzzy control system based on the human sensation of thermal comfort. Fuzzy systems proceedings, 1998. IEEE world congress on computational intelligence, the IEEE international conference, vol.1

[10] Pasino, K.M., Yurkovich, S. (1998). Fuzzy Control. United State of America: Addison Wesley;

[11] Yue, W., Biaobiao, Z., Jiabin, L., and K. -L. D. (2011). Fuzzy Logic and Neuro-fuzzy Systems: A Systematic Introduction. International Journal of Artificial Intelligence and Expert Systems (IJAE), Volume (2) : Issue (2)

NIPES-NCEE Conference Proceedings
The 2nd International Conference 15th-17th Feb. 2023
337-350
www.nipesjournals.org.ng

INFLUENCE OF DIFFERENT CURING CONDITIONS ON SOME PROPERTIES OF NIGERIAN BUILDING AND ROAD REASERCH INSTITUTE (NBRRI) LETERITE INTERLOCKING BRICKS

*Sule, H. J. A. B. Shehu., Moyi, Z. Nazifi, A.

Nigerian Building and Road Research Institute (NBBRI) Northwest Zonal Office Kano
*Email of the corresponding author: sulehussainijido@gmail.com

Abstract

The study aimed to determine the influence of different curing conditions on some properties of Nigerian building and road research institute (NBRRI) literate interlocking bricks. The constituent materials were tested and batched by weight, using mix ratio of 1:6, i.e., one part of cement to six parts of fine aggregate (lateritic soil) as recommended in the Nigerian National Building Code and Nigerian Building and Road Research Institute. The bricks with dimensions 250 × 130 × 220 mm3 were casted using NBRRI semi-automatic brick production machine. The bricks were cured using eight different curing conditions. The seven curing conditions used in the study are Condition "A": covering of bricks with tarpaulin with sprinkling of water twice a day (morning and evening). Condition "B": wet curing throughout (by complete immersion in portable water and covering with tarpaulin). Condition "C": complete covering with air and water tight polythene bags. Condition "D": covering with wet hessian and polythene sheet. Condition "E": keeping under dry laboratory conditions. Condition "F": keeping in open air under direct sunshine. Condition "G": keeping in open air under shed. For all other curing conditions, bricks were tested for bulk density, water absorption, durability and compressive strength at the end of every curing period. . It was concluded that the highest gain in average bulk density, water absorption, durability and compressive strength was recorded for bricks complete covered with air and water tight polythene bags. The lowest gain was recorded for the specimens cured in open air under direct sunshine. Based on results of tests, curing condition "C" is tested to be use in curing NBRRI interlocking bricks, if effective gain in strength and durability of the bricks needs to be attained.

Keywords*; Curing condition, interlocking bricks, water absorption, and compressive strength.*

1.0 Introduction

Literate brick is the simplest and most olden of all building materials that has been use for housing constructions in rural areas as well as in some urban areas for many centuries. The global nature of the economy according to [1,15,16] has increased the use of literate as a building material. Durability, relatively low cost, good sound and heat insulation, acceptable fire resistance, adequate resistance to weathering and good-looking appearance are the most acceptable properties offered by literate bricks as a building materials [2,17,18,19]. Interlocking bricks is a unique newly improved walling material designed and fabricated using cement as stabilizing agent mixed with literate soil in a predetermined proportion in order to increase strength of literate. NBRRI interlocking brick is an improved brick using NBRII technology which was designed to interlock with one another. The bricks do not require mortar usage during bricklaying work. Since they do not require mortar, the bricklaying work is faster and requires less skilled labour as the conventional blocks [3,11,13,14].

NBRRI INTERLOCKING BRICKS

Strength and durability of NBRRI literate bricks can be attained through adherence to right curing technique. Curing simply means the practise of keeping the literate bricks moist (control of temperature and moisture) so as to allow complete hydration in order to ensure gain in full durability and strength [4]. Curing should begin immediately after the finishing operation. If poor curing is adopted, the water vaporises and hydration stops, resulting in a low-strength laterite bricks. If sufficient moisture isn't retained in the curing environs, the laterite bricks won't develop extreme compressive strength, and cracking may occur. Durability of the laterite bricks may also be reduced due to inadequate hydration of the cementations material. Ambient atmospheric conditions can unfavourably affect the thermal and moisture structure of freshly casted literate bricks. Avoidance of the loss of water from the literate bricks is very significance not only because of the loss in the improvement of strength, but also because it leads to plastic shrinkage, increased permeability and reduced resistance to abrasion.

Advantages of proper curing includes, reduced permeability and attack by chemicals; prevents formation of plastic shrinkage cracks, caused by rapid surface drying; more water-tight bricks, increases abrasion resistance as the surface brick will have a higher strength and significant reduction in scaling problems. Several researchers have reported that cement-stabilised literate can be used in building and road construction [5,10,12]. The earlier study carried out by the Nigerian Building and Road Research Institute (NBRRI) involved the production of literate bricks that were used for the construction of a bungalow [6]. The mix ratio adopted for bricks production according to NBRRI standard was 1:6, i.e., one part of cement to six parts of fine aggregate (lateritic soil). NBRRI suggested the following minimum specifications as requirement for literate bricks, a bulk density of 1810 kg/m^3, water absorption of 12.5%, a compressive strength of 1.65 N/mm^2 and a durability of 6.9% with a maximum cement content fixed at 5%.

NIPES-NCEE Conference Proceedings
The 2nd International Conference 15th-17th Feb. 2023
337-350
www.nipesjournals.org.ng

Curing of literate bricks and concrete according to Leet and Bernal (1997) can be influenced by continuous spraying water over the literate bricks, covering the literate bricks and with water proofing sheets, spraying with coatings or leaving forms in place and covering the exposed surface. Shetty (2005), summarized that, water curing is subdivided into pounding, wet covering, immersion, spraying or fogging, membrane curing and application of heat. An additional means of curing is called water barrier method. The methods used include covering the surface of the literate bricks and concrete with overlapping polyethylene sheeting.

To ensure effective curing of stabilized interlocking bricks, Adams (2001) suggested the use of tarpaulin to shield green bricks for twenty-four hours, before uncovering temporarily to permit for watering twice a day (morning and evening), for 28 days. However, the method of curing described above requires a lot of water for curing and cannot be practice effectively where there is shortage of portable water, which is normally the situation in most rural communities in Nigeria.

According to Nader, Shebang, and Shayanfar (2017), on their work. ‘‘Comparison of different curing effects on concrete strength’’. The curing regimes employed were: immersion in drinking water; covering with wet hessian and polythene sheet; keeping under dry laboratory conditions; keeping in open air; curing compound and steam curing. Except for steam curing system, the specimens of which were tested at the age of three days, for all other curing conditions, the compression tests were performed at the age of 28 days. It has been found that the curing system greatly influences the concrete strength. While the highest gain in compressive strength was recorded for cubes covered with wet Hessian and polythene sheet, the lowest gain in compressive strength was recorded for the specimens’ cure using steam curing.

2.0 Materials and Methods

2.1 Materials

Materials used in the production of interlocking bricks comprises of laterite, cement and water.

Cement: The cement used is the Ordinary Portland Cement (Dangote Cement) with properties conforming to BS 12 [6,7,8]. The brand of cement was obtained from kofar ruwa market in Kano.

Water: Water for mixing and curing was bore-hole water fit for drinking, obtained from NBRRI zone office Kano, which was free from any amounts of oils, acids, alkalis, sugar, salts and organic materials or other substances as specified in BS 3148 (1980).

Literate soil: The literate sample used was collected at a depth of 1.5 m to 2.5 m from an existing borrow pit from Dawakin tofa 34km from Kano state, Nigeria. The literate was sieved with a 6mm sieve size and spread indoors for about a week in order to keep tchem as dry.

Mix ratio: The mix ratio of the literate brick was 1:6 by volume, i.e., one part of cement to six parts of fine aggregate (lateritic soil) as recommended in the Nigerian National Building Code and Nigerian Building and Road Research Institute.

2.2 Methodology

Preparation of Literate Samples

The literate sample were obtained from an existing borrow pit from dawakin tofa local government area, 34km from Kano state, Nigeria. The sample were air –dried for seven days in a cool, dry place, samples were taken and used for sieve analysis test. Atterberg's limits test was performed in accordance with specification of BS 1377. The literate sample for brick production was sieved using a wire mesh screen with aperture of about 6 mm in diameter. Fine materials passing through the sieve were collected for use while those retained were thrown away.

LITERATE SOIL

2.3 Production of NBRRI lateritic interlocking bricks

NBRRI interlocking bricks were produced using NBRRI semi-automatic brick production machine. The machine produce bricks with dimension of 230mm x230mm x120 mm. Recommended amount of dry literate and cement were systematically mixed together using shovels on a clean concrete platform. The dry mixture was spread again to receive water which was added gradually while mixing, using a watering can, until the optimum moisture content of the mixture was attained in addition to a uniform consistency.

NBRRI SEMI-AUTOMATIC BRICK PRODUCTION MACHINE

The production method comprises of batching, mixing and compaction of Literate. All the processes were carried out with reference to the International labour organization manual Nigerian Building and Road Research institute. Batching of literate, cement and water was done according to NBRRI standard. The bricks were cured for 3, 7, and 28 days using different curing method. Tests and experiments were carried out at the NBRII laboratory North-west zonal office, Kano.

NBRRI BRICKS AFTER CURING

In order to investigate the influence of curing conditions of NBRRI interlocking bricks. Five bricks were chosen for every curing regime and tested for bulk density, water absorption, durability and compressive strength. The curing regimes employed were:

Condition “A”: covering of bricks with tarpaulin with sprinkling of water twice a day (morning and evening).

Condition “B”: wet curing throughout (by complete immersion in portable water and covering with tarpaulin).

Condition “C”: complete covering with air and water tight polythene bags.

Condition “D”: covering with wet hessian and polythene sheet.

Condition “E”: keeping under dry laboratory conditions.

Condition “F”: keeping in open air under direct sunshine.

Condition “G”: keeping in open air under shed.

3.0 Testing Procedure

The bricks were tested for bulk density, water absorption, durability and compressive strength at the end of every curing period.

3.1 Bulk density test

Bulk density also called apparent density or volumetric density is the total mass of the brick, water and air per unit volume. The bulk densities of the brick samples were tested at the end of curing ages and carried out in accordance to Nigerian Industrial Standard (NIS 87, 2004). Five brick samples were selected at random, each sample was weighed and recorded. The volume of the brick sample was determined as the product of its length, breadth and height. The density of the brick sample was computed as;

Bulk density = $\frac{m}{v}$ Kg/m^3

Where:

M = Mass of the literate brick. V = Volume of the literate brick.

3.2 Durability Test

Durability of the bricks was determined through abrasion test, to determine bricks resistance to wearing due to environmental factors like wind and rain. The test was conducted in accordance with Association of State Highway and Transportation Official (AASHTO-T 96,2010). The test was conducted at 7-day, 14-day and 28 day curing ages. five bricks from each batch was weighed and weight was recorded as M_1. The bricks were then place on a smooth and firm surface and then wire-brushed to and fro on the surfaces for 50 times. To ensure uniform load on wire brush, a 3Kg brick was secured firmly at the back of the wire brush, the bricks was weighed, and their weight was recorded as M_2. The durability of the brick sample was computed as;

$$Durability\ (\ Abration)\% = (\frac{\text{Diff.in weight}}{\text{Original weight}} \quad \times \frac{100}{1}\ )$$

$$Durability\ (\ Abration)\% = \frac{\text{m1} - m2}{\text{m1}} \quad \times 100\%$$

Where

M_1 = mass of original bricks M_2 = mass of abraded bricks

3.3 Water Absorption Test

Water absorption test was conducted after the bricks had attained the curing ages of 7-day, 14-day and 28 – day. Five bricks were selected at random and weighed and their weight recorded as dry mass M_d, (dry mass) for each brick. These bricks were then immersed completely in reservoir containing clean water for 24 hours. The bricks were remove and reweighed and their weight recorded as M_w(wet mass) for each brick. The water absorption of the brick sample was computed as;

The percentage of water absorption by the bricks could be computed as;

$$wa = \frac{\text{ws} - wd}{\text{wd}} \ \times 100$$

Where

W_a = percentage of moisture absorption. W_s = weigh of soaked brick. W_d = weigh of dry brick

3.4 Compressive Strength test

Compressive strength of literate brick was determined at age of curing ages using compressive strength testing machine. The compressive strengths of the literate bricks were determined after 7, 14 and 28 days of curing accordance with BS 1881-116-1983. Each literate brick was crushed and the average compressive strength of the five literate bricks were calculated. The compressive strength was computed as:

Compressive strength = $\frac{P}{A}$ N/mm^3

Where:

P = crushing load in (KN), and A = cross-sectional area (mm$^{3)}$

4.0 Results

4.1 Result of sieve analysis

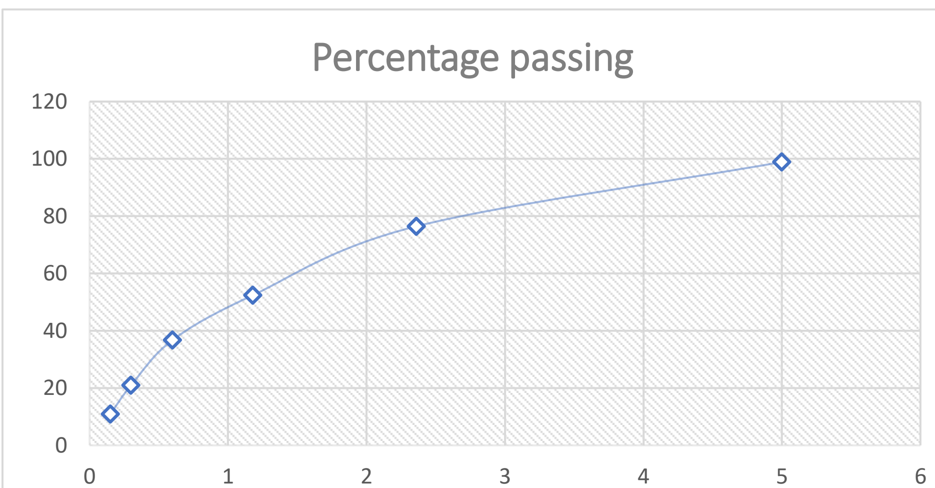

Fig 1: Result of sieve analysis

Particle size distribution of literate used in brick production is as presented in Fig. 1. The literate used in the study was an A-2-6 soil using the AASHTO system of soil classification implying that the soil has gravel, sand and silt fines.

Table 2: Physical properties of literate soil used

Properties	Value
Colour	Reddish Brown
Specific gravity	2.59
Liquid limit (%)	46
Plastic limit (%)	30
Plasticity index (%)	16
Condition of sample	Air Dried
Bulk density Kg/m^3	1388

4.2 Bulk density test

The average bulk density of bricks cured under the different conditions for 7, 14 and28 curing days are presented in Fig 2. The study observed highest Average bulk density in bricks cured using condition “C” (covering bricks with air and water tight polythene bags) with average bulk density of 1785Kg/m^3 at 28 days curing age. This closely followed by condition “A”: covering of bricks with tarpaulin with sprinkling of water twice a day (morning and evening), Condition “D”: covering bricks with wet hessian and polythene sheet, condition “B”: wet curing throughout (by complete immersion in portable water and covering with tarpaulin), “G”: keeping in open air under shed and condition “E” keeping under dry laboratory with average bulk density with 1779Kg/m^3, 1974Kg/m^3,1720Kg/m^3, 1668Kg/m^3 and 1654Kg/m^3 respectively. Bricks cured using conditions F: keeping in open air under direct sunshine condition with average compressive strength of 1642Kg/m^3 had recorded lowest average bulk density. These results indicated that curing of bricks by complete covering with water and air tight polythene bags produced better result, which approximately satisfied the minimum bulk density of 1810 kg/m^3 with a maximum cement content fixed at 5%as recommended by NBRRI.

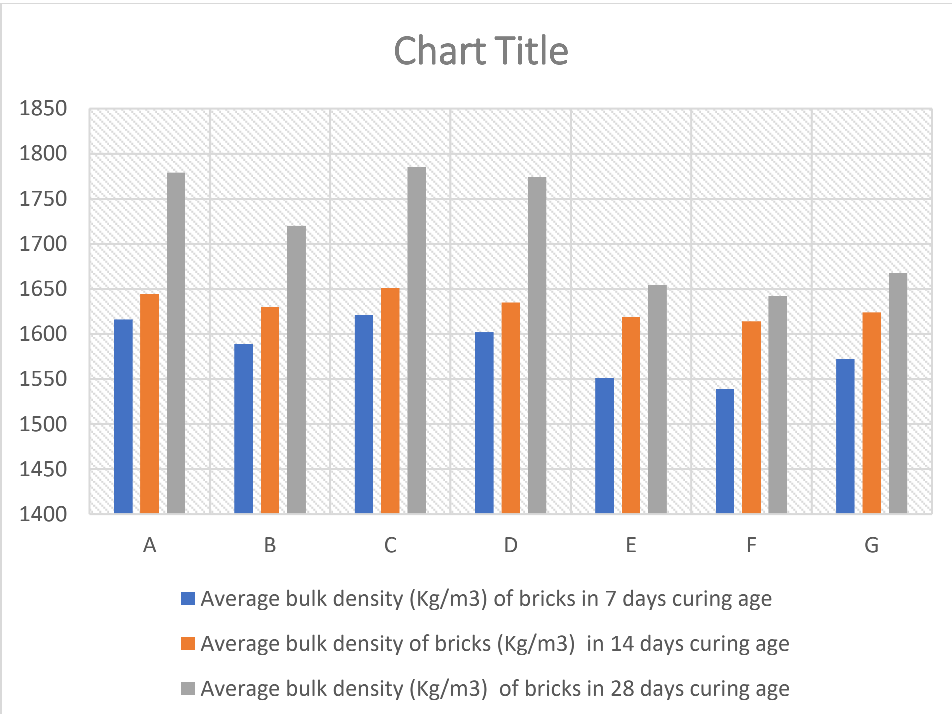

Figure 2: Bulk density test result

4.3 Durability test

The durability of bricks cured under the different conditions for 7, 14 and 28 curing days are presented in Fig 3. The study observed highest durability in bricks cured using condition “C” (covering bricks with air and water tight polythene bags) with average durability of 6.8% at 28 days curing age. Thus, closely followed by condition “A”: covering of bricks with tarpaulin with sprinkling of water twice a day (morning and evening), Condition “D”: covering with wet hessian and polythene sheet, condition “B”: wet curing throughout (by complete immersion in portable water and covering with tarpaulin), “G”: keeping in open air under shed and condition E: keeping under dry laboratory with average compressive strength of 6.5%, 6.2%, 6.0%, 5.7% and 5.5% respectively. Bricks cured using conditions “F”: keeping in open air under direct sunshine condition with average durability of 5.3%had recorded lowest average durability. These results indicated that curing of bricks by complete covering with water and air tight polythene bags produced better result, which approximately satisfied the minimum durability of 6.9% with a maximum cement content fixed at 5% recommended by NBRRI.

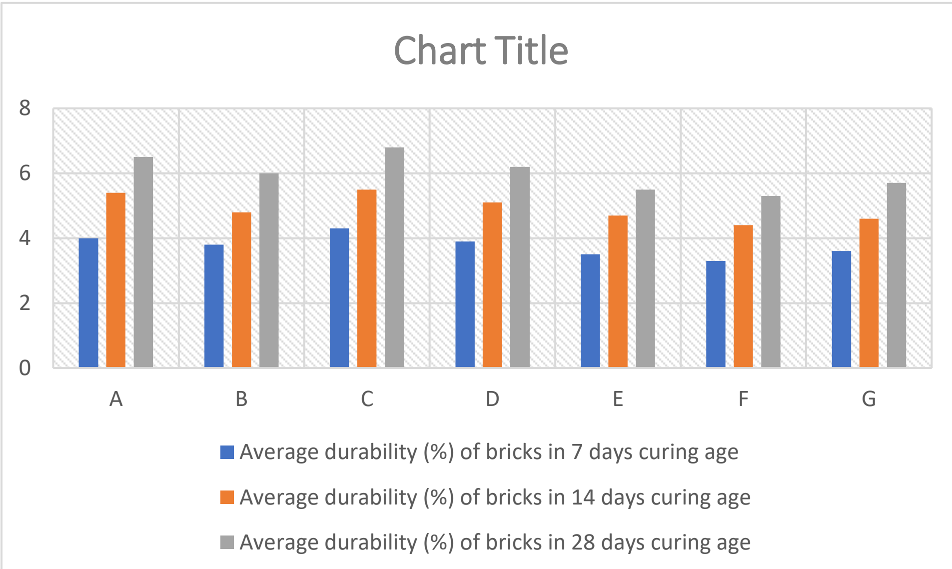

Figure 3: Durability test result

4.4 Water absorption test

The results of water absorption test using the different curing conditions at 7, 14 and 28 curing ages are presented in Figure, 4. The study observed lowest water absorption in bricks cured using condition "C" (by covering completely with air and water tight polythene bags). The average water absorption of 12.4% at 28 days curing age was recorded. These results indicated that curing of bricks by complete covering with water and air tight polythene bags produced better result, which approximately satisfied the minimum durability of 12.5% with a maximum cement content fixed at 5% recommended by NBRRI. The lowest water absorption values associated with these method of curing can be attributed to less evaporation of moisture from such bricks due to exposure as compared with the other methods where high moisture loss occur. However, the study suggested that, among the curing systems employed covering the bricks completely with air and water tight polythene bags appears to have the highest attainable water absorption. The water absorption of bricks cured using condition "A": covering of bricks with tarpaulin with sprinkling of water twice a day (morning and evening), Condition "D": covering with wet hessian and polythene sheet, condition "B": wet curing throughout (by complete immersion in portable water and covering with tarpaulin),"G": keeping in open air under shed, Condition E: keeping under dry laboratory and conditions "F": keeping in open air under direct sunshine observed the water absorption values of 12.4%, 12.6%,12.8%, 12.9%,13.1% and 13.2% respectively. The study also revealed that where water is scarce, covering of bricks with tarpaulin with sprinkling of water twice a day (morning and evening) and covering with wet hessian and polythene sheet are recommended for use. However, where water is available, complete immersion is recommended.

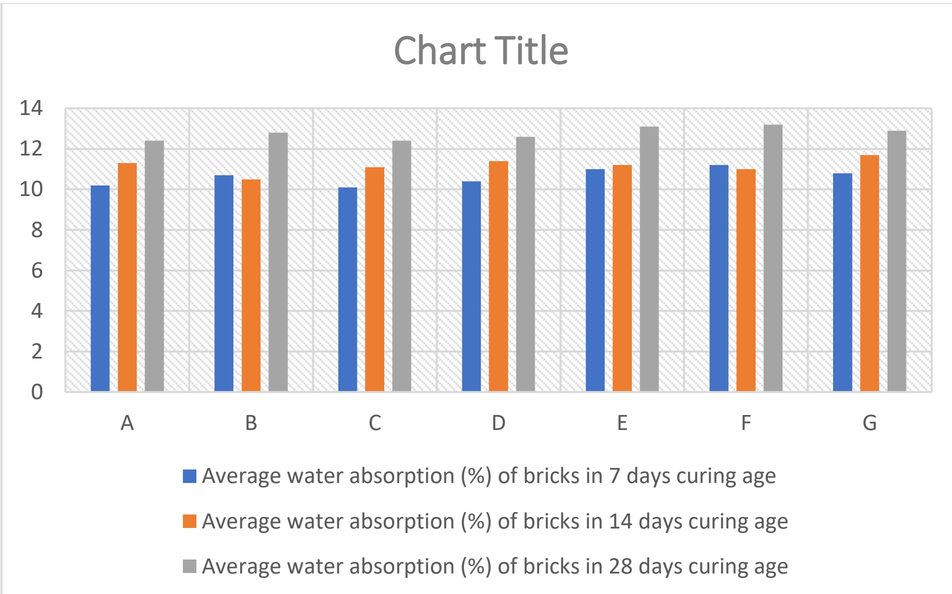

Figure 4: Durability test result

4.5 Compressive Strength

The compressive strengths of bricks cured under the different conditions for 7, 14 and28 curing days. The study observed highest compressive strength in bricks cured using condition "C" (covering bricks with air and water tight polythene bags) with average compressive strength of 1.62N/mm^3 at 28 days curing age, which approximately satisfied the minimum durability of 1.60N/mm^3 with a maximum cement content fixed at 5% recommended by NBRRI. The highest compressive strength obtained with curing condition "C" can be attributed to non-evaporation of moisture from bricks covered with air and water tight polythene bags that provided approximately 100 % relative humidity, while at the same time ensuring relatively stable temperature, as reported by Rigassi, (1995) which ensures effective hydration of cement as observed with moisture retained in the polythene bags during the removal of bricks for test. This result closely followed by condition "A": covering of bricks with tarpaulin with sprinkling of water twice a day (morning and evening), Condition "D": covering with wet hessian and polythene sheet, condition "B": wet curing throughout (by complete immersion in portable water and covering with tarpaulin), "E": keeping under dry laboratory and "G": keeping in open air under shed and condition with average compressive strength of 1.60N/mm^3, 1.58N/mm^{3}N/mm^3,1.54N/mm^3, 1.50N/mm^3 and 1.46N/mm^3 respectively. Bricks cured using conditions "F": keeping in open air under direct sunshine condition with average compressive strength of 1.40N/mm^{3}had recorded lowest compressive strength. This might be due to loss of moisture from the bricks during covering and uncovering for watering of bricks, in addition to moisture loss to the open direct sunshine on which the bricks were kept, such loss in moisture may have affected the hydration of cement and strength.

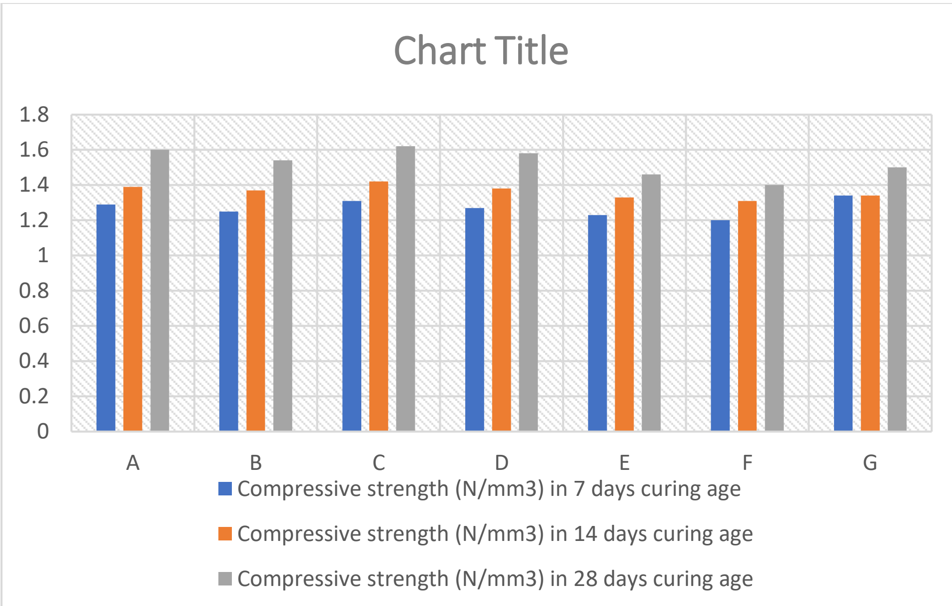

Figure 5: Compressive strength test result

5.0 Conclusion

Based on the findings from this work, it can be concluded that:

1) Different curing systems have different influences on the bulk density, water absorption, durability and compressive strength of NBRRI interlocking bricks.

2) Among the curing systems employed in this research, covering bricks completely with air and water tight polythene bags produced the highest bulk density, water absorption, durability and compressive strength.

3) In comparison with covering bricks completely with air and water tight polythene bags, keeping bricks in open air under direct sunshine, produced lower bulk density, water absorption, durability and compressive strength.

4) Curing of bricks by complete covering with air and water tight polythene is suggested for practice, where water is not freely accessible.

References

[1] ASHTO - T 96 -02 (2010): Standard Method of Test for Resistance to Degradation of small size coarse Aggregate by Abrasion and Impact in the Los Angeles Machine (ASTMC 131-01), Washington D.C. USA.
[2] Akeem A. R.; Olugbenro O. F, and K. J. Adeyeye, (2012). Production and Testing of Lateritic Interlocking Block. *Journal of Construction in Developing Countries*. 17(1) 2012, 33–48.
[3] Baba S, W.; Zanna A. L, Mustapha, M. M. (2013). Properties of Compressed Stabilized Earth Blocks (CSEB) For Low- Cost Housing Construction. *International Journal of Sustainable Construction Engineering & Technology.* Vol. 4, No 2, 2013.
[4] BS 12: (1996). "Specification for Portland Cement". British Standard Institution, London.
[5] BS 1377 Methods of Testing Soils for Civil Engineering Purpose. British Standards Institution, London, 1990.
[6] BS 1881 Part 116, (1983): Methods for determining compressive strengths of concrete cubes, British Standard Institution, 2 Park Street, London.
[7] BS 3148 (1980): Tests for water for marking Concrete, British Standards Institutions, British Standard House, 2 Park Street, London, WIY 4AA.
[8] Chippy M. and Sangeetha S, (2018). Review on Polyethylene Lateritic-Clay Brick. *International Research Journal of Engineering and Technology (IRJET).* Vol. 05, pp 761-765.
[9] Adam, E. (2001) Compressed Stabilised Earth Block Manufactured in Sudan, Grapho print, for UNESCO, Paris, France.
[10] Joel M. And Edeh, Joseph E. (2013). Effect of Curing Condition On Some Properties of Cement Stabilized Lateritic Interlocking Bricks. *Journal advanced Materials Research*. Vol. 824, Pp. 37-43.
[11] Leet, K.M and Bernal, D. (1997). Reinforced Concrete Design. Mc-Graw-Hill, New York.
[12] Naderi, M. Sheibani, R. and Shayanfar, M. A. (2005). Comparison of Different Curing Effects On Concrete Strength. 3rd International Conference On Concrete & Development. Pp. 507-516.
[13] Madedor, A.O and Dirisu, A. O (1992): "Research and development in the promotion of standards and specifications for stabilized soil blocks", Nigerian Building and Road Research Institute (NBRRI), Lagos.
[14] Madedor, A.O. and Dirisu, A. O. (1992): "Research and development in the promotion of standards and specifications for stabilized soil blocks", Nigerian Building and Road Research Institute (NBRRI), Lagos.
[15] MetCalfe, J. B. (1977): A laboratory investigation of strength/age relations of five soils stabilized with white hydrated lime and ordinary Portland cement RN/3435/JBM, DSIR, RRI.
[16] MuhamadZulkapnain, Z. (2014). Properties of Compress Stabilised Interlocking Block Using Laterite Soil with Different Cement - Aggregate Ratio. Thesis Submitted in Partial Fulfilment of the Requirements for The Award Of The Degree Of Bachelor Of Civil Engineering. Faculty of Civil Engineering & Earth Resources. University MalaysiaPahang**.**
[17] NIS 87 (2004): Standard for sandcrete blocks, Nigerian Industrial Standard, approved by Standard Organization of Nigeria**.**
[18] Shetty,S.M. (2005). Concrete Technology; Theory and Practice, Scand and company Ltd, RamNagar, New Delhi.
[19] Rigassi,V.(1995). Compressed Earth Bricks: Manual of Production. Vol. 1. CRA Terre-EAG. Vilefontaine, Cedex, France.

NIPES-NCEE Conference Proceedings
The 2nd International Conference 15th-17th Feb. 2023
351-360
www.nipesjournals.org.ng

OCCUPATIONAL EXPOSURE LEVELS OF ELF MAGNETIC FIELD ASSESSMENT IN 330 KV SWITCHYARD OF HYDRO-PLANT AND GAS-PLANT STATIONS IN NORTH-CENTRAL NIGERIA

Ocheni, Abdullahi Ugbede Usman*[1, 2]; Oyedum, Onyedi David[2]; Nwohu, Mark Ndubuka[3]; Moses, Abiodun Stephen[2]

[1]Department of Physics, University of Maiduguri, Nigeria
[2]Department of Physics, Federal University of Technology, Minna
[3]Department of Electrical and Electronics Engineering, Federal University of Technology, Minna
Corresponding email: oauusman@unimaid.edu.ng

Abstract
The ardent quest for electricity that affects virtually all human activities has evolved the speculation of its adverse effect on human health when exposed to the associated electromagnetic field. Occupational exposure levels of the strength of extremely low frequency (ELF) magnetic field in five 330 kV switchyard of Hydro-plant and Gas-plant generation stations with similar infrastructures were investigated, assessed and analysed. The entire switchyard measurements of ELF magnetic field were performed with reference to three observation heights of 1.0, 1.5 and 1.8 m above ground level via spot measurements technique in segmented manner using Extech 480826 triple-axis EMF metre in conformity to IEEE standards, and occupational exposure computed from the mean of the three observation heights for each spot. The data obtained were subjected to analysis using One-way ANOVA SPSS package. The results demonstrated occupational significant differences of ($p < .001$) between 330 kV switchyards of Shiroro Hydro-plant and Geregu Phase II Gas-plant, significant differences of ($p = .045$) between switchyards of Geregu Phase I Gas-plant and Geregu Phase II Gas-plant, and also significant differences of ($p < .001$) in occupational exposure was demonstrated between switchyards of Jebba Hydro-plant, Kainji Hydro-plant when separately compared to Geregu Phase I and Geregu Phase II Gas-plants. However, non-significant differences occurred between switchyards of Shiroro Hydro-plant and Jebba Hydro-plant, Kainji Hydro-plant and Geregu Phase I Gas-plant, and Jebba Hydro-plant with Kainji Hydro-plant. This study has revealed the prevalence of electropollution in occupational environment and variation in the strength of ELF magnetic field between switchyards personnel might encountered at instant of the measurements.

1.0 Introduction
Electrical infrastructure, such as transmission lines, substations and its facilities are regarded as main sources of manmade extremely low frequency (ELF) magnetic field which are of high strength close to source [1]. These sources of radiated ELF magnetic field are known as electropollution [2] or electrosmog [3] and have contributed to the level of environmental pollution in the atmosphere, in which the modern society exists and develops [4]. In Nigeria, the operational frequency of generated electricity is 50 Hz, which lies in the range of extremely low frequency (3 – 300 Hz) [5]. The results from epidemiological surveys have established that the intensity of ELF magnetic field from manmade sources are in manifold higher when compared to the intensity of natural sources [6].

The strongest occupational exposure to extremely low frequency magnetic field that form the fundamental part of the operating mechanism can be found in work environments where electricity is generated, transmitted or distributed [7, 8]. The systems expectedly emit very high ELF magnetic fields, because of the magnitude of electric current that pass through the system [9].

These form part of the reasons why the average exposures of magnetic field in occupational environment are found to be greater in electric utility than in other occupations [10]. And since limited number of people are exposed to these fields due to professionalism [11], and the field limits in occupational environments stipulated safety regulations [12]. Therefore, there should be need to embark on assessment of ELF magnetic field strength in switchyards vicinity, compare strength and determine the level of exposure workforce encounter in their day-to-day task. Since ELF magnetic field cannot be easily screened by human body because of the resemblance of permeability in both air and skin. Therefore, the study was aimed at determining whether the magnitude of the emitted field lies within the occupational reference thresholds set by ICNIRP for environmental safety.

Evidences from epidemiological studies of people who live or work around electric power stations [13], have revealed that prolonged excessive exposure to extremely low frequency magnetic field induces electric field within the human body and if there exist potential differences within it causes a current to flow due to its conductive nature [14,10]. The biological effects appear to cause or promote certain forms of leukaemia and brain tumours [15]. In view of these, the wide usage of electricity and its associated appliances have raised the question of electropollution and health risk associated with it [16].

The International Agency for Research on Cancer (IARC) based on the evidence gathered from international research [17], has classified ELF magnetic fields into category 2B, corresponding to the category of agents that are "possibly carcinogenic to humans" [18], that might transform normal cells into cancer cells [19]. And to support the claim World Health Organisation (WHO) through the International EMF Project has established the International Commission on Non-Ionising Radiation Protection (ICNIRP) which releases periodically recommendations, and the present occupational reference level is set at 1 mT [7]. However, scientists of the International Electromagnetic Fields Alliance (IEMFA), advised nations of the globe should adopt lower exposure guidelines of 0.1 µT to guard current public health and that of future generations in order to reduced exposure limits of radiated electromagnetic fields from electrical power and telecommunications technologies [20].

In Nigeria, several studies on ELF magnetic field transmission lines environment have been carried out in recent times, thus, accenting the presence of extremely low frequency magnetic field. However, from published literatures it were observed that there are scarce studies on comparative analysis in the strength of ELF magnetic fields emission in switchyards of generating plant of the study areas. Therefore, it is noteworthy to embark on assessing the magnitude ELF magnetic field in the transmission switchyards using spot measurements technique to fill the existing research gap.

In this study, One-way analysis of variance (ANOVA) was used to analyse the significant differences for the strength of ELF magnetic field level in 330 kV of North-Central, Nigeria to determine whether the personnel performing their day-to-day task in each switchyard are exposed to the same environmental hazard within the vicinity.

Figure 1 indicate the study areas on map of Kogi and Niger State, Nigeria.

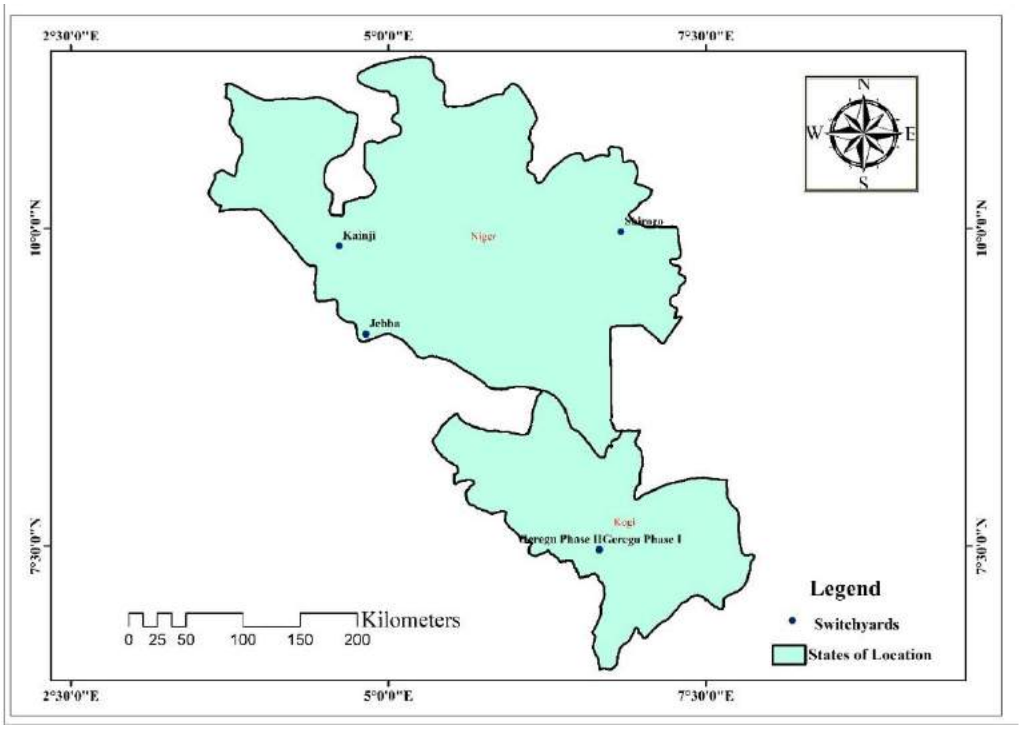

Figure 1: Map of the Study Areas

The studies were conducted in five 330 kV transmission switchyard stations. The stations are Geregu phase I switchyard at (7.470116ºN, 6.658052ºE) generation source from three gas turbines with installed capacity of 345 MW, Geregu phase II switchyard at (7.472133ºN, 6.659133ºE) generation source from three gas turbines with installed capacity of 507 MW both located in Kogi state while Kainji switchyard at (9.861044ºN, 4.613103ºE) generation source from eight turbines with installed capacity of 760 MW, Jebba switchyard at (9.168045ºN, 4.821214ºE) generation source from six turbines with installed capacity of 578 MW and Shiroro switchyard at (9.972474ºN, 6.830333ºE) generation source from four turbines with installed capacity of 600 MW all located in Niger state, Nigeria.

1.2 Governing laws of magnetostatic fields emission

The electric field and magnetic field produced by power facilities are usually uncoupled, due to the fact that ELF field varies so slowly in time that Maxwell's equations are generally converted into the electrostatic and magnetostatic equations [21], and their effects to the human body can be studied and computed independently of one another [22]. Magnetostatic is magnetic field phenomenon produced by steady currents [23]. There are two laws governing the phenomena of magnetostatic field emission in space close to sources:

A. Biot-Savart's law

This law is also referred to as point source model. The current-carrying conductors are modelled as point source if length of conductors or conductor spacing is much smaller than observation distance [13]. The magnetic field of a steady current is expressed by Biot-Savart law as [23]:

$$\vec{B} = \frac{\mu_o}{4\pi} \int \frac{Id\vec{l} \times \hat{r}}{r^2} \tag{1}$$

where $\mu_o = 4\pi \times 10^{-7} \mathrm{T} \cdot \mathrm{m/A}$ is the permeability of free space, I is the line current, $d\vec{l}$ is a differential element of the conductor in the direction of current, r is the distance between an observation point and a source point and $\hat{r}$ is a distance vector. The law specifies the direction and the magnetic field strength in the vicinity of conductor carrying-current [24].

B. Ampere's circuit law

This law is also referred to as long-conductor source model. The current-carrying conductors are modelled as long-conductor source if conductors are much larger than observation distance, as well as conductor spacing is much smaller than observation distance [13]. In power systems, magnetic field occur around the current-carrying conductor [25]. This symmetrical magnetic field generated by current distribution around the conductor can be determine by application of Ampere's law [26]:

$$B = \frac{\mu_o I}{2\pi r} \tag{2}$$

where B is the magnetic field, I is the current flow through the long-conductor, μ_o is the permeability of free space and $2\pi r$ is the circumference of the magnetic field generated by current through a long-conductor.

2.0 Methodology

The instrument used for the measurement of extremely low frequency magnetic field was Extech 480826 triple-axis EMF metre manufactured by Extech Instrument. It was calibrated to flat frequency response, with frequency bandwidth of 30 to 300 Hz and sampling time of approximately 0.4 s. The three modes of selection with corresponding basic accuracy are 20 µT (4 %), 200 µT (5 %) and 2000 µT (10 %), and measured field isotropically with detachable external magnetic field probe.

The field probe for the Extech 480826 Triple-Axis EMF metre during the measurement of ELF magnetic field was mounted on special designed "field probe stand" constructed to correspond to three observation heights of 1.0, 1.5 and 1.8 meters of interest. The estimated standard for the occupational exposure was obtained by computing the mean from the three observation heights at each spot of measurement.

The field probe stand was mounted along with the sensor placed at the successive position in segmented manner in switchyard vicinity for detection and measurement of fields intensity. What informed the construction of the field probe stand was to have corresponding uniformity in height for measurement of the field levels throughout the survey, to guaranty degree of accuracy and stability of field reading. The mounted sensor was directly connected to the detector that displayed the values through 1m length sensor cable, which processed the signal from the probe. The resultant rms vector magnitude of unperturbed extremely low frequency magnetic field in three orthogonal directions was computed according to Institute of Electrical and Electronics Engineers [IEEE] 644-1994 standards for measurement procedure [27]:

$$\mathrm{B} = \sqrt{\mathrm{B}_\mathrm{x}^2 + \mathrm{B}_\mathrm{y}^2 + \mathrm{B}_\mathrm{z}^2} \tag{3}$$

3.0 Results and Discussion

After exclusion of erroneous data that failed to meet the criteria for evaluation, a total of 767 data field were assessed and analysed for the five 330 kV switchyards of Hydro-plants and Gas-plants. The statistical analysis of the field data was performed using the IBM SPSS Statistics package (IBM version 21.0, USA). One-way analysis of variance (ANOVA) with significant level set at (*P* - value $\leq$ .05) was performed to compare the mean strength in ELF magnetic field generated between the switchyards with similar infrastructures, which operate at the same highest national voltage level of 330 kV. The essence of using ANOVA for analysis was to determine whether switchyard influences the level of ELF magnetic field generated within the vicinity. Table 1 presents summary of descriptive statistics, Test for Homogeneity of Variance, Robust test of Equality of Means and the Games-Howell Post Hoc test of Multiple Comparison of occupational exposure to ELF magnetic field level in the 330 kV switchyards of the electric generation stations in North-central, Nigeria.

Table 1: Statistical Descriptive Data and Games-Howell Post Hoc Test in 330 kV Switchyards for ELF Magnetic Field Measurements

	Descriptive Statistics			Test of Homogeneity of Variance		Robust Tests of Equality of Means	
330 kV Switchyard	**N**	**Mean μT**	**Std. Deviation**	**Levene Statistics**	**Sig.**	**Welch**	**Sig.**
Shiroro Hydro-plant	183	5.0555	4.76172	16.842	.000	31.885	.000
Jebba Hydro-plant	164	5.7843	3.28311				
Kainji Hydro-plant	170	6.1780	3.18878				
Geregu Phase I Gas-plant	124	3.9473	3.21017				
Geregu Phase II Gas-plant	126	2.9426	2.42697				

330 kV Switchyards of Generation Stations		**Mean Difference**	**Sig.**	**95% Confidence Interval**	
				Lower Bound	**Upper Bound**
Shiroro Hydro-plant	Geregu Phase II Gas-plant	2.11285	.000	.9788	3.2469
Jebba Hydro-plant	Geregu Phase I Gas-plant	1.83699	.000	.7775	2.8965
	Geregu Phase II Gas-plant	2.84171	.000	1.9211	3.7624
Kainji Hydro-plant	Geregu Phase I Gas-plant	2.23066	.000	1.1923	3.2690

	Geregu Phase II Gas-plant	3.23538	.000	2.3394	4.1314
Geregu Phase I Gas-plant	Geregu Phase II Gas-plant	1.00472	.045	.0139	1.9956

* The mean difference is significant at the 0.05 level

The One-way between-switchyards ANOVA was performed with occupational ELF magnetic field as the dependent variable and generation switchyards as the independent variable. The results revealed significant differences between switchyards with Levene's statistic of $F(4,762) = 16.842$, $p < .001$ and, Kainji Hydro-plant switchyard ($N = 170$, $M = 6.18$, $SD = 3.19$) was observed to have the highest mean occupational exposure to ELF magnetic fields, while Geregu Phase II Gas-plant switchyard ($N = 125$, $M = 2.94$, $SD = 2.43$) was observed to have the least occupational exposure to extremely low frequency magnetic field.

Since the Levene's statistical test was significantly different at ($p < .001$), therefore, assumption for homogeneity of variance have been violated. So, the Null Hypothesis "there was no significant difference in occupational ELF magnetic field exposure level in 330 kV switchyards of both hydro-plants and gas-plants" stand rejected. The Welch robust test of equality of mean was then employed for the analysis because it is robust to violation of homogeneity of variances.

The Welch robust test of equality of mean demonstrated that the switchyards occupational exposure to ELF magnetic field level had statistically significant differences of ($p < .001$) between them.

To determine the specific groups that differed in exposure levels, Multiple comparison of Game-Howell Post Hoc tests was performed by assuming nonequality of variances for the five switchyards to identify which switchyard are significantly different from the other. As revealed in Table 1, the mean and 95% confidence intervals for emission level demonstrated Jebba Hydro-plant and Kainji Hydro-plant switchyards to have statistically significant differences of ($p < .001$) when independently compared to both Geregu Phase (I & II) Gas-plant switchyards, while Shiroro revealed significant difference of ($p < .001$) with Geregu Phase II Gas-plant and, significant difference of ($p = .045$) was observed between switchyards of Geregu Phase I and Geregu Phase II Gas-plant. However, nonsignificant differences were observed between switchyards of Shiroro, Jebba and Kainji Hydro-plants when compared with each other and between switchyards of Shiroro Hydro-plant and Geregu Phase I Gas-plant.

The means occupational exposure to extremely low frequency magnetic field in 330 kV switchyards of Kainji Hydro-plant (6.18 µT), Jebba Hydro-plant (5.78 µT) and Shiroro Hydro-plant (5.06 µT) were found to be significantly high when compared to 330 kV switchyards of Geregu Phase I (3.95 µT) and Geregu Phase II (2.94 µT). However, these exposure levels are still far below the expected set limit of 1 mT for occupational exposure proposed by ICNIRP. These results have revealed that the personnel working in switchyards at voltage level of 330 kV are not exposed to the same level of ELF magnetic field.

Medical research has shown that exposure to ELF magnetic field above safe limits can have a significant detrimental effect on health. The short-term exposure might cause nervous system disorder, abnormal cell activity, muscle pain and other effects while the long-term exposure might cause risk of neurodegenerative diseases [28]. Further studies revealed that it causes physiological change in human tissues [29], like neurological, cardiovascular disorders and low sperm count in the workers [30], because the nervous system has bioelectric properties that make it more vulnerable to be influenced by electromagnetic fields [31]. The possible effects on health are reinforced by the submission of WHO and IARC that time weighted average exposure to ELF magnetic field levels greater than 0.3 µT increases the likelihood of leukaemia [32].

5.0 Conclusion

The One-way ANOVA performed for the five 330 kV switchyards of Hydro-plants and Gas-plants to determine the density of ELF magnetic fields in the studied locations revealed that there exist significant difference in occupational exposure levels between switchyards. Even though the level of ELF magnetic field emission in the five switchyards have been found to be lower than the recommended permissible set limits of 1 mT by ICNIRP guidelines, there still exist variance in occupational exposure levels encountered by workforce. With government efforts for stability in power supply, the ELF magnetic field in the switchyards are expected to rise in future with increased load demand. Therefore, it is suggested that constant monitoring of fields level should be undertaken to detect high risk zone for possible avoidance to prolonged exposure for safe working environment.

References

[1] D. Urban, L. Tjong and K. Karipidis, "Measurement of extremely low frequency electric and magnetic fields associated with electricity supply and distribution infrastructure," Australian Radiation Protection and Nuclear Safety Agency (ARPANSA), 619 Lower Plenty Road, Yallambie, Melbourne, 2014.

[2] I. J. Al-Faqeeh, M. Abu-Jafar and I. R. Abdelraziq, "The effect of the electromagnetic radiation from high voltage transformers on students health in Hebron district.," *International Journal of Geology, Agriculture and Environmental Sciences,* vol. 3, no. 1, p. 75–81, 2015.

[3] P. Nassiri, M. R. Monazzam, M. Yunesian, M. H. Sowlat, M. H. Safari, S. Momen Bellah Fard and S. A. Hosseini, "Extremely low frequency magnetic flux densities measured near hospital in Tehran," *International Journal of Environmental Research,* vol. 5, no. 4, p. 1035–1040, 2011.

[4] H. Jalilian, K. Najafi, M. R. Monazzam, Y. Khosravi and Z. Zamanian, "Assessment of static and extremely low-frequency magnetic fields in the electric-powered trains," *International Journal of Occupational Hygiene,* vol. 9, no. 2, p. 105–112, 2017.

[5] P. Rathebe, C. Weyers and F. Raphela, "Exposure levels of ELF magnetic fields in the residential areas of Mangaung metropolitan municipality," *Environ Monit Assess,* vol. 190, no. 544 , p. 1–9, 2018.

[6] Sudarti, L. Nuraini, T. A. Saleh and T. Prihandono, "The analysis of extremely low frequency (ELF) electric and magnetic field exposure biological effects around medical equipments," *International Journal of Advanced Engineering Research and Science (IJAERS),* vol. 5, no. 7, p. 289–296, 2018.

[7] R. Stam, "The Revised Electromagnetic Fields Directive and Worker Exposure in Environments with High Magnetic Flux Densities," Annal of Occupational Hygiene 2014, vol. 58, no. 5, p. 529–541, 2014.

[8] J. Vila, J. D. Bowman, L. K. L. Richardson, D. L. Conover, D. McLean, S. Mann, P. Vecchia, M. Tongeren and E. Cardis, "A source-based measurement database for occupational exposure assessment of electromagnetic fields in the interocc study: A literature review approach," Annals of Occupational Hygiene, vol. 60, no. 2, p. 184–204, 2016.

[9] S. Özen, "Evaluation and measurement of magnetic field exposure at a typical high-voltage substation and its power lines," *Radiation Protection Dosimetry,* vol. 128, no. 2, p. 198–205, 2008.

[10] G. Kulkarni and W. Z. Gandhare, "Proximity effect of high voltage transmission lines on humans," *ACEEE Int. J. on Electrical and Power Engineering,* vol. 3, no. 1, p. 28–32, 2012.

[11] M. Kokoruš, S. Delić, A. Mujezinović, M. Muratović and A. Čaršimamović, "Analysis of the possible solutions for the reduction of electric and magnetic fields near 400 kV overhead transmission lines," *Environmental Impact II,* vol. 181, p. 225–236, 2014.

[12] R. W. Habash, "Electromagnetic fields and radiation: Human bioeffects and safety," CRC Press, Ottawa, Ontario, Canada, 2001.

[13] I. O. Habiballah, M. M. Dawoud, K. Al-Balawi and A. S. Farag, "Magnetic field measurement & simulation of A 230 kV substation.," in *Proceedings of the International Conference on Non-Ionising Radiation at UNITEN (ICNIR 2003) Electromagnetic Fields and Our Health,* Kuala Lumpur, Malaysia, 2003.

[14] S. Helhel and S. Özen, "Evaluation of residential exposure to magnetic field produced by power lines near homes and working environments," *International Journal of Engineering and Applied Sciences (IJEAS),* vol. 2, no. 3, p. 1–10, 2010.

[15] L. Battistelli, A. Geri and G. Veca, "Magnetic field shielding of underground power cables in urban areas: A real-life example," *Boundary Elements,* vol. XXVII, no. 39, p. 527–540, 2005.

[16] Y. R. Ahuja, S. Sharma and B. Bahadur, "Autism: An epigenomic side-effect of excessive exposure to electromagnetic fields," *International Journal of Medicine and Medical Sciences,* vol. 5, no. 4, p. 171–177, 2013.

[17] C. Roldán-Blay and C. Roldán-Porta, "Quick calculation of magnetic flux density in electrical facilities," *Applied Sciences*, vol. 10, no. 891, 2020.

[18] International Agency for Research on Cancer [IARC], "IARC monographs on the evaluation of carcinogenic risks to humans: Non-ionising radiation, part 1, static and extremely low frequency (ELF) electric and magnetic fields," IARCPRESS, Lyon, France, 2002.

[19] H. Liu, G. Chen, Y. Pan, Z. Chen, W. Jin, C. Sun, C. Chen, X. Dong, K. Chen, Z. Xu, S. Zhang and Y. Yu, "Occupational electromagnetic field exposures associated with sleep quality: A cross-sectional study," *PLOS ONE,* vol. 9, no. 10, p. e110825, 2014.

[20] O. Johansson, A. Fragopoulou, Y. Grigoriev, L. Margaritas, L. Morgan, E. Richter and C. Sage, "The Seletun Scientific Statement," The International Electromagnetic Fields Alliance [IEMFA], Oslo, Norway, 2011.

[21] W. Tourab and A. Babouri, "Measurement and modelling of personal exposure to the electric and magnetic fields in the vicinity of high voltage power lines," *Safety and Health at Work (SH@W),* vol. 7, no. 2016, p. 102–110, 2015.

[22] A. Laissaoui, B. Nekhoul, K. Kerroum, K. K. Drissi and D. Poljak, "On the rotationally-cylindrical model of the human body exposed to ELF electric field," *Progress in Electromagnetics Research M,* vol. 29, p. 165–179, 2013.

[23] D. J. Griffiths, Introduction to Electrodynamics, 3rd ed., R. Alison and D. Kim, Eds., New Jersey: Prentice Hall, Upper Saddle River, New Jersey 07458, 1999.

[24] I. N. Ztoupis, I. F. Gonos and I. A. Stathopulos, "Calculation of power frequency fields from high voltage overhead lines in residential areas," in *Paper presented at the 18th International Symposium on High Voltage Engineering*, Seoul, Korea, 2013.

[25] C. Kocatepe, C. F. Kumru and E. Taslak, "Analysis of magnetic field effects of underground power cables on human health," in Paper presented at the 5th International Symposium on Sustainable Development (ISSD 2014), Sarajevo, Bosnia and Herzegovina, 2014.

[26] N. O. M. Sadiku, Elements of Electromagnetics, 3rd ed., Philadelphia, US: Saunders, 1989.

[27] Institute of Electrical and Electronics Engineers [IEEE] Standards Coordinating Committee 39 , "IEEE recommended practice for measurements and computations of electric, magnetic and electromagnetic fields with respect to human exposure to such fields 0 Hz to 100 kHz," IEEE 3 Park Avenue, New York, NY 10016–5997, USA, 2010.

[28] N. Raghu, M. N. Krishna, K. Nagendra and V. N. Trupti, "Survey of electromagnetic field near EVH lines and their health hazards," in Paper presented at the International Conference on Smart Grids, Power and Advanced Control Engineering (ICSPACE2017), Bangalor, India, 2017.

[29] S. Bhattacharjee, "Protective Measures to Minimize the Electromagnetic Radiation," Advance in Electronic and Electric Engineering, vol. 4, no. 4, pp. 375-380, 2014.

[30] O. Aliyu, I. Maina and H. Ali, "Analysis of electromagnetic pollution due to high voltage transmission lines," Journal of Energy Technologies and Policy, vol. 2, no. 7, p. 1–10, 2012.

[31] J. Huang, T. Tang, G. Hu, J. Zheng, Y. Wang, Q. Wang, J. Su, Y. Zou and X. Peng, "(2013) Association between exposure to electromagnetic fields from high voltage transmission lines and neurobehavioral function in children," PLoS ONE, vol. 8, no. 7, p. 1–10, 2013.

[32] World Health Organisation [WHO], "Exposure to Extremely Low Frequency Fields," WHO|Electromagnetic fields and public health, 2007.

NIPES-NCEE Conference Proceedings
The 2nd International Conference 15th-17th Feb. 2023
361-378
www.nipesjournals.org.ng

3D MODELLING OF A RECONDITIONED PISTON OF A SINGLE-CYLINDER FOUR-STROKE DIESEL ENGINE BY USING SOLIDWORKS SOFTWARE

Festus Oamen Isaac[1], Otunuya Obodeh[2] and Osagie Ighodalo[3]

[1]Faculty of Engineering, Department of Mechanical Engineering, Edo State University, Uzairue. isaac.oamen@edouniversity.edu.ng
[2]Faculty of Engineering and Technology, Department of Mechanical Engineering, Ambrose Alli University, Ekpoma. Edo State. engobodeh@yahoo.com
[3]Faculty of Engineering and Technology, Department of Mechanical Engineering, Ambrose Alli University, Ekpoma. Edo State. oighodalo@yahoo.com
Corresponding email: isaac.oamen@edouniversity.edu.ng

Abstract
This paper explains a 3D modelling of a reconditioned or thermal barrier-coated piston of a single-cylinder four-stroke diesel engine using the ZS1115NM diesel engine specifications. Due to the upsurge of counterfeit spare parts in the market, meeting the original equipment manufacturer (OEM) standards requires a reconditioning process. The reconditioned piston is a thermal barrier coated one with a ceramic material that enables it to withstand high gas combustion temperatures without cracking. A piston converts thermal energy to mechanical energy in an internal combustion engine (ICE). The methodology the was sizing and modelling of the conventional piston, topcoat and bond-coat layers and finally assembling them to get a reconditioned piston using Solidworks Computer-Aided Design (CAD) software. The material chosen for the piston (substrate) is an aluminium alloy designated as A92618 or simply A2618, due majorly to its high coefficient of thermal expansion (CTE) which enables the piston to withstand high thermal stress without cracking or failure. The ceramic material chosen is a 7.5% yttria-stabilized zirconia (7.5% Y2O3-ZrO2) which is the topcoat with low thermal conductivity and a high coefficient of thermal expansion (CTE) on a bond-coat metallic material called Nickel Chromium Aluminium Cobalt Yttria (NiCrAlCoY) which are practically thermally plasma sprayed on the crown of the substrate. The chosen thickness from the literature of the topcoat layer is 0.35 mm and that of the bond-coat layer is 0.15 mm. Also, from the literature, the major reason for the thermal barrier-coating (TBC) of a diesel engine piston crown using a ceramic material was to improve its performance by increasing the brake power and the brake thermal efficiency including reducing the brake-specific fuel consumption (BSFC) and emissions.

***Keywords**: 3D modelling, ZS1115NM, Original equipment manufacturer, SOLIDWORKS 2013, A2618, 7.5% Yttria-stabilized zirconia, Nickel Chromium Aluminium Cobalt Yttria, brake specific fuel consumption.*

1.0 Introduction
The thermal barrier-coatings (TBCs) are advanced ceramic materials applied on metallic surfaces of aero-engine, turbine and spark and compression-ignition engine parts (cylinder liner, cylinder head, valves, piston crown, etc.), which work at very high temperatures [1]. Coatings help to insulate metallic parts from heavy and excessive heat loads using thermally insulating materials which withstand reasonable temperature difference between the combustion chamber and coating surfaces. This results to high operating temperatures on the metallic or component surfaces. Coatings also reduce the problems of oxidation and thermal fatigue in order to extend the life span

of the machine components. Modern coating systems behave as barriers to heat transfer through metallic surfaces so as to protect engine parts from oxidation and hot corrosion [2,3].

The piston in an internal combustion engine (ICE) is a round piece of metal that converts the rotary motion of the crank-shaft into a reciprocating motion in the cylinder and exerts a force on the air-fuel mixture contained in the cylinder [4]. Piston has compression and oil control rings preventing oil from entering the combustion-chamber including the fuel air from mixing with the oil [5]. Most fitted pistons in engine cylinders have piston rings [6]. Two or more compression rings are acting as seals or barriers between the piston and cylinder-wall. There are also one or two oil control-rings below the compression-rings (Figure 1). The piston head may be flat, bulged or otherwise shaped. Pistons which are either forged or cast have rounded shapes [5]. The preferred common materials for petrol and diesel engine pistons are aluminium alloys because they possess high thermal conductivity, low density, simple machinability, high-reliability, simple fabrication processes and very good recycling-characteristics [7].

Figure 1 The different parts or elements of the piston

The single-component coating has not satisfied some multifunctional requirements of some engine parts. As a result, a complex thermal-barrier-coating structure was introduced. Research from the 1970s focused on a preferred coating system that comprises three separate layers on the substrate to achieve long-term improvement in the control of oxidation and corrosion at high temperatures [8,9]. Firstly, we have the topcoat layer which is made of ceramic material having low thermal conductivity for good thermal insulation for hot engine metallic parts Secondly, the bond-coat-layer which is made of a metallic alloy and placed directly on the substrate to hold the ceramic topcoat layer on the substrate. Finally, we have the thin thermally-grown-oxide (TGO) layer which provides good adherence between the ceramic topcoat layer and the bond-coat-layer [10]. When the thermal barrier-coating (TBC) is subjected to high temperatures the thermally grown oxide (TGO) layer which consists of alumina then protects the substrate from thermal oxidation and corrosion by serving as an oxygen diffusion barrier [2]. The thermal barrier-coatings (TBCs) are normally applied on the cylinder head, cylinder liner, piston crown, piston rings and valves by plasma spray method mainly to reduce the heat loss to the engine cooling-jacket [11,12]. Coating these engine parts with ceramic material also help to reduce the negative effects of wear, friction, heating, corrosion and oxidation [13,14]. Ceramic materials have higher thermal durability than metals [15]. Low-thermal conductivity ceramic materials are used to control temperature-distribution and heat flow in a system [16]. Thermal barrier-coatings provide room for higher thermal efficiencies of the engine, reduced emissions and improved combustion [17,18]. In addition, ceramic materials show better wear characteristics than other materials.

Adnan et al. [19] conducted a test on a single-cylinder, indirect injection Ricardo E6-MS/128/76 type diesel engine. They coated the cylinder head, valves and piston with $MgO–ZrO_2$ layer having 0.35 mm thickness on a NiCrAl bond-coat layer also having 0.15 mm thickness. They discovered that in low-heat-rejection (LHR) diesel-engine the NOx emissions were reduced by about 40% and the brake specific fuel consumption (BSFC) also reduced by about 6% compared to the conventional engines when injection timing was retarded to 340^0 crank-angles before top dead centre (TDC) to that of a conventional engine. Ekrem et al. [20] compared a conventional engine with a LHR engine. They used $MgZrO_3$ as a coating material for the diesel piston and $CaZrO_3$ for the cylinder head and valves. The piston was coated with $MgZrO_3$ having a thickness of 350 μm on a NiCrAl bond-coat-layer with 150 μm thickness. The results obtained showed that the combustion gas temperature for the LHR engine was increased by approximately 65 ^{0}C while the BSFC and particulate emissions were reduced by about 6% and 40%, respectively as compared to a conventional engine. Rohini and Prema [17] reviewed thermal barrier-coating (TBC) on the same diesel engine performance to improve thermal efficiency by reducing specific fuel consumption (SFC) and exhaust emissions [21]. They were able to make a comparison between a standard diesel engine and a low-heat-rejection (LHR) engine. Experimental results from various researchers show improvement in efficiency and rate of specific fuel consumption. Navin et al. [22] analyzed the performance and emission of a thermal barrier-coated engine by using palm oil biodiesel and diesel as fuels. They prepared TBC using a series of a mixture consisting of different blend ratios of yttria-stabilized zirconia ($Y_2O_3.ZrO_2$) and aluminium oxide-silicon oxide (Al_2O_3-SiO_2) via plasma spray coating method. Their experimental results revealed the mixtures of TBC with 60% $Y_2O_3.ZrO_2$ + 40% Al_2O_3-SiO_2 had excellent nitrogen oxide (NO), carbon monoxide (CO), carbon dioxide (CO2), and unburned hydrocarbon (UBHC) reductions when compared with other blend-coated pistons [23].

This is the process whereby a powder feedstock is injected into a high-temperature plasma-jet where finely divided metallic and non-metallic materials are deposited in a molten or semi-molten state on a prepared substrate [24,25]. It is used as an effective and economical method for producing ceramic-coatings on metallic-substrates and production of bulk-powders from spheroidization [26]. The plasma spray-coating system is shown in Figure 2 while the spraying-gun system is displayed in Figure 3. The system consists of a power unit, gas supply unit, spraying-gun, powder-supply unit, cooling-system and control unit [25,27].

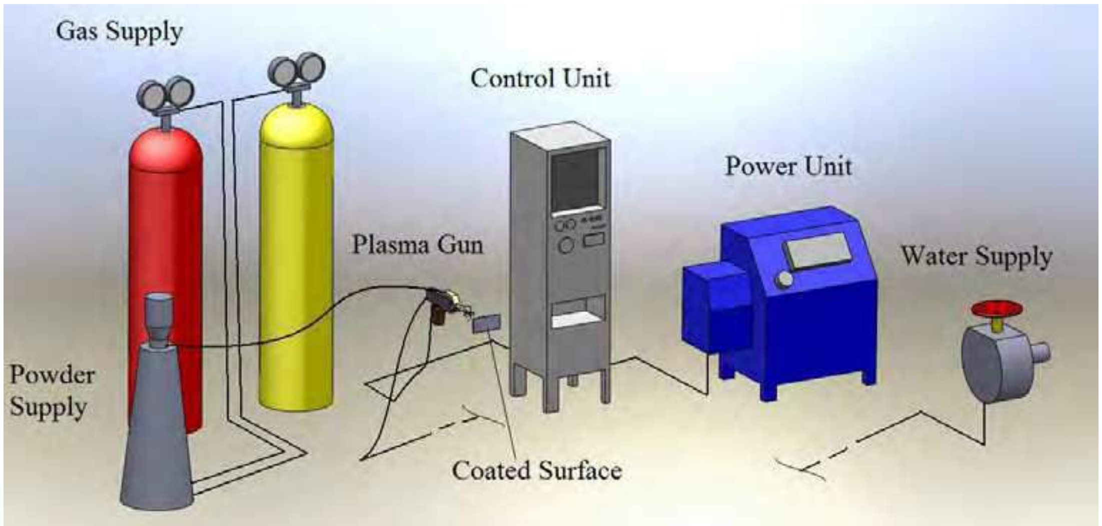

Figure 2 Plasma spray-coating system

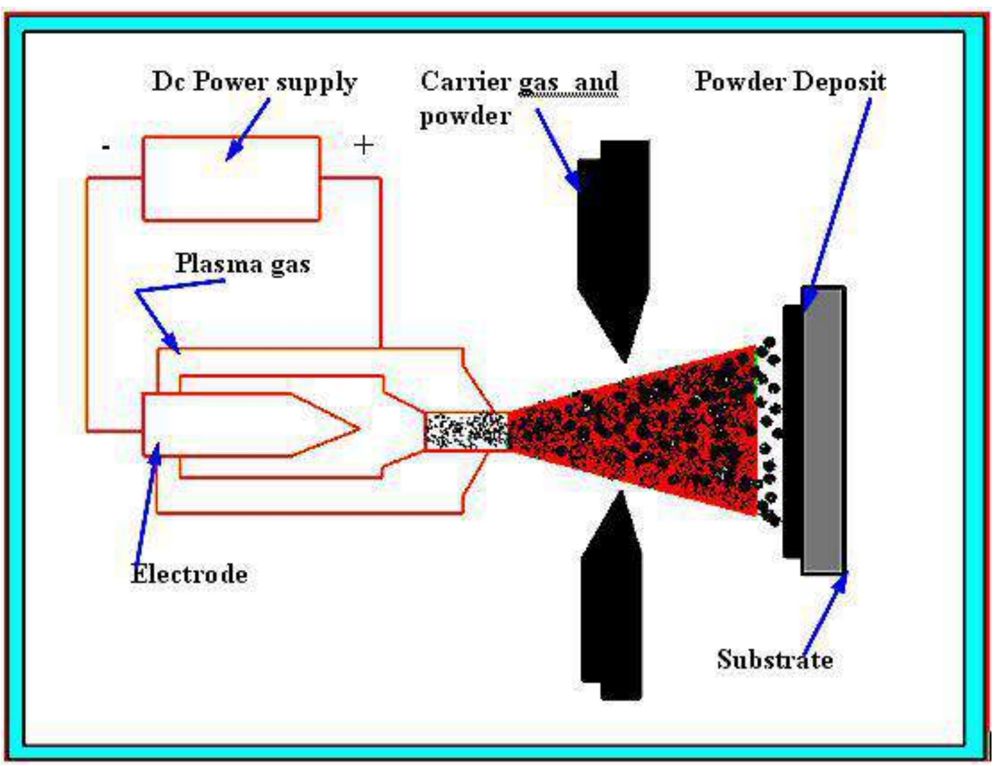

Figure 3 Plasma spraying-gun system

The plasma spray-coating is conducted either in an atmospheric or vacuum condition. When conducted in a vacuum condition, the plasma flame expands to 20 cm for more intensive coating to be obtained. The plasma spray-coating is the most widely accepted method of coating [25,28]. Figure 4 shows some coated piston tops.

(a) **(b)**

Figure 4 Ceramic coated piston tops

2.0 Materials and Methods

2.1 Materials

The three (3) materials used for the 3D modelling were a metal substrate called the aluminium alloy piston A2618, a metallic bond-coat of thickness 0.15 mm called the Nickel Chromium Aluminium Cobalt Yttria (NiCrAlCoY) with a chemical composition of Bal Ni, 17.5% Cr, 5.5% Al, 2.5% Co, 0.5% Y_2O_3; and ceramic topcoat also of thickness 0.35 mm called the Yttria Stabilized Zirconia (7.5% Y_2O_3-ZrO_2) [27]. This paper is part of our PhD work [27].

2.2 Methods

2.2.1 The design of the piston elements

Figure 5 shows the cross-sectional view of conventional or uncoated piston [27].

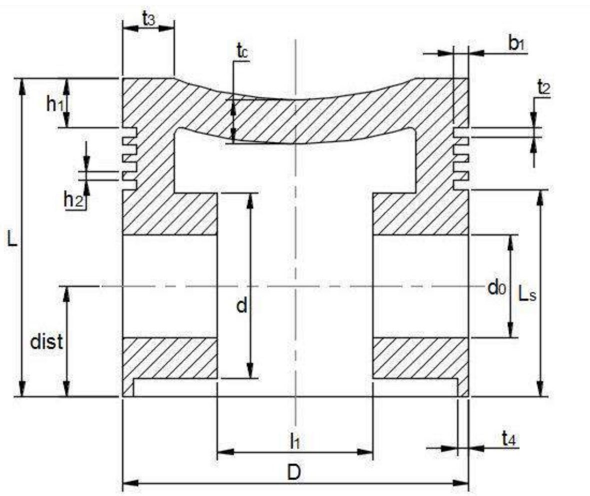

Figure 5 Cross-section of the model conventional piston

2.2.1.1 Design of the thickness of the piston head or crown, t_C:

According to Grashoff's formula, the piston head thickness t_C is given by,

$$t_C = \sqrt{\frac{3p_{max}D^2}{16\sigma_y}} \quad (1)$$

Where p_{max} is the maximum gas pressure (Pa),
D = the cylinder bore or outside diameter of the piston (m), σ_y = the permissible or yield tensile stress (strength) for the piston material (Pa)

2.2.1.2. The number of piston rings:

From Figure 2, we have total number of rings = 4 (number of compression rings = 3 and number of oil ring = 1)

2.2.1.3 Design of the radial thickness of the piston ring t_1:

Consider Eq. (2) for the design of piston ring radial thickness.

$$t_1 = D\sqrt{\frac{3p_w}{\sigma_p}} \quad (2)$$

Where p_w = allowable radial pressure of the gas on the cylinder wall taken as 0.025 MPa
σ_p = permissible bending or tensile stress for cast iron rings = 84 MPa

2.2.1.4 Design of the axial thickness of piston ring, t_2:

Also, consider Eq. (3) for the design of piston ring axial thickness.

$$t_2 = \frac{D}{10n_R} \text{ or } = 0.7t_1 \quad (3)$$

Where n_R = number of rings taken as 4

2.2.1.5 Determining the length of the piston pin in the connecting rod bushing, l_1

Eq. (4) gives the length of the piston pin.

$$l_1 = 0.45D \quad (4)$$

2.2.1.6 Design of the width of the piston top land h_1:

$$h_1 = 1.2\ t_C \quad (5)$$

2.2.1.7 Design of the width of other piston ring lands h_2:

$$h_2 = 0.75t_2 \quad (6)$$

2.2.1.8 Determining the piston barrel:

Piston Barrel thickness t_3 at the top end

$$t_3 = 0.03D + b_1 + 4.5 \quad (7)$$

$$b_1 = t_1 + 0.4 \quad (8)$$

Where b_1 = radial depth of the piston ring groove (mm)

The piston barrel thickness t_4 at the open end

$$t_4 = 0.25\ t_3 \quad (9)$$

2.2.1.9 Design of the length of the piston and piston skirt:

Length of the piston skirt, $l_s = 0.6\ D$ (10)

Total Length of Piston L = Length of the piston skirt + Length of the ring section + Top land

$$= l_s + (4\ t_2 + 3\ h_2) + h_1 \quad (11)$$

The length of the piston usually varies from D and 1.5D.

2.2.1.10 Design of the diameter of the piston boss and pin:

Outside diameter d_0 of piston pin:

$$d_0 = 0.3D \quad (12)$$

Piston Boss diameter $d = 1.5\ d_0$ (13)

Although, d_0 is given in the owner's manual. The value is 36 mm.

The inside diameter d_1 of the piston pin:

$$d_1 = 0.6\ d_0 \quad (14)$$

2.2.1.11 Design of the centre of the pin:

The centre of the pin is 0.02D to 0.04D above the centre of the skirt.

Centre of pin $= 0.04D + 0.5\ l_s$ (15)

The specifications for designing and modelling the conventional piston of the diesel-engine with the help of SOLIDWORKS software were that of the ZS1115NM single-cylinder, inline and four-stroke direct injection diesel engine manufactured by Changchai Company Ltd, China. The engine specifications are given in Table 1 [29].

Table 1 engine specification

Item	**Specification**
Engine model	ZS1115NM
Type	Single cylinder, four stroke, horizontal type, direct injection
Cylinder bore (D) (mm)	115
Piston stroke (L_S) (mm)	115
Piston displacement (V_s) (litre)	1.19
Compression ratio (c.r)	17:1
Rated output/brake power (b.p)(kW)	15.7
Rated speed (N)(Rev/min)	2200
Brake specific fuel consumption (bsfc) (g/kWh)	≤ 244.8
Specific lube oil consumption (g/kWh)	≤ 2.04
Lubricating method	Single circuit
Cooling method	Water cooled, evaporative
Cooling system	Radiator, natural convection
Starting method	Electric starting or hand cranking
Fuel injection pressure (MPa)	18.13 ± 0.49

Net weight (kg)	205
Overall dimension (L x W x H) (mm)	965 x 457 x 713
Mean piston speed (c_m) (m/s)	8.433
Fuel injection timing before TDC	22^0
Fuel type	Diesel
Chemical formula	$C_{14.4}H_{24.9}$
Connecting rod length (L_R) (mm)	258.5
Intake valve closes after TDC	38^0

Equations (1) – (15) can only be used in designing the piston if the maximum gas pressure p_{max} is known. The maximum gas pressure from our PhD work was 10.2 x 10^6 N/m^2 or 10.2 N/mm^2 [27]. The yield tensile strength of the material used for the piston, σ_t = 372 N/mm^2 [27]. Table 2 summarizes the sizes obtained from the design of the piston elements.

Table 2 size of piston parameters

S/N	Piston element	Size obtained (mm)
1	Cylinder bore, D	115
2	Thickness of the piston head, t_C	8.25
3	Radial thickness of the piston ring, t_1	3.436
4	Axial thickness of the piston ring, t_2	2.405
5	No of the piston rings, n_R	4
6	Width of the top land, h_1	9.9
7	Width of the ring land, h_2	1.80375
8	Radial depth of the piston ring groove, b_1	3.836
9	Thickness of the piston barrel at the top end, t_3	11.786
10	Thickness of the piston barrel at the open end, t_4	2.9465

11	Piston pin diameter, d_0	34.5
12	Diameter of the piston boss, d	51.75
13	Length of Skirt, l_s	69
14	Total length of the piston, L	93.93
15	Centre of pin above the centre of the skirt	39.10
16	Inside diameter of the piston pin, d_1	20.7
17	Length of the piston pin in the connecting rod bushing, l_1	51.75

2.3 Solidworks modelling of the conventional piston

The sizes obtained from the design of the piston elements in Table 4 were used in modelling the conventional piston in Solidworks CAD Software [28,30]. Figures 6 and 7 show the views of the modelled conventional piston.

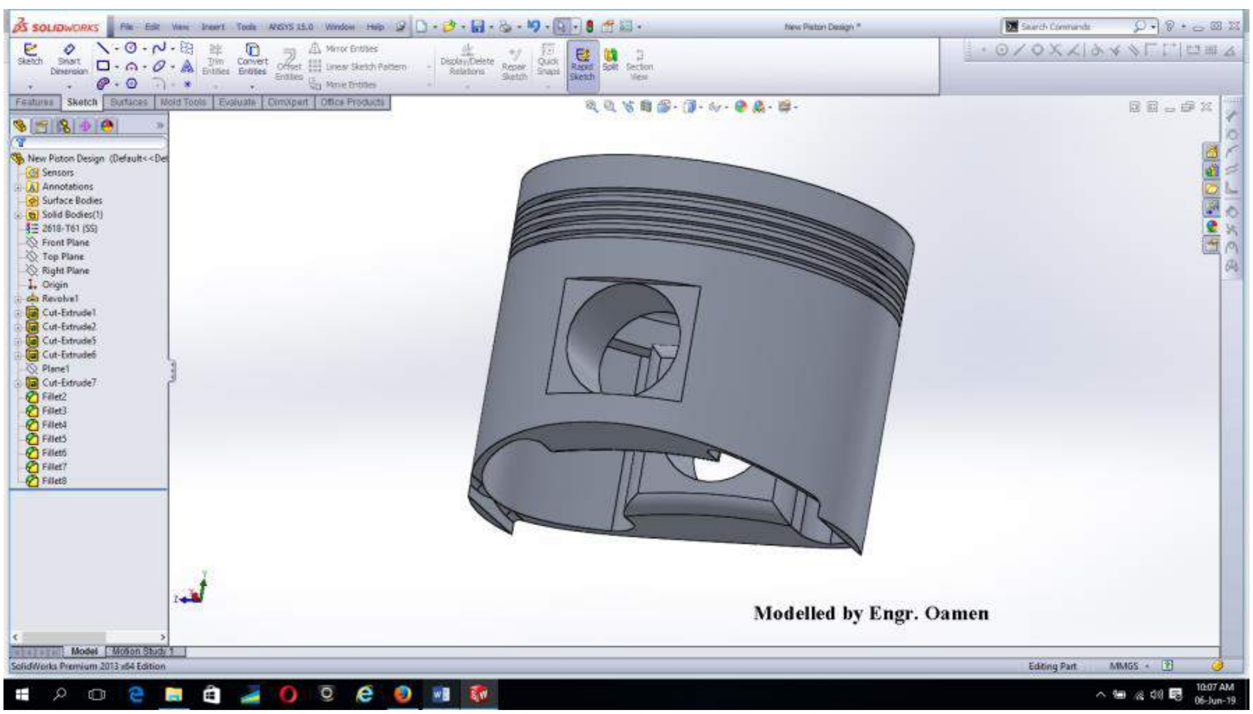

Figure 6 (a) The rotated view of the 3D modelled conventional piston

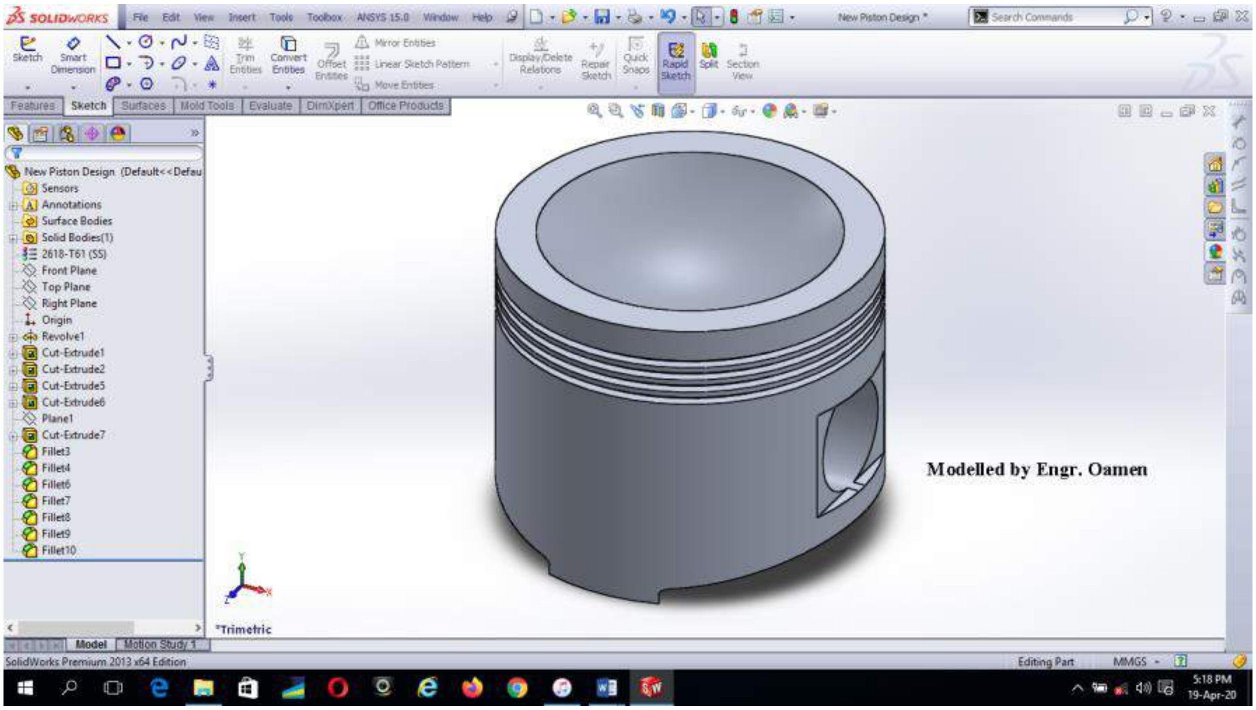

Figure 6 (b) The isometric view of the 3D modelled conventional piston

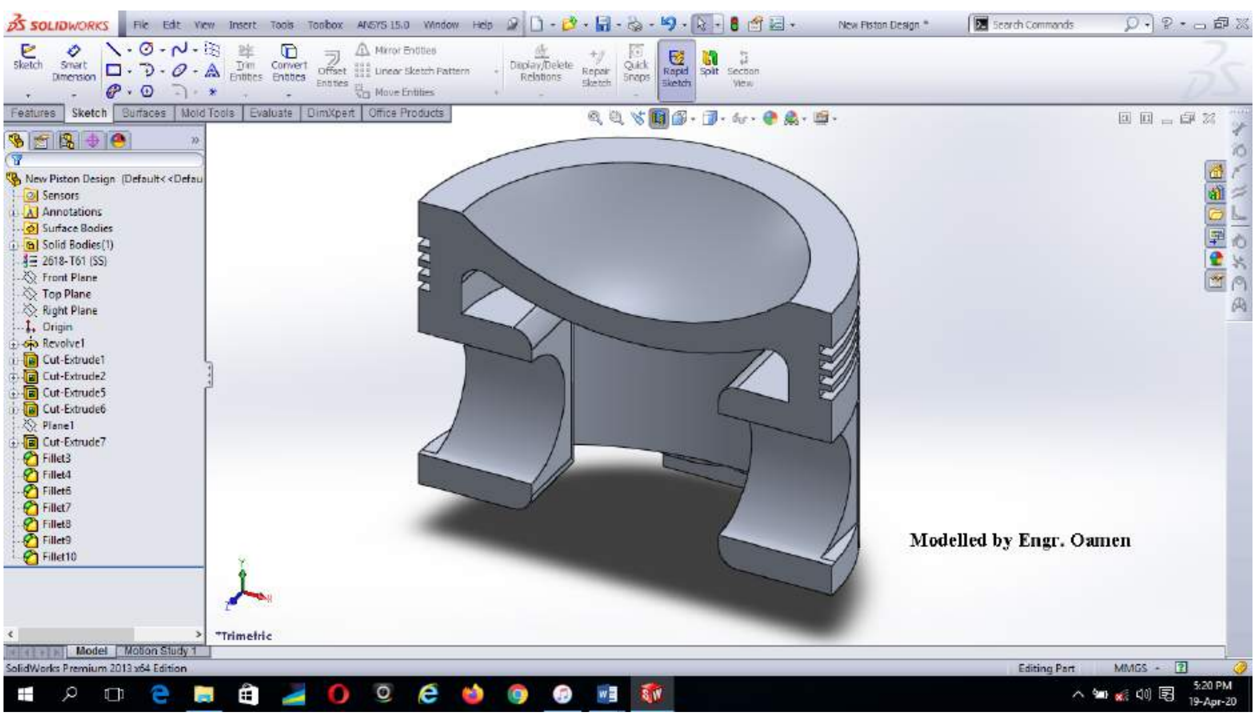

Figure 6 (c) The half view of the modelled conventional piston

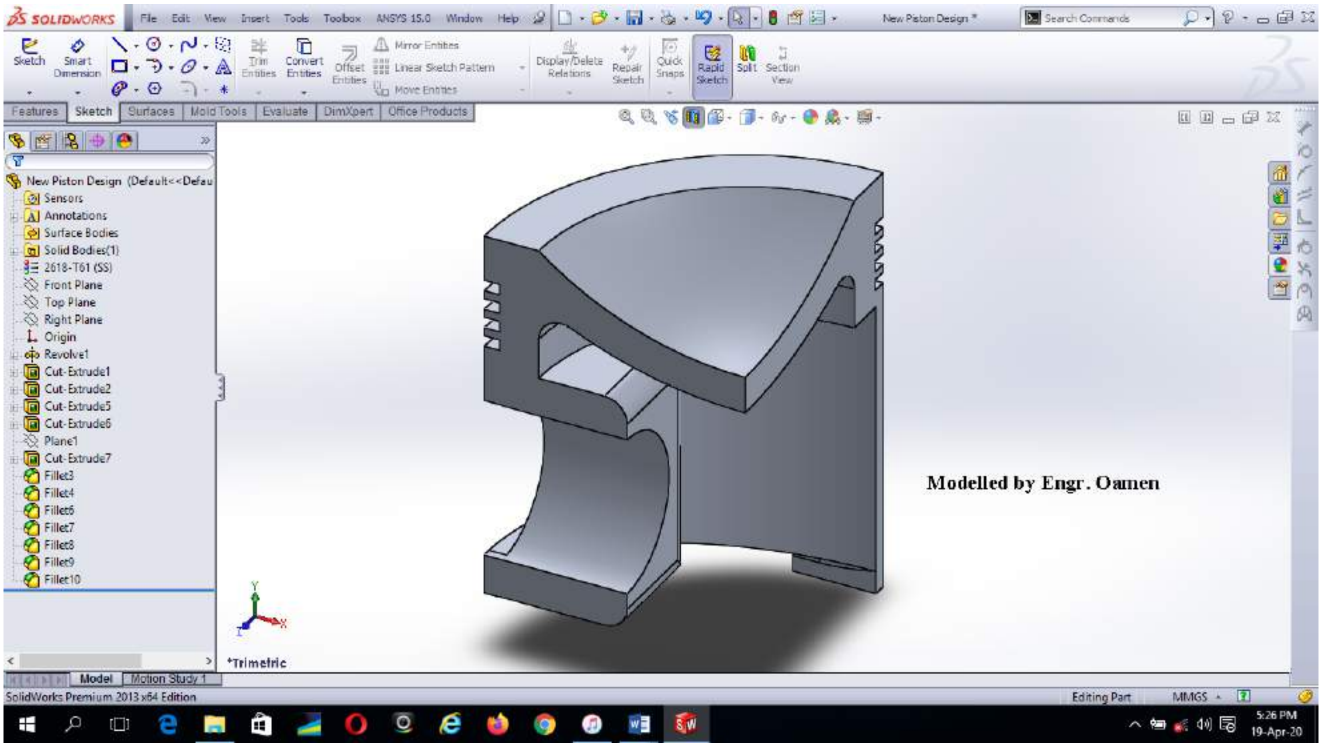

Figure 6 (d) The quarter view of the modelled conventional piston

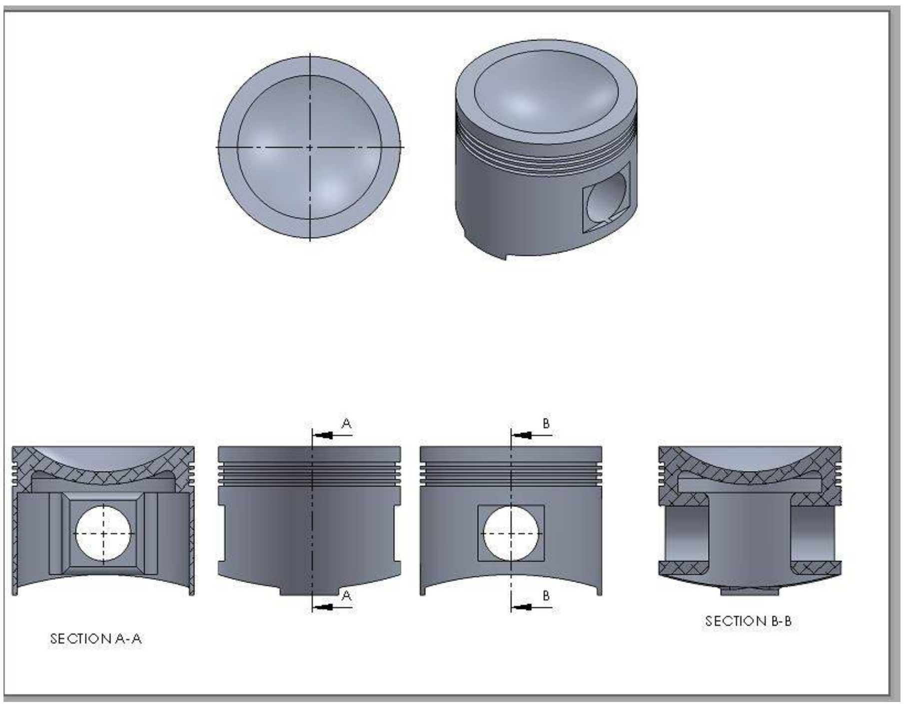

Figure 7 The sectional view of the modelled conventional piston

NIPES-NCEE Conference Proceedings
The 2nd International Conference 15th-17th Feb. 2023
361-378
www.nipesjournals.org.ng

2.4 Solidworks modelling of the bond-coat layer

The bond-coat layer of 0.15 mm thick was modelled in SolidWorks software. See Figure 8.

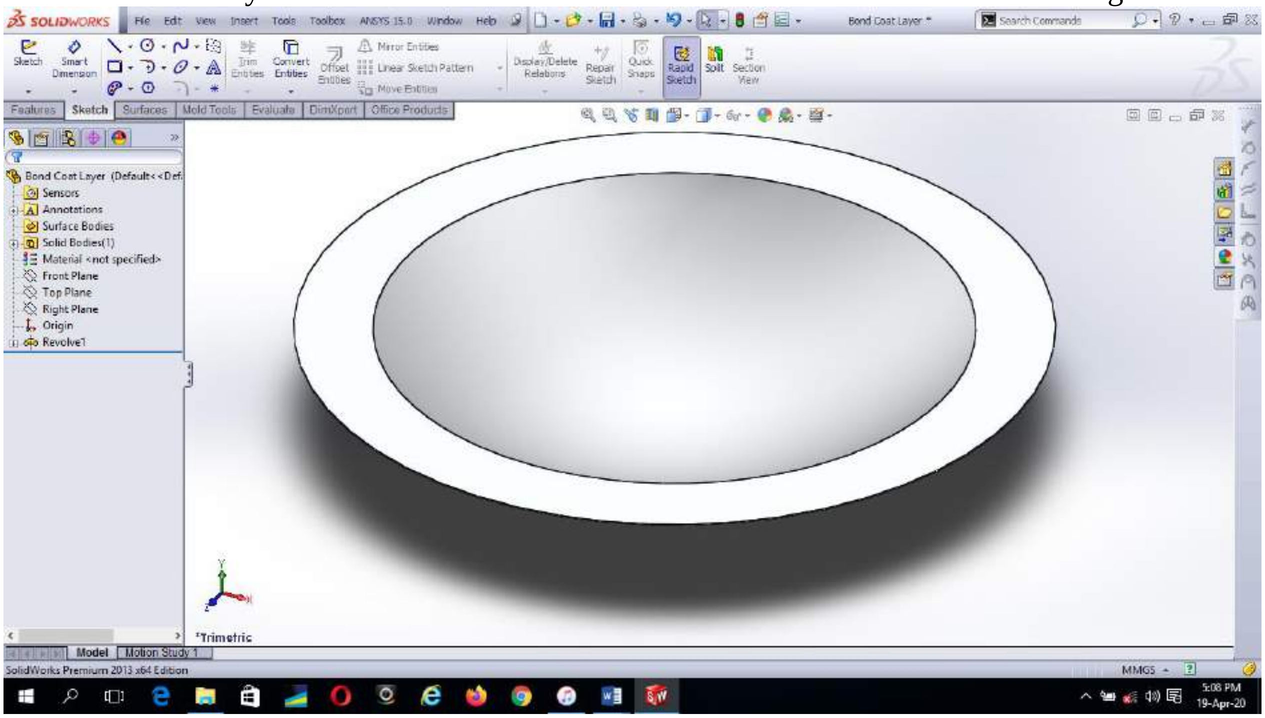

Figure 8 The modelled isometric view of the bond-coat layer of 0.15 thickness

2.5 Solidworks modelling of the topcoat layer

The topcoat layer of 0.35 mm thick was modelled in SolidWorks software. See Figure 9.

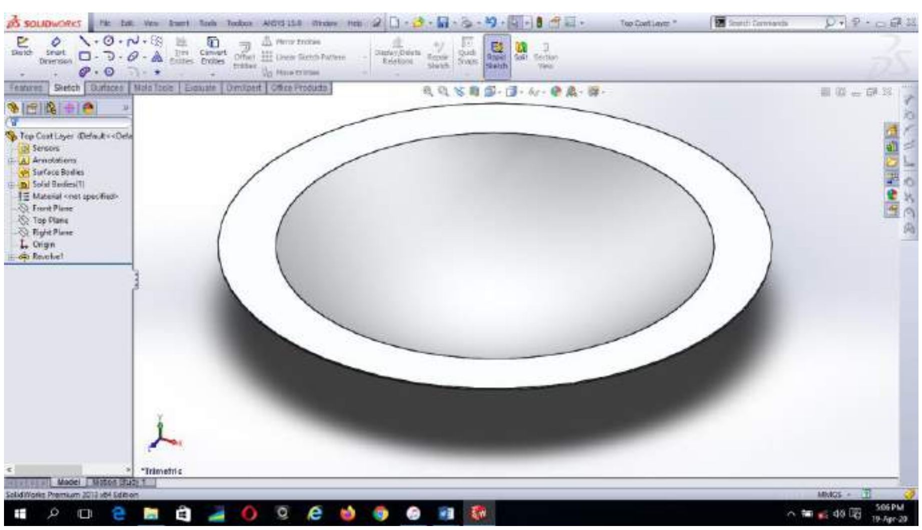

Figure 9 The modelled isometric view of the topcoat layer of 0.35 thickness

2.6 Solidworks assembling of the conventional piston, bond and topcoats layers

The assembling of the piston, bond-coat and topcoat layers was also carried out using the SolidWorks software. Figures 10 and 11 show the views of the modelled reconditioned piston.

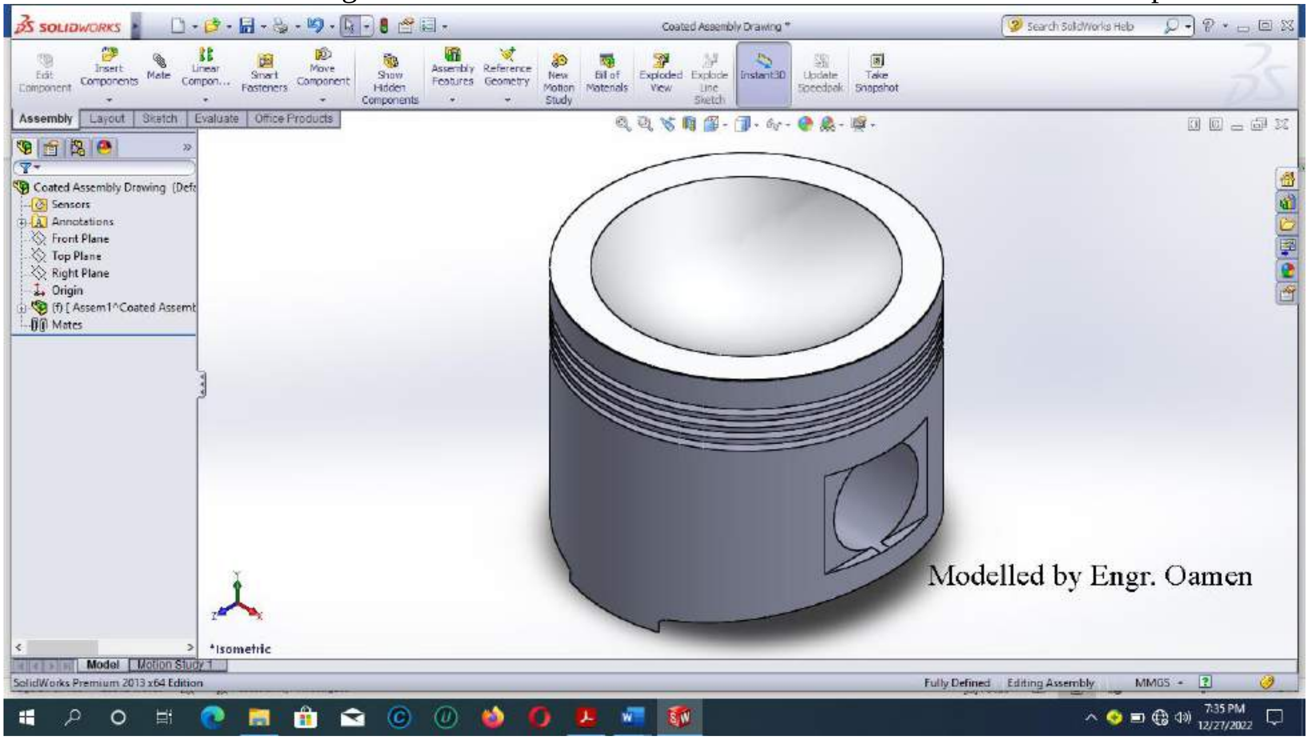

Figure 10 (a) The assembly view of the reconditioned piston with bond and topcoat layers

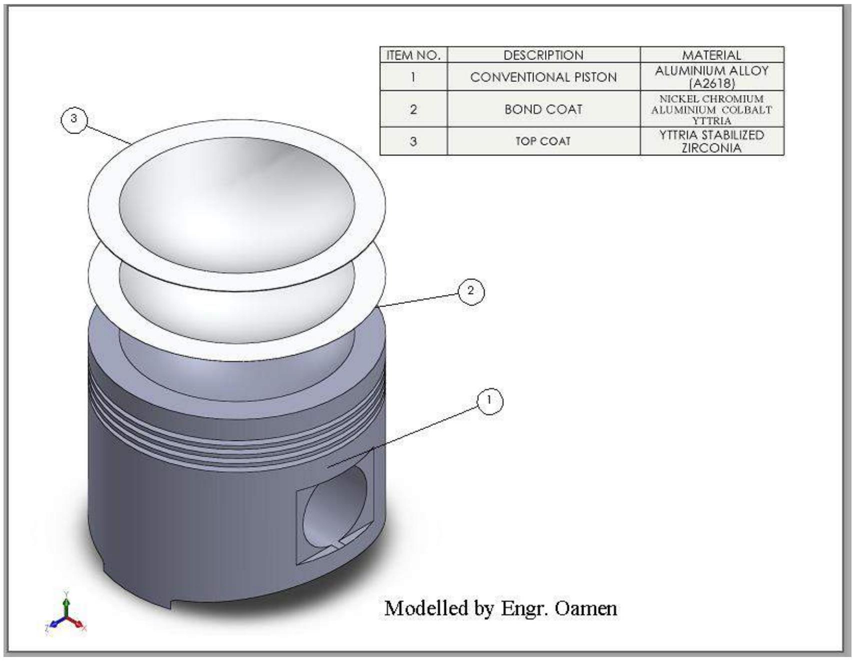

Figure 10 (b) The exploded view of the reconditioned piston with bond and topcoat layers

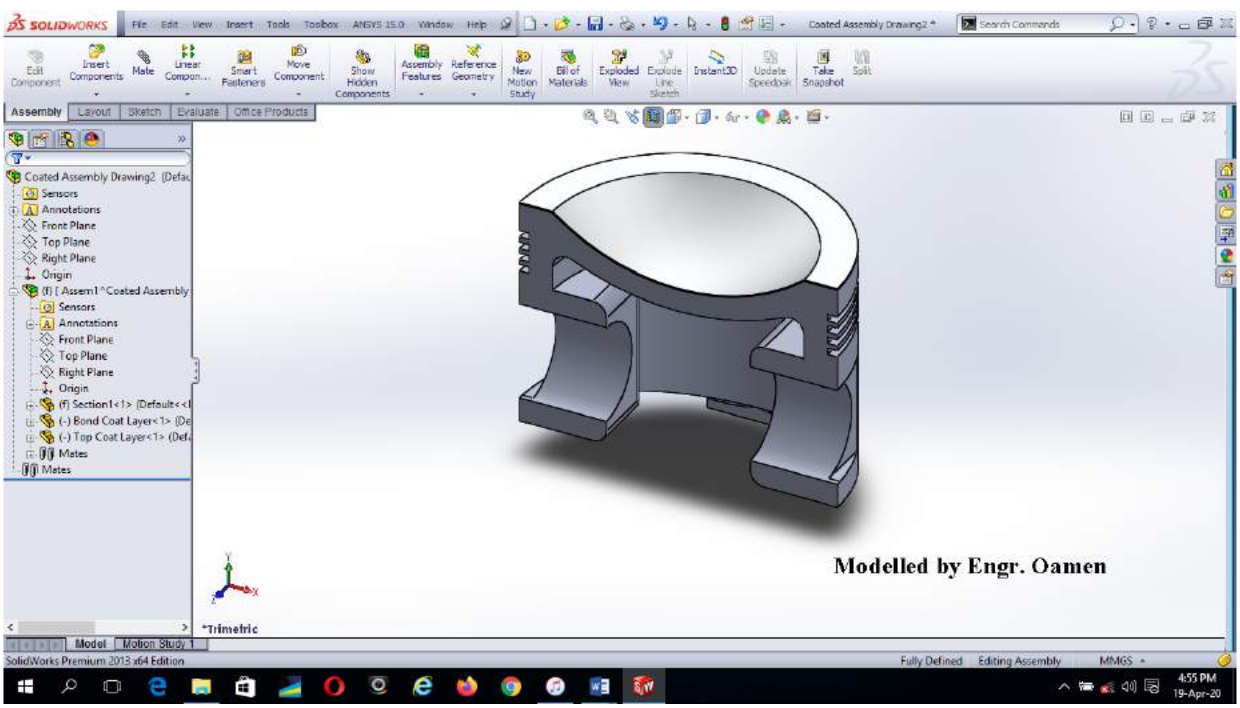

Figure 10 (c) The half assembly view of reconditioned piston with bond and topcoat layers

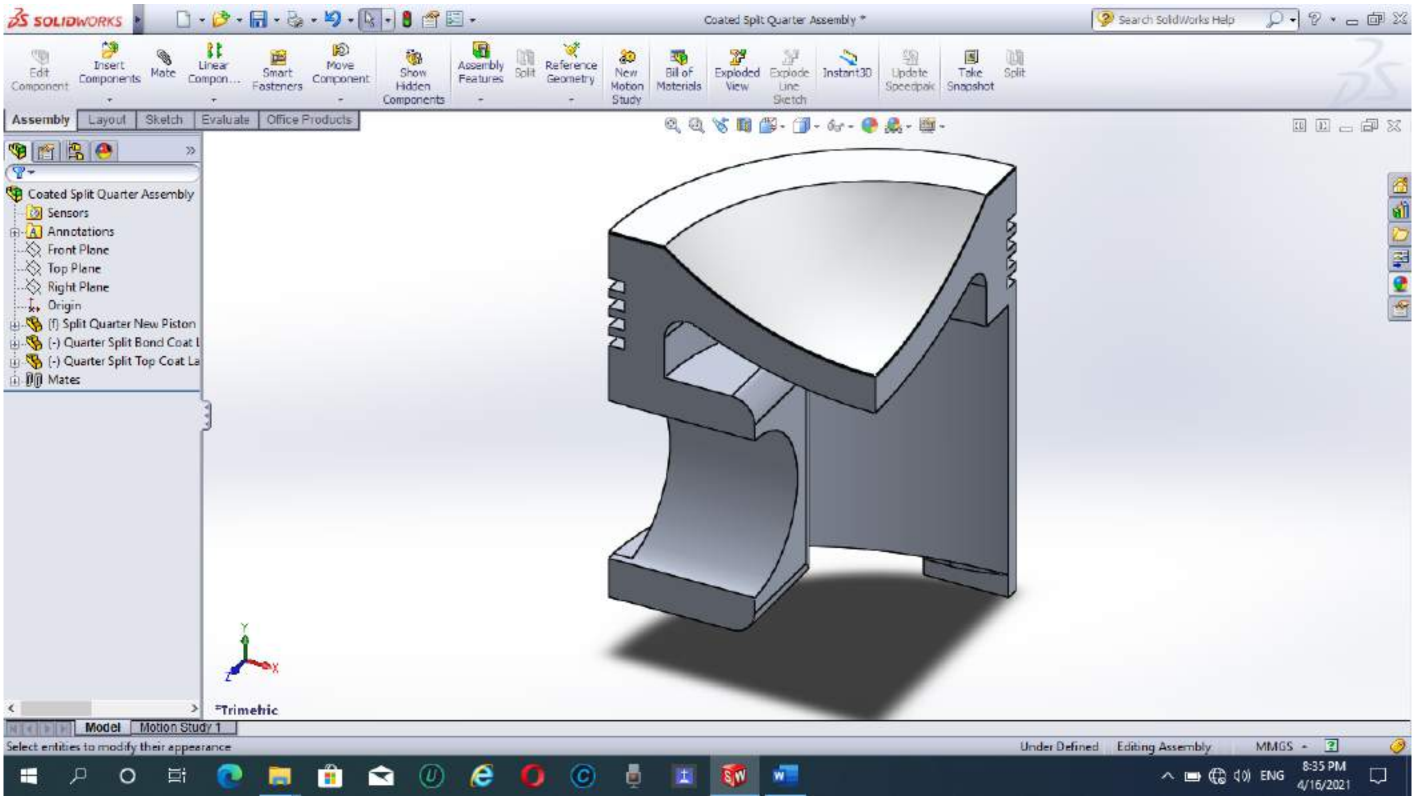

Figure 10 (d) The quarter assembly view of reconditioned piston with bond and topcoat layers

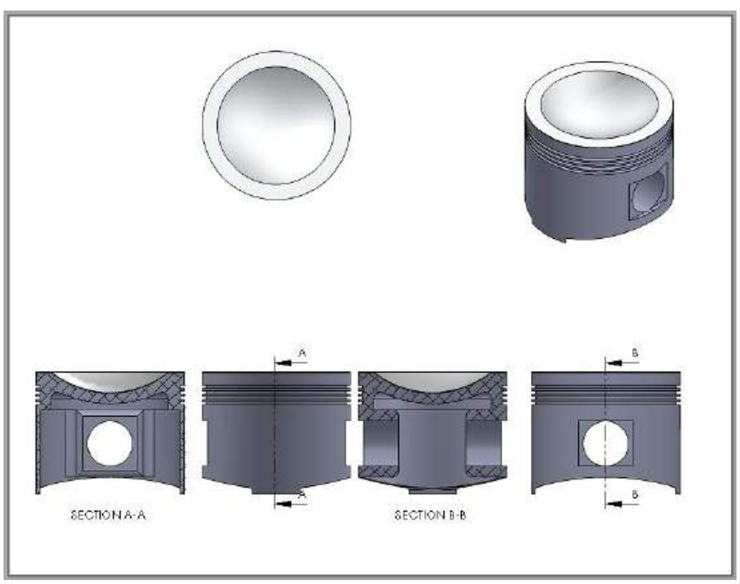

Figure 11 The sectional assembly view of reconditioned piston with bond and topcoat layers

3.0 Results and Discussion

Figures 6 to 11 show the results of modelling conventional and reconditioned pistons of the ZS1115NM single-cylinder, inline and four-stroke direct injection diesel engine using SOLIDWORKS 2013 CAD. This modelling provides the next stage involved in the reconditioning or coating of diesel engine pistons for improved performance.

4.0 Conclusions

Due to the upsurge of counterfeit spare parts in the market, meeting the original equipment manufacturer (OEM) standards requires a reconditioning process. Having modelled the thermal barrier-coated piston of a single-cylinder, inline and four-stroke direct injection diesel engine using SOLIDWORKS 2013 CAD, it could be concluded that with given engine specification suitable materials for designing and modelling a reconditioned piston of diesel engine are chosen and the model reconditioned.

References

[1] Ekrem, B. (2008). Thermal Analysis of Functionally Graded Coating AlSi Alloy and Steel Pistons. Journal of Energy Conversion and Management 202(16):325-336.
[2] Ramos, J. I. (1989). Internal Combustion Engine Modeling, 2nd ed. USA: Taylor and Francis 1-278.
[3] Heywood, J. B. (1988) Internal Combustion Engine Fundamentals, International Ed. USA: McGraw-Hill Book Company 1- 930.
[4] Dolan, J. A. (1991). Motor Vehicle Technology and Practical Work, Reprinted ed. Ibadan: Heinemann Educational Books Ltd 1-700.
[5] Röhrle, M. D. (1995). Pistons for Internal Combustion Engines – Fundamentals of Piston Technology, 2nd ed. Germany: Verlag ModerneIndustrie 1-70.
[6] Shirisha, G. S., & Sravani, D. K. (2016). Thermal Analysis of IC Engine Piston Using Finite Element Method. International Journal of Mechanical Engineering and Computer Applications 4(1):200-209.
[7] Lokesh, S., Suneer, S. R., Taufeeque, H., & Upendra, K. (2015). Finite Element Analysis of Piston in ANSYS. International Journal of Modern Trends in Engineering and Research (IJMTER) 2(4):619-626.
[8] Davis, J. R. (2004). Handbook of Thermal Spray Technology. USA: ASM International 1-347.
[9] Anders, T. (2017). Thermal Barrier-Coatings for Diesel Engines, 1st ed. Sweden: KTH Royal Institute of Technology 1-180.
[10] Pierz, P. M. (1993). Thermal Barrier-Coating Development for Diesel Engine Aluminium Pistons. Surface and Coatings Technology 61(1):60-66.
[11] Swati, S. C., & Vinayak, H. K. (2013). Piston Strength Analysis Using FEM. International Journal of Engineering Research and Applications 3:124-126.
[12] Deovrat, V., Ameya, P., Sampada, M., Nikita, S., & Atul, D. (2014). Design Analysis and Optimization of Piston and Determination of its Thermal Stresses Using CAE Tools. International Journal for Research in Applied Science and Engineering Technology (IJRASET) 3(5):273-277.
[13] Büyükkaya, E. (1994). Ceramic Coating Application and Performance Analysis in a Diesel Engine. Unpublished Msc Thesis. Istanbul Technical University, Turkey 1-80.
[14] Dipayan, S., Susenjit, S., & Samar, C. M. (2017). Thermo-mechanical Analysis of a Piston with Different Thermal Barrier-Coating Configuration. International Journal of Engineering Trends and Technology (IJETT) 48(6):335-349.

[15] Sridhar, K., Reji, R. K., & Narasimha, M. (2013). Thermal Barrier Analysis in Diesel. International Journal of Modern Engineering Research (IJMER) 3(3):1435-1441.
[16] Rohini, A., & Prema, S. (2020). A Review on Thermal Barrier-Coating for Diesel Engine and its Characteristics Studies. International Conference on Thermo-fluids and Energy Systems 1473:1-11.
[17] Ansari, F. A., & Dhanajay, Y. (2022). Review Paper on Simulation, Analysis and Validation on Thermal Barrier Coated Piston of Diesel Engine. International Research Journal of Modernization in Engineering Technology and Science 4(2):260-270.
[18] Adnan, P., Halit, Y., Can, H., & Ahmet, K. (2005). The Effects of Injection Timing on NOx Emissions of a Low Heat Rejection Indirect Diesel Injection Engine. Journal of Applied Thermal Engineering 25:3042–3052.
[19] Ekrem, B., Tahsin, E., & Muhammet, C. (2006). Effects of Thermal Barrier-Coating on Gas Emissions and Performance of a LHR Engine with Different Injection Timings and Valve Adjustments. Journal of Energy Conversion and Management 47:298–1310.
[20] Ekrem, B., & Muhammet, C. (2007). Thermal Analysis of a Ceramic Coating Diesel Engine Piston Using 3-D Finite Element Method. Journal of Surface and Coatings Technology 202:398–402.
[21] Navin, R., Mohammad, A. K., Mahendra, V., & Yew, H. T. (2021). Effect of Thermal Barrier-Coating on the Performance and Emissions of Diesel Engine operated with Conventional Diesel and Palm Oil Biodiesel. Coatings 11(692):1-14.
[22] Masera, K., & Hossain, A. K. (2019). Combustion Characteristics of Cottonseed Biodiesel and Chicken Fat Biodiesel Mixture in a Multi-Cylinder Compression Ignition Engine. SAE Tech 4:1-14.
[23] Khor, K. A., Murakosh, Y., Takahashi, M., & Sano, T. (1995). Plasma Spraying of Titanium Aluminide Coatings: Process Parameters and Microstructure. Journal of Materials Processing Technology 48:413–419.
[24] Isaac, F. O. (2022). A Review of Coating Methods and their Applications in Compression and Spark-Ignition Engines for Enhanced Performance. FUOYE Journal of Engineering and Technology 7(2):217-221.
[25] Malmberg, S., & Heberlein, J. (1993). Effect of Plasma Spray Operating Conditions on Plasma Jet Characteristics and Coating Properties. Journal of Thermal Spray Technology 2(4):339–344.
[26] Kuldeep, S., & Jakhar, O. P. (2014). The Behaviour of Temperature on Insulated ($MgZrO_3$) Diesel Engine Piston with ANSYS. International Journal of Emerging Technology and Advanced Engineering 4(8):692-695.
[27] Isaac, F. O. (2021). Unpublished Ph.D Dissertation, Ambrose Alli University, Ekpoma.
[28] Isaac, F. O., & Abu, L. (2022). Modelling of a Conventional Piston of a Single-Cylinder Four-Stroke Diesel Engine by Using SolidWorks. FUOYE Journal of Engineering and Technology 7(1):65-68.
[29] ZS1115NM. (2015). Single Cylinder Diesel Engine Owner's Manual. Changchai Company Ltd, China 1-40.
[30] James, B. D. (2016). Engineering Design and Graphics with SOLIDWORKS, 1st ed. Boston: Pearson 1-829.

NIPES-NCEE Conference Proceedings
The 2nd International Conference 15th-17th Feb. 2023
379-392
www.nipesjournals.org.ng

A COMPARATIVE STUDY OF PRE-TREATMENT AND HYDROLYSIS ON CORN COB AND CASSAVA BAGASSE FOR THE PRODUCTION OF BIOBUTANOL

Authors: Engr. I.P. Egharevba and Eboka Ifeoma Christy

Department of chemical engineering, University of Benin, Benin city, Edo state.
Email address: imuetinyan.egharevba@uniben.edu and
Ifeoma.eboka@eng.uniben.edu

ABSTRACT

The global population and industrialization have increased energy demand. This study focused on biobutanol production for biofuels and other high-value products. This study compares corn cob and cassava bagasse biobutanol production. Due to their estimated hemicellulose, cellulose, and lignin content, corn cob and cassava bagasse, both waste products, are suitable biobutanol feedstocks. Lab analysis did this. Dilute sulfuric acid and enzymatic hydrolysis produced fermentable sugar. The response surface methodology was used to optimize the sulfuric pretreatment's concentration, temperature, and time. This was done to recover lots of fermentable sugars from both feedstocks. At 760C, 31 minutes, and 4.3% (w/w) hydrogen sulfide, total sugars in corn cob and cassava bagasse showed their highest response, which was 804.23 mg/L and 807.28 mg/L, respectively. Enzymatic hydrolysis using cellulase and beta-glucosidase enzymes was performed under these conditions. Within the first 24 hours after hydrolysis, there was an overall increase of 15% in the total sugars. Because of the findings of this research, it is possible to draw the conclusion that corncob bagasse and cassava bagasse are two excellent and environmentally friendly feedstock options for the production of biobutanol.

1 INTRODUCTION

The world's transportation system is reliant on fossil fuels, and with crude oil prices soaring, demand for fossil fuels continues to grow. However. Demand for fossil fuels will not be met because they are a finite resources. When compared When compared to other wind and solar power, biomass can be instantly converted into petroleum products known as "biofuels.". The energy source will contribute to meeting the transportation fuel requirement.[1]**.** Agricultural product such as sugarcane, cassava, maize, are use for the production of biofuels. Nigeria is the 11th largest maize producer and Africa's 2nd largest maize producer. Nigeria's maize production climbed from 931 thousand tonnes in 1971 to 11,500 thousand tonnes in 2020, expanding at a 7.57 percent yearly pace. The annual maise grain production will leave a corn cob residue which can be utilized in sugar production[2].

The most potential feedstock is lignocellulosic material, which is a renewable natural resource. It is common in many poor countries for agricultural wastes to not be completely disposed of, and this has resulted in environmental contamination.[3]. For the development of biofuels that may be used as an alternative to fossil fuels, lignocellulosic biomass is the highest plentiful and renewable substance on the planet.[4] .The three main steps for the process of lignocellulosic biomass conversion into different value-added products: pre-treatment, enzymatic hydrolysis and fermentation. Cellulose, hemicelluloses and lignin are the three natural polymers composed mainly with lignocellulosic biomass.[5]

Pretreatment is a critical step in the conversion of complicated carbohydrate polymers into fermentable sugars. It is accomplished by making cellulose more available to the enzymes that convert the complex carbohydrate polymers into fermentable sugars. The final step is to destroy up the lignin polymers and cause the crystalline structure of cellulose to become disrupted. Several of today's biomass pretreatments (such as ethanol organosolv pretreatment, dilute acid pretreatment, and ammonia recycling percolation) are designed to separate the various biomass components (lignin, hemicellulose, and cellulose) into distinct processing streams. It has been shown that the eradication of lignin and/or hemicellulose can significantly lessen the reluctance of biomass to be broken down by enzymes. [6]
Lignocellulose can be hydrolyzed to yield simple sugars, which can be obtained either enzymatically by (hemi)cellulolytic enzymes or other acids, or chemically by sulfuric acids, depending on the method used. Despite the fact that fewer fermentation inhibitor products are produced, enzymatic hydrolysis is becoming a more preferred method due to the fact that it requires less energy and operates in a more benign environment. The deconstruction of lignocellulose by enzymes is complicated because it has various structural characteristics that make it extremely refractory. In addition to the complex network produced by cellulose, hemicellulose, and lignin, some enzymes can be absorbed by condensed lignin, resulting in a reduction in hydrolysis yield due to non-specific connect by the enzymes. [7]. All kinds of wastes from agriculture and forestry as well as grasses and other woody materials are all examples of lignocellulosic resources that have significant potential for use in biofuel generation [8]. Typically, the majority of agricultural lignocellulosic biomass is composed of around 10 percent to 25 percent lignin, 20 percent to 30 percent hemicellulose, and 40 percent to 50 percent cellulose, with the remaining 10 percent to 25 percent being hemicellulose[3].

2 MATERIALS AND METHODS

Manual size reduction, drying, grinding, and sieving are all part of the sample preparation procedure. This was done to get the sample ready for hydrolysis and pretreatment. Corn cob and cassava bagasse purchased from Uselu market was sun dried for 30 days. The sample was sun dried to minimize moisture, facilitate size reduction, and save oven energy. It was milled and sieved after drying to achieve a fine particle with a wide surface area with a particle size characteristic of 1.50mm. Larger sizes were machined down to the desired dimensions. The sample was ground into powder to improve surface area and hence aid contact between the sample and the chemical. Prior to usage, the sample was stored in an airtight bag and kept dry environment

2.1 Characterization analysis

The amount of cellulose, hemicellulose, and lignin in corn cob and cassava bagasse was analyzed, and the results are presented as dry weight units in Table 1. Cellulose, hemicelluloses, and lignin make up the composition of corn cobs and cassava bagasse at 0.5% NaOH alkaline concentration, as shown in Table 1. The primary structural component of plant cell walls is cellulose. Cellulose is a highly crystalline material, which contributes significantly to its resistance to enzymatic hydrolysis. Hemicellulose acts as a link between cellulose and lignin, thereby increasing the rigidity of the cellulose-hemicellulose-lignin network. Hemicellulose is a heteropolymer composed of five-carbon sugars (such as xylose and arabinose) and six-carbon sugars (e.g. mannose, glucose, and galactose). Hemicellulose's molecular weight is lower than cellulose's. Lignin is a very complex molecule composed of three types of phenolic acids (p-coumaryl, coniferyl, and sinapyl alcohol) linked in a three-dimensional structure that makes lignin especially difficult to hydrolyze [9]. Pretreatment with sulfuric acid could increase the surface area and porosity, which are advantageous for enzymatic hydrolysis of lignocelluloses. Consequently, the biomass level fractions for hemicellulose, cellulose, and lignin are displayed;

Table 1; Composition analysis of corn cob and cassava Bagasse

COMPOSITION (0.5 of NaOH Concentration0	**Corn Cob (Content %)**	**Cassava Bagasse (content %)**
Cellulose	59.69%	75%
Hemicellulose	30%	16%
Lignin	3.33%	3.33%

2.2 Dilute Acid Pretreatment . The process begins with the pretreatment of the biomass, then moves on to the enzymatic hydrolysis to produce simple sugars, then moves on to the fermentation of the simple sugars to produce biofuels, and finally moves on to the separation of the end product. [10]

Before being transferred to a conical flask to begin the pre-treatment process for both cassava bagasse and maize cob, 5g of each feedstock were weighed on an analytical weighing scale. Following that, the samples were added to a 100ml solution of sulfuric acid that was made by mixing various concentrations of H2S04 with 100ml of water. the sample was taken out of the autoclave and allowed to cool after the solution had been heated in it for various amounts of time.

All experiments with pretreatment were done three times. The solid and liquid components were separated using the Buchner funnel and filter paper. Following neutralization of the pH, the solid residue was washed with distilled water and dried for use in further study. 3 ml of the filtrate was metered out with a syringe and put to a boiling tube following filtration. Additionally, 1ml of DNS solution was measured and added to the boiling tube's measured filtrate. The boiling tube's solution was heated on a hot plate and brought to a boil for five minutes. The absorbance of the solution was then determined using a UV spectrophotometer.

The efficacy of the pretreatment was measured by measuring the sugar content of the liquid fraction known as hydrolysate. The amount of sugar released from the degradation of cellulose, hemicellulose, and lignin was measured after the pretreatment.. [11]

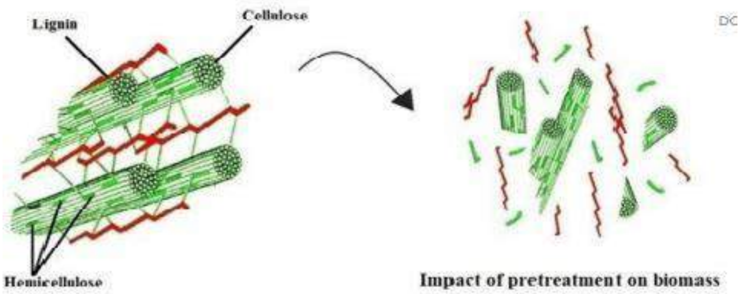

Figure 1: Schematic of goals of pretreatment on lignocellulosic material [12]

Pretreatment is a critical step in the development of successful cellulose conversion techniques. The pretreatment of cellulosic biomass, as illustrated in the schematic diagram of Fig. 1, is necessary to alter the structure of the biomass in order to make cellulose more available to the enzymes that transform carbohydrate polymers into fermentable sugars[11]

2.3 Design of experiment

The experiment was set up with a central composite design with three factors. Optimizing the CCD's reactions through response surface analysis. The acid content (1-3%), temperature (100^{o}C134°C), and time (trial duration) were each coded as one of three levels to be improved (10-30 minutes). Listed in Table 3.3 are the coded and uncoded factors (A, B, and C) and their corresponding levels. For the purpose of optimizing pretreatment with Response Surface Methodology, total sugars yield was selected as the response (RSM). As many as twenty iterations of the experimental design were conducted. Design Expert was used to do an ANOVA and create response surface plots. Numerical optimization was used to find the optimal value of the independent variables for the best possible response.[13]

Y = a1X1 + a2X2 + a3X3 + a11X12 + a22X22 + a33X32 + a12X1X2 + a13X1X3 + a23X2X3 + a0 where Y = total sugars (g/L), a_i = the linear coefficients, a_{ii} = the quadratic coefficient, a_{ij} = the cross-product coefficients, and a_0 = the model constant.

The quadratic model was used to determine fit while the F and t-test was used in illustrating the significance of response

Table 2; coded and acutal levels

Variables	Units	Symbols	Coded and actual levels		
			-1	0	+1
Temperature	°C	A	40	70	100
Time	Min	B	30	45	60
Acid concentration	%	C	1	5	10

2.4 Appropriate model determination

We chose the best model after examining linear, cubic, two-factor interaction, and quadratic models because it was statistically meaningful and offered the most accurate definition of the relationship between the response and the input variables (independent variables). Tables 4.3a and 4.3b display the summary statistics for the model. As demonstrated, the quadratic model has the highest predicted and adjusted R2 value. The quadratic model best describes the relationship between the response and the independent variables, so this is the conclusion to be drawn. **Table 3: model summary statistics on corn cob and cassava bagasse**

Source	**Sequential p-value**		**Lack of fit p-value**		**Adjusted R^2**		**Predicted R^2**		
	Corn cob	**Cassava Bagasse**	**Corn cob**	**Cassava Bagasse**	**Corn cob**	**Cassava Bagasse**	**Corn cob**	**Cassava Bagasse**	
Linear	0.7985	0.7548	<0.0001	<0.0002	-0.1168	-0.1046	-0.3441	-0.4065	
2FI	0.9590	0.8514	<0.0001	<0.0001	-0.3438	-0.02820	-1.8478	-1.8478	
Quadratic	**<0.0001**	**<0.0001**	**0.0002**	**0.1886**	**0.9422**	**0.9446**	**0.7729**	**0.9422**	**Suggested**
Cubic	0.9978	0.9822	<0.0001	0.0223	0.9056	0.9128	-5.4721	-3.1434	**Aliased**

2.5 Modeling and Analytical review using RSM

Using central composite design varied with acid concentration, time and temperature, the actual and predicted values of the factors A (Temperature), B (Concentration) and C (time) as designed with Design Expert 13 and their corresponding outputs are shown in table 4

Table 4: The experimental responses of the dependent variable Y (sugar yield in mg/L). Experimental vs. predicted yield.

Run	Temperature ^{0}C	Acid conc %	Time Mins	Response sugar yield for cassava bagasse Mg/L		Response sugar yield for corn cob Mg/L	
				Actual	**Predicted**	**Actual**	**Predicted**
1	70	5.5	40	850.871	965.242	901.357	923.594
2	87.8381	2.82428	51.8921	405.507	427.437	432.581	476.667
3	52.1619	8.17572	51.8921	514.705	552.419	389.714	436.926
4	70	1	40	665.867	611.259	380.689	334.344
5	40	5.5	40	123.488	50.108	419.946	369.883
6	70	5.5	40	984.262	965.242	924.421	923.594
7	87.8381	8.17572	51.8921	752.954	776.856	604.499	642.358
8	70	10	40	911.336	853.621	570.101	510.933
9	52.1619	8.17572	28.1079	348.652	406.145	504.326	534.848
10	70	5.5	40	984.262	965.242	924.421	923.594
11	87.8381	8.17572	28.1079	366.250	408.598	522.375	566.781
12	70	5.5	40	984.262	965.242	924.421	923.594
13	70	5.5	40	984.262	965.242	924.421	923.594

14	87.8381	2.82428	28.1079	373.469	415.177	398.738	426.133
15	52.1619	2.82428	51.8921	220.548	257.622	337.371	367.573
16	100	5.5	40	233.911	194.968	543.922	488.472
17	70	5.5	40	984.262	965.242	924.421	923.594
18	70	5.5	20	635.114	556.224	766.942	720.217
19	52.1619	2.82428	28.1079	411.824	467.345	453.788	490.538
20	70	5.5	60	722.968	689.535	739.157	680.369

2.6 Statistical analysis of experimental data

Using the response surface methodology, the effect of independent variables (temperature, time, and concentration) on the response (sugar yield) was quantified. It was determined that the polynomial equation of second degree best represents the relationship between independent variables and the response. Equation 4.1 is expressed in terms of coded factors and is used to forecast the response for given levels of each factor. High levels of factors are coded as +1 by default, while low levels are coded as -1. **By comparing the coefficients, the coded equation is useful for determining the relative impact of the factors.**

Yield of corn cob = $923.59 + 35.29A + 52.50B - 11.85C + 24.08AB + 43.37AC + 6.26BC - 174.80A^2 - 177.11B^2 - 78.95C^2$ Equation 1

Yield of cassava bagasse = $965.24 + 43.07A + 72.05B + 39.63C + 13.66AB + 55.50AC + 89.00BC - 297.94A2 - 82.31B2 - 121.04C2$ Equation 2

The final equation in terms of actual factors

Predictions of the outcome for a given set of input levels can be made using the equation expressed in terms of the actual factors. For this purpose, it is important to specify the levels in the original units for each consideration. Because the coefficients are scaled to satisfy the units of each factor and the intercept is not at the center of the design space, this equation should not be used to determine the relative impact of each factor.

Sugar yield of corn cob = $-2806.12365 + 67.93166A + 248.55268B + 28.26899C + 0.504600AB +$

0.204469AC + 0.196759BC – 0.549352A2 -24.73855B2 -0.558253C2 Equation 3

Sugar yield of cassava bagasse = +4332.45812 + 121.46363A + 21.481319B + 38.10912C + 0.2860698AB + 0.261609AC + 2.79698BC -0.936337A^2 -11.49639B^2 – 0.855905C^2 Equation4

2.7 Response surface plots

The sugar yield-optimal conditions for acid pretreatment are the focus of my design. We used a three-dimensional plot and contour plots to compare independent and dependent variables in order to reach this conclusion.After acid pretreatment, a visual observation can be made between (Temperature, Time, and Acid concentration) for the total sugars via the response surface plot. In order to maximize the post-pretreatment total sugar yield, a 3D surface response plot and a 2D contour plot are used to optimize the fermentation variables [14]. The 3D plots' shape reveals important interactions between the variables studied. The dome-shaped plots suggest that there is mutual interaction between variables. Other patterns in the scatter plot suggested highly significant interactions between the variables. [15].

(A) (B) (C)

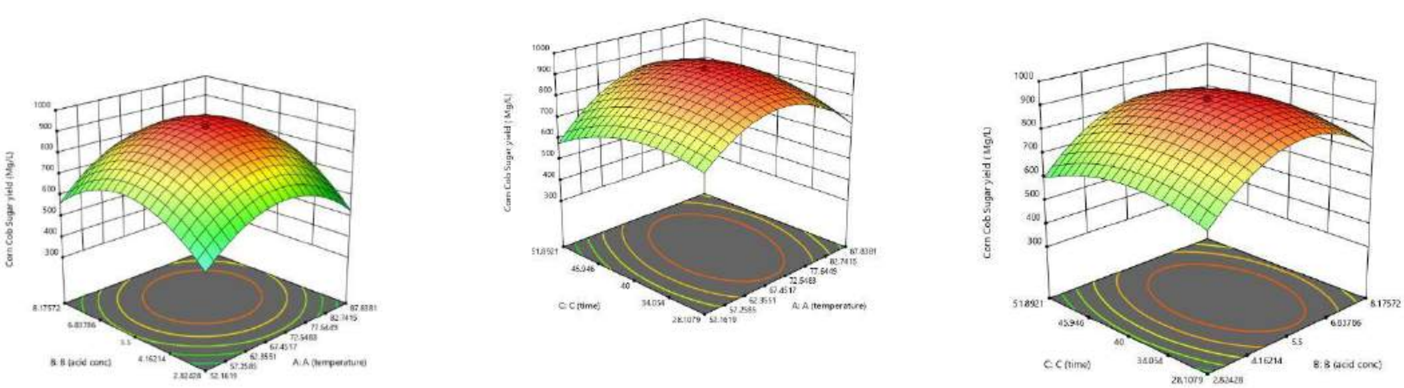

(D) (E) (F)

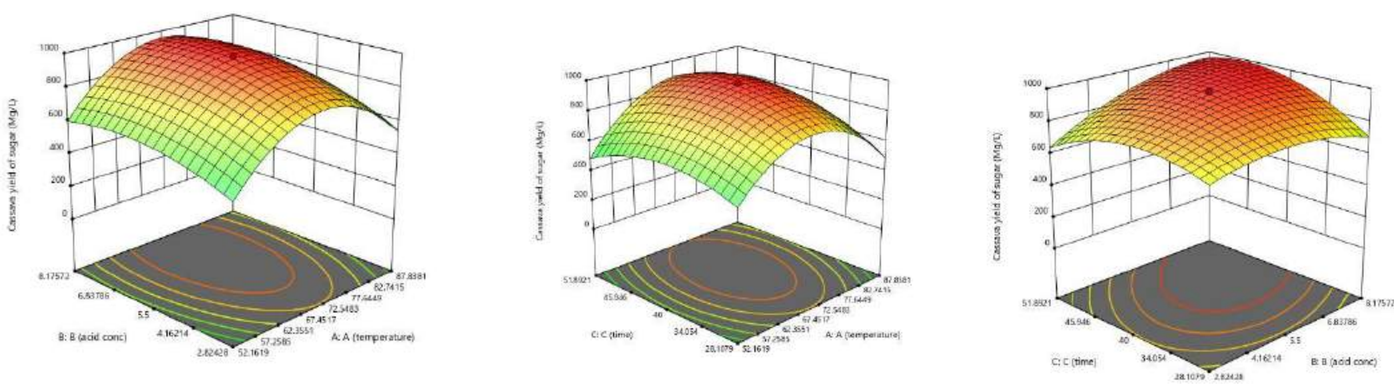

Figure 2;3D response surface plot of (A) interaction between temperature and acid concentration for corn cob;(B) interaction between time and temperature for corn cob;(C0 interaction between time and acid concentration for corn cob; (D) interaction between temperature and acid concentration for cassava bagasse; (E) interaction between time and temperature for cassava bagasse; (F) interaction between time and acid concentration for cassava bagasse

2.8 ANOVA for response surface quadratic model Table 5: Analysis of Variance Table on Corn cob

Source	**Sum of Squares**	**Df**	**Mean Square**	**Fvalue**	**p-value**	
Model	9.210E+05	9	1.023E+05	35.42	< 0.0001	Significant
A-Temperature	16975.96	1	16975.96	5.88	0.0358	
B-Acid concentration	37641.97	1	37641.96	13.03	0.0048	
C-Time	1916.75	1	1916.75	0.6635	0.4343	
AB	4640.47	1	4640.47	1.61	0.2337	
AC	15050.78	1	15050.78	5.21	0.0456	
BC	313.58	1	313.58	0.1085	0.7486	
A^2	4.404E+05	1	4.404E+05	152.43	<0.0001	

B^2	4.521E+05	1	4.521E+05	156.49	<0.0001	
C^2	89824.49	1	89824.49	31.09	0.0002	
Residual	28446.10	10	2888.94			
Lack of Fit	28446.10	5	5689.22	64.17	0.0002	Not Significant
Pure Error	443.31	5	88.66			
Cor Total	9.499E+05	19				

The **Model F-value** of 35.42 indicates that the model is statistically significant. There is a 0.01% possibility that an F-value of this magnitude could be caused by noise.

P-values less than 0.05 indicate significant model terms. In this instance, the model terms A, B, AC, A^2, B^2, and C^2 are significant. Values exceeding 0.1000 indicate that the model terms are not statistically significant. If your model contains numerous insignificant terms (excluding those required to support hierarchy), model reduction may improve it.

The **Lack of Fit F-value** of 64.17 indicates that Lack of Fit is statistically significant. There is only a 0.02% possibility that such a high Lack of Fit F-value could be caused by noise. A significant lack of fit is undesirable; the model should fit.

Table 6: Analysis of Variance on Cassava bagasse

Source	**Sum of Squares**	**Df**	**Mean Square**	**Fvalue**	**p-value**	
Model	1.637E+06	9	1.819E+05	36.96	< 0.0001	Significant
A-Temperature	25330.34	1	25330.34	5.15	0.0467	
B-Acid concentration	70904.71	1	70904.71	14.41	0.0035	
C-Time	21452.46	1	21452.26	4.36	0.0634	
AB	1491.75	1	1491.75	0.3031	0.5940	

AC	24638.15	1	24638.15	5.01	0.0492	
BC	63367.23	1	63367.23	12.88	0.0049	
A^2	1.279E+05	1	1.279E+05	259.93	<0.0001	
B^2	97630.52	1	97630.52	19.84	0.0112	
C^2	2.111E+05	1	2.111E+05	42.90	< 0.0001	
Residual	49215.07	10	4921.51			
Lack of Fit	34387.44	5	6877.49	2.32	0.1886	Not Significant
Pure Error	14827.63	5	2965.53			
Cor Total	1.686E+06	19				

The **Model F-value** of 36.96 indicates that the model is statistically significant. There is a 0.01% chance that an F-value of this magnitude could be caused by noise.
P-values less than 0.05 indicate significant model terms. In this instance, the model terms A, B, AC, BC, A^2, B^2, and C^2 are significant. Values exceeding 0.1000 indicate that the model terms are not statistically significant. If your model contains numerous insignificant terms (excluding those that are necessary for hierarchy), model reduction may improve it.

The Lack of Fit F-value of 2.32 indicates that the Lack of Fit is not statistically significant compared to the standard error. This high Lack of Fit F-value has an 18.86% chance of occurring due to noise. Non-significant mismatch is desirable; we want the model to fit.

2.9 Hydrolysis

It is necessary to go through the pre-treatment phase in order to alter the structure of the cellulose and make it more amenable to the enzymatic hydrolysis process. The feedstocks was heated in a dilute solution of H_2SO_4 while it was being processed in the autoclave. In order to accomplish the goal of increasing the substrates' surface area, this significantly reduced the amount of hemicellulose and lignin that was present. Because of this, the feedstock was able to be more easily accessed by the enzyme during the hydrolysis phase. However, the samples that were acid pretreated produced a greater amount of sugars. This demonstrates that diluted acid is an appropriate choice for a good pre-treatment, as it is also an economical choice. Using the RSM model and carrying out statistical optimization allowed for the determination of the conditions that are optimal. Maximum yields of fermentable sugars concentration were found to be 804.23 mg/L for corn cob and 807.28 mg/L for cassava bagasse. The conditions that produced the optimal levels of the factors were a pre-treatment time of 31 minutes at a temperature of $76.5^{0}C$ with a concentration of 4.3% (w/w) H_2SO_4.

In order to guarantee the highest possible sugar yield from the hydrolysis process, the samples were pre-treated with the optimal conditions obtained from H_2SO_4 pre-treatment. After that, the samples were neutralized with NaOH, and the PH was brought up to a value of 4.8, to satisfy the condition of cellulase enzyme as determined by [16].The results of sugar yield from enzymatic hydrolysis using fixed amount (10ml) of cellulase and beta- glucosidase enzymes, after samples were kept at 50℃ for 24 hours are 924.8645mg/L and 928.3743mg/L for corn cob and cassava bagasse respectively.

3 CONCLUSIONS

The exploration of agricultural wastes as a renewable and sustainable energy source was the result of a search for an alternative that could either replace or supplement the existing energy source for fermentable sugars. This energy source is then used in the production of biofuel and other value-added products. The production of biobutanol from corn cobs and cassava bagasse, both of which are readily available as waste products, was the primary focus of this research. RSM was utilized to achieve optimum results in the pretreatment process. According to the findings of this study, the lignin and extractives were effectively removed by H_2SO_4 pretreatment. This resulted in an increase in the accessibility of substrates for the enzymes, which in turn led to an apparent improvement in the efficacy of the enzymatic hydrolysis.

References

[1] M. Köpke and P. Dürre, "Biochemical production of biobutanol," *Handb. Biofuels Prod. Process. Technol.*, pp. 221–257, Jan. 2011, doi: 10.1533/9780857090492.2.221.

[2] R. Chandra, H. Takeuchi, and T. Hasegawa, "Methane production from lignocellulosic agricultural crop wastes: A review in context to second generation of biofuel production," *Renew. Sustain. Energy Rev.*, vol. 16, no. 3, pp. 1462–1476, 2012, doi: 10.1016/j.rser.2011.11.035.

[3] T. Shahzadi *et al.*, "Advances in lignocellulosic biotechnology: A brief review on lignocellulosic biomass and cellulases," *Adv. Biosci. Biotechnol.*, vol. 2014, no. 03, pp. 246–251, Jan. 2014, doi: 10.4236/ABB.2014.53031.

[4] J. Cai *et al.*, "Review of physicochemical properties and analytical characterization of lignocellulosic biomass," *Renew. Sustain. Energy Rev.*, vol. 76, no. October 2016, pp. 309–322, 2017, doi: 10.1016/j.rser.2017.03.072.

[5] A. Kumar *et al.*, "A review of factors affecting enzymatic hydrolysis of pretreated lignocellulosic Biomass," *Res. J. Chem. Environ.*, vol. 22, no. 7, 2018, Accessed: Oct. 06, 2021. [Online]. Available: https://www.researchgate.net/publication/326236093

[6] Y. H. P. Zhang, J. Hong, and X. Ye, "Chapter 14 Cellulase Assays," *Business*, vol. 581, pp. 213–231, 2009, doi: 10.1007/978-1-60761-214-8.

[7] G. P. Maitan-Alfenas, E. M. Visser, and V. ria M. Guimarães, "Enzymatic hydrolysis of lignocellulosic biomass: Converting food waste in valuable products," *Curr. Opin. Food Sci.*, vol. 1, no. 1, pp. 44–49, 2015, doi: 10.1016/j.cofs.2014.10.001.

[8] F. H. Isikgor and C. R. Becer, "Lignocellulosic biomass: a sustainable platform for the production of bio-based chemicals and polymers," *Polym. Chem.*, vol. 6, no. 25, pp. 4497–4559, Jun. 2015, doi: 10.1039/c5py00263j.

[9] S. Satimanont, A. Luengnaruemitchai, and S. Wongkasemjit, "Effect of temperature and time on dilute acid pretreatment of corn cobs," *Int. J. …*, vol. 6, no. 0, pp. 333–337, 2012, [Online]. Available: http://www.idconline.com/technical_references/pdfs/chemical_engineering/Effect of Temperature.pdf

[10] G. Brodeur, E. Yau, K. Badal, J. Collier, K. B. Ramachandran, and S. Ramakrishnan, "Chemical and Physicochemical Pretreatment of Lignocellulosic Biomass : A Review," vol. 2011, 2011, doi: 10.4061/2011/787532.

[11] N. Mosier *et al.*, "Features of promising technologies for pretreatment of lignocellulosic biomass," vol. 96, no. 2005, pp. 673–686, 2022, doi: 10.1016/j.biortech.2004.06.025.

[12] S. Rahmati *et al.*, "Pretreatment and fermentation of lignocellulosic biomass: Reaction mechanisms and process engineering," *React. Chem. Eng.*, vol. 5, no. 11, pp. 2017–2047, 2020, doi: 10.1039/d0re00241k.

[13] O. Yildirim, B. Ozkaya, M. Altinbas, and A. Demir, "Statistical optimization of dilute acid pretreatment of lignocellulosic biomass by response surface methodology to obtain fermentable sugars for bioethanol production," *Int. J. Energy Res.*, vol. 45, no. 6, pp. 8882–8899, 2021, doi: 10.1002/er.6423.

[14] H. A. Emeko, A. O. Olugbogi, and E. Betiku, "Appraisal of artificial neural network and response surface methodology in modeling and process variable optimization of oxalic acid production from cashew apple juice: A case of surface fermentation," *BioResources*, vol. 10, no. 2, pp. 2067–2082, 2015, doi: 10.15376/biores.10.2.2067-2082.

[15] E. Betiku, H. A. Emeko, and B. O. Solomon, "Fermentation parameter optimization of microbial oxalic acid production from cashew apple juice," *Heliyon*, vol. 2, no. 2, 2016, doi: 10.1016/j.heliyon.2016.e00082.

[16] A. Boonsombuti, K. Tangmanasakul, J. Nantapipat, K. Komolpis, A. Luengnaruemitchai, and S. Wongkasemjit, “Production of biobutanol from acid-pretreated corncob using Clostridium beijerinckii TISTR 1461: Process optimization studies,” *Prep. Biochem. Biotechnol.*, vol. 46, no. 2, pp. 141– 149, 2016, doi: 10.1080/10826068.2014.995810.

NIPES-NCEE Conference Proceedings
The 2nd International Conference 15th-17th Feb. 2023
393-412
www.nipesjournals.org.ng

REINFORCEMENT OF POLYMER MATRIX COMPOSITES USING NANOPARTICULATE RICE HUSK ASH

Nafisat Tijjani[1], Mastura Shehu Tofa[2], Ibrahim Abdullahi[3], Auwal Salisu Yunusa[4], Ishaq Bala Adam[5].

[1,4]Department of Mechatronics Engineering Technology, School of Technology, Kano State Polytechnic, P.M.B 3348, Kano State, Nigeria.

[2]40 NNDC Quarters, Hotoro GRA, Kano State, Nigeria.

[3]Department of Mechanical Engineering, Faculty of Engineering, Bayero University Kano, Kano State, Nigeria.

[5]Department of Mechanical Engineering Technology, School of Technology, Kano State Polytechnic, P.M.B 3348, Kano State, Nigeria.

Corresponding author's E-mail: nafisattijjani19@gmail.com

Abstract
Polymer matrix composites (PMC) are widely used as structural materials for different engineering applications. They provide better mechanical properties than the unreinforced polymers. Composites formed by addition of nanoparticles provide even more enhanced mechanical properties due to their higher surface area to volume ratio, and their better adhesive strength in contrast with those formed with micro particles. Treated plant fibres from some common agricultural wastes have been found to be suitable for reinforcing PMC due to their low density, low cost, high strength and stiffness. Rice husk is an agricultural waste found in abundance that can be utilised as reinforcing material when incinerated. The aim of this paper is to investigate the effect of addition of nanoparticulate Rice husk ash (RHA) in plastic composites for strength enhancement. RHA was produced by completely burning rice husk to ashes in a furnace at 700ºC for 4 hours. It was then cooled and the ashes were ground using mortar and pestle then sieved to 75µm and further ground for 11hours in Laboratory Ball Mill to get the RHA nanoparticulates. X-Ray Fluorescence (XRF) Technique was used to determine of the chemical composition of the RHA. Micrographs of the RHA were produced using Scanning Electron Microscope (SEM), and ImageJ software was used for characterisation of the particles. RHA nanoparticles having mean diameter of 21nm were used for the composite production. Composites test samples were produced by manual mixing with 2 wt%, 4 wt%, 6 wt%, 8 wt% and 10 wt% RHA reinforcement, in cast iron mould. The mixing ratio for the composite samples were 0-10 wt% added at 2 wt% interval, and 5:1 catalyst-accelerator mixing ratio. Methyl ethyl ketone peroxide (MEKP) was used as catalyst, and cobalt napthalate as accelerator. The test samples were subjected to tensile strength tests and flexural strength tests. The results from the tests carried out showed maximum improvement of Ultimate Tensile Strength (UTS), Tensile Modulus (TM) and Modulus of Rupture (MOR) at 2 wt% RHA reinforcement when compared with the unreinforced polyester. A decline in the properties was observed with further increase in RHA.

***Keywords**: Polymer Matrix Composite, Nanoparticulate, Rice Husk Ash, Ultimate Tensile Strength, Flexural Strength.*

1.0 Introduction

Composites are two or more materials combined with the intent of getting a unique material or desirable properties of the constituent materials such that the property cannot be found in a single naturally existing material [1,2,3]. Rapid growth especially in the manufacturing industries, has lead to the demand for materials with improved properties in terms of strength, stiffness, low cost of production and sustainability. Choice of materials to a great extent has been influenced by right combination of desirable properties for a specified application.

1.1 Plant Based Natural Fibers and Fillers

Fillers and fibers generally improve high strength modulus requirements in composites. Fibers can be natural or synthetic. The natural fiber can come from plants and are cellulose based; such as cotton and flux, or from animals and are protein based; such as wool and silk [4]. According to Yap et al. (2020), natural fibers possess more economic advantages than the synthetic. Natural fibers are also lightweight, renewable, and biodegradable.

In order to reduce the cost of the production, Yap et al. (2020) suggested the use of waste material as fillers in composites. The use of abundant agricultural wastes to produce environment-friendly materials can serve as an alternative. Plant fibres from common agricultural waste are found to be suitable for reinforcing plastics due to their low density, low cost, high strength and stiffness characteristics. With a total rice production of the world estimated to about 495.9 metric tons as of 2018/2019, with approximately 123.87 metric tons of rice husk produced, the use of rice husk has a great potential. Furthermore, rice husk being one of the abundant agricultural wastes when incinerated or openly disposed, poses great danger to human health and the environment. To reduce such negative effect, rice husk can be utilised in production of composites.

1.2 Classification of Composites

According to Subrahmanya et al. (2018), composites are broadly classified based on type of matrix as Polymer Matrix Composites (PMC), Ceramic Matrix Composites (CMC) and Metal Matrix composites (MMC). The Polymer Matrix Composites (PMC) are made up of different types of organic polymers. They consist of short or continuous fibers with the several reinforcing agents. The matrix in PMC adheres the fibers together for transfer of load between them such that mechanical loads are supported by the fibers. Consequently, mechanical properties such as fracture toughness, high strength and stiffness are improved. Moreover, PMC reinforced with natural fibers have a higher resistance and interfacial bonding between them, which helps to maintain their chemical and mechanical identities.

General development in composites, has been decrease in size of filler material; from macro to meso and micro to nano. The field of nanotechnology has recently gained significant attention for wide applications in different fields such as medicine, Food production, construction, automobile and electrical industries [4,5,6,7,8]. Din et al. (2019) further explained that PMC, CMC, and MMC, are also sub-categorized as Polymer Matrix Nanocomposites (PMNC), Ceramic Matrix Nanocomposites (CMNC), and Metal Matrix Nanocomposites (MMNC) when they are formed from nanoparticles respectively. The PMNC, the CMNC, and the MMNC present enhanced properties when compared with composites fabricated at the micro scale. Addition of nanoparticles in small quantities as reinforcement has shown observable effects on physical and mechanical properties of composites. Similarly, significant improvements have been observed in optical property, electrical conductivity, thermal conductivity, mechanical properties (stiffness, strength, wear and heat resistance), surface appearance and good barrier for gases on addition of nanoparticles in composites [9,10,11,12].

1.3 Composites Formation Techniques

Formation of composites can be facilitated with the aid of a catalyst and an accelerator. The accelerators are used in small quantities to enhance the efficiency of catalyst. Hussain et al. (2006) explained that different techniques can be used for formation of composites using the combination of a binder and a reinforcement material. Some of the techniques use close moulds, as found in Resin Transfer Moulding (RTM) technique, while use of open moulds is adopted in some others, such as the Wet lay-up and the Vacuum Resin Transfer Moulding (VARTM) techniques. On the other-hand, for formation of contours of complex forms and high quality complex structures, the Fiber Placement and Autoclave Processing techniques are used respectively. To obtain good nanoparticle arrangement and dispersion at low cost in large volume, the Pultrusion production process can be adopted.

Burleson et al. (2004), Clemens et al. (2017), and Joel and Vikas (2015) have identified some techniques that are used for characterization and measurement of nanoparticles. These are; the Scanning Electron Microscopy (SEM), the Transmission Electron Microscopy (TEM), X-ray Diffractometry (XRD), and the Small Angle X-ray Scattering (SAXS). They further explained that the SEM and the TEM can measure nanoparticles down to 1 nm. Din et al. (2019) further added that, other advanced techniques such as the Atomic Force Microscopy (AFM), Scanning Tunnelling Microscopy (STM), Fourier Transformed Infrared Spectroscopy (FTIR), X-ray Photoelectron Spectroscopy (XPS), Nuclear Magnetic Resonance (NMR), and Differential Scanning Calorimetry (DSC) have also been used recently for quantitative characterization of nanoparticles in nanocomposites.

2.0 Methodology

2.1 Materials and Equipment

The materials used for the production of the plastic composite are: polyester resin, rice husk, Methyl ethyl ketone peroxide (MEKP), and Cobalt-nephthalate. The Rice Husk was sourced from Kura Local Government Area of Kano State, Nigeria. The Polyester resin serves as the matrix, the rice husk ash as serves as the filler, Methyl ethyl ketone peroxide (MEKP) as catalyst, and Cobalt-nephthalate as accelerator. The proportion of the matrix and filler is taken at 0 wt%, 2 wt%, 4 wt%, 6 wt%, 8 wt% and 10wt% of RHA. While the catalyst to accelerator ratio was 5:1.

The equipment used for the preparation of the polymer matrix composite are: the furnace, the mortar and pestle, the weighing balance, micrometer screw gauge, a lint free cloth, distilled water, a measuring cylinder, cast-iron mould, a Universal Testing Machine (Cussons Technology P5030), a mechanical sieving machine, and a Laboratory ball mill (BICO-395-50 12INDRUM 3PH). While for the chemical analysis the X-Ray Florescence machine (Thermo scientific Advant'X 1200 Model), and Scanning Electron Microscope (BOC Edwards K950X) used, with ImageJ for characterisation of the particles.

2.2 Rice Husk Ash Preparation

The Rice husk was manually blown to remove dirt, stones and rice particles from the husk. The husk was completely burnt to ashes in a furnace at 700ºC for 4 hours. After cooling, the ash was ground using mortar and pestle, sieved to 75µm and 2kg of the RHA was further ground for 11hours in Bico Ball Mill with 285 iron balls of 20kg running at 450rpm (revolutions per minute) with a balls charge ratio of 10:1 to obtain the RHA nanoparticulates.

2.3 RHA Chemical Composition and Characterization

Chemical composition and characterization of the RHA nanoparticles was carried out after obtaining the RHA nanoparticles. The RHA particles were first viewed under scanning electron microscope after ball milling, and micrographs were produced. The particles were then characterized using imageJ. The RHA particles appeared to be spherical in shape, and some of the particles which appeared boldly are shown with the arrows in figure 1 below.

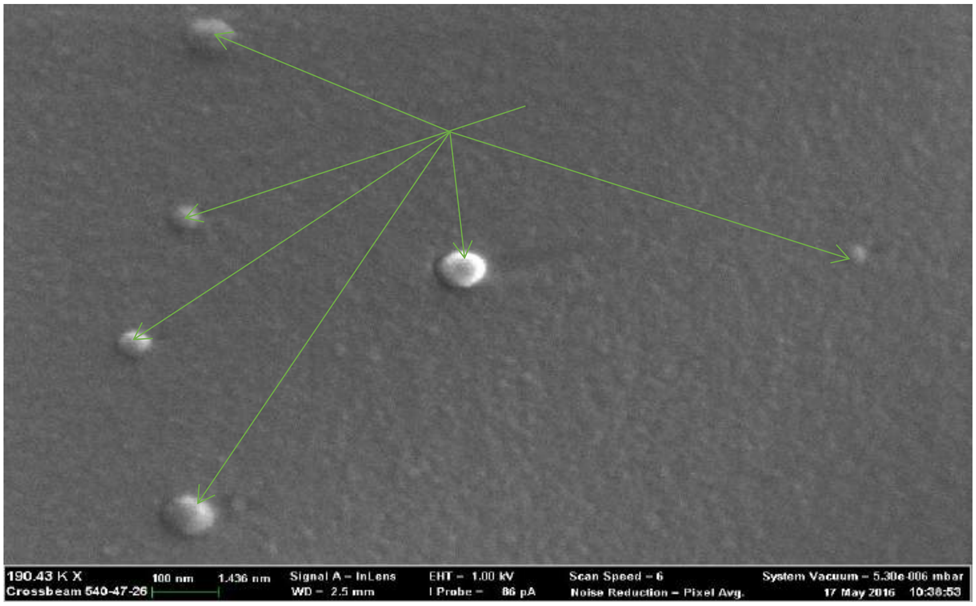

Figure 1: A Micrograph Showing Spherical Nature of the Rice Husk Ash Particles

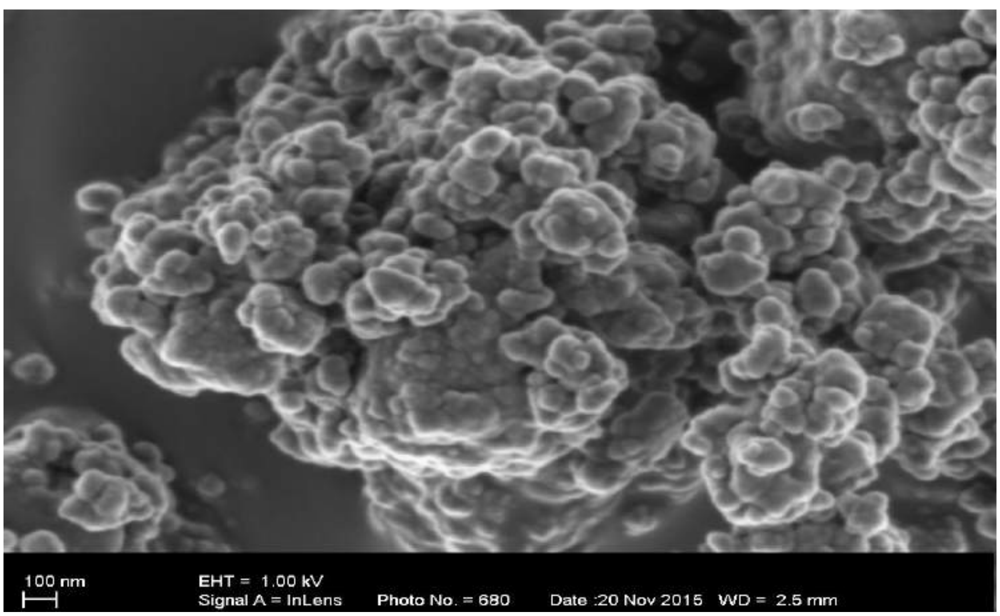

Figure 2: RHA Nanoparticles Micrograph

The characteristics obtained from the micrograph using the ImageJ, are tabulated below:

Table 1: RHA Particles Size Characterization Result

Characteristic	Area of Particle (nm²)	Circularity	Aspect Ratio	Roundness	Solidity
Mean	1467.63	0.578	2.146	0.558	0.735

Figure 2 was used for the particle characterisation and the results shown in Table 1. Imputing value of the mean area of particles from table 1 above in formula for calculating area of sphere, the mean diameter of the RHA particles was found.

Area of RHA particle, A $=\pi d^2$

Where d is the mean diameter of RHA particle

And π =3.1415

Therefore; $d = \sqrt[2]{\frac{A}{\pi}}$

Imputing the values for A and π

$$d = \sqrt[2]{\frac{1467.63}{\pi}}$$

$$d \approx 21nm$$

The X-Ray Fluorescence (XRF) Technique was used to determine of the chemical composition of the RHA. The RHA was first pulverized, then pelletized before being loaded in the XRF machine for twenty minutes, after which data generated is collated automatically on the computer attached to the XRF machine. The chemical composition of the RHA determined by X-Ray Fluorescence (XRF) is tabulated below:

Table 2: Chemical Composition of Rice Husk Ash

S/No.	**Chemical composition**	**Percentage**
1	SiO_2	87.22
2	K_2O	1.12
3	CaO	2.12
4	Al_2O_3	0.70
5	MgO	1.18
6	Fe_2O_3	1.68
7	NiO	0.20
8	MnO	1.06
9	P_2O_5	0.87
10	TiO_2	0.46
11	S	0.04
12	ZrO_2	0.01
13	Cr_2O_3	0.03
14	LOI	1.06
15	Others	2.25

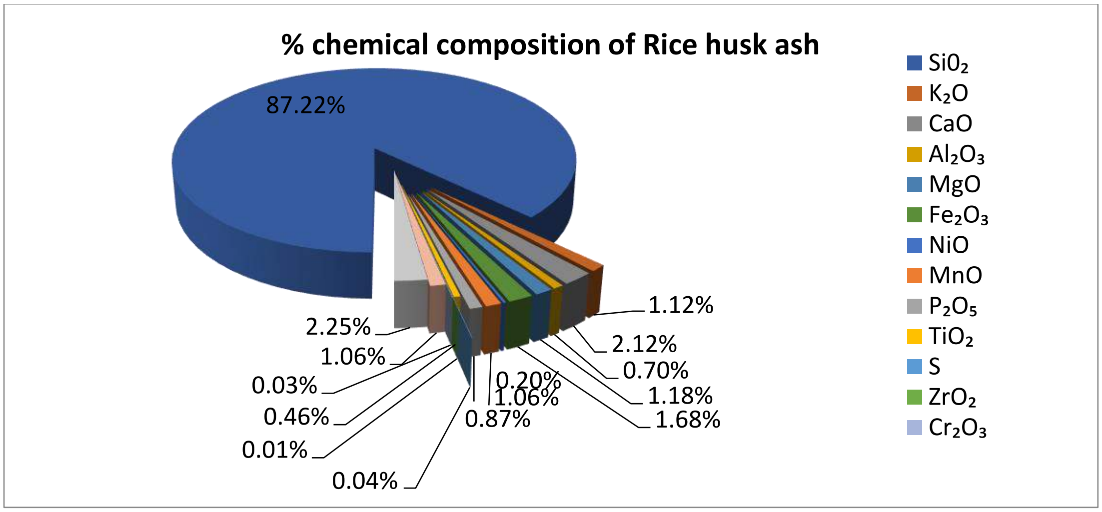

Figure 3: Rice Husk Ash Chemical Composition

2.4 Polymer Matrix Composite Preparation and Analysis

The composite was prepared using stir mixing technique. It was produced in a cast iron mould using the nanoparticulate RHA as reinforcement, and matrix of polyester resin along with methyl ethyl ketone peroxide (MEKP) as catalyst and cobalt napthalate as accelerator. The RHA was added and mixed in the composite samples from 0 -10 wt% addition at 2 wt% interval, and 5:1 as the catalyst-accelerator mixing ratio. The morphology of the nanoparticulate RHA was analysed using micrographs produced by the Scanning Electron Microscope (SEM). The RHA nanoparticles are sputter coated to make a thin conductive cover for high quality imaging. The SEM gave high resolution by using electromagnets in place of lenses. It used electron instead of light to form images and allowed much control over the degree of magnification.

2.5 Strength Tests

Two different tests for strength where conducted in this work; the Flexural strength tests and Tensile strength tests. For each of the two tests, there is a varied wt% of RHA from 0-10 wt%, at an interval of 2 wt%. This means that the tests where carried-out at 0 wt%, 2wt%, 4 wt%, 6 wt%, 8 wt%, and 10 wt% RHA, and for every wt% variation of RHA, the test was conducted with five different samples. Thus, a total of 60 samples were produced; 30 samples for tensile strength tests, and 30 samples for flexural strength tests. 5 samples each for tests at 0 wt%, 2 wt%, 4 w%, 6 wt%, 8 wt% and 10 wt% of RHA for the two different test.

Flexural Strength Test: A three-point loading system test was employed according to ASTM D-790 to determine the flexural properties of the composites. Rectangular specimens of size 130mm by 20mm by 5mm were subjected to strain rate of 0.1mm/mm/min and span length of 80mm on a Universal testing machine. The test was terminated for each sample at break and the modulus of rupture was calculated using the values obtained.

Tensile Strength Test: Tensile strength test was conducted following the ASTM D638-02 standard. Dumbbell shaped specimens of thickness 4.1mm, original width of 18.5mm and original distance between gauge marks of 78.5mm were used. The Ultimate Tensile Strength (UTS), the percentage elongation at break ($\%EL_b$) and the Young's modulus or tensile modulus (E) of the samples were determined.

3.0 Results and Discussion

3.1 Flexural Strenght Test

The Flexural Strength or modulus of rupture (MOR) was calculated at break for each sample using:

$$MOR, \sigma_{fm} = \frac{3PL}{2bd^2}$$

Where:

$\sigma_{fm} =$ Flexural strength (MPa)

P= Load (Force) at break (N)

L= Support span (mm)

b= width of sample (mm)

d= depth or thickness of sample (mm)

The values of Force and Deformation at breaking were obtained from the tests, and the MOR of all the samples was calculated and the results tabulated below:

Table 3: Flexural Test Results of Various Compositions of Nanoparticulate RHA Plastic Composite

RHA wt%	Sample Number	Force at peak (kgf)	Deformation at Break (mm)	Modulus of Rupture (Mpa)	Average Modulus of Rupture (Mpa)
0	1	30.082	3.723	70.800	44.256
	2	9.1775	0.949	21.599	
	3	21.108	2.357	49.680	
	4	16.825	2.048	39.600	
	5	16.825	1.328	39.600	
2	1	21.516	1.314	50.640	46.224
	2	23.963	2.176	56.400	
	3	18.049	1.123	42.480	
	4	15.806	1.115	37.200	
	5	18.865	1.601	44.400	
4	1	16.825	2.037	39.600	32.640
	2	15.194	1.810	35.760	
	3	9.789	0.830	23.040	
	4	12.848	0.925	30.240	
	5	14.684	1.115	34.560	
6	1	6.832	0.550	16.080	18.528
	2	9.687	1.203	22.800	
	3	9.177	0.896	21.600	
	4	9.585	0.731	22.560	
	5	4.079	0.382	9.600	

8	1	5.914	0.535	13.920	16.176
	2	9.177	0.890	21.600	
	3	7.546	0.807	17.760	
	4	6.628	0.602	15.600	
	5	5.099	0.570	12.000	
10	1	8.260	0.959	19.440	12.672
	2	3.365	0.428	7.920	
	3	7.852	0.992	18.480	
	4	3.161	0.346	7.440	
	5	4.283	0.638	10.080	

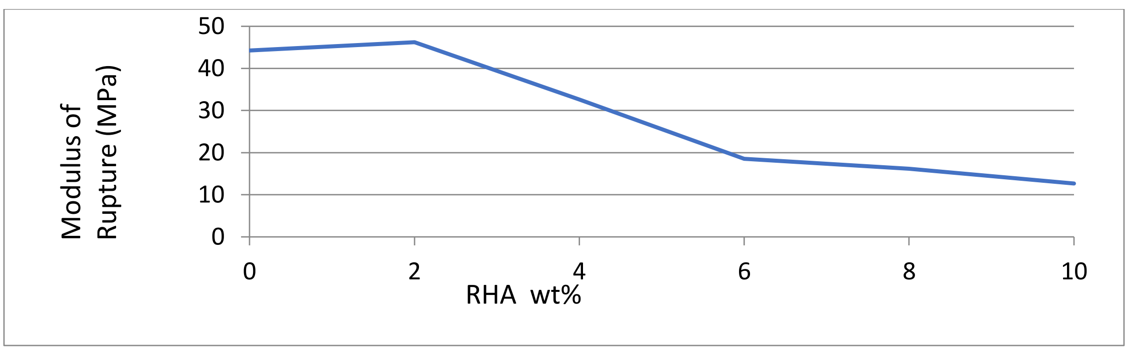

Figure 4: Modulus of Rupture (MPa) Against RHA wt% Loading

From the results in Table 4, the average value of MOR for the composite ranged from 46.22 MPa to 12.67 MPa with the unreinforced polyester having 44.26 MPa. A slight improvement of MOR has been observed in the composite with 2 wt% RHA, and a decline with further increase in RHA content.

3.2 Tensile Strength Test

The tensile stress at break or the Ultimate Tensile Strength (UTS) was calculated as:

$$UTS = \frac{P}{b_o \times d_o}$$

Where:

P = load at break of composite specimen (N)

b_o = original width of composite (mm)

d_o = original thickness of composite (mm)

From the tensile test results, Young's modulus or tensile modulus (E) was calculated as follows:

$$E = \frac{uts}{\varepsilon}$$

Where:

uts = ultimate tensile strength

ε = strain

And percentage elongation at break ($\%EL_b$) was calculated as:

$$\%EL_b = \frac{L - L_o}{L_o} \times 100 \qquad (9)$$

Where;

L = distance between gauge mark at break

L_o = original distance between gauge marks

Ultimate tensile strength (UTS) for sample 1 of 0wt% RHA was calculated using equation.

$$UTS = \frac{P}{b_o \times d_o}$$

$$UTS = \frac{85.8 \times 9.80665}{18.5 \times 10^{-3} \times 4.1 \times 10^{-3}} = 11.071 MPa$$

Similarly, UTS for all the other samples were calculated and the results tabulated below.

Young's modulus or tensile modulus (E) was calculated using equation:

$$E = \frac{uts}{\varepsilon}$$

strain, $\varepsilon = \frac{L - L_o}{L_o}$ but $L - L_o$ is elongation at break

$$\varepsilon = \frac{1.314}{78.5} = 0.017$$

$$E = \frac{uts}{\varepsilon} = \frac{11.071}{0.017} = 661.407MPa$$

And percentage elongation at break ($\%EL_b$) was calculated using the equation:

$$\%EL_b = \frac{L - L_o}{L_o} \times 100$$

$$= \frac{1.314}{78.5} \times 100 = 1.674\%$$

Similarly, strain, %EL and TM were calculated for all the other samples and results were tabulated in Table 5.

Table 4: Tensile Test Result of Various Compositions of Nanoparticulate RHA Plastic Composite

RHA wt%	Sample Number	Load at Break (kgf)	Elongation at Break (mm) $L - L_o$	% Elongation at break	Ultimate Tensile Strength (MPa)	Strain E	Tensile Modulus (MPa)
0	1	85.800	1.314	1.674	11.071	0.017	661.407
	2	75.100	1.520	1.936	9.691	0.019	500.464
	3	67.600	1.532	1.952	8.723	0.013	670.981
	4	61.200	1.378	1.755	7.897	0.018	449.862

	5	75.300	1.140	1.452	9.716	0.015	669.063
2	1	92.200	1.733	2.208	11.897	0.022	538.901
	2	85.100	1.248	1.590	10.981	0.016	690.704
	3	101.600	2.379	3.031	13.110	0.030	432.590
	4	82.903	1.292	1.646	10.697	0.016	649.957
	5	92.284	1.052	1.340	11.908	0.013	888.561
4	1	72.400	1.446	1.842	9.342	0.018	507.162
	2	70.100	2.209	2.814	9.045	0.028	321.439
	3	67.200	1.670	2.127	8.671	0.021	407.596
	4	71.200	1.187	1.512	9.187	0.015	607.584
	5	88.400	2.619	3.336	11.407	0.033	341.896
6	1	61.200	2.818	3.590	7.897	0.036	219.982
	2	51.600	1.299	1.655	6.658	0.017	402.362
	3	58.500	1.145	1.459	7.549	0.015	517.520
	4	73.000	2.150	2.739	9.420	0.027	343.923
	5	74.900	2.011	2.562	9.665	0.026	377.265
8	1	63.900	2.010	2.561	8.245	0.026	322.019
	2	68.000	2.260	2.879	8.774	0.029	304.774
	3	56.500	1.248	1.590	7.290	0.016	458.575
	4	54.963	2.091	2.664	7.092	0.027	266.252
	5	60.500	2.880	3.669	7.807	0.037	212.784
10	1	43.600	1.877	2.391	5.626	0.024	235.288
	2	51.700	1.660	2.115	6.671	0.021	315.471
	3	28.800	1.100	1.401	3.716	0.014	265.202

	4	45.683	3.815	4.860	5.895	0.049	121.293
	5	33.100	0.553	0.704	4.271	0.007	606.289

Table 5: Summary of Tensile Test Result of Various Compositions of Nanoparticulate RHA Plastic Composite

RHA wt%	Average force at peak (kgf)	Average Elongation at Break (mm)	Average Ultimate Tensile Strength (Mpa)	Average Percentage Elongation (Mpa)	Average Tensile Modulus (Mpa)
0	73.000	1.377	9.420	1.754	577.342
2	90.817	1.541	11.719	1.963	640.142
4	73.860	1.826	9.531	2.326	441.147
6	63.840	1.885	8.238	2.401	375.626
8	60.773	2.098	7.842	2.672	315.752
10	40.577	1.801	5.236	2.294	311.542

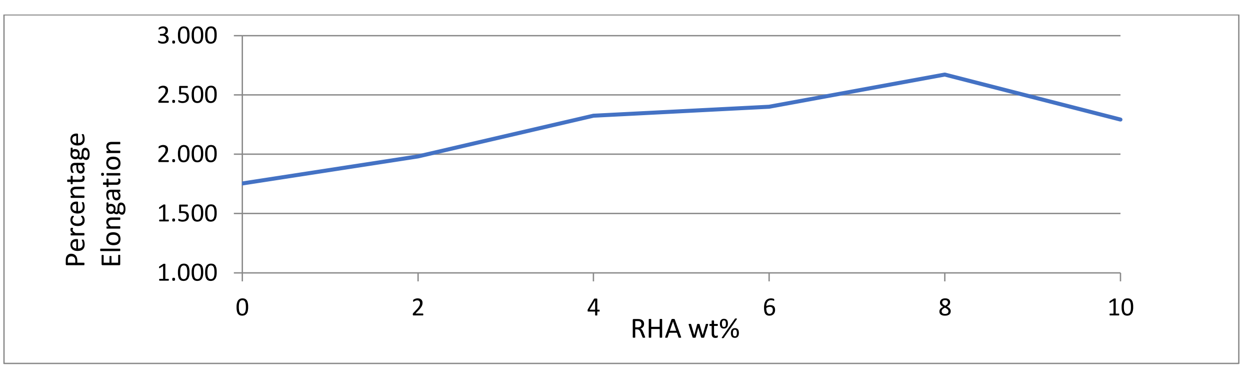

Figure 5: Percentage Elongation (%) against RHA wt% Loading

Figure 5 indicates that percentage elongation of the reinforced composites were greater than that of unreinforced samples. The percentage elongation was found to continuously increase with increase in RHA wt% loading from 1.75% of the unreinforced sample to a maximum of 2.67% at 8 wt% RHA, with a decline from 2.67% at 8 wt% RHA to 2.29% at 10 wt% RHA loading. It can be suggested that the increase in RHA helps support stress absorbed by the matrix, hence the increase in percentage elongation with increase in RHA wt% loading.

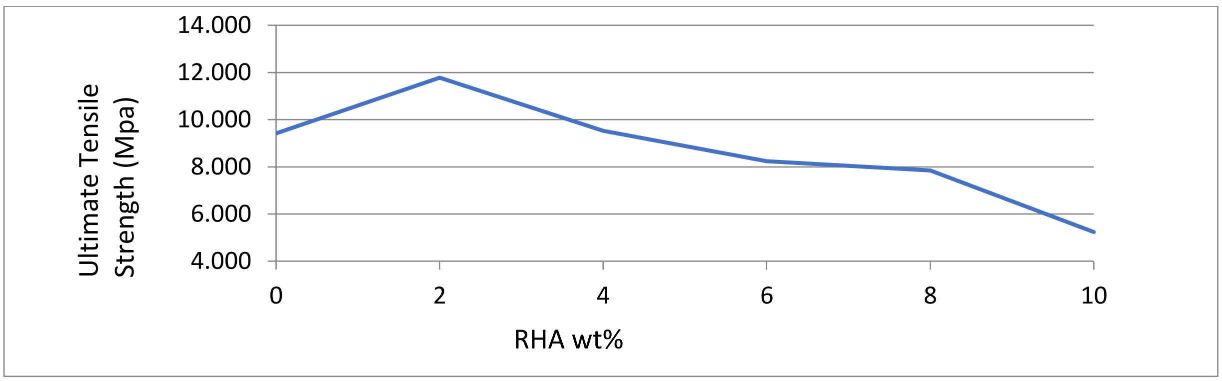

Figure 6: Ultimate Tensile Strength (MPa) against RHA wt% Loading

Ultimate Tensile Strength (UTS), increased from 9.420 Mpa at 0 wt% RHA, to 11.719 Mpa at 2 wt% RHA. There is a sharp decline in the UTS with further increase in RHA wt% loading, thus suggesting best spatial distribution of RHA with a 2 wt% RHA content. This can be attributed to the characteristic of Rice Husk which is easy agglomeration and the weak interface between filler and matrix, which cause more filler particle clusters at higher filler loading. Thus, UTS was found to be highest at 2 wt% RHA loading with a value of 11.719 Mpa. With increase in RHA wt% loading, decrease in UTS is realised. Decrease in strength of composites is associated with high content of filler material in works of Kusmono et al. (2008), Wu et al. (2007) and Eva et al. (2014).

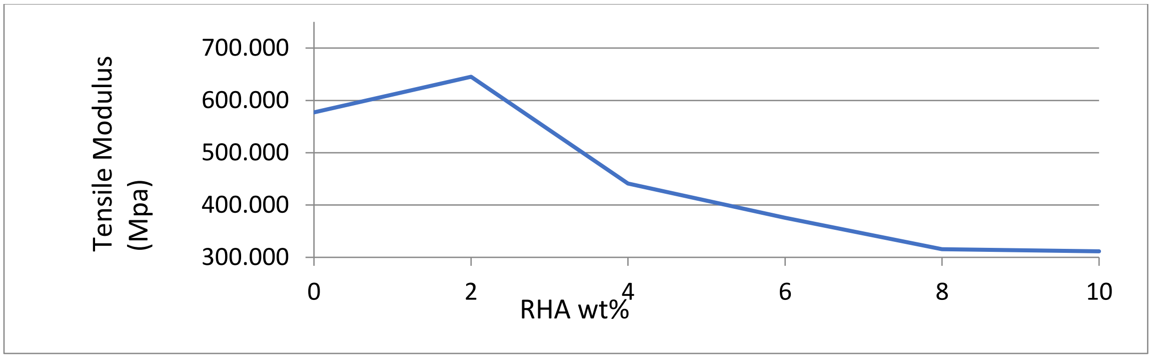

Figure 7: Tensile Modulus (MPa) against RHA wt% Loading

Figure 7 shows that the TM improved at 2 wt% RHA loading when compared with the unreinforced polymer. TM is highest at 2 wt% RHA loading with a value of 640.142 Mpa. This shows that stiffness has improved with 2 wt% RHA. A sharp decline was observed with further increase in RHA content. This decline is likely due to filler particle clustering. The same suggestion was made by Peng et al. (2012).

3.3 Contrast between strength properties of Unreinforced and Reinforced Polymer Matrix Composite

From the strength tests conducted and the results obtained, the table below presents values of the strength properties of the pure cast (Unreinforced) polyester and the reinforced PMC. It also gives the maximum value the properties and wt% of RHA at that value.

Table 6: Contrast between strength properties of Unreinforced and Reinforced Polymer Matrix Composite

Properties	Values for Pure Cast (Unreinforced) Polyester	Maximum Values for Reinforced PMC	wt% of RHA at Maximum Values for Reinforced PMC
Ultimate tensile strength (MPa)	9.420	11.719	2.000
Percentage Elongation at break (%)	1.754	2.672	8.000
Tensile Modulus (MPa)	577.342	640.142	2.000
Modulus of Rupture (MPa)	44.256	46.224	2.000

4.0 Conclusion and Recommendations

The mechanical properties test results showed maximum improvement of Ultimate Tensile Strength (UTS), Tensile Modulus (TM) and Modulus of Rupture (MOR) at 2 wt% RHA reinforcement when compared with the unreinforced polyester, and a decline with further increase in RHA content. The samples with 2 wt% RHA were found to have UTS of 11.719 MPa, TM of 640.142 MPa and MOR of 46.224 MPa. Therefore, it can be concluded that to improve the strength the PMC using nanoparticulate RHA, a small quantity of RHA (2 wt% RHA) is sufficient.

Several researchers have agreed that the morphology of materials has significant influence on their strength, and mechanical properties in general [13,14,15,16,17,18,19]. Composite's microstructure will show any spatial distribution or clustering of the RHA content in the PMC at varying load. This will make it possible to draw conclusions on the influence of the structural arrangement of RHA nanoparticles in the composite on the strength on the PMC. Hence, it is recommended that future research is conducted on analysis of microstructure on nanoparticulate RHA PMC.

References

[1] ASTM D638-02, American Society of Testing and Materials standard test method for tensile properties of plastic. Book of standard volume1402 Wood West Conshohocken PA 19428-2959 United States.

[2] ASTM D790 - 02, American Society for Testing Materials. Standard test method for flexural properties of plastics, ASTM international, West Conshohocken, PA 19428-2959, United States.

[3] Burleson D. J., Driessen M. D., & Penn R. L. (2004) characterisation of environmental nanoparticles. Journal of environmental science and health 39(10):2707-2753

[4] Callister, Jr. W. D., Rethwisch, D. G., & Balasubramaniam, R. (2014) *Callister's Material Science and Engineering* (2nd ed.). New Delhi: Wiley

[5] Clemens, H., Mayer, S., & Scheu, C. (2017). Microstructure and Properties of Engineering Materials: From Fundamentals to Applications. 10.1002/9783527684489.ch1

[6] Din, S. H., Shah, M. A., Sheikh, N. A., & Mursaleen, M. (2019). Nano-Composites and their Applications: A review. Characterization and Application of Nanomaterials. 2. 10.24294/can.v2i1.875.

[7] Eva, M., G., Basuki, W., Nurdin, B., & Harry, A. (2014). Preparation and characterisation of Rice Husk Ash as filler material in to Nanoparticles on HDPE thermoplastic composite. Journal of Chemistry and material research 6(7):14-25

[8] Hussain, F., Mehdi, H., Masami, O., & Russel, E.G. (2006). Polymer matrix Nanocomposites. Journal of composite materials 40(17):1555-1557

[9] Joel, F., & Vikas, M. (2015). Synthensis of polymer nanocomposite: Review of various techniques. First Edition published by Wiley- VCH Verlag GmbH and Co KGaA

[10] Kusmono, Z., A., Mohd, I., Chow, W., Takeichi, S., & Rochmadi, T. (2008).Enhancement of properties of PA/PP nanocomposites via organic modification and compartibilizer. IM.J Polym. 2(9):655

[11] La Mantia, F. P., Tzankova D. N., Morreale M., & Vaca G. C. (2004). Green composite of organic materials recycled postconsumer polyethylene. Polymer International. 53:1888-1891

[12] La Mantia, F.P., & Morreala, M. (2011). Green Composite: A brief review. Elsevier science direct Part A 42:579-588

[13] Leandro F.C., Omar P. V., Marco A. C., Marley B. R., & Jose R. M. (2011). Modelling the young modulus of nanocomposites: neural network approach. International joint conference in nueral networks. Pontificia Universida de catolica do Rio de Janeiro's IEEE Trans Nueral Netw vol. 5

[14] Maulida, S. D., & Faisal, B. (2015). The tensile strength properties effect of rice husk ash as on the composite of plastic drinking bottle. International Journal of Science and Technology Research 4:66-69

[15] Murugan, S.S. (2020). Mechanical Properties of Materials: Definition, Testing and Application. International Journal of Modern Studies in Mechanical Engineering, 6, 28-38.

[16] Subrahmanya, K., Yashas, T. G., Sanjay, M. R., Madhu, P., P, SenthamaraiKannan, P., & Yogesha, B. (2018). Polymer Matrix-Natural Fiber Composites: An Overview. Cogent Engineering. 5. 1446667. 10.1080/23311916.2018.1446667.

[17] Thomas, H., & Dorothee, V.S. (2010). Polymer Nanoparticles Composites: from synthesis to modern applications. Journal of material chemistry and physics 3:3468-3517

[18] Wu, Q., Lei Y., Clemons, C., M., Yao, F., Xu, Y., & Lian, K. (2007). Properties of ADPE/Caly/wood nanocomposites. Journal of plastic Technology 27:108-115

[19] Yap, S., Sreekantan, S., Hassan, M., Sudesh, K., & Ong, M. T. (2020). Characterization and Biodegradability of Rice Husk-Filled Polymer Composites. Polymers. 13. 104. 10.3390/polym13010104.

NIPES-NCEE Conference Proceedings
The 2nd International Conference 15th-17th Feb. 2023
413-422
www.nipesjournals.org.ng

DESIGN AND FABRICATION OF A TWIN DISC METALLOGRAPHIC POLISHING MACHINE

Unueroh U.G., Akhabue O.B., and Ogbeifun I.E.

Department of Mechanical Engineering,
University of Benin, Benin City, Nigeria.

Abstract

One of the most helpful pieces of equipment for grinding and polishing metallic samples so that their physical makeup may be examined under a microscope is the metallographic specimen polishing machine. In metallography, to obtain a smooth surface, the metallographic machine which compose of rotating plates and it forces are used, polishing is the final process of the precipitating part of the test. Polishing is often used to enhance the glossy, smooth workpiece, prevent the contamination of medical equipment, remove oxidation, or prevent pipe corrosion. Polishing is the process of rubbing or chemically removing a smooth and shiny surface to reveal a surface with a high specular reflection. The essence is to produce a simple and affordable piece of apparatus that can be used in research centres, laboratories, and workshops of Nigerian higher institutions and can serve as an alternative to the imported and costly polishing machines currently in use. The design uses motor-powered grinding wheels of appropriate composition to be rotated against a marked-out area of a sample metal piece to be polished and subsequently etched for metallographic purposes. A considerably chemically inactive liquid does the etching in Nita solution comprising nitric acid and ethanol. Mainly dependent on the type of metal being polished, water is used for flushing the polished area to ensure a smooth polished surface that retains the original microstructural composition and arrangement inherent in the original sample as it where before polishing. The polishing wheels are fine-grained and dense structured abrasive materials bonded together with an appropriate bonding agent. Provision is made for wheel insertion and removal from the motor spindle to accommodate different wheel types- either with a soft grinding abrasive material for polishing hard metals or hard grinding abrasive material for soft metals. A tank will also be incorporated into the machine to aid the flow of fluid needed for this experimentation. Thus, with the locally fabricated polishing machine from this project, it is possible to etch different types of metals for proper surface exposure for optical or electron microscopic investigations and analysis.

1. Introduction

The study of metals' physical structure and components, generally employing microscopy, is known as metallography. Various processes of grinding, polishing, and etching are used to prepare the surface of a metallographic specimen. Following separation, it is frequently studied using optical or electron microscopy[15].

It can also be described as the study of the internal structure of materials, metals, and alloys and the relationship of structure to composition and physical, chemical, and mechanical characteristics, which is known as metallography[16]. Many methods for determining internal structure have been developed, but microscopically investigations have always been the most significant. Throughout the history of metallography, they have been performed using an optical microscope [16].

Polishing is the process of rubbing or chemically removing a smooth and shiny surface to reveal a surface with a high specular reflection. Polishing is a step-by-step process. The first stage starts with rough polishing, and each subsequent level uses finer emery paper of increasing grades to achieve the desired finish. Metal is removed during this stage [13].

Fine polishing, which includes minimal or minor metal removal, is introduced in the second stage. It is usually used to remove scratches on the surface of the specimen.

In order to make plates free of defects for a microscopic inspection of metal microstructures, polishing is employed in metallography and metallurgy. The usage of automated polisher equipment is advised to achieve adequate graphite retention. This technology enables constant control of the needed weight on the time for each preparation stage and the specimens and in contrast to hand specimen preparation. This equipment also enables homogeneous specimen alignment against the preparation surface, influencing graphite retention [10]. To avoid the possibility of pulling out of the graphite phase, the number of grinding and polishing stages should be kept to a minimum [1].

At increasingly more acceptable levels, abrasive particles remove material from the specimen surface until the required metallographic surface quality is attained. Several metallographic preparation machines for grinding and polishing are available, each satisfying a particular set of preparation quality, capacity, and repeatability requirements [5].

Disc polishing machines are commonly used to polish metallography samples for microscopic investigation of diverse metal structures. Disc Polishing Machines produce a clean, without scratch, reflective surface appearance that allows metallographic perception to be corrected. Polishing is the final stage in achieving a flat, smooth, without scratch, reflective look[8][12]. A surface of this type is necessary for subsequent correct qualitative and quantitative metallographic interpretation. The machine is powered by the motor spindle, which is attached to the motor shaft through a friction mechanism. Polishing discs are installed and fixed by a nut on the shaft. For smooth operation, the shaft contains two bearings inserted into a bearing holder [10].

Finally, etching is the process of selective chemically attacking the surface of a polished object to reveal its micro-structural properties (grain boundary, phases, precipitates, and other micro-structure components). A widespread misconception is that a polished surface has a bright mirror finish, but most bright mirror surfaces are buffed [1].

The development of a twin-disc metallographic polishing machine will contribute tremendously to the successful polishing of metallographic materials. This machine overcomes the tediousness, time-consuming, messy, nasty, and discouragement in manual polishing. In addition, this machine improves accuracy high-volume processing and discourages local hand polishing.

Leonardo da Vinci was a scientific and technology pioneer, designing equipment to build optical instruments. In fact, he envisaged equipment between 1513 and 1517 to polish and grind telescope mirrors, which were made of bronze at the time. But unfortunately, it appears that Leonardo da Vinci did not build his idea during his lifetime as he has done with many of his previous projects [3][13].

Progress in optics theory and proficiency in the manufacturing of quality glass led to the emergence, particularly in Italy, of artisans specializing in the making of lenses for medical glasses, microscopes, field glasses, refractors, and so on in the early 17th century. During the period, specialized instruments were constructed to aid opticians' jobs, namely machines based on the ideas discovered by Descartes, Huygens, Hooke, Helvelius, Cherubin d'Orleans, and others. The lens polishing devices of Huygens (1683) and Cherubin d'Orleans (1670) were significant examples of this era [4][17].

Since Galileo popularized it, the refractor was dominant until the nineteenth century. Leonardo da Vinci's notion of utilizing a mirror to make an astronomical instrument was neglected until Jacques Grégory (1663), who was subsequently followed by Isaac Newton, resurrected it with the reflecting telescopes that retain their names this day. The original telescope mirrors were hand-shaped tiny metal disks. However, as they grew, it became necessary to shape and polish them using machines. The early amateur astronomers were the most prominent in this historical history [3][17].

William Herschel (1738-1822) constructed a polishing mechanism in 1788 that allowed him to finish a 50' mirror in 1789. Unfortunately, there is no description of the device that William Herschel maintained a secret up until his passing. He merely asserts that the need for its development was a result of the several workers—up to a dozen men—needed to complete his larger mirrors. Nonetheless, a tiny polishing machine he created may be exhibited at his museum in Bath, England [3][17].

Following in the footsteps of William Herschel, Lord Rosse (1800–1867), a wealthy landowner and amateur astronomer, started construction on a 183 cm bronze mirror for his telescope in 1843, which is still visible in Ireland. The Parsonstown Leviathan is still in use today. To do this, he used a polishing device, which he described in 1841 for the benefit of the Royal Society [6][17].

Later, another hobbyist, a wealthy trader named William Lassell (1799-1880), utilized a polishing machine to make large-sized mirrors (notably a 122cm mirror set up in Malta in 1855). However, during the story, we meet experts such as Henry Draper (1837-1882), who was one of the first to cut mirrors using Leon Foucault's theories. For this reason, about 1850, he created the machine based on Lord Rosse's invention from 1840, which served as a model for a long time. Today, this sort of equipment is still recognized by its name [3][17].

The same equipment was later improved and used by George Willis Ritchey, first in the United States (particularly for the 2.5-meter mirror for the Mount Wilson Hooker telescope), and then in France at the optics lab of the Dina foundation at the Paris Observatory. He left behind two machines after his time in France, along with the idea for a bigger machine with an 8-meter capacity, which was never realized. The polishing device used by George Willis Ritchey at his American workshop (1890). G.W. Ritchey built a two-meter polishing machine for the Dina laboratory at the Paris Observatory (from 1924). G.W. Ritchey designed the eight-meter machine [3][17].

Bernhard Schmidt (1879-1935) employed a different sort of machine. Due to his low financial resources, its motions were actuated with the foot. Despite this, he continued to produce high-quality mirrors. With the development of huge telescopes at professional observatories in the twentieth century, polishing equipment grew in size and sophistication. In that regard, computer science enabled significant breakthroughs by creating novel procedures mastered by specialized corporations (Zeiss, REOSC). For example, mirror cleaning and figuring robots of the same kind employed in the care sector are controlled by computers. The motions and pressures are thereby regulated, as are the deformations of the stand for mirror and lap polishing (these are known as the stressed-mirror or stressed-lap techniques). Furthermore, the deployment of such robots enables modifications to the machine's software based on the data acquired[11][17].

Reference to the use of machines early in modern amateur astronomy is discovered. Indeed, Paul Vincart reports one of them in an edition of the Belgian Astronomical Society's (Société Belge d'Astronomie) periodical "Ciel et Terre" as early as August 1922. In the 1930s, in the United States, Albert Ingalls covered many machines in his foundational work (Amateur Telescope Making). In France, details of similar devices may be found in an issue of the SAF (Société Française d'Astronomie) magazine "Astronomie" dealing with the 108th session of the committee in charge of instruments in February 1958 [17].

Amateur mirror manufacturers have been researching the benefits of machines for a very long time. Names like Pierre Bourge, Félix Bacchi, and, more recently, Dany Cardoen come to mind. But in our country, these strategies have never enjoyed the same level of acceptance as they have on the other side of the Atlantic. This occurrence may be explained by the fact that these tools were never included in Jean Texereau's "La fabrication du télescope d'amateur," the holy book of French amateur mirror producers. Because of the recent growth of Internet exchanges, one may read numerous testimonies from amateurs who have benefited from the community of amateur creators. Jean Texereau's Draper and Hindle machines were featured in L'Astronomie magazine in 1958 [11][17].

These devices were eventually employed as allies by independent professional mirror producers. For example, one of them was utilized by the late Roger Mosser in France decades ago. The same may be said today of Franck Grière (Mirro-Sphère) and JeanMarc Lecleire (Astrotélescope) [17].

One such example is Carl Zambuto, a professional who voluntarily imparts his wisdom and strategies to the American amateur community. Romano Zen, an Italian, and Mike Lockwood, another American, should be noted [17].

Therefore, in the design of our machine, it was taken into account the limitations of previous works in the field. The design aims to address these issues by operating at a moderate speed, which has been shown to increase the machine's lifespan and durability, while also improving the quality of the polished materials. Therefore, these design enhancements render the machine ideal use.

The machine also features added versatility with each polishing disc connected to a separate electric motor, allowing for simultaneous operation or individual operation as needed. The presence of a protective electric motor device (fuse) helps mitigate the impact of fluctuating and inconsistent power supply, increasing its overall reliability. The rotational speed can be regulated using an electric motor regulator, further contributing to its versatility and adaptability.

In this design work, we will be considering the following:

This project aim is to design and fabricate a laboratory twin disc metallographic polishing machine that can be used for grinding and polishing metallic materials in the metallographic laboratory.

In order to achieve the stated aim, the following objectives shall be met; to design and model the components of the machine, to fabricate a machine using materials that are readily available locally that can polish metals in a lab, to inputs a lagging material to help reduce heat loss during polishing, to design a machine that may be utilized everywhere, to evaluate the machine's performance with selected relatively cheap materials and whose service areas apply to the design.

2. Materials and Method

The design was aimed at fulfilling the following goals: manufacturing a decent and quality dual-component machine with a high probability of efficiency, raw material availability, and machine cost.

The choices of the material and component used here are based on the consideration of the following factors, cost analysis of the material, the durability of the materials, availability of the materials, properties of the material such as; physical properties, thermal properties, comparable properties, chemical properties, and mechanical properties.

Table of material used and selection criteria

S/N	MACHINE COMPONENTS	CRITERIA FOR MATERIAL SELECTION	MATERIAL SELECTED	REASONS FOR SELECTION
1.	Frame (Metal Casing)	Should be able to endure the machine's eccentric motion while in operation.	Square bar Mild steel	It is not prone to twisting, can tolerate vibration, and maintains strong stability.
2.	Shafts	It should be able to withstand the force and weight of the other components that are linked to it.	Cylindrical bar Stainless steel	Capability to tolerate twisting caused by a torque moment and compressive force caused by the weight of other components linked to it.

3.	Pillow Bearing	Should be able to withstand machine and motor torque.	Mild Steel	Adjustment is simple, and appropriate alignment is achieved.
4.	Wooden Disc	Should be able to withstand machine and motor torque.	Softwood	Ability to rotate quicker, lightweight, corrosion resistance, easy to make, and easily accessible
5.	Metal Clip	Should be able to withstand machine and motor torque.	Galvanized steel	Simple to grasp
6.	Bush Bearing	Should be able to withstand machine and motor torque.	Mild steel	Easy to adjust and good Alignment
7.	Cover Plate	Should be able to endure the machine's eccentric motion while in operation.	Galvanized steel	Significant strength, ductility, and toughness
8.	Tap And Pipe	Should be capable of assisting in transferring water from the polishing disc during the polishing process.	Stainless steel	Significant strength and corrosion resistance.
9.	Polishing Disc Casing	Should be able to endure the eccentric movement of the polisher disc and shield the machine body from splashing water.	Mild steel	Considerable strength and corrosion resistance

2.1 Machine Fabrication for the Plucking Component

The sequence of fabrication for the machine is outlined as follows: assembly of the frame structure, fabrication of the table support, integration of electric drive motors, installation of bearings on the rotational shaft, attachment of the polishing disc, addition of the required tapping mechanisms, connection of the water supply hose, finalization of the construction process, application of a protective paint coating.

The machine frame has an overall dimension of **30 inches by 20 inches**, providing a sturdy base for the various components. The table stand, measuring **21 inches by 18 inches**, was designed to provide optimal support for the electric motor, shaft, bearings, tap, and polishing discs. Two high-capacity **1119W** electric motors with a rotation speed of **2800** rpm were integrated to ensure the appropriate level of performance. The motors were securely fastened to the frame using hex head bolts and nuts. The shaft, with a diameter of 25mm and a length of 15mm, was erected at the center of the mainframe, supported by two bearings, and securely attached at the top and bottom of the frame through brazing. The polishing plates were attached to the base of the frame and joined to the shaft end via a hexagonal bolt.

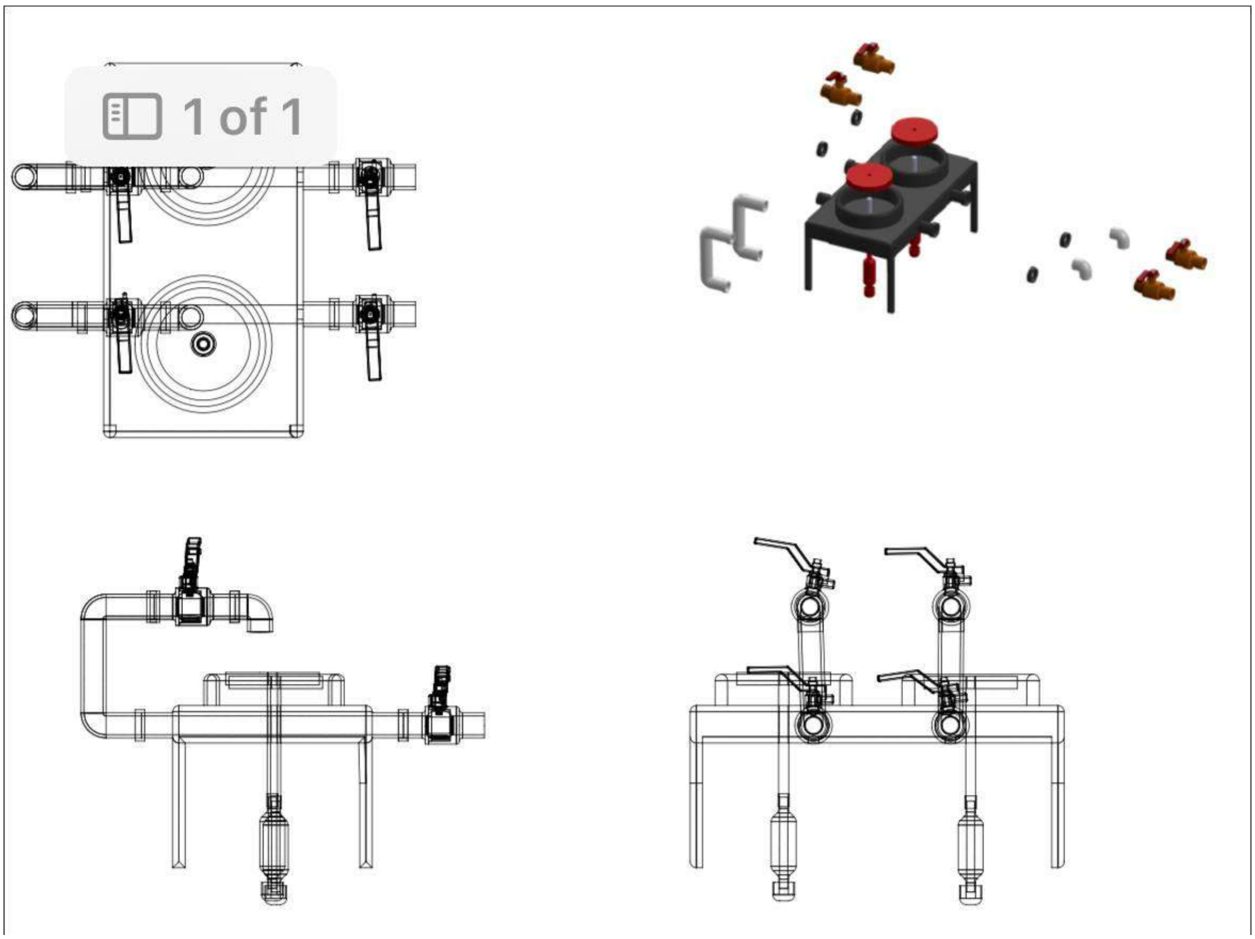

Figure 1: The orthographic view of the polishing machine

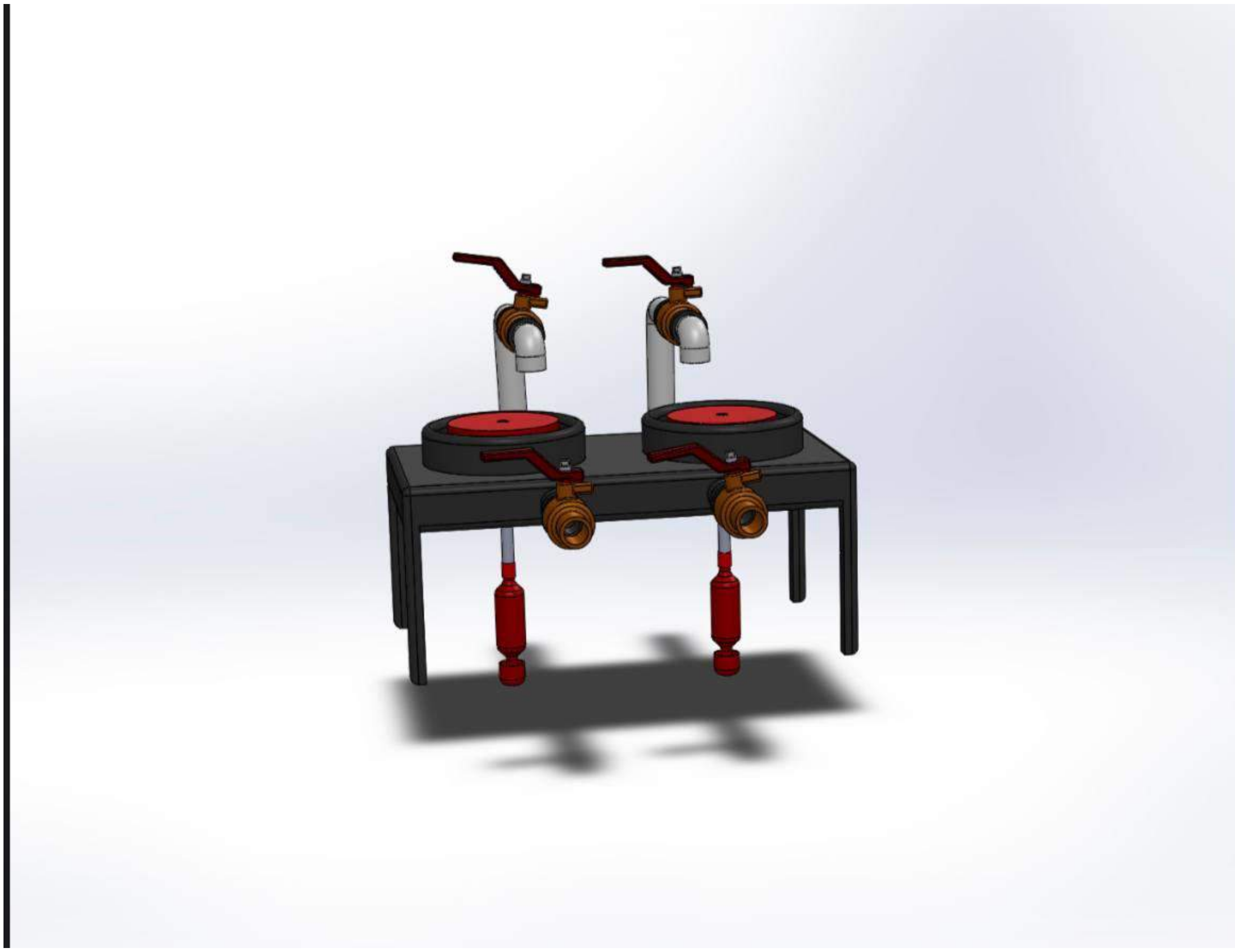

Figure 2: The isometric view of the polishing machine

2.2 Principle of Operation

Additionally, during operation, the material to be polished is placed on the rotating polishing disc in a secure manner. The tap is activated to regulate the temperature and maintain optimal conditions during the polishing process. The rotational motion of the polishing disc is driven by the shaft, which rotates against the stationary frame. The speed of rotation can be precisely controlled to accommodate the unique requirements of each individual polishing cycle, providing versatility and flexibility in the polishing process.

3.0 Results and Discussion

The polishing discs could work simultaneously. The load to be carried by the motor was already calculated in the design stage. Two separate motors were used for each polishing disc. A shiny, smooth surface of the mild steel metal sample was obtained with no presence of scratches. After cleaning the etchant, a darker surface was observed which made observation under the microscope easier by revealing microstructural details that were not evident to the naked eyes. This was aas a result of the mirror-like finish imparted on the polished surface. No observable change occurred after the application of an etchant to an unpolished surface stainless steel surface which was polished and etched with the nital solution was cloudy, which signified that the wrong etchant was used on the sample.

4.0 Conclusion and Recommendation

This project report has successfully showed the design of a locally fabricated metallographic grinding and polishing machine. The machine can be used for efficient grinding and polishing of samples for metallographic testing. The objectives of this project which is to design and fabricate an affordable laboratory metallographic polishing machine that can be used for grinding and polishing of metallic materials in the metallographic laboratory saves one the cost and inconvenience of purchasing an imported machine. It doesn't require any highly priced part for its maintenance.

Also, another objective was to produce a machine that is easy to operate and requires minimum maintenance. The overall procurement cost technically eliminates expenses that will arise from inflated prices of imported goods and also import duties and clearing fees. The machine weighs approximately 32 kg, and the polishing disc has a speed of 2333.3 rev/min.

Water flow must be properly controlled so as to ensure that the abrasive particles from the sample while polishing would not damage area for inspection and also to avoid unnecessary splash. The voltage used to operate the machine should not be less than 220 volts in order for the machine to perform efficiently. The shaft adjuster should be used to ensure that the gear and pinion are properly aligned. A sample holder could be integrated into the machine for ease of use. Instead of manual sample holding, which is hazardous to the machine operator's safety. Because of its light weight and low water reactivity, composite polymer material could be used as the polishing disc. A VARIAC Transformer should be used to reduce and increase the speed

References

[1] Akinlabi, O., Abel, B. and Emmanuel, O.O., 2018. Development of a laboratory metallographic grinding/polishing machine. Advances in Research, pp.1-13.
[2] Arvid, P. (1945). Ball and Roller bearing Engineering, S.H Burbank and Co., Incorporated Philadelphia. Pp78-86.
[3] Baucon, A., 2010. Leonardo da Vinci, the founding father of ichnology. Palaios, 25(6), pp.361-367.
[4] Buckley, J.P., 1934. Metallographic polishing machine. U.S. Patent 1,972,086.
[5] Erinle, T.J., Awopetu, O.O. and Ukoba, O.K., 2011. Development of metallographic specimen polishing machine. The Pacific Journal of Science and Technology, 12(2), pp.69-81.
[6] Friedrich, S., E Leitz Inc, 1937. Polishing machine. U.S. Patent 2,080,880.
[7] Greene, N.D., Rudaw, P.S. and Lee, L., 1966. Principles of metallographic etching. Corrosion Science, 6(8), pp.371-379.
[8] Kern, W. and Deckert, C.A., 1978. Chemical etching. Thin film processes, 1.
[9] Khurmi R.S. and Gupta J.K. 2005. Machine Design, Eurasia Publishing House (PVT) Ltd.: Ram Nagar, New Delhi, India. 110-055

[10] Nur, R., Suyuti, M.A. and Madjid, M., 2020, July. Development of polishing machine for preparation metallographic specimen with re-manufacturing. In IOP Conference Series: Materials Science and Engineering (Vol. 885, No. 1, p. 012016). IOP Publishing.
[11] Pawar, S.B. and Koli, S.K., 2016. Design and fabrication of bar polishing machine. International Research Journal of Engineering and Technology (IRJET), 3(6), pp.255-258.
[12] Petzow, G. ed., 1999. Metallographic etching: techniques for metallography, ceramography, plastography. ASM international.
[13] Samuels, L.E., 2003. Metallographic polishing by mechanical methods. Asm International.
[14] Shugley, J.E. 1980. Design of Machine Element. (5th Edition). McGraw-Hill Publishing Co.: New York, NY.
[15] Vander, G.F., 1999. Metallography, principles and practice. ASM international.
[16] Vander, G.F., 2012. Applied metallography. Springer Science & Business Media.
[17] Vijayan, N., Raj, S.A., Muthirulan, V., Sachidananda, K.H., 2019. Design and fabrication of a continuous polishing machine. Journal Européen des Systèmes Automatisés, Vol. 52, No. 5, pp. 485-493. https://doi.org/10.18280/jesa.520507.

NIPES-NCEE Conference Proceedings
The 2nd International Conference 15th-17th Feb. 2023
423-435
www.nipesjournals.org.ng

STRATEGIES FOR EFFECTIVE APPLICATION OF THE LEAN TECHNIQUES IN MATERIALS WASTE MINIMIZATION

[1]Yusuf, Alaya; [2]Mohammed, Aisha L.; [3]Ruth, O. Umesi & [4]Isyaku L.M

[1,2,3,4] Department of Quantity Surveying, Federal Polytechnic, Bida

Corresponding Email:- [1]ysfalaya@yahoo.com, [2]kawuaisha77@gmail.com, [3]ruthomozokpia@gmail.com

Abstract

The existing lean framework have proven complicated to implement and fail to consider specific context of building construction and materials waste minimization in a Nigeria. Thus, this research aims to fill this gap by developing a lean framework for material waste minimization in building projects in Abuja, with a view to minimizing the endemic problems of material waste in building construction projects in Nigeria. The study adopted a survey design approach using quantitative method but the model developed was validated using qualitative interviews. Data were collected using well-structured questionnaire administered to 320 respondents including, project managers, contractors, heads of waste management departments, and consultants of 80-active building construction sites that are practicing lean within Abuja, using Judgemental sampling method. A total of 189 questionnaires were retrieved from 320 administered. From the study, it was revealed that training of construction personnel on lean, use of more efficient construction equipment, good coordination to avoid over-ordering and Just-in-time operations, were the key action points for lean application in material waste minimization. The study developed lean-framework for material waste minimization in building projects. Based on the findings, the study recommended proper implementation of the lean framework developed in this study, as it would translate into a drastic reduction in the quantity of material waste generation in building construction projects.

***Keywords**: Building project, Construction industry, Relative importance index, Lean*

INTRODUCTION

The construction industry plays an indispensable role in any nation's economic growth by contributing to the national Gross Domestic Product (GDP) [1]. However, the industry is consideredas apolluter of the environment, since construction activities contribute to environmental degradation through resource depletion, air pollution, and generation of material waste [1].

Lean construction is a holistic concept that promotes the elimination of waste and has been adopted in several countries around the world with significant benefits achieved [2].

Lean construction is a concept that originated from the manufacturing industry, whose main principles are the elimination of wastes in any production process and activities to cause a reduction in the process cycles, an improvement in product quality and increment in efficiency of projects [3]. However, waste from the lean concepts does not only include material waste but all kinds of wastes that can be generated in the production process. Such wastes include delay; over-processing and ordering, excess motion, labour and inventory, defects and so on [3].

Lean production philosophy which was developed by the Toyota production system has been successful in achieving maximum profits and value for money to customers [4]. Adoption of the lean philosophy in the construction industry became necessary because of the needs to meeting project objectives (cost, quality and timely completion); the need to reduce uncertainty and waste in the production process,by adding value to construction activities; and the need to meet clients' needs [5,6,7,8].

STATEMENT OF THE PROBLEM

Construction material waste is a global problem as highlighted by Saidu and Shakantu (2017), it was asserted that 10-15% of materials delivered to construction sites which generates 164m tonnes of construction waste annually. In Nigeria, the problem of material waste remains unresolved and requiring urgent attention in the construction industry. This problem as posited by Saidu and Shakantu (2017) and reiterated by Umar (2019) that the amount of materials used in buildings building projects significantly predicts the quantity of generated waste in Nigeria.

Babatunde (2012) emphasised that the problem of construction material waste is well known in Nigeria, but seems not to be given the recognised attention it deserves and thus, building construction sector is often classified at the bottom of the ranking of reports regarding the efficiency of the production management techniques [10]. Hence, there is insufficient empirical data on its application in the Nigerian construction industry, hence a research sought to investigate the strategies for effective application of the lean techniques in materials waste minimization.

RESEARCH QUESTION

To address the highlighted problem, the following research questions must be duly answered:

i. What are the strategies for effective application of the lean techniques in materials waste minimization?
ii. What lean framework can be developed to effectively minimize material waste in building projects?

LEAN CONSTRUCTION

Lean Production (LP) was developed by Toyota production system in the 1950s led by Engineer Ohno who was committed to eliminating waste [11]. The term "lean" was coined by the research team working on international auto production to contrast it with craft and mass forms of production [12]. The core concept behind LP is to enable the flow of value creating work steps while eliminating non-value steps (waste) by focusing on fast cycle times. When waste is removed from the production process, cycle times drop until physical limits are reached. Value-adding activities are however, first improved through internal continuous improvement and fine-tuning of existing machinery. Only after these improvement potentials are realised, then major involvements in new technology are considered. The concept was adopted in the construction industry as it has close peculiarities with the manufacturing industry, and this is called the Lean Construction.

Fewings (2013) defined lean construction as a tool for elimination of waste from the design and production processes of a construction project using Lean principles by minimizing activities that do not add value to the product and services and creating more time for those that add value, Lean Construction maintains a continuous pursuit of improvement throughout the design, construction, operation and maintenance stages of a construction project to satisfy the client's requirements. In addition to making the construction process more effective, efficient and profitable, it brings effective value and risks management into construction companies and challenges the belief that cost, time and quality management cannot be concurrently pursued [3].

Lean Construction Techniques Relevant to Building Construction Projects

Lean Construction does not imply the imposition of Lean manufacturing techniques on construction process [13], but rather the development of techniques and tools that conform to Lean construction principles and applying them in project delivery [3]. The fundamental differences between manufacturing and construction processes in terms of the operations, planning and task execution makes it impossible for Lean manufacturing tools to be directly implemented in construction [14].

Bashir (2013) asserts that lean construction techniques are the different features or practices adopted in applying a Lean construction tool. In other words, Lean techniques are subsets of lean construction tools. A Lean construction tool comprise of one, two or more Lean techniques.

Last planner system: Last Planner System (LPS) aims to change the focus of control from the workers to the flow of work, better assignments to direct works through continuous learning, and corrective action, and to cause the work to flow across production units in the best achievable sequence of rate [15]. It is a system of production control, introduced in 1992 by Glenn Ballard, that emphasizes the relationship between scheduling and production control to improve flow of resources [16].

Value stream mapping (VSM): The VSM is a tool used for flowcharting lean processes. VSM also offers illustrations of the information flows, processes, and the control in the work flow [17]. The tool is used to visually represent the product flows. Possessing an understanding of the production processes, material flows, and information flows that make up the construction process, in order to apply the Lean process that is essential. VSM facilitates the understanding of this phenomenon.

Work organisation: The 5Ss forms the foundation for lean and continuous improvement. The main idea behind the 5Ss is to acquire, maintain and improve the standard set-up, organisation and design of the workplace and ensure that safety is intact, together with operating efficiently and decreasing waste, all done in an organized manner [18].

Visual management (VM): Visual Management ensures that things can easily be viewed. VM is based on the fact that most people respond to visual prompts and get more involved in things that they can see clearly and understand. All over an organisation, VM can be used to immediately communicate unambiguous happenings, so it can be quickly understood. Construction sites are utilising VM in various forms, for instance, on board signs for hazardous or dangerous situations, and color-coding of fire extinguishers and electrical wiring etc [19].

Just-in-time (JIT): Just after the conclusion of the World War II, the Toyota Production System spawned a new management philosophy called theJIT comprising three facets: people, plant, and systems. From its origins in keeping inventory levels in check, it subsequently developed into a managerial philosophy that broadened to encompass the tasks of maximising quality, while minimizing costs, of deliverables [20].

Standardised work: Standardised work forms the foundation for continuous improvement in lean production while standardising both the product and process [21]. Included in the standardisation is that the production rate for each process be the same as it take time with no variability; that a particular task be performed in the same manner throughout; to decrease set-up time and process time variation, product design is standardized; and to allow for continuous production, inventory is standardised. Each productis distinct in lean construction; thus, the production system is adopted. Visual management, i.e. postingproject information such as schedule and cost; workplace organisation.

Partnering: Partnering is a long-term commitment which includes two or more organisations with the aim to achieve a particular business objective together by obtaining the maximum potential of the resources available at each point [22,23]. The foundation of partnership is based on achievement of common targets, understanding the values and expectations of the other partner(s) and, importantly, trust. Partnerships yield common benefits that may include cost effectiveness and increased efficiency, greater innovation, and the improvement of quality products and services on a constant basis [24]. Partnering as an effective and innovative concept for project organisation; and the rewards of partnering come in the form of cost reduction and lesser conflict in the construction industry.

Daily huddle meeting: The daily huddle meeting requires another change in culture; a culture where the project manager has the discipline to prepare and implement a plan versus the typical culture of waiting for a problem to occur and then reacting to the problem. This planning change is implemented during the execution phase of the project by holding daily meetings to coordinate work activities. The huddle-up meeting is a great communication tool and can be used to address other project issues such as weather, environment, security, quality, or schedule. The huddle-up meeting provides a format to communicate coordination, quality, security, and schedule issues that must be addressed and, like safety, critical issues may require a work pause or stop work order until they are remedied; a warning may be issued for lesser events [25].

Procedures for Lean Techniques Application in Material Waste Minimization

Pre-implementation phase

Successful lean implementation relies heavily on the efficient “starting” of the implementation process. This will certainly require the company to ensure that all necessary foundations are taken place to enable a successful and sustainable lean implementation [26].First of all, management must begin to show leadership and demonstrate that it is committed to the project by elaborating the lean policy and setting up lean objectives. Furthermore, lean objectives must align with the strategic global policy of the organization. Then, the management is responsible for the establishment of “Lean Team”. As a small business, the lean team should not contain many individuals; however, it must be a multifunctional team. The next step is the training of the lean team. This training should be conducted by a lean expert consultant to provide an initial boost for the introduction of lean culture within the team. The first task of the team is the delimitation of the perimeter of action by choosing the top priority value stream. This can be performed using the product/process matrix or simply by Pareto analysis. The proper selection of the initial perimeter of action is crucial to focus resources and maximize gains. Once the initial perimeter is selected, the team has to develop a master plan of lean implementation. This master plan should include both a schedule and a budget [2].

Implementation phase (execution)

The implementation phase focuses on performance improvement at all levels of the organisation. This phase begins with a "warming up" step in with the lean team takes care on upgrading workforce and organising workstations to enable the deployment of other lean practices. First, the lean team needs to educate people and train them in lean practices and tools in order to get workforce acquainted with lean and prepare them for change. Afterwards, teams are oriented to the shop floor in order to build the sense of ownership and responsibility necessary for the improvement [27].

Post-implementation phase (generalisation)

The Post-implementation phase plays a critical role in completing lean implementation project and ensuring continuous improvement. First, the company needs to measure the progress it is making toward their goals [28] relying on scoreboard that contains lean Key Performance Indicators (KPI's) identified previously. Once the lean objectives are achieved, best ways to complete tasks should be capitalised, standardised and share. This step is paramount because it allows locking in the gains obtained in the execution phase. Afterwards, lean team must tackle another perimeter starting with establishment of new master plan for lean implementation.

Complete lean transformation phase

This is the final phase documenting the new lessons learned and scope changes resulted during execution, establishment of new lean standards and planning of continuous improvement. To accomplish lean transformation, the organisation must ensure that all necessary changes to the established requirements are implemented. This process aims to optimise the results of lean practice prior to the process of standardisation or future utilisation of the practice. Expanding the scope of lean implementation is an indicator of continuous improvement whereas stakeholder's involvement at all levels must be included. Moreover, the standardised lean practice must be ratified by the key stakeholders [5].

Challenges Facing Lean Implementation in Material Waste Minimization

A significant barrier identified was the unwillingness of the management in the contracting firms to train their workers about lean construction techniques, which is also linked to legislative bottlenecks against the training of workers, especially foreign workers in the country [29]. Furthermore, there is high averseness to change, or to embrace new ideas or innovations such as lean construction among the contracting organisations, while there is an unfavorable procurement system which pushes the risks involved in implementing new ideas to only the contractors[29].

Table 1: Challenges in application of lean techniques for material waste minimization

S/No	Challenges for the application of lean techniques for material waste minimization	Authors
1	Lack of training, Lack of top management support and commitment; Lack of equipment; Lack of client and supplier involvement; Unsuitable organisational structure and Lack of technical skills	Shang and Pheng (2014)
2	Poor project definition; Lack of supply chain integration; Long implementation period; Lack of buildable designs;Lack of long-term commitment to change and innovation; Lack of agreed implementation methodology; Lack of buildable designs and Extensive use of subcontractors	Omran and Abdulrahman (2015)
3	Delay in materials delivery; Materials scarcity; Poor communication; Difficulty in understanding concepts; Incomplete designs	Olamilokun (2015)
4	Inadequate pre-planning and Lack of standardisation	Agyekum (2012).

Source: Researcher's Field Survey, 2023.

Strategies for Addressing the Challenges of Applying Lean Techniques in Material Waste Minimization

These are the different ways of addressing the challenges to Lean Construction practice. The challenges have to be addressed in order to realize the targeted benefits. This section of the framework presents strategies that could be used in overcoming the challenges. In an attempt to identify ways of addressing these challenges, Suresh *et al.* (2012) identified creation of Lean awareness programs, staff training and education on Lean techniques, and government policies. There seems to be inadequate strategies reported in the literature. Thus, it becomes necessary to explore other strategies that could be used to address the numerous challenges.

To overcome the principal barriers to lean construction, universally applicable solutions are proposed. As the most pervasive barrier to implementing lean construction, the greatest effort should be concentrated on traditional practices in the Saudi Arabian construction industry. Within construction organizations, the management should be open to and committed to making changes in the construction field [30]. According to Devaki and Jayanthi(2014) this could be achieved by making changes to the culture in construction organizations to accommodate lean construction principles as part of organisational policy. If this were to occur, employees and organizational partners would be compelled to embrace a lean construction culture. However, as part of cultural changes, Bashir *et al.* (2015) suggested that construction organizations should use very simplified terms to convey ideas about lean construction in the organization policy. Similarly, as part of a commitment to lean construction practices, the management should acquire necessary managerial skills to oversee the successful implementation of lean construction during project delivery [31].

RESEARCH METHODOLOGY

Design in research is the overall plan for connecting the research problems to the pertinent empirical research. It articulates what data is required, what methods are going to be used to collect and analyse the data [32,33,34]. This study adopted a survey design approach using structured questionnaire in the form of quantitative data.

Data were collected through structured questionnaire administered to respondents within Abuja, the Federal Capital Territory (FCT) of Nigeria. Abuja was selected because is one of the epicentre of construction activities in Nigeria. The sample frame include 25 Civil Engineers, 35Quantity Surveyors and 30 architects. The sample covers construction companies domiciled in Idu Industrial Area, Abuja. This make the work as representative as possible, non-probability sampling technique was adopted in the administration of questionnaire in the study area.

Analysis

Table 2: Challenges in the application of lean techniques for material waste minimization

Challenges in the application of lean techniques for material waste minimization	RII	Ranking
Lack of appropriate training on lean	0.95	1
Poor site communication	0.87	2
Lack of top management support and commitment	0.86	3
Poor project definition	0.85	4
Long implementation period	0.83	5
Delay in materials delivery	0.80	6
Materials scarcity	0.80	6
Lack of supply chain integration	0.79	8
Lack of long-term relationship with suppliers	0.79	8
Unsuitable organizational structure	0.78	10
Lack of agreed implementation methodology	0.78	10

Difficulty in understanding concepts	0.77	12
Lack of equipment	0.76	13
Lack of technical skills	0.76	13
Dependency of onsite design components rather than standardized components	0.76	13
Inadequate pre-planning	0.75	16
Lack of client and supplier involvement	0.75	16
poor designs	0.74	18
Incomplete designs	0.74	18
Lack of long-term commitment to change and innovation	0.72	20
Lack of standardisation	0.70	21
Lack of buildable designs	0.70	21
Extensive use of subcontractors	0.70	21
The fragmented nature of the construction industry	0.60	23

Source: Researcher's Field Survey, 2023.

Table 4.3: Strategies for effective application of lean techniques in material waste minimization

Strategies for material waste minimization through lean techniques	**MIS**	**Ranking**
Training of construction personnel on lean	4.42	1
Use of more efficient construction equipment	4.29	2
Good coordination between store and construction personnel to avoid over-ordering	4.15	3
Just in time operations	4.10	4

Regular education and training of personnel on how to handle materials on site	4.08	5
Proper storage of materials on site	4.07	6
Change of attitude of workers towards the handling of materials	4.07	6
Vigilance of supervisors	4.02	8
Adherence to standardized dimensions	3.97	9
Checking materials supplied for right qualities and volumes	3.95	10
Employment of skilled workmen	3.88	11
Early and prompt scheduling of deliveries	3.85	12
Mixing, transporting and placing of concrete at the appropriate time	3.86	12
Accurate and good specifications of materials to avoid wrong ordering	3.79	13
Adoption of proper site management techniques	3.78	14
Careful handling of tools and equipment on site	3.73	15
Weekly programming of works	3.67	16
Accurate measurement of materials during batching	3.65	17
Encourage re-use of waste materials in projects	3.65	17
Access to latest information about types of materials on the market	3.64	19
Purchasing raw materials that are just sufficient	3.59	20
Minimizing rate of design changes	3.55	21
Using materials before their expiry dates	3.48	22

Source: Researcher's Field Survey, 2023

DISCUSSION OF FINDINGS

As regarding to possible strategies for addressing the identified challenges, findings revealed that the top rated strategies includes: training of construction personnel on lean, use of more efficient construction equipment, good coordination between store and construction personnel to avoid over-ordering. The least rated strategies includes: using materials before expiry date, purchasing raw materials that are just sufficient and minimizing rate of design changes. These findings are in line with the findings of Vilasini *et al.* (2011); Marwa (2013); Vidhate and Salunkhe (2018); Archana *et al.* (2017) and Subramani *et al.* (2018).

According to Ingle and Waghmare (2015), proper training and implementation of lean concepts and practices can be successfully adopted in construction projects and has increased keen interest from many organised players in the industry. It was clearly seen that the enabling factors included commitment of top management and site management, as well as the culture and systems of the organisation will be main forces for the success of lean construction in India. Likewise, review of industry case studies has shown that implementation of lean construction principles facilitates company‘s progress and engenders sustainable innovation practices in construction design and assembly.

Subramani (2018) further states that even though the prevalent theory of production (or specifically, theory of construction) is seen as counterproductive, leading to added costs and reduced overall performance, the huge positive impact of lean implementation on sustainable innovation within construction have been quantified and provided proof of sustainability outcomes in terms of reduced waste, effort and time.

According to Bashir *et al.*(2015), rather than an aggressive and one-off implementation approach, a step by step, or simplified implementation of lean construction is necessary to enable operators to adapt to the technological sophistications involved. These sophistications can also be reduced by supporting the implementation of lean construction with visualization mechanisms such as Building Information Modelling (BIM) to enable operators to easily monitor the process [35]. Furthermore, the government has a role to play to overcome the technological barrier to lean construction, especially to enact policies that will make lean methods more feasible [36]. For instance, such policy would set an agenda and provide a direction for construction organizations to identify and implement feasible lean construction methods [37,38,39,40].

CONCLUSION

The most important procedures for implementing the lean techniques at pre-construction stage are: establishment of lean policy/objectives, establishment of lean team and training, establishment of lean development master plan, result monitoring and diagnosis of lean cultural level. However, at the construction stage, the most important procedures are implementation of piloted projects, development of lean model and analyses of the current situation and extension, lean parameters, and establishment of lean policy/objectives. It is concluded further that lack of appropriate training, poor communication and lack of top management support and commitment are the key challenges for lean techniques implementation in building projects.

The best possible strategies for waste minimization through lean techniques are training of construction personnel on lean, use of more efficient construction equipment and good coordination between store and construction personnel to avoid over ordering.

RECOMMENDATIONS

From the findings and conclusion, the study makes the following recommendations:

1. The study also recommends that challenges like lack of appropriate training, poor communication, lack of top management support and commitment, and poor project definition should be given close attention when implementing lean techniques in building construction projects.
2. The study recommends that, to effectively apply lean techniques in building projects, the following strategies must be put into consideration: training of construction personnel on lean, use of more efficient construction equipment, good coordination between store and construction personnel to avoid over-ordering and just in time operations.
3. The lean framework developed in this study is recommended to the Nigerian construction industry, particularly the building sectors for minimizing material waste.

REFERENCES

[1] Agyekum, K. (2012). *Minimizing materials wastage at the construction stage of a project through the implementation of lean construction*. Kumasi, Ghana: Kwame Nkrumah University of Science and Technology.

[2] Ansah, R. H. Sorooshian, S. Mustafa, S. & Duvvuru, G. (2016). Lean Construction tools. Proceedings of the 2016 International conference on industrial engineering and operations management Detroit, Michigan, USA. *IEOM Society international;* 1(3):141-143.

[3] Archana, M. S. Renuka, S. M. & KarthigaiPriya, T. (2017). Identification and Analysis of Lean Techniques in Indian Construction Projects. *Journal of Mechanical and Civil Engineering;* 14 (2): 62-69.

[4] Arditi, J. (2016). Applying Lean Construction to Concrete Construction Projects. A Master's Project Report Presented to the Faculty of the Department of Engineering Technology College of Technology University of Houston.

[5] Ayarkwa, J. Agyekum, K. & Adinyira, E. (2012). Exploring Waste Minimization Measures in the Ghanaian Construction Industry. *Built Environment Journal*, 8(2), 22-30, 2011.

[6] Aziz, R.F. & Hafez, S.M. (2013). Applying Lean Thinking in Construction and Performance Improvement. *Alexandria Engineering Journal*, 52 (4), 679-695.

[7] Babalola, O., Ibem, E. O. & Ezema, I. C. (2019) Lean construction: an approach to chieving sustainable built environment in Nigeria. 3rd International Conference on Science and Sustainable Development (ICSSD). *Journal of Physics:* 1(2):9-10.

[8] Babatunde, S. O. (2012) Quantitative Assessment of Construction Material Wastage in Nigerian Construction Sites. *Journal of Emerging Trends in Economics and Managent Sciences* 3 (3), 238-241.

[9] Bajjou, M.S., Anas, C. & Ennadi, A. (2019). Development of a Conceptual Framework of Lean Construction Principles: An Input-Output Model. *Journal of Advanced Manufacturing Systems*, 18(1), 1–34. DOI: 10.1142/S021968671950001X.

[10] Bashir A. M., Suresh S., Oloke, D. A., Proverbs, D. G. & Gameson R. (2013). Application of Lean Construction Tools in the UK Contracting Companies- Findings from Qualitative Studies. *Proceeding for Architectural Technology Institute Conference*, Pennsylvania University.

[11] Devaki, M.P & Jayanthi, R. (2014). Barriers to implementation of lean principles. *International Journal of Engineering Research Technology*; 3, 1189–1192.

[12] Fewings, P. (2013) *Construction Project Management: An Integrated Approach,* 2nd ed., London: Spon Press.
[13] Forbes, L. H. & Ahmed, S. M. (2011). Modern Construction: Lean Project Delivery and Integrated Practices. *Boca Raton,* FL: CRC Press Inc.
[14] Harris, E. C. (2013). Global Construction disputes: A longer resolution global construction report. Kwww.echarris.com/contact solution.
[15] Ingle, A, & Waghmare, A. P. (2015). Advances in Construction: Lean Construction for Productivity enhancement and waste minimization. *International Journal of Engineering and Applied Sciences (IJEAS)*; 2(11): 2394-3661.
[16] Kokate, P. B., & Darade, R. (2018) Cost Control Techniques for Construction Project. *International Research Journal of Engineering and Technology (IRJET*), 5(6), 2433-2436.
[17] Kumar, U.V & Ramasamy, G. (2016). A Critical Study of Various Lean Techniques inPractice and Developing a Framework forDifferent Construction Building Projects. *International Journal of Chemical Sciences,* 14 (1), 175-187.
[18] Lee, C. Y. (2004). TQM in small manufacturers: an exploratory study in China. *International Journal of Quality & Reliability Management,* 21(2), 175-197.
[19] Maru, A.A. (2015). Lean construction in civil engineering and project management: Case study Analysis of UT Arlington College Park. *American journal of civil engineering*, 3, 70 – 74.
[20] Marwa G.S (2013). *Improving project performance using lean construction in Egypt: A proposed Framework*. The American University in Cairo School of Sciences and Engineering Construction and Architectural Engineering. A thesis submitted in partial fulfillment of the requirements for the Degree of Master of Science in Construction Engineering
[21] Moghadam, M. (2014). Lean-Mod: An Approach to Modular Construction Manufacturing Production Efficiency Improvement.Doctor of Philosophy, University of Alberta, Edmonton, Alberta.
[22] More, V. D., Charhate, Shrikant. & Sinha, M. (2016). Lean construction techniques in Indian construction industry: Some analysis. *International Journal of civil engineering research*, 7(1), 59-65.
[23] Mostafa, S., Dumrak, J., & Soltan, H. (2013). A framework for lean manufacturing implementation. *Production & Manufacturing Research: An Open Access Journal,* 1, 44-64.
[24] Muhammad, M., Chinyio, E. & Abdulaziz, S. A. (2017) The awareness and implementation of lean models in Nigerian construction. Proceedings of the 3rd NWUSCIAIA
[25] O'connor, R. & Swain, B. (2013). Implementing Lean in construction: Lean tools and techniques an introduction.Published by CIRIA, Classic House, 174–180 Old Street, London, EC1V 9BP, UK. ISBN: 978-0-86017-732-6.
[26] Ogunbiyi, O.E. Oladapo, A.K. & Jack, S. G. (2012). A review of lean concept and its application to sustainable construction in the UK. *International Journal of Sustainable Construction Engineering & Technology (ISSN: 2180-3242),* 4 (2), 66-87
[27] Olamilokun, O. (2015). Investigating Facilitators and Barriers for Adopting Lean Construction Principles in the Nigerian Building Consulting Firms. *InternationalJournal of Innovative Research and Development, 4*(12), 237-239.
[28] Omran, A., & Abdulrahim, A. (2015). Barriers to Prioritizing Lean Construction in the Libyan Construction Industry. *Acta Technica Corviniensis-Bulletin of Engineering, 8*(1): 53-64.
[29] Puvanasvaran, P., Megat, H., Hong, T. S., Razali, M. M., & Magid, H. A. (2010). Lean process management implementation through enhanced problem solving capabilities. *Journal of Industrial Engineering andManagement,* 3(3), 447-493.
[30] Saidu, I. & Shakantu, W.M.W. (2017). Predicting the Volume of Material Waste: A Case of ongoing Building Projects in Abuja, Nigeria. *The West African Built Environment Research Conference (WABER), Ghana*, 16th-18th August, 2017.
[31] Sarhan, J.G. Xia, B. Fawzia, S. & Karim, A. (2017). Lean construction implementation in the Saudi Arabian construction industry. *Construction Economics and Building*, 17(1), 46-69.
[32] Sarhan, S. (2013) 'Barriers to Implementing Lean Construction in the UK Construction Industry. *The Built & Human Environment Review*, 6(1), 1-11

[33] Shang, G., & Pheng, L. S. (2014). Barriers to lean implementation in the construction industry in China. *Journal of technology management in China, 9*(2), 155-173.
[34] Sorooshian, S. (2014). Delay-based Reliability Analysis on Construction Projects. *Life Science Journal*, 11(3): 104– 113.
[35] Subramani, T., Shanu, K., Akhil, R., Najeeb, A.M., & Rajan, J.K. (2018). Lean Technology and aste Minimization in Construction Industry using SPSS. *International Journal of Emerging Trends & Technology in Computer Science (IJETTCS);* 7(2): 2278-6856.
[36] Suresh, O., Khodeir, L. M. & Othman, R. (2018). Examining the interaction between lean and sustainability principles in the management process of AEC industry. *AIN SHAMs Engineering Journal*, 1627-34.
[37] Umar, A. (2019). Development of material waste prediction model for building construction works in Abuja, Nigeria. Unpublished MTech Thesis, submitted to Postgraduate School in partial fulfilment for the requirement of Master of Technology, in Quantity Surveying, Federal University of Technology, Minna.
[38] Van Wyk, M. M., & Toale, M. (2015). *Research Design. Educational research: An African approach*, Oxford University Press, Cape Town.
[39] Vidhate, T. & Salunkhe, A. (2018). General overview of Lean Management in Construction Industry. *International Research Journal of Engineering and Technology (IRJET*, 5(7):234-236.
[40] Vilasini, N, Neitzert, T.R&Gamage, J.R. (2011). Lean Methodology to Reduce Waste in a Construction Environment. *15th Pacific Association of Quantity Surveyors Congress*23 – 26 July 2011, Colombo, Sri Lanka. Pages 555-564

NIPES-NCEE Conference Proceedings
The 2nd International Conference 15th-17th Feb. 2023
436-447
www.nipesjournals.org.ng

DEVELOPMENT OF LEAN FRAMEWORK FOR EFFECTIVE MINIMIZATION OF MATERIALS WASTE IN BUILDING PROJECTS

[1]Mohammed, Aisha L., [2]Ruth, O. Umesi, [3]Yandalu, Mohammed Manko, &[4]Yusuf, Alaya

[1,2,4] Department of Quantity Surveying, Federal Polytechnic, Bida

[3]Department of Quantity Surveying, Niger State Polytechnic, Zungeru, Niger State

Corresponding Email:- [1]kawuaisha77@gmail.com, [2]ruthomozokpia@gmail.com , [3]manko3638@yahoo.com [4]ysfalaya@yahoo.com

Abstract

Lean framework have proven complicated to implement and fail to consider specific context of building construction and materials waste minimization in a Nigeria. Thus, this research aims to fill this gap by developing a lean framework for material waste minimization in building projects in Abuja, with a view to minimizing the endemic problems of material waste in building construction projects in Nigeria. The study adopted a survey design approach using quantitative method but the model developed was validated using qualitative interviews. Data were collected using well-structured questionnaire administered to 320 respondents including, project managers, contractors, heads of waste management departments, and consultants of 80-active building construction sites that are practicing lean within Abuja, using Judgemental sampling method. A total of 189 questionnaires were retrieved from 320 administered. From the study, it was revealed that training of construction personnel on lean, use of more efficient construction equipment, good coordination to avoid over-ordering and Just-in-time operations, were the key action points for lean application in material waste minimization. The study developed lean-framework for material waste minimization in building projects. Based on the findings, the study recommended proper implementation of the lean framework developed in this study, as it would translate into a drastic reduction in the quantity of material waste generation in building construction projects.

***Keywords**: Building project, Construction industry, Relative importance index, Lean*

INTRODUCTION

The construction sector world over, contributes to the realisation of about 50 percent of the total capital, being the second employer in the country. It is also an engine for technology, innovation and overall development [1].

Lean construction is a holistic concept that promotes the elimination of waste and has been adopted in several countries around the world with significant benefits achieved [2]. Lean construction is a concept that originated from the manufacturing industry, whose main principles are the elimination of wastes in any production process and activities to cause a reduction in the process cycles, an improvement in product quality and increment in efficiency of projects [3]. However, waste from the lean concepts does not only include material waste but all kinds of wastes that can be generated in the production process. Such wastes include delay; over-processing and ordering, excess motion, labour and inventory, defects and so on [3].

The construction industry plays an indispensable role in any nation's economic growth by contributing to the national Gross Domestic Product (GDP) [4]. However, the industry is considered as a polluter of the environment, since construction activities contribute to environmental degradation through resource depletion, air pollution, and generation of material waste [4].
Lean production philosophy which was developed by the Toyota production system has been successful in achieving maximum profits and value for money to customers [5]. Adoption of the lean philosophy in the construction industry became necessary because of the needs to meeting project objectives (cost, quality and timely completion); the need to reduce uncertainty and waste in the production process, by adding value to construction activities; and the need to meet clients' needs [6,7,8,9].

STATEMENT OF THE PROBLEM

Babatunde (2012) emphasised that the problem of construction material waste is well known in Nigeria, but seems not to be given the recognised attention it deserves and thus, building construction sector is often classified at the bottom of the ranking of reports regarding the efficiency of the production management techniques [13]. Hence, there is insufficient empirical data on its application in the Nigerian construction industry, hence a research sought to investigate the strategies for effective application of the lean techniques in materials waste minimization.
Construction material waste is a global problem as highlighted by Saidu and Shakantu (2017), it was asserted that 10-15% of materials delivered to construction sites which generates 164m tonnes of construction waste annually. In Nigeria, the problem of material waste remains unresolved and requiring urgent attention in the construction industry. This problem as posited by Saidu and Shakantu (2017) and reiterated by Umar (2019) that the amount of materials used in buildings building projects significantly predicts the quantity of generated waste in Nigeria.

RESEARCH QUESTION

To address the highlighted problem, the following research questions must be duly answered:

iii. How can lean framework be developed to effectively minimize material waste in building projects?
iv. What are the strategies for effective application of the lean techniques in materials waste minimization?

LEAN CONSTRUCTION

Fewings (2013) defined lean construction as a tool for elimination of waste from the design and production processes of a construction project using Lean principles by minimizing activities that do not add value to the product and services and creating more time for those that add value, Lean Construction maintains a continuous pursuit of improvement throughout the design, construction, operation and maintenance stages of a construction project to satisfy the client's requirements. In addition to making the construction process more effective, efficient and profitable, it brings effective value and risks management into construction companies and challenges the belief that cost, time and quality management cannot be concurrently pursued [3].

Lean Production (LP) was developed by Toyota production system in the 1950s led by Engineer Ohno who was committed to eliminating waste [14]. The term "lean" was coined by the research team working on international auto production to contrast it with craft and mass forms of production [15]. The core concept behind LP is to enable the flow of value creating work steps while eliminating non-value steps (waste) by focusing on fast cycle times. When waste is removed from the production process, cycle times drop until physical limits are reached. Value-adding activities are however, first improved through internal continuous improvement and fine-tuning of existing machinery. Only after these improvement potentials are realised, then major involvements in new technology are considered. The concept was adopted in the construction industry as it has close peculiarities with the manufacturing industry, and this is called the Lean Construction.

Concept of waste in building construction projects

Many approaches are used within different sectors to depict what waste is. As a business approach, waste is seen as an opportunity, whereas the local authorities in charge of waste management see it as service. On the other hand, households and government officials see it as a problem whereas the academicians see it as an unattended issue. Whatever way, waste is termed as a material that has been used and no longer wanted, either because they have no more value or they no longer serve any desired function [16].

Waste in construction has been defined in different ways by different studies. According to the new production philosophy, waste should be understood as any inefficiency that results in the use of equipment, materials, labour, or capital in larger quantities than those considered as necessary in the production of a building. This may include both the incidence of material losses and the execution of unnecessary work, which generates additional costs but do not add value to the product [17,37,38,39,40].

Classification of waste in building construction projects

Nagapan and Rahman (2012) asserts that waste is a product or material that is unwanted. Waste is also defined as any materials by product of human and industrial activity that has no residual value. Construction waste can be clustered into two groups namely the physical and non-physical waste.

i. Physical waste in the construction industry

According to Nagapan and Rahman (2012), physical construction waste can be defined as a mixture of inert and non-inert materials arising from construction, excavation, renovation, demolition, roadwork and other construction-related activities.

ii. Non-physical waste

On the other hand, waste can be defined as non-value adding works. The term non value-adding activity is used to differentiate between physical construction waste found on-site and other waste which occurs during the construction process. This type of waste is also referred to by other researchers as intangible waste, in-direct waste or non-physical waste [18,19].

Causes of Materials Waste in Building Construction Projects

Adewuyi and Otali (2013) asserts that the causes of construction material waste can be measured and evaluated using a large number of construction phase related factors, such as design and documentation, materials procurement and management, site management practices and site supervision including environmental conditions. The first set is related to designers and client's requirements: the people who consider the functional requirement of the building. The second set is related to construction team and contractors: people who consider the build ability and maintainability of the building. The third set is related to the site supervisors and the site operatives: people who are directly involved in the art of putting the raw materials together to form the building envelop. The origin of construction material waste according to Alhajj and Hamani (2011) revolves around four major sources namely, handling of materials, procurement of materials, culture and operation. These waste sources are each having their related waste causes as shown in Figure 2.1 on the origin of construction waste.

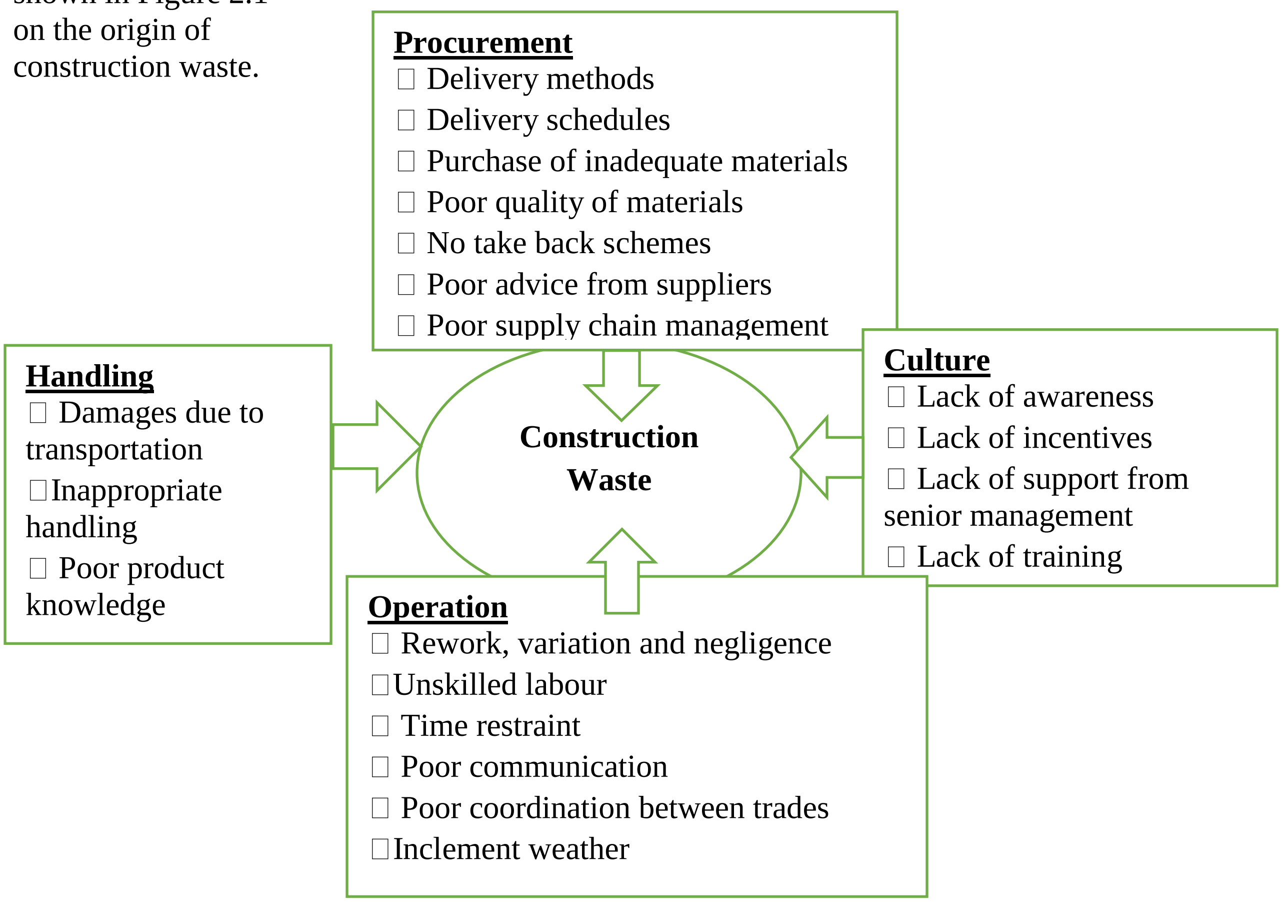

Figure 2.1: Origins of construction waste

Source: Alhajj and Hamani (2011).

Alhajj and Hamani (2011) concluded that most of the causes of waste are due to design issues. It is thus agreed that the process of waste minimization must be started at the early stages of the project. A survey conducted by Saunders and Wynn (2004) showed that improper design resulting in excessive cut-offs is one of the major causes of material waste.

Challenges Facing Lean Implementation in Material Waste Minimization

A significant barrier identified was the unwillingness of the management in the contracting firms to train their workers about lean construction techniques, which is also linked to legislative bottlenecks against the training of workers, especially foreign workers in the country [20]. Furthermore, there is high averseness to change, or to embrace new ideas or innovations such as lean construction among the contracting organisations, while there is an unfavourable procurement system which pushes the risks involved in implementing new ideas to only the contractors [20].

Table 1: Challenges in application of lean techniques for material waste minimization

S/No	Challenges for the application of lean techniques for material waste minimization	Authors
1	Lack of training, Lack of top management support and commitment; Lack of equipment; Lack of client and supplier involvement; Unsuitable organisational structure and Lack of technical skills	Shang and Pheng (2014)
2	Poor project definition; Lack of supply chain integration; Long implementation period; Lack of buildable designs;Lack of long-term commitment to change and innovation; Lack of agreed implementation methodology; Lack of buildable designs and Extensive use of subcontractors	Omran and Abdulrahman (2015)
3	Delay in materials delivery; Materials scarcity; Poor communication; Difficulty in understanding concepts; Incomplete designs	Olamilokun (2015)
4	Inadequate pre-planning and Lack of standardisation	Agyekum (2012).

Source: Researcher's Field Survey, 2023

Strategies for Addressing the Challenges of Applying Lean Techniques in Material Waste Minimization

These are the different ways of addressing the challenges to Lean Construction practice. The challenges have to be addressed in order to realize the targeted benefits. This section of the framework presents strategies that could be used in overcoming the challenges. In an attempt to identify ways of addressing these challenges, Suresh *et al.* (2012) identified creation of Lean awareness programs, staff training and education on Lean techniques, and government policies. There seems to be inadequate strategies reported in the literature. Thus, it becomes necessary to explore other strategies that could be used to address the numerous challenges.

To overcome the principal barriers to lean construction, universally applicable solutions are proposed. As the most pervasive barrier to implementing lean construction, the greatest effort should be concentrated on traditional practices in the Saudi Arabian construction industry. Within construction organizations, the management should be open to and committed to making changes in the construction field [21,35,36,37]. According to Devaki and Jayanthi(2014) this could be achieved by making changes to the culture in construction organizations to accommodate lean construction principles as part of organisational policy. If this were to occur, employees and organizational partners would be compelled to embrace a lean construction culture. However, as part of cultural changes, Bashir *et al.* (2015) suggested that construction organizations should use very simplified terms to convey ideas about lean construction in the organization policy. Similarly, as part of a commitment to lean construction practices, the management should acquire necessary managerial skills to oversee the successful implementation of lean construction during project delivery [22,32,33,34].

RESEARCH METHODOLOGY

Design in research is the overall plan for connecting the research problems to the pertinent empirical research. It articulates what data is required, what methods are going to be used to collect and analyse the data [23,29,30,31]. This study adopted a survey design approach using structured questionnaire in the form of quantitative data.

Data were collected through structured questionnaire administered to respondents within Abuja, the Federal Capital Territory (FCT) of Nigeria. Abuja was selected because is one of the epicentre of construction activities in Nigeria. The sample frame include 25 Civil Engineers, 35Quantity Surveyors and 30 architects. The sample covers construction companies domiciled in Idu Industrial Area, Abuja. This make the work as representative as possible, non-probability sampling technique was adopted in the administration of questionnaire in the study area.

Analysis

Table 2: Challenges in the application of lean techniques for material waste minimization

Challenges in the application of lean techniques for material waste minimization	RII	Ranking
Lack of appropriate training on lean	0.95	1
Poor site communication	0.87	2
Lack of top management support and commitment	0.86	3

Poor project definition	0.85	4
Long implementation period	0.83	5
Delay in materials delivery	0.80	6
Materials scarcity	0.80	6
Lack of supply chain integration	0.79	8
Lack of long-term relationship with suppliers	0.79	8
Unsuitable organizational structure	0.78	10
Lack of agreed implementation methodology	0.78	10
Difficulty in understanding concepts	0.77	12
Lack of equipment	0.76	13
Lack of technical skills	0.76	13
Dependency of onsite design components rather than standardized components	0.76	13
Inadequate pre-planning	0.75	16
Lack of client and supplier involvement	0.75	16
poor designs	0.74	18
Incomplete designs	0.74	18
Lack of long-term commitment to change and innovation	0.72	20
Lack of standardisation	0.70	21
Lack of buildable designs	0.70	21
Extensive use of subcontractors	0.70	21
The fragmented nature of the construction industry	0.60	23

Source: Researcher's Field Survey, 2023.

Table 4.3: Strategies for effective application of lean techniques in material waste minimization

Strategies for material waste minimization through lean techniques	MIS	Ranking
Training of construction personnel on lean	4.42	1
Use of more efficient construction equipment	4.29	2
Good coordination between store and construction personnel to avoid over-ordering	4.15	3
Just in time operations	4.10	4
Regular education and training of personnel on how to handle materials on site	4.08	5
Proper storage of materials on site	4.07	6
Change of attitude of workers towards the handling of materials	4.07	6
Vigilance of supervisors	4.02	8
Adherence to standardized dimensions	3.97	9
Checking materials supplied for right qualities and volumes	3.95	10
Employment of skilled workmen	3.88	11
Early and prompt scheduling of deliveries	3.85	12
Mixing, transporting and placing of concrete at the appropriate time	3.86	12
Accurate and good specifications of materials to avoid wrong ordering	3.79	13
Adoption of proper site management techniques	3.78	14
Careful handling of tools and equipment on site	3.73	15

Weekly programming of works	3.67	16
Accurate measurement of materials during batching	3.65	17
Encourage re-use of waste materials in projects	3.65	17
Access to latest information about types of materials on the market	3.64	19
Purchasing raw materials that are just sufficient	3.59	20
Minimizing rate of design changes	3.55	21
Using materials before their expiry dates	3.48	22

Source: Researcher's Field Survey, 2023

DISCUSSION OF FINDINGS

As regarding to possible strategies for addressing the identified challenges, findings revealed that the top rated strategies includes: training of construction personnel on lean, use of more efficient construction equipment, good coordination between store and construction personnel to avoid over-ordering. The least rated strategies includes: using materials before expiry date, purchasing raw materials that are just sufficient and minimizing rate of design changes. These findings are in line with the findings of Vilasini *et al.* (2011); Marwa (2013); Vidhate and Salunkhe (2018); Archana *et al.* (2017) and Subramani *et al.* (2018).

According to Ingle and Waghmare (2015), proper training and implementation of lean concepts and practices can be successfully adopted in construction projects and has increased keen interest from many organised players in the industry. It was clearly seen that the enabling factors included commitment of top management and site management, as well as the culture and systems of the organisation will be main forces for the success of lean construction in India. Likewise, review of industry case studies has shown that implementation of lean construction principles facilitates company‘s progress and engenders sustainable innovation practices in construction design and assembly.

Subramani (2018) further states that even though the prevalent theory of production (or specifically, theory of construction) is seen as counterproductive, leading to added costs and reduced overall performance, the huge positive impact of lean implementation on sustainable innovation within construction have been quantified and provided proof of sustainability outcomes in terms of reduced waste, effort and time.

According to Bashir *et al.*(2015), rather than an aggressive and one-off implementation approach, a step by step, or simplified implementation of lean construction is necessary to enable operators to adapt to the technological sophistications involved. These sophistications can also be reduced by supporting the implementation of lean construction with visualization mechanisms such as

Building Information Modelling (BIM) to enable operators to easily monitor the process [24]. Furthermore, the government has a role to play to overcome the technological barrier to lean construction, especially to enact policies that will make lean methods more feasible [10].For instance, such policy would set an agenda and provide a direction for construction organizations to identify and implement feasible lean construction methods [25,26,27,28].

CONCLUSION

The most important procedures for implementing the lean techniques at pre-construction stage are: establishment of lean policy/objectives, establishment of lean team and training, establishment of lean development master plan, result monitoring and diagnosis of lean cultural level. However, at the construction stage, the most important procedures are implementation of piloted projects, development of lean model and analyses of the current situation and extension, lean parameters, and establishment of lean policy/objectives. It is concluded further that lack of appropriate training, poor communication and lack of top management support and commitment are the key challenges for lean techniques implementation in building projects.

The best possible strategies for waste minimization through lean techniques are training of construction personnel on lean, use of more efficient construction equipment and good coordination between store and construction personnel to avoid over ordering.

RECOMMENDATIONS

From the findings and conclusion, the study makes the following recommendations:

4. The study also recommends that challenges like lack of appropriate training, poor communication, lack of top management support and commitment, and poor project definition should be given close attention when implementing lean techniques in building construction projects.
5. The study recommends that, to effectively apply lean techniques in building projects, the following strategies must be put into consideration: training of construction personnel on lean, use of more efficient construction equipment, good coordination between store and construction personnel to avoid over-ordering and Just in time operations.
6. The lean framework developed in this study is recommended to the Nigerian construction industry, particularly the building sectors for minimizing material waste.

REFERENCES

[1] Agyekum, K. (2012). *Minimizing materials wastage at the construction stage of a project through the implementation of lean construction*. Kumasi, Ghana: Kwame Nkrumah University of Science and Technology.

[2] Ansah, R. H. Sorooshian, S. Mustafa, S. & Duvvuru, G. (2016). Lean Construction tools. Proceedings of the 2016 International conference on industrial engineering and operations management Detroit, Michigan, USA. *IEOM Society international;* 1(3):141-143.

[3] Archana, M. S. Renuka, S. M. & KarthigaiPriya, T. (2017). Identification and Analysis of Lean Techniques in Indian Construction Projects. *Journal of Mechanical and Civil Engineering;* 14 (2): 62-69.

[4] Arditi, J. (2016). Applying Lean Construction to Concrete Construction Projects. A Master's Project Report Presented to the Faculty of the Department of Engineering Technology College of Technology University of Houston.

[5] Ayarkwa, J. Agyekum, K. & Adinyira, E. (2012). Exploring Waste Minimization Measures in the Ghanaian Construction Industry. *Built Environment Journal*, 8(2), 22-30, 2011.

[6] Aziz, R.F. & Hafez, S.M. (2013). Applying Lean Thinking in Construction and Performance Improvement. *Alexandria Engineering Journal*, 52 (4), 679-695.

[7] Babalola, O., Ibem, E. O. & Ezema, I. C. (2019) Lean construction: an approach to chieving sustainable built environment in Nigeria. 3rd International Conference on Science and Sustainable Development (ICSSD). *Journal of Physics:* 1(2):9-10.

[8] Babatunde, S. O. (2012) Quantitative Assessment of Construction Material Wastage in Nigerian Construction Sites. *Journal of Emerging Trends in Economics and Managent Sciences* 3 (3), 238-241.

[9] Bajjou, M.S., Anas, C. & Ennadi, A. (2019). Development of a Conceptual Framework of Lean Construction Principles: An Input-Output Model. *Journal of Advanced Manufacturing Systems*, 18(1), 1–34. DOI: 10.1142/S021968671950001X.

[10] Bashir A. M., Suresh S., Oloke, D. A., Proverbs, D. G. & Gameson R. (2013). Application of Lean Construction Tools in the UK Contracting Companies- Findings from Qualitative Studies. *Proceeding for Architectural Technology Institute Conference,* Pennsylvania University.

[11] Devaki, M.P & Jayanthi, R. (2014). Barriers to implementation of lean principles. *International Journal of Engineering Research Technology*; 3, 1189–1192.

[12] Fewings, P. (2013) *Construction Project Management: An Integrated Approach,* 2nd ed., London: Spon Press.

[13] Forbes, L. H. & Ahmed, S. M. (2011). Modern Construction: Lean Project Delivery and Integrated Practices. *Boca Raton,* FL: CRC Press Inc.

[14] Harris, E. C. (2013). Global Construction disputes: A longer resolution global construction report. Kwww.echarris.com/contact solution.

[15] Ingle, A, & Waghmare, A. P. (2015). Advances in Construction: Lean Construction for Productivity enhancement and waste minimization. *International Journal of Engineering and Applied Sciences (IJEAS)*; 2(11): 2394-3661.

[16] Kokate, P. B., & Darade, R. (2018) Cost Control Techniques for Construction Project. *International Research Journal of Engineering and Technology (IRJET*), 5(6), 2433-2436.

[17] Kumar, U.V & Ramasamy, G. (2016). A Critical Study of Various Lean Techniques inPractice and Developing a Framework forDifferent Construction Building Projects. *International Journal of Chemical Sciences,* 14 (1), 175-187.

[18] Lee, C. Y. (2004). TQM in small manufacturers: an exploratory study in China. *International Journal of Quality & Reliability Management,* 21(2), 175-197.

[19] Maru, A.A. (2015). Lean construction in civil engineering and project management: Case study Analysis of UT Arlington College Park. *American journal of civil engineering*, 3, 70 – 74.

[20] Marwa G.S (2013). *Improving project performance using lean construction in Egypt: A proposed Framework*. The American University in Cairo School of Sciences and Engineering Construction and

Architectural Engineering. A thesis submitted in partial fulfillment of the requirements for the Degree of Master of Science in Construction Engineering

[21] Moghadam, M. (2014). Lean-Mod: An Approach to Modular Construction Manufacturing Production Efficiency Improvement.Doctor of Philosophy, University of Alberta, Edmonton, Alberta.

[22] More, V. D., Charhate, Shrikant. & Sinha, M. (2016). Lean construction techniques in Indian construction industry: Some analysis. *International Journal of civil engineering research*, 7(1), 59-65.

[23] Mostafa, S., Dumrak, J., & Soltan, H. (2013). A framework for lean manufacturing implementation. *Production & Manufacturing Research: An Open Access Journal,* 1, 44-64.

[24] Muhammad, M., Chinyio, E. & Abdulaziz, S. A. (2017) The awareness and implementation of lean models in Nigerian construction. Proceedings of the 3rd NWUSCIAIA

[25] O'connor, R. & Swain, B. (2013). Implementing Lean in construction: Lean tools and techniques an introduction.Published by CIRIA, Classic House, 174–180 Old Street, London, EC1V 9BP, UK. ISBN: 978-0-86017-732-6.

[26] Ogunbiyi, O.E. Oladapo, A.K. & Jack, S. G. (2012). A review of lean concept and its application to sustainable construction in the UK. *International Journal of Sustainable Construction Engineering & Technology (ISSN: 2180-3242),* 4 (2), 66-87

[27] Olamilokun, O. (2015). Investigating Facilitators and Barriers for Adopting Lean Construction Principles in the Nigerian Building Consulting Firms. *InternationalJournal of Innovative Research and Development, 4*(12), 237-239.

[28] Omran, A., & Abdulrahim, A. (2015). Barriers to Prioritizing Lean Construction in the Libyan Construction Industry. *Acta Technica Corviniensis-Bulletin of Engineering, 8*(1): 53-64.

[29] Puvanasvaran, P., Megat, H., Hong, T. S., Razali, M. M., & Magid, H. A. (2010). Lean process management implementation through enhanced problem solving capabilities. *Journal of Industrial Engineering andManagement*, 3(3), 447-493.

[30] Saidu, I. & Shakantu, W.M.W. (2017). Predicting the Volume of Material Waste: A Case of ongoing Building Projects in Abuja, Nigeria. *The West African Built Environment Research Conference (WABER), Ghana*, 16th-18th August, 2017.

[31] Sarhan, J.G. Xia, B. Fawzia, S. & Karim, A. (2017). Lean construction implementation in the Saudi Arabian construction industry. *Construction Economics and Building*, 17(1), 46-69.

[32] Sarhan, S. (2013) 'Barriers to Implementing Lean Construction in the UK Construction Industry. *The Built & Human Environment Review*, 6(1), 1-11

[33] Shang, G., & Pheng, L. S. (2014). Barriers to lean implementation in the construction industry in China. *Journal of technology management in China*, *9*(2), 155-173.

[34] Sorooshian, S. (2014). Delay-based Reliability Analysis on Construction Projects. *Life Science Journal*, 11(3): 104– 113.

[35] Subramani, T., Shanu, K., Akhil, R., Najeeb, A.M., & Rajan, J.K. (2018). Lean Technology and aste Minimization in Construction Industry using SPSS. *International Journal of Emerging Trends & Technology in Computer Science (IJETTCS);* 7(2): 2278-6856.

[36] Suresh, O., Khodeir, L. M. & Othman, R. (2018). Examining the interaction between lean and sustainability principles in the management process of AEC industry. *AIN SHAMs Engineering Journal*, 1627-34.

[37] Umar, A. (2019). Development of material waste prediction model for building construction works in Abuja, Nigeria. Unpublished MTech Thesis, submitted to Postgraduate School in partial fulfilment for the requirement of Master of Technology, in Quantity Surveying, Federal University of Technology, Minna.

[38] Van Wyk, M. M., & Toale, M. (2015). *Research Design. Educational research: An African approach*, Oxford University Press, Cape Town.

[39] Vidhate, T. & Salunkhe, A. (2018). General overview of Lean Management in Construction Industry. *International Research Journal of Engineering and Technology (IRJET*, 5(7):234-236.

[40] Vilasini, N, Neitzert, T.R&Gamage, J.R. (2011). Lean Methodology to Reduce Waste in a Construction Environment. *15th Pacific Association of Quantity Surveyors Congress*23 – 26 July 2011, Colombo, Sri Lanka. Pages 555-564.

NIPES-NCEE Conference Proceedings
The 2nd International Conference 15th-17th Feb. 2023
448-459
www.nipesjournals.org.ng

ANALYSIS OF THE IMPACT OF FUKUSHIMA DAIICHI NUCLEAR ACCIDENT ON THE WORLD TODAY AFTER A DECADE

BubakariI Joda[1], Mohammed Joda Bello[2] and Kabiru Abubakar Yahya[3]

[1,3] Department of Electrical/Electronic Engineering School of Engineering Federal Polytechnic, Kaltungo. [1]bilkhalisa@gmail.com and [3]kabiruayahya@gmail.com
[2] Nigerian Nuclear Regulatory Headquarter Abuja. [2] hammanjoda2002@yahoo.com

Abstract

This paper provides detailed analysis on the causes and present-day influence of the aftermaths of March, 2011 (a decade ago) Fukushima Daiichi Nuclear Power Plant (FDNPP) accident is thoroughly reviewed. The impacts of the accident on the future of the nuclear energy industry, together with its health, energy security, psycho-social and ecological effects are the main consequences of the accident studied. Some proposed measures posited by some organizations, research groups and governments' agencies to curtail the lasting effects of the accident and avert its reoccurrence were also analyzed. The main sources of information used in conducting this study are official reports, academic papers and mass media reports.

KEY WORDS*: Nuclear Power Plant, Fukushima Daiichi, nuclear energy, energy security, psycho-social and ecological effects*

1.0 Introduction

Great East Japan Earthquake off the Pacific coast of Japan termed *Tohoku*, on March, 11th 2011 generated vehement tsunami waves that overpowered the Fukushima Daiichi nuclear power plant (FDNPP) protective barriers. Sequel to that, heat sinks, primary and backup power systems of the 6-unit power plant were inundated. This led to cascade of events that ultimately resulted in equipment malfunction, reactors meltdown and releasing of nuclear materials to environment thereby causing one of the three world worst nuclear accident in history [1, 2]. Japanese nuclear regulatory body; Nuclear and Industrial Safety Agency (NISA) declared that FNA was at Level-5 of International Nuclear and Radiological Event Scale (INES) same level as the 1986 Chernobyl accident [3, 4]. The released radionuclides severely affected large area of terrestrial and aquatic habitat. This tsunami caused about 15,900 confirmed fatalities and 3100 missing persons [5].

The earthquake and tsunami have not only effected the environment, but resulted in the simultaneous loss of about 30,600 MW, primarily in the northeast part of Japan (8800 MW of nuclear, 15,800 MW of thermal, and 6000MW of hydroelectricity) representing 13.4% of the country's total electricity capacity [6].

Fukushima Daiichi NPP was not the only power plant hit by the earthquake (as shown in Fig. 1), other NPPs along Japan's north-eastern coast like Higashidori, Onagawa, Fukushima Daini and Tokai Daini NPPs were equally stroke, though not as severe as FDNPP.

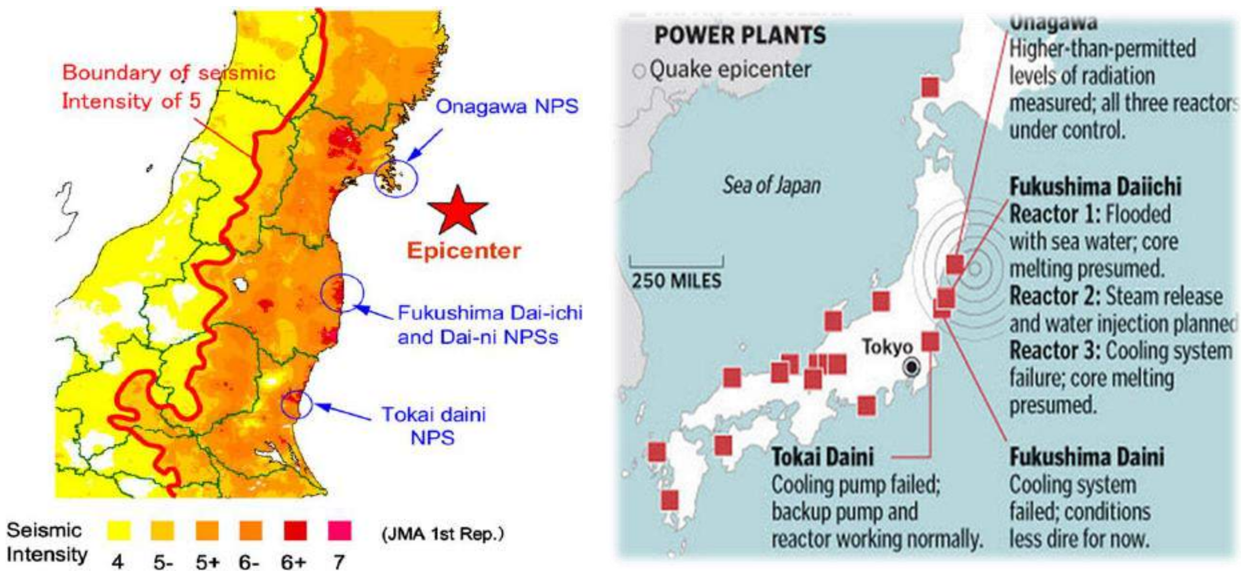

(a) Seismic intensities during the main shock. (b) State of NPPs following the accidents

Figure1 Intensities of the tsunami and its impacts on the NPPs [7].

1.1 Fukushima Daiichi Nuclear Power Plant (FDNPP) at the Time of the Accident

Fukushima Daiichi nuclear power plant (FDNPP) has six generating units (1-6) with boiling water reactors, all situated about 180km from the earthquake's epicenter. The first unit of the power plants was constructed in 1967 under TEPCO's turnkey contract with General Electric (GE) [3]. According to the operator; Tokyo Electric Power Company (TEPCO), at the time of the accident three boiling water reactors of Units 1, 2 and 3 (whose working principles is schematically described in Fig. 2) were fully operational delivering 460 MW, 784 MW and 784 MW of electric power respectively. While the reactors of the remaining three units were shut down for refueling or inspection purpose.

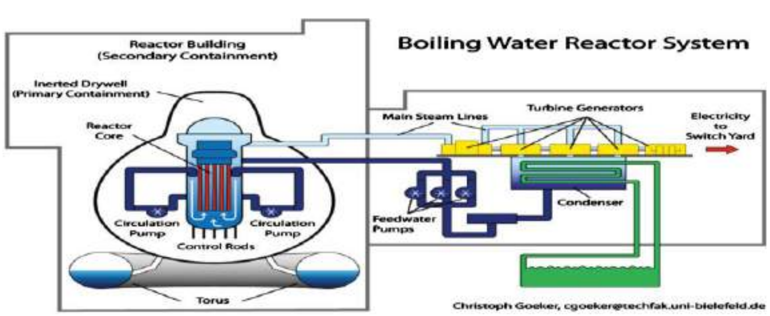

Figure 2 Schematics of boiling water reactor [7].

When the tsunami hit the FDNPP, the cooling system ought to have minimized the reactors' residual decay heat. Notwithstanding, it soon ended up noticeably clear that not exclusively was electric power from the transmission grid inaccessible because of earthquake harm, additionally that the plant's backup generators for emergency electric power were annihilated by the wave.

2.0 Causes of the Accident

Following the Tohoku earthquake, the colossal flooding due to the tsunami destroyed the FDNPP's seawater cooling pumps, emergency diesel generator, electrical systems and power supply to units 1, 2 and 3, hence causing a complete station blackout. Due to absence of heat removal mechanism, the reactor core confinement pump in the long run quit working [8]. Excessive overheating led to melting of the core material and formation of large amounts of hydrogen gas. Three huge oxy-hydrogen gas explosions subsequently destroyed buildings and led to the release of the nuclear materials [5].

Some findings reveal that five notices of tsunamis at the FDNPP had been disregarded by the nuclear administrator and regulators since 2000 [7]. TEPCO, FDNPP operator, had a record of safety defilements for years. Mostly especially in 2002, TEPCO self-proclaimed that in the vicinity of 1997 and 2002, on somewhere in the range of 200 events, support gives an account of nuclear plants had been adulterated [7]. In a press statement, TEPCO officials stated that "…*keenly (we) feel the responsibility for the accident and are determined to engage in business operation with safety on the top priority to prevent future recurrence*".

Hence it was argued that the accident was not a natural disaster, but the regulatory failures. Fukushima Nuclear Accident Independent Investigation Commission (NAIIC) narrowed down the reasons for the mishap to operator's failure to meet basic safety requirements [8]. This is in contrast to the other two worst NPP accidents; the 1979 Three Mile Island and 1986 Chernobyl that were primarily caused by either equipment malfunction, miscommunication or human error [9].

3.0 Impact of the Accident

The impact of FDNPP accident in light of medical, energy security and economic and radio-ecological effects are reviewed in this section, with special attention to short- and long-term global energy-security and policy.

3.1 Health Impact

Even though 80% of the released radionuclides from FDNPP accident were transported over the Pacific Ocean, the remaining 20% were deposited over Japanese coastal region [10, 4]. Sequel this, people and other inhabitants of the area were exposed to Iodine-131 (*131I*), Caesium-134 (*134Cs*) and Caesium-137 (*137Cs*) that either inhaled or ingested with contaminated food. These are considered the most genuine present and future wellbeing hazard for the neighborhood masses. Due to long half-life of *137C* (30years), it implies its long term exposure. Their effect observed over these six years is thyroid cancer most especially in children, increased risk of diabetes and mental health problem in adult less than 40 years [11]. That was the reason the Japanese Nuclear Emergency Response Headquarters (NERHQ) asked evacuees under 40 years to leave the stay-away departure zone and consistently be taking iodine prophylaxis to reduce the radioiodine uptake into the thyroid organ and along these lines diminish the danger of thyroid malignancy and heart diseases [5]. In 2014, a case 10-mm nodule of thyroid cancer was observed in an area 70km from FDNPP [12].

3.2 Psycho-social Impact

Following the Government's order of evacuating 146,520 residents from the area of high radiation, number of psycho-social and posttraumatic stress in the evacuees, normal populace and FDNPP workers has been observed in the last six years. Among which are post-traumatic stress, anxiety, ruptured social link and depression due to the changed lifestyle. Stigmatization and bullying have been observed in individuals exposed to radiations [1]. For six years after the accident, many people under the age of 40 emigrated from the affected areas, which not only resulted in excessive eradication additionally a quick maturing of the rest of the populace, as distinctively observed in Minamisoma City [14].

3.3 Impact on Global Energy Security and Economy

The decision to shut down all the nation's 54 nuclear reactors, with an aggregate limit of 48,960MW, after the mishap, has dropped the supply of power from nuclear power in the nation from 31.2% in February 2011 to zero in May 2012. Consequent to that, need for an alternative energy sources in Japan, like natural gas has drastically increased [6].

However, due to its natural resources deficiency, Japan continue to import huge amount petroleum product. As a consequence of this decision, Japan's annual import of liquefied natural gas skyrocketed to 81.8million tones as against 69.2million tones before the accident. Fig. 3 depicts fuel consumption for power generation by Japan's thermal power plan pre and post FDNPP mishap.

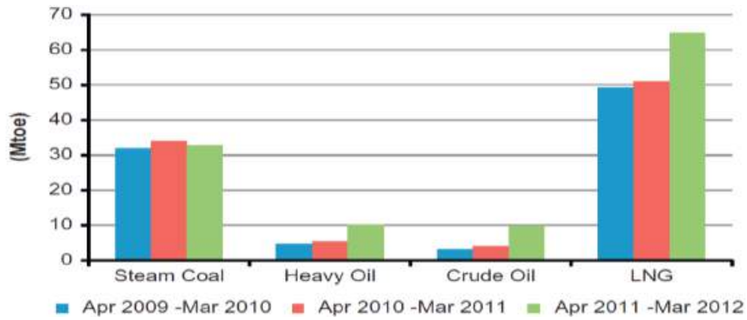

Figure 3 Fuel consumption for electricity generation in Japan [13]

The fuel utilization of substantial oil, unrefined petroleum, and condensed flammable gas (LNG) a year after the mishap (April 2011– March 2012) had expanded by 87.7%, 143.1%, and 26.7%, respectively, contrasted with a similar period preceding the mischance. This expanded interest for these energy sources has greatly affected the global accessibility and affordability of LNG which eventually affects the advertise cost of different sorts of energy.

Similar decision of shutting down all or some of their NPPs was taken by many countries like Germany, Switzerland, Belgium and Italy few days after FDNPP accident [6]. Yet in other countries, such as the United Kingdom, no drastic change occurred [2]. With the current global energy supply closely interconnected, the combined effect of securing an alternative energy sources in all of these countries has significantly altered the pattern of energy consumption in many other countries thereby influencing their energy security. Shutting down large number of NPP in the world has equally caused the price of Uranium and share costs of organizations required in the uranium business to fall drastically. For instance, uranium oxide (U_3O_8) costs tumbled from \$68.24/lb in March 2011 to \$49.99/lb quickly after the seismic tremor were still around \$50/lb in May 2012 [16].

FDNPP accident has instigated open's interest for extra security measures while constructing NPP. This has greatly increased the NPP construction costs and longer construction times [7]. This longer constructional time coupled with more stringent regulations eventually discouraged investors and lenders from taking an interest in the developing new NPP ventures.

3.4 Topographical and Ecological Effect

FDNPP accident has detrimentally impacted on adjacent groups because of radioactive defilement of land and groundwater that brought about long haul clearing of individuals from their homes, ranches, businesses and groups [11]. ^{137}Cs with physical half-life of about 30years and deposition densities of 1,000 *kBq/m2* – 10,000 *kBq/m2* recorded, hence is the primary concern due its potential prolonged impact on the ecosystem [1]. Among the terrestrial ecosystems, 70% (mainly forest) of the land is contaminated. A land is said to be contaminated if has a surface radiation level of above 40kBq/m2 [3]. In natural systems, artificial radioactive elements are consumed by plants and animals serving as important minerals and nutrients. This implies that these radionuclides are cycled and recycled through living organisms in the food web. Thus, Fukushima derived radionuclides will remain a threat to living organisms for a prolonged time period.

4.0 Suggested Measures

To curtail the existing effect of the FDNPP accident and prevent the reoccurrence of similar accident, some measures (policy making and/or technical) are posited by some organizations. In this study, these measures are classified as either curative or preventive.

4.1 Curative Measures

These are measures taken to alleviate the severity of the accident, stop its widespread among neighboring communities and bring back FDNPP to normalcy. To prevent further contamination of leaching groundwater, frozen soil barrier has been constructed. However, in July 2016 TEPCO admitted that they are "*technically incapable of blocking off groundwater with the frozen wall*" due the failure of the wall in stopping the groundwater from streaming in and blending with to a great degree radioactive water inside the smashed reactor structures [14].

Several attempts were made to clean up the site of the NPP accident, but the company tasked with the responsibility has admitted that all its attempts are to no avail due to extremely high levels of radiation beyond human survival. So remote controlled robots are used to ascertain the level of the damage. The most recent robots sent were designed by Toshiba to 73sievert of radiation, in any case, the level inside the reactor was as of late recorded at 530 Sieverts, hence the robot kept failing five times faster than planned.

TEPCO resolved to pumping water continuously (about 400 tons everyday) through the three reactors to cool the melted fuel and picks up the radiation. The contaminated water is diverted to decontamination facilities. Due to the inability of the radiation filters in the decontamination chamber to remove all the radiations, all the water is now stored in thousands of tanks. Authorities are deciding to dilute this huge amount of contaminated water and dumb it in an ocean, however local fishermen are utterly against the idea [14].

About 6000 cleanup workers and robots are carefully removing shattered mass of crushed concrete, pipes and hoses. About 200,400*m3* of rubble has so far been removed.

4.2 Preventive Measures

To prevent the reoccurrence of similar accidents, some measures are put in place by government agencies and research groups. Neglecting five warnings of tsunamis at the FDNPP signifies that NISA is not acting autonomously as it supposed to. A valid nuclear watch dog must be an autonomous organization, and therefore must not be under a government ministry. Else intrigue amass governmental issues could impact the safety regulators decisions. NISA was a casualty itself to some degree in view of its joined part as both industry promoter and industry controller, which genuinely undermined its ability as a nuclear safety guard dog. It is therefore suggested that all nations with regular citizen nuclear energy projects ought to make a quick top to bottom audit of the nation's regulatory framework and make their nuclear regulators truly independent.

Upon receipt and confirmation of an incident exceeding a foreordained level and formed into a nuclear emergency circumstance, the Head of Government shall declare “Nuclear Emergency Situation” in light of it and direct important agencies to take crisis reaction measures, for example, protecting or departure and preventive stable iodine prophylaxis administration. In a situation where the radiation is not very high, consideration need to be given to whether protective actions can reasonably be taken. In either case, doses of radioactive materials and radiation risks must be controlled within specified limits.

Adequate protection mechanisms against external events need be considered while siting and designing an NPP and such should be considered in the plant safety analysis. The protective mechanism should incorporate a robust tsunami warning system that will trigger immediate operator actions. A periodic evaluation of the impact of external threats to NPP configuration, critical safety systems and operation need to be carried out regularly.

An autonomous accident management system like mobile power, compressed air or water supplies should be put in place in case of total loss of off-site power or loss of all heat sinks. These systems should be situated in a safe place and together with means for their rapid transfer them to the affected sites.

In nuclear sites, Emergency Response Centers need to be accommodated in an on-site, robust, appropriately shielded, ventilated and well equipped buildings. These centers should have sufficient secure communication links to control rooms and other places on-site and off-site.

It is proposed in this study, using high-power lasers to cut down debris thereby helping the clean-up workers clear the residual nuclear fuel. Use of submersible robots with resilient shielding that can be used to measure radiation level under water. Additional feature that can make the robots more robust in radiation detection and fuel removal is shape-changing. The robot should assume long and straight shape while passing through a narrow passage.

Opinions:

Theoretically, nuclear transmutation involves transformation of one isotope into another isotope or another element by changing its nuclear structure as depicted and exemplified in the following equations:

$$^{A}X + {}^{1}_{0}n \rightarrow {}^{A+1}X$$

- The new isotope (^{A+1}X) may:
  - be stable to radioactive decay
  - have a shorter half life
  - spontaneously fission into fission products
  - be subsequently transformed by further neutron captures

$$\begin{array}{lllll} {}^{129}\mathrm{I} + \mathrm{n} \rightarrow & {}^{130}\mathrm{I} \rightarrow & {}^{130}\mathrm{Xe} + \mathrm{n} \rightarrow & {}^{131}\mathrm{Xe} + \mathrm{n} \rightarrow & {}^{132}\mathrm{Xe} \\ & (12.4\ \mathrm{h})\beta & \text{stable} & \text{stable,} & \text{stable,} \end{array}$$

This technique can be applied by providing optimum neutron beams with a calculated flux to a predetermined waste.

For liquid wastes stored in many tanks, NISA in collaboration with international water resources organizations should devise a regulatory and legal framework that will enable TEPCO release the contaminated waters into the ocean at a regulated amounts and predetermined intervals of time.

5.0 **Lessons Learnt**

1: There is a need to ensure that in considering external natural hazards:

- ✓ the siting and design of nuclear plants should include sufficient protection against infrequent and complex combinations of external events and these should be considered in the plant safety analysis - specifically those that can cause site flooding and which may have longer term impacts;
- ✓ plant layout should be based on maintaining a ‘dry site concept’, where practicable, as a defence-in-depth measure against site flooding as well as physical separation and diversity of critical safety systems;
- ✓ common cause failure should be particularly considered for multiple unit sites and multiple sites, and for independent unit recovery options, utilizing all on-site resources should be provided;
- ✓ any changes in external hazards or understanding of them should be periodically reviewed for their impact on the current plant configuration; and
- ✓ an active tsunami warning system should be established with the provision for immediate operator action.

2: For severe situations, such as total loss of off-site power or loss of all heat sinks or the engineering safety systems, simple alternative sources for these functions including any necessary equipment (such as mobile power, compressed air and water supplies) should be provided for severe accident management.

3: Such provisions as are identified in Lesson 2 should be located at a safe place and the plant operators should be trained to use them. This may involve centralized stores and means to rapidly transfer them to the affected site(s).

4: Nuclear sites should have adequate on-site seismically robust, suitably shielded, ventilated and well equipped buildings to house the Emergency Response Centres, with similar capabilities to those provided at Fukushima Dai-ni [Fukushima-1] and Dai-ichi [Fukushima-2], which are also secure against other external hazards such as flooding. They will require sufficient provisions and must be sized to maintain the welfare and radiological protection of workers needed to manage the accident.

5: Emergency Response Centres should have available as far as practicable essential safety-related parameters based on hardened instrumentation and lines such as coolant levels, containment status, pressure, etc., and have sufficient secure communication lines to control rooms and other places on-site and off-site.

6: Severe Accident Management Guidelines and associated procedures should take account of the potential unavailability of instruments, lighting, power and abnormal conditions including plant state and high radiation fields.

7: External events have a potential of affecting several plants and several units at the plants at the same time. This requires a sufficiently large resource in terms of trained experienced people, equipment, supplies and external support. An adequate pool of experienced personnel who can deal with each type of unit and can be called upon to support the affected sites should be ensured.

8: The risk and implications of hydrogen explosions should be revisited and necessary mitigating systems should be implemented.

9: Particularly in relation to preventing loss of safety functionality, the robustness of defence-in-depth against common cause failure should be based on providing adequate diversity (as well as redundancy and physical separation) for essential safety functions.

10: Greater consideration should be given to providing hardened systems, communications and sources of monitoring equipment for providing essential information for on-site and off-site responses, especially for severe accidents.

11: The use of IAEA Safety Requirements (such as GS-R-2) and related guides on threat categorization, event classification and countermeasures, as well as Operational Intervention Levels, could make the off-site emergency preparedness and response even more effective in particular circumstances.

12: The use of long term sheltering is not an effective approach and has been abandoned and concepts of ‘deliberate evacuation’ and ‘evacuation-prepared area’ were introduced for effective long term countermeasures using guidelines of the ICRP and IAEA. IAEA.

13: The international nuclear community should take advantage of the data and information generated from the Fukushima accident to improve and refine the existing methods and models to determine the source term involved in a nuclear accident and refine emergency planning arrangements.

14: Large scale radiation protection for workers on sites under severe accident conditions can be effective if appropriately organized and with well led and suitable trained staff.

15: Exercises and drills for on-site workers and external responders in order to establish effective on-site radiological protection in severe accident conditions would benefit from taking account of the experiences at Fukushima.

16: Nuclear regulatory systems should ensure that regulatory independence and clarity of roles are preserved in all circumstances in line with IAEA Safety Standards.

6.0 **Conclusion**

In this study, the impact of FDNPP accident on the future of the nuclear energy industry, together with its health, energy security, psycho-social and ecological effects of the accident are studied. Even though the accident was instigated by a natural disaster, many believe to a large extent that the operator, TEPCO is keenly responsible for the accident [18]. The tsunami that lead to the accident led to about 15,900 confirmed fatalities, 3100 missing persons and over 160,000 evacuated from the area, though 13% of which have resumed back.

The decision to shut down many nuclear reactors in Japan and other countries, has drastically increased the need for an alternative energy sources, globally. As a result, the availability and affordability of LNG was significantly affected. It also resulted in sudden decline in the price of U3O8 of $68.24/lb before the accident to $49.99/lb immediately after.

Number of preventive and curative measured were posited by many research groups and government agencies to contain the effect of the accident and avert its reoccurrence. Some additional measures and techniques that may help in cleaning up the contaminated area are also proposed in this study.

References

[1] S. Burnie, "Radiation Reloaded: Ecological Impacts Of The Fukushima Daiichi Nuclear Accident 5 Years Later," Greenpeace, Kendra Ulrich, March, 2016.

[2] T. P. P. T. Edwin Latréa, "Public Opinion Change After The Fukushima Nuclear Accident: The Role Of National Context Revisited," *Energy Policy,* Vol. 104 , P. 124–133, 2017.

[3] "The Fukushima Daiichi Accident Technical Volume 1: Description And Context Of The Accident," International Atomic Energy Agency,, Vienna, August 2015.

[4] A. B. T. E. J. Georg Steinhauser ⁎, "Comparison Of The Chernobyl And Fukushima Nuclear Accidents: A Review Of The Environmental Impacts," *Science Of The Total Environment,* Vol. 470–471, P. 800–817, 2014.

[5] O. H. F. Y. Hamada N, "Safety Regulations Of Food And Water Implemented In The First Year Following The Fukushima Nuclear Accident," *J Radiat Res,* Vol. 53, P. 641–671, 2012.

[6] L. H. Masatsugu Hayashi, "The Fukushima Nuclear Accident And Its Effect On Global," *Energy Policy* , Vol. 59, P. 102–111, 2013.

[7] X. X.-C. Qiang Wang, "Accident Like The Fukushima Unlikely In A Country With Effective Nuclear Regulation: Literature Review And Proposed Guidelines," *Renewable And Sustainable Energy Reviews* , Vol. 17, P. 126–146, 2013 .

[8] D. J. A. A. P. M. D. J. L. H. V. W. Fabienne Grallaa, "The Impact Of Nuclear Accidents On Provisioning Ecosystem Services," *Ecological Indicators,* Vol. 41, P. 1–14, 2014.

[9] G. Masahiko Aoki, "A Comparative Institutional Analysis Of The Fukushima Nuclear Disaster Lessons And Policy Implications," *Energy Policy,* Vol. 53, P. 240–247, 2013.

[10] *. J. P. L. A. H. L. A. Y. O. B. O. C. C. Olivier Evrard A, "Radiocesium Transfer From Hillslopes To The Pacific Ocean After The Fukushima Nuclear Power Plant Accident: A Review," *Journal Of Environmental Radioactivity 148 (2015) 92e110,* Vol. 148, Pp. 92-110, 2015.

[11] "Fukushima Five Years On," World Health Organization, March 2015. [Online]. Available: Www.Who.Int/Ionizing_Radition/A_E/Fukushima/Faqs-Fukushima/En/ . [Accessed 30 April 2017].

[12] A. M. Tremonti., "The Current," Cbc Radio , 09 March 2017. [Online]. Available: [Www.Cbc.Ca/Radio/Thecurrent/The-Current-For-March-9-2017-1.4015605/Fukushima-6-Years-After-Japan-S-Worst-Nuclear-Disaster-1.40157722. [Accessed 30 April 2017].

[13] "Electricity Generated And Purchased (Bulletin) .Availableat," The Federation Ofelectric Power Companies Of Japan (Fecj), [Online]. Available: /Http://Www.Fepc. Or.Jp/English/News/Generated_Purchased/Index.Htmls.. [Accessed 30 April 2017].

[14] M. Rich, "Struggling With Japan's Nuclear Waste, Six Years After Disaster," The Newyork Times, 11 March 2017. [Online]. Available: Https://Mobile.Nytimes.Com/2017/03/11/World/Asia/Struggling-With-Japans-Nuclear-Waste-Six-Years-After-Disaster.Html. [Accessed 03 March 2017].

[15] A. K. Y. O. Y. O. Masaaki Yamaguchi, "Predicting The Long-Term 137cs Distribution In Fukushima After The Fukushima Dai-Ichi Nuclear Power Plant Accident: A Parameter Sensitivity Analysis," *Journal Of Environmental Radioactivity* , Vol. 135 , Pp. 135-146, 2014.

[16] K. Y. M. S. T. T. Ishikawa K, "Depopulation With Rapid Aging In Minamisoma City After The Fukushima Daiichi Nuclear Power Plant Accident.," *J. Am Geriatr Soc*, Vol. 60, P. 2357–8., 2012.

[17] "Uxc Nuclear Fuel Price Indicators," 24 April 2017. [Online]. Available: Https://Www.Uxc.Com/P/Prices/Uxcprices.Aspx. [Accessed 30 April 2017].

[18] The Guardian News Paper "Four Former Tepco Executive Have Been Ordered By A Court To Pay A 94.8billion Dollars," 13 July 2022. [Online]. Available: Https:// Https://Www.Theguardian.Com/World/2022/Jul/13/Fukushima-Nuclear-Disaster-Ex-Bosses-Of-Owner-Tepco-Ordered-To-Pay-Yen-13tn-Tokyo-Court#:~:Text=7%20months%20old-,Fukushima%20nuclear%20disaster%3a%20ex%2dbosses%20of%20owner%20tepco,Ordered%20to%20pay%20%C2%A513tn&Text=A%20court%20in%20japan%20has,Nuclear%20power%20plant%20in%202011. [Accessed 10 February 2023].

NIPES-NCEE Conference Proceedings
The 2nd International Conference 15th-17th Feb. 2023
460-465
www.nipesjournals.org.ng

ACQUISITION OF EMPLOYABILITY SKILLS THROUGH TECHNICAL AND VOCATIONAL EDUCATION: A VITAL INVESTMENT FOR SUCCESS IN THE 21ST CENTURY WORKFORCE

Jamilu Saleh

Department of Technical Education, Hassan Usman Katsina Polytechnic,
Katsina State, Nigeria.

Abstract

As the number of Technical Vocational Education (TVE) graduates continues to rise, so does the unemployment rate among youths in many countries, particularly in developing nations. To address this issue, TVE graduates must possess the employability skills required by the 21st century workforce in order to secure employment.

The aim of this paper is to highlight the significance of TVE and employability skills. The paper examines the needs of employers in the 21st century and the crucial role of acquiring employability skills in TVE institutions. The conclusion is that TVE institutions must prioritize the development of employability skills by integrating them into their curriculum. This will ensure that TVE graduates possess the necessary skills to succeed in the 21st century workforce.

***Key words**: Employability Skills, Technical Vocational Education, 21st Century Workforce.*

INTRODUCTION

Employability skills are the non-technical skills that are in high demand by employers and necessary for success in the modern workforce. Technical vocational education (TVE) has been identified as an important source for acquiring these skills. TVE programs typically provide hands-on training and experience in specific technical trades and industries, but also have the potential to develop broader employability skills such as communication, teamwork, and problem-solving. According to Robinson, *et al.,* (2007) there is a great demand for educated people with general employability and specialized technical skills. Workers in the 21st century need skills such as problem-solving and analytic, decision-making, organization and time management, risk-taking, and communication to be employable in the workforce.

Acquiring employability skills through TVE can be a valuable investment for individuals seeking to enter or advance in the workforce. Research has shown that individuals with strong employability skills are more likely to be hired, retained, and promoted, leading to better long-term career outcomes.

.

Vocational and Technical Education Definition:

Technical Vocational Education (TVE) is defined as that type of education which fits the individual for gainful employment in recognized career as semi-skilled workers or technicians or sub-professionals [1]. According to the UNESCO Technical and Vocational Education and Training (TVET), provides individuals with the practical skills and knowledge needed for specific trades, crafts, or careers. The International Labour Organization (ILO) defines it as a form of education that focuses on preparing individuals for employment in specific trades, crafts, or careers through the provision of practical skills and knowledge. Meanwhile, the World Bank states that TVE emphasizes practical and theoretical training for specific trades and industries.

Employability skills Definition:

Employability skills are defined as the basic academic, personal, and teamwork skills that employers expect from their employees and are expected to be developed by the educational system. As per Munro (2007), these skills involve the ability to contribute to work efficiency, good oral and written communication, and critical thinking, which form the foundation of academic and workplace success. Bennett (2006) stated that employability skills include not only the desired attributes of employees but also the basic requirements for employment. The skills are considered as non-technical and are referred to as "transferable skills," "soft skills," or "generic skills". The definition of employability skills refers to the combination of abilities, knowledge, and characteristics that make a person appropriate and successful in a job. This includes everything from technical skills to personal traits that enable a person to secure and excel in employment. According to Clarke (2007), employability skills consist of basic skills, thinking skills, resource skills, information skills, interpersonal skills, system and technology skills, and personal qualities. Employability skills are necessary for getting, keeping, and doing well on a job, and they include areas such as managing resources, communication, team work, problem-solving, and job retention [2]. These skills are generic in nature and are necessary for success in the job market regardless of the employee's career path, educational background, or employment level [3]. Employability skills are crucial for producing a productive workforce and for success in education and all professions. Robinson and Garton (2008) defined employability skills as those essential skills necessary for getting, keeping, and doing well on a job and the skills, attitudes, and actions that enable workers to get along with others and make critical decisions. Overtoom (2000) referred to employability skills as transferable core skill groups that are necessary for effective job performance in the 21st century. Employability skills are also referred to as key skills, core skills, life skills, essential skills, key competencies, necessary skills, and transferable skills [4].

According to Lynch (2000), there is a "tremendous need" to understand the skill sets required by industry for TVE graduates. This is because, as Robinson et al. (2007) and Slusher et al. (2010) agree, workers in the 21st century need certain skills to be employable, such as problem-solving and analytical skills, decision-making, time management and organization, risk-taking, and effective communication [5]. And also Lynch (2000:7) suggests that preparing for one's occupation should start in high school.

Challenges in Developing Employability Abilities

In the workplace, technical skills are the methods and techniques used to perform specialized or practical tasks that can be easily measured and quantified. These skills are easier to train in TVE (Technical and Vocational Education) graduates compared to employability skills, which are referred to as core skills, generic skills, or nontechnical skills. These skills, including interpersonal skills, problem solving, and decision making, are important for the 21st century workforce but not easily taught in schools [6]. Technical and employability skills are complementary and superior performers possess both specialized technical skills and generic employability skills [7,8].

Technical skills are considered "hard skills" related to a particular organization or industry, such as machine operation and computer protocols, while employability skills are crucial for the 21st century workforce [9]. Employability skills are supposed to be acquired by everyone in the industry and are seen as important for success in any occupation [10]. However, TVE graduates may struggle with employability skills such as motivational skills, communication skills, interpersonal skills, critical thinking, and problem solving, leading to dissatisfaction among employers [11,12,13]. According to a study by Mohamed & Mohd (2005), TVE graduates had a low perception of the relevance of their course content to employability skills and felt that their course did not instill enough of these skills. Employability skills are not job-specific but are skills that are applicable across all industries and jobs, from entry-level positions to top management [9]. One challenge is the lack of awareness of the importance of employability skills. Many individuals may not realize that these skills are just as important, if not more so, than technical abilities in securing and succeeding in a job. Another challenge is the mismatch between the skills that employers desire and those that workers possess. A study by the Manpower Group found that 42% of employers globally struggle to find workers with the necessary skills. This highlights the need for individuals to continuously update and improve their employability skills to meet the demands of the job market. Lastly, there may be a lack of access to opportunities for individuals to develop their employability skills. For example, some individuals may not have access to on-the-job training or professional development programs that can help them acquire and improve these skills.

21st Century Workforce Employers' Requirements

21st century workforce employers have specific requirements to ensure their employees have the necessary skills and knowledge to perform in an ever-evolving work environment. These requirements are shaped by advances in technology, changing demographics, and the increasing pace of business operations. Graduates of TVE programs are being evaluated not only on their qualifications and certificates but also on their personalities. According to Branine (2008), the selection of TVE graduates varies from one employer to another and depends on the job offered. Employers usually conduct face-to-face interviews, telephone interviews, and online testing to assess the communication and computer technology skills of the candidates. Personal traits such as honesty, flexibility, self-direction, positive work ethic, and the desire to learn and be trained also play an important role in being employed as per Phani-Ram Challa (2007). Quek (2005) highlights the importance of transferring the learning from the classroom to the workplace to meet work demands. However, the unemployment rate among youths, especially in developing countries, has increased as the number of TVE graduates has significantly increased. Employers find it challenging to recruit potential workers who possess both technical and employability skills, as stated by Robinson (2000). The continuous changes in knowledge and skills due to globalization and the job market demand have resulted in the changing demands for skills in the 21st century workforce. According to Mohd Saleh, et al. (2010), globalization is creating new skill sets to respond rapidly to market demands, including interpersonal, technology, and communication skills.

Globalization has changed the international situation and has made human resources play a crucial role in boosting a country's development and infrastructure, as per Mohd Saleh, et al. (2010). Graduates with generic skills and knowledge will benefit from integration into the 21st century workforce, but those lacking skills and knowledge will fall behind, as emphasized by many researchers, including Dench (1997), Hunt & Baruch (2003), and Nabi (2003).

Employers are no longer interested in hiring graduates who only have specialized skills and lack employability skills, as per Zinser (2003). Organizations expect high levels of ability and thinking from graduates in performing tasks in the workplace and only select those who demonstrate knowledge and skills. Graduates must be able to continuously adapt to changes in environment, technology, and markets to maintain their knowledge and skills and remain competitive in the workforce. Organizations need highly trained employees with a combination of academic, technical, and social skills to meet the demands of an ever-changing world.

Technical Vocational Education Institutions and Employability Skills

The development of employability skills is crucial in Technical Vocational Education (TVE) institutions as it plays a significant role in ensuring that youths and school leavers are able to compete effectively in the job market. According to Kwok (2004), the competitiveness of individuals in the labor market depends on both their vocational competence and their employability skills. These skills must be developed to the extent that individuals are able to find suitable employment and adapt to changes in technology, organizations, and society [13].

Acquiring employability skills should be a focus for students during their time in TVE institutions or schools. These skills can be taught through classroom instruction or hands-on experiences both in and outside of the classroom. However, it takes a significant amount of time to develop employability skills as they are abstract in nature. Knight & Yorke [1] define employability skills, also known as “generic skills,” as the personal attributes, understanding, and achievements that make an individual successful in their employment choices and career development. To be employable, individuals must have a combination of both employability skills and technical skills. While having just employability skills may not be enough to secure employment, having only technical skills may not be enough to contribute to the growth and development of the organization. Employability skills must be redefined to include a balance of both generic and technical skills [11]. Achieving employability skills through Technical Vocational Education Institutions (TVETs) requires a combination of hands-on training, real-world experience, and support from both educators and employers. The World Bank states that “hands-on learning experiences are a key component of TVET programs, providing students with the opportunity to apply what they have learned in a practical setting.” This practical experience, combined with the support of educators, is essential for developing the skills and knowledge necessary for success in the job market. TVETs can also foster the development of employability skills through close partnerships with local employers. The Organisation for Economic Co-operation and Development (OECD) notes that “partnerships with employers are essential for ensuring that TVET programs are relevant and aligned with the needs of the labor market." These partnerships provide students with opportunities to network, make valuable connections, and gain real-world experience talent-shortage. In addition to hands-on training and partnerships with employers, TVETs can also support the development of employability skills through the implementation of a strong curriculum. According to the International Labour Organization (ILO), "an effective TVET curriculum should include not only technical skills but also a range of soft skills, such as communication, teamwork, and problem-solving." This combination of technical and soft skills is essential for success in the job market.

Conclusion

Technical Vocational Education institutions must prioritize the development of employability skills in their students to keep up with the demands of the 21st century workforce. These skills, which are highly valued by many organizations, should be integrated into the curriculum to ensure that graduates have the necessary skills for employment. Failure to focus on these skills may result in graduates who are unable to find employment and contribute to the economic development of their country. In today's rapidly changing job market, it is crucial that workers have the ability to adapt and stay ahead of the curve. This requires a combination of technical skills and employability skills, which are essential for workers to contribute to the growth and development of their country. Developing countries, in particular, require a large number of high-skilled workers to boost their economy and transition into a high-income society.

Thus, it is crucial for TVE institutions to make every effort to equip their students with the necessary employability skills for success in the workforce. In this way, graduates will have the tools they need to thrive in a constantly changing job market and contribute to the economic development of their country.

References

[1] Bennett, T.M. (2006). Defining the Importance of Employability Skills in Career/Technical Education. Dissertation ProQuest Information and Learning Company.
[2] Kwok, M. (2004). Towards an Understanding of Employability Skills Development Among University Graduates for Workplace Entry. Manitoba: The University of Manitoba.
[3] Ali, F.A., Long, Y., Zainol, F.A., & Mansor, M. (2012). Student's Self-Perceived Importance of Employability Skills Needed: A Case Study in University of Sultan Zainal Abidin (Unisza), Malaysia. Proceedings of the 2nd International Conference on Management, 11th-12th June, Langkawi Kedah, Malaysia.
[4] Audu, R., Kamin, Y. B., & Saud, M. S. (2013). Acquisition of Employability Skills in Technical Vocational Education: Necessity for the 21st Century Workforce. Australian Journal of Basic and Applied Sciences, 7(6), 9-14. doi: 10.9734/ajbas/2013/6789
[5] International Labour Organization (ILO). (2021). Technical and Vocational Education and Training (TVET). Retrieved from https://www.ilo.org/skills/tvet/lang--en/index.htm
[6] European Centre for the Development of Vocational Training. (2015). Employability skills for the future: A European framework.
[7] Lynch, R.L. (2000). High School Career and Technical Education for the First Decade of the 21st Century. Journal.
[8] Kathleen, C. (2005). Developing Employability Skills. Regional Educational Laboratory. School Improvement Research Series (SIRS).
[9] Branine, M. (2008). Graduate Recruitment and Selection in the UK. Career Development International, 13(6), 497-513.
[10] Hunt, J.W., & Baruch, Y. (2003). Developing Top Managers: The Impact of Interpersonal Skills Training. Journal of Management Development, 22(8), 729-752.
[11] Clarke, J. (2007). Employability Skills and the Financial Services Training Package. Australia: Department of Education Science and Training.
[12] Cheng, Y.C. (2004). Fostering Local Knowledge and Human Development in Globalization of Education. The International Journal of Education Management, 18(1), 7-24.
[13] Brown, D. J., & Lauder, H. (2017). The global skills gap: The future of work in the knowledge-based economy. Palgrave Macmillan.

NIPES-NCEE Conference Proceedings
The 2nd International Conference 15th-17th Feb. 2023
466-472
www.nipesjournals.org.ng

THE EFFECT OF TECHNICAL AND VOCATIONAL EDUCATION ON ECONOMIC DEVELOPMENT AND SOCIAL MOBILITY IN KATSINA STATE, NIGERIA

Jamilu Saleh

Department of Technical Education, Hassan Usman Katsina Polytechnic, Katsina State, Nigeria.

Abstract

The role of Technical and Vocational Education (TVE) in Nigeria is crucial for improving employment prospects, contributing to the country's economic growth, and developing human resources. The government is working to overcome challenges such as funding and outdated curricula by incorporating technology into new technical colleges and offering hands-on training through apprenticeships. This paper discusses the benefits of TVE in promoting social mobility, reducing poverty and youth unemployment and contributing to overall economic development. The paper also highlights ongoing challenges such as lack of access to quality education and shortage of skilled workers in Katsina state, where specific difficulties include a shortage of academic staff, inadequate facilities, and limited resources for modern equipment. The conclusion and recommendations include increasing funding for infrastructure and resources, implementing updated curricula, providing training for academic staff, emphasizing hands-on experience, integrating technology, strengthening the role of the National Board for Technical Education, addressing the lack of access to quality education and disconnect between education and work, investing in human capital development, promoting TVE to women and girls, and addressing challenges in the education system.

***Key words**: Technical and Vocational Education, Economic Development, Social Mobility, Katsina State, Nigeria.*

INTRODUCTION

In the 21st century, the world is rapidly changing and becoming more interconnected, with increased competition and interdependence. This is due to several forces that are transforming the world of work. The growing demand for skilled workers, combined with a rising global unemployment rate, has led to an increased interest in Technical, Vocational Education and (TVE). Technical Vocational Education and programs offer comprehensive education that includes the study of technology and related sciences, as well as the acquisition of practical skills, attitudes, and knowledge related to various economic and social sectors. The objectives of technical education in Nigeria, as outlined in its national policy, include the acquisition of skills and competencies necessary for economic development, as well as the imparting of technical knowledge and vocational skills to individuals to make them economically self-reliant. The recent financial crisis has exposed weaknesses in the global economic system, leading to a reduction in job creation and a sharp increase in youth unemployment. Young people, particularly in regions like the Middle East, Africa, South Asia, and Latin America, are disproportionately affected by this trend.

Overview of Technical and Vocational Education

Technical and Vocational Education (TVE) in Nigeria aims to equip individuals with practical skills and knowledge in a specific trade or industry, to improve their employment prospects and contribute to the country's economic growth.

According to the National Policy on Education [1], "Technical and vocational education is an important aspect of education for self-reliance and is designed to provide individuals with the skills required for employment and entrepreneurship.

In recent years, the Nigerian government has made efforts to prioritize and improve TVE. The Minister of Education, stated in a 2019 press release that, "The Federal Government is committed to revamping the technical and vocational education system in the country in order to meet the demands of the 21st century job market. However, the implementation of effective TVE programs in Nigeria still faces challenges, such as a lack of funding, outdated curricula, and a negative perception of vocational education. These issues have led to low enrollment in TVE programs and a shortage of skilled workers in the country.

Despite these challenges, the Nigerian government continues to work towards improving the TVE sector, with initiatives such as the establishment of new technical colleges and the integration of technology in vocational training. Katsina State, is home to a number of technical and vocational education programs. These are designed to provide students with the necessary skills and knowledge to excel in the labor market upon graduation. The programs range from basic skills development to more advanced training for those seeking to pursue a career in a specific sector.

At the basic level, the government provides technical and vocational training to students in secondary schools. This equips the youth with the required skills needed to further their studies or secure employment in their chosen field. The courses range from basic automotive repair and welding to more advanced courses such as plumbing, electricity and masonry.

At a higher level, the government provides more advanced training opportunities. This includes certificate programs, as well as diploma and degree programs at the higher education level. These courses are targeted towards individuals who already have basic skills and are looking to further their education in a particular field. These courses are typically divided into both theoretical and practical components, with students receiving the necessary skills and knowledge to become experts in their chosen field.

In addition to traditional technical and vocational education, Katsina State also offers a variety of apprenticeship programs. These programs are designed to give students hands-on experience in a particular field, while allowing them to gain valuable knowledge and experience. Apprenticeships can range from short-term placements, to more comprehensive programs that span several years.

Role of TVE in Economic Development

Economic development refers to positive changes in the economy that lead to an improvement in the standard of living. Sustainability involves maintaining these changes indefinitely, balancing economic and social progress, addressing cultural differences, and respecting ecological limits [2]. Achieving economic development and sustainability requires sustained efforts across various areas, such as human capital development, critical infrastructure, regional competitiveness, social inclusion, health and safety, and more.

The growth of technological advancements has led to an increased demand for workers with advanced skills, as new technologies are knowledge- and skill-intensive [3]. The benefits of technological progress may not be fully realized without ongoing skill acquisition [4]. Education and training play a crucial role in promoting knowledge, innovation, and the spread of new production methods [5]. In a rapidly changing technological environment, adaptability is crucial for maintaining competitiveness and keeping labor and capital employed [6].

Technical and vocational education (TVET) provides practical and career-focused training to students, equipping them with in-demand skills (International Labour Organization). UNESCO recognizes its benefits for the economy and poverty reduction and has made it one of its top four priorities. TVET has a significant impact on human resource development and contributes to individual and societal growth, including economic and social participation, technology, democracy, and ecological awareness. A skilled workforce enables global competitiveness and economic growth, as well as improved career paths and earning power for individuals (UNESCO).

Oladepo (1998) emphasizes the significance of technical and vocational education, stating that it provides individuals with the necessary skills, attitudes, and knowledge to participate in the business community and become self-reliant. This sentiment is echoed by (Tukur, Kaigamma, and Saidu 2004), who view vocational and technical education as a crucial tool for future empowerment. If properly implemented, the current educational system that prioritizes vocational and technical education has the potential to drive economic development and bring about positive change in society. Ozoemana (2013) also recognizes the dynamic nature of vocational and technical education and its role in promoting economic and industrial growth, job creation, and poverty reduction. Dawudo (2000) adds that vocational and technical education is a crucial factor in a nation's economic prosperity and political influence.

The economic importance of technical and vocational education has become increasingly pressing in light of social and economic crises, high dropout rates, and a changing workforce. As a result, many developing nations have made vocational and technical education a priority in their educational reform agendas. In Nigeria, for example, the Federal Government has established a National Implementation and Monitoring Committee to integrate out-of-school boys into the basic education program and develop special vocational schools that will provide both basic and vocational education. The goal is to produce well-rounded and productive individuals who will contribute to their communities and the nation's economic development.

Vocational and technical education has several benefits for the economic and technological development of a country such as Nigeria. Firstly, it empowers individuals with the skills needed to enhance their productivity and drive national economic development [7]. Secondly, these programs are more adaptable to the rapidly changing skills and technology landscape than traditional academic programs [8]. Thirdly, graduates of vocational schools have better employment prospects and are better equipped to enter the workforce than those from academic secondary schools [9]. Fourthly, these graduates have critical thinking, problem-solving, and entrepreneurial skills that are essential for success in a knowledge-based economy and globalized world [10,11]. Lastly, vocational education reduces youth unemployment and juvenile delinquency by providing individuals with the skills needed to be self-employed [3].

Impact of TVE on Social Mobility

Vocational and technical education (TVE) has been shown to have a positive impact on social mobility, allowing individuals to move up the social and economic ladder through acquiring in-demand skills and improving their job prospects. According to the International Labour Organization, TVET can be critical in promoting economic development by providing the skills necessary for employment and entrepreneurship, enabling individuals to improve their financial stability and achieve a better standard of living. TVET has been recognized as a key tool for reducing poverty and promoting equality by providing access to higher-skilled and better-paying jobs. UNESCO has made technical education one of its top four priorities, recognizing its benefits in promoting economic development and reducing poverty [4].

In addition to its impact on employment and income, TVET can also have positive effects on individual well-being and self-esteem. A study by Ashton et al. (1999) found that education and training play a vital role in promoting knowledge, innovation, and the spread of new production methods, leading to increased creativity and improved self-esteem and confidence.

In the context of globalization, the relationship between employers and employees is expected to change. The traditional notion of stable or lifelong employment is no longer applicable, and the retention of employees is more likely to be based on the skills and knowledge they bring to the company to create a competitive advantage [5]. In this new market, visionary leadership and innovative management and organizational principles are required. The outdated command-and-control management system commonly used by Nigerian organizations will not be effective in this new environment. The education, training, and employment policies must be updated. Employers need to recruit "knowledge" workers for higher-skilled jobs, requiring the education system to produce graduates with relevant knowledge, critical and higher-order skills, and proper attitudes.

In order to remain competitive, bold steps must be taken to upgrade vocational and technical education in Nigeria. This includes developing manpower through organized learning activities to improve performance, personal growth, and the organization. Human resource development (HRD) is a dynamic, ongoing, empowering process that aims to improve the performance of organizations by maximizing the efficiency and performance of its people. HRD develops employees' knowledge, skills, motivations, attitudes, and work environment.

However, there are challenges to realizing the full impact of TVET on social mobility, including a lack of access to high-quality vocational education, a disconnect between the educational system and the world of work, and a shortage of skilled workers. Addressing these challenges will be critical in ensuring that the benefits of TVET are realized and that individuals have the opportunity to improve their social and economic standing.

Challenges and Opportunities of TVET in Katsina State

The population of Katsina state in Nigeria was estimated to be 459,022 in 2007 and has 10 state-run vocational schools and one skills acquisition center, in addition to 6 federal government-run skills acquisition centers and a few privately-owned vocational centers. Despite the existence of these institutions, technical and vocational education (TVE) in Katsina state faces challenges such as a shortage of academic staff, inadequate workshop facilities, and limited resources for acquiring modern equipment and materials. These challenges are exacerbated by the insufficient number of properly equipped workshops, outdated equipment and facilities, and the lack of teaching materials and research facilities.

According to Alamu (2011), "efforts need to be made by the government and stakeholders to encourage and develop technical and vocational education in Katsina state for the economic development of the country." However, there are opportunities for the development of TVE in Nigeria. The growing demand for skilled workers in Nigeria's industries and the potential to improve social mobility provide significant opportunities for TVE to contribute to economic growth and development [6].

In 2012, the Nigerian Ministry of Education launched the Technical Education and Skills Development (TESD) program to provide technical training to school-aged and adult learners, with a focus on providing opportunities for women and girls. The government has established the National Board for Technical Education (NBTE) to set standards for technical and vocational training in Nigeria. To improve TVE in Nigeria, the government must invest in infrastructure, equipment, and qualified instructors and provide support for women and girls interested in technical and vocational training. The government must also ensure that all technical and vocational training centers adhere to the standards set by the NBTE.

The acquisition of skills enhances productivity, leading to increased output and income, both in wage employment and self-employment. This is because work is often a team effort, and the productivity of one worker is dependent on the productivity of others. The more training a worker receives, the more they can learn from their colleagues and the more efficiently they can collaborate in areas such as production, innovation, distribution, and sales [1].

Technical and Vocational Education and Training (TVET) can contribute to occupational competence by teaching appropriate skills and training in the use of local technology. It should also reflect the basic needs of its beneficiaries. TVET can contribute to individual, community, and national development by: building confidence and potential in learners through relevant programs; fostering self-sufficiency and independence through hands-on training; equipping students with the necessary skills and knowledge to prepare them for the workforce; developing inclusive programs that lead to social and economic development; and providing practical training that aligns with community expectations, cultural norms, economic conditions, and national goals.

Conclusion

Technical and Vocational Education (TVE) plays a critical role in promoting economic growth, reducing poverty and unemployment, and providing individuals with in-demand skills. The Nigerian government is working to improve TVE, but faces challenges such as funding, outdated curricula, and negative perception. The Technical Education and Skills Development (TESD) program and the National Board for Technical Education (NBTE) have been established to provide technical training and set standards for technical and vocational education. Despite the challenges, TVET is essential for human capital development and aligning with national goals. The acquisition of skills through TVET leads to increased productivity and income, and the benefits of TVET must be fully realized through addressing issues such as lack of access to quality education, disconnect between education and work, and shortage of skilled workers.

Recommendations:

1. Increase funding for TVET to improve infrastructure, equipment, and resources.
2. Implement updated curricula to align with current in-demand skills and technology.
3. Provide training and development opportunities for academic staff to improve their skills.
4. Emphasize hands-on experience through apprenticeship and practical training programs.
5. Encourage technology integration in TVET to prepare students for the future workforce.
6. Strengthen the role of the National Board for Technical Education (NBTE) in setting standards for TVET.
7. Address challenges such as lack of access to high-quality education and disconnect between education and work.
8. Invest in human capital development through HRD to improve performance and efficiency in TVET.
9. Promote TVET to women and girls through programs like TESD
10. Address challenges such as lack of access to high-quality education and disconnect between education and work.

References

[1] Ashton, D., Green, F., & Ross, F. (1999). Education, training and employment: Exploring the evidence. Institute for Employment Studies.
[2] Enebe, K. (2000). Manpower development and employment generation in Nigeria. Journal of Applied Sciences and Environmental Management, 4(1), 33-40.
[3] Edukugho, E. (2011). Nigeria: Rectors meet, tackle challenges facing technological education. Vanguard, 29 September 2011.
[4] Federal Republic of Nigeria (2004). National policy on education (Revised). Lagos, NERDC Press.
[5] Henry O. Owolabi. (2003). Technical and vocational education in Nigeria. Emola-Jay Communications Inc.
[6] International Labour Organization. (n.d.). Technical and Vocational Education and Training (TVET). [Online]. Available from https://www.ilo.org/global/topics/education-and-skills-development/lang--en/index.htm.
[7] International Labour Office. (2011). Global employment trends for youth: 2011 update. Geneva.
[8] Lourdesamy, L. (2000). The role of education and training in promoting economic development. Journal of European Industrial Training, 24(4), 145-151.
[9] Muhammad, B. A. (2012). Integrating e-learning in technical and vocational education: A technical review. International Journal of Academic Research in Business and Social Sciences, 2(5).
[10] UNESCO. (n.d.). Technical and Vocational Education and Training (TVET). [Online]. Available From https://en.unesco.org/themes/technical-and-vocational-education-and-training-tvet
[11] Alamu, S. A. (2011). The state of science and technology infrastructure in secondary schools in Nigeria. Journal of Educational and Social Research, 2(8), 56-66.

NIPES-NCEE Conference Proceedings
The 2nd International Conference 15th-17th Feb. 2023
473-489
www.nipesjournals.org.ng

ON MAGNETIC MOMENT AS A NOVEL FEATURE IN THE DIRECT PRODUCTION OF MAGNETIC MONOPOLES AT THE LARGE HADRON COLLIDER (LHC) VIA DRELL-YAN PHOTON SUB-CHANNEL INTERMEDIATION

D. Dosu, O. Ebomwonyi

Department of Physics, University of Benin, Nigeria
Corresponding Author: osarodion.ebomwonyi@uniben.edu

Abstract

This study proposed magnetic moment as an explanation for the observed differences in the signature recorded in the Electromagnetic Calorimeter (ECAL) crystals at the LHC's compact muon solenoid (CMS), using 000000fb"-1 of 13TeV proton-proton collision data. Registrations of kinematics parameters, such as kinetic energy, transverse momentum, and pseudorapidity for the results interpreted in the Drell-Yan production models for monopoles with spins 0 and 1/2, were generated and studied. A confidence level upper limit of 0000- 00000fb was set on the cross-section of the Dirac magnetic monopole's production. We considered masses between 500GeV and 4500GeV

***Keywords**: Magnetic moment, Monopoles, Pseudorapidity, Efficiency analysis, Drell-Yan mechanism.*

1. Introduction

Paul Dirac's paper on magnetic monopoles [1] proposed the existence of particles that carry a single magnetic pole; either north or south, a revolutionary idea at the time because it implied that the fundamental building blocks of the universe were not just electric charges, as had been previously believed, but also magnetic charges. The paper questioned the validity of Maxwell equations of classical electrodynamics for lack of symmetry in electro-magnetic duality. Equation (1) to Equation (4) are the Maxwell equations of classical electrodynamics.

$$\nabla . E = \frac{\rho_e}{\epsilon_0} \qquad (1)$$

$$\nabla . B = 0 \qquad (2)$$

$$\nabla \times E = -\frac{\partial B}{\partial t} \qquad (3)$$

$$\nabla \times B = \mu_0 \epsilon_0 \frac{\partial E}{\partial t} \qquad (4)$$

Dirac's compelling theoretical evidence fixes the asymmetry in Equations (1) and (2) by positing that

$$\nabla . B = \rho_m \quad (5)$$

The symmetry between electric and magnetic fields in the source-free Maxwell equations, suggests the possibility of electric charges having magnetic counterparts known as magnetic monopoles. The symmetrised Maxwell equations are invariant under rotation in the plane of the electric and magnetic fields, and a direct observation of single magnetic monopoles will have far reaching consequences, most notably an explanation to the electric-charge quantization.

According to Dirac [1], when a monopole moves through space, it generates a magnetic field around it. However, this field is singular at the location of the monopole, which is physically impossible. To resolve this problem, Dirac proposed the existence of a line-like defect called a Dirac string, which carries the singularity of the magnetic field. The monopole is then located at the end of the string, and the field is non-singular everywhere else. Dirac's theory was based on the mathematical framework of quantum mechanics and relied on the existence of a particular type of field called a gauge field. The idea of magnetic monopoles was later incorporated into grand unified theories (GUTS); which attempt to unify the fundamental forces of nature.

The Dirac strings are hypothetical topological defects that are associated with magnetic monopoles in gauge theories and were introduced by Paul Dirac as a way to reconcile the existence of magnetic monopoles with the observed absence of singularities in the electromagnetic field.

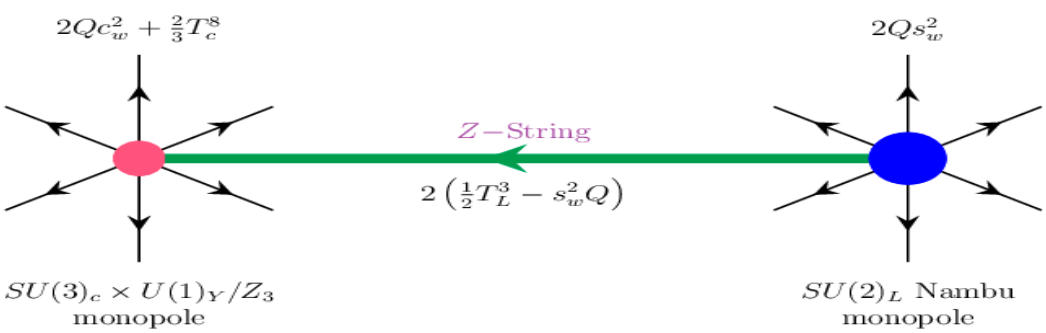

Fig. 1: A doubly charged coloured Dirac monopole (pink) and a Nambu monopole (blue) connected by a Z-string with magnetic flux T [2]

Dirac further theorized that the quantization of electric charge could be understood as a consequence of angular momentum, with his argument deriving the quantization condition; a relationship between electric and magnetic charge to be

$$ge = n\hbar \, {}^{c}\!/_{2} \quad (6)$$

where g is the magnetic charge, e is the elementary charge, n is an integer, and $\hbar$ is the reduced Planck constant. This could be extended to derive the fundamental magnetic charge on the mopnopole, called Dirac charge, to be

$$g_D = \hbar \, {}^{c}\!/_{2e} = {}^{e}\!/_{2\alpha} \qquad (7)$$

Dirac's argument predicts the fundamental magnetic charge to be

$$q = N g_D e c, \qquad (8)$$

here, we have set q in SI units and g_D a dimensionless quantity, that is,

$$g_D = \frac{1}{2\alpha} = 68.5e \qquad (9)$$

where $\alpha = \frac{1}{137}$ is the fine structure constant.

The force between a monopole and an anti-monopole is $(137/2)^2$, which is 4700 times greater than the force between an electron and a positron. This force between the monopole pairs is much stronger, hinting at the difficulty of finding these fermions in nature [3,4].

Grand Unified Theories extend beyond the standard model and aim at unifying the three gauge interactions SU(3), SU(2), and U(1). 't Hooft [3] showed that specific spontaneously broken gauge theories have non-singular classical solutions that lead to magnetic monopoles in quantum theory, hence independently predicting the existence of monopoles as a twist or knot defect in the GUT Higgs field.

Although the monopoles appearing in grand unification theories typically have masses of the order of the unification scale, i.e, $10^{16} GeV$, some extensions of the standard model predict electroweak monopoles (which obey Schwinger's quantization condition that $g_2 q_1 - g_1 q_2 = \frac{2nh}{\mu_0}$) with masses as low as $4TeV$. Possibilities of generating monopoles of different mass scales have been predicted via stages of symmetry breaking

$$SO(10)\xrightarrow{M_1}SU(4)\times SU(2)\times SU(2)\xrightarrow{M_2}SU(3)\times SU(2)\times SU(1).$$

If monopoles were to exist, we expect they would have a unique magnetic moment that would be distinct from that of other magnetic particles. By measuring the magnetic moment of a sample, it would be possible to identify the presence of monopoles and determine their properties, such as their spin, mass, and charge. These monopoles would be very massive and would have been produced in large numbers in the early universe, but would be very rare today due to their large mass. The mass of the magnetic monopole is a hypothetical particle treated as a free parameter. When considering the Dirac monopole, a parameter that is readily considered due to its known ionizing property is the dE/dx significance measurement. The rack registered due to dE/dx is a parabolic path, curved in the $r-z$ plane due to the candidate's interaction with the magnetic field in the inner tracker detector.

The transfer of momenta in an individual interaction then depends on the charge and mass of the target particle, the velocity and charge of the projectile, and the impact parameter generated during the collision. The general equation which gives information about energy deposition is known as the Berthe-Bloch equation

$$-dE/dx = K\frac{Z}{A}\frac{Z^2}{\beta^2}[l\frac{2m_ec^2\beta^2\gamma^2}{I}-\beta^2] \tag{10}$$

In the case of a monopole such as the one produced at the LHC; we consider them to be a relatively heavy particle with a mass of the border of a few TeV. Such a monopole is expected to lose energy only through ionization [5]. The Berthe-Bloch equation is modified for the monopole with charge $q_m = gec$ to become

$$-dE/dx = K\frac{Z}{A}g^2[l\frac{2m_ec^2\beta^2\gamma^2}{I_m}+\frac{K(|g|)}{2}-\frac{1}{2}-B(|g|)] \tag{11}$$

To make important deductions, we consider the kinematics parameters; pseudorapidity, transverse momentum and azimuthal distribution for spin models 0 and $1/2$. The $spin-0$ monopole, being scalar, has no magnetic moment while the $spin-1/2$ fermionic monopole couples minimally with its magnetic moment generated through spin interaction. Furthermore, the $spin-1/2$ magnetic monopole models are augmented by the presence of spinor magnetic moment terms with an introduced dimensionless phenomenological parameter $\tilde{k}=0$ [6]. Since the detector acceptance is dependent on the monopole energy and angular distributions, cross-sections are constrained with some model dependence.

1.1 Production mechanisms for magnetic monopole candidates via the Drell-Yan mechanism

The Drell-Yan (DY) mechanism is a process by which a quark and an antiquark annihilate each other, producing a lepton and an antilepton. The lepton and antilepton then combine to form a virtual photon, which subsequently decays into a pair of leptons.

Spin-0 monopoles interact via the Lagrangian

$$L = -\frac{1}{4} F^{\mu\nu} F_{\mu\nu} + (D^{\mu}\varphi)^{\dagger}(D^{\mu\varphi}) - M^{2}\varphi^{\dagger}\varphi \qquad (10)$$

and the covariant derivative which couples its scalar field (φ) to the photon field A_μ with field strength

$$F_{\mu\nu} = \partial\mu + igA\mu \qquad (11)$$

is given by

$$D_\mu = \partial_\mu + igA_\mu, \qquad (12)$$

with

$$L_{4pt} = g^2 A^{\mu}\varphi^{\dagger}A_{\mu}\varphi \qquad (13)$$

guiding our choice of vertex.

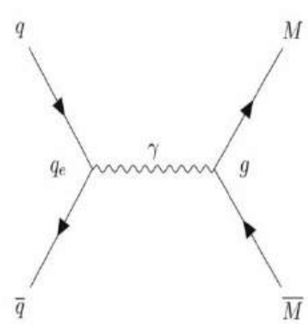

Fig. 2: Feynman diagram for the production of monopoles via the DY production mechanism

This work offers experimental evidence for the case of the magnetic moment as a deciding parameter in the registrations of spin-0 and spin- ½ monopole candidates in the ECAL. This experimental study is novel and appearing in literature for the first time to the best of our knowledge. Plots for generator-level kinematics were contrasted for the compact muon solenoid

(CMS)-generated monopole masses which ranged from $1TeV$ to $4.5TeV$. We also compared the results for efficiency analysis.

2.0 Methodology

The Compact Muon Solenoid (CMS) experiment is one of four detectors built at crossing sites of the LHC beams and is one of two general-purpose detectors (the other being ATLAS) which have been designed to explore the physics opportunities presented by the LHC. Thus, the initial goal of the CMS detector is to study several Higgs boson production modes, which can be explored with the detector

The detector has a beam spacing of 25ns, and beam crossing occurs in the CMS detector at a rate of 40 million per second (40MHz). An additional complication is the approximately 25 interactions that occur with each beam crossing - this generates 1 billion events in the CMS detector every second. To extract physics from these interactions, it is vital to have fast electronics and very good resolution (proton-proton interactions are very messy and produce hundreds or thousands of particle candidates) and, because these events occur far too quickly to all be recorded and would take up vast amounts of disk space to store what are, for the majority, uninteresting events, very precise "triggering" is required.

2.1 On Monopole signature and identification in the CMS detector

2.1.1 Data Generation cycles, analysis, and Monte-Carlo experiment

The ultimate aim of this experiment, data generation cycles, and analysis are to ensure that only the monopole's signature gets registered in the electromagnetic calorimeter (ECAL)

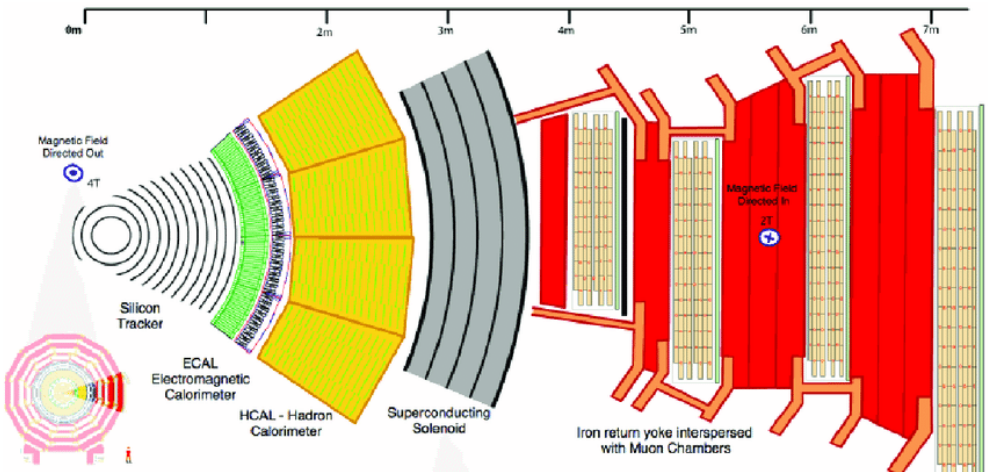

Fig.3: CMS Detector [7]

2.2 Analysis Strategy

2.2.1 Monopole Tracking Recognition

This analysis strategy uses a track combiner algorithm, instead of the SM-oriented standard tracking algorithm because the monopole behaves differently from standard model (SM) particles.

2.2.2 Track Ionization

We then proceed to measure the ionisation of the track as identified via the TCA. The monopole, due to its high mass can be easily predicted by the Berthe relationship to deposit energy at a high rate, hence it's dE/dx measurement is high. The background noise are also factored in and instead of the standard dE/dx which is an harmonic average of dE/dx, we instead measure dE/dx significance, which is a combination of total number of strips and fractions of unsaturated strips. [3]

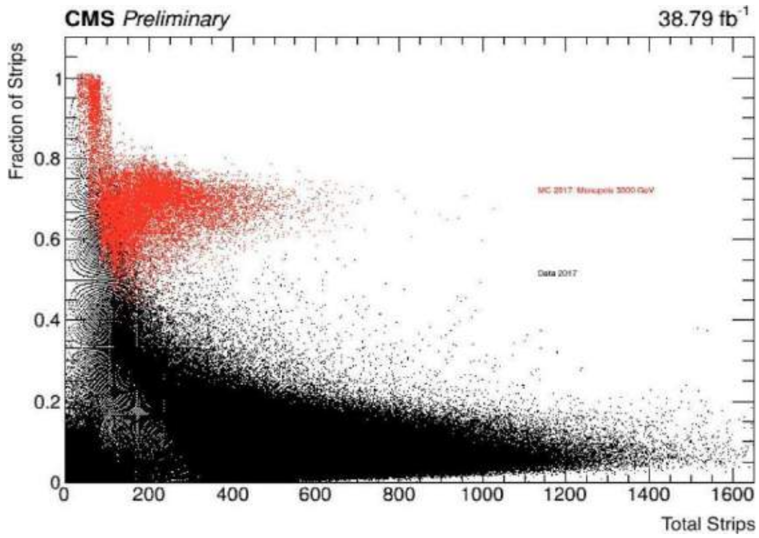

Fig. 4: Applying the $^{dE}/_{dx}$ significance cut shows a clearer discrepancy from the standard $^{dE}/_{dx}$ cut

2.2.3 Track Curvature

Relatively small curvature in the track path is observed for monopoles with energy high enough to transverse the electromagnetic calorimeter, this explains why the $r-z$ curvature recorded in the tracks of monopoles are quite insignificant.

2.2.4 Electromagnetic Calorimeter Cluster Finding

It is expected that the monopole candidates studied in this analysis will lose most, if not all their energy in the ECAL by the ionization we have described. Also, a consequence of having almost all its energy deposited in the ECAL implies that the next layer in the CMS detector set-up. That is, the Hadronic Calorimeter (HCAL) will register few or no monopole deposit. The cluster shape for monopole candidates are tracked in the ECAL crystals using two clustering algorithms: the Hybrid algorithm and the Island algorithm. The monopole, unlike the SM particles that deposits their energy in several crystals, deposits all of its charge (about 5000 times that of the electron) in the ECAL, what this implies is that the ratio of seed crystal energy to that in the 5 x 5 crystal will approximate to 1. The Island and Hybrid algorithm are used for this analysis.

2.2.5 Trigger Selection

HLTPhoton200 v* was used for 2017 and 2018 datasets, with traverse energy (ET) as $200GeV$. It is worth mentioning too, that due to the L1 spike killer algorithm, the analysis considers monopole candidates that do not deposits all their energy into the central crystal.

2.2.6 Monopole Identification

In addition to the aforementioned parameters, we require that the distance between the monopole track and the extrapolated ECAL cluster be less than 0.5. We then bring these characteristics together to form the basis of our selection criteria:

Table 1: Pre-selection cuts for monopole matching

Pre-Selections	Parameter	Cut
Parabolic Fit	$\lvert RZPar0\rvert \rightarrow Z_0 = \lvert d\rvert$	< 10 cm
	$\lvert RZPar1\rvert \rightarrow \eta_0 = \lvert f\rvert$	< 999 cm
	$\lvert RZPar2\rvert \rightarrow \rho - Z$ curvature $= \lvert g\rvert$	$0.005\ \mathrm{cm}^{-1}$
Matching Fit	$\triangle R$	< 0.5
	HCAL Isolation	< 10 GeV
Circular Fit	$\lvert XYPar0\rvert \rightarrow d = \sqrt{(a-c)^2 + b^2} - \lvert c\rvert$	< 0.6 cm
	$\lvert XYPar2\rvert \rightarrow \lvert\Phi_0 - arctan\frac{b}{c-a}\rvert$	< 10

Table 2: Analysis selection cut applied to identify monopole candidates that passed the pre-test

	Parameter	Threshold
Analysis Cuts	Energy Deposit in the ECAL	> 200 GeV
	HLT_Photon200_v^*	Pass
Loose Cuts	dE/dx_{Sig}	≥ 7
	$F51$	> 0.60
Discriminating Cuts	dE/dx_{Sig}	≥ 9
	$F51$	> 0.85

The CMS experiment simulates, analyzes, and reconstructs data using specialized software referred to as CMS software (CMSSW). To create MC simulations and to reconstruct data chosen by the trigger system, the CMSSW combines algorithms. This search takes into account physics processes like PDFs, harmonization, underlying event, and parton showers in order to produce the necessary output.

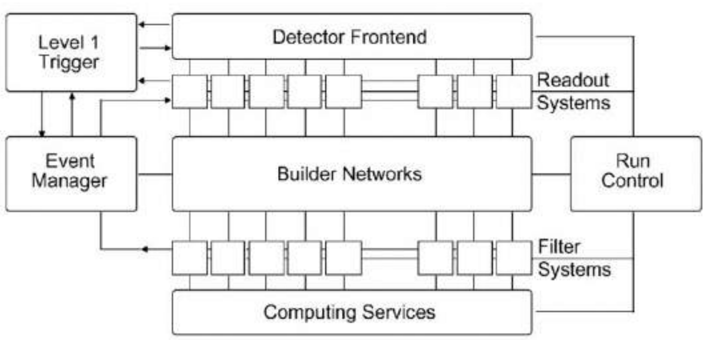

Fig. 5: CMS trigger and data acquisition system

NIPES-NCEE Conference Proceedings
The 2nd International Conference 15th-17th Feb. 2023
473-489
www.nipesjournals.org.ng

2.2.7 Signal Efficiency

The signal efficiency analysis [3] is done in the order that the loose pre-selection (trigger selection and then the energy cut) are first applied. Monte Carlo samples for the full RUN II for mass points $1\,TeV$ to $4.5\,TeV$ were generated to study the selection efficiency. The candidates that pass these cuts are then checked against the tighter selection of ${dE}/{dx}$ signal and F51,

where,

$$Relative\ efficiency = \frac{number\ of\ events\ after\ selections}{number\ of\ events\ after\ selections\ except\ the\ mentioned\ cut} \tag{14}$$

$$Signal\ efficiency = \frac{number\ of\ events\ after\ all\ selection\ cuts}{number\ of\ events\ after\ selections\ before\ selections\ applied} \tag{15}$$

3.0 Results and Discussion

Table 3: Efficiency analysis result for spin-1/2 mass 1000*GeV*

1000 Photon200	CutFlow	Relative eff		1000 NoTrg	CutFlow	Relative eff
Generated ev	16889			Generated ev	16889	
TRG	773	4.58%		TRG	16844	99.73%
QualityCuts	759	98.19%		QualityCuts	13997	83.10%
ECut	684	90.12%		ECut	5741	41.02%
F51Cut	368	53.80%		F51Cut	4785	83.35%
dEdXSigCut	366	99.46%		dEdXSigCut	4738	99.02%
Signal efficiency	0.0216709		0.0011204152	Signal efficiency	0.280538	
	0.04576943573					
	N1Cuts				N1Cuts	
No TRG	5035	0.0726912		No TRG	5035	0.941013
No Quality	520	0.703846		No Quality	5674	0.835037
No ECut	598	0.61204		No ECut	8706	0.544222
No F51Cut	673	0.543834		No F51Cut	5631	0.841414
No dEdXSig	485	0.754639		No dEdXSig	5093	0.930296

Table 4: Efficiency analysis result for spin-0 mass 1000*Gev*

Spin 0	1000 HLT_Photon200	CutFlow	Relative efficiency		1000 NOTRG	CutFlow	Relative efficiency
	Generated ev	9500			Generated eV	9500	
	TRG	859	0.09042105		TRG	9492	99.91%
	QualityCuts	847	0.98603		Quality cuts	8878	93.53%
	ECut	803	0.94805		ECuts	5910	66.57%
	F51Cut	449	0.55915		F51Cuts	4875	82.49%
	dEdXSigCut	448	0.99777		dEdxsigCut	4833	99.14%
	Signal efficiency	0.0471579			Signal efficiency	0.508737	
		N1Cuts	Relative eff		N1Cuts		Relative efficiency
	No TRG	5216	0.0858896		No TRG	5216	0.926572
	No Quality	607	0.738056		No Quality	5503	0.878248
	No ECut	692	0.647399			7416	0.651699
	No F51Cut	800	0.56			5837	0.827994
	No dEdXSig	586	0.764505			5277	0.915861

Table 5: Efficiency analysis result for spin-1/2 mass 2000*GeV*

2000 Photon200	CutFlow	Relative eff		2000 NoTrg	CutFlow	Relative eff
Generated ev	17629			Generated ev	17629	
TRG	1028	5.83%		TRG	17584	99.74%
QualityCuts	1009	98.15%		QualityCuts	15014	85.38%
ECut	930	92.17%		ECut	7319	48.75%
F51Cut	537	57.74%		F51Cut	5955	81.36%
dEdXSigCut	531	98.88%		dEdXSigCut	5873	98.62%
Signal efficiency	0.0301208		0.00128729545	Signal efficiency	0.333144	
	0.05723523739					
	N1Cuts				N1Cuts	
No TRG	6320	0.084019		No TRG	6320	0.929272
No Quality	709	0.748942		No Quality	6835	0.859254
No ECut	776	0.684278		No ECut	9430	0.6228
No F51Cut	911	0.582876		No F51Cut	7143	0.822204
No dEdXSig	684	0.776316		No dEdXSig	6419	0.91494

Table 6: Efficiency analysis result for spin-0 mass 2000*GeV*

2000 Photon200	CUTFLOW	RELATIVE EFFICIENCY		2000 NO TRG	**CUT FLOW**	RELATIVE EFFICIENCY
GENERATED eV	14000			GENERATED eV	14000	
TRG	1420	10.143		TRG	13992	99.943
QUALITY CUT	1411	99.366		QUALITY CUT	13278	94.897
ECUT	1333	94.47		ECUT	9912	74.649
F51CUT	764	57.314		F51CUT	8059	81.305
DeDxSIG_CUT	759	99.345		DEDXSIG_CUT	7970	98.896
SIGNAL EFFICIENCY	0.0542143			SIGNAL EFFICIENCY	0.569286	
	CUTFLOW	RELATIVE EFFICIENCY		2000 NO TRG	CUT FLOW	RELATIVE EFFICIENCY
NO TRG	8791	86.338		NO TRG	8791	90.661
NO QUALITY	1032	73.547		NO QUALITY	9191	86.715
NO ECUT	1097	69.189		NO ECUT	10972	72.6394
NO F51CUT	1318	57.587		NO F51CUT	9768	81.593
NO DEDXSIG	1011	75.074		NO DEDXSIG	8913	89.419

Table 7: Summary of efficiency analysis results for both spin-1/2 and spin-0

1000GeV	**Spin-1/2 (16889 entries)**	**Spin-0 (9500 entries)**
TRG	4.58%	9.042%
F51	53.80%	55.92%
dE/dXsigcut	99.46%	99.78%
2000GeV	Spin-1/2 (17629 entries)	Spin-0 (14000 entries)
TRG	5.83%	10.14%
F51	57.74%	57.31%
dE/dXsigcut	98.88%	99.35%

NIPES-NCEE Conference Proceedings
The 2nd International Conference 15th-17th Feb. 2023
473-489
www.nipesjournals.org.ng

3.1 Generator Level Kinematics

The generated kinematics plot for monopole data sets 1000GeV-4500GeV is displayed in the plots for transverse and total momentum distribution for spin-1/2 monopole candidates.

3.2 Pseudorapidity

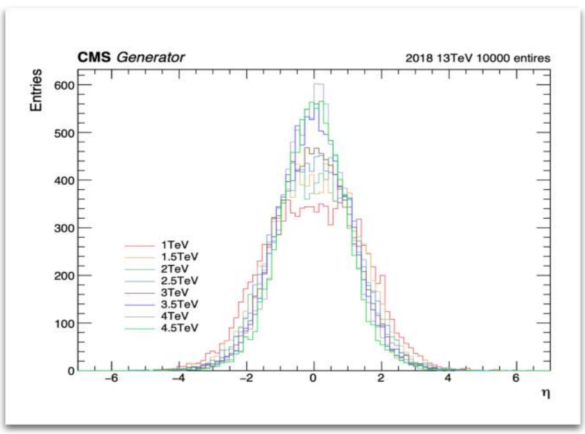

Fig. 6: Spin-1/2 monopole

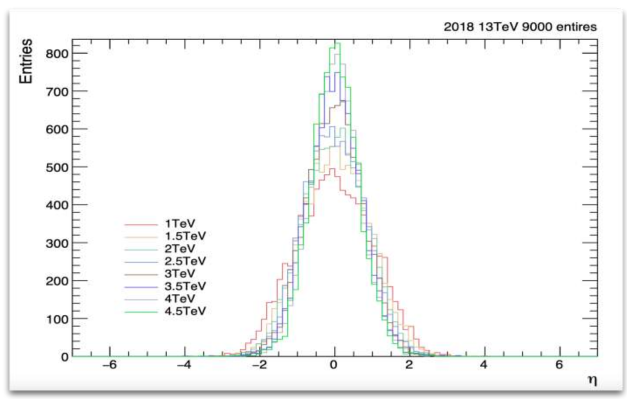

Fig. 7: Spin-0 monopole

3.3 Transverse momentum

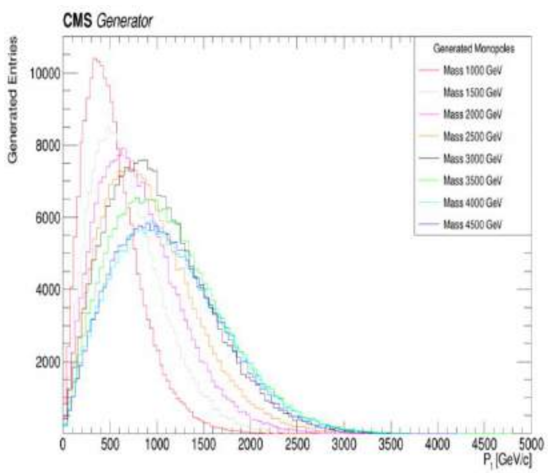

Fig. 8: Spin-1/2 monopole

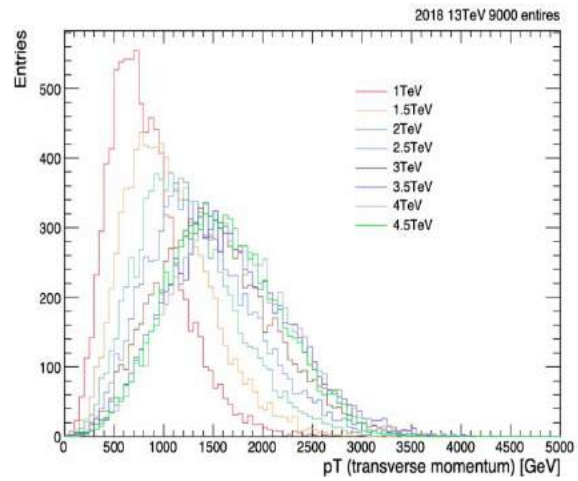

Fig. 9: Spin-0 monopole

3.4 Azimuthal distribution (ϕ)

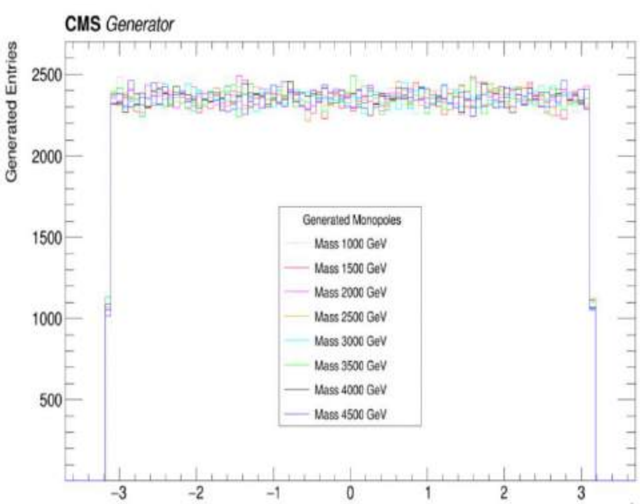

Fig. 10: Spin-1/2 monopole

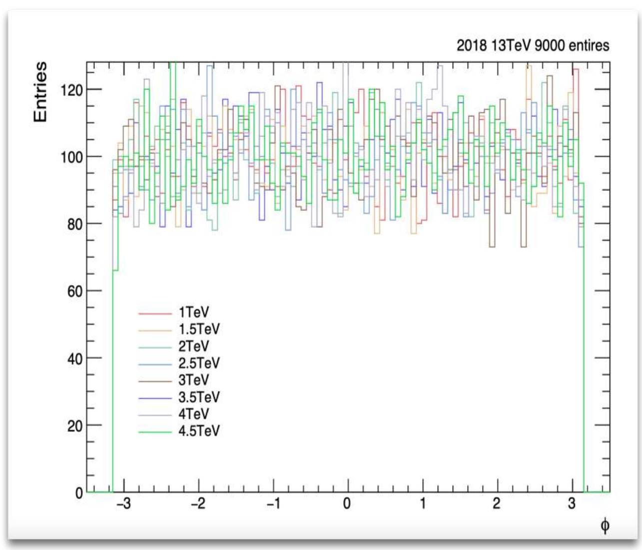

Fig. 11: Spin-0 monopole

From the results of the efficiency analysis shown in Tables 3-6, we observe that the offline selection cuts have efficiencies greater than 50% and 90% for F51 and dE/dx significance, respectively. Also, the trigger selection for Spin-1/2 has efficiency lower than 10%, even after the offline selections are applied (Table 7). We present two mass points; 1000 GeV and 2000 GeV, to explain a question that may arise from comparing the relatively lower number of generated entries for the 1000 GeV spin-0 mass. The closeness in range for the 2000 GeV mass shows that the efficiency of registration for the spin-0 monopole candidate is higher than the spin-1/2 irrespective of the number of generated entries.

In Figures 6 and 7, the plotted histogram for pseudorapidity is seen to have a harder registration and is more centrally registered ($-2< \eta < 2$) for the spin-0 monopole than in the case of the spin-1/2 monopole ($-3<\eta < 3$).

In Figures 8 and 9, it is seen that monopoles have high transverse momentum. Also, the registration for the spin-0 monopole is again observed to be harder than that of spin-1/2. No difference except for harder registration in the case of spin-0 monopoles is observed in the azimuthal distributions (Figures 10 and 11) due to the expected conservation of azimuthal symmetry.

We conclude that the observed higher efficiencies of the spin-0 monopole candidates are a consequence of it being a scalar particle, thereby causing it to not interact with the tracker system as would the spin-1/2 fermionic monopoles.

Conclusion

Conclusion

This paper explores how the existence of a magnetic monopole would explain the quantization of electric charge and symmetries, Maxwell's equations of electromagnetism, and modifications to the Lorentz force. We also reinstate the moments to be an important parameter in the observed registrations for the selected cases of spin-0 and spin-1/2. This is justified by presenting ROOT generated results for pseudorapidity, azimuthal distribution, transverse momentum and contrasted cases in efficiency analysis.

Acknowledgment

I wish to thank my supervisors as a summer student at CERN: Albert De Roeck, Mai El Sawy, Srimanob Noraphat, Afsar Abbas, and Lin Shih, for introducing me to the research area and guidance. I also acknowledge the CERN and the CMS department for the data used in this work.

References

[1] P.A.M. Dirac (1931). Quantised singularities in the electromagnetic field. Proc. Roy. Soc. A 133, 60-72.
[2] George_Lazarides_Dirac_plus_Nambu_Monopolesin_the_Standard_Model.https://www.researchgate.net/publication/352435675
[3] M.M. Hassan El Sawy (2020). Search for Magnetic Monopoles in the CMS experiment at the Large Hadron Collider (LHC). https://cds.cern.ch/record/2744867.
[4] G. 't Hooft (1974). Magnetic Monopoles in Unified Theories. Magnetic monopoles in unified gauge theories. Nucl. Phys. B 79, 276–284.
[5] A. De Roeck, A. Katre, P. Mermod, D. Milstead, T. Sloan (2012). Sensitivity of LHC experiments to exotic highly ionising particles. The European Physical Journal C 72. 1434-6052.
[6] S. Baines, N.E. Mavromatos, V.A. Mitsou, J.L. Pinfold, A. Santra (2018). Monopole production via photon fusionand Drell-Yan processes: MADGRAPH implementation and perturbativity via velocity-dependent coupling and magnetic moment as novel features. Eur. Phys. J. C 78: 966, doi:10.1140/epjc/s10052-018-6440-6.
[7] A. Seiden (2012). Characteristics of the ATLAS and CMS detectors. Phil. Trans. R. Soc. A370, 892–906.

NIPES-NCEE Conference Proceedings
The 2nd International Conference 15th-17th Feb. 2023
490-500
www.nipesjournals.org.ng

PRiSM METHODOLOGY AND PROJECT SUCCESS: A STAKEHOLDERS' PERSPECTIVE

Musa Mohamed[1] and Jato, Peter Igorigo[2]

Department of Project Management Technology, School of Innovative Technology, Federal University of Technology, Minna, Niger State, Nigeria
Musamoh@futminna.edu.ng[1]
digijat@yahoo.com[2]

Abstract.

In business, success is the only language stakeholders understand. This may be due to investment of scarce resources with the anticipation that the business or project will deliver the expected values and benefits to meet strategic business objectives. Traditionally, project success is measured with respect to the Iron Triangle, but the question is: is the concept still effective? It does, how do we assess projects whose deliverables are delivering value and benefits, yet cost thrice their original budget and twice their schedule, for instance? How effective is the concept now, with respect to the myriad sustainability challenges around the world? This research therefore, aims to examine PRiSM methodology, an all-inclusive and sustainable methodology, and its impact on project success from the perspective of stakeholders executing projects in Nigeria's tertiary educational sector. The outcome of the study suggests that the PRiSM approach could result in improved collaboration and communication, better project planning and execution and will contribute to a high likelihood of project success. Nevertheless, using sustainable building techniques and materials is one of the main obstacles to adopting the PRiSM approach, along with the need for a cultural shift, lack of understanding about new methodologies and technologies, lack of senior management support, and others. Cost of implementation, complexity, difficulty in measuring success and resistance to change are some of it draw backs. The findings show that professionals need to acquire new skills and retrain in cutting-edge, sustainable techniques and technologies. There is also significant evidence that respondents would use the PRiSM approach if they possess the requisite knowledge and skill. Though this research focused on the construction sector, it opens up opportunities for further studies in other sectors, such as Oil and Gas, Manufacturing, Pharmaceuticals and others. This information could be helpful to project management experts in understanding these sustainability challenges and strategising and seizing opportunities to increase the project success rate while reducing the carbon footprint.

***Keywords**: PRiSM Methodology, Project Success, Project Performance*

1. INTRODUCTION

Projects result in new products, services, or outcomes, and using them could positively or negatively affect people or organisations. As benefits mount, stakeholders become increasingly concerned about the project's success. Project success is the creation of sustainable business value [1,2,3,4,5], through effective project management. It is also the degree to which a project satisfies the sated requirements. On the other hand, according to PMI (2021), project management is guiding the project work to achieve the intended outcome, however, Kerzner H. (2017), opines successful project management as achieving a continuous stream of project objectives within time, within cost, at the desired performance/technology level, while utilizing the assigned resources effectively and efficiently, and having the results accepted by the customer and/or stakeholders.

However, climate change and sustainability requirements appear to have modified the standard concept of project success assessment due to the effects of the deliverables on the environment, and by extension the society and economy. Interestingly, several methodologies and technologies are evolving to enhance project performance; one of such is Sustainable Project Management. According to Silvius, G. (2017), "Sustainable Project Management is the planning, monitoring and controlling of project delivery and support processes, with consideration of environmental, economic and social aspects of the life-cycle of the project's resource, processes, deliverables and effects, aimed at realising benefits for stakeholders and performed in a transparent, fair and ethical manner that includes proactive stakeholder participation". Therefore, in the present equation for project success, the project management methodology (PMM) is a key consideration. The definition by Silvius may have provided the foundation for Green Project Management (GPM), a global organisation advocating for sustainability in project management to create the P5 standard; People, Planet, Prosperity, Process, and Product as the benchmark for attaining sustainability. Each P5 element describe the specific actions a project manager will take to deliver sustainable project in a sustainable manner.

The aim of this paper is to conduct an exploratory study of stakeholders' perception of PRiSM methodology and its impact on project success in tertiary educational institutions in Nigeria, specifically, to investigate stakeholders' opinion of PRiSM methodology, factors affecting the adoption of PRiSM methodology and to determine how PRiSM methodology influences project success. The research is organised into sections; the methodology section explains the method employed by describing the relevant data required, the design strategy employed, the study population, the sample size and the study technique. Finally, the findings and discussion section present a content analysis of the five thematic areas of the study, while the paper concludes with a recommendation for further study.

2. METHODOLOGY

After conducting a desktop literature review to identify the potential project success factors, sixty-eight (68) elements were found which were divided into five groups based on themes. These were encoded into closed-ended questionnaires. The structured questionnaire was organised into two sections, A and B. Section A deals with the respondents' demographic information. In contrast, section B has five thematic parts designed to provide answers to the research questions. For example, in section B, part 1 comprises the conceptual development of PRiSM methodology; Part 2 contains stakeholders' perception of PRiSM methodology; Part 3 includes the factors militating against the adoption of PRiSM methodology; Part 4 includes the impact of PRiSM methodology on project performance; and Part 5 contains project delivery performance. These thematic areas were rated by respondents using a 5-point Likert scale.

2.1. Sources of Data

The Primary data was gathered from the responses through questionnaires obtained from contractors, consultants and other professionals. In contrast, desk-top literature was gathered from books, journals and online sources related to the topic of the study.

2.2. Sampling Technique and Sampling Size

The sample size for this study was drawn from professionals in the tertiary education sector. Due to the characteristics of the population, a two-stage sampling technique was used. First, a random sampling procedure was used to select those to whom the research instruments were administered. This was used in selecting the targeted construction professionals that directly execute projects in the tertiary institutions without any biases or loop-sidedness as every professional has every chance of involvement, as applied in the study of Muhammed et al. (2022a).

Cochran's Equation was used to determine the sample size. Random sampling for an undefined population using the Cochran formula in Equation (3.1), where p = 0.5, i.e., the maximum variability at a 95% confidence level. The value of 95% is used because the researcher needs to know the variability in the proportion of the actual users of PRiSM methodology in the construction industry. In Equation (3.1), e is the precision desired for the sample size at $\pm$5 per cent, z is the abscissa of the standard curve given as 1.96 and q is represented by (1 – p), which is equivalent to 0.5. Matto et al. (2021), Anosike (2021), and Muhammed et al. (2022a) used the Equation in their works.

Cochran (1963)

$$n_0 = \frac{Z^2pq}{e^2} \qquad \text{(Eqn. 3.1)}$$

Thus

$$n_0 = \frac{1.96^2(0.5*0.5)}{0.05^2} \qquad \text{(Eqn. 3.2)}$$

$$n_0 = 384$$

Thus, the Equation calculates the minimum sample size to be **384**.

2.3. Data Collection Instrument

A close-ended questionnaire was used for this study. As described earlier, the format of the questionnaires, which were aligned to meet the research objectives, has two main parts or sections, A and B. The researcher used this method because it was cheap even when the sample size was large [6,7,8,9,10]. In addition, it frees biases of the interviewer, and respondents had sufficient time to give good answers; thus, the outcome could be steadier and more consistent. Section A deals with the respondents' demographic information, while section B has five thematic parts designed to answer the research questions. These thematic areas are made up of factors to be rated by the respondents using a 5-Point Likert.

2.4. Method of Data Analysis

The study employed only descriptive analysis. Descriptive statistics use charts, tables, and mean and standard deviation to describe the magnitude of the respondents' demographic features and the relationship between the variables involved.

3. RESULTS AND FINDINGS

A total of 239 construction professionals (163, 68.2%) were males, while (76, 31.8%) were females. The result implies that there is a gender imbalance which may be due to the challenging nature of construction work.

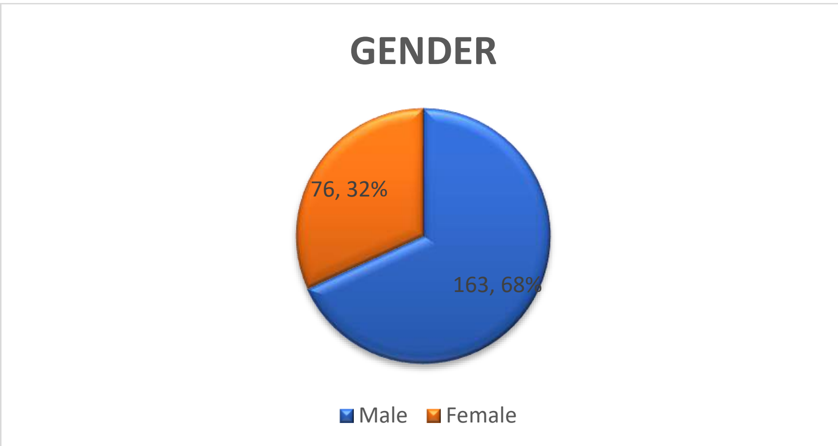

Figure 1: Gender of respondents

The age demography shows that (34, 14.2%) were within the age bracket of 20-30 years; (56, 23.4%) were within 31-40 years; (74, 31%) were within 41-50 years; (48, 20.1%) were within 51-60 years; while (27, 11.3%) were 61 years and above. The result implies that the respondents with an age bracket of 31 to 60 years constituted the more significant and active population.

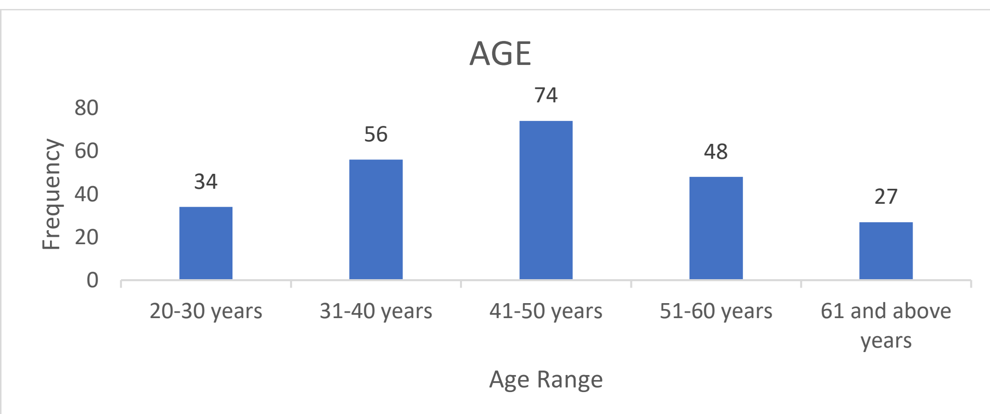

Figure 2: Ages of respondents

The professional demography of respondents was (46, 19.2%) were project managers, quantity surveyors (25, 10.5%); architects (30, 12.5%); engineers (81, 33.9%); site managers (21, 9%); estate surveyors (10, 4%) and urban and regional planners (26, 10.9%). The result indicates that most of the respondents are engineers since they constitute the profession with the most significant number of participants.

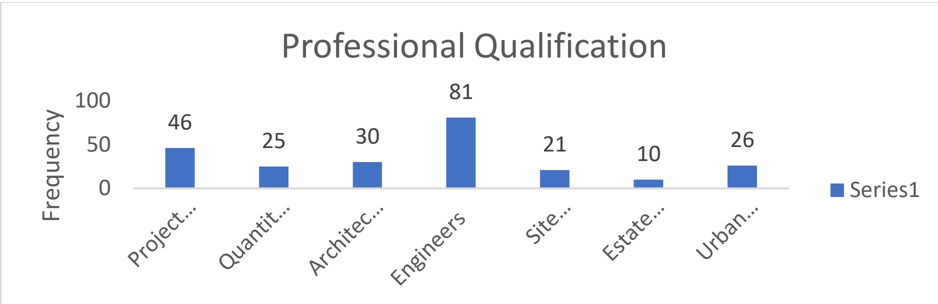

Figure3: Professional qualification of respondents

The academic demography shows that (25, 10.5%) hold National Diploma; (68, 28.5%) hold HND; (77, 32.2%) hold a first Degree; (55, 23%) hold Master's while (14, 5.8%) hold PhD. The result reveals that most respondents entered the construction industry after their first degree.

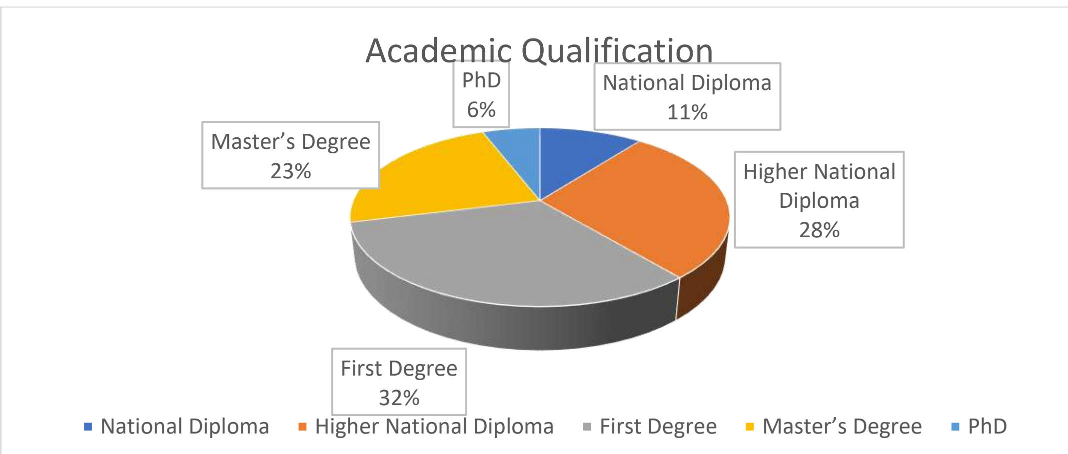

Figure 4: Academic qualification of respondents.

The following sections present the findings of stakeholders' opinions on each of the five thematic areas in which PRiSM methodology could impact the execution of physical infrastructural projects in the Nigeria construction section.

3.1. Factors Affecting PRiSM Methodology Development

Respondents strongly agree that seven factors hinder the development of the PRiSM methodology which are; lack of desire for change (89.5%); inadequacy of innovativeness (75.7%); project managers' insufficient thinking capacity (79.5%); sufficiency in the use of traditional project management methodologies (81.2%); lack of adaptability (81.2%); insufficient research and development (74.5%), and comfortability in the use of traditional project management methods (80.8%). These factors collectively indicate an 80.3% agreement on average that they affect the development of PRiSM methodology, as presented in Table 1.

Table 1: Factors affecting PRiSM methodology development

Factors Affecting PRiSM Methodology Development	SD	D	I	A	SA

Lack of Desire for Change	5	4	5	11	214
Inadequacy of Innovativeness	20	12	13	13	181
Project Managers Insufficient Thinking Capacity	37	4	5	3	190
Sufficiency in the usage of Traditional Project Management Methodologies	5	32	5	3	194
Lack of Adaptability	5	4	33	3	194
Insufficient Research and Development	13	16	9	23	178
Comfortability in the usage of Traditional Project Management Methodologies	11	6	6	23	193
Total (Percentage)	96 (5.74%)	78 (4.66%)	76 (4.54%)	79 (4.72%)	1344 (80.33%)
Mean	0.4013	0.3264	0.3179	0.3305	5.6234

3.2. Stakeholders' perception of PRiSM Methodology

The perception of stakeholders regarding PRiSM methodology shows that 84.5% strongly agree that they have never heard of PRiSM methodology. 70.7% said they have heard of the methodology, only 37.7% said they know other methodologies. Again, while 44.8% said they hardly use any methodology in their project, 44.8% said they want to use the methodology but need access. 15.6% said they needed help understanding the methodology. However, despite its newness, 84.5% are willing to use it but said they lack knowledge, while 59.4% said they do not like it. 70.7% said they think of it often, and just 37.7% are strongly positive that PRiSM methodology may improve their workflow. In comparison, 85.3% are affirmative that it can improve collaboration and communication, whereas 61.5% think it can assist in better project planning. There is a 58.5% strong agreement that the above factors influence stakeholders' perception of PRiSM Methodology, as indicated in Table 2.

Table 2: Factors affecting stakeholders; perceptions of PRiSM methodology

Stakeholders' Perception of PRiSM Methodology	SD	D	I	A	SA
I have never heard about PRiSM Methodology	0	0	0	37	202
I have heard about PRiSM Methodology	18	18	17	17	169
I only know about other Methodologies	149	0	0	0	90
I hardly use any Methodology in my Projects	0	132	0	0	107
I want to use PRiSM Methodology but have no access	0	0	132	0	107
I Don't Understand PRiSM Methodology	35	52	17	97	38
I don’t like PRiSM Methodology	0	0	0	97	142
I want to try PRiSM Methodology but have no knowledge of it	0	0	0	37	202
I think about PRiSM Methodology Often	18	18	17	17	169
I think PRiSM Methodology can improve my work	149	0	0	0	90

PRiSM Methodology can improve collaboration and communication	0	20	8	7	204
PRiSM Methodology can assist in Better Project Planning and Execution	4	40	0	48	147
Total (Percentage)	373 (13.08 %)	280 (9.82%)	191 (6.70 %)	357 (12.52 %)	166 7 (58. 5%)
Mean	1.5606	1.1715	0.799 1	1.4937	6.97 48

3.3. Factors militating against the adoption of PRiSM Methodology in the execution of construction projects in the tertiary education sector in Nigeria.

A total of 25 factors were identified militating against adopting the PRiSM methodology. While each factor is necessary, only the top ten factors will be analysed for convenience. As shown in Table 3, 24.3% of the respondents strongly agree that advocacy and awareness are factors militating the adoption of PRiSM methodology. Fifty-nine point four per cent think the company's existence (experience) as a factor, whereas 77.8% said its staff strength in the construction business. Conversely, only 4.2% think the physical structure of the construction firm (organogram) hinders the adoption of the methodology. Again, 53.1% strongly agree that access to affordable tools and applications and the presence of quality construction experts, respectively, could be factors. While 27.2% believe that supportive ICT infrastructure could be a factor, 62.3% attribute it to legislation/legal requirements. Respondents strongly agree that commitment and support from top management (84.5%), and strengthening and implementation mechanism (77%), respectively, could also be factors. Analysing the 25 factors, 50.7% on average strongly agree that these factors contribute to the hindrance of PRiSM adoption, as shown in Table 3.

Table 3: Factors militating against the adoption of PRiSM methodology in the Nigerian tertiary education sector

Factors militating against the adoption of PRiSM methodology in the Nigerian tertiary education sector	SD	D	I	A	SA
Advocacy and Awareness	25	42	17	97	58
Company's Existence in Years (Experience)	0	0	0	97	142
Staff Strength of Construction Business	18	18	17	0	186
Physical structures of the Construction Firm	149	0	0	80	10
Accessibility to Affordable Tools and Applications	0	112	0	0	127
Presence of Quality Construction Experts	0	0	132	0	127
Supportive ICT Infrastructure	35	35	17	87	65

Legislation/Legal Requirement	0	0	0	87	149
Commitment and backing from Top management	0	0	0	37	202
Strengthening and Implementation Mechanism	18	18	17	0	184
Ability to operate the Project Management software packages	139	0	0	0	100
Economic Incentives	0	122	0	0	117
Construction Standards	0	0	122	17	100
Knowledge Sharing	35	35	17	87	65
Changes in the Construction Process	0	0	0	124	115
Cost Inconsistencies	0	0	17	37	185
Regulator Mechanisms	18	35	17	0	169
Level of Government Support for Project Management tools	149	0	0	0	90
Supportive Policies and Legislation on Project Management Tools in Nigeria	0	149	0	0	90
Resource Efficiency	0	0	139	0	100
Competitive Advantage	35	35	17	104	48
Computer literate level of construction stakeholders	0	0	0	97	142
Awareness of the benefits of Software use	17	0	0	17	205
Level of Change Management Procedure Within Construction Firm	18	35	17	0	169
Confidence Level of Software technology usage by Industry stakeholders	139	0	17	0	83
Total (Percentage)	795 (13.27 %)	636 (10.62 %)	563 (9.39 %)	968 (16.16 %)	3028 (50.67%)
Mean	3.3264	2.6611	2.3556	4.0502	12.6694

3.4. PRiSM Methodology Impacts

According to the respondents' preferences in table 4, seven factors were identified that could impact PRiSM methodology. Thirty-three point five per cent infer that there is a high chance of projects being delivered on time using the PRiSM methodology; 44.8% also affirm that there is a high chance of projects delivered on cost using same. Surprisingly, only 15.9% strongly agree that projects are highly likely to be delivered on the scope. Again, 56.5% are optimistic that there is a high chance of projects progressing without scope changes during the project life cycle. In comparison, 70.7% think there is a high chance of projects progressing as planned using the PRiSM methodology.

Further, 38.9% believe there are high chances of innovative ways of managing projects using the PRiSM methodology. In comparison, 49% are satisfied that there is a high chance that project managers understand the project better using the PRiSM methodology. Overall, there is a confidence level of 44.2% affirmative that PRiSM methodology impacts project delivery.

Table 4: PRiSM methodology impacts

PRiSM Methodology Impacts	SD	D	I	A	SA
There is a high chance of Projects being delivered on time using the PRiSM Methodology	0	142	0	17	80
There is a high chance of Projects delivered on cost using the PRiSM Methodology	0	0	132	0	107
There is a high chance of Projects delivered on the scope using the PRiSM Methodology	52	35	17	97	38
There is a high chance of Projects being delivered without scope changes during the project life cycle using the PRiSM Methodology	0	17	0	87	135
There is a high chance of Projects being delivered as planned using the PRiSM Methodology	18	18	34	0	169
There are high chances of innovative ways of managing projects using the PRiSM Methodology	129	17	0	0	93
There is a high chance that Project Managers understand the project better using the PRiSM Methodology	0	122	0	0	117
Total (Percentage)	199 (11.89%)	351 (20.98%)	183 (10.94%)	201 (12.01%)	739 (44.17%)
Mean	0.9163	1.3938	0.7657	0.8828	3.5105

3.5. Project Delivery Performances

Seven factors are identified to contribute to project delivery performance. Amongst these, respondents are confident that projects are delivered on time using the PRiSM methodology (37.7%); projects are delivered on cost using the PRiSM methodology (15.9%); Projects are delivered on the scope using the PRiSM methodology (52.3%); Projects are delivering without scope changes during the project life cycle using the PRiSM methodology (77.4%); Projects are delivering as planned using the PRiSM methodology (77.8%); Projects are managed innovatively using the PRiSM methodology (30.5%) and Projects are understood better using the PRiSM methodology (37.7%). These factors show a 47% affirmative that the above factors influence project delivery performance, as depicted in table 5.

Table 5: Project delivery performance

Project Delivery Performances	SD	D	I	A	SA
Projects are delivered on time using the PRiSM Methodology	17	0	132	0	90
Projects are delivered on cost using the PRiSM Methodology	35	52	17	97	38
Projects are delivered on the scope using the PRiSM Methodology	0	0	17	97	125
Projects are delivered without scope changes during the project life cycle using the PRiSM Methodology	0	0	0	54	185
Projects are delivered as planned using the PRiSM Methodology	18	18	17	0	186
Projects are managed innovatively using the PRiSM Methodology	166	0	0	0	73
Projects are understood better using the PRiSM Methodology	0	149	0	0	90
Total (Percentage)	236 (14.11%)	219 (13.09%)	183 (10.94%)	248 (14.82%)	787 (47.04%)
Mean	0.9874	0.9163	0.7657	1.0377	3.2929

4. CONCLUSION

This research concludes that PRiSM methodology could manage climate change through the reduction of carbon footprint in Nigeria's building industry. It further concludes that construction professionals in Nigeria's building industry are change-averse and, as a result are missing out on the advantages and benefits new or sustainable methods offer. First, it shows a need for more knowledge in sustainable project management and senior management support. Secondly, PRiSM methodology could deliver the project with minimal scope changes and provide a schedule, cost efficiency, and specification. Furthermore, it shows a link between project success and PRiSM methodology. However, cost of implementation, complexity, difficulty in assessing success are some of it draw backs. A significant limitation of the research is the unavailability and access to data on construction firms executing projects in the tertiary educational sector in Nigeria.

5. RECOMMENDATION

This study recommends that:

2. There is a need for construction professionals to be ready, willing and open to new and innovative technologies and methodologies.
2. There is a need for top management's full support and encouragement in the deployment of new methodologies such as training and knowledge hunting, and information sharing.
3. Knowledge of PRiSM methodology, adoption and implementation should be vigorously pursued.
4. Government and stakeholders in the building industry should collaborate to standardise PRiSM as the de facto methodology for infrastructure project implementation.

5.1. Contribution to Knowledge

This study considers the versatility and benefits of the PRiSM methodology. It is an awakening call to stakeholders of the importance of social, economic, and environmental dimensions while also ensuring that scope, time, cost and quality are not negatively impacting the execution of the projects.

5.2. Areas of further study

As projects are executed in different industries, every industry may have its project management peculiarities. Therefore, while this study focused on stakeholders' perception of PRiSM methodology on project success in the construction industry, its influence on project delivery in other industries, such as manufacturing, oil and gas, pharmaceuticals, and others, would be a valuable study.

REFERENCES

[1] Kerzner, H., (2017). Project Management: A Systems Approach to Planning, Scheduling and Controlling (12th Ed. ed.). Hoboken, New Jersey.: John Wiley & Sons, Inc.
[2] Project Management Institute. (2021). A Guide to the Project Management Body of knowledge, Newton Square, PA: Author
[3] Silvius, G. (2017). 'Sustainability as a New School of Thought in Project Management Journal of Cleaner Production 166, 1479-1493.
[4] Muhammed, A. O., Muhammed, A. A., Yakubu, H. A., Suleiman, A., & Adam, A. (2022a). Assessment of Factors Affecting Contractors Tendering Success for Construction Projects in North-Central Nigeria. International Journal of Real Estate Studies, 16(1), 87–99. https://doi.org/10.11113/intrest.v16n1.155.
[5] Anosike, N. M. (2021). Views of construction professionals on the causes and remedies of building collapse in Nigeria. International Journal of Engineering Technologies and Management Research, 8(6), 68-85. doi:10.29121/ijetmr.v8.i6.2021.976.
[6] Matto, M. C., Ame, A. M., & Nsimbila, P. M. (2021). Influence of contract management on value for money procurement in Tanzania. Int. J. Procurement Management, Vol. 14, No.6
[7] Cochran, W. G. (1963). Sampling Technique, 2nd ed.; John Wiley and Sons Inc.: New York, NY, USA.
[8] Monca, Gutierrez (2014). Applying PRiSM methodology in the Canadian Construction Sector.
[9] Quan, P., Bilge, E., & Yesemin, Nielsen (2022). Project Management for Sustainable Buildings: A comprehensive Insight into the Relationship to Project Success.

NIPES-NCEE Conference Proceedings
The 2nd International Conference 15th-17th Feb. 2023
501-511
www.nipesjournals.org.ng

ANAEROBIC CO-DIGESTION OF PALM OIL EFFLUENT AND FOOD WASTE

Ejiroghene Kelly Orhorhoro[*1], Silas Oseme Okuma[2], Samuel Batet[2]

[1]Department of Mechanical Engineering, General Abdulsalami Abubakar College of Engineering, Igbinedion University, Okada, Edo State, Nigeria
[2]Department of Mechanical Engineering, Nigeria Maritime University, Okerenkoko, Delta State, Nigeria

Corresponding email: ejiroghene.orhorhoro@iuokada.edu.ng

Abstract
The yearly expansion of oil palm plantations in Nigeria is accompanied by an increase in the number of palm oil mills that produce crude palm oil (CPO) from fresh fruit bunches (FFB). In Okada alone, there are several palm oil mills, and Igbinedion University just acquired a palm oil farm that is currently undergoing development. The production process in a palm oil mill consists of sterilization, stripping, clarification, and palm kernel oil recovery. This generates solid waste and liquid waste. The liquid waste (i.e., palm oil effluent), when discharged directly into the environment without proper treatment, can pollute the environment, emitting greenhouse gases (GHG) that cause global warming. In this study, palm oil mill effluent and food waste were evaluated for biogas production under. Food waste and palm oil effluent from Okada town were co-digested in a fixed dome anaerobic digester at a mesophilic temperature range. The highest cumulative biogas yield was achieved from the co-digestion of palm oil effluent and food waste. Besides, the digestates obtained at the end of the complete hydraulic retention time were odourless, which is an indication of thorough treatment of the palm oil effluent. More so, such digestates can serve as organic manure for Okada palm oil farms.

Keywords*: Palm oil effluent, Food waste, co-digestion, biogas yield, mesophilic temperature*

1.0 Introduction
Palm oil is one of the vital commercial crops for edible oil production. Palm oil mill effluent (POME) is the wastewater characterized by thick yellowish liquid and high organic contents, having chemical oxygen demand (COD) and biochemical oxygen demand (BOD) respectively [1, 2]. These are major concerns in environmental pollution due to their adverse effects on many forms of life. The direct discharge of POME into the environment is a matter of concern for both toxicological and aesthetic reasons. The majority of the palm oil mills use the addition of water during the extraction process of crude palm oil (CPO) from the fresh fruit bunch (FFB) [3]. As a result, a considerable amount of wastewater will be generated and disposed of in ponds, drainage systems, streams, and rivers [4–8]. However, POME is suitable for generating electricity through biogas. POME has a low pH (pH 3.4–5.2) because it contains many organic acids produced by the initial fermentation process. It has a high concentration of total solids (40,500 mg/l) and a high concentration of suspended solids (18,000–46,011 mg/l). The concentration of oil and grease ranges from 4,000–9,341 mg/l, depending on milling processes [9–12]. The characteristics of POME depend on the quality of the raw material (fresh palm-oil fruit bunches) and the efficiency of palm oil extraction processes [13]. POME has become a commodity rather than undesirable wastewater, providing energy cost savings and additional income for the palm oil mills (POMs).

The main reasons for its suitability for anaerobic digestion are its high organic content, which is relatively easily digestible, and its low toxicity to the working microorganisms. POME supply is dependable both in terms of quality and quantity. POME composition also falls into the optimal range of C/N ratios (20–30) [14–16].

Municipal solid wastes (MSW) are generated and dumped indiscriminately in Nigeria due to poor implementation of standards, thus causing environmental and public health hazards [17-20]. Food waste (FW) that is a component of MSW is defined as consumable food for humans that is thrown, decayed, deteriorated, or infested by pests that originate at any stage [21]. Food waste (FW) is inevitably generated throughout the whole food supply chain (FSC), from production to packaging, processing to distribution, and finally through consumption [22]. The disposal of FW poses an environmental issue due to the emission of methane gas and hence must be handled properly. As it is a suitable feedstock for AD, waste can be transformed into energy via a sustainable method. In this study, anaerobic digestion (AD) of FW is being investigated as a more sustainable method involving waste to energy (WTE) technology. The AD process is a technology that recovers energy and nutrients from organic waste streams in usable forms in the absence of oxygen [23, 24]. It is a sustainable, renewable, and zero-carbon form of energy supply. The anaerobic digestion process can be used to recover some of this energy in the form of biogas, typically a mixture of flammable gases with a composition of 40–70% CH_4, 20–60% CO_2, and 5–10% of other gases, which include siloxane [25-28]. The ratio of CH_4 to CO_2 is normally stable in the reactor; any variation in the ratio is due to a process imbalance. The quality of biogas generated by organic waste materials does not remain constant but varies with the period of digestion [29-31]. In the absence of the process, there is an uncontrolled release of methane to the atmosphere due to the biodegradation of organic matter at open waste dump sites. Annually, natural biodegradation of organic matter is estimated to release 500–800 million tons of methane gas into the atmosphere [32]. Therefore, this study is focused on the anaerobic co-digestion of palm oil effluent and food waste

2.0 Materials and Methods

2.1 Substrates Collections

The palm oil mill effluent (POME) and food waste (FW) were collected from the palm oil processing mill and households in Okada town. The POME was stored in a tightly closed 50-liter water container. The POME and FW were analyzed for total solids, volatile solids, carbon/nitrogen (C/N) ratio, chemical oxygen demand (COD), and pH.

2.2 Preparation of Substrates

The stored POME in 50-liter containers and food waste were taken out of the cool room. The substrate was thawed until its temperature increased to room temperature. Pre-treatments were carried out on the food waste. This includes mechanical and thermal pre-treatment. The mechanical treatment involves reducing the size of the food waste. The food waste was passed through a grinder. Reduction in particle size increases the solubilisation of organic material [33]. The surface area exposed to contact with microorganisms also increases. Thus, the degradability of organic material increases, enhancing methane generation. Thermal pre-treatment such as sterilization was also conducted on the FW prior to anaerobic co-digestion [34]. The thermal pre-treatment before AD causes the breakdown of complex molecules such as polysaccharides and proteins into smaller molecules and releases the organic content into the liquid phase. Sterilization is carried out at 121°C [35] and a portion of the stored POME was measured using a measuring cylinder. After being measured (30 liters), the ground FW (20 kg) was poured into a bucket to be mixed with POME. The mixture was continuously stirred in the bucket for proper mixing. After that, the mixture was charged into a fixed-dome anaerobic digester.

Experimental Setup

An anaerobic co-digestion bioreactor was used to co-digest the POME and FW. The bioreactor is a 100-liter fixed-dome anaerobic digester. The experiment was conducted at a mesophilic temperature range of 36°C–38°C. A 10.55 mm external diameter, a 10 mm internal diameter, a pressure gauge, a thermometer, and a 0.25 inch internal diameter valve of U-tube were connected to the fixed dome digester. Pressure testing was carried out on the digester, and this was mainly to look out for possible leakages. A plastic gas bag was used for biogas collection. Prior to charging the digesters with the substrates, the U-tube was charged with tap water at a marked level. Nitrogen gas was purged through to expel oxygen from the digester and make it airtight in order to ensure anaerobic conditions in the headspace of anaerobic digesters [36]. The prepared mixture was charged into the digester and allowed for anaerobic co-digestion to take place for a complete hydraulic retention time. The digesters were then attached to a biogas bag for gas collection. The gas generated was measured daily using the water displacement method by reading the volume of water displaced in the U-tube, which is equal to the volume of gas generated. The total solids (TS), volatile solids (VS), pH, C/N ratio and COD were determined using standard method [37].

3.0 Results and Discussion

3.1 Results of Characteristics of Substrates

Table 1 shows the results of the characterization of the substrates used in anaerobic co-digestion. It shows the changes in pH, COD, TS, VS, and C/N ratio at the start, after 10 days, and at the completion of the hydraulic retention time (46 days). The pH of the collected POME substrate was acidic (weak acidic, 5.30), and the pH of the collected FW substrate was alkaline (weak alkaline, 8.76). However, their mixture was tending toward neutrality (7.04 m) at day 10 of co-digestion, and this neutrality was maintained to the end of the hydraulic retention time (HRT). The neutral pH obtained is an indication of a stable anaerobic co-digestion process [38-39]. Thus, methanogenesis bacteria that will enhance optimum biogas production are in favor, and this has consequently resulted in a continuous increase in cumulative biogas yield, as shown in Table 2.

Table 1 Characteristics of the prepared substrates used in anaerobic co-digestion

S/N	Parameters	POME Substrates	FW Substrates	Mixed POME and FW Substrates	Co-Digested POME and FW Slurry	
					After 10 Days	After 46 Days
1	pH (m)	5.30	8.76	7.65	7.04	7.00
2	COD (g)	4.50	1.23	4.15	3.05	1.55
3	TS (%)	4.78	10.12	9.75	ND	ND
4	VS (%)	3.36	86.75	87.45	ND	ND
5	C/N ratio	22.85	28.94	23.45	ND	ND

*ND—Not Determined

Furthermore, the COD of the POME substrates was determined at 4.50 g at the starts, while the COD for FW was obtained at 1.23 g. The COD of the mixture of the combined POME and COD was obtained at 4.15g, and after 10 days and 46 days of co-digested COD, it was recorded at 3.05 g and 1.55 g, respectively. There was a decrease in the COD of the co-digested substrates throughout the process, and this was an indication of COD removal. The removal of COD brought about an increase in biogas yields. According to El-Mashad and Zhang [40], biogas production increases with an increase in COD removal, which can be well explained by the fact that the methanogenic consortium acclimated very well, which consequently led to the co-digestion of the substrates under anaerobic conditions. Also, to confirm if the experiment was conducted at mesophilic slurry temperature, the temperature of the digester was monitored daily, as shown in Figure 2. It was observed that the experiment was actually conducted at an optimum mesophilic temperature range. According to Ebunilo *et al.* [41], temperature is considered one of the most important variables for process stability, as anaerobic bacteria populations can only survive in certain temperature ranges. Besides, sudden changes and fluctuations in the process temperature lead to inhibition of bacteria populations. Thus, the digestion and co-digestion of substrates in a biogas digester should be run at a stable mesophilic temperature range of 35°C–38°C that can bring about optimum biogas production.

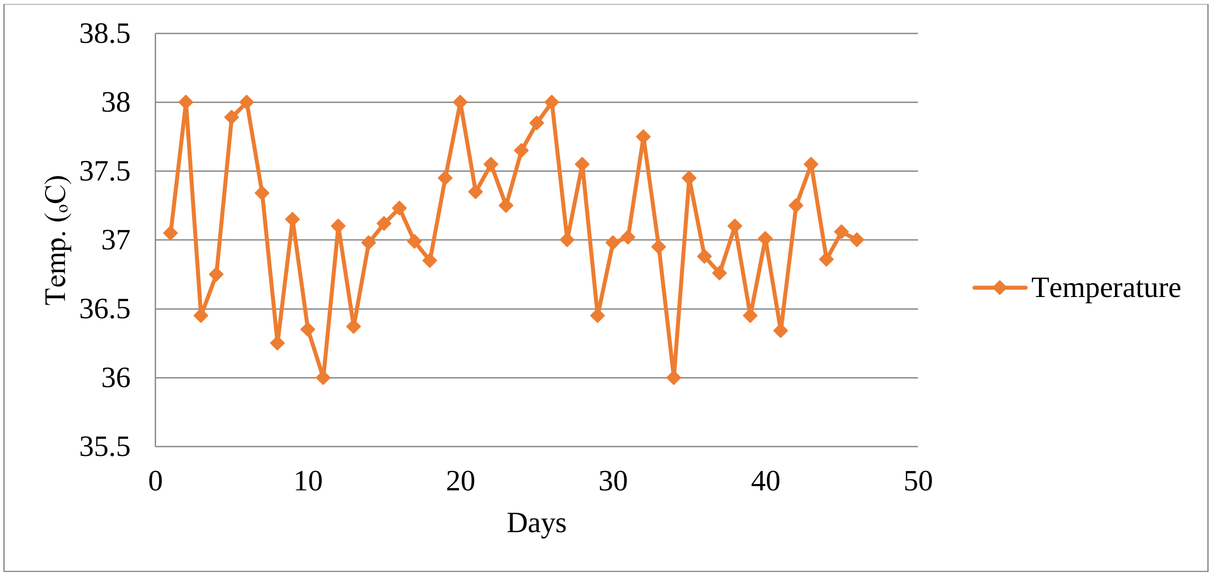

Figure 1 Evaluation of the effect of mesophilic temperature

3.2 Results of Cumulative Biogas Yield

The result of the cumulative biogas yield is shown in Table 2 and Figure 2. There was a continuous increase in biogas yield until the end of HRT. Thus, an alternative method of improving biogas yields from the AD process is co-digestion. Co-digestion leads to stabilization and improved nutrient utilization for a variety of substrate compositions [42]. Co-digestion of different substrates leads to improved biogas yield because of positive synergisms that establish the digestion medium and supply missing nutrients [43]. Apart from the advantages derived from easier handling of mixed wastes, it can help establish the required moisture contents of the substrates [44, 45].

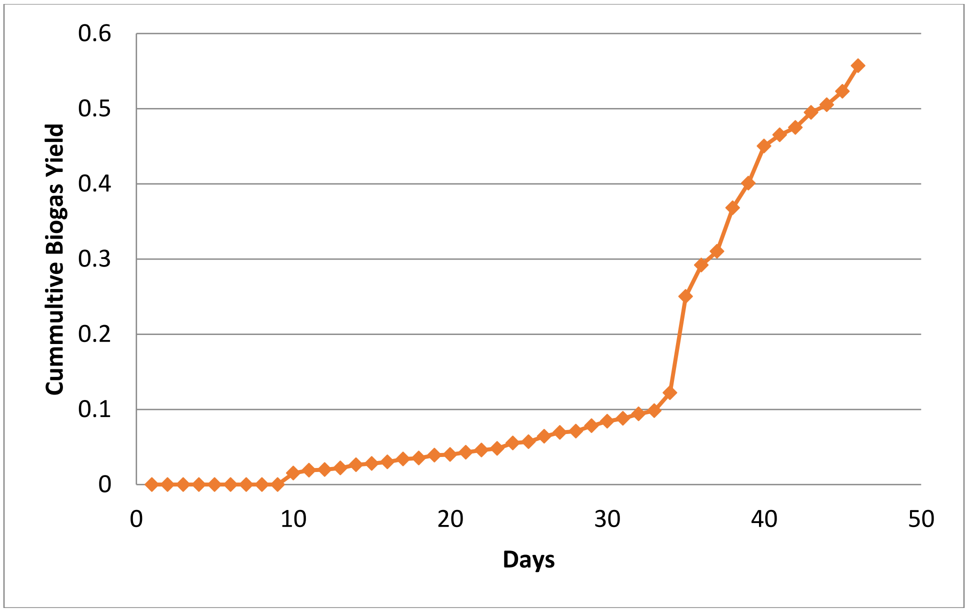

Figure 2 Evaluation of cumulative biogas yield

Table 2 Result of cumulative Biogas Yield

Day	Temp (^{0}C)	Remark	Cumulative Biogas Yield (m^3)
1	37.05	No gas	0.00
2	38.00	No gas	0.00
3	36.45	No gas	0.00
4	36.75	No gas	0.00
5	37.89	No gas	0.00
6	38.00	No gas	0.00
7	37.34	No gas	0.00
8	36.25	No gas	0.00
9	37.15	No gas	0.00
10	36.35	Yellow flame	0.015
11	36.00	Blue flame	0.019
12	37.10	Blue flame	0.020
13	36.37	Blue flame	0.022
14	36.98	Blue flame	0.026
15	37.12	Blue flame	0.028
16	37.23	Blue flame	0.030
17	36.99	Blue flame	0.034
18	36.85	Blue flame	0.035

19	37.45	Blue flame	0.039
20	38.00	Blue flame	0.040
21	37.35	Blue flame	0.043
22	37.55	Blue flame	0.046
23	37.25	Blue flame	0.048
24	37.65	Blue flame	0.055
25	37.85	Blue flame	0.057
26	38.00	Blue flame	0.064
27	37.00	Blue flame	0.069
28	37.55	Blue flame	0.071
29	36.45	Blue flame	0.078
30	36.98	Blue flame	0.084
31	37.02	Blue flame	0.088
32	37.75	Blue flame	0.094
33	36.95	Blue flame	0.098
34	36.00	Blue flame	0.122
35	37.45	Blue flame	0.250
36	36.88	Blue flame	0.292
37	36.76	Blue flame	0.310
38	37.10	Blue flame	0.368
39	36.45	Blue flame	0.401
40	37.01	Blue flame	0.450
41	36.34	Blue flame	0.465
42	37.25	Blue flame	0.475
43	37.55	Blue flame	0.495
44	36.86	Blue flame	0.505
45	37.06	Blue flame	0.523
46	37.00	Blue flame	0.557

4.0 Conclusion

The anaerobic co-digestion of palm oil mill effluent with food waste effectively improves the biogas production of There was a continuous increase in biogas production after the tenth day of recorded biogas yield, and the cumulative biogas yield was obtained at 0.557 m^3 at the end of the hydraulic retention time. The mesophilic temperature of the fixed dome digester was stable throughout the process, and an optimum mesophilic temperature range was recorded. The study shows that POME and food waste can be converted into useful energy rather than the direct discharge of POME and indiscrimate dumping of food waste in the environment, as is currently practiced by POME industries and households in Okada town.

References

[1] Najafpour, G., Yieng, H.A., Younesi, H., & Zinatizadeh, A. (2005). Effect of organic loading on performance of rotating biological contactors using palm oil mill effluents. *Process Biochem.,* 40: 2879-84

[2] Suksong, W., Kongjan, P., Prasertsan, P., Imai, T., & O-thong, S. (2016). Optimization and microbial community analysis for production of biogas from solid waste residues of palm oil mill industry by solid-state anaerobic digestion. *Bioresour Technol.,* 214:166-74.

[3] O-Thong, S., Boe, K., & Angelidaki, I. (2012). Thermophilic anaerobic co-digestion of oil palm empty fruit bunches with palm oil mill effluent for efficient biogas production. *Appl Energy,* 93:648-54.

[4] Orhorhoro, E. K., Ebunilo, P. O. B., and Sadjere, E. G., (2017). Determination and Quantification of Household Solid Waste Generation for Planning Suitable Sustainable Waste Management in Nigeria. *International Journal of Emerging Engineering Research and Technology,* 5(8): 1-9

[5] Sosnowski, P., Wieczorek, A., Ledakowicz, S. (2003). Anaerobic co-digestion of sewage sludge and organic fraction of municipal solid wastes. *Adv. Environ Res.,* 7:609–16

[6] Edelmann, W., Engeli, H., Gradenecker, M.(2000). Co-digestion of organic solid waste and sludge from sewage treatment. *Water Sci Technol.,* 41:213–21.

[7] Ejiroghene Kelly Orhorhoro, Emmanuel E. Lindsay, Joel O. Oyejide (2022). Analysis and Evaluation of a Three-Stage Anaerobic Digestion Plant for Management of Biodegradable Municipal Solid Waste. *International Journal of Engineering Research in Africa,* 60: 75-87. doi:10.4028/p-a24obb

[8] Luostarinen, S., Luste, S., & Sillanpää, M. (2009). Increased biogas production at wastewater treatment plants through co-digestion of sewage sludge with grease trap sludge from a meat processing plant. *Bioresour Technol.,* 100:79-85.

[9] Chin, M.J., Poh, P.E., Tey, B.T., Chan, E.S., & Chin, K.L. (2013). Biogas from palm oil mill effluent (POME): opportunities and challenges from Malaysia's perspective. *Renew. Sustain. Energy Rev.,* 26: 717–726

[10] Loh, S.K., Lai, M.E., Ngatiman, M., Lim, W.S., Choo, Y.M., Zhang, Z., & Salimon, J. (2013). Zero discharge treatment technology of palm oil mill effluent. *J. Oil Palm Res.,* 25: 273–281.

[11] Wu, T.Y., Mohammad, A.W., Jahim, J.Md., & Anuar, N. (2010). Pollution control technologies for the treatment of palm oil mill effluent (POME) through end-of-pipe processes, J. Environ. Manag., 91: 1467–1490

[12] Wang, J., Mahmood, Q., Qiu, J.P., Li, Y.S. Chang, L.N., Chi, L.N., & Li, X.D. (2015). Zero discharge performance of an industrial pilot-scale plant treating palm oil mill effluent. *BioMed Res. Int.,*: 1–9.

[13] Rupani, F.P., Singh, R.P., Ibrahim, M.H., & Esam, N. (2010). Review of current palm oil mill effluent (POME) treatment methods: vermicomposting as a sustainable practice. *World Appl. Sci. J.,* 11: 70–81.

[14] Wang, X., Yang, G., Feng, H., Ren, G., & Han, X. (2012). Optimizing feeding composition and carbon–nitrogen ratios for improved methane yield during anaerobic co-digestion of dairy, chicken manure and wheat straw, Bioresour. Technol., 120: 78–83.

[15] Habiba, L., Hassib, B., & Moktar, H. (2009). Improvement of activated sludge stabilisation and filterability during anaerobic digestion by fruit and vegetable waste addition. *Bioresour. Technol.*, 100: 1555–1560.

[16] Kayhanian, M. (1999). Ammonia inhibition in high-solids biogasification: an overview and practical solutions. *Environ. Technol.*, 20: 355–365.

[17] Orhorhoro, E.K., Ebunilo, P.O.B., and Sadjere, E.G. (2017). Determination and Quantification of Household Solid Waste Generation for Planning Suitable Sustainable Waste Management in Nigeria. *International Journal of Emerging Engineering Research and Technology,* 5(8): 1-9

[18] Owamah, I.H., Izinyon, O.C., Igbinewekan, P. (2015). Characteristics and quantification of solid waste generation in the Niger Delta Region of Nigeria: a case study of Ogbe-Ijoih community in Delta State. *Journal of Material Cycles and Waste Management,* 19(1): 366-373

[19] Igbinomwanhia, D.I., Obanor, A.I., Olisa, Y.P. (2017). Characterisation of Domestic Solid Waste for the Determination of Waste Management Option in Amassoma, Bayelsa State, Nigeria". J. Appl. Sci. Environ. Manage, 18(2): 211-215

[20] Igoni, A.H., Ayotamuno, M.J., Eze, C.L., Ogaji, S.O.T., and Probert, S.D. (2008). Designs of anaerobic of digesters for producing biogas from municipal solid-waste. *Appl. Energ.,* 85: 430-438

[21] Food and Agriculture Organisation. E-conference: Utilization of Food Loss andWaste asWell as Non-Food Parts as Livestock Feed'|FAO. 2015. Available online: http://www.fao.org/save-food/news-and-multimedia/events/detail-events/en/c/325893/

[22] Zin, N.M., Saim, M., Suhaimi, A.H.M.S. (2018). Household food wastage prevention in Malaysia: An Issue Processes Model perspective. *Econ. Technol. Manag. Rev.,* 13, 51–62

[23] Gaida, D., Wolf, C., Meyer, A., Stuhlsatz, J., Lippel, T., Bäck, T., Bongards, M. and McLoone, S. (2012). State estimation for anaerobic digesters using the ADM1. *Water Science and Technology,* 66 (5), 1088

[24] Ge, X., Matsumoto, T., Keith, L., and Li, Y. (2014). Biogas energy production from tropical biomass wastes by anaerobic digestion. Bioresource Technology, 169: 38–44

[25] Franco, C., Gianluca, C., Alessandro, P., Valentina, C. (2015). Lignocellulosic biomass feeding in biogas pathway: state of the art and plant layouts. *Energy Procedia (Science Direct),* 81: 1231 – 1237

[26] Ray, N. H. S., Mohanty, M. K., and Mohanty, R. C. (2013). Anaerobic digestion of kitchen waste: Biogas production and pretreatment waste, a review. *International Journal of Scientific and Research Publication,* 3: 11-18

[27] Orhorhoro E.K., Orhorhoro, O.W., Atumah, E.V. (2018): "Performance Evaluation of Design AD System Biogas Purification Filter. *International Journal of Mathematical, Engineering and Management Sciences,* 3(1): 17–27

[28] Ebunilo, P.O., Orhorhoro, E.K., Adegbayi, O.A. (2016). Investigation of the purification of biogas from domestic wastes using local materials in Nigeria. *International Journal of Scientific & Engineering Research,* 7(2): 505-515

[29] Ejiroghene Kelly Orhorhoro, Emmanuel E. Lindsay, Joel O. Oyejide (2022). Analysis and Evaluation of a Three-Stage Anaerobic Digestion Plant for Management of Biodegradable Municipal Solid Waste. *International Journal of Engineering Research in Africa,* 60: 75-87. doi:10.4028/p-a24obb

[30] Qiao, W., Yan, X., Ye, J., Sun, Y., Wang, W., and Zhang, Z. (2011). Evaluation of biogas production from different biomass wastes with/without hydrothermal pretreatment. Renewable Energy, 36: 3313-3318

[31] Orhorhoro E.K., Ebunilo, P.B., Sadjere E.G. (2017). Effect of Organic Loading Rate (OLR) on BiogasYield Using a Single and Three-Stages Continuous Anaerobic Digestion Reactors. *International Journal of Engineering Research in Africa,* 39: 147-155. Doi:10.4028/www.scientific.net/JERA.39.147.

[32] Esposito, G, Frunzo L, Liotta, F, Panico, A. and Pirozzi, F. (2012). BMP tests to measure the biogas production from the digestion and co-digestion of Complex organic substrates. Open Journal of Environmental Engineering, 5: 1–8.

[33] Krishna, D., Kalamdhad, A.S. (2014). Pre-treatment and anaerobic digestion of food waste for high rate methane production–A review. *J.Environ. Chem. Eng.,* 2, 1821–1830

[34] Ariunbaatar, J., Panico, A., Esposito, G., Pirozzi, F., Lens, P.N.L. (2014). Pretreatment methods to enhance anaerobic digestion of organic solid waste. *Appl. Energy*, 123: 143–156

[35] Lee, B., Park, J.G., Shin, W.B., Kim, B.S., Byun, B., Jun, H.B. (2019). Maximizing biogas production by pretreatment and by optimizing the mixture ratio of co-digestion with organic wastes. *Environ. Eng. Res.*, 24: 662–669

[36] Hassan, M.A., Yacob, S. and Shirai, Y. (2004).Treatment of palm oil wastewaters. In: Wang, L.K., Hung, Y., Lo, H.H. and Yapijakis, C.,editors. *Handbook of industrial and hazardous wastes treatment*. New York. Marcel Dekker,Inc. 719– 36.

[37] Raposo, F., Fernández-Cegrí, V., De la Rubia, M.A., Borja, R., Béline, F., Cavinato, C., Ganesh, R. (2011). Biochemical methane potential (BMP) of solid organic substrates: evaluation of anaerobic biodegradability using data from an international interlaboratory study. *J. Chem. Technol. Biotechnol.,* 86:1088-98

[38] Orhorhoro, E.K., Ebunilo, P.O., and Ikpe, A.E., (2016). Effect of pH on Anaerobic Digestion (AD) of Organic Municipal Solid Waste in Benin City, Nigeria. *Journal of the Nigerian Association of Mathematical Physics,* 36(01): 369-374

[39] Paramagurua, G., Kannanb, M., Lawrencec, P. (2017). Effect of pH on Biogas Production through Anaerobic Digestion of Food Waste. *Journal of Advanced Engineering Research,* 4(1): 59-62

[40] El-Mashad, H.M., and Zhang, R. (2010). Biogas production from Co-digestion of dairy manure and food waste. *Bioresource Technology,* 101: 4021-4028

[41] Ebunilo, P.O., Orhorhoro, E. K., Oboh, V., Onochie, P. U (2016). Effect of Temperature on Biogas Yields Using South-South Nigeria as a Case Study. *International Journal of Technology Enhancements and Emerging Engineering Research,* 4(3): 50-54

[42] Zhou, Q., Shen, F., Yuan, H., Zou, D., Liu, Y., Zhu, B., and Li, X. (2014). Minimizing asynchronism to improve the performances of anaerobic co-digestion of food waste and corn stover. *Bioresource Technology*, 166: 31–36. http://dx.doi.org/10.1016/j. biortech.2014.04.074

[43] Zhou, P., Elbeshbishy, E., and Nakhla, G. (2013). Optimization of biological hydrogen production for anaerobic co-digestion of food waste and wastewater biosolids. *Bioresource Technology*, 130, 710–718

[44] Zhang, Y., Banks, C. and Heaven, S. (2012). Co-digestion of source segregated domestic food waste to improve process stability. *Bio-resource technology,* 114: 168-178

[45] Mahanty, B., Zafar, M. and Park, H.S. (2013). Characterization of Co-digestion of industrial sludges for biogas production by artificial neural network and statistical regression models. *Environ Technol.*, 34: 2145–2153

NIPES-NCEE Conference Proceedings
The 2nd International Conference 15th-17th Feb. 2023
512-521
www.nipesjournals.org.ng

OPTIMIZATION OF BIOGAS YIELD BY THE COMBINATION OF ALGAL BIOMASS AND FOOD WASTE

Ejiroghene Kelly Orhorhoro[*1], Joel Oluwayomi Oyejide [2], Tega Emmanuel Erokare [3]

[1]Department of Mechanical Engineering, General Abdulsalami Abubakar College of Engineering, Igbinedion University, Okada, Edo State, Nigeria
[2]Department of Mechanical Engineering, Federal University of Petroleum Resources, Effurun, Delta State, Nigeria
[3]Department of Agricultural and Biosystems Engineering, Faculty of Engineering, Delta State University of Science and Technology, Ozoro, Nigeria

Corresponding email: ejiroghene.orhorhoro@iuokada.edu.ng

Abstract
The possibility of algal biomass as a source of liquid and gaseous biofuels has been the subject of considerable discussion among researchers recently. Researchers totally agreed that algae have the potential to become a viable aquatic energy crop with a higher energy potential compared to that from either terrestrial biomass or municipal solid waste. In this study, an experimental biogas optimization via the use of algal biomass and food wastes as feedstock for biogas production was investigated. The collected algal samples were digested separately and co-digested with food waste collected from Igbinedion University restaurants using a batch bioreactor. The operating conditions of the biogas reactor were closely monitored. The results showed that the bioreactor was kept within a 37 ± 1°C mesophilic temperature range. Besides, average daily biogas yield of FW=0.21 m3, FWAB=0.26 m3, and AB=0.14 m3 was obtained. With higher biogas yield recorded with the co-digestion of food waste and algal biofuel (FWAB), there is huge potential for biogas production from algae biomass.

Keywords: *Algal Biomass, Food Waste, Anaerobic Digestion, Biogas, Batch Bioreactor*

1.0 Introduction
Algae are a large and very diverse group of organisms, ranging from simple unicellular microalgae to giant macroalgae. The morphology of macroalgae or seaweeds resembles that of terrestrial plants, but the biochemical composition is significantly different. The major carbon storage products in terrestrial plants are starch and fructose [1–3], which can be easily converted to biogas. The use of algae as a source of biofuels has been on the increase for the past 50 years, and this is due to the potential biomass yield of algae and cultivation systems that do not compete for land or fresh water with terrestrial crops [4, 5]. Nevertheless, despite the huge potential and the depth of research on its usability, there are no commercial-scale quantities of economically viable fuel from either micro- or macroalgae [6]. Besides, the dilute concentrations of microalgae in their growth medium and the high water content (80–90%) of algae impact adversely on the energy balance of processes that depend on dry biomass [7–10]. One of the critical challenges in achieving energy return from microalgae is harvesting and concentrating the algae [11–13]. This is because of several factors, including the small size of microalgae (30 m) [14]; the dilute nature of the microalgal suspension (0.02–0.05% dry solids) [15, 16]; the small differences in density of the algal cells relative to that of the growth medium [17]; and the negative charge on the surface of algal cells that results in dispersed, long-lasting algal suspensions [18–20]. Drying the harvested

biomass is also a highly energetic process and can use the equivalent of the vast majority of potential energy in the biomass [21, 22]. Algae are thus unattractive for direct combustion, pyrolysis, and gasification that require dry biomass due to the high energy inputs for moisture removal, but suitable for processes that use wet biomass [23-25] such as the biogas technology via anaerobic digestion and co-digestion.

Furthermore, the incessant high cost of fuel coupled with an increasing awareness of greenhouse gas emissions and global warming have promoted an interest in further anaerobic digestion process (ADP) research and industrial applications [26–31]. The ADP is viewed not only as a method for treating biodegradable organic wastes, sewage biosolids, livestock manure, and concentrated wastes from the food industry but also as a vital source of renewable fuel [32–35]. Different agricultural crops and terrestrial and aquatic plants have been reported in the past as an appropriate feedstock for AD [36–37]. Indeed, the National Algal Biofuels Technology Roadmap 2010 noted that anaerobic digestion is an underutilized technology for algal biofuel production that eliminates several of the key obstacles that are responsible for the current high costs associated with algal biofuels, and as such may be a cost-effective methodology [38–42]. Therefore, this present study is focused on the optimization of biogas yields by the combination of algal biomass and food waste.

2.0 Materials and Methods

The following materials and methods were applied in this study.

2.1 Materials

The materials and equipment used in this study include algal biomass, food waste, a batch bioreactor, a thermometer, a water plastic, a pressure gauge (accuracy ±0.02), a 100kg universal weighing scale (accuracy ±200 g), a gas bottle, a rubber hose, a manual compressor unit, a gas analyzer, and a pH meter.

2.1 Methods
Figure 1 shows the process diagram.

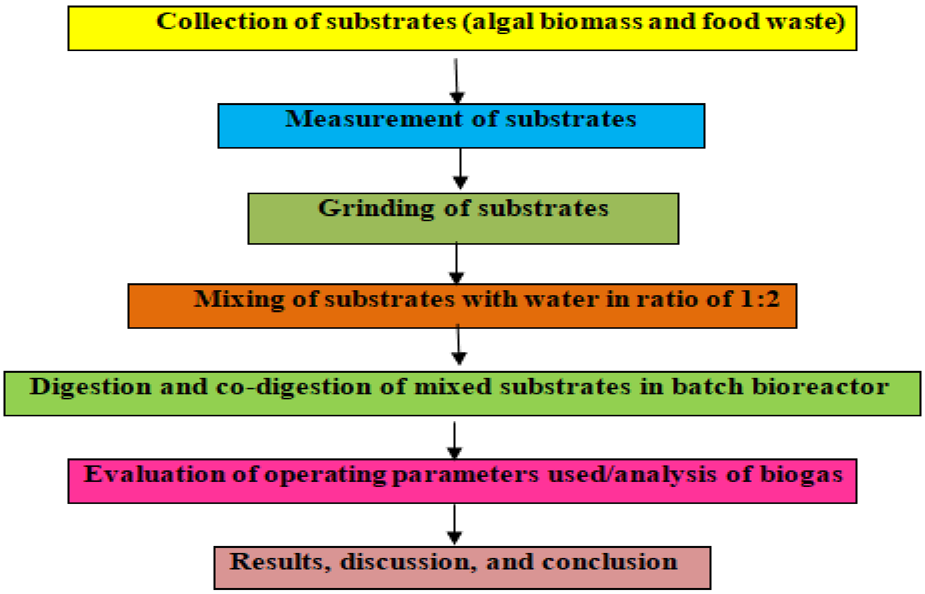

Figure 1 Process diagram

This section involves the collection of substrates used and the determination of the quantity of biogas it yields. The collected food wastes from Igbinedion University's Okada restaurant were ground into small particles mainly to increase their surface area and then mixed with water in a ratio of one to two (1:2). The sizes of substrates have direct effects on their anaerobic digestion in the bioreactor, and this calls for size reduction by grinding [43, 44]. Reduction of substrate sizes leads to an increased surface area for microbes to act on, thus improving the efficiency of the digester [44]. The mixture is loaded into the bioreactors and sealed. The bioreactor's content was stirred several times per day with the aim of mixing the substrates inside the digester for optimum biogas yield. Research has shown that biogas yield drops when stirring is completely avoided [45]. More so, stirring helps to break down the scum formed on the surface of the bioreactor contents and prevents the bacteria from becoming stagnant [46]. Besides preventing the formation of swimming layers and sediments, stirring also brings the microorganisms (MOs) into contact with the feedstock particles, facilitates the up-flow of gas bubbles, and homogenizes the distribution of heat and nutrients through the whole mass of substrates. The pressure, pH, and temperature readings were monitored using a thermometer, pH meter, and pressure gauge. The yielded biogas was analyzed for its composition using a gas chromatograph.

3.0 Results and Discussion

4.1 Comparative Analysis of Biogas Yield

Figure 2 shows the comparative analysis of biogas yield for a period of fifty days for co-digestion of a combination of food waste and algal biomass (sample = FWAB) and separate digestion of algal biomass (sample = AB) and food waste (sample = FW). Optimum biogas yields were observed for the combination of algal biomass and food waste (i.e., sample = FWAB) compared to separate digestion (i.e., sample = AB and sample = FW). More so, the highest biogas yield was equally observed in the combination of FWAB and was followed by FW and AB, respectively. All these point to the fact that algal biomass can be used to optimize biogas yields. Besides, this further confirms the reports of past researchers that suggested the use of algal biomass for biogas production through anaerobic digestion [4, 6, 7, 12, 19]. The results of the average daily biogas yield, as shown in Figure 3, confirm that sample FWAB yielded more biogas as compared to samples AB and FW. This confirms once again that the co-digestion of food waste with algal biomass will optimize biogas production.

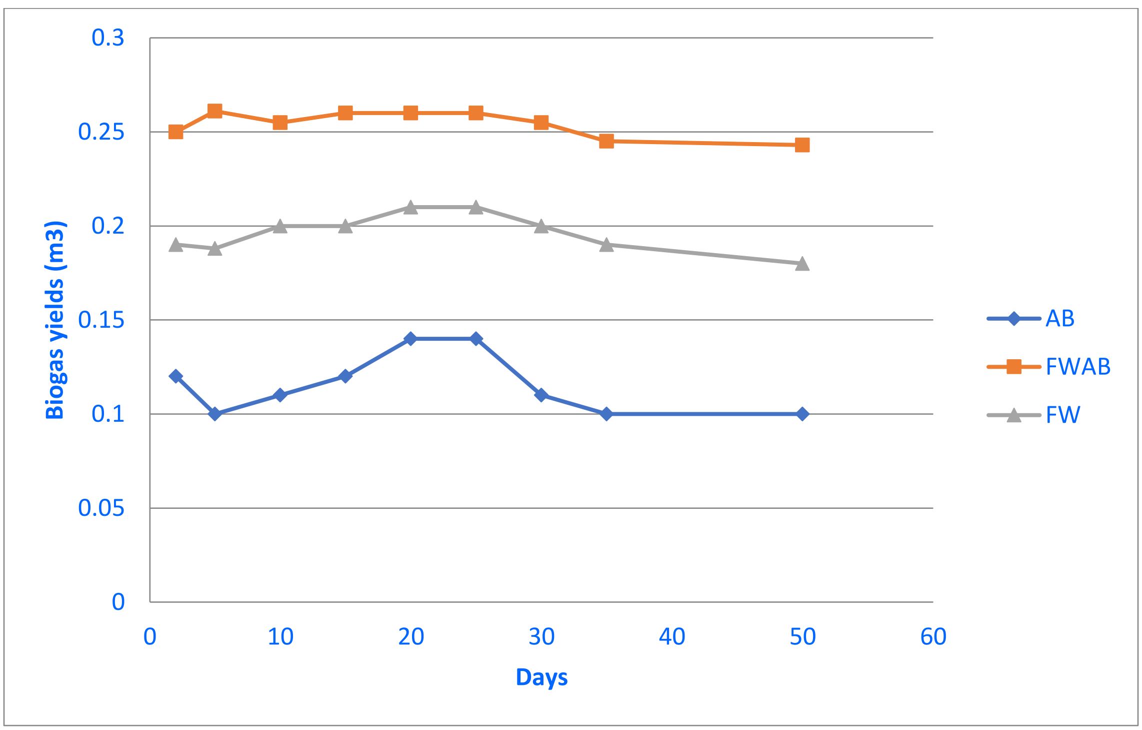

Figure 2 Evaluation of optimum biogas yield

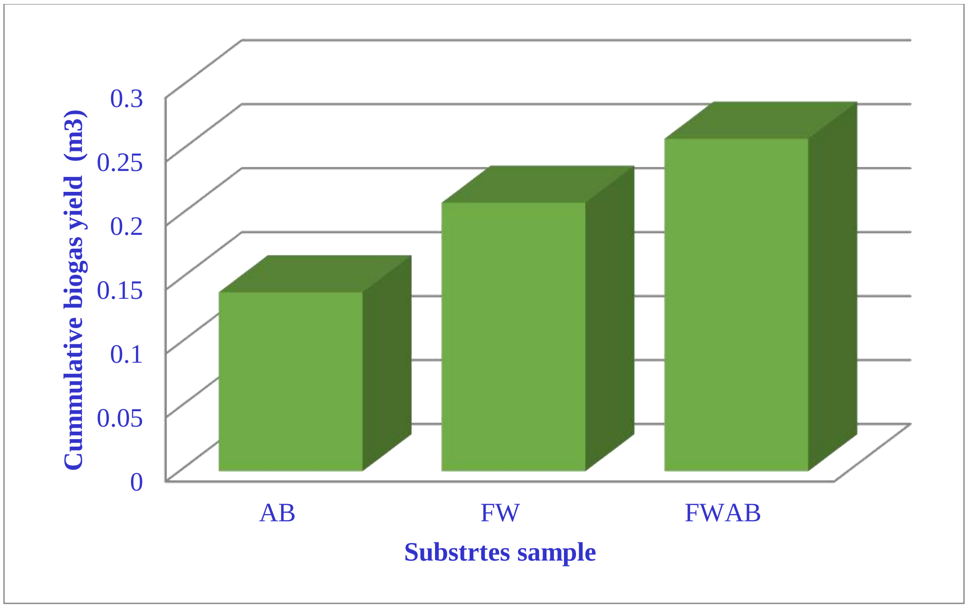

Figure 3 Comparative analysis of cumulative biogas yield

4.2 Evaluation of Effect of Temperature

Temperature is considered one of the most important variables for process stability, as anaerobic bacteria populations can only survive in certain temperature ranges. Besides, sudden changes and fluctuations in the process temperature lead to inhibition of bacteria populations. Therefore, for efficient results and stable anaerobic digestion plant operation to be attained, controlling the process temperature is always required [47]. The anaerobic digestion process can be operated in one of these three temperature ranges with the corresponding bacteria population. However, the mesophilic temperature range is preferred for most anaerobic digestion plants [47]. The main reasons for this are that the anaerobic digestion performance of psychrophilic and thermophilic bacteria is slower than that of mesophilic bacteria. Also, it is difficult to maintain anaerobic digestion plants under psychrophilic temperature conditions due to the low process temperature. Furthermore, thermophilic bacteria are known to be very sensitive to disturbances, which require costly process monitoring and control [45]. In general, optimum mesophilic temperature brings about shorter hydraulic retention time (more production of biogas) since more methanogenic bacteria are working upon the substrate [48]. To evaluate the effects and impact of mesophilic temperature on different substrates used in this research, a comparative analysis of the effect of mesophilic temperature was carried out (Figure 4). The outcome revealed that optimum mesophilic temperature ranges were used in this study, which agreed with the research work of [48]. Thus, temperature did not impart a negative effect on the results. Besides, it was observed that the temperature variation was 37 ^{o}C and approximately the same across each of the samples experimented with.

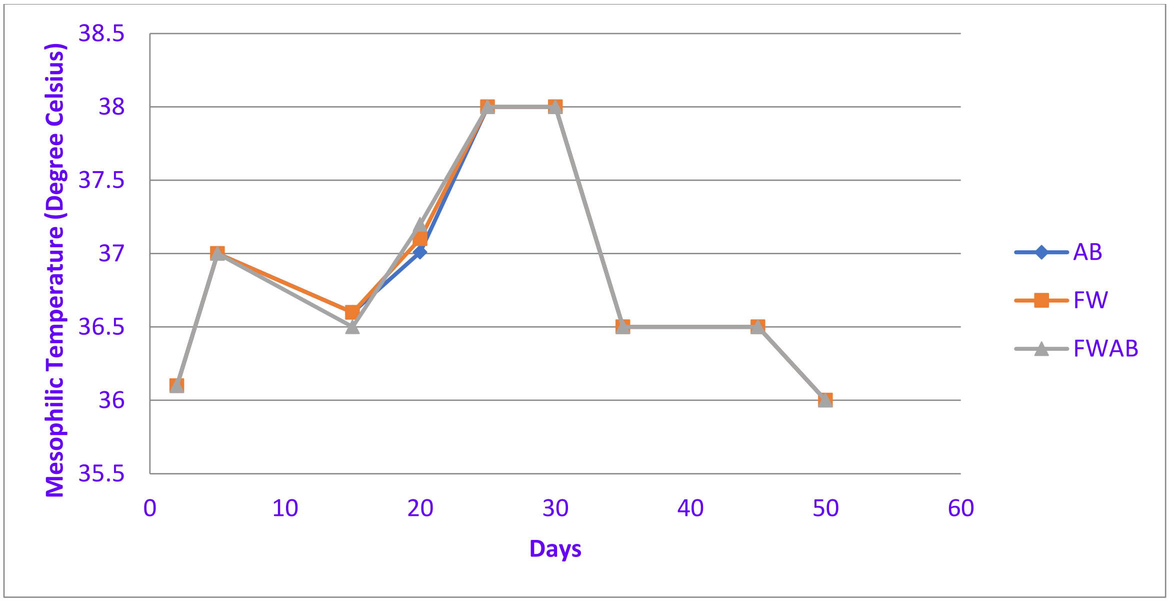

Figure 4 Evaluation of temperature on biogas yield

4.3 Evaluation of Effect of pH

Furthermore, the pH value of a stable anaerobic digestion process ranges between six and nine [49]. Methanogenesis, which is the stage at which methane is produced, is very sensitive to acidity. As a result, a pH range that is beneficial to methane-forming bacteria is required to reduce the toxicity of both free ammonia and free volatile acids [50, 51]. High or low pH values decrease or stop the activity of methane-forming bacteria. As shown in Figure 5, the pH readings of sample FWAB are within neutrality (pH = 7 m), and this is an indication of a healthy environment that favors optimum biogas yield. But this was not the case when the substrates were digested separately (i.e., samples AB and FW).

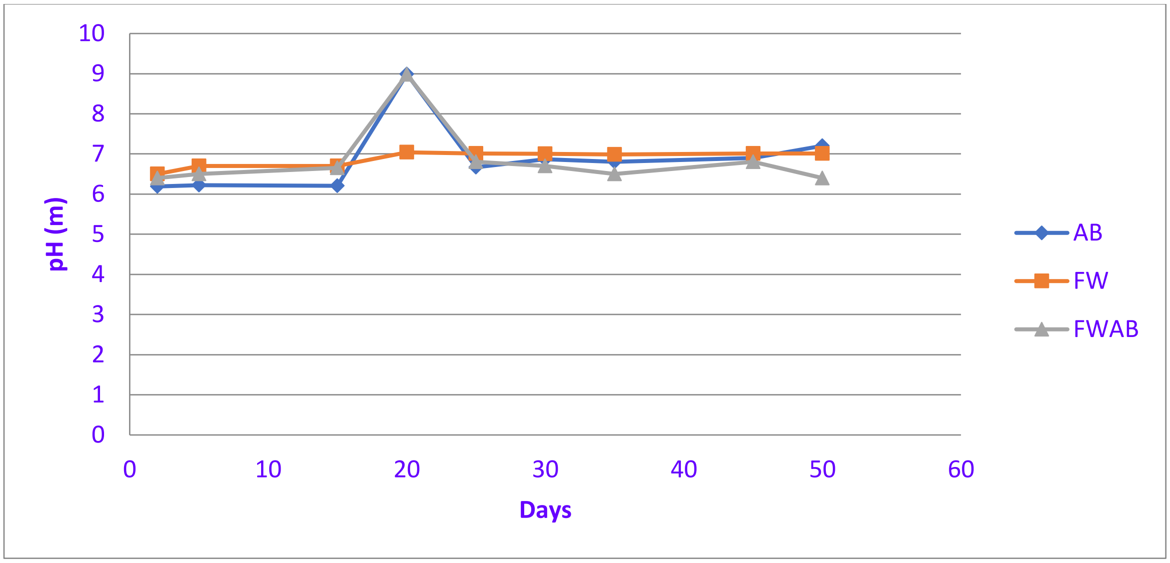

Figure 5 Evaluation of effect of pH on optimum biogas yield

4.0 Conclusion

Algal biomass represents a potential green bioenergy source for the production of biomethane when processed using biogas technology. In this study, optimization of biogas yield by the combination of algal biomass and food waste was investigated. The results obtained show the potency of algal biomass as an important substrate for biogas production. It was observed that an average daily biogas yield of FW=0.21 m^3, FWAB=0.26 m^3, and AB=0.14 m^3 was obtained. Besides, more biogas yield was recorded with the co-digestion of food waste and algal biofuel (FWAB). Thus, there is huge potential for biogas production from algae biomass.

References

[1] Chapin F.S., Schulze E., Mooney H.A. (1990). The ecology and economics of storage in plants. *Annu Rev Ecol Syst*., 21(1):423–447. doi: 10.1146/annurev.es.21.110190.002231

[2] Zeeman S.C., Kossmann J., Smith A.M. (2010). Starch: its metabolism, evolution, and biotechnological modi fi cation in plants. Annu Rev Plant Biol 61:209–234. doi: 10.1146/annurevarplant-042809-112301

[3] Somerville C., Bauer S., Brininstool G., Facette M., Hamann T., Milne J., Osborne E., Paredez A., Persson S., Raab T., Vorwerk S, Youngs H (2004) Toward a systems approach to understanding plant cell walls. Science 306(5705): 2206–2211. doi: 306/5705/2206[pii]10.1126/science.1102765

[4] Chen H., Qiu T., Rong J., He C., Wang Q. (2015). Microalgal biofuel revisited: An informatics-based analysis of developments to date and future prospects. *Appl. Energy*, 155, 585–598

[5] Kerrison P.D., Stanley M.S., Edwards M.D., Black K.D., Hughes A.D. (2015). The cultivation of European kelp for bioenergy: Site and species selection. *Biomass Bioenergy*, 80, 229–242

[6] Milledge J.J., Harvey P.J. (2016). Potential process 'hurdles' in the use of macroalgae as feedstock for biofuel production in the British Isles. *J. Chem. Technol. Biotechnol.,* 91, 2221–2234

[7] Milledge J.J., Heaven S. (2014). Methods of energy extraction from microalgal biomass: A review. *Rev. Environ. Sci. Biotechnol*., 13, 301–320

[8] Milledge J.J., Smith B., Dyer P., Harvey P. (2014). Macroalgae-Derived Biofuel: A Review of Methods of Energy Extraction from Seaweed Biomass. *Energies.,* 7, 7194–7222

[9] Sills D.L., Paramita V., Franke M.J., Johnson M.C., Akabas T.M., Greene C.H., Tester J.W. (2012). Quantitative Uncertainty Analysis of Life Cycle Assessment for Algal Biofuel Production. *Environ. Sci. Technol.,* 47, 687–694

[10] Fasaei F., Bitter J.H., Slegers P.M., Van Boxtel A.J.B. (2018). Techno-economic evaluation of microalgae harvesting and dewatering systems. *Algal Res.,* 31, 347–362

[11] Collet P., Helias A., Lardon L., Steyer J.P., Bernard O.(2015). Recommendations for Life Cycle Assessment of algal fuels. *Appl. Energy,* 154, 1089–1102

[12] Milledge J.J., Heaven S. (2013). A review of the harvesting of micro-algae for biofuel production. *Rev. Environ. Sci. Biotechnol.,* 12, 165–178

[13] Wang S.K., Stiles A.R., Guo C., Liu C.Z. (2015). Harvesting microalgae by magnetic separation: A review. *Algal Res.,* 9, 178–185

[14] Molina Grima E., Belarbi E.H., Acien-Fernandez F.G., Robles-Medina A., Yusuf C. (2003). Recovery of microalgal biomass and metabolites: Process options and economics. *Biotechnol. Adv.,* 20, 491–515

[15] Zamalloa C., Vulsteke E., Albrecht J., Verstraete W. (2011). The techno-economic potential of renewable energy through the anaerobic digestion of microalgae. *Bioresour. Technol.,* 102, 1149–1158

[16] Uduman N., Qi Y., Danquah M.K., Forde G.M., Hoadley A. (2010). Dewatering of microalgal cultures: A major bottleneck to algae-based fuels. *J. Renew. Sustain. Energy,* 2, 012701.

[17] Reynolds C.S. (1984). The Ecology of Freshwater Phytoplankton; Cambridge University Press: Cambridge, UK,.

[18] Edzwald J.K. (1993). Algae, bubbles, coagulants, and dissolved air flotation. *Water Sci. Technol.,* 27, 67–81.

[19] Moraine R., Shelef G., Meydan A., Levi A.(1979). Algal single cell protein from wastewater-treatment and renovation process. *Biotechnol. Bioeng.,* 21, 1191–1207.

[20] Packer M. (2009). Algal capture of carbon dioxide; biomass generation as a tool for greenhouse gas mitigation with reference to New Zealand energy strategy and policy. *Energy Policy.,* 37, 3428–3437

[21] Bruton T., Lyons H., Lerat Y., Stanley M., Rasmussen M.B. (2009). A Review of the Potential of Marine Algae as a Source of Biofuel in Ireland; Sustainable Energy Ireland: Dublin, Ireland

[22] Milledge J.J., Staple A., Harvey P. (2014). Pyrolysis of Invasive Seaweed Species. In Proceedings of the British Phycological Society Annual Meeting, Galway, Ireland, 25–27 June.

[23] Horn, S.V. (2000). Bioenergy from Brown Seaweeds; Norwegian University of Science and Technology (NTNU):Trondheim, Norway.

[24] Murphy F., Devlin G., Deverell R., McDonnell K. (2013). Biofuel Production in Ireland An Approach to 2020 Targets with a Focus on Algal Biomass. *Energies 2013,* 6, 6391–6412

[25] Milledge J.J., Staple A., Harvey P. (2015). Slow Pyrolysis as a Method for the Destruction of JapaneseWireweed, Sargassum muticum. *Environ. Nat. Resour. Res*. 2015, 5, 28–36

[26] Orhorhoro E.K., Ebunilo, P.B., Sadjere E.G. (2017). Effect of Organic Loading Rate (OLR) on BiogasYield Using a Single and Three-Stages Continuous Anaerobic Digestion Reactors. *International Journal of Engineering Research in Africa,* 39: 147-155. Doi:10.4028/www.scientific.net/JERA.39.147.

[27] Jha, A. K., Li, J., Nies, L. and Zhang, L. (2013). Research advances in dry anaerobic digestion process of solid organic wastes. *Africa Journal Biotechnology,* 10: 14242-14253

[28] Jonas, L., Simon, Z., Hans, O., and Andreas, L. (2014): ―Effect of different pH-values on process parameters in two-phase anaerobic digestion of high-solid substrates. *Journal Environmental Technology,* 36(2): 12-20

[29] Orhorhoro E.K., Orhorhoro O.W., Atumah E.V. (2018). Performance Evaluation of Design AD System Biogas Purification Filter. *International Journal of Mathematical, Engineering and Management Sciences*, 3: 17–27. Doi: 10.33889/IJMEMS.2018.3.1-003.

[30] Paramagurua, G., Kannanb M., Lawrencec P., Thamilselvand D. (2017). . Effect of total solids on biogas production through anaerobic digestion of food waste. *Desalination and Water Treatment,* 63: 63–68.

[31] Karthikeyan, O.P. and Visvanathan, C., (2012). Bio-energy recovery from high-solid organic substrates by dry anaerobic bio-conversion processes: a review. *Rev. Env. Sci. Biotechnol.,* 12: 257-284.

[32] Katare, S. and Dal C.R. (2016). Biogas Purification and Enrichment through Stepped Scrubbing. *International Journal of Engineering Sciences and Research Technology,* 5(7): 795-799

[33] Orhorhoro E.K., Ebunilo P.O., Sadjere E.G. (2017). Development of a Predictive Model for Biogas Yield Using Artificial Neural Networks (ANNs) Approach. *American J. of Energy and Power Eng.,* 4: 71-77.

[34] Orhorhoro, E.K, Orhorhoro, O.W and Ebunilo, P.O. (2016). Analysis of the effect of Carbon/Nitrogen (C/N) ratio on the performance of biogas yields for non-uniform multiple feed stock availability and composition in Nigeria. *International Journal of Innovative Science, Engineering & Technology,* 3(5): 119-126

[35] Orhorhoro, E.K., Ebunilo, P.O., and Ikpe, A.E., (2016). Effect of pH on Anaerobic Digestion (AD) of Organic Municipal Solid Waste in Benin City, Nigeria. *Journal of the Nigerian Association of Mathematical Physics,* 36(1): 369-374

[36] Ejiroghene Kelly Orhorhoro, Emmanuel E. Lindsay, Joel O. Oyejide (2022). Analysis and Evaluation of a Three-Stage Anaerobic Digestion Plant for Management of Biodegradable Municipal Solid Waste. *International Journal of Engineering Research in Africa,* 60: 75-87. doi:10.4028/p-a24obb

[37] Nimas, M.S., Minming, Z., Zhezi, Z., and Dongke, Z. (2017): ―Effect of Biochar Addition and Initial pH on Hydrogen Production from the First Phase of Two-Phase Anaerobic Digestion of Carbohydrate Food Waste. *Energy Procedis-Elsevier Journal,* 105: 379-384

[38] Wang S., Wang Q., Jiang X.M., Han X.X., Ji, H.S. (2013). Compositional analysis of bio-oil derived from pyrolysis of seaweed. *Energy Conv. Manag.,* 68: 273–280

[39] Jankowska E.. Sahu A.K., Oleskowicz-Popiel P. (2017). Biogas from microalgae: Review on microalgae's cultivation, harvesting and pretreatment for anaerobic digestion. *Renew. Sustain. Energy Rev.,* 75: 692–709

[40] Solé-Bundó M., Garfí M., Matamoros V., Ferrer, I. (2019). Co-digestion of microalgae and primary sludge: Effecton biogas production and microcontaminants removal. *Sci. Total Environ.*

[41] Oliveira J.V., Alves M.M., Costa J.C. (2015). Optimization of biogas production from Sargassum sp. using a design of experiments to assess the co-digestion with glycerol and waste frying oil. *Bioresour. Technol., 175*: 480–485

[42] Angelidaki I., Karakashev D., Alvarado-Morales M. (2017). Anaerobic Co-Digestion of Cast Seaweed and Organic Residues, Technical University of Denmark: Lyngby, Denmark

[43] Shahriari, H., Warith, M., Hamoda, M., and Kennedy, K. (2013): ―Evaluation of single vs. staged mesophilic anaerobic digestion of kitchen waste with and without microwave pretreatment. *Journal of Environmental Management,* 125: 74–84

[44] Orhorhoro, E.K., Ebunilo, P.O.B., and Sadjere, E.G. (2017). Design of Bio-Waste Grinding Machine for Anaerobic Digestion (AD) System. *European Journal of Advances in Engineering and Technology,* 4 (7): 560-568

[45] Edmond, D., Etleva, J., Valdete, V., Erta, D., and Enkeleida, S. (2017). Temperature and Stirring Effect of Biogas Production from Two Different Systems. *American Journal of Energy Engineering,* 5(2):6-10

[46] Yaqin, Y., and Xiwu, L. (2013). Effect and mechanism of stirring on cyanobacteria anaerobic fermentation for biogas production. *Journal of Food, Agriculture and Environment (JFAE),* 11(3-4): 1954-1959

[47] Osita, O.O., and Lawan, U. G. (2014). The Optimum Mesophilic Temperature of Batch Process Biogas Production from Animal-based Wastes. *Research Journal of Applied Sciences, Engineering and Technology,* 8(16): 1772-1776

[48] Ebunilo, P.O., Orhorhoro, E. K., Oboh, V., Onochie, P. U (2016). Effect of Temperature on Biogas Yields Using South-South Nigeria as a Case Study. *International Journal of Technology Enhancements and Emerging Engineering Research,* 4, (3): 50-54

[49] Chrish, K. (2013). Variation of methane and carbon dioxide yield in a biogas plant‖. MSc Thesis report 2013. Department of Energy Technology Royal Institute, Royal Institute of Technology Stockholm, Sweden

[50] Jonas, L., Simon, Z., Hans, O., and Andreas, L. (2014): ―Effect of different pH-values on process parameters in two-phase anaerobic digestion of high-solid substrates‖. Journal Environmental Technology, 36(2): 12-20

[51] Orhorhoro, E.K., Ebunilo, P.O., and Ikpe, A.E., (2016). Effect of pH on Anaerobic Digestion (AD) of Organic Municipal Solid Waste in Benin City, Nigeria‖, Journal of the Nigerian Association of Mathematical Physics, 36(1): 369-374

NIPES-NCEE Conference Proceedings
The 2nd International Conference 15th-17th Feb. 2023
522-535
www.nipesjournals.org.ng

DESIGN AND FABRICATION OF AN ELECTRIC BICYCLE FROM RECYCLED MATERIALS

Umukoro Emmanuel Oghenerukevwe, Onobun Osegiele Emmanuel, Avweromre Ogheneruemu Isaiah, Okhueleigbe Oselu Divine and Godspower Linus Sunday

Department of Mechanical Engineering, University of Benin, P.M.B 1154, Benin City, Nigeria.

Corresponding email: emmanuel.umukoro22@gmail.com, Sunday.linus@uniben.edu

Abstract

Electric vehicles (EVs) have long been recognized as a sustainable and efficient mode of transportation, but their high cost and limited customization options have hindered widespread adoption. This research project aims to address this issue by designing and fabricating an affordable and customizable electric bicycle using a converted car alternator as an electric motor.

The design and fabrication process followed a systematic approach, including research and sourcing of materials, conversion of a used car alternator into an electric motor, creation of a 3D model using computer-aided design software, and fabrication and testing of prototypes. The resulting electric bicycle is not only affordable and customizable but also meets all necessary safety and performance standards.

The electric bicycle designed in this project is a significant step towards addressing the problem of high cost and limited customization options in EVs and brings us closer to a greener future with more accessible and sustainable transportation options. The use of a converted car alternator as an electric motor also reduces waste by repurposing existing resources.

In this report, we present the details of the design and fabrication process and the results of our testing, making it a valuable resource for those interested in sustainable transportation, electric vehicles, and alternative energy.

Keywords*: Electric Vehicle, Green Energy, Pedelec, Alternator, Motor, Bicycle.*

1.0 Introduction

Transportation plays a crucial role in our daily lives and its impact on the environment and sustainability has never been more important. Due to the rapidly dwindling resources of gasoline, diesel, and natural gas, the energy crisis is one of the biggest issues facing the globe today. Another factor that contributes to the economic decay manifests in the form of large amounts of automobile waste that litter in the Nigerian landscape, since there are no regulations regarding the quality and quantity of vehicles that can be imported and a lack of technology to deal with automotive waste. The majority of vehicles imported into Nigeria are rickety and are mostly out of use. [1]. The recent innovations in the automobile industry as seen in Europe and the United States are geared toward the mass production and adoption of eco-friendly 'greener' electric vehicles, a consequence of this would result in the mass inflow of used vehicles to developing countries, Nigeria inclusive. The popular dump site for these vehicles in a developing country like Nigeria are at undeveloped plots of land set aside for car mechanics, popularly known as a Mechanic village. The trade at these sites includes repair and maintenance of automobile and they engage in trade of spare parts. [2].

The adoption of clean energy automobile vehicles should also be encouraged in developing countries so they can be on par with the economic developments in developed countries. [3] proposes that the hybrid bicycle market has enormous growth potential in the automotive sector. Bicycles were the most popular form of transportation during the movement toward environmentally friendly technologies, and when fuel prices have increased and environmental concerns have been taken into account, we have to admit that using a bicycle for short trips is much preferable to using a motor vehicle.

The Electric bicycle is a hybrid vehicle with an electric engine that power motion. They serve as a cheaper, eco-friendly mode of transportation to overcome the daily hassle of traffic jam and helps people get to their destination fast without increased effort while providing better maneuverability than cars. The main concept for the electric bicycle's motion cycle involves attaching a motor that is battery powered and can be regulated to switch on during rough terrains and turned off to pedaled to recharge the batteries while moving over smooth or flat terrains. The high cost of and limited customization options of electric vehicles have been a barrier to its widespread adoption. However, in this research project we tend to address this issue by designing and fabricating an affordable and customizable electric bicycle using a converted car alternator as an electric motor.

In principle the viability of using an automobile alternator for high powered applications like a wind energy system is still being discussed but it can be converted to a powerful dc motor for powering an electric bicycle. An intriguing secret is hidden by the vehicle alternator. They are recognized as the component that transforms internal combustion energy into the electricity required to power everything else, but they can also function independently as an electric motor. These alternators in order to reduce the greater AC voltage to 12V for the automotive electrical systems, usually comes with a rectifier and regulator pack system. They take the shape of a 3-phase alternator with the magnetic component supplied by an electromagnet on the rotor. On the inside, they have two connections to a set of brushes that feed the rotor coils through a set of slip rings, three connections to the stator coils, which appear to be universally wired in a delta configuration. They have an incredibly large capacity, and estimates place its motor power at several horsepower [4].

2.0 Methodology

In order to accomplish the project's goal, relevant material was researched, and various bicycle fabrication configurations were examined and taken into consideration to build a fully functional pedal assisted (pedelec) bicycle. To effectively carry out the project, three design concepts were proposed as regards the placement of the electric motor in designing the pedelec as analyzed below:

Concept One: Front Hub Motor Design

An e-bike with a front hub motor has the motor mounted to the front fork of the wheel. The bike has a good weight balance as a result of the placement of the battery and motor. This gives the bike a good balance and makes it simple to ride. The engine pulls the bike forward as soon as you begin cycling once it is turned on, allowing you to rapidly begin cycling. Front hub motors are usually lighter than rear hub motors by 2 to 5 pounds, they also allow for additional drivetrain options including belt drive, 1X gearing, and internal gear hubs. The drawbacks to their usage stem from them being less durable and giving a rougher riding experience with poor traction.

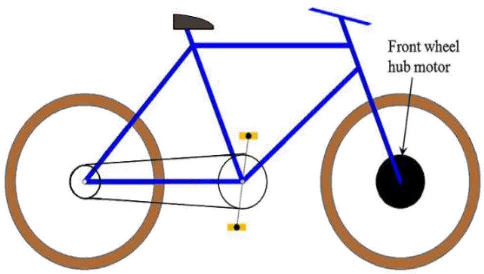

Figure 24 Front Hub Motor design

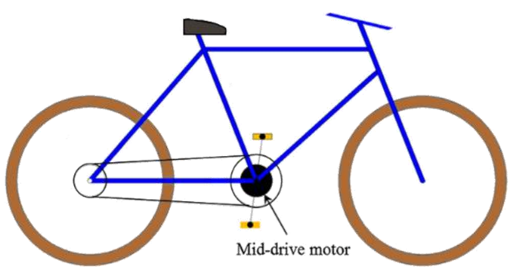

Figure 25 Middle Drive Design

Concept Two: Mid-Drive Motor Design

A mid-drive motor is positioned low and in the middle of the electric bicycle, improving weight distribution. The front and rear wheels are simpler to remove because of the Electric Bicycle's centrally positioned motor. They offer improved weight distribution and easier are often easier to maintain. They fall short in their ability to generate noise while riding and they get hot quickly.

Concept Three: Rear Hub Motor Design

In this configuration the bike's rear wheel houses the rear hub motor. These motors start working as soon as you start pedaling and are quieter than mid-drive motors, making it simple to begin going. Because the bike's back-end houses both sorts of motors, this side is a little heavier than the front and provides the motor with a lot of pushing power that aids in forward motion.

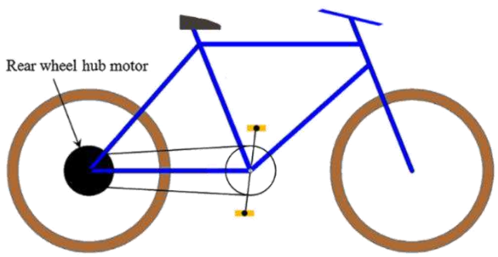

Figure 3 - 26 Rear Hub Motor

Design Methodology

The design concept adopted for this research work was an hybrid of the rear hub concept with the application of a drive train overdrive system for delivering high torque for smoother ride experience.

Figure 4 final design of the E-bike with mounted motor

Motor Housing Mount - Design and Materials:

The motor mount is made from mild steel, which is a strong and durable material that is resistant to corrosion and fatigue. It is of rectangular shape with slanted protruding legs that are connected to the rear wheel tires. It is made from a 28cm in length, 15 cm in breadth and 3.5 cm width, made from length-angle iron of 3mm thickness. The mount is attached to the frame using bolts and welding joints has a slot for the motor axle to fit into.

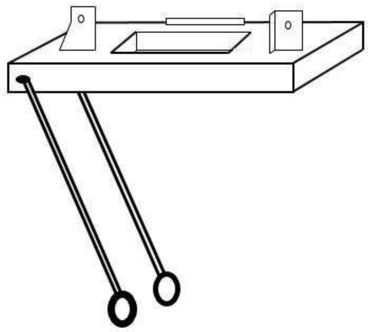

Figure 5 Isometric sketch of motor housing

Alternator To Dc Motor Conversion:

a. The unwanted components of the alternator were removed, these components includes the motor housing, the voltage regulator, the diode rectifier and the brush assembly.

b. The power supply to the alternator was connected using a solder and wire, this is done after converting the alternator to a star coil winding.

c. Test for motor functionality was carried out, to ensure the motor output match the needed power and toque output to allow for motion.

d. once the desired output was obtained the brushes were adjusted and the commutator cleaned, then all damaged parts were replaced.

Analysis Of the Transmission System

Gear Ratio:

The gear ratio is the relationship between the number of teeth on the chainring and the number of teeth on the sprocket. It determines the resistance of the pedals and the speed of the bicycle.

$$\text{Gear ratio} = \frac{Number\ of\ teeth\ on\ chainring}{Number\ of\ teeth\ on\ the\ sprocket} \quad [5]$$

Pedal – Rear Wheel Drive
Number of teeth on chainring = 43
Number of teeth on rear wheel sprocket = 15
Gear Ratio for pedal drive = 43/15 = 2.86 ~ 3: 1
Motor - Rear Wheel Drive

Number of teeth on motor sprocket = 16
Number of teeth on rear wheel sprocket = 21
Gear Ratio for motor drive = 16/21 = 1: 1.3 (Overdrive mechanism)
The higher gear ratio in the pedal drive signifies that the pedal drive provides faster acceleration and better torque, while the lower gear ratio of the motor drive provides a higher top speed as opposed to torque.

Figure 6 Transmission system for pedal and motor drive

Electrical Control System

The Fabricated charging system comprises of a Step-down transformer that converts 220v AC into 12V, this voltage is then passed through a Rectifier block that converts the 12V AC into 12V DC current which becomes sufficient for charging the batteries in parallel.

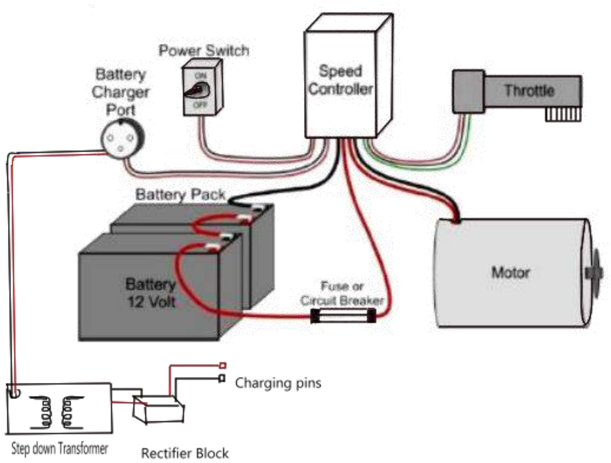

Figure 727 Circuit representation of the fabricated Electric bicycle

Battery Specifications

The electric bicycle is a pedal-assist e-bike designed for urban commuting. The battery system plays a critical role in the performance and reliability of the e-bike.
Battery Type: Lead-acid batteries
Capacity: There are 5 12V 8 amps batteries connected in series for use, A total of 48V (4 batteries) is used for powering the electric bicycle, the last battery is for the motor rotor.
Charge time: The battery can be charged when connected in parallel and can be charged fully in approximately 5 hours. When in use the battery can last up to 3 hours on full use.
Weight: Each battery weight 1.8kg, hence total battery weight is 9kg

Figure 8 a battery weight measurement, b battery charger weight

Usage Manual and Safety Guidelines for the Fabricated E-Bicycle

1. Familiarize yourself with the bicycle: Before riding the bicycle, it is important to familiarize yourself with the various components and controls, including the pedals, handlebars, brakes, and any other features.
2. Check the safety of the bicycle: Before riding the bicycle, it is important to perform a basic safety check to ensure that the bicycle is in good condition. This can include checking the brakes, tires, and other components for wear or damage, and making sure that all lights and reflectors are working properly.
3. After successfully mounting the electric bicycle with safety gear on, it is important to pedal the bicycle so as to ensure the chain and sprockets are properly positioned before switching on the motor switch to allow for throttle mode.
4. Use the pedal-assist feature appropriately: The pedal-assist feature on a pedelec can provide an extra boost of power to help you ride up hills or cover longer distances. It is important to use this feature appropriately, such as only activating it when needed.
5. Pedal the bicycle: While the pedal-assist feature can be helpful, it is important to remember that it is still important to pedal the bicycle yourself. Relying solely on the pedal-assist feature can result in a less effective workout and may cause the battery to drain more quickly. Also, remember to charge the batteries with the charging module provided in the correct sequence.
6. Stay alert and ride defensively: As with any bicycle, it is important to stay alert and ride defensively when using a pedelec. This includes keeping an eye out for pedestrians, vehicles, and other hazards, and taking appropriate action to avoid collisions or accidents.

Maintenance Manual for Fabricated Electric Bicycle

Proper maintenance is important to ensure the safe and reliable operation of your fabricated electric bicycle. This manual provides guidelines for the routine maintenance. It is important to follow these guidelines to help extend the life of your bicycle and ensure that it performs at its best.

Routine Maintenance

a) **Check the tire pressure regularly**: Proper tire pressure is important for the safety and performance of your pedelec. It is a good idea to check the tire pressure at least once a week, using a tire pressure gauge to ensure that the pressure is within the recommended range.
b) **Lubricate the chain**: The chain is an important component of your pedelec and it is important to keep it lubricated to prevent rust and wear. It is a good idea to apply a light coat of bike-specific chain lubricant every few weeks, or more frequently if the bicycle is used in wet or dirty conditions.
c) **Clean the bicycle regularly**: It is a good idea to clean your pedelec regularly to remove dirt and grime that can accumulate on the frame, components, and drivetrain. Use a soft brush and a mild soap solution to clean the bicycle, and be sure to dry it thoroughly afterward.
d) **Check and tighten bolts and nuts**: It is important to regularly check the bolts and nuts on your pedelec to ensure that they are tightened to the correct torque. Use a torque wrench to tighten any bolts or nuts that are loose, and replace any that are stripped or damaged.

e) **Inspect the brakes**: The brakes are an important safety feature on your pedelec, and it is important to regularly inspect them to ensure that they are functioning properly. Check the brake pads for wear, and adjust or replace them as needed.

Other Maintenance

i. **Replace worn or damaged components**: If you notice any components that are worn or damaged, it is important to replace them as soon as possible. This can include components such as tires, tubes, chains, and brake pads.
ii. **Charge the battery regularly**: The battery is an important component of your pedelec, and it is important to keep it charged to ensure that the bicycle is ready to ride. It is a good idea to charge the battery at least once a week, or more frequently if the bicycle is used frequently.
iii. **Store the bicycle properly**: When not in use, it is important to store your pedelec in a dry, protected location to help prevent rust and other damage. If possible, store the bicycle indoors or in a covered area, and avoid leaving it in direct sunlight or extreme temperatures.

3.0 Results and Discussion

The electric bicycle design focused on maximizing the efficiency and performance of the electric drivetrain while minimizing the weight and cost of the vehicle.

To achieve these goals, we obtained a high-efficiency BLDC (brushless DC) motor with a rated power output of 250 watts and a torque of 0.8 Nm. We also used 5 lead acid batteries with a capacity of 12 volts each and 8 amp-hours, which were sized to provide a range of approximately 30-40 kilometers (depending on the terrain and rider input).

Overall, the results of the testing for a cyclist of 73kg showed that the electric bicycle performed well in a range of conditions, with a top speed of approximately **15-20 km/h,** a **0-15** km/h acceleration time of approximately 6 seconds, and a range of approximately 25-30 km on a single charge.

The handling and stability of the bicycle were also found to be excellent, with smooth and responsive steering and a comfortable and stable ride. To provide for better brake functionality a stronger V-clamp break was used, and to give extra stability to the rear wheel, a bigger hub was installed to support the weight of the Electric bicycle.

The mechanical power of the BLDC motor was calculated using the equation:

$$P = \omega \times T \qquad [6]$$

where P is the mechanical power (in watts), ω is the angular velocity of the motor (in radians per second), and T is the torque (in newton-meters). The angular velocity of the motor was calculated using the equation:

$$\omega = (2\pi \times n) / 60 \qquad [6]$$

where ω is the angular velocity (in radians per second), n is the speed of the motor (in revolutions per minute), and 2π is the constant equal to approximately 6.28.

The speed of the motor was measured to be 2852 rpm, with an electric power rating for our motor being 250 watts, and the torque of the motor was measured to be 0.837 Nm

Torque Transmitted to real wheel becomes:

$P = 2 \times \pi \times N \times T / 60$

$250 = 2 \times \pi \times 2852 \times T /60$

$T = 0.837$ N m

Using these values, the angular velocity of the motor was calculated to be 314.16 radians per second (

$\omega = (2\pi \times 2852) / 60) = 298.66$ radians per second

The mechanical power of the motor was then calculated to be approximately

0.837 Nm x 298.66 radians per second = 249.98 watts.

This result indicates that the BLDC motor has a mechanical power output of approximately 249.98 watts at a speed of 2852 rpm and a torque of 0.837 Nm.

It can be observed that there is an overdrive system as the speed transferred from the electric motor to the rear wheel through the chain drive is greater but with a reduced torque.

Table 1 overdrive comparison for motor and rear wheel

Component	Speed (rpm)	Torque (Nm)
Electric motor output	2852	0.837
Rear wheel	3000	0.796

Test Results

The test was conducted using a range of rider weights and the data obtained from each test ride are as follows:

Table 2 Test Results and Values

Rider	Weight (kg)	Power output (W)	Maximum speed (km/h)	Battery life (h)
1	67.0	240	21.9	2.4
2	77.4	248	21	2.0
3	65.8	235	22.3	2.5
4	60.1	220	24	2.8
5	75.0	247	22	2.3
6	100.0	261	12	0.89

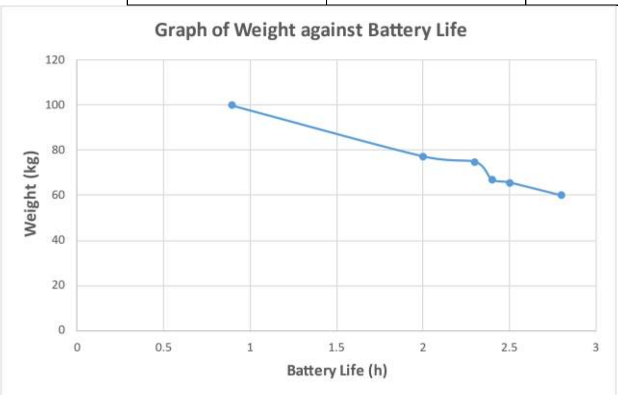

Figure 9 Result graph for cyclist weight vs battery life

4.0 Graphical Modelling and Design for the fabricated E-bike

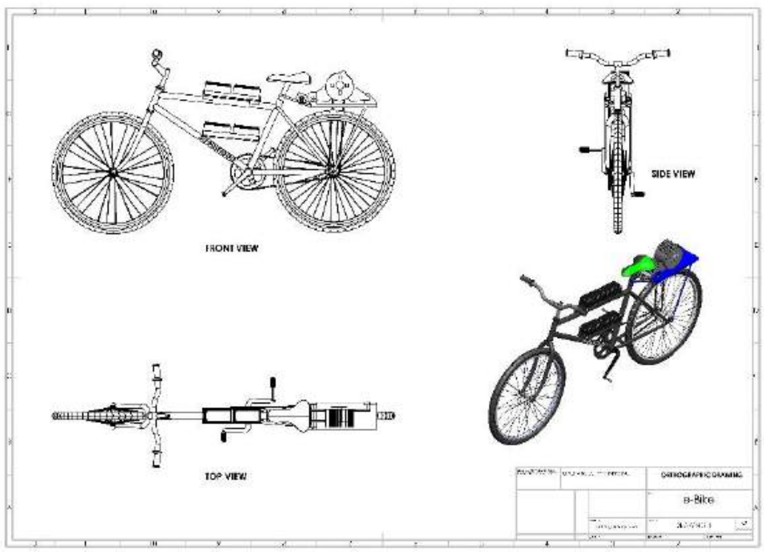

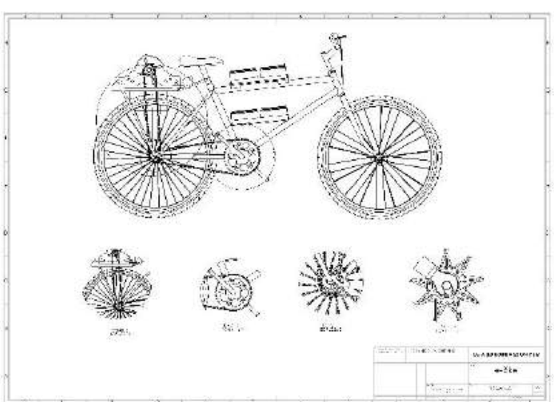

5.0 Conclusion

The design, analysis, and fabrication of an electric bicycle is a complex and challenging task that requires a thorough understanding of electrical and mechanical engineering principles. By using the latest technologies and materials, and following a rigorous design and testing process, it is possible to create an electric bicycle that is reliable, efficient, and capable of meeting the needs of a wide range of users. The results of this project demonstrate that it is possible to design and build an electric bicycle that is cost-effective, environmentally friendly, and capable of providing an enjoyable and convenient transportation option for commuters, recreational riders, and people with disabilities, at the breath addressing the issue of high cost and limited customization options in electric vehicles.

References

[1] J. K. Nduka, H. I. Kelle, e. c. ogoko and p. c. okafor, "Review of Environmental and Public Health Impact of Automobile Wastes and Automobile Transportation in Nigeria," 2019. [Online]. Available: https://www.intechopen.com/chapters/68599. [Accessed 23 october 2022].

[2] M. Nwachukwu, H. Huan and K. Achilike, "Integrated study for automobile wastes management and environmentally friendly mechanic villages in the Imo River basin, Nigeria," *African Journal of Environmental Science and Technology,* vol. iv, no. 4, 2010.

[3] V. Kumar, A. Karthik , A. Roshan and A. Kumar, "Design and Implementation of Electric Assisted Bicycle with Self Recharging Mechanism," *International Journal of Innovative Research in Science, Engineering and Technology,* vol. iii, no. 5, pp. 485-486, 2014.

[4] J. List, "CAR ALTERNATORS MAKE GREAT ELECTRIC MOTORS; HERE'S HOW," 2020. [Online]. Available: https://hackaday.com/2020/01/16/car-alternators-make-great-electric-motors-heres-how/. [Accessed 23 october 2022].

[5] B. John, Electrical Circuit Theory and Technology (2nd Edition), London: Routledge, 2003.

[6] R. Hibbeler, Engineering Mechanics, Upper Saddle River, New Jersey: Pearson Prentice Hall, 2009.

NIPES-NCEE Conference Proceedings
The 2nd International Conference 15th-17th Feb. 2023
536-544
www.nipesjournals.org.ng

DESIGN AND INSTALLATION OF A CAPACITY LIMITING RFID ACCESS CONTROL SYSTEM

Moluno Richie Chukwunalu, Oyakhilome Lordson Osenegame, Ika Kevwe Ntow, Fidelis Endurance David, P.O Olagbegi

Department of Mechanical Engineering, University of Benin, P.M.B. 1154, Benin City, Nigeria

Corresponding emails: olagbegi@uniben.edu, molunorichie@gmail.com

Abstract

Radio Frequency Identification (RFID) access control systems are a vital component of any security system. They are used to control access to restricted areas and to ensure that only authorized personnel are allowed access. The use of RFID access control systems helps to reduce the risk of unauthorized access and to increase the safety and security of a facility. Capacity limiting RFID access control systems are designed to limit the number of people who can access a facility at any given time. This is important for ensuring that only the required number of personnel are allowed access to the restricted area. It also helps to reduce the risk of overcrowding in areas where large numbers of people are allowed access.

This project involves the design and installation of a capacity limiting RFID access control system to improve security and safety in an area at the Faculty of Engineering. The system was designed to utilize Radio Frequency Identification (RFID) technology to identify and authenticate users, as well as limit the number of users who can access the area at any given time. The system was designed to be flexible and customizable, allowing for the addition of extra hardware and software components as needed. The installation of the system include the setup of the RFID readers, the configuration of the software, and the integration of the system with existing security systems.

The project was successfully installed at the e-library of the Mechatronics Engineering with a limiting number of twenty (20) persons. It is expected that the system will provide an effective, efficient, and secured solution to controlling access to the area while also limiting the number of people that can access the e-library at any given time.

Keywords: *RFID, Readers, Transponders, Tags, Beacons*

1.0 Introduction

The need to control access to various organizations has led to the development of access control systems. These systems are installed at entrances and other locations within the organization to allow only authorized individuals to enter and to regulate the flow of people in crowded areas. The system can be enhanced to track movements and restrict access to sensitive areas [1].

One technology that can be used to create an access control system is radio frequency identification (RFID), a wireless technology. RFID has been widely used for automating a range of tasks, from home control to industrial automation. The hardware of an RFID-based access control system consists of RFID readers and electronic tags [2].

Radio Frequency Identification (RFID) has been in use for many years, with its origins dating back to World War II when German pilots discovered that the radio signals reflected back from their planes changed as they rolled back to base. This allowed the ground radar team to distinguish between German and Allied planes, marking the first use of passive RFID technology. Over time, RFID has become one of the most important Automatic Identification and Data Capture (AIDC) technologies. However, it also presents higher privacy and security compared to other AIDC technologies due to its ability to anonymously communicate over longer distances and the potential to reveal sensitive information about the tagged objects [3].

Other alternatives to the RFID access control systems are, IOT based systems, facial recognition systems and Bluetooth based access control systems [4]. After considering their merits and demerits, RFID based systems can top in terms of cost, durability and ease of installation.

Currently, at the Faculty of Engineering, University of Benin, Benin City, there are little to no methods in place to control both crowded spaces and access to restricted areas. The commonly employed method of access control used here are manual door locks, this lacks effective crowd control or capacity limiting measures.

After considering the needs in this case study, we have been able to outline the following key issues:

- **i.** Overcrowding: The number of people in restricted areas can exceed the designed sitting capacity, leading to a non-conducive environment (e.g., school library).
- **ii.** Unauthorized access: There may be unauthorized access to sensitive areas (e.g., offices, server rooms, storehouses).

The following issues have been identified as the main challenges in the current process of access control and capacity limiting. While this list in not exhaustive, it serves as the starting point for this project.

The aim of this project is to design and install an RFID access control system that can effectively implement capacity limiting and improve crowd control, resulting in efficient process.

2.0 METHODOLOGY

The design was made while considering the following attributes:

- Minimal cost
- Ease of installation

- Durability

Aside the above-mentioned attributes, the efficiency of operation and authorization is also an important factor.

2.1 CONCEPT

This concept consists RFID-based access control. The major components are;

- The electromagnetic lock
- Counting and de-counting device
- RFID reader
- Power source
- Micro controller

Other components can be added to improve the system, some of which are *(alarm/buzzing system, database system, LCD's and LED's).*

The hardware components of the capacity limiting RFID access control system are organized around the microcontroller, which acts as the system's "brain." Outputs, such as locks, GSM modules, buzzers, LCDs, and LEDs, are used for controlling the access. The RFID reader captures data from the RFID tag and transfers the signal to the microcontroller, which processes and extracts the valuable data. The authorization process is then carried out, and if authorized, the current count is incremented by the counting device. If the count exceeds the capacity, access will be denied. Unauthorized access will also be denied.

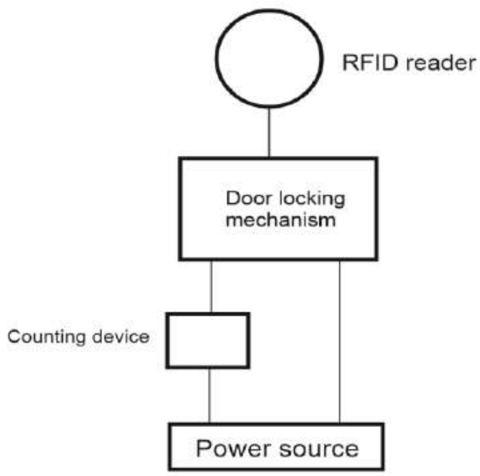

Figure 1 Basic Model diagram

2.2 THE PROTOTYPE

The counting device serves as a critical circuit breaker in the capacity limiting RFID access control system, providing a link between the power source and the door locking mechanism. If an authorized user attempts to access a restricted area and the counting device determines that the current number of people within the area exceeds the predetermined capacity limit, it will cut off the power supply to the door locking mechanism. This action will prevent the door from unlocking, effectively denying access to the user.

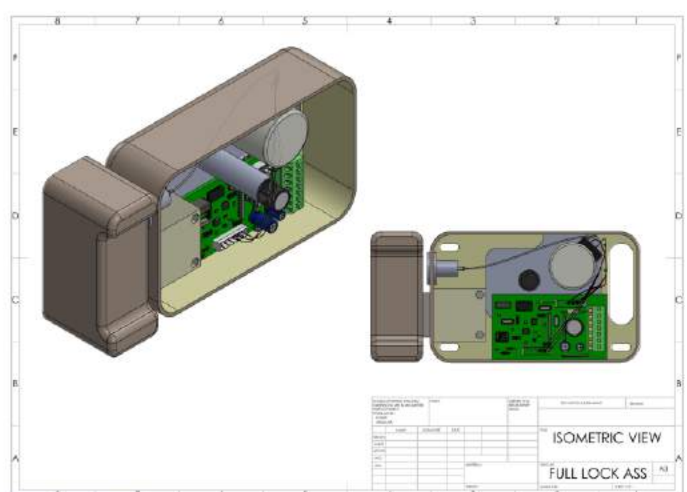

Figure 2 3D model view for door locking mechanism

The RFID based access control system was selected based on its relatively lower cost of maintenance, ease of installation and durability. The required materials were bought before installation began.

2.3 Installation

First the door hinges were fastened firmly to the wall. This will allow proper alignment of the door locking mechanism.

Once the door was standing firm, the damper was installed to enable un aided closing of the door when opened.

Figure 3 Door damper fixed in place

The door locking mechanism together was then attached to the door, alignment was carried out to allow the steel lock mate firmly with the hole.

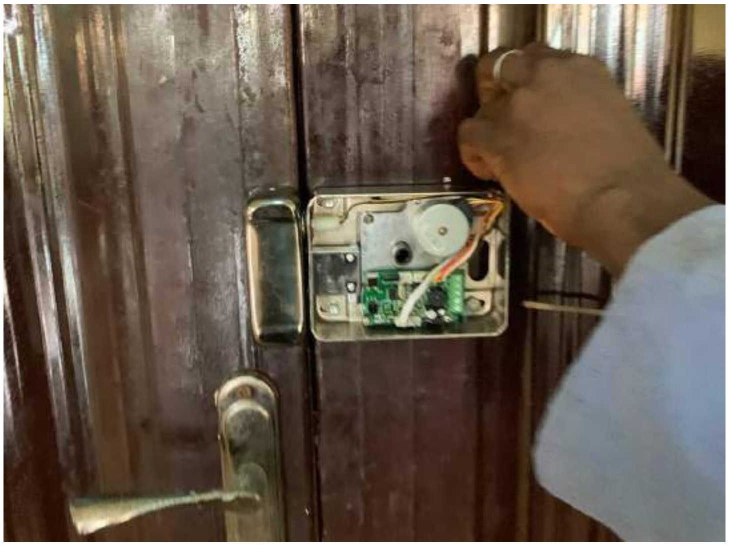

Figure 4 Door locking mechanism fixed in place

The only component of the system exposed to the outer part of the door is the RFID reader, since this is where the users tag will be placed to begin the authentication process

Figure 5 RFID tag

The counting device was then coupled, it detects incoming and outgoing persons by using laser beams aligned directly with a potentiometer. When there is any significant interruption with the beam path, it counts or decants based on the direction passed.

Figure 6 Coupled counting/decounting device

3.0 Results and Discussion

The capacity limiting RFID access control system was designed and installed at the e-library of the Mechatronics Engineering Department. The system was tested for efficiency and effectiveness, and the results are presented below.

The results of the study indicate that the capacity limiting RFID access control system was successful in controlling the flow of individuals entering and exiting a designated area. The system utilized RFID technology to allow entry only to individuals with authorized access, and also to limit the number of people allowed in the area to a specified capacity.

3.1 RFID Tag and Reader Configuration

The RFID system was configured using 13.56 MHz RFID readers and tags, which were compatible with the microcontroller. The RFID readers were set up to read data from the RFID tags, which were attached to the users' ID cards. The tags were programmed with unique identification numbers that were stored in the microcontroller. The system was configured to allow only authorized personnel to access the e-library.

3.2 Counting and Decounting System

The counting and de-counting system was designed to limit the number of people who could access the e-library at any given time. The system was set up to increment the count each time an authorized user accessed the e-library and decrement the count when a user exited the e-library. When the count reached the capacity limit of twenty (20), the system denied access to any additional users until the number of users within the e-library dropped below the capacity limit.

The implementation of the capacity limiting RFID access control system has many practical applications. For example, it could be used in public spaces such as museums, libraries, and theaters to prevent overcrowding and ensure that visitors have a more enjoyable and safer experience. It could also be used in workplaces to restrict access to certain areas and improve overall security.

In addition, the study highlights the importance of utilizing the appropriate technology when designing access control systems. The use of RFID technology in this system allowed for the efficient and accurate identification of authorized individuals, while also providing the necessary functionality to limit capacity.

However, it is important to note that the implementation of such a system requires careful consideration of various factors, such as cost, maintenance, and user experience. For instance, the cost of purchasing and installing the necessary hardware and software may be prohibitive for some organizations. Additionally, the system may require regular maintenance to ensure that it continues to operate effectively.

Furthermore, there may be concerns around privacy and data security associated with the use of RFID technology in access control systems. Organizations must ensure that appropriate measures are in place to protect the personal information of individuals who are using the system.

Overall, the study demonstrates that the capacity limiting RFID access control system has the potential to provide a viable solution for controlling access to designated areas. However, further research is needed to explore the feasibility and effectiveness of implementing such systems in different contexts and environments.

4.0 CONCLUSION

We were able to achieve our objectives.

- **a)** The RFID access control device was relatively easier to install from scratch.
- **b)** Cost of installation was minimal as compared to other alternative methods of implementation
- **c)** The capacity limiting feature was implemented and passed tests successfully
- d) Major device can be detached from the doors and coupled

References

[1] Harri, N. (2011) The Study of Business Opportunities and Value add of NFC application in Security Access Control Solution. Master thesis, Department of Business administration, Kemi-Tornio, pp 17-19.

[2] Mohammad Yamin, Xu Huang, Dharmedra Sharma (2007) Wireless and Sensor Technology and Crowd Management. Faculty of Information Sciences and Engineering, University of Canverra ACT 2601 Australia.

[3] Degen, Christoph. (2021). Inductive coupling for wireless power transfer and near-field communication. EURASIP Journal on Wireless Communications and Networking. 2021. 10.1186/s13638-021-01994-4.ze

[4] Riabi, H. K. B. Ayed and L. A. Saidane, "A survey on Blockchain based access control for Internet of Things," 2019 15th International Wireless Communications & Mobile Computing Conference (IWCMC), 2019, pp. 502-507, doi: 10.1109/IWCMC.2019.8766453.

NIPES-NCEE Conference Proceedings
The 2nd International Conference 15th-17th Feb. 2023
545-554
www.nipesjournals.org.ng

DESIGNING SMART-INTELLIGENT SYSTEM FOR TEACHING-LEARNING 6-11 YEARS ROBOTIC PROGRAMMING

Ibuomo R. Tebepah

Department of Computer Science, University of Africa
Paper Presented at the 2nd International Conference of Nigerian Institution of Professional Engineers and Scientist on Engineering Trends in Science & Engineering towards industry 4.0 Revolution, Benin City, Edo State

Abstract

This paper aims in designing a smart-intelligent educational system that will aid self-study and same time serve as a teaching tool for teachers. The criterion used as the design base were derived after a critical review, comprising usage, analysis of end users experience, and articles of existing application and IDEs for children within the age bracket. The design comprises components such as user analysis, log files, database, initial user data input, provisioning and hybrid machine learning algorithms that facilitates the smartness and intelligence of the system. Though the design was not demonstrated in this paper, it however created a framework for its subsequent development.

Introduction

Modern teaching-learning is becoming more flexible, interactive and adaptive [1,5] with the application of technology and utilization of smart mobile devices to access digital resources. This has made learning activities seamless, available and personalized (adaptive) to the learner.

Smart learning is used to describe learning that occurs through the medium of digital devices, application which is believed to increase retention. It is learning in the digital age. However, different authors and researchers have different understanding or usage of the concept.

Smart is taken as an abbreviation which means Self-directed, Motivated, Adaptive, Resource-enriched, Technology-embedded education according to Kim and Kim (2013). It is a well thought out concept that encapsulates the entirety of learning – objectives, resources, content, context, and presentation. Thus, smart solutions are bundles of different apps which each app performing a specific task or rather help a learner in achieving a specific goal or performing a learning activity.

There are other simplified description as published in the work of Galimullina, Ljubimova, and Ibatullin (2019), defining it as a technology-supported environment for learning. The technology enhanced learning (TEL) model of [2] is similar to Galimullina, Ljubimova, and Ibatullin (2019) view. By these, it can be generalized that the use of technology makes the learning process smart, if all other factors are not put into consideration or held constant.

An aspect of smart learning that of interest to technologist is the level of intelligence of the system, the ability of the system to automatically make decisions and adapt itself to different learning requirement and specifications without any direct input from the user. That means the system is able to support and analyse exiting data and blend seamlessly to the intelligent learning space [3], with no reference (independent) to the users. Speaking of technology applications especially in relation to smart and intelligent system, artificial intelligence serves as the vehicle through which it is achieved. Smart-intelligent systems as powered by AI in the form of machine learning and deep learning algorithms which the capability of processing both structured and unstructured data.

Cui (2022) research applied an AI enabled smart system called integrated multimedia teaching model (IMTM), a comprehensive smart educational resource that enhances users' capacity in listening and oral expression. The infiltration of artificial intelligence in our world has brought to clarity many supposedly challenges [4], with the integration and extensive applications of new generation computing technologies such as deep learning, cloud computing, big data, there has been a great leap forward in every sector including education. An education being the bedrock or foundation of technology (founded on research) has been greatly influenced, and it is almost becoming impossible to conduct teaching-learning without the use of some sort of technology. The application of machine learning in solving human and machine complex problems, and its success can be attributed to the support of computing capabilities and the technology that backs such processes.

Whereas, learners could easily adapt or transfer knowledge gained in using mobile devices for conventional purpose, teachers sometimes have the challenge of knowledge transfer. This can be attributed to several factors such as variation of time spent on surfing the internet, interest in social media activities, level of technology savviness, and interest.

In understanding learners' level of participation of intelligent teaching, Valks et al (2021) empirical study considers AI usefulness, interactive reward, satisfactory support and enjoyment for dynamic activities within the system. Notably of the system is the need for smart resource allocation which enables control and effective management of resources.

However, it was also observed that despite the high possibility of knowledge transfer of amongst learners when giving the opportunity to use teaching-learning application, learners are reluctant. The reasons could be generalized as interest and content presentation. This does not imply by any means that smart-intelligent system should not be used, but rather, better adaptive techniques and learning pedigree should be considered when designing such applications. Also, the age grade of the supposed learners is an important attribute that should be captured within the design. The instance of Change et al (2020) used virtual characters as intelligent tutors in teaching simple geometry to children. It is an embedded system that uses the combination of augmented reality and mobility, which created a pleasurable experience in the children influencing them to memorizing processes and figures subconsciously.

Shadiev and Yi (2022) work explained and demonstrated learning activities using unmanned aerial vehicle (UAV), involving collection of data, learning how to fly working in the field with UAV and programming. The main advantage of using UAV in learning according to their work is accessing data from inaccessible or dangerous locations, collecting and delivering temporal and spatial resolution information quickly.

Cho, Lee, and Kim (2022) work experimented with students studying architecture, having different perceptions and experiences in using remote learning systems. Their perceptions were based on the environment (platform) that is being used especially for programmes and courses that traditionally designed for a face-to-face studio method of teaching-learning process.

The suggestions from Radosavljevic, Radosavljevic, and Jelic (2019) work in creating a smart classroom using technology was aimed at replicating the familiar traditional classroom setting that makes learning process easier for both students and teachers. The technology powered classroom should enable the presentation of various teaching materials and relevant, necessary for personalized learning group learners, mobile and virtual learning related activities. The smart-intelligence should be able to provide adjustment for the individual students through the implementation of specific algorithms in ML that is able to analyse the context of learning, its environment and individual activities and adopt to the scenario

In all, the aim of structured learning peculiar and usually tailored towards to achieving the ideology of the locality.

Method

The study reports on the process of designing a framework for a smart-intelligent system using the unified modelling language tools. It identified the components that comprises the system as; classes, interfaces, virtual tutor, MLAs, lesson content, content presentation, log analysis, user dashboard, and data store. Since it is a smart-intelligent framework, there were specific consideration as each component was designed to suit the age grade of 6-11 years. These considerations include; concentration span, rate of assimilation of new conceptions, difficulty level of content, presentation perception (look-and-feel of the environment/platform), and subject matter.

In the case of the age grade factor consideration, the random sampling observation (RSO) technique was used. This technique randomly samples the sample set (35), spanning through the 6-11 years age grade, and were observed while they used digital devices. Ordered questions were asked as each child used it for various activities. In situations where the respondent is more than one, there was frequent interaction between and amongst them, with very similar responses. The collated responses of the respondents formed the attributes/variables that were taken to cognizance in the design. This process justified and authenticated the variables as determinants.

At the end of each RSO, the results were weighted along the main learning pedagogy; which are cognitive, pyscho-motor and affective. The weighting entailed how each identified attribute strengthens the learning domain.

Results

The results are showing in diagram form as seen in figure 1, figure 2, figure 3, and figure 4

Framework Design

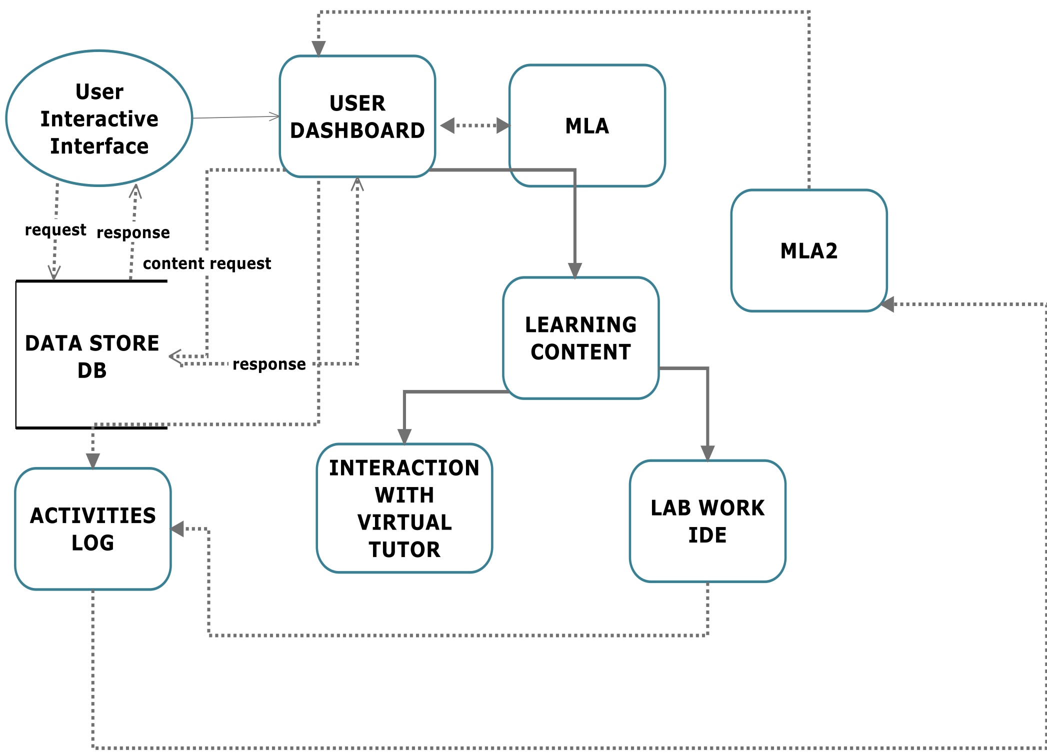

Figure 1: smart-intelligent architecture

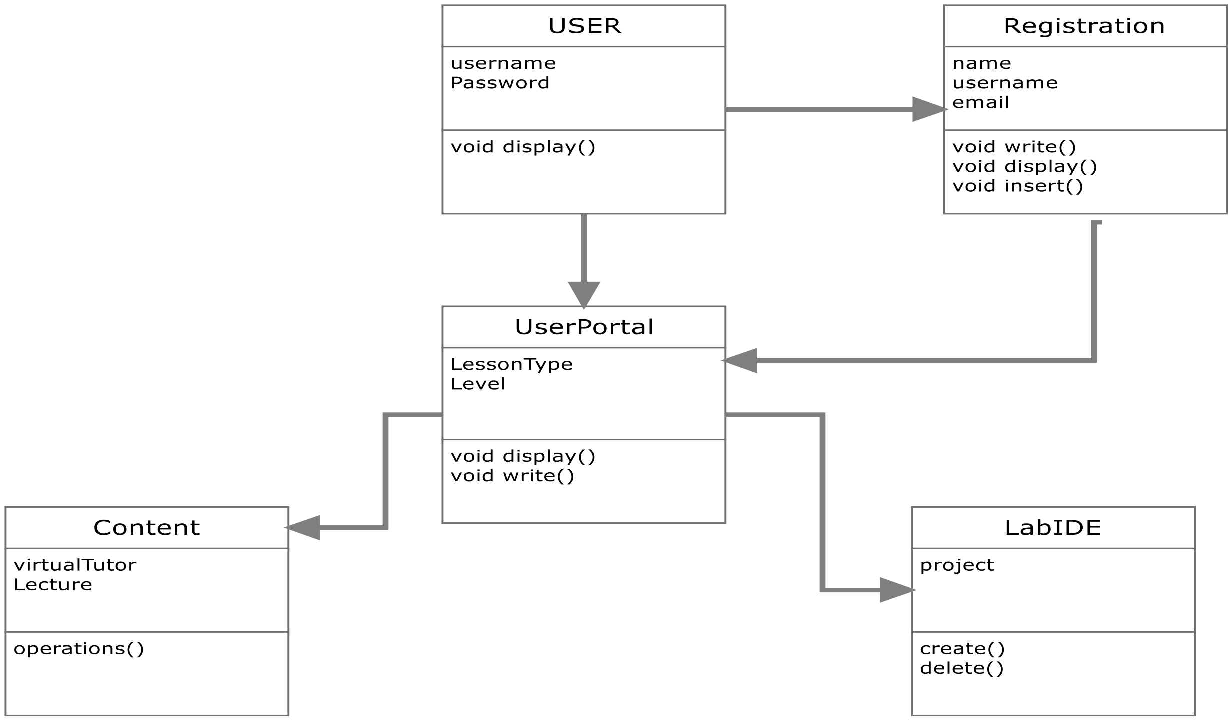

Figure 2: basic class structure

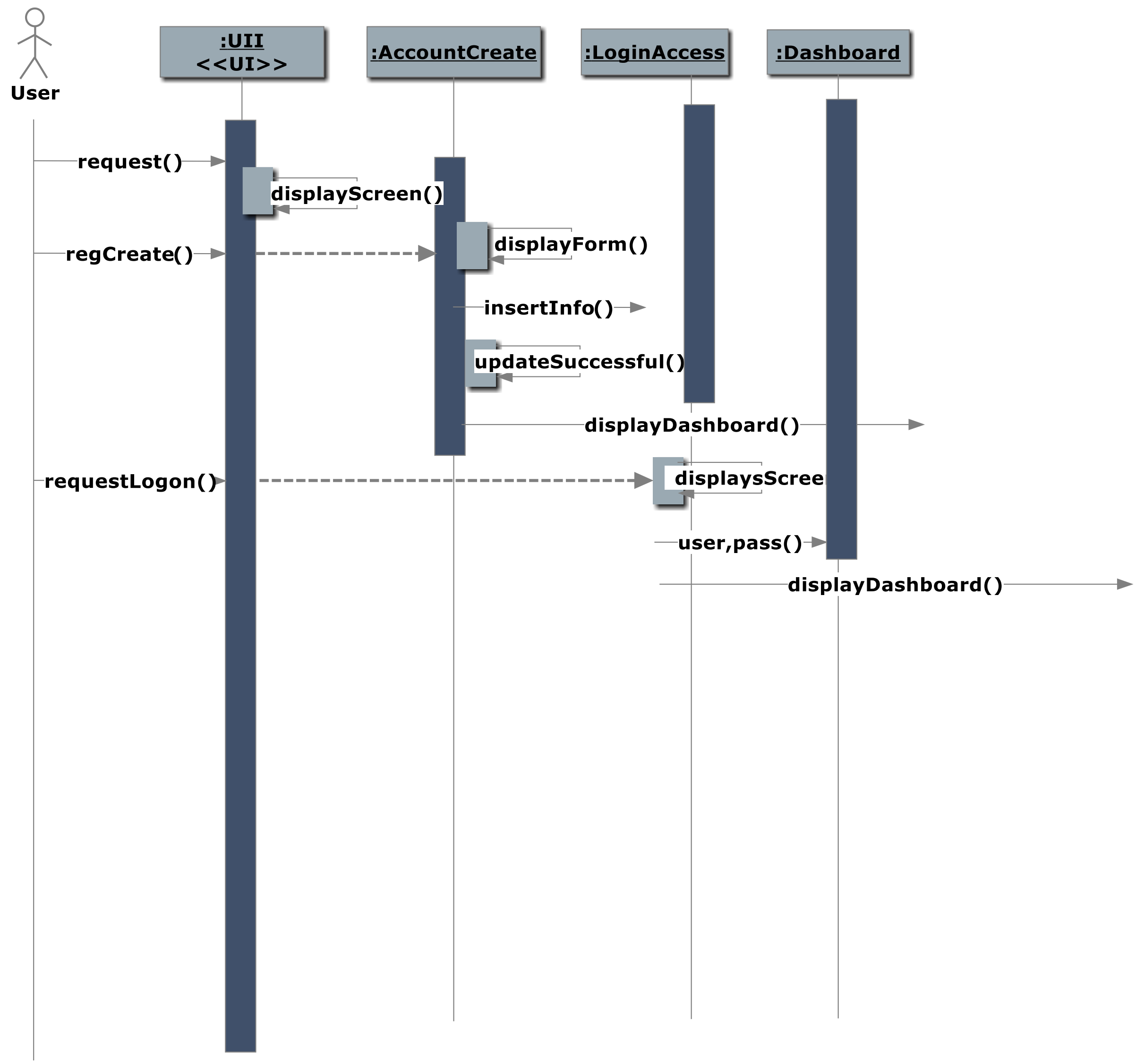

Figure 3: The System Sequence Diagram

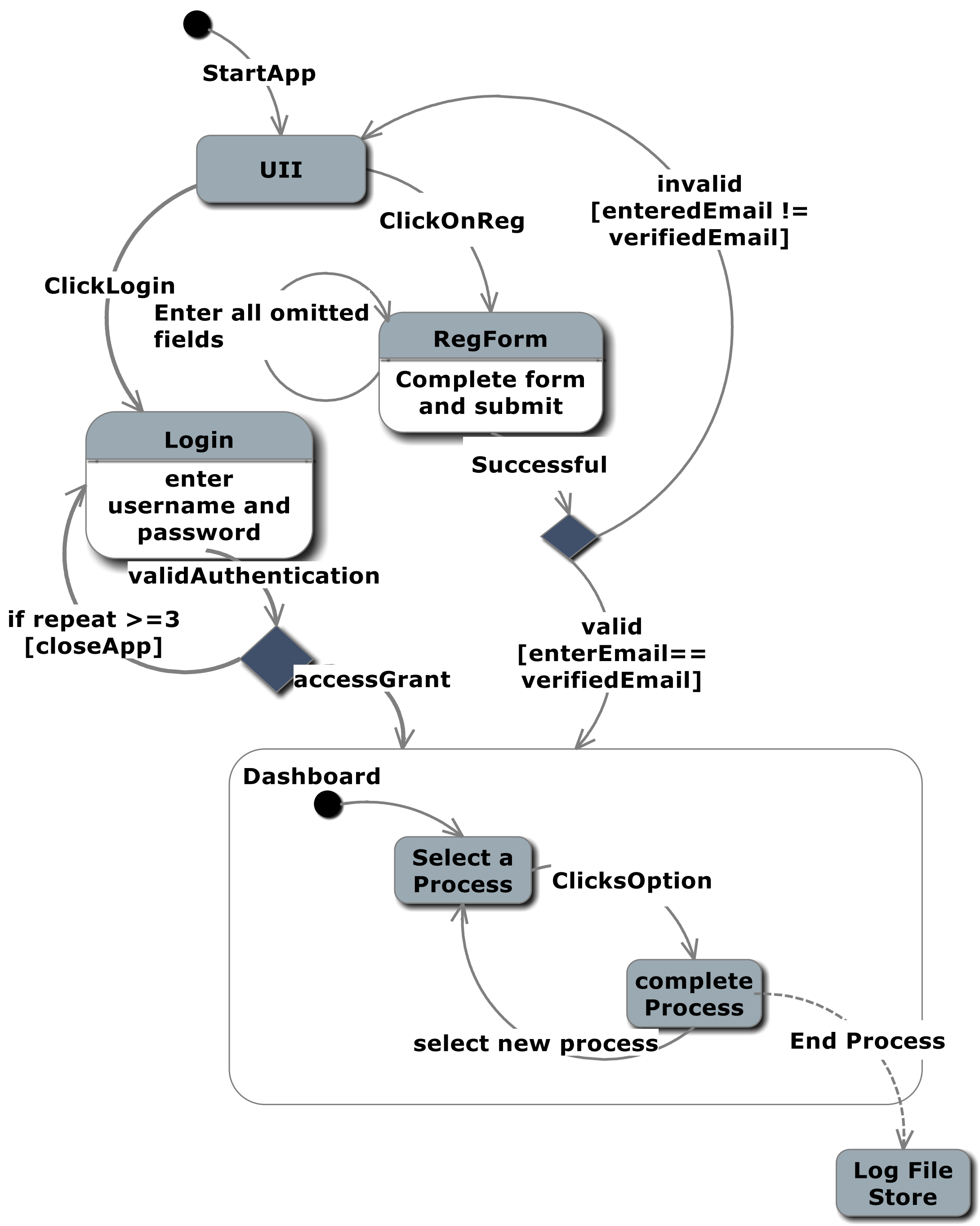

Figure 4: System Process State Diagram

Discussion

User Interactive Interface (UII): The UII component is the first displayed page at the start of the application and it contains sub-components such as the welcome, registration and login. It also includes a description of the app, with its name on the page. The page brings up a pop-up chatbot when it notices inactivity after 59 seconds of app initiation. As a user hovers on each subcomponent, a brief description of the component is displayed that serves as a guide on what the component is used for.

The registration subcomponent as the name implies is to enable prospective or intending user of the app to create an account that will be provisioned through authentication via email. The registration is a necessary requirement, without it, a user will not gain access. The content of the registration subcomponent is displayed in form format requesting for basic user details.

Login subcomponent contains label, textFields for the username and password with a submit button. With the label, the user knows where to input their username and password. The submit button is created to read and transfer text inputted in the textFields to the appropriate and corresponding data fields in a specific table within a database.

User Dashboard (UD): The user dashboard is activated when a user successfully logs onto the system. It is the user profile page. The dashboard is the main working component of the user as it contains several subcomponents; username, logout button, update profile, learning content, level, and feedback. Each of these is taking to logical conclusion, thereby completing a specific task. For instance, the learning content though a subcomponent within the dashboard, yet is a major component as it has several elements embedded in it.

Machine Learning Algorithm (MLAs): This is a logical component as it exists virtually within the dashboard. That means that its effect is seen or determine when the dashboard is viewed, and it makes learner centric suggestions. MLAs are presented in form of mathematical model, giving the designers and the programmers to create appropriate variable for each symbol for computation.

Data Store (DS): Data store houses all of the data within the app. The stored data includes; user details and learning content that are presented in different format and medium. DS contains both structured and unstructured data. Registration details and learning content are presented in structured manner, while the log files (activities log) are unstructured.

Activities Log (AL) otherwise known as log files is an unstructured data that captures user activities. It is the totality of user interaction with the app, which is used to postulate UX. These are used consequently to determine or proposed possible activities for the user. For instance, if in the activities log, it has been determined that a user has completed the basic lesson of a particular learning content, when next they login, the system will suggest a different learning content or a high level of the previously completed lesson. If it was not completed, they system also suggest to the user to complete the outstanding lesson before proceeding to the next level.

Learning Content (LC) component is made up of the learning material/resources that is presented in different format (multimedia and text). Content is planned, prepared following the teaching-learning objectives by trained specialist on the subject matter and uploaded. Uploaded materials can be downloaded or viewed only. It is arranged according to the difficulty level – basic, intermediate and advance. It is expected that a learner starts from the basic, however, limit is not placed as a learner can choose to start from any level. Content is further broken down into various lessons. The number of lessons for a specific topic depends on how broad (coverage) it is. It is expected that every lesson is presented starting from the rudimentary to the sophisticated, and it should be a buildup of prerequisite topics. Thus, lessons are arranged in a systematic and sequential order, making it easy for learners to follow.

Interaction with virtual tutor has two possibilities; real time teacher which is possible through a request form, and a robot virtual tutor. Learners are at liberty to make their choice. The expected virtual classroom is to take the pattern or setting of the traditional classroom.

Lab Work IDE (LWI) component was included present an all-in-one app; for learning and practice environment. Each lesson is required to be accompanied by a laboratory work. The essence is to drive in the principles and skill learnt in the course of taking the lesson. Children of the age in view can easily get distracted and bored when they are a passive.

Classes

The class structure is the transposition of the various components into programmable units. Each component is represented in a single class with inner classes and extended classes. This makes it possible for abstraction and encapsulation of events and actions that protects the user. Figure 2 is a basic representation of the app. The name of the class is displayed at the top, followed by the attributes (variable names and types), and the method (action).

Each class though distinct, yet interfaces with other classes seamlessly in a sequential order, giving the app a modularized and subset outlook. The implication is that the component can function in a sectional way independent of other component, but yet can be conjugated to form a singular entity.

System Sequence

The system sequence is a representation of functional modalities. It shows how activities are expected to be done. In figure 3, the rectangle boxes represent the different classes/interfaces on which the activities are being performed. It also shows the end of the activity. Thus, each task or activity is carried out within a class.

Process State

The Process State (PS) represent the transaction state of the system. That is how processes are initiated, handled and ended. It shows the mechanisms of error handling or correction, gradual or quantitative easing of processes if there is an abrupt interruption.

Conclusion

This study reported on the designing of a smart-intelligent system that would enable learners within the age 6-11 years to develop independent learning skill using robotic programming as the subject matter (learning content). The developed framework can be implemented on different subject content and multiple contents, for different age grades. It is adaptable, flexible, and robust enough to accommodate mobility, web enabled, and standalone depending on the implementation. The designed framework allows for IDE integration, making it easy for practical or laboratory exercises to be done with ease without necessarily depending on a third-party IDE.

It is usable by both teachers and learners, and can be deployed at home and places of learning when implemented.

References

[1] Cui, Q. (2022). Multimedia teaching for applied linguistic smart education system. *International journal of Human-Computer Interaction, 39* (1)

[2] Hwang, G., Tang, K., & Tu, Y. (2022). How ai supports nursing education: profiling the roles, applications and trends of ai in nursing education. *Interactive Learning Environment*

[3] Knox, J. (2020). Artificial intelligence and education in china. *Learning, Media and Technology* https://doi.org/10.1080/17439884.2020.1754236

[4] Valks, B., Artesteijn, M., Koutamanis, A., & Heijer, A. (2021). Towards a smart campus: supporting campus decisions with internet of things applications. *Building Research & Information*, *49* (1)

[5] Yang, Y., Zhang, H., Chai, H., & Xu, W. (2022). Design and application of intelligent teaching space for blended teaching. *Interactive Learning Environment*

NIPES-NCEE Conference Proceedings
The 2nd International Conference 15th-17th Feb. 2023
555-562
www.nipesjournals.org.ng

ANALYSIS OF THE RHEOLOGICAL CHARACTERISATION OF HIGH TEMPERATURE HIGH PRESSURE WATER BASED MUD USING RHEOLOGICAL MODELS

Odiri Jude Ogheneyerovo[1], Paul O. Ogbeide[2]

Department of Petroleum Engineering
University of Benin
[1]jude.odiri@eng.uniben.edu, paulogbeide@gmail.com[2],

Abstract
This paper examines the rheological characterization of the High Temperature and High Pressure Water Based Mud using rheological models. The goal was to find the most appropriate model that effectively characterizes the HT HPWBM. The Power Law model, the Bingham Plastic Model, the Hershel-Buckley Model, and the Casson Model are only a few of the mathematical models that have been used to describe the rheology of non-Newtonian fluids. To get accurate findings for pressure drops and hydraulic calculations, the optimum rheological model that accurately represents the shear stress-shear rate analysis must be used. Hence, in this study two fluids are used, the base fluid formulation represented as sample 1 and the base fluid formulation with an addition of KCl and aging is represented as sample 2. By using standard conversion factors and a variety of non-Newtonian models, the dial readings from the viscometer were then translated into stresses. The degree of deviation of each model from the measured stress, the absolute average percentage error (ϵAAP) was used and at the end, the Hershel-Bulkley rheological model was found to be the model with the least value of error. Hence, it is the most appropriate model as it was able to characterize the mud behaviour of the sample fluids with the lowest error relative to the other models across the entire shear rate conditions.

1.0 Introduction
"The effectiveness or the performance of the drilling fluid is dependent also on their rheological properties that is, the material properties that govern the specific way in which the deformation or flow behaviours occur" [1]. The rheological properties of the drilling fluid, or the material characteristics that control the particular manner in which deformation or flow behaviors occur, are also a factor in the drilling fluid's efficiency or performance [2]. The characteristics of the rock formation plays a critical role in the selection of a drilling fluid type during drilling while taking into account its financial and environmental implications. The drilling industry has historically used two different types of drilling fluids: water-based fluid and oil-based fluid.
Water-based fluid is cost-effective and easily formulated hence it is commonly utilized as a drilling fluid while oil-based fluid is more costly compared to water-based fluid. There are unique considerations while using OBF, cost and environmental factors are some of these.(the proper disposal of cutting to separate any potential environmental contaminations). As a result, when creating OBF, the type of oil utilized must be considered. Research has been done to identify and create oils that help lessen environmental issues. Consequently, a synthetic oil-based fluid with excellent biodegradability and low toxicity was found. But the issue still bothers on the toxicity of the fluid and its lubricity and other drilling parameters that leads to a safe drilling operation.

HP WBMs are particulary advantageous compared to conventional water based systems [3] because they provide faster ROPs, torque and drag reduction, shale inhibition, and improved wellbore stability with reduced environmental impact compared to inverted emulsion-based fluid counterparts [4,5]. The faster ROPs of HP water-based drilling fluids are typically attributed to the low-colloidal solids content- less than 10% by volume of solids [6,7] and formations that help minimize bit balling and accretion. HP WBMs typically are provided by chemical additives that suppress hydration, reduce pore pressure transmission, and encapsulate drilling cuttings. The key features of HPWBM systems include high shale stability, clay and cuttings inhibition, rate-of-penetration (ROP) enhancement, minimized bit balling and accretion, torque and drag reduction, and environmental compliance [8].

2.0 Methodology

The following mathematical models are used to describe the rheology of the sample fluid. These are:

1. Power Law model
2. Bingham Plastic model
3. Hershel Buckley Model
4. Casson Model

Table 1 Rheological Models and Formula

Rheological Models	Formula
Power Law	$\tau = k\gamma n$
Bingham Plastic	$\tau = \tau_o + \mu_p$
Herschel-Bulkley	$\tau = \tau_{OH} + k_H\, \gamma^{nH}$
Casson	$\tau^{\frac{1}{2}} = k_{oc}^{\frac{1}{2}} + k_c^{\frac{1}{2}} y^{\frac{1}{2}}$

Table 2: Samples Base Formulation at 14.0 lb/gal(Galindo A. et al. 2015).

Material	Quantity
Water (bbl)	0.79
pH buffer (lbm/bbl	4.5
KCl (lbm/bbl)	8.0

Rheology modifier (lbm/bbl)	1.0
High temperature polymer (lbm/bbl)	7.0
Thinner (lbm/bbl)	3.0
Barite (lbm/bbl)	311.0

Method of Data Analysis

The model parameters were gotten with the use of the mathematical model equations and then subsequent plotting of graph of log τ versus log γ gives the parameters 'n' and 'k' for the Power Law Model.

The Plot of $\log(\tau - \tau_{OH})$ against log γ gives the parameters 'n' and 'k' for the Hershel-Bulkley Model.

The plot of ($\tau^{0.5}$) versus ($\gamma^{0.5}$) gives the yield stress for the Casson Model (k_{oc}) and the Casson plastic viscosity (k_c).

The Bingham plastic model parameters are gotten by solving for the value of normal yield stress and plastic viscosity.

Descriptive graphs and charts were employed in the analysis.

Calculated stress values were gotten by the use of the different rheological model stress equations.

Finally, the measures of deviation of model stresses from calculated stresses in Pascals were measured with the use of Absolute average percentage error and comparisons were made regarding the calculated value of errors.

3.0 Analysis and Results

Analysis of Fluid Sample 1

Table 3: Viscometer Readings for Sample 1 (Kay A. Galindo et al. 2015).

Speed (RPM)	Dial Readings(lb/100ft2)	Shear Rate (s-1)
600	35.8	1022
300	23.1	511
200	20.2	340.06

100	15.9	170.30
6	7.6	10.22
3	6.8	5.11

Stress Equations for all Models for Sample 1

- τ = 1.9937 $\gamma^{0.2939}$ for the power law model
- τ_o = 5.304 + 0.006477γ for the Bingham plastic Model
- τ = 3.47 + 0.20314 ($\gamma^{0.6027}$) for the Herschel-Bulkley Model
- $\tau^{0.5}$ = $1.2281^{.5}$ + $0.05676^{0.5}$($\gamma^{0.5}$) for Casson Model

Table 4: Calculated Values of Stress Using Different Rheological Models for Sample 1

Speed (RPM)	Dial (lb/ft2)	Shear rate (S^{-1})	Measured (Pa)	PLRM (Pa)	BPRM (Pa)	HBRM (Pa)	CRM (Pa)
600	35.8	1022	18.258	15.2805	11.92349	16.70096	76.11764
300	23.1	511	11.781	12.46421	8.613747	12.18286	42.169
200	20.2	340.06	10.302	11.05819	7.506569	10.28654	30.26737
100	15.9	170.30	8.109	9.024306	6.407033	7.963125	17.78522
6	7.6	10.22	3.876	3.947639	5.370195	4.294502	3.496269
3	6.8	5.11	3.468	3.220066	5.337097	4.012951	2.711798

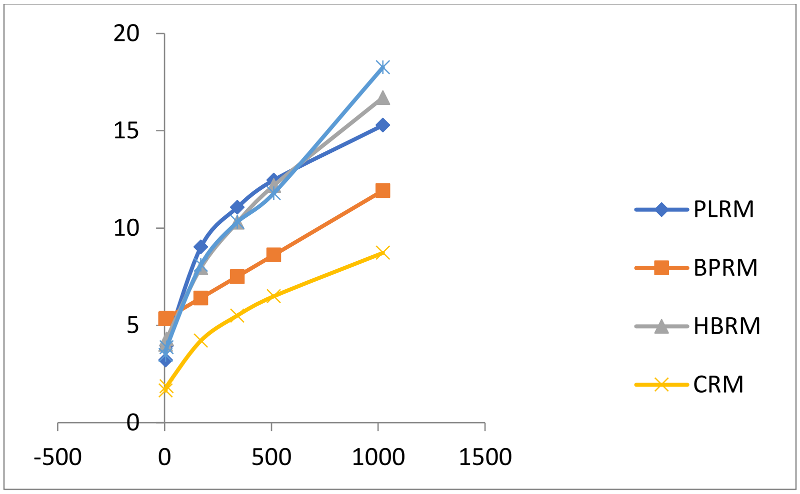

Fig 1: Relationship of Shear Stress-Shear Rate Graph of Different Models for Sample 1

Analysis of Fluid Sample 2

HT HPWBM + KCl
Static Aging (ºF/hours) = 400/16
Table 5 Viscometer Readings for Sample 2 [6].

Speed (RPM)	Dial Readings(lb/100ft2)	Shear Rate (s-1)
600	98	1022
300	63	511
200	49	340.06
100	33	170.30
6	10	10.22
3	8	5.11

Stress Equations for all Models

- $\tau = \tau = 1.5637\gamma^{0.4845}$for the power law model
- $\tau_o = 14.28 + 0.01785\gamma$ for the Bingham plastic Model
- $\tau = 4.08 + 0.2274\ (\gamma^{0.7709})$ for the Herschel-Bulkley Model
- $\tau^{0.5} = 2.446^{0.5} + 0.2393^{0.5}(\gamma^{0.5})$ for the Casson Model

Table 6: Calculated Values of Stress Using Different Rheological Models for Sample 2

Speed (RPM)	Dial (lb/ft2)	Shear rate (S-1)	Measured (Pa)	PLRM (Pa)	BPRM (Pa)	HBRM (Pa)	CRM (Pa)
600	98	1022	49.98	44.89856	32.5227	51.58903	150.8661
300	63	511	32.13	32.09101	23.40135	31.92275	81.22069
200	49	340.06	24.99	26.34463	20.35007	24.42073	57.11766
100	33	170.30	16.83	18.84417	17.31986	16.01531	32.20214
6	10	10.22	5.1	4.822058	14.46243	5.444508	4.98708
3	8	5.11	4.08	3.44654	14.37121	4.879672	3.633319

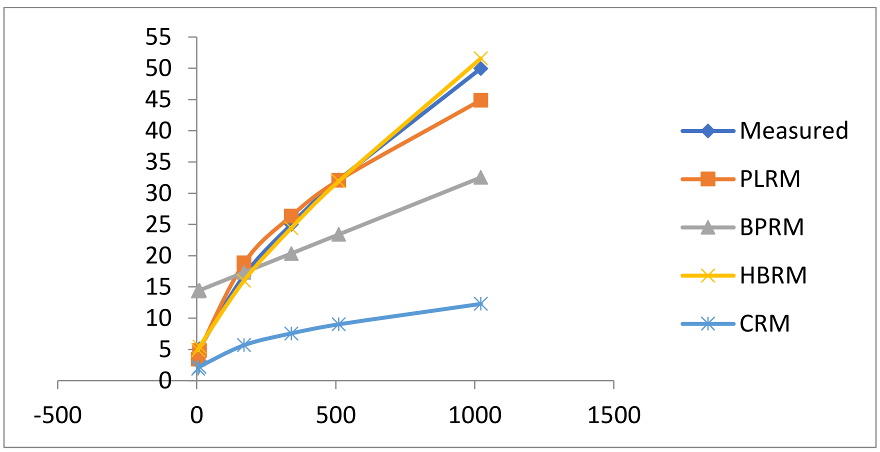

Fig 2: Relationship of Shear Stress-Shear Rate Graph of Different Models for Sample 2

Calculation of Values of Deviation of Models From Measured Stresses
The degree of each model's departure from the observed stresses was really predicted using the Absolute Average Percentage Error, ϵ_{AAP} .

The ϵ_{AAP} is given by the equation,

$$\epsilon_{AAP} = \left[\frac{1}{N}\Sigma \left| \frac{(\tau_{measured} - \tau_{calculated})}{\tau_{measured}} \right|\right] * 100$$

Table 7: Absolute Average Percentage Error (ϵAAP) of the Rheological Models

Mud Samples	PLRM	BPRM	HBRM	CRM
Sample 1	8.29	33.69	6.73	153.26
Sample 2	8.11	86.56	6.22	97.95

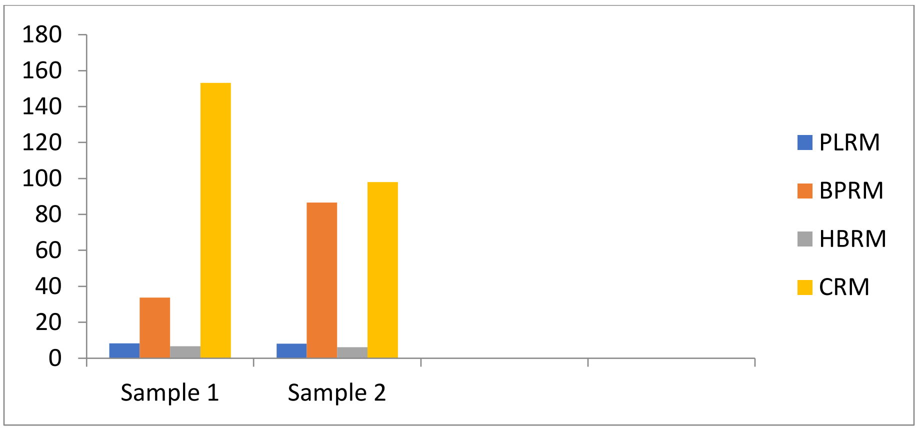

Fig 3: Values of Absolute Average Percentage Error of Rheological Models

4.0 Conclusion

From the above analysis and investigations, the following conclusion can be inferred,

1. The Hershel Bulkley Model best characterizes the fluid's behaviour across the entire low and high shear rate conditions.
2. The Power law model next best characterizes the fluid's rheology due to the polymer inherent in its composition.
3. The Bingham Model does not predict accurately the behaviour of the drilling fluid as it gives low shear stress values at high shear rate and high stress values at low shear rates conditions.
4. The Casson Model gives a very high stress at shear rate and very high stress at low shear rate conditions. Hence, poorly predicts the rheological behaviour of the drilling fluid.

REFERENCES

[1] Al-Ansari, A., Yadav, K., Anderson, D. et al . 2005. Diverse Application of Unique HP Water Based Mud Technology in the Middle East. Presented at the SPE/IADC Middle East Drilling Technology Conference and Exhibition, Dubai, United Arab Emirates, 12-14 September. SPE-97314-MS, http://dx.doi.org/10.2118/97314-MS.

[2] Becker, R.G.; Morgan, W.C.; Chin, J.E.; and Griffith, J.,2003, "Improved Rheology Model and Hydraulics Analysis for Tomorrow's Wellbore Fluids Application." Society of Petroleum Engineers, Tulsa,Oklahoma.

[3] Caenn R and Chillingar G V 1996 Drilling fluids: state of the art. Journal of Petroleum Science and Engineering 14, 3-4 p. 221-30.

[4] Carpenter, Chris."High Performance Water Based Drilling Fluids Offshore Cameroon". JPet Technol 66.(2014): 120-122. doi: https://doi.org/10.2118/0214-0120-JPT

[5] Kay A. Galindo, Weibin Zha, Hui Zhou, and Jay P. Deville. High Temperature, High Performance Water-Based Drilling Fluid for Extreme High Temperature Wells. Presented at the SPE International Symposium on Oilfield Chemistry held in th Woodlands, Texas USA, 13-15 April 2015. SPE-173773-MS. https://doi.org/10.2118/173773-MS

[6] L. Figura and A. Teixeira, Food Physics. [New York]: Springer-Verlag Berlin Heidelberg, 2007, p. page 117.

[7] Montilva, J., van Oort, E., Brahim, R. et al, 2007. Using a Low-Salinity High Performance Water-Based Drilling Fluid for Improved Drilling Performance in Lake Maracaibo. Presented at the SPE Annual Technical Conference and Exhibition, Anaheim, California, USA, 11-14 November, SPE-110366-MS. http://dx.doi.org/10.2118/110366-MS.

[8] Rodriguez, S.Y., Arenas, R.D.J., Sierra, H. et al, 2010. Breaking Old Paradigms With the Use of High-Performance WBM Systems. Presented at the SPE Latin Kay A. Galindo, Weibin Zha, Hui Zhou, and Jay P. Deville. High Temperature, High Performance Water-Based Drilling Fluid for Extreme High Temperature Wells. Presented at the SPE International Symposium on Oilfield Chemistry held in the Woodlands, Texas USA, 13-15

NIPES-NCEE Conference Proceedings
The 2nd International Conference 15th-17th Feb. 2023
563-574
www.nipesjournals.org.ng

EFFECT OF REACTION TEMPERATURE ON THE TOTAL PETROLEUM HYDROCARBON OF BIODIESEL PRODUCED FROM WASTE COOKING OIL USING A HETEROGENOUS CATALYST

George Oluwafemi Joseph and ENGR. DR. Mrs E.T Akhihiero

Chemical Engineering University of Benin, Benin, Nigeria
Email: George_oluwafemi@yahoo.com

Abstract

The continuous increasing demand for energy and the decrease in petroleum reserves has led to the search for alternative fuels which are renewable and sustainable. Biodiesel a renewable fuel has proven to be more useful in combustion engine than the petro-diesel because of its biodegradability and smoother combustibility. Transestrification of waste cooking oil to biodiesel was carried out with methanol to oil molar ratio of 8:1 using activated carbon from coconut shell as catalyst. The temperature of the reaction was varied. The total petroleum hydrocarbon (TPH) of the biodiesel produced were determined at reaction temperatures of 400C, 500C and 600C,while biodiesel properties produced at 400C, 450C, 500C, 550C and 600C were also determined. The concentrations of total petroleum hydrocarbon for biodiesel at of 400C, 500C and 600C were 1652.65, 9629.803 and 9608.752 respectively. Total petroleum hydrocarbon explains the nature of the oil used in the transesterification and hence the quality of the biodiesel produced. Higher temperature of above 500C does not favor the presence of some hydrocarbon in the fuel produced. The properties of the biodiesel produced conform to ASTMD 6751.

***Keywords**: Biodiesel, Waste cooking oil, Total petroleum hydrocarbon, Coconut shell, Methanol, NaOH*

1.0 Introduction

Researchers has developed a wide variety of efficient and novel waste recycling technologies in an effort to recover resources and maximize the transformation of trash into useful components and finished goods [1].

Sustainable industrialisation throughout the past decade has been driven by factors like a growing population, new technologies, more generous investment incentives, greater trade and capital liberalization, and new finance sector innovations. Researchers and industrialists face the task of delivering low-cost, environmentally friendly resources that meet modern manufacturing techniques in order to keep up with the increasing demand for raw materials brought on by the current industrial revolution. So, WCO stands for "waste cooking oil," which refers to used oil and fat from the kitchen. WCOs are commonplace in both commercial and domestic kitchens, especially those serving food. Population growth is causing a rapid increase in the quantity of WCO generated by households and food service establishments [2]. WCO can, however, be turned into biodiesel for use in a variety of applications if it is first catalyzed using a number of different types of agricultural waste [3]. With its low emissions and desirable chemical features like non-toxicity and biodegradability, biodiesel made from renewable resources is one of the most enticing alternative fuels being developed at the moment [4].

Additionally, unlike non-renewable fuel, biodiesel fuel may be used in any standard diesel engine (petroleum or diesel). Aside from being quickly depleted, the nitrogen, sulfur, and carbon oxides, lead, and hydrocarbons released during combustion are also negative aspects of using nonrenewable fuel [5]. The optimal production of biodiesel involves the assessment of the amount of total petroleum hydrocarbon (TPH) present at each temperature state, which leads us to the definition of TPH:

Total Petroleum Hydrocarbons, also known as TPH, is used to describe petroleum, often known as crude oil. Petroleum is composed of thousands of distinct components. The fact that practically all of them contain hydrogen in addition to carbon is what gives them their name: hydrocarbons. The percentage of crude oil that is comprised of petroleum hydrocarbons ranges from fifty to ninety-eight percent, depending on the origin of the petroleum, and is considered an essential component [6,16,17,18]. TPH is released into the environment as a result of industrial releases, oil spill occurrences, or the disposal of waste materials from domestic or commercial use. Oil spills in coastal seas are typically caused by ship operations, tanker collisions, oil exploration, and oil production. Crude oil spills are a frequent occurrence in the oil industry, particularly in offshore drilling, transportation, and transfer. Second, the hazardous effluent flow from petroleum refineries is a well-documented contributor to pollution [7,19]. The amount of oil spills is still a problem for the environment, despite the fact that statistics show a definite declining trend in the frequency of oil spills over the previous 50 years. There have been more than 140 large spills, totaling over 7 million tons of hydrocarbon oil spilled into the environment [8]. An estimated one thousand tons of petroleum hydrocarbon oil will be lost in 2020 owing to tanker spills. It's the same sum as in 2012 and 2019. The list of recent and global oil spills includes over 200 incidents, both on land and at sea. Every year, millions of tons of petroleum are released into the ocean due to both natural seepages and human-caused oil spills [9,20,21,22,23,24].

Fundamentally, engineering is a field that has shown us how to become problem solvers in the ever-changing environment we live in. The environmental impact of waste cooking oil disposal and the potential for its reuse as a resource has been of great concern. In contrast, finding a renewable energy source that can replicate the features and components of petro diesel is a problem that needs to be solved. In response, scientists realized they could use waste cooking oil as a feedstock to produce biodiesel. The total petroleum hydrocarbon of the biodiesel produced is the main factor in determining the characteristic grade of this futuristic goldmine obtained from this feat. Thus, it is imperative it be of the best quality standard thereby obtaining the temperature at which the total petroleum content is optimum in order to aid in the production of the best biodiesel.

1.1 Waste cooking oil

When food is prepared and fried using edible vegetable oil, a byproduct is waste cooking oil (WCO). When people talk about WCO, they are usually referring to oil used for deep frying, edible fat mixed with kitchen rubbish, or oily wastewater sent directly into sewers. Used vegetable oils and animal fats are readily available worldwide, especially in developed countries. However, the term used or waste cooking oil differs in meaning from person to person but in totality it means an oil that has loosed it functionality and regarded as trash.

Oils and fats present a significant management challenge due to the evident difficulty of disposing of them and the potential for contamination of water and land resources. The Energy Information Administration estimates that daily generation of spent cooking oil in the United States totals roughly 100 million gallons, or 9 pounds per person [11].

While some of this waste cooking oil is recycled into soap, the vast majority is simply dumped into the environment. Cities have a bad habit of dumping WCO in sewers, drains, open areas, rivers, and woodlands, where it can generate foul odors, clog drainage pipes, damage concrete, and harm both terrestrial and aquatic ecosystems. Foam formation, an increase in the organic load on water sources, difficulties in wastewater treatment, a decrease in dissolved oxygen levels, and a shift in the equilibrium of the environment are all possible results of improper disposal of WCOs [10].

Due to the similarities between the two countries, it was decided to assume that the annual per capita production of waste cooking oil in Canada is 9 pounds. Statistics Canada estimates that 33 million people currently reside in Canada. Therefore, it is possible that Canada generates about 135,000 tons of used cooking oil annually. An annual output of 700,000-1,000,000 tons of wasted cooking oil was recorded across EU member states [12]. There are around 200,000 tons of discarded cooking oil produced every year in the UK [13]. Reducing environmental contamination caused by the massive amounts of waste cooking oils unlawfully thrown into rivers and landfills is a key benefit of using biodiesel as a petrodiesel alternative made from waste cooking oil [14]. Some solutions have been proposed for dealing with WCO that would lessen their impact on the environment, including better management, disposal, minimization, recycling, conversion, utilization, valorization, and remediation. Utilizing waste cooking oil for biodiesel production could help cut emissions of carbon dioxide, nitrogen oxide, and other pollutants. Most of the carbon in biomass-derived fuel is biogenic and renewable. Used cooking oil is one of the cheapest and most readily available sources for biodiesel production. The cost of feedstock contributes for around 70-80% of the entire cost of manufacturing biofuel, hence WCO has been recognized as a feasible strategy to reduce this cost. WCO is widely available, low-cost, yields a lot of usable product, and doesn't harm the ecosystem. Several technologies have also been developed to chemically and biologically transform WCO into biofuels. Because the cost of feedstock is one of the primary concerns with the process, using waste cooking oil considerably increases the economic sustainability of biodiesel production.

Every fuel sample are made up of hydrocarbons, basically total petroleum hydrocarbon in its entirety explains the hydrocarbons that makes a fuel has a good quality. The quality in terms of how it burns in diesel engines and other characteristic properties. Thus, total petroleum hydrocarbon basically gives information about the quality of the biodiesel produced, the more it is in amount the better characteristic quality the biodiesel possesses.

In addition, for the immense availability of methanol for the transesterification process, biogas can be a good source in aiding the process of biodiesel production by inhibiting the dearth of this important constituent as production scale advances.

2.0 Methodology

Esterification of waste cooking oil

The waste cooking oil was measured using the measuring cylinder to the 500ml mark, which was poured into the round bottom flask and methanol at the 125ml mark quantity were added to the flask at a ratio 1:4. The mixture was kept on the magnetic stirrer for an hour with a steady temperature of 60^0C whereby 1% of H_2SO_4 was added during the rigorous mixing process. After an hour, the mixture was poured into a separating funnel which was kept standing for 24hrs for the separation process to occur. The sole aim of this process was to reduce the free fatty acid (FFA) in the used cooking oil so as to hinder the formation of soap in the transesterification process to the biodiesel which is the desired end point we are interested in.

Transesterification of waste cooking oil

The weighing balance was used to measure 55g of the waste cooking oil into the conical flask at the ratio 8:1, which was continuously stirred on the magnetic stirrer with the simultaneous addition of heat. 1g of NaOH was added and 2g of the catalyst was added likewise. From the ratio used, the amount of methanol added was calculated and 16.56g of methanol was added into the conical flask for the transesterification process to occur which yielded the Biodiesel production. The process was repeated at varying temperatures which were at 40^0,45^0,50^0,55^0, and 60^0

2.1 Preparation of catalyst

During the experiment, the coconut shell was subjected to the carbonization process, and a chemical activation approach was employed. To activate the carbonized coconut shell, phosphoric acid was utilized.

Experimental Procedure

After being sun-dried and then placed in the oven at temperatures between 100 and 300 degrees to eliminate excess moisture, the raw material samples of coconut shells were rinsed with distilled water to remove any inorganic material that might be present. The sample was dried, then broken into smaller pieces in preparation for the carbonization process in the muffle furnace.

Carbonization Process

A horizontal programmable furnace was used to carbonize the raw material sample. The 60.61g shell sample was placed in the center of a quartz boat. Until the target carbonization temperature (500 degrees) was reached, the sample was heated at a steady rate of 6 degree/min using a flowrate of 100 mL /min of nitrogen. So, we kept it at 500 degrees for an entire hour. Following carbonization, just around 40g remained a reduction of about 34% in mass.

Activation Process

After the carbonization process, char samples were chemically activated using phosphoric acid (H_3PO_4).Impregnation was done using 100 ml of 0.5M solution of phosphoric acid mixed with 30g of the carbonized shell. The mixture was kept soaked for 72hrs to allow for proper activation and then removed from the solution. The activated carbon was washed till neutral with distilled water to remove excess phosphoric acid. It was properly dried in the oven for an hour at 105^0C which was afterwards taken into the muffle furnace for further activation process aiding the surface area and pore formation.

3.0 Results and Discussion

Total petroleum hydrocarbon analysis

For the GC analysis, materials were extracted using a modified version of the USEPA 8015 technique for diesel range organics (DRO). The instrument used for the analysis was the HP5890 PLUS II with the detector as flame ionization detector. The composition at various temperatures is displayed in the table below.

Table 1: Total petroleum hydrocarbon concentration at varying temperature

TPH	Concentration(µg/L)		
	40^0C	50^0C	60^0C
n-octane	<0.01	180.5389	221.8381
n-nonane	101.0506	1.866286	0.209383
n-decane	106.9504	5.364262	143.5602
n-undecane	0.163120	27.51849	<0.01
n-dodecane	637.8479	1374.535	243.0964
n-tridecane	8.603761	0.697638	16.06723
n-tetradecane	8.426814	1187.820	70.37475
n-pentadecane	71.72041	198.9259	235.6981
n-hexadecane	98.02745	2153.429	1633.884
n-heptadecane	81.31296	44.62819	5.444186
Pristane	182.8537	85.18941	39.51925
n-octadecane	175.3982	24.16912	2197.611
Phytane	39.06693	24.97422	8.298555
n-nonadecane	24.08437	504.3024	98.14532
n-eicosane	24.52543	2233.245	2562.736

n-heneicosane	8.148551	453.5538	264.3281
n-docasane	15.56609	991.2703	1636.659
n-tricosane	2.101071	47.02346	23.34783
n-tetracosane	0.343233	<0.01	111.7804
n-pentacosane	0.857689	25.61895	3.288261
n-hexacosane	0.560919	43.64406	12.89782
n-heptacosane	2.901913	4.126324	5.915126
n-octacosane	2.934670	4.126324	5.915126
n-nonacosane	0.587658	9.978404	8.923421
n-tricontane	2.821470	0.818808	1.806131
n- hentriacontane	40.64845	0.646767	1.109832
n-dotriacontane	2.872587	0.254951	5.432951
n-titriacontane	12.27344	4.540271	55.05294
∑ TPH	1652.65	9629.803	9608.752

However, it can be deduced that from the compilation of the data shown in table 1 above, the transesterification process carried out at temperature of 50^0 C produced the best quality in terms of the amount of total petroleum hydrocarbons present.

Physicochemical Properties of Biodiesel from waste cooking oil

Temperature(^{0}C)	Flash point	pH	Density (g/ml)	Acid Value(mgKOH/g)	Viscocity
40	----------	6.70	870	0.672	--------------
45	----------	6.52	879	0.543	---------------
50	142.5	6.86	890	0.562	4.43

55	----------	6.62	882	0.520	--------------
60	-----------	6.70	891	0.690	---------------
ASTM D6751	130 min	6.5-6.8	880-890	0.5-0.6	1.9-6.0

The diesel range organics that were produced by the biodiesel ranged from n-octane to ntitriacontane (C_8 - C_{33}). These diesel organics are the essential defining qualities of the biodiesel produced. It was observed that the functional group largely represented was the alkane group, having various petroleum hydrocarbons being present. Also, due to their primary presence in crude oil, pristane and phytane are considered to be one of the most important constituents which gives a proper overview of the source of biodiesel and its constituent quality. Their significance stems from the fact that their presence possesses characteristic importance in the biodiesel produced. However, despite the biodiesel produced deriving its feedstock from waste cooking oil, it possesses a number of characteristics that are distinct from those of its counterpart, crude oil.

Chromatogram of the total petroleum hydrocarbon

Chromatogram at 40 degrees temperature

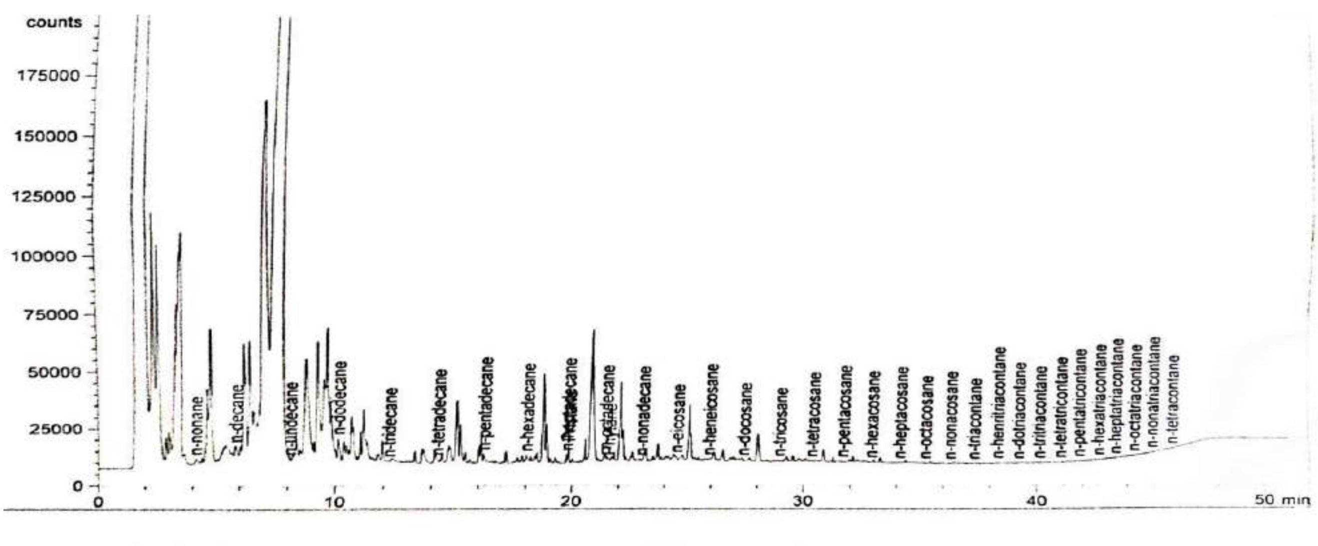

The chromatogram of the biodiesel produced at a temperature of 40 degrees, which contained a total petroleum hydrocarbon content of 1652.65µg/L

Chromatogram at 50 degrees

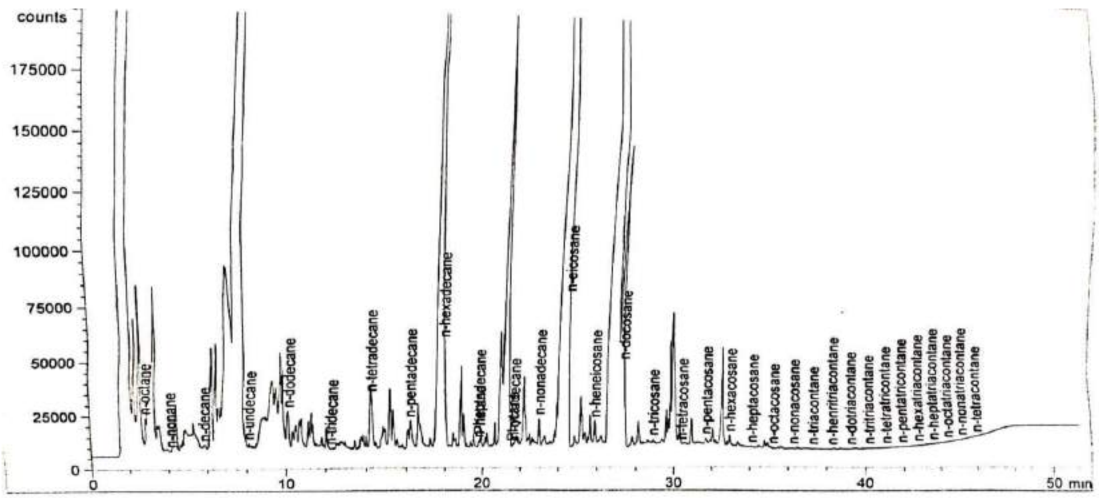

The chromatogram for the biodiesel produced at 50 degrees, which was the temperature that achieved the optimum total petroleum hydrocarbon composition with a content of 9629.803µg/L

Chromatogram at 60 degrees

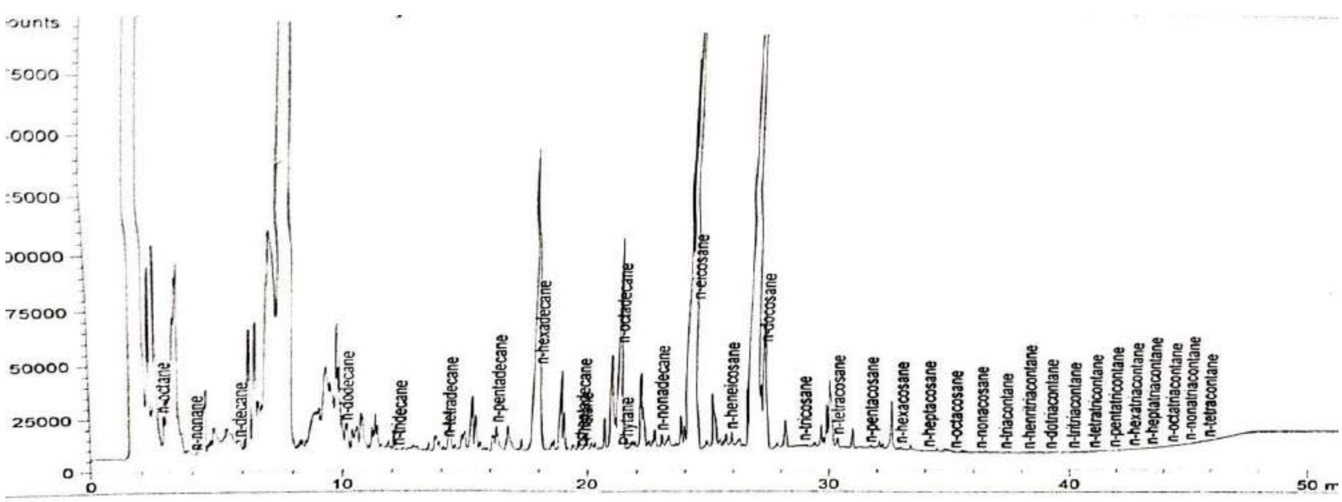

The chromatogram achieved at 60 degrees, containing a total petroleum hydrocarbon of 9608.752µg/L

However, from the chromatogram of the biodiesel achieved at varying temperatures the abundance count is seen to be on the vertical axis while time which served as an important function was on the horizontal axis, these parameters aided in obtaining the amount of the total petroleum hydrocarbon present at each temperature phase. Thus, ascertaining the temperature with the highest quality.

Thus, it could be inferred that at 40 degrees the total petroleum hydrocarbon content, TPH was very low which was caused as a result of the insufficient temperature for the transesterification process due to the source of it feedstock, waste cooking oil. And, at 60 degrees the TPH content reduced slightly due to some hydrocarbons evaporating from the system. But, at 50 degrees the biodiesel with the highest quality was obtained having the highest total petroleum hydrocarbon content.

In conclusion, an increase in temperature favored the reaction process.

CONCLUSION

In this paper, emphasis has been given on the Biodiesel, as a potential and sustainable substitute for petro diesel. Thus, it brought about elucidating it several aspects which are stated below:

1. Biodiesel has been proven the best substitute to fossil fuel. It is superior to petroleum based fuels because it is renewable, biodegradable, and non-toxic.

2. The influence of temperature on the total petroleum hydrocarbon was kinetically important, which was carried out at 40, 50 and 60 degrees. The best results were obtained at 50°C. That is, the analysis satisfactorily achieved its aim by obtaining the temperature with the highest total petroleum hydrocarbon content, with the composition of each individual hydrocarbon summing up to obtain the total petroleum hydrocarbon present in the varied temperature.

3. Transesterification is more common in the production of biodiesel than other conversion processes, such as micro-emulsification and pyrolysis.

4. WCO is expected to be more important in the future production of biodiesel than other edible and non-edible oils because of its low cost and wide availability. However, WCO requires several pre-treatment steps to eliminate solid impurities and reduce FFA and water contents. The pre-treatment process may include a washing step, centrifugation, flash evaporation, and acid esterification.

5. Several types of catalysts have been used widely for esterification reaction, such as homogenous catalysts (acidic and basic), heterogeneous catalysts (acidic and basic), and enzymes. Base homogenous catalysts face a large challenge in terms of the FFA and water contents in the oil. Therefore, a two-step process may overcome this challenge.

6. Methanol is used in the transesterification process because of its wide availability, high activity, and low cost. The methanol/oil molar ratio was one of the variables that had more influence on the process. Within the range of molar ratios employed, the best results were obtained for an 8:1 ratio.

Reference

[1] J. Orsavova, L. Misurcova, J.V. Ambrozova, R. Vicha, J. Mlcek, Fatty acids composition of vegetable oils and its contribution to dietary energy intake and dependence of cardiovascular mortality on dietary intake of fatty acids, Int. J. Mol. Sci. 16 (2015) 12871– 12890, https://doi.org/10.3390/ijms160612871.
[2] Chen Y, Xiao B, Chang J, Fu Y, Lv P, Wang X. Synthesis of biodiesel from waste cooking oil using immobilized lipase in fixed bed reactor. Energy Conversion and Management 2009;50:668–73.
[3] Wan Omar WNN, Saidina Amin NA. Optimization of heterogeneous biodiesel production from waste cooking palm oil via response surface methodology. Biomass and Bioenergy 2011;35:1329–38
[4] Demirbas A. Progress and recent trends in biodiesel fuels. Energy Conversion and Management 2009;50:14–34.
[5] Al-Dhabaan, F.A. Morphological, biochemical and molecular identification of petroleum hydrocarbons biodegradation bacteria isolated from oil polluted soil in Dhahran, Saud Arabia. Saudi journal of biological sciences 2019, 26, 1247-1252
[6] Cai, Y.; Wang, R.; Rao, P.; Wu, B.; Yan, L.; Hu, L.; Park, S.; Ryu, M.; Zhou, X. Bioremediation of Petroleum Hydrocarbons Using Acinetobacter sp. SCYY-5 Isolated from Contaminated Oil Sludge: Strategy and Effectiveness Study. Int. J. Environ. Res. Public Health 2021, 18, 819.
[7] Li Y, Zhao Y, Peng S, Zhou Q, Ma LQ (2010) Temporal and spatial trends of total petroleum hydrocarbons in the seawater of Bohai Bay, China from 1996 to 2005. Mar Pollut Bull 60:238–243
[8] Speight JG (2011b) Production, properties and environmental impact of hydrocarbon fuel conversion. In: Advances in clean hydrocarbon fuel processing. Woodhead Publishing, Cambridge, pp 54–82 www.deq.state.ok.us/factsheet/land/TPH. 2018..
[9] Chen Y, Xiao B, Chang J, Fu Y, Lv P, Wang X. Synthesis of biodiesel from waste cooking oil using immobilized lipase in fixed bed reactor. Energy Conversion and Management 2009;50:668–73.
[10] Wan Omar WNN, Saidina Amin NA. Optimization of heterogeneous biodiesel production from waste cooking palm oil via response surface methodology. Biomass and Bioenergy 2011;35:1329–38
[11] Demirbas A. Progress and recent trends in biodiesel fuels. Energy Conversion and Management 2009;50:14–34.
[12] Al-Dhabaan, F.A. Morphological, biochemical and molecular identification of petroleum hydrocarbons biodegradation bacteria isolated from oil polluted soil in Dhahran, Saud Arabia. Saudi journal of biological sciences 2019, 26, 1247-1252
[13] Cai, Y.; Wang, R.; Rao, P.; Wu, B.; Yan, L.; Hu, L.; Park, S.; Ryu, M.; Zhou, X. Bioremediation of Petroleum Hydrocarbons Using Acinetobacter sp. SCYY-5 Isolated from Contaminated Oil Sludge: Strategy and Effectiveness Study. Int. J. Environ. Res. Public Health 2021, 18, 819.
[14] Li Y, Zhao Y, Peng S, Zhou Q, Ma LQ (2010) Temporal and spatial trends of total petroleum hydrocarbons in the seawater of Bohai Bay, China from 1996 to 2005. Mar Pollut Bull 60:238–243
[15] Speight JG (2011b) Production, properties and environmental impact of hydrocarbon fuel conversion. In: Advances in clean hydrocarbon fuel processing. Woodhead Publishing, Cambridge, pp 54–82 www.deq.state.ok.us/factsheet/land/TPH. 2018.
[16] Chen Y, Xiao B, Chang J, Fu Y, Lv P, Wang X. Synthesis of biodiesel from waste cooking oil using immobilized lipase in fixed bed reactor. Energy Conversion and Management 2009;50:668–73.
[17] Wan Omar WNN, Saidina Amin NA. Optimization of heterogeneous biodiesel production from waste cooking palm oil via response surface methodology. Biomass and Bioenergy 2011;35:1329–38
[18] Demirbas A. Progress and recent trends in biodiesel fuels. Energy Conversion and Management 2009;50:14–34.

[19] Al-Dhabaan, F.A. Morphological, biochemical and molecular identification of petroleum hydrocarbons biodegradation bacteria isolated from oil polluted soil in Dhahran, Saud Arabia. Saudi journal of biological sciences 2019, 26, 1247-1252
[20] Cai, Y.; Wang, R.; Rao, P.; Wu, B.; Yan, L.; Hu, L.; Park, S.; Ryu, M.; Zhou, X. Bioremediation of Petroleum Hydrocarbons Using Acinetobacter sp. SCYY-5 Isolated from Contaminated Oil Sludge: Strategy and Effectiveness Study. Int. J. Environ. Res. Public Health 2021, 18, 819.
[21] Al-Dhabaan, F.A. Morphological, biochemical and molecular identification of petroleum hydrocarbons biodegradation bacteria isolated from oil polluted soil in Dhahran, Saud Arabia. Saudi journal of biological sciences 2019, 26, 1247-1252
[22] Cai, Y.; Wang, R.; Rao, P.; Wu, B.; Yan, L.; Hu, L.; Park, S.; Ryu, M.; Zhou, X. Bioremediation of Petroleum Hydrocarbons Using Acinetobacter sp. SCYY-5 Isolated from Contaminated Oil Sludge: Strategy and Effectiveness Study. Int. J. Environ. Res. Public Health 2021, 18, 819.
[23] Li Y, Zhao Y, Peng S, Zhou Q, Ma LQ (2010) Temporal and spatial trends of total petroleum hydrocarbons in the seawater of Bohai Bay, China from 1996 to 2005. Mar Pollut Bull 60:238–243
[24] Speight JG (2011b) Production, properties and environmental impact of hydrocarbon fuel conversion. In: Advances in clean hydrocarbon fuel processing. Woodhead Publishing, Cambridge, pp 54–82 www.deq.state.ok.us/factsheet/land/TPH. 2018.

NIPES-NCEE Conference Proceedings
The 2nd International Conference 15th-17th Feb. 2023
575-581
www.nipesjournals.org.ng

DESIGN AND CONSTRUCTION OF AN AUTOMATIC PAPER SHREDDER WITH A CROSS-CUT PATTERN

[1] Ikuemonisan, Victor Oluwaseyi and [2] Ashiedu, Festus Ifeanyi

[1, 2] Department of Mechanical Engineering, Federal University of Petroleum Resources Effurun, Delta State Nigeria.
[1] Email: victorikus@gmail.com
[2] Email: ashiedu.ifeanyi@fupre.edu.ng

Abstract

A Paper Shredder can be used to shred or cut documents made of Paper or Plastic into tiny strips. Private businesses use it to shred sensitive papers, such as contracts, into tiny pieces or rubble. As a result, these gadgets secure information while reducing environmental waste. This research work focuses on the Design and Construction of an Automated Paper Shredder with a Cross-Cut Pattern. In order to actualize the set objectives, the design has been divided into two; mechanical and electronic control units. The Paper Shredding Machine will achieve a shredding dimension of 4x23 mm using the cross-cutting technique. In addition, the fabrication process will involve procedures like metal shaping, welding, machining, and the usage of mechanical fasteners. The Cutting Blades and Shafts will consist of Medium Carbon Steel (Gear). The machine will use an Arduino Nano Microcontroller, a Programmable Integrated Circuit to control the Machine's Operation. Other significant sections for this design include the Power Supply, Blades, DC Motor, Microcontroller, Indicator, and many more. When completed, the machine will be subjected to a Paper Shredding Test using a Cross-Cutting Technique to validate its Performance and Calibrate it for efficient operation.

***KEYWORD**: Affordability, Ease of Operation, Documents Security, Safety Improvement.*

1.0 INTRODUCTION

Documents are made of paper, which frequently contains sensitive information. To keep this information out of the wrong hands, it is necessary to destroy materials. The best course of action is to completely destroy the paper before discarding it. Shredders can be categorized as either household or industrial, depending on their intended usage [1]. Paper shredders are frequently categorized as consumer shredders because consumers utilize them the most. This shredder will consist of a microcontroller (Arduino Nano), two cutting shafts fitted with multiple cutting blades, LEDs, etc. By limiting the number of landfills, documents, and paper can be more easily transported to the recycling center after destruction, which helps protect the environment [2], [8], [10].

Shredders for documents are increasingly in demand in recent times. However, the most common shredders do not completely destroy the papers which leads to the ability to rearrange these shredded documents leading to the exposure of sensitive information [5]. Many design techniques have been explored for shredder machine designs for various purposes [3] [9] [13], [11].

The aim of this project is to design and construct a paper shredding machine using a cross-cut technique. This involves: researching previous shredder machine components, such as the blades, frame, and transmission system; implementing an engineering sketch for dimensioning, selecting and assembling the appropriate electronic components for the automation, and evaluating the performance of the developed system using a standardized paper shredder.

This calls for the use of Programmable logic circuit as an interface for controlling mechanical movements through electronic systems. Several paper shredding machines use strip cutting, particle cutting, cross-cutting, and many more.

A thorough analysis of the construction and operation of paper shredder machines was conducted [12]. The numerous components of the cutting system, transmission, and frame were each thoroughly examined. The study focused on the individual parts' types, features, size, alignment, benefits, and drawbacks. Additionally, covered in the study are the motion study and stand analysis in ANSYS-15 as well as the construction of the 3D model of various elements of Dassault Systems' solid works. To overcome the problem of a strip of paper coming back with the blade, a Stripper finger component was added to the design.

Using a shredder that cuts this trash and turns it into nourishing fertilizer, [6] proposed a machine to improve the conventional technique of disposing of agro waste. The suggested device is an add-on for a KAMCO Tera-track 4W tractor, which supplies input power and support for the shredder. For chipping and powdering operations, numerous types of cutting blades (rotary, triangular, and screw blades) are available.

Also, an affordable, practical, and time-saving atomized paper shredder was developed [1]. The device eliminates constraints like time reduction and increased paper shredding per time. Eliminating paper backflow along cutting blades lowers noise and vibration. An enhancement was sought for the procedure of decreasing the buildup of post-consumer plastic waste. He created a system with carefully chosen characteristics to enhance current equipment.

Another author [4] presented the blades of the paper shredder that had serrated cutting edges that were formed by bending. This could be done by two methods. The blade body and serrated edge of the first approach were produced and punched together from the same base material. There were considerable production costs involved, and even premium materials were needed. The second method used serrated cutting edges that were thickened especially to conserve material.

To prevent the cut material from accumulating around the blade shaft, stripper bars or fingers were provided between the blades of each shaft in the cutter zone [15]. The stripper's finger was received in this instance on the stripper block in the spaces between the blades. Due to the fingers' engagement with the support ribs of the opposing housing, the necessary stability was reached. The Stripper block was an injection mold component, making it easy to make, simple to build, and inexpensive.

2.0 METHODOLOGY

The purpose of this activity is to analyze, design, and assemble the electronic circuit of the gadget using readily available components and linking each part together. There are two primary categories for the hardware and software components that make up the paper shredder. The blades, bearings, electric motor, shaft assembly, and microcontroller unit make up the hardware interface. The Arduino IDE and Proteus software, which function as a circuit simulator, are also a part of the software package. The machine will have a power button to set it in ready-to-operate mode, while an infrared (IR) remote and a push button will be used to initiate the paper shredding mechanism.

Also, the machine operation could be halted using either the IR remote or the push button to alter the mechanism of operation. An indicator on the machine will show the state in which it is operating.

The paper shredding machine will use a combination of cross-cut and particle-cut techniques. The reason for this is to ensure that the efficiency of the cutting technique outperforms previously designed systems that focused solely on an approach. With the aforementioned paper techniques for this research work, it is expected to produce an efficient, safe, and reliable method of destroying sensitive documents.

Figure 1 below shows the components of the automated shredder machine. The components highlighted in Figure 1 are a combination of the electronic hardware and the mechanical materials required for the development of the research work.

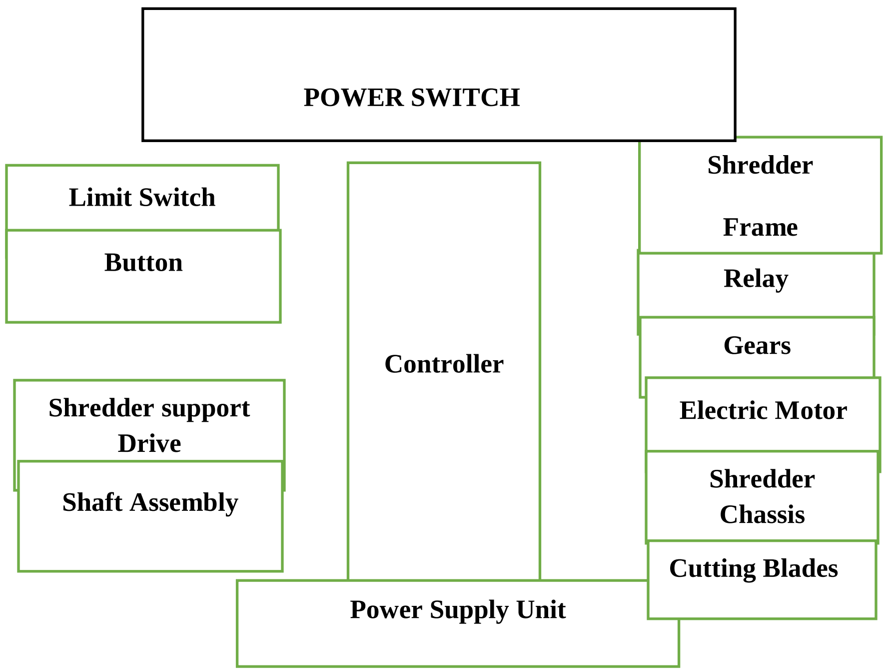

Figure 1: Block Diagram of an Automated Paper Shredding Machine

2.0.1 The Shredder

The shredder will consist of different parts which include;

- **Electric Motor:** The electric motor transfers the required power in a forward rotation to shred paper. The electric motor used for this project rotated at a speed of 1450 revolutions per minute and has a power rating of 80 watts (0.08 kW).
- **The Blades:** The blade, which is a circular cutting blade, actually shreds the paper into strips. This design used a blade that was 1.5mm thick and constructed of medium carbon steel. The inside diameter of the blade will be converted into a hexagonal shape on a lathe in order for the intended shaft to fit. A total of 112 washers and 56 washers will be put on each shaft.

- **Bearings**: To lessen friction, this machine utilizes dip groove ball bearings, which will be situated at either end of the main shaft.
- **Shaft Assembly:** A shaft assembly is made up of gears, washers, and blades. The washer, which is shaped like a conventional ring, serves just to line and lock the blades so that they don't move when the machine is in use. There will be 20 of them in total, and two of them will have lock nuts. The primary shaft gear is composed of the size and two spur gears.

The main section of the paper shredding machine is the machine frame, which serves as a support structure for other machine parts, especially the moving parts. The frame for this design will be made of mild steel with a 4 mm thickness and measured 1100 mm by 700 mm by 500 mm. The major structural elements of the machine are the mainframe, left base, right base, shredder support, and gear support.

Several factors will be put into consideration during the fabrication of the machine

i. Torque of the machine
ii. Shaft diameter
iii. Power determination
iv. Bearing selection
v. Gear module
vi. Determination of the cutting force

2.0.2 Advantages of Cross-cut pattern Shredder over Others

i. Ability to shred papers with staples and Clips without blade damage
ii. Ability to shred thicker materials like cardboard
iii. Ability to obscure the information more completely
iv. Cross-cut Shredder cuts into tiny pieces not larger than 4 x 23 mm

2.1 Cutting Force

Cutting force (Fc) = τ x t (1)

Tensile strength = 3.6 N/mm

Shear strength (τ) = 80% of tensile strength

τ = 80/100 x 3.6 = 2.88N/mm.

Considering a thickness of 4 mm

Fc = 1.42 x 4 = 4.8 N

Using a factor of safety of 3

Fc = 2.84 x 3 = 8.52 N

Considering the shaft as one with a uniformly distributed load,

The force at the cutting spot is 8.52 N and it is distributed at an interval of 12mm on the shaft with the cutting blades.

$$P = \frac{aq}{n+1} \quad [9] \qquad (2)$$

n = the degree of parabola =0
q =8.52 N
12mm, a = 320mm
$\therefore$ p =$\frac{8.52\times320}{12}$ = 227.2 N = total cutting force
Cutting power (PC) = total cutting force (FTC) x cutting speed (SC)
PC = 227.2 x 0.28 = 63.616 W
Using a factor of safety of 3 from standard values
PC = 63.616 x 3 = 190.85 W

- Transmitted power (PT) = cutting power (Pc) + power loss in belt (PLB) + power loss in gear (PLg) + power loss in bearing (PLb)

PT = 190.85 + 0.05 PT + 0 + 0.62 (3)
PT - 0.05 PT = 191.47
0.95 PT = 191.47
PT = 191.47/0.95
PT = 201.55 W
Using a standard module of 3mm and rotational speed of 900 rpm
Using.
The ratio of the basic dynamic load rating to the equivalent dynamic bearing load is given as
$^{C}/_{P}$ =10.3
C = 10.3 x P
P= 1 x FrA = 191.47 N
Therefore, C = 10.3 x 191.47= 1972.141 N

2.2 CUTTING AND PRECISION TOOLS

- **Grinding machine**: The mild steel pan and the shaft holding the blades will be converted to a diameter of 50 mm and stepped down to a diameter of 25 mm from both ends to a length of 40 mm using the grinding machine and a cutting disc.
- **Measuring Tape**: The shaft and mild sheet metal will be measured with a tape rule.
- **Vernier Caliper**: It will be used to gauge the blade and gears' interior diameters.
- **Bending Machine**: The mild steel sheet metal will be folded into a rectangular shape using the iron bender.
- **Chalk**: Chalk will be used to mark out the mild steel sheet metal's measured length; the medium carbon steel shaft and other components relied on that measurement.
- **Drilling machine**: the drilling machine will be used to drill holes in the metal sheet.
- **Bench vice**: The workpiece was primarily held in place throughout the cutting operation using the vice.
- **Welding Machine**: The machine frame and the metal sheet were both welded using an electric welding machine.

2.3 DESIGN INTERFACING

- **Riveting:** Using a riveting gun and pin, the supporting rollers that help the machine move will be attached to the machine frame.
- **Deslagging:** Following the completion of the welding process, the impurities from the welded frame will be removed using a wire brush and a chipping hammer.
- **Electrical System:** The driving shaft was connected to the 80-watt (0.08kw) electric motor, and other electrical connections like the cable and plug were also made. The shredder support had an electric motor positioned inside of it.
- **Mechanical Fasteners**: bolts and nuts were used to firmly secure the electric motor and shaft to the shredder support as well as to the shafts.
- **Painting**: To enhance the finished machine's aesthetics, black oil paint was applied.

3.0 RESULTS AND DISCUSSION

The Shredder will be put into use right after completion. The machine will be powered by an electrical source; the electric motor will supply the required electrical energy, and the gears will convert the electrical energy into mechanical energy, reducing the speed of the electrical motor to the desired speed required by the paper shredder to successfully shred the papers into strips. The intermeshing washers, which will be sandwiched between the strip-forming rollers grab and drag the paper sheet to create the shreds.

There are possible unforeseen errors or faults which may have occurred during the fabrication of the machine. However, such faults will be addressed in the ensuing redesign as part of a continuous design process.

4.0 EVALUATION OF THE PERFORMANCE OF THE AUTOMATIC PAPER SHREDDING MACHINE

The evaluation of the performance of the paper shredding machine will be carried out using a software simulator and comparison analysis by calibrating the developed paper sheet shredding machine against a standard.

5.0 CONCLUSION

This research will produce an efficient low-cost automated paper shredding machine using cross-cut and strip-cutting techniques machine capable of thoroughly shredding sensitive and discarded documents.

REFERENCES

[1] Ankit, B. R, Vinayak D.W and Bhushan. G.P., (2018): "Design and Fabrication of Paper Shredder Machine" International Journal for Research in Applied Science and Engineering Technology, Volume 6, Issue 10.
[2] Auti, S.M., Sheth, J., Tulasyan, P. Gaikwad, A., Bagwe, P., (2020): Design of Shredder Machine for ELV Tyres, In Vasudevan H., Kottur V., Raina A.: (eds) Proceedings of International Conference on Intelligent Manufacturing and Automation, Lecture Notes in Mechanical Engineering.
[3] Ekman, R. (2018): Development of a Plastic Shredder, Master Thesis, Sweden, Lund University.
[4] Gu-Ming Zeng, 2006, "Blade of Paper Shredder", US 2008/0040934A1.
[5] Kumaran, P., Lakshmi Narayanan, N., Martin, A.V., George, R., and Jojo, J. (2020): Design and analysis of shredder machine for e-waste recycling using CATIA, IOP Conf. Series: Materials Science and Engineering, 993.
[6] Nithyananth, S., Samuel, L., Mathew, N. and Suraj, S.,(2014) "Design of waste Shredder Machine" International Journal of Engineering search and Applications, Volume 4, Issue 3(version 1), pp 487-491.
[7] Olukunle, T. A., (2016) " Design consideration of a plastic shredder in Recycling process" International Journal of Mechanical Aerospace, Industrial, Mechatronics, and Manufacturing Engineering Volume 10, No 11.
[8] Onyeyili, I.O., (1998), "A Fundamental Course in Engineering Mechanics". Snaap Press ltd.
[9] Pavankumar, E., Baskaran, S., Prithivirajan, R., Vinoth Kumar, S., Karpagaraj, A. (2021): Development of Multifunctioning Organic Waste Shredding Machine for Natural Compost, In: Arockiarajan A., Duraiselvam M., Raju R. (eds) Advances in Industrial Automation and Smart Manufacturing. Lecture Notes in Mechanical Engineering.
[10] Pedraza-yepes, C., Pelegrina-romero, M.A., Pertúz-martínez, G.J. (2018): Analysis by Means of the Finite Element Method of the Blades of a PET Shredder Machine with Variation of Material and Geometry, Contemporary Engineering Sciences, Vol.11, No. 83, pp. 4113-4120.
[11] Reddy, S., Raju, T. (2018): Design and Development of mini plastic shredder machine, IOP Conf. Series: Materials Science and Engineering, 455.
[12] Siddique. F, Patil, H., Raut. S, Wadake, O. and Tandel, S., (2017) "Design and Fabrication of Paper Shredder Machine" International Journal of Scientific and Engineering Research, Volume 8, Issue 3.
[13] Vatskicheva, M.M., Valkov, M.(2013): Existing structures of multi-purpose shredders and guidelines for their improvement, Proceedings of the University of Mining and Geology "St. Ivan Rilski", Sofia, Bulgaria.
[14] Vatskicheva, M., Grigorova, I.(2017): Study of two-shaft shredder for crushing of concrete, rubber, plastic and wood, Journal of International Scientific Publications: Materials, Methods & Technologies, Vol. 11, pp. 238-253.
[15] Willi S., (1995) "Blade and Stripper assembly for a paper shredder", US Patent 5400978.

NIPES-NCEE Conference Proceedings
The 2nd International Conference 15th-17th Feb. 2023
582-595
www.nipesjournals.org.ng

DESIGN AND FABRICATION OF A FIREFIGHTING DEVICE

Asemota Esosa, Otobiogeh Pope, Azamosa Harry, Egware Henry, and Unuareokpa Omozee

Department of Mechanical Engineering, Faculty of Engineering, University of Benin, Edo state, Nigeria.
Phone: +2349021557243, +2348155612627, +2348061226282
Email: a_esosa@yahoo.com, omozee.unuareokpa@uniben.edu

Abstract

Fire, a very vital substance in the advancement of the human species, has proven to be almost as destructive as it is useful. With the increased concepts of engineering devices aimed to ensure the safety of the human race in this world, this project is one that not only aims at saving lives but also ensures the protection of property from the raging claws of fire. Made from a combination of various technologies, this device was created with the purpose of extinguishing fire while being wirelessly controlled.

The main systems that make up this device focus on mobility, and obstacle avoidance through the use of a controller, visual aid, and flame extinguishing. Mobility is achieved through the use of motors, chain drives, sprockets, and a 12V battery all fused with programmable logic and circuit integration. Obstacle avoidance is made possible through the use of a wireless controller and a receiver. A Wi-Fi camera connected to a mobile phone was used to relay visuals to the controller to aid the movement of the device. Also, the flame extinguisher uses CO2 as a main source to extinguish the fire, it was also designed to be able to use water as the main extinguishant in the event of a lack of CO2. With these systems, we were able to create a low-cost device that would aid firefighters in the war against fire.

***Keywords**: Firefighting, Design and Fabrication, Extinguisher, Wirelessly controlled, Water.*

1.0 INTRODUCTION

Fire, a discovery that has both helped and hindered mankind's survival, has been a central focus of human attention for 1.5 million years. While it has played a vital role in technological advancement, it has also been responsible for some of the worst casualties ever recorded by man, like the Peshtigo fire of 1871 in which 1500 deaths were documented [1]. Over time, various firefighting techniques and approaches have been invented, from leather belts to modern-day water pumps, hydrants, and chemicals. The introduction of a team of specially trained firefighters equipped with the knowledge of fire behavior was a crucial turning point in man's fight against fire outbreaks. This was followed by the realization that although all fires were alike, they were not the same, and the classification of fire into six different classes [2]. This project aims to build on this realization.

Despite the advent of firefighters and their pressurized water pumps, firefighters still lose their lives while in action. An average of 75 firefighters die annually in the United States while fighting fires, with the statistics indicating that the certainty of death increases with each fire incident [3]. This highlights the need for better ways to protect firefighters and prevent casualties. Additionally, there have been recent introductions of firefighting devices to aid in fighting fires from inaccessible sources, but their efficacy is still under question.

This study aims to address this problem by exploring the development and improvement of device firefighting systems to enhance their effectiveness and efficiency in combating fire outbreaks, thereby reducing the risk to the lives of firefighters. The objectives are to:

i. To design a CAD model of the mini firefighter device using Solidworks
ii. To fabricate a model of the mini firefighter device
iii. To test run the functionality of the model in real-time fire incidents

The significance of this study lies in its potential to improve firefighting efforts, reduce fire damage and casualties, and protect the lives of firefighters.

2.0 METHODOLOGY

In the design of this firefighting device, the following concepts were considered, deliberated upon, and thoroughly analyzed before a decision was made. For the analysis, we considered both the pros and cons of all the concepts and then constructed a decision matrix using factors such as cost, complexity, ease of use, ease of maintenance, environmental impact and sustainability, performance, etc.

2.1 DESIGN CONCEPTS

CONCEPT ONE: **FIREFIGHTER MACHINE USING PLASTIC TANK STORAGE**

In this concept, the direction of the machine is controlled with an aid of a remote and navigated with a 360 degrees Wi-Fi camera mounted at the center of the chassis accessed via using Wi-Fi connection with your smartphone. The fluid tank pump is made of plastic material and contains an extinguishant that can spray at least one meter when the button is pressed. The machine's arm is fixed and not able to lift the spray nozzle upward and downward [4].

Figure 28: The first concept [4]

Advantages of Concept One

i. The system is simple.
ii. Visuals for the operator is possible

Disadvantages of Concept One

i. The device arm is fixed which makes it hard to give off fire in other directions.
ii. Fire possess a danger to the camera and plastic storage of the machine since there are not fireproof.

CONCEPT TWO: FIREFIGHTER MACHINE USING AN EXTERNAL STORAGE TANK

In this concept, there is no extinguishant tank, the extinguishant is transmitted into the machine by the use of a hose from an external stationary storage tank and the extinguishant is pumped at high pressure and used to put off the fire. The pump nozzle moves up, down, and side to side horizontally. Directions are navigated through a remote control and a radio wave camera [5].

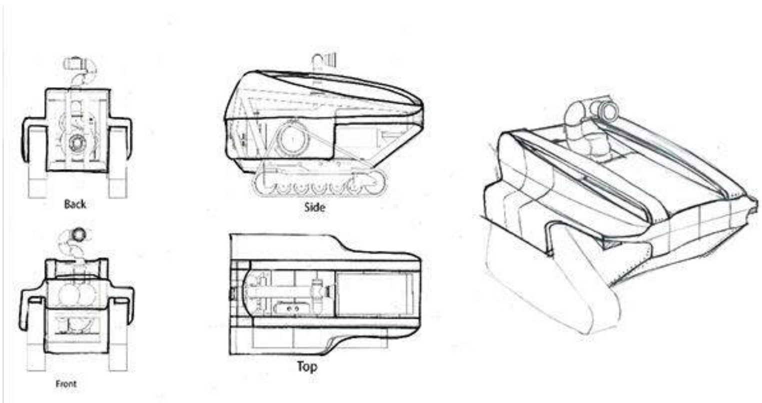

Figure 2: Orthographic projection of the second concept [5]

Figure 3: The second concept [5]

Advantage of Concept Two

i. The system is simple.
ii. Enough storage tanks would be available to stop the fire.
iii. Lightweight due to the absence of a sitting storage tank

Disadvantages of Concept Two

i. The length of the hose determines how far the machine can go to stop the fire, which could be a hindrance to the operation.
ii. Hose can get burnt during operation if the right fire-resistant material is not used.

CONCEPT THREE: USE OF A MOVEABLE NOZZLE AND STORAGE TANK

In this design, the fire extinguisher is incorporated into the device, making it a lot easy to put out the fire. The presence of a storage tank on the machine means the extinguisher would be carried by the machine and not transported through a hose, which would have been a limitation while fighting the fire, as the length would have been. With visual aid, the operator is also able to see where the device is moving, in other to avoid obstacles, put off the fire, and return safely to the operator.

Figure 4: The third concept

Advantages of Concept Three

i. Presence of a portable storage tank eliminates the need for a hose connection which would have had the limitation of length and cost.
ii. Presence of motion visual aid which helps when encountering obstacles.

Disadvantages of Concept Three

i. The complexity of the machine.
ii. Weight complications due to the inclusion of the storage tank.

2.2 DECISION MATRIX

A decision matrix is a useful tool for comparing and evaluating different conceptual designs for a firefighting machine. To create a decision matrix for this purpose, we would start by identifying the key factors that we would consider when choosing between these different concepts. These include things like:

i. Performance and effectiveness in extinguishing fires
ii. Cost and ease of maintenance
iii. Ease of use and control by firefighter
iv. Size and weight of machine
v. Environmental impact and sustainability

Designs	Performance and effectiveness	Cost and ease of maintenance	Ease of use and control	Size and weight	Environmental impact	Total score
Design 1	4	3	4	2	4	17
Design 2	3	4	3	4	4	18
Design 3	5	3	5	2	5	20

In this decision matrix, the scores are assigned on a scale of 1 to 5, with 1 being the lowest and 5 being the highest. By reviewing this matrix, one can see how each design compares across the different evaluation criteria and it can be seen that design 3 is relatively the best fit for this project.

2.3 PROTOTYPE FABRICATION

CHASSIS

Figure 7: The chassis

The chassis was mainly made from 23inches length square pipe used as the base framework with an 18-inch length square pipe used as a cross member for the front axle rollers and back axle tires. The 5 inches diameter rollers were used for the front tires, while the 8 inches diameter rollers were used as the back tires.

MOTOR

Figure 8: DC motor

2 motors were used, and one motor was used to transmit rotation motion with the help of a sprocket chain attached to a drive wheel. The diameter of the sprocket of the chain motor was twice as small as the sprocket in the drive wheel. Therefore, enabling the drive wheel to rotate twice the speed of the drive motor. The other was laid under the chassis which helped to aid the left and right directional movement for reverse and turning.

PUMP

Figure 9: 12 Volts pump

And the extinguishant is connected to a 12-volt high-pressure centrifugal extinguishant pump, which has an impeller inside the pump that uses centrifugal force to push the extinguishant at high pressure from the extinguishant jet or nozzle.

FLUID TANK

Figure 10: Fluid storage tank

We bought a 3kg gas cylinder and converted it by making a hole close to the button and welded a 2-inch galvanized pipe on that hole, thereby creating a passage for the extinguishant to go into the gas cylinder, this served as the extinguishant inlet for the reservoir, making it our extinguishant reservoir for the machine. Another hole was cut close to the top of the machine in a horizontal manner which served as an outlet for the extinguishant and connected to the pump.

ELECTRICAL CONNECTIONS

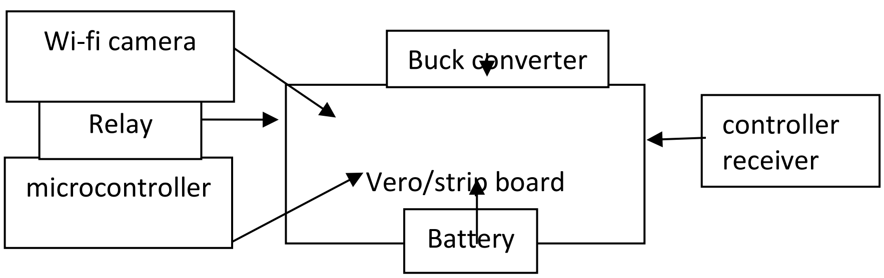

A Solderless Vero breadboard was used as the main frame for the circuit connection. A 12volt powered battery was connected to light up the breadboard and an Atmega328p-u microcontroller was attached. An LM259 12volt step-down dc-dc buck converter module was also connected to the board to help control the voltage supplied to the board and the components on it. Relay terminals were connected to each component and a Mosfet semiconductor was used to help control the amount of voltage entering the components. The Controller receiver was also connected to the board to help in the feedback response to the controller. An Esp cam board that housed the Wi-Fi camera was also connected to the board which aided visuals to the operator.

CONTROLS
WIRELESS CONTROLLER

Figure 11: Wireless controller

The control commands are sent to the firefighting machine with the help of a wireless remote control. With 6 buttons in the remote control, four buttons are used to steer to the left, to the right, move forward and backward, one button to activate the extinguishant to off the fire, and one other button to move the direction for the pump (180° degrees horizontal and vertical movement).

WI-FI CAMERA

Figure 12: Wi-Fi camera

The Esp cam download board was connected to the Eps cam 32 which was then fixed to the veroboard with the use of ribbon cables.

Figure 13: Front view of the completed device **Figure 14: Back view of the device**

2.4 DESIGN CALCULATIONS

For the detailed design analysis of this machine, we would be making some assumptions:
Surface area of the fire = 6m^2
Thickness of the flames = 0.5cm
Pressure required of the water tank would be

$P = \frac{Weight\ of\ the\ tank}{Surface\ Area\ of\ the\ tank}$ [6]

$P = \frac{3 \times 9.81}{15m^2}$

P = 1.962N/m^2

Stress expected on the tank
Volume of fluid extinguishant = 4.7m^3
Weight of the fluid extinguishant = 1.962×10^3N

γ = Specific weight = $\frac{weight}{Volume}$

= 0.417N/m^2

$\emptyset = {}^{F}/_{A}$ [6]

$= \frac{1.962 \times 10^3}{\frac{\pi \times d^2}{4}}$

Taking the diameter of the tank as 0.8m

$$\emptyset = 3.9KN/m^2$$

Pressure Required Of The Nozzle

For our calculations, we would be assuming the minimum conditions required of the flow to extinguish a fire.

i. The minimum flow rate required to extinguish a class A fire using water as an extinguishant is $0.0075m^3/s$ [7].
ii. The assumed minimum diameter for our nozzle is 2.2cm.
iii. The assumed initial pressure is 379.2KPa, which is the usual factory set pressure of a 12volts pump [8]
iv. The outlet diameter of a 12v pump is usually 1.9cm
v. We assume a constant flowrate across the pipe

Using Bernoulli's equation for finding flowrate

$Q = A \times V$ [9]

$$0.075 = \frac{\pi 0.019^2}{4} \times V_1$$

$$V_1 = 264.5m/s$$

$$0.075 = \frac{\pi 0.022^2}{4} \times V$$

$$V_2 = 19.73m/s$$

Using

Bernoulli's equation for pressure to calculate the pressure required at the nozzle, we have

$P_1 + \frac{1}{2}\rho v_1^2 + \rho g h_1 = P_2 + \frac{1}{2}\rho v_2^2 + \rho g h_2$ [9]

So

$$P_2 = P_1 + \frac{1}{2}\rho v_1^2 + \rho g h_1 - \frac{1}{2}\rho v_2^2 - \rho g h_2$$

Taking h_1 as 0 since it is the ground level and h_2 as 40cm - the projected height of our nozzle from the ground.

$P_2 = 35$MPa

This is the required pressure predicted for our machine's nozzle (using the above-listed conditions) to successfully extinguish a class A fire.

3.0 RESULTS AND DISCUSSIONS.

We selected a refractory material to help protect the device from fire, which would in turn improve its effectiveness in certain situations, but this was not possible as the material kept on interfering with our control signals to the device. A suggestion was made to use pyrex glass to act as the refractory material due to its high resistance to heat, but this was not feasible as glassblowing it to fit the skeletal structure of our device was not only cost-demanding but also time intensive.

We were able to achieve a flow rate intensive enough to extinguish the various fires we set up the flow rate we achieved can be calculated from the Bernoulli equation stated below.

To determine the flow rate of our nozzle we would make use of Bernoulli's equation which states that the sum of kinetic, potential, and pressure energies of a fluid in a system is constant.
For a nozzle, the Bernoulli equation can be expressed as:
Q = $AV \times \sqrt{2}g(h1 - h2)$ [10]
where:

i. Q is the flow rate of the nozzle (volume per unit time)
ii. A is the cross-sectional area of the nozzle $= \frac{\pi d^2}{4}$
iii. v is the velocity of the fluid through the nozzle = $19.73 m/s$
iv. g is the acceleration due to gravity
v. h1 and h2 are the heights of the fluid at the inlet and outlet of the nozzle, respectively

Q = $(0.00038) \times 19.73 \times \sqrt{2} \times 9.81(0.4 - 0)$
Q = $0.021 m^3/s$
Our wireless controls worked perfectly well and we were able to achieve a working distance of 15 metres from the firefighting device, which ensures the optimum safety of the firefighter.
The camera functioned without a hitch and connected to our phones seamlessly, giving us a view of what the device sees, this was very useful in tight corners that were not easily accessible.

4.0 GRAPHICAL MODELLING

Figure 5: The chosen concept

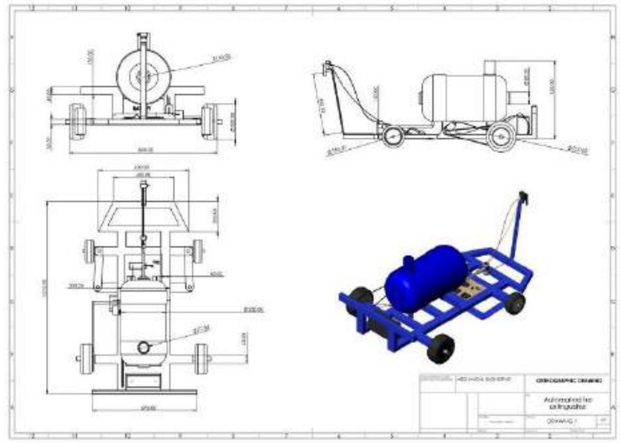

Figure 6: Detailed design of the chosen concept

5.0 CONCLUSION AND RECOMMENDATIONS

Though we were limited to subpar material due to cost, we were able to make the machine to a satisfactory level. The mechanical parts of the device were fabricated perfectly, and the movement of the device to and fro in the operation of firefighting was smooth. Also, the electrical parts and controller were all coupled and connected seamlessly to each other; with the use of Arduino, we were able to make the wireless control possible and effective, the controls worked perfectly well and we were able to achieve a working distance of 15 metres from the firefighting device, which ensured the optimum safety of the firefighter. The camera provided proper visuals and allowed us to extinguish the fire without physically seeing it, while the battery lasted about 3 hours of constant use before needing to the recharged. In all, not only was the device effective in doing its job, it was also cost-effective.

RECOMMENDATIONS

i. The use of mild steel for the fabrication was solely due to cash constraints and should not be used for further developments of this project.
ii. The placing of the camera can be made better, as we experienced some form of obstruction since it was placed behind the nozzle arm.
iii. The circuit board should be covered properly, to avoid damage in the event of an erratic fire.
iv. A better wireless technology should be used for the control in the event of mass production, as the Bluetooth technology employed could only offer perfect control at a distance of 15 metres away.

REFERENCES

[1] E. (. Bush, "Fighting Fire!: Ten of the Deadliest Fires in American History and How We Fought Them by Michael L. Cooper (review)," in *Bulletin of the Center for Children's Books.*, 2014, pp. 67. 353-353. 10.1353/bcc.2014.016….

[2] M. Dickinson, "What Are the 5 Different Classes of Fires?," 2021. [Online]. Available: https://vanguard-fire.com/what-are-the-5-different-classes-of-fires/. [Accessed 10 10 2022].

[3] R. F. Fashy and M. L. Joseph, " Firefighter Fatalities in the United States," NFPA, 2019.

[4] A. Mohammed, "digitalcommons.cwu.edu/undergradproj/124," 13 October 2020. [Online]. Available: https://digitalcommons.cwu.edu/undergradproj/124. [Accessed 23 November 2022].

[5] C.Ryan,"behance.net,"march2016.[Online].Available: https://www.behance.net/gallery/61944891/Unmanned-Firefighting-Robot-Conceptual-Design?locale=en_US. [Accessed 23 November 2022].

[6] R. Hibeller, Engineering Mechanics: Statics (14th ed.), Pearson Education Inc, 2016.

[7] National Fire Chief Council, "Control Measure - Flowrates," 2022. [Online]. Available: https://www.ukfrs.com/guidance/search/flow-rates#:~:text=Relying%20on%20pressure%20alone%20as,prevent%20fire%20growth%20and%20spread.&text=This%20shows%20that%20an%20estimated,minimum%20to%20extinguish%20the%20fire.. [Accessed 3rd December 2022].

[8] Amazon, "KOLERFLO 12V DC Fresh Water Pump," 2022. [Online]. Available: https://www.amazon.com/KOLERFLO-Pressure-Agriculture-Applications-FL42-5-0-12/dp/B09196SLT3. [Accessed 1 12 2022].

[9] Y. A. Cengel and J. M. Cimbala, Fluid Mechanics: Fundamentals and Applications (4th ed.), McGraw-Hill Education, 2018.

[10] R. W. Fox, A. T. McDonald and P. J. Pritchard, Introduction To Fluid Mechanics (8th ed.), John Wiley & Sons, 2011.

NIPES-NCEE Conference Proceedings
The 2nd International Conference 15th-17th Feb. 2023
596-610
www.nipesjournals.org.ng

PREDICTION OF HOUSEHOLD SOLID WASTE GENERATION IN OKADA TOWN USING ARTIFICIAL NEURAL NETWORKS

Ejiroghene Kelly Orhorhoro[1*], Andrew Amagbor Erameh[2], Joseph Eka Efia[3]

[1,2,3]Department of Mechanical Engineering, General Abdulsalami Abubakar College of Engineering, Igbinedion University, Okada, Edo State, Nigeria

Corresponding email: ejiroghene.orhorhoro@iuokada.edu.ng

Abstract
There is a poor waste management policy in Nigeria, just like in other sub-Saharan African countries, and solid waste generated is improperly disposed of in our environment. Waste from most towns in Nigeria is sometimes discharged into adjoining streams without treatment due to poor implementation of standards, thus causing environmental and public health hazards. Also, one cannot ascertain the quantity of solid waste generated in Okada town, hence this study. The materials used for this study include a weighing balance, hand gloves, a nose mask, and a black polyethylene bag labeled in the following order: sample A-food waste, sample B-plastic and rubber waste, sample C-glass waste, sample D-paper waste, sample E-metal waste, and sample F-other waste. The solid waste generated in Okada town was randomly collected from different households after a period of seven days (one week), and the quantity of household solids generated was measured after sorting with a weighing balance. A stratified random sampling (SRS) method was applied. Artificial Neural Networks (ANNs) was used to predict the solid waste generated daily. From the results of the waste survey carried out, a total of 318.879 kg of household solid waste was generated per week by 100 households, consisting of 334 people. It was observed that an R2 value of 0.99621 was obtained for the training set. Furthermore, R2 values of 0.98253 were obtained for the testing set, 0.99560 for the validation test, and 0.99834 for the all-data set. As determined, all the values were found to be high and close to 1. Also, there was a close correlation between the data used in the validation process and the predicted values of household solid waste generated. This affirmed that the ANNs were capable of predicting household solid waste generation.

Keywords: *Household Solid Waste, Stratified Random Method, Artificial Neural Network, Prediction, Food Waste*

1.0 Introduction
The problem of solid waste (SW) generation in developing countries is a major concern for governments and society. The generated SW is difficult to manage in Nigeria, especially with increasing population pressure and social-economic pressure [1-5]. Solid waste is useless and unwanted products in their solid state, discarded by members of society. Most towns and cities in African countries spend 20–50% of their environmental budget on solid waste management and only 20–80% of the waste is collected. Nigeria's towns and cities are today struggling to clear heaps of solid waste from their environment. Strategic centres of attraction in the country are now taken over by the messy nature of unattended heaps of solid waste emanating from society. Both towns and city officials are unable to prevent the unlawful dumping of solid waste, and this is a clear violation of the clean air and health edicts in their environmental sanitation laws and regulations [6-8]. Solid waste is generated in all sorts of ways, and the volume of its generation depends on the consumption pattern and industrial and economic structures in place [9, 10]. Past research work has shown that developed countries with fast-growing economies are mostly faced with a high volume of solid waste generation [11]. For instance, it was observed that solid waste

generated in China increased by 9% annually from 1979 to 1995, a period associated with rapid economic growth, and this is expected to double by 2030 [12].

Furthermore, household solid waste generated in Nigeria generally consists primarily of the following waste components: food remnants, plastics, paper, textile, metal, and glass [2], and the annual generation rate is 25 million tonnes at a daily rate of 0.24-0.66 kg/day/person [13-16]. As reported by [17-19], the Artificial Neural Networks (ANNs), also called *neurocomputing,* is a computational network that bears the relationship between numerous simple computational elements called artificial neurons, which perform a nonlinear function of their inputs. It is composed of groups of interconnected processing elements known as neurons, and the links between these neurons are known as weights and biases. The higher the weight of an artificial neuron, the stronger the input obtained [20, 21]. By adjusting the weights of an artificial neuron, one can obtain the output for specific inputs. It is formed in three layers (i.e., input layer, hidden layer, and output layer), and each layer consists of one or more nodes represented by small circles. The lines between the nodes indicate the flow of information from one node to the next node [22-24].

2.0 Materials and Methods

The following materials and equipment were used; polyethylene bags (labeled in the following order; Sample A-food waste, Sample B-plastic and rubber waste, Sample C-glass waste, Sample D-paper waste, Sample E-metal waste, and Sample F-other waste), weighing balance, noise mask, and groove. The black polyethylene bag is used to collect domestic solid waste. Figure 1 shows the summary of the procedures adopted in the household solid waste survey.

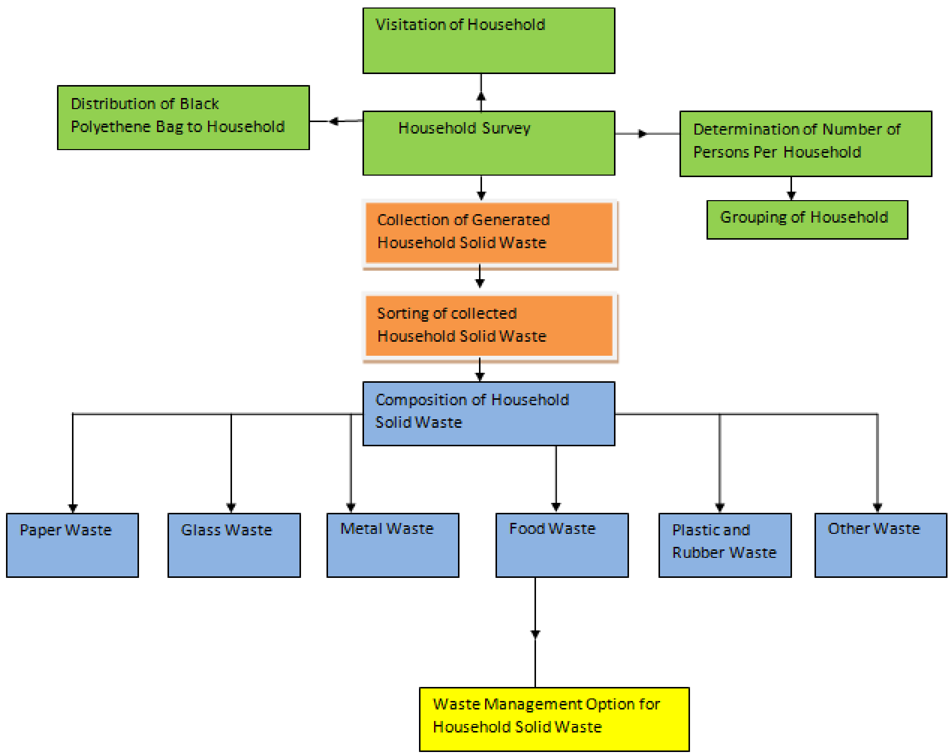

Figure 1 Household Solid Waste Survey

One hundred (100) households were used in this study, and the household family size was selected after initial visitation. The solid waste was collected randomly from different households located in Okada town after a period of seven days. The quantity of solid generated was measured after sorting with a weighing balance, and the stratified random sampling (SRS) method was adopted. The technique is a sampling method based on population determination and characterization. It involves the process of separating members of the population into matching subgroups before sampling, and in so doing, every element in the population is given to only one stratum [25]. Figure 2 shows the procedures to be followed in developing the ANNs model.

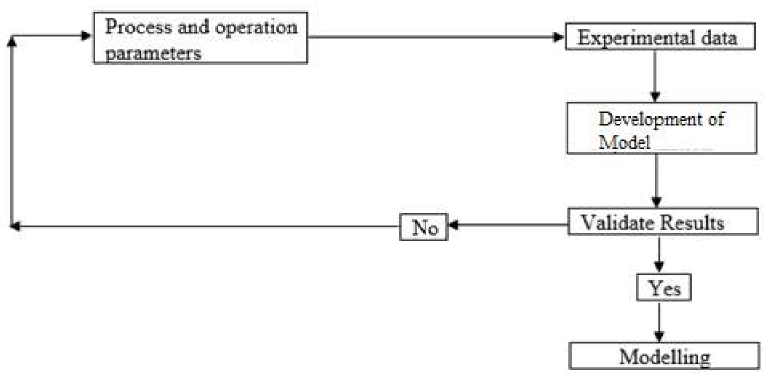

Figure 2 Modelling framework

The ANNs was fully utilized as a tool for modelling the prediction and optimization of household solid waste generated in Okada town. It was developed using the ANN toolbox of MATLAB 2014 software. The input (i.e., sample A-sample F) and target data were gotten from the experiment and then organized in a Microsoft Excel Spreadsheet. The ANNs architecture is designed in terms of the components of the neural network and its operations. Both the number of neurons and the number of layers in each layer were recognized. The multilayered feed forward architecture was used for designing the ANN model, and the Levenberg-Marquardt back propagation training algorithm (trainlm) was used for the training. It consists of at least three layers of nodes, and each node is a neuron that uses a nonlinear activation function, with the exception of the input node. The networks are comprised of 6 input layers, 10 hidden layers, and 1 output layer, thus making a three-layer layout. The architecture of the ANNs model was computed using 10 dissimilar numbers of hidden neurons in the hidden layer (i.e., from 1 to 10 neurons) for the three different trials of data separation (i.e., % of training set: % of validation set: % of testing set), including 50%: 25%: 25%. The back-propagation network (BPN) is by far the most widely used training algorithm for a multilayer feed forward neural network. It contains the output layer with nodes representing the dependent variables that are being modelled, hidden layers that contain nodes to support capturing the nonlinearity in the data, and the input layer consisting of nodes that represent input variables to the problem. Figure 3 shows the ANNs architecture.The generated household solid waste in Okada town was collected and use to validate the ANNs model.

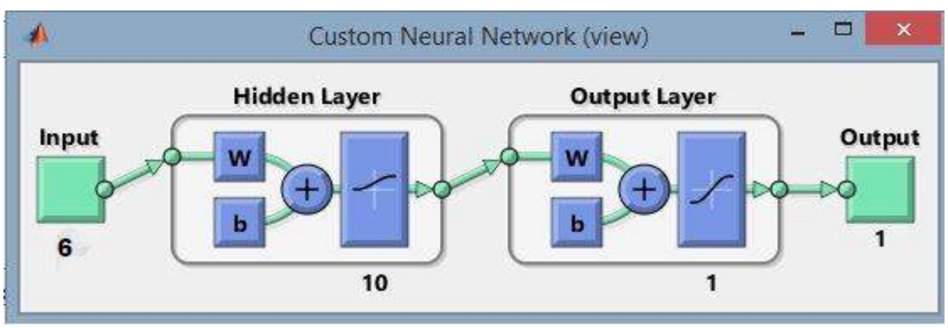

Figure 3 ANNs architecture

3.0 Results and Discussion

Table 1 shows the results of the different compositions of household solid waste generated in Okada town for a total number of 100 households.

Table 1 Composition of household waste generated in Okada Town

S/N	Number of family member	Sample A	Sample B	Sample C	Sample D	Sample E	Sample F
1	7	0.273	0.091	3.510	0.112	0.133	0.091
2	4	0.156	0.052	2.655	0.064	0.076	0.052
3	5	0.195	0.065	2.695	0.080	0.085	0.065
4	3	0.117	0.039	1.020	0.042	0.057	0.039
5	8	0.304	0.096	4.667	0.128	0.136	0.104
6	3	0.114	0.039	1.017	0.048	0.057	0.039
7	3	0.113	0.037	2.019	0.044	0.058	0.036
8	5	0.190	0.065	3.700	0.080	0.095	0.065
9	3	0.117	0.036	2.014	0.042	0.051	0.039
10	6	0.228	0.072	4.034	0.084	0.102	0.078
11	4	0.156	0.052	3.897	0.064	0.076	0.052
12	9	0.942	0.108	5.042	0.126	0.153	0.117
13	5	0.190	0.060	3.690	0.070	0.085	0.065
14	3	0.117	0.039	1.017	0.048	0.057	0.039
15	2	0.078	0.026	1.680	0.032	0.038	0.039
16	4	0.156	0.052	1.359	0.056	0.068	0.048
17	13	1.494	0.156	6.394	0.169	0.221	0.117
18	7	0.266	0.093	3.371	0.112	0.133	0.840
19	10	0.980	0.120	3.380	0.140	0.170	0.110
20	5	0.195	0.063	2.690	0.080	0.095	0.065
21	8	0.304	0.093	5.699	0.120	0.152	0.096

22	9	0.742	0.104	4.039	0.126	0.153	0.098
23	5	0.195	0.067	1.690	0.080	0.084	0.063
24	4	0.156	0.053	1.361	0.064	0.059	0.043
25	7	0.566	0.089	3.369	0.112	0.135	0.082
26	6	0.628	0.069	3.035	0.096	0.103	0.051
27	5	0.795	0.068	2.710	0.081	0.095	0.061
28	4	0.156	0.057	1.354	0.057	0.076	0.059
29	5	0.190	0.068	3.710	0.083	0.090	0.061
30	4	0.156	0.051	1.400	0.057	0.076	0.047
31	5	0.190	0.063	2.700	0.079	0.091	0.076
32	3	0.117	0.038	1.720	0.048	0.057	0.051
33	7	0.866	0.086	3.359	0.109	0.119	0.081
34	4	0.156	0.051	1.399	0.058	0.076	0.049
35	4	0.157	0.050	1.410	0.067	0.078	0.051
36	3	0.119	0.034	1.698	0.047	0.059	0.031
37	4	0.159	0.050	2.401	0.054	0.069	0.049
38	2	0.078	0.029	0.686	0.034	0.038	0.027
39	5	0.581	0.061	2.609	0.081	0.083	0.067
40	4	0.153	0.053	1.401	0.068	0.076	0.051
41	4	0.160	0.051	1.398	0.067	0.069	0.060
42	3	0.115	0.036	1.730	0.039	0.071	0.036
43	6	0.227	0.066	3.041	0.084	0.102	0.063
44	5	0.182	0.063	2.701	0.083	0.075	0.060
45	4	0.155	0.051	1.403	0.059	0.077	0.047

46	3	0.114	0.033	1.702	0.040	0.072	0.039
47	5	0.184	0.062	2.690	0.082	0.080	0.062
48	3	0.117	0.039	1.789	0.041	0.051	0.037
49	2	0.079	0.027	1.691	0.035	0.038	0.027
50	6	0.229	0.067	2.051	0.079	0.096	0.092
51	7	0.267	0.088	2.309	0.098	0.119	0.081
52	8	0.302	0.096	2.712	0.112	0.136	0.101
53	8	0.305	0.093	4.719	0.109	0.144	0.106
54	5	0.186	0.063	1.687	0.078	0.095	0.064
55	6	0.225	0.067	2.065	0.088	0.108	0.073
56	5	0.180	0.063	2.673	0.077	0.079	0.063
57	6	0.225	0.069	2.075	0.078	0.110	0.076
58	4	0.160	0.053	1.413	0.057	0.069	0.053
59	3	0.120	0.035	1.703	0.043	0.052	0.037
60	5	0.186	0.062	1.702	0.081	0.093	0.066
61	6	0.230	0.066	2.109	0.077	0.076	0.078
62	4	0.156	0.054	1.425	0.060	0.074	0.052
63	5	0.182	0.067	2.669	0.062	0.092	0.065
64	7	0.266	0.089	3.319	0.111	0.118	0.091
65	9	0.342	0.108	4.042	0.126	0.153	0.108
66	3	0.117	0.037	1.713	0.048	0.057	0.039
67	5	0.187	0.036	2.690	0.080	0.085	0.066
68	3	0.116	0.036	1.803	0.048	0.054	0.037
69	4	0.156	0.057	1.406	0.064	0.068	0.049

70	3	0.117	0.040	1.699	0.048	0.057	0.034
71	5	0.188	0.068	2.700	0.079	0.080	0.062
72	6	0.227	0.067	3.190	0.079	0.102	0.073
73	8	0.303	0.094	4.704	0.112	0.144	0.097
74	3	0.124	0.037	1.813	0.049	0.057	0.040
75	4	0.162	0.055	1.402	0.059	0.072	0.057
76	2	0.077	0.029	0.680	0.029	0.038	0.027
77	2	0.081	0.027	1.599	0.032	0.039	0.031
78	6	0.222	0.067	4.189	0.069	0.084	0.070
79	3	0.117	0.036	1.020	0.042	0.060	0.042
80	3	0.111	0.034	1.019	0.049	0.057	0.047
81	4	0.166	0.057	1.500	0.065	0.080	0.063
82	5	0.187	0.069	3.690	0.088	0.750	0.067
83	6	0.224	0.066	3.190	0.069	0.112	0.082
84	4	0.161	0.057	2.501	0.057	0.068	0.048
85	3	0.122	0.039	1.041	0.048	0.054	0.042
86	5	0.186	0.069	3.690	0.078	0.095	0.067
87	7	0.262	0.090	4.323	0.089	0.119	0.091
88	7	0.265	0.085	5.334	0.098	0.126	0.094
89	6	0.529	0.063	4.034	0.096	0.084	0.084
90	8	0.810	0.096	5.704	0.112	0.104	0.106
91	5	0.177	0.067	3.701	0.080	0.095	0.061
92	4	0.160	0.055	2.512	0.064	0.069	0.051
93	3	0.112	0.040	1.128	0.048	0.057	0.040

94	7	0.259	0.083	2.317	0.098	0.103	0.063
95	5	0.184	0.060	3.687	0.070	0.091	0.045
96	6	0.227	0.064	4.099	0.096	0.109	0.074
97	8	0.800	0.959	5.709	0.112	0.123	0.106
98	6	0.225	0.062	4.189	0.096	0.084	0.084
99	8	0.305	0.093	2.712	0.113	0.126	0.106
100	11	0.418	0.132	4.718	0.154	0.176	0.132
∑	507	27.173	7.289	260.021	7.604	9.534	7.258
WG_{PHH}		0.272	0.073	2.600	0.076	0.095	0.073
WG_{PP}		0.054	0.014	0.513	0.015	0.019	0.014

*WG_{PHH}-Solid waste generated per household, *W_{GPP}-Solid waste generated per person

Table 1 shows the results obtained from household solid waste generation in Okada town, Edo State, Nigeria. The components of household solid waste generated include food left over, plastic and rubber, paper, wood, carbon, leather, textile material, glasses, ferrous metals, metal cans, and ceramics, and 0.629 kg of household solid waste was generated per person per day. Also, a total of 318.879 kg of household solid waste was generated per week by 100 households, consisting of 507 people. Thus, 3.189 kg of household solid waste was generated per household on a daily basis. By percentage composition, food waste has the highest percentage (73% and 75%) as depicted in Figure 4 and Figure 5.

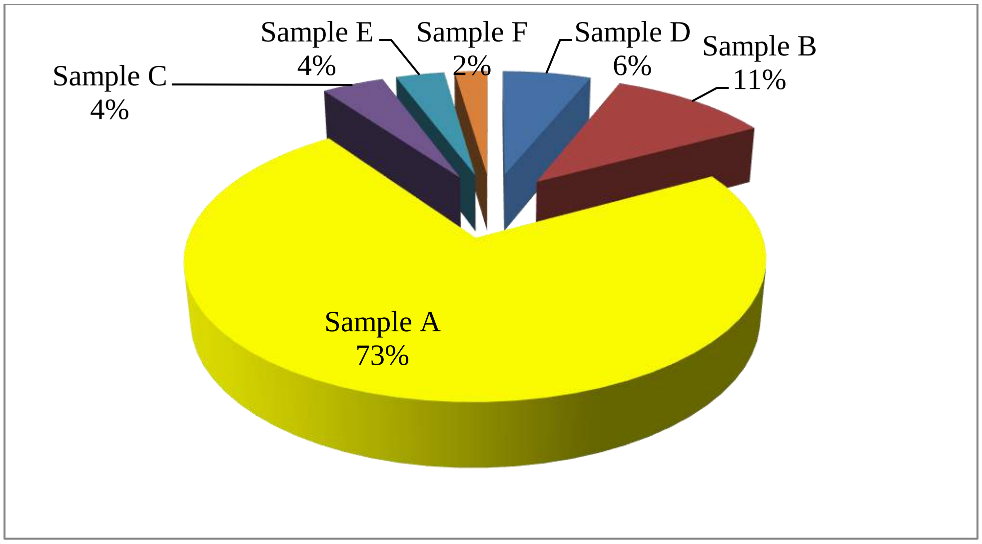

Figure 4 Percentage composition per household solid waste generated in Okada town

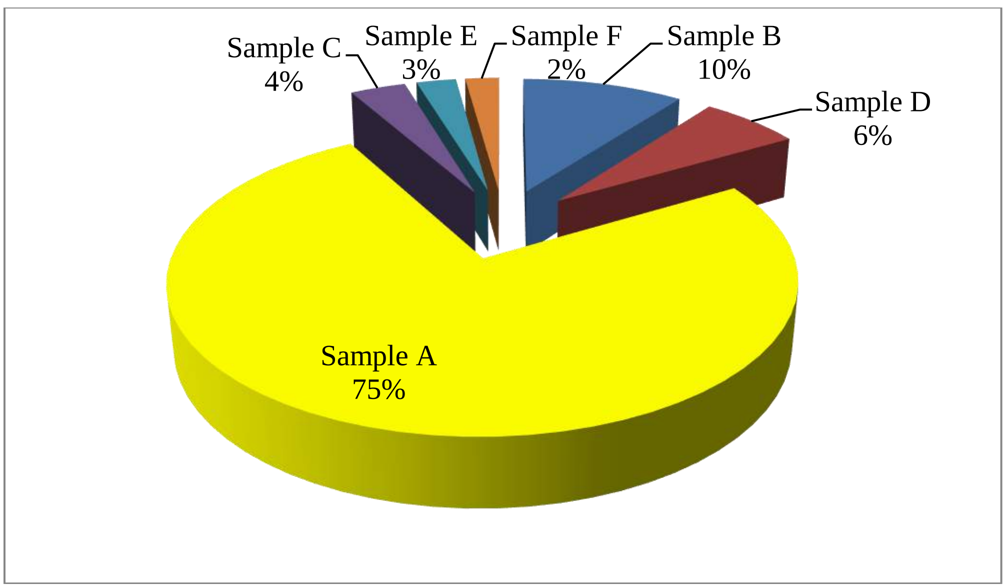

Figure 5 Percentage compositions per person solid waste generated in Okada town

The composition of food waste consists mainly of food left-over, vegetables, fish and meat waste, fruits, peels (cassava, yam, potato, orange, pawpaw, banana, plantain, etc.). In comparison with the work of other researchers, Igbinomwanhia *et al.* [26] reported a seventy-eight (78%) percentage composition of the generated food waste in the Benin metropolis. In the same line, Owamah *et al.* [27] reported a percentage composition of 77% and 87% of food waste for municipal solid waste characterization in Nigeria. Benjamin *et al.* [28], on the other hand, reported a fifty-two percent (52%) composition of generated food waste. The artificial neural networks with the lowest mean squared error (MSE) for validation was chosen, and this was based on the results of the different trials of the neural network model. The correlation between the targets and the outputs is represented by the regression (R^2) value, and a bigger regression (R^2) value close to one (1) is an indication of a good relationship, while a zero R^2 value designates a random relationship. Table 2 shows the results of the ANNs model performance using a data separation of 50%, 25%,and 25% for training, testing, and validation. It was observed that the best validation performance of the ANNs that produced the slightest value of MSE was 5.0123e-008 as revealed in Figure 6, and this agreed with the work of Behera *et al*. [29] and Yetilmezsoy *et al.* [18] that reported a lower MSE as the basic criterion for determining the training accuracy of the network.

Table 2 Results of the ANN Model

Data	Percentage of Separation (%)	Number of Data	R^2
Training	50	50	0.99621
Testing	25	25	0.98253
Validation	25	25	0.99560
All	100	100	0.99834

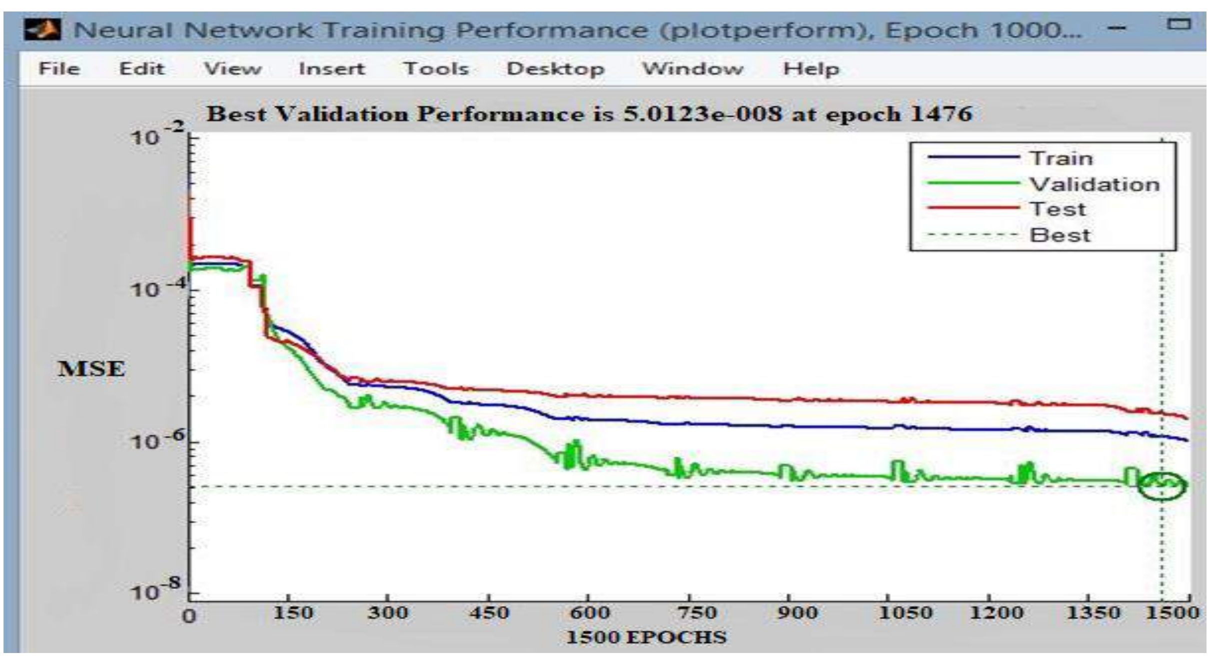

Figure 6 Performance Curve of ANN

The least value of MSE obtained during performance validation of the ANNs was 5.0123e-088 and this occurred at 1476 epochs. Also, a relatively high coefficient of determination (R^2) value of 0.99560 for validation was obtained, and this value is close to 1. Since the R^2 values obtained are close to 1, the prediction of the ANNs model was linearly correlated. Figure 7 shows the regression plots of the designated ANNs for validation, testing, and training, for all data sets. As shown in Figure 7, the regression plots and the expected neural network have a close relationship between the targets and the output. Besides, the R^2 values of the training set (0.99621), the testing set (0.98253), and the validation set (0.99560), and the all-data set (0.99834) were found to be high and close to 1.

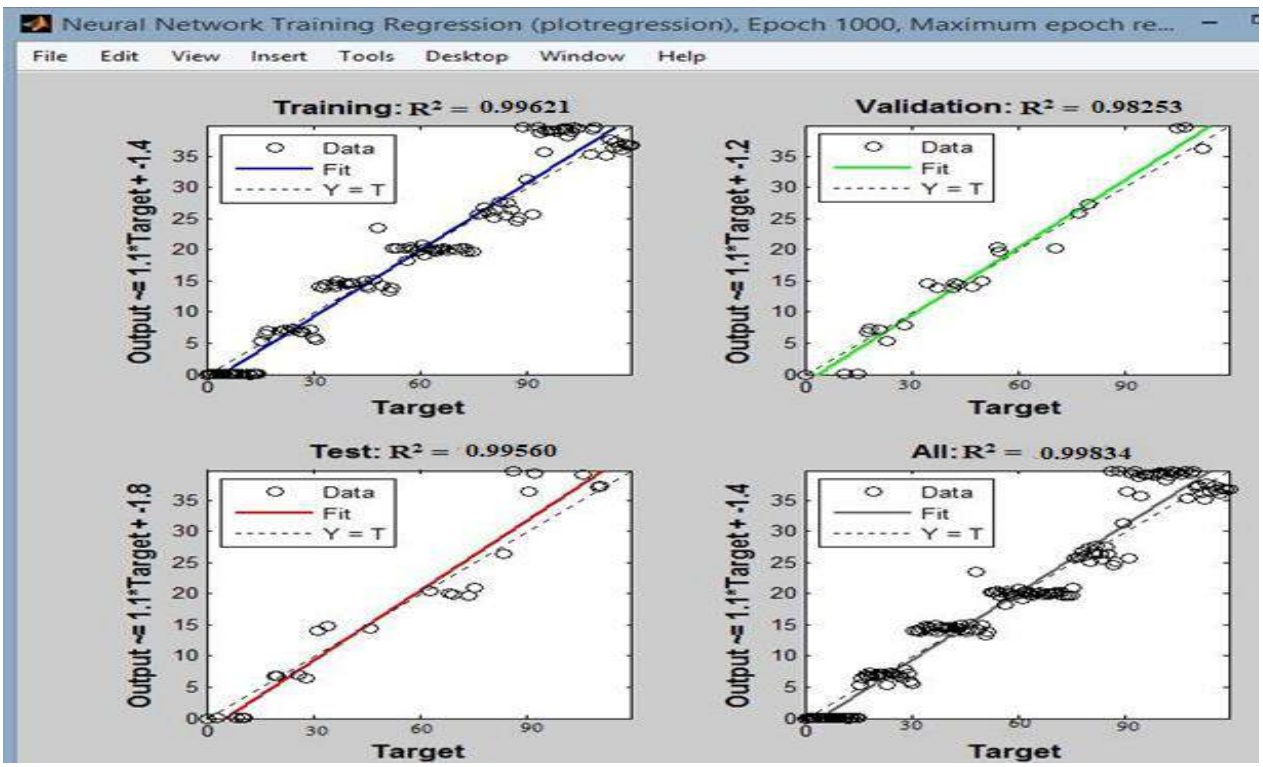

Figure 7 The regression plots of the ANN Model

Figure 8 shows the results of the actual and predicted household solid waste by the developed ANNs model. The ANNs successfully predicted household solid waste generation. Therefore, the ANNs learned the relationship between the input and the output in the solid waste generation stream very well.

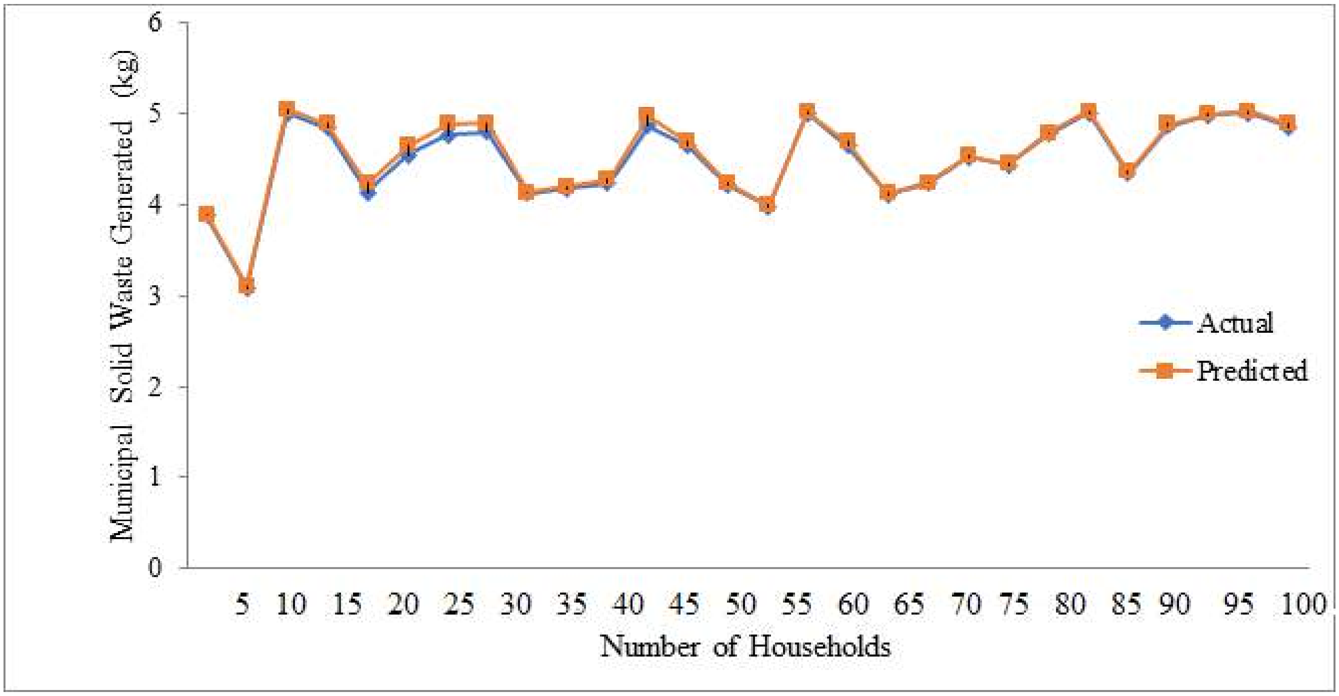

Figure 8.Actual versus Predicted Municipal Solid Waste by ANN

4.0 Conclusion

The household solid waste generation survey of Okada town, Edo State, Nigeria revealed that the components of household solid waste generated include food left over, plastic and rubber, paper, wood, carbon, leather, textile material, glasses, ferrous metals, metal cans, and ceramics. Also, 0.629 kg of household solid waste was generated per person per day, and a total of 318.879 kg of household solid waste was generated per week by 100 households consisting of 507 people. By composition, food waste has the highest percentage (73% and 75%). A relatively high coefficient of determination (R^2) value of 0.99560 for validation was obtained and the R^2 values of the training set (0.99621), the testing set (0.98253), the validation set (0.99560) and the all-data set (0.99834) were found to be high and close to 1.

References

[1] Omole, F.K., and Alakinde, M.K. (2013). Managing the Unwanted Materials: The Agony of Solid Waste Management in Ibadan Metropolis, Nigeria. *International Journal of Education and Research*, 1(4),1

[2] Orhorhoro, E.K., Ebunilo, P.O.B., and Sadjere, E.G. (2017). Determination and Quantification of Household Solid Waste Generation for Planning Suitable Sustainable Waste Management in Nigeria. *International Journal of Emerging Engineering Research and Technology,* 5(8): 1-9

[3] Alejandro, V., and Eder, P. (2014). End-of-Waste Criteria for Waste Plastic for Conversion. Joint Research Centre (JRC) European Commission. Report EUR 26843 EN, JRC91637, doi: 10.2791/13033, p.47, ISBN

978-92-79-40944-8. Luxembourg: Publications Office of the European Union. [Online] Available from: https://ec.europa.eu/jrc/sites/default/files/2014-jrc91637_.pdf.

[4] Adewole, A.T. (2009). Waste Management towards Sustainable Development in Nigeria. ACase Study of Lagos State. *International NGO Journal*, 4 (4):174

[5] Akintokun, P.O., Adekunle, I.M., Adekunle, A.A., Akintokun, A.K., and Arowolo, T.A. (2011). Recycling of organic wastes through composting for land applications; A Nigerian experience. *Waste management & research*, 29(6): 582-93. doi10.1177/0734242X10387312

[6] Momodu, S.N., Dimuna, K.O., Dimuna, J.E. (2011). Mitigating the impact of Solid Wastes in Urban Centres in Nigeria. *J. Hum. Ecol.*, 34(2), 125-133

[7] Kadafa, A.A., Latifah, A., Abdullah, HS., and Wan nur A. (2012). A Review on Municipal Solid Waste Management in Nigeria. *Journal of American Science,* 8(12): 975-982

[8] Orhorhoro, E.K., and Oghoghorie, O. (2016). Review on Solid Waste Generation and Management in Sub-Saharan Africa: A Case Study of Nigeria. *J. Appl. Sci. Environ. Manage.*, 23 (9): 1729-1737. DOI: https://dx.doi.org/10.4314/jasem.v23i9.19

[9] Anwar, J., Habib, A., Haslenda, H., Saeed, I.A., and Ramli, M. (2014). Municipal Solid Waste Management and Potential Revenue from Recycling in Malaysia. *Modern Applied Science,* 8(4): 37-49

[10] Ebunilo, P.O., Atuma, E.V., Orhorhoro, E.K., (2021). Performance Evaluation of a Developed Dried Grass Shredding Machine for Composting. *Advanced Engineering Forum,* 40: 73-82. https://www.scientific.net/AEF.40.73

[11] Hoornweg, D., Bhada-Tata, P. (2012). What a Waste: A Global Review of Solid Waste Management. Urban Development Series Knowledge Papers, World Bank. pp.7. [Online] Available from: http://siteresources.worldbank.org/inturbandevelopment/Resources/3363871334852610766/What_a_Waste 2012_Final.pdf.

[12] Antanasijevic, D., Pocajt, V., Popovic, I., Redzic, N., Ristic, M. (2013). The forecasting of municipal waste generation using artificial neural networks and sustainability indicators. *Sustain Science,* 8: 37-46

[13] Orhorhoro, E.K., Lindsay, E.E., Oyejide, J.O. (2022). Analysis and Evaluation of a Three-Stage Anaerobic Digestion Plant for Management of Biodegradable Municipal Solid Waste. *International Journal of Engineering Research in Africa,* 60, 75-87

[14] Hoornweg, D., Thomas, L., Otten, L. (2014). Composting and its Application in Developing Countries. Urban Waste Management Urban waste management. Working Paper 8, Urban Development Division, Washington DC, World Bank. http://www.worldometers.info/word-population/nigeria-population/, [Accessed September 13th, 2019]

[15] Igbinomwanhia, D.I., Ohwovoriole, E.N., Ejovo, N. (2012). A study of the constraints to Residential Solid Wastes Management in Benin Metropolis, Nigeria. *Journal of Emerging Trends in Engineering and Applied Science (JETEAS),* 3(1): 103-107,.

[16] Orhorhoro, E.K., Oyejide, J.O. (2020). Modelling of Biogas Yield from Anaerobic Co-digestion of Food Waste and Animal Manure using Artificial Neural Networks. *Applications of Modelling and Simulation*, 4: 81-88

[17] Tardast, A. Rahimnejad, M. and Najafpour, G. (2014). Use of Artificial Neural Network for the prediction of bioelectricity production in a membrane less microbial fuel cell. *Fuel*, 117: 697–703

[18] Yetilmezsoy, K., Turkdogan, F. I., Temizel, I., Gunay, A., (2012). Development of ANN-Based Models to Predict Biogas and Methane Productions in Anaerobic Treatment of Molasses Wastewater. I*nternational Journal of Green Energy*, 10 (9): 885-907

[19] Yeshona, S., Funmilayo, F., Evariste, B. and Gueguim, K. (2017). Artificial neural networks: an efficient tool for modelling and optimization of biofuel production (a mini review). B*iotechnology & Biotechnological Equipment,* 31(2): 221-235

[20] Orhorhoro, E.K., Ebunilo, P.O.B., and Sadjere, E.G. (2017). Development of a Predictive Model for Biogas Yield Using Artificial Neural Networks (ANNs) Approach. *American Journal of Energy and Power Engineering*, 4(6), 71-77

[21] Sewsynker, Y., Gueguim, K.E.B., Lateef, A. (2015). Modelling of biohydrogen generation in microbial electrolysis cells (MECs) using a committee of artificial neural networks (ANNs). *BiotechnolBiotechnol Equip*, 29(6): 1208–1215

[22] Elnekave, M., Celik, S.O. and Tatlier, M. (2012). Artificial Neural Network predictions of Up flow Anaerobic Sludge Blanket (UASB) Reactor Performance in the treatment of citrus juice wastewater. *Pol J Environ Stud.*, 21(1), 49–56

[23] Harper, W.F. and Taewoo, Y. (2013). Using electronic signals and neural networks to monitor the performance of an anaerobic bioreactor. *Int J Water Res Environ Eng.*, 5(9), 521–532

[24] Mahanty, B., Zafar, M. and Park, H.S. (2013). Characterization of Co-digestion of industrial sludges for biogas production by artificial neural network and statistical regression models. *Environ Technol.*, 34, 2145–2153

[25] Shahrokh E.M., Dougherty, E.R. (2014). Effect of separate sampling on classification accuracy. *Bioinformatics*, 30 (2): 242–250

[26] Igbinomwanhia, D.I., Obanor, A.I., Olisa, Y.P. (2017). Characterisation of Domestic Solid Waste for the Determination of Waste Management Option in Amassoma, Bayelsa State, Nigeria. *J. Appl. Sci. Environ. Manage.*, 18(2): 211-215

[27] Owamah, I.H., Izinyon, O.C., Igbinewekan, P. (2015). Characteristics and quantification of solid waste generation in the Niger Delta Region of Nigeria: a case study of Ogbe-Ijoih community in Delta State". Journal of Material Cycles and Waste Management,19(1): 366-373

[28] Benjamin, T.A., Emmanuel, E.O., and Gideon, A.D. (2014). Characterisation of Municipal Solid Waste in the Federal Capital, Abuja, Nigeria. *Global Journal of Science Frontier Research: Environment and Earth Science*, 14, (2): 1-7

[29] Behera, S. K., Meher, S. K., Park, H. S. (2014). Artificial Neural Network model for predicting methane percentage in biogas recovered from a landfill upon injection of liquid organic waste. *Clean Technologies and Environmental Policy*: 1-11.

NIPES-NCEE Conference Proceedings
The 2nd International Conference 15th-17th Feb. 2023
611-622
www.nipesjournals.org.ng

DESIGN AND CONSTRUCTION OF GAS-FIRED SINGLE DRUM TOMATO PASTE DRYING MACHINE

Babatunde. O. Jayeoba* & Babatunde. A. Olaifa

Department of Science Laboratory Technology, Federal Polytechnic, Ilaro, Ogun State, Nigeria
*Corresponding author email: babatunde.jayeoba@federalpolyilaro.edu.ng;

Abstract

Preservation of goods is a paramount application of mechanical engineering that result from the basic principle of physics of heat and interaction with matter in meeting the demand for the solution to sustainable development goals problems of hunger alleviation, food insecurity, wastage of agricultural resources such as perishable goods are problems to be solved technologically. This study aimed at design and construction of mechanical gas-fired single drum drying system for preservation and processing of tomato paste to proffer solution through agricultural resources management. Dehydration and moisture removal from tomato paste was carried out with designed and constructed gas-fired single drum drying system. The design was made through a computer aided design application AutoCAD with well analysed dimensions before it was constructed with the aid of welding, fitting and coupling using studied materials based on thermal properties and its effect on product consumption (mild steel, iron, galvanised stainless steel) for maximum efficiency. After a careful construction of subsystems, it was coupled where heat energy was supplied through an adjustable gas cylinder. The system was tested igniting the heat source which was channelled through the burner into the drum, tomato paste was gradually released from a reservoir into the heated rotating drum with constant temperature of 50oC at bone drying conditions, after a complete revolution the dried paste is scrapped into the underneath tray. The sample was analysed and found to have specific energy consumption and drying efficiency varied from 2.29 to 3.72 MJ/kg water and 67.8 to 83.8%, respectively. For commercial preservation of tomato paste, there is need to increase the dimensions of the design and construction to meet up with large scale drying of goods in order for implementation of mandates concerning sustainable development goals (SDG).

***KEYWORDS**:* *Mechanical, gas-fired single drum, thermal, AutoCAD, Sustainable development goal (SDG)*

1.0 INTRODUCTION

The economy of a nation hinges on the food security where this quest has made every society to look into sustainability of resources for economy development. One of such programmes that has been established in meeting the sustainable development goals has the following as mandates; alleviation of hunger, food security, nutrition improvement and promotion of agricultural resources as it is available in (SDG, No.2, 2030) with proposed date of accomplishment before 2030. Because of these mandates of sustainable development goals (SDG), the world has shifted major research attention towards the preservation of food in order to bridge the of food shortage, scarcity and unavailability of perishable goods throughout the year. And of such food materials are vegetables (tomatoes) that are perishable and their methods of processing and preservation have called for the attention of mechanical engineers in fabrication of systems that will assist in actualizing the sustainable development goals (SDGs) [1].

Among the processing techniques to preserve perishable goods and make it available throughout the seasons of the year is drying, vegetable drying involves the removal or reduction of moisture content to the barest minimum that makes the vegetable inhabitable for spoilage microorganism without destroying nutritious tissues, edibility or aesthetic appearance of the fruit. Drying means include traditional drying methods such as drying by direct sunlight or for example in the case of small amounts of food, drying over a kitchen fire [2].

There are more advanced drying techniques which involves artificial means, most of these are sophisticated in process/drying parameters control of the sample, they also possess higher capacity with varieties of product processing/drying [3].

Artificial drying systems have their own demerits such as high capital investment for production implication, this is because of higher energy consumption, maintenance of equipment and spare part replacement cost. Also, technical-know-how is another challenge which may not be readily available.

Mechanised techniques are usually applicable for use in urban or peri-urban areas where there is better access to these inputs. Some techniques involve use of solar dryers, drum dryer [4]; [5].

The quest for security and sustainable economy development has been a pivot of research for the mechanical engineers in proffering solution to food wastage and alleviate hunger by designing and fabrication of efficient systems for food processing and preservation. Among the important perishable goods that needs urgent attention of mechanical engineers in processing are tomatoes (Lycopersicum *esculentum*) [6].

Tomatoes are important items to human health and nutrition because of the reason that they contain essentials like vitamin C, potassium, vitamin K, fiber, carbohydrate and antioxidants, which are beneficial in mitigating the risk of cancer and heart diseases. Unfortunately, tomatoes are not only periodic but highly perishable [7]. Consequently, there is always an unreasonable gap between harvest and off-season periods because they are often being consumed rapidly during harvest period due to lack of storage facilities especially in the rural communities of developing countries like Nigeria where there is limited access to electricity. According to [8], tomatoes are being cultivated virtually across the country but most predominantly grown in the northern Nigerian towns such as Zaria, Jos, Gombe, Kano, Maiduguri and the south west towns like Ogbomosho and Ibadan but unfortunately, the peasant farmers and traders incur a lot of losses during harvest peak owing to low prices which are traceable to surplus, poor storage facilities, lack of electricity, poor road network for transporting the items to urban areas and ultimately because the harvest periods are often characterized by low sun intensity cum high relative humidity which in addition to wind blow, insects and pests infestation makes direct/open sun-drying often inefficient. It is highly paradoxical that 29,000 metric tons of tomatoes are being wasted in three states of Northern Nigeria while Nigeria imports 26,000 metric tons of tomato paste annually [9], [10]. Hence, it is highly imperative to source for alternative means of preserving this food material so as to provide a larger market which would afford tomatoes consumers and traders opportunities to purchase it on a year round basis and also return a higher profit for rural and suburban farmers of developing countries. Meeting the demand for the solution to sustainable development goals problems of hunger alleviation, food insecurity, wastage of agricultural resources such as perishable goods are problems to be solved technologically [11]. Drying process is very important in processing and preserving agricultural products cum many others particularly in developing countries. This study designs and construct mechanical gas-fired single drum drying system for preservation and processing of tomatoes to proffer solution through agricultural resources management in rural areas that have no access to infrastructural facilities such as electricity.

This study aimed at design and construction of gas-fired single drum tomato paste drying machine, the aim was achieved through the followings as objectives: the system's architecture framework was designed using software computer aided design application software (AutoCAD), construction and assembling of the subsystems through welding and fitting, and functional/efficiency analysis of the drying machine and assessment of working parts.

2.0 METHODOLOGY

This section of the study highlights and discuss functions of materials necessary for the design and construction of gas-fired single drum tomato paste drying machine, the methodology adopted in the design and construction is also presented in the chapter of the study in terms of welding and fitting of parts with subsystems. Table 1 shows the materials/parts/components with the dimensions as used for the construction of the system.

Table 1: Dimension/Specifications and Quantities of the Materials/Parts Used for Fabrication

S/N	**Materials/Part**	**Quantity**	**Dimension/Specification**
1	Mild Steel (Body Frame)	Three standard size	560mm x 520mm and 700mm
2	Drum Roller (Iron Rod)	One sheet	Ø 30mm x 560 mm
3	Drum Cover	2	Ø 40mm x 250mm
4	Drum (Galvanised Stainless steel)	Half-sheet	(Ø260 x 400) x 2mm
5	Flange drum	2	260mm x 285mm

6	Collector	Half-sheet	520 mm by 560mm
7	Scrapper (Galvanised Stainless steel)		30mm by 560 mm long
8	Angular bar	3 standard length	50 mm x 50 mm
9	Paint	Lump	Finishing
10	Pillow Bearings	2	Ø 30mm
11	Ball bearings	2	Ø 10 x 22 mm
12	Bolts and nuts	4	M12 x 30
13	Funnel	1	Ø 160mm x 120 mm
14	Funnel valve (flat bar)	1	22 x 300 mm
15	Outlet funnel pipe	1	Ø40mm x 320 mm
16	Teflon Outlet Tomato Cover	2	(Ø 35 x 6 x 12thick)mm
17	Burner pipe	1	30mm (diameter) by 560 mm
18	Hose clip	2	16mm
19	Gas Hose	1	Ø 10 mm x 1000mm
20	Gas Hole pipe	1	Ø 10mm x 120 mm
21	Gas cylinder	1	12 kg
22	Regulator	1	
23	Drum handle (mild steel)		300mm

2.1 System Design using AutoCAD

The system was designed with the aid of computer aided design application software (AutoCAD) with appropriate dimensions as indicated in Table 2.1 where necessary. Figures 1 show different views (exploded, isometric and dimensional descriptions of the system.

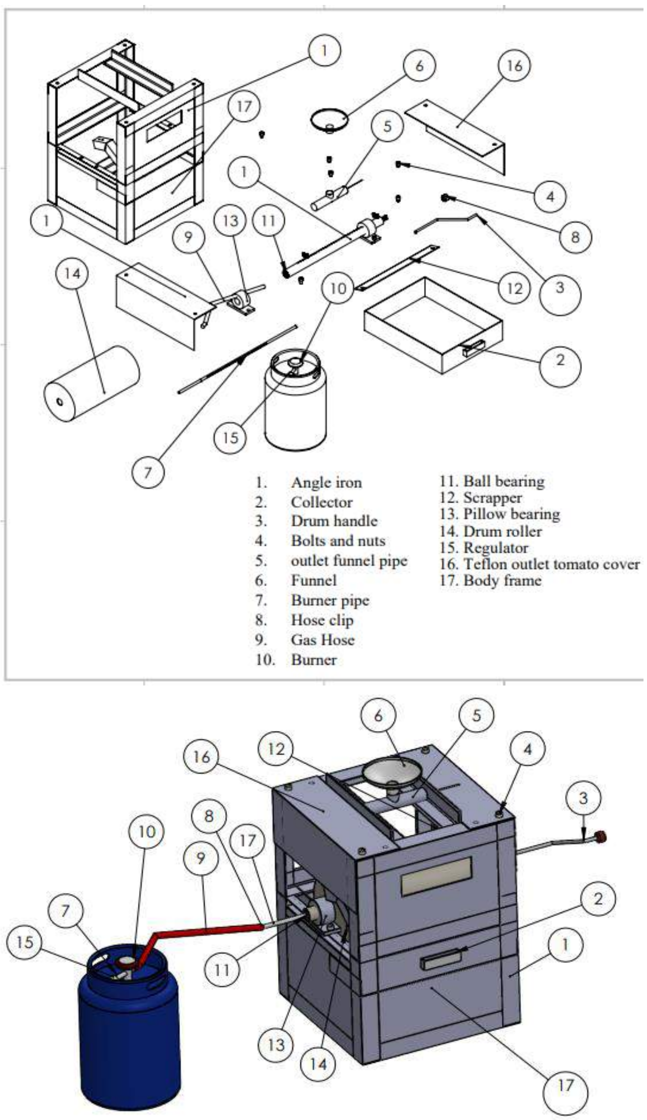

1. Angle iron
2. Collector
3. Drum handle
4. Bolts and nuts
5. outlet funnel pipe
6. Funnel
7. Burner pipe
8. Hose clip
9. Gas Hose
10. Burner
11. Ball bearing
12. Scrapper
13. Pillow bearing
14. Drum roller
15. Regulator
16. Teflon outlet tomato cover
17. Body frame

Figure 1: Exploded and Isometric Views of Gas-fired Single Drum Drying Machine.

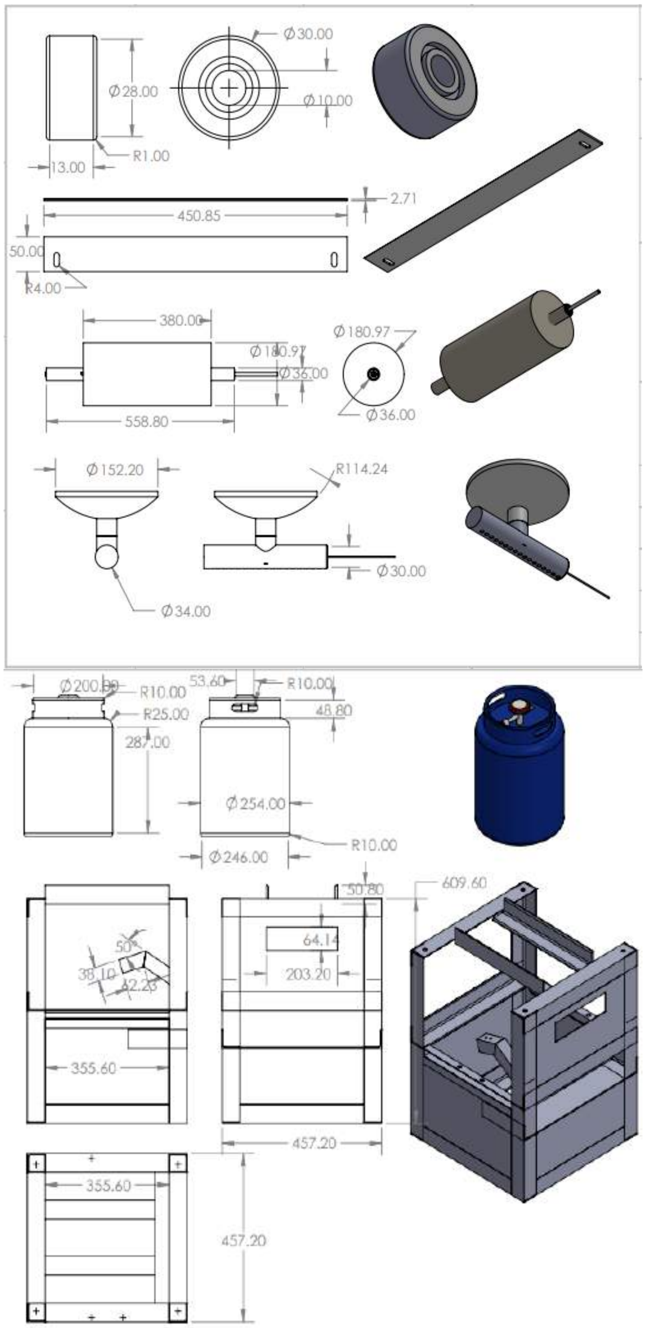

Figure 2: AutoCAD Exploded View and Dimensional Description of the System.

The system comprises of three major subsystems namely: the mechanical framework that serves as housing, the rotating drum and the energy source (gas cylinder). The mechanical framework of the dryer was designed in a rectangular volume shape with the dimension 600mm x 560mm and 800mm for length, breath and height respectively.

2.2 System Fabrication Techniques

This section of the study described the step by step workshop practices in the design and construction of gas-fired single drum tomato paste dryer, this includes all necessary bench work activities and engineering procedures. The system was constructed through cutting, fitting, coupling and welding of the parts by following the design indicated in Figures 1. The whole system is broken down into sub-systems for easy construction, the sub-systems are: the static body (mechanical framework, sample scrapper and collector, the moving drum, the heat energy source.

2.2.1 Construction of System Housing Framework

The design was actualized physically by cutting a mild steel sheet into parts based on the design dimensions for the frame work.

The joints are welded together with welding machine and carved out with essential openings and hangers for handling and fixing of other sub-systems such as the drum, collector and scrapper. The framework was filed for finishing smoothness and painted to prevent corrosion.

2.2.3 Rotating Drum

This part is dynamic and has contact with the sample being dried, the drum is cylindrical in shape made with galvanized stainless steel, the volume of the cylindrical drum is having the following dimensions (Ø260 x 400) x 2mm in diameter, height and thickness respectively. The drum is covered at both ends with stainless material having a dimension of Ø 40mm x 250mm.

The drum is suspended within the body and fixed to an angular bar of dimension 50 mm x 50 mm where it is being rotated through two pairs of pillow and ball bearings of dimension Ø 30mm, and Ø 10 x 22 mm respectively. Figure (1) shows the dimensional view of single drum gas-fired drying machine.

3.0 RESULTS AND DISCUSSION

This section of the study highlights and discuss the results gotten from the design of the system following the construction procedures with the use of materials stated in chapter three of this study. Based on the design, the subsystems (dryer framework, drying rolling drum and gas cylinder as heat source) were constructed using the materials listed in previous section as shown in Plate I.

Plate I: Single Drum Dryer Subsystems

From the different subsystems, a whole system was assembled for complete system where the drum is fitted into the framework with scrapping bar attached in partial contact with the drum as shown in Plate II.

3.1 Constructed Single Drum gas-fired Dryer

Plate II: Coupling of Single Drum Gas-fired Tomato Paste Dryer Subsystems

3.2 Performance Evaluation

Some mass of fresh fully ripe (red) tomatoes purchased from a nearby local market in Ota, Ogun state, Nigeria.

The fresh tomato sample were first washed, wiped with a clean dry cloth, then blended and processed to make sample paste. The sample was weighed prior to application of single drum dryer and monitored.

The paste was then poured into the constructed drying machine reservoir from where it was channelled into the perforated pipe funnel.

After the initiation of the combustion process by igniting the gas (propane/butane) fuel, the preheating of the single drum under no-load condition continued until the drum temperature that would be in contact with sample sprayed on it reached 50^{o}C which was maintained for the drying procedure with the aid of a heat control unit (HCU) of the gas-burner. The sample was then uniformly dropped from the reservoir on the heated drum, through the perforated pipe funnel which is rotated intermittently for regular heat transfer or distribution into the sample. The drying process continued while the scrapper scraps the dried tomato sample from the drum, and the collector receives it beneath.

The sample was weighed and monitored with the aid of an electronic weighing balance. This procedure continued until there was no more noticeable variation in the weight of the dried paste. At this point, the final weight of the dried tomatoes was recorded to be 1.4 kg and the total drying period was estimated. Samples of both the dried paste and the fresh ones were thereafter analysed.

3.2.1 System Evaporation Rate,

The evaporation rate of free water can be estimated by the following relationship shown in equation (4.1), where dM/dt is the rate of moisture removal per unit drum surface (kg H_2O/hr m^2)

$$\frac{dM}{dt} = 30 \cdot 94 V^{0.8} \Delta P \tag{4.1}$$

where $\Delta P = P_s - P_a$ (Atm) is the difference between the vapour pressure at product surface P_s and the vapor pressure in the ambient air P_a, V is the velocity of ambient air (m/s). The drying rate within period/section is controlled by moisture diffusion as well as heat transfer.

Alternatively, water removal rate may be estimated from an energy balance equation:

$$\frac{dM}{dt} = 3.6 \frac{h(T_W - T_{evp})}{L} \tag{4.2}$$

where T_w is temperature of the drum surface (°C), T_{evp} is temperature of evaporating surface (°C), L is latent heat (kJ/kg H_2O), and ***h*** is an overall heat transfer coefficient (W m^{-2} $^oC^{-1}$). The value of ***h*** varies between 200 and 2,000 (W m^{-2} $^oC^{-1}$), depending on the type and the thickness of the film being dried.

3.2.2 Physical Characteristics

The comparison between the physical properties of the pre-drying (fresh) tomatoes paste and those of the post-drying (dried) ones is presented. It is evident from this data that the weight of the tomatoes decreased with increasing drying time. This trend which is consistent with those in the literature can be reasonably traced to the removal of water content (dehydration) during drying.

3.2.3 System Drying Rate, D

The average rate of drying in the drum was estimated from (4.3) as the ratio of the change in mass of tomatoes to the drying time:

$$D = \frac{\Delta M_T}{\tau_d \,(\text{min})}, \qquad \Delta M_T = M_{T,i} - M_{T,f} \tag{4.3}$$

D = Drying rate gram/minute, $M_{T,i}$ = Initial mass of tomatoes before drying, (g), $M_{T,f}$ = Final mass of tomatoes after drying, (g), τ_d = Total drying time, (minute)

3.2.4 System Thermal Analysis

Heat Energy required (used) to evaporate water from the tomatoes, $qdrying$

The amount of heat energy actually used to effect drying by evaporating (removing) the required moisture from the tomatoes was determined from the addition of the heat energy required to raise the temperature of 5 kg of tomatoes to the drum design maximum temperature and that required to remove moisture which is mathematically represented in (6):

$$Q_{Drying} = \left(M_{T,i} \times c_{p,t} \times \Delta T\right) + \left(M_w \times L_v\right)$$
$$\Delta T = T_{sd} - T_i$$

where

$\boldsymbol{Q_{Dryi}}$ = Heat energy required for drying, (kJ), $M_{T,i}$ = Initial mass of tomatoes to be dried, (kg)

$C_{p,}$ = Specific heat of tomatoes, (4.6 kJ/kg ^oC as reported by [10]

T_{sd} = Safe drying temperature required for tomatoes, (65^{o}C) (design condition)

Ti = Mean ambient temperature (28^{o}C) (design condition)

Lv = Latent heat of vaporization (of liquid water at 50 ^{o}C = 2381.9 kJ/kg from the steam table)

4.0 CONCLUSION

This study has been able to design and construct a single drum gas-fired tomato paste drying machine, this is in order to technologically adopt engineering means in solving societal problems of preservation, wastage and economic standard.

Single drum gas-fired tomato paste drying machine was designed on AutoCAD application software with dimensions and materials that were readily available within reach, the design was transformed into construction based on the appropriate dimensions through critical analysis in terms of food contamination and economic importance.

The system is stress free and more efficient compared to charcoal-fired or steam-fired single drum dryer. The temperature that regulate the heat energy channeled into the drum can also be monitored through the burner regulator depending on the sample being dried.

The complete system was tested for calibration and analysis was carried out regarding the machine thermal energy conversion efficiency, sample dehydration/moisture removal performance and sample physical characteristics.

It can be concluded that with the application of this mechanical single drum gas-fired tomato paste dryer, perishable goods such as tomato can be preserved from wet paste form into dried form.

It is highly recommended that the design and construction of single drum gas-fired tomato paste drying machine should be adopted as a technological means of drying tomato paste in rural or any other similar environment because of its independency on electricity. It can be manually operated through mechanical means, as it also efficiently utilizes energy.

For commercial preservation of tomato paste, there is need to increase the dimensions of the design and construction to meet up with large scale drying of goods in order for implementation of mandates concerning sustainable development goals (SDG).

REFERENCES

[1] Mavis, O. A., Joyce, A. A., Firibu, S., Luis, A., Luis, A. E., & Subramaniam, S. (2014). Effect of pretreatment on physicochemical quality characteristics of a dried tomato (Lycopersicon esculentum), *African Journal of Food Science*, vol. 8, no. 5, pp. 253 - 259.

[2] Constanza, C., Juan, P. V., Julián, Q., & Andrea, M. (2020). Effect of Drum-Drying Conditions on the Content of Bioactive Compounds of Broccoli Pulp, *Foods*, vol. 9, pp. 1224 – 1237.

[3] Devahastin, S. & Mujumdar, A. S. (2006). Indirect Dryers," in *Handbook of Industrial Drying*, 4th ed., Boca Raton, CRC Press, 2006, pp. 137-149.

[4] Kalogianni, E., Xynogalos, V., Karapantsios, T., & Kostoglou, M. (2002). Kalogianni, E., Xynogalos, V.,Effect of feed concentration on the production of pregelatinized starch in a double drum dryer., *Food Science and Technology,* vol. 35, no. 8, pp. 703 - 714

[5] Deepika, A., & Darshan, P. (2014). Effect of solar tunnel and freeze drying techniques on the organoleptic acceptability of products prepared incorporating okara (soy by-product)., *International Journal of Food and Nutritional Sciences,* vol. 3, no. 3, pp. 10 - 13.

[6] Bag, S. K., Mishra, H. N., & Srivastav, P. P. (2011). Optimization of process parameters for foaming of bael (Aegle marmelos L.) fruit pulp, *Food and Bioprocess Technology,* vol. 4, no. 8, pp. 1450 - 1458.

[7] Jyoti, D. R. (2014). Effect of pre-drying treatments on quality characteristics of dehydrated tomato powder., *International Journal of Research in Engineering and Advanced Technology,* vol. three, pp. 1 – 7.

[8] McGriffen, M. E., Pantome, D. J., & Maisuna, J. B. (1994). Path analysis of tomato yield components in relation completion with block and eastern nightshade.," *Journal of America Society of Horticultural Science,* vol. 119, pp. 6 - 11.

[9] Mbi, Interviewee, Ndee Amaugu Minaj Broadcasting International Television. [Interview]. 18 October 2008.

[10] Ehiem, J. C., Irtwange, S. V., & Obetta, S. E. (2009). Design and Development of an Industrial Fruit and Vegetable Dryer, *Journal of Applied Sciences,* vol. 1, no. 2, pp. 44-53.

[11] Sharda, S. (2013). Studies on effect of various operating parameters and foaming agents-drying of fruit and vegetables., *International Journal of Modern Engineering Research*, vol. 3, no. 3, pp. 1512 – 1519.

[12] Sahni, E. K., & Chaudhuri, B. (2012). Contact drying: A Review of Experimental and Mechanistic Modeling Approaches, International Journal of Pharmaceutics, vol. 434, no. 1, pp. 334-348.

NIPES-NCEE Conference Proceedings
The 2nd International Conference 15th-17th Feb. 2023
623-634
www.nipesjournals.org.ng

BIODESULFURIZATION OF DIESEL BY GROUNDNUT SHELL ACTIVATED CARBON COATED *Pseudomonas stutzeri*.

Pambani Reuben[1], Aberuagba Folorunso[2]

[12]Department of Chemical Engineering, Federal University of Technology Minna, Niger State,

Nigeria.

Corresponding Author: pamelee23@gmail.com[1]

Abstract

The combustion of sulfur containing fuel produce substances that are harmful to the environment and this has led to a lot of researches aimed at reducing the sulfur content of fuels to a level that is environmentally friendly.The sulfur content of hydrodesulfurized fuels which is the conventional method of removing sulfur from fuels are still high due to the presence of some sulfur compounds that are either recalcitrant or refractory.Biodesulfurization which plays a complimentary role to hydrodesulfurization is slow just like other bioreactions. For biodesulfurization to play the complimentary role effectively, there is need to make it faster. In this research, activated carbon was produced from groundnut shell. The structural morphology and functional group present were investigated using scanning electron microscope (SEM) and fourier transform infrared (FTIR) spectroscopy respectively. The produced activated carbon was coated with an isolated pseudomonas stutzeri. The role of the activated carbon on the biodesulfurization activity of the pseudomonas stutzeri on diesel was investigated. The specific surface area (SBET) of the produced activated carbon was calculated by applying the BET equation to the adsorption data to be 1250 m2/g. The result from this study showed a high level of desulfurization of 92% for coated bacteria as compared to 70% for uncoated bactaeria which is due to the high surface area of the activated carbon and the functional group created during activation.

Keywords*: Activated carbon, Pseudomonas stutzeri , SEM, FTIR, biodesulfurization*

1.0 Introduction

Petroleum has been considered as the world's number one source of energy but due to its sulfur content, it has become necessary for the refiners to reduce the sulfur content to the barest minimum. This is due to the fact that sulfur oxides resulting from combustion of fuels can cause atmospheric pollution, acid rain and global warming. In order to have a clean atmospheric air, or to reduce air pollution from the transport sector, sulfur has to be removed from the fuel. It is therefore the desire of the United State Environmental Protection Agency (EPA) that the sulfur content of petroleum products, diesel as a case study should not exceed 15 ppm [1].

Hydrodesulfurization (HDS) is used to remove sulfur from hydrocarbons in petroleum refineries which require either increasing reactor residence time, or carrying out reactions under higher temperature and pressure [2]. However, the catalysts used in HDS are not active enough to remove refractory sulfur compounds like dibenzothiophene and its derivatives. In the aspect of Non-HDS technology, reverse is the case as it does not require higher hydrogen and energy consumption. Researchers have shown in the past few years that the use of microorganisms might increase the biodesulfurization yield [3,4]. Biodesulfurization as a non-HDS is an HDS alternative method which is used to achieve ultra clean fuels. Although different researchers have isolated bacteria capable of removing sulfur from petroleum, but this activity is unlikely to be sufficient for commercial applications where the requirement is for microorganisms with high activity and broad selectivity for different sulfur compounds [5,13]. In order to achieve this requirement, there is a need to increase the rates of biodesulfurization of currently used bacteria.

Activated carbons are still in wide-use for adsorption of pollutants within gaseous and liquid phases. Numerous economic and industrial sectors, such as food and beverage processing, chemical, pharmaceutical, petroleum, mining, nuclear, automobile, and vacuum manufacturing employ this material within their processing units. Some of these applications are very demanding with regard to the surface chemistry and characteristics of these carbon adsorbents [6].

In biotechnological processes, Kinetic equations which describe the activity of microorganism or an enzyme on a particular substrate are very important in understanding many phenomena. According to Olsen, (2006), description of a true behavior of a system can be done by obtaining an accurate estimate of the kinetic parameters in the models. The estimates of Michaelis-Menten kinetic parameters k and KM can be calculated by fitting data to either the derived form of Michaelis-Menten equation [7] or the integrated form of the same equation as reported by Goudar and Delvin (2001).

Kinetic studies of the four reactions of the 4S route have been reported in the literature, not as a reaction network but as single reactions. Several works have shown that desulfurization kinetics is only described as the DBT disappearance rate [8,9,10]. Other researchers also used Michaelis–Menten equation as a model equation for biodesulfurization process [11].

However, in this work, *Pseudomonas stutzeri* was isolated from the soil samples as a bacterium that feed on sulfur. Also, this work produced activated carbon from groundnut shell to coat the surface of the bacteria and the biodesulfurization activity of the bacteria and that of the activated carbon coated bacteria was investigated.

1.2 Statement of the Problem

Researchers have shown that alkylated dibenzothiophenes are the major sulfur component in the conventional hydrodesulfurization treated oil fraction due to the fact that they are highly recalcitrant to chemical catalyst. According to Moheballi and Ball (2016), biodesulfurization technology should be viewed as complementary technology to remove recalcitrant molecules present in hydrodesulfurization-treated oils. In line with the above statement, more research need to be carried out on desulfurization of petroleum fractions in order to meet up with the lower sulfur level (15-10ppm) as regulated by United state environmental protection agency [12].

1.3 Aim and Objectives

The aim of this work is to biodesulfurize diesel through groundnut shell activated carbon coated bacterium that could utilize sulfur compounds.

Specific Objectives

The specific objectives are:

- To isolate microorganism that can feed on sulfur.
- To produce activated carbon from groundnut shell
- To coat the bacterium with activated carbon produced from groundnut shell.
- To study the difference between the rates of desulfurization using groundnut shell activated carbon coated bacterium and uncoated bacterium.
- To develop a kinetic model for the biodesulfurization of diesel

1.4 Scope of the Study

The following scope has been strictly adhered to:

- Removal of sulfur compound from the substrates without distorting significantly their carbon framework by extracellular enzymes activities of the microorganisms.
- Production of activated carbon from groundnut shell by chemical activation method.
- Coating of Pseudomonas Stutzeri with activated carbon produced from groundnut shell
- Obtaining experimental results from the action of the coated and uncoated bacterium on diesel.

1.5 Significance of the Study

- Activated carbon was produced from readily available groundnut shells which are dumped into the environment and serve as pollutants.

- Fuel containing recalcitrant and refractory sulfur molecules desulfurized better with activated carbon coated Pseudomonas Stutzeri than the uncoated bacteria.

2.0 Materials and Reagents

Sterile tubes, sterile eppendorf PCR tubes, sterile pipette, Petri dishes, inoculating loop, conical flask (100mL, 250mL, 500mL), microscopic slides, test tube rack, measuring cylinder (10mL, 50mL, 100mL, 500mL, 1000mL), filter paper/absorbent paper, hand gloves (nitrile), sterile pipette tips (10, 100, 1000µ1), face shield, cotton wool**.** Eppendorf centrifuge (Hermle Z-300), thermo cool microwave oven (MS-2480EG), incubator (bacteriological type), microscope, PCR cycler, Autoclave (HIRAYAMA), micro centrifuge, gel electrophoresis set, UV trans illuminator, vortex, weighing balance, Bunsen burner, Rotary shaker (Gallenkamp), DNA extraction kit (Promega), Gas Chromatograph. DNA marker, electrophoresis grade agarose, MgCl2 (25mM), 3% hydrogen peroxide, 50mM EDTA, Mannitol salt agar, Brain-Heart Infusion (BHI) broth, Sodium hypochlorite,70% ethanol, isopropanol, 10mg/mL iysozyme, 10mg/mlL lysostaphin, ethidium bromide solution (10mg/mL) Taq DNA polymerase, genomic DNA (5ng/µl), dNTP mix (2mM each of dATP, dCTP, dGTP, and dTTP), oligonucleotide primers (5µM), 0.5X TBE buffer, sodium chloride, normal saline.

2.1 Sterilization and antiseptic techniques

Before conducting the experiment all glass wares were washed thoroughly in detergent solution, rinse in clean tap water and air-dried before placing them in an oven. The sterilization temperature in the oven was 170 ^oC for a minimum of three hours. Also the work bench area and drawers for keeping experimental materials were washed and sterilized by mopping item with 70 % ethanol solution.

2.1.1 Sample collection

The soil contaminated with diesel was collected in the following places: Modibbo Adama University of Technology's diesel store, administrative block generator room, Computer Centre generator room, and A.A Abdulkadir Filling Station along Numan-Mubi Road, Yola, Adamawa State, Nigeria. Diesel sample (1L) was collected from Total Filling Station along Mohammed Mustapha way, Jimeta, Yola, in new plastic container. All the samples were collected in sterile polythene bags. The collected diesel was sterilized to destroy organism that might be present.

2.1.2 Isolation of bacterium

The culture media with compositions (peptic animal digest tissue 5 mg/L, Sodiun chloride 5 mg/L, beef extract 1.5 mg/L, yeast extract 1.5 mg/L, pH 7.4, temperature 35 ^{0}C, 1Litre distilled water) were prepared by dissolving 13 g of the growth media in 1000 mL distilled water and were gently heated to dissolve completely. Then 5 g of each soil sample was mixed with 10 mL of distilled water before a serial dilution of 10^{-1} to 10^{-5} were carried out and incubated for 3 days. The colonies formed after incubation was then sub cultured onto nutrient agar for identification. The colony was then isolated, purified and transported to the Chevron Biotechnology Centre MAUTECH, Yola where it was confirmed.

2.1.3 Gram reaction

A thin smear of pure isolate was prepared on a clean grease-free slide. It was air-dried and heat-fixed by passing it horizontally over a Bunsen flame three times. Then, the smear was flooded with crystal violet stain for one minute and rinsed with sterile distilled water. Lugol's iodine was then poured onto the smear for one minute before washing gently with sterile distilled water. The iodine is a mordant; it fixes the crystal violet stain firmly into the cell (Kareem, 2010). The smear was then decolorized with 70 % ethanol briefly and immediately rinsed with water. The smear was counter-stained with safranin for 20-30 seconds and then rinsed with water. The slide was blotted dry with a piece of filter paper and finally allowed to air-dry. It was examined under oil immersion objective of the light microscope (Davies *et al*., 2007).

2.1.4 Hydrogen sulfide test

Hydrogen sulfide can be produced in small amounts from sulfur-containing amino acids like cysteine by a large number of bacteria in carbohydrate media. Hydrogen sulphide produces on contact with lead acetate a black precipitate, indicated by a visible black-colored reaction on the hydrogen sulfide paper strip. The lead acetate procedure is more sensitive than any other method for detecting hydrogen sulfide production and was used in this study. In this method, the lead acetate paper was dipped into the the growth culture for 3 minutes, the formation of black patches on the lead acetate paper indicated the production of lead sulfide as a result of H2S production.

2.1.5 DNA extraction

DNA Extraction Procedure was adopted from the manual of promega DNA Extraction Kit procured:

1 mL of an overnight culture was added to 1.5 mL micro-centrifuge tube.

It was centrifuged at 13,000 rpm for 2 minutes to pellet the cells and remove the Supernatant.

The cells were re-suspended thoroughly in 480µl of 50 mM EDTA.

Appropriate lytic enzyme(s) was added to the suspended cell pellet in a total volume of 120 µl, and gently pipette to mix it.

The sample was incubated at 37 ^{0}C for 30 minutes and centrifuged for two minutes at 13,000 rpm and removed the supernatant.

600 µL of nucleilysis solution was added and gently pipette until the cells were re – suspended.

The sample was incubated at 80^{0}C for 5 minutes to lyse the cells; then cool to room temperature.

3 µL of RNase solution was added to the cell lysate and invert the tube 2 times to mixed it.

The sample was then incubated at 37 ^{0}C for fifteen minutes and cooled at room temperature.

200 µL of protein precipitation was added to the RNase-treated cell lysate and vortexvigorously at high speed for twenty seconds to mix the protein precipitation solution with the cell lysate.

The sample was then incubated on ice for 5 minutes.

The sample was centrifuge at 13 000 rpm for three minutes.

The supernatant containing the DNA was transferred to a clean 1.5ml centrifuge tube containing 600 µL of room temperature isopropanol.

The sample was then gently mixed by inversion until the thread-like strands of DNA form a visible mass.

The sample was centrifuged at 13,000 rpm for two minutes.

The supernatant was carefully pour off on clean absorbent paper and drained the tube, followed by adding 600µL of 70% ethanol and the tube was inverted gently several times to wash the DNA pellet.

It was then centrifuge at 13,000 rpm for two minutes and carefully aspirated the ethanol.

The tube was drain on clean absorbent paper and allowed the pellet to air-dry for ten fifteen minutes.

100µL of DNA Rehydration Solution was added to the tube and rehydrate the DNA by incubating at 65ºC for one hour.

2.1.6 Gel electrophoresis

2 % agarose solution was prepared by measuring 2 g of agarose powder and mixed with 100 ml of 1X Tris-borate (TBE) in flask.

The flask was covered and microwave for two minutes and allowed to cool down for 5 minutes.

5µg/ml of ethidium bromide was added to the solution after it has cooled

Both the open sides of the gel casting tray was sealed.

Sample comb was inserted around the gel casting tray and form sample wells and agarose solution was pour into it carefully to avoid air bubbles

The casting tray was allowed for twenty minutes at room temperature.

The comb and tape was then gently removed after the agarose solution gelled accordingly.

The gel casting tray with the solidified agarose was transferred into the electrophoresis chamber.

TBE buffer solution was poured into the electrophoresis chamber to cover the gel.

The DNA samples was mixed with gel loading dye (loading buffer) and was carefully loaded into the wells using micropipette.

The electrophoresis chamber was covered and the negative side of the electrophoresis chamber was on the same side as the wells.

The electrophoresis chamber was connected to an electric current for two hours thirty minutes at a constant voltage of 70 V.

The gel was then removed from the chamber and the tray, the fragments was visualised with UV-trans illuminator.

2.1.7 Polymerize chain reaction (PCR)

The PCR mixture for the first reaction contained 12.5 µL of a 2X master mix containing Taq buffer (10Mm Tris–HCl, pH 8.3, 50Mm KCl, 1.5Mm $MgCl2$), 200 µL of each dNTP 2.5 units of Taq DNA polymerase, PCR primers and 5 µL of DNA template and water in a final volume of 25 µL. In the second reaction, the same master mix was used but with different primer concentration with two µL DNA template from the first reaction in a 25 µL reaction volume. The PCR was run in a gene Amp PCR system. A 2 % agarose gel stained with ethidium bromide was used to run for visualization of the PCR product.

2.1.8 DNA sequences

Sequencing of the amplified DNA was performed by HTDS 3500 DNA Sequencer and the sequences were compared using the Genbank (National Center for Biotechnology Information, NCBI).

2.1.9 Preparation of Activated Carbon

Activated carbons (AC) were prepared from groundnut shell by following procedures: firstly, the groundnut shells obtained from a local milling site in wukari, Taraba State were washed with water to remove dirt and other contaminants, oven-dried at 110 °C for 12 h then grounded and sieved to fractions with average particle size of 1.0 mm. Secondly, the prepared groundnut shell were carbonized at 400 °C under nitrogen flow (300 mL min^{-1}) for 90 min. The resulting samples were impregnated with NaOH (weight ratio 1/3) and dried at 120 °C for 12 h. Then, the preparative process was followed by heating at 400 °C for 20 min under nitrogen atmosphere at a flow rate of 300 mL min^{-1}; thereafter the temperature was raised to the temperature of 650 °C for 60 min to activate the obtained material. Finally, the activated product was grounded, neutralized by 0.1 M HCl solution and washed several times with hot distilled water to a constant pH (6.6–7.0). The washed activated carbon samples were dried under vacuum at 120 °C for 24 h and stored in a container.

2.2.1 Characterization of activated carbons

The surface functional groups of AC samples (ACs) were identified by fourier transform infrared spectroscopy using an IR Prestige 21, Shimazu, operating in the range of 4000–500 cm^{-1} and employing the KBr pellet method.

The morphology of the AC was obtained with a field emission scanning electron microscopy. The specific surface area (S_{BET}) was calculated by applying the BET equation to the adsorption data.

2.2.2 Bacterium Coating with Activated Carbon

In this aspect, the microorganism capable of removing Dibenzothiophene was coated with groundnut shell activated carbon. Fifteen milliliters of the activated carbon suspension (15g of activated carbon per liter of saline water) was mixed with 100 mL of a cell suspension (25g of cells per liter of saline water). The microbial cells were coated by adsorbing the activated carbon. The coated cells were concentrated on the side of the vessel containing the suspension and separated from the suspension medium.

2.2.3 Desulfurization Experiment

Biodesulfurization was carried out using the process as described thus: 20 mL of diesel was separately mixed with 10 mL of sulfur-free phosphate buffer of pH 7 containing 0.5 mL of the cells suspension in sterile distilled water and 2 % w/v glucose solution in a 250 mL flask. The flask was incubated on a Gallenkamp rotary shaker at 150 rpm for 5 hours in a temperature of 36 °C. Small amount of the reaction mixture were withdrawn at a regular intervals of 5 hours to monitor the concentration of DBT (original sulfur compound). For analysing the supernatant using Gas Chromatography (Model 3800), it should not have any contamination (like free bacteria) which would damage the GC column. The experiments were also conducted for 10, 15, 20, 25, 30, 35, 40, 45, and 50 hours in duplicates. However, this procedure was used for both coated and uncoated cells of *pseudomonas stutzeri up-1 strain*. Uncoated bacterium was used as control in order to determine the differences between the two.

2.2.4 Determination of Sulfur Content

The concentrations of various sulfur compounds were determined by gas chromatography (Model 3800) using a WCOT FUSED SILICA column and a flame ionization detector. The flow rate of the nitrogen carrier gas was 15 mL/min. The injector and detector temperature was maintained at 250 ^{0}C and 350 ^{0}C respectively. Sulfur-containing organic compounds: namely; benzothiophene and dibenzothiophene were run as standards and used to identify the peaks in diesel samples for both the control and experimental designs.

3.0 Results and discussion of results

3.1 Identification of micro organism

The microorganism used for desulfulrization of diesel in this research was identified via biochemical test and confirmatory test. The cell of the bacterium appeared small, slender rods and united in pairs and short chains. It has two polar flagella and actively motile as observed under the microscope

3.1.1 Biochemical Tests

Biochemical tests carried out on the isolated microorganism showed that the isolate has rod shape and raised elevation on nutrient agar with cream colour. It was observed to be Gram-negative due to their inability to retain the purple colour of the basic stain and, therefore, appeared pink under the light microscope. The isolate was also positive to the hydrogen sulfide test due to the present of black coloration of the lead acetate test paper.

Bacteria taxonomy relies on characterization, classification and nomenclature. Therefore, Series of biochemical tests were carried out on the isolated microorganism in order to identify the bacterium. Generally, visualization of bacteria at microscopic level is facilitated by the use of stains, which react with some components present in the cell. The isolate was found to have rod shape and observed to have a multiple polar flagella. The results from the gram reaction of the biochemical test showed a red pink colour as viewed by microscope on adding ethanol which confirmed that the bacterium is gram-negative. The blackening of the lead acetate strip showed a positive result indicating that H2S was produced. The production of H_2S shows that the bacterium is capable of desulfurizing sulfur from the substrates (DBT and BT).

3.1.2 Confirmatory Test

The DNA extracted was amplified by sequencing in which the molecular scheme followed identification for phylo-genetics affiliation of biocatalyst16S RNA genes using the sequence of the forward primer (16Sf) 5- AGAGTTTGATCCTGGCTCAG-3.The amplified pragment was compared with NCBI Genbank database where it was confirmed as *pseudomonas strutri up-1 strain*. *Pseudomonas* strutri strain UP-1 16S ribosomal RNA gene, partial sequence

GenBank: AY364327.1

GCCTAACACATGCAAGTCGAGCGGATGAGTGGAGCTTGCTCCATGATTCAGCG
GCGGACGGGTGAGTAATGCCTAGGAATCTGCCTGGTAGTGGGGGACAACGTTT
CGAAAGGAACGCTAATACCGCATACGTCCTACGGGAGAAAGTGGGGGATCTT
CGGACCTCACGCTATCAGATGAGCCTAGGTCGGATTAGCTAGTTGGTGAGGTA
AAGGCTCACCAAGGCGACGATCCGTAACTGGTCTGAGAGGATGATCAGTCACC
TGGAACTGAGACACGGTCCAGACTCCTACGGGAGGCAGCAGTGGGGAATATT
GGACAATGGGCGAAAGCCTGATCCAGCCATGCCGCGTGTGTGAAGAAGGTCTT
CGGATTGTAAAGCACTTTAAGTTGGGAGGAAGGGCAGTAAGTTAATACCTTGC

TGTTTTGACGTTACCGACAGAATAAGCACCGGCTAACTTCGTGCCAGCAGCCG
CGGTAATACGAAGGGTGCAAGCGTTAATCGGAATTACTGGGCGTAAAGCGCG
CGTAGGTGGTTCGTTAAGTTGGATGTGAAAGCCCCGGGCTCAACCTGGGAACT
GCATCCAAAACTGGCGAGCTAGAGTATGGCAGAGGGTGGTGGAATTTCCTGTG
TAGCGGTGAAATGCGTAGATATAGGAAGGAACACCAGTGGCGAAGGCGACCA
CCTGGGCTAATACTGACACTGAGGTGCGAAAGCGTGGGGAGCAAACAG

The Sequence Length was measured to be 1,356bp.

Separation of DNA fragments for cleared visualization was done by Agarose gel electrophoresis. Although DNA was invisible to the eye, therefore fluorescent dyes with an affinity for DNA were used. Upon excitation, fluorescent dyes absorbed the energy of UV light and emit lower energy visible light. This means that on illuminating the gel with UV light after electrophoresis, the DNA fragments fluoresced and appeared as bright bands on a dark background.

4.0 Conclusion

The following conclusions were made at the end of biodesulfurization process of diesel:

1. *Pseudomonas strutri* up-1 has been isolated from the soil samples as the bacteria that feed on sulfur with high activity and stability to remove sulfur from organic compounds that commonly exist in diesel oil.

2. The produced activated carbon had a size range of 0.5mm to 1mm. There was a high level of desulfurization of 92% for coated bacterium as compare to 70% for uncoated bacterium. This clearly indicated that groundnut shell activated carbon can enhance the activity of biodesulfurization of diesel which is attributed to the high surface area.

References

[1] Acuña-Argüelles, M. E., Olguin-Lora, P and Razo-Flores, E. (2003). Toxicity and Kinetic Parameters of the Aerobic Biodegradation of the Phenol and Alkylphenols by a Mixed Culture. *Biotechnol. Lett*. **25**: 559 - 564.

[2] Denome S.A., Oldfield, C. Nash, L.J. and Young, K.D. (1994). Characterization of the desulfurization genes from *Rhodococcus* sp. strain IGTS8, J. Bacteriol. 176 : 6707– 6716.

[3] Folsom B, Schieche, D., Di Gracia P., Wener, J. and Palmer, S. (1999). Microbial Desulfurization of Alkyl-Dibenzothiophenes from A Hydrodesulfurized Middle Distillate By *Rhodococcus Erythropolis* I-19, Appl. Environ. Microbiol. 65: 4967– 4972.

[4] Goudar, C. T. and Delvin, J. F. (2001). Nonlinear Estimation of Microbial and Enzyme Kinetic Parameters from Progress Curve Data. *Wat. Environ. Res*. **73**: 260-265.

[5] Grossman, M. J., Lee, M. K., Prince, R. C., Minak-Bernero, V., George, G. N. and Pickering,
I. J. (2001). Deep desulfurization of Extensively Hydrodesulfurized Middle
II. Distillate Oil by *Rhodococcus Sp*. Strain ECRD-1. Appl Environ Microbiol 67, 1949–1952

[6] Guobin, S., Huaiying, Z., Jianmin, X., Guo, C., Wangliang, L., and Huizhou, L., (2006). Biodesulfurization of Hydrodesulfurized Diesel Oil with *Pseudomonas* Delafieldii R-8 from High Density Culture. Biochem. Eng. J. 27, 305-309.

[7] Kobayashi M., K. Horiuchi, O.Yoshikawa,K. Hirasawa,Y. Ishii, K. Fujino, H. Sugiyama, and K. Maruhashi, (2001). Kinetic Analysis of Microbial Desulfurization of Model and Light Gas Oils Containing Multiple Alkyl Dibenzothiophenes, Biosci. Biotechnol. Biochem. 65 298–301

[8] Luo M., J. Xing, Z. Gou, S. Li, H. Liu, and J. Chen, (2003). Desulfurization of Dibenzothiophene by Lyophilized Cells of *Pseudomonas Delafieldii* R-8 In The Presence of Dodecane, Biochem. Eng. J. 13:1–6.

[9] Mayank A., Pritam K.D., Jaykumar B. B., and Arup J. B. (2016). Physical Insight into
I. Ultrasound-Assisted Biodesulfurization Using Free and Immobilized Cells of *Rhodococcus Rhodochrous* MTCC 3552. Chemical Engineering Journal 295:254– 267

[10] Mc Farland, B.L., Boron, D.J., Deever, W., Meyer, J.A., Johnson, A.R. and Atlas, R.M. (1998). Biocatalytic sulfur removal from fuels: applicability for producing low sulfur gasoline. *Crit. Rev. Microbiol.*, 24: 99-147.

[11] Mohebali, G., Ball, A. S.,(2016). Biodesulfurization of Diesel Fuel- Past, present and Future perspective. International Biodeterioration & Biodegradation 110: 163-180

[12] Olsen S**.** (2006). Applications of Isothermal Titration Calorimetry to Measure Enzyme Kinetics and Activity in Complex Solutions. Thermochim. Acta ***448****: 12–18.*

[13] Yang J, and Marison WI. (2005). Two-stage process design for the biodesulfurization of a model diesel by a newly isolated *Rhodococcus globerulus* DAQ3. Biochem Eng 27:77–82.

NIPES-NCEE Conference Proceedings
The 2nd International Conference 15th-17th Feb. 2023
635-649
www.nipesjournals.org.ng

ENERGY PERFORMANCE MODELING OF A LOCAL GAS POWER PLANT IN NIGERIA

A.J. Peters* and O.O. Ighodaro

Department of Mechanical Engineering, University of Benin, Nigeria.
*Corresponding author. Email: abasifreke.peters@gmail.com

Abstract

The Energy performance characteristics of a local power plant in Nigeria, operating at design and part load conditions was evaluated. Differences in part load performance, due to various factors in operation were investigated using EBSILON® Professional. Various part load operation strategies including variation in ambient temperature, variation of fuel and air flow, variation of expected output, variation in efficiency of components were considered while maintaining constant turbine exhaust temperature. The mass flow, air flow ratios under different load conditions (30% to 110%) nominal power was determined. Data were also collected from the power plant through direct observation from the monitoring screen of the human machine interface, log-books and manufacturer's manuals.. Variation in air ratio in the combustion chamber also enabled the regulation of the maximum temperature of the cycle and achieved specified power output. The results also showed that the power plant with higher design performance exhibited less efficiency degradation during part load operation. The efficiency of the turbine power plants was strongly affected by the pressure ratio, the air-fuel ratio, the ambient temperature, and the isentropic efficiencies.

Keywords*: Modeling, Simulation, Off-design, Thermodynamic Performance, EBSILON®, Design Performance*

1 Introduction

Global power generation from fossil fuels predominates till date [3]. The development of any economy, as well as standard of living of the general public depends on accessibility to, and availability of power. An increase in the use of power for commercial purposes is also important for sustainable development [9]. Therefore, the growing demand for non-renewable natural resources for power generation by the current energy conversion technologies, and the environmental impact due to global warming, waste disposal and flue gas emissions, has necessitated the need to improve the design and operation of energy systems, which prevents the release of substances capable of harming the environment.

The design of a gas turbine design is centered on certain distinguishing components, including the turbine geometry, flow rate, inlet and outlet pressures, dimensions, and performance [1]. However, alterations in power demands and turbine loses implies that turbines operate at reduced efficiencies. Hence, analysis and modeling of power generation system is of engineering interest and essential for the efficient utilization of energy resources. A simple gas turbine cycle (SGTC) is the most common cycle employed by most power plants for power generation. It is environmentally advantageous with short construction lead time and is characterized by low capital cost compared with steam power plants [9]. However, low efficiency due to limitations resulting from lower compression ratio and thermal properties of hot gas path limits the turbine inlet temperature. The problem of sustainability of energy has necessitated the need to improve on the existing gas turbine technology.

Sustainability in the use of gas turbines for power generation in gas turbines is a function of improved efficiency. Efficiency is very key because it affects other aspects of the sustainability of energy which includes cost value, efficient use of resources, enhanced design and analysis, energy security and a better environment. One way to improve the efficiency of a power plant is by combining gas turbine and a steam turbine to result in a combined cycle or combined with a steam generator to produce heat in a cogeneration plant, or combined heat and power (CHP) plant. A major setback to this, however, is the availability of space in already installed power plants. Carrying out modifications on the simple gas turbine cycle can improve its efficiency considerably. Some of the modifications which have been made on the SGTC are regeneration, reheating and intercooling. Apart from design efficiency, the off-design performance of gas turbines is equally important, since they ordinarily function at part load conditions for a significant portion of their lifetimes [5]. Regardless of gas turbine configurations, performance generally degrades with a reduction in power. For this reason, enhancing the part load performance for improving fuel economy, is paramount. Reports on off-design performance analysis of gas turbines have been previously reported [6], [8], [10], and [2].

Most power plants operate under off-design conditions as a result of variation in load or ambient conditions or both [7]. In comparison with design point performance, the understanding of part-load behavior is insufficient due to its complexity. In this study therefore, the part load performance characteristics of Omoku gas turbine was evaluated. Part load operation strategies included variations in ambient temperature, fuel, and air flow, expected output and efficiency of components, while maintaining constant turbine exhaust temperature. A model of the gas turbine cycle power plant was developed and simulated using EBSILON® Professional 13.0 software in design and part load operations.

2. Materials and Methods

2.1 Study area

2.1.1 The Omoku gas power station

The 150 MW gas power plant used in this study is situated in Omoku community, Ogba/Ndoni/Egbema Local Government Area, with a total population of approximately 33,000 people in the northern part of River State, Nigeria. It is located in the south coastal area of Nigeria with geographic coordinates on Longitude: 6º39ʾ24ʾʾE ad Latitude: 5º20ʾ37ʾʾN. It is among the power stations under the National Integrated Power Project (NIPP) scheme, managed by the Niger Delta Power Holding Company. The community is not linked with the national power grid due to its remote nature, hence a 132 kV switchyard is being used for electricity distribution. Natural gas powers the power plant due to its proximity to raw materials, occasioned by the presence of oil multinational oil companies.

The plant has 6 generating 25 MW GE heavy duty gas turbines, with a combined installed capacity of 150 MW.

2.1.2 Data collection

Data were collected from the gas plant (GE FRAME 5—MS 5001 PA—Single Shaft) via direct observation from the monitoring screen of the human machine interface (HMI), log-books and manufacturer's documentation. Relevant plant and working fluid parameters were obtained from appropriate thermodynamic tables.

2.1.3 Omoku gas turbine cycle

The turbine is a simple cycle, single shaft gas turbine, made of an inlet, seventeen stages of axial compressor, two stages of axial turbine, combustion chamber which comprises 10 cans arranged in an annular order, exhaust, and support systems. Figure 1 shows the schematic and temperature-entropy (T-S) diagram.

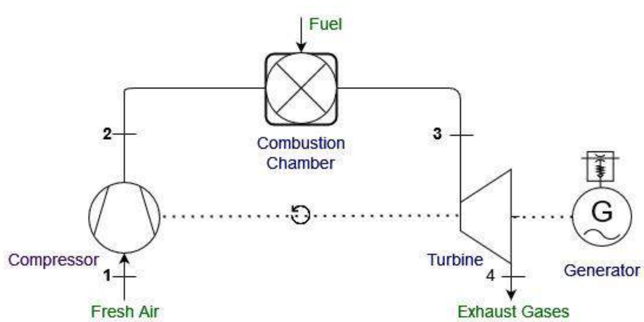

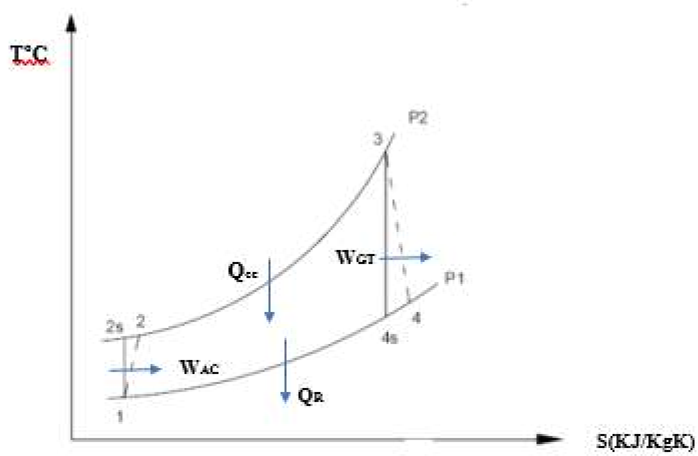

Figure 1 Schematic and T-S Diagram of Omoku Gas Turbine Power Plant

2.3 Energy balance for the simple gas turbine cycle

(a) ***Actual compressor work for the simple cycle gas turbine***

Turbines and compressors are steady flow devices. A balance between the energy in the fluid entering the compressor and that exiting the compressor will give the compressor work.

$$\dot{W}_{AC} = \dot{m}_a(h_2 - h_1) = \dot{m}_a c_{p,a}(T_2 - T_1) \quad (1)$$

Where $\dot{m}_a$ (kg/s) is mass flow rate of the air at the inlet of AC, T_1 is the compressor inlet temperature, $c_{p,a}$is the specific heat capacity of air.

(b) Combustion Chamber

$$\dot{Q}_{CC} = \dot{m}_f H_f \eta_{cc} = \dot{m}_{fg} h_3 - \dot{m}_a h_2 \equiv \dot{m}_{fg} c_{p,g} T_3 - \dot{m}_a c_{p,a} T_2 \quad (2)$$

$$\dot{m}_{fg} = \dot{m}_f + \dot{m}_a \quad (3)$$

Where $\dot{Q}_{CC}$ is heat added into the combustion chamber, $c_{p,g}\left(\frac{KJ}{KgK}\right)$ is the specific heat capacity flue gas, η_{cc} is efficiency of the combustion process, $\dot{m}_{fg}$ and $\dot{m}_f$ are mass flow rate of flue gas and fuel respectively.

(c) Gas Turbine

$$\dot{W}_{GT} = \dot{m}_{fg}(h_3 - h_4) = \dot{m}_{fg} c_{p,g}(T_3 - T_4) \quad (4)$$

Where $\dot{W}_{GT}$ is the work done by the turbine.

(d) Heat Rejected

$\dot{Q}_R = \dot{m}_{fg} c_{p,g} T_4 - \dot{m}_a c_{p,a} T_1$ (5)

Net Work, $\dot{W}_{net} = \dot{W}_{GT} - \dot{W}_{AC}$ (6)

Thermal Efficiency, $\eta_{therm} = \frac{\dot{W}_{net}}{\dot{Q}_R}$ (7)

Heat rate, , $HR = \frac{3600}{\eta_{therm}}$ (8)

2.3 Modeling and simulation with EBSILON® professional

Ebsilon, an abbreviated form of Energy balance and simulation of the load response of power generating or process controlling network structures, is a mass and energy balance calculation program for thermodynamical cycles. It is based on standard components, which are used for modeling common power plants; and programmable components used for modeling complex power plants processes with user-defined behaviour.

The basic control elements and tool bars (Figure 2) are the standard toolbar, component bar for selecting a component from a category, component wizard bar for accessing components classified by numbers, Ebsilon bar for starting simulations, and zoom bar for zooming in the model and finding objects.

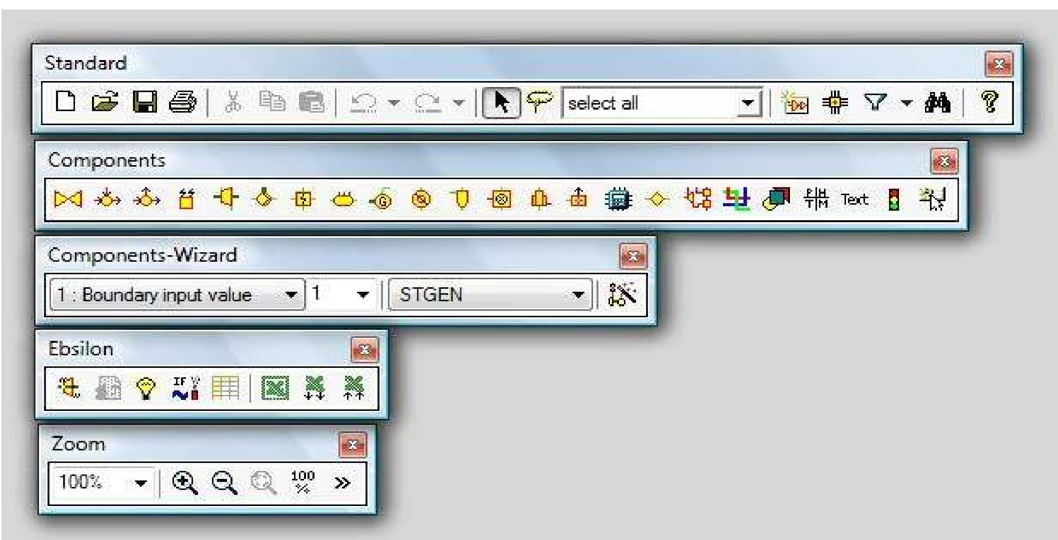

Figure 2 The basic control elements and tool bars of Ebsilon Software

2.4 Gas turbine GE MS 5001 in off-design

Off-design performance refers to the performance of an engine other than the design point [2]. Temperature, fuel and air flows were selected for the off-design performance of the gas plant. The following assumptions, according [4] were made:

i. The kinetic and potential energy losses were neglected in the system.

ii. The system operated under a steady state and steady flow condition.

iii. Combustion taking place in the combustion chamber was complete.

iv. Fuel and air were ideal gases.

v. The composition of air at the inlet of the compressor were 79 % N_2 and 21 % O_2.

vi. Air compressors and gas turbines operated at adiabatic condition.

2.4.1 Variation of ambient temperature

The variation of ambient temperature produced a change in the turbine behaviour because the air entering the turbine changed its properties, such as density, humidity, and flow rate. In this study, a 5% variation in humidity was assumed when the temperature changed; while variations in density and air flow for different cases (10°C, 20°C, 30°C, and 40°C) were considered.
As example, the calculations for the case at 40°C is described below:

Table 1 Density values obtained in each case are as shown.

T_{amb} (°C)	ρ (kg/m³)	φ (%)
10	1.246	120
20	1.204	110
30	1.163	100
40	1.127	90

At 40°C, we get a mass of air of 118.63kg/s, which is smaller than in nominal conditions of 122.319kg/s. The new air flow must be set at the compressor entrance using the "boundary value input" as we explained earlier. The temperature has to be changed also.
In every case of partload we will now have new conditions of temperature and mass flow. Ebsilon calculates by itself the amount of fuel which has to be burnt in the combustion chamber. The parameter which determines the amount of fuel is the air ratio.

The air ratio (called ALAM in Ebsilon and represented in tables as λ) is a parameter in the combustion chamber which enables the regulation of the maximum temperature of the cycle. The air ratio is defined as the ratio between the mass of air and the stoichiometric mass of air for a known fuel flow. By changing the air ratio, an order is given to the combustion chamber to accept more or less fuel. This means that the maximum temperature of the cycle, after the combustion chamber changes also. This creates a measure to achieve either higher or lower temperatures by varying the air ratio. If the air ratio is increased, more air is accepted in reference to the stoichiometric air and the maximum temperature of the cycle decreases. The exhaust temperature of the turbine decreases as well. If the air ratio decreases, the temperatures increase.

Variation of fuel and air flows

When an amount of power smaller than in nominal conditions is enough for satisfying the demand, the gas turbine can work in partload as well. First, the pursued objective is to determine how much power is needed. Then to achieve a variation in power, taking into cognizance the aim of keeping the exhaust temperature of the gas turbine constant; basically, for the benefit of a heat recovery steam generator to be coupled at the exhaust of the gas turbine unit. To adjust the exhaust temperature, the air ratio is varied.

In this case the criteria followed establishes a constant exhaust temperature while the range of power is between the 50 % of the load and nominal conditions. To obtain a constant exhaust temperature, the air ratio was varied in the same way that we have already explained when the gas turbine works in an ambient with changing temperatures. To obtain the required power, the mass of air has to be changed as well, taking into account that the smaller amount of air the less power is delivered. Depending on the required power, Ebsilon calculates by itself the amount of fuel necessary for ensuring that the gas turbine delivers exactly that amount.

For 80% load case:

The amount of power obtained in nominal condition is 26.809 MW. In this case we need the 80% of the nominal power, which is $0.8 \times 26.809 = 21.447$ MW. To reach that amount, the air ratio and the mass of air entering the compressor was varied. That also implies variation in mass of fuel, and the value at 80% load case was obtained. This value is represented as P_{aprox} and the ratio P_{aprox}/P_o represents the ratio with which the delivered power is obtained. If the P_{aprox}/P_o coincides with the partload needed, then the delivered power is exactly the required amount. In the case of 80%, the ratio P_{aprox}/P_o is exactly 80%, which means that the numbers obtained are correct.

In Figures 3 and 4, the model of the gas turbine working at nominal conditions of GE MS 5001 in design conditions and 80% nominal power are shown.

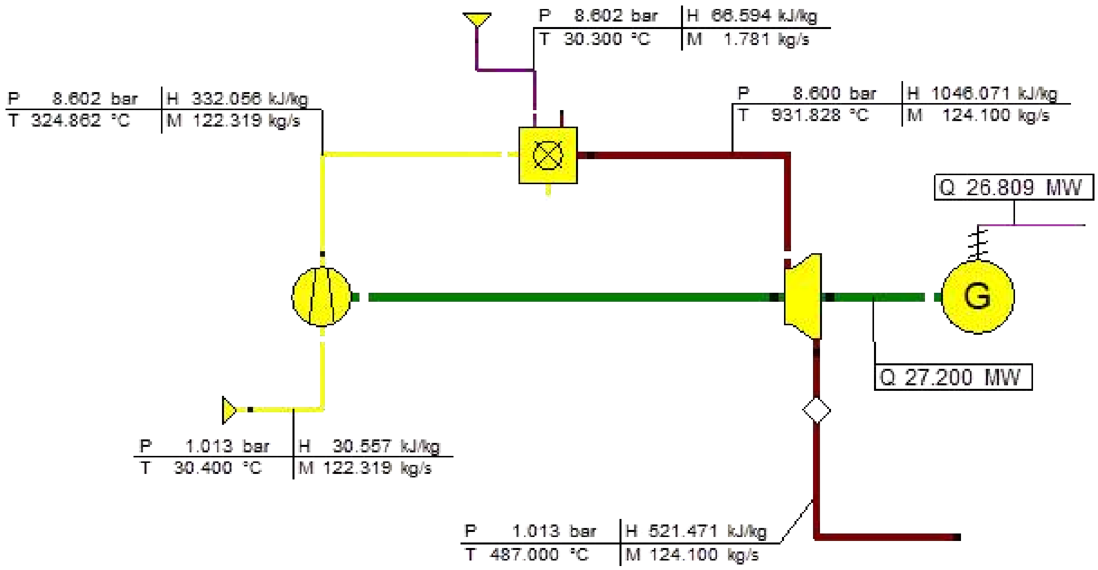

Figure 3 Model of GE MS 5001 in Design Conditions

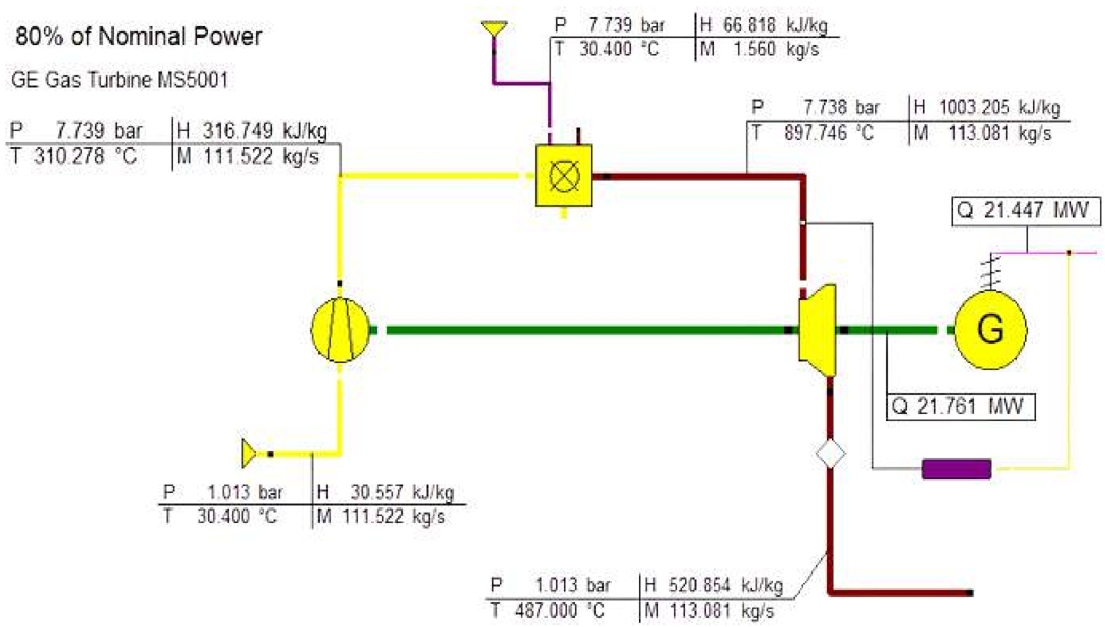

Figure 4 Gas Turbine working at 80 % of Nominal Power

Result and discussions

Temperature simulation in off-design

Table 2 and Figure 5 show the simulation of the exhaust and inlet temperatures of the gas turbine according to the criteria followed for establishing the temperatures in off-design. As shown in Tables 4 and 5, the power of the gas turbine is higher when the ambient conditions are colder due to the fact that a bigger amount of gas is expanded in the turbine and the pressure ratio is higher than in nominal conditions. That makes the gas turbine power output higher in rainy seasons, while in dry season it decreases. In the analysis, an average of 2.73 MW drop in power output for 10^{o}C increase in ambient temperature is obtained. The power of the gas turbine is higher when the ambient conditions are colder due to the fact that a greater amount of gas is expanded in the turbine, and the pressure ratio is higher than in nominal conditions. This makes the gas turbine power output higher in rainy seasons, while in dry seasons, it decreases. In the analysis, an average of 2.73 MW drop in power output for 10^{o}C increase in ambient temperature is obtained.

In a combined cycle power plant, the energy in the exhaust gases of the gas turbine is transferred to the steam cycle by using a HRSG. The exhaust gases of the gas turbine have a large amount of energy when they are leaving the turbine with a temperature of over 487 ˚C. The parameters which define the HRSG are set for the design case that means that the surfaces of the heat exchangers are designed according to these conditions. At other conditions, they are of course constant. For adequate performance of a combined cycle power plant the conditions of the steam cycle should remain constant. In consequence the outlet temperature (TOT) of the gas turbine should be as constant as possible independent of the ambient temperature.

Table 2 Temperature variation in Off-design

***Tamb* (◦C)**	***λ***	***TIT* (˚C)**	***TOT* (˚C)**
20	3.773	968.21	447.0
30	3.890	968.15	487.0
40	4.004	618.56	487.0
50	4.178	543.98	487.0

Table 3 Mass flows in Off-design

Tamb **(◦C)**	$\dot{m}_{air}$ **(kg/s)**	$\dot{m}_{fuel}$ **(kg/s)**	$\dot{m}_{gas}$ **(kg/s)**
20	101.35	1.588	102.91
30	106.29	1.585	107.88
40	111.28	1.612	112.90
50	116.99	1.645	118.64

Table 4 Parameters obtained in Off-Design

Tamb **(◦C)**	λ	**Power (*MWe*)**
20	3.773	32.328
30	3.890	29.588
40	4.004	26.809
50	4.126	24.119

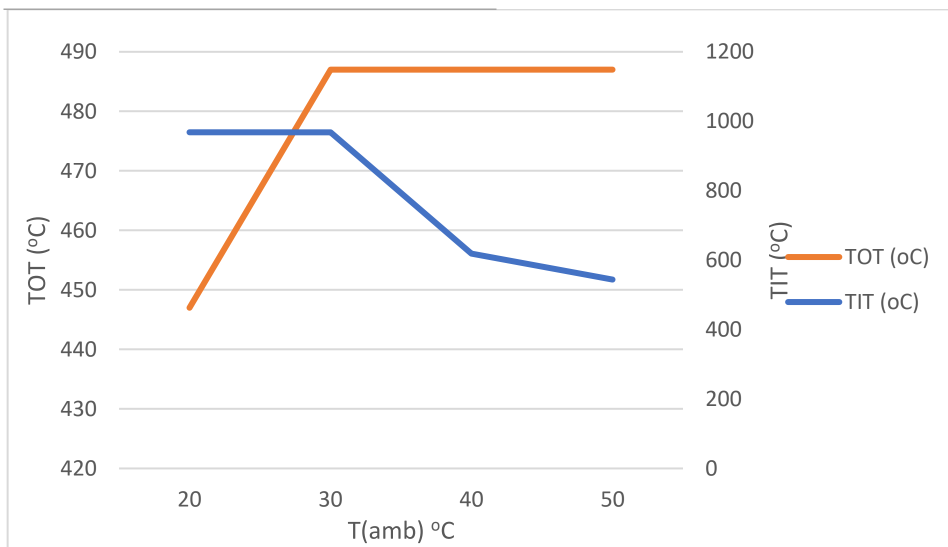

Figure 5 Temperature Simulation in Off-design

Variation of fuel and air flows

Figure 6 shows the simulation of the gas flow and exhaust temperature when the performance of the gas turbine varies from 30 % to 110 % of the nominal power.

- The ratio M_{gas}/M_{gas0} represents the variation of the gas flow with regards to the nominal gas flow.
- The ratio T_{exh}/T_{exh0} represents the variation of temperature with regards to the exhaust temperature in design conditions.

In Table 5, the different values obtained for every parameter are shown in each case of the off-design:

- The parameter Off-design represents the ratio between the necessary power and the nominal power.
- The parameter P_{aprox} is the power that in reality is obtained in the turbine in each case.
- The ratio P_{aprox}/P_0 represents how close we are at obtaining the off-design percentage necessary.

Table 5 Variation of Parameters in Off-design when the power is specified

Off-design	P_0 (MW)	P_{aprox}(MW)	$\dot{m}_{air}$(kg/s)	$\dot{m}_{fuel}$(kg/s)	$\dot{m}_{gas}$(kg/s)	λ	Texh (◦C)
110.00%	27.500	27.500	116.921	1.744	118.664	3.890	487.0
100.00%	25.000	25.003	106.292	1.585	107.877	3.890	487.0
90.00%	22.500	22.500	101.739	1.487	103.226	3.970	487.0
80.00%	20.000	20.000	96.865	1.385	98.250	4.057	487.0
70.00%	17.500	17.500	74.404	1.110	75.514	4.240	487.0
60.00%	15.000	15.000	63.775	0.951	64.726	4.343	487.0
50.00%	12.500	12.500	53.146	0.793	53.938	4.459	487.0
40.00%	10.000	10.000	42.517	0.634	43.151	4.592	450.0
30.00%	7.500	7.500	31.887	0.476	32.363	4.749	432.0

From Table 5, the amount of fuel is decreasing at the same time as the amount of air. The fuel decreases slower compared with the variation of air flow. The decrease of the amount of air entering the compressor leads to a constant outlet turbine temperature, can be seen in Figure 6.

Table 6 Relative parameters in off-design

Paprox/P0	***Mgas/Mgas0***	***Texh/Texh0***
110.0%	99.6%	101.0%
100.0%	100.0%	100.0%
90.0%	95.7%	100.0%
80.0%	91.1%	100.0%
70.0%	86.1%	100.0%
60.0%	80.7%	100.0%
50.0%	74.6%	100.0%
40.0%	67.7%	92.4%
30.0%	60.4%	88.7%

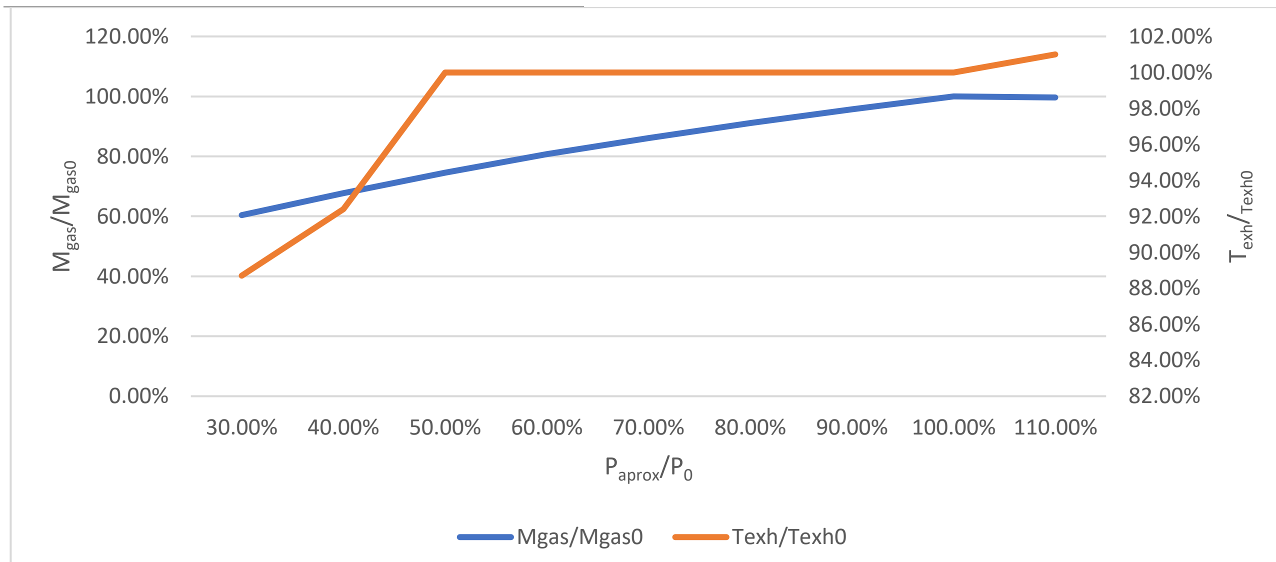

Figure 6 Temperature and Mass flow behaviour in off-design for a specific power

As shown in Figure 7, less mass goes through the turbine when we move into off-design operation, which implies that, the air flow, and the fuel flow decreases.

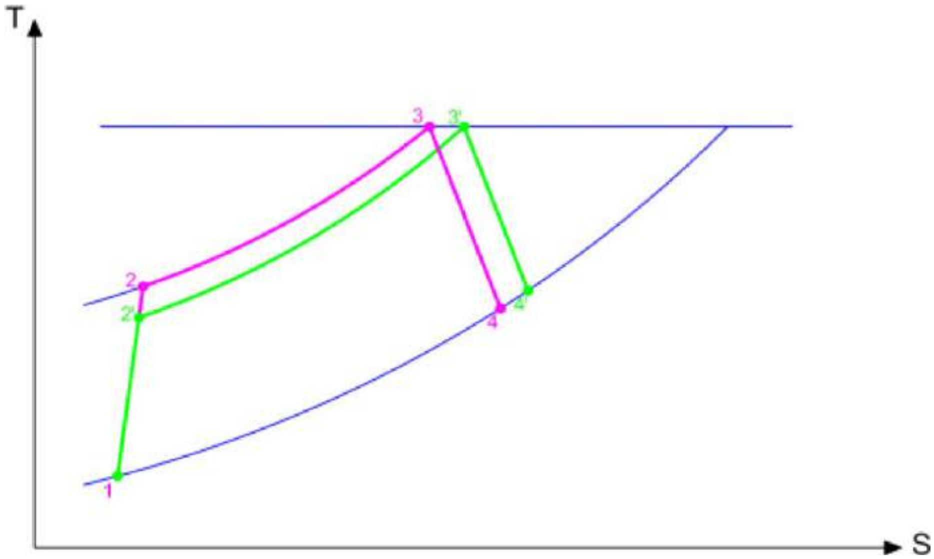

Figure 7 Comparison between the T-S diagrams for the gas turbine accepting less air

In the Figure 7, the cycle 1-2'-3'-4' represents the gas turbine working with less air. In the graphic, we can see that when the air flow is small the compression process is shorter, and the combustion is longer until reaching the maximum temperature in the cycle. This new "longer" combustion in process 2'-3' means that the amount of fuel burnt is bigger than in process 2-3. Technically, the mass of air entering the compressor is controlled by changing the orientation of the blades at the entrance (inlet guides vanes).

Variation of efficiency in components

As earlier mentioned, the gas turbine efficiency depends only on the pressure ratio and the nature of the working fluid. Working in off-design conditions means changes in the pressure ratio of the gas turbine and in its power output. But also, the other components of the gas turbine working in off-design suffer a change in their performance which has to be taken into account in the overall efficiency of the gas turbine.

In Ebsilon, compressors and turbines have an established default value of isentropic efficiency. The isentropic efficiency in a compressor or a turbine is a comparison between the real power obtained or consumed and the isentropic case. The default isentropic efficiency for turbines is 0.9 and for compressors is 0.85 and in off-design these values are defined by some correction curves. The variation of isentropic efficiency is directly proportional to the change of mass flow which is going through the compressor or turbine.

Conclusion

EBSILON Professional software was employed to model and simulate the Omoku gas turbine model. Modeling was done for both design and off-design scenarios to offer parameters that gas turbine model manufacturers would often not provide. The generated model validation results was in good agreement. Additionally, the data gathered will be beneficial for the installed gas turbine model thermodynamic and environmental evaluations. From the analysis, it was deduced that the power of the gas turbine is higher when the ambient conditions are colder due to the fact that a bigger amount of gas is expanded in the turbine and the pressure ratio is higher than in nominal conditions. This makes the gas turbine power output higher in rainy seasons, while in dry seasons it decreases. The power outputs at different ambient temperatures were simulated, indicating a drop in power output with increase in ambient temperature. An average of 2.73 MW drop in power output for 10◦C increase in ambient temperature was obtained.

The mass flow, air flow ratios under different load conditions (30% to 110% of nominal power simulation) show a decrease in the amount of fuel and air. However, fuel decreases slower compared with the variation of air flow at an average of 0.115 to 5.393 respectively. The decrease of the amount of air entering the compressor led to a constant outlet turbine temperature with variation in load case between 100% to 40%. Also, with less mass (air and fuel flow) going through the turbine when in off-design operation, the compression process is shorter, and the combustion is longer until reaching the maximum temperature in the cycle. This implied that more fuel is burnt. Technically, the mass of air entering the compressor can be controlled by changing the orientation of the blades at the entrance (inlet guides vanes). The results also showed that gas turbines with higher design performance exhibit less efficiency degradation during off-design operation. The efficiency of Gas Turbine power plants is strongly affected by the pressure ratio, the air-fuel ratio, the ambient temperature, and the isentropic efficiencies.

References

[1] Chandra, H., Arora, A., Kaushik, S.C., Tripathi, A. and Rai, A. (2011). Thermodynamic analysis and parametric study of an intercooled-reheat closed-cycle gas turbine on the basis of a new isentropic exponent. *International Journal of Sustainable Energy,* 30(2): 82-97.

[2] Ebigenibo, G.s. and Nweke, P. (2020). Off-design performance analysis of gas turbines. *Global Journal of Engineering and Technology Advances*, 4(2): 001-010

[3] Kabeyi, M. J. B. and A. O. Oludolapo (2020). *Managing Sustainability in Electricity Generation*. Paper presented at the 2020 IEEE International Conference on Industrial Engineering and Engineering Management, Singapore, Singapore, 14-17 December 2020, 2020, IEEM20-P-0

[4] Khani, L., Mohammad, S. M., Chitsaz, A., & Marc, A. R. (2016). Exergy and Exergeoeconomic Evaluation of a New Power/Cooling Cogeneration System Based on a Solid Oxide Fuel Cell. *Energy*, 64-77.

[5] Kim, T. and Hwang, S. (2006). Partload performance analysis of recuperated gas turbine considering engine configuration and operation strategy. *Energy*, 31(2-3): 260-277

[6] Lazzaretto, A. and Toffolo, A. (2001). Analytical and neural network models for gas turbine design and off-design simulation. *International Journal of Applied Thermodynamics*, 4(4): 173-182

[7] Lebele-Alawa, B.T. and Le-ol, A.K.(2015). Improved design of a 25mw turbine plant using combined cycle application. *Journal of Power and Energy Engineering*, 3(8): 1-14.

[8] Lee, J.J., Kang, D.W. and Kim, T.S. (2011). Development of a gas turbine performance analysis program and its application. *Energy Procedia*, 36(8): 5274-5285.

[9] Mohamed, K. M. (2005) *Parametric Analysis of Advanced Combined Power Generation Systems.* M.Sc. Thesis, University of New Brunswick.

Tiwari, A.K., Basan, M. and Islam, M. (2012). Effect of operating parameters on the performance of combined cycle power plant. *Open Access Scientific Reports*, 1: 351. doi:10.4172/scientificreports.351

[10] Yang, C., Huang, Z. and Ma, X. (2017). Comparative study on off-design characteristics of CHP based on GTCC under alternative operating strategy for gas. *Energy*, 145: 1-9

NIPES-NCEE Conference Proceedings
The 2nd International Conference 15th-17th Feb. 2023
650-653
www.nipesjournals.org.ng

PHOTOCATALYTIC DEGRADATION OF DYE (SIMULATED METHYLENE BLUE) OVER MO-CO /ZNO CATALYST

J. A. Aminu[1], U.G. Akpan[2].

Department of Chemical Engineering, Federal University of Technology Minna, Nigeria. joeadeoluaminu@gmail.com

Abstract

This present study is aimed at producing an improved photo catalyst for efficient degradation of dye constituents. This study seeks to evaluate the degradation potential of Mo-Co/ZnO bi-catalyst on dye effluent.

Dyes are applied in the textile industry, plastics, paints, pharmaceutical industries amongst many others. The use of dyes to solve problems and needs of man such as food, clothing and shelter, creates other problems such as pollution of water as most industries which use dye in their operations discharge dye effluent into streams and rivers which causes harm to the aquatic life in the ecosystem. Dyes are very problematic to decolorize via the existing methods owing to their compound structure and breakdown mechanism.

Therefore, there is need to device an efficient and effective method to remove and degrade the accompanied constituents of dye effluent before being discharged into the environment. In this research, the degradation of dye effluent under sun light was investigated using developed Mo-Co supported on ZnO photo catalyst. This was achieved through development and characterization of ZnO particle using chemical route, formulation and characterization of Mo-Co/ZnO via impregnation method, Photo catalytic degradation of dye effluent under sunlight, evaluation of the kinetic and the degradation isotherm parameters.

The developed catalyst (Mo-Co/ZnO) was used to degrade methylated blue dye under various conditions and parameters. Time, catalyst dosage and dye concentration was varied to measure the performance of the catalyst. It was discovered that degradation occurred more at higher time, lower catalyst dosage and lower concentration of dye.

1.0 Introduction

The application of dye, an organic compound has been widely employed in various areas including leather, textile, paper, cosmetics, printing, food, petroleum, paints and in pharmaceuticals.

The existence of these noxious dyes is possible threat to aquatic ecosystem as they release substances that decrease the photo-synthesis process in aquatic plant. Due to the harmful effect of the dye effluent into the surrounding ecosystem, the removal of the constituents' chemicals is therefore important.

Dyes are very problematic to decolorize via the existing methods owing to their compound structure and breakdown mechanism. Therefore, the discharge of such wastes containing diverse dyes and their breakdown products into the environmental components is critically undesirable.

Among numerous approaches, photo catalytic degradation for organic dyes and chemicals has been established as one of the most significant and green technologies for wastewater remediation techniques. In this process, the organic pollutants are effectively and directly degraded in the presence of photo catalyst, through photo catalytic oxidation–reduction reactions.

2.0 Methodology

This was achieved through development and characterization of ZnO particle using chemical route, formulation and characterization of Mo-Co/ZnO via impregnation method, Photo catalytic degradation of dye effluent under sunlight, evaluation of the kinetic and the degradation isotherm parameters.

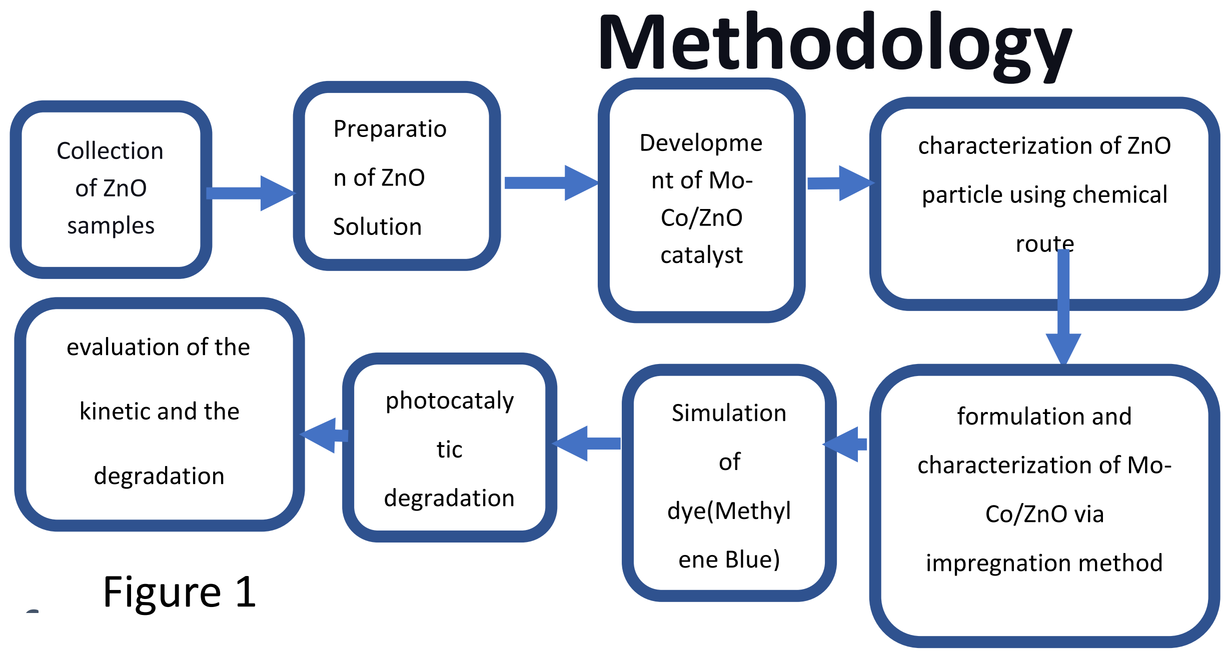

Figure 2: Methodology used in carrying out experiment

3.0 Results and Discussion

Contact time (minutes)	Percentage degradation (%)
10	68.70
20	72.52
30	75.39
40	75.62
50	77.12
60	84.50

.
Table1: Effect of contact time on the photo-catalytic efficiency of Mo-Co ZnO-supported catalyst

Table 1 shows the effect contact time on the photo-catalytic efficiency of Mo-Co ZnO-supported catalyst in methylene blue dye degradation.
A time-dependent degradation capacity of the catalyst was observed, with best time being 60 minutes at which a percentage degradation of 84.50% was obtained. The least percentage degradation was observed at 10 minutes with a percentage degradation was 68.70%

Catalyst dosage (g)	Percentage degradation (%)
0.50	89.91
1.00	81.26
1.50	79.54
2.00	78.46
2.50	71.83

Table2: Effect of Catalyst dosage on the photo-catalytic efficiency of Mo-Co Zn-supported catalyst
Table2 shows the effect of catalyst dosage on the photo-catalytic efficiency of Mo-Co Zn-supported catalyst in methylene blue dye degradation is shown in table 2.
The efficiency of the catalyst was found to be maximum at lower adsorbent as the maximum degradation (89.91%) was observed catalyst dosage of 0.50 g. Percentage degradation was observed to decrease with increase in adsorbent dosage.

Dye concentration (mg/L)	Percentage degradation (%)
20	92.17
40	90.13
60	78.59

80	**78.59**
100	**70.90**

Table3: Effect of dye concentrations on the photo-catalytic efficiency of Mo-Co ZnO supported catalyst.

Table 3 shows the dye concentration significantly affects the photo-catalytic efficiency of the catalyst. The optimum dye concentration was observed to be 20 mg/L at which percentage degradation of the dye was calculated to be 92.17%.

5.0 Conclusion

Mo-Co/ZnO is a very good photo catalyst. Higher contact time, lower catalyst dosage and lower concentration of dye improve the effectiveness of the catalyst and higher degradation of dye occurs.

References

[1] Al-Mashaqbeh, A., El-Eswed, B., Banat, R., Khalili, F.I. (2018). Immobilization of organic dyes in geopolymeric cementingmaterial, *Environ. Nanotechnol. Monit. Manage*., 10, 351–359.

[2] Andronic, L. & Duta, A. (2008). The Influence of TiO_2 Powder and Film on the Photodegradation of Methyl Orange,*Materials Chemistry and Physics*, 112,1078-1082. doi:10.1016/j.matchemphys.2008.06.059.

[3] Iwasaki, M., Hara, M., Kawada, H., Tada, H. & Ito, S. (2000). Cobalt Ion-Doped TiO_2 Photocatalyst Response to VisibleLight,*Journal of Colloid and Interface Science*, 224, 202-207. doi:10.1006/jcis.1999.6694

[4] Kumar, A.& Pandey, G. (2017). A review on the factors affecting the photocatalytic degradation of hazardous materials.*Mater. Sci. Eng. Int. J.*, 1, 1–10.

[5] Krishnakumar, B.,Hariharan, R., Pandiyan, V.,Aguiar, A.&Sobral,A.J. (2018). Gelatin-assisted g-TiO_2/BiOI heterostructure nanocomposites for azo dye degradation under visible light, *J. Environ. Chem. Eng.*, 6, 4282–4288.

[6] Khan, J.,Sayed,M., Ali,F.&Hasan, M. K. (2018). Removal of Acid Yellow 17 Dye by Fenton oxidation process, Z. *Physik. Chemie.*,232, 507–525.

[7] Legerská,B., Chmelová,D.&Ondrejovič, M. (2018). Decolourization and detoxification of monoazo dyes by laccase from the white-rotfungus *Trametes versicolor, J. Biotechnol*., 285, 84–90.

NIPES-NCEE Conference Proceedings
The 2nd International Conference 15th-17th Feb. 2023
654-663
www.nipesjournals.org.ng

EVALUATION OF BIOGAS PURIFICATION FILTER

[1]Zakariya M.A., [2]Idi S. and [1]Isodje E.

[1]Department of Petroleum and Natural Gas Processing, Petroleum Training Institute, Effurun, Nigeria.

[2]Department of Welding Engineering and Offshore Technology, Petroleum Training Institute, Effurun, Nigeria.

[3]School of Industrial Continuous Education, Petroleum Training Institute, Effurun, Nigeria.

E-mail: *[1]zakariya_a@pti.edu.ng , [2]idi_su@pti.edu.ng , [3]isodje_e@pti.edu.ng

corresponding author email*

Abstract
Biogas purification is a vital production process of biogas. It entails the removal of impurities so as to improve the quality of methane produced. In this research work, the evaluation of biogas purification filter was carried out. A cylindrical filter made from polyethene outer casing was fitted with sponge containing silica gel, iron fillings and calcium oxide in three separate layers respectively. This was used to purify biogas yielded from the anaerobic digestion of cow dung and cassava peels. The results obtained were analysed for percentage composition of biogas and the activeness of the purifier. The results showed an improvement in the percentage composition of methane from 67.56 % to 89.20 %. More so, there was dropped in the percentage composition of carbon (IV) oxide, water vapour, hydrogen sulphide, and other gaseous impurities (siloxane, carbon (II) oxide, nitrogen) from 31.03 %, 0.69 %, 0.20 %, 0.53 % to 10.75 %, 0.00 %, 0.00 %, and 0.05 %. These results simply showed that the purification filter can be used for processing produced biogas.

Keywords: *Biogas, Purification, Percentage Composition, Methane, Impurities*

1.0 Introduction
The demand for energy globally has been progressively increasing currently for the past decades [1-2]. This is due to rapid population growth, industrialization, and technological advancement [3-5]. In addition, energy security, economic growth, and environmental protection are the main drivers of national energy policies in any country in the world towards sustainable development [6-7]. The need for exploring new sources of energy which are renewable as well as being environmentally friendly cannot be overemphasized. Biogas technology offers an attractive platform to utilize certain categories of biomass for meeting our energy needs if it is properly harnessed [8-13]. Biogas is produced in many different environments, including landfills, sewage sludge and during anaerobic degradation of organic material [14-16]. In Nigeria, various cellulosic biomass (kitchen organic domestic wastes, cattle dung, agricultural waste etc) are readily available and can be utilized in the production of biogas [17]. Nigeria biogas potential is estimated at 25.53 billion m^3 per year [18].
Biogas can be used to generate electricity, cook, etc but the large volume of carbon (IV) oxide (CO_2) produced with it reduces the heating value of the gas. Besides, it also increases compression and transportation overall costs and thus reduces its economic usability [19-22]. Therefore, purification is required because it allows for a wider variety of uses, either for heat and electricity, or for vehicle and generators fuels. However, for use as a fuel, purification to remove carbon

dioxide (CO_2) and hydrogen sulphide (H_2S) is urgently required, because H_2S corrodes vital mechanical components within engine if it is not removed [23]. On the other hand, CO_2 has a huge negative effect on biogas usage quality, thus removing CO_2 increases the heating value and leads to bio-methane quality, similar to natural gas [24]. The hydrogen sulphide might be present in small quantities but its presence usually prohibits the direct use of these gases because of its toxic properties, the formation of SO_2 upon combustion (acid rain), and the problems it (usually) gives in downstream processing [39]. Besides, H_2S is frequently encountered in the field of odour monitoring because of its high odorous power [40].

2.0 Methodology

2.1 Materials

The following materials were used in this research work:

i. Biogas gas mild steel digester with temperature and pressure gauge attached
ii. Blend of cow dung and cassava peels substrates
iii. Silical gel
iv. Quicklime (CaO)
v. Iron oxide
vi. Weighing scale
vii. Manual compressor
viii. Purification filter
ix. Gas analyzer
x. Local sponge

2.2 Methods

The digester is a 0.25 m^3 capacity and made with mild steel was used. It has an inlet valve for charging of slurry [25], thermometer for taking the temperature of the slurry [26], pressure gauge for taking the gas pressure [27], outlet valve for discharge of slurry [25], stirrer for intermittent stirring of slurry [28], a view glass that is positioned between the slurry and gas section, and gas discharging valve for evacuation of biogas are all connected to the digester. The substrates were grinded to reduce the sizes to smaller sizes as reported by [29] and mixed with water in a ratio of 1:2 [30]. The slurry in the digester was stirred continuously [28] and left for anaerobic digestion to take place. The pressure gauge was monitored for the production of biogas and flame test was immediately carried out once the pressure gauge indicates an increase. Flame test is very necessary because is an indication of production of bio-methane. The production of yellow flame shows that bio-methane production has started and blue flame confirms adequate bio-methane production [31]. At that stage purification to evaluate the developed biogas purification filter becomes necessary. The raw biogas and purified biogas were evaluated for the percentage composition of methane and other components present. Figure 1 shows the arrangement of the biogas purification filter as recommended by [31-33] while Figure 2 isometric view [36]. Figure 3 shows the picture of the purification filter.

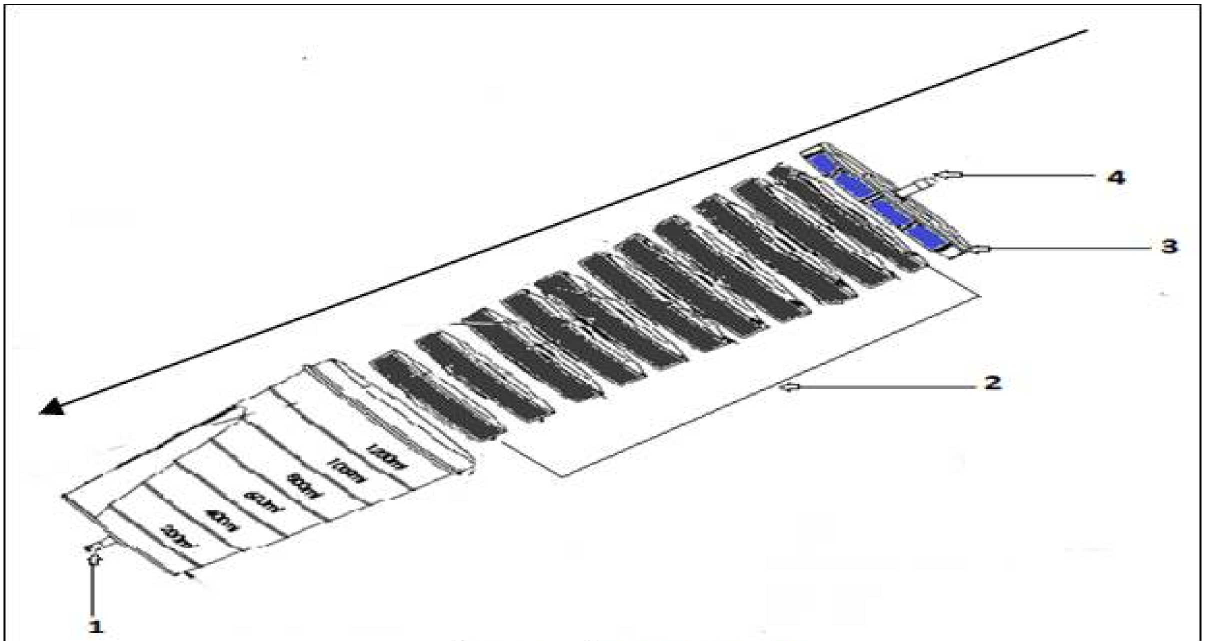

S/N	DESCRIPTION
1	Outlet nipple
2	Purifiers (Silica gel, quicklime, Iron oxide)
3	Cover
4	Inlet nipple

Figure 1. Arrangement of the biogas purification filter

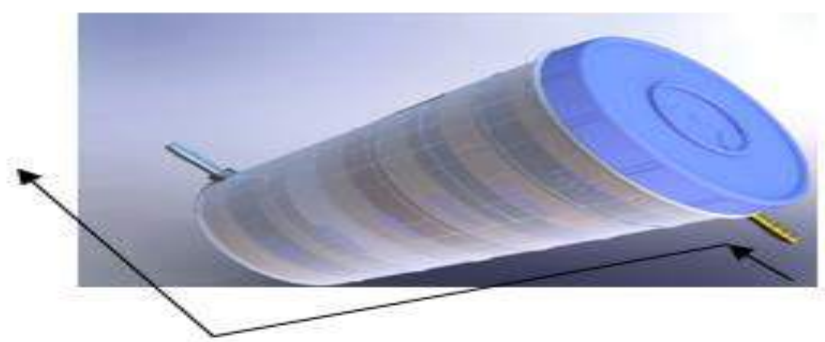

Figure 2. Isometric view

Figure 3. Picture of purification filter

3.0 Results and Discussion

The purifiers were impregnated on separate iron sponges and placed in the plastic container biogas purification filter. The arrangement was carried out as; the sponge with silica gel was inserted first followed with, quicklime and iron oxide. Water easily reacts with carbon (iv) oxide and hydrogen sulphide, thus, it is obligatory for the removal of water vapour due to the formation of hydrogen trioxosulphate (VI) acid from sulphur (IV) oxide which have the following effects; corneal haze, breathing difficulty, eye irritation, heart failure, etc. [37]. Also, the sponge inserted with quicklime will help to purify carbon (IV) oxide. The control set up consists of silica gel, iron fillings and calcium oxide. The biogas evacuated was purified with both test materials filter and control setup filter. The chemistry of the processes is shown in Equation (1)-Equation (5) [31-32]. Equation (1)-Equation (3) shows the removal of water vapour and carbon (iv) oxide while Equation (4) shows the removal of hydrogen sulphide.

$$2CaO(s) + 2H_20\ (g) + 4\ CO_2\ (g) \longrightarrow 2(HCO_3)_2(s) \quad (1)$$

$$CaO(s) + H_2O\ (l) \longrightarrow Ca(OH)_2\ (aq) \quad (2)$$

$$Ca(OH)_2(aq) + CO_2\ (g) \longrightarrow 2Ca(HCO_3)_2\ (s) \quad (3)$$

The equation below shows the reaction for the removal of hydrogen sulphide using iron oxide.

$$FeO(s) + H_2S\ (g) \longrightarrow FeS + H_2O\ (g) \quad (4)$$

Table 1 shows the result of flame test. Production of biogas was observed on the 14th days with indication of pressure reading (0.32 Bar). The pressure builds up continue to increase till 22nd days (0.87 Bar) before drop in pressure in 23rd day (0.55 Bar). The dropped in pressure is an indication of unhealthy environment for methanogenesis forming bacteria, thus biogas evacuation is required as reported by [25, 27]. The sequence follow will increase and dropped in pressure. More so, the formation of blue flame on the 17th day was a confirmation of proper production of bio-methane.

Table 1. Results of flame test

Day	Pressure (Bar)	Temp. (^{0}C)	Remarks
1	0.00	35	No gas
2	0.00	36	No gas
3	0.00	38	No gas
4	0.00	33	No gas
5	0.00	37	No gas
6	0.00	36	No gas
7	0.00	35	No gas
8	0.00	36	No gas
9	0.00	35	No gas
10	0.00	37	No gas
11	0.00	37	No gas
12	0.00	38	No gas
13	0.00	36	No gas
14	0.32	37	No flame
15	0.40	36	Yellow flame
16	0.41	36	Yellow flame
17	0.50	32	Blue flame
18	0.56	34	Blue flame
19	0.59	33	Blue flame
20	0.65	35	Blue flame
21	0.70	35	Blue flame
22	0.83	36	Blue flame
23	0.55	37	Blue flame
24	0.57	35	Blue flame
25	0.59	36	Blue flame
26	0.70	35	Blue flame
27	0.76	37	Blue flame

28	0.88	34	Blue flame
28	0.57	35	Blue flame
29	0.73	35	Blue flame
30	0.87	34	Blue flame
31	0.55	37	Blue flame
32	0.60	36	Blue flame
33	0.63	34	Blue flame
34	0.78	35	Blue flame
35	0.89	36	Blue flame
36	0.51	37	Blue flame
37	0.56	36	Blue flame
38	0.64	35	Blue flame
39	0.78	37	Blue flame
40	0.84	35	Blue flame
41	0.85	36	Blue flame
42	0.84	33	Blue flame
43	0.84	31	Blue flame
44	0.51	30	Blue flame
45	0.63	34	Blue flame
46	0.66	35	Blue flame
47	0.75	33	Blue flame
48	0.42	35	Blue flame
49	0.43	35	Blue flame
50	0.51	34	Blue flame

Table 2 shows the gas analysis of biogas production before and after purification with the biogas purifier.

Table 2. Result of biogas percentage composition analyser

S/N	Raw biogas percentage composition					After purification with biogas purification filter				
	CH_4	CO_2	H_2S	H_2O	Others	CH_4	Co_2	H_2S	H_2O	Others
1	67.55	31.01	0.69	0.21	0.54	89.20	10.75	0.00	0.00	0.05
2	67.54	31.04	0.69	0.20	0.53	89.22	10.74	0.00	0.00	0.04
3	67.57	31.03	0.70	0.19	0.51	89.17	10.77	0.00	0.00	0.06
4	67.58	31.02	0.67	0.21	0.52	89.20	10.75	0.00	0.00	0.05
$\sum$	270.24	124.1	2.75	0.81	2.10	356.79	43.10	0.00	0.00	0.20
Ave	67.56	31.03	0.69	0.20	0.53	89.20	10.75	0.00	0.00	0.05

The constituents of raw biogas, biogas purified with the purification filter are depicted in Table 2. The results show that the percentage composition of raw biogas, carbon (IV) oxide, hydrogen sulphide and other gaseous components that consists of hydrogen, oxygen, nitrogen, carbon (II) oxide, siloxane, ammonia, benzene, toluene, and xylene [35-38] are 67.56 %, 31.03 %, 0.69 %, 0.20 %, 0.53 %. However, after purification, there was an improvement in the percentage composition of bio-methane the percentage composition obtained be 89.20 %. On the other hand, there were decreased in the percentage composition of carbon (IV) oxide (10.75 %,) while hydrogen sulphide and water vapour were completely removed. The increase in the percentage composition of bio-methane confirmed the removal of impurities from the biogas while the decrease in the compositions of carbon dioxide and water vapour confirms purifying ability of the filter [31, 32, 34].

4.0 Conclusion

Biogas is urgently needed as a fuel substitute for firewood and other fossil fuels that have huge negative effect on the ozone layer. However, without the technology of the filter, biogas usage would be hampered as results of impurities contain in it. In this study, evaluation of homemade biogas purification was successfully carried out. The homemade purifier was developed using an existing literature. Silica gel, quicklime and iron oxide were embedded in sponge which serves as support before properly arranged in the purifier casing. The outcome showed that the filter was successfully used in purification of impure (raw) biogas. Thus, it can be concluded that the homemade purification system was very active and thus can be used for the purification of biogas.

References

[1] Orhorhoro, E.K., Emmanuel E.L., Oyejide O.J. (2019). Analysis and Evaluation of a Three-Stage Anaerobic Digestion Plant for Management of Biodegradable Municipal Solid Waste. *International Journal of Engineering Research in Africa,* 60: 75-87

[2] Ferrer I., Garfi M., Uggetti E., Ferrer-Marti L., Calderon A. and Velo E. (2011). Biogas production in low-cost household digesters at the Peruvian Andes. Biomass and Energy, 35:1668-1674

[3] Finn, H., Rune, B. and Bernt, L. (2013). Adapting Dynamic Mathematical Models to a Pilot Anaerobic Digestion Reactor. *Modeling, Identication and Control*, 34(2): 35-54

[4] Ge, X., Matsumoto, T., Keith, L., and Li, Y. (2014). Biogas energy production from tropical biomass wastes by anaerobic digestion. *Bioresource Technology*, 169: 38–44

[5] Nigeria Electricity Regulatory Commission, Power Sector Outlook in Nigeria, Governments Renewed Priorities, ww.nigeriapowerreform.org, 2014, Accessed 29th June, 2019.

[6] Samuel O.D., Okwu M.O, Oyejide O.J., Ebrahim T., Asif A., Mohammad K. (2020): 'Optimizing biodiesel production from abundant waste oils using a hybrid of semi empirical equation and grey wolf optimizer algorithm'. Elsevier – Fuel, Fuel 281 (2020) 118701, 1-13, DOI: 10.1016/j.fuel.2020.118701

[7] Paramagurua, G., Kannanb, M. Lawrencec, P. Thamilselvand, D. (2017). Effect of total solids on biogas production through anaerobic digestion of food waste. *Desalination and Water Treatment*, 63: 63–68.

[8] Grimberg, S.J., Hilderbrandt, D., Kinnunen, M., Rogers. S. (2015). Anaerobic digestion of food waste through the operation of a mesophilic two-phase pilot scale digester–assessment of variable loadings on system performance. *Bioresource technology*, 178: 226-229

[9] Adelekan, B.A. and Adelekan, I.O. (2004). Health Implications of Household Energy Use in Selected Nigerian Towns. *Nigerian Journal of Renewable Energy, Sokoto Energy Research Centre*, 12(1& 2): 138-146

[10] Appels L., Baeyens J., Degreve J., Dewil R. (2008). Principles and potential of the anaerobic digestion of waste-activated sludge. *Progress in Energy and Combustion Sci.*, 772 – 777

[11] Authayanun S., Aunsup P., Im-orb K., Arpornwichanop A. (2013). Systematic analysis of proton electrolyte membrane fuel cell systems integrated with biogas reforming process. *Chemical Engineering Transactions*, 35, 607-612

[12] Odeyemi, O. (1981). Biogas from *Eupatorium odorantum*, an alternative cheap energy source for Nigeria". In Global impacts of Applied Microbiology, 6th International Conference, 246-252

[13] Oyejide O.J., Ogie N.A. and George B.J. (2021): 'Artificial Neural Network Model for Prediction of Biogas Yield from Anaerobic Co-Digestion of Decomposable Wastes.' 2nd International Conference on Electrical Power Engineering / Training Workshop (ICEPENG), May 18-22.

[14] Catsbery J. and Kempen G.J (1990). Long-term operation of a biofilter for simultaneous removal of H_2S and NH_3. *Air & Waste Management Association*, 52: 1389-1398

[15] Cavenati S., Grande, C.A., Rodrigues, A.E. (2005). Upgrade of methane from landfill gas by pressure swing adsorption. *Energy & Fuels*, 19, 2545-2555

[16] Ojolo, S.J., Oke, S.A., Animasahun, O.K., and Adesuyi, B.K. (2007). Utilization of poultry, cow and kitchen wastes for biogas production: A comparative analysis. *Iranian J. Environ. Health Sci. Eng*, 4, 223-228

[17] Oyejide O.J., Orhorhoro E. K., Atadious D. (2018): 'Mathematical Modeling Of Biogas Yield From Anaerobic Co-Digestion Of Organic Waste And Pig Dung.' International Journal of Engineering Science Invention (IJESI)5(7): 30-38.

[18] Chima C.N., Jude N.O., Justina C.O. and Ekpewerechi S.A. (2013). Biogas potential of organic waste in Nigeria. Journal of Urban and Environmental Engineering, 7(1): 110-116

[19] Kim S., Kim H.T. (2004): "Optimization of CO_2 absorption process with MEA solution. *Carbon Dioxide Utilization for Global Sustainability,* 153: 429-434

[20] Kohl, A. L., and Riesenfeld, F. C. (1979). Gas Purification, 3d ed. - Ed., Gulf Pub. Co., Book Division, Houston

[21] Schattauer, A., Abdoun, E., Weiland, P., Plochl, M. and Heiermann, M. (2011). Abundance of trace elements in demonstration biogas plant. *Bio-systems,* 108 (1): 57-65

[22] Yuan, W. X. and Bandosz, T. J. (2007). Removal of Hydrogen Sulphide from Biogas on Sludge-Derived Adsorbents. *Fuel*, 86(17-18): 2736-2746

[23] Yuan W. X., and Bandosz T. J. (2007). Removal of Hydrogen Sulphide from Biogas on Sludge- Derived Adsorbents. *Fuel*, 86(17-18), 2736-2746

[24] Appels L., Baeyens J., Degreve J., Dewil R. (2008). Principles and potential of the anaerobicdigestion of waste-activated sludge. *Progress in Energy and Combustion Sci.,* 772 – 777

[25] Ebunilo, P.O., Aliu, S.A. and Orhorhoro, E.K. (2015). Performance Study of a Biogas Pilot Plant using Domestic Wastes from Benin Metropolis. *International Journal of Thermal & Environmental Engineering volume,* 10(2):135-141

[26] Ebunilo, P.O., Orhorhoro, E. K., Oboh, V., Onochie, P. U (2016). Effect of Temperature on Biogas Yields Using South-South Nigeria as a Case Study. *International Journal of Technology Enhancements and Emerging Engineering Research,* 4(3): 50-54

[27] Orhorhoro, E.K., Ebunilo, P.O., Tamuno, R.I., and Essienubong, I.A. (2016). The Study of Anaerobic Co-Digestion of Non-Uniform Multiple Feed Stock Availability and Composition in Nigeria. *European Journal of Engineering Research and Science, (EJERS),* 1(1): 39-42

[28] Mussoline, W., Esposito, G., Lens, P., Garuti, G., Giordano, A. (2012). Design considerations for a farm-scale biogas plant based on pilot-scale anaerobic digesters loaded with rice straw and piggery wastewater. *Biomass Bioenerg.,* 46: 469-478

[29] Orhorhoro, E.K., Ebunilo, P.O.B., and Sadjere, E.G. (2017). Design of Bio-Waste Grinding Machine for Anaerobic Digestion (AD) System. *European Journal of Advances in Engineering and Technology,* 4 (7): 560-568

[30] Ebunilo, P.O., Ukwuaba, S.I., Owunna, I.B., Sadgere, E.G. and Orhorhoro, E.K. (2016). Evaluation of cow dung and talinum triangulare as a seeding agent for the production of biogas from domestic wastes in Warri metropolis. *International Journal of Scientific and Engineering Research,* 7(3): 633-641

[31] Ebunilo, P.O., Orhorhoro, E.K., Adegbayi, O.A. (2016). Investigation of the purification of biogas from domestic wastes using local materials in Nigeria. *International Journal of Scientific & Engineering Research*, 7(2): 505-515

[32] Osunde, P.O., Ebunilo, P.O.B., and Orhorhoro, E.K. (2017). Preliminary Evaluation of a Biogas Purification Filter Suitable for use in Nigeria. *Journal of Scientific and Engineering Research*, 4(10): 125-134

[33] Orhorhoro E.K., Orhorhoro, O.W., Atumah, E.V. (2018). Performance Evaluation of Design AD System Biogas Purification Filter. *International Journal of Mathematical, Engineering and Management Sciences*, 3(1): 17–27

[34] Orhorhoro Ejiroghene Kelly, Arhore Oghenegare, and Okuma Silas Oseme (2020). Determination and removal of siloxane in energy recovery of biogas from municipal solid waste. *Journal of Sustainable Energy & Environment*, 11: 93-100

[35] Herout, M., Malaťák, J., Kučera, L., and Dlabaja, T. (2011). Biogas composition depending on the type of plant biomass used. *Res. Agr. Eng.*, 57(4): 137–143

[36] Ray, N. H. S., Mohanty, M. K., and Mohanty, R. C. (2013). Anaerobic digestion of kitchen waste: Biogas production and pretreatment waste, a review. *International Journal of Scientific and Research Publication,* 3: 11-18

[37] Simonyan K.J. and Fasina O. (2013). Biomass resources and bioenergy potentials in Nigeria. *Africa Journal of Agricultural research,* Vol. 8(40): 4975-4989

[38] Franco, C., Gianluca, C., Alessandro, P., Valentina, C. (2015). Lignocellulosic biomass feeding in biogas pathway: state of the art and plant layouts. *Energy Procedia (Science Direct)*, 81: 1231 – 1237

[39] Maat H., Hogendoornb J.A., Versteeg G.F., (2005). The removal of hydrogen sulfide from gas streams using an aqueous metal sulfate absorbent. Part I. The absorption of hydrogen sulfide in metal sulfate solutions, *Separation and Purification Technology*, 43: 183–197

[40] Zaouak O., Ben Daoud A., Fages M., Fanlo J.L. and Aubert B., (2012): High Performance Cost Effective Miniature Sensor for Continuous Network Monitoring of H_2S. *Chemical Engineering Transactions*, 30: 325-330

NIPES-NCEE Conference Proceedings
The 2nd International Conference 15th-17th Feb. 2023
664-672
www.nipesjournals.org.ng

PERFORMANCE EVALUATION OF A BIOMASS BRIQUETTE STOVE BURNER

[1]Ajiboluwa A.A., [2]Enakireru E.E. and [3]Akinfaloye A.O.

[1]Department of Mechanical Engineering, Federal University of Petroleum Resources, Effunrun, Nigeria
[2, 3]Department of Mechanical Engineering, Petroleum Training Institute, Effurun, Nigeria.

E-mail:* [1]ajiborisha.abisoye@fupre.edu.ng, [2]enakireru_ee@pti.edu.ng, [3]akinfaloye_ao@pti.edu.ng

corresponding author email*

Abstract

This research work is focused on the design and construction of biomass briquette stove burner. The designed and constructed biomass briquette stove burner is a circular section and consists of chimney, smoke ring, air inlet, combustion chamber, fuel loading section, and ash tray. The briquette stove was constructed using locally available materials. Materials selected and used for this research work include; mild steel casing, clay, and fiberglass. The combustion chamber was design to ensure that optimum concentrate of flame and heat is conveyed to the cooking utensils for maximum efficiency. Biomass briquette produced from corncob was used for testing of the stove burner. The performance of the biomass briquette stove burner was evaluated by comparing burning the briquette using biomass briquette stove and burning in open air. The performance test results show that maximum thermal efficiency of 76.27% was obtained with the system.

Keywords: *Biomass, Briquette stove, Design, Construction, Thermal efficiency, Combustion Chamber*

1.0 Introduction

The availability of affordable energy and its efficient utilization for both domestic and commercial usage is very vital, if not the most critical factor in developmental activities of any nation. It is one of the essential factors for continuous development and economic growth of a nation [1, 2]. However, increase in urbanization, industrialization, technological advancement etc., in Nigeria have resulted in energy demand among increasing population estimated at 187,896,647 persons [3]. The growing population and technological developments have shown that the present sources of energy in use are not adequate [4-6]. Besides, increasing demand for wood and fossil fuel with limited availability has resulted in environmental pollution [7]. Availability of energy for cooking remains a major concern for average Nigerian and sub-Sahara Africa countries [8]. In Nigeria, Agricultural land covered approximately 745,000km^2 of the total land area, and about 41.2% of the Agricultural land is arable land, 11.3% forest area and 3.3% permanently cropped area [9-11]. About 70% of Nigerian populations are involved in Agricultural production with more than 70% of the farming population practicing subsistence Agricultural farming [12]. An estimate of 48% of the country's population lives in the rural areas with more than 70% of the country's population living below the poverty line. The source of energy is wood fuel and fossil fuel which has contributed to desertification, deforestation and erosion in the country [13, 14]. Nonetheless, as wood fuel supplies diminish due to over dependency [15], there is now increase in physical or economic encumbrances in sustaining even a minimal daily fuel supply among Nigerian populace. The use of firewood and mismanagement of the existing energy resources (Agricultural residues) is creating human and environmental crisis in Nigeria [16]. Traditionally, wood in form of fuel wood, twigs and charcoal has been the major source of renewable in Nigeria, accounting for about 51% of the total annual energy consumption; the other sources of energy include natural gas (5.2%), hydroelectricity (3.1%), and petroleum products (41.3%) [17].

The degradation and depletion of the forest reserve base has major effects on other sectors of the economy. The disappearance of forest cover leads to erosion, soil degradation and unfavorable hydrological changes [18]. The decreasing availability of fuel wood, coupled with the ever-rising prices of kerosene and cooking gas in Nigeria, draw attention to the need to consider alternative sources of energy for domestic and cottage level industrial use in the country [19]. Such energy sources should be renewable and should be accessible to the poor, thus this research work. Biomass resources in Nigeria according to the Food and Agricultural Organization [20-22] are described as organic non-fossil materials of biological origin, which can be identified as agricultural crops**,** grasses and shrubs, residues and wastes (agricultural, forestry, municipal and industrial). Biomass energy resources of Nigeria stated by Energy Commission of Nigeria [17] are estimated to be about 144 million tons per year.
Biomass briquette includes; elephant and spear class, ground nut shells, solid waste, agricultural waste and other organic materials. They are commonly used for electricity generation, heating and cooking fuel in developed countries such as USA, China, France, etc., and developing countries such as India [1, 21]. The composition of the briquettes varies due to the availability of raw materials. The raw materials are gathered and compressed into briquette using briquette machine in order to burn longer and make transportation easier [21, 23]. Biomass briquetting represents a set of technologies for the conversion of biomass residues into a convenient fuel [24]. A briquette stove is a stove that burns compacted biomass briquette materials to generate heat for residential and sometimes industrial spaces. By steadily feeding fuel into a burning pot area from a storage container, the fuel creates a constant flame that requires little or no physical adjustments. The special advantage of the briquette stove is that inside the house the smoke emission is minimal, because the cook does not have to tend the fire all the time [24]. Briquette fuels are fuels made from compacted organic matter or biomass [24]. Briquettes was introduced and its use as domestic fuel is gradually taking over the conventional use of firewood and charcoal as it is more economical, made from waste products of processed biomaterials and it is environmentally friendly as most briquettes produced emits less poisonous gases e.g. carbon monoxide compared to firewood. Briquettes can be made from any of five categories of biomass: industrial waste or co-products, food waste, agricultural residues, energy crops and virgin lumber [24].

2.0 Methodology

The designed and constructed biomass briquette stove burner is a circular section and consists of chimney, smoke ring, air inlet, combustion chamber, fuel loading section, and ash tray. The combustion chamber has a dimension of diameter 160mm, height 350mm and thickness of 10mm. The chimney has a dimension of diameter of 10mm and height of 80mm. The chimney is attached to the smoke ring, and the smoke ring is connected to the combustion chamber. The fuel loading door, air inlet, and ash tray are all attached to the combustion chamber. The briquette stove was constructed using locally available and standardized materials. Materials selected and used for this research work includes; mild steel, clay, and fiberglass. The hearth of the combustion chamber is made of clay, the outside of which is lined with fiberglass and encased in a mild steel casing. The outlet is at the base of the combustion chamber. The base of the biomass briquette stove consists of a door for loading fuel (biomass briquette) into the combustion chamber, and four openings which serve as combustion air inlets to the chamber. A drawer is integrated at the base to expedite the removal of ash which would have collected at the tray. The top of the stove consists of the pot seat, refractory rings of dissimilar diameters to house different sizes of pot, and a chimney. The pot seat is designed such that the pot sinks to a depth below the top- most level of the stove. The refractory ring selected for use has the same internal diameter that is equal to the external diameter of the cooking pot. By this, there is little or no clearance between the pot and the ring. The chimney is made of mild steel and integrated at the margin of the top of the stove to remove smoke and other by-products of combustion out of the cooking environment.

2.1 Biomass Briquette Carrier

The biomass briquette carrier was constructed from mild steel sheet, it is cylindrical in shape and perforated all round for the purpose of passage of air for proper combustion. It has diameter 20cm and height 8cm. The circumference and volume of the biomass briquette carrier was calculated using equation (1), and equation (2).

$$\mathrm{C} = \pi \mathrm{D} \tag{1}$$

$$\mathrm{C} = \frac{22}{7} \times 0.02 = 0.0629\mathrm{m}$$

$$V = \pi \mathrm{D}^2 \frac{\mathrm{h}}{4} \tag{2}$$

$$V = \frac{22}{7} \times 0.02^2 \times \frac{0.08}{4} = 2.514^{-5} m^3$$

2.2Insulating Material

The insulating material used was fiber glass, and it was used to insulate the wall of the combustion chamber. The fiber glass was arranged using a binder into a texture similar to wool. The procedure traps many small pockets of air between the glass. The trapped air pockets result in high thermal insulation properties. Due to its thermal and acoustic properties, the fiber glass is one of the most widely used forms of insulation. It has maximum service temperature of about 250^{o}C [7, 20, 26].

2.3Thermal Efficiency

The thermal efficiency of the biomass briquette stove burner depends largely on how well the quantity of heat generated is conveyed from the point of combustion to the pot. The designed was such that the fuel bed to pot distance was close as possible to minimize heat losses and maximize heat transfer. If the distance between the fuel bed and pot is too far, heat will be loss from the system, thus improper heating obtained [27]. The procedure and formula used in the calculations were based on the approach used by Adamu [27]. The burning rate, R, corrected for the moisture content of the fuel was calculated using equation (3).

$$R = \frac{100(\mathrm{W_i} - \mathrm{W_f})}{(100+\mathrm{M})\mathrm{t}} \quad (3)$$

Where,
Wi= initial weight of fuel at start of test (kg)
W_f= final weight of fuel at end of test (kg)
M = moisture content of fuel (%)
t = total time taking for burning fuel (s)
The Eindhoven formula was applied to determine the thermal efficiency of the biomass briquette stove burner. The Eindhoven formula for calculating stove efficiency as given by Nwakaire and Ugwuishiwu, [28] is given in equation (4).

$$\mathrm{N_f} = \frac{M_w \mathrm{C}(\mathrm{T_f} - T_i)}{\mathrm{M_f E_f}} \quad (4)$$

Where,
Nf= Biomass Briquette stove burner efficiency
Mw=Initial mass of water in the pot (kg)
M_f=Mass of water evaporated during the experiment (kg)
Cw=Specific heat capacity of water=4.186 (kJ kg–^{10}C)
Ti=Initial temperature of water (°C)
Tf=Final temperature of water (°C)
E_f=Calorific value of fuel =15641.4 (kJ kg–1) [22]
Figure 1 shows the isometric view of the constructed biomass briquette stove burner.

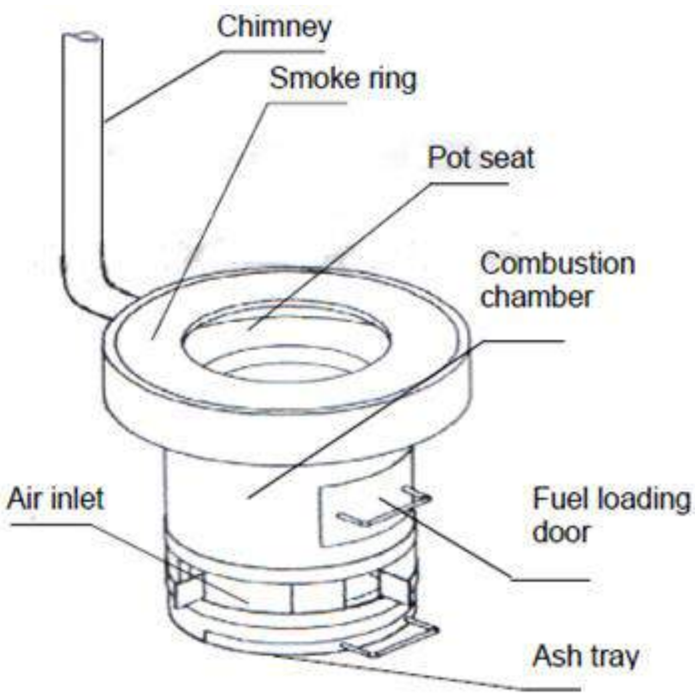

Figure 1. Isometric View of Biomass Briquette Stove Burner

3.0 Results and Discussion

The testing of the biomass briquette burner stove was carried out as followed:

3.1Burning Biomass Briquette Material in Open Air

In burning the briquette biomass material in open air, the tester starts with the biomass briquette stove burner at room temperature and uses a pre-weighed bundle of briquette to heat a measured quantity of water in a standard pot.

3.2Burning Biomass Briquette Material using Stove Burner

In the main testing, the burning of the biomass briquette material was done using a biomass briquette stove burner. The corncob briquette was loaded through the fuel loading door and ignited in the combustion chamber and fired using the air inlet port. This test was carried out using different time duration. The temperature readings were measured using maximum and minimum thermometer incorporated in the combustion chamber. The result obtained was tabulated in Table 1.

Table 1. Result of Burning in Open Air and Stove Burner

Burning in Open Air		Stove Burner	
Time (Minute)	Temperature (^{0}C)	Time (Minute)	Temperature (^{0}C)

0	25	0	25
2	35	2	48
5	43	5	59
8	57	8	74
11	67	11	83
14	80	14	94
17	110	17	100

*Quantity of Fuel used= 1.5kg; *Mass of water: 7.5kg; Briquette Material =Corncob

Figure 2 shows the briquette material produced from corncob, and it was used for the testing.

Figure 2. Briquette Material produced from Corncob.

Figure 3 shows the variation in temperature change in burning biomass briquette using stove burner and burning in open air without stove burner. The results obtained showed that water started boiling earlier when biomass mass briquette stove was used (14 minutes), unlike when the water was boiled in open air. It took the water 17 minutes to boil in open air. Also, improved temperature was obtained with briquette stove burner, and this is an indication of trapped hot air within the combustion chamber. However, the case was not the same when the biomass produced from corncob was burnt in open air. The temperature reading values obtained was smaller in comparison to the one obtained with biomass briquette stove. This confirmed the inability of the system to trap the hot air with the burning area unlike the stove burner that has a well-designed combustion chamber.

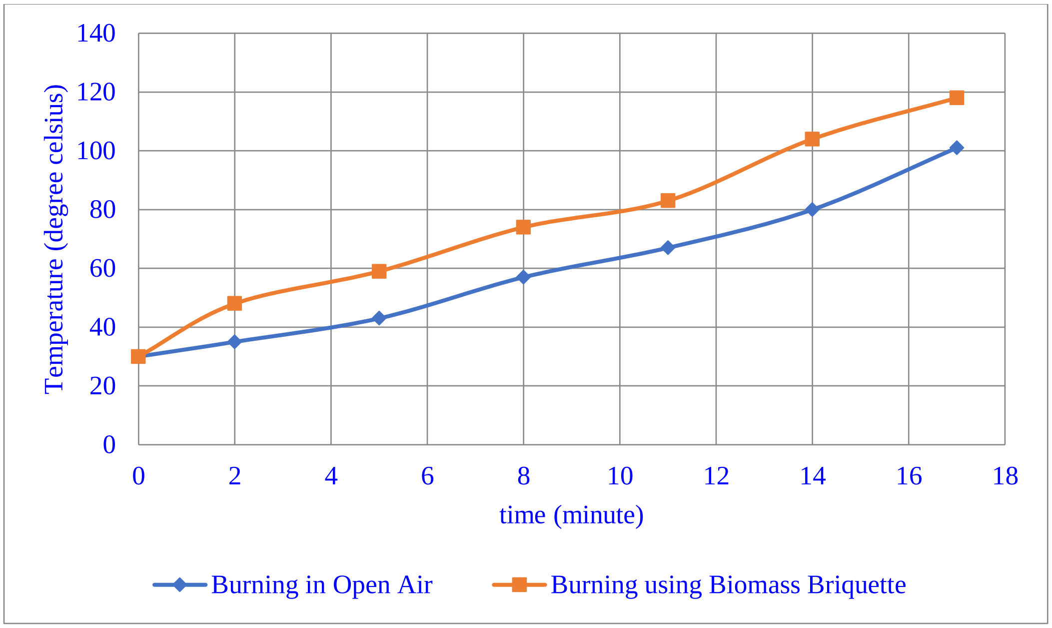

Figure 3. Variation in temperature change with and without Briquette Stove Burner

The thermal efficiency of the biomass briquette stove burner was evaluated using equation (4)

$$N_f = \frac{M_w C_w (T_f - T_i)}{M_f E_f} \times 100 = \frac{7.5 \times 4.186 \times 95}{0.25 \times 15641.4} \times 100 = 76.27\%$$

4.0 Conclusion

The biomass briquette stove was successfully designed and constructed using locally available materials; mild steel, fiberglass, and clay. These materials were used to construct the combustion chamber, briquette pot, stove body, stove base and chimney. Performance evaluation was carried out to determine the thermal efficiency of the stove, its heating ability. The outcome of the results obtained showed that the designed stove for this research work was within performance range. The biomass briquette produced from corncob has minimal smoke emission and the smoke emitted was properly channeled out through the chimney making the stove safe for domestic usage.

References

[1] Oyejide O. J., Okwu M.O. and Tartibu L.K. (2019). Adaptive design and development of a modular water hyacinth briquette stove, Energy Sources, Part A: Recovery, Utilization, and Environmental Effects. Tailor & Francis Grp, LLC, ISSN 1556-7036.

[2] Akinbami, J.F.K. (2001). Renewable Energy Resources and Technologies in Nigeria: Present Situation, Future Prospects and Policy Framework. Migration and Adaptation Strategies for Global Changes 6: pp. 155 – 181

[3] HDR (2015). Work for Human Development". Human Development Report 2015, Retrieved from http://hdr.undp.org/sites/default/files/2015_human_development_report.pdf, Accessed 12th June, 2016

[4] Orhorhoro, E.K, Orhorhoro,O.W. and Ebunilo, P.O. (2016). Analysis of the effect of carbon/nitrogen (C/N) ratio on the performance of biogas yields for non-uniform multiple feed stock availability and composition in Nigeria. International Journal of Innovative Science, Engineering & Technology, Vol. 3 Issue 5, 119-126

[5] Energy Information Administration (EIA) (2012). Biofuels issues and trends, USDA Washington, DC 20585. www.eia.gov/biofuels/issuestrends/pdf/bit/pdf.

[6] IEA Bioenergy, 2015. IEA Bioenergy Task 37 - Country reports summary 2015. https://www.google.com/search.

[7] Orhorhoro E.K., Oyejide J.O., and Abubakar S.A. (2018). Design and construction of an improved biogas stove. Arid Zone Journal of Engineering, Technology and Environment, 14(3):325-335.

[8] Orhorhoro E.K., and Lindsay E.E., Oyejide J.O. (2022). Analysis and Evaluation of a Three-Stage Anaerobic Digestion Plant for Management of Biodegradable Municipal Solid Waste. International Journal of Engineering Research in Africa, 60: 75-87

[9] Simonyan K.J. and Fasina O. (2013). Biomass resources and bioenergy potentials in Nigeria. Africa Journal of Agricultural research, Vol. 8(40), pp. 4975-4989

[10] Ebunilo P.O., Orhorhoro E.K., and Atumah V.E. (2020). Performance Evaluation of a Developed Dried Grass Shredding Machine for Composting. Advanced Engineering Forum, 40; 73-82

[11] Ebunilo P.O., Orhorhoro E.K., and Atumah V.E. (2021). Design analysis of a modular grass shredding machine. Journal of Engineering for Development; Vol. 13(2): 18-30

[12] Attah, A.W. (2012). Food Security in Nigeria: The role of Peasant Farmers in Nigeria. An International Multidisciplinary Journal, Ethiopia, 6(4), Serial No.27, pp.173-190

[13] Sambo, A.S. (2006). Renewable energy electricity in Nigeria, The way forward. Paper presented at the Renewable Electricity Policy Conference held at Shehu Musa Yarádua Centre, Abuja. pp. 11-12

[14] Orhorhoro E.K., Okonkwo, M.C., Oghoghorie O., and Onogbotsere, M.E. (2017). Design and Fabrication of an Improved Low Cost Biomass Briquetting Machine Suitable for use in Nigeria. International Journal of Engineering Technology and Sciences (IJETS), Vol.8 (1)

[15] CIA (Central Intelligence Agency), (2012). The World factbook, Nigeria, http://www.cia.gov/library/publications/the world -factbook/index.html, Accessed 24th, August 2015

[16] Ebunilo, P.O., Sadjere, E.G., Owunna, I.B., and Okonkwo, M.C. (2015). Analysis and Design of a Low-Cost Biomass Briquetting Machine. First University of Benin Annual Research Day (UBARD) Conference, pp.649-651

[17] Akinbami, J.K. (2011). Renewable Energy Resources and Technologies in Nigeria: Present Situation, Future Prospects and Policy Framework. Mitigation and Adaptation Strategies for Global Change 6: pp155-188. Kluwer Academic Publishers. Netherlands.

[18] World Bank, (2004): "Nigeria: Federal Government Economics Reform Governance Project" Volume 1.

[19] Chaney, I.J.O., Clifford, M.J., and Wilson, R. (2010). An experimental study of the combustion characteristics of low density biomass briquettes**,** Fuel processing technology, Progress in Energy and Combustion Science, 30,2, 219–230

[20] Food and Agriculture Organization (2008). The state of food and agriculture. Biofuels: Prospects, risks and opportunities. Food and Agriculture Organization of the United Nations Publication. Rome.128

[21] Yahaya, D.B., and Ibrahim, T.G. (2012). Development of rice husk briquettes for use as fuel;Research Journal in Engineering and Applied Sciences 1(2), pp.130-133

[22] Energy Commission of Nigeria (ECN) (2003). National Energy Policy.www.energy.gov.ng. Accessed on 12th August

[23] Nwakaire. J.N., and Ugwuishiwu B.O. (2015). Development of a Natural Cross Draft Gasifier Stove for Application in Rural Communities in Sub-Saharan Africa. Journal of Applied Sciences, 15: 1149-1157

[24] Biomass briquettes (2015). American Heritage Dictionary of the English Language, Fifth Edition. Copyright 2011 by Houghton Mifflin Harcourt Publishing Company. Published by Houghton Mifflin Harcourt Publishing Company. Retrieved, August 24, 2017, from http://www.thefreedictionary.com

[25] Natindco, (2015). Insulating Products. Retrieved on October 10, 2015 from http://natindco.in/insulating-products/glasswool

[26] Sule S., Oyejide O.J, Akusu O.M. (2019): **'Design, Construction, and Simulation of a Solar Fish Dryer'**. International Journal of Trend in Scientific Research and Development (ijtsrd), 3(2), 239-244. DOI: https://doi.org/10.31142/ijtsrd20299

[27] Adamu, S. (2012). Design, Construction and Performance Evaluation of Dual Source Cooking stove. Final Year Project, Department of Agricultural and Bioresources Engineering, Federal University of Technology, Minna, 2012

[28] Nwakaire, J.N., and Ugwuishiwu, B.O. (2015). Development of a Natural Cross Draft Gasifier Stove for Application in Rural Communities in Sub-Saharan Africa. Journal of Applied Sciences, 15, pp.1149-1157

NIPES-NCEE Conference Proceedings
The 2nd International Conference 15th-17th Feb. 2023
673-682
www.nipesjournals.org.ng

DEVELOPMENT OF A COMPRESSION MOLDING MACHINE FOR RECYCLING PLASTIC WASTES

[1]Abubakar S.A., [2]Abdullahi A. and [3]Zakariya M.A.

[1]Department of Mechanical Maintenance, Directorate of Services, Petroleum Training Institute, Effurun, Nigeria.

[2]Department of Electrical & Electronics Engineering, Petroleum Training Institute, Effurun, Nigeria.

[3]Department of Petroleum and Natural Gas Processing, Petroleum Training Institute, Effurun, Nigeria.

E-mail: *[1]abubakar_sa@pti.edu.ng, [2]abdullahi_a@pti.edu.ng, [3]zakariya_a@pti.edu.ng

corresponding author email*

Abstract
A compression molding machine capable of recycling plastic wastes was developed from locally available raw materials. The machine consists mainly of the following units; threaded screw, hopper, heater, heating chamber, forming chamber, steel frame, and control switch. The plastic wastes were loaded through the hopper and heated within an experimental temperature of 220^0C and under a pressure of 4 MN/m^2. The compression molding machine was tested and evaluated for optimum performance. The force due to pressure was calculated as 142.14KN and the total force obtained as 142.58KN. Also, the threaded screw speed was calculated as 6mm/sec and the volume low rate was obtained as $1.178 \times 10^{-5} m^3/sec$. The compression mold was able to successfully compress the molten plastic wastes materials. The outcome of the mould formed showed that the machine can be used to recycled plastic wastes in a small scale.

Keywords: *Development, Plastic Wastes, Compression Mould Machine, Recycling, Temperature*

1.0 Introduction
Plastic wastes constitute a menace to our environment and biodiversity thus there is high need to build equipment for recycling as a way to minimize their dangerous effects. Plastic wastes are part of the general municipal solid wastes which are unwanted material collected from households and commercial organizations. The general municipal waste consists of a mix of combustible and non-combustible materials, such as paper, plastics, food waste, glass, defunct household appliances and other non-hazardous materials. Advances in technology, lifestyle changes and may other factors affecting human living has resulted in the use of polymer materials such as plastics for the production of goods such as packaging materials, water and mineral containers, fluid sachets, sanitary wares, clothes, electronics, home wares etc. however; these materials after use and time eventually degrade and are disposed with no proper treatment or recycling and they constitute environmental mess and hazards [1-5]. In order to reduce or eradicate emissions and other problems arising from the poor use and disposal of plastic materials many countries have adopted recycling processes that can be used to convert these wastes materials into other semi-finished or finished products. Recycling is an aspect of environmental engineering that deals with the development of technically reasonable solutions to environmental problems by designing, fabricating and maintaining equipment (machines) to recycle wastes produced by municipalities and private industries [6-7]. A plastic recycling machine/ equipment is that which performs the

function of melting (such as compression moulding machine), crushing, grinding etc., of plastic materials (thermoplastics and thermosets) into granules for the production of new products.
Compression moulding is a well-known technique to make variety of composite products. It is a closed moulding process with high pressure application. In compression moulds, base plate is stationary while upper plate is movable. Reinforcement and matrix are placed in the metallic mould and the whole assembly is kept in between the compression moulder. Heat and pressure is applied as per the requirement of composite for a definite period of time. The material placed in between the moulding plates flows due to application of pressure and heat and acquires the shape of the mould cavity with high dimensional accuracy which depends upon mould design [8-9]. The versatile nature of this technology has made several researches in the past to adopt the techniques. For instance, Nor, [10] carried out a mechanical system design of compression moulding**.** The study emphasized the development of hydraulic system for compression moulding machine in order to make it fastest in production of thermoplastics products. Orhorhoro *et al.* [11] carried out the design and fabrication of compression moulding machine for plastic waste recycling in Nigeria. The machine consists mainly of threaded screw, hopper, heater, heating chamber, forming chamber, steel frame, and control switch. The raw materials (waste plastics) were loaded through the hopper and heated within a temperature range of 180^0C-220^0C and under a pressure of 3.77 MN/m^2. Jagushte *et al* [12] designed and fabricated a pneumatic compression moulding machine for fiber reinforced polymer (FRP) composites. In their design, temperature of specimen dies can be controlled automatically by using sensors and by using FRL (filter, regulator and lubricator) unit, the pressure can be controlled. The low density, high strength and high stiffness to weight ratio, fiber reinforced composite materials are manufactured by the machine are low cost. However, the machine was limited to samples only in the form of dumbbell shapes. In this present work, compression moulds machine is designed and this is meant to tackle the problem of producing an effective compression moulding machine from local materials in order to make them more readily available for use in recycling as well as to increase the number of articles to be made per time.

2.0 Methodology

The concept for the compression mould making machine was first developed from a series of concepts. The selected concept is to design the machine with an integration of two concepts which entails a transfer of the plasticized stock from a heat chamber into a square mould cavity, this cavity contains a certain amount of coolant to cause faster rate of heat transfer from the control volume of the cavity to the surroundings by convection [11, 12, 13]. The plastic wastes to be recycled attain a molten state at a particular temperature before being poured into the cavity and then hydraulically compressed by a piston head. The molten material then cures at a lower temperature and shorter time instead of cooling slowly due to ordinary natural flow of air.

2.1 Conceptual Design

Before the conceptual design for the compression moulding machine was drawn, proper consideration was made to specify and identify some problems which could hindered effective performance of the system. Thus, effort was put to identify these factors and limitations as put together; energy utilization, functionality, reliability, heat resistance, durability, simplicity, portability and space, cost, and safety. The design concept as shown in Figure 1 had a frame supporting a hydraulic press, spring, upper mould, lower mould, water cooling reservoir, heating crucible and a chimney. The operations required to produce the squared shaped plastic products by compression moulding include mould preparation, heating the material up to melting temperature, pressurizing the material in the mould, cooling and ejecting the product from the mould. It is important to note that the heating was done in a crucible outside the mould. The plasticized stock was placed in the mould and compressed hydraulically, where it flows to take the shape of the mould.

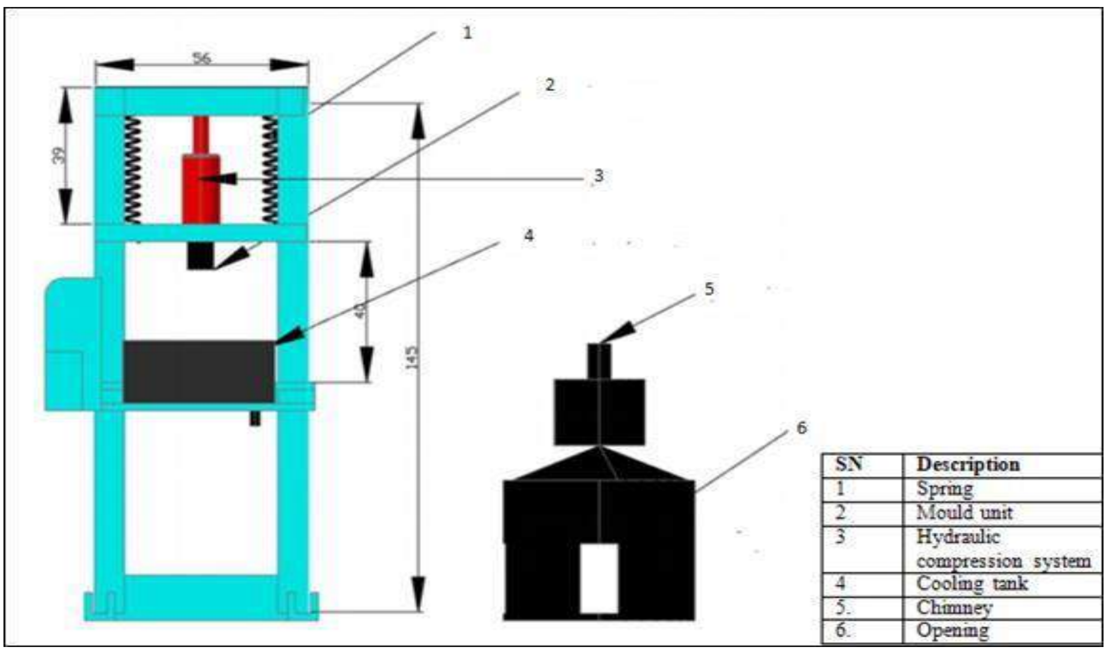

Figure 1: Design Concept

2.2 Configuration of the Compression Moulding Machine

The compression moulding machine comprises of two vertical columns of C beam cross-sections (designated C100 × 6 according to ASME) joined together by two horizontal beams of C beam cross sections at both ends. Fixed to these vertical columns are a C beam cross section and a I beam cross section beam at offset distances of 450mm and 100mm from the upper beam labelled X and Y respectively. The beam labelled X supports the spring units, upper mould and the hydraulic press, while the Y beam supports the cooling unit and lower mould, which was designed according to its individual load configuration to avoid fail by yielding, while determining the maximum deflections and the maximum bending stress. The maximum shear stress according to the Von-Mises failure criteria is also determined. The vertical beams are subjected to the same load configuration and thus designed to prevent instability by buckling. The stress and strain analysis of the mould is also done with respect to mechanical properties. The cooling unit is designed as an effective heat exchanger for the required curing temperature. The components of the hydraulic press are designed to avoid failure by the bending stress due to the applied load. Mild steel was selected as a material based on its properties such as high bending and tensile strength, its compatibility with operations like machining and cost. The compression mould making machine is shown in Figure 2 while more a representation in the orthographic views is shown in Figure 3.

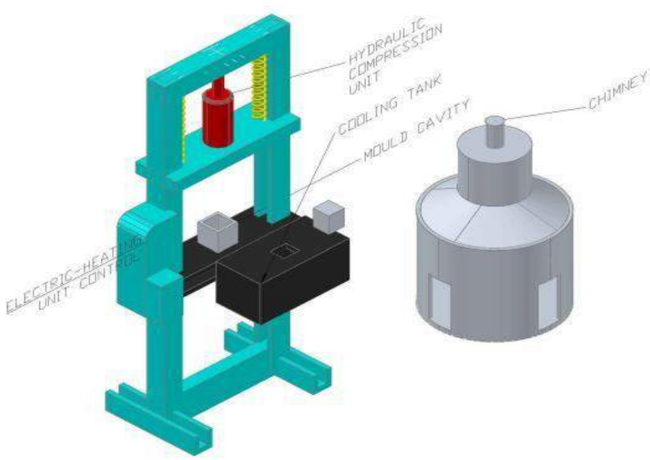

Figure 2: An Isometric View of the Compression Mould Machine

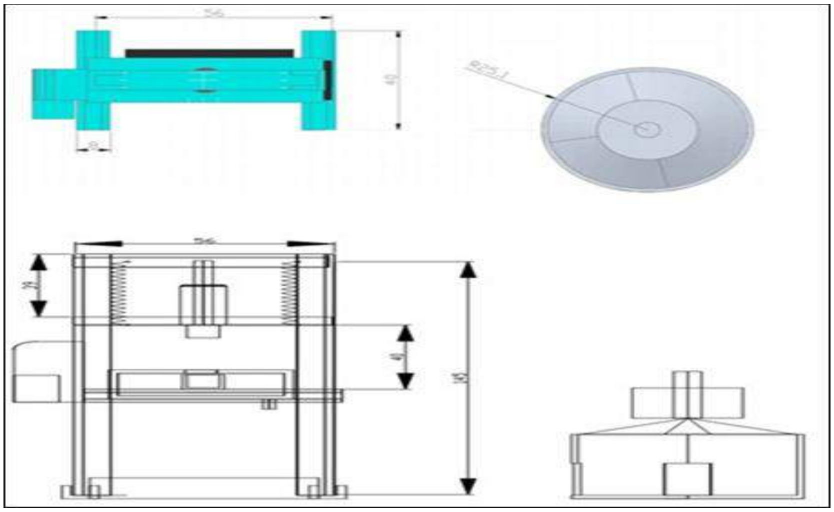

Figure 3: An Orthographic View of the Compression Mould Machine

2.3 Design Specification

The following design specifications were drawn:

i. A temperature of 220^0C machine
ii. A mould size of 400mm by 400mm by 150mm square electrical wall plate
iii. An airtight in both heating chamber and mould forming chamber
iv. A pressure of 15.8MPa
v. Forming strength of machine equals to 32N and is greater than common polymers force (10~34 Mpa of common polymers)
vi. A compression mould that can process 5kg of waste plastic per operation

2.4 Design of Mould

The mould is square in shape as showed in Figure 4.

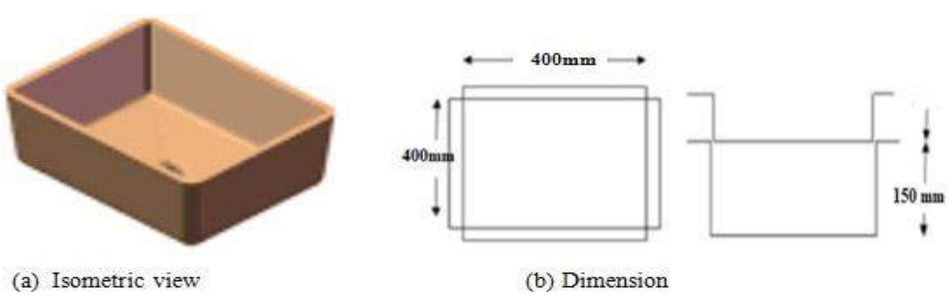

Figure 4: View of the Mould

The total surface area and volume of the mould chamber is given as the total surface area and volume of a rectangular geometry as depicted in Equation (1) and Equation (2).

$A_m = 2BL + 2LH + 2HB$ (1)

$V_m = L X B X H$ (2)

where,

A_m = Total surface area of the mould

V_m= Volume of the mould

$A_m = 2 X 0.4 X 0.4 + 2 X 0.4 X 0.15 + 2 X 0.15 X 0.4 = 0.56m^2$

$V_m = 0.4 X 0.4 X 0.15 = 0.024m^3$

2.5 Stress and Strain Analysis of the Mould

As shown in Figure 5 is the possible stress distributions in the mould.

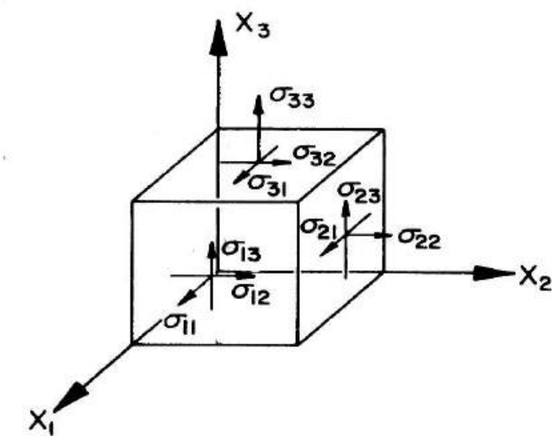

Figure 5: Stress Distribution in Mould

Longitudinal Strain (Extension) along the x-axis

$\varepsilon_x = \frac{\sigma x}{E}$ (3)

Transverse Strains (Contraction) along the y and z –axes

This transverse strains (contraction) along the y and z –axes which are related to the Poisson's ratio:

$\varepsilon_y = \varepsilon_z = -\nu\varepsilon_x = \frac{-\nu\varepsilon_x}{E}$ (4)

Applying the principle of superposition (x-axis)

$\varepsilon_x = \frac{1}{E}[\sigma_x - v(\sigma_y + \sigma_z)$ (5)

The strain along the y and z axis can therefore be written as:

$E_y = \frac{1}{E}[\sigma_y - v(\sigma_x + \sigma_z)$ (6)

$E_z = \frac{1}{E}[\sigma_z - v(\sigma_x + \sigma_y)$ (7)

The shearing stresses acting on the unit cube produce shearing strains as follows;

$\tau_{xy} = G\gamma_{xy}$ (8)

$\tau_{yz} = G\gamma_{yz}$

(9)

$\tau_{xz} = G\gamma_{xz}$ (10)

For Hooke's law to apply in 2- Dimension, Equation (5) - (6) reduces to Equation (11)

$\varepsilon_y = \varepsilon_z = -E\,\varepsilon_x$ (11)

Also,

$K = \frac{-E}{3(1-2\nu)}$ (12)

2.6 Volume Flow Rate

The volume flow rate is given by Equation (13).

Volume flow rate Q = Area x Velocity

(13)

Assumption;

Flow is Newtonian and Isothermal

That is;

Q = AV

2.7 Distance between the Torpedo and Barrel

$x = \pi\left(R^2 - r^2\right)$ (13)

2.8 Force due to Pressure

$F = \pi r^2 p$ (14)

Where;

F = Force due to pressure

r=internal radius

2.9 Surface Area of Torpedo

$SA = \pi DL$ (15)

Where;

SA= surface area of Torpedo

2.10 Viscous Drag Force

$VDF = \pi DL\,\tau$

(16)

Where;

VDF = Viscous drag force
D = External diameter of barrel
τ =shear stress

2.11 Total Force

$$TF = F + VDL \quad (17)$$

Where;
TF = Total force
F = Force due to pressure
VDL = Viscous drag force

3.0 Results and Discussion

In this study, compression moulding machine for recycling of plastic wastes was successfully developed. The result of the estimated threaded screw speed was determined as 6mm/sec and this result agreed with the research work of [11]. The value was estimated based on the average values of five (5) different threaded screw speeds (i.e., 6.5 mm/sec, 5.5 mm/sec, 6 mm/sec, 5.8 mm/sec, and 6.02 mm/sec). This speed was sufficient enough to compress the formed plastic mould at 220^{o}C as suggested by [11]. The volume low rate was obtained as 1.178 x 10^{-5}m^3/sec. Also, the force due to pressure was calculated as 142.14KN and the total force obtained as 142.58KN. These results agreed with the research work of [11]. The various weights of the plastic feed stocks and the formed product were weighed respectively. The time and temperature for melting of the plastic and the solidification of the formed products was also recorded. Figure 1 shows the bar-chart of the comparative analysis of solidification time of cooling in water and air. Cooling with water produced less solidification time and this was due to water high heat capacity (an ability to absorb).

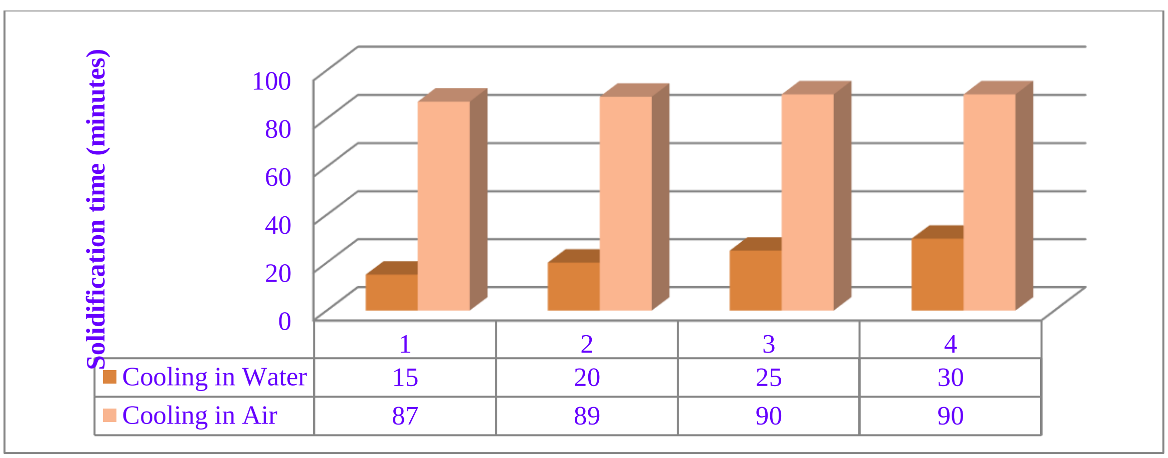

Figure 6: Bar-Chart Showing Comparative Analysis of Solidification Time

4.0 Conclusion

The compression moulding process is one of the non-conventional processes in plastic engineering sector; the process is most suitable for easy flow material. In this study, a compression moulding machine for the process and recycling of plastic waste materials was successfully developed. The machine was evaluated for performance and test results showed that the objectives of the project work were achieved. Besides, the test evaluation showed a good improvement in cooling with water instead of air. Therefore, with the development and successfully testing of the prototype which proved that the production of quality plastic products in commercial quantities is possible, the use of compression moulding machine for recycling of plastic wastes in Nigeria is a welcome development.

References

[1] United Nations Environment Programme (UNEP) (2009). Converting Waste Plastic into a resource. United Nations Environmental Programme Division of Technology, Industry and Economics International Environmental Technology Centre. 10, 12-73.

[2] Apurva, J.C. (2013). Use of Plastic Waste in Flexible Pavements. International Journal of Application or innovation in Engineering & Management (IJAIEM). PravatibaiGenbaMoze College of Engineering, Pune.Vol. 2 (4), 540.

[3] Oyejide O.J., Ogie N.A. and George B.J. (2021). Artificial Neural Network Model for Prediction of Biogas Yield from Anaerobic Co-Digestion of Decomposable Wastes. 2nd International Conference on Electrical Power Engineering / Training Workshop (ICEPENG 2021), May 18-22, 2021.

[4] Ionescu, G., Rada, E.C., Ragazzi, M., Marculescu, C., Badea, A., Apostol, T. (2013). Integrated municipal solid waste model using advanced pretreatment and waste to energy processes. Energ. Convers. Manag., 76, 1083–1092.

[5] Benjamin, T.A., Emmanuel, E.O., Gideon, A.D. (2014). Characterisation of Municipal Solid Waste in the Federal Capital, Abuja, Nigeria. Global Journal of Science Frontier Research: Environment and Earth Science, 14, (2), 1-7

[6] Wright, T.S.A. (2002). Definitions and frameworks for environmental sustainability In higher education.International journal of sustainability in higher education, 2002. 3(3), 203-220.

[7] Brandup (1996). Recycling and Recovery of plastic, 1996

[8] Kamal M. R. (2009). Compression moulding technology and fundamentals. 1st ed. Munchen, Germany: Hanser Publications.

[9] Sungnam H. (2017). Influence of Curing Conditions on the Strength Properties of Polysulfide Polymer Concrete, College of Engineering, Sungkyunkwan University, Natural Sciences Campus, 2066 Seobu-Ro, Jangan-Gu,Suwon-Si 16419, Gyeonggi-Do, Korea.

[10] Nor, A. (2016). Mechanical System Design of Compression Moulding. Mechanical System Design, 1-8

[11] Orhorhoro, E.K., Atumah, E.V., Ayodele, S.A. (2016). Design and Fabrication of Compression Molding Machine for Plastic Waste Recycling in Nigeria. International Academic Journal of Innovative Research 3(1), 1-20

[12] Jagushte G. S., Nilesh K.,Pravin J. ,Abhishekh G., Rameshwar C.,(2017). Fabrication of Pneumatic Compression Moulding Machine for FRP Composites. 4(7)

[13] Atadious D. and Oyejide O.J, (2018). Design and Construction of a Plastic Shredder Machine for Recycling and Management of Plastic Wastes. International Journal of Emerging Engineering Reaserch 5(9): 1379-1385

NIPES-NCEE Conference Proceedings
The 2nd International Conference 15th-17th Feb. 2023
683-688
www.nipesjournals.org.ng

CORROSION INHIBITION OF LOW CARBON STEEL USING LEAVES EXTRACTS OF PHYLLANTHUS AMARUS IN ACIDIC MEDIUM

[1]Uti L.O., [2]Idim A.I. and [3]Nji C.A.

[1]Department of Petroleum Engineering and Geosciences, Petroleum Training Institute, Effurun, Nigeria.
[2]Department of Electrical & Electronics Engineering, Petroleum Training Institute, Effurun, Nigeria.
[3]Department of Petroleum Engineering, Federal University of Petroleum Resources, Effurun, Nigeria.

E-mail: [1]uti_lo@pti.edu.ng, [2]idim_ai@pti.edu.ng, * [3]ayafornjichristianlee@rocketmail.com

corresponding author email*

Abstract
Organic corrosion inhibitors are widely used in industry because of their effectiveness at wide range of temperatures, compatibility with protected materials, good solubility and relatively low toxicity. In this study, the inhibitive action of leaves extracts of Phyllanthus amarus on low carbon steel corrosion in acidic medium was investigated using weight loss. The corrosion inhibition experiment was performed by setting up reactors containing low carbon steel coupon with variable concentrations of plant extract and 500ml of 2.5M tetraoxosulphate (VI) acid solution. The study revealed that the leaves extracts of Phyllanthus amarus was an efficient inhibitor and was most effective as the concentration increased from 0, 1.0, 2.0, 3.0 % v/v respectively.

Keywords: *Low Carbon Steel, Corrosion, Inhibitor, Phyllanthus Amarus, Weight Loss*

1.0 Introduction
Palm A number of organic and inorganic compounds have been studied as inhibitors to prevent metals from corrosive attacks. Several heterocyclic compounds have been reported by researchers [1-5] in the past as corrosion inhibitors and the screening of synthetic heterocyclic compounds is still being continued. Also, quite a lot of other inorganic inhibitors that includes chromate, zinc, polyphosphate, and nitrite were used as corrosion inhibitors [6]. Besides, molybdate, phosphates, phosphonocarboxylic acids and polymers were used as inhibitors, along with metal ions especially zinc ion (Zn^{2+}). Though many synthetic compounds showed good anticorrosive activity, most of them are highly toxic to both human beings and environment. These toxic effects and ecological problems are associated with the discharge of such materials have resulted in the development of other efficient and environmentally acceptable inhibitors. Hence the recent trend is the search for environmentally friendly inhibitors. Furthermore, due to the hazardous effects of most synthetic inorganic inhibitors and restrictive environmental regulations, researchers have focused on the need for the design of cheap, non-toxic and environmentally benign natural products as corrosion inhibitors [7-10]. Natural organic compounds which are either synthesized or extracted from aromatic herbs, spices and medicinal plants have played major roles in this regard [11-14]. This area of research is of much importance because in addition to being environmentally friendly and ecologically acceptable, that can be extracted by simple procedures with low cost [4, 8, 15]. The plant extracts are rich sources of naturally synthesized chemical compounds that can be produced

by simple processes at low cost and are biodegradable in nature. The application of naturally extracted compounds from leaves or seeds as corrosion inhibitors have been widely reported by several authors [4, 8, 15-18].

Corrosion is an electrochemical process by which metallic surfaces react with their environment causing the metal to lose its material properties due to surface deterioration [12, 19-20]. Corrosion process is a natural process that results in considerable waste of industrial investment. This phenomenon is noticed in various types of surfaces, thus, causing a major economic loss in the industrial sector. Corrosion control involves different aspects such as environmental, economic and technical. The use of inhibitors is one of the most practical methods for protecting metal against corrosion, especially in acidic media [4, 8, 21-23]**.** As acidic media, hydrochloric acid (HCl) and sulphuric acid (H_2SO4) are often used as industrial acid cleaners and pickling. Acid solutions are used in the most important industrial applications in etching and acid cleaning [8]. Because of the general aggressiveness of acid solutions, the practice of inhibition is commonly used to reduce the corrosive attack on metallic materials.

2.0 Methodology

2.1 Preparation of the leave's extracts of phyllanthus amarus

The collected leaves of phyllanthus amarus were dried in a laboratory oven at a minimal temperature to avoid loss of main organic components of the plant. A Retsch Planetary Ball Mill PM 400 was used for the grinding of the phyllanthus amarus leaves. The grinding jars are arranged eccentrically on the sun wheel of the planetary ball mill. The direction of movement of the sun wheel is opposite to that of the grinding jars in the ratio 1:-2 (or 1:-2.5 or 1:-3) as recommended by [8]. The difference in speeds between the balls and grinding jars produces an interaction between frictional and impact forces, which releases high dynamic energies. The interplay between these forces produces the high and very effective degree of size reduction of the planetary ball mill. After the pulverizing, 260 g of the ground phyllanthus amarus leaves was taken in 1000 ml round bottom flask and enough quantity of ethanol was added as a solvent for extraction. The round bottom flask was covered with a stopper and left for two days [8]. The extract obtained was later heated on a water bath at a temperature of 60^oC until most of the ethanol evaporated. Tetraoxosulphate (VI) acid of 0.25M concentration was poured into beakers at a constant volume of 200ml. The phyllanthus amarus leave extract was added to the beakers. The inhibition test solutions were prepared to obtain 1.0, 2.0, 3.0% v/v respectively. The experiment was carried out for the duration of fifteen (15) days. At interval of three (3) day, the samples were washed in distilled water, dried and weighed. The weight loss and rate of corrosion were evaluated.

2.2 Weight Loss and Corrosion Rate

The prepared low carbon steel samples were used for the experiment to determine the weight loss and corrosion rate of the low carbon steel in acidic corrosion environment, which was performed at room temperature. The various steel samples were weighed with an analytical weighing balance and recorded as (W_I) before being immersed into the corrosion environment. After three days interval, each of the steel samples were retrieved, properly cleaned and allowed to dry for about five minutes. They were then placed on a weighing balance to record their final weights (W_F). This procedure was repeated for the remaining sample for a period of 15 days. Equation (1) was used to calculate the weight loss.

$$W_L = W_i - W_f \quad (1)$$

where,

W_L = Weight loss

W_I = Initial weight

W_F = Final weight

Equation (2) was used to calculate the corrosion rate of low carbon steel.

$$C_R = \frac{87.6 W_L}{DAT} \quad (2)$$

Where;

C_R = Corrosion Rate (mm/y)

W = Weight loss (mg)

D = Density of Low Carbon Steel = 7.85g/cm^3

A = Area of medium carbon steel samples used (cm^2)

T = Exposure time to corrosion environment (days)

2.3 Low Carbon Steel Sample Preparation

The low carbon steel samples 30 mm diameter were used as coupons for the corrosion rate and weight loss. Initially, the coupons were mechanically polished with abrasive papers and was degreased in ethanol, dried, weighed and stored in the desiccator.

3.0 Results and Discussion

The samples were exposed to acidic medium for a duration of fifteen (15) days. Corrosion activities and its rate on the test samples were evaluated by visual observation via corrosion rate measurement using weight loss. Effect of corrosion on the low carbon steel immersed in the acidic medium were observed to occurred after a day of exposure. Weight loss was monitored at the interval of three (3) days. The results obtained were used to determine the corrosion rate of the low carbon steel coupon samples used in this study. Visual inspection indicated that corrosion processes started with color transformation to yellow deposits in the first two days and this was a confirmation of presence of ions concentration in the sample of the corrosion environment [20]. With the prolong exposure of the samples, the yellow deposits turned dark brown coloration that surrounded the surface of the samples of low carbon steel [19]. Figure 1 and 2 show the plot of weight loss and corrosion rate of the low carbon steel exposed in acidic corrosion environment. The results showed that the weight loss decreased with the concentration of phyllanthus amarus leaves extract that served as an inhibitor in this study. It was observed that the control sample without any trace of organic phyllanthus amarus leaves extract inhibitor (0.0 % v/v) has the highest weight loss recorded while the samples immersed in the 3.0 % v/v phyllanthus amarus leaves extract inhibitor has the lowest weight loss recorded. More so, it was observed that weight loss increases from day 1 and become peak on day 6 before the gradual decrease to day 15.

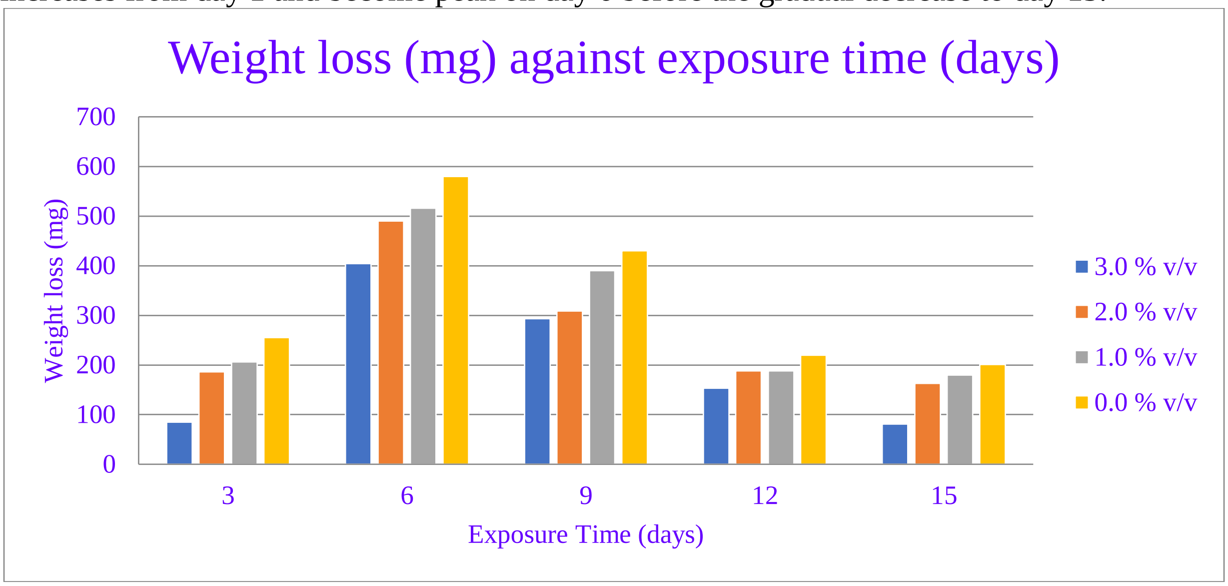

Figure 1. Weight Loss against Exposure Time

From figure 2, the corrosion rate of all the samples increases steadily for the first six (6) days with the peak on the 6th day. This was followed by continuous decrease in the corrosion rate of all the samples. However, the corrosion rate of the samples become partially uniform after the twelve (12) days and the pattern remain the same for the remaining fifteen (15) days. The decreased in the corrosion rate of all the samples between the period of 6th day and 15th day can be attributed to the aggressiveness of the chemical reactivity, transport properties of the corrosion medium, pH of the corrosion medium which is within neutral, concentration of the corrosion species in the used sea water, and most importantly the metallurgy of the alloy sample and temperature of the tetraoxosulphate (VI) acid which served as the corrosion medium as reported by [8, 21-23].

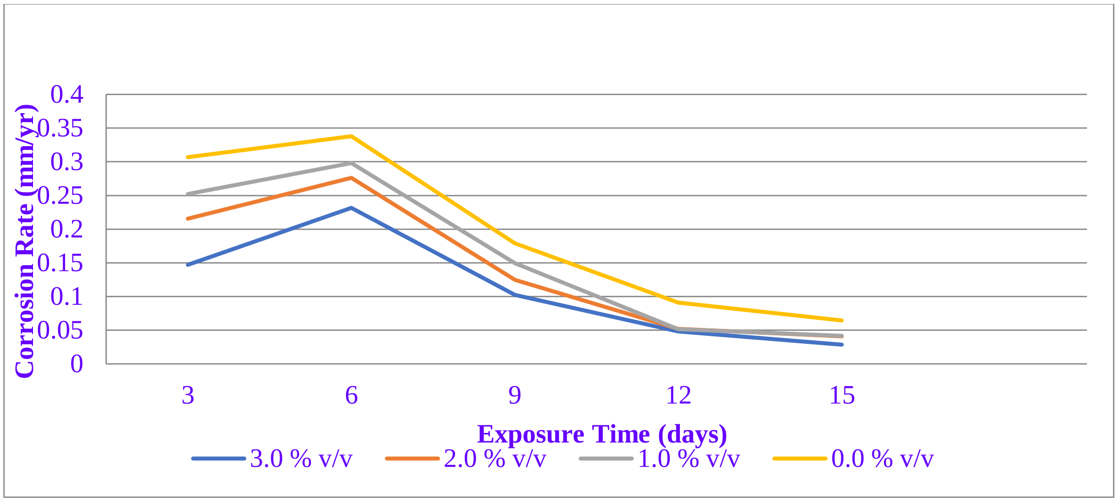

Figure 2. Corrosion Rate against Exposure Time

4.0 Conclusion

In this study, the corrosion inhibition of low carbon steel using leaves extracts of phyllanthus amarus in acidic medium was investigated. From the findings from the study, it can be concluded that low carbon steel samples experienced fast weight loss and corrosion rate at beginning of exposure to corrosion environment. With continuous exposure, there tend to be a constant decreased in weight loss and corrosion rate. Furthermore, the concentration of the extracts of phyllanthus amarus leaves play a crucial role in the corrosion environment. Increase in the concentration of the organic inhibitor led to a decreased in both the weight loss and corrosion rate of the low carbon steel. Therefore, extracts of phyllanthus amarus leaves is a good organic inhibitor.

References

[1] Ayeni .F.A. Aigbodion, V.S. & Yaro. S.A. (2007). Non-Toxic plant extract as corrosion inhibitor for Chill cast Al-Zn-mg alloy in caustic Soda solution, Eurasion Chem Tech Journal, 9: 1-31

[2] Bao J. Y., Cai M., Sun G., Wang and Corke. H (2005). Anthocyanins, Flavonoid and Free Radical Scavenging Activity of thines Baybery (Myrial rubia) extracts and their colour properties and stability. Journal of Agric Food Chem. 53: 2327-2332.

[3] Brunner, J.H., (1994). Direct spectrophometry dertermination of saponin. Animal Chemistry 34:1314- 1326

[4] Onwuamaeze, I.P., Oyejide O.J., and Salisu S. (2018). The Effect of Annealing on the Microstructure and Mechanical Properties of Welded Carbon Steel. Nigeria Research Journal of Engineering and Environmental Sciences. 3(1), 96-102

[5] Bouklah, M., and Hammouti, B. (2006); Thermodynamic characterization of steel corrosion or the corrosion inhibition of steel in sulphuric acid solutions by Artemisia. Port. Electrochim. Acta, 24: 457 – 468.

[6] Craig B.D., Lane R.A., Rose D.H (2006), "Corrosion Prevention and Control: A Program Management Guide for Selecting Materials". 2nd Ed., Advanced Materials, Manufacturing, and Testing Information Analysis Center: 61-109, 221-244.

[7] Ambrish Singh, Eno E. Ebenso, and M. A. Quraishi(2012). Corrosion Inhibition of Carbon Steel in HCl Solution by Some Plant Extracts, 1: 1235-12401

[8] Atadious D, Bankole W. J. and Oyejide O. J (2018). Behavioral Corrosion Mechanism of Hot Worked Mild Carbon Steel Immersed in various Acidic Environments. International Journal of Advances in Scientific Research and Engineering (ijasre) 4(12): 31-39.

[9] Znini, M., Bouklah, L., Majidi, S., Kharchouf, A., Aouniti A., Bouyanzer B., Hammouti B. (2011). Chemical composition and inhibitory effect of Mentha spicata essential oil on the corrosion of steel in molar hydrochloric acid. Int. J. Electrochem. Sci., 691-704

[10] Chauhan L.R., Gunasekaran G. (2007). Corrosion inhibition of mild steel by plant extract in dilute HCl medium. Corros. Sci, 49, 1143–1161

[11] Solomon M.M., Umoren S.A., Udosoro I.I., Udoh A.P. (2010). Inhibitive and adsorption behaviour of carboxymethyl cellulose on mild steel corrosion in sulphuric acid solution. Corros. Sci, 52: 1317–1325

[12] Orhorhoro E.K., Erameh A.A., and Adingwupu A.C. (2018). Evaluation of the effect of tempering on the corrosion susceptibility of low carbon steel in sea water. Nigerian Research Journal of Engineering and Environmental Sciences, 3(1): 409-415

[13] M'hiri, N., Veys-Renaux D., Rocca E., Ioannou I., Boudhrioua, N.M., Ghoul M. (2016). Corrosion inhibition of carbon steel in acidic medium by orange peel extract and its main antioxidant compounds. Corros. Sci., 10: 55–62.

[14] Qiang Y., Zhang S., Guo L., Zheng, B. Xiang, S. Chen, S. (2017) Experimental and theoretical studies of four ally imidazolium-based ionic liquids as green inhibitors for copper corrosion in sulfuric acid. Corros. Sci., 119: 68–78

[15] Ei-Etre A.Y. (2007). Inhibition of acid corrosion of carbon steel using aqueous extract of olive leaves. J. Colloid Interface Sci., 314: 578–583.

[16] Orubite K.O., Oforka N.C. (2004). Inhibition of the corrosion of mild steel in hydrochloric acid solutions by the extracts of leaves of Nypa fruticans Wurmb. Mater. Lett, 58: 1768–1772

[17] Roslliza R., and Wan Nik W.B. (2010). Improvement of corrosion resistance of A6061 alloys by tapioca in seawater. Journal of current Applied Physics 10: 221-229

[18] Sanda B.S. (2011). Effect of Bitter Leaf Extracts on in-vitro corrosion behavior of some surgical implants in simulated body fluids. Department of metallurgical Engineering, Ahmadu Bello University Zaria.

[19] Okuma S.O., Orhorhoro E.K., and Tamuno R.I. (2020). Corrosion evaluation on mild steel in different selected media. International Journal of Engineering Applied Sciences and Technology, 5(3):33-38

[20] Oyejide J.O., Orhorhoro E.K., Ogie A.N., and Idi S. (2017). Investigation of the Effect of Annealing on the Corrosion Resistance of Medium Carbon Steel in Sea Water, Journal of Emerging Trends in Engineering and Applied Sciences (JETEAS), 8(5): .219-224

[21] Malik A.U., Ahmad S., Andijani I. (1999). Corrosion behavior of steels in Gulf seawater environment, Saline Water Conversion Corporation, 123: 205-213

[22] Lee J.S., Ray R.I., Lemieux E.J., Falster A.U., and Little B.J. (2004). An evaluation of carbon steel corrosion under stagnant seawater conditions, Biofouling, 20 (4/5): 237-247

[23] Pruthviraj R.D., Prakash C.H. (2013). Somasheklariah, Mild Steel Corrosion Inhibition by Plant Extract in 0.1 M Hydrochloric Acid Solution, Sch. J. Eng. Tech., 1(3):169-171

NIPES-NCEE Conference Proceedings
The 2nd International Conference 15th-17th Feb. 2023
689-710
www.nipesjournals.org.ng

SPATIAL-TEMPORAL ASSESSMENT OF GROUNDWATER QUALITY AROUND A MUNICIPAL OPEN WASTE DUMPSITE IN BENIN CITY SOUTH-SOUTH NIGERIA

Idehen, Osaretin Friday [1] and Emeribe Chukwudi Nnaemeka [2]

[1]Department of Geography and Regional Planning, Igbinedion University, Okada, Edo State, Nigeria.

[2]National Centre for Energy and Environment, University of Benin, Benin City, Nigeria

Corresponding Author: idehen.osaretin4@iuokada.edu, 08027112883

Abstract

The spatio- temporal analyses of the physico- chemical and microbiological properties of groundwater samples from four (4) boreholes was carried out to establish the groundwater quality around Ikhueniro Open Waste Dumpsite in Benin City, South- South Nigeria. The boreholes were purposively selected in a North, South, East and West direction to ensure spatial spread. Leachate and groundwater samples were taken in both dry (January, 2019) and wet (May, 2019) seasons. Standard equipment and laboratory procedures were used to determine the physical, chemical including heavy metals and microbiological parameters of the leachate and groundwater samples. The physico-chemical and microbiological characteristics of leachate samples from the dumpsite showed high pollution potentials as well as marked seasonal variation. Laboratory results revealed that the concentration of PH, TDS, Ca, Mg, No2, No3, Fe, Mn, and Cd of all the groundwater samples exceeded the allowable limits of World Health Organization (WHO) for drinking water. Besides, the concentration of COD in the groundwater samples from Sampling Point two (2) also surpassed WHO standard limit for drinking water. However, laboratory analyses showed that there was no trace of Total Heterotrophic bacteria Counts (THC) and Total Coliform Counts (TCC) in the groundwater samples around the dumpsite. With the exception of PH values, laboratory results of the physico- chemical properties of groundwater samples generally showed obvious seasonal variation in terms of higher concentration in the rainy season than in the dry season. Specifically, the concentration of Bicarbonate (HCO3) ranged from 45.3mg/l to 72.0mg/l in the dry season and 48.3mg/l to 85.4mg/l in the rainy season. The study therefore revealed that the groundwater around Ikhueniro Open Dumpsite was polluted and unfit for drinking. It was however recommended that there is an urgent need for periodic monitoring and assessment of groundwater quality around Ikhueniro Open Dumpsite and beyond. In Nigeria, this can be achieved by putting in place appropriate groundwater governance structure to ensure the sustainable management of groundwater resource

Key Words*: Ikhueniro waste dumpsite, Groundwater water quality, Leachate, groundwater quality parameters.*

Introduction

Water is essential to life, the environment and socio- economic development of society. Life and civilization depend on the availability of water. Water is a common denominator among the five fundamental human wants (water, food, health, education and peace). Water is used in households, industries and agriculture but also for energy, transport and recreation. The sustainable development of society is inherently tied to the availability of water [1,2,3].

The earth's overall water resources are put at about 1.36 thousand million cubic kilometers of water. The vast majority of this is contained in the oceans and seas (about 97.2 percent) but too salty for human consumption. It is estimated that about 2.8 percent is available as fresh water on the earth. Of the 2.8 percent fresh water, 2.2 percent is available as surface water. Of the available surface water (2.2 percent), 2.15 percent is freshwater locked up as polar ice or ice cap, 0.6 percent as groundwater, 0.01 percent in lakes and streams and the remaining 0.01 percent occurs in other forms [4,5].

However the most abundant and usable freshwaters are largely hidden beneath the ground. Subsurface water accounts for just under 99 percent of the total volume of freshwater presently circulating on the earth. Surface water (rivers, lakes or wetlands) amount to less than 1 percent of the total, the balance of 0.16 percent is in the form of atmospheric moisture [6]. By implication groundwater is therefore a veritable source of freshwater for the use of man

The water beneath the ground surface contained in the void or spaces in rock or bedrock fractures is termed groundwater. Groundwater is the water that lies in aquifers under the earth surface. Groundwater originates from precipitation which infiltrates through the soil profile and accumulates on the aquifer. The aquifer is a water bearing porous rock layer from which water can be tapped [7,8,9]. Above the aquifer is the water table where atmospheric pressure.is equivalent to groundwater pressure. Groundwater forms an important component of the water cycle and its quantity and quality depend are factors of rock type, precipitation, soil cover, topography and the state of the environment [10,11,12].

In Nigeria groundwater has become a valuable renewable resource. The failure of public water supply and poor quality of surface water sources have made a great number of people, institutions and industries to resort to groundwater exploitation [13]. Besides, low financial cost required for harnessing groundwater resources, its availability to where water is required and natural quality are impacting many advanced and less developed countries turning to subsurface sources of water for households and industrial uses [14].

On account of the rapidly growing population and urbanization in the last decades, there has been a rapid rise in water shortages in Nigeria [13]. In Benin City, Edo State, South- South Nigeria, the problem has been exacerbated by the outright neglect of the State Water Resources Agency. This has snow-balled into the proliferation of boreholes across the State especially Benin City and it's environ. However, the rapid urbanization and population growth has also heralded increased generation of domestic, commercial and industrial wastes. In fact the generation of municipal solid waste in term of volume has shown a positive relationship with population growth, urbanization, economic development, improved living standards or social status of the population across the globe [15].

Across the world waste generation poses serious environmental, economic and social problems [16]. The production of leachate from waste dumps is a function of the amount of rainwater percolating through the refuse as well as the variety of solid waste, regional hydrology, dumpsite age, humidity, temperature and oxygen availability [17,18]. Taylor and Allen (2006) concluded that the by- products of waste ultimately become part of the hydrological system of an area. Groundwater in areas around dumpsites has apple chance of contamination from leachate generated from adjacent waste dumpsites. Once groundwater is contaminated, it poses health hazard to local resource users and the environment.

The problem of waste management in the Benin City is becoming more serious as urbanization is engulfing the wastes dump sites (Plate 1). The groundwater quality in the adjoining areas may have been compromised from leachate percolation because of proximity to the sites. The health impact of groundwater contamination from leachate percolation on the resource users is well documented across the world [19]. According to Fetter (2007), solid waste dumps in wet zones are more likely to produce larger volume of leachate than in the desert areas. By implication the hot, humid climatic characteristic of Benin City and environs favour the generation of leachate in solid waste dumpsites and the ultimate impact on groundwater quality. The dumpsite for this study at Ikhueniro and adjoining areas along the Benin City Bypass near Benin- Agbor Road was chosen because urbanization has caught up with it. As a result of rapid urbanization, the Ikhueniro Wastes Dumpsite is now engulfed by human settlements and business activities. In Nigeria the monitoring and surveillance of groundwater quality is grossly inadequate. Relevant information or data on status of groundwater quality in this area in Benin City is highly needed to ensure the wellbeing of the present and future population in line with Goal Six (Clean Water and Sanitation) of Sustainable Development Goals (SDGs). The aim of this study is to investigate groundwater quality around Ikhueniro solid waste dumpsite and its implication for sustainable development.

Material and Methods

Study Area: This study is on Ikhueniro Open Wastes Dump Site and adjoining areas in Benin City, Edo State, South- South Nigeria. The Ikhueniro Open Waste Dump Site is located in the outskirts of the city. It is situated along Benin City Bypass near Benin- Agbor Express Road. The Ikhueniro Open Waste Dump Site (Latitudes 60 19’ 31.663’’- 60 19’ 43.968 N and Longitude 50 44’ 45.77’’- 50 44’ 53.741 E) covers an area of about 60,834.78m2 (0.6834741km2). It is the largest waste dumpsite in Benin City. Benin City is located on a fairly low- lying plain covered with porous sand. The Benin City Plain is an extension of the vast Coastal Plains which form the Southern fringe of Nigeria. The Coastal Plains are generally below 150 meters in height. Benin City is drained by two rivers, Ikpoba River in the north- east and Ogba River in the south- west.

The geology of the study area is similar to other parts of Niger Delta Basin as reviewed by Short and Strauble (1967), Asseez (1967), and Reijers et al., (1996). The area is uniformly underlain by the porous Benin geologic formation. The young sedimentary deposit is made up of tertiary scarp of Benin. The Benin formation has a depth of about 762.5m and lain on top of the Agbada formation, which is made of sand stone and rough sand [20]. The Benin Formation comprises of up to 200m of sands with shales, clays and gravel. This multi- aquifer geologic formation extends to the coastal belts. The Benin geologic formation is more permeable than the Deltaic Plains. The depth of the water table ranges from 3 to 15m beneath the ground surface. The seasonal fluctuations or variations ranges from 2.1 to 3.6m. Since the Benin geologic structure is largely sandy and permeable, the actual potential ranges between 150 and 1400m3/d/m [21,22].

Figure 1: Location of Ikhueniro Open Dumpsite in Benin City, Edo State.

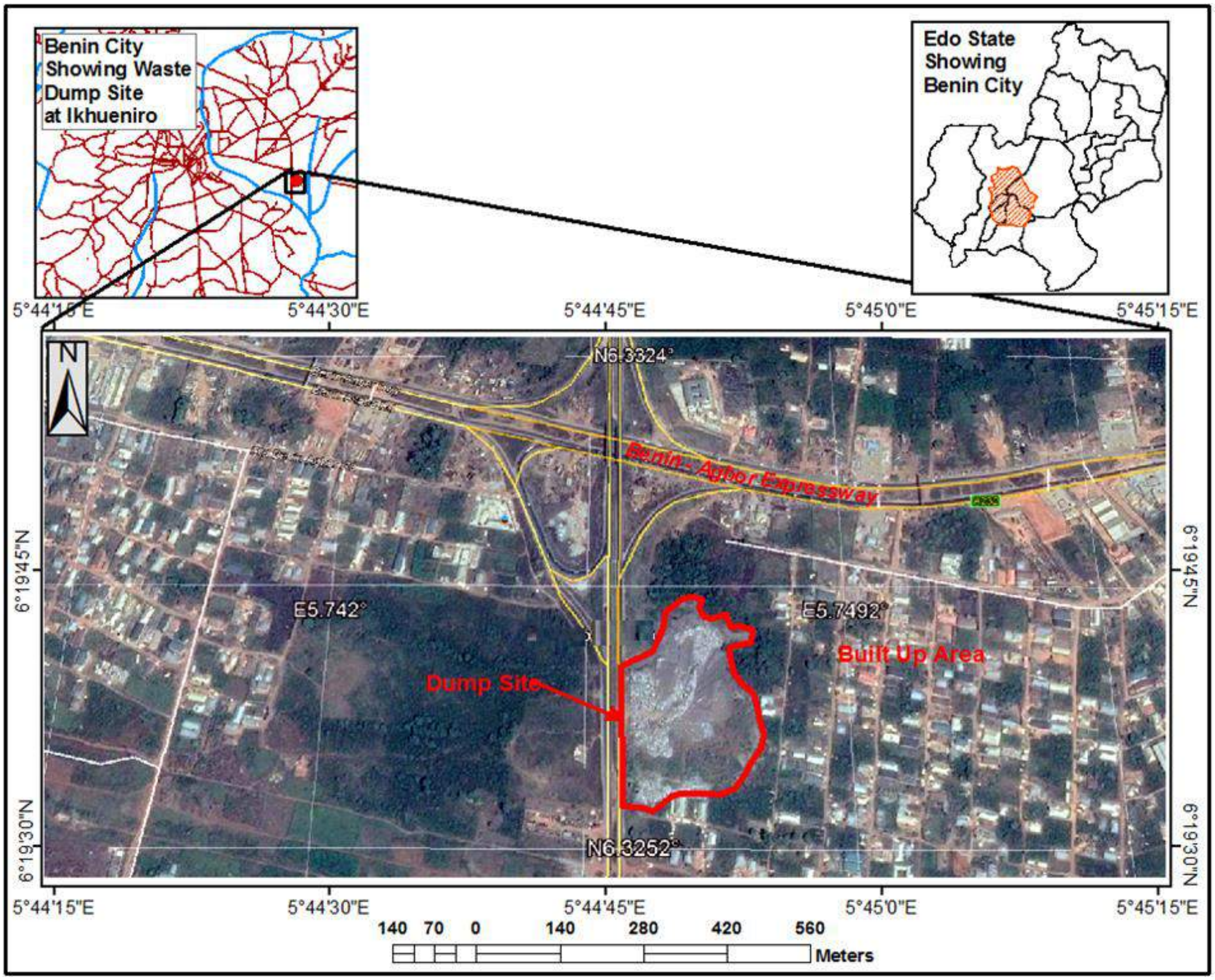

Source: Google Earth and Modified by the Researcher, 2019

Available hydrological data show a relationship between the confining aquifers in the coastline and the unconfined aquifers of the Benin Formation. The aquifers depth increases towards the interior while the confining rock formation reduces in thickness [23].

Benin City falls within rain forest climate belt of southern Nigeria, which is characterized by wet and dry seasons. The climatic belt has a bimodal rainfall pattern characterized by long, rainy season that begins in early March and terminates in early November while the dry season commences from early November and ends in March. Rainfall in Benin City is characteristically of high intensity with double maxima in July and September. However, between the double maxima, there is a brief dry period known as 'August Break' [24]. The rainfall pattern of the area is influenced by the north motion and retreat of the Inter- Tropical Discontinuity [25].

Oteze (2011) reports that rainfall records for 104years for Benin City showed annual rainfall ranged from 1228mm to 3039mm, with a mean of 2100mm and a 15-year annual mean evapotranspiration of 1026nn while the mean monthly temperature is about 280c.

Figure 2: Edo State Geological Formations Showing Ikhueniro Dump Site.

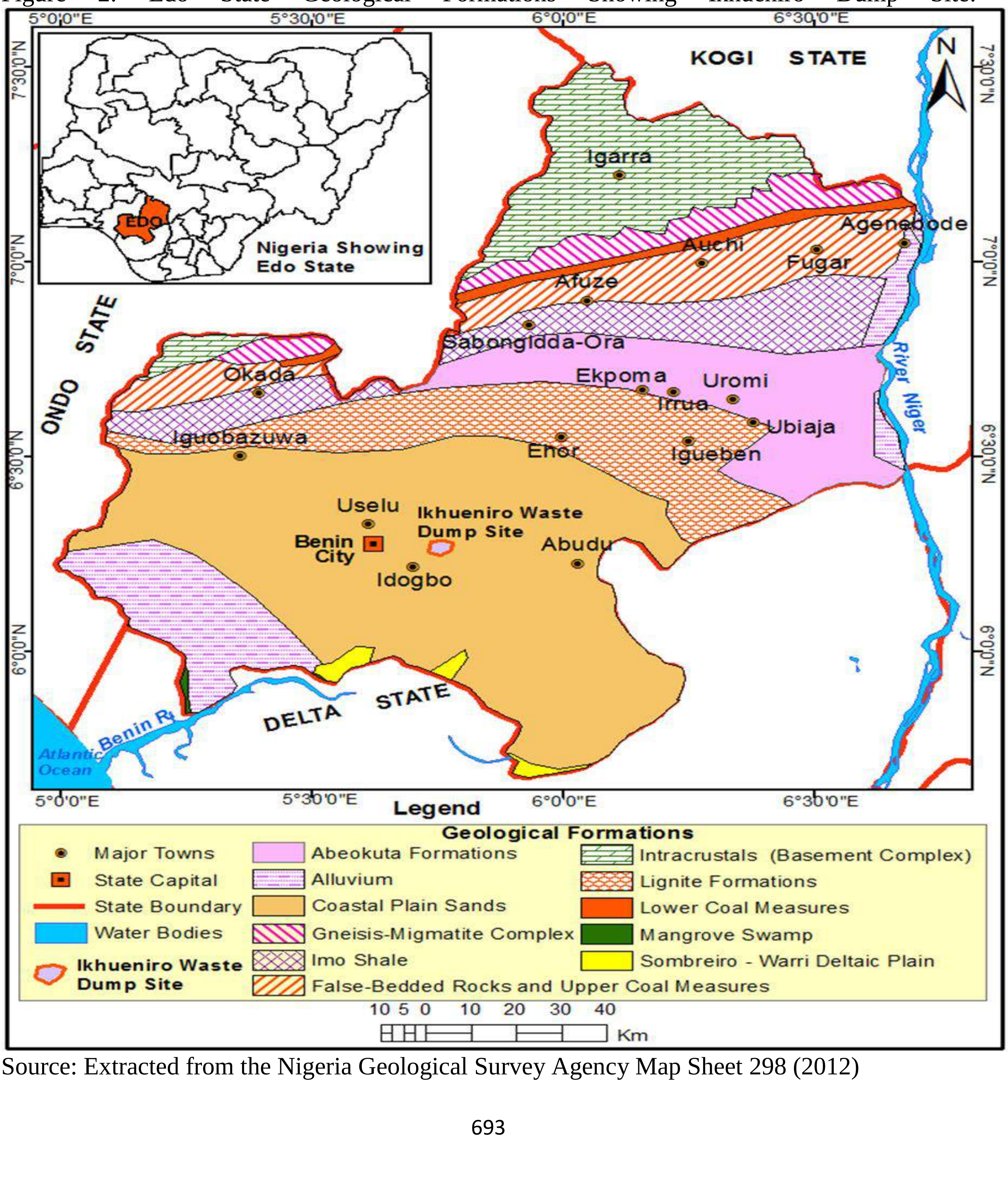

Source: Extracted from the Nigeria Geological Survey Agency Map Sheet 298 (2012)

Sampling and Laboratory Analyses

The purposive sampling technique was used to select the boreholes from which groundwater samples were collected. Purposive sampling has been found to be efficient when limited numbers of samples can serve as primary data sources because of the nature of research design and aim of the research [26]. Four (4) boreholes were selected for this study. The first sampling of leachate and groundwater was carried out in the dry season (15th January 2019). The second leachate and groundwater specimen was collected in the rainy season (7th May, 2019). The spatial distribution of groundwater sampling points or stations are shown in figure 3.

Since the dumpsite does not have leachate gathering device, leachate specimens were collected from the base of heaps of wastes where leachate flow out by gravity. In the dry season leachate was extracted from soil samples collected from the dumpsite with the aid of a soil hugger. The soil sample was mixed with distilled water to extract leachate. In this study, eight groundwater samples were collected from four boreholes within a radius of 1.5km from the solid wastes dump. Two samples (one each in rainy and dry season) were collected from purposively sampled four (4) wells around Ikhueniro Wastes Dump Site on the basis of north, south, east and west direction. The selected boreholes for groundwater sampling were also influenced by the willingness of the house owners to allow their boreholes to be used for the study. The selected Sampling Stations or boreholes include, 1 (north), 2 (east), 3 (south) and 4 (west) as shown in figure 3. This sampling pattern of boreholes' selection was to enhance spatial spread and the likely flow of groundwater. Leachate and groundwater specimens were stored in pre acid – rinsed polyethylene containers. The containers were further washed with the aid of distilled water and rinsed again with the samples at the site. The sampling bottle was corked after filling with samples using lids and kept in a cool box and was taken to the laboratory for analyses.

Plate 1: Ikhueniro Waste Dump and Urban Encroachment

Table 1: Geo- Spatial Attributes of Groundwater Sampling Stations

Sampling Stations	Latitudes (North)	Longitudes (East)	Elevation	Distance from center of Dump Site
1	6^{O} 19' 49.339"	5^{O} 44' 53.119"	80meters	297.12meters
2	6^{O} 19' 37.234"	5^{O} 44' 54.061"	79meters	178.37meter
3	6^{O} 19' 23.531"	5^{O} 44' 0.39"	85meters	465.19meters
4	6^{O} 19' 51.964"	5^{O} 44' 30.339"	85meters	693.88meters

Source: Fieldwork, 2019.

Figure3: Ikhueniro Open Dump Site and Ground Water Sampling Stations

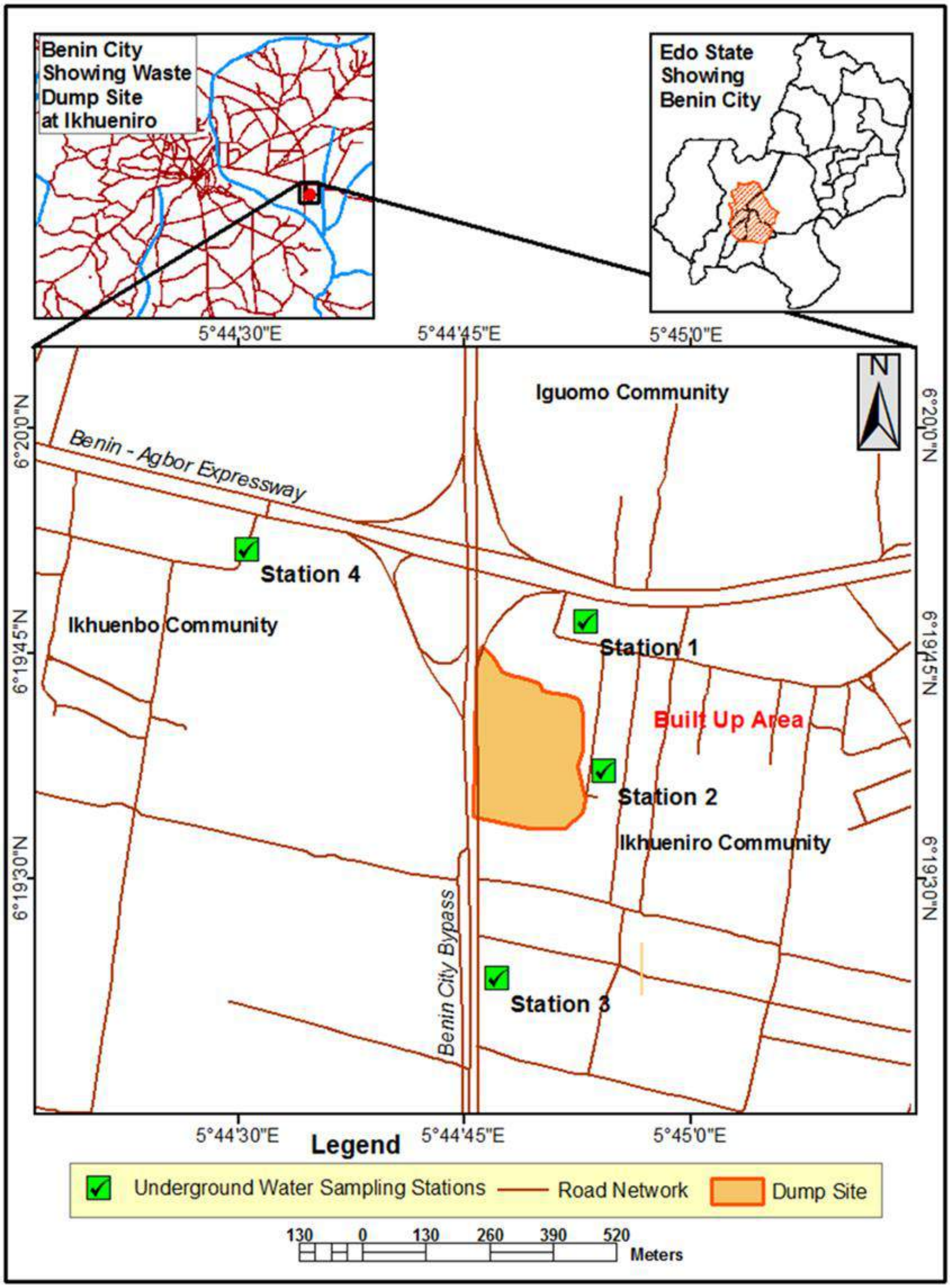

The physical parameters of the groundwater samples were determined in- situ. Alkalinity, Acidity, Total Suspended Solid (TSS) Total Dissolved Solid (TDS), Dissolved Oxygen (DO), Biochemical Oxygen Demand (BOD), Chemical Oxygen Demand (COD), Colour, Salinity, Bicarbonate (HCO3), Sodium (Na), Potassium (k), Calcium (Ca), Magnesium (Mg), Chlorine (Cl), Phosphorus (P), Ammonium (NH4N), Nitrate (NO3), Nitrite (NO2), and Sulphate (SO4) were determined using the American Public Health Association Methods (APHA, 2005). The analyses of heavy metals including Iron (Fe), Manganese (Mn), Zinc (Zn), Copper (Cu), Chromium (Cr), Cadmium (Cd), Nickel (Ni), Lead (Pb) and Vanadium (V) was done by Flame Atomic results were compared with the World Health Organization (WHO) standard for drinking water.Absorption Spectrophotometry. The microbiological properties of groundwater and leachate samples were also determined. The standard plate count (SPC) and most probable number (MPC) were used to determined Total Heterotrophic bacteria Counts and Total Coliform Counts respectively.

Results and Discussion

Descriptive Characteristics of physico-chemical parameters of Groundwater samples in both the Dry and Rainy Seasons

The results of the descriptive statistics of the physico-chemical parameters of Groundwater samples in both the dry and rainy Seasons are presented in Table 1 and 2 respectively. From both tables, it can be seen that standard deviation and standard errors of estimation from mean are generally within or below mean distribution, an indication of normal distribution. According to Anyadike (2009) a standard deviation (or σ) is a measure of how dispersed the data is in relation to the mean. Low standard deviation means data are clustered around the mean, and high standard deviation indicates data are more spread out. A standard deviation close to zero indicates that data points are close to the mean, whereas a high or low standard deviation indicates data points are respectively above or below the mean. With respect to the tables below, it can be said that our results are normally distributed and this has implications for planning as the tables give normal distribution of quality parameters.

Table 2: Descriptive statistics of physico-chemical parameters of Groundwater samples (Dry season)

	Mean	SE	SD	SV	Range	Min	Max	Sum	Confidence Level (95.0%)
pH	5.15	0.08	0.173	0.03	0.4	5	5.4	20.6	0.27
EC	25.9	7.5	15.1	226.8	33.4	12.8	46.2	103.4	23.9
Salinity	0.012	0.003	0.007	0.0005	0.015	0.006	0.021	0.05	0.010
TDS	13	3.67	7.4	54.0	16.5	6.4	22.9	52	11.7
DO	1.4	0.07	0.14	0.02	0.3	1.3	1.6	5.6	0.22

BOD_5	0.72	0.08	0.17	0.029	0.4	0.5	0.9	2.9	0.27
COD	6.5	2.89	5.7	33.5	12.9	2.1	15	26	9.2
HCO_3	55.8	5.7	11.5	131.4	26.7	45.3	72	223	18.2
Na	0.44	0.078	0.155	0.024	0.37	0.25	0.62	1.79	0.24
K	0.107	0.023	0.046	0.002	0.11	0.06	0.17	0.43	0.07
Ca	4.84	0.64	1.27	1.62	2.94	3.72	6.66	19.35	2.02
Mg	2.48	0.288	0.57	0.33	1.21	11.89	3.1	9.94	0.92
Cl	60.2	3.79	7.59	57.7	17.7	53.2	70.9	240.7	12.08
P	0.043	0.008	0.017	0.0003	0.043	0.021	0.064	0.174	0.028
NH_4N	0.23	0.014	0.028	0.0008	0.054	0.201	0.255	0.921	0.045
NO_2	0.20	0.044	0.089	0.0079	0.214	0.10	0.317	0.806	0.14
NO_3	0.411	0.086	0.172	0.029	0.385	0.255	0.64	1.65	0.27
SO_4	0.78	0.031	0.062	0.0039	0.15	0.71	0.85	3.11	0.09

Table 2 : Descriptive statistics of physico-chemical parameters of Groundwater Samples (Rainy season)

	Mean	SE	SD	SV	Range	Min	Max	sum	Confidence Level (95.0%)
pH	5.28	0.21	0.42	0.18	0.90	5.00	5.90	21.10	0.67
EC	31	14	28	770	61	10	71	123	44
Salinity	0.014	0.006	0.013	0.000	0.028	0.004	0.032	0.055	0.020
TDS	15.43	6.91	13.83	191.18	30.20	5.20	35.40	61.70	22.00
DO	1.8	0.1	0.1	0.0	0.3	1.6	1.9	7.0	0.2
BOD_5	1.03	0.03	0.05	0.00	0.10	1.00	1.10	4.10	0.08

COD	8.2	4.5	9.0	80.8	19.2	2.4	21.6	32.8	14.3
HCO_3	62.53	8.02	16.04	257.37	36.60	48.80	85.40	250.10	25.53
Na	0.598	0.116	0.232	0.054	0.560	0.320	0.880	2.390	0.368
K	0.14	0.02	0.05	0.00	0.11	0.10	0.21	0.56	0.08
Ca	5.8	0.8	1.6	2.5	3.3	4.9	8.2	23.3	2.5
Mg	2.6	0.3	0.6	0.3	1.3	2.0	3.3	10.6	0.9
Cl	70.90	7.24	14.47	209.45	35.45	53.18	88.63	283.61	23.03
P	0.057	0.010	0.021	0.000	0.051	0.030	0.081	0.226	0.033
NH_4N	0.282	0.017	0.034	0.001	0.079	0.251	0.330	1.126	0.054
NO_2	0.32	0.08	0.16	0.03	0.35	0.19	0.54	1.26	.25
NO_3	0.750	0.122	0.245	0.060	0.514	0.561	1.075	2.998	0.389
SO_4	0.263	0.180	0.359	0.129	0.739	0.062	0.801	1.050	0.572

The Seasonal Variations of the Physico- chemical. Heavy Metals and Microbiological Properties of Leachate Samples from Ikhueniro Waste Dump.

The summary of the results of seasonal variation of the physical, chemical and microbiological properties of leachate is presented in table 3. From table 3, the physical parameters of P^H Electricity Conductivity, Salinity, colour, Turbidity, Total Suspended Solid (TSS), and Total Dissolved Solid (TDS) depict marked season variation with higher concentration in the wet season than the dry season. The results of P^H values of the leachate sample obtained varies from 7.8 in the dry season to 7.9 in the rainy season. Similarly, the results of Salinity of leachate samples showed higher concentration in the rainy season (1.357g/l) than the dry season (0.439g/l). The levels of TSS and TDS of leachate samples varied from 14.4mg/l to 18.0mg/l and 485mg/l to 1500mg/l in the dry season to rainy season respectively.

Table 3: Laboratory Results of Leachate Samples for Dry and Wet Seasons

Parameters/ Variables	Dry season	Wet season
P^H	7.8	7.9
EC	970	3000
Sal.	0.439	1.357
Col.	8.7	10.8
Turb.	11.3	15.3
TSS	14.4	18.0
TDS	485	1500
DO	3.1	3.5
BOD	5.8	7.0
COD	121.6	148.0
HCO_3	912.2	2696
Na	74.7	122.3
K	60.1	84.0
Ca	526.2	812.0
Mg	154.8	200.4
Cl	401.4	903.9
P	1.325	1.871
NH_4N	1.075	3.031
NO_2	0.845	1.220
NO_3	2.701	5.801
SO_4	4.401	1.53

Fe	4.111	5.657
Mn	1.102	1.780
Zn	2.415	3.422
Cu	0.177	0.210
Cr	0.075	0.095
Cd	0.061	0.088
Ni	0.052	0.065
Pb	0.088	0.111
V	0,042	0.051
THC	14	20
Total Coliform	4	9

All the chemical parameters and heavy metals of leachate samples with the exception Sulphate (SO_4), showed higher concentration in the wet season than the dry season. The results of Bicarbonate (HCO3) of leachate samples obtained clearly indicated higher levels for the rainy season (2696mg/l) than the dry season (912.2mg/l). The levels of Chlorine (Cl) of leachate showed similar patterns of higher concentration in the rainy season (903.9mg/l) than the dry season (401.4mg/l). However, the results of Sulphate (SO_4) of leachate samples indicated higher levels for the dry season (4.401mg/l) than the rainy season (1.53mg/l). The concentration of Cadmium and Zinc of leachate samples varied from (0.088mg/l) to (0.061mg/l) and (3.422mg/l) to (2.415mg/l).the rainy season to dry season respectively. The microbiological parameters of leachate samples- the Total Heterotrophic bacteria Counts and Total Coliform Counts also highlighted apparent season variation from (14 to 20) ×103cfu/ml and from (4 to 9) MPN/100ml in the dry and wet seasons respectively.

The Seasonal Variations of the Physico- chemical and Microbilogical Properties Groundwater Samples Around Ikhueniro Waste Dump.

The results indicated that the EC levels of groundwater samples was higher in the dry for stations 1, 3 and 4 with the exception of Station 2. The salinity levels of groundwater samples from Stations 1 and 4 was higher for dry season than the rainy season. Salinity levels of groundwater samples in Station 1 ranged from 0.007mg/l to 0.006mg/l and Station 4 ranged from 0.006mg/l to 0.004mg/l during dry and rainy seasons respectively. On the other hand, groundwater samples from Station 2 showed higher levels in the wet season (0.032mg/l) than the dry season (0.021mg/l). Besides there was no seasonal difference of salinity levels of the groundwater samples from Station 3. However, groundwater samples in Station 2 recorded the highest levels of salinity and may not be unconnected to its proximity to the dumpsite.

TDS concentration in groundwater samples for stations 1, 3, and 4 showed higher values in the dry season than the rainy season. However, just as in the case of EC, groundwater samples in station 2 indicated higher level in the wet season (35.4mg/l) than during the dry season (22.9mg/l

The results of laboratory investigation revealed that the groundwater samples recorded higher DO concentration in the rainy season than during the dry season. For both seasons groundwater samples from station 3 recorded the highest concentrations.

Table 4: Groundwater Samples Laboratory Results for Dry Season

	St-1	St. - 2	St. – 3	St. -4	WHO limits
Ph	5.4	5.1	5	5.1	6.5-8.5
EC	16.3	46.2	28.1	12.8	≤1000
Salinity	0.007	0.021	0.013	0.006	NS
Colour	ND	ND	ND	ND	≤15
Turbidity	ND	ND	ND	ND	≤5
TSS	ND	ND	ND	ND	0
TDS	8.6	22.9	14.1	6.4	500- 1000
DO	1.3	1.4	1.6	1.3	≤5
BOD_5	0.8	0.7	0.5	0.9	1-5
COD	4.9	15	4	2.1	1-5
HCO_3	51.4	72	54.3	45.3	40-150
Na	0.42	0.62	0.5	0.25	≤200
K	0.09	0.17	0.11	0.06	NS
Ca	4.32	6.66	4.65	3.72	75-200
Mg	2.11	3.1	2.84	1.89	30-100
Cl	57.2	70.9	59.4	53.2	≤240
P	0.047	0.064	0.042	0.021	≤0.3
NH_4N	0.255	0.255	0.201	0.21	≤1.5

NO_2	0.103	0.317	0.211	0.175	≤3
NO_3	0.305	0.64	0.445	0.255	45-50
SO_4	0.76	0.855	0.79	0.705	200-400
Fe	0.945	1.504	1.24	0.756	≤0.1
Mn	0.096	0.315	0.184	0.084	≤0.05
Zn	0.514	0.688	0.512	0.409	≤3
Cu	0.041	0.072	0.061	0.031	≤1
Cr	0.018	0.04	0.021	0.013	≤0.05
Cd	0.015	0.017	0.02	0.011	≤0.005
Ni	0.008	0.015	0.012	0.003	≤0.02
Pb	0.031	0.05	0.038	0.024	≤0.05
V	0.005	0.011	0.009	0.001	≤0.010
THC	ND	ND	ND	ND	≤150
Total Coliform	0	0	0	0	0

From stations 2 and 3, there is an apparent seasonal variation of BOD levels in all the groundwater samples investigated with the rainy season concentrations higher than that of dry season Chemical Oxygen Demand (COD): The COD measures the Oxygen amount that is used during reactions in a water sample. It is the quantity of oxygen needed to breakdown organic carbon to carbon dioxide and water [27].

Table 5: Groundwater Samples Laboratory Results for Wet Season

	St-1	St. – 2	St. – 3	St. -4	WHO limits
pH	5.9	5.1	5	5.1	6.5-8.5
EC	14.3	70.9	27.7	10.3	1000
Salinity	0.006	0.032	0.013	0.004	NS
Colour	ND	ND	ND	ND	≤15
Turbidity	ND	ND	ND	ND	≤5
TSS	ND	ND	ND	ND	0
TDS	7.2	35.4	13.9	5.2	500- 1000
DO	1.6	1.7	1.9	1.8	≤5
BOD_5	1	1	1.1	1	1-5
COD	4	21.6	4.8	2.4	1-5
HCO_3	54.9	85.4	61	48.8	40-150
Na	0.55	0.88	0.64	0.32	≤200
K	0.11	0.21	0.14	0.1	NS
Ca	5.14	8.2	5.1	4.88	75-200
Mg	2.38	3.26	2.91	2.01	30-100
Cl	70.9	88.63	70.9	53.18	≤240

	St-1	St. – 2	St. – 3	St. -4	WHO limits
P	0.055	0.081	0.06	0.03	≤0.3
NH_4N	0.27	0.33	0.275	0.251	≤1.5
NO_2	0.218	0.54	0.312	0.19	≤3
NO_3	0.561	1.075	0.801	0.561	45-50
SO_4	0.082	0.801	0.105	0.062	200-400
Fe	1.181	1.983	1.462	0.896	≤0.1
Mn	0.18	0.411	0.214	0.122	≤0.05
Zn	0.57	0.705	0.633	0.471	≤3
Cu	0.047	0.081	0.069	0.039	≤1
Cr	0.025	0.042	0.03	0.022	≤0.05
Cd	0.018	0.028	0.021	0.014	≤0.005
Ni	0.009	0.018	0.015	0.005	≤0.02
Pb	0.038	0.057	0.043	0.031	≤0.05
V	0.007	0.014	0.011	0.004	≤0.010
THC	ND	ND	ND	ND	≤150
Total Coliform	0	0	0	0	0

Note: $TS = TSS + TDS$

The results of groundwater investigation showed that Bicarbonate (HCO_3) levels ranged from 45.3mg/l to 72.0mg/l in the dry season and 48.8mg/l to 85.4mg/l in the rainy season. Laboratory investigations also revealed a seasonal pattern of the concentration of Sodium (Na) in the groundwater samples. In the rainy season, the levels of Na varied from 0.32mg/l to 0.88mg/l and 0.25mg/l to 0.62mg/l in the dry season. Groundwater quality investigation around the dump site revealed marked seasonal variation of Potassium with greater levels in the rainy season than the dry season. Investigation revealed that during the dry season, Calcium (Ca) levels of groundwater samples ranged from3.72mg/l to 6.66mg/l and 4.88mg/l to 8.20mg/l in the rainy season.

The concentration of Mg in groundwater samples also indicated seasonal variation with higher concentration in the wet season (2.01mg/l to 3.26mg/l) than the dry season (1.89mg/l to 3.10mg/l). Chlorine (Cl) levels of groundwater samples for dry and rainy seasons ranged from 53.2mg/l to 70.9mg/l and 53.18mg/l to 88.63mg/l respectively. The concentration of phosphorus of the groundwater specimens ranged from 0.021mg/l to 0.064mg/l for dry season and 0.030mg/l to 0.081mg/l in the rainy season. The results of P concentration of the leachate sample obtained in figure 18 varies from 1.325mg/l in the dry season to 1.871mg/l in the rainy season.

Ammonia (NH_4N) levels also showed the pattern of greater concentration in rainy season (0.251mg/l to 0.330mg/l) than for dry season (0.201mg/l to 0.255mg/l). From the study the Nitrite (NO_2) concentration in the groundwater samples varied from 0.103mg/l to 0.317mg/l in the dry season and 0.218mg/l to 0.540mg/l during the rainy season The laboratory results showed that Nitrate (NO_3) levels was very low in all the groundwater samples investigated. The minimum and maximum nitrate concentration recorded during the dry season was 0.255mg/l and 0.640mg/l respectively. In the rainy season, Nitrate levels varied from 0.561mg/l to 1.075mg/l. Also groundwater samples from the closest sampling station to the dump site (station 2) recorded the highest nitrate and nitrite levels for both seasons.

The laboratory results in the study indicated seasonal pattern of nitrite and nitrate concentrations of leachate samples from the dumpsite. The nitrite levels of leachate showed higher concentration in the rainy season (1.22mg/l) than the dry season (0.845mg/l). The levels of nitrate of leachate samples also varied from (5.801mg/l) in the rainy season to (2.701mg/l) in the dry season. Sulphate (SO4): Sulphate is an ion commonly found in groundwater. It could result naturally from air, rainwater, soil or rocks as well as anthropogenic sources such as mining and wastes.

Total Heterotrophic bacteria Counts (THC) and Total Coliform Counts (TCC) are used to give a general indication of the health or sanitary condition of public or domestic water supply. The TCC refers to the bacteria in the soil and water in contact with human or animal waste. The THC is an anaerobic bacteria test in water to detect all bacteria in drinking water. It is the overall bacteriological quality of drinking water (Nazak, et al, 2015). The laboratory results indicated that there was no trace of Total Heterotrophic bacteria Counts (THC) and Total Coliform Counts (TCC) in the groundwater samples around Ikhueniro waste dumps as shown in tables 3 and 4 respectively. Field investigation revealed that the average depth of the boreholes (sampling points) in the area is 225 feet (67.57m). The depth of the boreholes could be responsible for the absence THC and TCC in the groundwater samples. Fetter (2007) observed that the deeper the aquifer the less the probability of microbe and bacteria to survive. Besides, Meybeck et al (1996) concluded that the depth of the overlying unsaturated zone can help forestall the levels of inflow of micro- organisms and other pollutants into groundwater. The laboratory results of microbiological analysis of groundwater samples and leachate from the dumpsite for dry and wet seasons are presented in tables 6 and 7 respectively.

Table 6: Results of Microbiological Analyses for Dry Season

Sampling Point	Total Heterotrophic bacteria Counts (x10^3 cfu/ml)	Total Coliform Counts (MPN/100ml)
1	0	0
2	0	0
3	0	0
4	0	0
Leachate	14	4

Table 7: Results of Microbiological Analyses for Wet Season

Sampling Point	Total Heterotrophic bacteria Counts (x10^3 cfu/ml)	Total Coliform Counts (MPN/100ml)
1	0	0
2	0	0
3	0	0
4	0	0
Leachate	20	9

The Seasonal Characteristics of the Concentration of Heavy Metals of Groundwater Samples Around Ikhueniro Waste Dump

. The results of Iron (Fe) concentration in sampled groundwater around the dump site revealed that values ranged from 0.756mg/l to 1.504mg/l during the dry season and that of the wet season varied from 0.896mg/l to 1.983mg/l. Groundwater samples from station 2, the closest to the dump site recorded the highest iron concentration in both seasons.. Again, investigation revealed that samples of groundwater from station 2 recorded the highest levels of manganese for both rainy (0.411mg/l) and dry (0.315mg/l) seasons. This may not be unconnected with its nearness to the dump site.

Investigations revealed that Zinc (Zn) concentration in groundwater samples was higher in the wet season (0.471- 0.705) mg/l than the dry season (0.409- 0.688) mg/l.). From the results monitored, Copper (Cu) levels of sampled groundwater varied from 0.031mg/l to 0.072mg/l in the dry season and 0.039mg/l to 0.091mg/l in the rainy season. Just as reported for iron, manganese and zinc, groundwater samples from station 2 recorded maximum concentration of copper in the study (0.081mg/l 0.072mg/l for rainy and dry seasons respectively. Laboratory results for chromium showed that concentration was higher in the rainy season than the dry season. In the wet season chromium concentration was between 0.022mg/l and 0.042mg/l and varied from 0.013mg/l to 0.040mg/l in the dry season. Besides, the groundwater samples from station 2 recorded the highest levels of chromium in the study. Groundwater monitoring results indicated concentration of cadmium at trace level of 0.011mg/l to 0.020mg/l in the dry season and 0.014mg/l to 0.028mg/l in the rainy season. Results (figure 31) monitored for nickel showed that concentration was greater in the rainy season than the dry season. In the wet season nickel concentration was between 0.005mg/l and 0.018mg/l and ranged from 0.003mg/l to 0.015mg/l in the dry season. Moreover, the groundwater samples from station 2 recorded the maximum concentration of nickel in the study.

Lead (Pb) is a hazardous metal because it has destructive effects on the kidney and brain. From the study concentration of lead in the groundwater samples 0.024mg/l to 0.050mg/l and 0.031mg/l to 0.057mg/l during dry and rainy seasons respectively. The results indicated that vanadium concentration varied from 0.001mg/l to 0.011mg/l and 0.004mg/l to 0.014mg/l during dry and rainy seasons respectively.

Generally the higher concentration of water quality indicators of the groundwater samples in the rainy season than the dry season around Ikhueniro waste dumps corroborated previous studies done in different areas by De et al. (2017) and Barjinder et al. (2013) and Dhundi et al. (2011).

Comparison of the Observed Properties of Groundwater and WHO Benchmark for Drinking Water.

The summary of the results and the applicable World Health Organization [28,29,30] recommended guideline values for drinking water quality are presented in tables 4 and 5. From the results in tables 4 and 5, the concentration of P^H, TDS, Ca, Mg, NO_2, NO_3, Fe, Mn, and Cd of all the groundwater samples fell outside the maximum standard limit World Health Organization for drinking water. The levels of Vanadium (V) in the groundwater samples from sampling points 4 and 5 surpassed the maximum limits of WHO for drinking water. Besides, COD concentrations in the groundwater samples from sampling point 4 also surpassed WHO maximum permissible limit for drinking water. The values of P^H observed in all the groundwater samples for dry season ranged from 5.0 to 5.4 and 5.0 to 5.9 in the rainy season. The scale of the P^H measurements runs from 0-14, with 7.0 considered neutral. The P^H values below 7.0 are considered acidic and the values above are considered bases. The P^H is an essential factor in determining the health and suitability of a water source. The P^H values showed that the groundwater samples from the study are acidic and therefore the results fell below the WHO acceptable limit of 6.5 – 8.5 for drinking water.

The TDS values of the groundwater samples from the Sampling Stations varied from 6.4mg/l (Station 4) to 22.9mg/l (Station 2) in the dry season and from 5.2mg/l (Station 4) to 35.4mg/l (Station 2) in the wet season. The TDS concentrations of the groundwater samples in all the stations for both seasons fell outside the permissible limit of WHO (500- 1000mg/l). The Calcium (Ca) levels of groundwater samples ranged from3.72mg/l to 6.66mg/l in the dry season and 4.88mg/l to 8.20mg/l in the rainy season. The Ca levels of the groundwater sample fell far below the WHO standard of 75- 200mg/l for drinking water.

Conclusions

In summary the groundwater around Ikhueniro open dump site was found to be polluted by PH, TDS, Ca, Mg, NO2, NO3, Fe, Mn, Cd and to a lesser extent COD and V. The concentrations of these contaminants exceed the WHO allowable standard limit for drinking.

From the study the groundwater and leachate samples recorded higher levels of pollution during the wet season compared to dry season and thus suggest that groundwater contamination is enhanced by rainy season.

The study also revealed that significant differences existed in the contamination levels based on the distance of the sampling point from the dump site. The concentration of most of the physico-chemical variables was highest in borehole closest to the dump site. The pollution levels therefore decreases with the increase in distance of borehole from the dump site.

It is important to note that from laboratory analysis there was no trace of Total Heterotrophic bacteria Counts (THC) and Total Coliform Counts (TCC) in the groundwater samples in the study area. Field investigation revealed that the average depth of the boreholes (sampling points) in the area is 225 feet (67.57m). The depth of the boreholes may be responsible for the absence THC and TCC in the groundwater samples. Fetter (2007) observed that the deeper the aquifer the less the probability of microbe and bacteria to survive. However leachate samples showed substantial concentration of THC and TCC.

Furthermore, as there is no natural or other possible reason for high concentration of these contaminants in the groundwater samples, it can be concluded that the leachate generated from the Ikhueniro open waste dump site has significant impact on the groundwater quality around the dump site.

Recommendations

Proper methods of waste disposal should be put in place. For example at the household level, Proper segregation of wastes should be done to ensure that all organic waste or matter can be composted and then used as manure or fertilizer. Besides, waste can be recycled into valuable products for the use of the people.

In addition, immediate attention is needed towards the continuous monitoring, assessment and remediation of the groundwater around the Ikhueniro open dump site to prevent further water quality retardation.

The dump site should be upgraded to sanitary landfills to forestall leachate percolation to the aquifer.

There is also the need to for the establishment of 'Buffer Zones' around the existing dump sites or landfill in the context of groundwater exploitation.

The depth of boreholes around dumpsites and beyond should be regulated to ensure that groundwater of the best quality is tapped. The depth should reflect the attributes of local geology or aquifers.

Groundwater governance institutional framework should be restructured to ensure best practice in Nigeria. Groundwater governance institutions such as Federal Ministry of Water Resources (FMWR), Federal Ministry of Environment (FME), Nigeria Hydrological Service Agency (NIHSA), Federal Environmental Protection Agency (FEPA) et cetera should be re-organized and properly funded to ensure regular monitoring, assessment and better management of the Country's groundwater resources.

REFERENCES

[1] Adelana, S. M.A.; Olasehinde, P. I.; Bale, R. B.; Virbka, P.; Edet, A. E.; and Goni, I. B. (2008). An Overview of the Geology and Hydrogeology of Nigeria In: S.M.A. Adelana and A. M. MacDonald (eds), Applied Groundwater Studies in Africa, IAH, CRC Press, Balkema, The Netherland, pp. 171- 198.

[2] Anyadike, R.N.C. (2009) Statistical Methods for the Social and Environmental Sciences. Spectrum Books, Ibadan.

[3] APHA, (2005). Standard Method for the Examination of Water and Wastewater, 2nd Edition, APHA, Washington DC.

[4] Asseez, L.O. (1967) "Review of the Stratigraphy Sedimentation and Structure of the Niger Delta, in Geology of Nigeria (Ed). C.A. Kogbe, 259-272.

[5] Davie, T. (2008). "Fundamentals of Hydrology" (2nd edition), Rouledge: London.

[6] Dawei, H. (2010). Concise Hydrology, Ventus Publ., UK.

[7] Dohare, D., Deshpande, S. and Kotiya, A. (2014). Analysis of Groundwater Quality Parameters: A Review, Research Journal of Engineering Sciences, Vol. 3(5), 26- 31.

[8] Esmaeilil, M., karbassi, A. R., Baghvad, S. A. and Bejman, A. H. (2010). Potential of Natural Bed Soil on Absorption of Heavy Metals in Industrial Waste Landfill, International Journal of Science and Technology, 7(3): 545- 552.

[9] Fetter, C. W. (2007). Applied Hydrogeology, 2nd Edition, Marril Publ, New Delhi.

[10] Herschy, R. W. (1998). World Water Balance in Herschy, R. W. and Fairbridge, R. W. (eds), Encyclopaedia of Hydrology and Water Resources, Kluwer Academic, Boston, pp. 787- 788.

[11] Iloeje, N. P. (1973). Geography of Nigeria: Longman Nigeria Limited.

[12] Jhamnani, B. and Singh, S. k. (2009). Groundwater Contamination Due to Bhalaswa Landfill Site in New Delhi, International Journal of Civil and Environmental Engineering, 1(3).

[13] Martins, O. (2001). Water Resources Management and Development in Nigeria- Issues Challenges in a New Millennium: An Inaugural Lecture Delivered at the University of Agriculture, Abeokuta, Aug., 2001.

[14] Meybeck, M., Kuusisto, E., Makela, A. and Malkki, E. (1996). Water Quality, in: Water Quality Monitoring. A Practical Guide to the Design and Implementation of Fresh Water Quality Studies and Monitoring Programmes, Edited by Jamie Bartram and Richard Balance published on Behalf of United Nations Environment Programme and World Health Organisation.

[15] Nazak, A.; Ali, Z. and Amir, H. M. (2015). The Interaction Between Heterotrophic Bacteria and Coliform, Fecal Coliform, Fecal Streptococci Bacteria in the Water Supply Network. Iran Journal of Public Health, Vol. 44, 12: 1685- 1692.

[16] Nirmala, D. and Jagath, G. (2013). Leachate Characterization and Surface Groundwater Pollution at Municipal Solid Waste Landfill of Gohagoda, Sri Lanka, International Journal of Scientific and Research Publications, Vol. 3(11).

[17] Nwajide, C.S (2006). A guide for geological field trips to Anambra state and related sedimentary basins in south eastern Nigeria, PTDF Chair., University of Nigeria, Nsukka.

[18] Odjugo, P. A. O. (2012). Valuing the cost of environmental degradation in the face of changing climate: Ephasis on flood and erosion in Benin City, Nigeria, African Journal of Environmantal Science and Technology, Vol 6(1), pp. 17- 27

[19] Oteze, G.E. (2011). Water supply, ground water and flood control in Benin City, presented at the NMGS, Benin Chapter sensitization workshop on water resources management and its implication Benin City 22nd March.

[20] Papadopoulou, M. P. (2001) Numerical Modeling of the Environmental Impact of Landfill Leachate Leakage on Groundwater Quality. Field Application Environmental Model Asses, pp. 12: 43- 54.

[21] Raghunath, H.M.(2008). "Hydrology, Principles, Analysis and Design" (2nd edition), New Age International Publishers: New Delhi.

[22] Rees, J., Winpenny, J. and Hall, A.W. (2008). Water as a Social and Economic Good, Tec Background Paper, NO 12, Global Water Partnership.
[23] Reijers, T.J.A., Petters, S.W., Nwajide, C.S (Eds.) (1996).The Niger Delta Basin, SPDC Corporate Reprographic Services, Warri.
[24] Salami, L. (2012). Leachate Characterization Assessment of Groundwater Quality: A case of Solous Dumpsite in Lagos State, PhD Seminar Paper, Lagos State University, Epe, Lagos, Nigeria.
[25] Salami, L., Fadayini, M. O. and Madu, C. (2014). Assessment of a Closed Dump Site and Its Impact on Surface and Groundwater Integrity: A Case Study of Oke Afa Dumpsite, Lagos, Nigeria, IJRRAS,, 18(3).
[26] Sharholy, M., Ahmed, K., Vaishya, R. and Gupta, R. (2007). Municipal Solid Waste Characteristics and Management in Allahabad, India, Journal of Waste Management, 27(4), 490- 496.
[27] Short, K.C., Stauble, A.J., (1967). Outline of geology of Niger Delta, Bull. American Association of Petroleum Geologist: 54(5):761-779.
[28] Taylor, R. and Allen, A. (2006). Waste Disposal and Landfill Potential Hazards and Information Needs, In World Health Organization (WHO) (Eds), Protecting Groundwater for Health, Managing the Quality of Drinking Water Resources, 339- 360.
[29] Tods, D. K. (1980). Groundwater Hydrology, 2nd Edition, New York, John Wiley.
[30] World Health Organization (2006). Guidelines for Drinking- Water Quality, First Addendum to 3rd Edition, Vol. 1, Recommendation, Geneva.

NIPES-NCEE Conference Proceedings
The 2nd International Conference 15th-17th Feb. 2023
711-724
www.nipesjournals.org.ng

A REVIEW ON THE MOST APPROPRIATE ALTERNATIVE FUELS FOR AUTOMOBILES

Igbunu Inikori O., Amanda Charles, Ovuru Derick P., Aduwenye Bawo K.

Department of Mechanical Engineering, University of Benin, P.M.B 1154, Benin City, Nigeria.

Abstract

There is an increase in research to encourage the usage of alternative fuels in automobiles due to the depletion of oil sources and certain environmental concerns. Some fuel sources will stand out in this regard with particular benefits, while others will not. Choosing the alternative fuel source that is best for automobiles in the present environment is essential, and understanding the characteristics of various forms of energy is also very essential for recommending an alternative fuel. In this research, a comprehensive review is carried out on existing literature on the benefits, drawbacks, environmental impact, and effects on human health, availability, and economic implications of alternative fuels. This was to determine the fuel that is most appropriate for use in automobiles. The alternative energy sources for vehicles considered are LPG, CNG, hydrogen, biodiesel, ethanol and methanol, electric vehicles, hybrid, and fuel cell vehicles. The study reveals that alcohol (butanol, methanol, ethanol, and fossil fuels) are the most affordable alternative fuels, but electric and fuel cell cars stand out for their environmental advantages. Hydrogen can be sourced easily and is an important fuel source for internal combustion engines and fuel cell vehicles. The study concludes that while there is no one-size-fits-all solution, a combination of alternative fuels can provide a path towards reducing dependence on fossil fuels and mitigating the negative impacts of transportation on the environment. The research highlights the need for investment in research and development and supportive policies and infrastructure, to accelerate the transition towards a cleaner and more sustainable transportation sector.

Keywords: *Alternative fuel, fossil fuel, environmental impact, energy, internal combustion engine.*

1.0 Introduction

Fossil fuels, such as gasoline and diesel, have been the primary source of energy for transportation for many decades. However, the extraction, refinement, and use of these fuels have significant environmental impacts.

The burning of fossil fuels releases carbon dioxide (CO2) and other greenhouse gases into the atmosphere, which contribute to global warming and climate change. The transportation sector is one of the largest contributors of CO2 emissions globally, accounting for nearly 25% of total emissions [1].

In addition to emissions from the combustion of fossil fuels, the extraction and refining process also have significant environmental impacts. For example, oil spills from offshore drilling and pipeline leaks can cause harm to marine life and the environment [2]. Refining crude oil into gasoline and diesel fuel also produces air pollution, including emissions of sulfur dioxide, nitrogen oxides, and particulate matter [3].

Fossil fuels are also non-renewable resources, meaning that they will eventually run out [4]. The continued dependence on fossil fuels also contributes to geopolitical instability, as nations compete for access to limited supplies [5].

The use of fossil fuels in transportation has a significant impact on the environment, contributing to global warming and climate change, air pollution, and environmental degradation. It is therefore important to consider transition to alternative fuels that are more sustainable and might have a lower impact on the environment.

Alternative fuels for automobiles refer to fuels that can be used as substitutes for traditional gasoline and diesel fuels. Some of the common alternative fuels are ethanol, biodiesel, compressed natural gas (CNG), liquefied natural gas (LNG), hydrogen fuel cells, electricity, and propane.

Alternative fuels for cars are becoming more popular due to rising transportation demand and the need to lessen the carbon imprint. Although the typical gasoline-powered internal combustion engine has long dominated the automotive industry, it has several disadvantages, including significant pollutants and reliance on limited oil supplies. Finding alternative fuels that are more cost-efficient, sustainable, and ecologically benign is becoming increasingly popular as a result. This study seeks to give a general overview of the best alternative fuels for cars and assess their potential in terms of price, emissions, availability, and infrastructure. The paper's conclusion and recommendation will include an analysis of alternative fuels' effects on the environment and a decision about which fuel is best for cars.

The use of alternative fuels in the automotive industry has gained significant attention in recent years due to concerns over energy efficiency and environmental sustainability. According to a report by the International Energy Agency [6], transportation is responsible for over 20% of global energy-related carbon dioxide emissions. As such, there is a growing need to find alternative fuels that are not only more energy efficient but also have a lower impact on the environment.

Several alternative fuels have been proposed, including electricity, ethanol, biodiesel, hydrogen, natural gas, and propane [7]. Each of these fuels offers a unique set of advantages and challenges, and the most suitable alternative fuel depends on various factors such as local availability, infrastructure, and vehicle technology.

For instance, electric vehicles (EVs) are becoming increasingly popular due to advancements in battery technology and the growth of charging infrastructure [8]. EVs produce zero tailpipe emissions, making them a cleaner alternative to traditional internal combustion engine vehicles [9].

Ethanol, a biofuel made from crops, is another alternative fuel that is gaining popularity [2]. Biodiesel, made from recycled cooking oil, animal fats, or vegetable oils, offers similar performance to diesel fuel and can be used in any diesel engine without modification [10].

Hydrogen is a zero-emission fuel that can be used in fuel cell vehicles [11]. While hydrogen offers significant environmental benefits, the limited availability of hydrogen refuelling infrastructure and high production costs remain challenges to widespread adoption [12-19].

These alternative fuels will be seen in more detail during the course of this research paper and the advantages and disadvantages will be seen as well.

In conclusion, alternative fuels for automobiles offer a promising path towards a cleaner and more sustainable future for the automotive industry. However, further research and development are needed to overcome the challenges associated with each alternative fuel and to ensure their widespread adoption [20-31].

2.0 Petroleum and the Oil Sector in the World

The petroleum and oil sector has long been the dominant source of fuel for the global transportation sector, powering the majority of the world's cars, trucks, and other vehicles. However, the continued use of petroleum-based fuels has raised several environmental and sustainability concerns, including air pollution, greenhouse gas emissions, and dependence on finite resources. In response to these challenges, alternative fuels for automobiles have emerged as a potential solution.

Petroleum is the most commonly used fuel in vehicles right now. Some of the major advantages are there are matured technologies for fuel extraction and because of well-developed combustion engines. Some disadvantages include the fact that they are non-renewable sources of energy, it takes very long to form fossil fuels, air pollution and global warming.

While the oil industry remains a major player in the global economy, alternative fuels such as electric batteries, hydrogen, biofuels, and natural gas are gaining traction as viable options for powering the world's transportation sector. These alternative fuels offer several benefits over traditional petroleum-based fuels, including reduced emissions, increased energy security, and decreased dependence on finite resources [32].

Despite these advantages, the widespread adoption of alternative fuels for automobiles faces several challenges, including the lack of infrastructure, higher upfront costs, and technical barriers. However, many governments around the world have begun to implement policies to encourage the adoption of alternative fuels, including tax incentives, research and development investments, and regulations to reduce emissions from the transportation sector [33].

In conclusion, the petroleum and oil sector has long dominated the global transportation sector, but alternative fuels are emerging as a potential solution to the environmental and sustainability challenges posed by traditional petroleum-based fuels. While the widespread adoption of alternative fuels faces several challenges, the potential benefits of these fuels have led many governments to implement policies to encourage their development and adoption.

3.0 Alternative Fuels and The Past

The use of alternative fuels in automobiles has a long history, dating back to the early 20th century. In the early days of the automobile industry, gasoline was not the only fuel option available. A variety of alternative fuels were used in vehicles, including electricity, ethanol, and even steam.

One of the earliest alternatives to gasoline was electricity, which was used to power electric vehicles (EVs) in the late 19th and early 20th centuries. At the turn of the 20th century, EVs were the preferred mode of transportation for many city dwellers, as they were clean, quiet, and easy to operate [34-40]. However, the discovery of vast reserves of cheap oil and the development of the internal combustion engine ultimately led to the decline of EVs, and gasoline became the dominant fuel for transportation.

Another alternative fuel that has been used in the past is ethanol, which is made from fermented crops such as corn, sugarcane, and barley. Ethanol has been used as a fuel for vehicles for over a century and was even used in the early days of the automobile industry as a blending component for gasoline [41]. Despite its long history, the use of ethanol as a transportation fuel only gained widespread popularity in recent decades as a result of concerns over oil dependence and climate change.

Finally, steam engines were also used in the early days of the automobile industry. Steam-powered vehicles were some of the first vehicles to be mass-produced, and they were used for both personal and commercial transportation [42-45]. However, internal combustion engines (ICEs) eventually replaced steam engines due to their lower cost and greater efficiency.

In conclusion, the use of alternative fuels in automobiles has a long history, dating back to the early days of the automobile industry. While gasoline ultimately became the dominant fuel for transportation, various alternative fuels such as electricity, ethanol, and steam were used in the past and continue to play a role in the transportation sector today.

3.0 ALTERNATIVE FUELS

A. Biodiesel

Biodiesel is a renewable, clean-burning diesel fuel made from biological materials, such as vegetable oils and animal fats. It is considered an alternative fuel because it can be used in diesel engines without any modifications, and it produces fewer emissions compared to conventional diesel fuel.

Biodiesel is produced through a chemical process called transesterification, where the glycerol molecule is separated from the fatty acids found in the biological material. This results in the

formation of methyl esters (the chemical name for biodiesel) and glycerol. The methyl esters are then blended with conventional diesel fuel to create biodiesel.
The use of biodiesel as a transportation fuel has several benefits, including:

- Renewable and sustainable: Biodiesel is made from renewable resources, making it a sustainable alternative to conventional diesel fuel.
- Reduced emissions: Biodiesel produces fewer emissions compared to conventional diesel fuel, including fewer greenhouse gas emissions, particulate matter, and toxic air pollutants.
- Biodegradable: Biodiesel is biodegradable, which means that it breaks down much faster than conventional diesel fuel in the event of a spill.
- Energy independence: Biodiesel can be produced from a variety of domestic resources, reducing the dependence on foreign oil.

Despite these benefits, there are also some challenges associated with the use of biodiesel, including:

- Cost: Biodiesel is generally more expensive than conventional diesel fuel, due to the cost of producing the biological materials and the transesterification process.
- Feedstock availability: The availability of feedstock, such as vegetable oils and animal fats, can be limited and subject to price volatility.
- Engine compatibility: Some older diesel engines may not be compatible with biodiesel, as the fuel can cause compatibility problems with certain materials used in the fuel system.

Overall, biodiesel is a promising alternative fuel that offers several benefits over conventional diesel fuel.

B. Methanol

Methanol is a colourless, volatile, and flammable liquid that has been used as an alternative fuel for several decades. It is a simple alcohol composed of carbon, hydrogen, and oxygen, and it can be produced from a variety of feedstocks, including natural gas, coal, and biomass.

One of the main advantages of methanol as a fuel is that it can be easily produced from renewable and low-cost feedstocks. This makes it a potentially attractive option for countries looking to reduce their dependence on petroleum and to transition to a more sustainable energy mix.

Another advantage of methanol is that it can be used in a variety of applications, including as a fuel for internal combustion engines and as a feedstock for the production of other fuels and chemicals. Methanol can also be blended with gasoline to produce a fuel with improved combustion properties and reduced emissions.

In terms of its environmental impact, methanol is considered to be a cleaner fuel than gasoline. When burned, methanol releases less greenhouse gas emissions than gasoline, and it also produces fewer toxic pollutants such as nitrogen oxides (NOx) and particulate matter.

Despite its advantages, there are also some challenges associated with the use of methanol as a fuel. For example, it has a lower energy density than gasoline, which means that vehicles powered by methanol require larger fuel tanks to store the same amount of energy as gasoline. Additionally, methanol can be more corrosive than gasoline, which can lead to issues with fuel systems and other engine components.

C. Ethanol

Ethanol is a bioalcohol that is widely used as an alternative fuel for transportation and energy production. It is a renewable and domestically produced fuel that is made from crops such as corn, sugarcane, and wheat, as well as from agricultural and forestry waste.

One of the main advantages of ethanol as a fuel is that it is renewable and domestically produced, which makes it an attractive option for reducing dependence on foreign oil and reducing greenhouse gas emissions. When burned, ethanol produces fewer emissions than gasoline, including carbon monoxide, volatile organic compounds, and particulate matter. Additionally, ethanol is a high-octane fuel, which can improve engine performance and efficiency.

Ethanol can be blended with gasoline to create a fuel known as E10 (10% ethanol and 90% gasoline) which can be used in standard gasoline engines without modification. Higher ethanol blends, such as E85 (85% ethanol and 15% gasoline), are available for use in Flex Fuel vehicles, which are specifically designed to run on fuels containing higher percentages of ethanol.

However, there are also some challenges associated with the use of ethanol as a fuel. For example, ethanol has a lower energy density than gasoline, which means that vehicles require a larger volume of ethanol to store the same amount of energy as gasoline. This results in reduced fuel efficiency and increased fuel costs for consumers. Additionally, the production of ethanol from crops like corn can have negative impacts on food prices and can be resource-intensive.

D. Compressed Air

Compressed air energy storage (CAES) is a technology that stores energy in the form of compressed air. This technology involves compressing air and storing it in underground cavities, such as depleted natural gas fields, or in above-ground tanks. When the stored air is needed, it is released and expanded through a turbine, generating electricity.

One of the main advantages of CAES as a form of energy storage is its high efficiency. Unlike batteries, which can lose a significant amount of energy as heat during charging and discharging, CAES can store and release energy with minimal losses. Additionally, CAES can provide a large amount of stored energy in a relatively small amount of space, making it well-suited for use in urban areas where space is limited.

Another advantage of CAES is that it can be used to store energy from renewable sources, such as wind and solar power, which can be intermittent and unreliable. By storing energy when it is abundant and releasing it when it is needed, CAES can help to stabilize the power grid and ensure that energy is available when it is needed.

Despite these advantages, there are also some challenges associated with the use of CAES. For example, the technology requires a large amount of energy to compress air, which can limit its overall efficiency. Additionally, the release of compressed air can also produce significant noise, which can be a problem in densely populated areas

E. Hydrogen

Hydrogen is a promising alternative fuel for transportation, and many researchers and industries have been exploring its use in fuel cell vehicles. Fuel cell vehicles use hydrogen as a fuel to generate electricity through a chemical reaction with oxygen, which powers an electric motor.

One of the main advantages of hydrogen as a fuel for transportation is that it produces zero emissions when used in a fuel cell vehicle. Unlike internal combustion engines, which produce harmful pollutants such as carbon monoxide and nitrogen oxides, fuel cell vehicles produce only water vapor as a byproduct. Additionally, hydrogen is a versatile fuel that can be produced from a variety of sources, including natural gas, biomass, and water, making it a potentially renewable and sustainable option.

Another advantage of hydrogen as a fuel is its high energy density. Hydrogen has a much higher energy content than traditional battery technologies, which means that hydrogen-powered vehicles have the potential to have a longer driving range and faster refueling times compared to electric vehicles.

However, there are also some challenges associated with the use of hydrogen as a fuel. For example, the production and storage of hydrogen can be expensive, and there is currently a limited infrastructure for producing and distributing hydrogen fuel. Additionally, the development of fuel cell vehicles and hydrogen refueling infrastructure is still in its early stages, which makes it difficult for consumers to adopt the technology.

F. Natural Gas (CNG & LNG)

Natural gas is a promising alternative fuel for transportation, and has been used as a fuel for vehicles for many years. Natural gas vehicles (NGVs) are powered by compressed natural gas (CNG) or liquefied natural gas (LNG), and can offer several advantages compared to conventional gasoline or diesel vehicles.

One of the main advantages of natural gas as a fuel is its low cost. Natural gas is typically less expensive than gasoline or diesel, which makes it an attractive option for fleet operators and individual consumers. Additionally, natural gas has a lower carbon content compared to gasoline or diesel, which means that NGVs produce fewer greenhouse gas emissions when used as a fuel.

Another advantage of natural gas as a fuel is its abundance. Natural gas is widely available in many countries, and is produced domestically in many regions, which reduces dependence on foreign oil. Additionally, natural gas can be produced from a variety of sources, including conventional natural gas wells, coalbed methane wells, and shale gas formations, making it a potentially sustainable and renewable option.

However, there are also some challenges associated with the use of natural gas as a fuel for transportation. For example, the infrastructure for producing and distributing natural gas as a fuel for vehicles is still limited in many areas, which makes it difficult for consumers to adopt the technology. Additionally, natural gas vehicles are typically more expensive than conventional gasoline or diesel vehicles, which can be a barrier to adoption.

G. Propane (LPG – Liquefied Petroleum Gas)

Propane, also known as liquefied petroleum gas (LPG), is a popular alternative fuel for vehicles. It is a clean-burning and domestically-produced fuel that offers several benefits compared to traditional gasoline and diesel fuels.

Advantages of using propane as a vehicle fuel include:

- Lower emissions: Propane produces fewer harmful emissions compared to gasoline and diesel, which makes it a more environmentally-friendly fuel. When used as a vehicle fuel, propane reduces carbon monoxide, hydrocarbon, and nitrogen oxide emissions by approximately 20-30%.
- Lower fuel costs: Propane is typically less expensive than gasoline or diesel on a per-gallon basis. This can result in significant cost savings for consumers, particularly for those who cover a lot of miles in their vehicles.
- Improved engine performance: Propane is a high-octane fuel that provides a consistent and reliable power source for vehicles. It helps to improve engine performance and provides a smoother, quieter ride compared to gasoline or diesel.
- Domestic production: Propane is domestically produced in the United States, which reduces dependence on foreign oil.
- Wide availability: Propane is widely available in the United States and can be found at a large number of fueling stations. This makes it a convenient fuel option for many drivers.

However, there are also some disadvantages of using propane as a vehicle fuel, including:

- Lower energy density: Propane has a lower energy density compared to gasoline and diesel, which means that vehicles need more fuel to travel the same distance.
- Range limitations: Vehicles running on propane typically have a shorter range compared to gasoline or diesel vehicles. This can be a problem for long-distance travelers.
- Refueling infrastructure: Although propane is widely available, the refueling infrastructure is not as developed as for gasoline and diesel. This can make it more difficult for drivers to find a propane refueling station, particularly in rural areas.

Propane is a clean-burning, domestically-produced alternative fuel that offers several advantages for vehicles, including lower emissions, lower fuel costs, improved engine performance, and widespread availability. However, it also has some disadvantages, such as lower energy density, range limitations, and a less-developed refueling infrastructure.

H. Electricity

Electricity is a rapidly growing alternative fuel for vehicles. Electricity is considered as an alternative fuel under energy policy act of 1992. Electricity is a type of alternative fuel for vehicles that is rapidly growing in popularity due to its various benefits and benefits to the environment. Electric vehicles (EVs) operate by storing electrical energy in batteries, which are then used to power an electric motor. The electrical energy is generated from renewable sources, such as wind or solar power, or from conventional sources, such as coal or natural gas. The electric vehicle converts electric energy stored in batteries to mechanical energy using electric motors. It offers several advantages over traditional gasoline and diesel fuels.

Advantages of using electricity as a vehicle fuel include:

- Zero emissions: Electric vehicles produce zero tailpipe emissions, making them a clean and environmentally-friendly alternative to gasoline and diesel vehicles.
- Low operating costs: The cost of charging an electric vehicle is typically less than the cost of refueling a gasoline or diesel vehicle, which can result in significant cost savings for consumers.
- Improved efficiency: Electric vehicles are highly efficient, with energy conversion rates of up to 80-90%, compared to 20-30% for gasoline or diesel vehicles. This translates into longer driving ranges and lower energy costs.
- Quiet operation: Electric vehicles are known for their quiet operation, which makes them an ideal choice for city driving.
- Reduced dependence on fossil fuels: By using electricity as a vehicle fuel, drivers can reduce their dependence on finite fossil fuels, and support the growth of renewable energy sources.

However, there are also some disadvantages of using electricity as a vehicle fuel, including:

- High upfront costs: Electric vehicles can be more expensive than gasoline or diesel vehicles, particularly when considering the cost of the batteries.

- Limited driving range: Electric vehicles have a limited driving range compared to gasoline or diesel vehicles, which can be a problem for long-distance travelers.
- Charging infrastructure: Although charging infrastructure is rapidly growing, it is still not as developed as the refueling infrastructure for gasoline and diesel. This can make it more difficult for drivers to find a charging station, particularly in rural areas.

Electricity is a promising alternative fuel for vehicles that offers several advantages, it has the potential to reduce dependence on fossil fuels, reduce harmful emissions and more. However, there are also some disadvantages, such as high upfront costs, limited driving range, and a less-developed charging infrastructure.

This is a major challenge in a country with not enough electricity like Nigeria and some other African countries.

I. Fuel Cell

A fuel cell is a form of battery that produces electricity through the electro-chemical reaction of fuel and oxygen, as opposed to burning fossil fuels. Energy can be produced from hydrogen using a technology called fuel cells. In a fuel cell, hydrogen can be used directly as fuel. [46-52]

Fuel cells are a type of alternative fuel for vehicles that convert hydrogen gas into electricity, which is then used to power an electric motor. Fuel cells offer several advantages over traditional gasoline and diesel fuels, and are considered to be a promising alternative for the transportation sector.

Advantages of using fuel cells as a vehicle fuel include:

- Zero emissions: Fuel cells produce zero tailpipe emissions, making them a clean and environmentally-friendly alternative to gasoline and diesel vehicles. The only byproduct of a fuel cell is water vapor.
- Long driving range: Fuel cell vehicles have a longer driving range compared to battery electric vehicles, which can be a problem for long-distance travelers.
- Fast refueling: Fuel cell vehicles can be refueled in a matter of minutes, which is much faster than charging an electric vehicle.
- Efficient energy conversion: Fuel cells have energy conversion rates of up to 60%, which is higher than the 20-30% conversion rate of gasoline and diesel vehicles.
- Reduced dependence on fossil fuels: By using hydrogen as a vehicle fuel, drivers can reduce their dependence on finite fossil fuels and support the growth of renewable energy sources.

However, there are also some disadvantages of using fuel cells as a vehicle fuel, including:

- High upfront costs: Fuel cell vehicles can be more expensive than gasoline or diesel vehicles, particularly when considering the cost of the fuel cell stacks and hydrogen storage systems.

- Limited hydrogen infrastructure: The hydrogen refueling infrastructure is not as well developed as the gasoline or diesel refueling infrastructure, which can make it more difficult for drivers to find a refueling station.
- Hydrogen production: Currently, the majority of hydrogen is produced from fossil fuels, which negates some of the environmental benefits of using fuel cells as a vehicle fuel. However, hydrogen can also be produced from renewable sources, such as wind or solar power.

Fuel cells are a promising alternative fuel for vehicles that offer several advantages, including zero emissions, long driving range, fast refueling, efficient energy conversion, and reduced dependence on fossil fuels. However, there are also some disadvantages, such as high upfront costs, limited hydrogen infrastructure, and the challenge of producing hydrogen from renewable sources.

4.0 Conclusion

In conclusion, there are several alternative fuels available for use in automobiles, each with its own unique advantages and disadvantages as we can see during the course of this research paper. Some of the most promising alternative fuels include electricity, propane, and fuel cells.

Electricity is a clean and efficient alternative fuel for vehicles, with zero tailpipe emissions and high energy conversion rates. However, EVs can be more expensive than gasoline or diesel vehicles, and have a limited driving range compared to gasoline or diesel vehicles. EVs are not really recommended In African countries where electricity is less stable, it can also be relatively expensive.

Propane is a domestically produced alternative fuel that is widely available and has a low carbon footprint. Propane vehicles have lower emissions than gasoline or diesel vehicles, and are less expensive to operate than EVs. However, propane vehicles have a limited driving range compared to gasoline or diesel vehicles.

Fuel cells are a promising alternative fuel for vehicles that offer several advantages, including zero emissions, long driving range, fast refueling, and efficient energy conversion. However, fuel cell vehicles can be more expensive than gasoline or diesel vehicles, and the hydrogen refueling infrastructure is not as well developed as the gasoline or diesel refueling infrastructure.

Based on these factors, it is recommended that individuals and organizations consider their specific needs and requirements when choosing an alternative fuel for their vehicles. For those looking for a clean and efficient alternative to gasoline or diesel, an EV may be the best option. For those looking for a domestic alternative fuel with a low carbon footprint, propane may be the best choice. For those looking for a long driving range and fast refuelling, a fuel cell vehicle may be the best option. Cheaper options may include methanol and ethanol.

Ultimately, the best alternative fuel will depend on individual circumstances and priorities. While there is no one-size-fits-all answer, the study's findings suggest that a combination of alternative fuels can pave the way to lowering reliance on fossil fuels and minimizing the harmful effects of our regular fossil fuels on the environment. The study emphasizes the necessity of spending money on research & development, as well as on legislation and infrastructure that would hasten the transition to a cleaner and more sustainable transportation industry.

5.0 References:

[1] International Energy Agency. (2020). Transportation. Retrieved from https://www.iea.org/topics/transportation
[2] U.S. Department of Energy. (2019). Fossil fuels - non-renewable energy. Retrieved from https://www.energy.gov/science-innovation/energy-sources/fossil-fuels
[3] U.S. Environmental Protection Agency. (2021). Oil spills. Retrieved from https://www.epa.gov/oil-spills
[4] U.S. Energy Information Administration. (2021). Fossil fuels. Retrieved from https://www.eia.gov/energy/fossil-fuels/
[5] European Alternative Fuels Observatory. (2021). Electric vehicles. Retrieved from https://www.afdc.energy.gov/vehicles/electric_vehicles.html
[6] International Energy Agency. (2020). Transportation. Retrieved from https://www.iea.org/topics/transportation
[7] National Biodiesel Board. (2020). Biodiesel basics. Retrieved from https://www.biodiesel.org/about-biodiesel/biodiesel-basics
[8] National Renewable Energy Laboratory. (2019). Alternative fuels data center. Retrieved from https://www.afdc.energy.gov/
[9] U.S. Department of Energy. (2019). Electric vehicles. Retrieved from https://www.energy.gov/eere/electricvehicles/electric-vehicles
[10] U.S. Department of Energy. (2021). Hydrogen and fuel cells. Retrieved from https://www.energy.gov/eere/fuelcells/hydrogen-and-fuel-cells
[11] U.S. Energy Information Administration. (2021). Renewable & alternative fuels. Retrieved from https://www.eia.gov/topics/renewable_sources/renewable_alternative_fuels/
[12] Cantrell, J. (2017). A brief history of the steam engine. Retrieved from https://www.popularmechanics.com/technology/news/a25860625/steam-engine-history/
[13] Sperling, D., & Gordon, D. (2009). Two billion cars: Driving toward sustainability. Oxford University Press.
[14] U.S. Department of Energy. (2020). Ethanol: A renewable fuel made from corn and other plant materials. Retrieved from https://www.energy.gov/eere/bioenergy/ethanol-renewable-fuel-made-corn-and-other-plant-materials
[15] Department of Energy. (2021). Alternative Fuels Data Center. Retrieved from https://afdc.energy.gov/fuels/
[16] International Energy Agency. (2021). Alternative fuels for road transport. Retrieved from https://www.iea.org/reports/alternative-fuels-for-road-transport
[17] The National Renewable Energy Laboratory (NREL). Detailed information on biodiesel production, properties, and performance, as well as information on the benefits and challenges of using biodiesel as a transportation fuel. Retrieved from https://www.nrel.gov/
[18] The U.S. Department of Energy's Alternative Fuels Data Center (AFDC). Comprehensive information on alternative fuels, including biodiesel. Retrieved from https://afdc.energy.gov/
[19] The American Biodiesel Board (ABB). Information on the production, properties, and benefits of biodiesel, as well as the latest industry news and research: https://www.biodiesel.org/
[20] The European Biodiesel Board (EBB). Information on the production, properties, and benefits of biodiesel. Retrieved from https://www.ebb-eu.org/
[21] Methanol Institute. (n.d.). About Methanol. Retrieved from https://www.methanol.org/about-methanol

[22] United States Department of Energy. (n.d.). Alternative Fuels Data Center - Methanol. Retrieved from https://afdc.energy.gov/fuels/methanol
[23] Wu, Y., Fan, X., & Ma, L. (2017). Methanol as a transportation fuel: Status, challenges and prospects. Renewable and Sustainable Energy Reviews, 68, 638-646.
[24] Zhang, X., Zhang, D., & Wei, D. (2018). Methanol as a promising alternative fuel for transportation: A review. Renewable and Sustainable Energy Reviews, 81, 2307-2319.
[25] Thomas, R. J., & Holmberg, M. (2017). Life cycle greenhouse gas emissions of methanol and diesel fuels used in heavy-duty vehicles in the United States. Journal of Cleaner Production, 142, 1418-1425.
[26] U.S. Department of Energy. (n.d.). Alternative Fuels Data Center - Ethanol. Retrieved from https://afdc.energy.gov/fuels/ethanol_blends.html
[27] National Renewable Energy Laboratory. (n.d.). Ethanol. Retrieved from https://www.nrel.gov/research/ethanol.html
[28] Renewable Fuels Association. (n.d.). Ethanol Basics. Retrieved from https://www.ethanolrfa.org/resources/ethanol-basics/
[29] Al-Sadat, A. H., & Yusoff, I. (2017). Ethanol as an alternative fuel: A review of current status and prospects. Renewable and Sustainable Energy Reviews, 70, 13-22.
[30] Zhang, Y., & Fan, W. (2018). Life cycle assessment of corn-based ethanol production in the United States. Journal of Cleaner Production, 172, 2703-2712.
[31] International Energy Agency. (2017). Compressed Air Energy Storage (CAES). Retrieved from https://www.iea.org/reports/compressed-air-energy-storage-caes
[32] U.S. Department of Energy. (n.d.). Energy Storage Systems - Compressed Air Energy Storage. Retrieved from https://www.energy.gov/eere/storage/compressed-air-energy-storage
[33] Li, Y., & Wang, J. (2019). Compressed air energy storage systems: A review. Renewable and Sustainable Energy Reviews, 106, 136-149.
[34] Stine-Morrow, E. A. L., & Basu, S. (2017). Compressed air energy storage and the future of renewable energy. Renewable and Sustainable Energy Reviews, 69, 489-501.
[35] Fan, Z., Li, Y., Li, J., & Wang, J. (2017). A comprehensive review of compressed air energy storage systems. Applied Energy, 189, 708-719.
[36] U.S. Department of Energy. (n.d.). Hydrogen & Fuel Cells. Retrieved from https://www.energy.gov/eere/fuel-cells/hydrogen-and-fuel-cells
[37] National Renewable Energy Laboratory. (n.d.). Hydrogen and Fuel Cells. Retrieved from https://www.nrel.gov/research/hydrogen-fuel-cells.html
[38] European Commission. (2021). Hydrogen as a fuel for transport. Retrieved from https://ec.europa.eu/info/strategy/priorities-2019-2024/european-green-deal/actions-being-taken-eu/hydrogen-fuel-transport_en
[39] Haeseong, J., & Jang-Juan, L. (2019). A review of hydrogen fuel cell vehicles: Current status and future prospects. Renewable and Sustainable Energy Reviews, 102, 796-808.
[40] Lim, H. S., Kim, J., & Kim, S. (2019). Current status and future prospects of hydrogen as an energy carrier. Renewable and Sustainable Energy Reviews, 107, 343-360
[41] U.S. Department of Energy. (n.d.). Natural Gas Vehicles. Retrieved from https://www.afdc.energy.gov/fuels/natural_gas.html
[42] Natural Gas Vehicles for America. (n.d.). Benefits of Natural Gas. Retrieved from https://www.ngvamerica.org/benefits/
[43] Natural Gas Europe. (2021). Natural Gas Vehicles. Retrieved from https://www.naturalgaseurope.com/natural-gas-vehicles
[44] Ahn, K. J., & Lee, J. H. (2017). Natural gas vehicles: Status, challenges, and prospects. Energy Policy, 104, 449-456.
[45] Kumar, A., & Dale, B. E. (2016). Natural gas as a transportation fuel: Benefits and challenges. Renewable and Sustainable Energy Reviews, 55, 807-816.
[46] National Renewable Energy Laboratory. (2019). Understanding Electric Vehicle Charging. Retrieved from https://www.nrel.gov/docs/fy19osti/75188.pdf

[47] Union of Concerned Scientists. (2021). Electric Cars: Pros and Cons. Retrieved from https://www.ucsusa.org/resources/electric-cars-pros-and-cons
[48] International Energy Agency. (2021). Global EV Outlook 2021: Energy Access Outlook. Retrieved from https://www.iea.org/reports/global-ev-outlook-2021-energy-access-outlook.
[49] National Renewable Energy Laboratory. (2021). Hydrogen and Fuel Cells. Retrieved from https://www.nrel.gov/hydrogen/
[50] US Department of Energy. (2021). Fuel Cells: What You Need to Know. Retrieved from https://afdc.energy.gov/fuels/fuel_cells.html
[51] Union of Concerned Scientists. (2021). Fuel Cells: Pros and Cons. Retrieved from https://www.ucsusa.org/resources/fuel-cells-pros-and-cons
[52] International Energy Agency. (2021). Global Fuel Cell Outlook 2021. Retrieved from https://www.iea.org/reports/global-fuel-cell-outlook-2021.

NIPES-NCEE Conference Proceedings
The 2nd International Conference 15th-17th Feb. 2023
725-741
www.nipesjournals.org.ng

A COMPARATIVE INVESTIGATION OF THE EFFECT OF DRY QUENCHING AND WET QUENCHING ON THE CORROSION SUSCEPTIBILITY OF AISI 1018 STEEL IN MARINE ENVIRONMENT

O. Awheme[1, *], G. O. Okosun[2], T. Uwanogho[3], K. O. Urhibo[4], G. Ojeru[5]

[1,2,3,4,5] Mechanical Engineering Department, University of Benin, P.M.B 1154, Benin City, Nigeria

*Corresponding author Tel.: +2348066772354

E-mail address: oghenerobo.awheme@uniben.edu

Abstract

This paper presents the result on the investigation of the effect of dry and wet quenching on the corrosion susceptibility of low carbon steel exposed to seawater. The samples of the steel were subjected to heat treatment involving austenizing at 870oC, the soaking time was 13 minutes, then dry quenching was done in ash and sand and wet quenching was done in oil and water to room temperature, there were control samples which were not heat treatment (as-received). The microstructural examinations were carried out. The weight loss and corrosion rate were calculated at 10 days interval for 40 days after immersion in marine environment. Eight samples were dry quenched another eight were wet quenched and four were the control sample. The results obtained from the samples immersed in the seawater showed that the samples from wet quenching medium showed the lowest weight loss of 0.08g for water and 0.114g for oil, followed by samples from dry quenching medium which gave 0.297g for sand and 0.353g for ash, and then the control sample gave the highest weight loss to be 0.385g. The samples from wet quenching medium also showed the lowest corrosion rate of 0.033mm/yr for water and 0.069mm/yr for oil, followed by samples from dry quenching medium which gave 0.122mm/yr for sand and 0.13mm/yr for ash and then the control sample which gave the highest corrosion rate to be 0.144mm/yr. The corrosion test results indicated that the wet quenched steel showed better corrosion resistance over the entire exposure periods when compared to the dry quenched and the control steel samples. It was therefore recommended that the samples specifically from water quenching medium are preferred over other quenching medium for corrosion resistance in marine environment for low carbon steel.

Keywords: *Dry Quenching, Wet Quenching, AISI 1018 Steel, Corrosion, Marine environment*

1. Introduction

Steel, a major alloy element containing carbon and iron is known to be one of the most important elements in engineering industries because of the wide range of applications especially plain carbon steel [1]. Plain carbon steel is a type of steel which contains very small amount of impurities or alloying elements and their biggest advantage is the fact that they have very low cost of production [2]. Low carbon steel has carbon content of 0.002% - 0.25%. Low carbon steel is the most common type of steel as its price is relatively low while it provides material properties that are acceptable for many applications. It is neither externally brittle nor ductile due to its low carbon content. It has lower tensile strength and malleable [2].

Heat treatment involves the application of heat, to a material to obtain desired material properties (e.g. mechanical, corrosion. electrical, magnetic, e-t-c.). During the heat treatment process, the material usually undergoes phase microstructural and crystallographic changes [3]. The purpose of heat treating carbon steel is to change the mechanical properties of steel, usually ductility, hardness, yield strength tensile strength and impact resistance. The electrical, corrosion and thermal conductivity are also altered during heat treatment process. Heat treatment uses phase transformation during heating and cooling to change a microstructure in a solid state. In heat treatment, the processing is most often entirely thermal and modifies only structure [4, 5].

Corrosion is the passage of metal into a chemically combined state and it occurs naturally immediately after a metal has been extracted from its ore [6, 7]. It is the gradual destruction of materials by chemical and/or electrochemical reaction with their environment. Corrosion in other words is the disintegration of engineering material into its constituent atom due chemical reaction with its environment [2]. In marine environment corrosion is more effective than in terrestrial environment because of its pH, oxygen concentration, presence of salts and other element such as chloride, sulphate etc [8, 9]. There are different types of corrosion but the major kind of corrosion that occurs in marine environment includes galvanic corrosion pitting corrosion and crevice corrosion [10]. The effect of corrosion cuts across all industries. In the oil and gas industry, the cost attached to corrosion is about $1.4 billion in oil and gas exploration and production [11].

Marine environment is simply salt water environment, they include the oceans, seas bays, estuaries, and other major water bodies, including their surface interface and interaction, with the atmosphere and with land seaward of the mean high mark. The selection of a proper material, for engineering purposes in marine environment, is one of the most difficult problems for the designer. The best material is one which serves the desired objective at the minimum cost. Marine environment enhances the rate of corrosion [12]. Due to the corrosiveness of the marine environment and the susceptibility of low carbon steel to corrosion, there is therefore the need to investigate the effect dry quenching and wet quenching on the corrosion susceptibility of AISI 1018 steel in marine environment.

Materials and methods

2.1. Materials

The materials used for this research work is mild steel (AISI/SAE 1018), with the chemical composition shown in Table 1 was sourced from Premium Steel and Mines Company Limited located in Ovwian Aladja, Delta State).

2.2. Methods

2.2.1. Chemical Analysis of Sea Water

The sea water sample was gotten from Lekki Beach Lagos State. The chemical analysis of the sea water was carried out at the Department of Chemistry, University of Benin. The results of the analysis are shown in Table 2.

2.2.2 Chemical Analysis of Ash

The ash that was used for the dry quenching medium was wood ash, the analysis was carried out at the Department of Chemistry, University of Benin. The results of the analysis are shown in Table 3.

2.2.3 Test Samples Preparation for Heat Treatment

The low carbon steel was machined with the aid of a lathe machine and been a rib steel it was first de-ribbed on a lathe machine for easier calculation. First it was mounted on a 3 jaw chuck, facing was done to smoothen the surface and lastly it was de-ribbed. The sample was cut into 30 pieces; each piece was 50 mm in length and 14 mm in diameter. The sample was divided into three groups, first group is for dry quenching involving ash and sand, the second is for wet quenching involving water and oil and the third is for control samples for both dry and wet quenching.

2.2.4 Heat Treatment

The heat treatment was carried out using a muffle furnace. The sample were heated to an austenitic temperature of 870^{o}C with a soaking time of 13 minutes. The samples for dry quenching were then cooled in ash and sand to room temperature and the sample for wet quenching were cooled in water and oil to room temperature while the control samples were not heat treated.

2.2.5 Determination of Corrosion Susceptibility from Weight Loss Measurements

The samples from the various quenching medium and the control samples were fully immersed in seawater in separate containers and well labeled. The one from ash quenching medium was labeled 'ASH', the one from sand was labeled 'SAND', the one from oil was labeled 'OIL' and the one from water was labeled 'WATER'. The samples were immersed in sea water for 40 days, but their initial weight was gotten using an electronic weighing balance before it was immersed in the sea water environment. The weight losses of the samples (a measure of difference between the original mass of the sample before immersion, M_1 and the mass of the same sample after exposure, M_2) were determined at an interval of 10 days. Corrosion rate was determined using the standard relation given by [13]:

$$Cr = \frac{K * \Delta W}{A * T * \rho} \quad (1)$$

Where;

Cr = corrosion (penetration) rate in mm/yr; ΔW = Weight loss in gram

A = Exposed surface are of coupon in cm^2; ρ = Density of steel in $g/cm^3 = 7.86 g/cm^3$

T = Time of exposure in hours; k = Constant for unit conversion = 8.76×10^4

Since the samples are cylindrical in shape, the total exposed area is given by:

$$A = 2\pi r^2 + 2\pi rl \quad (2)$$

Where r is the radius of the samples and l is the length.

The results of the weight loss and corrosion rate are presented in Figure 1, 2 and 3 respectively.

2.2.6 Microstructural Examination

In this experiment, the heat treatment and the control samples were examined. The samples were grinded at one end using 220, 320, 400, 600, 800 and 1000 grit papers. It was rotated at 90° when changing from one grade of paper to the other, until a very smooth surface was obtained. The surfaces were then polished using silicon carbide of 0.3 micron. This process continued until the surfaces had a mirror finish, sensibly free from surface roughness from cutting and grinding. The surfaces of the specimens were now etched using 2% Nital to reveal the grain boundaries. Etching involves cleaning the surface of the specimen with nitric acid solution further in order to clear the specimen surface of any disturbance. Optical metallurgical microscope fitted with a photographic device was used for the microstructural examination. The micrography was done at a magnification of x 200. The results are shown in Figure 4 – Figure 8.

3. Results and Discussion

3.1 Results

Table 1: Chemical composition of the low carbon steel substrate

Elements	C	Mn	Si	P	S	Cr	Cu
Composition (W %)	0.18	0.66	0.25	0.0445	0.047	0.21	0.023

Table 2: Results of Chemical Analysis of the Sea Water Sample

pH	7.38
Electronic conductivity (us/cm)	31.9
Total Alkalinity (mg/l)	0.00
Salinity (mg/l)	0.020
Total dissolved solid	1.60
Cl (mg/l)	177.5
SO_4 (mg/l)	42.918
Ca (mg/l)	51

Na (mg/l)	8200
Mg (mg/l)	0.12

Table 3: Chemical Analysis of the ASH Samples

pH	12.13
Electronic conductivity (us/cm)	15.53
Total Alkalinity (mg/l)	1456
Salinity (mg/l)	0.010
Total dissolved solid (mg/l)	0.78
Cl (mg/l)	71
SO_4 (mg/l)	-
Ca (mg/l)	0.00
Na (mg/l)	66.2
Mg (mg/l)	0.00

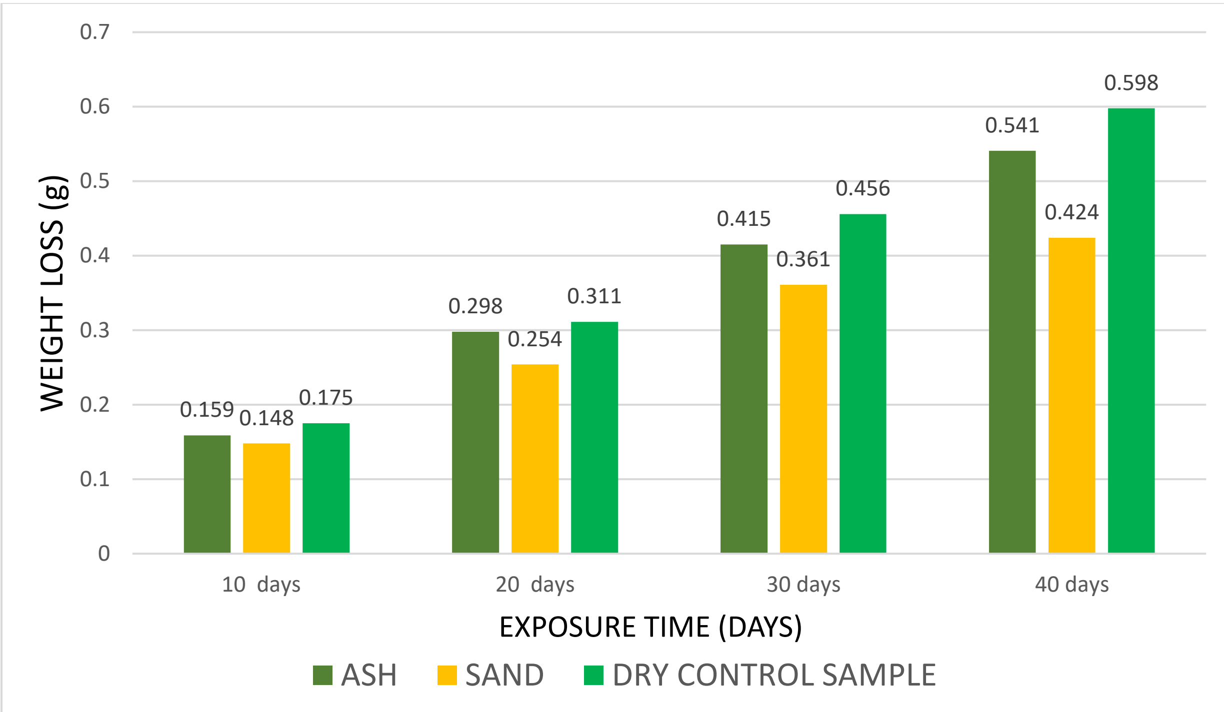

Figure 1: Plot of Weight Loss Against Exposure Time for The Dry Quenched and Control Samples with Constant Soaking Time Immersed in Marine Environment

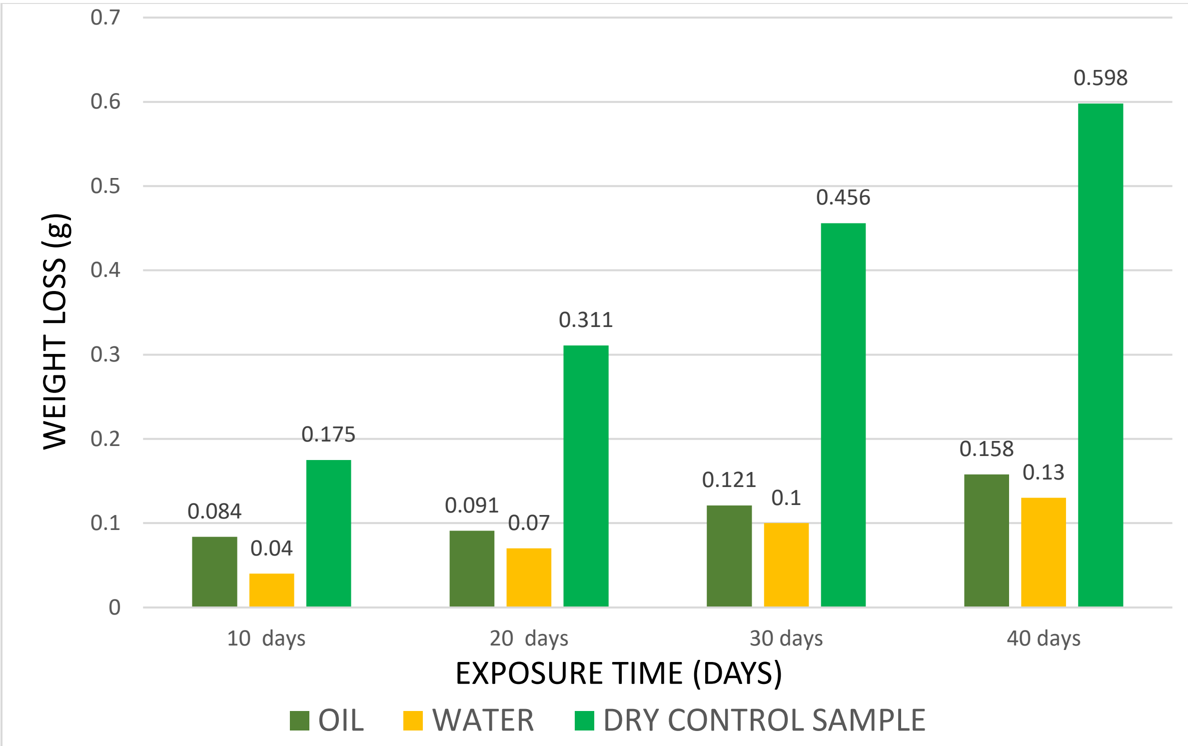

Figure 2: Plot of Weight Loss Against Exposure Time for The Wet Quenched and Control Samples with Constant Soaking Time Immersed in Marine Environment

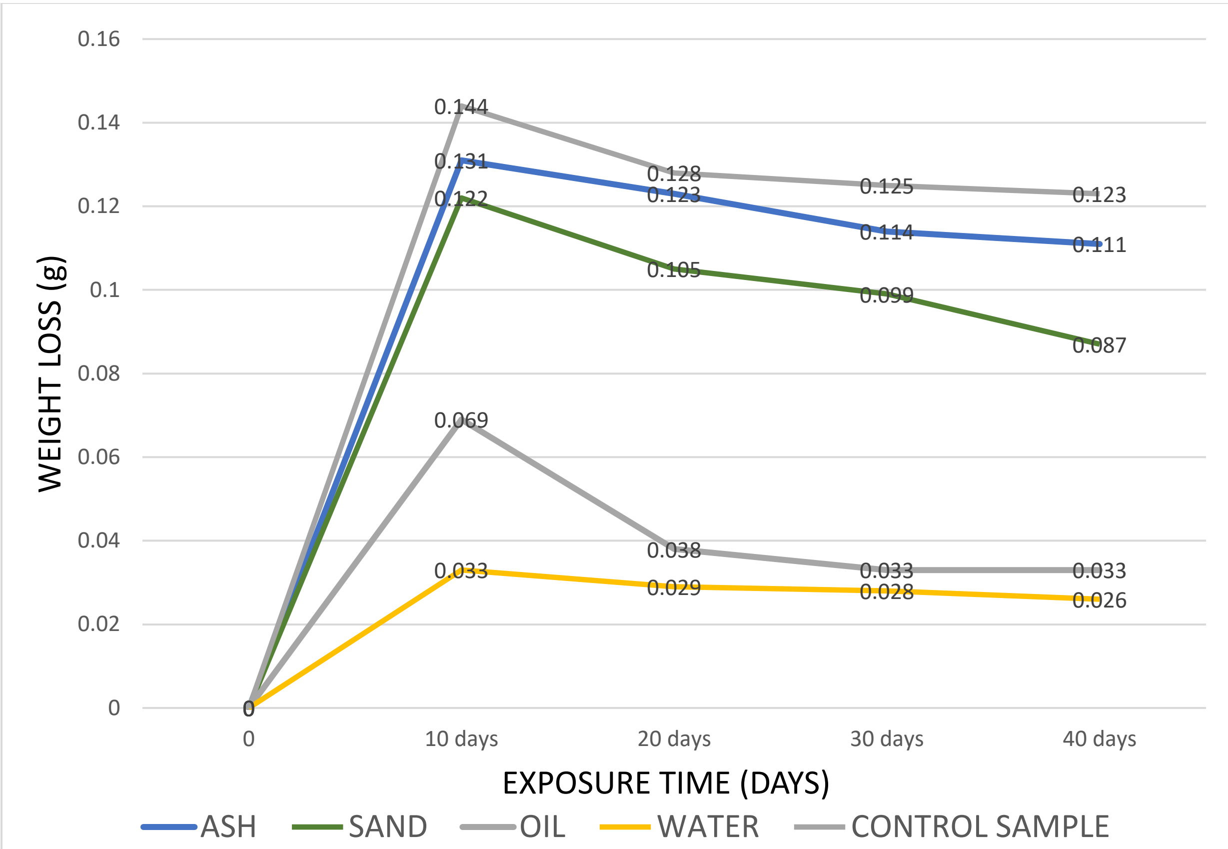

Figure 3: Plot of Corrosion Rate Against Exposure Time for The Heat Treated and Control Samples Immersed in Marine Environment

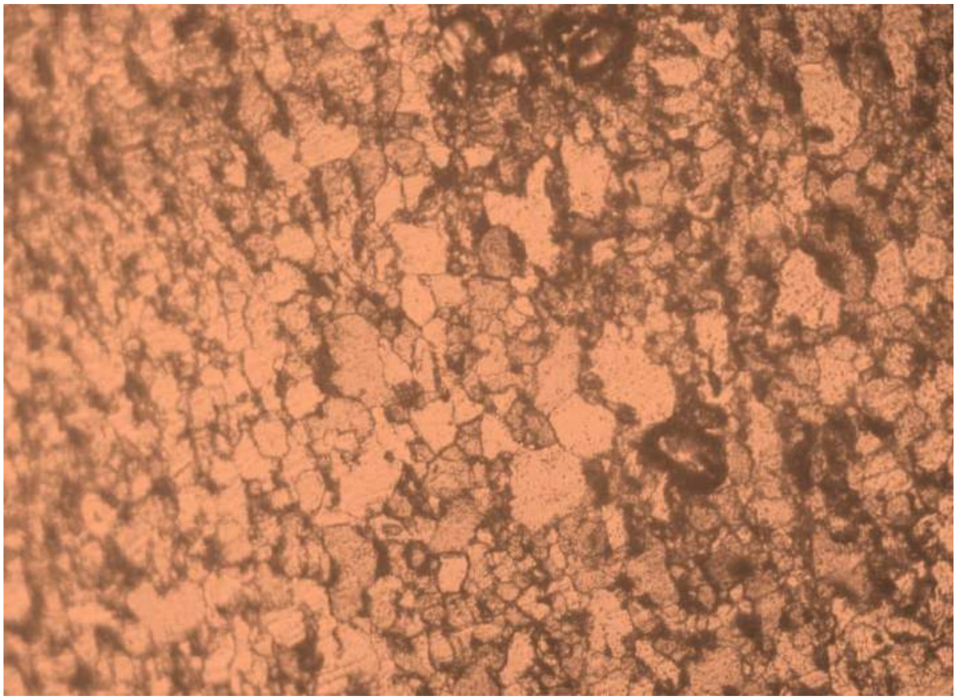

Figure 4: Optical microstructure of Control Samples after 40 days of Immersion in Marine Environment

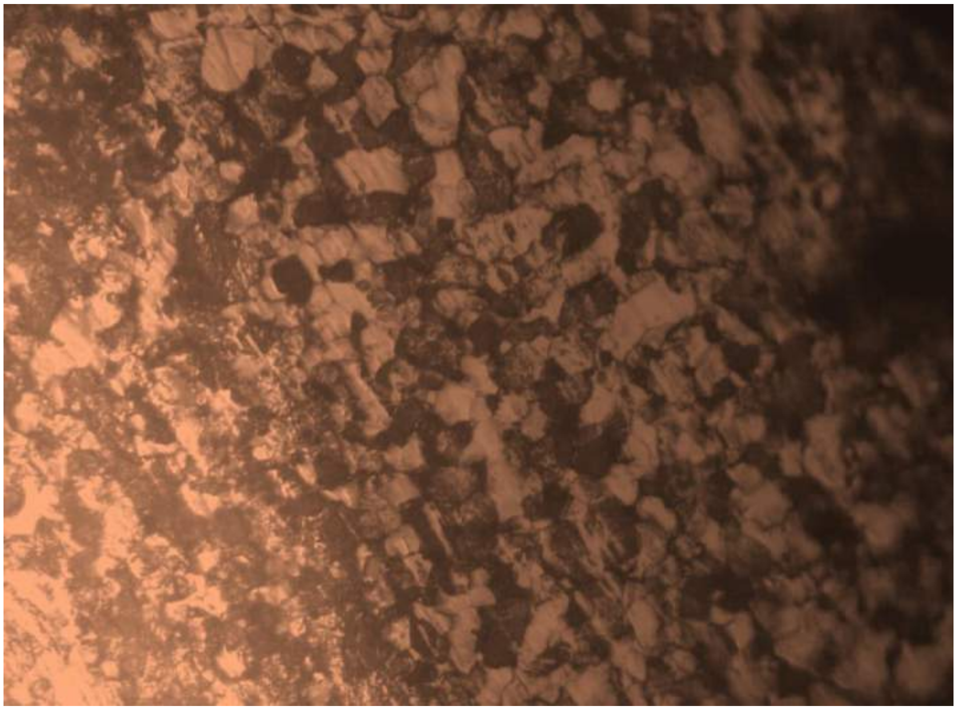

Figure 5: Optical microstructure of Ash Quenched Samples after 40 days of Immersion in Marine Environment

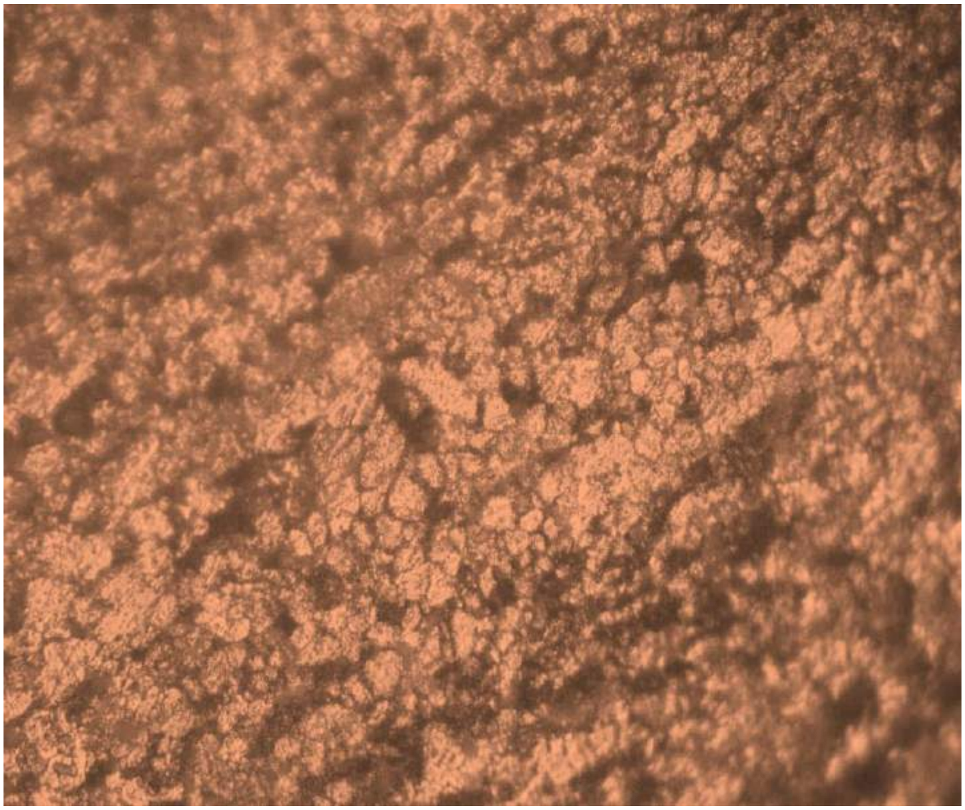

Figure 6: Optical microstructure of Sand Quenched Samples after 40 days of Immersion in Marine Environment

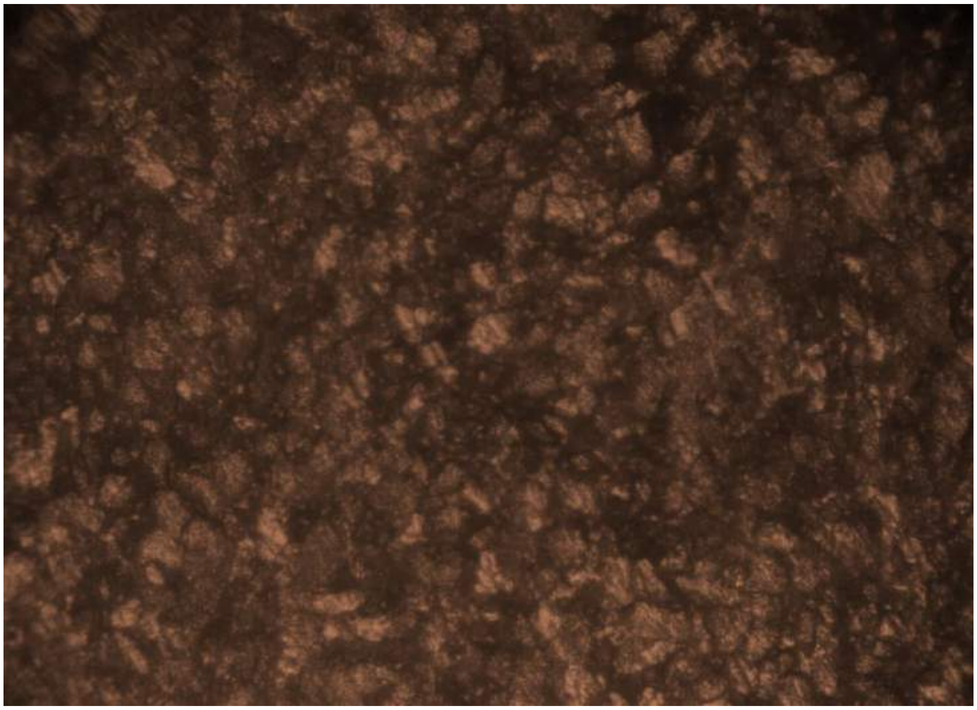

Figure 7: Optical microstructure of Water Quenched Samples after 40 days of Immersion in Marine Environment

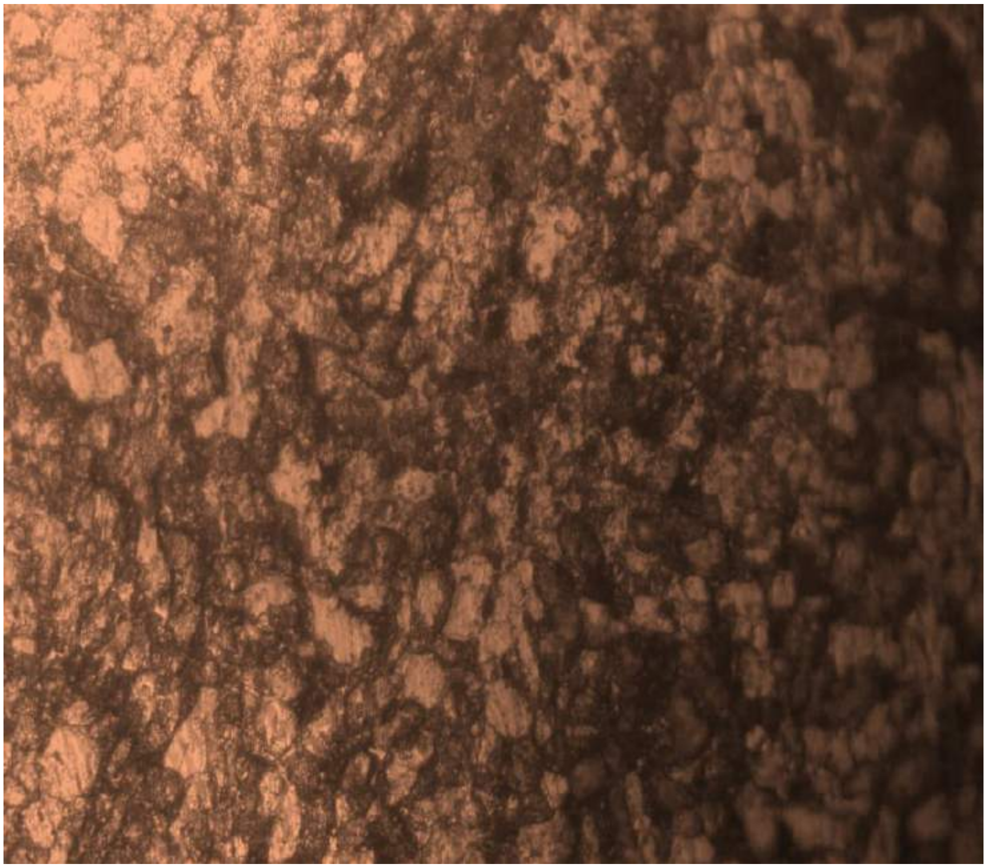

Figure 8: Optical microstructure of Oil Quenched Samples after 40 days of Immersion in Marine Environment

3.2 Discussion

3.2.1 Effect of the cooling medium on the corrosion behavior of the low carbon steel of 0.18%C in marine environment

The results of the investigation showed the existence of corrosion, because weight loss were evident, as it was observed that the weight loss increases with increase in exposure in time for the samples [14]. The weight loss of the samples was in the order: control sample > sample from ash quenching medium > sample from sand quenching medium > sample from oil quenching medium > sample from water quenching medium. This shows that control sample has a higher weight loss followed by the ash sample, then the sand sample then oil sample and finally the water sample. This evident is shown in Figure 1 and Figure 2, which showed the average weight loss of the control sample to be 0.385g, the ash sample to be 0.353g, the sand sample to be 0.297g, the oil sample to be 0.114g, while the water sample to be 0.08g.

The corrosion rate was observed to decrease with increase in exposure time for all the samples [15]. This can be seen from Figure 3, where the corrosion rate was found to increase rapidly with peak corrosion rate in the first 10 days of immersion in marine environment then after, it began to reduce gradually. The high rate of corrosion of all the samples could be attributed to the absence of passive films. But as the exposure time in days increases the samples begin to form a protective film and corrosion products. In quenching, the cooling medium is of great importance, when low carbon steel is quenched faster the strength increases thereby increasing the corrosion resistance [16]. From the investigation, this observation was evident in all the quenched samples with the water quenched samples displaying the least weight loss and also with the highest corrosion resistance.

3.2.2 Effect of Cooling Medium on The Microstructure of the Low Carbon Steel

From the result of the investigation, it can be seen clearly that the heat treatment processes have varied effect on the microstructure of low carbon steel. From Figure 4 to Figure 8, it is evident that the control samples produce a coarser ferrite and cementite microstructure, the ash samples produce coarse ferrite and cementite microstructure, the sand samples produce ferrite and cementite microstructure, water samples produce a martensitic microstructure with finely dispersed cementite and oil samples produces a coarse cementite microstructure in the ferrite matrix. The microstructure from water quenching medium produces the least corrosion rate followed by the microstructure of oil, sand, ash and then control sample with the highest corrosion rate. This is in agreement with the findings of [17] who in his research work observed that the more the cementite were uniformly dispersed in ferrite microstructure the more corrosion resistance it becomes The cooling media has a remarkable effect on the microstructure at room temperature [18-20].

4. Conclusion

From the results of the investigation carried out, the following conclusions were made:

1. The Control sample were more susceptible to corrosion than the heat treated steel samples in the marine environment.

2. The wet quenched steel sample had the best resistance to corrosion with regards to its corrosion rate when compared with the dry quenched samples.

3. The microstructure of the heat treated samples remarkably affects their susceptibility to corrosion attack.

References

[1] P. J. Cunat (2004). Alloying Elements in Stainless Steel and other Chromium-Containing Alloys. *Euro Inox*, *2004*, pp.1-24.

[2] R. Nyborg (2003). Corrosion Control in Oil and Gas Line. Institute for Energy Technology (ISE), Material and Corrosion Technology Department, 2nd Edition Norway.

[3] T. V. Rajan, C. P. Sharma and A. Sharma (1989). Heat Treatment Principle and Technique, Practice Hall of India. Private Ltd, New Delhi pp. 36- 58. In Senthilkumar T. and Ajiboye T. K. (2012). Effect of Heat Treatment Processes on the Mechanical Properties of Medium Carbon Steel. Journal of Minerals & Materials Characterization & Engineering, Vol. 11, No.2 pp.143-152, 2012.

[4] W. Hai-Yan, L. Jian-Hua, P. Gui-Rong and W. Wen-Kui (2010). Effects of High-Pressure Heat Treatment on the Solid-State Phase Transformation and Microstructures of Cu61. 13Zn33. 94Al4. 93 Alloys. *Chinese Physics B*, *19*(9), p.096203.

[5] B. V. Feujofack Kemda, N. Barka, M. Jahazi and D. Osmani (2021). Modeling of Phase Transformation Kinetics in Resistance Spot Welding and Investigation of Effect of Post Weld Heat Treatment on Weld Microstructure. *Metals and Materials International*, *27*, pp.1205-1223.

[6] U. Trdan, M. Hočevar and P. Gregorčič (2017). Transition from Superhydrophilic to Superhydrophobic State of Laser Textured Stainless Steel Surface and its Effect on Corrosion Resistance. *Corrosion Science*, *123*, pp.21-26.

[7] P. R. Roberge (2019). *Handbook of Corrosion Engineering*. McGraw-Hill Education.

[8] B. Valdez, M. Schorr, R. Zlatev, M. Carrillo, M. Stoytcheva, L. Alvarez, A. Eliezer and N. Rosas (2012). Corrosion Control in Industry. *Environmental and Industrial Corrosion-Practical and Theoretical Aspects*.

[9] K. A. Chandler (2014). *Marine and Offshore Corrosion: Marine Engineering Series*. Elsevier.

[10] J. E Pepper and D. F. Clark (1979). The Corrosion, Cleaning, Inspection and Repair of Storage Tanks in Crude Oil Service Bahrain. Society of Petroleum Engineers. DIO: https://doi.org/10.2118/7760-MS.

[11] H. K. Gerhadus, P. H. Michiel, C. C. Brongers, G. Niel (2001). Corrosion Costs and Preventive Strategies in the United. PUBLICATION NO. FHWA-RD-01-156: NACE, USA.

[12] G. Nayar Kishor, H. Sharqawy Mostafa, D. Banchik, Leonardo, LV. Ienhar and H. John (2016). “Thermophysical Properties of Seawater: A Review and Correlations that Include Pressure Dependence”. Desalination. 390: 1 – 24. Dio:10.1016/j.desal.2016.02.024.

[13] O. Awheme, G. U. Unueroh and I. M. Ibrahim (2018). "The Effect of Tempering Temperature on Corrosion of AISI 1045 Steel in 1M Sodium Chloride Environment. *Nigerian Journal of Technology (NIJOTECH).* Vol. 37, No. 3, pp. 640-646.

[14] E. Franzoni and E. Sassoni (2011). Correlation between Microstructural Characteristics and Weight Loss of Natural Stones Exposed to Simulated Acid Rain. *Science of the Total Environment*, *412*, pp.278-285.

[15] S. B. Lalvani and G. Zhang (1995). The Corrosion of Carbon steel in a Chloride Environment due to Periodic Voltage Modulation: Part I. *Corrosion Science*, *37*(10), pp.1567-1582.

[16] W. D. Jr. Callister (2007). Materials Science and Engineering: An Introduction (7th Edition). New York, USA: John Wiley & Sons, Inc.

[17] A. Kaynar, S. Gunduz and M. Turkmen (2013). Investigation on the Behaviour of Medium Carbon and Vanadium Microalloyed Steels by Hot Forging Test. *Journal of Materials and Design,* 51, 819-825.

[18] J. Han, A. K. da Silva, D. Ponge, D. Raabe, S. M. Lee, Y. K. Lee, S. I. Lee and B. Hwang, (2017). The Effects of Prior Austenite Grain Boundaries and Microstructural Morphology on the Impact Toughness of Intercritically Annealed Medium Mn Steel. *Acta Materialia*, *122*, pp.199-206.

[19] S. S. Al-Bermani, M. L. Blackmore, W. Zhang and I. Todd (2010). The Origin of Microstructural Diversity, Texture, and Mechanical Properties in Electron Beam Melted Ti-6Al-4V. *Metallurgical and Materials Transactions a*, *41*, pp.3422-3434.

[20] F. Ochoa, J. J Williams and N. Chawla (2003). Effects of Cooling Rate on the Microstructure and Tensile Behavior of a Sn-3.5 wt.% Ag Solder. *Journal of Electronic Materials*, *32*, pp.1414-1420.

NIPES-NCEE Conference Proceedings
The 2nd International Conference 15th-17th Feb. 2023
742-759
www.nipesjournals.org.ng

DEVELOPMENT OF AN ENVIRONMENTAL WASTE INFORMATION MANAGEMENT SYSTEM

[1]Amannah, Constance Izuchukwu and [2]Olorunda, Sunkanmi

[1&2]Department of Computer Science, Ignatius Ajuru University of Education Port Harcourt, Nigeria

E-mail: aftermymsc@yahoo.com

Abstract

Environmental pollution has been a major problem in the country, due to improper disposal of waste. As a result of the increase in urbanization coupled with the infrequent environment sanitation exercises some of the drainage systems in the country have been turned into dumps of all sorts of solid waste. The aim of the study was to develop of an environmental waste information management system. This study essentially modeled a waste management system using web-based technology, garbage truck weighing mechanisms, helping waste management agents in monitoring position of waste in the environment. The methodology adopted in the stud was the Object-Oriented System. It is adopted because it is an effective, efficient, reliable, reusable and a faster way of developing systems. The study was implemented using Hyper pre-processor (PHP) programming language linking it up with Microsoft Structured Query Language (MySQL) in Xamp and Javascript. The testing phase integrated the software application with the external computer peripherals devices in order to check how components interact with one another and with the system as a whole. This is also called End to End scenario testing. User have to create an account with the system before user can login. The study developed an environmental waste information management system, integrated the environmental waste information management system, implemented the environmental waste information management system and evaluated environmental waste information management.

1.0 Introduction

Waste Information management is the collection, transport, processing waste treatment, recycling or disposal of waste materials, usually ones produced by human activity, in an effort to reduce their effect on human health or local aesthetics or amenity. Many method of waste reduction had evolved over the years and the way they are done varies from one country to another and also with respect to the type of waste generated as well as the countries productivity strength. In Nigeria the only system that has just been launched is an automated web-based Early Warning System (EWS), which could be used in dealing with the destructive effects of persistent flooding in the country and this was launched in Lagos in the year 2011. This is an effort to combat the adverse effect of climate change for sustainable development, food security, and the wellbeing of the people. The major weakness of this system is its inability to show a spatial view of the waste collection sites and the appropriate collection time, to prevent overflow and blocking of drainages which results in flooding. In the proposed system user will register enter his house location where a waste user will send a message to the agent for deposition of the waste while some user can schedule out time and date for pick up at their place.

Environmental pollution has been a major problem in Nigeria, due to improper disposal of waste which has contributed to environment degradation. As a result of increased urbanization and infrequent environment sanitation exercises, urban resident dump solid wastes carelessly or haphazardly; anywhere they deem fit. Such disturbing tendencies and attributes many seem incomprehensible; if we desire to live in healthily environment. Some of the drainage system in the county has been turned into a dump site for human and all sorts of solid waste, with the constant pollution of the environment it is evident that human beings are being affected health wise thus calling for help and solution mechanisms. The current garbage collection management involves individuals who walk from, and to every household giving receipt of payments for garbage collection service. To get the service of the individuals or company, a resident or flat caretaker has to look for them and request for their service. For disposal, the collectors mainly consisting of youths, pick the waste and disposal it in landfills, some of whom are not even legal hence leading to pollution and environmental degradation.

The aim of this study was to develop environmental waste information management system. The following are the objectives of the study, to;

i. develop mechanism to report waste disposal within homes
ii. integrate the waste disposal mechanism with the database for effective information processing
iii. implement the integrated waste disposal mechanism using high level programming language
iv. test the integrated waste disposal mechanism.

This study will educate the general public, stakeholders in environmental management, student, and government and policy makers on the problems of solid waste management in Nigeria. This research will also serve as a resource base to other scholars and researchers interested in carrying out further research in this field.

There are categories describe to you in detail, so if you have a lipstick that you spent, he throws himself into the category of combustion, but after you remove it from the packaging and plastics dumped into the category of ‘small plastic and metal. Japan is a country-specific, because with 127 million people, on average, 336 people live in an area of 1 km^2. Logically Japan has to take care of as little use of land for the purpose of disposal. In the world’s major cities, there are 3.5 kg of waste per capita a day. With increased population and living standards, the waste also increases. According to the Basel Convention, the world annually produces about 4oo.ooo.ooo tons of hazardous waste. Military waste and radiochemical industry, which uses various raw materials and products that have hazardous properties is especially present. The production of hazardous waste can occur in combat, destruction of chemical plants in NHB accidents (transport, storage, accidents, natural disasters, and natural disasters) and so on. The harmful and dangerous contaminants working environment includes the physical (solid waste, dust, noise, vibrations), chemical (aerosols, gases, vapors, fumes, dust, waste), radiation (ionizing, UV, oils, infrared, radar, laser, ultrasound, x-ray) and biological (viruses, bacteria, mold, fungi, parasites, insects, rodents). Anthropogenic substances go into the environment in different ways. Wastewater is discharged into surface and underground waterways and basins.

Solid waste is stored in special landfills, buried and deposited in abandoned mines. Agriculture uses fertilizers and pesticides (about 70,000 different harmful and hazardous substances, and the list is supplemented annually with new 900-1000 terms). Synthesized new compounds that are not found in the working environment and living organisms are able to decompose (PVC materials). It is estimated that close to 40 million plastic bottles and bags, a large number of lost and discarded fishing nets, nylon and others float on seas and oceans [1].

A huge number of wastes are created by technological and technical activities, but several types are re-used: metal, plastic, paper, glass. A number of issues from environmental protection consider the re-use of materials: to reduce the need for primary raw materials, reduce the pollution of water and soil. Industrial waste is divided into;

i. Scrap,

ii. Waste wood,

iii. Waste plastics and other materials,

iv. Industrial waste. Ecologically beneficial and comprehensive technologies that reduce the amount of the primary production are developing. Non-waste technology should provide:

v. Development and production of new products, taking into account the possibility of re-use; - processing of production and everyday waste into new products; - The use of closed systems of industrial water supply [2].

Since solid waste consist of several types of waste, it is important to briefly examine the various forms and types of solid waste. Municipal Solid Waste (MSW) Municipal Waste as waste from households, as well as any other waste which, because of it nature or composition is similar to waste from households. This broader definition therefore considers waste from commercial premises to be municipal, where it is similar in composition to household waste.

MSWs are difficult to manage as the components are diverse, with materials such as metal, paper, glass and other organics mixed together [3]. Similarly, a study [4] revealed that the characteristics of MSW depend largely on the source however, in some countries, Turkey for example; nearly more than half of all MSW are recyclable materials while the recyclable constituents such as cardboard, paper, glass and plastics make up a significant percentage of the total municipal solid waste. The compositions of municipal solid include materials such as soil, garden and food waste, wood, paper, ashes, plastics, textiles and rubber [5]. They concluded that, municipal solid wastes are a collection of wastes that are mainly from household and commercial sources. Similarly, [6] added that, MSW mainly consist of food and garden waste, textiles, paper or cardboard, plastics, glass and metals. They argued that, due to the composition of MSW, the waste could easily be used for energy recovery or the production of fuel. Argued that, unlike other waste streams that are more homogeneous with a good percentage of each material, the composition of municipal solid waste are diverse and are generally prone to changes from city to city and country to country.

Construction Waste Solid waste from the construction industry one of the main waste streams in many countries. In Hong Kong, construction waste amounted to about 29,674.013 metric tons per day [7]. They pointed out that, most of the construction wastes produced in the country included both inert and non-inert materials. Furthermore, [8] pointed out that the huge volume of solid waste generated by the construction industry in Hong Kong is as a result of the limited availability of land in the country. They added that as a result of the boom in the construction of multi-story buildings in the city about 21.5 million tons of construction waste was produced in 2005. Similarly SEPA [9] reported that although the construction industry contribute about £10 billion to the Scottish economy yearly, the sector also produced a large percentage of solid waste which range from concrete, wood, metals, plastics, soils, glass among other materials. SEPA estimated that the industry generate about nine million tons of waste annually.

A similar trend is observed across the EU, the volume of construction waste is on the increase and the wastes produced are significantly high when compared to the total waste generated. For instance, figures from Eurostat, it is revealed that in 2008 Construction waste in the UK account for about 100,999,493 tons while in 2010, the sector contributed about 105,560, 291 tons of waste. Similarly, France produced 252,979,840 tons and 260,225,886 in 2008 and 2010 respectively while construction waste in Germany was 197,206,500 and 190, 990,217 tons in 2008 and 2010. Cumulatively the 27 member countries of the EU produce about 871,370,000 and 859,870,000 in 2008 and 2010 respectively [10]. European Environment Agency [11] reported that overall about 31% of all waste produced in the EU annually are construction waste. A report [12] revealed that construction and industrial waste amounted to about 50% of all waste produced in the EU in 2006. A study [13] found that on the average about 15% of solid waste land filled in Australia are generated from construction activities annually.

The huge waste produced by the construction industry in Australia adds to the cost of construction projects, mainly due to the strict control of landfills in Australia [14]. Most construction waste are produced from design/detailing errors, design changes, packaging waste, unused scrap materials among others. Similarly, [5, 8] observed that a good percentage of construction waste produced in the Netherland includes plastics, metal, wood and stones mainly from demolition and re construction activities. Furthermore, Barros and others found that apart from other waste produced during construction, about 1 million tons of sand is produced as waste annually, some of which are recycled.

Industrial wastes as waste produced as a result of the processing of raw materials for the production of new products. They pointed out that these could be in factories, mines or even mills. It has been reported that in Malaysia, Indonesia and Thailand a large percentage of the total solid waste arising is from palm oil processing [11]. The report found that, annually about 3.2 million metric tons of solid waste is produced in Thailand from the palm oil industry. The corresponding value for Malaysia and Indonesia 47 and 40 million tons respectively, the waste produced by the industry includes bunches fruits shells and palm. Different types of wastes produced by the industries; they added that some of the wastes are toxic while others are non-toxic.

Agricultural Solid Waste Generally, Agricultural solid wastes are many and are beyond the scope of this study. However, [13] noted that agricultural wastes are wastes arising from activities such as the rearing of livestock, sowing of plants and from milk production. Agricultural waste materials include animal manure, various crop residues and silage effluent. Agricultural wastes are mostly reusable in the energy and industrial sector. However, reported that inappropriate management of agricultural waste may lead to environmental hazard for example; high application of manure on land could pollute surface and ground water.

Commercial Waste Commercial waste is an important waste stream especially considering the vast amount of solid waste generated from this sector. In Northern Ireland, about 1.5 million tons of solid waste was generated by commercial and industrial activities in 2005. The report added that, commercial activities produced more than half of the total solid waste produced for that year. The result of a survey of industrial and commercial businesses in England [12, 14] shows that commercial waste accounted for about 11% of the total waste produced in 2002. Similarly, in Scotland, a survey [5] showed that retailing, wholesales, hotels and restaurants produced the largest volume of commercial waste in Scotland in 2006. The survey revealed that some areas of the country with a large concentration of businesses produced more business waste than other areas with fewer businesses. Glasgow and Clyde particularly produced higher percentages of waste than other areas. On the overall [5, 6] revealed that in 2009, the commercial sector contributed about 29% of the total waste to the total volume of controlled waste generated in Scotland. Commercial solid wastes are solid or semi-solid wastes produced as a result of activities in stores, restaurants, markets, offices, hotels, motels, print shops, service stations, auto repair shops among others [7].

A report [5, 6] pointed out that the retail sector covers various commercial activities from the sales of vehicles to household items in or outside stores. The report added that, most wastes produced from the sector are non-metallic with composition ranging from packaging materials to animal and vegetable waste. Generally, the type of materials sold influences the type of waste produced. A survey of grocery stores in Quebec, Canada, revealed that materials such as fruits, baked products, seafood, packaging materials and other frozen products make up a large amount of waste from grocery stores.

A report [10] pointed out that in 2008 alone; the retail sector generated about 1.4 million tons of packaging and food waste in the UK. In 2005 commercial activities such as retailing, wholesaling, public administration, real estates and other business activities produced about 459,285 tons of waste in Northern Ireland. A survey in Mexicali, Mexico [1, 9] revealed that a single store in Mexicali generated about 5,375kg of cartons and 339kg of plastics per week.

A survey [8, 9] pointed out that, one supermarket chain in Quebec spends about $6 million for waste disposal. Hence, suggested that, supermarkets should consider recycling and reusing as a waste management tool in other to recover some operational cost. 5. Waste Management Human interactions with the environment (human activities) have always resulted in waste production. However, [3, 9] reported that waste production and management was not a major issue until people began living together in communities.

It is obvious that there are certain factors that prevent environmental factors from developing and flourishing. It is not a fairy tells that despite the degradation of valuable land resources and creation of long-term environmental and human health problems, uncontrolled open dumping of waste products are still prevalent in most developing countries, which Nigeria is not excluded which indeed desperately need immediate action due to the associated detrimental effects to our communities and the environment. Most Nigerians are carefree about wastes management, and there is not enough awareness created to enable the citizens show a good deal of concern and take active part in preserving the environments.

There is no doubt that illiteracy forms part of the wastes management problems. When the citizens are literate, they will be more informed and able to take quality decisions that affect themselves and the generality of the people. When the citizens are not literate, they will not be able to comply with existing rules and regulations governing the effective disposal of wastes; they will also have very wrong attitudes to waste disposal initiatives. They will not be able to read some sign posts, such as “Do not dump wastes here”. They will not have both administrative and managerial personnel skilled that will efficiently plan and have the needed legal framework required to handle serious environmental issues regarding wastes management and improvements. The issue of rapid population growth is yet one of the problems affecting effective wastes management in Nigeria. This is because, as the population increases, so are wastes recklessly generated and the environment ultimately polluted, especially when there are no effective wastes disposal systems in place to cope with the quantity or volume of wastes generated daily. Additionally, the Nigerian citizens are very poor and do not have the sufficient funds to invest on infrastructure development that will enable them evacuate and recycle the wastes generated.

In concord to the above statement, a survey in Hong Kong, as [11, 12] claimed, revealed that the lack of interest to reuse waste in the hotel industry is as a result of the cost associated with the purchase of recycling materials. This goes to mean that lack of funds makes useless any other plans or measures put in place to curtail or curb the rate of wastes disposal within the environments irrespective of the country involved. The issue of uncontrolled urbanization will not be overlooked, as this seriously affects the environment and the populace, and lack of effective legal framework need not be overlooked to improve wastes management systems in Nigeria. Furthermore, the Nigerian government attitude towards the education sector poses another serious problem. It is when the educational institutions are adequately funded and research grants provided that scientific research will adequately take place. In a system where the education sectors are in shamble, with weak political will on the part of leading state officials, and the corruptive tendencies inbuilt in the political leaders, much room will be created for inefficient systems for data management and inaccurate planning for wastes management and disposal systems in Nigeria. Oftentimes, despite some laudable government agencies, plans and programs, because of problems of finance and its management strategies they fail woefully.

Stran land filling is the final destination of most waste produced from waste treatment and processing facilities. Strange, added that, other technologies merely serve the purpose of volume reduction or treatment before final disposal. There are different forms of approach to waste management. He added that, wastes streams with different characteristics may require different management approach. For instance, industrial waste might contain more hazardous materials than municipal waste streams. Hence, the management of these two waste streams might differ [13, 14].

Although waste management might differ between countries, there are some basic processes or paths that waste management needs to follows. These paths are illustrated in Figure 1, the study reported that, wastes generated must be gathered and stored by the generator in a place.

The municipal authorities or their agents collect the waste from the point of storage, for transportation to processing or disposal sites. The study added that, in some instances, the waste generators separate the waste into various materials from where they are collected for recycling by the recycling industries. Development embraces the following meanings: (1) development as structural transformation; (2) human development; (3) development of democracy and governance, and (4) development as environmental sustainability. But Development involves the positive changes that society has experienced throughout history, and still experiences; while Sharpley [9] in his contribution stated that development outlines the plans, policies, programs and activities undertaken by certain institutions, governments and other governmental and non-governmental organizations. Nevertheless, before delving into the nitty-gritty of the subject matter, it will be pertinent to define and explain the conceptual meaning of the major terms as listed hereunder. Waste: Waste, as asserted by [10, 13] is an essential product of human activities.

In concord, [11] posited that most human activities generate waste. According to researchers, the term “waste” is to a very large degree subjective in meaning, as the term is open to several interpretations and also influenced by personal opinion. This stems from the fact that a substance can only be regarded as a waste when the owner labels it as such. This is particularly true because one individual may regard a substance as waste, while another may view the same substance as a resource. As in the pre-historic times, as [8] noted that waste wasn’t a problem as the quantity generated was not much in commensurate with the small population, and immense amount of land was available to accommodate and also absorbed the waste generated without any form of degradation.

Nevertheless, in the sixties, the rate of waste started increasing due to the movement of persons from rural to urban areas, and in addition to- industrial revolution. This migration led to population explosion and industrial wastes led to variety in composition of wastes generated [13]. The production of wastes today remain a major source of concern to human existence, as the situation is no more the same; the pace and magnitude of waste generation have been constantly on increase, and so does the variety of the wastes (such as metals and glass) began to appear in large quantities. This unending increase in waste, which are indiscriminately littered and openly dumped on major roads, streets and corners have formed breeding grounds for rats and other pets in Nigeria. In concord, [14] also noted that it is no longer news that Nigerian cities are inundated with the challenges of unclean solid wastes. This act and uncontrolled manner of waste disposal by the generality of the public is currently posing great risk to human health, as several outbreaks of epidemics are recorded daily in our communities, thereby causing high death tolls in the country.

However, let us examine how some scholars defined the term “Waste”. Waste according to [13] is referred to as any matter, which has no further use, based on the composition (e.g., garbage, trash, junks, domestics or ashes), and it may be domestic, non- hazardous, hazardous or infectious. It has been conceptualized/ as the useless by-product of human activities, which physically contains the same substances that are available in the useful product.

Waste as an essential product of human activities, but also the result of inefficient production processes whose continuous generation is a loss of vital resources. In conclusion, wastes are materials whose owners no longer have a need for. Waste Management: Researches have shown that waste production is as a result of human interactions and/or activities with the environment. As [9] reported in his research that waste production and management was not a major issue until people began living together in communities. Subsequently also, as population and purchasing power of citizens increased worldwide, more goods were produced to meet the increasing demands, thereby leading to the production of more wastes. These continuous productions of waste resulting from human activities, have overburdened the environment. It has been affirmed that the production of waste materials have remained a major source of worry as it has always been since primitive period. In modern times, most developing or underdeveloped countries in various communities face lots of health and environmental pollution challenges in relation to daily wastes generation. This, among others is as a result of improper or irregular waste management systems in Nigeria. What really constitutes a waste has been a problem to scholars of this discipline, as there are several opinions to what constitute a waste. Irrespective of the fact that the word is subjective in meaning, as it is open to several interpretations and also influenced by personal opinions and subsequently no one-size-fits-all definition so far nevertheless, it is important to provide some acceptable definitions for the purpose of this paper.

2.0 Methodology

A web based mechanism is developed to store the history of the driver and various records related to waste. In this application, we also used image processing to measure the waste index of a particular dumping site. The waste index can be low, medium, or high. A dumper truck database is generated in the system so that data and details of dumper truck ID, meeting date, meeting time of garbage collection, and so on are collected. This technique keeps track of all the truck drivers' activities and the waste gathering system of waste management. This system allows on-time waste gathering and also allows automobile trace through database along with of Global Positioning System (GPS) automation. The GPS employs satellites to determine a vehicle, person, or other assets' precise position and records the asset's position at regular intervals. The trucks' details are then forwarded to the data centers with are mote correspondence interface. With the help of the tracking system, the authorities of a waste management organization can keep track of their vehicles. Our system provides an optimized path for collecting waste, which saves much time and increases the efficiency of the work done. In this system, we have used the Arduino UNO micro-controller. Sensors are connected with the microcontroller for processing. Ultrasonic sensor ranges from 2cm to 400cm measurement function of noncontact. Moisture sensors are also used to detect whether the waste is wet or dry.

2.1 Justification of the proposed system

The following are the merits of the proposed system over the existing systems;

i. automated updating of waste position in the database
ii. fast information retrieval from the database
iii. accuracy in information recording
iv. effective waste location monitory

2.2 Method Adapted in the study

This research work adopted Object-Oriented System Development Methodology (OOSDM). This method views, models and implements the proposed system as a collection of interacting classes and objects. OOSDM is adopted because it an effective, efficient, reliable, reusable and a faster way of developing systems.

3.0 Architecture of the Proposal System

The system consists of smart trash bins with a real-time monitoring system which integrates multi-choices, such as ultrasound distance, along with a transmission module. Low energy use was considered throughout the design process. Each node is consequently supposed to be powered by multiple sources; for instance, solar energy or batteries. For flexibility, we have designed hardware that can use either energy source, as trash bins are often put in places where direct sunlight is not available. Selection of the best electronic components for their interconnection and for energy efficiency strategies during the employment of the methods was considered. Furthermore, technical solutions will enable turning off nodes (or parts of them) when they do not work. Once principal components of the node has been chosen, the overall design was targeted at their integration. The data are used to track and predict the status of the trash over each period. Furthermore, they will be used to calculate the optimal path, accordingly. The predicted state of each trash bin can be examined, based on assigned training data. It is, then, reviewed to refresh the appropriate waste fill level, which is an essential input parameter of the optimal path algorithm

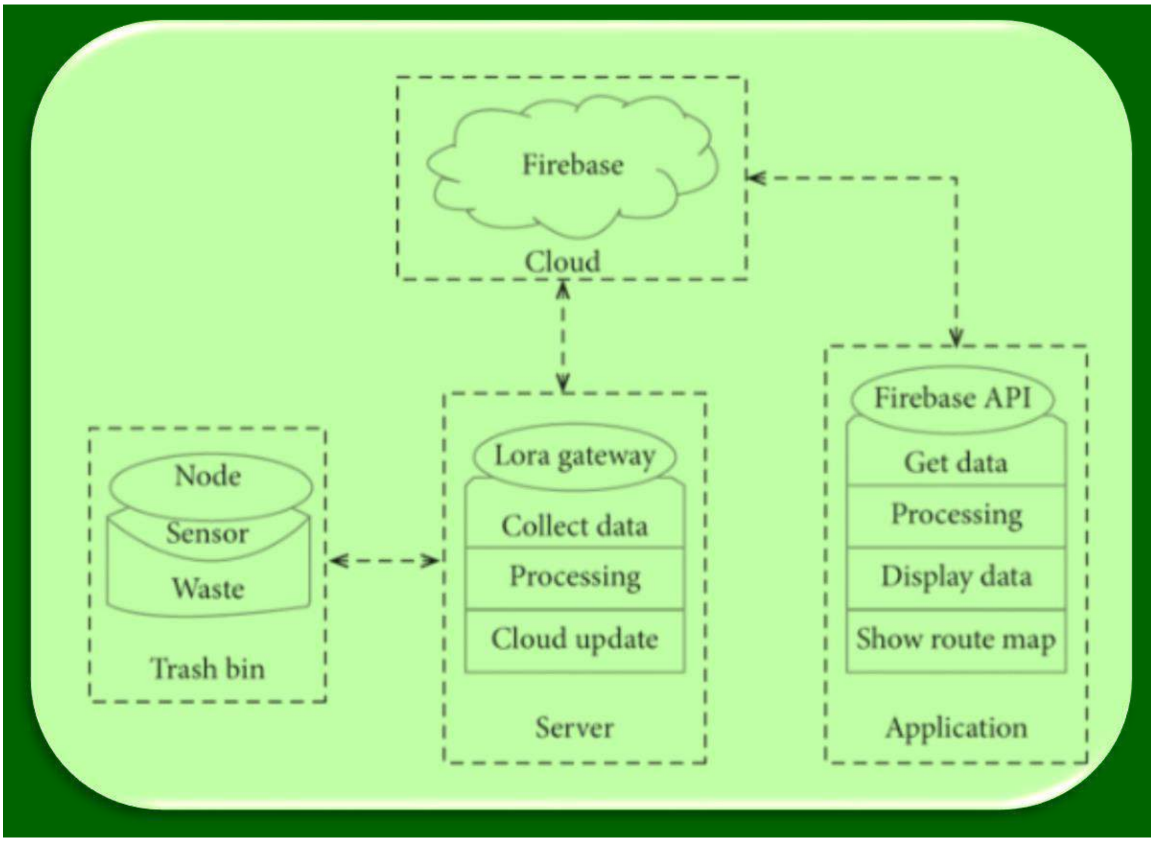

Figure 1: Architecture of Design Proposed System

NIPES-NCEE Conference Proceedings
The 2nd International Conference 15th-17th Feb. 2023
742-759
www.nipesjournals.org.ng

3.1 Input design of the proposed system

The input of the system includes fields like: house address, GPS location, phone and size of the waste. The input is entered through any keyboard.

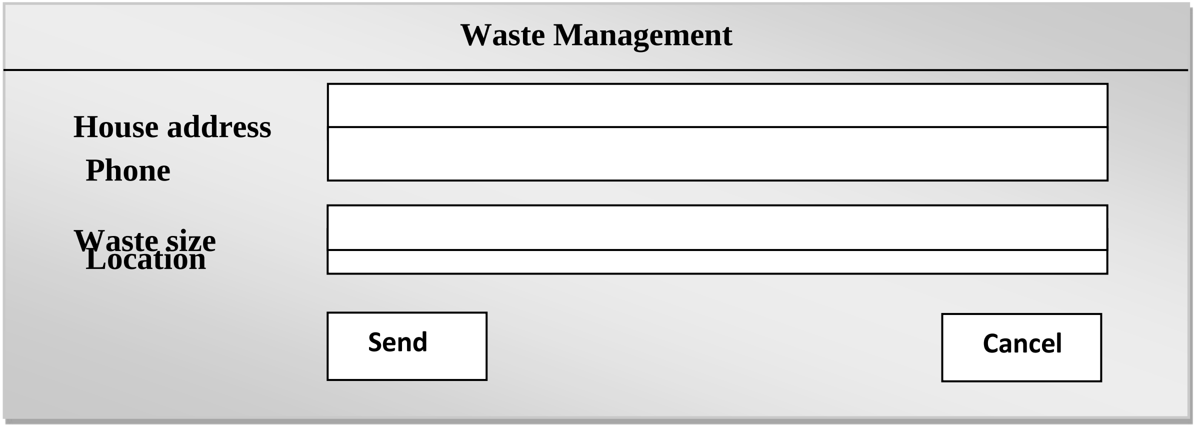

Figure 2 Input Design of the Proposed System

3.2 Process Model Design

The design model showed all the graphical design of the proposed system for the developer to use in the data flow process in the proposed system. The design tools used were USE-CASE diagram, sequence diagram, class diagram and program flowchart.

The Sequence Diagram of the system

In the waste management system, the sequence diagram is used to model and visualize the logic behind the sophisticated function, operation and procedures. Where the user send the data needed to company database, the waste management company retrieve the data and also makes confirmation on the database, check the available service and send a reply to the user.

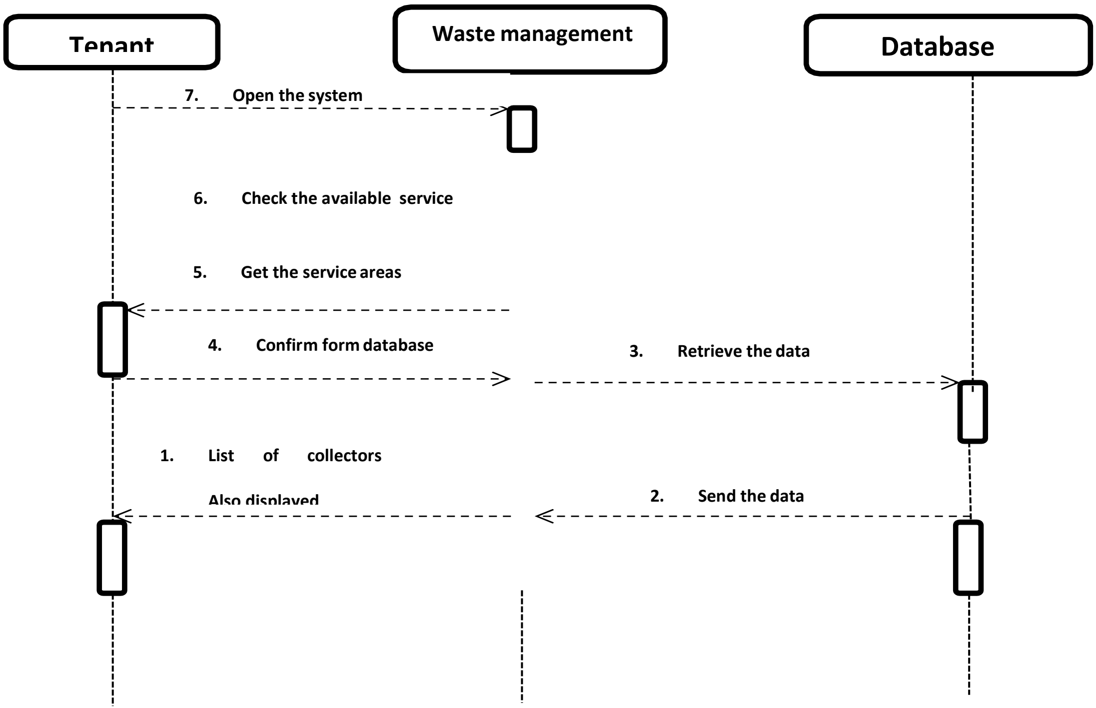

Figure 2 Sequence Diagram Design of the Proposed System

Class Diagrams

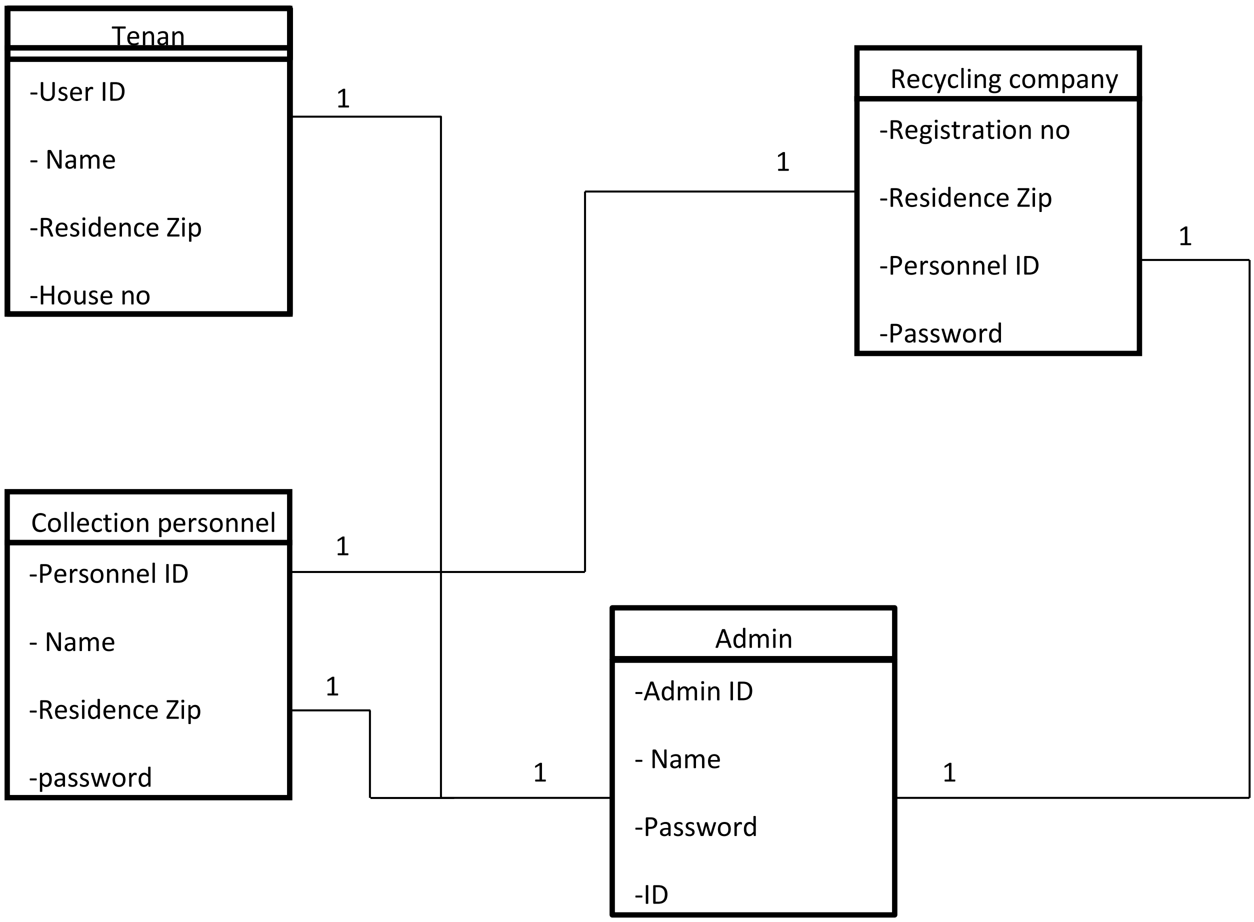

Figure 3 Class Diagram of the Proposed System

USE-CASE Diagram

The **USE-CASE** depict an admin in the waste management system. The other users will be indirect users.

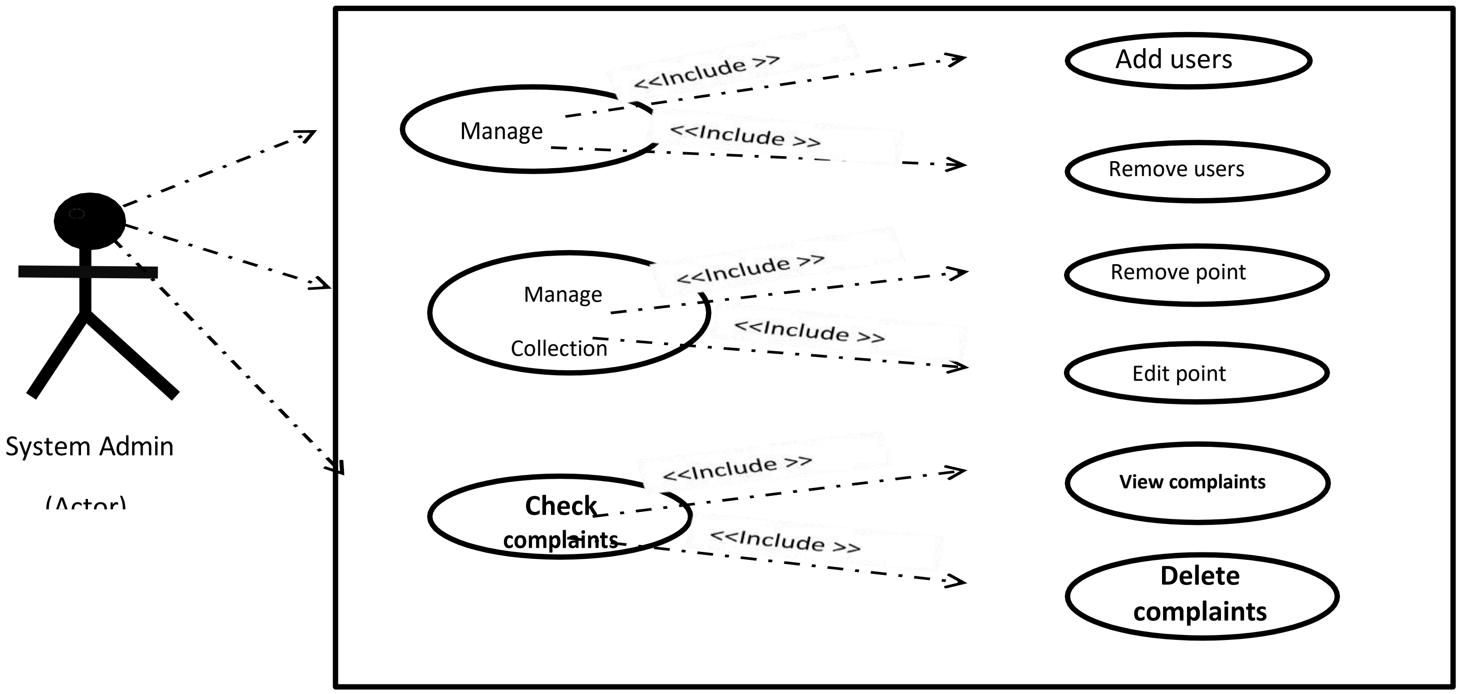

Figure 4 USE-CASE Diagram of the Proposed System

Algorithm of the proposed system

The state of algorithm is recursive, it can search and fill value simultaneously,

Hence, the steps involved in this program include:

1. Start
2. Login
3. If login= valid then
4. Search for waste
5. Display location
6. Update system
7. else
8. Stop

3.3 Output design of the proposed system

The output of the system is based on the required input sent by the user to the system admin who in turn sends work to be done.

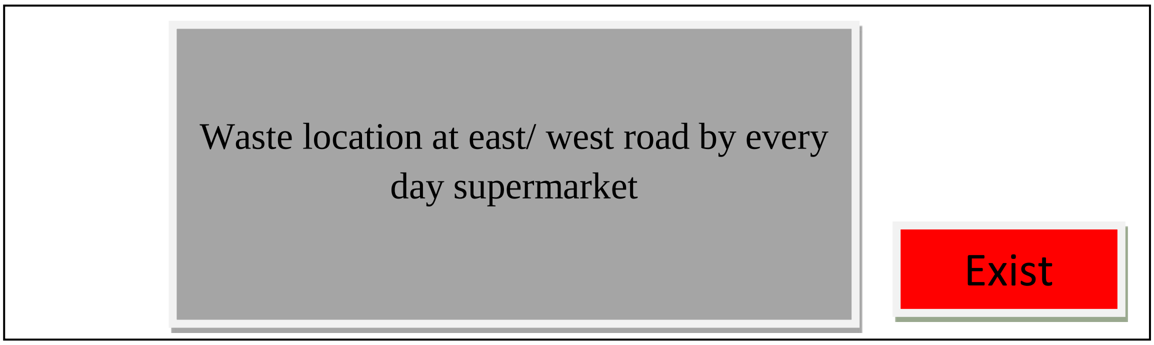

Figure 7 Output Design of the Proposed System

Figure 5 Output design of the proposed system

Database design of the proposed system

The propose system was design to implement environment information management system for easy disposal of waste in our environment. The database server provides controlled access and rapid transaction processing to meet the requirements of the client. The user of the new system have to create an account with the system before user can login. User login information is secured on a cloud server which helps in avoiding unauthorized access from the outside world. User can make request of waste disposal from the waste management company and also cancel or decline request. The waste management company will also have to accept the request as the admin of the system.

These record will be used to grant or deny user access to the smart cities environment.

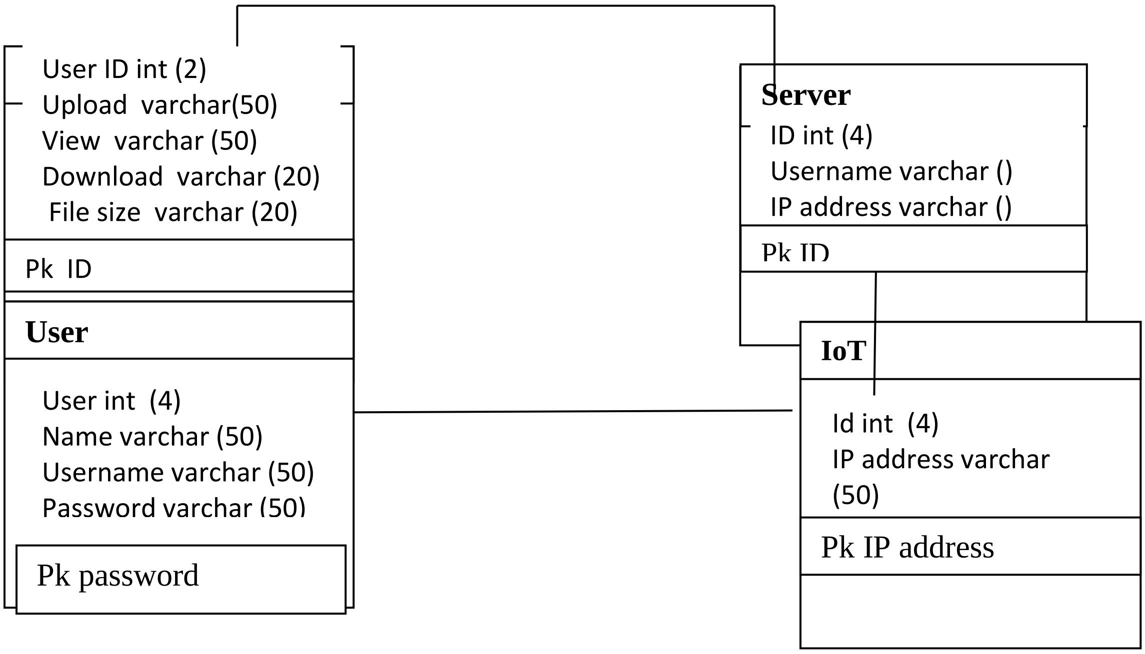

Figure 7 Logical Data Model

Table 1: Registration table of system products

SIN	**Fields**	Datatype	**Constraint**
1	Address	Varchar (30)	
2	Waste size		
2	Phone Number:	Varchar(15)	Primary Key

Table 2 login table

S/N	**Fields**	**Datatype**	**Constraint**
1	Id	Integer	
2	Username	Varchar(50)	
3	Password	Varchar(50)	Primary Key

Table 3 Logical Database Description of the proposed system

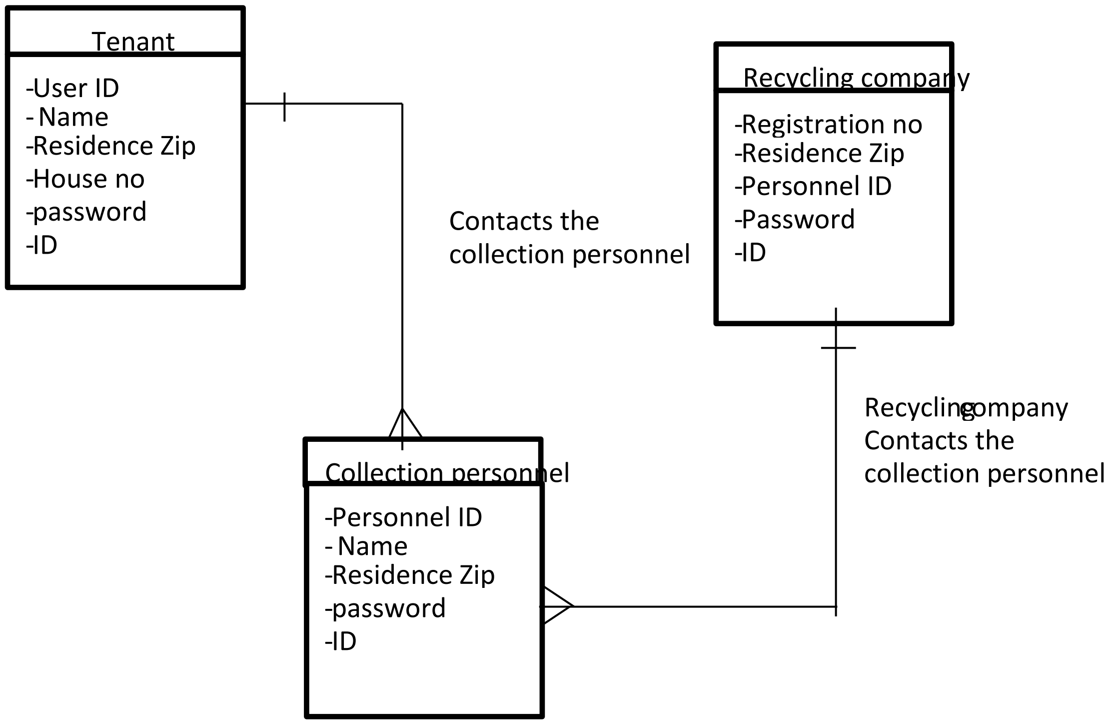

4.0 Results and Discussion

The study achieved its aim, it; developed an environmental waste information management system, integrated the environmental waste information management system, implemented the environmental waste information management system and evaluated environmental waste information management

The admin and new user's login page is one of the input stages where the admin and new user's input their login details which are their email and passwords. The user's input their information which is later processed and outputted through a computer system. Integrated the environmental waste information management system: The functionality of the system was integrated into the waste management system using PHP. The implementation of this model was done using PHP, MySQL and JavaScript. PHP was also best-suited for the implementation of the system. After the design, integration and implementation of the proposed system were made, it was evaluated and tested using a Xampp Server.

5.0 Summary and Conclusion

Summary

Environmental pollution has been a major problem due to improper disposal of waste which has contributed to environment degradation. Urban resident dump solid wastes carelessly or haphazardly; anywhere they deem fit. Some of the drainage system in the county has been turned into a dump site for human and all sorts of solid waste, with the constant pollution of the environment it is evident that human beings are being affected health wise thus calling for help and solution mechanisms. The aim of this project was to develop environmental waste information management system.

This work is essentially intended to model a waste management system in our environment, using web-base technology, garbage truck weighing mechanisms, helping waste management agent in monitoring position of waste in the environment. The basic design tools were USE-CASE diagram, sequence diagram, class diagram and program flowchart.

Hyper preprocessor (PHP) was used to implement this system because, it has high-performance graphic and statistic computing, it is object-oriented and it is good for modeling of systems, including software development, mobile applications, web application and large systems development.

During the testing of the proposed system, the following were targeted:

The fully integrated software applications including the external computer peripherals devices, were tested in order to check how components interact with one another and with the system as a whole (This is also called End to End scenario testing)
Verification through thorough testing of every input in the application to check for desired outputs.

User have to create an account will the system before user can login. User login information is secured on a cloud server which helps in avoiding unauthorized access from the outside world

5.2 Conclusion

In this work, we successfully developed an environmental waste information management system for easy disposal of waste in our environment. Internet was used to support the auto-integration of an environmental waste management system. This system will help improve and manage waste in an effective and efficient manner where User have to create an account with the system before user can login. User login information is secured on a cloud server which helps in avoiding unauthorized access from the outside world, this allows the user access services which is the primary reason for using the system which allows them to request and decline service from the waste management company.

REFERENCE

[1] Assamoi B, & Lawryshyn, Y. (2012). The environmental comparison of landfilling vs. incineration of MSW accounting for waste diversion. J. Waste Management 32(1): 1019-1030

[2] Arena U, Mastellone ML, & Perugini F. (2003). Chemical Engineering Journal 96(1-3): 207-222. Assamoi B, Lawryshyn, Y (2012).

[3] Barlaz, M., 1998: Carbon storage during biodegradation of municipal solid waste components in laboratory-scale landfills. *Global Biogeochemical Cycles*, 12(2), 373-380.

[4] Barlaz, M., R. Green, J. Chanton, R.D. Goldsmith, and G. Hater, (2004): Evaluation of a biologically-active cover for mitigation of landfill gas emissions. *Environmental Science and Technology*, 38(18), 4891-4899.

[5] Bates, J. & Haworth A., (2001): Economic evaluation of emission reductions of methane in the waste sector in the EU: Bottom-up analysis. Final Report to DG Environment, European Commission by Ecofys Energy and Environment, by AEA Technology Environment and National Technical University of Athens as part of Economic Evaluation of Sectoral Emission Reduction Objective for Climate Change, 73.

[6] Beck-Friis, B.G. (2001). *Emissions of ammonia, N_2O, and CH_4 during composting of organic household waste.* PhD Thesis, Swedish University of Agricultural Sciences, Uppsala, 331.

[7] Berge, N., D. Reinhart, & Townsend T, (2005): A review of the fate of nitrogen in bioreactor landfills. *Critical Reviews in Environmental Science and Technology*, 35(4), 365-399.

[8] Bernache-Perez, G., S. Sánchez-Colón, A.M. Garmendia, A. Dávila-Villarreal, and M.E. Sánchez-Salazar, (2001): Solid waste characterization study in Guadalajara Metropolitan Zone, Mexico. *Waste Management & Research*, 19, 413-424.

[9] Bingemer, H.G. and P.J. Crutzen, (1987): The production of CH_4 from solid wastes. *Journal of Geophysical Research*, 92(D2), 2182-2187.

[10] Binner, E., (2002): The impact of mechanical-biological pretreatment on the landfill behaviour of solid wastes. Proceedings of the workshop on Biowaste, Brussels, April 8-10, (2002). 16.

[11] Bockreis, B. & Steinberg I. (2005): Influence of mechanical-biological waste pre-treatment methods on gas formation in landfills. *Waste Management*, 25, 337-343.

[12] Bogner, J., C. Scheutz, J. Chanton, D. Blake, M. Morcet, C. Aran, & P. Kjeldsen, (2003): Field measurement of non-methane organic compound emissions from landfill cover soils. Proceedings of the Sardinia '03, International Solid and Hazardous Waste Symposium, published by CISA, University of Cagliari, Sardinia.

[13] Wilson, D. C. (2007). Development drivers for waste management. Waste Management & Research the Journal of the International Solid Wastes & Public Cleansing Association Iswa, 25(3), 198-207.

[14] The environmental comparison of landfilling vs. incineration of MSW accounting for waste diversion. J. Waste Management 32(1): 1019-1030

NIPES-NCEE Conference Proceedings
The 2nd International Conference 15th-17th Feb. 2023
742-759
www.nipesjournals.org.ng

COMPARISON BETWEEN TEMPERATURE DISTRIBUTION IN AXISYMMETRIC AND 3D MODELS OF A DIESEL ENGINE PISTON CROWN USING FINITE ELEMENT METHOD IN ANSYS SOFTWARE

Festus Oamen Isaac[1], Otunuya Obodeh[2] and Osagie Ighodalo[3]

[1]Faculty of Engineering, Department of Mechanical Engineering, Edo State University, Uzairue. isaac.oamen@edouniversity.edu.ng
[2]Faculty of Engineering and Technology, Department of Mechanical Engineering, Ambrose Alli University, Ekpoma. Edo State. engobodeh@yahoo.com
[3]Faculty of Engineering and Technology, Department of Mechanical Engineering, Ambrose Alli University, Ekpoma. Edo State. oighodalo@yahoo.com
Corresponding email: isaac.oamen@edouniversity.edu.ng

Abstract
This paper presents the comparison between the steady-state thermal analysis using the finite element method (FEM) of an axisymmetric (2D) and 3D models, respectively of a conventional or uncoated piston of a single-cylinder four-stroke diesel engine using the ZS1115NM diesel engine specification. The methodology involves sizing the piston elements before being modelled in SOLIDWORKS 3D Computer-Aided Design (CAD) software. After modelling in SolidWorks, a quarter view of the model was imported into ANSYS Workbench for steady-state thermal analysis. Similarly, an axisymmetric (2D) model was also created in Mechanical ANSYS Parametric Design Language (APDL) for the same steady-state thermal analysis. The material chosen for the piston (substrate) is an aluminium alloy designated as A92618 or simply A2618, due majorly to its high coefficient of thermal expansion (CTE) which enables the piston to withstand high thermal stress without cracking or failure. The triangular discretization of the 3D quarter model produced 8904 elements and 15872 nodes and that of the axisymmetric (2D) model was 372 elements and 859 nodes. The 3D quarter model produces finer mesh than the axisymmetric one and the maximum surface temperature obtained in the 3D model was 1249 K and that in the axisymmetric one was 1232.7 K. It is seen that the temperature distribution in the ANSYS 3D simulation decreases faster as heat is being conducted away from the piston to ensure its long-life span. This is again seen in the minimum temperature of the 3D model which is 438.30 K as compared to the axisymmetric model having 546.01K.

Keywords: *3D model, ZS1115NM, Axisymmetric model, SOLIDWORKS CAD, A2618, ANSYS Workbench.*

1.0 Introduction
The pistons convert thermal energy to mechanical energy in an internal combustion engine [1]. They also serve to transmit gas forces via connecting rod to the crankshaft. They are sealed with piston rings in the combustion chamber against gas leakage to the crankcase, prevent the infiltration of oil from the crankcase into the combustion-chamber, and also remove the absorbed combustion heat to the cylinder-liner and the cooling oil [2]. The preferred common materials for petrol and diesel engine pistons are aluminium alloys because they possess high thermal conductivity, low density, simple machinability, high-reliability, simple fabrication process and very good recycling-characteristics [1,3]. The continuing advancement of modern diesel and petrol engines resulted to specific objectives for more piston development [2]. The objectives are to reduce piston weight, increase mechanical and thermal loads' capacity, lower friction including improved scuffing-resistance, etc. In addition, the basic requirements for

durability, low-noise level and minimum oil-consumption need to be considered. These goals may only be achieved by a targeted-combination of very high-performance aluminium materials for piston production, novel piston designs and the application of innovative coating systems [4]. There are ongoing improvements recorded with cast and forged aluminium alloys where it was seen that aluminium piston materials still offer great optimization potential and will continue to play a dominant role as piston material in the future [1].

Pistons in internal combustion engines (ICE) face high mechanical and thermal loads [3]. The mechanical (pressure) loads on the piston result from extreme pressure cycles with peak pressures of up to 200 bar in the combustion-chamber and huge forces-of-inertia which are caused by extremely high-acceleration during the reciprocating-motion of pistons [5]. Similarly, the thermal (temperature) loads on the piston are due to the combustion process with very high gas temperatures in the combustion-chamber ranging from 1800°C to 2600°C depending on the type of engine, gas exchange, fuel, compression, and air-fuel ratio [3]. Exhaust gases have temperatures ranging from 500°C to 800°C [5]. The mode of combustion heat transfer to the chamber walls and piston top is primarily by convection [6]. The heat is then discharged by the water-cooling of the chamber-walls and by the oil-cooling of the piston. More heat absorbed by the piston top is transferred by the piston-area. The remaining heat is removed by the lubricant impinging on the underside of the piston. See Figure 1 for the resulting temperature profile within the piston [7].

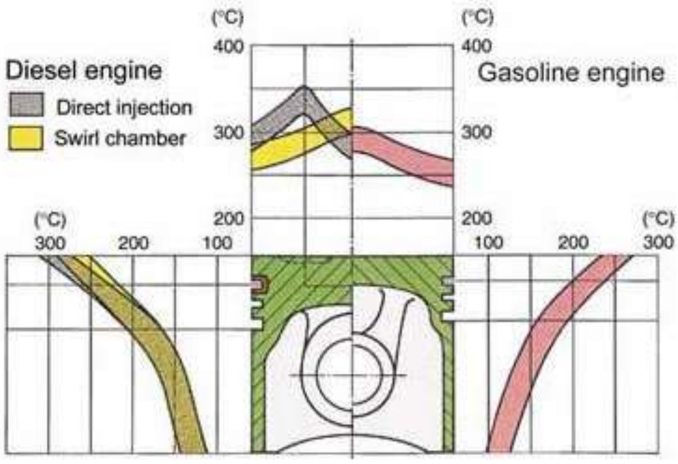

Figure 1 Operating temperatures in automotive engines under full load

A finite element method is a numerical tool for evaluating approximate solutions to a large class of engineering-problems [8]. It considers the solution region to comprise many small, interconnected, sub-regions or elements and gives a piece-wise approximation to the governing equations (the complex partial differential equations) are reduced to either linear or nonlinear simultaneous equations [8,9]. Hence, the finite element discretization (i.e., dividing the domain or continuum into several smaller regions) procedure reduces the continuum problem, which has an infinite number of unknowns, to one with a finite number of unknowns at specified points referred to as nodes [10]. Because the finite element method allows us to form elements, or sub-regions, in an arbitrary sense, a close representation of the boundaries of complicated domains is possible [9].

There are many methods used for finite element formulation but for this paper finite element formulation with linear triangular elements method was used [8]. The linear triangular element was chosen because it is used for the formulation of three-dimensional engineering problems [10]. The major disadvantage associated with using rectangular elements is that they do not conform to curved boundaries. In contrast, triangular elements are better suited to approximate curved boundaries [8].

2.0 Materials and Methods

2.1 Materials

In selecting the substrate material for designing the piston of a ZS1115NM single-cylinder, horizontal and four-stroke direct injection diesel engine, the following qualities of materials were considered [3,11]:

(a) Strength to withstand the high-pressure;
(b) Minimum weight to withstand the inertia-forces;
(c) Good heat conductivity to reduce the risk of detonation and allow higher compression ratios;
(d) High coefficient of thermal expansion: The substrate material has a high coefficient of thermal expansion (CTE) to prevent cracking or failure of the piston;
(e) Effective oil-sealing in the-cylinder;
(f) Sufficient bearing area to prevent-undue wear;
(g) High-speed reciprocation without-noise;
(h) Sufficient rigid construction to withstand thermal-and-mechanical distortions; and
(i) Sufficient support for the piston-pin.

The above qualities require an aluminium alloy for the piston material. The piston material used for the axisymmetric and 3D models was a metal substrate called the aluminium alloy piston A2618 [12,13]. This paper was part of our PhD work [11]. Note that for an isotropic elastic material, the thermal conductivity in all three directions is constant, i.e., $k_r = k_\theta = k_z = k$ [11]. However, an axisymmetric problem is independent of the angle θ. Again, note that the radial (r) and axial (z) coordinates that specified axisymmetric were considered X and Y coordinates in the ANSYS software program [14]. Tables 1 and 2 show the chemical composition and mechanical/physical properties of the A2618, respectively [12,13].

Table 1 Chemical composition of A2618 aluminium alloy

S/N	Alloying elements	Percentage composition (%)
1	Copper	2.3
2	Manganese	1.6
3	Iron	1.1
4	Nickel	1.0
5	Silicon	0.18

6	Titanium	0.07
7	Aluminium	93.75

Table 2 Mechanical/physical properties of A2618 aluminium alloy

S/N	Property	Value
1	Mass density (ρ)	2760 kg/m^3
2	Yield tensile strength (σ_y)	372 MPa
3	Ultimate tensile strength (σ_u)	441 MPa
4	Compressive strength (σ_c)	441 MPa
5	Shear strength (τ_s)	260 MPa
6	Fatigue strength	125 MPa
7	Young modulus (E)	74.5 GPa
8	Shear modulus (G)	27 GPa
9	Poisson's ratio (ν)	0.33
10	Thermal conductivity (k)	146 W/mK
11	Coefficient of thermal expansion (α)	22.3 x 10^{-6}/K
12	Specific heat (c)	875 J/kgK
13	Liquidus temperature	638 ^{0}C

2.2 Methods

2.2.1 Design of the piston elements

Figure 2 shows the cross-sectional view of a conventional piston with its elements [15,16].

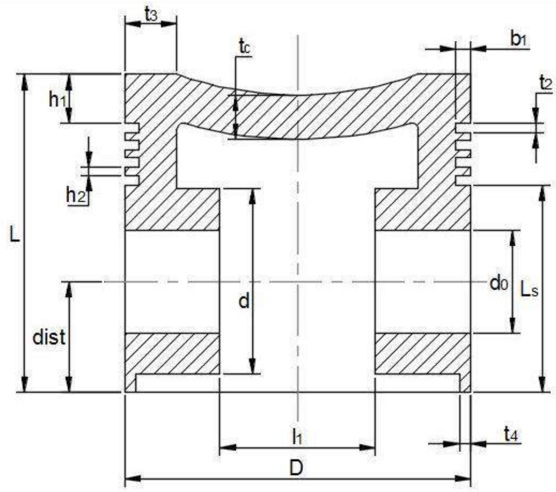

Figure 2 Cross-section of the model conventional piston

2.2.2.1 Design of the thickness of the piston head or crown, t_C:

According to Grashoff's formula, the piston head thickness t_C is given by,

$$t_C = \sqrt{\frac{3p_{max}D^2}{16\sigma_y}} \tag{1}$$

Where p_{max} is the maximum gas pressure (Pa),
D = the cylinder bore or outside diameter of the piston (m), σ_y = the permissible or yield tensile stress (strength) for the piston material (Pa)

2.2.1.2. The number of piston rings:

From Figure 2, we have total number of rings = 4 (number of compression rings = 3 and number of oil ring = 1)

2.2.1.3 Design of the radial thickness of the piston ring t_1:

Consider Eq. (2) for the design of piston ring radial thickness.

$$t_1 = D\sqrt{\frac{3p_w}{\sigma_p}} \tag{2}$$

Where p_w = allowable radial pressure of the gas on the cylinder wall taken as 0.025 MPa
σ_p = permissible bending or tensile stress for cast iron rings = 84 MPa

2.2.1.4 Design of the axial thickness of piston ring, t_2:

Also, consider Eq. (3) for the design of piston ring axial thickness.

$$t_2 = \frac{D}{10n_R} \text{ or } = 0.7t_1 \quad (3)$$

Where n_R = number of rings taken as 4

2.2.1.5 Determining the length of the piston pin in the connecting rod bushing, l_1

Eq. (4) gives the length of the piston pin.

$$l_1 = 0.45D \quad (4)$$

2.2.1.6 Design of the width of the piston top land h_1:

$$h_1 = 1.2\ t_C \quad (5)$$

2.2.1.7 Design of the width of other piston ring lands h_2:

$$h_2 = 0.75t_2 \quad (6)$$

2.2.1.8 Determining the piston barrel:

Piston Barrel thickness t_3 at the top end

$$t_3 = 0.03D + b_1 + 4.5 \quad (7)$$

$$b_1 = t_1 + 0.4 \quad (8)$$

Where b_1 = radial depth of the piston ring groove (mm)

The piston barrel thickness t_4 at the open end

$$t_4 = 0.25\ t_3 \quad (9)$$

2.2.1.9 Design of the length of the piston and piston skirt:

Length of the piston skirt, $l_s = 0.6\ D$ (10)

Total Length of Piston L = Length of the piston skirt + Length of the ring section + Top land

$$= l_s + (4\ t_2 + 3\ h_2) + h_1 \quad (11)$$

The length of the piston usually varies from D and 1.5D.

2.2.1.10 Design of the diameter of the piston boss and pin:

Outside diameter d_0 of piston pin:

$$d_0 = 0.3D \quad (12)$$

Piston Boss diameter $d = 1.5\ d_0$ (13)

Although, d_0 is given in the owner's manual. The value is 36 mm.

The inside diameter d_1 of the piston pin:

$$d_1 = 0.6\ d_0 \quad (14)$$

2.2.1.11 Design of the centre of the pin:

The centre of the pin is 0.02D to 0.04D above the centre of the skirt.

$$\text{Centre of pin} = 0.04D + 0.5\ l_s \quad (15)$$

The specifications for designing and modelling the conventional piston of the diesel-engine with the help of SOLIDWORKS software were that of the ZS1115NM single-cylinder, inline and four-stroke direct injection diesel engine manufactured by Changchai Company Ltd, China. The engine specifications are given in Table 1 [11,17].

Table 3 Engine specification

Item	Specification
Engine model	ZS1115NM
Type	Single cylinder, four stroke, horizontal type, direct injection
Cylinder bore (D) (mm)	115
Piston stroke (L_S) (mm)	115
Piston displacement (V_s) (litre)	1.19
Compression ratio (c.r)	17:1
Rated output/brake power (b.p)(kW)	15.7
Rated speed (N)(Rev/min)	2200
Brake specific fuel consumption (bsfc) (g/kWh)	$\leq$ 244.8
Specific lube oil consumption (g/kWh)	$\leq$ 2.04
Lubricating method	Single circuit
Cooling method	Water cooled, evaporative
Cooling system	Radiator, natural convection
Starting method	Electric starting or hand cranking
Fuel injection pressure (MPa)	18.13 ± 0.49
Net weight (kg)	205
Overall dimension (L x W x H) (mm)	965 x 457 x 713
Mean piston speed (c_m) (m/s)	8.433
Fuel injection timing before TDC	22^0
Fuel type	Diesel
Chemical formula	$C_{14.4}H_{24.9}$

Connecting rod length (L_R) (mm)	258.5
Intake valve closes after TDC	38^0

Eqs. (1) – (15) can only be used in designing the piston if the maximum gas pressure p_{max} is known. The maximum gas pressure from the literature was 10.2 x 10^6 N/m^2 or 10.2 N/mm^2 (Isaac, 2023). The yield tensile strength of the material used for the piston from Table 2 is $\sigma_y = 372\ N/mm^2$ [11]. Table 4 summarizes the sizes obtained from the design of the piston elements.

Table 4 Size of piston elements

S/N	Piston element	Size obtained (mm)
1	Cylinder bore, D	115
2	Thickness of the piston head, t_C	8.25
3	Radial thickness of the piston ring, t_1	3.436
4	Axial thickness of the piston ring, t_2	2.405
5	No of the piston rings, n_R	4
6	Width of the top land, h_1	9.9
7	Width of the ring land, h_2	1.80375
8	Radial depth of the piston ring groove, b_1	3.836
9	Thickness of the piston barrel at the top end, t_3	11.786
10	Thickness of the piston barrel at the open end, t_4	2.9465
11	Piston pin diameter, d_0	34.5
12	Diameter of the piston boss, d	51.75
13	Length of Skirt, l_s	69
14	Total length of the piston, L	93.93
15	Centre of pin above the centre of the skirt	39.10
16	Inside diameter of the piston pin, d_1	20.7
17	Length of the piston pin in the connecting rod bushing, l_1	51.75

2.2.3 Solidworks 3D model of the piston

The sizes obtained from the sizing of the piston elements in Table 4 were used in a 3D model of the piston in Solidworks CAD Software [11,15] Figures 3, 4 and 5 show the different views of the 3D model.

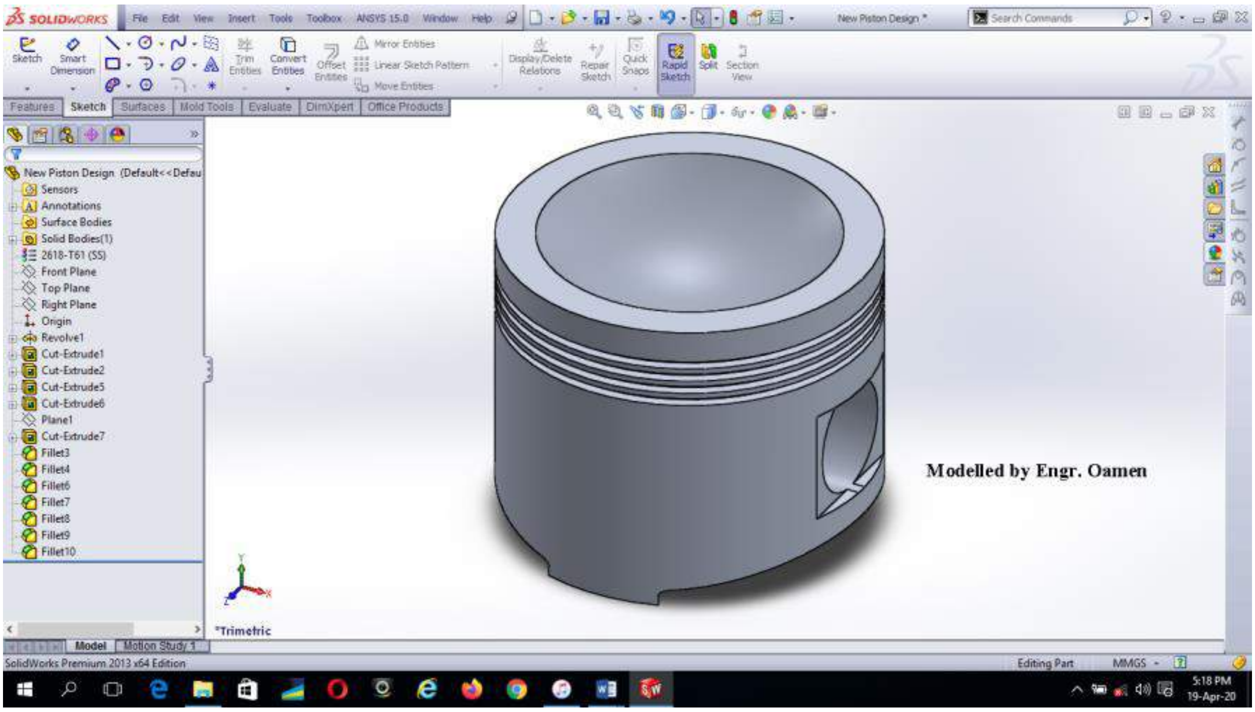

Figure 3 The isometric view of the 3D model

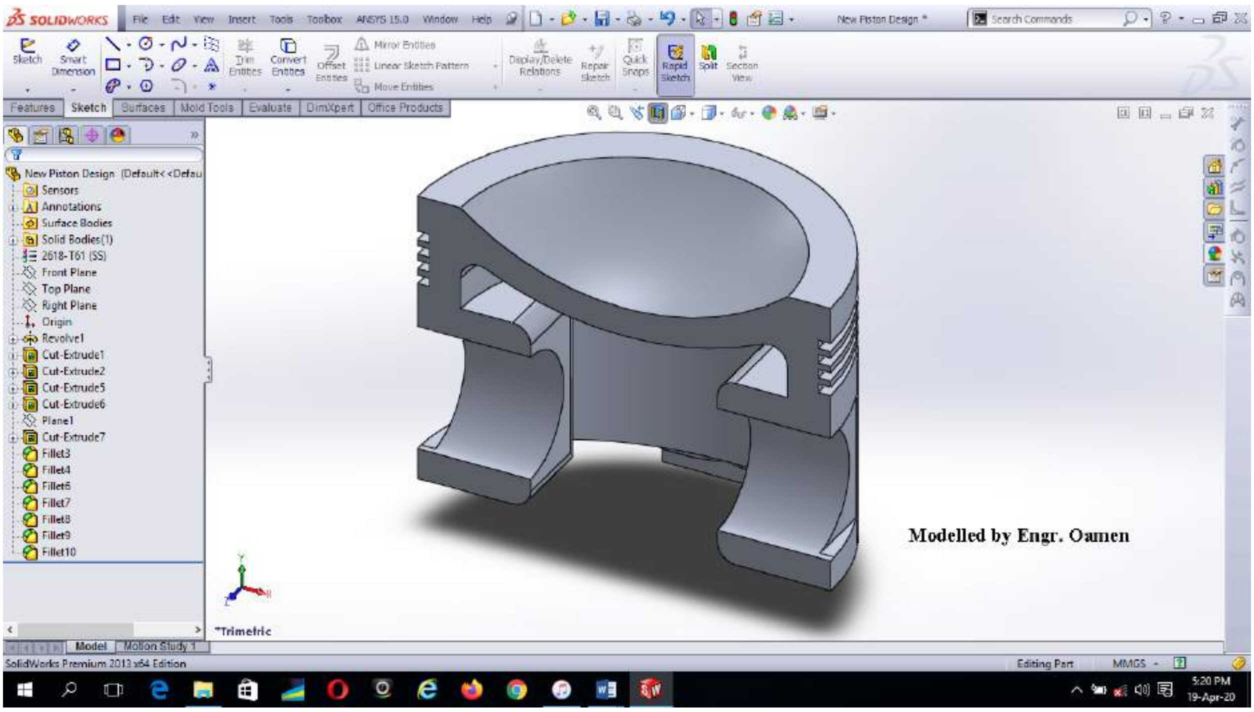

Figure 4 The half view of the 3D model

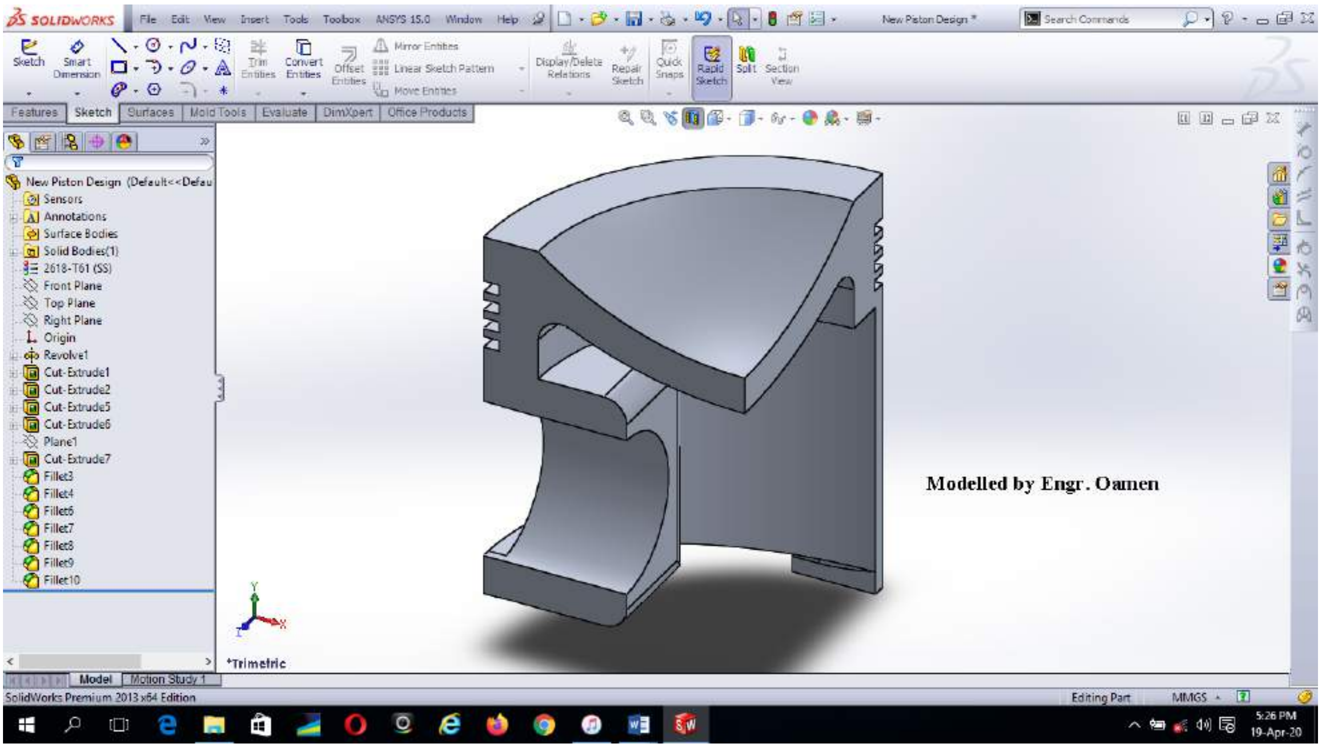

Figure 5 The quarter view of the 3D model

2.2.4 Axisymmetric (2D) model using ANSYS software

ANSYS is one of the most widely used commercial finite element programs [14]. ANSYS make use of three methods of solving problems. Engineering problems are solved in ANSYS finite element analysis (FEA) software by creating an input data file using a text editor such as Notepad; solving interactively using the ANSYS Graphical User Interphase (GUI) and solving by combining text file input and interactive solution methods. For this paper, the GUI method was used. The general process of FEA by using the software was divided into three main phases: preprocessing, solution and general postprocessing, refer to the flowchart in Figure 6 [11].

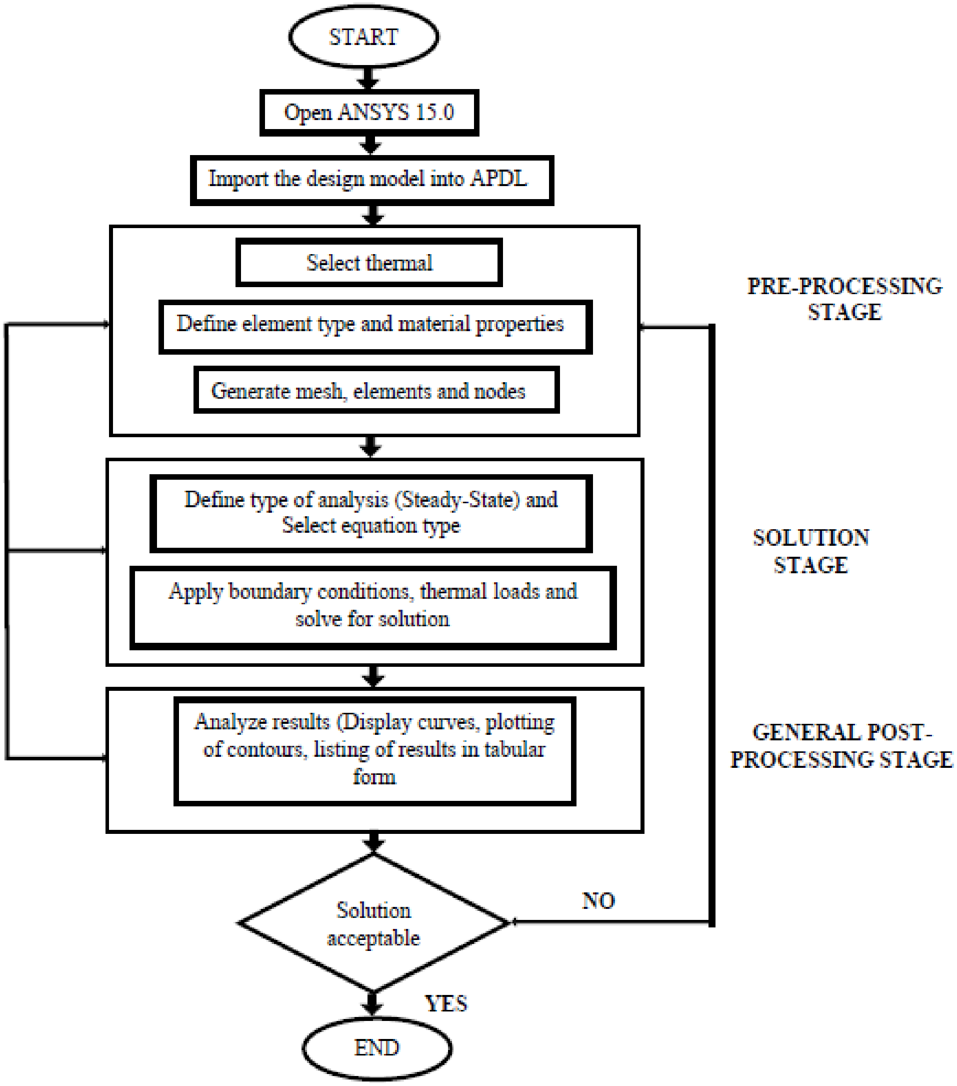

Figure 6 Flowchart of FEA for steady-state thermal by ANSYS

Using the flowchart in Figure 6, the axisymmetric model was created below [11]:

(a) Specifying preferences using the following step:
ANSYS Main Menu ≫ Preferences ≫ Select ≫ Thermal ≫ h-method ≫ OK
Refer to Figure 7.

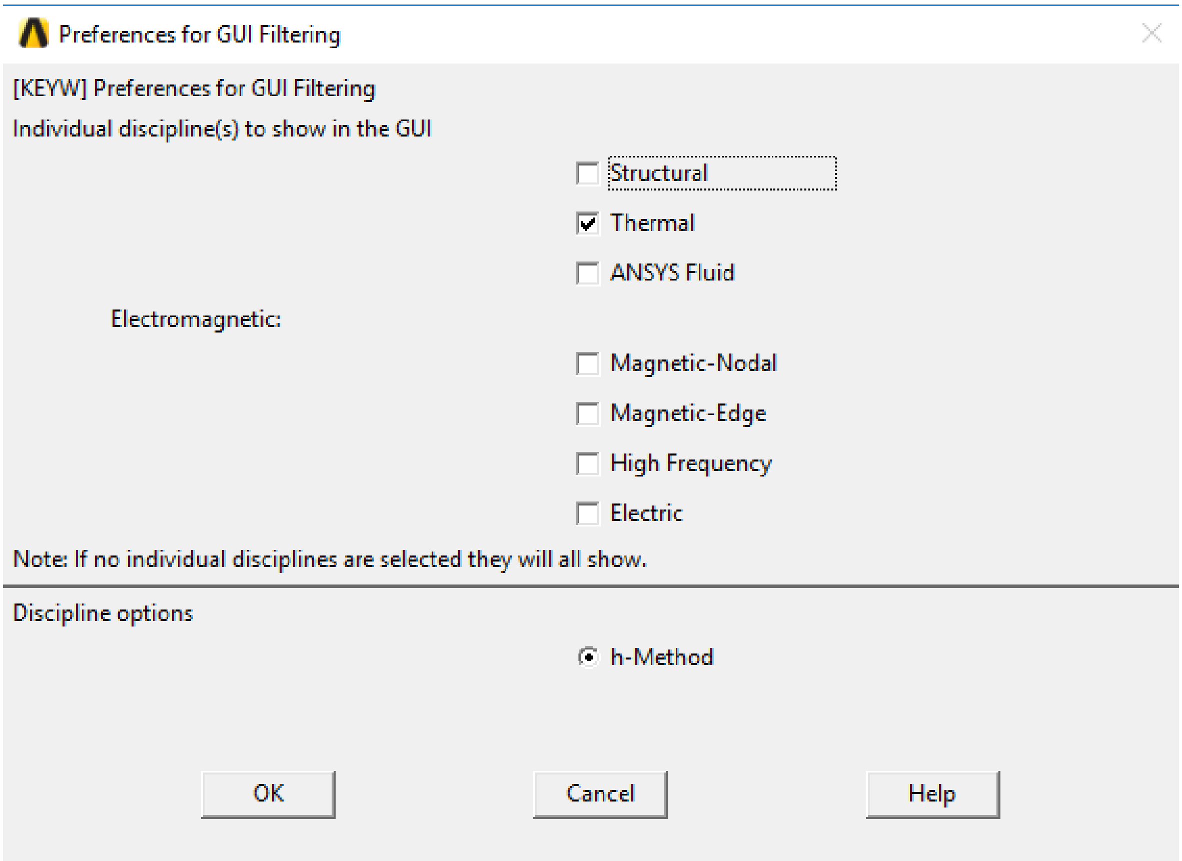

Figure 7 Preferences for GUI filtering dialog box for thermal analysis

(b) Specifying the element type (ET command) using the following step:
We selected the element type by doing the following on the software.
Main Menu ≫ Preprocessor ≫ Element Type ≫ Add/Edit/Delete

i. Clicked on *Add.*
ii. Selected Solid from the left list and 8node 77 (PLANE77) from the right list; clicked on OK.
iii. Clicked on *Option* and selected *Axisymmetric* under Element behavior K3
iv. Clicked on *OK* and *Close.* Refer to Figures 8, 9, 10 and 11.

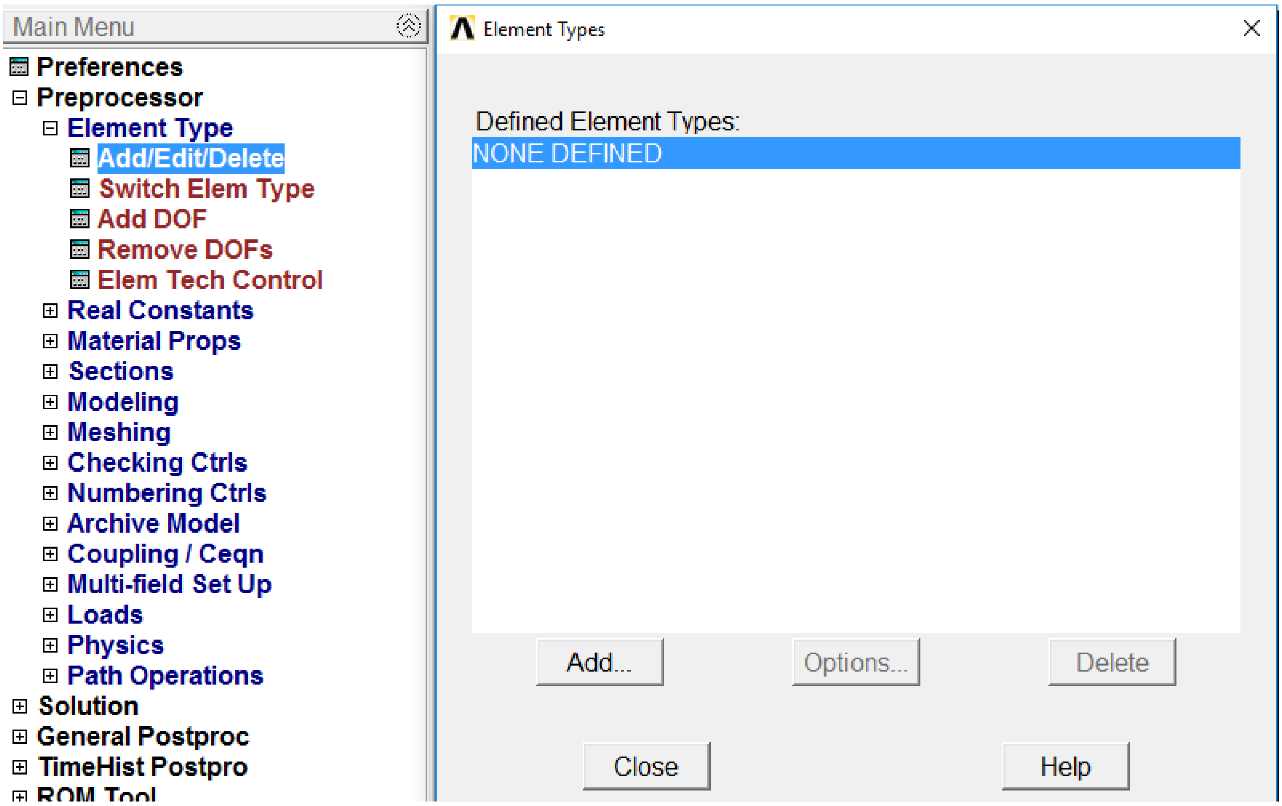

Figure 8 Added element

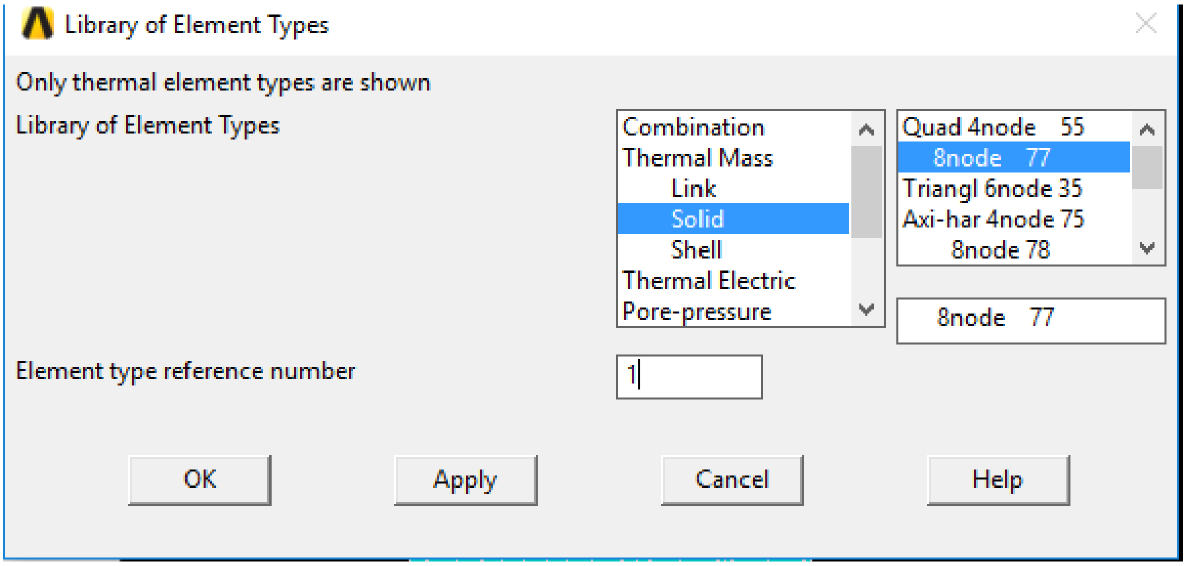

Figure 9 Selecting element type

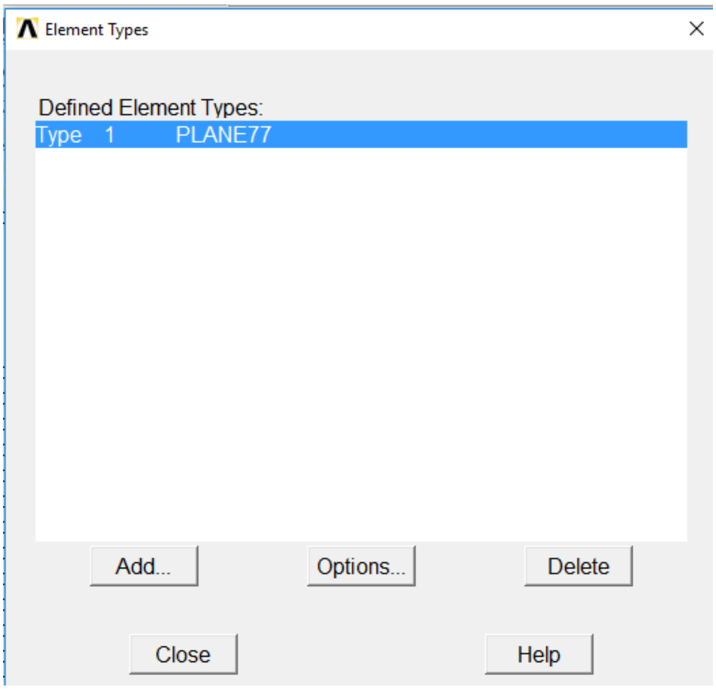

Figure 10 Element type selected

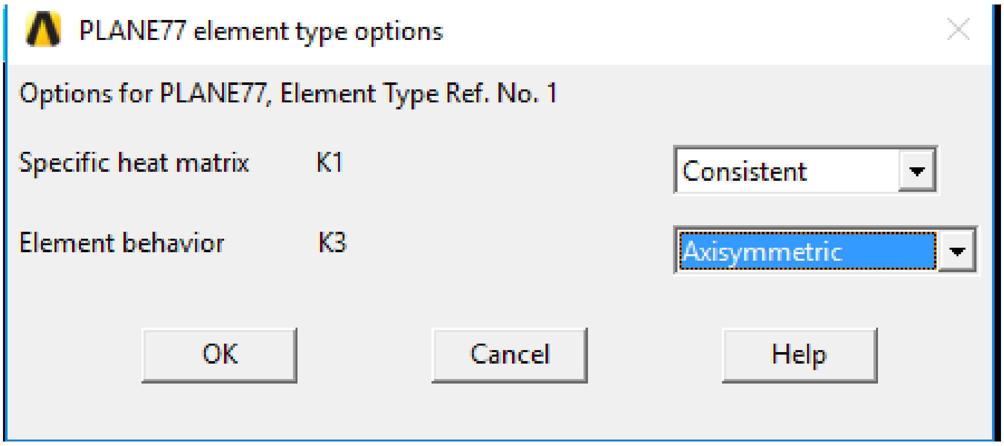

Figure 11 Axisymmetric option selected

(c) Specifying material properties (MP command) using the following step:
The material properties for A2618 from Table 2 were entered in this section.
Main Menu ≫ Preprocessor ≫ Material Props ≫ Material Models ≫ Thermal [11]

i. In the *Define Material Model Behavior* dialog box, in the right window, we double-clicked on *Thermal*, *Conductivity*, and, finally, *Isotropic*, which brought up another dialog box.
ii. Entered *0.146* for *KXX*, and clicked on *OK*.
iii. Double-clicked on *Density*.
iv. Entered *2.76E-006* for DENS.
v. Double-clicked on *Specific Heat.*
vi. Entered *875* for C.

vii. Closed the *Define Material Model Behavior* dialog box by using the following menu path:
Material ≫ Exit. Refer to Figures 12, 13, 14 and 15.

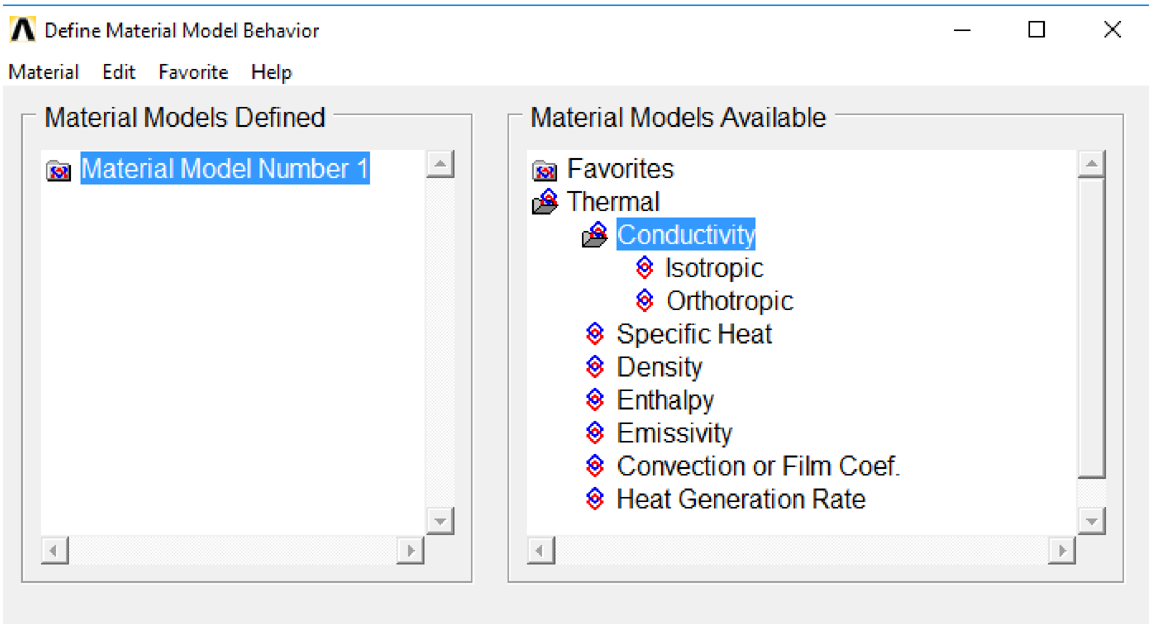

Figure 12 The material models defined

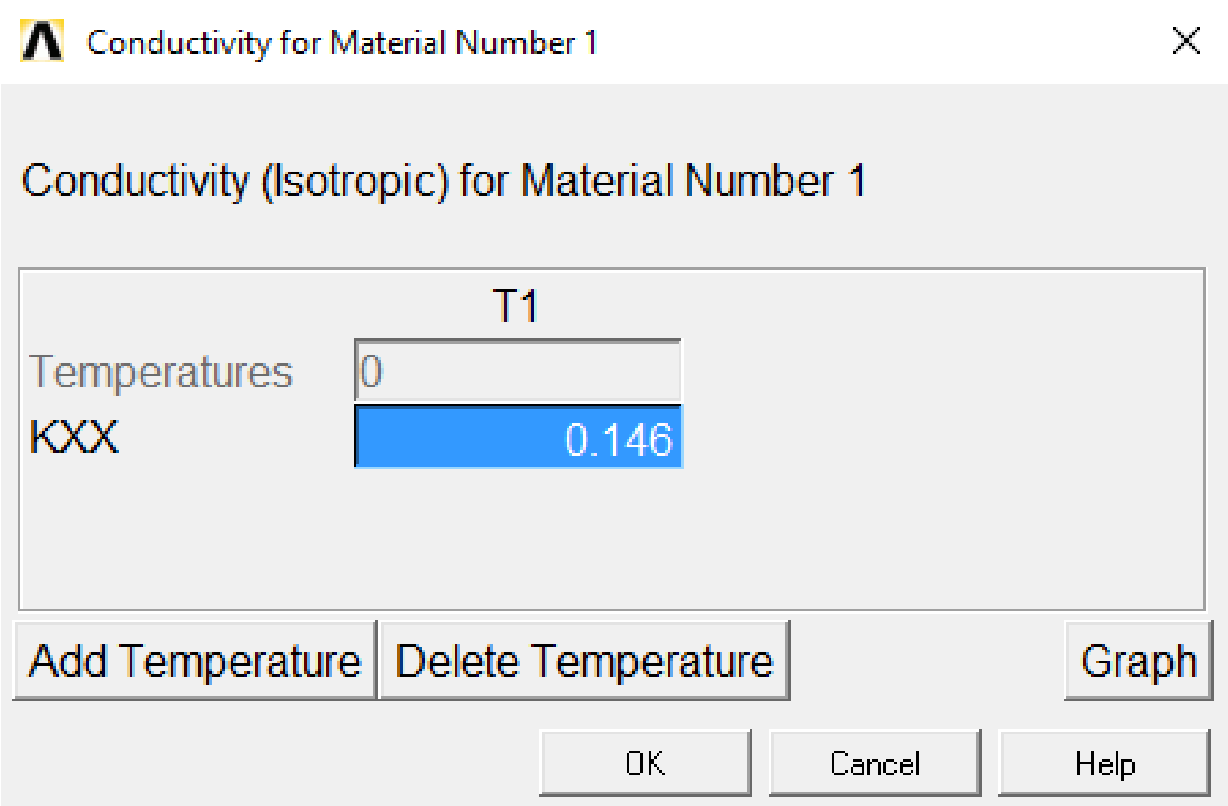

Figure 13 Entered thermal conductivity of material

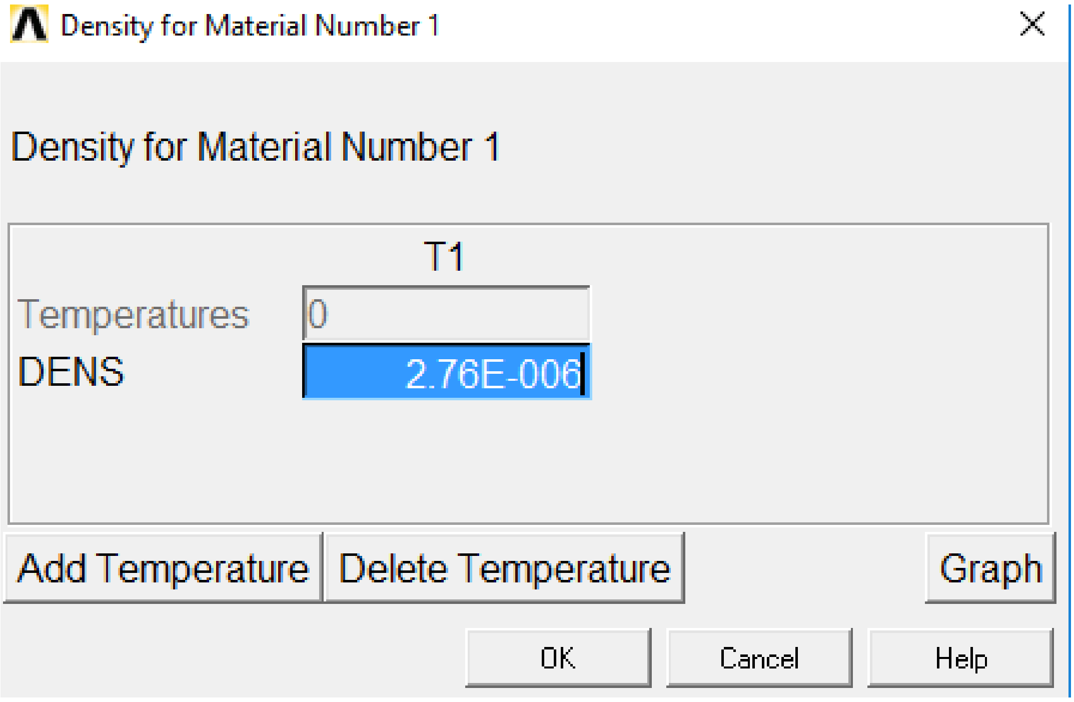

Figure 14 Entered density of material

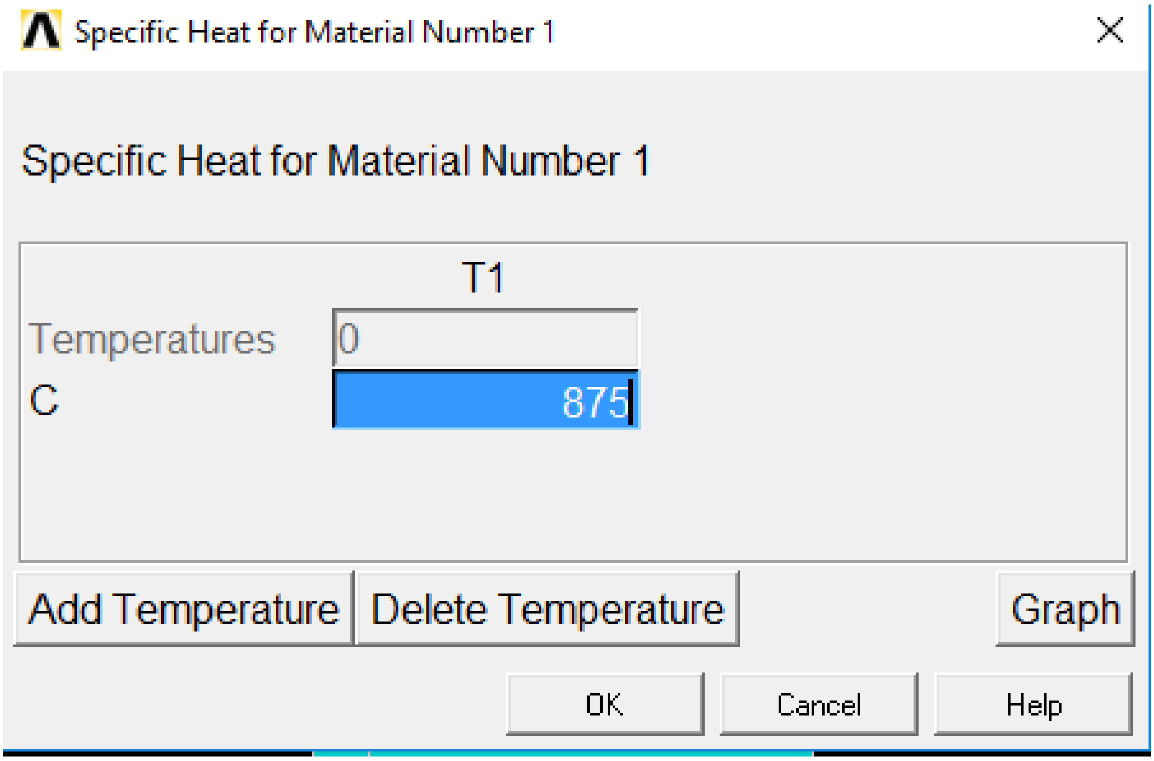

Figure 15 Entered specific heat of material

NIPES-NCEE Conference Proceedings
The 2nd International Conference 15th-17th Feb. 2023
760-783
www.nipesjournals.org.ng

Using the sizes from Table 4, the axisymmetric model was developed in Mechanical APDL. See Figure 16.

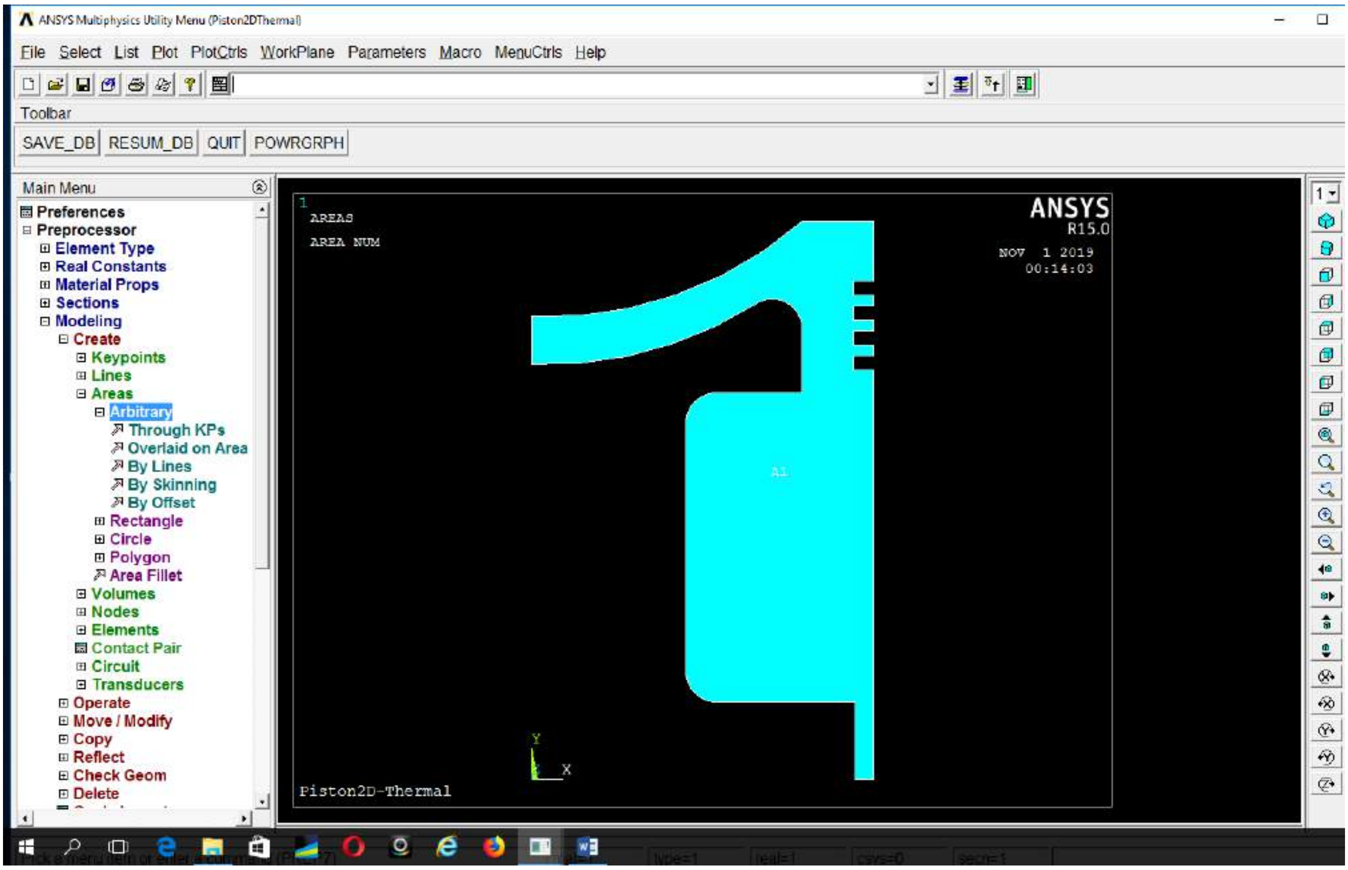

Figure 16 The area created

2.3.5 The meshing of the 3D and axisymmetric models

After importing the 3D model into ANSYS workbench, and selecting element type 20node 90, it was meshed automatically into 8904 elements and 15872 nodes. See Figures 17 and 18 [11].

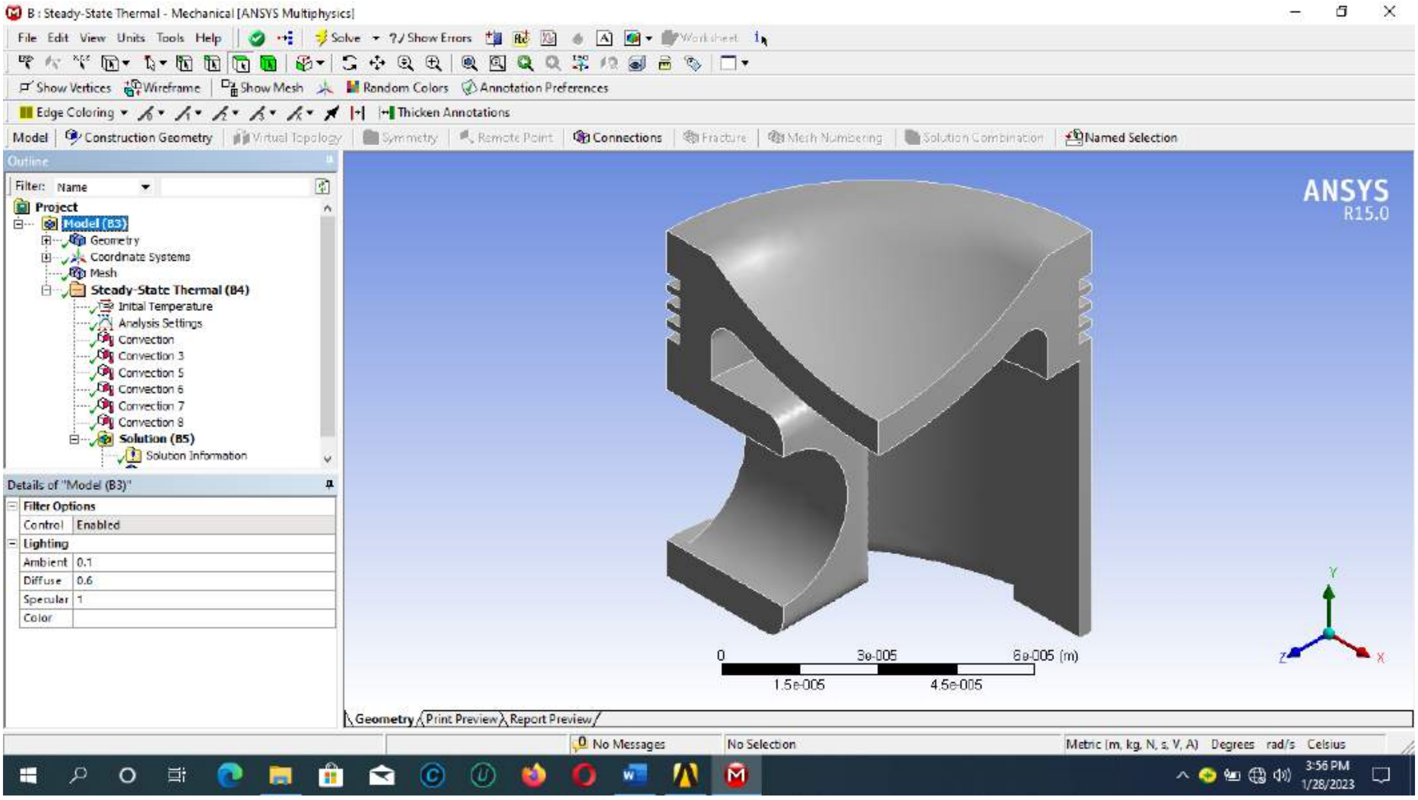

Figure 17 The 3D model imported into ANSYS workbench from SolidWorks

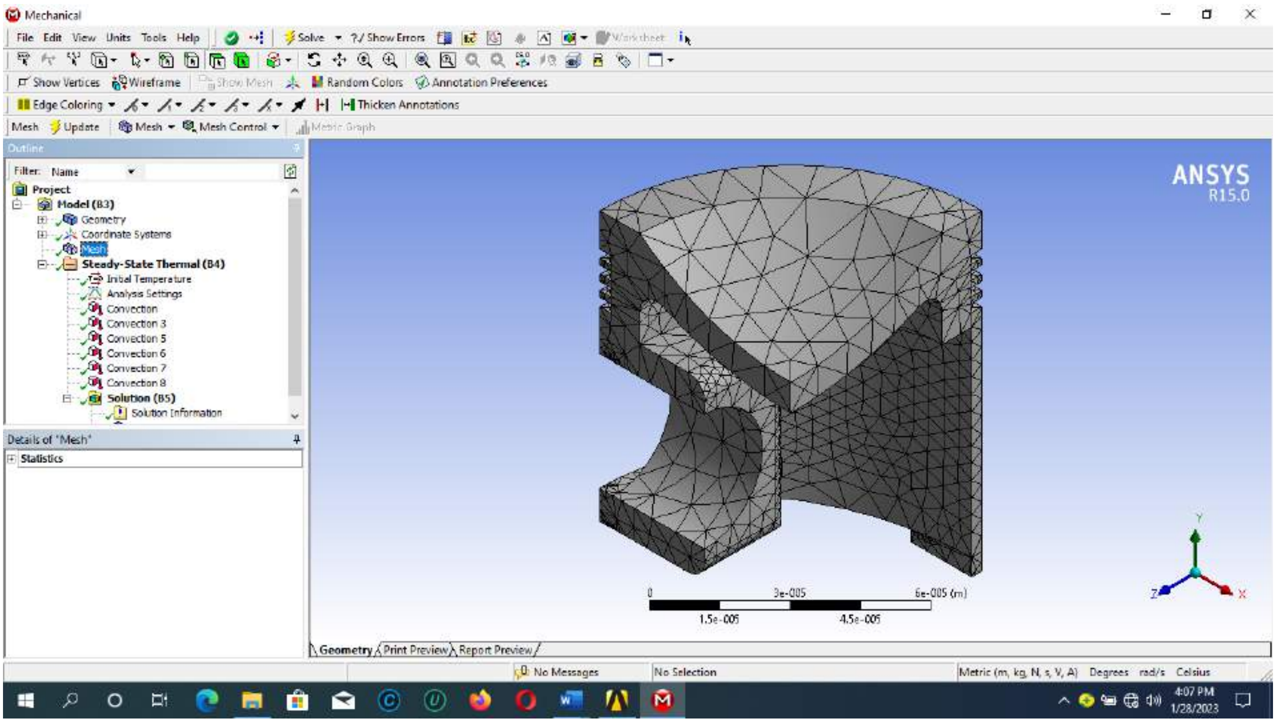

Figure 18 The 3D quarter model meshed automatically into 8904 elements and 15872 nodes

Similarly, the axisymmetric model was also meshed automatically into 372 elements and 859 nodes. See Figure 19.

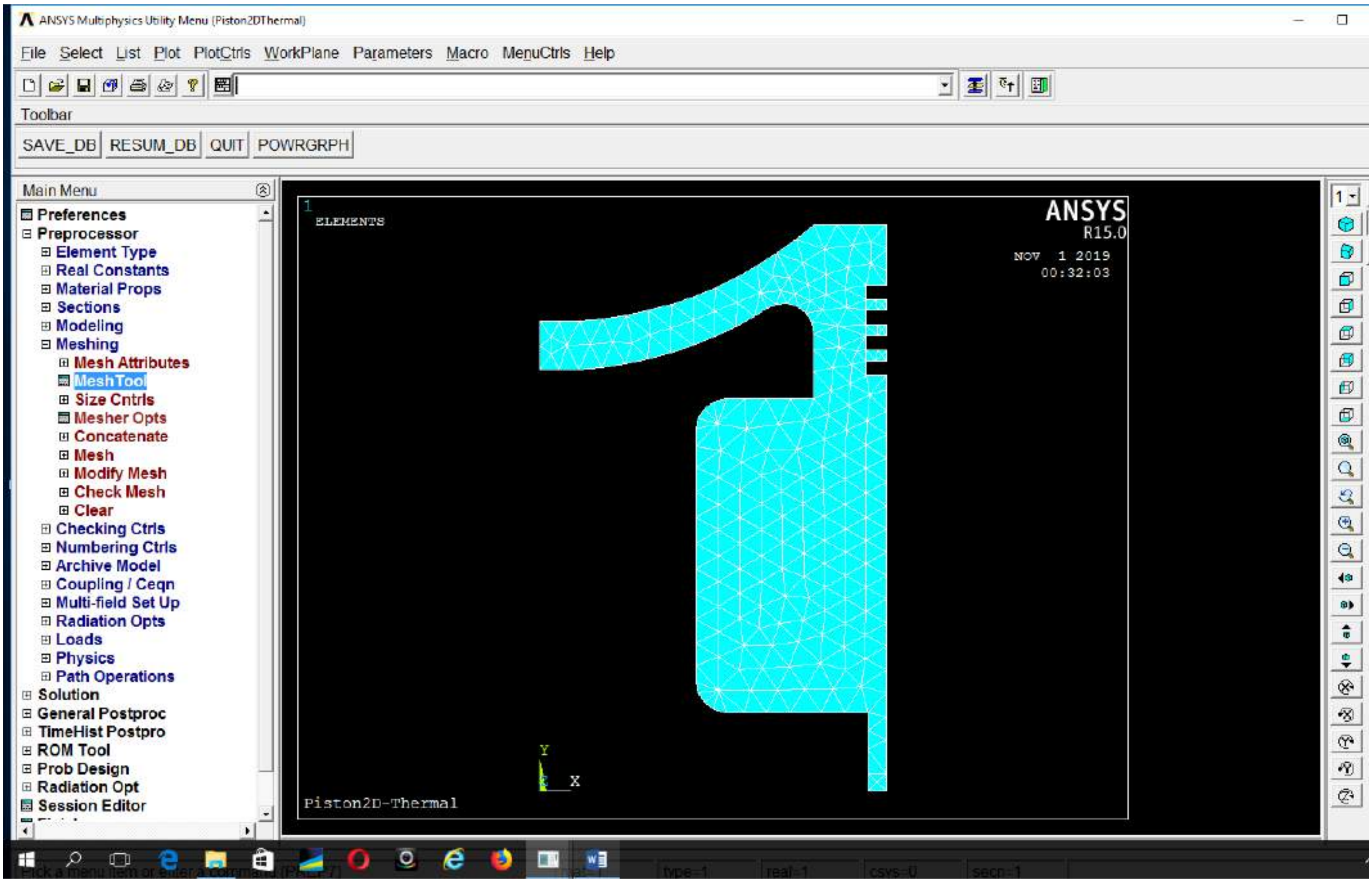

Figure 19 Axisymmetric Model meshed automatically into 372 elements and 859 nodes

2.3.6 Application of boundary conditions and thermal loads

Table 5 shows the piston thermal boundary conditions for the steady-state thermal analysis [11].

Table 5 The piston thermal boundary conditions

Thermal boundary	Bulk temperature (K)	Heat transfer coefficients (W/mm²K)
Top of Piston	$T_g = 3059.43$	$h_g = 5.39x10^{-4}$
Under Piston Crown (Lubricating oil coolant)	$T_{oil} = 393$	$h_{oil} = 6.95x10^{-4}$

Side of Piston (Water film coolant)	$T_{water} = 353$	$h_{water} = 2x10^{-4}$

The temperature of the oil (T_{oil}) in the crankcase from the literature is assumed to be 120^0C with a calculated heat transfer coefficient (h_{oil}) of 695.224 W/m^{2}K and that of the water film (T_{water}) assumed to be 80^0C with a heat transfer coefficient (h_{water}) of 200 W/m^{2}K [18].

The ANSYS solution produced the following contour plots for the axisymmetric and the 3D models, respectively. See Figures 20 and 21, respectively.

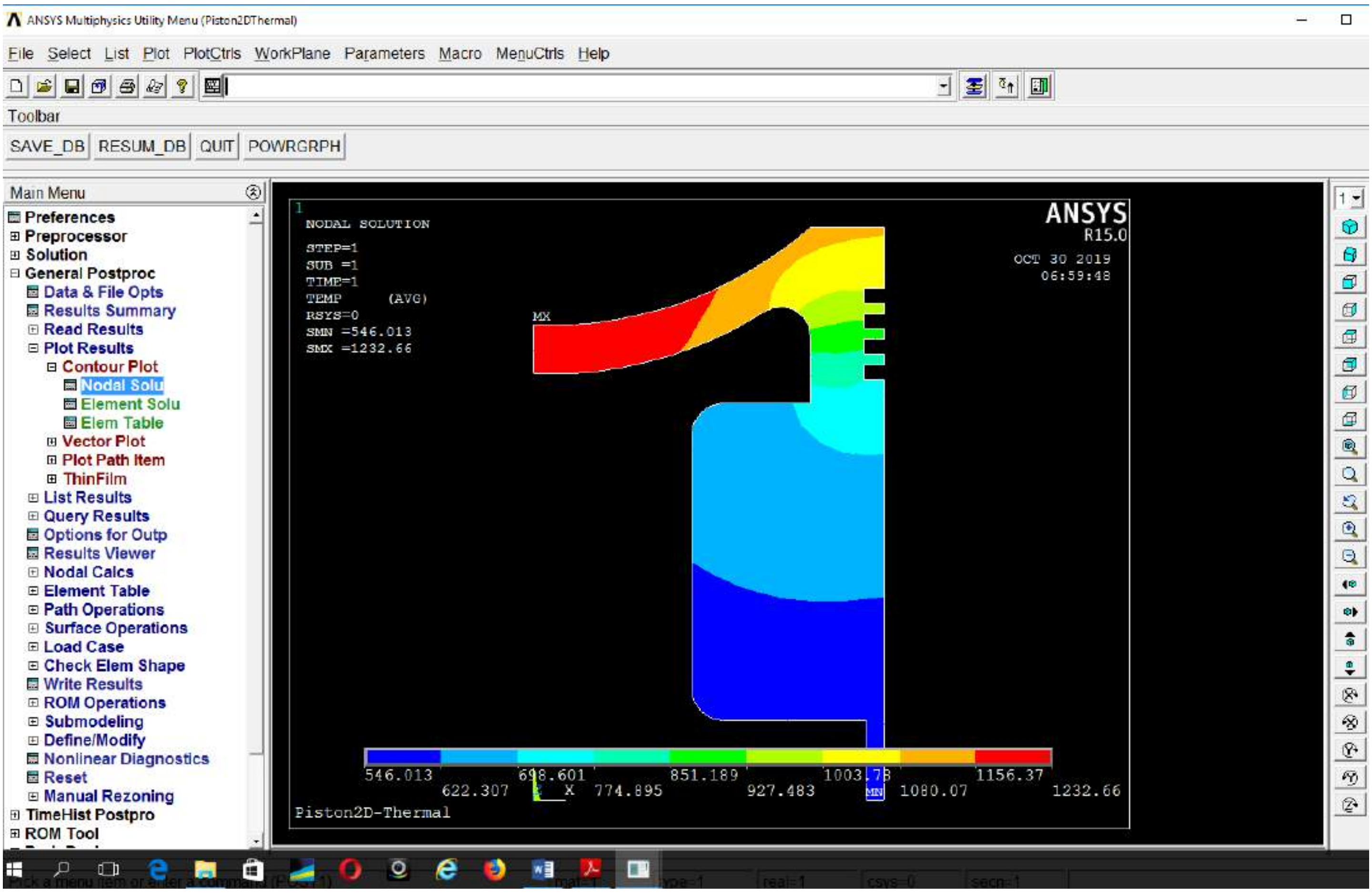

Figure 20 The contour plot of temperature distribution in the axisymmetric model

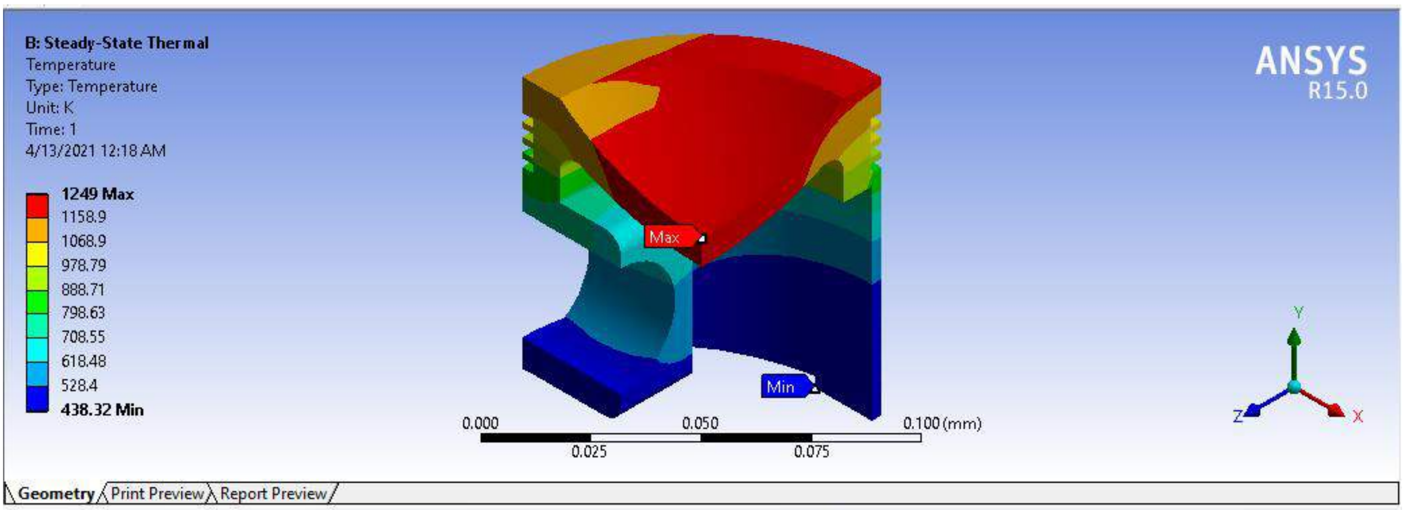

Figure 21 The contour plot of temperature distribution in the 3D quarter conventional piston

3.0 Results and Discussion

Table 6 shows the comparison of the results of the axisymmetric and the 3D models, respectively which were taken from the contour plots in Figures 20 and 21, respectively.

Table 6 Comparison of ANSYS simulated temperature distribution 2D Results with 3D results

Piston position on contour plot	ANSYS simulated 2D results (K)	ANSYS simulated 3D results (K)	Percentage deviation (%)
1	1232.70	1249.00	1.31
2	1156.40	1158.90	0.21
3	1080.07	1068.90	-1.04
4	1003.80	978.80	-2.55
5	927.50	888.70	-4.37
6	851.20	798.60	-6.59
7	774.90	708.60	-9.36
8	698.60	618.50	-12.95
9	622.31	528.40	-17.77

10	546.01	438.30	-24.57

Using Table 6, the graph of temperature distribution for the two models against piston position on the contour plots is plotted in Figure 22. This shows the comparison of nodal temperature distribution of axisymmetric model (2D) with the 3D model.

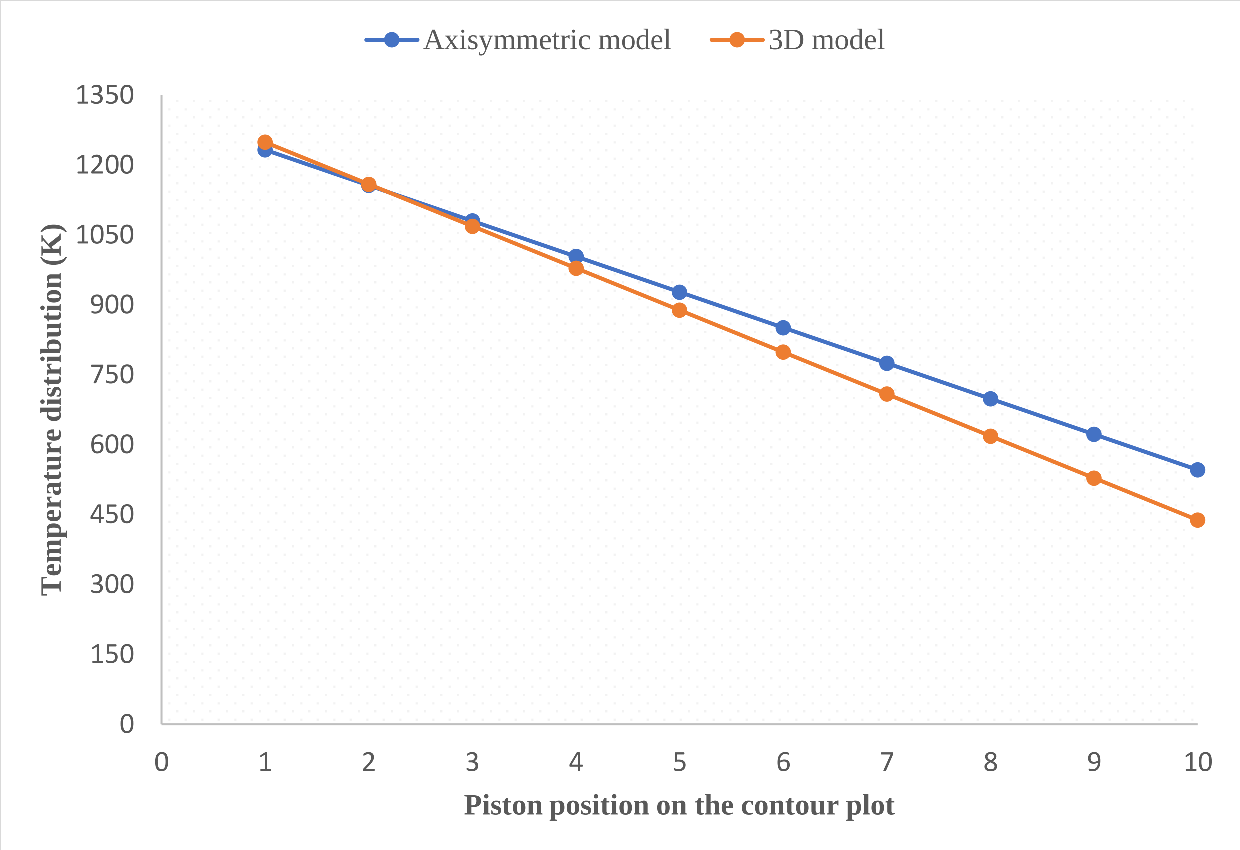

Figure 22 Comparison of temperature distribution in the axisymmetric model with the 3D model

The variation of temperature with piston position on the contour plots for the two models is presented in Figure 22. From Figure 22, with the axisymmetric (2D) model the minimum temperature which is 546.01 K is at the bottom part of the piston skirt while the maximum temperature which is 1232.70 K is on the piston crown's centre. However, with the 3D model, the minimum temperature which is 438.30 K is also at the bottom part of the piston skirt while the maximum temperature which is 1249.00 K is also at the piston crown's centre. The 3D model has a higher surface temperature on the piston crown centre and the lower temperature at the bottom part of the piston skirt. Figure 22 also shows that the 3D model conducts heat faster away from the piston due to the fast reduction in the temperatures from the top (piston crown) to the bottom (piston skirt). This will help to increase the life span of the piston.

4.0 Conclusions

The axisymmetric and 3D models of a conventional aluminium alloy piston (A2618) of a single-cylinder four-stroke diesel engine using the ZS1115NM diesel engine specification were successfully created. The steady-state thermal analysis for temperature distribution was done in ANSYS commercial software. The variation of temperature in the 3D model showed more accurate results because of more elements and nodes than the axisymmetric one. The maximum surface temperature on the piston top for the axisymmetric model was 1232.70 K while that for the 3D model was 1249 K. However, the percentage deviation of the two results in Table 6 was satisfactory. The two models have approximately the same brake thermal efficiency of 60 %.

References

[1] Lokesh, S., Suneer, S. R., Taufeeque, H., & Upendra, K. (2015). Finite Element Analysis of Piston in ANSYS. International Journal of Modern Trends in Engineering and Research (IJMTER) 2(4):619-626.

[2] Shirisha, G. S., & Sravani, D. K. (2016). Thermal Analysis of IC Engine Piston Using Finite Element Method. International Journal of Mechanical Engineering and Computer Applications 4(1):200-209.

[3] Dolan, J. A. (1991). Motor Vehicle Technology and Practical Work, Reprinted ed. Ibadan: Heinemann Educational Books Ltd 1-700.

[4] Akalin, O., & Newaz, G. M. (1998). A New Experimental Technique for Friction Simulation in Automotive Piston Ring and Cylinder Liners. SAE Paper 981407.

[5] Tadala, A., Naresh, K., Abdul, K., & Purushotham, A. K. (2016). Analysis of Four-Stroke Single-Cylinder Engine Piston by Using Aluminium Alloys (Al-GHS 1300, Al-Sic- Graphite, A6061 and Pure Aluminium). International Journal of Mechanical Engineering (SSRG-IJME) 3(1):4-12.

[6] Mahajan, K. S., & Deshmukh, S. H. (2016). Structural and Thermal Analysis of Piston. International Journal of Current Engineering and Technology 5:22-29.

[7] Ganesan, V. (2007). Internal Combustion Engines, 3rd ed. New Delhi: Tata McGraw-Hill Publishing Company Ltd 1-645.

[8] Roland, W. L., Perumal, N., & Kankanhalli, N. S. (2004). Fundamentals of the Finite Element Method for Heat and Fluid Flow, 2nd ed. UK: John Wiley and Sons Ltd 1-356.

[9] Bhavikatti, S.S., 2005. Finite element analysis. New Delhi: Age International Publishers Ltd, 1-347.

[10] David, V. H. (2004). Fundamentals of Finite Element Analysis, 1st ed. New York: McGraw-Hill Companies, Inc., 1-505.

[11] Isaac, F. O. (2023). Unpublished PhD Dissertation, Ambrose Alli University, Ekpoma 1-328.

[12] Ashby, M.F., 1999. Materials selection in mechanical design, 2nd ed. London: Butterworth- Heinemann, 1-513.

[13] Ashby, M. F. (2005). Materials Selection in Mechanical Design, 3rd ed. London: Butterworth-Heinemann, 1-602.

[14] Kent, L. L. (2005). ANSYS Tutorial, 1st ed. USA: Schroff Development Corporation Publications, 1-186.

[15] Isaac, F. O., & Abu, L. (2022). Modelling of a Conventional Piston of a Single-Cylinder Four-Stroke Diesel Engine by Using SolidWorks. FUOYE Journal of Engineering and Technology 7(1):65-68.

[16] Ansari, F. A., & Dhanajay, Y. (2022). Review Paper on Simulation, Analysis and Validation on Thermal Barrier Coated Piston of Diesel Engine. International Research Journal of Modernization in Engineering Technology and Science 4(2):260-270.

[17] ZS1115NM, 2015. Single-Cylinder Diesel Engine Owner's Manual. Changchai Company Ltd, China 1-40.

[18] Puran, S., & Deb, A. P. (2015). Structural and Thermal Analysis of Different Piston Materials with Cooling (Due to Combustion Pressure) Using Finite Element Analysis. International Journal of Automotive Engineering and Technologies 4(2):110-117.